HELLENIC REPUBLIC
National and Kapodistrian University of Athens

School of Medicine

First Department of Orthopaedic Surgery
"Attikon" University General Hospital
Chairman: Prof. Panayiotis J. Papagelopoulos, MD, DSc, FACS

DOCTORATE THESIS

Optimising Personalised Orthopaedic Operations Through Digital Design and 3D Printing

by

Ioannis I. Mavrodontis

BSc Mechanical Engineering, MSc Advanced Manufacturing

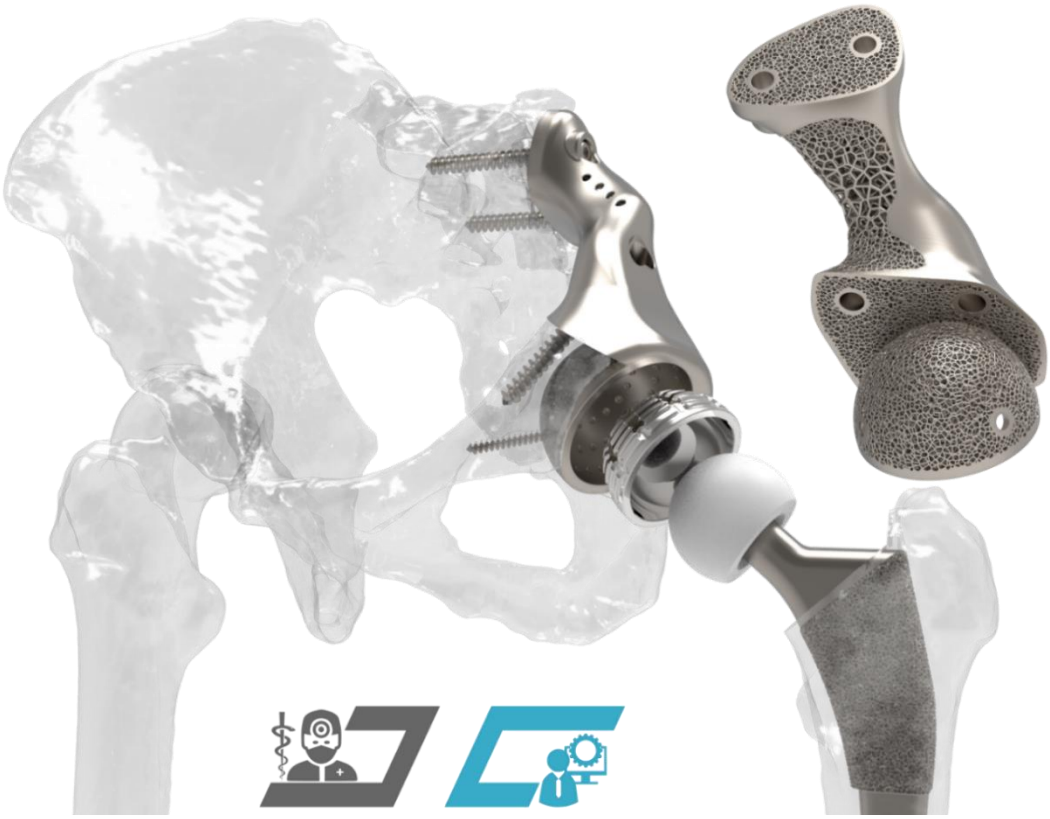

Athens, March 2024

ΕΛΛΗΝΙΚΗ ΔΗΜΟΚΡΑΤΙΑ
Εθνικό και Καποδιστριακό Πανεπιστήμιο Αθηνών
Ιατρική Σχολή

Α' Ορθοπαιδική Χειρουργική Κλινική
Πανεπιστημιακό Γενικό Νοσοκομείο «Αττικόν»
Διευθυντής: Καθηγητής Παναγιώτης Ι. Παπαγγελόπουλος, MD, DSc, FACS

ΔΙΔΑΚΤΟΡΙΚΗ ΔΙΑΤΡΙΒΗ

Βελτιστοποίηση Εξατομικευμένων Ορθοπαιδικών Επεμβάσεων δια Ψηφιακού Σχεδιασμού και 3D Εκτύπωσης

του

Ιωάννη Ι. Μαυροδόντη

BSc Μηχανολόγος Μηχανικός, MSc Προηγμένες Κατασκευές

Αθήνα, Μάρτιος 2024

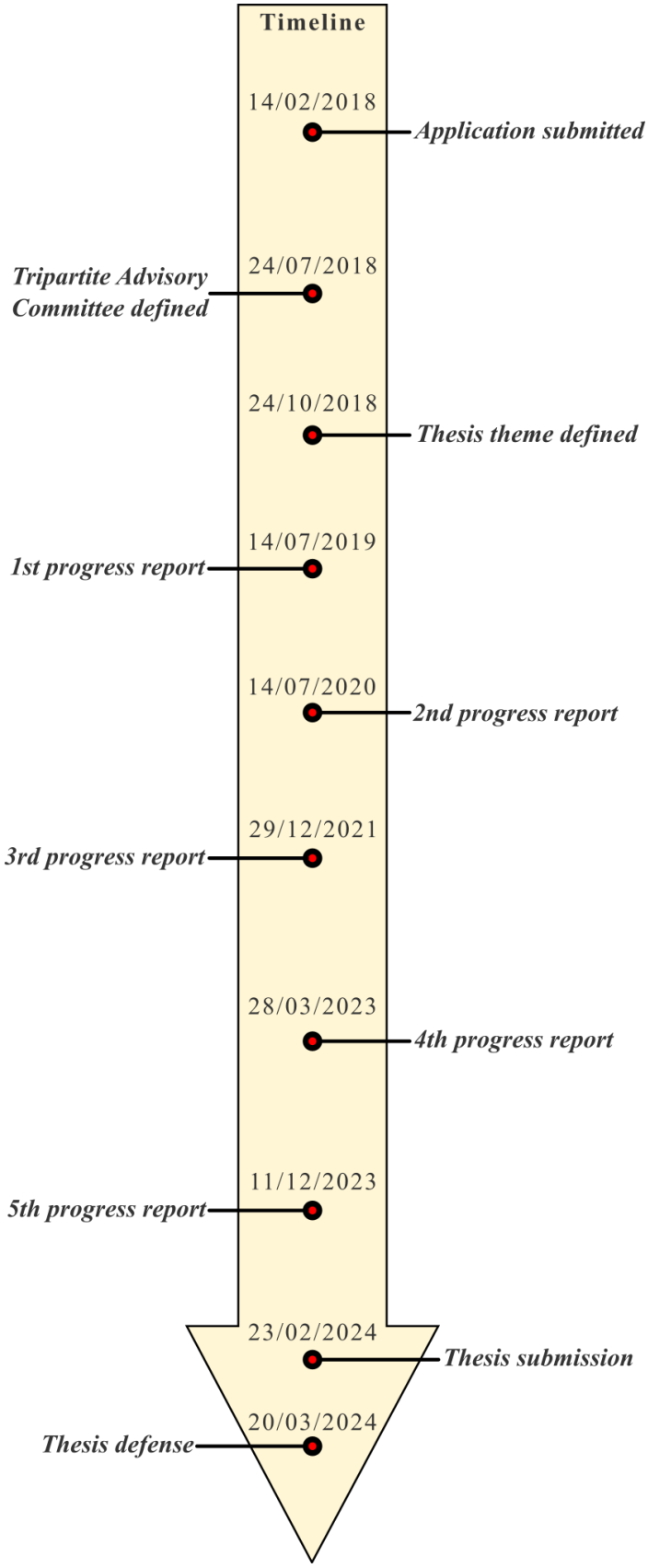
Timeline
14/02/2018
Application submitted
24/07/2018
Tripartite Advisory Committee defined
24/10/2018
Thesis theme defined
14/07/2019
1st progress report
14/07/2020
2nd progress report
29/12/2021
3rd progress report
28/03/2023
4th progress report
11/12/2023
5th progress report
23/02/2024
Thesis submission
20/03/2024
Thesis defense

Tripartite Advisory Committee

Panayiotis J. Papagelopoulos (Supervisor)

Professor and Chairman, First Department of Orthopaedic Surgery, School of Medicine, National and Kapodistrian University of Athens

Olga D. Savvidou

Professor, First Department of Orthopaedic Surgery, School of Medicine, National and Kapodistrian University of Athens

Vasileios A. Kontogeorgakos

Associate Professor, First Department of Orthopaedic Surgery, School of Medicine, National and Kapodistrian University of Athens

---

Main Researcher

Ioannis I. Mavrodontis

BSc Mechanical Engineering, MSc Advanced Manufacturing

Collaborating Clinics and Laboratories

Orthopaedic Research and Education Center "Panayiotis N. Soucacos"

"Attikon" University General Hospital, First Department of Orthopaedic Surgery, National and Kapodistrian University of Athens

Seven-member Committee of Inquiry

Panayiotis J. Papagelopoulos (Supervisor)

Professor and Chairman, School of Medicine, National and Kapodistrian University of Athens

Theodore G. Papaioannou

Professor, School of Medicine, National and Kapodistrian University of Athens

Olga D. Savvidou

Professor, School of Medicine, National and Kapodistrian University of Athens

Andreas F. Mavrogenis

Professor, School of Medicine, National and Kapodistrian University of Athens

Constantinos I. Stergiou

Professor, Mechanical Engineering, University of West Attica

Vasileios A. Kontogeorgakos

Associate Professor, School of Medicine, National and Kapodistrian University of Athens

Olympia G. Papakonstantinou

Associate Professor, School of Medicine, National and Kapodistrian University of Athens

Score: Excellent (7/7)

Prof. Nikolaos Arkadopoulos

Dean of School of Medicine, National and Kapodistrian University of Athens

Hippocrates Oath

I swear by Apollo Healer, by Asclepius, by Hygieia, by Panacea, and by all the gods and goddesses, making them my witnesses, that I will carry out, according to my ability and judgment, this oath and this indenture.

To hold my teacher in this art equal to my own parents; to make him partner in my livelihood; when he is in need of money to share mine with him; to consider his family as my own brothers, and to teach them this art, if they want to learn it, without fee or indenture; to impart precept, oral instruction, and all other instruction to my own sons, the sons of my teacher, and to indentured pupils who have taken the Healer's oath, but to nobody else.

I will use those dietary regimens which will benefit my patients according to my greatest ability and judgment, and I will do no harm or injustice to them. Neither will I administer a poison to anybody when asked to do so, nor will I suggest such a course. Similarly, I will not give to a woman a pessary to cause abortion. But I will keep pure and holy both my life and my art. I will not use the knife, not even, verily, on sufferers from stone, but I will give place to such as are craftsmen therein.

Into whatsoever houses I enter, I will enter to help the sick, and I will abstain from all intentional wrong-doing and harm, especially from abusing the bodies of man or woman, bond or free. And whatsoever I shall see or hear in the course of my profession, as well as outside my profession in my intercourse with men, if it be what should not be published abroad, I will never divulge, holding such things to be holy secrets.

Now if I carry out this oath, and break it not, may I gain for ever reputation among all men for my life and for my art; but if I break it and forswear myself, may the opposite befall me.

Author's Curriculum Vitæ

Ioannis I. Mavrodontis

BSc, MSc, PhD Cand.

Passionate about engineering and especially the "mechanical world", although believe in inter-epistemic and multidisciplinary synergy for problem-solving. Specialized in medical devices and other parts, tools, assemblies, networks, and machinery research, design, and manufacture. Interested in design optimization methodologies and biomimesis. Able to manage and carry out challenging custom-made projects from scratch to completion.

"Everything flows" -Heraclitus

Work Experience

2022- **Senior Mechanical Design Engineer**
Korr. (Kalithea, 17675 Attica, Greece. tothekorr.com)
Custom physical and digital user experience solutions

R&D of physical transaction and interaction devices:
- Brainstorming new ideas, principles of operations, and mechanisms.
- Proof-of-concept realization, testing, and experimentation.
- Detail 3D CAD of mechanical components, assemblies, and tools.
- Technical and financial evaluation of manufacture/production methodology.
- Prototyping and assembling for design evaluation and iteration.

2021-2022 **Senior Mechanical Design Engineer**
Printec Group (Moschato, 18344Attica, Greece. printec.com)
Custom physical and digital user experience solutions

R&D of physical transaction and interaction devices:
- Brainstorming new ideas, principles of operations, and mechanisms.
- Proof-of-concept realization, testing, and experimentation.
- Detail 3D CAD of mechanical components, assemblies, and tools.
- Technical and financial evaluation of manufacture/production methodology.
- Prototyping and assembling for design evaluation and iteration.

2018-2021 **Head of Engineering Design & Manufacture**
Insol Ltd (Aspropirgos, 19300 Attica, Greece. insol.com.gr)
Fully automated solutions and machinery for the food industry
End-to-end project engagement to deliver bespoke turn-key systems:
- Technical and financial offers preparation as per the client's requirements.
- R&D and detail 3D CAD/CAM of mechanical components, assemblies, and tools.
- P&ID diagrams composition followed by detailed equipment and piping networks 3D design conforming to hygienic standards.
- Market research and communication with partner material suppliers.
- BOM, manufacturing drawings generation, and production planning.
- Design and production process inspection and troubleshooting to deliver optimal solutions.
- Installation and start-up supervision.

2015-2016 ***Mechanical Design & Manufacture Engineer***
Axon Engineering SA (Oinofyta, 32011 Viotia, Greece. axoneng.gr)
Complex aerospace and military components

High-precision assemblies, parts, tools design, and fabrication:
- 3D CAD design.
- Programming CNC machining operations (CAM).
- Manufacturing planning.
- Production inspection and supervision.
- Packaging design.

2014 **Apprentice Mechanical Engineer**
Hellenic Aerospace Industry (Schimatari, 32009 Viotia, Greece. haicorp.com)
Manufacturer and MRO of aeronautical components
- Hands-on MRO, testing, and installation of aircraft propellers (Lockheed Hercules C-130, Bombardier CL-215 & CL-415).
- Design and manufacture molds for advanced composite parts.

2013 **Associate Mechanical Design Engineer**
Maria Liakou Civil Engineering Office
- Buildings inspection.
- 2D Mechanical layouts design.

Education

2018-2024 **PhD Candidate**
National and Kapodistrian University of Athens, School of Medicine (Athens, 11527 Attica, Greece. uoa.gr), First Department of Orthopaedic Surgery at "Attikon" University General Hospital (Chaidari, 12462 Attica, Greece. attikonhospital.gov.gr)
PhD title:
Optimizing Personalized Orthopaedic Operations Through Digital Design and 3D Printing

2016-2017 **MSc Advanced Manufacturing (Grade: Distinction)**
University of Strathclyde (G11XQ Glasgow, United Kingdom. strath.ac.uk)
MSc dissertation title:
Optimised additive manufacturing of biomimetic orthopaedic implants

2010-2015 **BSc Mechanical engineering (Grade: First-class honours 82%)**
University of West Attica (Egaleo, 12244 Attica, Greece. uniwa.gr)
BSc dissertation title:
Additive manufacturing technologies. Design, manufacture and operation of a material extrusion machine ("Morpheas" 3D printer)

Personal Skills

Mother tongue: Greek, Russian

Other languages: English language certificates: *University Of Michigan ECPE, IELTS 7/9*

Digital Competence
- Operating systems: *Linux, Apple Macintosh, MS Windows*
- Office suites: *Open, MS, Google Docs.*
- Image processing & Graphics: *Adobe Photoshop, Illustrator, Premier and After Effects, Gimp, Inkscape.*
- CAD/CAM/CAE: *Autodesk Autocad, Inventor and Fusion 360, DS Catia and Solidworks, Siemens NX and Solidedge, Missler TopSolid, Blender, Robert McNeel & Associates Rhiniceros, 3D System's Freeform Plus, nTopology, Vero Edgecam, ANSYS.*
- Programming: *C, html5, G-code, Mathworks Matlab, NI Labview.*
- Other: *PC-based CNC controllers (LinuxCNC, ArtSoft Mach3), LaTeX/XeLaTeX word processing, 3DSlicer, Materialise MIMICS & 3-matic, 3D printing process planning software.*

Other skills

- Strong organizational and managerial skills with a responsive problem-solving focus.
- Fast learner and adaptable to work under pressure with no supervision.
- Engineering and optimization techniques emphasizing on cost, time, quality, function, and aesthetics.
- Analytical thinking for systematic engineering design from conceptualization to materialization.
- Theoretical and hands-on expertise oin traditional and advanced manufacturing technologies.
- Experience with mechatronic systems and programming micro-controllers.
- 3D Printing for rapid prototyping and end-manufacturing.
- User-oriented proposal presentations and quotations preparation.
- Technical and financial feasibility studies.

Additional Info

Honours and awards

- Scott advanced manufacturing scholarship *(University of Strathclyde, 2016).*
- Fully funded place *(University of Strathclyde, 2016).*
- Award for achieving the best average semester grade *(State Scholarships Foundation, 2013).*
- Award for achieving the best average semester grade *(State Scholarships Foundation, 2014).*

Seminars

- "Labview programming: Measuring and systems control", 30 hours seminar, University of West Attica.

Driving licence

A, B

Design & Manufacture Projects

- Autonomous line-following robot.
- "Morpheas" material extrusion 3d printer.
- "Rabbitron" agricultural robot.
- "Nanobot" 6 DOF micro-milling machine tool.
- ATM module redesign for 3d printing.
- Dual material extrusion 3d printer "Morpheas #2".
- Patient lifting and transferring hoist EasyGo Lift.
- Custom orthopaedic and orthodontic devices.
- Cheese and yogurt production lines.
- Cheese cube cutting machine.
- Milk heating systems.
- Milk and cream pasteurizing systems.
- Cheese packaging line.
- Sanitary silos and mixing tanks.
- Sanitary and ancillary piping networks and valve clusters.
- Optimised 3d printing of patient-specific biomimetic orthopaedic implants.
- Face shields against COVID-19 pandemic: 3D Printing & Injection Molding.
- User interaction and transaction devices.
- Pharmaceuticals venting machine.

Conferences and Publications

- Exhibitor and speaker @ Industrial Projects Conference 2017, University of Strathclyde's Technology and Innovation Centre. Title: "Feasibility Study: Additive Manufacturing in ATM design and manufacture".
- Exhibitor and speaker @ First Student Innovation Festival 2014, Piraeus University of Applied Sciences' Conference Center. Title: "Morpheas" 3D printing machine.
- Exhibitor and speaker @ Innovative Business Plans Competition 2014, Piraeus University of Applied Sciences' Conference Center. Title: "MorphoTech 3D labs: 3D printing machines and services".
- Speaker @ "Applied Biomechanics and 3D Technologies in Orthopaedics" Conference, Hellenic Association of Orthopaedic Surgeons, Athens, 2019. Title: "Optimising Orthopaedic Operations Through Synergy Between Orthopaedics-Mechanical Engineering".
- Speaker @ "Biomechanical, Biological & Technological Advancements in Orthopaedics" Conference, Metropolitan Hospital, Athens, 2019. Title: "3D (Bio)Printing (R)Evolution: Shifting from Reconstructive to Regenerative Orthopaedics".
- Papagelopoulos, P.J., Savvidou, O.D., Koutsouradis, P.K., Chloros, G.D., Bolia, I.K., Sakellariou, V.I., Kontogeorgakos, V.A., Mavrodontis, I.I., Mavrogenis, A.F. and Diamantopoulos, P., 2018. Three-dimensional Technologies in Orthopedics. *Orthopedics*, 41(1), pp.12-20.
- Mavrodontis, I.I., Trikoupis, I.G., Kontogeorgakos, V.A., Savvidou, O.D. and Papagelopoulos, P.J., 2024. Point-of-Care Orthopedic Oncology Device Development. *Current Oncology*, 31 (1), pp.211-228.
- Trikoupis, I.G., Mavrodontis, I.I., Papadopoulos, D.V., Goumenos, S.D., Georgouli, D.A., Gavriil, P.A., Melissaridou, D., Savvidou, O.D., Kontogeorgakos, V.A. and Papagelopoulos, P.J., 2024. 3D-printed glenoid implant reconstruction, after partial scapulectomy for malignant tumors. a case series. *European Journal of Orthopaedic Surgery & Traumatology.*

Teaching

- Helped in gaining approval and establishing the MSc program "Applied Biomechanics in Orthopaedics", National and Kapodistrian University of Athens, School of Medicine.
- Taught "Manufacturing processes & 3D printing of biomaterials" in 2020, module of MSc "Applied Biomechanics in Orthopaedics", National and Kapodistrian University of Athens, School of Medicine.

Volunteering

- Tree planting for Parnitha mountain reforestation.
- Beaches cleaning in West Attica.
- Face shields design, mass production, and packaging for COVID-19 pandemic.

Interests

- Cycling & hiking.
- Traveling.
- Reading & researching.
- "Maker culture".
- Drawing.

Author's Rights Declaration

© 2024 by Ioannis I. Mavrodontis. Some rights reserved.

The content of this doctorate Thesis is licensed under the terms of
Creative Commons Attribution – Non-Commercial - Share Alike 4.0 International License.
Due attribution to the author and title of this doctorate Thesis must always be made of the use of any material contained in, or derived from, this doctorate Thesis.

The approval of this doctorate Thesis from the School of Medicine of the National and Kapodistrian University of Athens does not imply acceptance of the author's opinions (Law 5343/1932, article 202, comma 2).

Statement of Academic Honesty

I declare that this submission is entirely my own original work.

I declare that, except where fully referenced direct quotations have been included, no aspect of this submission has been copied from any other source.

I declare that all other works cited in this submission have been appropriately referenced.

I declare that I have reviewed this submission and it complies with the departmental standards.

I understand that any act of academic dishonesty such as plagiarism or collusion may result in the non-award of my degree.

Signed

Dated

20th of March 2024

Abstract

The theme of this Thesis is the Point-of-Care (PoC) utilization of emblematic 3D technologies (3D digital design, 3D Printing (3DP), Virtual/Augmented/Mixed Reality (xR)) that enable the realization of scientifically amalgamated inter-epistemic schemes in a medical setting to simplify orthopaedic operations by complex pre-operative planning and (bio)mechanical engineering, thus delivering fast high-quality (in)tangible customized solutions to improve individualized patient healthcare.

The Thesis is structured in eight sections and many sub-sections to ultimately transition from the general to the specific part, whilst the reader is presented with a plethora of visual material. All required software and hardware means to develop individualized orthopaedic services and products at the PoC are covered and many details, step-by-step guidelines, and notes are provided to enable the fabrication of patient-specific orthopeaedic solutions featuring optimized biomimetic structures.

The state of the art is unfolded in the first section. The characteristics of individualized orthopaedic rehabilitation, inter-epistemic synergy and enabling technologies, and PoC 3D Units are covered.

In section two, the theme, approach, and structure are impressed, and the hypothesis is introduced, suggesting that inter-epistemic workflows exploiting the triad of 3D digital design, 3DP, and xR technologies could be disruptive for individualized orthopaedics, especially if routinely applied at or near the PoC.

Section three provides a critical literature review on the use of biomaterials in modern reconstructive orthopaedics and Tissue Engineering (TE) for regenerative medicine. Emphasis is given on manufacturing and 3DP techniques, including bibliography, historical background, features of 3DP technologies, process flow chain for 3DP, their characteristics, and potential. The adoption of advanced 3D digital design tools and 3DP for PoC 3D Units and their impacts on orthopaedics are highlighted. The potential of 3DP for boosting the design and materialization of optimized forms as well as associated challenges and issues are analyzed; biomimetic designs, architected endo and exo-structures, and meta-(bio)materials-by-design for mechanical and biological superiority. xR technologies and applications in orthopaedics are also discussed.

In section four, the research rationale is justified and the methodology to approach the initial hypothesis is set. A de-novo 15-step role-based end-to-end systematic inter-epistemic patient-specific orthopaedic product design workflow is created and applied to solve selected case studies at the PoC.

Two scenarios for PoC 3D Unit establishment and associated topics are discussed for distributed and localized manufacturing in section five; organizational structure and framework, online platform for data exchange, regulations and quality management system, hardware and software equipment, infrastructure and layout, and costing. A small hypodigmatic pilot PoC 3D Unit was established as per the available resources.

In section six, selected case studies are solved at the pilot PoC 3D Unit as per the 15-step inter-epistemic workflow set, utilizing advanced 3D digital design and optimization techniques, xR, and 3DP. Five oncological case studies about pelvic and sacrum tumor resection and reconstruction using patient-specific instrumentation and custom-made artificial endo-prostheses are presented. Anatomical structures, surgical instruments, and endo-prostheses were visualized digitally, virtually, and physically before issuing the final

documentation for approval to enable the materialization of the collaboratively developed solutions. The first case is analytically described step-by-step whilst justifying each selection and decision, and alternative design options are also being explored. For the other oncological cases, the final solutions are demonstrated. A case study on patient-specific orthotic devices using 3D scanning is also carried out.

The results are discussed in section seven and the conclusions and future work in section eight. The developed patient-specific solutions were successfully prototyped at the pilot PoC at acceptable clinical times and costs, whereas the end polymer and metallic parts that required industrial-grade machines were outsourced to external partners for production. 3DP of polymer anatomical models, surgical guides, and implant prototyping, along with xR systems for pre-operative planning and intra-operative (non-navigation) purposes can be implemented at relatively low initial capital investments and operating and maintenance costs. A plethora of trade-offs can be made for PoC 3D Units in terms of software and hardware equipment, layout, personnel, etc. It is orthological for interested healthcare facilities to commence with in-house 3D design and 3DP only for prototyping and outsourcing the end parts, and only if sufficient demand exists to implement in situ final manufacturing and increase their capacity. Investments should be rationalized and driven by clinical needs so that the collaboratively developed solutions are clinically and scientifically relevant and ultimately beneficial for each unique patient. Non-technical challenges (regulatory compliance, lack of directives, standards and quality management systems, need for skilled personnel) and technical limitations still hold 3D technologies from springboarding and should be addressed. As necessity drives invention and innovation, once the readiness of 3D technologies stops remaining under question and their costs in tandem with the required medical device development time will be further reduced, their PoC incorporation will accelerate orthopaedics into intelligent formats capable of unlocking mass-customization with high-quality end-results and increased patient satisfaction.

Healthcare was traditionally a non-engineering design and non-manufacturing sector as neither design nor manufacturing has been taking place in situ. As 3D design and manufacturing technologies are now being adopted, the transformation of healthcare facilities into decentralized design and/or manufacturing sites is viable. PoC 3D Units aiming at medical device development should be established accordingly to facilitate the symbiosis of healthcare professionals with skilled (bio)mechanical engineers to develop patient-specific devices at the PoC within acceptable lead times and costs. (Bio)mechanical engineers could enable orthopaedic surgeons to actively participate in medical device making at or near the PoC for clinical applications. Novel approaches by advanced 3D digital design and optimization, coupled with the freedom offered by 3DP should be embraced to architect (bio)meta-materials-by-design and develop smart medical devices for reconstructive orthopaedics, though there is a need to shift towards TE for regenerative medicine and other smart and innovative approaches.

Although related pitfalls are known to engineers, an increased awareness is suggested to explore and exploit the full potential of the 3D design-3DP-xR triad that introduces entirely new abilities for delivering medical devices at the PoC with greater customization, innovation in design, cost-effectiveness, and high quality.

Περίληψη

Η παρούσα Διδακτορική Διατριβή πραγματεύεται την αξιοποίηση εμβληματικών τρισδιάστατων (3D) τεχνολογιών (3D ψηφιακός σχεδιασμός, 3D εκτύπωση (3DP), εικονική/επαυξημένη/ανάμικτη πραγματικότητα (xR)) στο σημείο περίθαλψης (PoC), για την δημιουργία διεπιστημονικών συνεργειών που μπορούν να προσφέρουν ταχεία ανάπτυξη απτών ή/και μη απτών εξατομικευμένων λύσεων υψηλής ποιότητας και να μεταφέρουν το επίπεδο δυσκολίας και πολυπλοκότητας στον προεπεμβατικό σχεδιασμό, με αποτέλεσμα να απλοποιούνται οι ορθοπαιδικές επεμβάσεις, με απώτερο σκοπό την βελτίωση της παρεχόμενης ιατρικής φροντίδας σε κάθε μοναδικό ασθενή.

Η Διατριβή είναι δομημένη σε οκτώ κεφάλαια και αρκετά υποκεφάλαια για την μετάβαση από το γενικό στο ειδικό μέρος, ενώ παρουσιάζεται πληθώρα γραφικών στον αναγνώστη. Αναφέρονται όλα τα απαραίτητα υλικά και λογισμικά για την ανάπτυξη εξατομικευμένων λύσεων στο PoC, ενώ δίνονται οδηγίες βήμα-βήμα και σημειώσεις περί της ανάπτυξης και τελικά υλοποίησης εξατομικευμένων ορθοπαιδικών προϊόντων τα οποία εμπεριέχουν βελτιστοποιημένες βιομιμητικές δομές.

Στο πρώτο εισαγωγικό κεφάλαιο αναφέρονται τα χαρακτηριστικά της εξατομικευμένης προσέγγισης στην ορθοπαιδική, οι 3D τεχνολογίες που επιτρέπουν την δημιουργία της απαραίτητης διεπιστημονικής συνέργειας, αλλά και οι 3D Μονάδες που μπορούν να εγκατασταθούν μέσα ή δίπλα στα PoCs (νοσοκομεία, κλινικές).

Στο δεύτερο κεφάλαιο αποτυπώνεται το θέμα, η προσέγγιση, η δομή και η υπόθεση της Διατριβής, δηλαδή η έρευνα ωφέλειας της εφαρμογής της τριάδας 3D ψηφιακού σχεδιασμού-3DP-xR σε PoC 3D Μονάδες, υπό κατάλληλη διεπιστημονική συνέργεια ορθοπαιδικών-μηχανικών και βάση κατάλληλης συστηματικής μεθοδολογίας.

Το τρίτο κεφάλαιο περιλαμβάνει κριτική βιβλιογραφική ανάλυση περί των βιοϋλικών που χρησιμοποιούνται στην ορθοπαιδική και στην ιστομηχανική για αναγεννητική ιατρική. Ιδιαίτερη έμφαση δίνεται στις τεχνολογίες 3DP, και συγκεκριμένα στην σχετική βιβλιογραφία, ιστορική αναδρομή, κατηγορίες, σχεδιασμός για 3DP, χαρακτηριστικά και δυνατότητες. Αναφέρονται τα οφέλη ενσωμάτωσης προηγμένων εργαλείων 3D σχεδίασης και 3DP σε PoC 3D Μονάδες για την υλοποίηση βελτιστοποιημένων βιομιμητικών μέτα-προϊόντων που κατέχουν κατάλληλες εσωτερικές και εξωτερικές δομές για μηχανική και βιολογική υπεροχή, ενώ αναλύονται και σχετικές προκλήσεις. Τέλος, περιγράφονται οι εφαρμογές των xR τεχνολογιών στην ορθοπαιδική.

Στο τέταρτο κεφάλαιο, αιτιολογείται το σκεπτικό της έρευνας και τίθεται η μεθοδολογία προσέγγισης της αρχικής υπόθεσης. Δημιουργείται μια κατάλληλη και νέα συστηματική διεπιστημονική μεθοδολογία που περιλαμβάνει 15 βήματα για την ανάπτυξη εξατομικευμένων ορθοπαιδικών λύσεων, και εφαρμόζεται σε επιλεγμένα περιστατικά για την επίλυση μυοσκελετικών προβλημάτων.

Στο πέμπτο κεφάλαιο, περιγράφονται δυο σενάρια σχετικά με την ίδρυση κατάλληλης PoC 3D Μονάδας και αναπτύσσονται σχετικά θέματα για τοπική και διανεμημένη ανάπτυξη ορθοπαιδικών λύσεων, δηλαδή: δομή και πλαίσιο λειτουργίας, διαδικτυακή πλατφόρμα, κανονισμοί και συστήματα διασφάλισης και ελέγχου

ποιότητας, εξοπλισμός (υλικά, λογισμικά), κατόψεις και υποδομές, και κοστολόγηση. Τέλος, παρουσιάζεται η ίδρυση μιας μικρής υποδειγματικής PoC 3D Μονάδας χρησιμοποιώντας τους διαθέσιμους πόρους.

Το κεφάλαιο έξι αφορά τα επιλεγμένα περιστατικά τα οποία λύνονται χρησιμοποιώντας την διεπιστημονική μεθοδολογία 15 βημάτων και την υποδειγματική PoC 3D Μονάδα. Σε όλα τα περιστατικά χρησιμοποιήθηκαν προηγμένες μέθοδοι 3D σχεδιασμού, 3DP και xR. Για τα πέντε πρώτα ογκολογικά περιστατικά (όγκοι πυέλου και ιερού οστού) αναπτύχθηκαν ανατομικές δομές, εξατομικευμένα χειρουργικά εργαλεία και ενδοπροθέσεις 3D ψηφιακά, σε περιβάλλοντα xR, όπως επίσης υλοποιήθηκαν με 3DP για προεπεμβατικό έλεγχο πριν την τελική κατασκευή με 3DP. Το πρώτο περιστατικό αναλύεται λεπτομερώς βήμα-βήμα, δικαιολογώντας κάθε επιλογή και παρέχοντας εναλλακτικές για κάθε περίπτωση, ενώ για τα υπόλοιπα περιστατικά παρουσιάζονται οι τελικές λύσεις. Το έκτο περιστατικό αφορά 3D σάρωση, σχεδιασμό και υλοποίηση (3DP) εξατομικευμένου ορθοτικού προϊόντος (νάρθηκας χειρός).

Τα αποτελέσματα σχολιάζονται στο κεφάλαιο επτά και τα συμπεράσματα και μελλοντικές εργασίες δίνονται στο κεφάλαιο οκτώ. Όλες οι λύσεις που αναπτύχθηκαν, πρωτοτυποποιήθηκαν επιτυχώς στην μικρή υποδειγματική PoC 3D Μονάδα εντός κλινικά αποδεκτών χρόνων και κόστους, ενώ τα τελικά μεταλλικά και πολυμερή τεμάχια των λύσεων που απαιτούσαν βιομηχανικού τύπου 3D εκτυπωτές στάλθηκαν για κατασκευή σε εξωτερικούς συνεργάτες. Η 3DP πολυμερών ανατομικών μοντέλων, χειρουργικών εργαλείων και δοκιμαστικών εμφυτευμάτων, μαζί και η χρήση των τεχνολογιών xR για προεπεμβατικό σχεδιασμό και διεγχειρητική χρήση μπορεί να ενσωματωθεί σε νοσοκομεία και κλινικές με χαμηλό κεφάλαιο και με χαμηλό κόστος λειτουργίας και συντήρησης. Υπάρχουν πολλά διαφορετικά σενάρια PoC 3D Μονάδων που αφορούν την λειτουργία, εξοπλισμό, υποδομές, προσωπικό κ.ο.κ. Είναι ορθολογικό για τα ενδιαφερόμενα νοσοκομεία και κλινικές να ξεκινήσουν με 3D σχεδιασμό και 3DP για πρωτοτυποποίηση και ανάθεση τελικής κατασκευής σε εξωτερικούς συνεργάτες, και να ενσωματώσουν τελική κατασκευή μόνο εφόσον υπάρχει αρκετή ζήτηση. Οι επενδύσεις θα πρέπει να δικαιολογούνται και να οδηγούνται από τις κλινικές ανάγκες ώστε κάθε λύση που αναπτύσσεται να είναι κλινικά και επιστημονικά αποδεκτή και ευεργετική για κάθε μοναδικό ασθενή. Μη τεχνικές προκλήσεις (κανονισμοί, πρότυπα και συστήματα διαχείρισης ποιότητας, εξειδικευμένο προσωπικό) και τεχνικοί περιορισμοί εξακολουθούν να εμποδίζουν το PoC εφαλτήριο των 3D τεχνολογιών και πρέπει να αντιμετωπιστούν.

Καθώς η αναγκαιότητα οδηγεί την εφεύρεση και την καινοτομία, μόλις η ετοιμότητα των 3D τεχνολογιών σταματήσει να αμφισβητείται και το κόστος τους σε συνδυασμό με τον απαιτούμενο χρόνο ανάπτυξης ιατρικών προϊόντων μειωθεί περαιτέρω, η PoC ενσωμάτωσή τους θα επιταχύνει την ορθοπαιδική προς μια πιο έξυπνη κατάσταση για να ξεκλειδωθεί η μαζική προσαρμογή με υψηλή ποιότητα εφαρμογών και αυξημένη ικανοποίηση των ασθενών.

Οι ορθοπαιδικές κλινικές και τα νοσοκομεία είναι χώροι όπου εντός αυτών δεν αναπτύσσονταν ή/και κατασκευάζονταν εξατομικευμένες λύσεις. Καθώς οι 3D τεχνολογίες εξελίσσονται και είναι προσβάσιμες, είναι πλέον εφικτή η PoC ενσωμάτωσή τους. Τέτοιες PoC 3D Μονάδες θα πρέπει να ιδρύονται και να λειτουργούν κατάλληλα ώστε να εξυπηρετείται η συμβίωση ορθοπαιδικών και μηχανικών για την γρήγορη ανάπτυξη εξατομικευμένων λύσεων με χαμηλό κόστος και υψηλή ποιότητα. Οι μηχανικοί μπορούν να

επιτρέψουν την ενεργή συμμετοχή των ορθοπαιδικών στην ανάπτυξη κάθε λύσης. Καινοτόμες προσεγγίσεις προηγμένου 3D σχεδιασμό και βελτιστοποίηση, και 3DP μπορούν να εφαρμοστούν για την υλοποίηση μέτα-προϊόντων και «έξυπνων» συσκευών, ενώ μπορεί να δοθεί ιδιαίτερη έμφαση στις τεχνικές ιστομηχανικής και αναγεννητικής ιατρικής και σε άλλες επαναστατικές μεθοδολογίες αντιμετώπισης μυοσκελετικών παθήσεων.

Παρόλο που οι σχετικοί κίνδυνοι είναι γνωστοί στους μηχανικούς, προτείνεται αυξημένη ευαισθητοποίηση για να αποφευχθούν οι κίνδυνοι αλλά και για να εξερευνηθούν και να αξιοποιηθούν πλήρως οι δυνατότητες των 3D τεχνολογιών που εισάγουν νέες προσεγγίσεις με μεγαλύτερο βαθμό προσαρμογής σε κάθε ασθενή, καινοτομία στο σχεδιασμό, βέλτιστη σχέση κόστους-αποτελεσματικότητας και υψηλή ποιότητα.

Acknowledgments

I would like to express my sincere gratitude to Professor and Chairman of the First Department of Orthopaedic Surgery Panayiotis J. Papagelopoulos for his invaluable supervision and insightful guidelines throughout these years, boosting my motivation to carry out this research work. His dynamism and disruptive view on embracing emblematic 3D technologies and tools into the ecosystem of modern orthopaedic practice springboarded my understanding and made me emphasize the potential and prerequisites needed to practically form inter-epistemic synergies between (bio)mechanical engineering and orthopaedics for developing individualized orthopaedic rehabilitation products in situ, at the Point-of-Care.

I am deeply thankful to Professor Olga D. Savvidou and Associate Professor Vasileios A. Kontogeorgakos for their mentorship, who along with Professor and Chairman Panayiotis J. Papagelopoulos formed the Tripartite Advisory Committee. Their unwavering input of orthopaedic expertise and critique of this research shaped the methodology and methods used to approach the theme, investigate the hypothesis, and achieve the goals. A highly sought set of skills was acquired, as well as great experience to pursue a career either in academia or in industry.

My gratitude extends to the First Department of Orthopaedic Surgery, School of Medicine, National and Kapodistrian University of Athens, for providing me the opportunity to undertake a doctorate research program and enjoy cherished moments, from start to completion.

I eulogize and express my greatest respect and appreciation to my wife Megi and our little daughter Emmelia. Her unconditioned comprehension and encouragement these years acted like supportive energy injections that fed my passion to complete this research with zeal.

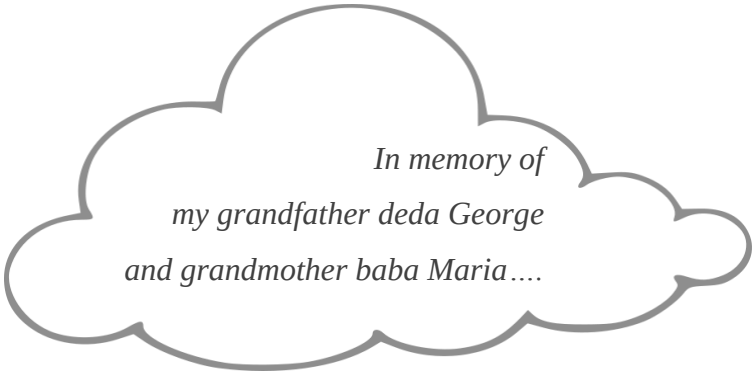
In memory of
my grandfather deda George
and grandmother baba Maria….

Table of Contents

GENERAL PART

1. Introduction: State of the Art 1

1.1 Individualized Orthop(a)edics 1

1.2 Inter-epistemic Synergy 6

1.3 Synergy-Enabling Technologies 10

1.4 Point-of-Care Units and 3D Technologies 17

2. About the Thesis 23

2.1 Theme, Approach and Structure 23

3. Critical Literature Review 26

3.1 Biomaterials: Osseointegration and Infection 26

3.2 Tissue Engineering for Regeneration 43

3.3 About Manufacturing and 3D Printing 48

3.3.1 Principle of Operation 52

3.3.2 Bibliography 56

3.3.3 Historical Background 60

3.3.4 3D Printing Technologies 68

3.3.5 Generic Process Flow Chain 77

3.3.6 Characteristics and Potential 81

3.4 About 3D Technologies in Orthopaedic Point-of-Care Units 94

3.5 3D Printing Applications and Impacts on Orthopaedics 108

3.6 3D Printing of Optimized Designs: Biomimesis 133

3.6.1 Biomimetic Meta-Materials-by-Design: Cellular and Functionally-Graded-Materials 142

3.6.1 Mechanical Performance Optimization 157

3.6.2 Biological Performance Optimization 175

3.6.3 Challenges and Defects in 3D Printing Biomimetic Designs 192

3.7 xReality in Orthopaedics 202

4. Approach and Contribution 213

4.1 Rationale of Research 213

4.2 Methodology 216
5. Point-of-Care 3D Unit 225
5.1 Introduction 225
5.2 Organizational Structure and Framework 227
5.2.1 SkeletoMy Online Platform 232
5.2.2 Regulations and Quality Management 240
5.3 Hardware and Software 252
5.3.1 Computer and Office Equipment 253
5.3.2 xR Equipment 255
5.3.3 3D Scanners 257
5.3.4 3D Printers and Materials 258
5.3.5 Software 266
5.4 Infrastructure and Layout 271
5.4.1 Thesis Available Resources – Constraints 276
5.5 Cost Analysis 278
5.6 Distributed and Localized Manufacturing 284
6. Case studies 292
6.1 Introduction and Assumptions 292
6.2 Bone Tumor Resection and Reconstruction 292
6.3 Pelvic Reconstruction 298
6.4 Case 1: Ilium and Hip Joint Reconstruction 302
6.4.1 Medical Imaging, Processing, Visualization and Diagnosis 302
6.4.2 Post-resection Medical Imaging 306
6.4.3 Post-resection Image Data Processing 306
6.4.4 (In)Tangible Anatomy Visualization 312
6.4.5 Rehabilitation Strategy and Task Clarification 328
6.4.6 Conceptual Design and Evaluation 333
6.4.7 Embodiment Design 340
6.4.8 Design Check 388
6.4.9 Detailed Design 391

6.4.10 Pre-operative Simulation 431
6.4.11 Final Check, Manufacturing, and Delivery 435
6.5 Case 2: Ilium-Acetabular and Hip Joint Reconstruction 436
6.6 Case 3: Acetabular and Hip Joint Reconstruction 444
6.7 Case 4: Sacrum Reconstruction 452
6.8 Sacral Tumor Resection 461
6.9 Case 5: Orthotic Device: Hand Splint 465
7. Results and Discussion 469
8. Conclusions and Future Research 489
9. References 495
10. Published Articles 588
11. Appendices 621
11.1 Appendix A: Timeline of Technology Advancements 621
11.2 Appendix B: Modern Devices and Tools in Orthopaedics 622
11.3 Appendix C: World Demographic Figures 631
11.4 Appendix D: Table of Disabilities in Population 633
11.5 Appendix E: Bone Architecture and Properties 634
11.6 Appendix F: Ashby's Material Property Charts 637
11.7 Appendix G: 3D Printing of Different Materials 639
11.8 Appendix H: Anisotropy of Material Extruded Products 641
11.9 Appendix I: 3D Printing and Software Market Landscape 642
11.10 Appendix J: 3D Printing in Series of Severe Cases 647
11.11 Appendix K: Bone tumor types and statistics 663
11.12 Appendix L: Anatomy of the pelvis 664
11.13 Appendix M: SkeletoMy website 672
11.14 Appendix N: Considerations for PoC manufacturers 680
11.15 Appendix O: Biomimicry Taxonomy 682

Table of Figures

Figure 1: Classification of orthopaedic practices 1
Figure 2: Schematic illustration of orthopaedic techniques evolution 2
Figure 3: Disease categories of prevalent conditions globally 3
Figure 4: Orthopaedic industry market....4
Figure 5: iTotal patient-specific knee replacement system 5
Figure 6: Engineering as a process for producing tangible and intangible solutions (engines) 7
Figure 7: Types of musculoskeletal joints....7
Figure 8: Leonardo da Vinci's anatomical drawings....8
Figure 9: Musculoskeletal system under orthopaedic and biomechanical points of view 9
Figure 10: Macroscopic inter-epistemic approach for orthopaedic products development 9
Figure 11: Inter-epistemic multi-disciplinary field of individualized orthopaedic products....10
Figure 12: Historical evolution of medical imaging, navigation, and robotic systems 11
Figure 13: Internal and external anatomy scanners 11
Figure 14: 3D software to design and optimize bespoke solutions 12
Figure 15: xR head-mounted displays and haptic devices....13
Figure 16: 3D printers and 3DPed anatomical models, jigs and prosthesis 13
Figure 17: Enabling technological tools for making individualized orthopaedic products....14
Figure 18: Processes, materials, and applications of 3DP of medical devices 16
Figure 19: Layer-by-layer manufacturing principle 17
Figure 20: In-hospital 3D labs using Materialise software as of December 2020....19
Figure 21: Questions to be addressed for the PoC 3D Unit....24
Figure 22: Thesis hypothesis, scope, objectives, goals, and tools....25
Figure 23: (Bio)materials science tetrahedron....27
Figure 24: Development of engineering materials over time 27
Figure 25: Typical biomaterials used in endo-prostheses....29
Figure 26: Bone-biomaterial interface interactions 30
Figure 27: Attributes of the ideal orthopaedic implant....31
Figure 28: Hip arthroplasty implants design considerations 32
Figure 29: Stages of fracture healing....33
Figure 30: Types of bone cells....34
Figure 31: Bone remodeling phases and cell types 35

Figure 32: Surface and properties modification techniques 37
Figure 33: Optimal pore size for biological and mechanical superiority. 39
Figure 34: Supra-cellular architecture with large and small pore sizes. 40
Figure 35: 3D Printed composite Ti-PE sternum and ribcage implant 40
Figure 36: 3D Printed Ti acetabular cup with cellular structures 40
Figure 37: Biofilm formation cycle and implant surface protection mechanism 42
Figure 38: Most common sterilization methods 43
Figure 39: Elements of Tissue Engineering 45
Figure 40: In vivo, in vitro TE approaches and construct types 46
Figure 41: Bone scaffold from natural bone and PCL powders 46
Figure 42: Properties of the “hyperelastic bone” 47
Figure 43: Envisiotec Bioplotter extrusion system and PCL products 47
Figure 44: Lithoz CeraFab S65 photocuring system and HA and TCP products 48
Figure 45: Parameters affecting the selection of manufacturing technologies 48
Figure 46: Manufacturing as a transformation system 49
Figure 47: Categorization of manufacturing technologies as per DIN 8580 50
Figure 48: Manufacturing processes categories and groups as per DIN 8580 50
Figure 49: Typical manufacturing process flow 51
Figure 50: Manufacturing technology selection based on material and shape 51
Figure 51: Complex forms and endo-features made with 3D metal printing 52
Figure 52: Kinematics of Additive Manufacturing/3DP 52
Figure 53: Making of a 3D laminated object 53
Figure 54: Impact of layer number on laminated product quality 53
Figure 55: Geometry types and impact of layer number on quality and accuracy 54
Figure 56: Repetitive principle of 3DP and object-building evolution 54
Figure 57: Support requirements based on selected build orientation 55
Figure 58: Support types based on 3DP technology 55
Figure 59: Web search interest of AM and 3DP terms 60
Figure 60: Annually published papers related to AM and 3DP listed on Scopus (unfiltered) 60
Figure 61: Topographic relief map 61
Figure 62: Willeme’s 2nd photo-sculpturing method 62
Figure 63: Nakagawa’s laminated forming tool 63
Figure 64: Munz’s machines 63
Figure 65: Ciraud’s powder jetting system 64

Figure 66: Housholder's machines 64
Figure 67: Kodama's layer photo-polymerization approaches and product 65
Figure 68: Herbert's photo-polymerization apparatus and product 65
Figure 69: Marutani's photo-polymerization apparatus 65
Figure 70: Andre's photo-polymerization systems 66
Figure 71: 3D Systems SLA-1 machine 67
Figure 72: BPM Technology Personal Modeler 67
Figure 73: Process flow chain for SL 68
Figure 74: Classifications of 3DP mechanisms for different materials and states 69
Figure 75: Binder Jetting principle, example machine, and product 70
Figure 76: Directed Energy Deposition principle, example machine, and product 70
Figure 77: Material Extrusion principle, example machine, and product 71
Figure 78: Material Jetting principle, example machine, and product 71
Figure 79: Powder-bed Fusion principle, example machines, and products 72
Figure 80: Sheet Lamination principle, example machine, and product 72
Figure 81: Sheet Lamination principle, example machine, and product 73
Figure 82: Examples of 3D printer types, uses, costs 77
Figure 83: Generic process flow chain for 3DP 78
Figure 84: Examples for each 3DP process category 79
Figure 85: "Morpheas" FFF 3DP machine and sample polymer parts 80
Figure 86: STL and AMF file structures 80
Figure 87: Tessellation quality and .stl file size 81
Figure 88: Ishigawa diagram of parameters affecting metal 3DP 82
Figure 89: Uses and users of 3DP 83
Figure 90: Product development phases: 3DP versus traditional manufacturing 83
Figure 91: Traditional manufacturing versus 3DP 86
Figure 92: 3D Printed topology optimized multi-material parts with embedded electronics 87
Figure 93: Topologically optimized, generatively designed, and consolidated 3D Printed parts 87
Figure 94: Generative design and topology optimization differences 88
Figure 95: Sources of micro-porosity in ME-based 3DP technologies 88
Figure 96: Surface treatments for finishing enhancement of 3D Printed parts 89
Figure 97: Hybrid additive-subtractive CNC machine tool 89
Figure 98: Anisotropy in mechanical properties of parts 3DPed with VP 90
Figure 99: Worldwide revenue from independent 3DP service providers 91

Figure 100: Trends in manufacturing systems....91
Figure 101: Production time and cost for 3DP versus traditional manufacturing processes....92
Figure 102: Hype Cycle for 3DP as of 2018....92
Figure 103: Potential impacts of 3DP on product offerings and supply chains....93
Figure 104: Immediate, likely, and future scenarios for 3DP in different industries....93
Figure 105: Measurement methods for 3D object reconstruction....95
Figure 106: Workflow for patient-specific products 3DP....96
Figure 107: Strengths, limitations, and applications of medical imaging and 3D scanning....96
Figure 108: Most frequently used technologies and materials for 3DP in orthopaedics....97
Figure 109: 3D Printed metal proximal tibia locking plate and polymer drill guide....98
Figure 110: 3D Printed splints at the PoC....98
Figure 111: Floorplans of hypothetical PoC 3D Unit indicating the various zones....99
Figure 112: Steps in creating a PoC 3D Unit....100
Figure 113: Regulations tree for custom-made, patient-matched, and adaptable medical devices.103
Figure 114: FDA-cleared 3DPed medical devices breakdown....104
Figure 115: PoC design and 3DP scenarios mentioned by the FDA....104
Figure 116: Feedstock materials costs and 3D printers used in orthopaedics....105
Figure 117: Workflow for patient-specific implants 3DP....107
Figure 118: Custom 3D Printed spinal prostheses. Source: (Willemsen et al., 2019)....107
Figure 119: Risk assessment for custom 3DPed spinal prostheses....108
Figure 120: Process and challenges of custom implant 3DP....109
Figure 121: 3DP applications in medicine....110
Figure 122: 3D Printed biomodel displaying osteoblastoma and planned resection margins....110
Figure 123:3DP applications in upper and lower extremity trauma....111
Figure 124: 3D Printed molds for making antibiotic-eluting spacers....112
Figure 125: 3DPed PSI for tibia osteotomies and pedicular sighting....113
Figure 126: Development process and 3DP patient-specific spine solutions....114
Figure 127: Process and 3DPed parts for one-step reconstruction after tumor resection....115
Figure 128: Foot bone reconstruction using 3D Printed jigs and endo-prosthesis....116
Figure 129: 3DPed scapula and calcaneus models for pre-operative plate preparation....116
Figure 130: 3D Printed multi-color and multi-material anatomical models....116
Figure 131: 3DP applications in joint, spine, pelvis, and other areas....117
Figure 132: 3D Printed custom Ti acetabular prosthesis and polymer drilling guide....117
Figure 133: Conventional (a) and PSI (b and c) sets for total knee arthroplasty....119

Figure 134: Published papers on 3DP/AM/Bioprinting listed on PubMed 121
Figure 135: 3DP in orthopaedics 122
Figure 136: 3D Printed orthotics 124
Figure 137: 3DPed endo-prosthesis filled with bone graft and covered with a vascularized flap ..125
Figure 138: 4D Printed stent shape morphing due to temperature change....126
Figure 139: 3DPed drug eluting endo-prostheses....126
Figure 140: Femoral stems with embedded electronics 127
Figure 141: 3D Printed femoral stems with embedded electronics....127
Figure 142: Condition monitoring after hip arthroplasty using embedded sensors....128
Figure 143: Three-axis model of manufactured products....129
Figure 144: Custom-made expandable endo-prostheses 130
Figure 145: Cases treated with custom 3DPed hemipelvic endo-prostheses 131
Figure 146: 3DPed custom Ti6Al4V hemi-pelvic endo-prostheses with porous features 132
Figure 147: Examples of structures found in nature....134
Figure 148: Examples of nature's "biological 3D printers" 135
Figure 149: 3DP enables biomimetic forms fabrication....138
Figure 150: 3DPed femoral head replicas as per the natural stress distribution....139
Figure 151: Biomimetic 3DPed wrist splint and pregnancy corset by N. Oxman 139
Figure 152: Evolution of biomaterials, smart biomaterials, and 3DP role 140
Figure 153: Endocultivation, in vivo, in vitro TE approaches 141
Figure 154: Internal and external stimuli used to enable biofunctionalities....141
Figure 155: Published records on Scopus on tissue "regeneration" and "replacement" 141
Figure 156: 3D-Bioplotter and bioconstructs 142
Figure 157: 3D ink (bio)printing within a supportive gel....142
Figure 158: Research challenges and solution domain of metamaterials 3DP....142
Figure 159: 3 2D polygons and 5 3D polyhedral that can fill space without distortion....143
Figure 160: Classification of cellular materials....144
Figure 161: Optimized helmet and shoe featuring cellular structures....144
Figure 162: Modelling methods for cellular structures generation 145
Figure 163: Characteristics of bending and stretch-dominated lattices....146
Figure 164: Trabecular bone as a reference to design cellular structures....147
Figure 165: 2D and 3D Voronoi diagrams. 148
Figure 166: Gyroid TPMS geometry and equation 149
Figure 167: Sheet and skeletal Gyroid TPMS. 149

Figure 168: Volume fraction and surface-to-volume of TPMS as a function of c. 149
Figure 169: Sheet and skeletal-based Gyroid unit cells with 50% relative density.....150
Figure 170: Different strut and pore sizes of sheet and skeletal Gyroids of same cell size. 150
Figure 171: Sheet and skeletal Gyroid TPMS blending for bone imitation. 151
Figure 172: Some unit cell geometries used to make lattice structures.....151
Figure 173: Voronoi tessellation for synthesizing trabecular-like designs 152
Figure 174: Selective and isotropic Voronoi tessellation 153
Figure 175: Voronoi-based irregular scaffold modeling 153
Figure 176: Voronoi designs compared to micro-CT scanned reference 154
Figure 177: Infill geometries generated by voxel-wise topology optimization.....154
Figure 178: Biomimetic networks by iterative network topology optimization.....155
Figure 179: Multi-body interpenetrating lattices 155
Figure 180: A biomimetic functionally graded airless tyre design: Michellin's Vision Concept ...156
Figure 181: Steps for manufacturing FGMs 156
Figure 182: Structures and types of FGMs 157
Figure 183: Multi-component phase diagrams for FGMs 157
Figure 184: 3DPed porous specimens and knee implant 158
Figure 185: Summary of orthopaedic surgical applications of FGMs 159
Figure 186: Admissible design space of unit cells for optimum parameters selection 160
Figure 187: Bone loss by stress shielding for fully dense and fully porous femoral stems 160
Figure 188: Relative density, modulus, and pore size for cellular Ti and Co-Cr alloys 161
Figure 189: 3DPed Ti femoral meta-implant with negative and positive Poisson's ratios 161
Figure 190: Mechanical properties and energy absorption of periodic and stochastic structures ...162
Figure 191: 3DPed non-auxetic fixed-porosity and functionally-graded Ti acetabular cups.....163
Figure 192: Mechanical performance of 3DPed porous Ti femoral stem 163
Figure 193: Geometrical and mechanical data for different 3DPed cell morphologies 164
Figure 194: Gyroid designs that approximate mechanical properties of cortical bone 164
Figure 195: Modulus of elasticity and strength of sheet and skeletal TPMSs.....165
Figure 196: Mechanical performance of 3DPed TPMS to make "synthetic bone".....166
Figure 197: Mimicking bone's anisotropy by TPMS designs 167
Figure 198: Optimal design spaces of 3DPed TPMS to make "synthetic bone".....168
Figure 199: Mimicking cortical and trabecular bone by TPMS designs 169
Figure 200: Topology-optimized 3DPed acetabular cage with graded porosity 170
Figure 201: Five variations of functionally-graded Gyroid TPMS 171

Figure 202: Density and cell grading for Gyroid and Diamond TPMS 171
Figure 203: 3DPed Ti/HA FGM trans-femoral fixation.....172
Figure 204: Tensile strength of 3DPed porous Ta with different porosities 172
Figure 205: Mechanical characteristics of different unit cells.....173
Figure 206: Mechanical characteristics of biodegradable metallic cellular architectures 173
Figure 207: Mechanical characteristics of standard metallic cellular architectures 174
Figure 208: Modulus of elasticity, yield strength, and fatigue strength for different unit cells 174
Figure 209: 3DPed porous implants with various architectures in literature 176
Figure 210: 3DPed porous implants with various architectures in literature 177
Figure 211: Commercialized and under research 3DPed porous implants.....178
Figure 212: 3DPed porous Ti implants filled with fibrin gel and loaded with BMP-2 179
Figure 213: Osseointegration of 3DPed porous Ti versus porous CoCr 180
Figure 214: Bone ingrowth in 3DPed tetrahedron and octet truss.....180
Figure 215: Mechanical-biological performance of 3DPed porous Ti with different pore sizes 181
Figure 216: Biological performance of 3DPed porous specimens with TnT and HA coating.....182
Figure 217: Biological performance of different 3DPed Ti porous scaffolds 182
Figure 218: Osseointegration of radial and ulnar endo-prostheses 183
Figure 219: Osseointegrated 3DPed porous Ti cervical cage.....183
Figure 220: Bacterial protection of 3DPed Ti implants.....183
Figure 221: Pros and cons of different materials used for bone scaffolds.....184
Figure 222: Composite 3DPed biomaterials for bone scaffolds 184
Figure 223: Metal, polymer, and ceramic 3DPed biomaterials for bone scaffolds 185
Figure 224: Biological comparison of 3DPed and traditionally made porous implants.....186
Figure 225: Biological comparison of 3DPed and traditionally made porous Ti cups 187
Figure 226: Radiological and histological evaluation of different 3DPed Ti pore architectures 187
Figure 227: Advantages of 3DPed 3D scaffolds 188
Figure 228: Osseointegration into 3DPed porous Ti with different porosities.....189
Figure 229: Mechanical and biological comparison of different Gyroid scaffolds.....189
Figure 230: Permeability of different unit cells, pore size, and porosity 191
Figure 231: Permissible design space of cellular solids for 3DP 193
Figure 232: Sintered unmelted particles on lattice produced by EBM and LBM 194
Figure 233: Multi-scale, multi-physics phenomena during PBF 3DP.....195
Figure 234: Structural and geometric defects of metallic parts 3D printed by PBF technologies ..196
Figure 235: Geometric errors of as-built compared to as-designed TPMSs 197

Figure 236: 3DPed cellular solids with different build orientations....198
Figure 237: Powder removal from cellular solids 3DPed by EMB....199
Figure 238: Scan strategies and optimal power-speed parameters for defect-free PBF 3DP....200
Figure 239: Effects of heat and chemical treatments on PBF 3DPed parts....201
Figure 240: Algorithmically-driven methods and machine learning for 3DP....201
Figure 241: Applications of VR in healthcare....202
Figure 242: Example VR Systems....203
Figure 243: Example of immersive VR simulator for shoulder arthroplasty....203
Figure 244: HMD, monitor and projection AR Systems....204
Figure 245: MR applications examples....205
Figure 246: VR, AR, and MR about the physical world....205
Figure 247: Reality-Virtuality continuum....206
Figure 248: Information flow and feedback loop in xR systems....206
Figure 249: Tracking methods in xR systems....207
Figure 250: Knee+ AR knee arthroplasty navigation system....209
Figure 251: Annually published articles on virtual/augmented/mixed reality on PubMed....209
Figure 252: Advantages and disadvantages of non-VR training options....210
Figure 253: 3D lower leg rendering and AR overlay with arrows indicating perforators....210
Figure 254: Intra-operative AR system for minimally invasive screws placement....211
Figure 255: Thesis hypothesis....215
Figure 256: Bottom-up and top-down approaches for custom 3DPed solutions....216
Figure 257: Thesis approach....217
Figure 258: “Iceberg” model of physical product-making....217
Figure 259: Inter-epistemic why-what-how orthopaedic product development process....217
Figure 260: Ideal implant development process....219
Figure 261: Double Diamond design process....219
Figure 262: Biomimicry design spiral....220
Figure 263: Systematic design, Double Diamond and Dw3DP-Df3DP....220
Figure 264: Thesis PoC inter-epistemic custom orthopaedic product development workflow....221
Figure 265: Ishigawa diagram for causes of low-quality 3D printed products....225
Figure 266: Organizational structure of the PoC 3D Unit....229
Figure 267: The scrum framework....231
Figure 268: PoC 3D Unit interactions, services, and product development....232
Figure 269: SkeletoMy logo and punch line....233

Figure 270: Options for users to communicate with the PoC 3D Unit....233
Figure 271: Scanning protocol for medical image data acquisition and submission....235
Figure 272: PixelMed Publishing's DicomCleaner interface....236
Figure 273: SkeletoMy's Terms of Use and Warranty Notes....237
Figure 274: User feedback report for SkeletoMy improvement....238
Figure 275: Reports sent to the user for approval of patient-specific products....239
Figure 276: SkeletoMy's flowchart to offer requested services to users....240
Figure 277: Contents of the ISO 13485 standard....246
Figure 278: Process mapping for 3DP and parameters impacting the 3DPed product....247
Figure 279: Risk management as per ISO 149671:2019....252
Figure 280: Computers, peripherals, power, networking, and office equipment of PoC 3D Unit....255
Figure 281: xR equipment of PoC 3D Unit....256
Figure 282: 3D Scanners of PoC 3D Unit....260
Figure 283: 3D Printers of PoC 3D Unit: high-temp ME....260
Figure 284: 3D Printers of PoC 3D Unit: ME....261
Figure 285: 3D Printers of PoC 3D Unit: low-cost ME and VP print farm....262
Figure 286: 3D Printers of PoC 3D Unit: VP....262
Figure 287: 3D Printers of PoC 3D Unit: (photo-polymer) MJ....263
Figure 288: 3D Printers of PoC 3D Unit: BJ....263
Figure 289: 3D Printers of PoC 3D Unit: plastic PBF....264
Figure 290: 3D Printers of PoC 3D Unit: metal PBF....265
Figure 291: 3D Printers of PoC 3D Unit: ceramic photocuring....266
Figure 292: 3D Printers of PoC 3D Unit: extrusion bioprinter....266
Figure 293: Software for the PoC 3D Unit....270
Figure 294: Single ground floor PoC layout concept for Scenario 1....271
Figure 295: Two-floor PoC layout concept for Scenario 1....272
Figure 296: Example of PoC workshop equipment for Scenario 1....273
Figure 297: Example of a two-floor PoC building concept for Scenario 1....274
Figure 298: Example of departments and rooms of the two-floor PoC for Scenario 1....275
Figure 299: Single ground floor PoC layout concept for Scenario 2....276
Figure 300: Single ground floor and two-floor PoC concept for Scenario 2....276
Figure 301: A small PoC Unit concept housed within an office of a HCF....277
Figure 302: Pilot PoC 3D Unit used in this Thesis....277
Figure 303: Equipment of pilot PoC 3D Unit used in this Thesis....278

Figure 304: Cost per part versus production volume for plastic manufacturing methods.....279
Figure 305: Evolution, classification, and perspectives of 3DP cost models.....281
Figure 306: Cost analysis per offered service from the PoC 3D Unit.....283
Figure 307: SkeletoMy cost analysis for requested services.....284
Figure 308: Business production strategies.....287
Figure 309: Centralized versus decentralized manufacturing network.....289
Figure 310: Centralized versus decentralized manufacturing example in the US.....290
Figure 311: Distributed manufacturing model for 3DP novel medical face masks.....290
Figure 312: Geographic location of the PoC 3D Unit.....291
Figure 313: Histologic form and sites of common bone tumors.....293
Figure 314: X-ray images of common bone tumor types.....293
Figure 315: Bone and soft tissue tumor diagnosis and biopsy algorithm.....295
Figure 316: Tumor diagnosis process flow chain and synergy.....295
Figure 317: Three pelvic bone components.....300
Figure 318: Timeline of pelvic reconstruction approaches.....301
Figure 319: X-ray, CT, and MRI image of the pelvic osteosarcoma site.....302
Figure 320: Siemens Somatom Definition Flash and scanning planes.....303
Figure 321: Pre-operative photorealistic views of 3D pelvic anatomy; hard and soft tissue.....303
Figure 322: 3D digital pre-operative anatomical pelvic model generation.....304
Figure 323: Enneking classification of pelvic tumor resections and planned resection.....305
Figure 324: 3D Slicer graphical user interface.....306
Figure 325: nnU-Net pipeline and structures recognized by Total Segmentator.....307
Figure 326: 3D digital post-resection anatomical pelvic model generation.....308
Figure 327: The Hounsfield unit scale.....309
Figure 328: As-generated surface mesh model of the post-resected pelvis and export settings.....309
Figure 329: Comparison of as-CT-scanned and solid-filled regions of the same slice.....310
Figure 330: Solid-filled post-resected surface mesh models and export settings.....310
Figure 331: Isolated solid-filled surface mesh model of post-resected pelvis and export settings.311
Figure 332: Initial (left) and simplified (right) mesh in Meshlab software.....311
Figure 333: Remeshing and simplification settings in Meshmixer and Meshlab software.....311
Figure 334: Photorealistic rendered views of post-resected pelvic anatomy.....312
Figure 335: Post-resected mesh model and DICOM data loaded in 3D Slicer.....313
Figure 336: Online and offline 3D surface mesh viewers.....314
Figure 337: Blender, Rhinoceros, Fusion 360, Spaceclaim, Freeform interfaces.....314

Figure 338: Post-resected pelvic mesh loaded into some viewers of mobile-based devices.....315
Figure 339: The high-end Varjo VR-3 and the Oculus Rift S VR headsets.....315
Figure 340: Post-resected pelvis as seen in Specto and Medical Imaging xR environments.....316
Figure 341: User with Rift S equipment immersed in VR environment.....317
Figure 342: Post-resected mesh model as-generated and as-loaded in Medical Imaging xR.....317
Figure 343: Microsoft Hololens 2 and Varjo XR-3 MR headsets.....318
Figure 344: Post-resected mesh model in AR Viewer and DICOM data in Medical Imaging xR..318
Figure 345: Creality CR-10s 3D printer and ColorFabb PLA/PHA filament properties.....319
Figure 346: Report, settings, and 3D paths for the post-resected model in Prusa Slicer.....320
Figure 347: Post-resected 3DPed pelvic model.....321
Figure 348: Post-processing example for surface quality enhancement.....322
Figure 349: Measurement comparison between the 3DPed and digital post-resected model.....323
Figure 350: Creality CR-10s versus the Bambu Lab X1 Carbon 3D printer.....324
Figure 351: Splitting, 3DP, post-processing and assembling the pelvic model.....325
Figure 352: Post-resected pelvic model anatomically split into 4 sections.....326
Figure 353: Alternative option for splitting the post-resected pelvic model split into 4 sections...326
Figure 354: Multiple 3DP of the post-resected pelvic model anatomically split.....327
Figure 355: Multiple 3DP of post-resected pelvic model split with alternative option.....327
Figure 356: Screenshot of Miro whiteboard used to define specifications on sticky notes.....332
Figure 357: Elements of Pugh's product design specifications.....332
Figure 358: Views of the post-resected pelvis in sketch-friendly format.....333
Figure 359: Drawing and marking the digital model in Medicalholodeck VR.....333
Figure 360: Evaluation criteria and SWOT analysis for each concept.....335
Figure 361: Bulky natural-like and low-profile design concepts.....336
Figure 362: Endo-prosthesis with and without integrated acetabular shell.....336
Figure 363: No-cutting and fine flat-cutting and reaming for perfect endo-prosthesis fit.....337
Figure 364: Physical clay modeling of the agreed endo-prosthesis concept.....338
Figure 365: Paper hand sketches of the agreed endo-prosthesis concept.....339
Figure 366: Screenshot of Miro whiteboard used to generate the mind map of concepts.....340
Figure 367: Transition from conceptual to detailed design via embodiment design.....341
Figure 368: Anatomically alignment of post-resected pelvic mesh model to cartesian space.....342
Figure 369: Measured offset between acetabula.....343
Figure 370: Cut planes and resultant flat surfaces on acetabulum rooftop and sacrum side.....344
Figure 371: Measured anteversion and abduction angles for acetabular shell placement.....344

Figure 372: Safe zone of anteversion and abduction angles for acetabular shell placement 345
Figure 373: Femoral head diameter measurement.....346
Figure 374: Normal repositioning of the left femur 346
Figure 375: Taper-lock and anti-rotation features of standard and dual mobility cups.....348
Figure 376: Cemented liner and cemented cup-liner combination options.....348
Figure 377: New left acetabulum center of rotation.....349
Figure 378: Endo-prosthesis acetabular shell part in the left reamed acetabulum 350
Figure 379: Selected femoral stem: DePuy Synthes' Tri-lock 351
Figure 380: Femoral neck cut and views of the stem inserted in the femoral canal.....352
Figure 381: Components of total left hip arthroplasty.....353
Figure 382: Multi-modal 3D digital model of the pelvis and reconstructive endo-prosthesis 353
Figure 383: Bone screw types and characteristics. 354
Figure 384: Custom porous bone screws 3DPed out of Ti alloy powder. 355
Figure 385: Points and orientation for screws insertion 356
Figure 386: Optimal and safe insertion points and lengths of acetabular screws.....356
Figure 387: Optimal insertion points of sacral screws 357
Figure 388: Healthy right ilium mirrored 357
Figure 389: Exported components to model the endo-prosthesis.....358
Figure 390: Conversion of triangular mesh model into solids 360
Figure 391: Models to design and simulate the custom solution.....361
Figure 392: Textured acetabular shell with two 4 mm cancellous screws holes.....361
Figure 393: Conversion of quadrilateral mesh model into a solid model.....362
Figure 394: Comparison of quadrilateral, triangular mesh, and solid models.....363
Figure 395: Cancellous bone screws modeled as per ISO 5835.....363
Figure 396: Endo-prosthesis modeling.....364
Figure 397: Endo-prosthesis fixed with bone screws 365
Figure 398: Photorealistic view of the implanted solution: endo-prosthesis and arthroplasty.....366
Figure 399: Ilium-like endo-prosthesis concept 367
Figure 400: Photorealistic rendering of the endo-prosthesis and arthroplasty components.....367
Figure 401: Drilling jig-trial endo-prosthesis instrument modeling.....368
Figure 402: Photorealistic rendering of the drilling jig-trial endo-prosthesis instrument 368
Figure 403: Reaming check tool modeling.....369
Figure 404: Photorealistic views of the reaming check tool.....369
Figure 405: Cutting jig and insert modeling.....370

Figure 406: Features cut for the unique fit of cutting jig on anatomy....370
Figure 407: Photorealistic rendered views of the cutting jig....371
Figure 408: Femoral head-cutting jig modeling....371
Figure 409: Photorealistic views of the femoral head cutting jig....372
Figure 410: Hip joint range of motion.....372
Figure 411: Kinesiology phases of walking. 372
Figure 412: Hip range of motion pattern during walking.....373
Figure 413: Active muscles during walking and hip joint motion during activities. 373
Figure 414: Muscles contribution on hip contact force during walking.....374
Figure 415: Loads acting on left acetabulum during dual and single-leg stance....377
Figure 416: Loads acting on the femur....377
Figure 417: Resultant hip joint force and moment profiles for different activities. 378
Figure 418: Workflow to generate multi-material volumetric meshes....379
Figure 419: Set-up for the two mechanical simulation studies....380
Figure 420: Von Mises Stresses on pelvis induced by right hip load....381
Figure 421: Von Mises Stresses on pelvis induced by left hip load....382
Figure 422: Pelvis, endo-prosthesis, and bone screws displacements induced by left hip load....382
Figure 423: Pelvis, endo-prosthesis, and bone screws displacements induced by right hip load....383
Figure 424: Von Mises stresses on endo-prosthesis and bone screws induced by right hip load ...383
Figure 425: Von Mises stresses on endo-prosthesis and bone screws induced by left hip load....384
Figure 426: Pelvis, endo-prosthesis, and screw displacements-stresses by combined loading....386
Figure 427: Resected mass and center of mass 387
Figure 428: Photorealistic views of extra stabilization options for the pelvic endo-prosthesis 387
Figure 429: Views and details of the extra stabilization options for the pelvic endo-prosthesis 388
Figure 430: Photorealistic views of preliminary solution featuring soft and hard tissue 389
Figure 431: 2D slices of the preliminary solution in 3D Slicer....389
Figure 432: 3D views of the preliminary solution in 3D Slicer 390
Figure 433: Ti6Al4V Grade 3 powder characteristics....391
Figure 434: PA 2201 Medical-Grade powder characteristics....392
Figure 435: Powder grains binding mechanisms....392
Figure 436: Powder-bed fusion-based 3D printers for polymer parts....393
Figure 437: Properties of parts 3D printed by EBM versus LBM technologies 395
Figure 438: EBM and LBM powder-bed fusion-based 3D printers....395
Figure 439: Generative design of endo-prosthesis 397

Figure 440: Final generatively designed and shape-optimized endo-prosthesis 398
Figure 441: Topology optimization setup.....399
Figure 442: Topology-optimized endo-prosthesis for left and right hip loading cases.....400
Figure 443: Topology-optimized endo-prosthesis for combined left-right hip loading.....401
Figure 444: Unit cell and foam characteristics 402
Figure 445: Formulas for relative modulus and strength cellular solids 404
Figure 446: Examples of software capable of cellular structure 3D modeling 405
Figure 447: Beam-based, stochastic, 2D plates, skeletal, and sheet TPMS libraries in nTop.....406
Figure 448: Types of cellular solids in nTop.....407
Figure 449: Examples of cellular structures generated by nTop 407
Figure 450: Endo-prosthesis porous optimization workflow 409
Figure 451: Voronoi complex pore size calculation workflow 410
Figure 452: Examples of Voronoi pattern with and without defined boundary limits to conform .411
Figure 453: Gradient region for the Voronoi pattern.....411
Figure 454: Ramp options to create point spacing and beam thickness gradients in nTop.....412
Figure 455: Examples of cellular infill-solid shell union with and without blending radius 412
Figure 456: Tolerance and file size of facet meshes (.stl) output from nTop.....413
Figure 457: Endo-prosthesis optimization with Voronoi complexes workflow in nTop 413
Figure 458: Mass, characteristics, and file size of the Voronoi-optimized endo-prosthesis 414
Figure 459: Voronoi-optimized endo-prosthesis photo-realistic, details, x-ray and section views.415
Figure 460: Stochastic Voronoi complexes designed for LBM and EBM 3DP technologies.....416
Figure 461: Generated slices for 3DP by nTop 416
Figure 462: Ti6Al4V skeletal Gyroid unit cell (40% relative density) homogenization graph 417
Figure 463: Characteristics of the skeletal, sheet, and mixed Gyroids.....418
Figure 464: Workflow to define admissible design space for skeletal Gyroid 3DP 419
Figure 465: Redefined, more suitable parameters of the skeletal Gyroid unit cell 420
Figure 466: Parameters of the sheet Gyroid unit cell 421
Figure 467: Sheet Gyroid-optimized endo-prosthesis views and details.....423
Figure 468: Mass, characteristics, and file size of the sheet Gyroid-optimized endo-prosthesis 424
Figure 469: Different approaches to mechanical simulation of cellular solids in nTop.....425
Figure 470: Characteristics of the field optimization design tool in nTop 427
Figure 471: Elastic deformation and failure mechanisms of cellular solids.....427
Figure 472: Results of hollow body mechanical simulation by loading the left hip socket 428
Figure 473: Results of hollow body mechanical simulation by loading the right hip socket.....429

Figure 474: Results of hollow body mechanical simulation by loading both hip sockets 430
Figure 475: Material Extrusion 3DP for pre-operative simulation and verification 431
Figure 476: Vat Photopolymerization 3DP of optimized endo-prosthesis in transparent material .432
Figure 477: 3DPed components of the final solution 432
Figure 478: 3DPed reamed, flat-cut, and drilled anatomical model.....433
Figure 479: 3DPed reaming check tool 433
Figure 480: 3DPed flat-cutting instrument.....433
Figure 481: 3DPed drilling jig-trial endo-prosthesis instrument.....434
Figure 482: 3DPed femur, femoral head cutting jig and stem with head.....434
Figure 483: 3DPed endo-prosthesis out of clear resin photopolymer 434
Figure 484: 3DPed endo-prosthesis, cemented, and final assembled solution.....435
Figure 485: CT scan indicating the tumor site.....437
Figure 486: Automatically generated hard and soft tissue by Total Segmentator in 3D Slicer 438
Figure 487: Planned resection and Enneking's classification 438
Figure 488: Photorealistic views of pelvic model and peripheral hard and soft tissue 439
Figure 489: Planned resected tissue, bone screws placement, and hip components 439
Figure 490: Patient-specific bone tumor and femoral head-cutting instruments.....440
Figure 491: Patient-specific endo-prosthesis trial and bone drilling instrument.....440
Figure 492: Solution with all components fixed on the anatomical model 441
Figure 493: Optimized endo-prosthesis with inter-connected porous architectures 442
Figure 494: 3DPed prototype parts for physical surgery simulation.....443
Figure 495: CT and MRI scans indicating the tumor site.....444
Figure 496: ICP alignment of CT and MRI-generated models 445
Figure 497: Generated models from CT and MRI scans combined 446
Figure 498: Photorealistic combined model 447
Figure 499: Planned bone resection and Enneking's classification.....447
Figure 500: Planned resected tissue, bone screws placement, and hip components 448
Figure 501: Patient-specific bone tumor and femoral head-cutting instruments.....448
Figure 502: Patient-specific endo-prosthesis trial and bone drilling instrument.....449
Figure 503: Solution with all components fixed on the anatomical model 449
Figure 504: Optimized endo-prosthesis with inter-connected porous architectures 450
Figure 505: 3DPed prototype parts for physical surgery simulation.....451
Figure 506: CT and MRI scans indicating the tumor site.....452
Figure 507: Generated models from CT scan.....453

Figure 508: Generated models from MRI scan and combined model 454
Figure 509: ICP alignment of CT and MRI-generated models 455
Figure 510: Photorealistic combined model 455
Figure 511: Planned resected tissue and Mayo Clinic's classification of sacral resections 456
Figure 512: En bloc sacral tumor resection and reconstruction with pedicle screw-rod system 456
Figure 513: Patient-specific bone tumor-cutting instruments 457
Figure 514: Pedicle screw-rod system reconstruction 457
Figure 515: Planned placement of bone screws for artificial endo-prosthesis reconstruction 458
Figure 516: Patient-specific endo-prosthesis trial and bone drilling instrument 458
Figure 517: Solution with all components fixed on the anatomical model 459
Figure 518: Optimized endo-prosthesis with inter-connected porous architectures 460
Figure 519: 3DPed prototype parts for physical surgery simulation 460
Figure 520: CT and MRI scans indicating the tumor site 461
Figure 521: Generated models from CT scan 462
Figure 522: Generated models from MRI scan and combined model 463
Figure 523: Planned resected tissue and Mayo Clinic's classification 464
Figure 524: Patient-specific bone tumor-cutting instruments 464
Figure 525: 3DPed prototype parts for physical surgery simulation 465
Figure 526: 3D hand scanning workflow 466
Figure 527: Individualized hand splint design flow 467
Figure 528: 3DPed hand splint 468
Figure 529: Two single-piece face shield designs for 3DP 469
Figure 530: Time and cost per stage of the inter-epistemic workflow 478
Figure 531: Pelvic tumor ablation education demo model 480
Figure 532: Two-part mold used for the injection molding of a two-piece face shield 482
Figure 533: Pelvic reconstructions using 3DPed endo-prostheses 485
Figure 534: Foot reconstructions using 3DPed endo-prostheses 486
Figure 535: Lower-limb reconstructions using 3DPed endo-prostheses 487
Figure 536: Upper-limb reconstructions using 3DPed endo-prostheses 488

Table of Tables

Table 1: Regulations and standards on medical devices 21
Table 2: Characteristics of biomaterials used in orthopaedics 28
Table 3: Book list on 3DP 56
Table 4: Process parameters, feedstock materials, and terms used for each 3DP category 73
Table 5: Advantages, disadvantages, and medical uses for each 3DP category.....75
Table 6: Advantages and disadvantages of 3DP technologies 84
Table 7: Book list on medical 3DP.....119
Table 8: Book list on biomimesis and Functionally Graded Materials 135
Table 9: List of standards on development, 3DP, and quality control of medical devices 248
Table 10: Computer equipment for the PoC 3D Unit.....253
Table 11: Office, power, networking and miscellaneous equipment for the PoC 3D Unit.....254
Table 12: xR equipment for the PoC 3D Unit 256
Table 13: 3D Scanners for the PoC 3D Unit 257
Table 14: 3D Printers and materials for the PoC 3D Unit.....258
Table 15: Software used in PoC 3D unit 267
Table 16: Characteristics of centralized and decentralized manufacturing networks. 287
Table 17: Indications and contraindications for limb salvage surgery. 296
Table 18: Advantages and disadvantages of biological and artificial reconstruction 297
Table 19: Specifications list for the pelvic endo-prosthesis and PSI.....329
Table 20: Comparison of EBM versus LBM.....394
Table 21: Objectives followed to achieve the goals and cover the literature gaps.....490

Glossary of Terms

3DP=3D Printing

AAOS=American Academy of Orthopaedic Surgeons

ABS=Acrylonitrile Butadiene Styrene

AcAl=AcideAlkali

AI=Artificial Intelligence

AJCC=American Joint Committee on Cancer's

AlAcH=AlkalieAcide Heat Treatment

AM=Additive Manufacturing

AMF=Additive Manufacturing File Format

AnH=Anodizing-heat Treatment

AO Foundation=Arbeitsgemeinschaft für Osteosynthesefragen

AR=Augmented Reality

ASA=Acrylonitrile styrene acrylate

ASME=American Society of Mechanical Engineers

ASTM=American Society for Testing and Material

BJ=Binder Jetting

BMP-2=Bone morphogenetic Protein 2

BMSCs=Bone Marrow Derived Mesenchymal Stromal Cells

B-Rep=Boundary Representation

CAD=Computer-Aided Design

CAE=Computer-Aided Engineering

CAM=Computer-Aided Manufacturing

CF=Carbon Fiber

CFD=Computational Fluid Dynamics

CHX=Chlorhexidine

CMM=Coordinate Measuring Machines

CNC=Computer Numerical Control

CT=Computed Tomography

CTA=Computed Tomography Angiography

DCB=Decellularized Bone

DED=Directed Energy Deposition

Df3DP=Design for 3D Printing

DfAM=Design for Additive Manufacturing

DICOM=Digital Imaging and Communications in Medicine

DIN=Deutsches Institut für Normung

DMLS=Direct Metal Laser Sintering

Dw3DP=Design with 3D Printing

DwAM=Design with Additive Manufacturing

EBM=Electron Beam Melting

ECM=Extracellular Matrix Molecules

EDM=Electrical Discharge Machining

EFFORT=European Federation of National Associations of Orthopaedics and Traumatology

EtO=Ethylene Oxide

EU=European Union

FDA=Food and Drug Administration

FEA=Finite Element Analysis

FFF=Fused Filament Fabrication

FGF-2=Fibroblast Growth Factor 2

FGM=Functionally Graded Material

GF=Glass Fiber

HA=Hydroxyapatite

HAOST=Hellenic Association of Orthopaedic Surgery and Traumatology

hASCs=Human Adult Adipose Stem Cells

HCF=HealthCare Facility

HDPE=High-Density Polyethylene

HIP=Hot Isostatic Pressing

HIPS=High Impact Polystyrene

HMD=Head-Mounted Displays

HU=Hounsfield Units

H2O2=Hydrogen Peroxide

IGES=Initial Graphics Exchange Specification

IL-12=Interleukin 12

IoT=Internet of Things

IR=Infrared Radiation

ISO=International Organization for Standardization

ISOLS=International Society Of Limb-Salvage

MC3T3-E1=Mouse Embryonic Osteoblast Precursor

MCP-1=Monocyte Chemoattractant Protein-1

MDR=Medical Devices Regulation

ME=Material Extrusion

MJ=Material Jetting

MPPA=Multivalent Polymer Peptide Antagonists

MR=Mixed Reality

MRI=Magnetic Resonance Imaging

MSTS=Musculoskeletal Tumor Society's

MTS=Musculoskeletal Tumor Society

NHS=National Health Service

NKUA=National and Kapodistrian University of Athens

NURBS=Non-uniform rational basis spline

PA=Polyamide=NYLON

PAEK=Polyaryletherketone

PBF=Powder-Bed Fusion

PC=Polycarbonate

PCL=Polycaprolactone

PCMX=Para Chloro Meta Xylenol

PDMS=Polydimethylsulphoxide

PDS=Polydioxanone

PE=Polyethylene

PEEK=Polyether ketone

PEG=Polyethylene glycol

PEGDA=Polyethylene glycol diacrylate

PEI=Polyethylenimine

PEKK=Polyetherketoneketone

PET=Polyethyleneterephthalate

PET=Positron Emission Tomography

PETG=Polyethylene Terephthalate Glycol

PGA=Polyglycolic Acid

PHMB=Polyhexamethylene Biguanide

PLA=Polylactic acid

PLGA=Polylactic-co-glycolic acid

PMMA=Polymethyl methacrylate

PoC=Point-of-Care

PP=Polypropylene

PS=Polysulfone

PSI=Patient-specific Instrument

PTFE=Polytetrafluroethylene

PU(R)=Polyurethane

QMS=Quality Management System

RGD=Arg-Gly-Asp (Arginylglycylaspartic acid)

rhBMP-2=Recombinant Human Bone Morphogenetic Protein-2

SEM=Scanning Electron Microscope

SL=Sheet Lamination

SLA=Stereolithography Apparatus

SLM=Selective Laser Melting

SLS=Selective Laser Sintering

STEP= Standard for the Exchange of Product Data

STL=Standard Tessellation Language

SWOT=Strengths, Weaknesses, Opportunities, Threats

TCP=Tri-calcium Phosphate

TE=Tissue Engineering

TGF-β2=Transforming Growth Factor-beta 2

TnT=Titania Nanotubes

TPE=Thermoplastic elastomer

TPMS=Triply Periodic Minimal Surface

TPU=Thermoplastic polyurethane

UHMWPE=Ultra High Molecular Weight PolyEthylene

US=Ultrasound

US=United States of America

UV=Ultraviolet

VP=Vat Photo-polymerization

VR=Virtual Reality

WHO=World Health Organization

xR=xReality, refers to VR, AR, MR

GENERAL PART

1. Introduction: State of the Art

1.1 Individualized Orthop(a)edics

"Prevention is better than cure" as Hippocrates of Kos (father of clinical medicine[1]) said. Nevertheless, all branches and specialties of medicine are continuously gaining knowledge and experience whilst seeking to incorporate new suitable technological tools to create an ecosystem with palettes of fast-track and high-quality monitoring, diagnostic, prognostic, and therapeutic techniques.

From ancient to modern times, Greece has been among the protagonists regarding the foundations and evolution of medicine, surgery, and orthopaedics *(Megaloikonomos et al., 2021)*. Orthop(a)edics[2] is composed of various practices *(Figure 1)* to reinstate the mechanics (form and function) of the musculoskeletal system due to congenital, developmental, degenerative, and traumatic anomalies and syndromes. Academic, clinical, and industrial contributions brought a gigantic anode over epochs as analogous operations *(Canale, Azar and Beaty, 2020)* and products *(Pal, 2014)* evolved greatly *(Le Vay, 1990; Peltier, 1993; Klenerman, 2002; Swarup and O'Donnell, 2016) (Figure 2)*.

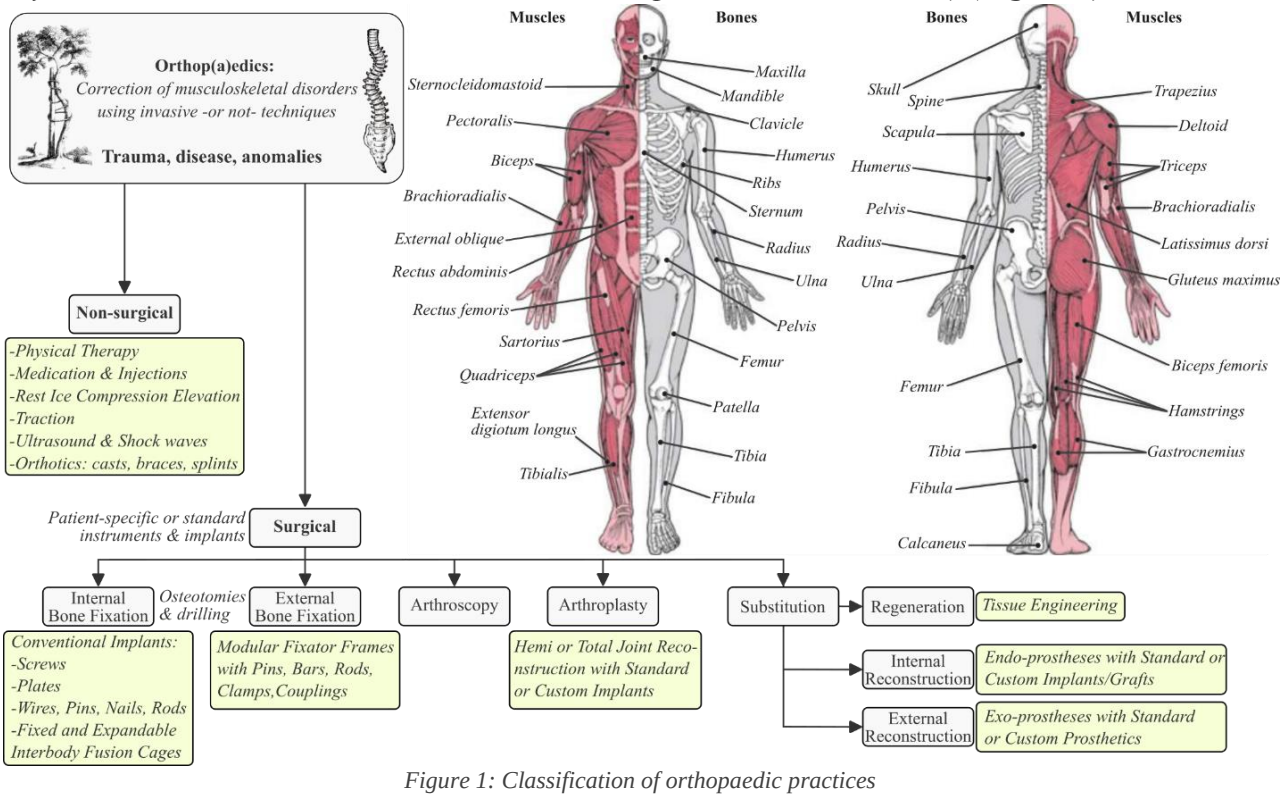

Figure 1: Classification of orthopaedic practices

Diachronically, humans had and have a built-in natural need to develop improved technological tools for multifarious applications to better satisfy the needs of society *(Appendix A)*.

[1] Clinical: from Greek *"κλινική"* (kliniké), from *"κλίνη"* (klíne; bed). Medicine: from Latin *"medico"*, from *"medeor"*, from Greek *"μέδω"* (médō; take care of).

[2] Orthopaedics was coined in 1741 by N. Andry (Dean of Faculty of Medicine, Paris), from Greek *"ορθός"* (orthós; correct) + *"παιδίον"* (pædíon; child) to describe correction/prevention of musculoskeletal deformities in children. Orthopedics, from *"ορθός"* (orthós; correct) + *"πεδώ"* (pedō; prevent a distortion) is etymologically more practical and generic, from Greek verb *"ορθοπ(ο/ε)δώ"* (orthop(o/e)dō; to walk uprightly) that is derived from *"πούς"* (poûs; foot in English, pes/pedis in Latin) *(Christodoulou, 2017)*.

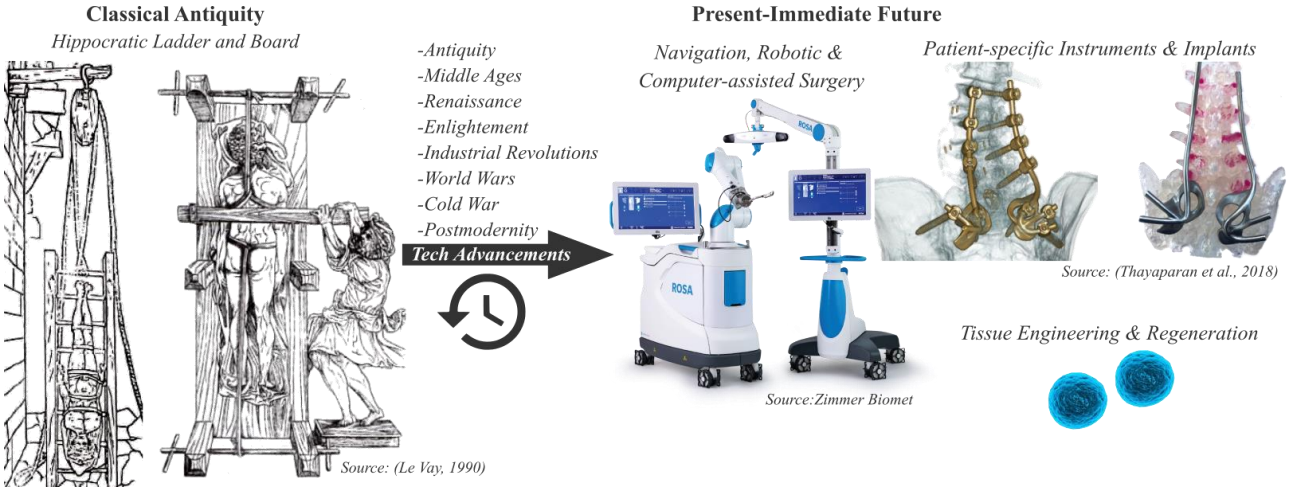

Figure 2: Schematic illustration of orthopaedic techniques evolution

Advancements in biomaterials and engineering science led to the emergence of enhanced products, consequently, clinical and surgical musculoskeletal rehabilitation techniques primed to reach a triumphant acme, whilst national and international orthopaedic associations[3] were formed to boost orthopaedic upgrades. *Appendix B* shows a collection of modern custom-made[4] and standard medical devices[5] used in orthopaedics, i.e. orthotics[6], implants[7], (mega)endo-prostheses[8], surgical tools and instruments, imaging devices, computer software, xR[9] devices.

[3] E.g. AAOS (American Academy of Orthopaedic Surgeons), EFORT (European Federation of National Associations of Orthopaedics and Traumatology), HAOST (Hellenic Association of Orthopaedic Surgery and Traumatology), AO Foundation (working group on bone fusion), MTS (Musculoskeletal Tumor Society), ISOLS (International Society Of Limb-Salvage), etc.

[4] As per the Medical Devices Regulation (EU) 2017/745, a custom device is *"any device specifically made in accordance with a written prescription of any person authorized by national law by virtue of that person's professional qualifications which gives, under that person's responsibility, specific design characteristics, and is intended for the sole use of a particular patient exclusively to meet their individual conditions and needs". "Mass-produced devices adapted to specific requirements are not considered custom-made".*

[5] According to the Medical Devices Regulation (EU) 2017/745 , a medical device is *"any instrument, apparatus, appliance, software, implant, reagent, material or other article intended by the manufacturer to be used, alone or in combination, for human beings for one or more of the following specific medical purposes: a) diagnosis, prevention, monitoring, prediction, prognosis, treatment or alleviation of disease/injury/disability, b) investigation, replacement or modification of the anatomy or of a physiological or pathological process or state, and c) providing information by means of in vitro examination of specimens derived from the human body, including organ, blood and tissue donations, and which does not achieve its principal intended action by pharmacological, immunological or metabolic means, in or on the human body, but which may be assisted in its function by such means".*

[6] From Greek *"όρθοσις"* (órthosis; correction), from *"ορθός"* (orthós; correct). *"An appliance that exerts external forces on parts of the body to support joints or correct deformities" (Oxford Dictionaries).*

[7] From Latin *"implantare"*, from *"in"* (in) + *"plantare"* (to plant). *"An object or material inserted or grafted into the body for (endo)prosthetic, therapeutic, diagnostic, or experimental purposes" (Dorland's Illustrated Medical Dictionary).*

[8] From Greek *"πρόσθεσις"* (prósthesis; addition), from *"προστίθημι"* (prostíthemi; add), from *"προς"* (prós; towards) + *"τίθημι"* (títhemi; place). *"An artificial substitute for a missing body part, used for functional, or cosmetic reasons, or both" (Dorland's Illustrated Medical Dictionary).* Refers to either internal placement (endo-prosthesis, usually seen as just prosthesis) or external placement (exoprosthesis, usually seen as just prosthetics).

[9] xR refers to Virtual Reality (VR), Augmented Reality (AR), Mixed Reality (MR) where sensations are simulated with head-mounted displays, screens, or multi-projected environments (sight, hearing) and haptics (touch). VR is *"a computer-generated simulation of a*

During the last decades, the number of people living on Earth has been growing at increasingly high rates with the life expectancy being extended, and so is the geriatric population *(Appendix C)*. The United Nations Population Division *(2019)* projects that the world population will rise from 7,7 billion in 2019 and hit 9,7 billion in 2050. These demographic patterns suggest an increase of people who will experience abnormal functioning for larger periods of their lives, and such shifts should alarm health policy planners to prioritize the preparation and adaptation of healthcare systems accordingly with adequate resources *(Cieza et al., 2020).*

The musculoskeletal disorders category contributes the most to the total number of disabilities recorded worldwide *(Figure 3) (Appendix D).* It is apparent that as orthopaedic disorders grow along with the aging population, more operations will be required to be performed.

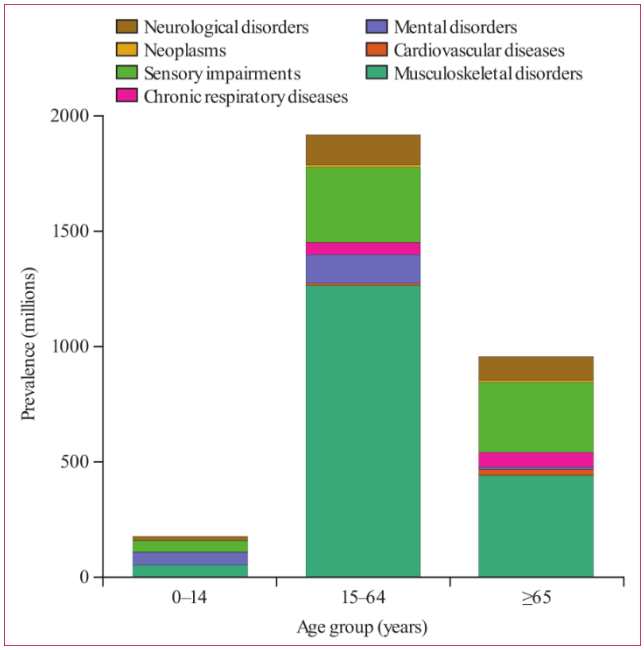

Figure 3: Disease categories of prevalent conditions globally . Source: (Cieza et al., 2020)

The orthopaedic industry reached $ 53,6 billion in 2021 *(Orthoworld, 2022)* with reconstructive and replacement being the most common types of surgeries *(Figure 4)*. A representative index reflecting these trends is arthroplasties[10], the registries of which are annually ascending in the EU[11] and worldwide[12], with the majority taking place in the hip and knee areas.

three-dimensional image or environment that can be interacted with in a seemingly real or physical way by a person using special electronic equipment, such as a helmet with a screen inside or gloves fitted with sensors" (Oxford Dictionaries). AR and MR superimpose computer-generated graphical information with the physical world on screens or the scene that the user is looking at *(Oxford Dictionaries)*. xR is used for training, pre-operative planning assistance, patient education, intra-operative guidance etc.

[10] From Greek *"ἄρθρον"* (árthron; joint) + *"πλάσσω"* (plásō; to form), meaning joint restoration.

[11] A collection of arthroplasty registries is listed in the Network of Orthopaedic Registries of Europe (NORE) (available at: https://www.efort.org/about-us/nore/research/).

[12] E.g. American Joint Replacement Registry (available at: https://www.aaos.org/registries), Australian (available at: https://aoanjrr.sahmri.com/annual-reports-2021), Canadian (available at: https://www.cihi.ca/en/canadian-joint-replacement-registry-cjrr), New Zealand (available at: https://www.nzoa.org.nz/nzoa-joint-registry).

The previous figures fuel the demand for orthopaedic rehabilitation products and imply that a great number of multifarious parts have to be manufactured to reflect and satisfy the diverse patients' needs. Thus, the respective orthopaedic products market has to resonate and expand analogously.

In our digital era where 4th industrial revolution[13] (industry 4.0) is being unfolded with serious impacts on societies and many markets including medicine, aspirations emphasize on transforming the traditional healthcare delivery system to individually serve each unique patient (mass-customization) at reasonable costs and lead times *(Javaid and Haleem, 2020; Paul et al., 2021)*. Hence, key players involved in orthopaedic products industry need to accelerate and optimize their products' life cycles and seek efficient and effective design and manufacturing methods that are essentially rapid, agile, and sustainable to serve the growing demand, whilst minimizing costs, lead times, material waste, and improving the supply by decentralizing manufacturing and embracing distributed and localized networks *(Emelogu et al., 2016; Moreno and Charnley, 2016)*.

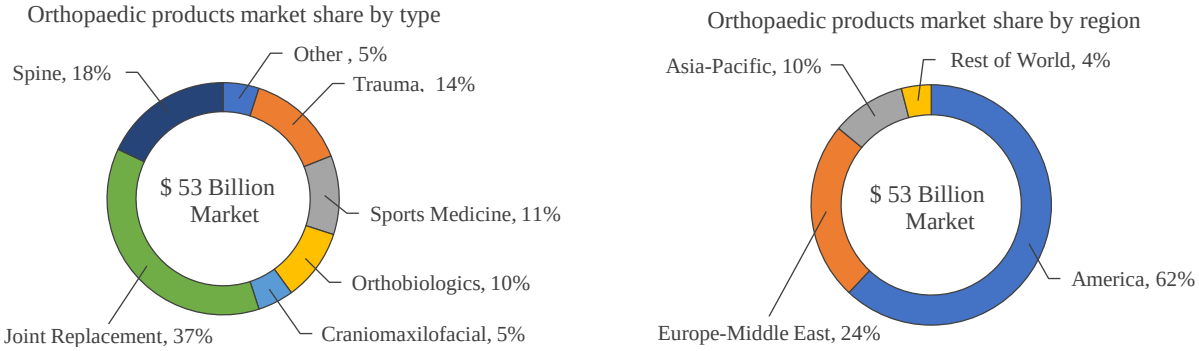

Figure 4: Orthopaedic industry market. Source: (Orthoworld, 2020)

Each patient is unique, thus individualized parameters must be factored in before any operation. Extreme conditions and special cases where no alternative solutions are available such as bone reconstruction for limb salvage after oncological resections *(Özger et al., 2022)* make it necessary that endo-prostheses and implants are tailored as per the unique patient's anatomy[14] and physiology. Even for routine surgeries, where implant manufacturers have always been offering off-the-shelf options for various types and sizes to select, both giants and smaller companies, are now shifting towards establishing patient-specific design and production services. A custom-made knee arthroplasty kit by Conformis (Conformis Inc., Massachusetts, US) is shown in *Figure 5*.

The customized approach in healthcare refers to *"fitting the method/product to the patient and not the patient to the method/product"*. Although orthopaedics has always been patient-centered,

[13] Industry 4.0 marks a shift towards data-intensive smart manufacturing systems. It is characterized by increased interconnectivity and virtualization, decentralized cyber-physical systems, Internet of Things (IoT), cloud computing, and Artificial Intelligence (AI).

[14] Originates from Greek *"ανατομή"* (anatomé; dissection), from *"ανά"* (aná; up) + *"τομή"* (tomé; cutting, section), from *"τέμνω"* (témnō; I cut, incise), meaning "cutting up" a body. *"The study of the structure of living organisms, especially of their internal parts by means of dissection and microscopical examination" (Oxford Dictionaries).*

until the emergence of specific enabling technologies (discussed next), it was not feasible or was extremely costly and time-consuming to match every product to each patient due to the lack of suitable software tools, imaging techniques, biomaterials, and manufacturing methodologies.

Individualized products are made to order just in time to simplify the operation for the clinician or surgeon with no stock required. *Appendix B* shows some customized parts and instruments.

Individualized medicine focuses on matching something different to suit the needs of a unique individual patient. Although the terms *personalized*[15] and *precision*[16] partially embody the individualization dimension and are used synonymously, they are debated, critiqued, and articulated in various ways and contexts, reflecting different views *(Erikainen and Chan, 2019; Iriart, 2019)*.

Figure 5: iTotal patient-specific knee replacement system. Source: Conformis

Granted orthological design, bespoke implantable solutions have the potential to provide a) superior mechanical performance in terms of properties tuning for failure prevention and operation free of stress shielding phenomena, tailored to the anatomical area to be applied (host bone), b) superior biological performance in terms of integration, promoting bone ingrowth to achieve osseointegration[17] and ultimately osteogenesis[18], with potential for Tissue Engineering (TE) applications for regeneration, c) optimum aesthetical outcomes with perfect anatomical fit, and d) optimum post-operative function with fast recovery, less complications, infection risks, and future interventions *(Li et al., 2012; Regis et al., 2015; Taniguchi et al., 2016)*.

[15] Does not exclusively indicate making something as per the needs of one individual patient as it also suggests tailoring to a subgroup of patients. The Council of European Union *(2015/C 421/03)* defines it as *"a patient-centered care model that takes into account the phenotypes and genotypes for matching the right therapeutic strategy, for the right person, at the right time, and/or to determine the predisposition to disease and/or to deliver timely and targeted prevention".*

[16] Defined as the prevention, investigation, and treatment of diseases based on a data ecosystem that seeks to taxonomize diseases as per the biology at a molecular or cellular level. Refers to the creation of drugs or medical devices that are unique to a patient, but mainly to coin classification of individuals into subgroups (also seen as *stratified medicine)* that differ in their susceptibility to a particular disease, in the biology or prognosis of those diseases they may develop, or in their response to a specific treatment.

[17] From Greek *"οστό"* (ostó; bone) + *"integration". "A direct structural and functional connection between ordered, living bone and the surface of a load-carrying implant" (Brånemark, 1985).*

[18] From Greek *"οστό"* (ostó; bone) + *"γένεσις"* (génesis; origin, mode of formation), meaning bone formation.

On the contrary, a tailored product requires extensive pre-operative planning and high specialist knowledge, higher development time and cost compared to its off-the-shelf counterpart, and last but not least, overthinking might cause the paralysis-by-analysis phenomenon.

1.2 Inter-epistemic Synergy

To fabricate patient-specific orthopaedic parts, suitable synergies[19] must be formed. Scientifically amalgamated schemes could categorically improve healthcare delivery. Multi and inter-disciplinary synergies among disciplines of medicine and health sciences are common, however, blends of disciplines originating from different sciences are essential to be explored and exploited, particularly for the development of standard or custom parts, i.e. orthopaedic surgery and mechanical engineering. Indeed, healthcare and engineering professionals are cooperating for the development of off-the-shelf medical devices that are accompanied by instructions for surgical or not techniques, but enabling inter-epistemic[20] (inter-scientific) synergies of high readiness level within a feasible context able to achieve routine application for custom-making, especially within the Healthcare Facility (HCF), is truly groundbreaking.

Human beings are charismatically gifted with intelligence and consciousness, which enable the activities of questioning, observation, exploration, reasoning, and creation. Hence, it is orthological to state that all humans are potential *engineers* with the natural (not the professional) hue of the word *engineering* that is both verb and noun.

As its Latin origin indicates, an *engineer*[21] invents or creates something to solve/satisfy a problem/need by *engineering*. Therefore, engineering produces a tangible or an intangible *engine* that solves a problem *(Figure 6)*. According to Kolaitis *(1964) "engineering is a multidimensional reasoning process with an extended semantic context, declaring a fuzzy blend of art and science that relates to technology in the most inventive, imaginative and creative points of view".*

Under the previous philosophical umbrella, and just to facilitate a path towards identifying a field for realizing a synergy between the professions of orthopaedics and mechanical engineering, the term *orthopaedic engineering* can be introduced, similarly to *mechanical engineering*[22] that is synthesized by the descriptive adjective *mechanical*.

---

[19] From the Greek *"συνέργεια",* from *"συν"* (sín; together) + *"έργο"* (érgo; work). "*The interaction or cooperation of two or more agents to produce a combined effect greater than the sum of their separate effects" (Oxford Dictionaries).*

[20] From *inter* (existing between) + the Greek *"επιστήμη"* (epistēmē; knowledge, science) meaning inter-scientific.

[21] Formerly "*ingineer",* from Latin *"ingenium"* (talent, devise), from *"in"* (in) + "*gignere"* (beget) *(Oxford Dictionaries).* The same applies in Greek, i.e. *"Μηχαν(ευτ)ικός"* (mechan(eft)ikós; engineer) from Greek *"μηχανεύομαι"* (mechanévome; engineering (verb)). Engineering (noun) is usually attributed in Greek as *"μηχανευτική"* (mechaneftiké; mechaneutics) or *"μηχανοτεχνία"* (mechanotechnía; mechanotechnics) *(Kolaitis, 1964)*.

[22] In Greek, *"μηχανολογία"* (mechanología; mechanology), from *"μηχανή"* (mechané; engine) + *"λόγος"* (lógos; root of logic), relates to the study of machines, mechanisms and systems involving forces and movement.

To fully define a common space where orthopaedic surgeons and mechanical engineers could harmonically and increasingly intersect, the field of biomechanics[23] has yet to be considered. Biomechanics falls under the scope of the mechanical engineering profession that is characterized by a broad gnostic sphere that deals with the (bio)mechanical as opposed to medical properties of the musculoskeletal system. Mechanical engineers study the static and dynamic performance of the musculoskeletal which is being treated as a highly complex hypodigmatic system with features and mechanisms that are perfectly forged and diachronically optimized by Mother Nature. The intelligent mechanical design hidden within us is truly admirable, e.g. hierarchical bone architecture *(Appendix E)*, and mechanics of bone joints *(Figure 7)*.

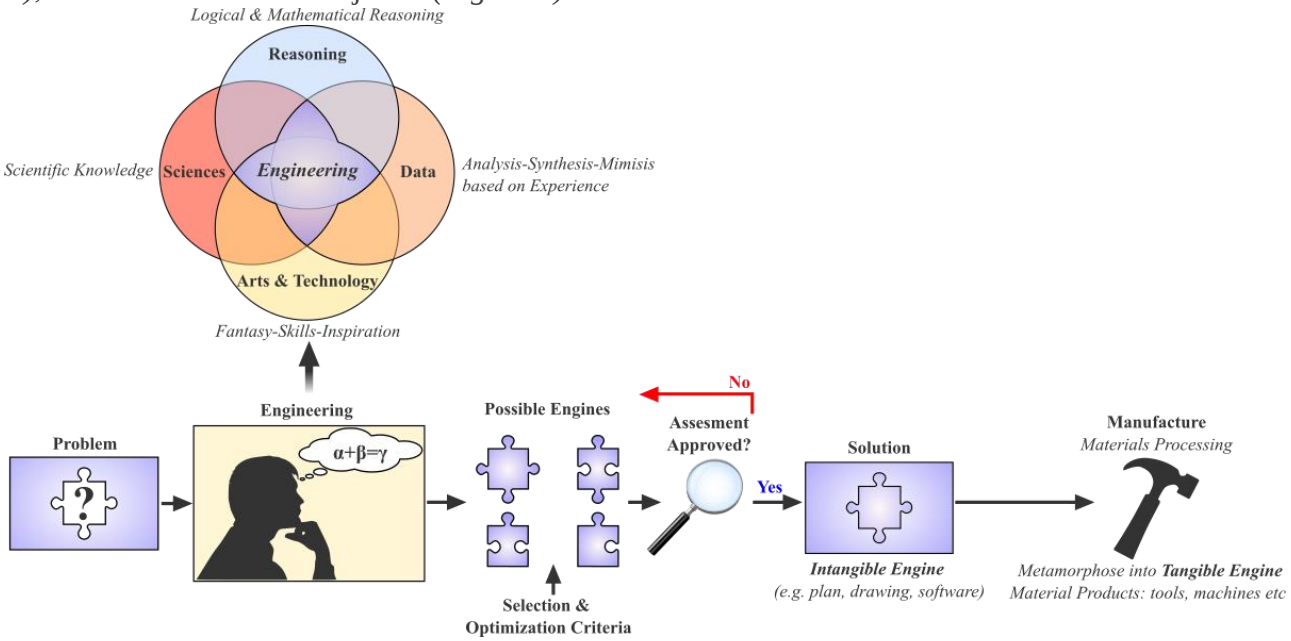

Figure 6: Engineering as a process for producing tangible and intangible solutions (engines)

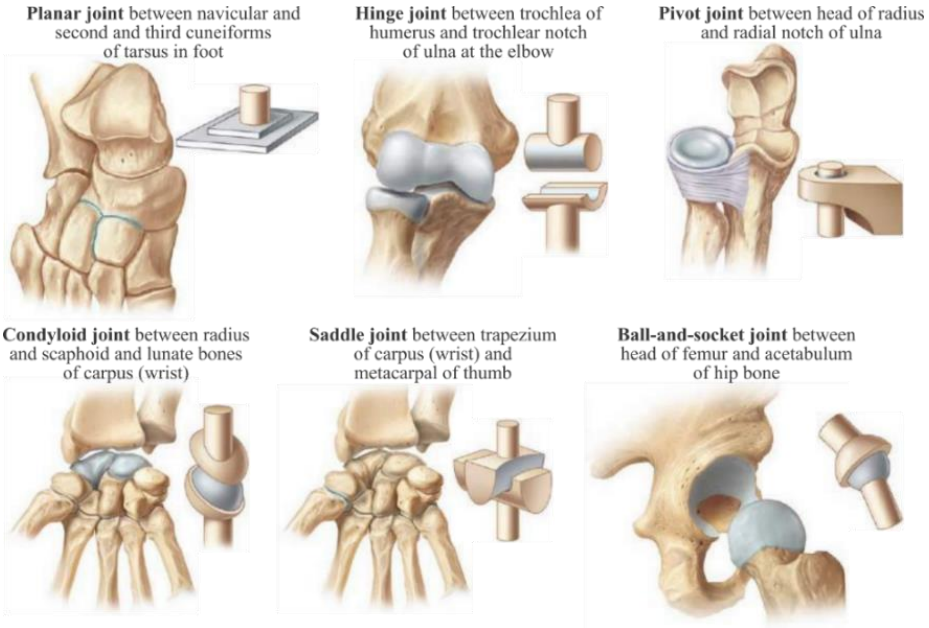

Figure 7: Types of musculoskeletal joints. Source: (Tortora and Derrickson, 2020)

[23] From the Greek *"βίος"* (víos; life) + *"μηχανική"* (mechaniké; mechanics), meaning the mechanical study of living systems.

A plethora of personalities with medical and mechanical engineering *(Figure 8)* backgrounds had biomechanical insights[24], triggering the genesis of intense interest in acquiring high scientific knowledge and experience about the forms and functions of the musculoskeletal system (*Mow and Huiskes, 2005).* This way, orthopaedics was enriched with novel (non)surgical therapies, whereas biomechanical and gait analyses were introduced and implemented, not only to normalize associated disorders but also to monitor and improve performance *(Baker, 2007; Klette and Tee, 2008).*

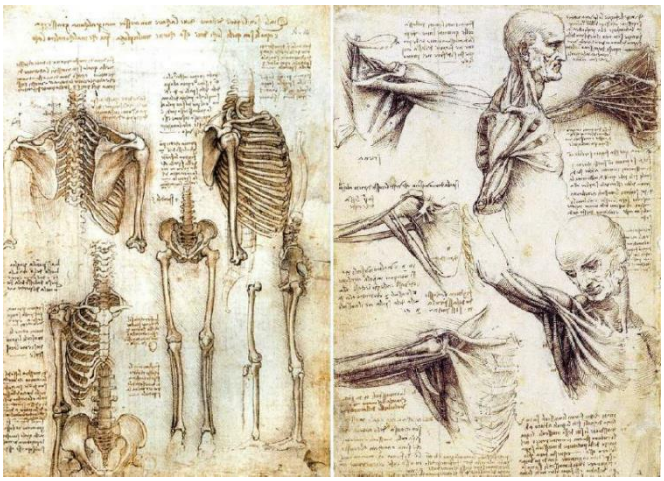

Figure 8: Leonardo da Vinci's anatomical drawings. Source: Royal Collection

Pragmatically, biomechanical studies are clinically relevant in orthopaedics, especially when implants and endo-prostheses are pursued *(Mavrogenis et al., 2017a).* Orthopaedic surgeons with (bio)mechanical backgrounds that are being assisted by mechanical engineers can analyze musculoskeletal mechanics and participate in the development process of orthopaedic devices actively by providing design principles, concepts, and specifications. Indeed, (bio)mechanical engineering finds applications in orthopaedics and contributes towards individualization *(Canciglieri and Trajanovic, 2022).*

Even though biomechanics addresses the musculoskeletal system from a different perspective *(Figure 9),* it forms a fundamental basis for interlinking orthopaedics with mechanical engineering. A synergy can be transpired and established within this particular space if both professions interfere effectively, efficiently, and sustainably based on a properly structured product development workflow. In this case, the orthopaedic surgeon will identify the problem, provide guidelines, and set the solution specifications, whereas the mechanical engineer will design and materialize the solution.

Figure 10 illustrates the macroscopic inter-epistemic approach for making standard or custom-made orthopaedic products. From initiation to completion, three questions have to be answered:

1. ***Why develop the solution?***: the musculoskeletal problem is identified and clarified by the orthopaedic surgeon, and the requirements of the solution are comprehended.

[24] E.g. Aristotle (mechanics of organisms), Galen (function of body parts), Leonardo da Vinci (engineering principles and anatomical illustrations), Vesalius (illustration of human body), Galilee (mechanical aspects of bone), Borelli (mechanics of organisms).

2. ***What to develop?***: the rehabilitation strategy and the product's functions and specifications are set by the orthopaedic surgeon.
3. ***How to develop the solution?***: it is the mechanical engineer who is responsible for applying a suitable tactic to design, optimize, manufacture, post-process, prepare and deliver the product as per the orthopaedic surgeon's guidelines and pre-set functions and specifications.

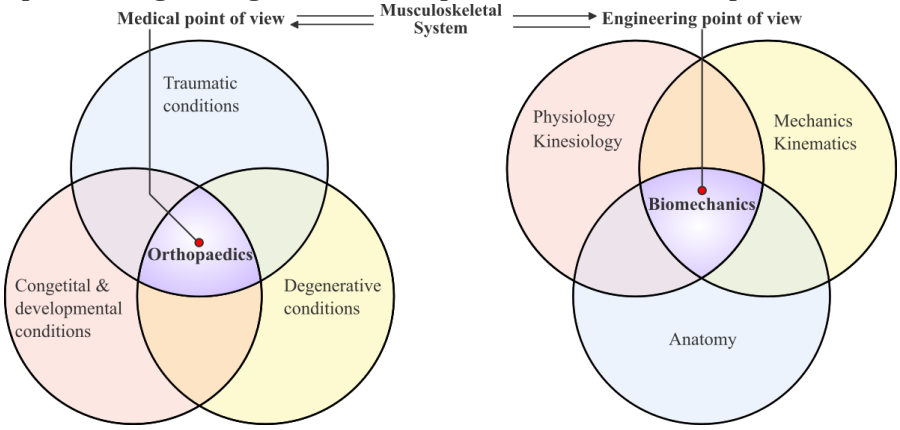

Figure 9: Musculoskeletal system under orthopaedic and biomechanical points of view

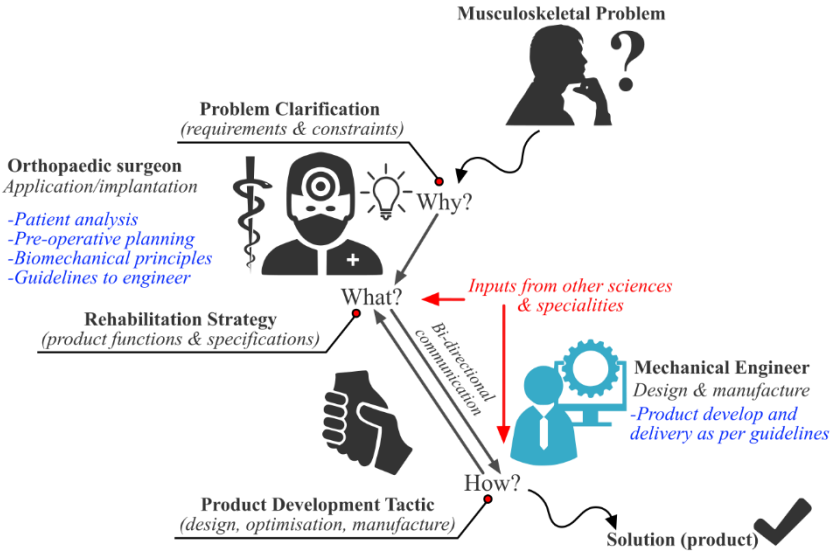

Figure 10: Macroscopic inter-epistemic approach for orthopaedic products development

Several sciences and disciplines are indeed in developing an individualized orthopaedic product. In addition to the orthopaedics-engineering synergy discussed, to enable materialization of patient-specific implantable or externally attachable parts, radiology, 3D imaging, and availability of suitable manufacturable biomaterials are elemental. *Figure 11* shows the inter-epistemic and multi-disciplinary landscape describing each role and the disruption that might be brought by regenerative medicine for artificially-induced biological tissue regeneration rather than the current bioinert reconstruction approaches.

For custom solutions, the improvement in clinical outcomes should justify the additional costs and time required to develop these particular solutions. A custom approach provides the best results when the outcome for the patient improves and the total cost goes down, whereas the opposite is the worse. Unfortunately, most unique patient-centric interventions in healthcare result in higher costs

with improved outcomes *(Iriart, 2019)*. As synergy-enabling technological tools are penetrating the industry and maturing into widely accessible tools at reasonable costs, the future holds digitalized and intelligent orthopaedics *(Pei, 2018; Zheng et al., 2018; Canciglieri and Trajanovic, 2022)* to become mainstream for making individualized and closer to nature parts for musculoskeletal reconstruction and tissue regeneration.

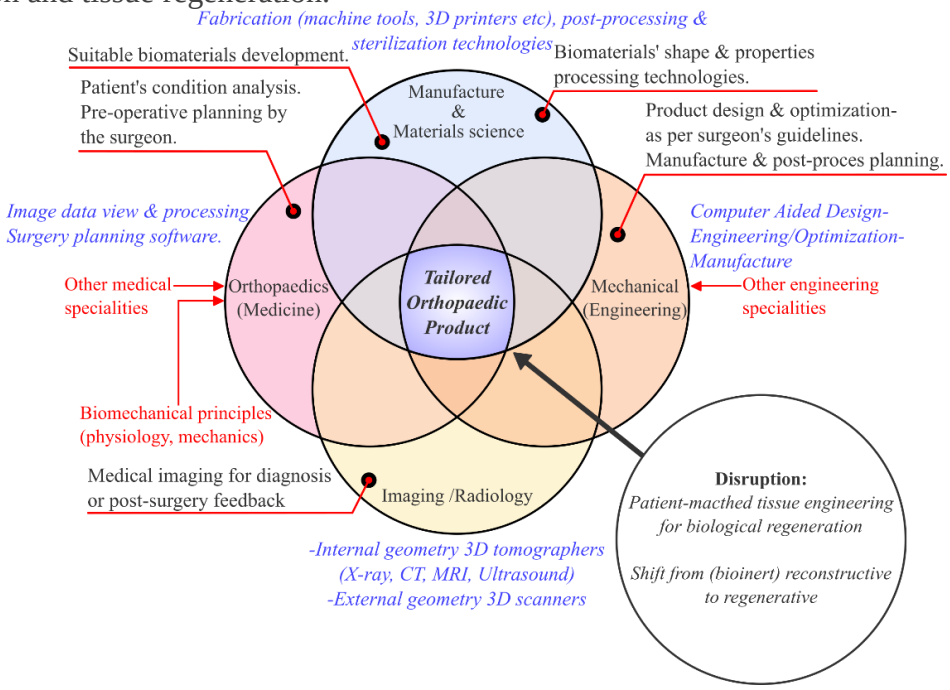

Figure 11: Inter-epistemic multi-disciplinary field of individualized orthopaedic products

1.3 Synergy-Enabling Technologies

The terms personalized, precision, intelligent, digital, image/template/computer-assisted/guided are attributed to orthopaedics to contextualize patient-specific treatments. 3D computer digital design, materialization, and implantation/application techniques of individually-matched orthopaedic products are enabled thanks to several technological tools *(see Appendix B) (Figure 17)*:

1. **3D (medical) imaging:** tomography[25] (external and internal forms) and 3D scanners[26] (external-only shape) for anatomical image data acquisition *(Figure 13)*. It is the most fundamental part as

[25] From Greek *"τομή"* (tomé; cutting, section) + *"γράφω"* (gráfō; write), meaning acquisition of cross-sections. Tomography technologies used for 3D medical anatomical imaging to non-invasively acquire cross-sectional images (slices) of the body's inside include **Computed Tomography (CT)** which utilizes X-rays, **Magnetic Resonance Imaging (MRI)** which is based on the emission of electromagnetic waves from the body when it is placed in a strong magnetic field and exposed to radiofrequency radiation, Nuclear medicine imaging where the radiation emitted from within the body is recorder rather than radiation generated by external sources, e.g. **Positron Emission Tomography (PET)** which is based on injecting radiopharmaceutical tracers and Gamma rays, **Ultrasound (US)** tomography where high-frequency sound waves are utilized, and **Fluoroscopy** which is based on X-rays to generate real-time moving images of the body's interior.

[26] A process of digitally acquiring data of the shape and appearance of a real object to be used to construct digital 3D models. There are two main categories: contact (e.g. Coordinate Measuring Machines (CMM)) and non-contact (active (emit radiation, light or sound to detect reflections or radiation passing through objects) or passive (do not emit radiation themselves, but rely on detecting reflected ambient radiation such as visible light).

the exact anatomy of the patient is visualized to serve as the basis for the other technologies to add value. 3D medical imaging can be used for diagnosis (pre-operative), live at the time of operation (intra-operatively), or post-operatively for assessment and follow-up.

Robotics and navigation systems: deployed for intra-surgical guidance and collaboration *(Jacofsky and Allen, 2016; Malham and Wells-Quinn, 2019; Mao et al., 2021) (see Appendix B).* Disruption is driven mainly by lowering equipment costs to allow wide adoption and accessibility. The historical evolution of medical imaging, computing, navigation, and robotic systems is pictured in *Figure 12.*

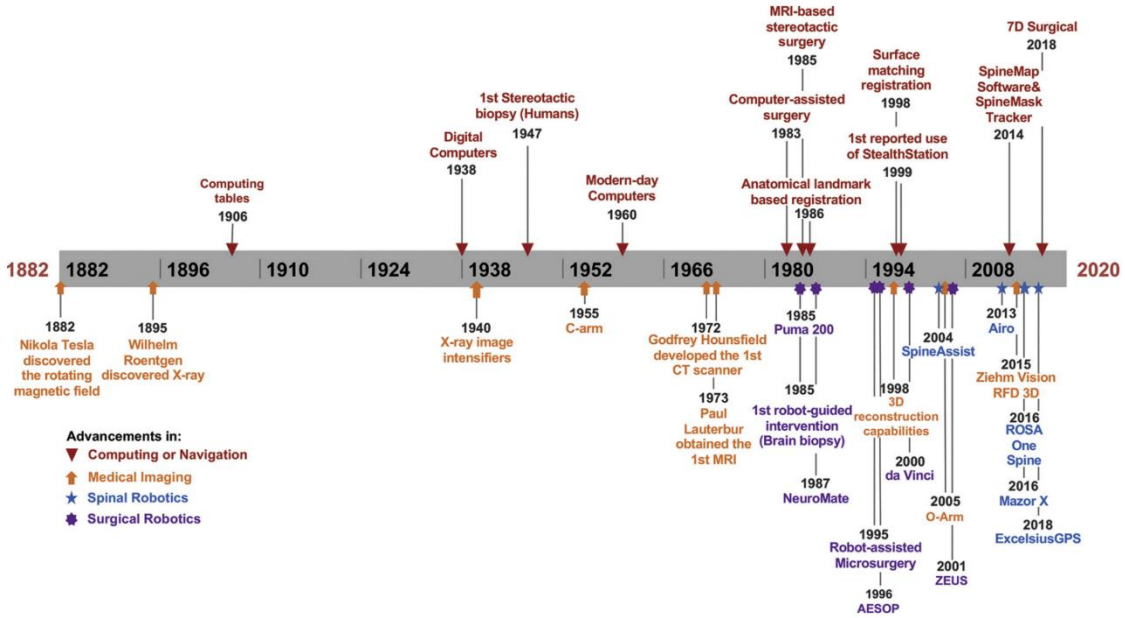

Figure 12: Historical evolution of medical imaging, navigation, and robotic systems. Source: (Mao et al., 2021)

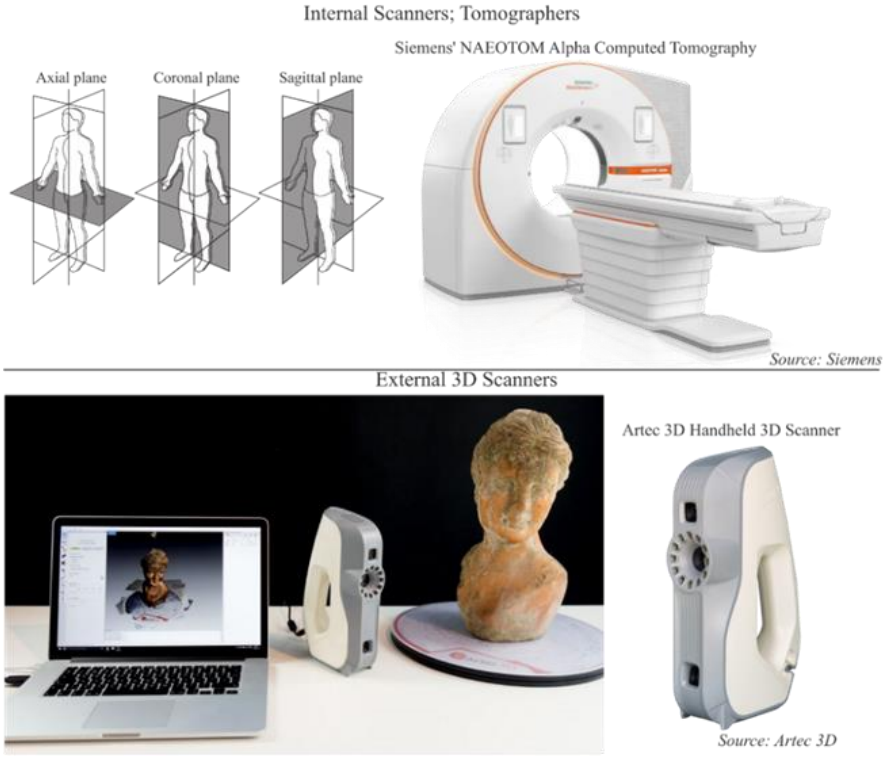

Figure 13: Internal and external anatomy scanners

2. **3D computer software to:** a) generate and manipulate medical image data[27], b) plan pre-operatively and navigate intra-operatively, and c) design products, simulate their performance, and topologically optimize[28] them *(Figure 14)*. Disruption is powered by algorithmic data-driven techniques and Artificial Intelligence (AI)[29].

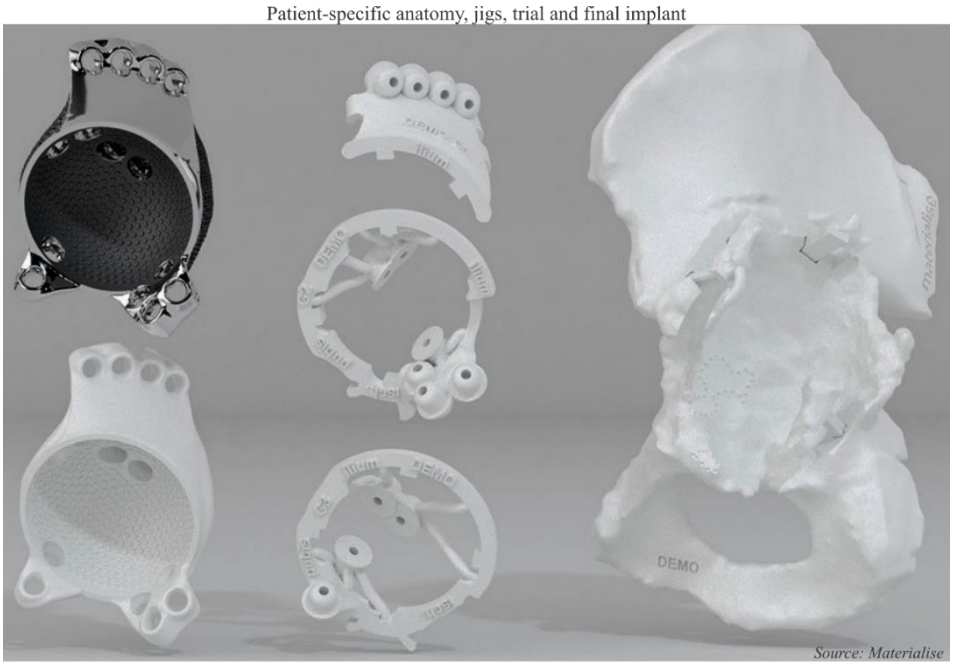

Figure 14: 3D software to design and optimize bespoke solutions

[27] Digital Imaging and Communications in Medicine (DICOM) is a worldwide standard to store, exchang and transmit medical images.

[28] Topology optimization is a mathematical (computational) method based on FEA that spatially optimizes the distribution of a given material within a defined design space, for a given set of loads, boundary conditions, and constraints to maximize the performance of the system. On the other hand, generative design is an iterative and evolutionary design exploration process that generates all possible permutations and alternative solutions, based on the design goals set, materials selected, applied loads, boundary conditions, and constraints (cost, manufacturing, etc).

[29] According to the European Commission's High-Level Expert Group on Artificial Intelligence *"Artificial intelligence (AI) refers to systems designed by humans that, given a complex goal, act in the physical or digital world by perceiving their environment, interpreting the collected structured or unstructured data, reasoning on the knowledge derived from this data and deciding the best action(s) to take (according to pre-defined parameters) to achieve the given goal. AI systems can also be designed to learn to adapt their behavior by analyzing how the environment is affected by their previous actions."*

3. **xR:** Virtual/Augmented/Mixed Reality (VR/AR/MR) devices (projectors, screens, head-mounted displays, haptics) for (semi)immersive reality-like experience to aid pre-surgery planning, simulation, and surgical navigation *(Figure 15)*. Disruption brought by Metaverse[30] rise.

Virtual reality goggles and haptic devices for surgery simulation

Source: FoundamentalVR

Augmented/Mixed reality goggles for surgery assistance

Source: Royal Phillips

Figure 15: xR head-mounted displays and haptic devices

4. **Biomaterial fabricators:** manufacturing techniques for biomaterials forming, e.g. Additive Manufacturing (AM)[31], a.k.a. 3D Printing (3DP)[32] *(Gibson, Rosen and Stucker, 2021) (Figure 16).* Disruption emerges as the available feedstock biomaterials and quality are increased, the costs and lead times are lowered, and the decentralized manufacturing model and Industry 4.0 evolve.

Stratasys' JT50 Photopolymer jetting 3D printer and product (anatomical replica)

Source: Stratasys

EOS' P 396 Powder Sitnering 3D printer and product (anatomical model & spine jigs)

Source: EOS

Concept Laser's M2 Powder Melting 3D printer and product (partial femoral implant)

Source: Concept Laser

Source: Stratasys

Source: Anatomics

Source: Virginia Cancer Specialists

Figure 16: 3D printers and 3DPed anatomical models, jigs and prosthesis

[30] From Greek *"μετά"* (metá; after, beyond (a prefix indicating transcendence)) + *"universe"*, meaning virtual-reality worlds and networks in which users can interact with other users within computer-generated environments.

[31] Additive Manufacturing (AM) is defined as *"a process of joining materials to make parts from 3D model data, usually layer upon layer, as opposed to subtractive and formative manufacturing methodologies" (ISO/ASTM, 2021).*

[32] 3D printing is typically associated with machines used for non-industrial purposes including personal use. It is often used as a de facto standard term interchangeably with AM. In this Thesis, it is used synonymously with AM.

To individually treat orthopaedic disorders requiring custom-made devices, a suitable development and materialization workflow should be applied. A prerequisite to manufacture/3DP a patient-specific orthopaedic device is a readily available 3D digital model of the device and to 3D design a device to specifically match a unique patient, the patient's anatomy has to be accurately acquired in 3D. In other words, the following workflow is followed to design, fabricate and implant/attach an individualized orthopaedic product:

Images of the patient's anatomy are obtained using 3D imaging techniques to virtualize the real anatomy.

↓

The acquired image data is processed to generate the digital 3D anatomy. Patient-specific products are 3D designed, and optimized, and the operation is modeled virtually for on-screen or xR simulation.

↓

The virtual anatomical replica and the virtual patient-specific products are realized using biomaterial fabricators (3DP) to simulate the operation physically and for final production.

↓

The sterilized products are delivered to the clinician/surgeon for implantation/attachment. The operation can take place with live computer guidance or robotic assistance.

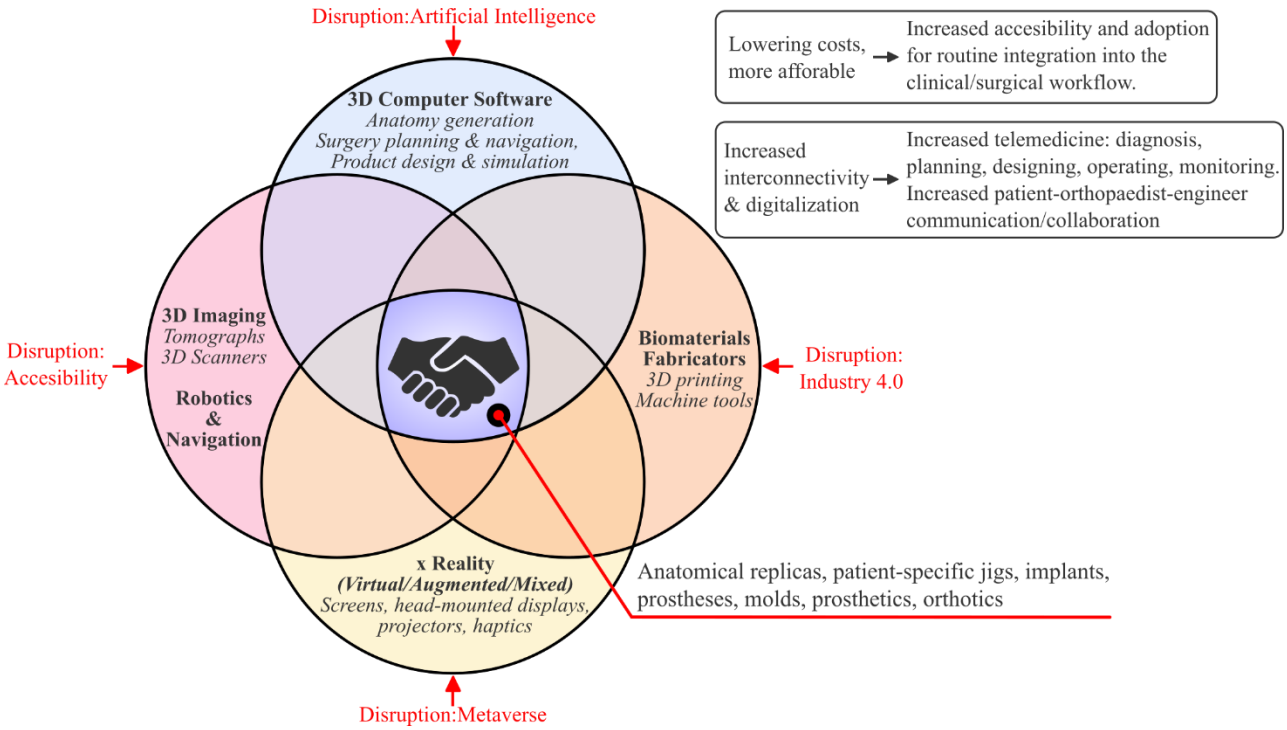

Figure 17: Enabling technological tools for making individualized orthopaedic products

Most of the aforementioned synergy-enabling technological tools that are now entering the home of orthopaedic industry, are sourced from other industries, traditionally found in the manufacturing industry, where were harnessed by professional engineers. These tools have the potential to "*make orthopaedic surgeons the designers"* granted that orthopaedic surgeons are assisted by skilled professional engineers.

The COVID-19 pandemic impacted orthopaedics and gave a glimpse into the future of digital orthopaedics as it catalyzed the need to adopt a new model of musculoskeletal healthcare delivery that embraces digital health tools *(Bini et al., 2020)*; 3D digital design, 3DP technologies, xR systems, patient engagement platforms, surgical scheduling applications, wearable sensor devices, data science, virtual physical therapy and telerehabilitation, telemedicine, chatbots, virtual/digital scribes.

In orthopaedics, the term *"3D digital technologies"* refers to a broad gnostic sphere that encompasses high-fidelity 3D medical image data acquisition hardware, surgical robotic manipulators, 3D computer software for detailed planning, simulation, design, and optimization of orthopaedic products, 3DP hardware for design materialization, and xR devices for immersive and augmented experience to facilitate pre-operative planning, training, and intra-operative guidance.

Indeed, computer-assisted orthopaedic surgery *(Haaker and Konerman, 2013; Sugano, 2018)* and 3D digital technologies are revolutionizing orthopaedic practice *(Papagelopoulos et al., 2018)* by enabling accurate planning, execution, and design of patient-specific devices using 3D software, followed by 3DP of these devices.

Similar to X-ray machines and CT scanners that changed 20th-century orthopaedics, advances in computer graphics and medical imaging paved the way to reach the current epoch of *Digital Surgery (Atallah, 2021)* and *Digital Anatomy (Uhl et al., 2021)* where the complex spatial relations of the human body are being visualized and processed in a computer-accessible digital format and matching anatomical parts are generated with powerful 3D tools to assist clinical diagnosis and modeling, design, simulation, treatment and guidance for more efficient rehabilitation strategies and tactics.

Considering the impacts of AI and Industry 4.0 *(Javaid and Haleem, 2020)*, and powered by the aforementioned emblematic 3D technologies, orthopaedics are undergoing a computational revolution, getting digitalized *(Pei, 2018)*, individualized (*Canciglieri and Trajanovic, 2022)* and evolving into an intelligent form *(Zheng, Tian and Zhuang, 2018)*.

Various 3DP processes and materials are used for different medical applications *(Figure 18)*. Orthopaedic devices are designed by engineers as per the orthopaedic surgeons' instructions to accurately and precisely match the patient's needs and then 3DPed to receive the tangible part within a short time. But still, this will be possible only if suitable equipment and infrastructure exist and granted that multi-disciplinary and inter-epistemic synergies are formed to enable the engineer-orthopaedic surgeon synergy for patient-specific product development.

Of the total value of 3DP products and services ($12,8 billion), the medical 3DP sector represents $1,65 billion *(Wohlers Associates, 2021a)*. Medical 3DP has impacted more than 3 million patients directly and more than 5 million indirectly, whilst the most growth is expected in customized devices, surgical planning, and development and prototyping areas *(ASME, 2020)*.

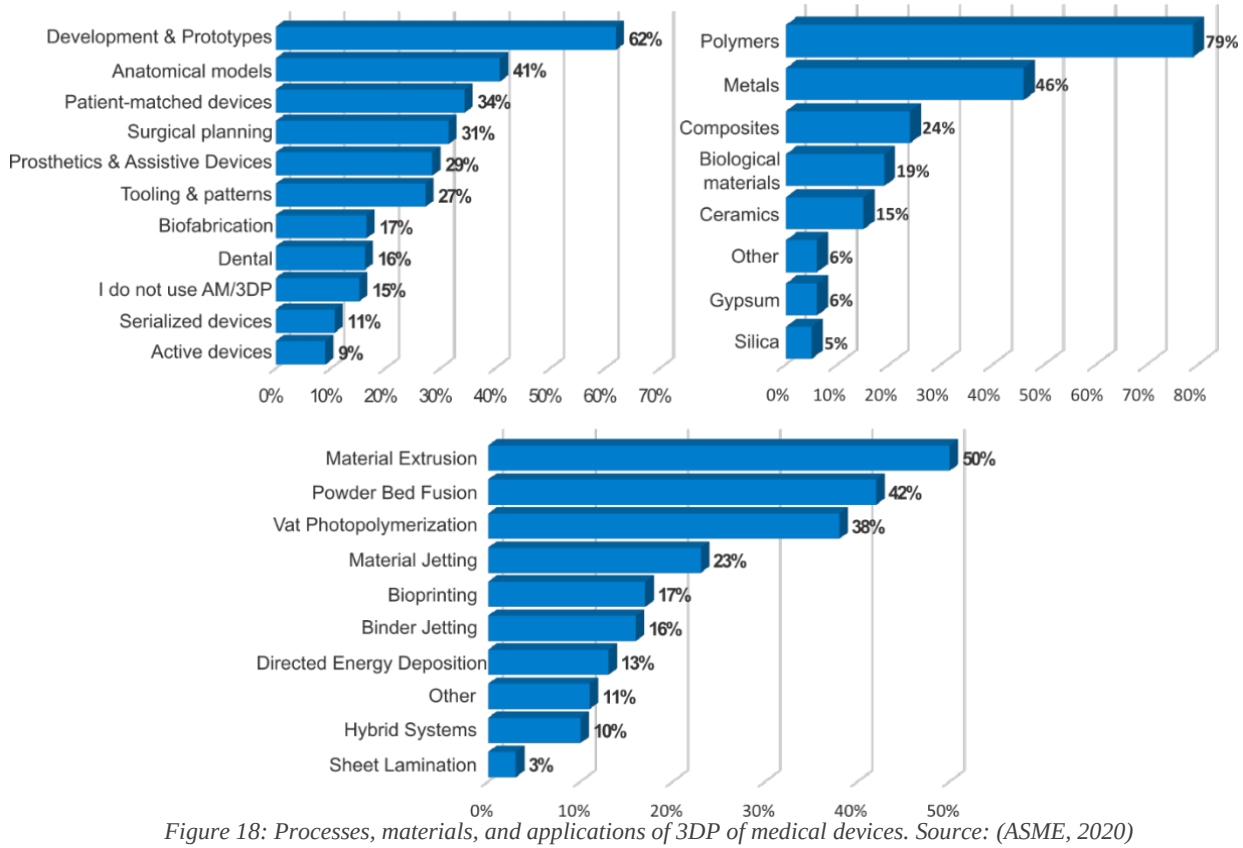

Figure 18: Processes, materials, and applications of 3DP of medical devices. Source: (ASME, 2020)

Emphasizing on the fabrication of orthopaedic implants, these are made of biomaterials with such properties and form to be safely, securely, and accurately fitted into the body *(Bose and Bandyopadhyay, 2016)*. Conventionally, these were shaped using classic formative and subtractive processes, and then post-processed and coated to meet the final specifications *(Özel et al., 2016)*. Selecting the optimal manufacturing technique is a multi-variable process, but 3DP is well-suited for fabricating unique patient-specific musculoskeletal substitution parts *(Munsch, 2017)*.

3DP is similar to reverse tomography, i.e. instead of digitizing the real object by scanning its cross-sections, the digital model is realized in a laminated 3D object by materializing and stacking the cross-sections of the digitally designed form *(Figure 14)*. Utilizing this layer-by-layer principle allows the forming extremely complex 3D geometries with intricate organic internal and external features that vary in material composition, density, and properties spatially across the part per se. This way, almost unlimited design freedom, and de novo innovation are available as manufacturing barriers are lifted, and the physical making of an object is now easier than the digital modeling of it. Hence, digital modeling and optimization become the bottleneck of innovative product making.

Medically approved 3DPed parts have been implanted worldwide *(Ventola, 2014; Di Prima et al., 2016; Lowther et al., 2019; Fogarasi, Snodderly and Di Prima, 2023)*, whereas research on 3DP applications in medicine is intense with numerous applications found in the literature *(Tack et al., 2016; Levesque et al., 2020; Kermavnar et al., 2021; Charbonnier, Hadida and Marchat, 2021; Salmi, 2021)*, e.g. anatomical replicas for pre-operative planning *(Marro, Bandukwala and Mak,*

2016), instruments for intra-operative guidance *(Dahake et al., 2016),* fixation implants *(Wang et al., 2017),* (mega)endo-prostheses *(Fukuda, 2015),* prosthetics and orthotics *(Manero et al., 2019; Ribeiro et al., 2019; Schwartz and Schofield, 2023),* TE constructs *(Munaz et al., 2016; Mandrycky et al., 2016; Poomathi et al., 2021),* drug delivery systems *(Prasad and Smyth, 2016).*

Figure 19: Layer-by-layer manufacturing principle. Source: Hasbro

3DP was successfully used in many industries. Indeed, it went mainstream recently, but actually appeared in the 1980s and improved remarkably ever since, both technologically and commercially *(Wohlers Associates, 2021a)*. Despite some limitations and technical flaws in 3DPed parts (though can be improved by post-processing, e.g. surface roughness, micro-porosity, dimensional inaccuracies) the method was called *"manufacturing revolution"* due to the ability to *"build something out of nothing"* and its special attributes and impacts on product offerings, life-cycles, business models, supply chains, and environment *(Markillie, 2012; Manyika et al., 2013; Grynol, 2015; Gao et al., 2015; Esmaeilian, Behdad and Wang, 2016).*

3DP is penetrating orthopaedics along with computer-guided and robotic-assisted surgery and is considered a game changer that could expand the horizons in the industry, driving it to a technologically higher level, enabling novel designs to be materialized *(Snyder, Cotteleer and Kotek, 2014; Shaffer et al., 2015).*

1.4 Point-of-Care Units and 3D Technologies

The previously listed revolutionary enabling technological tools that aid in:

1. Visualizing, simulating, and training on multifarious simple-to-complex cases, and
2. Designing and fabricating bespoke parts for pre-, intra- and post-clinical and surgical operations,

are becoming more and more reliable and higher in quality. But to dramatically boost their adoption and integrate them into the clinical and surgical workflow, they have to come at affordable costs. As these emblematic technologies are accelerating and maturing, the healthcare system will be transformed by implementing their routine use for patient-specific treatments, thus delivering better health to each individual and society.

That is the reason why increased awareness by orthopaedic surgeons is needed to explore and exploit the full potential of 3D digital design and 3DP techniques that introduce entirely new abilities

for manufacturing and delivering medical devices at the point-of-use, greater customization, innovation in design, and cost-effective quality solutions *(Shamsi et al., 2017)*. Thus, the way for the wide settlement of the so-called Point-of-Care (PoC) 3D units/labs is paved, as long as hindering challenges are lifted and proper Quality Management Systems (QMS) are introduced. PoC design and/or manufacturing refers to in-healthcare facility units that deal with on-site or near-site development of virtual or tangible products to assist orthopaedic operations.

3DP proved to have the suitable characteristics and potential to enable decentralized manufacturing at the point of interest. Technical, non-technical, and business-model-related challenges are causing a hysteresis for the wide diffusion and adoption of 3DP in medicine and orthopaedics. Fortunately, there are actions toward setting suitable roadmaps, solutions, and regulations to overcome these challenges *(Tavassoli., 2018; 2019).* In the quest to establish such PoC 3D Units in an orthopaedic setting, the frontiers involved are the following *(ASME, 2020)*:

1. Regulatory compliance[33], harmonized standards, and QMS[34] used to be issues but now are being addressed.
2. Available workforce, skills, knowledge, and training.
3. Available materials for 3DP and their biocompatibility.
4. Cost, speed, accuracy, repeatability, process validation, and verification for 3DP.
5. Misinformation and hype.
6. Integration with other technologies.
7. Intellectual property issues[35].
8. Digital security.

The COVID-19 pandemic caused by the SARS-CoV-2 virus revealed the weaknesses of modern healthcare systems as their capacity, supply, and workforce were challenged. It is known that necessity drives invention and innovation, hence, thanks to 3DP for distributed[36] and localized manufacturing, personal protective equipment, and other critical parts were produced at units in or near the PoC during the crisis *(Vakharia et al., 2021; Tareq et al., 2021; Sandhu et al., 2022)*. Hence, despite some safety concerns and challenges *(Singh, Venkatesh, and Deoghare, 2021)* units/labs

[33] In the EU, the Medical Devices Regulation (MDR) 2017/745 applies *(Official Journal of the EU, 2017)*. In the US, the FDA exempts custom-made orthopaedic devices from standard regulations *(FDA, 2014)*, has issued a discussion paper on 3D printing of medical devices at the point of care *(FDA, 2021)*, and guidance on technical considerations for 3DP medical devices *(FDA, 2017)*. Other topics on 3DP of medical devices and 3DP at the PoC are available at http://www.fda.gov/3DPrinting.

[34] The ASTM F42 and ISO's 261 committees are engaged with issuing 3DP standards on generic and medical applications of 3DP.

[35] The EU Commission carried out a study on the intellectual property implications of the development of industrial 3DP *(Mendis et al., 2020)*.

[36] Distributed manufacturing is a form of local decentralized model using a network of geographically dispersed facilities that are coordinated using information technology.

equipped with 3D design software and 3D printers, revealed their potential to rapidly adapt and deliver custom products undisturbed.

Powered by digital technologies that run on desktop and mobile platforms, PoC 3D Units can facilitate efficient collaboration, remote communication, and data sharing between patients-clinicians-engineers performance monitoring. These characteristics make PoC 3D digital design and 3DP ideal for aiding orthopaedic surgeons in therapeutic practices pre-operatively (prognosis, diagnosis), intra-operatively, and post-operative follow-up.

It is worth mentioning that it is not exclusively implied that a PoC 3D Unit both designs and manufactures tailored products; it could be either design-only or manufacture/3DP-only by assigning the design or manufacturing to contractors.

The number of healthcare centers utilizing the well-known FDA-approved image data processing, 3D planning, and design software Mimics Innovation Suite[37] (Materialise NV, Leuven, Belgium) *(Figure 20)*, reflects the global trend toward PoC 3D Units.

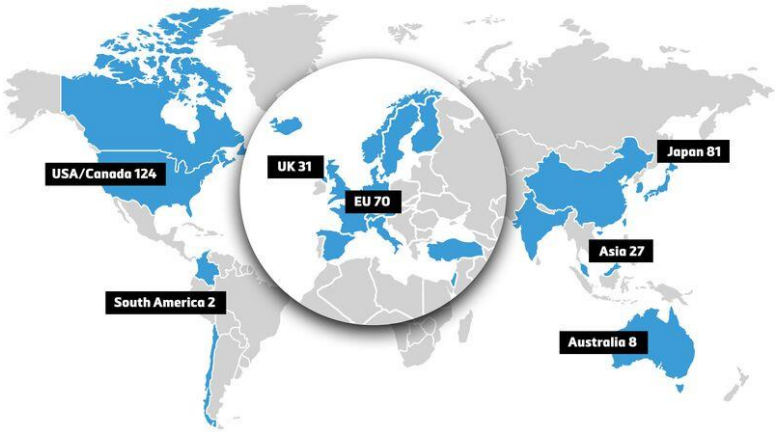

Figure 20: In-hospital 3D labs using Materialise software as of December 2020. Source: Materialise

Healthcare was traditionally a non-engineering design and non-manufacturing sector as neither design, nor manufacturing has been taking place in situ, but the fact that 3D design and manufacturing technologies are now being adopted from PoC 3D Units, are transforming HCFs into decentralized design and/or manufacturing sites. Fortunately, pitfalls related to such PoC 3D design and manufacturing are known to engineers and professionals working at industrial labs which have been the home to such technologies.

In a PoC 3D Unit equipped with software and hardware that personnel have the necessary knowledge and expertise to operate and use, innovative products can be fabricated as long as safety and effectiveness are guaranteed using proper quality control to ensure that product specifications are met with minimized patient risk *(FDA, 2021)*.

[37] Mimics Innovation Suite is an FDA-approved software used for medical image data processing, 3D analysis, operation planning and simulation, custom product design, finite element meshing, and 3D printing process planning. See https://www.materialise.com/en/medical/mimics-innovation-suite.

Early studies dealt with implantable patient-specific 3DPed products under technical, medical, and organizational perspectives, referring to the associated logistical, ethical, and legal challenges, and stressed that valid technical files with all necessary documents (technical and design considerations, risk analysis, manufacturing process, and labeling) are essential to ensure safety and legal validity of the patient-centric approach *(Willemsen et al., 2019).*

Researchers identified the feasibility of PoC 3DP in a hospital setting *(Calvo-Haro et al., 2021a; 2021b; Keller et al., 2021a; 2021b).* Most studies are focused on product design, manufacture, sterilization, and application, but few on the specifications and requirements of decentralized facilities for efficient and sustainable customized fabrication and biofabrication[38] *(Sanicola et al., 2020).* However, apart from the necessary inter-epistemic and multi-disciplinary synergy formation, the current main issues for implementing PoC 3D Units are economic and regulatory *(Serrano et al., 2020).* Studies show that individualized orthopaedic parts could be achieved within the acceptable time frame, provided that suitable equipment and infrastructure exist *(Teo et al., 2021).* As design and manufacturing techniques are streamlined in tandem with AI for automating processes, the range of orthopaedic applications will widen and ultimately the reliance on large centralized manufacturing plants and maintenance of expensive supply networks will be reduced.

Being able for in situ resource utilization for 3D design and/or manufacturing within or near the HCF for developing custom instrumentation and parts to aid in treating simple to extremely complex musculoskeletal anomalies is of high importance for the orthopaedic surgeon and the patient.

To realize how groundbreaking a PoC 3D Unit could be, one can imagine how such facilitates treating patients in remote and difficult-to-reach locations; instead of waiting for the delivery of custom or standard parts from centralized manufacturers using the traditional supply network, the part design and/or manufacturing could take place decentralized near or within the health center, close to the patient site. Thinking beyond Earth is even more paradigmatic as surgical or non-surgical operations in extraterrestrial missions are indeed very challenging due to minimum resources, nevertheless, individualized health care can be deployed in space via on-board biomaterial fabricators (3D (bio)printers) for materializing on-the-go patient-specific or standard instrumentation and other critical parts *(Rajput, 2021; Navarro et al., 2021).*

To develop custom-made orthopaedic devices and translate their development within the HCF, it is essential to overcome regulatory, intellectual property, ethical, technical, and economic challenges

[38] To restore tissue form and function, alternatively to bone grafting and permanent implants, biofabrication combines the body's regenerative abilities with bioactive factors and biodegradable biomaterials formed into complex shapes using technologies such as 3D bioprinting.

that are related to unique patient-specific medical devices, whereas education on new professionals should follow these trends.

US, EU, and Australian regulations and international standards to which medical devices must conform and adhere before their entrance to the market are summarized in *Table 1*.

Table 1: Regulations and standards on medical devices

Jurisdiction		Regulation
US	FD&C Act	Federal Food Drug and Cosmetics Act (FD&C Act) (Title 21 Chapter 9 of the United States Code). Emergency custom-made orthopaedic devices are exempted from standard regulations *(FDA, 2014).* Discussion papers on 3DP (e.g.*"3D Printing Medical Devices at the Point of Care" (FDA, 2021))* are available at http://www.fda.gov/3DPrinting.
EU	MDR	Regulation (EU) 2017/745 of the European Parliament and Council on medical devices. Emergency medical devices fall under Article 5.5 and custom-made devices under Annex XIII.
	IVD Regulation	Regulation (EU) 2017/746 of the European Parliament and Council on in vitro diagnostic medical devices.
	Cell and Tissue Directive	Directive 2004/23/EC of the European Parliament and Council on setting standards of quality and safety for the donation, procurement, testing, processing, preservation, storage, and distribution of human tissues and cells.
	ATMP Regulation	Regulation (EC) No 1394/2007 of the European Parliament and Council on advanced therapy medicinal products.
	Medicinal Products for Human Use Directive	Directive 2001/83/EC of the European Parliament and Council on the Community code relating to medicinal products for human use.
	EMA Regulation	Regulation (EC) No 726/2004 of the European Parliament and Council laying down on authorization and supervision of medicinal products for human and veterinary use.
Australia	The Act 1989	The Therapeutic Goods Act 1989 (Cth)
	Therapeutic Goods Regulation 1990	Therapeutic Goods Regulations 1990 (Cth)
	Medical Device Regulations 2002	Therapeutic Goods (Medical Devices) Regulation 2002 (Cth)
Organization		**Standards**
ISO		ISO's 11.040.40 standards catalogue is available at https://www.iso.org/ics/11.040.40/x/.
ASTM		ASTM's standards under Jurisdiction F04 are available at https://www.astm.org/get-involved/technical-committees/committee-f04/subcommittee-f04.
FDA		FDA's guidance documents available at https://www.fda.gov/regulatory-information/search-fda-guidance-documents, and recognized consensus standards to which FDA accepts a declaration of conformity (see https://www.accessdata.fda.gov/scripts/cdrh/cfdocs/cfStandards/search.cfm).

However, custom-made orthopaedic devices are most of the times of emergency concern and should be manufactured and delivered fast. As novel design and manufacturing technologies such as 3DP enable individualized products to be fabricated easily, rapidly, and economically compared to traditional methods, there was pressure towards jurisdictions for regulatory exemption of custom-made devices from exhaustive assessment and establish associated guidelines and standards.

The existing regulations and standards oversee the way medical devices are 3D designed and manufactured/3DPed. Such engineering methodologies with industrial roots should be effectively

framed around the healthcare system. Regulations on custom medical device development are uncertain but not unregulated as different jurisdictions around the world frame such exemptions differently and provide alternative clearance pathways, however, more adaptive frameworks about decentralized design and manufacture are needed to boost the adoption of PoC 3D Units from more health centers *(Horst and McDonald, 2020)*.

Harnessing 3DP for making unique composition, structure, and customizability needs further guidance to establish quality control measures for each device manufactured. Although regulatory hurdles can be navigated *(Morrison et al., 2015)*, ultimately, the evolution and synthesis of regulation and technology will define the maturation of PoC 3D design and 3DP.

The operation of a PoC 3D Unit lies at the intersection of healthcare providers, regulatory groups, engineers, and manufacturers who contribute to a common goal of providing quality and safety to patients. Recognizing the elements of a QMS and placing it under documentation is important to assure quality and safety, implement strategies for addressing errors (identification and mitigation), and improve consistency. Otherwise, the uncontrolled rapid growth of 3D technologies and the increasing complexity might put patients at increased risk for potential errors, decreased quality of the final product, and sub-optimal solution performance.

The Personalized Medical Devices authoring group of the International Medical Device Regulators Forum (IMDRF) *(2020)* recommended harmonized approaches for the application of existing regulatory pathways to medical devices intended for a particular individual, to offer significant benefits to the manufacturer, user, patient, and regulatory authorities. Eliminating differences between jurisdictions reduces the cost of gaining regulatory compliance and allows patients and healthcare professionals earlier access to new treatments and technologies.

In the US, section 520(b) of the Food, Drug, and Cosmetic Act (FD&C Act) describes the exemption of custom-made devices from regulatory control under certain circumstances involving life-threatening conditions with no alternative treatments available by allowing authorized healthcare professionals to provide design input and take responsibility for the safety and performance of the customized medical devices *(FDA, 2014)*. Custom-made medical devices in the EU are regulated as per Annex XIII, whereas emergency devices are developed within the HCFs as per Article 5.5 of the Medical Devices Regulation (MDR) 2017/745 *(Official Journal of the EU, 2017)*.

Compared to the orthopaedic reconstruction products, although legislation and standardization exist at some level, more challenging in the clinical translation are the tissue-engineered medical products used for tissue regeneration, the ethical concerns of which are argued *(Sekar et al., 2021)*. Ethical evaluation and legal regulation of 3D bioprinted living constructs cannot be thoroughly evaluated by standard clinical trials and current regulations *(Kirillova et al., 2020)*.

2. About the Thesis

2.1 Theme, Approach and Structure

Although the profession of (bio)mechanical design and manufacturing engineering is fundamental for standard or customized orthopaedic product development, until now, it was extremely intricate for an orthopaedic surgeon to address and achieve routine collaboration with (bio)mechanical engineers. Even more unusual, was for one to encounter the physical presence of (bio)engineering-based Point-of-Care (PoC) 3D Units/Labs within a healthcare facility aiming at instantly servicing orthopaedic operations by custom design and/or manufacturing.

Given the previous facts, the theme revolves around the emerged and emerging technological software and hardware toolsets for anatomical imaging, digital design, Virtual/Augmented/Mixed Reality (VR/AR/MR (xR)), and 3D Printing (3DP). More specifically, the scope is to assess the potential, performance, readiness, and viability of in situ or close-to-the-PoC utilization of these technologies to assist orthopaedic surgeons in rehabilitating musculoskeletal anomalies by realizing individualized solutions, together with the (bio)mechanical engineers, rapidly and at the lowest cost. Surgical operations can be simplified by mitigating as much complexity possible from the operating room and transferring that at the planning phase by preparing ((bio)mechanical engineering design and manufacturing) suitable products for each individual patient at the right time, before the operation, as per the orthopaedic surgeon's guidelines.

Establishing an in-hospital 3D Unit to support the distributed and localized manufacturing models for in situ production, that operates efficiently and effectively under a suitable framework and studying what hinders its feasibility is considered intriguing and challenging from both engineering and medical/clinical perspectives, and can lead to highly sought practical skills and knowhow.

The hypothesis that inter-epistemic workflows where such technologies are combined and inserted could be disruptive for individualized orthopaedics (especially if routinely applied at or near the PoC) will be investigated, and the qualitative and quantitative results will be fully explored. The roles of (bio)mechanical engineers in a PoC 3D Unit and how they could contribute to orthopaedic operations, the causes of hysteresis for adopting (bio)mechanical engineering design and manufacturing at the PoC, as well as the topics shown in *Figure 21* will be addressed.

Based on this formulated hypothesis, the strategy (goals) and tactic (objectives) are organized. The four goals set are epigrammatically:

1. Accent the inter-epistemic synergy for individualized orthopaedic services and optimized product development at the PoC 3D Unit under a holistic view.
2. Construct a systematic patient-specific design and manufacture methodology, and end-to-end guidelines, highlighting the critical parameters and challenges of each step of the workflow.

3. Set and present the characteristics of a hypodigmatic small 30 sqm pilot PoC 3D Unit in "Attikon" University General Hospital: organizational structure, framework for implementation, equipment, infrastructure and layout, and cost. Review PoC Unit's performance and sustainability under its potential for a decentralized manufacturing model, readiness for routine operation, challenges, and cost and time responsiveness.
4. Granted that bespoke digital, virtual, and physical solutions have been developed for some selected pragmatic pelvic and sacrum reconstruction case studies, novel, *"smart"* solutions and the need to shift from reconstructive to regenerative approaches will be discussed.

In the orthopaedic product market, many companies are currently offering custom solutions. Also, as will be critically presented, the published worldwide literature is highly active and reports a plethora of novel topics on the design, manufacture (3DP), and performance of patient-specific orthopaedic parts. On the other hand, the previous goals were set to cover the lack of literature to:

- Holistically deal with the implementation of a de novo inter-epistemic synergy at the PoC.
- Focus on the set-up requirements and assessment of a PoC 3D Unit per se *(see Figure 21)*.
- Methodically present a systematic end-to-end workflow for patient-tailored services and optimized product development and analyze each step applied whilst providing guidelines.

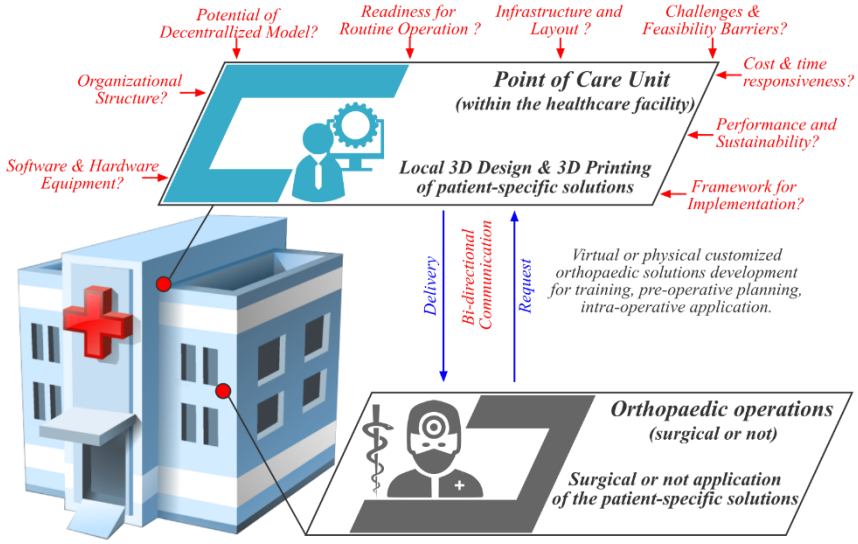

Figure 21: Questions to be addressed for the PoC 3D Unit

This Thesis will incorporate an appropriate scientific methodology and will seek to address and fill the knowledge gaps from an engineering point of view, exploring medical and biological, but focusing on mechanical and manufacturing aspects, to ultimately contribute to the research field of custom musculoskeletal treatment services delivery and products development.

Towards achieving the previous goals, six fundamental objectives had to be accomplished:

1. Review modern and 3DPable biomaterials used in individualized orthopaedic reconstruction.
2. Explore/exploit the potential of digital design, xR, 3DP, and 3D scanning in individualized orthopaedics.

3. Review requirements and characteristics of PoC 3D digital design, xR, 3DP, and 3D scanning.
4. Carry out scenarios with pragmatic cases (under hypotheses and assumptions and based on available budget and resources) by applying digital design, xR, 3DP, and 3D scanning technologies in situ, within the hospital environment. Select orthopaedic oncology and orthosis cases and treat them as currently ongoing pragmatic cases to be carried out by a pilot PoC 3D Unit set at the First Department of Orthopaedic Surgery, School of Medicine, NKUA.
5. Apply advanced design techniques and optimization algorithms for the custom solutions, inspired from and mimicking the cosmos of natural structures that are optimized for their assigned functions: biomimetic morphologies with heterogeneous architectures and topologically variable material density with gradient porous elements. Products incorporating biologically-inspired spongy endo- and exo-structures could reach superior mechanical and biological performance and minimize complications.
6. Evaluate and compare these technologies with traditional approaches based on mechanical and biological performance, and sustainability, and against technical, time, and economic criteria.

The required tools to deliver the results are 3D anatomical imaging devices (tomographers and scanners), xR devices, and 3D printers for parts materialization. Also, powerful enough computers capable of executing software for xR applications, processing the scanned image data, modeling (Computer-Aided Design (CAD)), simulating (Computer-Aided Engineering (CAE) with Finite Element Analysis (FEA)), optimizing the solutions digitally, and planning and simulating the manufacturing process (3DP) (Computer Aided Manufacturing (CAM)).

The hypothesis, scope, objectives, goals, and tools are summarized graphically in *Figure 22*.

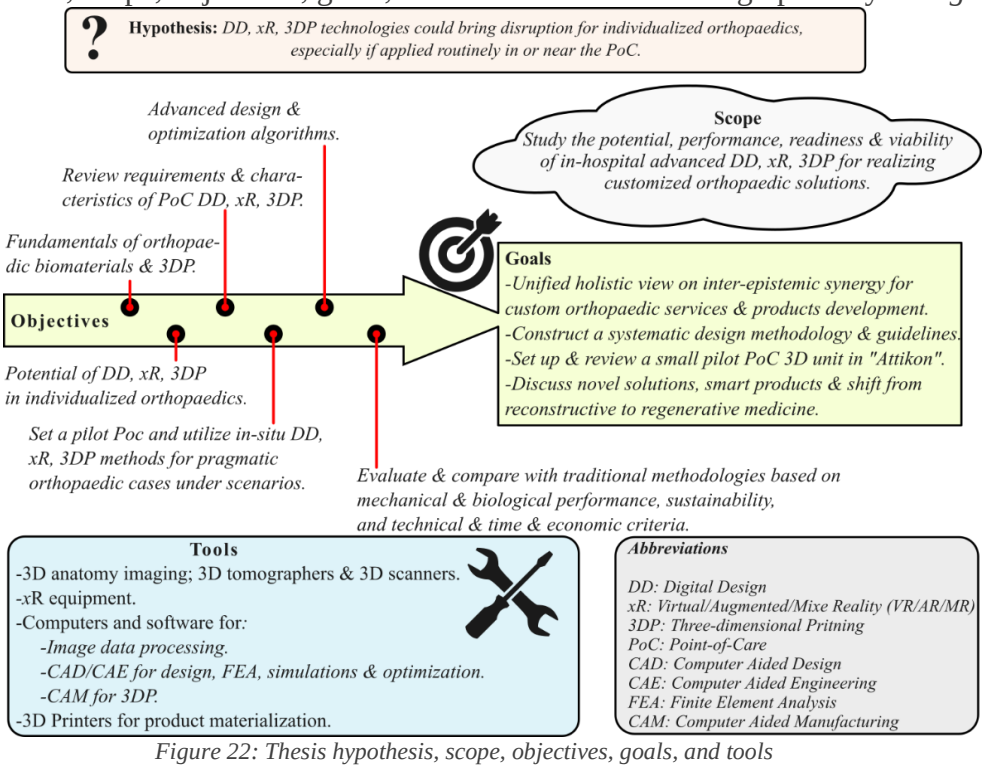

Figure 22: Thesis hypothesis, scope, objectives, goals, and tools

To scientifically research the validity of the stated hypothesis, approach the accomplishment of the set objectives, and achieve the goals, the Thesis was organized and structured as follows:

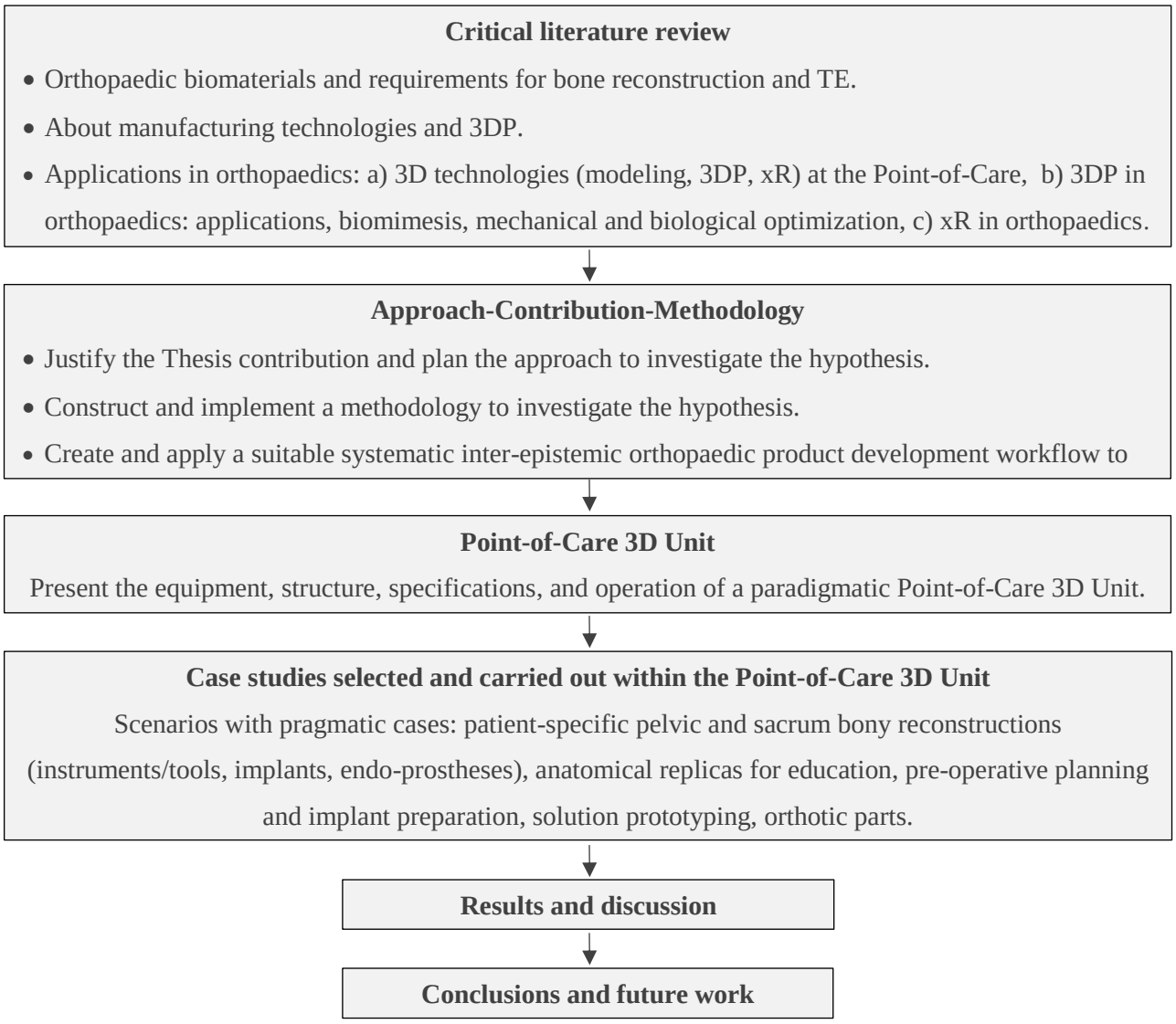

3. Critical Literature Review

3.1 Biomaterials: Osseointegration and Infection

All materials can be characterized by four independent criteria that are graphically placed at the corners of the so-called materials science tetrahedron *(Callister and Rethwisch, 2018) (Figure 23)*:

1. **Structure:** the fine micro and meso endo-structure of the material revealed by microscopy and the gross macro structure visible by the naked eye or low magnification levels.
2. **Properties:** the physical, chemical, mechanical, and other properties of the material.
3. **Performance:** how well the material performs in a particular application, e.g. technically, economically, biologically.
4. **Processing:** how well the material can be manufactured (formed into shapes and given desirable properties) and post-processed (surface finishing, sterilization, etc.).

For implantable orthopaedic products, the target is to select biomaterials able to achieve high performance, are easily processable, have maximum biocompatibility, and adequate strength for load-bearing applications.

The orthopaedic industry has been drawing biomaterials from the engineering materials palette that is continuously advancing over epochs (*Figure 24*). Thus, orthopaedic devices were always made of biomaterials that somewhat followed these engineering trends.

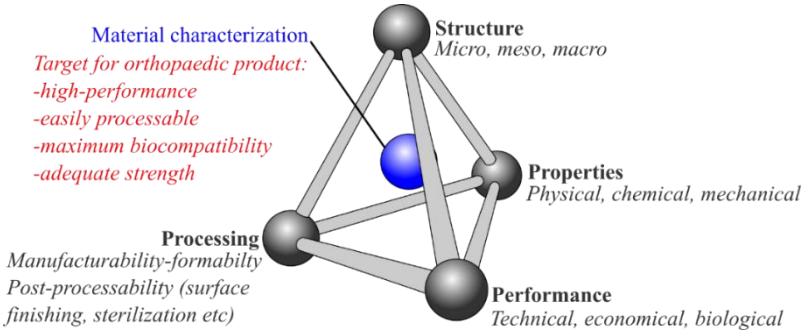

Figure 23: (Bio)materials science tetrahedron

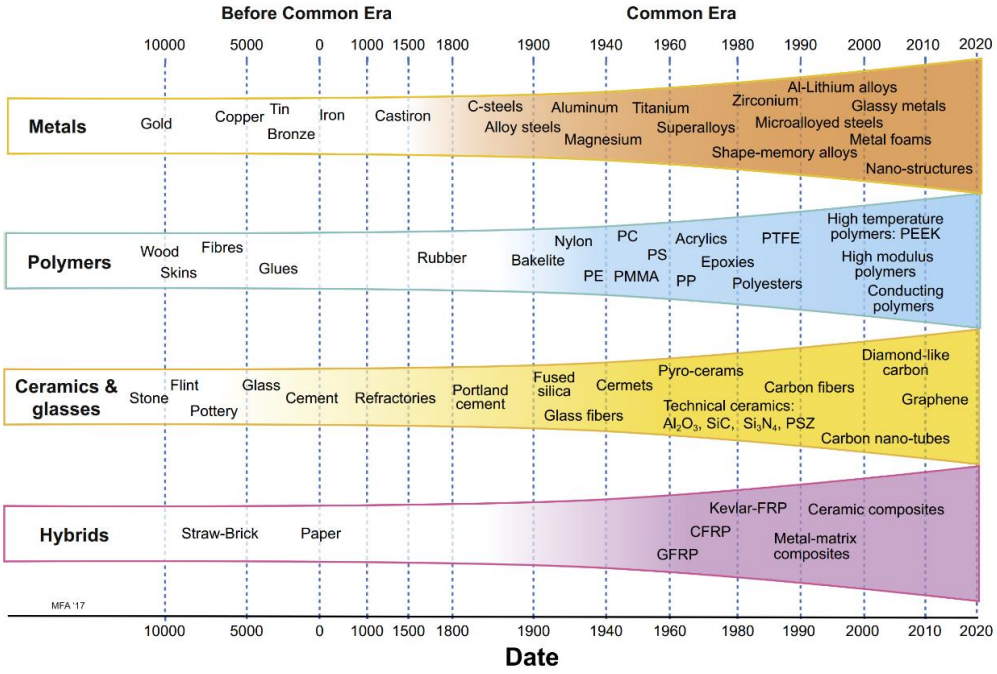

Figure 24: Development of engineering materials over time. Source: (Ashby, Shercliff and Cebon, 2019)

Focusing on orthopaedic implants, these must be made of biomaterials with suitable properties and anatomically matching form for a comfortable, safe, secure fit whilst being smoothly integrated into the host tissue *(Bose and Bandyopadhyay, 2016)*. Depending on the case, such devices are either temporarily or permanently placed and can be either movable (joints) or fixed *(Pal, 2014)*.

Biomaterials are *"natural or synthetic substances, capable of being tolerated permanently or temporarily by the human body" (Poitout, 2016)*. Biomaterials are classified into metals, ceramics, polymers, composites, natural materials, and grafts[39]. Biomaterials used in medicine have been

[39] Can be autograft (tissue transferred from one site of the body to another), allograft (transplantation between individuals of the same species), xenografts (transplantation between different species) *(Dorland's Illustrated Medical Dictionary)*.

extensively discussed by Ratner et al. *(2013)*. The basic characteristics and applications of biomaterial classes used to treat musculoskeletal disorders are summarized in *Table 2*.

Table 2: Characteristics of biomaterials used in orthopaedics

Material Class	Advantages	Disadvantages	Applications
Metals, e.g.: Stainless Steel 316L. Ti and alloys (Ti6Al4V). Co-Cr and Mo alloys. Ta, NiTi, and shape memory alloys.	Good ductility. High mechanical strength. Excellent fatigue resistance. Excellent fracture toughness. Good corrosion resistance. High availability. Relatively easy to fabricate. Easy to sterilize and autoclave.	Bioinert. High modulus of elasticity. Poor biocompatibility.	Load-bearing implants and bone replacement endo-prostheses. Instrumentation. Molds. Spinal correctors, plates, nails, screws, staples, wires.
Ceramics, e.g.: Ca phosphates (e.g. HA, TCP) Bioglass. Al oxides. Ti oxides. Zr, Ca aluminates.	Good biocompatibility. Composition can be tailored for bioactivity and bioresorption. Excellent corrosion resistance. Excellent wear and abrasion resistance. High compressive strength. Bone-like density and modulus. Easy to sterilize and autoclave.	Brittle. Low fatigue resistance. Low fracture toughness. Anisotropic mechanical properties. Difficult to form.	Metal implant coatings. Bone cements and fillers. Acetabular cup liners and femoral heads for arthroplasties. TE scaffolds for regeneration.
Polymers, e.g.: PMMA, PTFE, PEEK, PDMS, PLA**,** PCL**,** PDS**,** PET(G), PEG, PP**,** PS**,** PC, PE, P(L)GA, PU, PA(NYLON), PAEK, PEGDA, PEKK, PEI, ASA, HIPS, TPE.	Easy to manufacture and given a variety of forms. Available in various forms and states. Low density. Rate of bioresorption can be tailored.	Low mechanical strength. Uncontrolled degradation is of concern. Difficult to sterilize.	Sutures and bone cements. Artificial tendons. Bone substituting spacers. Liners in arthroplasties. Drug delivery carriers. Metal implant coatings. Bioabsorbable devices for bone regeneration. Instrumentation. Molds. Anatomical replicas. TE scaffolds for regeneration.
Natural, e.g.: Collagen, Hyaluronic acid, Human tissue-grafts, Living cells.	Available in human body and other biological systems. Extremely biocompatible.	Rejection by host body. Difficult to process and form.	Increase or substitute hard and soft tissue.

Choosing the right biomaterial requires identification of the application, the function of the product, and understanding of the benefits and drawbacks of each material as their specific characteristics and properties vary. For example, the following metals *(Kadakia et al., 2020a):*

- Stainless steel 316L: low cost, readily available with acceptable biocompatibility but with high modulus of elasticity (can lead to stress shielding of surrounding bone) and nickel content (possibility to induce allergic reactions), thus, it is mostly used temporarily for plates and screws.
- Ti alloys: modulus of elasticity similar to cortical bone (lower if porous) with excellent biocompatibility and high corrosion resistance. If porous, facilitates bony biological fixation, so it

is used for permanent implants to be integrated. However, if not coated (e.g. with TiN) and treated appropriately, its low wear resistance makes it poor for load-bearing articulating surfaces.

- Co-Cr alloys: high strength, excellent wear properties, high corrosion resistance, and low coefficient of friction. It can be spray coated with Ti to gain a porous surface. It finds applications in load-bearing articulating components.

Kuncická, Kokich and Lowe *(2017)* gave an extensive review of characteristics, processing, surface treatments, and new trends in metals and metal alloys used in joint replacement, whereas *Figure 25* presents the typical biomaterials that are most frequently used for making endo-prostheses to substitute bone tissue in different anatomical areas of the musculoskeletal system.

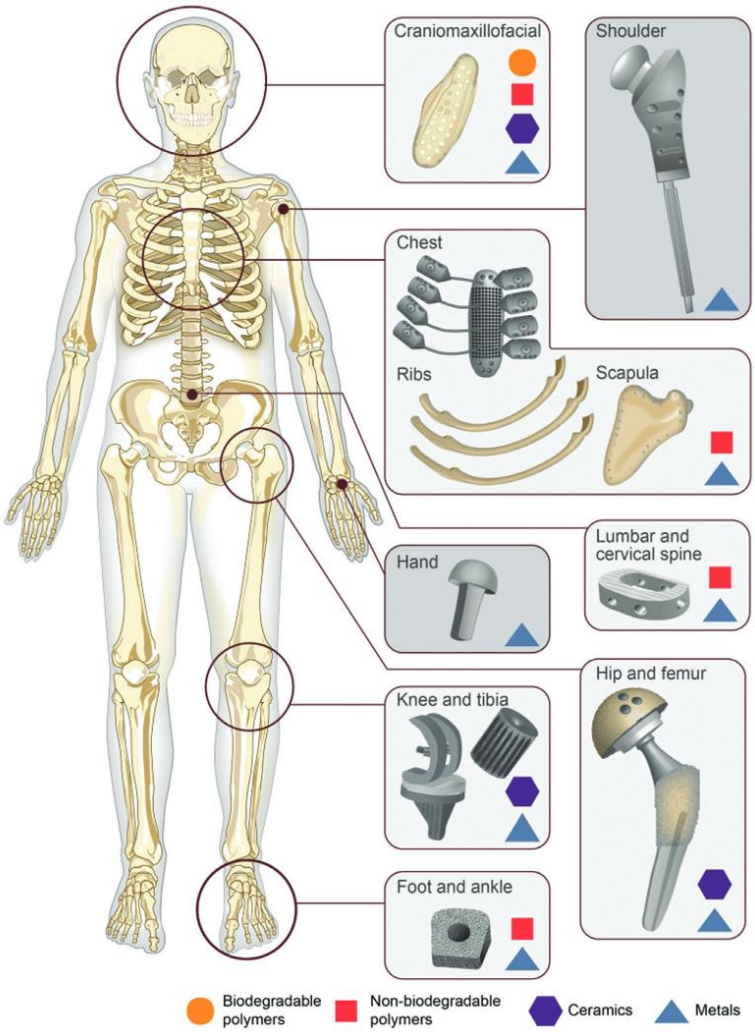

Figure 25: Typical biomaterials used in endo-prostheses. Source: (Garot, Bettega and Picart, 2021)

The so-called Ashby charts summarize graphically various properties of materials into charts. For example, *Appendix F* shows the Modulus of Elasticity versus Density and the Strength versus Density for technical and natural materials groups, including osseous tissue.

Navarro et al. *(2008)* presented a review of the evolution and generations of biomaterials used in orthopaedics: First generation (bioinert materials), 2nd generation (bioactive and biodegradable materials), 3rd generation (materials designed to stimulate specific responses at the molecular level).

Bone fixation or bone substitution implants (endo-prostheses) used in orthopaedic cases are categorized as per their functionality *(Özel et al., 2016):*

1. **Bioinert:** provide structural support with minimal response in the host tissue. They are neither rejected, nor recognized.
2. **Bioactive:** intense interfacial biological phenomena occur. Lifetime and effectiveness of artificial endo-prostheses can be increased by enabling some level of bioactivity (bone ingrowth through functionalized surface by coatings and/or textured porous surface).
3. **Biodegradable:** capable of degrading and absorbed in the host site whilst guiding the host tissue to grow through it and heal itself. Thus, overcoming issues related to permanent implants.
4. **Biomimetic:** mimic nature's hierarchical structures and mechanisms to actively repair tissue.

The interfacial interactions of biotolerant, bioinert, bioactive, and biodegradable biomaterials with the host bone tissue are schematically presented and described in *Figure 26*.

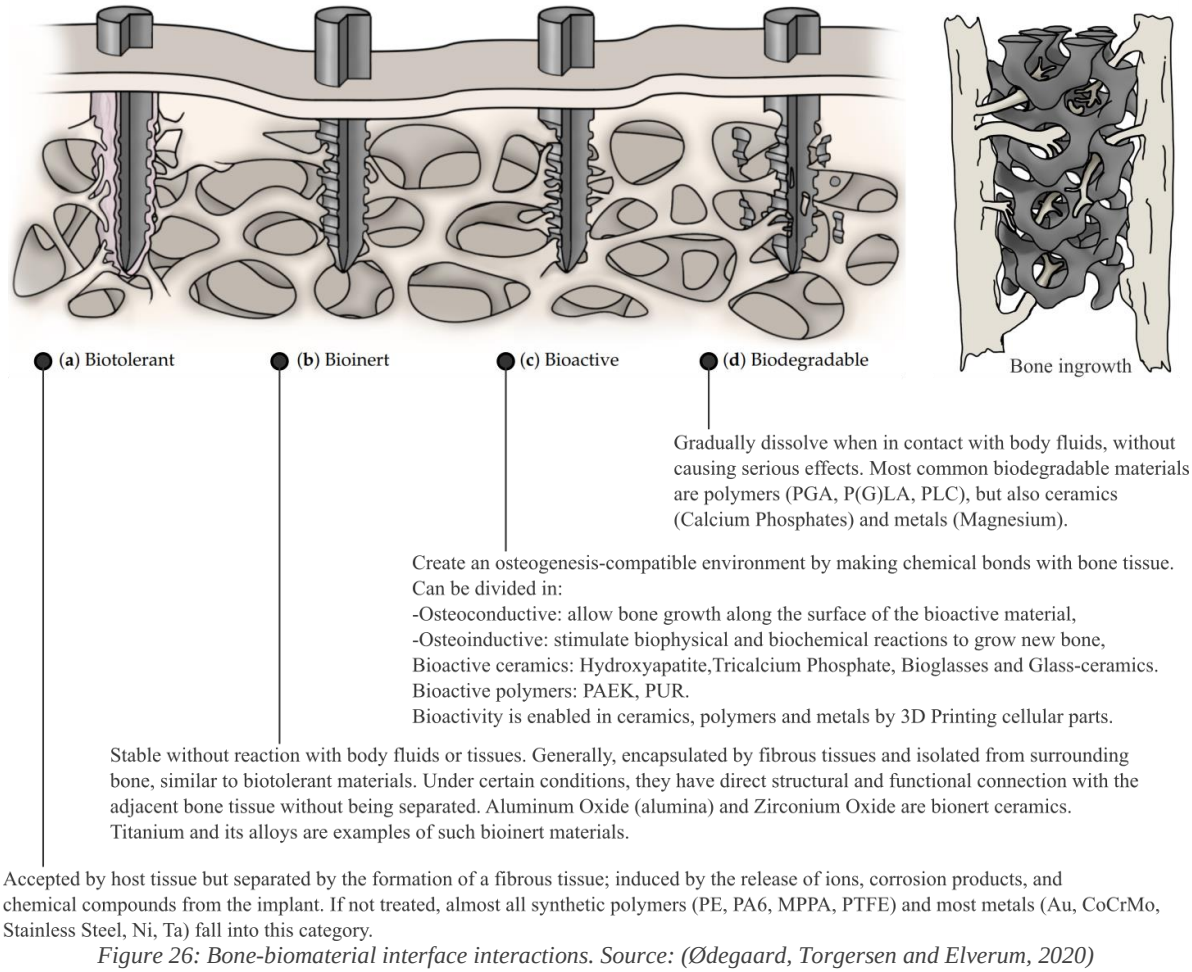

Figure 26: Bone-biomaterial interface interactions. Source: (Ødegaard, Torgersen and Elverum, 2020)

For optimal performance, risk minimization, and elimination of future surgical interventions, implants should conform to certain requirements *(Figure 27) (Ratner et al., 2013; Poitout, 2016; Özel et al., 2016; Li and Mai, 2017)*:

1. Anatomical matching shape and suitable surface characteristics based on the patient's anatomy, status, and condition of the host tissue that serves as the implant bed. Optimized exo-structures

can introduce porosity and offer high wettability for nutrient transports, and optimized endo-structures can be implemented to approach bone's mechanical performance.

2. Adequately bone adherence. Fixation points are selected as per bone quality and are usually accomplished using bone cement, screws, press-fitting, or scaffold surface structures (treatments, coatings, 3DP) within which bone can grow onto and into.
3. Resist sterilization and withstand the corrosive environment within the body, e.g. sodium chloride and pH variations lead to plastic breakdown and metal corrosion *(Hansen, 2008)*
4. Biological properties for osseointegration, anti-bacterial properties, and inflammation control.
5. Durable and wear-resistant with high fatigue strength whilst possessing bone-like mechanical properties. In case of large differences in moduli of elasticity compared to host tissue, the lack of mechanical stimuli can lead to bone resorption as a result of its remodeling process *(Wolff, 1986)* and implant loosening (stress shielding phenomenon *(Ridzwan et al., 2007)*).
6. Made of biocompatible materials without showing toxicity and triggering immune reactions.

The above requirements are illustrated in *Figure 27* as attributes of the ideal orthopaedic implant.

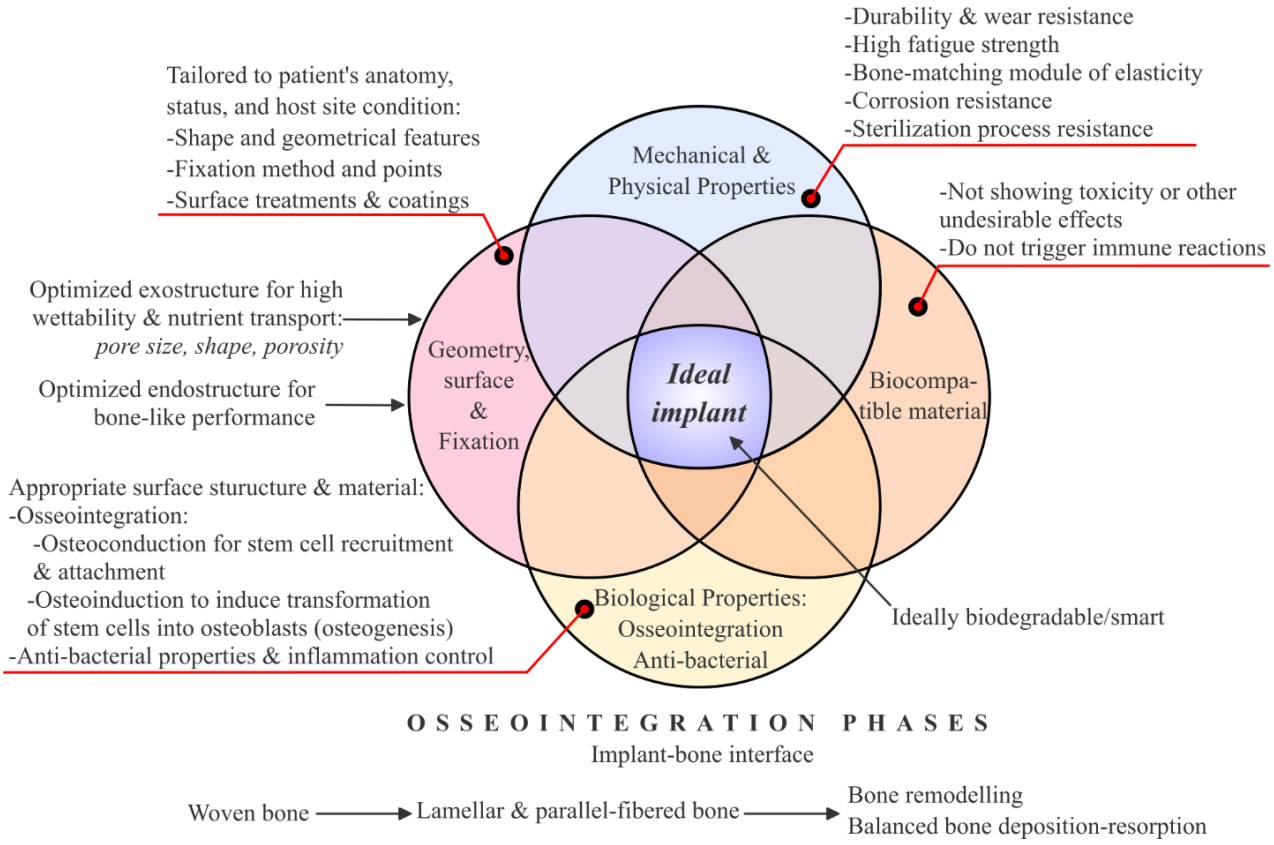

Figure 27: Attributes of the ideal orthopaedic implant

For example, *Figure 28* pictures the major design considerations and the required features of the hip-joint arthroplasty implants: femoral stem, acetabular shell, and liner.

Osteogenesis or ossification refers to the bone formation process and occurs:

1. In embryos and fetuses.
2. Until adult size is reached.

3. Throughout life during bone remodeling *(Figure 31).*
4. During the repair of small bone fractures.

Once bone fractures, granted immobilization, the fascinating biological process of bone healing commences (*Figure 29*). Four cell types are responsible for bone generation and maintenance *(Figure 30) (Tortora and Derrickson, 2020)*:

1. **Osteogenic:** originate from mesenchymal stem cells. Osteogenic or osteoprogenitor cells are the only bone cells capable of cell division and transformation into osteoblasts.
2. **Osteoblasts:** build the extracellular matrix of bone (deposition). Eventually, they become osteocytes and lining cells which might turn back into osteoblasts. Lining cells activate osteoclastic activity.
3. **Osteocytes:** mechano-sensors of bone to maintain normal bone tissue. Osteoblasts and osteoclasts are guided by them for the amount, time, and place of bone deposition or resorption.
4. **Osteoclasts:** originate from the fusion of many monocytes. They break down the extracellular matrix of bone (resorption) and help in the remodeling process.

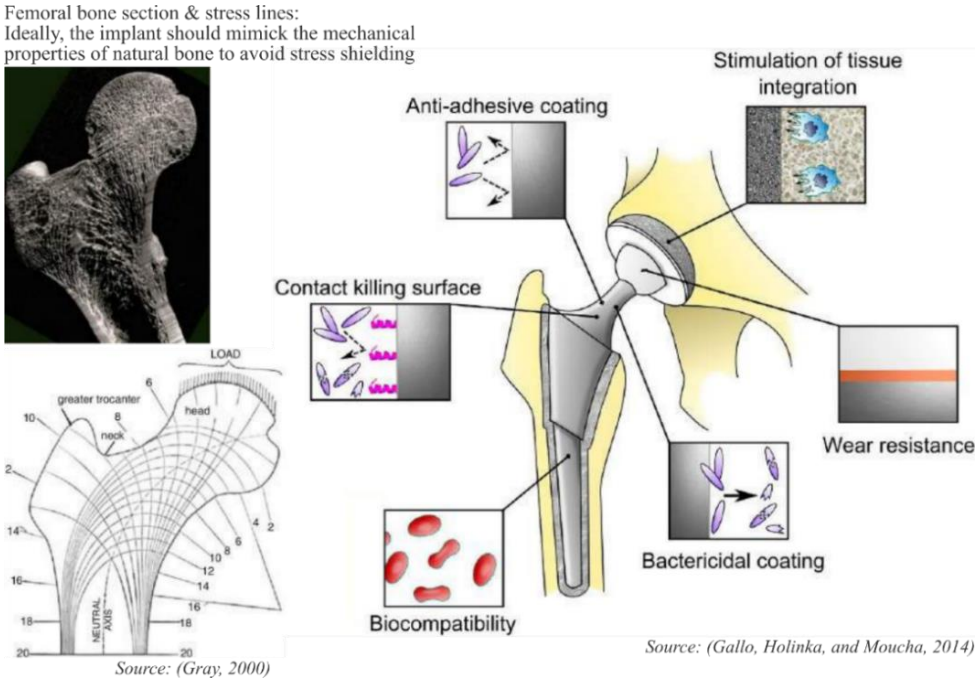

Figure 28: Hip arthroplasty implants design considerations

For small fractures, orthotic devices are used, whereas, in more critical situations, internal or external bone fixation practices are followed. In extreme conditions and difficult-to-treat oncological cases such as bony losses after tumor resections, self-healing is not possible and reconstruction procedures are applied. From head to toe, when and why to choose biological or artificial implant reconstruction of anatomical integrities depend on prognostic factors, technical considerations, short-to-long-term advantages and disadvantages, and other parameters: patient demographics, tumor properties, socioeconomic and psycho-socio-cultural factors, healthcare policies, capabilities of the medical institution, and surgeon's skills, knowledge, and experience *(Özger et al., 2022).*

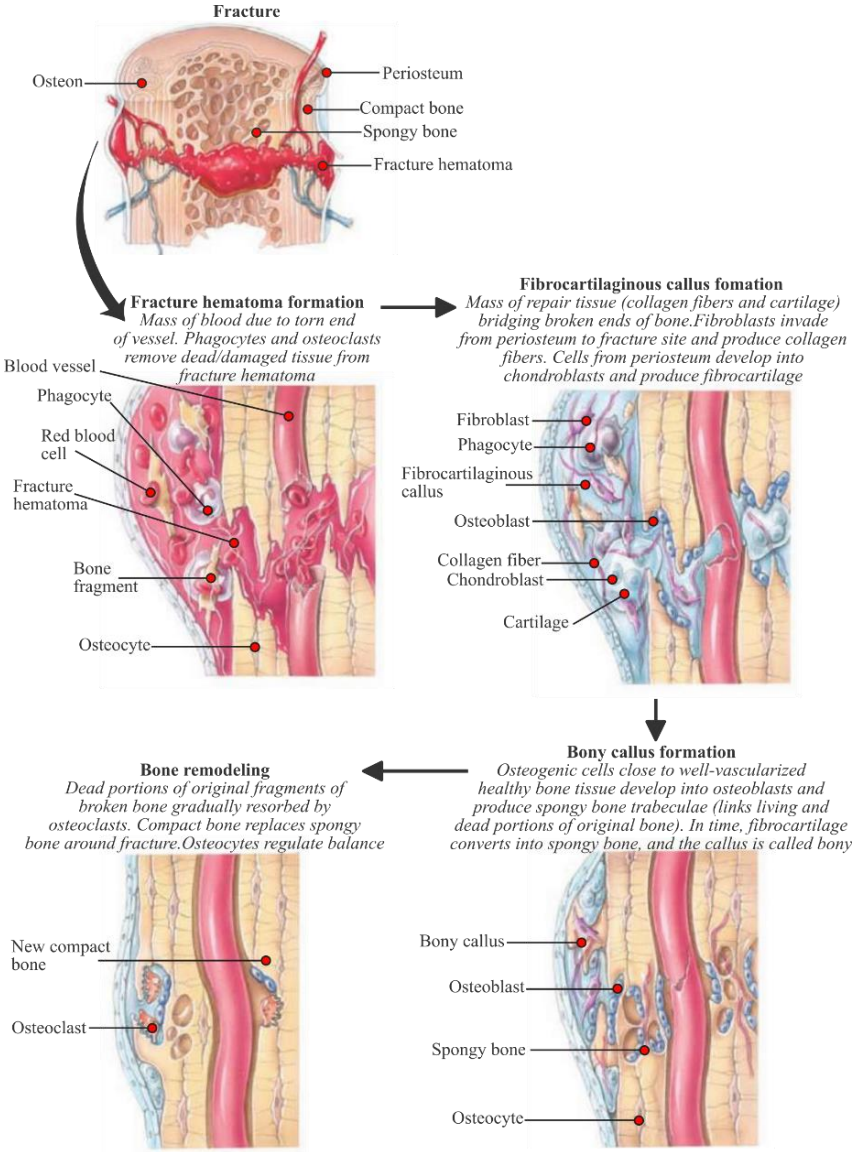

Figure 29: Stages of fracture healing. Source: (Tortora and Derrickson, 2020)

Osseous tissue can be substituted with *(Tunn, 2009; Ratner et al., 2013; Lewallen et al., 2015; Özger et al., 2022)*:

1. **Artificial endo-prostheses**: custom-made or readily available in standard or modular forms. Usually made of metals, are strong and reliable with low complication rates, and enable rapid return to full-weight bearing. However, long-term issues such as infection, disease, aseptic loosening, and mechanical failure should always be considered. Porous-coated or structurally porous endo-prostheses dramatically improve osseointegration. Expandable types also exist aiming at young patients whose tissue grows and remodels much faster.
2. **Biological grafts:** have offer biological reconstruction, restore bone stock, joint mechanics, and soft tissue attachments. These can be:

   a) Autografts: have excellent healing properties as they consist of native bone tissue moved from one site of the patient's body to another. Autografts are limited in availability and effective only for small losses. However, donor site morbidity (necrosis) and infections might occur.

b) Allografts: for big bone losses, fragments are taken from donors and post-processed before implantation. Compared to autografts, they have less mechanical integrity, are less osteoconductive, less osteoinductive, and not osteogenic because cells are usually removed. Allografts are selected as per the patient's needs and are available in various limited shapes and sizes. As non-native tissue, they might trigger immune rejection and transmit diseases.

3. **Graft substitutes:** allograft-based substitutes or artificially fabricated by TE techniques that are used to (re)generate tailored tissue. Such methods are still under development.

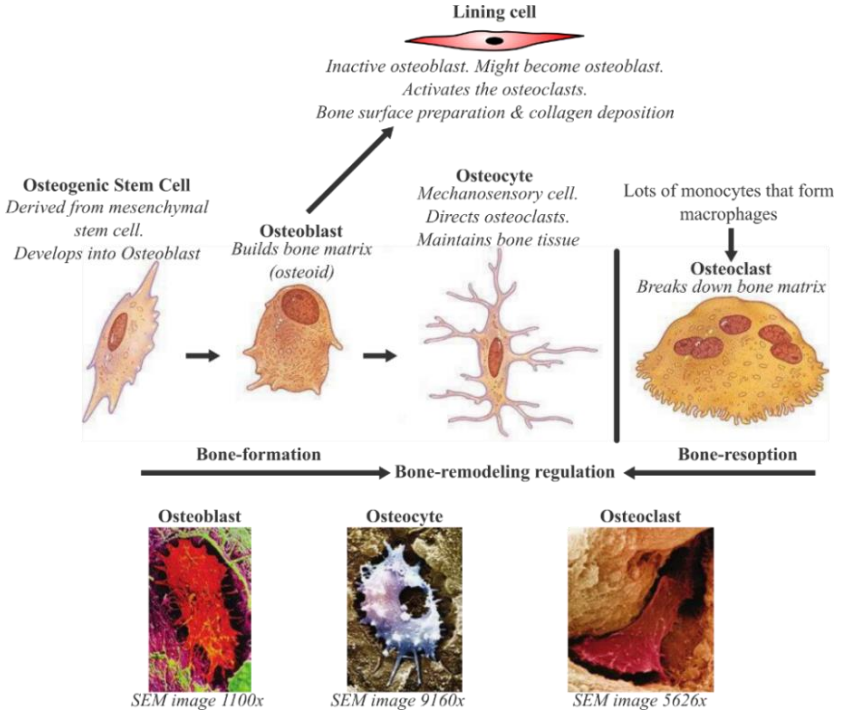

Figure 30: Types of bone cells

Artificial endo-prostheses are usually made of bioinert metals. However, recent advances in surface treatments, coating materials, and 3DP for making implants from hard to traditionally shape biocompatible materials with bone-inspiring spongy architecture and open-celled surfaces, are promising towards overcoming many associated issues and activating some level of bioactivity.

When special artificial endo-prostheses are used instead of grafts, biological reconstruction is not possible because biodegradable implants capable of load-bearing are not yet available in the market. In such cases, osseointegration is the goal: *"a direct structural and functional connection between ordered, living bone and the surface of a load carrying implant" (Brånemark, 1987)*. It characterizes a post-implantation condition where the implant is accepted by the body with the host osseous tissue grown into it through its specially designed scaffold structure. Osseointegration is achieved if the implant surface and the material per se are osteoconductive[40] and osteo-inductive[41] to stimulate cell

[40] Permit cell recruitment and attachment into the implant's structure *(Dorland's Illustrated Medical Dictionary)*, i.e. permit ingrowth.

[41] Process of inducing stem cells to differentiate into mature osseous tissue cells *(Dorland's Illustrated Medical Dictionary)*, i.e. stimulate growth of new bone.

activity (adhesion, proliferation, differentiation) and promote osteogenesis, and is a function of the material's biocompatibility, implant shape and surface characteristics, patient's age and status, host site condition, surgical technique, and timing/conditions of loading and mobility *(Li and Mai, 2017)*.

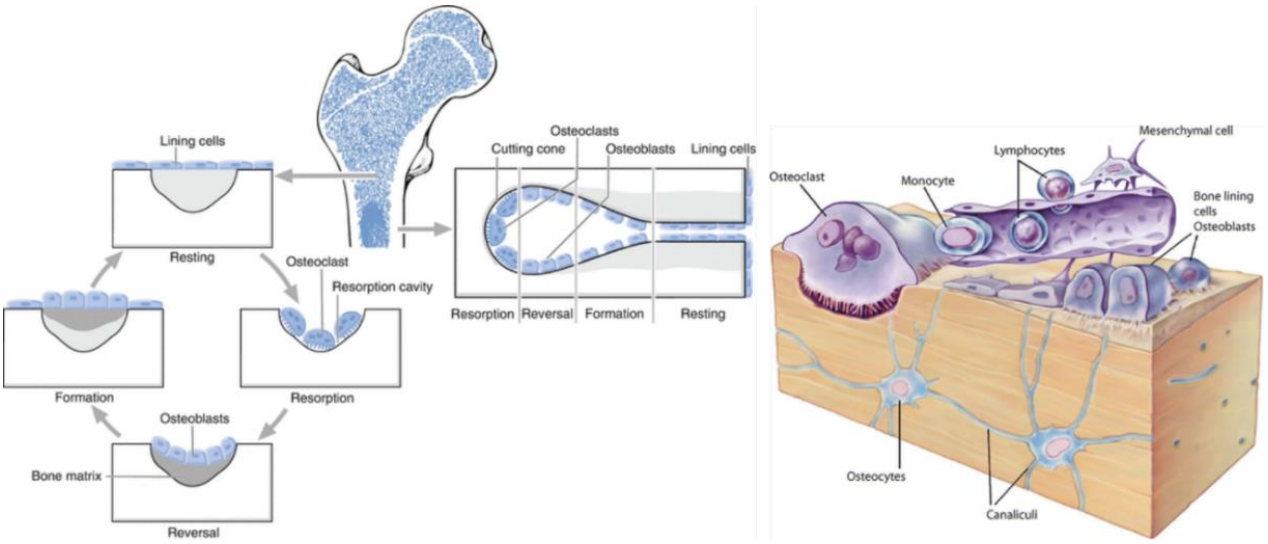

Figure 31: Bone remodeling phases and cell types. Source: (R. Bartl and C. Bartl, 2016)

An implant is considered osseointegrated when there is no progressive relative movement between the bone-implant with which it has direct contact. Mavrogenis et al. *(2009)* mentioned that *"osseointegration should be regarded not as an exclusive reaction to a specific implant material but as the expression on the endogenous basic regenerative potential of bone"* and stated that *"osseointegration is not the result of an advantageous biological tissue response but rather the lack of a negative tissue response"*.

Biologically driven design strategies, selection of suitable biocompatible materials, implant shape and geometrical features, and surface textures/coatings lead to controlled, guided, and rapid peri-implant bone healing.

T. and B. Albrektsson *(1987)* stated that implant integration or loss is dependent on the simultaneous control of several parameters and gave an excellent review of the concept, biomechanical and structural viewpoints, and experimental and clinical observations of osseointegration. Alvarez and Nakajima *(2009)* also reviewed clinical studies that verified osseointegrated porous metallic scaffolds.

Schenk and Buser *(1998)* have histologically researched the osseointegration of porous textured Ti implants and divided the process into three phases:

1. **Woven bone:** the implant's surface is penetrated by woven bone which emerges from the host bone that moves towards the implant (*distance osteogenesis)* and from direct deposition of new tissue (*contact osteogenesis).*
2. **Adaptation of bone mass to load:** the woven bone transforms into a well-defined lamellar and parallel-fibered pattern.

3. **Adaptation of bone structure to load:** remodeling occurs with balanced coordination of resorption (osteoclasts) and deposition (osteoblasts) activities coupled in space and time.

Granted porous architectures, post-implantationally, numerous phenomena occur at the bone-implant interface that might ultimately lead to the formation, penetration, and integration of a mineralized matrix *(Li and Mai, 2017)*. Greater and hydrophilic implant surfaces imply greater adsorption of proteins, tissue fluids, and adhesion of cells.

Interaction with the biological environment is allowed if bioactivity is enabled by surface-functionalization through coatings, impregnation, pollution, or physical surface texturing *(Ehrenfest et al., 2009; Muthaiah et al., 2022)*. Pragmatically, a surface-textured or coated endo-prosthesis to obtain porosity for cement-less implantation has higher overall survival and survival to infection compared to their solid counterparts attached with cement *(Pala et al. 2013)*.

Interestingly, the same biomaterial can be designed and manufactured with interconnected pore features to be osseointegrated (e.g. use for bone replacement) or not (e.g. temporary osteosynthesis usage). 3DPed bone-interfacing implants with graded or constant porous surface topographies have been observed to promote bone ingrowth and reach high osseointegration levels *(Van der Stok et al., 2015; Sarker, Leary and Fox, 2020; Park et al., 2020; Li et al., 2020; Brink and Lamerigts, 2020; Ren et al., 2021; Brogini et al., 2021; Gao et al., 2021; Wang et al., 2021).*

The osteointegration capacity is governed by the osteoconductive nature of the materials per se, and by the physicochemical surface properties that trigger cell interactions; roughness, micro and nano-topography, porosity, surface energy, and biomaterial characteristics. With 3DP, a biomaterial can be formed with integrated interconnected pores so that its surface is functionalized for increased osteoconductivity and osteoinductivity to promote osteogenic differentiation of stem cells and bone formation onto and into the pores. Hence, there is no need to implement coating techniques (e.g. spraying) to deposit metal particles (e.g. cpTi, CoCrMo) to obtain porous surface layers.

A surface can be activated by morphological, physicochemical, biochemical, and biological modifications. *Figure 32* summarizes the techniques used to alter the material's surface characteristics: electrical discharge, porosity, filler release, wettability, (bio)chemistry, topography.

At long-term follow-up, monoblock porous-coated Ti and Ta acetabular cups have demonstrated excellent radiographic and clinical outcomes and survivorship *(De Martino et al., 2016; Gerscovich, Schwing and Unger, 2017; Yeroushalmi et al., 2021)*. But instead of coating the implants to gain porosity, with 3DP, porosity can be integrated precisely under control, by implementing the cellular scaffold structures as designed and desired. Two 3DPed products by powder-bed fusion technology are shown in *Figure 36:* a composite porous bone-like PE-Ti6Al4V sternum-ribcage endo-prosthesis (by Anatomics (Anatomics Pty Ltd, Melbourne, Australia)) *(Kamel et al., 2020)* and a Ti6Al4V

acetabular cup (Delta-TT by Lima Corporate (Limacorporate S.p.A, Udine, Italy)) along with a similar 12 mm diameter 6 mm height scaffold specimen featuring multiplanar hexagonal cells (640 μm pore size, 65% porosity) mimicking the trabecular bone are shown in. The specimen was seeded with human adipose tissue-derived stem cells (hASCs) and the microscopy images reveal a plentiful calcified extracellular matrix on the specimen's surface.

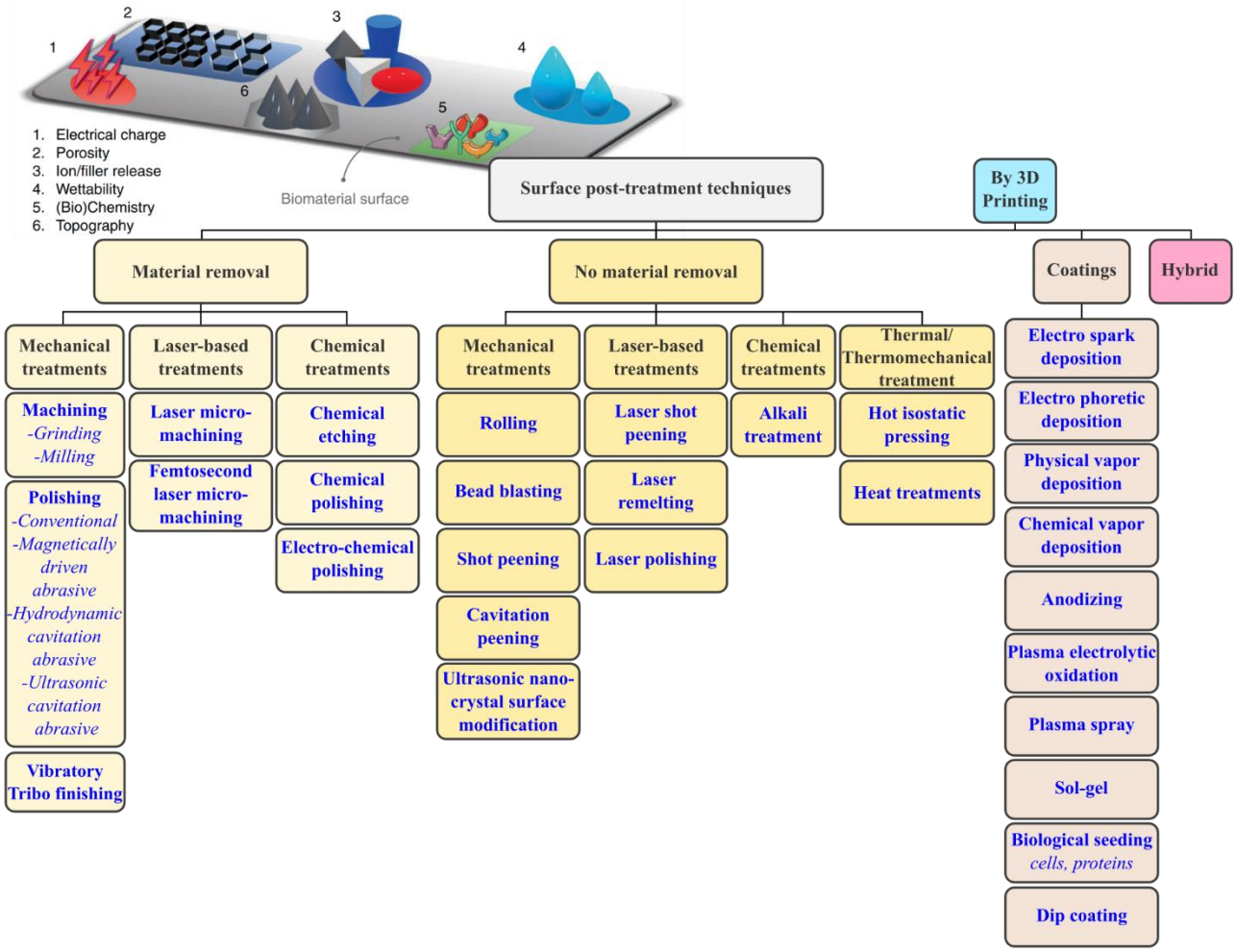

Figure 32: Surface and properties modification techniques. Source: (Kumbhar and Mulay, 2016; Liu et al., 2019; Florea et al. 2020; Maleki et al., 2021; Montoya et al., 2021; Ferraris and Spriano, 2021)

3DPed porous acetabular cups achieve better bone ingrowth and osseointegration, stable outcomes with high survival rates, great clinical improvements, and excellent initial biological fixation and performance *(Regis et al., 2015; Perticarini et al., 2015; Geng et al., 2020; Dall'Ava et al., 2019a; Huang et al., 2021b; Dall'Ava et al., 2021).* For biological superiority (enriched osseointegration) of orthopaedic endo-prostheses, the optimal surface pore architecture (porosity, strut thickness, pore size) should be selected whilst considering also the mechanical performance and manufacturability. More about biomimetic interconnected porous structures with suitable pore sizes and porosity investigated in the literature and enabled by 3DP are discussed in *Sub-section 3.6.*

Galois and Mainard *(2004)* and researches on casting techniques for making foam ceramic and metal products, defined the optimum pore size at 0,08-0,25 mm with pores over 0,5 mm showing

bone ingrowth discourage. Pore sizes of 0,1 mm serve better transport of metabolic wastes and induce cell attachment and osteochondral formation before osteogenesis, whereas pore sizes greater than 0,3 mm support better vascularization and oxygenation, favoring the formation of neo-capillaries and neo-bone tissue by direct osteogenesis and at the same time, lower porosity stimulates osteogenesis by suppressing cell proliferation and forcing cell aggregation, whereas high porosity and pore size result in greater bone ingrowth *(Karageorgiou and Kaplan, 2005)*. In other words, as pore size and porosity increase, vascularization benefits from the higher permeability for successful bone ingrowth and osteogenesis, whereas cell colonization for bone ingrowth and mechanical strength are not, because osteogenic protein adsorption and osteoblast cell colonization benefit from increased surface area but smaller pore sizes. As new geometries of interconnected porous architectures were being explored and 3DP techniques utilized for the materialization of such, new structures challenged these values and the suggested pore size started trending closer to 0,6 mm *(Karageorgiou and Kaplan, 2005; Palmquist et al., 2013; Regis et al., 2015; Taniguchi et al., 2016; Shah et al., 2016; Hara et al., 2016; Tan et al., 2017; Wild et al., 2018; Wang et al., 2019; Barba, Alabort and Reed, 2019).*

It is thus apparent that trade-offs can be made on the selection of optimal pore size-porosity-thickness to compose a porous structure. Tan et al. *(2017)* and Barba, Alabort and Reed *(2019)* addressed the mechanical and biological requirements that an orthopaedic implant should conform to and provided the charts shown in *Figure 33*, marking the range of optimal pore size between 0,3-0,6 mm as the best compromise between cell colonization and vascularization.

As both cell colonization and vascularization are required for bone regeneration within a scaffold structure, supra-cellular architectures with multiple tissue interfaces featuring a combination of large pores to facilitate vascularization and smaller pores to promote tissue maturation and formation (*Figure 34*) can be formed by blending suitable geometries or implementing gradients and materialized by 3DP *(Karageorgiou and Kaplan, 2005; Charbonnier, Hadida and Marchat, 2021)*. However, such architectures have to possess suitable mechanical properties and be manufacturable.

Osseointegration-boosting materials to coat, impregnate or pollute the implant's surface, include *(Goodman et al., 2013; Zhang et al., 2014a; Tejero, Anitua and Orive, 2014; Brogini et al., 2021)*:

- Calcium phosphates (Hydroxyapatite (HA) and Tri-calcium Phosphate (TCP)) and similar coatings. Bioceramics and composites are used for implant-making and coatings due to their high strength, hardness and wear resistance, biocompatibility, osteoconductiveness, and bacteriostasis *(McEntire et al., 2015)*. The impact of HA coatings was histologically verified decades ago *(Furlong and Osborn, 1991)*. HA coatings are similar to bone tissue topographically and compositionally, hence they act as a reservoir for the calcium required to build bone during bone regeneration and fracture healing. Such coatings are gradually resorbed and completely replaced

by new bone tissue, forming a solid connection. Hybrid HA coatings such as Bioactive Glass–nHA have also been developed *(Xie et al., 2010)*.

- The immobilization of molecules is another way to modify a surface to induce and modulate biological interactions at the tissue-implant interface, i.e. Extracellular Matrix Molecules (ECM) (e.g. Collagen 1), enzymes, biological peptides (e.g. Arg-Gly-Asp (RGD)), biodegradable polymers and hydrogel coatings, titanium nanotubes, growth factors as biologic coatings (e.g. Fibroblast Growth Factor 2 (FGF2), Transforming Growth Factor-beta 2 (TGF-β2), Bone morphogenetic protein 2 (BMP-2)), reactive hydroxyl groups, bisphosphonates, and Strontium.

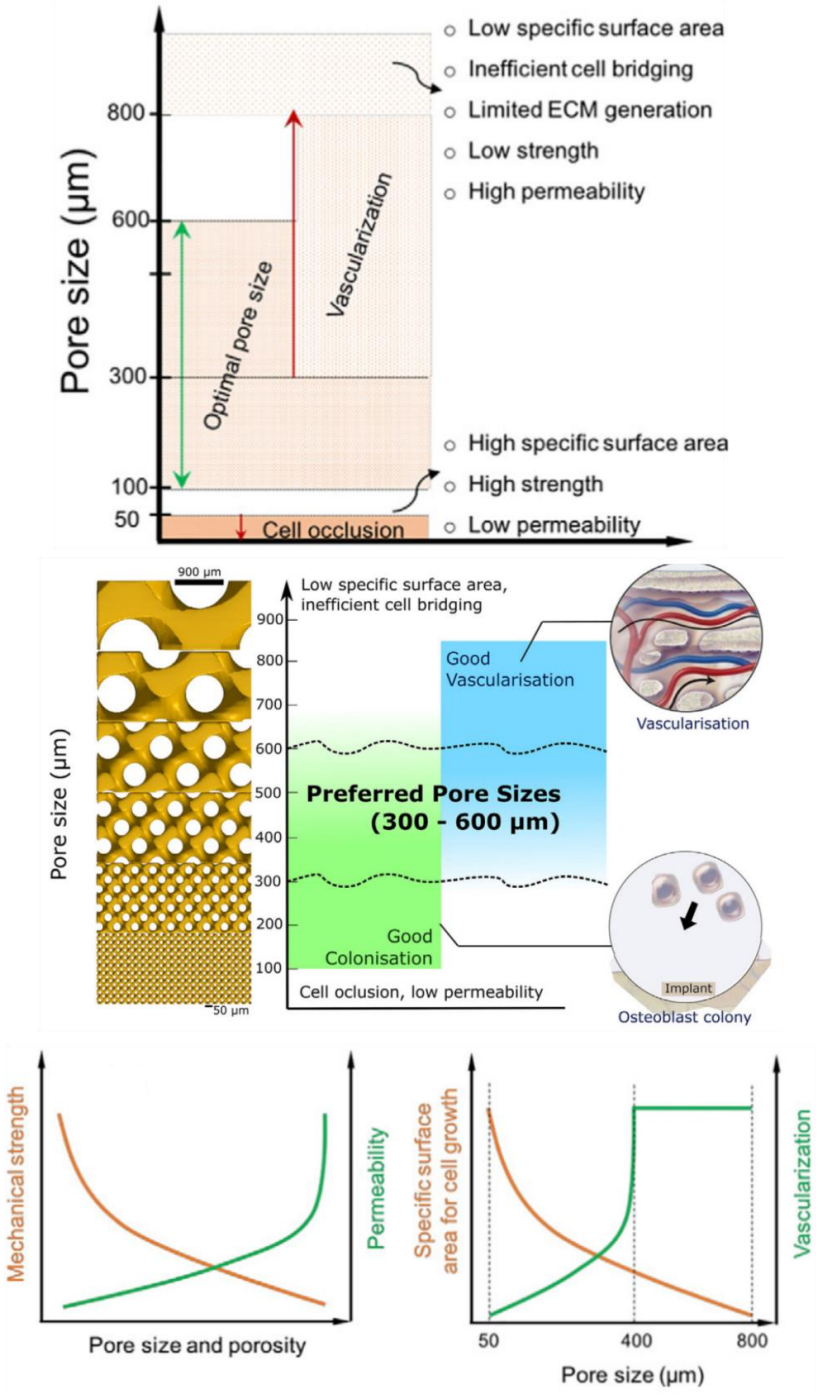

Figure 33: Optimal pore size for biological and mechanical superiority. Source: (Tan et al., 2017; Barba, Alabort and Reed, 2019)

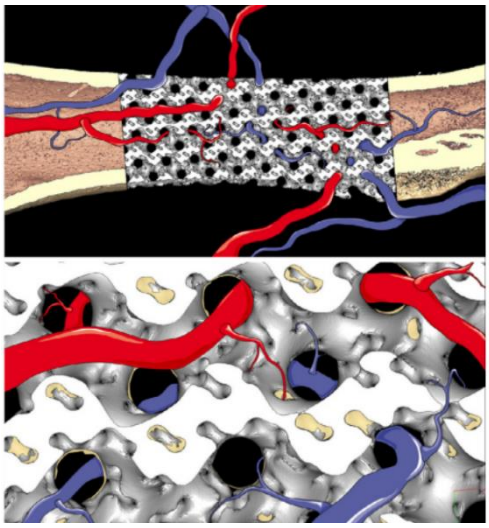

Figure 34: Supra-cellular architecture with large and small pore sizes. Source: (Charbonnier, Hadida and Marchat, 2021)

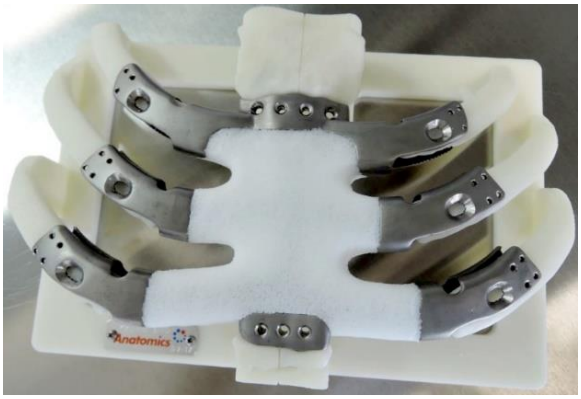

Figure 35: 3D Printed composite Ti-PE sternum and ribcage implant. Source: Anatomics

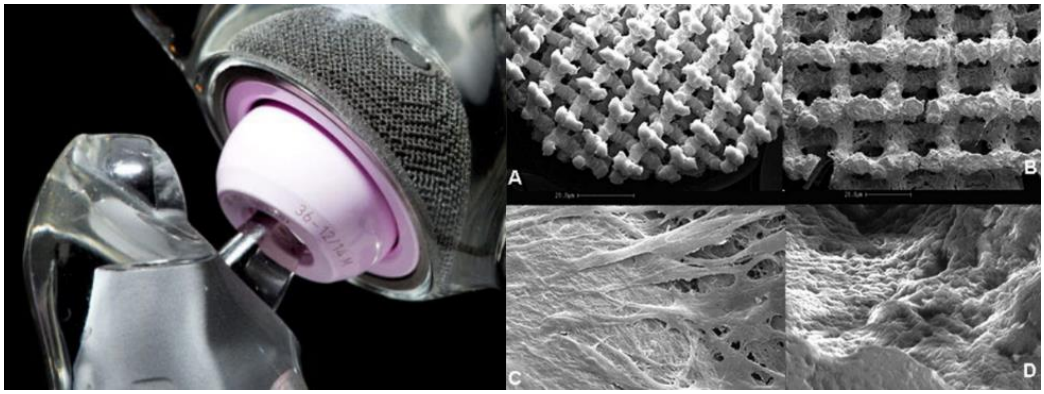

Figure 36: 3D Printed Ti acetabular cup with cellular structures. Source: GE Additive and (Gastaldi et al., 2010)

On the other hand, a surface that accelerates host cell adhesion also tends to promote similar bacterial activities as infecting microorganisms share the same adhesive mechanisms. To describe this *"competition"* of host cells versus bacteria to achieve adhesion, replication, and colonization, Gristina *(1987)* coined the phrase *"race for the surface"*. In this *"race"*, the goal is to win the host cells, creating a stable interface with implant and protecting from invading bacteria. Consequently, surfaces and coatings that advance osseointegration, indirectly inhibit bacterial infection, and surfaces and coatings that restrict bacterial activities indirectly assist osseointegration.

It is extremely important to address the implant-induced infections that have been the nemesis of orthopaedic surgery. Once bacteria colonize the implant's surface, a biofilm is created that

compromises its performance (*Figure 37*), repels host cells, and delays bone healing, leading ultimately to implant loosening and acute chronic infections of the underlying bone and the adjacent soft tissue. Implant-induced infections are the most serious complications as it is necessary for the implant to be removed and for the patient to undergo antibiotic therapy leading to prolonged suffering, substantial amputations, morbidity, and even mortality *(Goodman et al., 2013)*.

The infection rate of endo-prostheses after primary limb-sparing surgery is 8%-15% and following revision surgery is 43%, whilst amputation risk due to (mega)endo-prosthesis infection is 23,5%-87% *(Mavrogenis et al., 2011)*. In another study *(Mavrogenis et al. 2015)*, it was found that cement-less endo-prostheses have a higher survival rate, whereas endo-prostheses reconstruction might be infected in 8,6% of cases and 21% of the infected endo-prostheses are amputated.

Implantation of endo-prostheses includes long surgery times with extensive exposures and usually combined with immunosuppression, infections should be prevented, and if not, be diagnosed promptly and treated appropriately. Such microbial phenomena should be eliminated by proper sterilization procedures, antibiotic prophylaxis, aseptic management techniques, and the use of biomaterials coated with anti-bacterial layers or having anti-bacterial surface per se.

To avoid periprosthetic infections, it is necessary for orthopaedic implants and especially mega endo-prostheses to feature microbial-resistant layers with certain physiochemical surface characteristics to inhibit initial bacterial adhesion and subsequent biofilm formation. Usually, if the material per se cannot passively combat bacterial colonization, anti-infection coatings are applied onto the surface or into the porous surface layers. Coatings must fulfill several requirements for safe in vitro activity, efficacy, ease of use, and be readily available at acceptable costs *(Romanò et al., 2015)*. Coating materials should have suitable properties to offer three-lines-of-defence protection as shown in *Figure 37*. Such coating materials can be *(Goodman et al., 2013; Zhang et al., 2014a; Romanò et al., 2015; Trovarelli et al., 2019; Jahanmard et al., 2020; Donati et al., 2021; Savvidou et al., 2020; Xi et al., 2021; Lex et al. 2022)*:

1. Polymer coatings such as PEG, PE oxide, PMMA, hyaluronic acid, chitosan, cytokines/chemokines, biosurfactants, biodegradable polymers (PLA, PLGA, PDLLA), and hydrogels loaded with or without antibiotics.
2. Copper and silver coatings. Especially for the silver coatings, its ions lead to reduced infection rates, continuous long-term antimicrobial prophylaxis through continuous silver ion release, resistance to biofilm formation, and successful record in clinical use.
3. Others such as Nitric oxides, Ti oxides, organic agents (e.g. CHX, PCMX, PHMB), proteins such as MCP-1, IL-12, antiseptics and antimicrobial peptides with anti-microbial properties, bacteriophages, enzymes, Iodine, Selenium.

4. Antibiotics loaded into the implant's porous surface or into the coat layers, or via carriers impregnated with antibiotics such as bone cement.

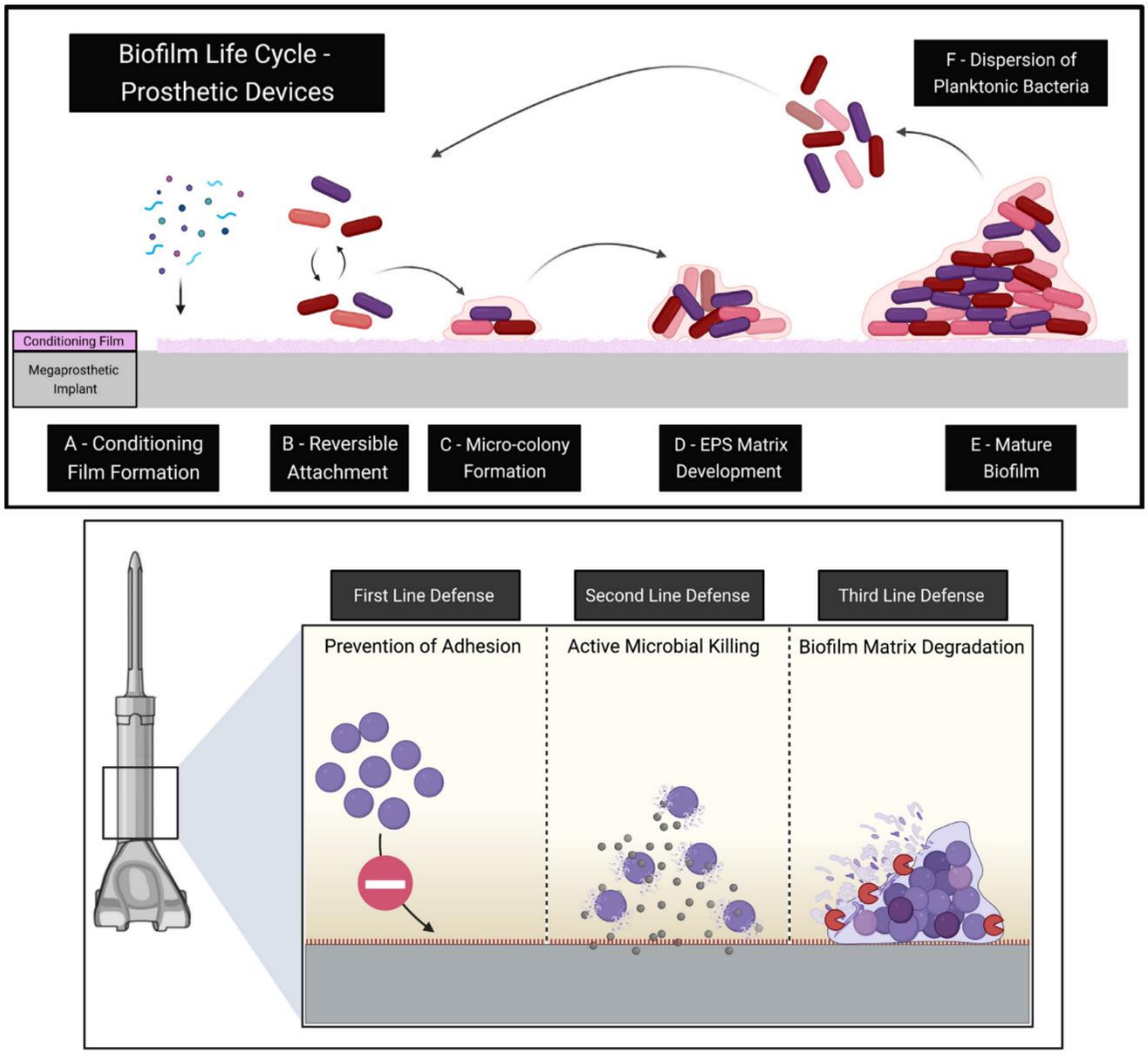

Figure 37: Biofilm formation cycle and implant surface protection mechanism. Source: (Lex et al., 2022)

Therefore, the implant's surface must be modified to be multifunctional with balanced osseointegrative and anti-bacterial properties *(Raphel et al., 2016; Contreras et al., 2021)*. Coquillat et al. *(2021)* reviewed metallic biomaterials with hybrid multifunctional coatings consisting of bioceramic and polymeric layers with hierarchical organization and drug-eluting capacity.

Regarding the sterilization of orthopaedic implantable device methods, many exist with each having advantages and disadvantages *(Rutala and Weber, 2013; 2016; Govindaraj and Muthuraman, 2015)*. *Figure 38* shows the most common methods.

Orthopaedic surgeons designed implants using materials with a successful record of industrial usage. Biomimetic structures with cellular features, and density and composition gradients open new dimensions for materials-by-design that are not just governed by composition itself. Such meta-(bio)materials will advance reconstructive surgery and will make tissue regeneration more feasible. Controllable topological interventions and tweaks at the micro/meso endo-structural scale, lead to controllable macroscopic properties variations across the volume of a monolithic material. Indeed, a

biomaterial can be both surface-functionalized to be osseointegrated and structurally-optimized and compositionally graded within to gain host-tissue matching mechanical properties. 3DP applications and techniques, as well as design optimization approaches for making biomaterials-by-design for patient-specific implants will be discussed in *Sub-section 3.6*.

Sterilization method	Advantages	Disadvantages
Steam	• Nontoxic to patient, staff, environment • Cycle easy to control and monitor • Rapidly microbicidal • Least affected by organic-inorganic soils among sterilization processes listed • Rapid cycle time • Penetrates medical packing, device lumens	• Deleterious for heat-sensitive instruments • Microsurgical instruments damaged by repeated exposure • May leave instruments wet, causing them to rust • Potential for burns
Hydrogen peroxide gas plasma	• Safe for the environment and health care worker • Leaves no toxic residuals • Cycle time is ≥28 min, and no aeration necessary • Used for heat- and moisture-sensitive items because process temperature <50°C • Simple to operate, install (208 V outlet), and monitor • Compatible with most medical devices • Only requires electrical outlet	• Cellulose (paper), linens, and liquids cannot be processed • Endoscope or medical device restrictions based on lumen internal diameter and length (see manufacturer's recommendations) • Requires synthetic packaging (polypropylene wraps, polyolefin pouches) and special container tray • Hydrogen peroxide may be toxic at levels >1 ppm TWA
100% ETO	• Penetrates packaging materials, device lumens • Single-dose cartridge and negative-pressure chamber minimizes the potential for gas leak and ETO exposure • Simple to operate and monitor • Compatible with most medical materials	• Requires aeration time to remove ETO residue • ETO is toxic, a carcinogen, and flammable • ETO emission regulated by states, but catalytic cell removes 99.9% of ETO and converts it to CO_2 and H_2O • ETO cartridges should be stored in flammable liquid storage cabinet • Lengthy cycle and aeration time
Vaporized hydrogen peroxide	• Safe for the environment and health care worker • It leaves no toxic residue; no aeration necessary • Cycle time, 55 min • Used for heat- and moisture-sensitive items (metal and nonmetal devices)	• Medical devices restrictions based on lumen internal diameter and length; see manufacturer's recommendations (eg, stainless steel lumen 1 mm diameter, 125 mm length) • Not used for liquid, linens, powders, or any cellulose materials • Requires synthetic packaging (polypropylene) • Limited materials compatibility data • Limited clinical use and comparative microbicidal efficacy data
Hydrogen peroxide and ozone	• Safe for the environment and health care worker • Uses dual sterilants, hydrogen peroxide and ozone • No aeration needed because of no toxic by-products • Compatible with common medical devices • Cycle time, 46 min • FDA cleared for general instruments, single-channel flexible endoscopes, and rigid and semirigid channeled devices	• Endoscope or medical device restrictions based on lumen internal diameter and length (see manufacturer's recommendations) • Limited clinical use (no published data on material compatibility, penetrability, organic material resistance) and limited microbicidal efficacy data • Requires synthetic packaging (polypropylene wraps, polyolefin pouches) and special container tray

Figure 38: Most common sterilization methods. Source: (Rutala and Weber, 2016)

The optimal implant satisfies all the previously stated requirements and is at least bioactive. In addition, for complete biological reconstruction, the ideal implant should be biodegradable and biomimetic to mimic the highly organized and dynamically changing hierarchical architecture and characteristics of bone *(Appendix E)*. Such implant types used to replace or regenerate tissue are being studied and are the main theme of TE for regenerative medicine *(Pallua and Suschek, 2011; Steinhoff, 2016)* where 3DP is currently a protagonist manufacturing method.

3.2 Tissue Engineering for Regeneration

As said, the biological goal of artificial bioinert load-bearing implants is osseointegration which is enabled by suitable surface modifications that allow activities to occur at the bone-implant interface. Even though biological fixation can be achieved in artificial scaffolds *(Alvarez and Nakajima, 2009)*, these continue to be non-biological and foreign bone substitutes.

Biodegradable/bioresorbable materials with sufficient biological and mechanical properties would be ideal options to be used as templates to guide organisms for true regeneration and osseous self-healing. Such approaches fall under the scope of TE for Regenerative Medicine *(Pallua and Suschek, 2011; Steinhoff, 2016)* which aims at either implanting a biomaterial able to stimulate

existing stem cells or developing constructs (scaffold, cells, signals) within bioreactors and then implant these constructs into the patient's body to be recognized as its own tissue.

TE refers to both hard and soft tissue and is defined as *"an interdisciplinary field that applies the principles of engineering and life sciences toward the development of biological substitutes that restore, maintain, or improve tissue function" (Langer and Vacanti, 1993)*. Its three fundamental pillars are *(Figure 39) (Ratner et al., 2013; Nukavarapu, Freeman and Laurencin, 2015):*

1. **Scaffolds:** act as substrates for cells and offer mechanical integrity. They have suitable structural and functional characteristics to be clinically applied, i.e.:
    a. Highly interconnected porous 3D structure with suitable pore morphology and surface to allow rapid vascular invasion, nutrient delivery and circulation, and cell attachment, proliferation, and differentiation for bone genesis.
    b. Made of biodegradable/bioresorbable biomaterials with tissue growth-matching rates. These can be either natural/tissue-derived or synthetic (metals, polymers, ceramics, composites).
    c. Maintain mechanical stability with properties that ultimately match implantation's site.
2. **Cells:** the building blocks of tissue that promote tissue healing and regeneration. They might be fed into an in vitro (outside of a living organism) construct before implantation using suitable signals or recruited in vivo (inside of a living organism). They might be either embedded within scaffolds (scaffold-based) or used per se to make scaffold-free constructs, or injected directly into the site. Additionally, they might be either differentiated or composed of stem cells taken from the patient (autologous) or other organisms (heterologous/allogenic).
3. **Signals:** used to stimulate growth by inducing cell proliferation and differentiation. Apart from the very important mechanical stimuli, these might be hormones, cytokines, growth factors, extracellular matrix molecules, cell surface molecules, and nucleic acids.

Figure 40 illustrates the in vivo and in vitro TE approaches, as well as the types of constructs that can be utilized. TE's quest to imitate and regenerate the bone structure involves many challenges as bone is a highly complex hierarchically arranged system *(Lanza et al.,2020) (Appendix E)*. Osseous tissue is capable of self-healing and regenerating but this ability is limited in amount. Only if we fully understand the regeneration process taking place at all levels (micro to macro) within our bodies, such fascinating tissue osteogenic activities would be possible to be triggered to occur in vivo or in vitro. By implanting suitable constructs into an organism, this outstanding attribute of bone can be harnessed for the host organism to be guided and instructed and *"build"* tissue where and as much necessary.

Engineered tissue constructs are populated with living cells and signal factors and possess the aforementioned properties to facilitate cells, and signaling activities, and promote osteogenesis.

These are made of natural or synthetic polymers, ceramics, and composites, to imitate bone's composition and structure: an abundant extracellular matrix composed of 25% water, 25% collagen fibers, and 50% crystallized mineral salts, mainly HA *(Tortora and Derrickson, 2020)*.

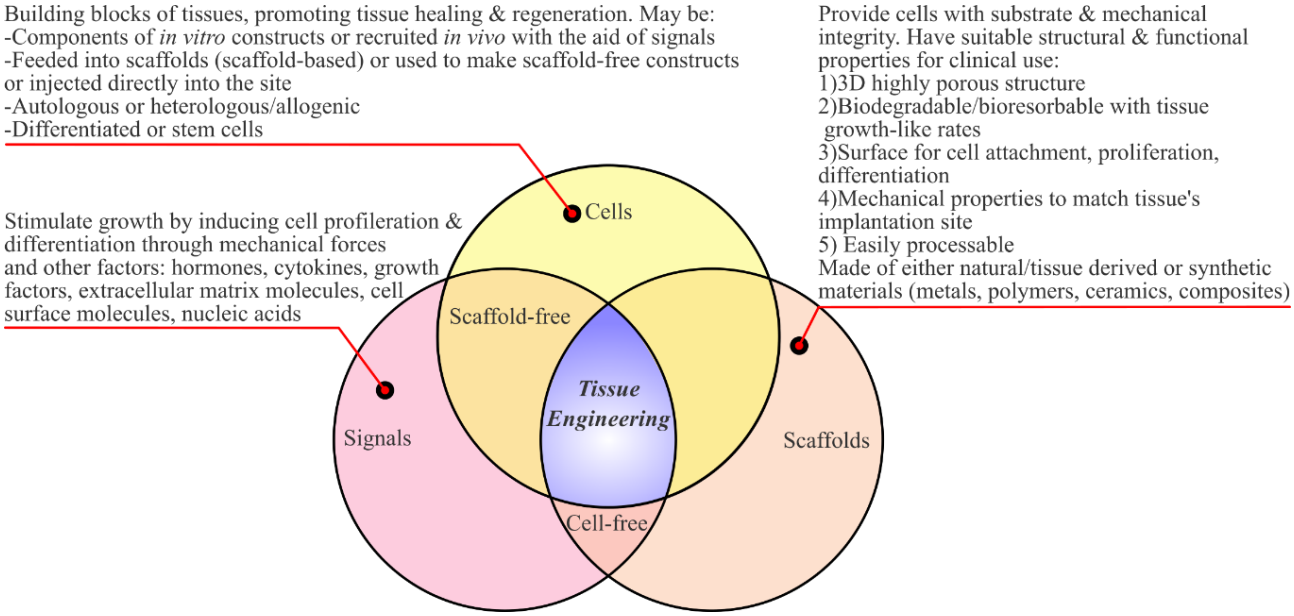

Figure 39: Elements of Tissue Engineering

Figure 41 pictures a 3DPed mandible bone scaffold made of Decellularized Bone (DCB) matrix powder and biodegradable polyester powder (Polycaprolactone (PCL)) *(Hung et al., 2016)*. The DCB offers the required proteins and growth factors to assist cell differentiation and adds roughness to help cell attachment and amplify the signals sent from growth factors.

Jakus et al. *(2016)* developed a 3DPed synthetic biomaterial, and evaluated it in vitro and in vivo: no immune rejection, rapidly vascularized, integrated with surrounding tissue, ossification, and new osteogenesis with no biological factors added. The so-called *"hyperelastic bone" (Figure 42)* is composed of 90% HA and 10% PCL or polylactic-co-glycolic acid, experience elastic mechanical properties (32-67% strain to failure, 4-11 MPa modulus of elasticity), is highly absorbent (50% porosity), maintained cell viability and proliferation, and induced osteogenic differentiation. This construct was 3DPed by Bioplotter (Envisiotec Gmbh (now Etek after acquisition by Desktop Metal), Gladbeck, Germany) shown in *Figure 43* along with some PCL products.

Thavornyutikarn et al. *(2014)* gave a literature review on biomaterials and characteristics of bone scaffolds and compared the production techniques for bone TE. They pointed out that material extrusion, photo-polymerization, and powder-based 3DP techniques are superior in making bone scaffolds because conventional methods (solvent casting, freeze-drying, thermally induced phase separation, gas foaming/supercritical fluid processing, textile technology (electrospinning), powder-forming processes, sol-gel techniques) have numerous inabilities and limitations: cannot make fully continuous interconnectivity and uniform pore morphologies spatially, the building process cannot

be controlled accurately and precisely (randomized), there is a need of organic solvents (toxic) to dissolve polymers and other chemicals, and porogens (toxic) to create the pores.

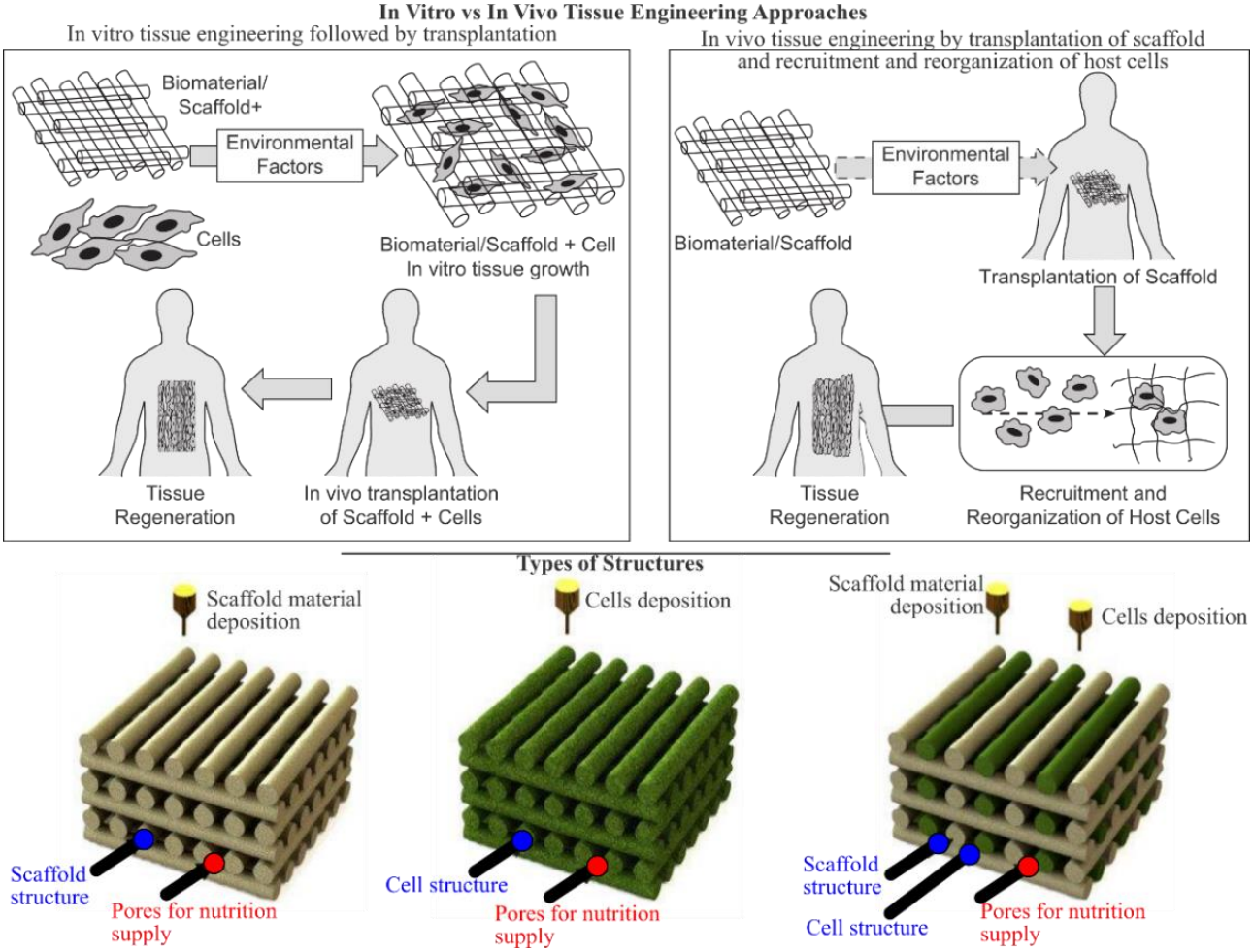

Figure 40: In vivo, in vitro TE approaches and construct types. Source: After (Ratner et al., 2013; Munaz et al., 2016)

Figure 41: Bone scaffold from natural bone and PCL powders. Source: John Hopkins Medicine

Figure 44 shows bioresorbable implants made of HA and TCP by 3DP CeraFab S65 (Lithoz Gmbh, Vienna, Austria) system utilizing LCM technology: ceramic-loaded liquid photocurable slurries are photo-polymerized layer-by-layer within a vat and then thermal post-processed and sintered to obtain a dense ceramic part.

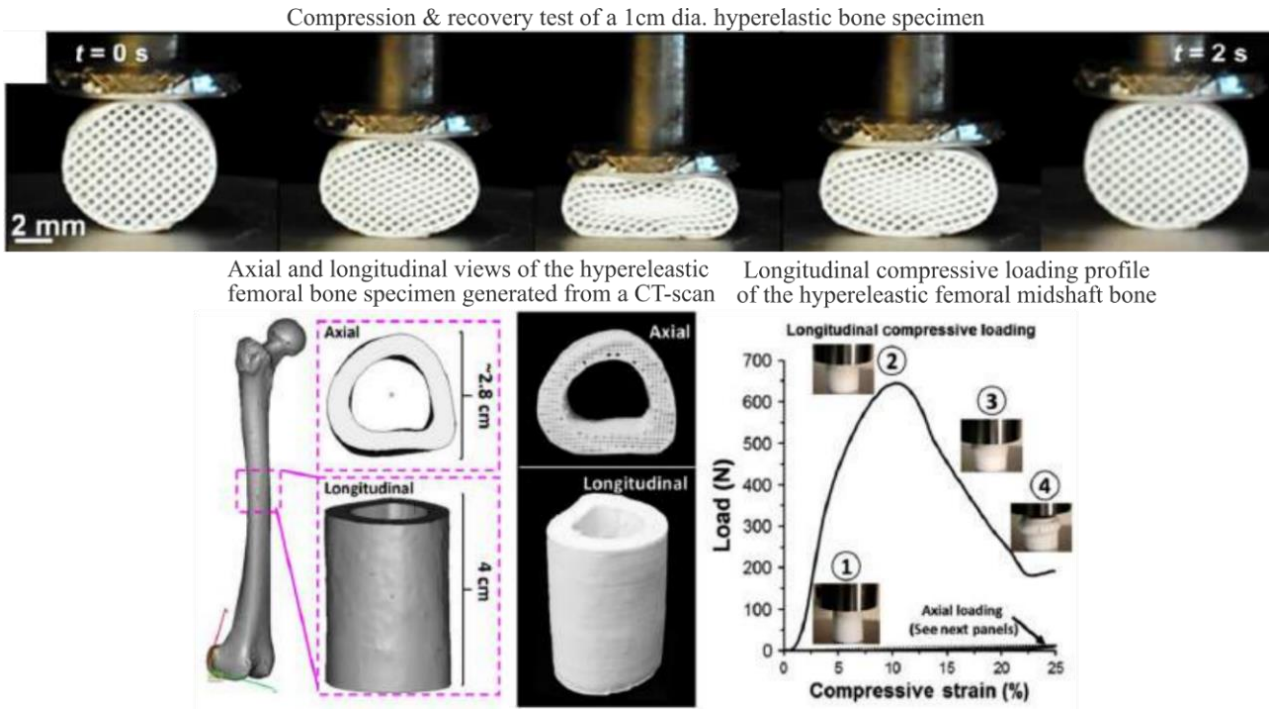

Figure 42: Properties of the "hyperelastic bone". Source: (Jakus et al., 2016)

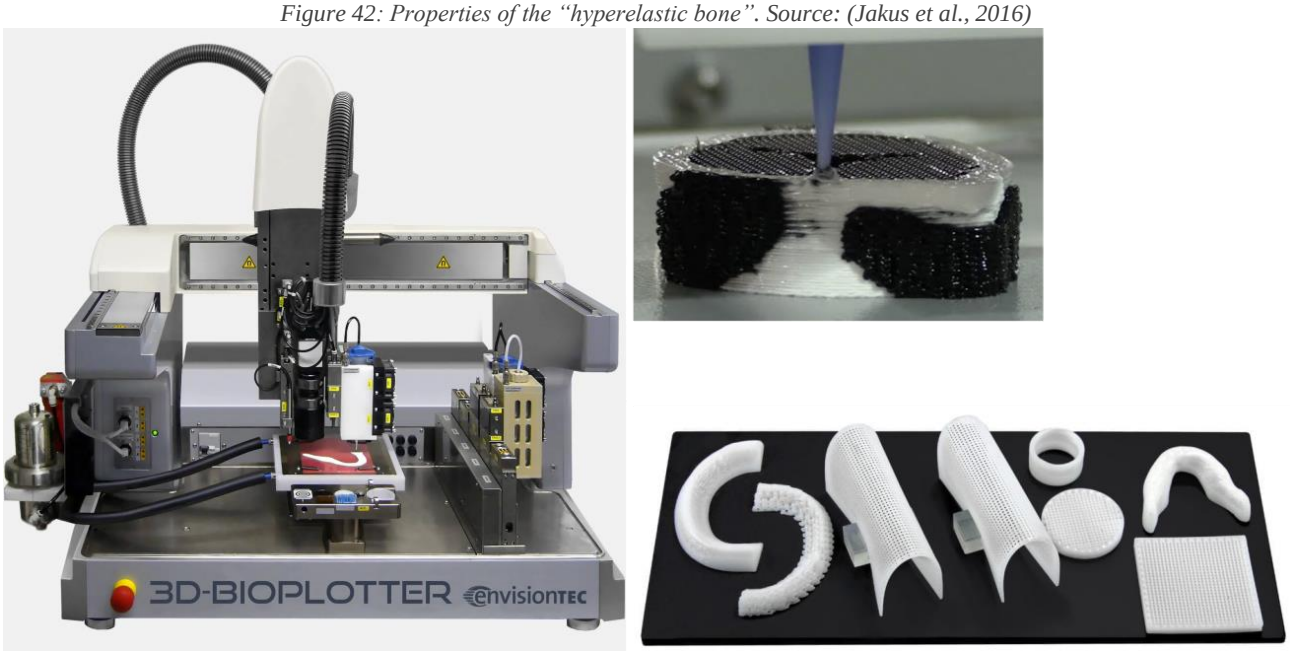

Figure 43: Envisiotec Bioplotter extrusion system and PCL products. Source: Envisiotec

3DP has great potential in TE and is being currently investigated intensively in academia and industry. It is used to make either scaffold-based constructs or scaffold-less by directly patterning living cells (bioprinting). 3DP techniques have been successfully used to make various complex structures via cell deposition, including functional living soft and hard tissue and artificial organs *(Mandrycky et al., 2016)*. Munaz et al. *(2016)* dealt with the feasibility of 3DP techniques for TE, presented recent advances in bio-inks and challenges in scaffold-based and scaffold-free approaches, whereas Ozbolat, Moncal and Gudapati *(2017)* evaluated the currently available material extrusion, droplet, and laser-based bioprinting technologies and machines.

Figure 44: Lithoz CeraFab S65 photocuring system and HA and TCP products. Source: Lithoz

Unfortunately, the production of custom-made bioresorbable TEed constructs able for bone tissue regeneration whilst capable of full load-bearing is still in its infancy and not yet readily available to replace artificial (metal mainly) endo-prostheses bone reconstruction procedures.

3.3 About Manufacturing and 3D Printing

There is a plethora of manufacturing technologies used to shape and offer certain properties to different materials *(Kalpakjian and Schmid, 2020)*. The parameters affecting the selection of the optimum production methodology *(Ashby, 2016)* are shown in *Figure 45*.

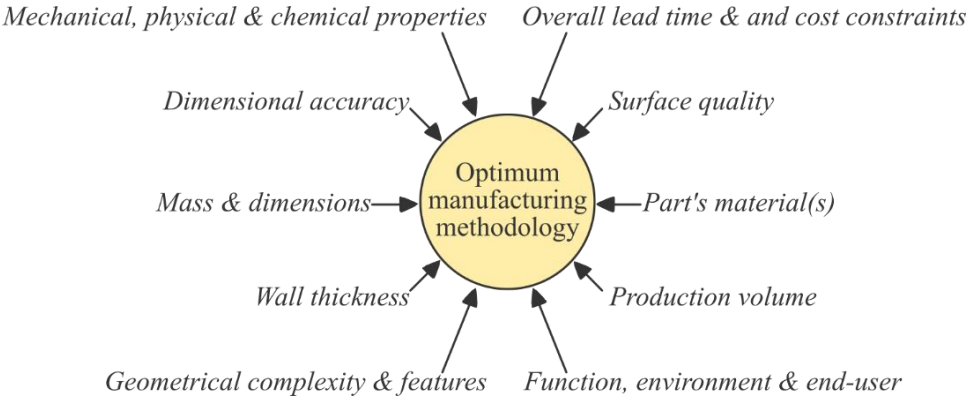

Figure 45: Parameters affecting the selection of manufacturing technologies

Manufacturing can be treated as a transformation process *(Hubka and Eder, 1988; Eder, 2008)* with material, energy, and information as inputs and outputs *(Figure 46)*. Within this context, based on the change of the material's mass, DIN 8580 *(2003)* categorizes all manufacturing techniques into six categories *(Figure 47)* with each being further divided into groups and sub-groups *(Figure 48)*.

The combination of several techniques is usually needed to fabricate end parts in low, medium or mass volumes. *Figure 49* illustrates a typical process flow. First, raw material is shaped using formative (e.g. casting, molding, powder, composite forming), Additive Manufacturing/3DP, or deformation methods. Then, secondary subtractive shaping and properties changing techniques take

place. Finally, material joining and finishing (surface treatments) methodologies are applied. Generally, subtractive technologies can be used for a) making the required tooling (molds, dies) for formative and deformation processes, b) finishing products made by formative, additive, and deformation processes for surface quality and dimensional accuracy improvements, c) direct shaping of the raw material if the geometry is suitable and the material machinable. Implants can be produced using different combinations of fabrication techniques, but there is always an optimum based on the desired criteria and requirements.

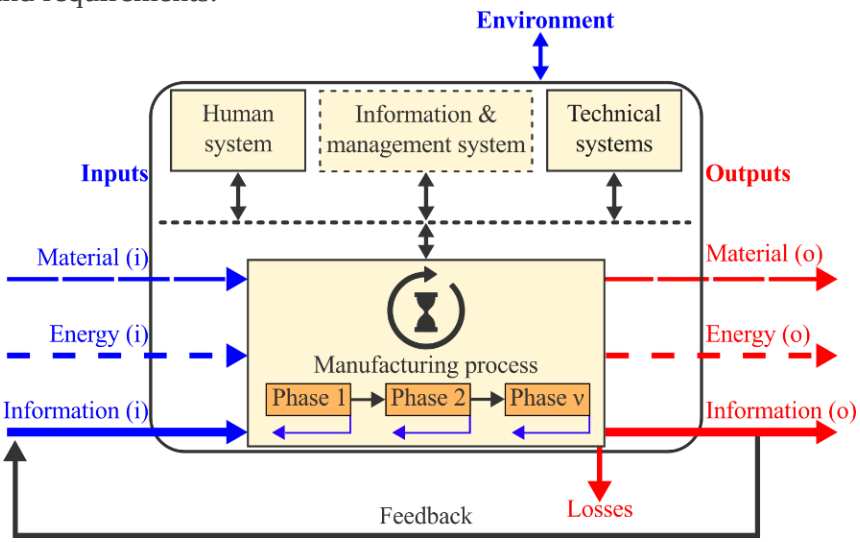

Figure 46: Manufacturing as a transformation system. Source: After (Hubka and Eder, 1988; Eder, 2008)

Figure 50 pictures a manufacturing technology selection table according to the desired material and geometry of the product. There are analogous tables about dimensional accuracy, surface quality, minimum wall thickness, and cost *(Ashby, 2016)*.

As per ISO/ASTM *(2021)*, Additive Manufacturing (AM)[42], also known as 3D Printing (3DP)[43] is defined as *"a process of joining materials to make parts from 3D model data, usually layer upon layer, as opposed to subtractive manufacturing and formative manufacturing methodologies".* It is a tool-less method used for the primary shaping of complex freeform products. The 3D geometry emerges from the selective and successive material addition, that takes place layer-wise, with each layer corresponding to a cross-section of the product to be fabricated. This principle allows extremely intricate geometrical features to be formed, both internally and externally.

Thinking of unique individualized orthopaedic implants with complex features that are matched to the patient, it is apparent that 3DP is an ideal candidate. *Figure 51* shows two examples of 3DPed parts with complex freeform internal and external features.

[42] Historical alternative terms include Rapid Prototyping/Manufacturing, Instant/Direct Manufacturing, Solid Freeform Fabrication, 3D Printing, Computer Aided/Digital/Automated/Desktop/Layer/Material Incress/Material Addition Manufacturing/Fabrication.

[43] 3D printing is typically associated with machines used for non-industrial purposes including personal use. It is often used as a de facto standard term interchangeably with AM. In this Thesis, it is used synonymously to AM.

Create cohesion	Preserve cohesion	Reduce cohesion	Increase cohesion	
1. Primary shaping	Shape changing			5. Coating
	2. Deformation	3. Subtractive	4. Joining	
	6. Properties Changing			
	Rearrange material particles	Remove material particles	Add material particles	

Figure 47: Categorization of manufacturing technologies as per DIN 8580

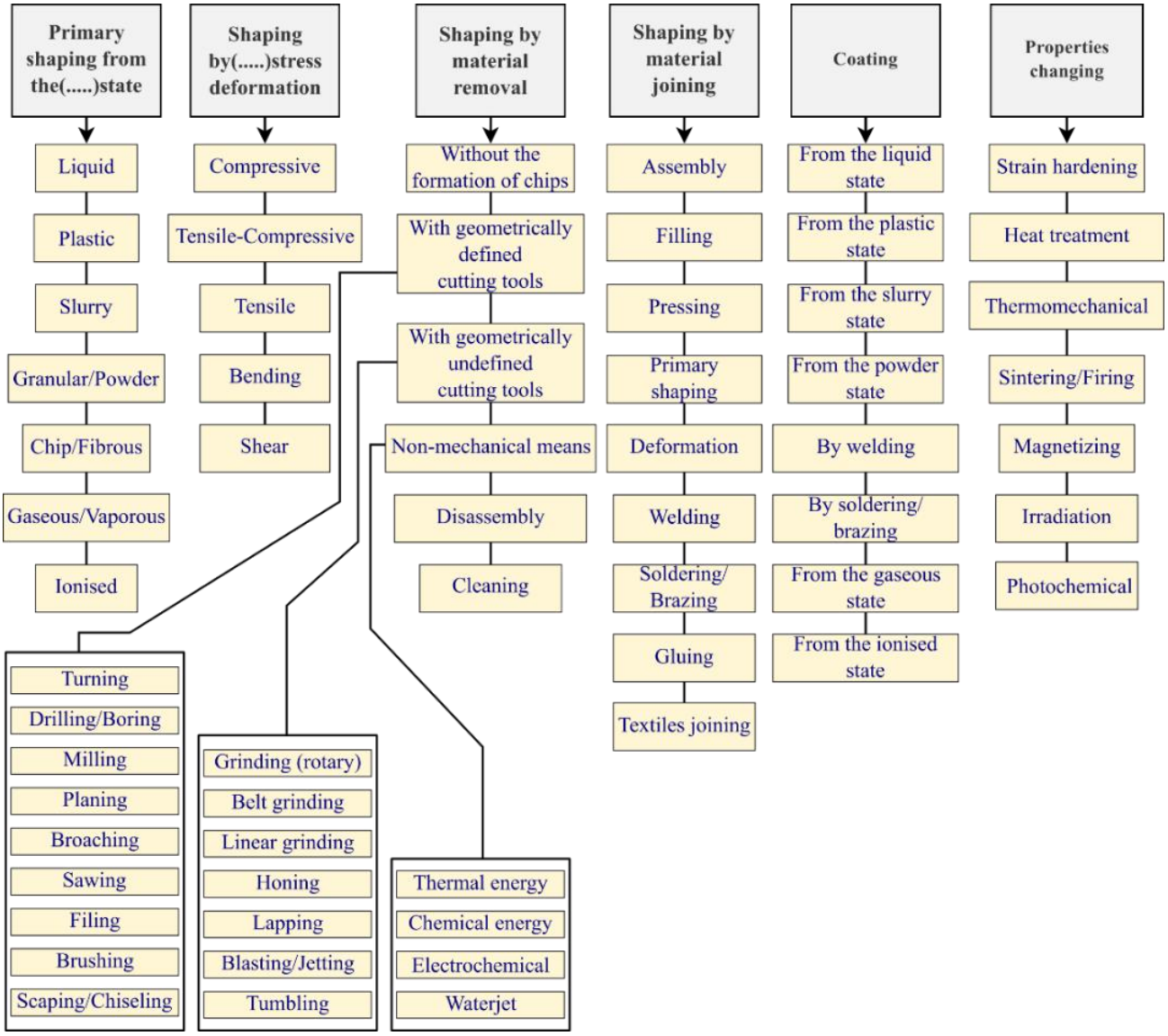

Figure 48: Manufacturing processes categories and groups as per DIN 8580

3DP technologies are capable of processing a wide palette and states of materials, to shape them into any forms with any geometrical features via single-step or multi-step 3DP *(Appendix G)*.

There is a plethora of 3DP technologies, each having different characteristics and potential regarding the product properties and material processing capabilities *(Gebhardt and Hötter, 2016; Gibson, Rosen and Stucker, 2021).* 3DP was introduced as a rapid prototyping technique, but eventually evolved and became capable of superior end-parts production (rapid manufacturing) out

of polymer, metal, ceramic, and composite materials at fluid[44], solid[45], or powder[46] states *(Kumar and Kruth, 2010; Ivanova, Williams and Campbell, 2013; Kotlinski, 2014; Bourell et al., 2017).*

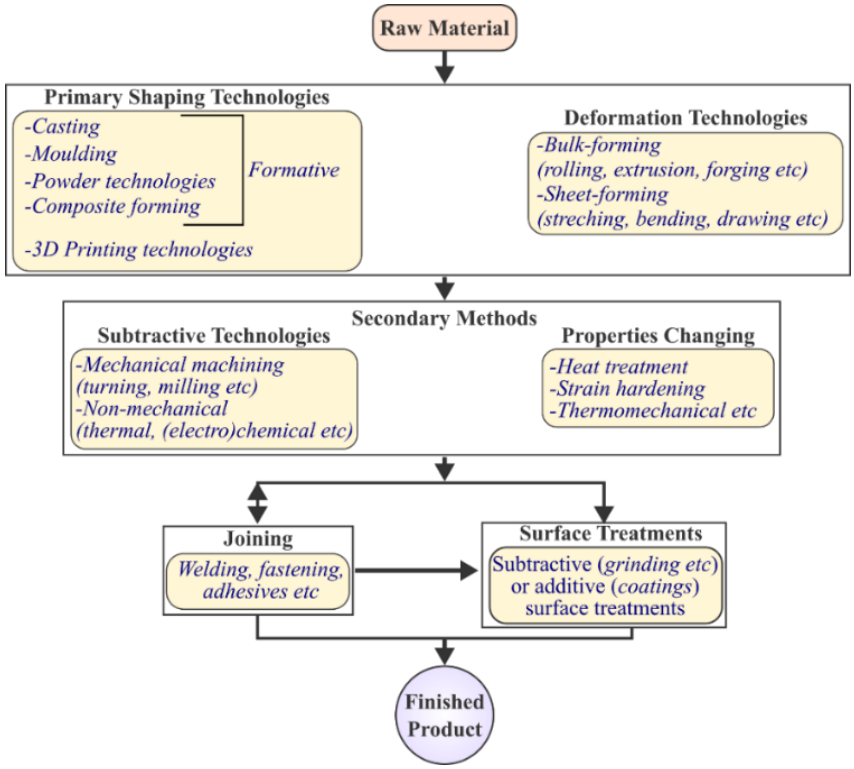

Figure 49: Typical manufacturing process flow. Source: After (Ashby, 2016)

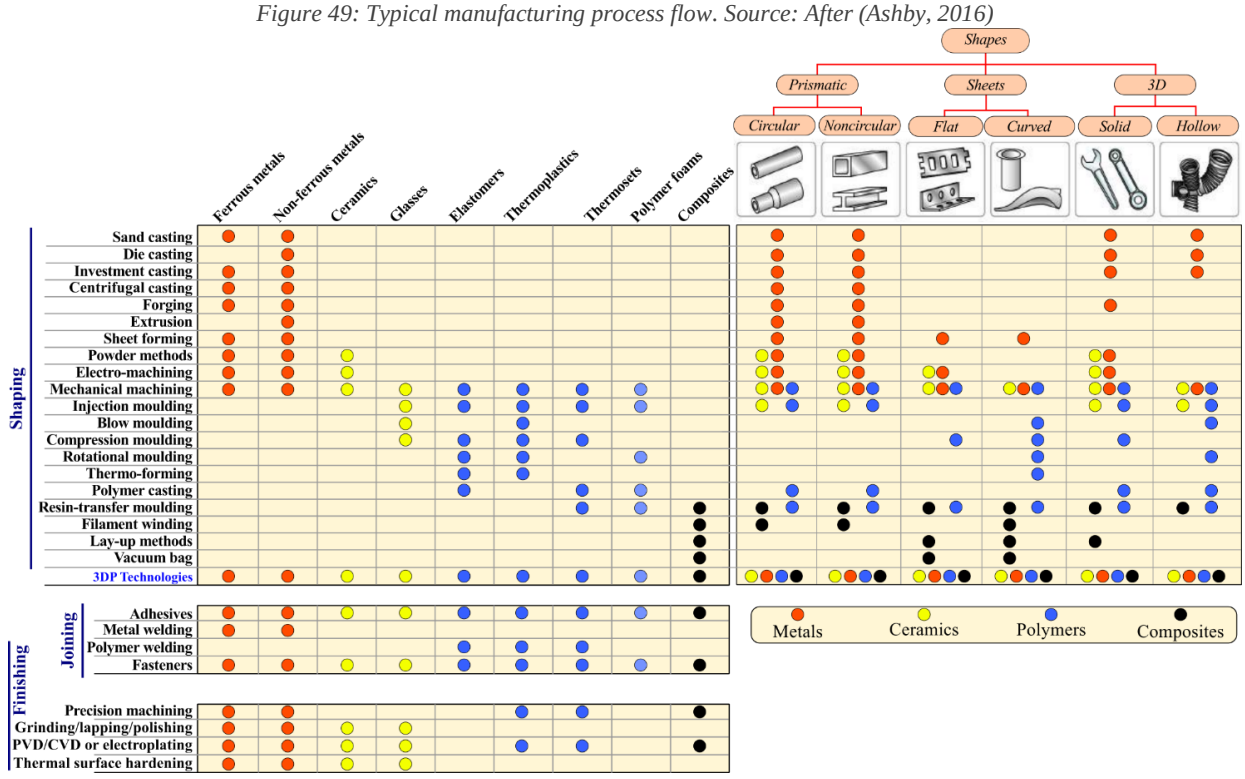

Figure 50: Manufacturing technology selection based on material and shape. Source: After (Ashby, 2016)

[44] Photo-polymers, thermoplastics, thermosetting, composites, gels, slurries, and even living cells.

[45] Wire/rods/pellets (metals, thermoplastics, and composites), sheets (paper, polymers, metals, ceramics, and composites).

[46] Metals, polymers, ceramics, composites.

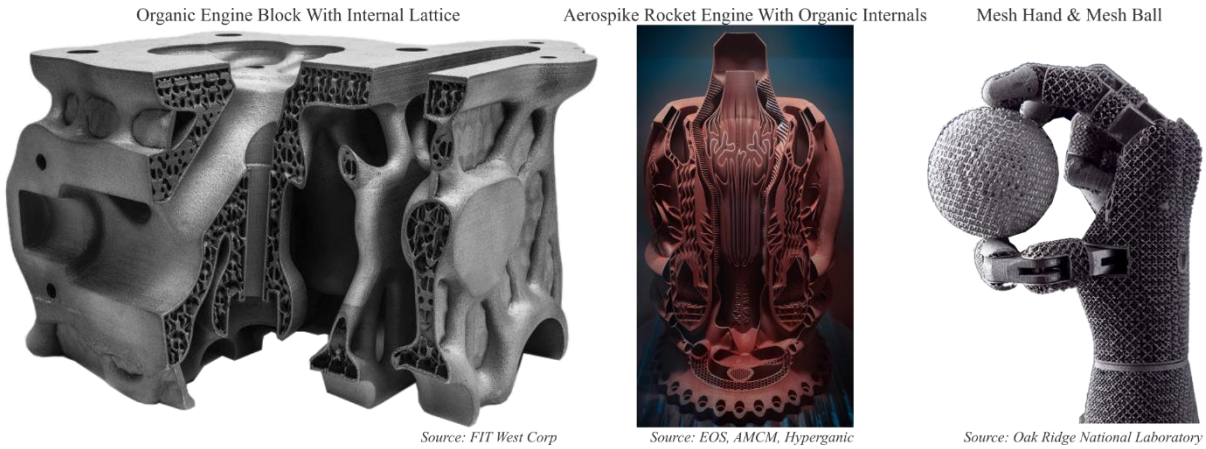

Figure 51: Complex forms and endo-features made with 3D metal printing

3.3.1 Principle of Operation

The fact that parts grow under control by selective material addition implies that any desired internal and external geometrical feature can be developed. Indeed, this is truly important as unlimited design freedom is enabled.

Based on the kinematics, the additive process can take place either in a layer-wise fashion or spatially *(Figure 52) (Kruth, 1991)*. The majority of 3DP technologies operate under layer-wise kinematics due to hardware and software simplicity. It would be logical to describe layer-based 3DP as a reverse tomography, i.e. instead of scanning the real object's cross-sections to acquire data and generate its digital model, the digital model's cross-sections are sent to a 3D printer to form a tangible object layer-by-layer.

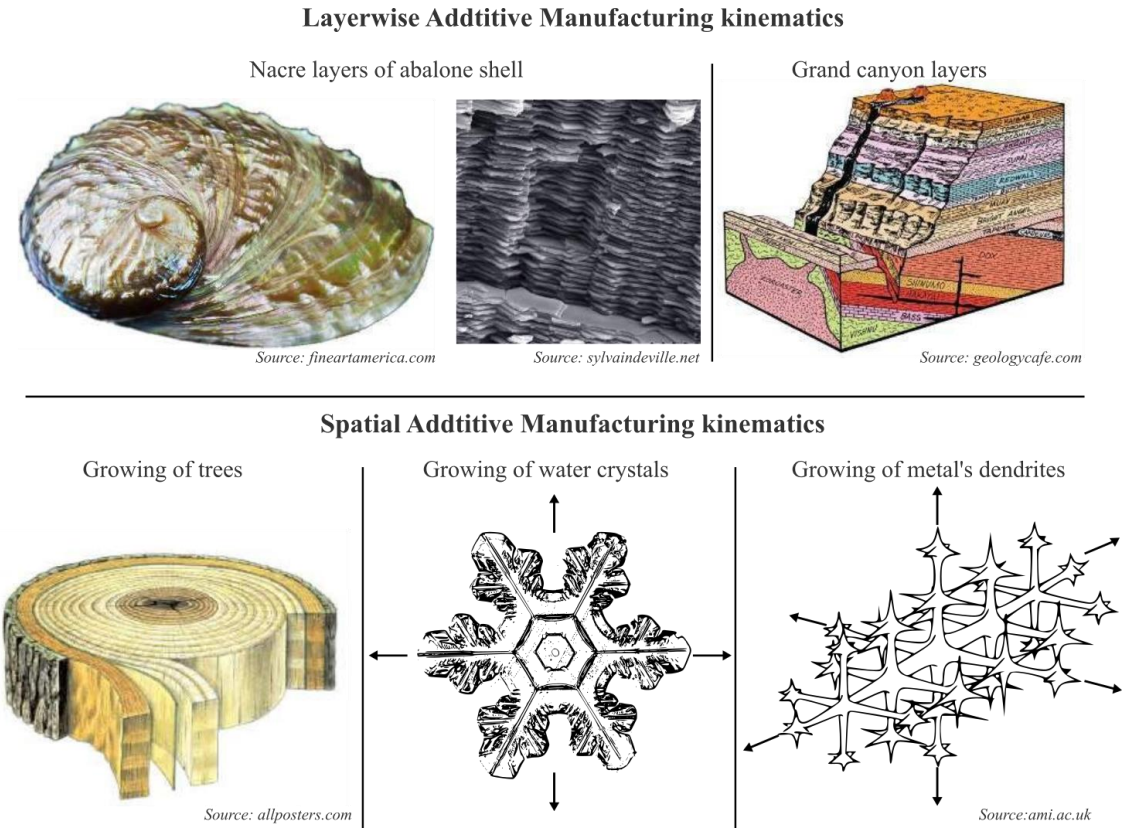

Figure 52: Kinematics of Additive Manufacturing/3DP

Any 3D object can be produced by building, stacking, and joining its cross-sectional layers *(Figure 53)*. It should be noted that the higher the number of cross-sectional layers used (density), the better the surface quality and dimensional accuracy of the laminated product *(Figure 54)*. According to this observation, geometries with flat surfaces about the slicing axis, are independent of the layer count, whereas inclined and curved surfaces suffer from the stair-stepping phenomenon *(Figure 55)*.

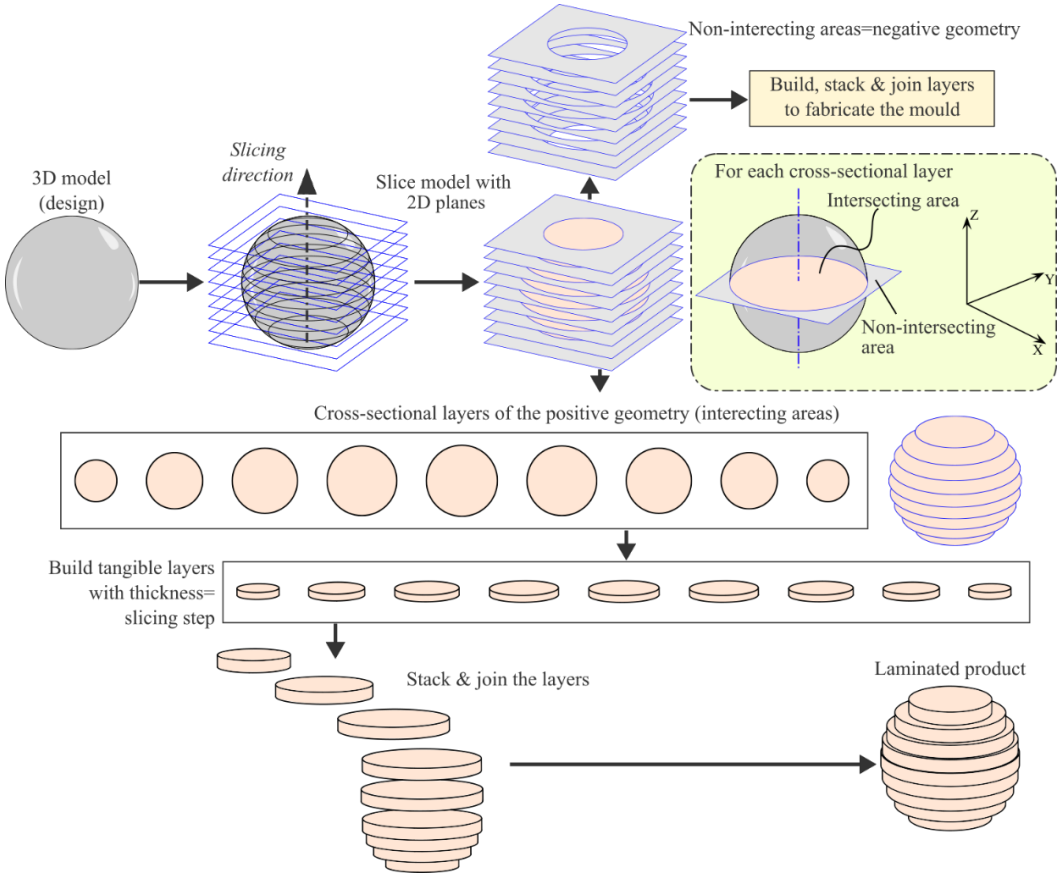

Figure 53: Making of a 3D laminated object

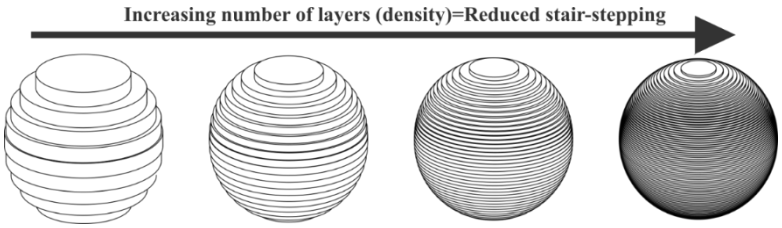

Figure 54: Impact of layer number on laminated product quality

3DP machines (3D Printers) operate autonomously under a repetitive form-and-bond principle utilizing various kinematics and mechanisms to accomplish the layer-forming and bonding process *(Figure 56)*. A 3D printer is composed of a built platform (bed) and a material processing head[47] that move relatively to each other to achieve movement along the x and y axes to build a layer, and along the z-axis (typically in the scale of tenths of micrometers) to process the next one. Layers are either

[47] Depends on the technology and machine used. Could be a cutting tool, extrusion, jetting, or radiation head where layers are built either by projecting the cross-sections at one go, or with a scanning system point-by-point.

build-then-bonded or build-bonded directly on top of the previous. The material of the layers can be self-bonded/fused (e.g. through heating), or using other agents such as glue.

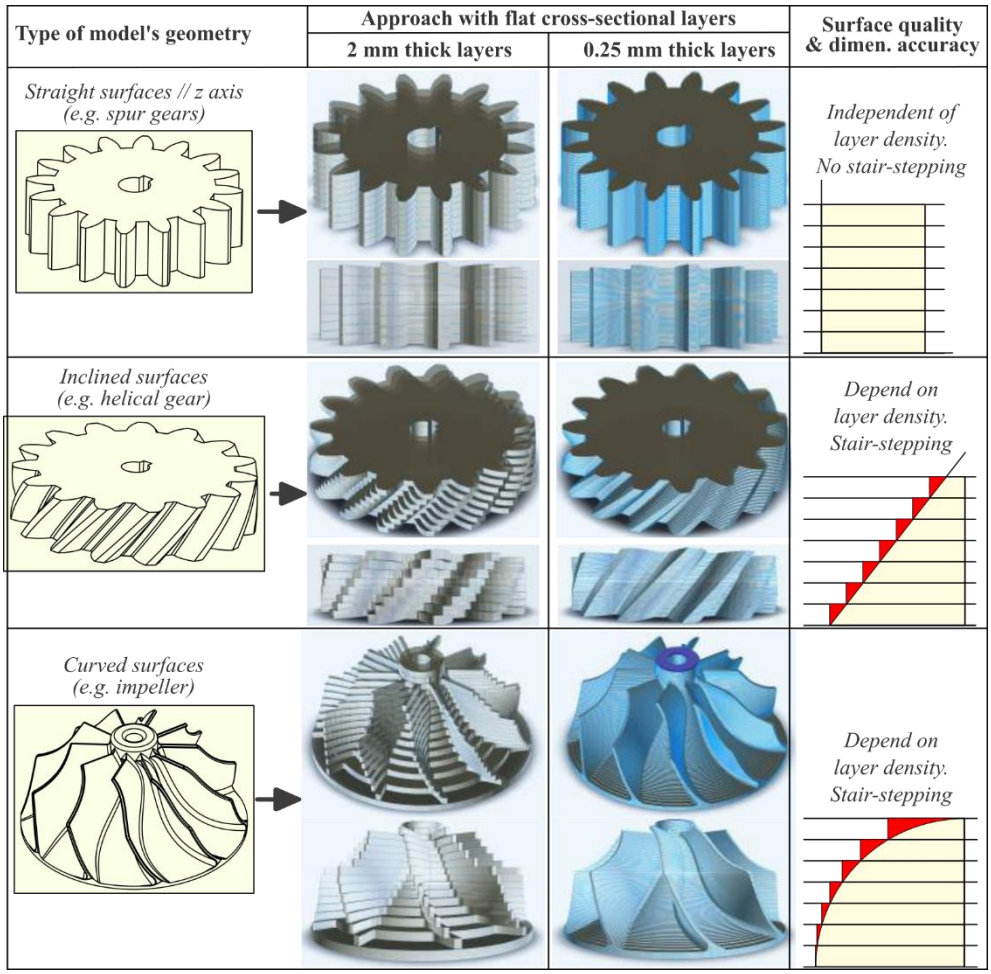

Figure 55: Geometry types and impact of layer number on quality and accuracy

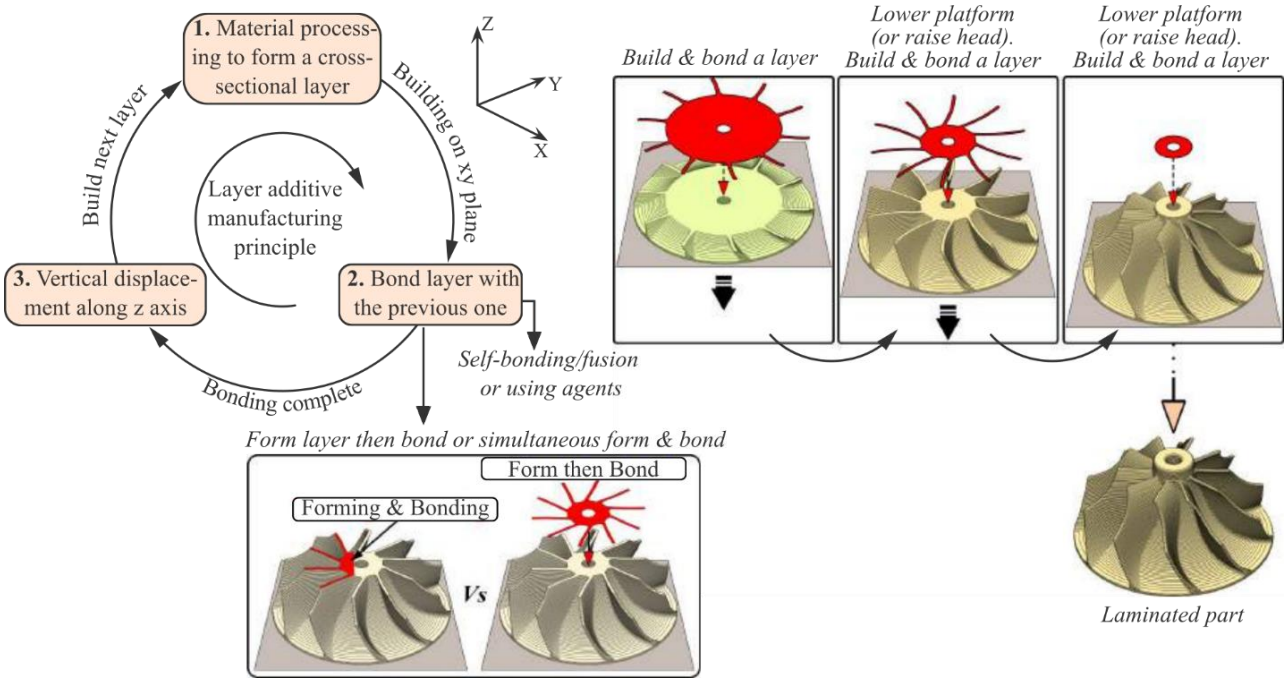

Figure 56: Repetitive principle of 3DP and object-building evolution

Based on the selected build orientation *(Figure 57)*, 3DP technology, machine characteristics, and the object's geometrical features, support structures might or might not be required *(Figure 58)*.

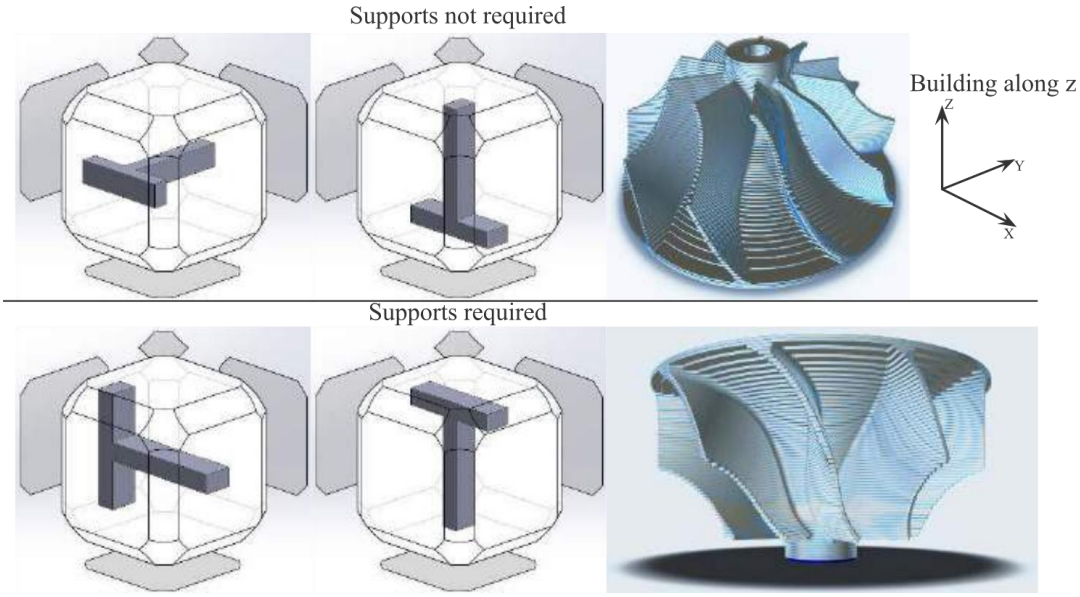

Figure 57: Support requirements based on selected build orientation

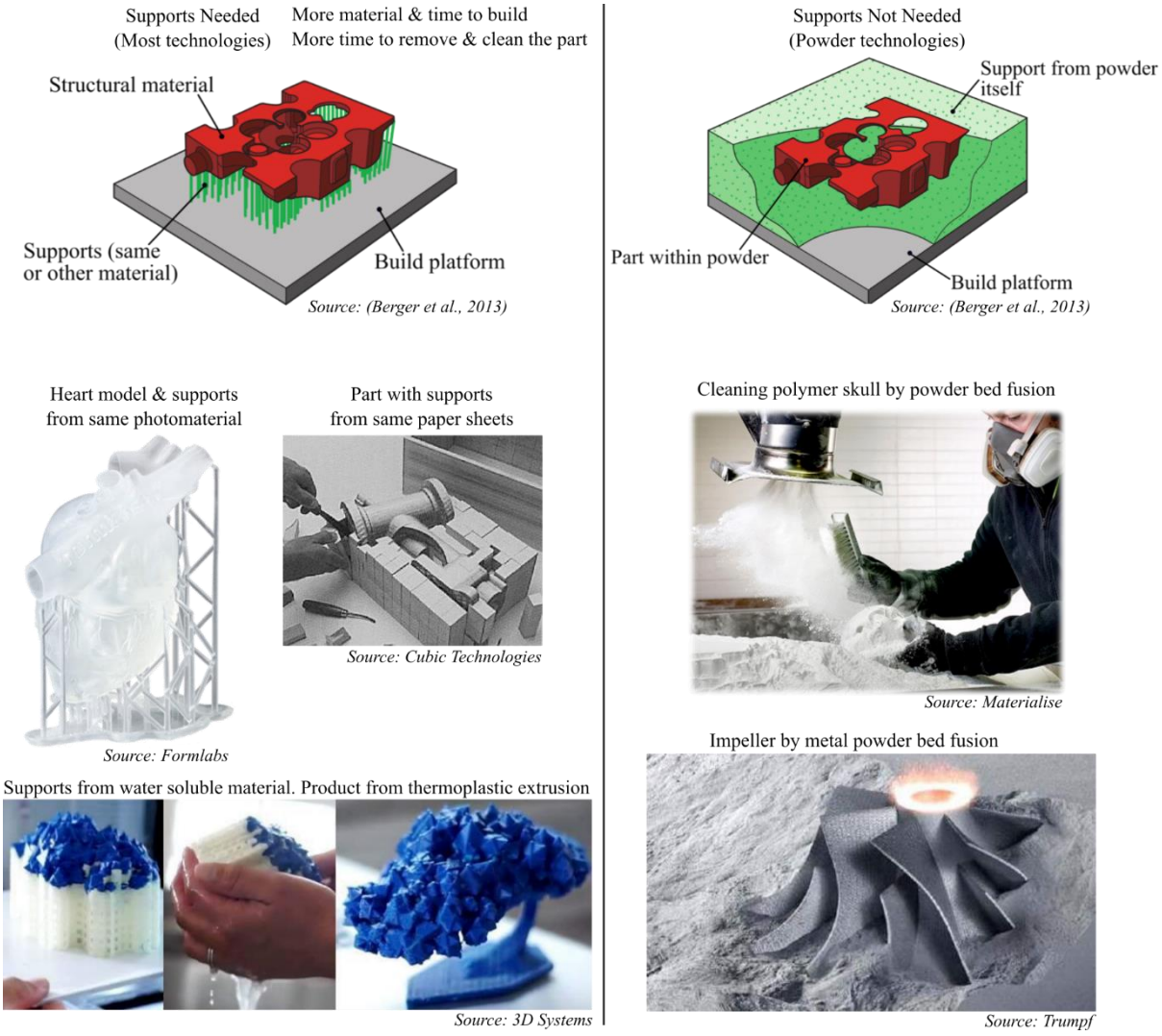

Figure 58: Support types based on 3DP technology

3.3.2 Bibliography

Kruth *(1991)* was the first to conduct a comparative analysis of the available 3DP technologies back in 1991. Later, numerous journal and conference papers, reports, and roadmaps on 3DP were published, reaching eventually a great total number. Such references are included in the 3DP-related books list shown in *Table 3*. The first book was introduced in 1992 but 3DP techniques and machines were described in papers and patents before as will be shown in the following historical *Section*.

Table 3: Book list on 3DP

Book Author/Editor & Year	Title
Jacobs, 1992; 1996 Hilton and Jacobs, 2000	Rapid Prototyping and Manufacturing: Fundamentals of Stereolithography. Stereolithography and Other RP and M Technologies. Rapid Tooling: Technologies and Industrial Applications.
Bjorke, 1992	Layer Manufacturing: A challenge of the Future.
Burns, 1993	Automated Fabrication: Improving Productivity in Manufacturing.
Wood, 1993	Rapid Automated Prototyping: An Introduction.
Kochan, 1993	Solid Freeform Manufacturing.
Johnson, 1994	Principles of computer automated fabrication.
SME, 1994	Rapid Prototyping Systems: Fast Track to Product Realization.
Gebhardt, 2013(First ed. 1995); 2012; 2014 Gebhardt and Hötter, 2016	Generative Additive Manufacturing and 3D Printing. Understanding Additive Manufacturing: Rapid Prototyping, Rapid Tooling, Rapid Manufacturing. Additive Manufacturing: 3D Printing for Prototyping and Manufacturing.
Chua and Leong, 2017 (First ed. 1997); 2015 Chua, Matham and Kim, 2016 Chua, Wong and Yeong, 2017 Chua, Yeong, Low, Tran and Tan, 2021	3D Printing and Additive Manufacturing: Principles and applications. Bioprinting: Principles and Applications. Lasers in 3D Printing and Manufacturing. Standards, Quality Control, and Measurement Sciences in 3D Printing and Additive Manufacturing. 3D Printing and Additive Manufacturing of Electronics.
Bernard and Taillandier, 1998	Le prototypage rapide.
Leu, 2000	Handbook of Rapid Prototyping and Layered Manufacturing.
Pham and Dimov, 2001	Rapid Manufacturing: The Technologies and Applications of Rapid Prototyping and Rapid Tooling.
Cooper, 2001	Rapid Prototyping Technology: Selection and Application.
Lu, Fuh and Wong, 2001	Laser-induced materials and processes for rapid prototyping.
McDonald, Ryall and Wimpenny, 2001	Rapid Prototyping casebook.
Varadan, Jiang and Varadan, 2001	Micro-stereolithography and other Fabrication Techniques for 3D MEMS.
Pique and Chrisey, 2001	Direct-Write Technologies for Rapid Prototyping Applications: Sensors, Electronics, and Integrated Power Sources.
Gibson, 2002; 2005 Gibson, Rosen and Stucker, 2021 (First ed. 2010)	Software Solutions for Rapid Prototyping. Advanced Manufacturing Technology for Medical Applications: Reverse Engineering. Software conversion and Rapid Prototyping. Additive Manufacturing Technologies.
Venuvinod and Ma, 2004	Rapid Prototyping: Laser-based and Other Technologies.
Grimm, 2004	User's Guide to Rapid Prototyping.
Noorani, 2005	Rapid Prototyping: Principles and Applications.
Kamrani and Nasr, 2006	Rapid Prototyping: Theory and Practice.
Hopkinson, Hague and Dickens, 2006	Rapid Manufacturing: An Industrial Revolution for the Digital Age.
Zah, 2006	Economics and Selection of Rapid Manufacturing.
Raja and Fernandes, 2008	Reverse Engineering: An Industrial Perspective.

Liou, 2008	Rapid Prototyping and Engineering Applications: A Toolbox for Prototype Development.
Bartolo and Bidanda, 2008a; 2008b Bartolo, 2011	Stereolithography: Materials, Processes and Applications. Biomaterials and Prototyping Applications in Medicine. Virtual Prototyping and Bio Manufacturing in Medical Applications.
Dahotre and Harimkar, 2008	Laser Fabrication and Machining of Materials.
Wang, Stoll and Conley, 2010	Rapid Tooling Guidelines for Sand Casting.
Bopp, 2010	Value Creation by Rapid Manufacturing.
Ringeisen, Spargo and Wu, 2010	Cell and Organ Printing.
Liebschner, 2010	Computer-Aided Tissue Engineering.
Narayan, Boland and Lee, 2010 Calvert and Narayan, 2011 Narayan, 2020 (First ed. 2013)	Printed Biomaterials: Novel Processing and Modeling Techniques for Medicine and Surgery. Computer Aided Biomanufacturing. Rapid Prototyping of Biomaterials.
Hoque, 2011a; 2011b	Advanced Applications of Rapid Prototyping: Technology in Modern Engineering. Rapid Prototyping Technology: Principles and Functional Requirements.
Breuninger, Becker, Wolf, Rommel and Verl, 2012	Generative Manufacturing via Laser Sintering.
Schmidt and Belegratis, 2013	Laser Technology in Biomimetics.
Berger, Hartmann and Schmid, 2013	Rapid Prototyping, Tooling, and Manufacturing
Hutchings and Martin, 2013	Inkjet Technology for Digital Fabrication.
Forgacs and Sun, 2013	Biofabrication: micro and nano fabrication, printing, patterning and assemblies.
Zhang, Fisher and Leong, 2015	3D Bioprinting and Nanotechnology in Tissue Engineering and Regenerative Medicine.
Bibb, Eggbeer and Paterson, 2015	Medical Modelling: The Application of Advanced Design and Rapid Prototyping Techniques in Medicine.
Atala and Yoo, 2015	Essentials of 3D Biofabrication and Translation.
Turksen, 2015	Bioprinting in Regenerative Medicine.
Gu, 2015	Laser Additive Manufacturing of High-Performance Materials.
Cho, Jang, Lee, Park and Patiet., 2015	Organ Printing.
Bandyopadhyay and Susmita, 2020 (First ed. 2016)	Additive Manufacturing.
Srivatsan and Sudarshan, 2016	Additive Manufacturing: Innovations, Advances, and Applications.
Ozbolat, 2016	3D Bioprinting: Fundamentals, Principles and Applications.
Brandt, 2016	Laser Additive Manufacturing: Materials, Design, Technologies, and Applications.
Dutta and Froes, 2016	Additive Manufacturing of Titanium Alloys: State of the Art, Challenges and Opportunities.
Muthu and Savalan, 2016	Handbook of Sustainability in Additive Manufacturing.
Daly, 2016	Socio-Legal Aspects of the 3D Printing Revolution.
Berg, Van der Hof and Kosta, 2016	3D Printing: Legal, Philosophical and Economic Dimensions.
Wimpenny, Pandey and Kumar, 2017	Advances in 3D Printing and Additive Manufacturing Technologies.
Farooqi, 2017	Rapid Prototyping in Cardiac Disease: 3D Printing the Heart.
Deepak, 2017	3D Printing in Medicine.
Mitchell, 2017	Bioprinting.
Milewski, 2017	Additive Manufacturing of Metals.
Redwood, Schöffer and Garret, 2017	The 3D Printing Handbook: Technologies, Design and Applications.
Rybicki and Grant, 2017	3D Printing in Medicine: A Practical Guide for Medical Professionals.
André, 2017	From Additive Manufacturing to 3D/4D Printing.
Thomas, Jessop and Whitaker, 2017	3D Bioprinting for Reconstructive Surgery.
Killi, 2017	Additive Manufacturing Design, Methods, and Processes.
Bhatia and Ramadurai, 2017	3D Printing and Bio-Based Materials in Global Health.

Yang, Hsu, Baughman, Godfrey, Medina, Menon and Wiener, 2017	Additive Manufacturing of Metals: The Technology, Materials, Design and Production.
Basit and Gaisford, 2018	3D Printing of Pharmaceuticals.
Al'Aref, Dunham, Mosadegh and Min, 2018	3D Printing Applications in Cardiovascular Medicine.
Godoi, Bhandari, Prakash and Zhang, 2018	Fundamentals of 3D Food Printing and Applications.
Zhang and Jung, 2018	Additive Manufacturing: Materials, Processes, Quantifications and Applications.
Gouge and Michaleris, 2018	Thermo-Mechanical Modeling of Additive Manufacturing.
Attene, Livesu, Lefebvre, Funkhouser, Rusinkiewicz, Ellero, Martinez and Bemano, 2018	Design, Representations, and Processing for Additive Manufacturing.
Bian, Shamsaei and Usher, 2018	Laser-Based Additive Manufacturing of Metal Parts: Modeling, Optimization, and Control of Mechanical Properties.
Niaki and Nonino, 2018	The Management of Additive Manufacturing.
Shishkovsky, 2018	Additive Manufacturing of High-performance Metals and Alloys - Modeling and Optimization.
Khademhosseini and Camci-Unal, 2018	3D Bioprinting in Regenerative Engineering: Principles and Applications.
Ovsianikov, Yoo and Mironov, 2018	3D Printing and Biofabrication.
Dipaola and Wodajo, 2019	3D Printing in Orthopaedic Surgery.
Gupta, 2019	3D Printing of Metals.
Tsoulfas, Bangeas and Suri, 2019	3D Printing: Applications in Medicine and Surgery.
Ahmad and Dutta, 2019	3D Printing Technology in Nanomedicine.
Sadasivuni, Deshmukh and Al-Maadeed, 2019	3D and 4D Printing of Polymer Nanocomposite Materials.
Leary, 2019	Design for Additive Manufacturing.
Dutta, Babu and Jared, 2019	Science, Technology and Applications of Metals in Additive Manufacturing.
Froes and Boyer, 2019	Additive Manufacturing for the Aerospace Industry.
Davim, 2019	Additive and Subtractive Manufacturing: Emergent Technologies.
Liou, 2019	Rapid Prototyping and Engineering Applications.
Bar-Cohen, 2019	Advances in Manufacturing and Processing of Materials and Structures.
Kumar, Zindani and Davim, 2019; 2020	Additive Manufacturing Technologies From an Optimization Perspective. Rapid Prototyping, Rapid Tooling and Reverse Engineering: From Biological Models to 3D Bioprinters.
Pei, Monzón and Bernard, 2019	Additive Manufacturing – Developments in Training and Education.
Kumar, Pandey and Wimpenny, 2019	3D Printing and Additive Manufacturing Technologies.
Devine, 2019	Polymer-Based Additive Manufacturing: Biomedical Applications.
AlMangour, 2019	Additive Manufacturing of Emerging Materials.
Afonso, Sousam, Torcato and Pires, 2019	Incremental Forming as a Rapid Tooling Process.
Guvendiren, 2019	3D Bioprinting in Medicine: Technologies, Bioinks, and Applications.
Cho, Kim, Jang, Gao, Han and Singh, 2019	3D Bioprinting: Modeling In Vitro Tissues and Organs Using Tissue-Specific Bioinks.
Cho, 2019	Biofabrication and 3D Tissue Modeling.
Diegel, Nordin and Motte, 2019	A Practical Guide to Design for Additive Manufacturing.
Chen, 2019	Extrusion Bioprinting of Scaffolds for Tissue Engineering Applications.
Ouyang, 2019	Study on Microextrusion-based 3D Bioprinting and Bioink Crosslinking Mechanisms.
Singh, Prakash and Singh, 2020	3D Printing in Biomedical Engineering.
Lamprou, 2020	3D Printing of Pharmaceuticals and Drug Delivery Devices.
Eyers, 2020	Managing 3D Printing.
Guvendiren and Serpooshan, 2020	3D Printing for Tissue Engineering and Regenerative Medicine.
Thomas and Singh, 2020	3D Printing in Medicine and Surgery.
Toit, Kumar, Choonara and Pillay, 2020	Advanced 3D-Printed Systems and Nanosystems for Drug Delivery and Tissue Engineering.
Friedrich and Walter, 2020	Structure and Properties of Additive Manufactured Polymer Components.
Yan, Shi, Zhaoqing, Wen and Wei,2020	Selective Laser Sintering Additive Manufacturing Technology.

Srivastava, Rathee, Maheshwari and Kundra, 2020	Additive Manufacturing: Fundamentals and Advancements.
Celik, 2020	Additive Manufacturing: Science and Technology.
Kumar, 2020	Additive Manufacturing Processes.
Leach and Carmignato, 2020	Precision Additive Metal Manufacturing.
Balasubramanian and Senthilkumar, 2020	Additive Manufacturing Applications for Metals and Composites.
Marques, Esteves, Pereira and Oliveira, 2020	Additive Manufacturing Hybrid Processes for Composites Systems.
Fisher, 2020	Additive Manufacturing of Metals.
Gokuldoss, 2020	Selective Laser Melting: Materials and Applications.
Chen, 2020	3D Printing and Ubiquitous Manufacturing.
Shunmugam and Kanthababu, 2020	Advances in Additive Manufacturing and Joining.
Nicolantonio, Rossi and Alexander, 2020	Advances in Additive Manufacturing, Modeling Systems and 3D Prototyping.
Crook, 2020	3D Bioprinting: Principles and Protocols.
Dave and Davim, 2021	Fused Deposition Modeling Based 3D Printing.
Singh, Prakash and Ramakrishna, 2021; 2022	Additive Manufacturing: Foundation Knowledge For The Beginners. Innovative Processes and Materials in Additive Manufacturing.
Yang, Lee and Vida, 2021	Cardiovascular 3D Printing: Techniques and Clinical Application.
Heinrich, 2021	3D Printing of Optical Components.
Suri, Tsioukas and Papadopoulos, 2021	3D Printing: Applications in Medicine and Surgery Volume 2.
Yang, Na, Shi, Tang, G. Zhang and F. Zhang, 2021	Multimaterial 3D Printing Technology.
Wake, 2021	3D Printing for the Radiologist.
Manjaiah, Raghavendra, Balashanmugam and Davim., 2021	Additive Manufacturing: A Tool for Industrial Revolution 4.0.
Pou, Riveiro and Davim, 2021	Additive Manufacturing.
Shi, Yan, Zhou, Wu, Wand, Yu and Ying, 2021	Materials for Additive Manufacturing.
Kumar, Voicu and Thakur, 2021	3D printable Gel-inks for Tissue Engineering.
Toyserkani, Sarker, Ibhadode, Liravi, Russo and Taherkhani, 2021	Metal Additive Manufacturing.
Ladani, 2021	Additive Manufacturing of Metals: Materials, Processes, Tests, and Standards.
Singh and Hussain, 2021	Additive Manufacturing with Functionalized Nanomaterials.
Gibbons, 2021	Additive Manufacturing of Metals.
Sing and Yeong, 2021	Process–Structure–Properties in Polymer Additive Manufacturing.
Leach and Carmignato, 2021	Precision Metal Additive Manufacturing.
Lancaster, Fortunato and Kolisnychenko, 2021	3D Printing of Non-Metallic Materials.
Song, Wen, Yan, Wei and Shi, 2021	Selective Laser Melting for Metal and Metal Matrix Composites.
Yan, Hao, Yang, Young, Z. Li and Y. Li, 2021	Triply Periodic Minimal Surface Lattices Additively Manufactured by Selective Laser Melting.
Yadroitsev, Yadroitsava, Plessis and MacDonald, 2021	Fundamentals of Laser Powder-bed Fusion of Metals.
Douglas, 2021	Bioprinting: To Make Ourselves Anew.
Rybicki, 2021	3D Printing in Medicine and Its Role in the COVID-19 Pandemic.
Sharma, Subburaj, Sandhu and Sharma, 2021	Applications of 3D printing in Biomedical Engineering.
Tayebi, Masaeli and Zandsalimi, 2021	3D Printing in Oral & Maxillofacial Surgery.
Kang, 2021	Clinical Atlas of 3D Printing Bone Reconstruction.
Kirihara and Nakata, 2021	Multi-dimensional Additive Manufacturing.
Rangappa, Gupta, Siengchin and Song, 2021	Additive and Subtractive Manufacturing of Composites.
Kasper, Egger and Lavrentieva, 2021	Basic Concepts on 3D Cell Culture.
Kalaskar, 2022	3D Printing in Medicine.
Podsiadły, 2022	Polymers for 3D Printing.
Zhang, Leong and Fisher, 2022 (First ed. 2015)	3D Bioprinting and Nanotechnology in Tissue Engineering and Regenerative Medicine.

Singh, 2022	4D Printing: Fundamentals and Applications.
Conti and Marino, 2022	Bioprinting: From Multidisciplinary Design to Emerging Opportunities.
Menezes, Misra and Kumar, 2022	Tribology of Additively Manufactured Materials.
Sandhu, Singh, Prakash, Subburaj and Ramakrishna, 2022	Sustainability for 3D Printing.
Weißenfels, 2022	Simulation of Additive Manufacturing using Meshfree Methods.
Kumar, 2022	Additive Manufacturing Solutions.
Salunkhe, Hussein and Davim, 2022	Applications of Artificial Intelligence in Additive Manufacturing.
Sandhu, Singh, Prakash, Sharma and Subburaj, 2022	Emerging Applications of 3D Printing During CoVID 19 Pandemic.
Khan and Jappes, 2022	Innovations in Additive Manufacturing.
Godec, Gonzalez-Gutierrez, Nordin, Pei and Alcázar, 2022	A Guide to Additive Manufacturing.

The interest in searching the terms *"Additive Manufacturing"* and *"3D Printing"* in Google engine and the total unfiltered annual accenting number of papers listed on Scopus for 3D Printing-related terms are graphically shown in *Figure 59* and *Figure 60* respectively.

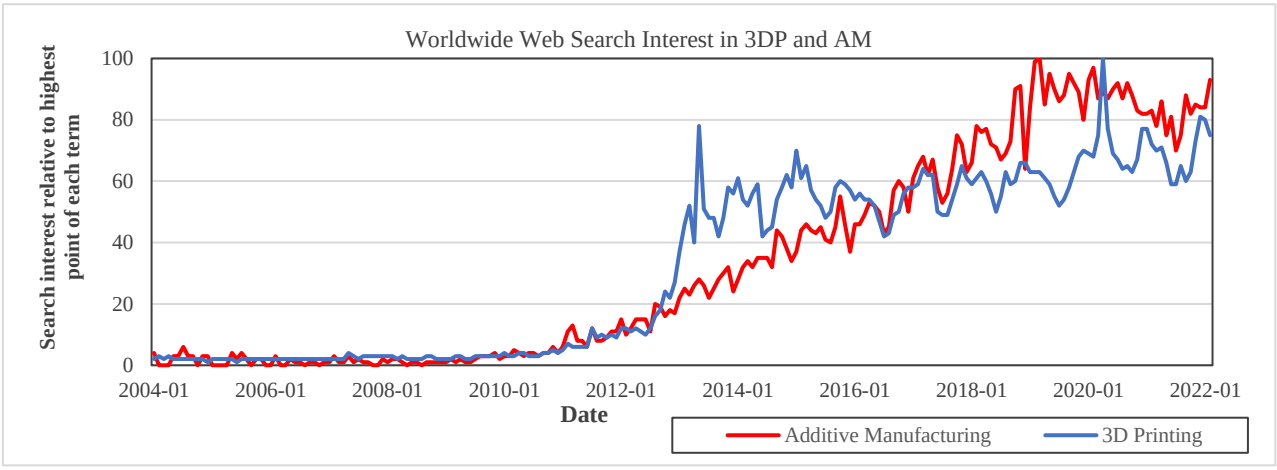

Figure 59: Web search interest of AM and 3DP terms. Source: Google Trends

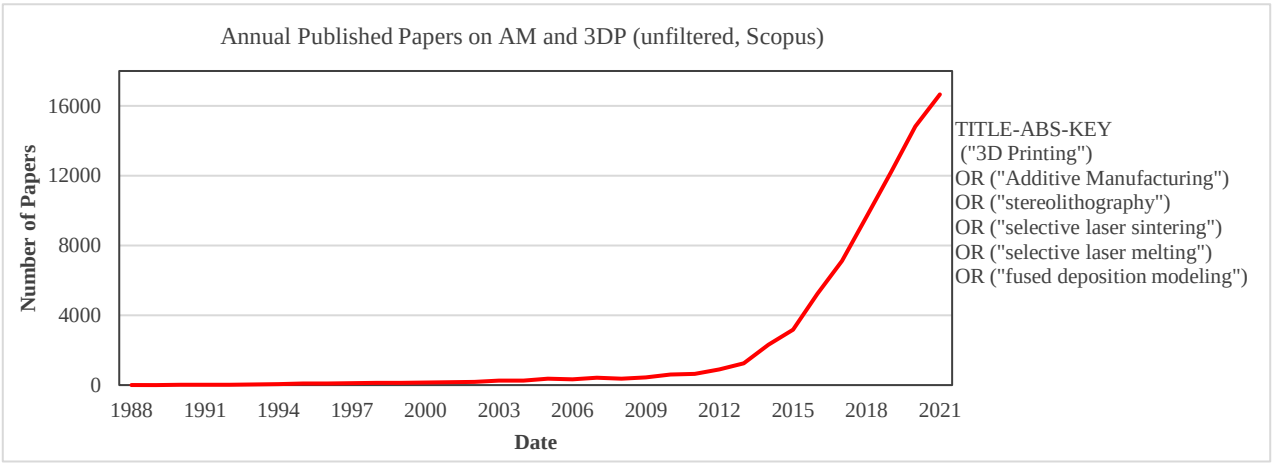

Figure 60: Annually published papers related to AM and 3DP listed on Scopus (unfiltered)

3.3.3 Historical Background

Growing parts layer-wise or spatially by selective material addition is not a new concept. In fact, this is how natural structures emerge and the philosophy behind the creation of biological organisms and living things.

Routes of modern 3DP technologies can be traced back to the days when structures like pyramids were formed. Indeed, this additive concept is utilized for the construction of every building today. Searching the literature and especially the worldwide patent databases, one can find plenty of concepts and machines for fabricating tangible 3D products by adding material instead of subtracting or using molds. Beaman et al. *(1977)* have shown that topographic and photo-sculpturing methodologies contributed and led to the introduction and development of modern 3DP machines.

The idea behind topographic maps is the use of isolines (contour lines), with each corresponding to a certain height. Blanther *(1892)* used this approach and described a method for producing relief maps by cutting the contour lines of a given terrain out of wax sheets. By stacking and joining the positive layers, a relief map emerges, whereas the negative layers can be used to compose a mold for making paper copies *(Figure 61)*.

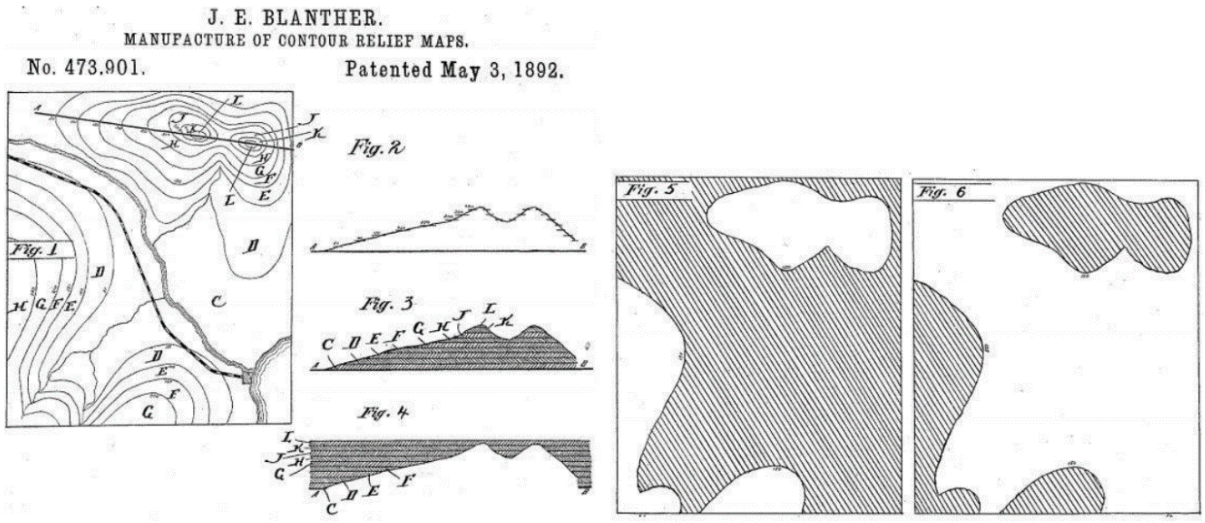

Figure 61: Topographic relief map. Source: (Blanther, 1892)

Similar topographic relief maps were also developed by Perera *(1940)* with paper sheets, Zang *(1964)* with transparent sheets within which topographic information is drawn and opaque sheets are interposed, and Gaskin *(1973)* who mentioned a geological device with removable parts to enable the presentation of the interior structure. Matsubara *(1974)* explained the use of photo-hardening polymers to make such parts: a mixture of photo-sensitive polymers and refractory powders (graphite, sand) is heated to form a layer, suitable light source selectively cures areas of each layer, and a solvent is used to remove the non-irradiated material. The contour layers are stacked and joined to form the 3D geometry.

Photo sculpturing is a technology developed during the mid-19th century for making 3D tangible copies of models with the aid of photographic machines and projectors. Their principles remind the modern reverse engineering techniques. Willeme *(1864)* applied two such operations. The first involved 24 photographic machines equally distributed around the model to be sculpted. Based on these 24 photographs, an artist sculpted every 1/24 of the model out of a material block. The second

method also required simultaneous multi-photography, but the 3D part emerged by stacking and joining sheets that were cut along the outlines of the model *(Figure 62)*.

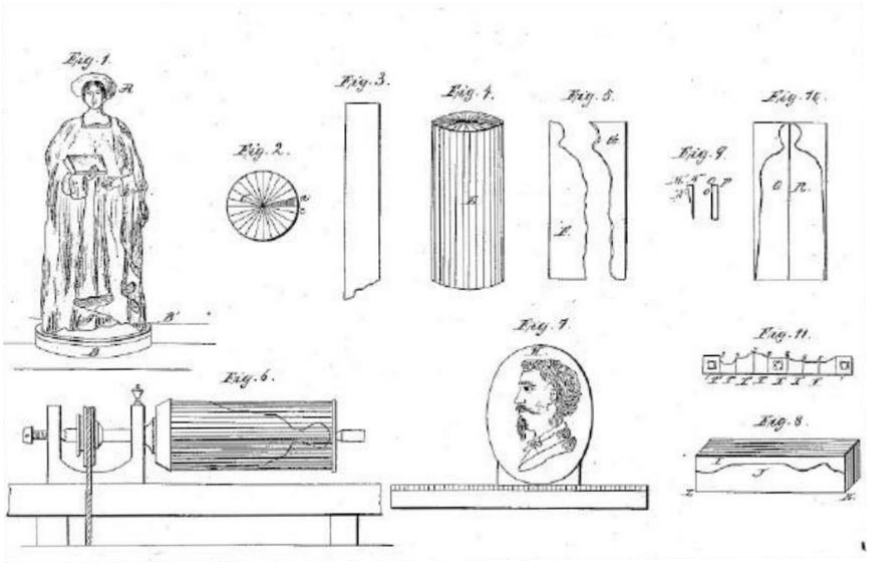

Source:US Patent No.43822, 1864

Source:George Eastman House

Figure 62: Willeme's 2nd photo-sculpturing method

Improved look-alike processes but with the projection of the model's photographs on the material to be sculpted were proposed by Smith *(1908)* and Heise *(1925)*, whereas Morioka *(1929)* described a series of such photographic and layer-wise techniques. Photo-chemical approaches with photo-sensitive materials and light sources were mentioned by Baese *(1904)* and later by Monteath *(1924)*.

Numerous authors described techniques for making laminated parts manually, e.g. Peacock *(1899)* for horseshoes, Palais *(1932)* for toys, Kojima *(1959)* for furniture, Frontera *(1967)* for artistic figures, Abbott *(1972)* for plastic propellers, J. Kirk and L. Kirk *(1976)* for decorative parts. DiMatteo *(1976)* wrote that by stacking layers, with each corresponding to a cross-section of the product to be formed, complex 3D geometries can be realized that are difficult or impossible by conventional manufacturing techniques, e.g. propellers, tools, and molds. He described a device for drawing the outlines of a model on sheets, that are then cut by mechanical or not means, stacked, and joined by glue or bolts to form a positive or negative (mold) shape.

Nakagawa *(1976)* showed that metal sheets can be utilized to produce various laminated forming tools *(Figure 63)* to be used in traditional shaping techniques. He used this approach to make molds with embedded cooling channels as well *(Himmer, Nakagawa and Anzai, 1999)*.

Systems for forming walls by concrete mixture deposition proposed by Kay *(1924)*, Urschel *(1943)*, and Ahart *(1951)*, as well as concepts like Reed's *(1958)* for producing circular walls by adding bricks and concrete layer-by-layer, share the same foundations as modern 3DP machines. Baker *(1925)*, mentioned the use of electric arc welding for shaping 3D parts layer-by-layer, whereas Ujjie *(1971)* for forming cylindrical tubes. Later, Brown et al. *(1982)* reported a technique for repairing and forming parts by metal powder or wire deposition with simultaneous melting by an

electric arc, laser beam or other means. Similar operations were proposed by Bronowski *(1986)*, Edmonds and McAnich *(1988)*, and others mainly from the aerospace and automotive sectors.

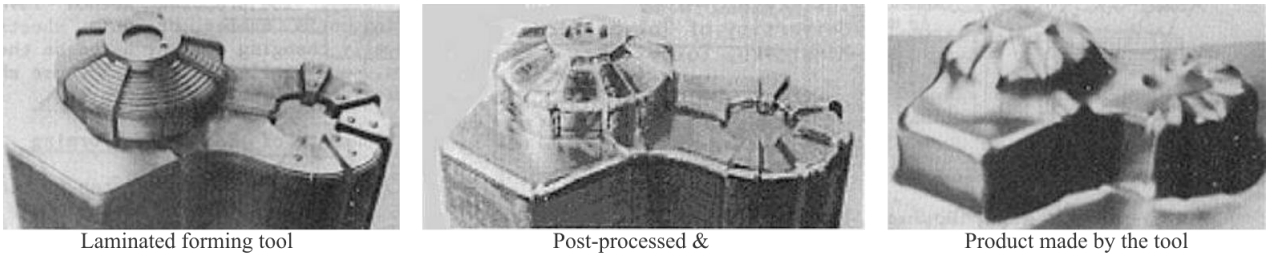

Figure 63: Nakagawa's laminated forming tool. Source: (Nakagawa ,1976)

Munz *(1956; 1968)* developed two interesting 3DP machines *(Figure 64)*. The first utilized a special photo-sensitive emulsion that is spread over a piston and selectively irradiated and hardened by a scanning system. Once a cross-sectional layer is formed, the piston is lowered, a new coat of emulsion is introduced and the process is repeated until the final 3D shape is grown inside the cylinder. The second machine operated under a similar principle; a thermoplastic material (structural) is extruded in a layer-by-layer manner through an orifice and a second material is incorporated to support the structural.

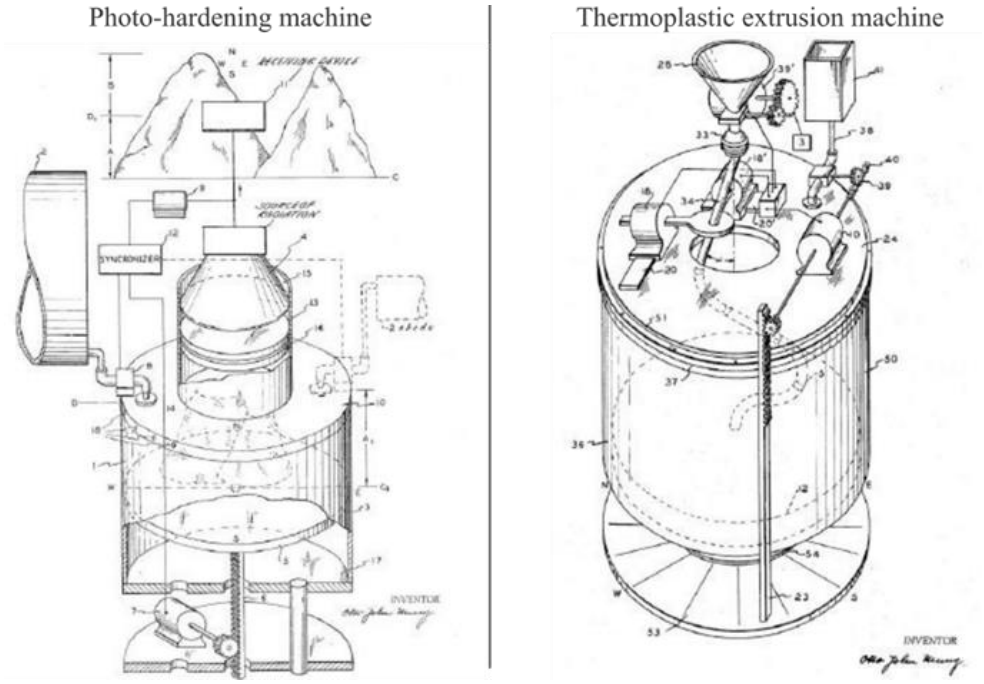

Figure 64: Munz's machines. Source: (Munz, 1956; Munz, 1968)

Ciraud *(1973)* mentioned a system for processing powder materials *(Figure 65)* where grains are deposited by gravity, magnetically, electrostatically, or jetted by an orifice whilst thermal energy (laser, electron beam, plasma) fuses them.

Swainson *(1971)* and researchers from the Battelle Memorial Institute laboratories *(Adamson, 1977; Schwerzel et al., 1984)* tried to develop systems capable of solidifying special fluid materials inside a vat. The material is selectively cured at the points where two laser beams interfere, hence, 3D parts can emerge either spatially or layer upon layer.

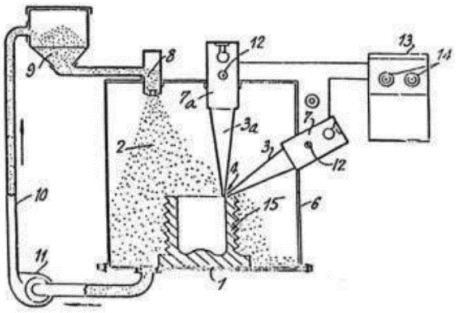

Figure 65: Ciraud's powder jetting system. Source: (Ciraud, 1973)

Housholder *(1981)* demonstrated two 3DP concepts *(Figure 66)*. The first processed and fused powder materials: the bed was coated with powder and selectively irradiated with focused thermal energy to fuse the grains. Masks with openings according to the shape of each cross-sectional layer or a scanning laser beam can be used. Once a layer has been fused, the bed moves down, new powder is introduced, and the process is repeated for all cross-sectional layers. Finally, the non-irradiated powder is removed and the part is received. The other system was based on material extrusion: two orifices were used to extrude one structural and one support material within the cells of a mesh. Once a layer is completed, the bed lowers and the process is repeated for all the other layers.

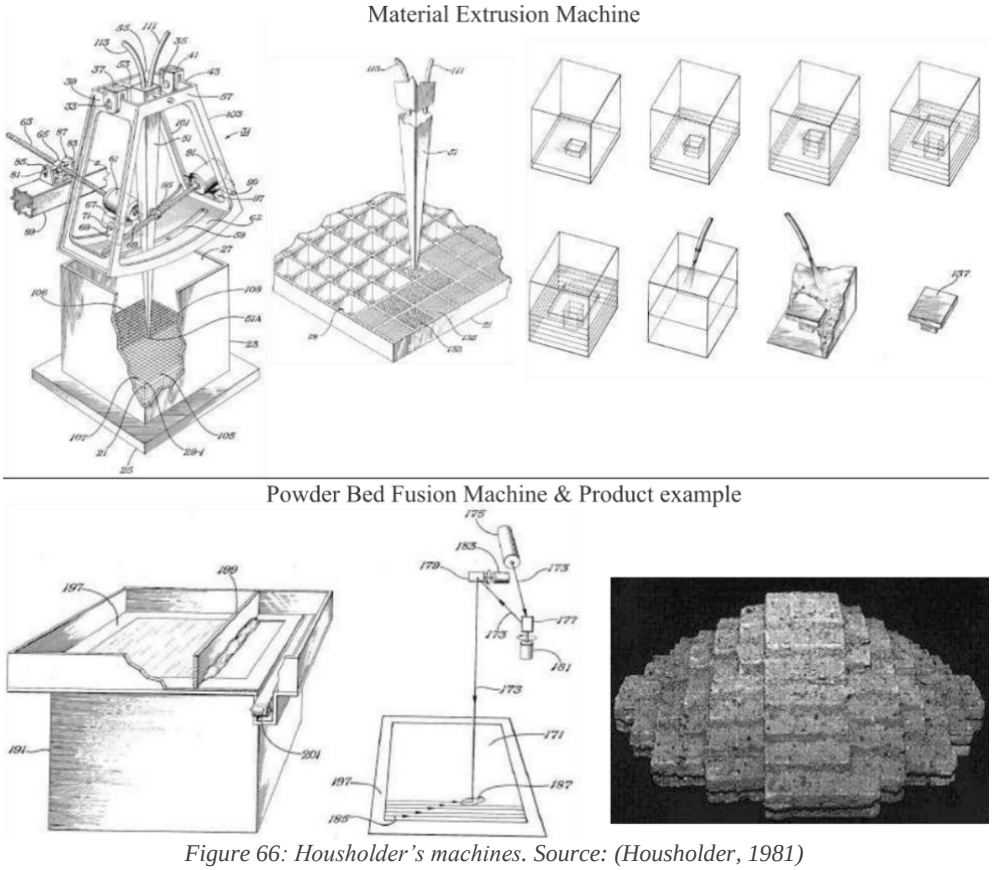

Figure 66: Housholder's machines. Source: (Housholder, 1981)

Kodama *(1980; 1981)* from Nagoya Municipal Industrial Research Institute developed a photo-polymer curing system to make 3D products. The main system operated as follows: the surface of the photo-polymer was selectively irradiated with ultra-violet radiation generated by Hg or Xn lamps, and hardened. Once a layer is formed, the platform where the part grows is moved down within the

photo-polymer and the process is repeated until the 3D geometry emerges. The use of masks and lamps from above or below the vat, or a scanning optical fiber also proposed *(Figure 67)*.

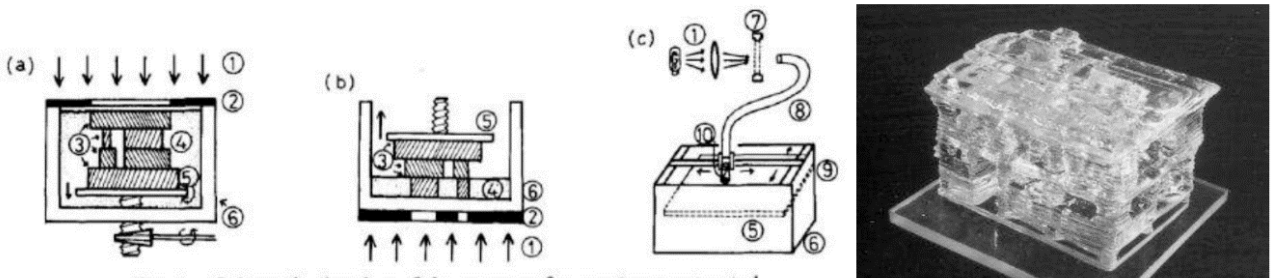

FIG. 1. Schematic sketches of three types of apparatus constructed in the present work. In this Fig. ① ultraviolet rays ② mask ③ solidified layers ④ liquid photo-hardening polymer ⑤ movable plate ⑥ receptacle ⑦ shutter ⑧ optical fiber ⑨ *XY* plotter and ⑩ optical lens. Exposure and shift of the movable plate is repeated in turn, and the solid model is grown on or under the plate.

Figure 67: Kodama's layer photo-polymerization approaches and product. Source: (Kodama, 1980)

Several photo-polymerization systems were later developed by:

- Herbert *(1982)* from 3M Graphic Technologies Sector Laboratory used an Ar laser beam and a scanning system to irradiate the photo-polymer. The part sits at the bottom of the vat and once a layer is cured, the whole vat is lowered, new material is added, and the process is repeated *(Figure 68)*. Herbert later published a review of such systems *(Herbert, 1989)*.

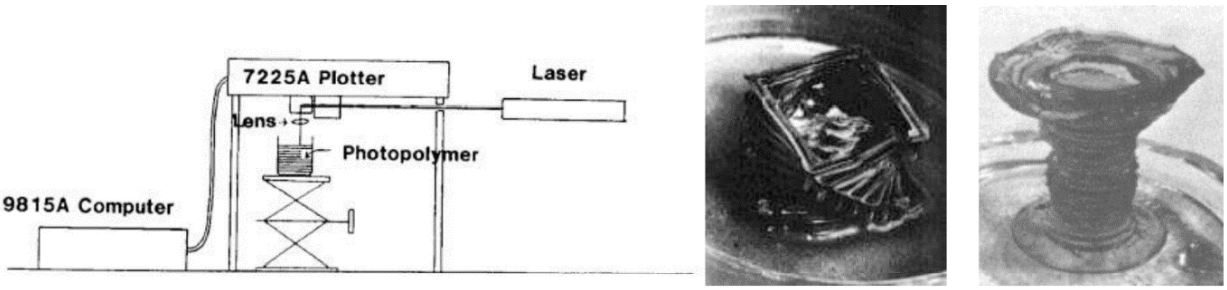

Figure 68: Herbert's photo-polymerization apparatus and product. Source: (Herbert, 1982)

- Marutani *(1985)* from Osaka Prefectural Industrial Research Institute used an optical fiber immersed in the photo-polymer to guide ultra-violet light *(Figure 69)*. This approach can achieve forms both layer-by-layer and spatially. Later, he published a series of papers regarding photo-polymerization techniques *(Nakai and Marutani, 1986; Marutani, 1990)* and helped Mitsubishi CMET to introduce the Solid Object Ultraviolet Laser Plotting (SOUP) machine.

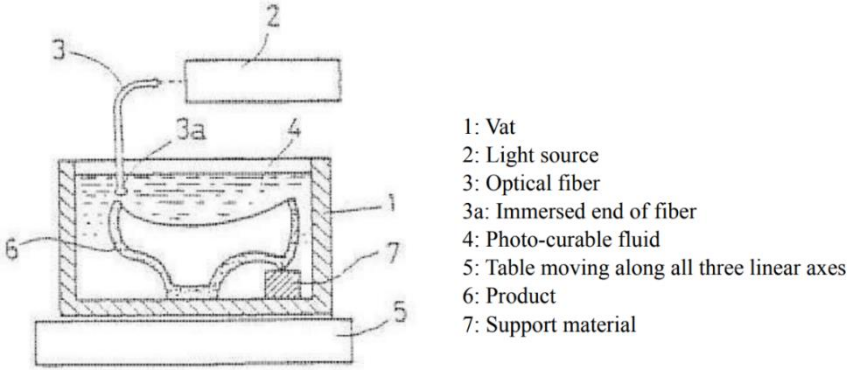

Figure 69: Marutani's photo-polymerization apparatus. Source: (Marutani, 1985)

- Andre from French National Center for Scientific Research, and Witte and Mehaute from Cilas-Alcatel *(1984)* presented fiber and optical-based systems *(Figure 70)*, later commercialized by Laser3D as StereoPhotoLithography (SPL) *(Allanic, Medard and Schaeffer, 1992).*

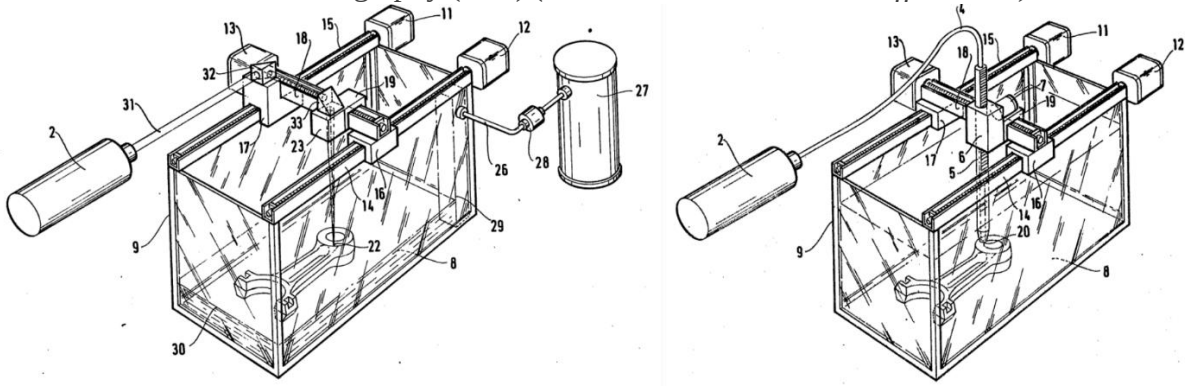

Figure 70: Andre's photo-polymerization systems. Source: (Andre, Witte and Mehaute, 1984)

- Hull *(1986)* from Ultraviolet Products described the Stereolithography technology and four possible machine configurations. He founded 3D Systems (3D Systems Inc., California, US) in 1986 and introduced the first-ever commercial 3DP machine called SLA-1 (StereoLithography Apparatus) *(Hull and Lewis, 1991) (Figure 71):* a HeCd laser beam was guided by a galvanometer driven dynamic mirror and scanned the surface of an acrylic based photo-polymer. The material was hardened and the operation was repeated for all cross-sectional layers. The part was received and introduced into a UV furnace for complete hardening. The basic process flow chain presented by 3D Systems is used today by the majority of 3DP technologies *(Figure 73).*

Masters *(1987)* mentioned a system for selectively jetting particles or molten material by a nozzle having three or more degrees of kinematic freedom. Thus, a 3D geometry can be formed either layer-wise or spatially. He founded Perception Systems in 1988 (renamed to BPM Technology (not in business), called the technology Ballistic Particle Manufacturing (BPM) *(Menhennett and Brown, 1996)*, and commercialized the Personal Modeler: a 5-axis thermoplastic jetting machine *(Figure 72)*.

In the late 80s, more laser scanning photo-polymerization systems were developed and commercialized worldwide: Solid Object Ultraviolet Laser Plotting (SOUP) by CMET (CMET Co. Ltd, Kanagawa, Japan), Solid Creation System (SGS) by D-MEC (D-MEC Ltd, Tokyo, Japan) (not in business), Solid Modeling System (SOMOS) DuPont (DuPont de Nemours Inc., Delaware, US) (product not in the market now), STEREOS by Electro Optical Systems (EOS Gmbh, Krailling, Germany) (product not in the market now). Light Sculpting's Design-Controlled Automated Fabrication (not in business) *(Fudim, 1988)* and Cubital's (Cubital Ltd, Ra'anana, Israel) (not in business) Solider *(Pomerantz et al., 1990)* used masks and UV lamps for layer projection instead of laser point scanning. Helisys (Helisus Inc., California, US) (not in business) introduced a paper sheet lamination-based technology called Laminated Object Manufacturing (LOM) *(Feygin, 1988)*, Stratasys (Stratasys Ltd, Minnesota, US) a polymer material extrusion machine based on Fused

Deposition Modeling (FDM) technology *(Crump, 1992),* Desk Top Manufacturing (DTM) (not in business) a powder-bed fusion based technology called Selective Laser Sintering (SLS) *(Deckard, 1989),* and Sachs et al. *(1993)* developed a binder jetting technology named 3D Printing that was later licensed to a series of companies. During the 90s and till nowadays, a vast number of 3DP technologies, materials, and machines appeared in the market *(Wohlers Associates, 2021a; Wohlers and Gornet, 2021),* and a plethora of associated patents have been granted, the annual number of which is growing as can be seen from the online Google Patents engine that searches through patent offices worldwide.

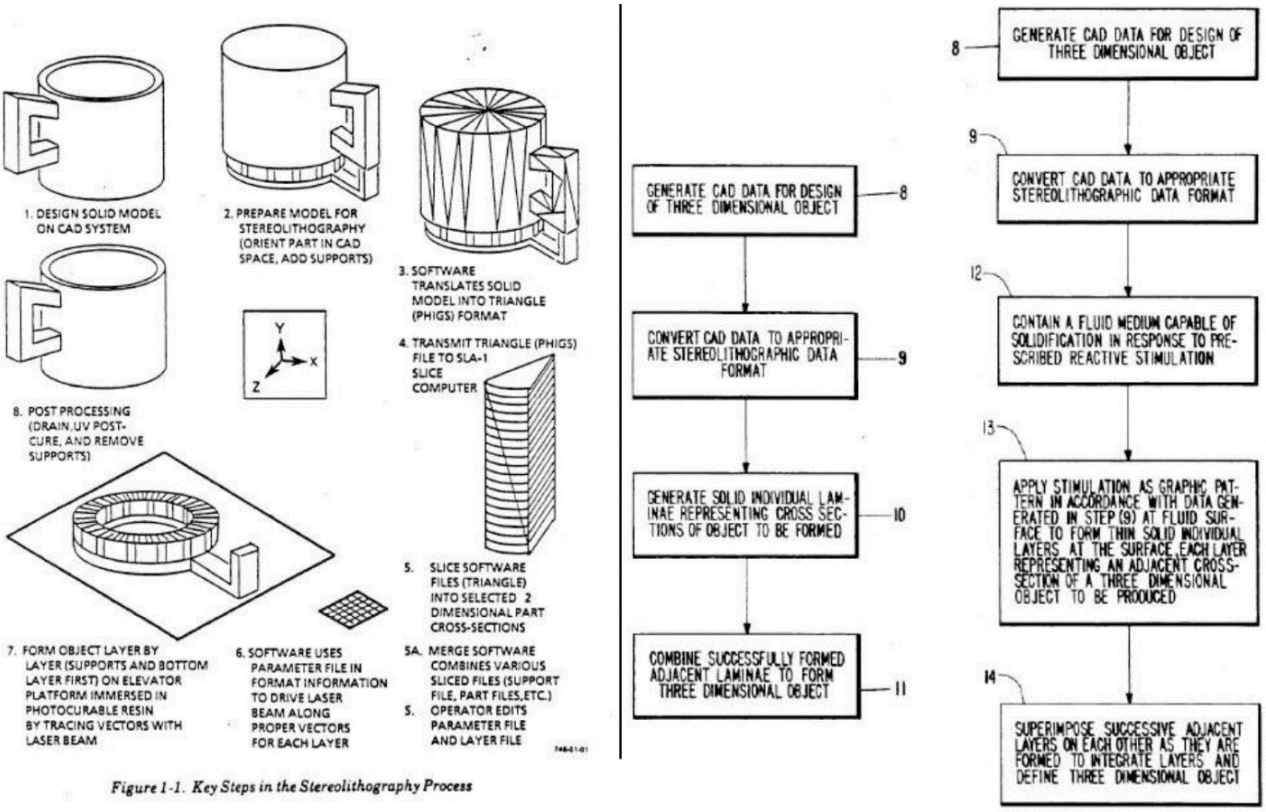

Figure 71: 3D Systems SLA-1 machine. Source: (Hull and Lewis, 1991)

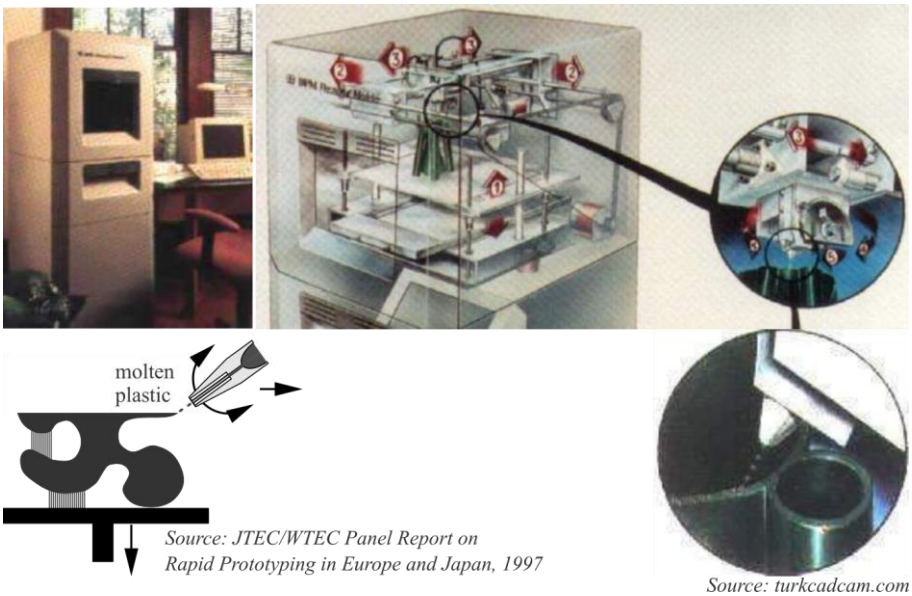

Figure 72: BPM Technology Personal Modeler

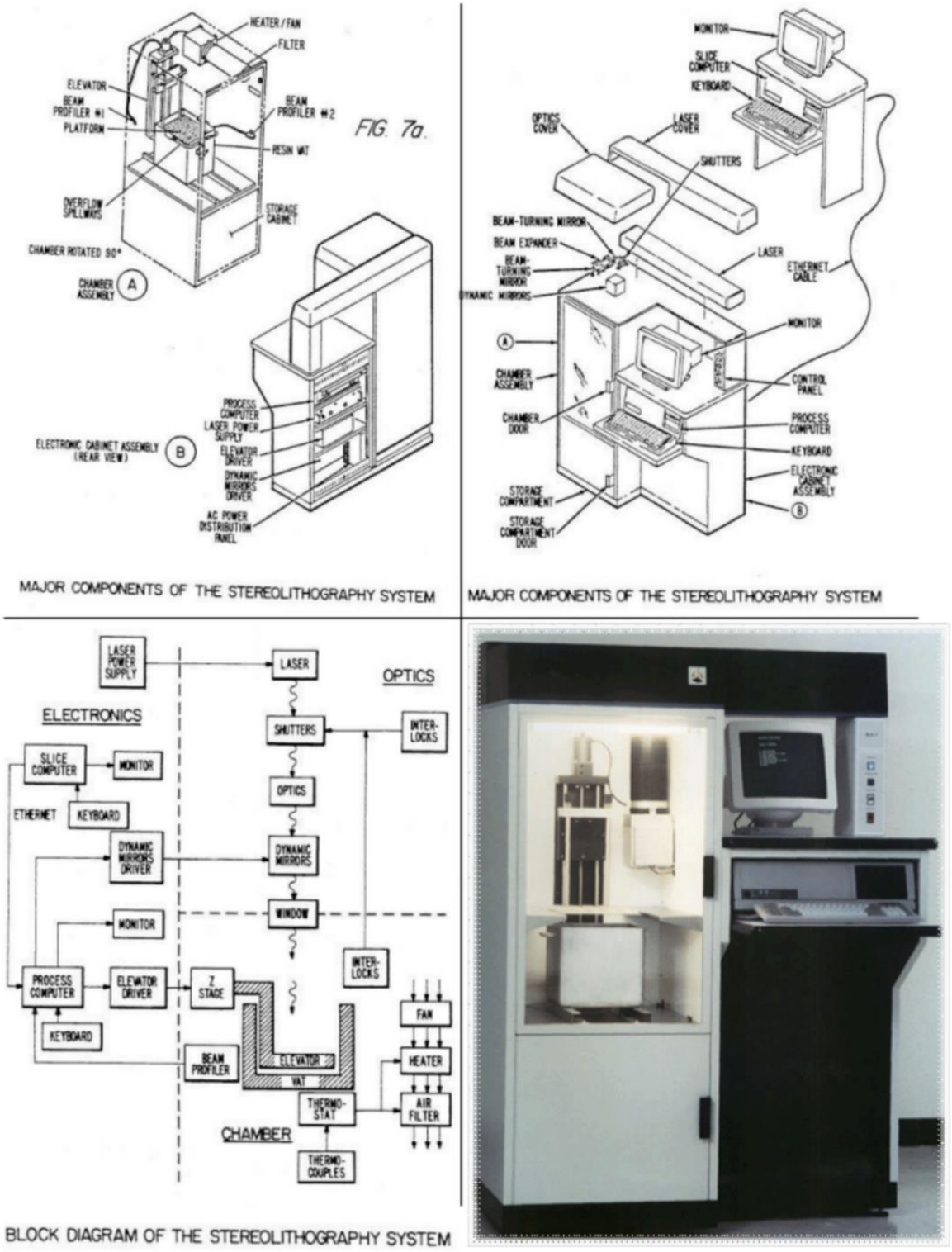

Figure 73: Process flow chain for SL. Source: (Hull and Lewis, 1991)

3.3.4 3D Printing Technologies

Single-step or multi-step 3DP *(Appendix G)* is utilized to materialize any form out of various material states, and a plethora of material suppliers, 3D printer manufacturers, post-processing services, and design software vendors compose the corresponding market landscape (*Appendix I*).

3DP technologies can be classified based on several criteria *(Kruth, 1991)*. Classifications of 3DP mechanisms for different materials and states are shown in *Figure 74*.

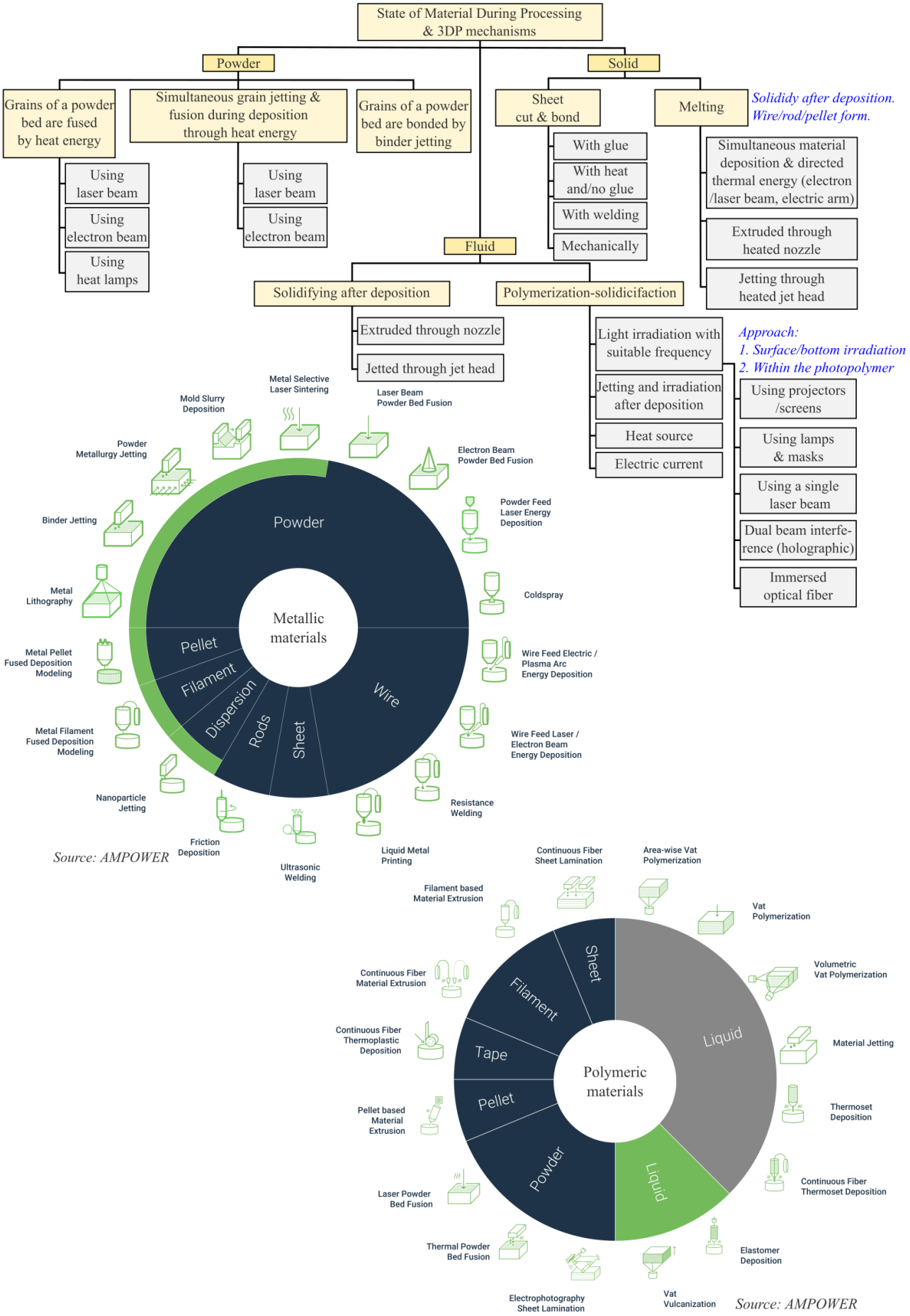

Figure 74: Classifications of 3DP mechanisms for different materials and states

ISO/ASTM *(2021)* categorizes 3DP into the following seven main teams:

1. **Binder Jetting (BJ):** a liquid bonding agent (glue) is selectively jetted and deposited on sand, polymer, metal, composite, or ceramic powders to join their grains *(Figure 75)*. For metals and ceramics further sintering and infiltration are required *(Appendix G)*. The powder itself supports the part and there are no thermal and mechanical influences to distort the shape.

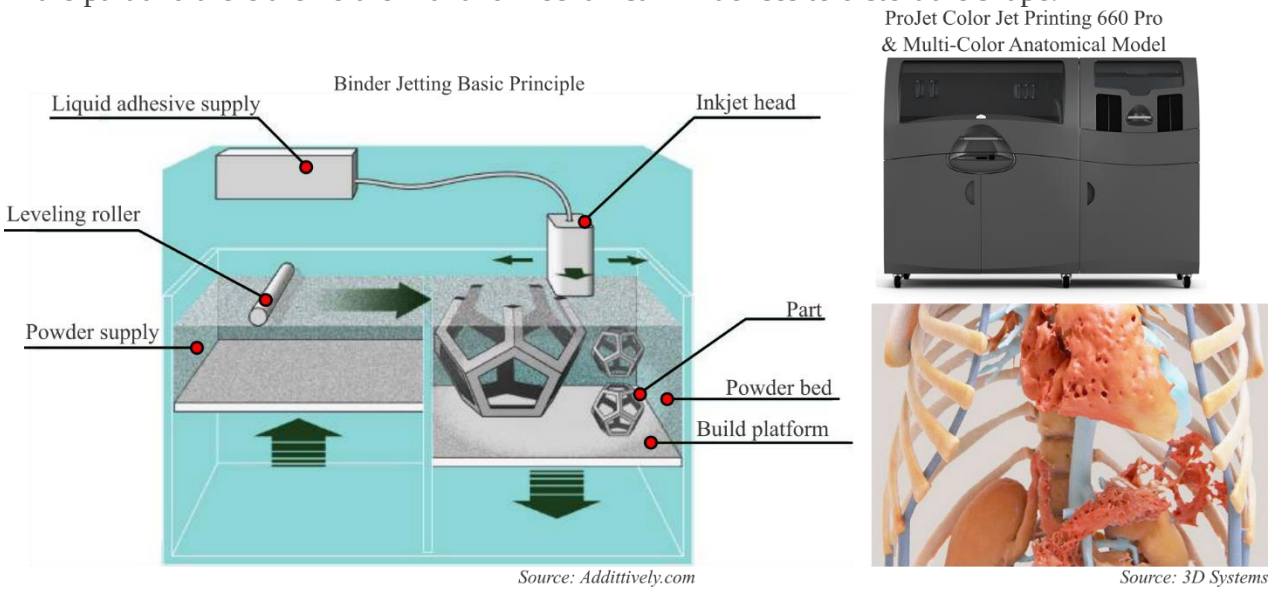

Figure 75: Binder Jetting principle, example machine, and product

2. **Directed Energy Deposition (DED):** focused thermal energy (electric arc, laser, electron beam, plasma) fuses the wire or powder material by melting it while it is being selectively deposited *(Figure 76)*. This approach was initially used for coating and repairing, then for shaping parts. Such hybrid additive-subtractive arrangements also exist *(Flynn et al., 2016)*.

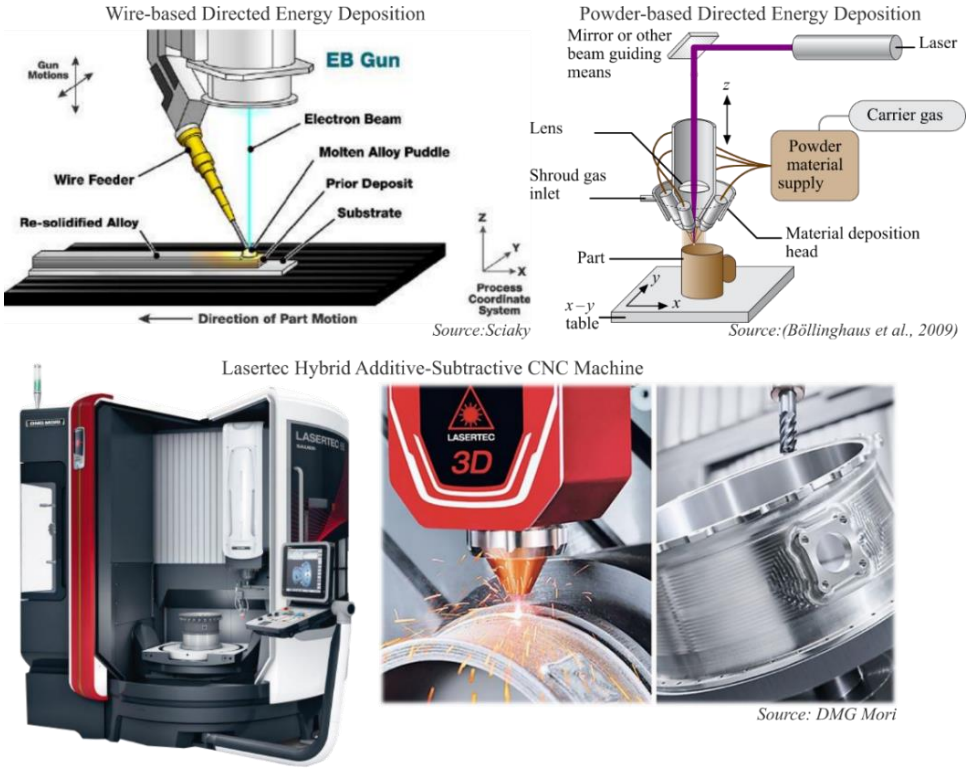

Figure 76: Directed Energy Deposition principle, example machine, and product

3. **Material Extrusion (ME):** polymers, low-temp metals, composites, and viscous liquids (slurries, gels) are selectively extruded and deposited on a build platform through one or more nozzles. A well-known extrusion process is the Fused Filament Fabrication (FFF) during which a thermoplastic filament is heated and extruded *(Figure 77)*. If support structures are needed, these are made from the same structural or secondary different material.

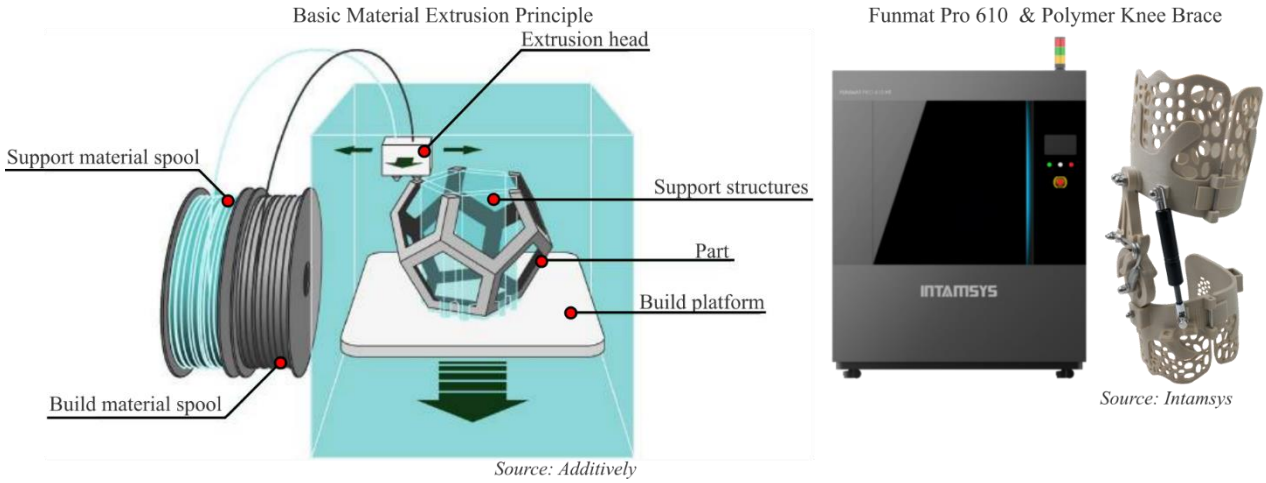

Figure 77: Material Extrusion principle, example machine, and product

4. **Material Jetting (MJ):** polymers, photo-polymers (extra photo-polymerization required), waxes, composites, inks, or metal droplets are selectively jetted and deposited on a build platform *(Figure 78)*. Support structures are made from the same structural or secondary different material.

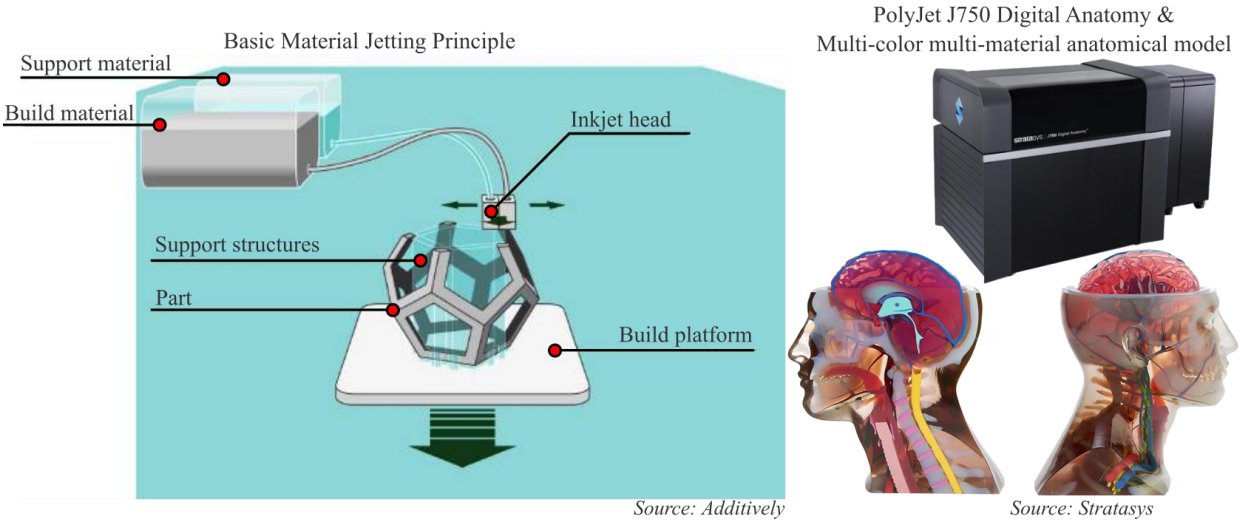

Figure 78: Material Jetting principle, example machine, and product

5. **Powder-bed Fusion (PBF):** thermal energy (e.g. laser or electron beam *(Figure 79)*) selectively fuses the grains of the polymer, metal, ceramic, or composite powder-bed. Support structures are required only for metal parts to avoid distortions.
6. **Sheet Lamination (SL):** paper, polymer, metal, ceramic or composite sheets are formed/cut, stacked, and bonded together *(Figure 80)*. The sheets can be formed/cut and then bonded or vice versa. Usually, the sheets themselves support the part.

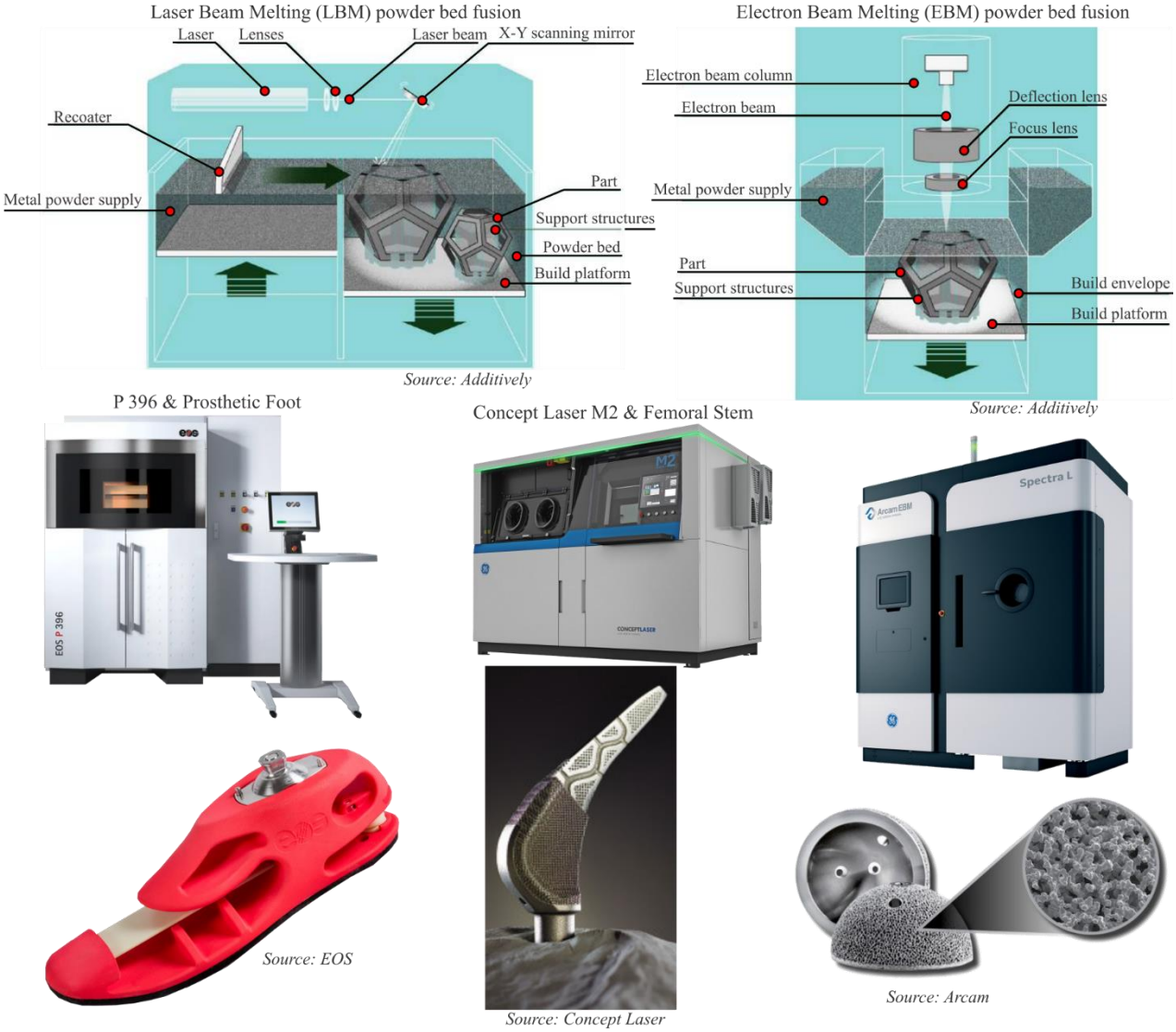

Figure 79: Powder-bed Fusion principle, example machines, and products

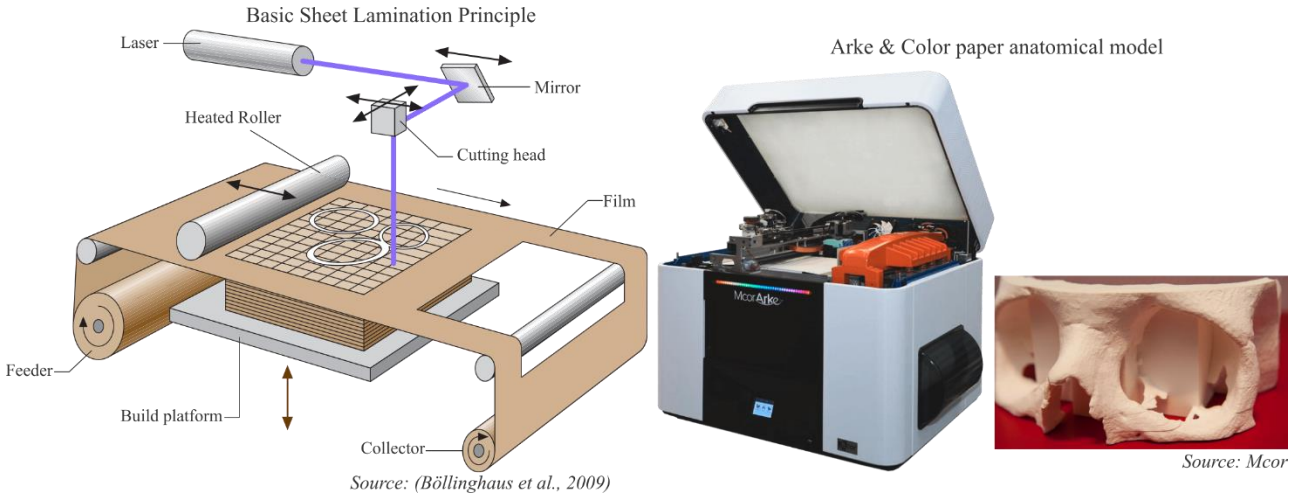

Figure 80: Sheet Lamination principle, example machine, and product

7. **Vat Photo-polymerization (VP)**: liquid photo-polymer, ceramic, or composite materials are selectively solidified by suitable light radiation beam: scanning *(Figure 81)* or whole layer projection/mask system being above (surface processing) or below the vat (processing starts from

the bottom). The process can also take place within the material by laser interference or by an immersed optical fiber. Support structures are required to avoid distortion of the part's shape.

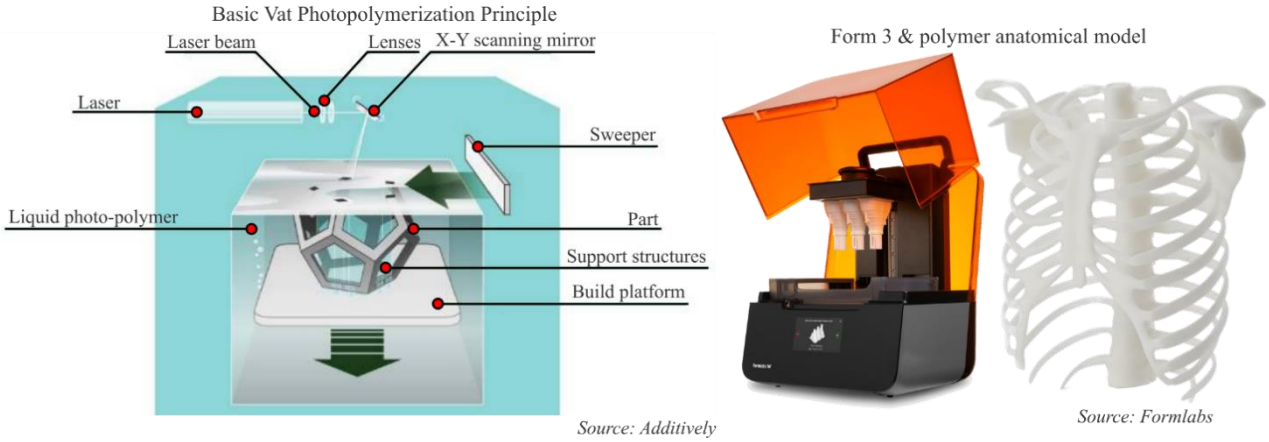

Figure 81: Sheet Lamination principle, example machine, and product

Figure 84 illustrates in-process example photos for every 3DP process category.

BJ, PBF, and SL technologies take place layer-wise, whereas DED, ME, MJ, and VP (within the material) both layer-wise and spatially as long as suitable kinematics are incorporated. The process teams describe basic principles of operation, hence, technologies falling under each category have different characteristics and potential (product's surface quality, dimensional accuracy, mechanical and physical properties, machine's production speed, build size, material processing capabilities), and involve diverse mechanisms and configurations to grow the part *(Gebhardt and Hötter, 2016; Gibson, Rosen and Stucker, 2021; Wohlers Associates, 2021a).*

Apart from the positioning accuracy and minimum layer thickness, *Table 4* summarizes the process parameters, available feedstock materials, and market terms for each 3DP category. The material states and processing steps for each 3DP process category are shown in *Appendix G*, whereas advantages, disadvantages, and orthopaedic uses of 3DP are listed in *Table 5*.

Table 4: Process parameters, feedstock materials, and terms used for each 3DP category

Category	Other Market Terms	Parameters	Feedstock Materials
BJ	*3D Printing (3DP), Color Jet Printing (CJP).*	*Powder and binder characteristics, inkjet head characteristics, binder flow rate, processing speed.*	*Starch & Plaster: for functional parts infiltration is needed (wax, epoxy, elastic urethanes, adhesive cyanoacrylate).* *Metals & Ceramics: de-bindering, sintering, infiltration, isostatic pressing (powder metallurgy techniques).* *Polymer powders glued by suitable liquid binder reacting at room temp (e.g. PMMA).* *Direct manufacturing of sand molds to be used in casting.*
DED	*Directed Light Fabrication (DLF), Laser Engineered Net Shaping (LENS), Direct Metal Deposition (DMD), Laser Direct Casting (LDC), Laser Metal Forming (LMF), Laser Consolidation*	*Degrees of kinematic freedom, laser type, power & spot size, speed & deposition flow rate, feedstock morphology, environment &*	*With appropriate atmospheric preparation & shield gas most metals: Ni superalloys, Steels, Stainless & Tool Steels, Ti, Al, Cu, Co alloys, refractory metals (Ta, W, Zr), some ceramics & ceramic or metal matrix composites.*

	(LC), LaserCast, LasForm (Laser Forming), Construction Laser Additive Directe (CLAD), Laser Metal Deposition (LMD), Laser Deposition Technology (LDT), Direct Metal Tooling (DMT), Laser Deposition Welding (LDW), Electron Beam Solid Free Form Fabrication (EBSFF), Electron Beam Free Form Fabrication (EBFFF), Electron Beam Additive Manufacturing (EBAM), Wire and Arc Additive Manufacturing (WAAM).	*thermal history control (heat buildup, reheating, peak temperatures, time at peak temperature, cooling rates).*	
ME	*Fused Deposition Modeling (FDM), Fused Filament Fabrication (FFF), Composite Filament Fabrication (CFF), Multiphase Jet Solidification (MJS), Contour Crafting (CC), Direct-Ink-Writing (DIW), Composite Filament Fabrication (CFF), Augmented Polymer Deposition (APD), Atomic Diffusion Additive Manufacturing (ADAM).*	*Nozzle size, extrusion flow rate, build speed, environment & nozzle temperature, feedstock characteristics & viscosity, thermal history control to prevent delamination & distortions.*	*Polymers: ABS, PLA, PA(Nylon), PETG, PC, PP, PPSF, PPSU, PEEK, some elastomers (TPU), HIPS, fiber-reinforced polymers.* *Composites: polymer binders blended with polymers, waxes, metals, and ceramics.* *Water-soluble materials: PVA, PEG.* *Viscous liquids: ceramic slurries, (hydro)gels, inks.* *Metal/ceramics with isostatic pressing & sintering.*
MJ	*Ballistic Particle Manufacturing (BPM), Wax Deposition Modeling (WSM), MultiJet Modeling (MJM), Shape Deposition Manufacturing (SDM), Polymer Jetting (Polyjet), Drop On-Demand (DOD), MultiJet Printing (MJP), NanoParticle Jetting (NPJ).*	*Inkjet head characteristics, jetting frequency, flow rate & speed, curing control, feedstock viscosity.*	*Polymers & photo-polymers (simultaneously photo-polymerization).* *Waxes, Composite inks & (hydro)gels.* *Low-temp metal droplets.* *Metal & ceramic mixtures (extra sintering step).*
PBF	*Selective Laser Sintering (SLS), Selective Laser Melting (SLM), Laser Beam Melting (LBM), Direct Metal Laser Sintering (DMLS), Direct Metal Printing (DMP), Laser Metal Fusion (LMF), Electron Beam Melting (EBM), Selective Mask Sintering (SMS), Selective Inhibition Sintering (SIS), High Speed Sintering (HSS), Selective Heat Sintering (SHS), Multi-Jet Fusion (MJF), Layered Powder Metallurgy (LPM).*	*Laser: power, spot size, pulse duration, frequency, wavelength.* *Layer scanning: speed, spacing, pattern, count.* *Powder: size & morphology, density, layer thickness, material.* *Temperature: chamber/bed/feeder temperature, temperature uniformity.* *Melt Pool: temperature gradient, lifetime, dimensions, viscosity & melt flow, stability, bailing, sputtering.*	*Polymers: PA, PAEK, PP, TPE, PS, PP, PC, PEEK, PCL, PGA, PLA, UHMWPE, PMMA.* *Metals: Al, Steels, Tool Steels, Stainless Steels, CoCr, Cu, Ti, Ni, Ta, Au, Pl, Mg.* *Ceramics: HA, CP, TCP, Zr, Si, Al & Ti oxides, bioceramics.* *Composites: mixtures with a variety of materials, PA(Nylon) blends, Polylactides mixtures for scaffolds.*

SL	*Computer-aided manufacturing of laminated engineering materials (CAM-LEM), Laminated Object Manufacturing (LOM), Selective Adhesive and Hot Press (SAHP), Paper Lamination Technology (PLT), Plastic Sheet Lamination (PSL), Selective Deposition Lamination (SDL), Selective Lamination Composite Object Manufacturing (SLCOM), Ultrasonic Consolidation (UC).*	*Sheet cutter tool characteristics, connecting means characteristics, and material properties.*	*Paper, polymer, metal, ceramic or composite sheets are cut, stacked & connected with glue, self-bonding or mechanically.*
VP	*Stereolithography (SLA), StereoPhotoLithography (SPL), Low Force Stereolithography (LFS), Solid Object Ultraviolet Laser Plotting (SOUP), Solid Modeling System (Somos), Solid Creation System (SCS), Laser Modeling System (LMS), Solid Laserdiode Plotter (SLP), Computer-Operated Laser-Active Modeling Machine (COLAMM), Digital Light Synthesis (DLS), Digital Light Processing (DLP), Solid Ground Curing (SGC).* *Slide And Separate (SAS), Lithography based Ceramic Manufacturing (LCM), MicroLightSwitch (MLS), Continuous Liquid Interface Production (CLIP), Daylight Polymer Printing (DPP).*	*Laser: power, spot size, radiation time, frequency, wavelength.* *Layer scanning: speed, spacing, pattern, count.* *Material: layer thickness, surface tension & viscosity, composition.*	*Rigid, soft, elastic photo-polymer resins (acrylate, epoxy, vinyl).* *Blends with ceramics, waxes, silicone etc.*

Table 5: Advantages, disadvantages, and medical uses for each 3DP category

Category	Advantages	Disadvantages	Uses
BJ	*Support-free process with no thermal & mechanical influences.* *Maximum volume utilization: stacking of multiple parts within powder.* *Multi-color parts.* *Low noise & low energy consumption.* *Binder mixture change on the fly.* *High speed & low cost.*	*Manual work, loose powder removal equipment & damaging danger.* *Extra steps are required for functional parts, metals & ceramics.* *Warpage & shrink if sintered.* *Poor accuracy, surface finish, porosity.*	*Multi-color anatomical models.* *Indirect parts production via sintering & infiltration.* *Indirect parts production via sand molds.* *Scaffolds for TE.*
DED	*Direct metallic & ceramic parts fabrication.* *Fully dense parts with fine-grained microstructure.* *Spatial multi axis deposition.*	*Reduced ability to produce small-scale features, poor surface quality & poor dimensional accuracy.*	*Coating & repairing, near-net shaping 3D parts, hybrid additive-subtractive solutions.*

	Can be combined with machining in situ or producing near net shapes. *High deposition rates.* *Repair high-technology components or adding material or coatings deposition.*	*Heat treatment for stress relief & machining to improve surface quality & accuracy.* *Overhangs require a multi-axis deposition head.* *Large & expensive machines with high energy consumption.*	
ME	*Multi-color & Multiple parts printing.* *Low-cost machine cost & materials.* *Low noise & low energy consumption & compact machines.* *One-step process for polymers (only supports removal & cleaning).* *Range of functional materials.*	*Low build speed.* *Low accuracy and resolution & increased stair-stepping.* *Visible seam lines.* *Overhangs require support structures from the same or different material.*	*(Multicolor) Anatomical models & surgical tools.* *Prosthetics & orthotics.* *Indirect production of metals.* *Indirect production via molds.* *Scaffolds for TE.*
MJ	*Multi-color & multi-material with spatially jetting option.* *Clear materials.* *Low noise & low energy consumption & compact machines.* *One-step process.* *High accuracy & surface quality.* *Fast process. Multiple parts printing.*	*Expensive machines & materials.* *Limited materials.* *Overhangs require support structures from the same or different material.*	*Multi-color multi-material anatomical models.* *Surgical tools.* *Prosthetics & orthotics.* *Indirect production via molds.* *Scaffolds for TE.*
PBF	*Range of materials.* *One-step process for direct fabrication & fully dense parts with high strength.* *Good accuracy but a rough surface.* *Fast direct polymer, metal & ceramic fabrication.* *Maximum volume utilization: stacking of multiple parts within powder. Polymers supports-free.*	*Large expensive machines & materials with high energy consumption.* *Metals might require heat treatment and support structures to avoid deformation.* *Extra steps if indirect manufacturing of metals & ceramics.* *Extra post-processing, cleaning equipment, de-powdering entrapped cavities.* *Particles baked on part.*	*Anatomical models & surgical tools.* *Prosthetics & orthotics.* *Direct & indirect implant production.* *Scaffolds for TE.*
SL	*Fast one-step process for direct fabrication.* *Mixed metallic & ceramic materials.*	*Limited design freedom & geometric complexity.* *Waste material.*	*Anatomical models.* *Direct fabrication with Ultrasonic Consolidation.*
VP	*Most accurate processes with excellent surface finish & accuracy.* *Projection methods are fast & single-step process.* *Transparent & translucent materials available.* *Multiple parts printed simultaneously.*	*Restricted to photosensitive materials.* *Post-curing might be needed.* *Supports are required to avoid distortions.* *Liquid monomer is hazardous waste.* *Need of holes to empty trapped liquid.* *Expensive machines & materials.*	*Anatomical models & surgical tools.* *Prosthetics & orthotics.* *Indirect implant production.* *Scaffolds for TE.*

Not all 3D printers are the same as their structure and characteristics vary even for the machines that are based on the same 3DP technology. Some are limited to prototype and concept model production and others for functional end parts. 3D printers are usually designated as fabbers for personal usage, office for professional applications, and production printers for shop floor utilization. Indicative costs of some 3D printers meant for different application levels are shown in *Figure 82*.

	Machine class			
Designation *	**Prototyper**		**Fabricator**	
	Personal 3D printer		Professional 3D Printer	Production machine Production 3D printer
	Fabber	Personal printer	Office printer	Production printer (Shop floor machine)
Use	Private, domestic	Semiprofes-sional office	Professional office or workshop	Professional, production or job shop
Usage levels (Fig. 1.7)				
▪ Prototypes Display models	X			
▪ Concept models		X		
▪ Functional prototypes			X	
▪ Final products				X
Construction material	Plastic	Plastic	Plastic	Plastic, metal, ceramic
Price level	500 to 4000 € [1 € ≈ 1.07 USD]	1000 to 10,000 €	20,000 to 70,000 €	130,000 to > 800,000 €
Example	Prusa Mendel	Dimension	Objet	Concept SLM

Figure 82: Examples of 3D printer types, uses, costs. Source: (Gebhardt and Hötter, 2016)

3.3.5 Generic Process Flow Chain

The generic workflow *(Gebhardt and Hötter, 2016; Gibson, Rosen and Stucker, 2021)* for additive layer materialization of parts from digital 3D data is described below (*Figure 83*):

A. The process starts with a 3D digital model that is either designed in CAD software or digitized for reverse engineering *(Raja and Fernandes, 2008)* using tomography, 3D scanning, Coordinate Measuring Machines (CMMs).
B. The desired digital model is then tessellated into a surface mesh format such as .stl or .amf to be imported into and manipulated by a dedicated 3DP process planning software.
C. The process planning involves the selection of operation parameters (e.g. slicing density and orientation, layer filling pattern, fabrication speed), creation of support structures, surface mesh slicing into 2D cross-sections, and machine-specific settings to generate the control code.

D. The 3D Printer is prepared and the layer-by-layer additive build commences.
E. The 3DPed product is received, removed from the platform, and cleaned. Further post-processing might be applied for quality and accuracy improvements before its application.

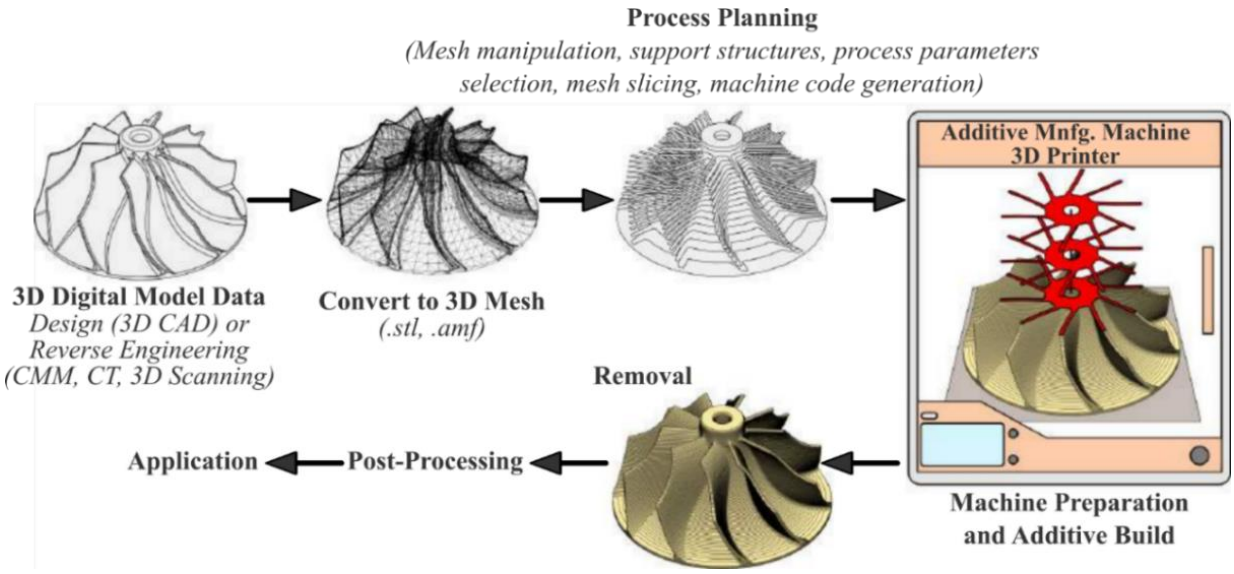

Figure 83: Generic process flow chain for 3DP

An extrusion-based FFF 3D printer called *"Morpheas"*[48] *(Mavrodontis, 2015)* and sample products after applying the aforementioned process flow chain are illustrated in *Figure 85*.

Tessellation is used to approximate a 3D geometry using polygons (triangles). Most CAD software are capable of exporting models in STL format (binary (smaller) or ASCII types). Selecting the desired tolerance (chord height), several flat triangles are generated to achieve this tolerance. Curved surfaces are better approximated by increasing the number of triangles. *Figure 87* shows the impact of triangle number on surface quality and STL file size. The STL (Standard Tessellation Language) was developed by Albert Consulting in 1987 for 3D Systems' (3D Systems Inc., California, US) SLA machines *(3D Systems, 1988)*, and is the standard format used by most 3DP technologies until today.

Digital 3D model data such as STEP[49] or IGES[50] describe curves and contain much geometrical information, once this data is converted into a facet surface body (e.g. STL), all information is lost and the geometry becomes just a surface mesh with flat triangles *(Gibson, Rosen and Stucker, 2021)* as shown in *Figure 86*. To deal with this issue, the Additive Manufacturing File format (AMF) was developed to generate curved polygons and store more geometrical data *(ISO/ASTM, 2020)*.

[48] Morpheas is a material extrusion-based 3D printer (Fused Filament Fabrication) designed and manufactured from scratch by I. Mavrodontis *(2015)* for his undergraduate Thesis project for research purposes.

[49] STEP is a widely used data exchange form which stands for "Standard for the Exchange of Product model data". It is based on ISO 10303 which represents 3D objects in CAD and provides related information.

[50] Initial Graphics Exchange Specification (IGES) is an ASCII-based textual format file format that allows the digital exchange of surface and solid model representations and other types of information among CAD systems.

Binder Jetting

Binder Jetting Process

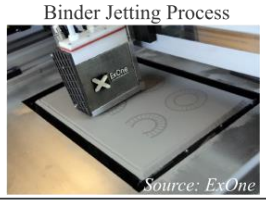

Binder Jetting Head

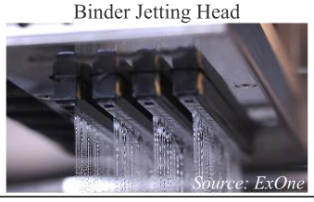

Directed Energy Deposition

Wire Deposition & Fusing Head

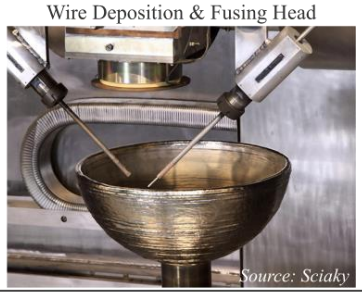

Powder Jetting & Fusing Head

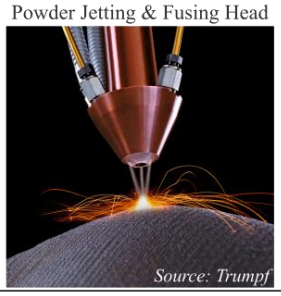

Material Extrusion

Slurries/Pastes/Cells/Hydrogels Bioprinting (HA, PCL etc)

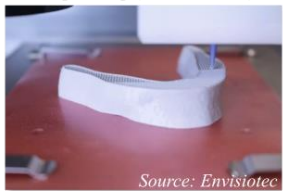

Freeform Reversible Embedding of Suspended Hydrogels

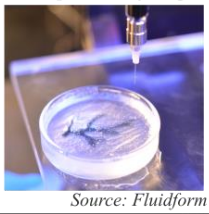

Source: Fluidform

Fused Filament Fabrication

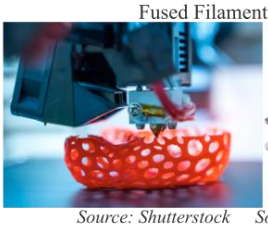

Source: Shutterstock

Source: MatterHackers

Material Jetting

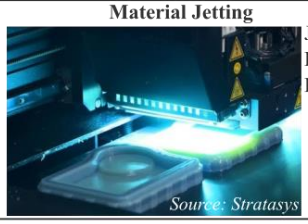

Jetting & Photopolymerization Process

Powder Bed Fusion

Powder Bed Fusion Process

Part Being Build Within Powder

Sheet Lamination

Plastic Sheet Cut & Bond

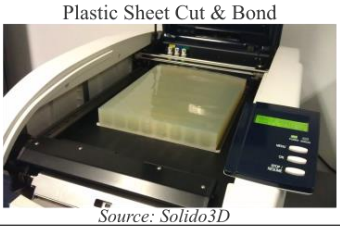

Source: Solido3D

Multi-colour Paper Cut & Glue

Vat Photopolymerization

Bottom-up Photopolymerization

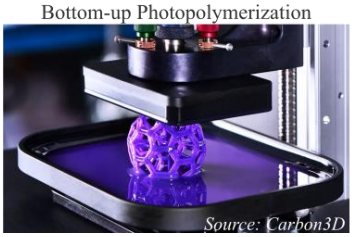

Top-down Photopolymerization

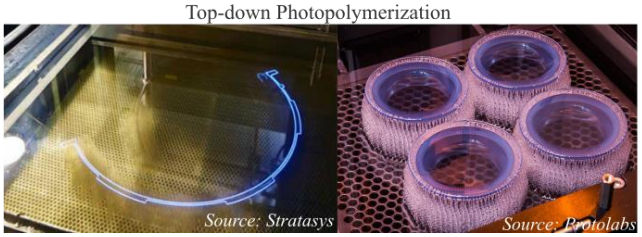

Figure 84: Examples for each 3DP process category

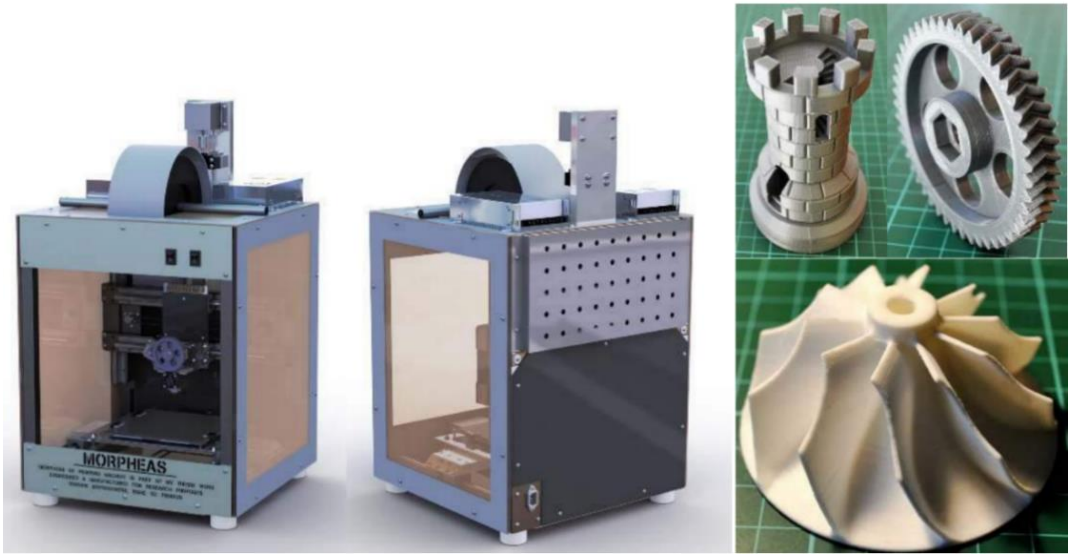

Figure 85: "Morpheas" FFF 3DP machine and sample polymer parts. Source: (Mavrodontis, 2015)

ASCII TYPE STL FILE (Larger file)

```
solid name
For each triangle
    facet normal ni nj nk
        outer loop
            vertex v1x v1y v1z
            vertex v2x v2y v2z
            vertex v3x v3y v3z
        endloop
    endfacet
.
.
endsolid name
```

BINARY TYPE STL FILE (Smaller file)

```
Header
Number of triangles
For each triangle
    n //for normal vector
    ni
    nj
    nk
    v1 //for vertex 1
    v1x
    v1y
    v2z //for vertex 2
    v2x
    v2y
    v3z //for vertex 3
    v3x
    v3y
    Attribute byte count
.
.
end
```

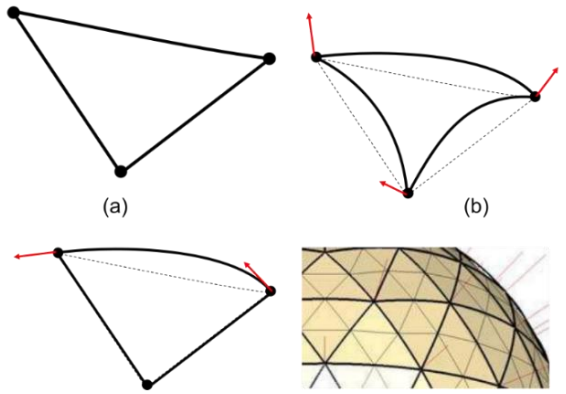

a) A default (flat) triangle patch (as in .stl)
b) A triangle curved using vertex normals
c) A triangle curved using edge tangents
d) Subdivision of a curved triangle patch into four curved sub-patches
e) An AMF file containing curved geometry

```
<?xml version="1.0" encoding="UTF-8"?>
<amf unit="millimeter">
  <object id="0">
    <mesh>
      <vertices>
        <vertex>
          <coordinates >
            ...
          </coordinates >
          <normal>
            <nx>0</nx>
            <ny>0.707</ny>   Only needed for
            <nz>0.707</nz>   curved surfaces
          </normal>
        </vertex>
        ...
        <edge>
          <v1>0</v1>
          <dx1>0.577</dx1>
          <dy1>0.577</dy1>
          <dz1>0.577</dz1>   Only needed for
          <v2>1</v2>         curved edges
          <dx2>0.707</dx2>   (rare)
          <dy2>0</dy2>
          <dz2>0.707</dz2>
        </edge>
        ...
      </vertices>

      <volume materialid="0">
        <triangle>
          ...
        </triangle>
        ...
      </volume>
    </mesh>
  </object>
</amf>
```

(e)

Figure 86: STL and AMF file structures. Source: (ISO/ASTM, 2020)

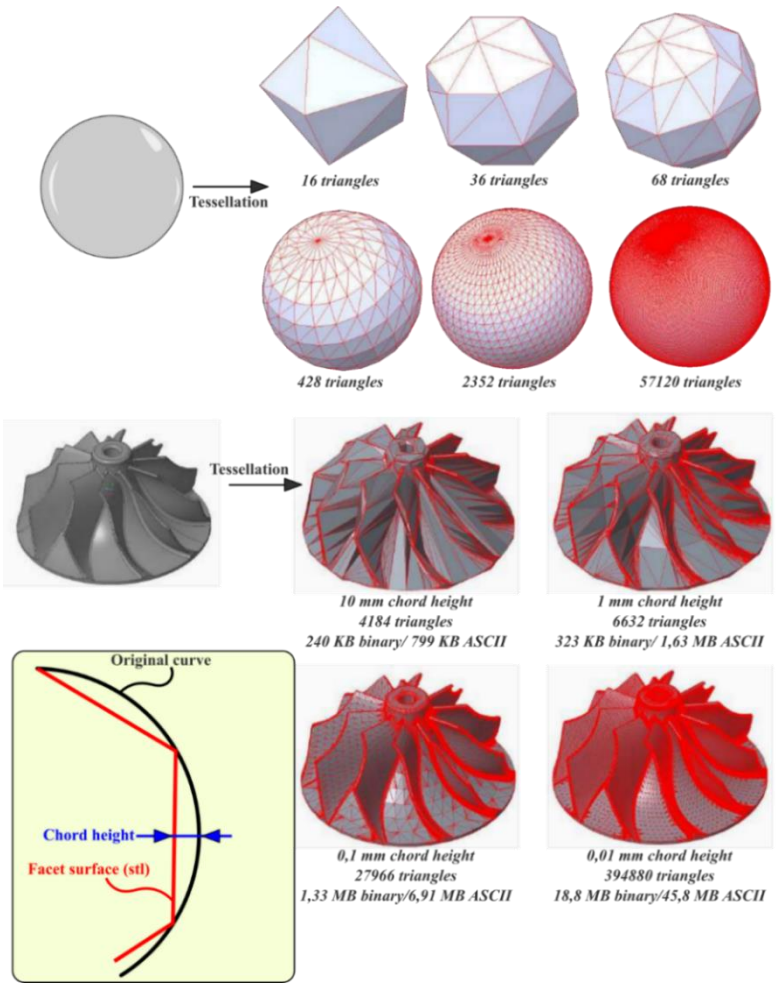

Figure 87: Tessellation quality and .stl file size

3.3.6 Characteristics and Potential

The quality of a 3DPed part (surface finish, dimensional accuracy, properties) is a function of:

1. **3D printer operator:** experience, expertise, and caution required.
2. **Part:** the CAD model features (e.g. smallest details, wall thickness) should be matched to the specifications and optimized for the 3DP technology to be used. The CAD data should be appropriately and accurately translated to a clean surface mesh model to facilitate error-free import into the process planning software.
3. **Pre-processing:** refers to the selection of parameters about the part(s) positioning, support structures (if applied), machine set-up, slicing, layer forming technique, and build orientation within the 3D printer. The previous parameters affect the 3DPed part's quality and thus should be optimized based on the desired criteria, e.g. maximize mechanical performance or surface quality, minimize production time or support structures *(Kulkarni, Marsan and Dutta, 2000; Pandey, Reddy and Dhande, 2003).*
4. **3D printer:** characteristics, condition, mechanisms, and structure of the 3D printer per se.
5. **Process:** machine-specific variables selected (e.g. scanning strategy, speed, power), hardware and software used to maintain the pre-set parameters and atmosphere.

6. **Material:** the handling of the material(s) and its behavior during the 3DP process that is affected by its mechanical, chemical, rheological, optical, and thermal properties.
7. **Post-processing:** part and supports removal, cleaning, accuracy, surface improvements (e.g. machining, polishing, coating), and (non)thermal treatments (*Wohlers Associates, 2021b).*

Figure 88 illustrates an Ishigawa diagram of the parameters affecting 3DP of metallic materials using laser-based PBF technologies.

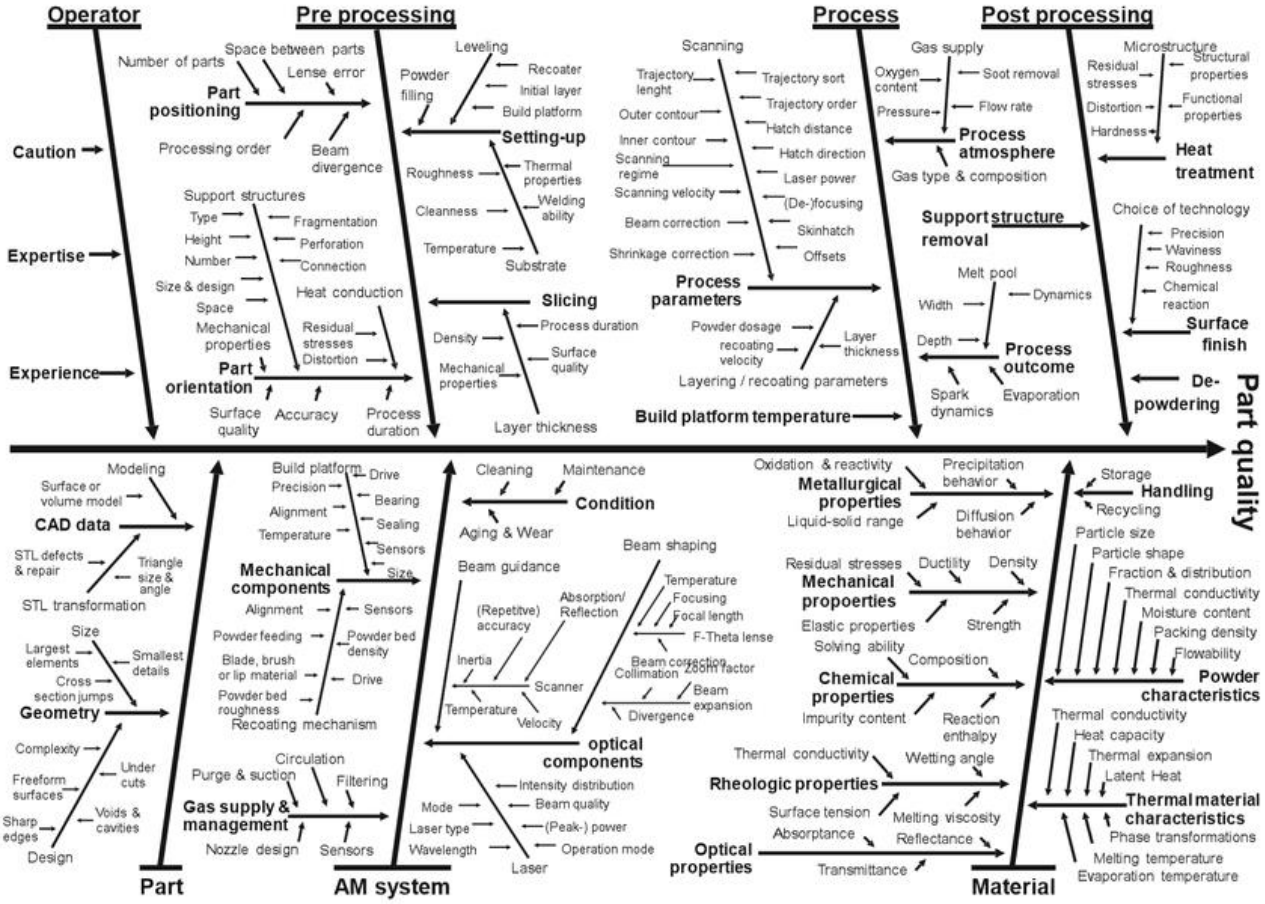

Figure 88: Ishigawa diagram of parameters affecting metal 3DP. Source: (Haberland, Siemens Industrial Turbomachinery AB)

Regarding the cost breakdown for a typical 3DPed object, the segments for the printing per se are 59%, 14% for pre-processing, and 27% for post-processing (*Wohlers Associates, 2021a).*

During the product design phase, Design for AM or 3DP (Df3DP) principles should be considered to deal with issues of 3DP for defect-free products with the desired properties *(Kranz, Herzog and Emmelmann, 2014; Thompson et al., 2016; Schnabel, Oettel and Mueller, 2017; ISO/ASTM, 2018; Diegel, Nordin and Motte, 2019; Leary, 2019*; *Renjith, Park and Okudan, 2019; Vaneker et al., 2020)* and Design with AM or 3DP (Dw3DP) *(Floriane et al., 2016)* approaches (e.g. topology optimization with biomimetic cellular structures) to fully explore and exploit 3DP capabilities.

3DP is successfully adopted for rapid prototyping, manufacturing, and tooling for various uses by many users including medicine *(Figure 89) (Petrovic et al., 2011; Lunsford et al., 2016; Salmi,*

2021, Wohlers Associates, 2021a). Numerous insights[51] and reports are calling 3DP a *"disruptive manufacturing force"* that could bring the next *"industrial revolution"* due to its groundbreaking and sustainable potential *(Markillie, 2012; Manyika et al., 2013; Grynol, 2015; Shaffer et al., 2015; Gao et al., 2015; Esmaeilian, Behdad and Wang, 2016; Ford and Despeisse, 2016).*

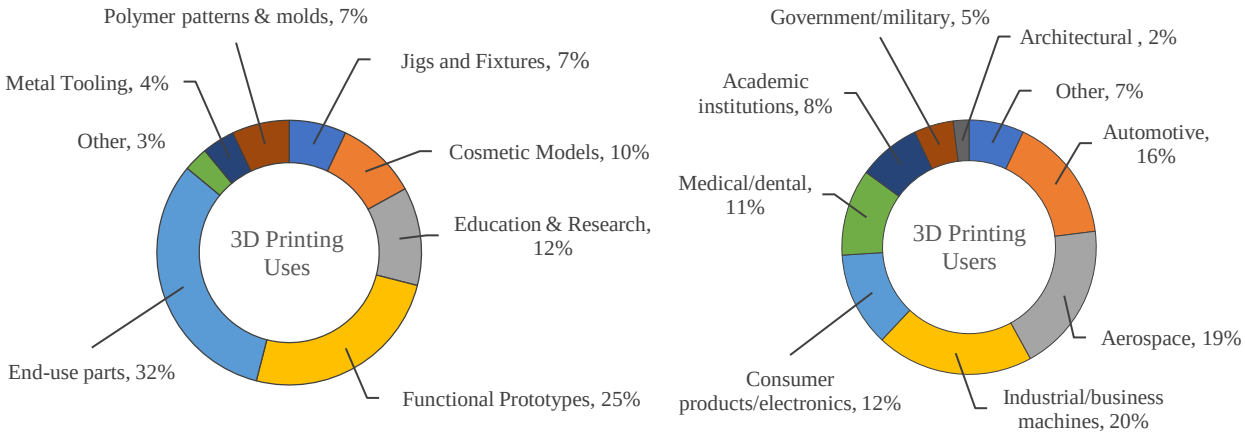

Figure 89: Uses and users of 3DP. Source: (Wohlers Associates, 2021a)

Implementing 3DP during product development leads to time and cost compressions due to fewer steps involved. In *Figure 90*, the application levels of 3DP technologies for rapid prototyping, rapid tooling, and rapid manufacturing are correlated to the phases of the traditional development process as described in the internationally accepted process chain of the German Association of Mechanical Engineers (VDI) VDI 2221 on the design of technical products and systems.

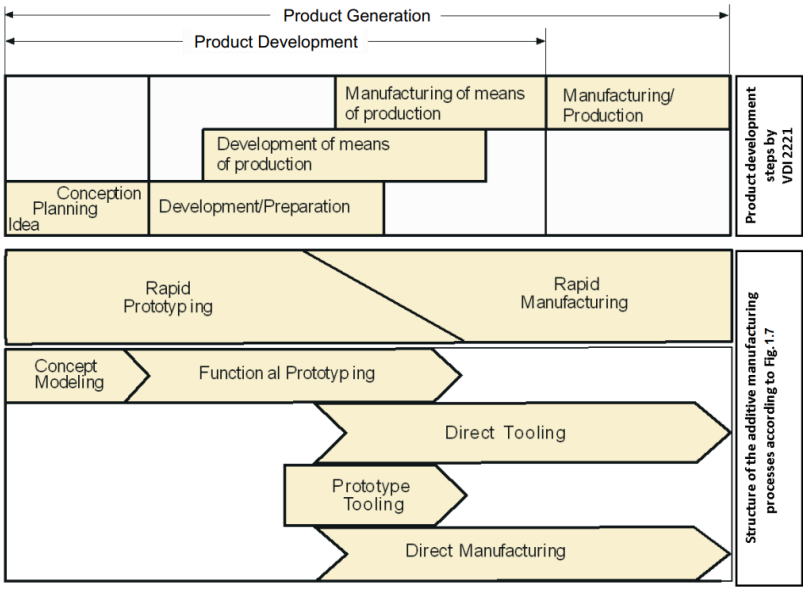

Figure 90: Product development phases: 3DP versus traditional manufacturing. Source: (Gebhardt and Hötter, 2016)

Of course, 3DP is not a panacea and should be used when it fits. As with any manufacturing methodology, 3DP has also limitations. The pros and cons of 3DP are mentioned in *Table 6* and in *Figure 91* the traditional manufacturing is compared to 3DP by addressing the life-cycle of products.

[51] A series of insight reports on 3DP was issued by Deloitte (https://www2.deloitte.com/us/en/insights/focus/3d-opportunity.html).

Table 6: Advantages and disadvantages of 3DP technologies

Pros	Cons
The tool-less automatic and flexible method offers time and cost savings through all product development stages.	The cost of production class 3D printers and feedstock materials are relatively still high.
Parts can be reduced in weight and miniaturized, and assemblies consolidated. Therefore, typical conventions for design for manufacture and assembly (DfMA) might be eliminated.	Not suitable for mass production, except if selected materials or geometries cannot or are difficult or expensive to manufacture otherwise.
As long as matching technologies and machines are selected, various materials can be processed, including biological.	Poor surface finish (stair-stepping) and dimensional inaccuracies.
More simplified in terms of process planning and operation compared to machining.	Product properties suffer from anisotropy (directional dependency expressed as differences in a material's physical properties along different axes) that is affected by the build orientation, layer scanning strategy, and 3D printer used itself.
Unique parts incorporating extremely intricate internal or external geometrical features are possible, even with embedded kinematic components. Generatively designed and topology optimized products can be materialized and *"smartness"* through biomimesis, multi-material processing, electronics integration (*Espalin et al., 2014; Thompson et al., 2016; Lehmhus et al., 2016; Panesar et al., 2017)* and shape-shifting/morphing (*"4D Printing") (Khoo et al., 2015; Momeni et al., 2017)* are enabled.	Quality control and assurance, certification, qualification, and regulations of special 3D printed parts used to be issues. Legislation and standardization on hardware, software, materials, pre/post-processing, quality control, and design for 3DP are in their infancy to promote penetration and adoption.
Economic and competitive for one-off and low production.	Micro-porosity on or within the parts.
Meta-materials fabrication that are governed by their structure design (materials-by-design) instead of just their composition. Functionalization-by-design can also be gradient/graded and topologically selective.	Expert personnel and skills required to design parts for 3DP. Operation of 3D printers is easier compared to machines used in traditional methods such as CNC machining: milling machines and lathes.

Can be used for near-net shaping followed by machining, or rapid tooling for classic processes.	Compared to traditional methods, the available materials palette is still limited. Each 3DP technology has its matching feedstock materials.
(Mass)Customization to individual's needs is enabled.	
Multiple and different parts can be built simultaneously, increasing productivity.	
Designs can be changed, and production re-set quickly on the fly with minimum complications.	
Autonomous 3DP machines can be implemented for the lights-out factories of the future manufacturing, also known as Industry 4.0.	
Inventories are reduced as parts are fabricated on-demand.	
Serves distributed and localized manufacturing models including cloud-based manufacturing and Internet-of-Things (IoT). Production can take place near or at the point of use, even deployed extra-terrestrially for supporting manned or unmanned space exploration missions by in situ resource utilization *(Sacco and Moon, 2019)*.	
No *"Achille's heel"* in difficult-to-form shapes, materials, and super-alloys *(Panwisawas, Tang and Reed, 2020)*.	
None, or negligible material waste.	
Majority of machines are safe, user-friendly, and low-noise.	
Serves reverse engineering workflows: the digitally acquired prototype's geometry can be physically duplicated easily.	

Design for Manufacturing and Assembly (DfMA) is a process followed by designers to tailor their designs to minimize manufacturing difficulties, time, and costs. The unique capabilities of 3DP lead to unique design opportunities and freedoms, hence Design for AM (DfAM) or 3DP (Df3DP) emerged to maximize product performance and other life-cycle objectives through the synthesis of shapes, sizes, hierarchical structures, and material compositions *(Rosen and Kim, 2021)*.

3DPed parts can exhibit complexity along different dimensions *(Rosen and Kim, 2021):* shape complexity (any shape customized hierarchically), material complexity (material distributed differently in different regions, resulting in different properties), and functional complexity (kinematic and/or other features can be embedded in the part with no assembly required).

The utilization of 3DP for fabricating topology and shape-optimized parts is one of the most intensively investigated research fields. To demonstrate the capabilities of 3DP, topologically optimized multi-material parts with embedded electronic components that could be tailored to any unique requirements are shown in *Figure 92*, whilst topologically optimized and generatively designed parts and assemblies consolidated into single parts are shown in *Figure 93*.

	Traditional Manufacturing	Additive Manufacturing
Production cost	Economies of scale can lead to very low unit-cost but require a large volume of sales of specific products	Unit cost does not vary much with scale, no cost imperative to sell large volumes of specific products
Design requirement	Strict design-for-manufacturability requirements restrict product design possibilities	Reduced design-for-manufacturability requirements allow novel designs
Specialized molds and tools	The fixed cost for product-specialized tools is distributed across all units produced	No fixed cost for product-specialized tools and molds
Production speed of order	Serial process that depends on the speed of the critical path, as well as the degree to which bottlenecks lead to queues	Parallel process that depends on the speed of a printer and the number of printers used
Delivery speed of order	Globalization of production entails long transportation lead times, reducing delivery speed	Localization of production enables fast delivery upon completion of order
Capacity utilization	Specialized equipment requires high volume in specific products to achieve adequate utilization	Flexible equipment requires volume across different products to achieve adequate utilization
Capacity expansion	Lumpy expansion opportunities imply that plants often operate at over/under capacity	Easier to adjust capacity to demand since capacity can be bought in smaller increments
Learning curve	Production process may require product-specific learning, generating economies of scale	Learning is machine-specific and applies to different products made on the machine
Forecasting	Detailed product mix forecasting can lead to insufficient statistical aggregation to make accurate predictions	Forecasting shifts to aggregate raw materials and capacity, making forecasting more accurate
Bill of materials	High parts count due to product portfolio proliferation and specialization of supply chain partners	Low parts count due to the ability to integrate parts in the printing process
Purchasing	Separate bill of materials in product portfolio can lead to a large number of suppliers and low volume in supplied components	Raw material needs reduce complexity of purchasing portfolio and allow efficient scale in purchasing with less demand volume
Transportation	Leveraging economies of scale requires aggregating global demand, increasing complexity of transportation of parts and finished goods	Localized production means less transportation of parts and finished goods; transportation needs focus on raw materials, where demand is more aggregated and transportable
Material use	Subtractive process leads to excess material and waste	Additive process leads to less excess material and waste; recycling of printed and other materials a promising possibility
Marketing	Reaching global markets requires investment in brand to create global awareness and trust	Local production allows tapping into social responsibility and local networks to create awareness and trust

Figure 91: Traditional manufacturing versus 3DP. Source: (Ben-Ner and Siemsen, 2017)

Topology optimization and generative design are often used interchangeably but it is not the same. Topology optimization refers to computational techniques that have been used for several decades *(Logo and Ismail, 2020)* for optimizing (based on FEA) the layout of a given material within a given design space, for a given set of loads, boundary conditions, and constraints to maximize the system's performance. On the other hand, generative design is an iterative and evolutionary design exploration process that generates all possible permutations and alternative solutions, based on the design goals set, materials selected, applied loads, boundary conditions, and constraints (cost, manufacturing, etc.). *Figure 94* shows a part optimized via both topology optimization and generative design approaches.

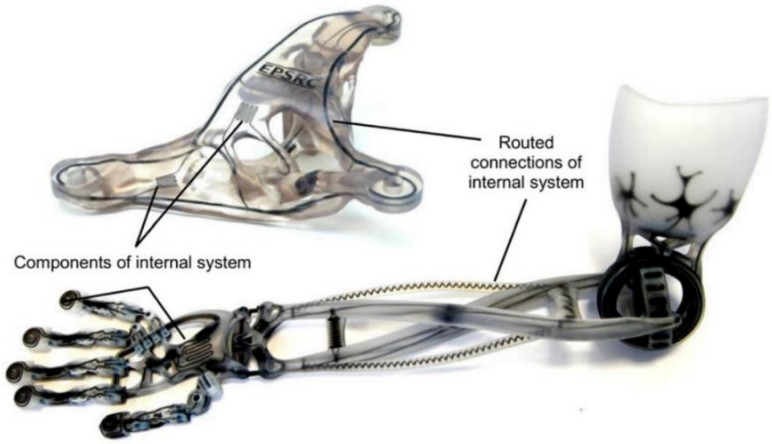

Figure 92: 3D Printed topology optimized multi-material parts with embedded electronics. Source: (Panesar et al., 2015)

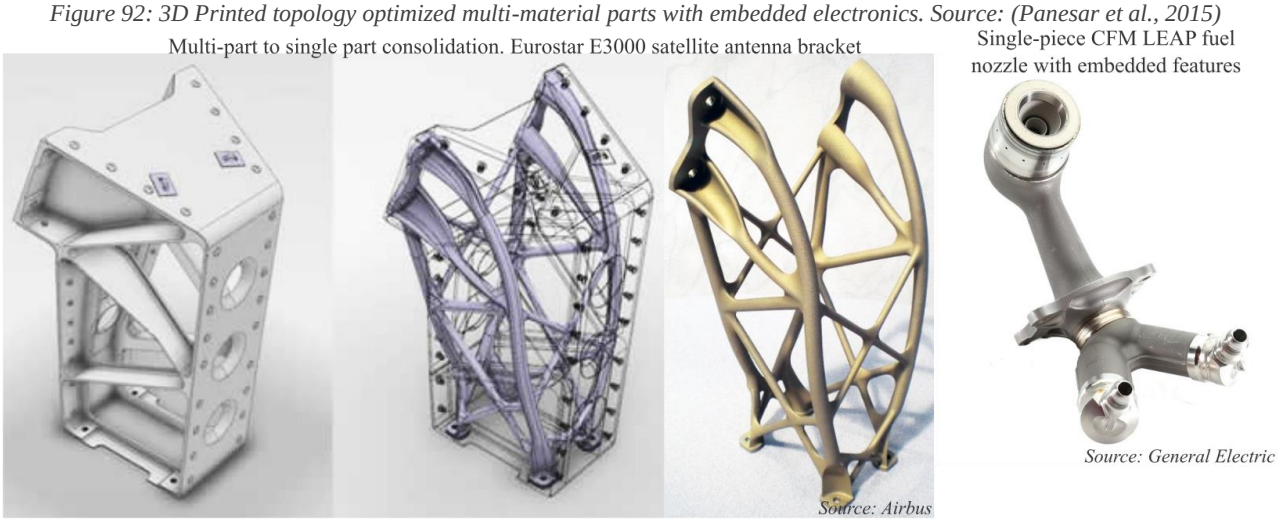

Figure 93: Topologically optimized, generatively designed, and consolidated 3D Printed parts

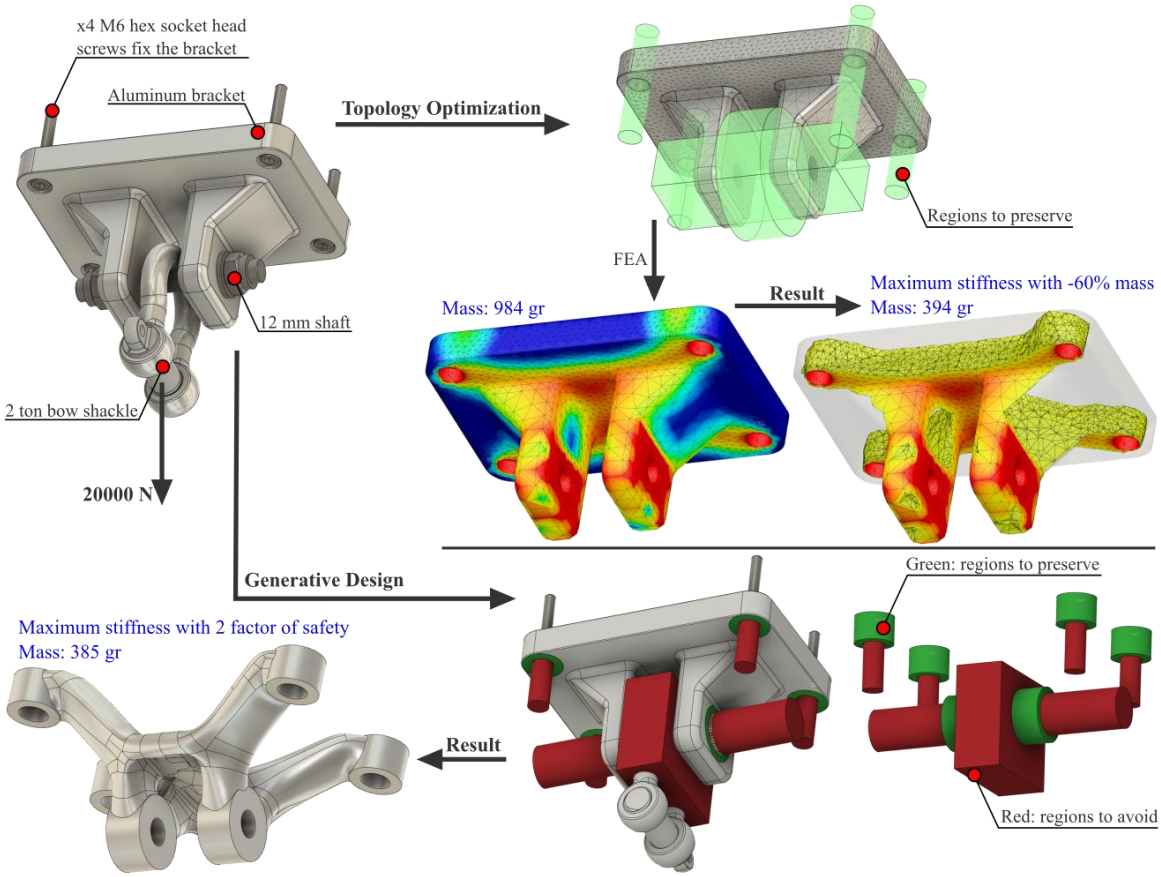

Figure 94: Generative design and topology optimization differences

Focusing on the technical flaws of 3DP, the following notes are bolded:

1. **Micro-porosity:** the fact that the process of 3DP occurs under a layer-by-layer fashion and each layer is scanned to be formed, leading to the creation of tiny pores. These pores, if not desired, can be infiltrated with filler materials (metal or ceramic) or the whole part can be isostatically pressed. *Figure 95* shows the pores that emerge from ME-based technologies, analogous material binding/fusion mechanisms take place in other 3DP technologies.

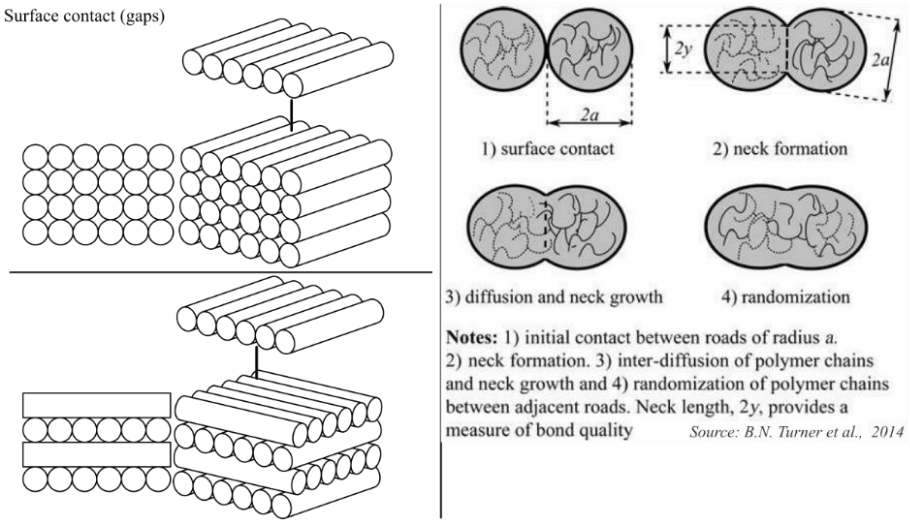

Figure 95: Sources of micro-porosity in ME-based 3DP technologies

2. **Surface finish and dimensional accuracy:** various post-processing techniques are deployed to deal with such imperfections (*Wohlers Associates, 2021b*). CNC machining is usually applied to

improve dimensional accuracy, whereas to deal with the stair-stepping phenomenon, abrasive/chemical treatments or coatings might apply *(Figure 96)*. It is important, before 3DP, to compensate the material to be removed or added so that the final after-treated dimensions are within the accepted range. Using 3DP for near-net shaping followed by integrated CNC machining, leads to highly flexible configurations capable of forming any desired shape with excellent surface finish and dimensional accuracy. Industry and academia have demonstrated such hybrid additive-subtractive machine tools *(Figure 97) (Flynn et al., 2016)*.

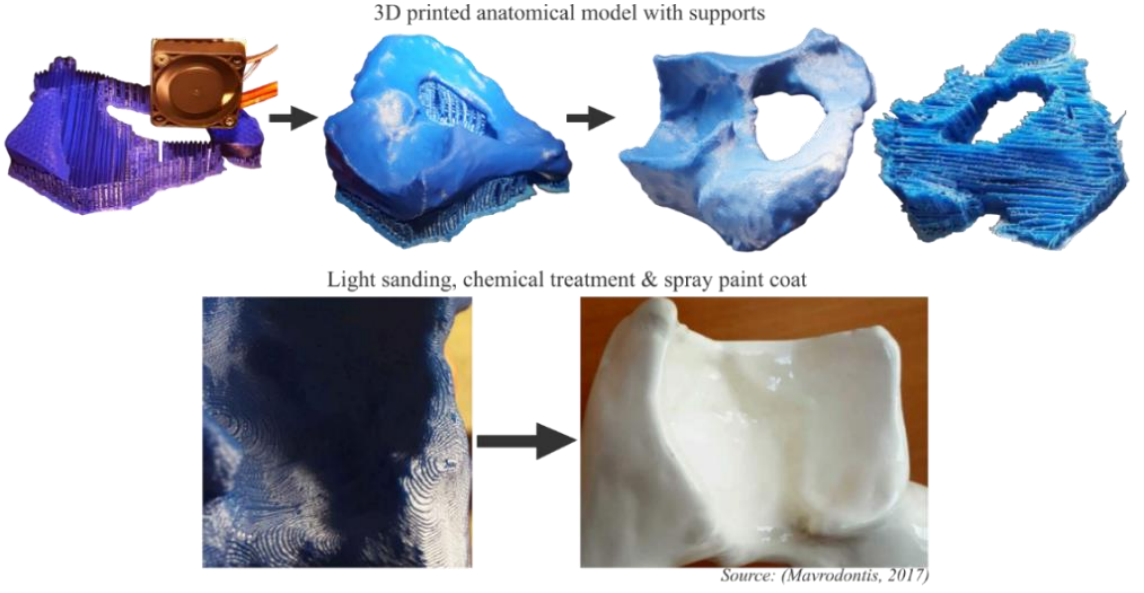

Figure 96: Surface treatments for finishing enhancement of 3D Printed parts

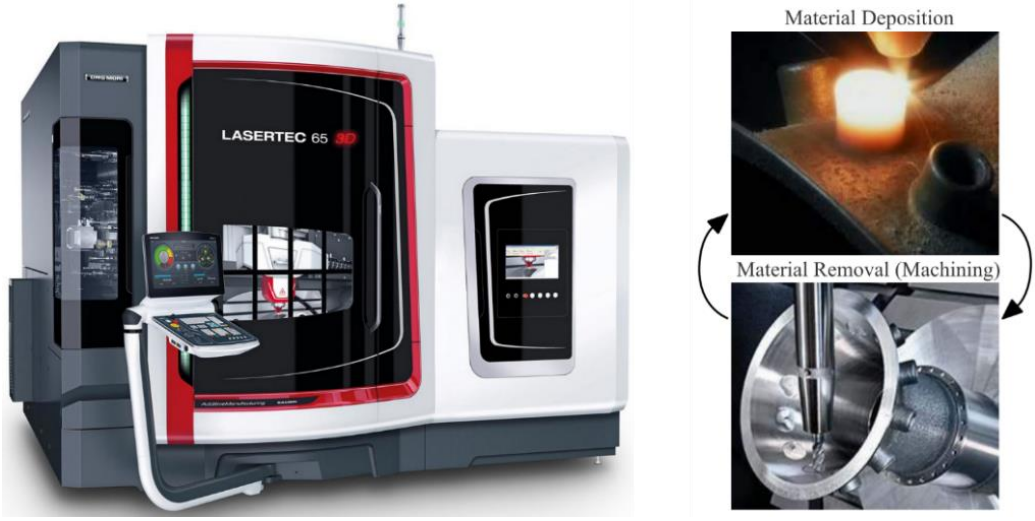

Figure 97: Hybrid additive-subtractive CNC machine tool. Source: DMG Mori

3. **Anisotropy:** due to the layer-wise nature of 3DP, the strategy of the layer forming and the selected build orientation are crucial parameters affecting the mechanical properties of the final product. Not all 3DP technologies produce the same degree of anisotropy, for example, *Figure 98* shows the differences in tensile strength in parts 3DPed in various build orientations and layer scanning techniques with VP, whereas *Appendix H* shows a similar study conducted in 2015 by Mavrodontis *(2015)* using the "*Morpheas"* ME machine.

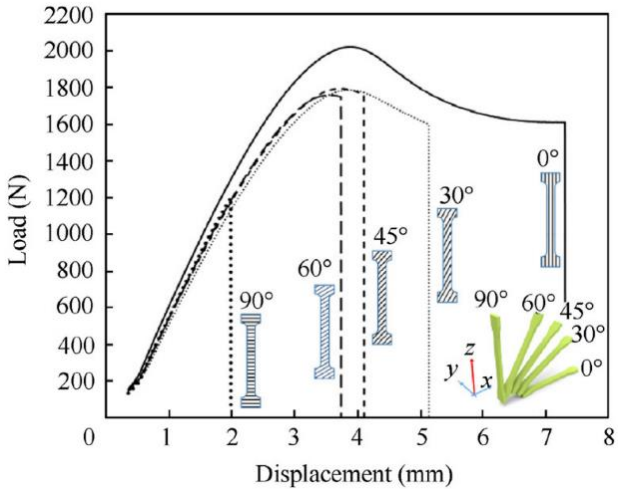

Figure 98: Anisotropy in mechanical properties of parts 3DPed with VP. Source: (Yang et al., 2018)

The 3DP industry reached $12,8 billion in 2020 (7,5% expansion, considerably lower than the 27,4% average growth over the last 10 years) and the independent service providers worldwide hit $5,3 billion of revenue *(Figure 99) (Wohlers Associates, 2021a).*

Academic and industrial research are also intensively active whereas a series of standards are being issued[52] and a plethora of associated patents[53] are applied every year with growing rates.

A hindering barrier that shields innovation are intellectual property protection issues *(Mendis et al., 2020).* Although patents protect inventors and companies, they restrict creative input and introduction of new and improved associated machines, materials, and processes and consequently widen 3DP applications for wide adoption.

The characteristic trends of manufacturing systems over time are shown in *Figure 100*. 3DP can positively impact these attributes, product offerings, and supply chains. The market structure can be affected by the technological and economic implications of 3DP *(Weller, Kleer and Piller, 2015)*, and products, supply chains, and business models can eventually evolve as shown in *Figure 103*.

Using 3DP, a part can be either produced per se as in conventional manufacturing methods, or improved functionally, or completely redesigned. Good candidate parts for 3DP are typically

[52] The recently established ASTM's F42 and ISO's TC216 Committee are dedicated to topics regarding 3DP, e.g. test methods, design, materials, processes, applications, data, terminology, environment, health and safety.

[53] As verified by the Google Patents engine that searches through international patent offices and from other reports, i.e. UK Intellectual Property Office *(2013),* Gridlogics Technologies *(2014),* IDA Science and Technology Policy Institute Report *(2014).*

produced in low volumes and have one or a combination of the following: complex geometries, custom geometries, and special variations of properties *(Rosen and Kim, 2020)*. 3DP proved to be time and cost-competitive *(Thomas and Gilbert, 2014)* while having a significant impact on a product's life cycle. But this is not always true as selecting the optimum technique implies that numerous parameters have to be weighted *(Figure 45) (Ashby, 2016; Kalpakjian and Schmid, 2020)*.

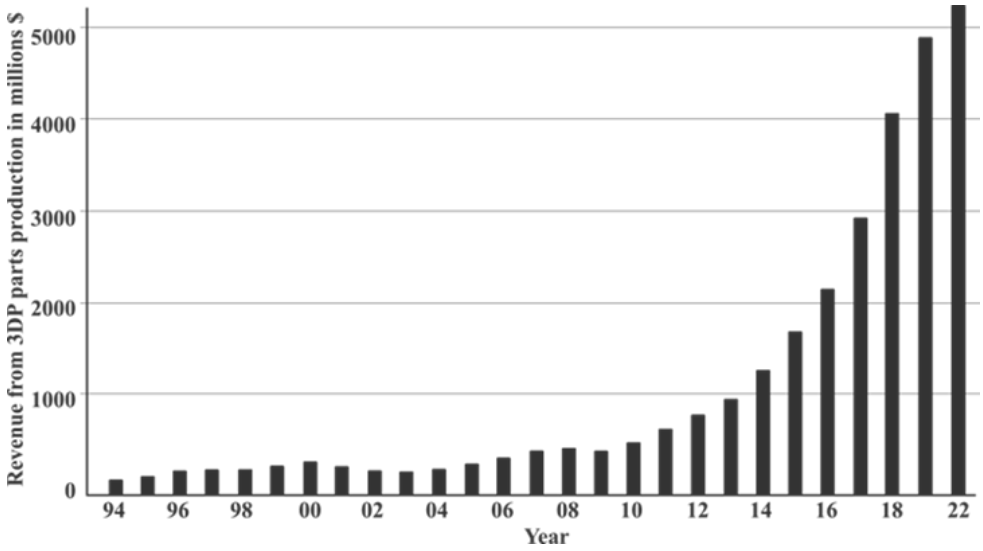

Figure 99: Worldwide revenue from independent 3DP service providers. Source: (Wohlers Associates, 2021a)

The qualitative graphs pictured in *Figure 101* compare 3DP to other methods requiring tooling (primary shaping like casting, forging, molding, and subtractive like CNC machining) in terms of time and cost versus production volume and complexity. It is clear that 3DP has unlimited design freedom but is effective for low to medium production volumes and/or the fabrication of complex geometries. To estimate the cost of 3DP production, several variables have to be set. Hopkinson and Dickens *(2003)* developed a model where the cost per part is independent of the production volume, whereas Ruffo et al. *(2006)* developed a more detailed model for better estimation in low production volumes and the 3DP cost curve has a decreasing saw tooth shape instead. Atzeni et al. *(2010; 2012)* showed that parts can be redesigned (optimized and consolidated) for 3DP for further cost and time savings, whilst offering superior performance. In any case, for improved time and cost-effectiveness, multiple and different parts should be built simultaneously in single print sessions *(Ruffo and Hague, 2007; Rickenbacher, Spierings and Wegener, 2013)*.

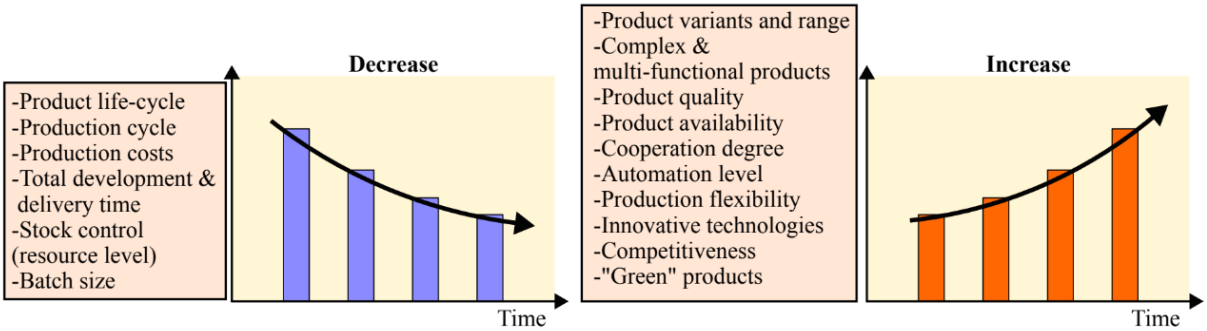

Figure 100: Trends in manufacturing systems. Source: After (Böllinghaus et al., 2009)

It should be underscored that each 3DP technology has different characteristics with different material processing capabilities, so the production time and cost vary as per the production volume and geometric complexity among 3DP technologies.

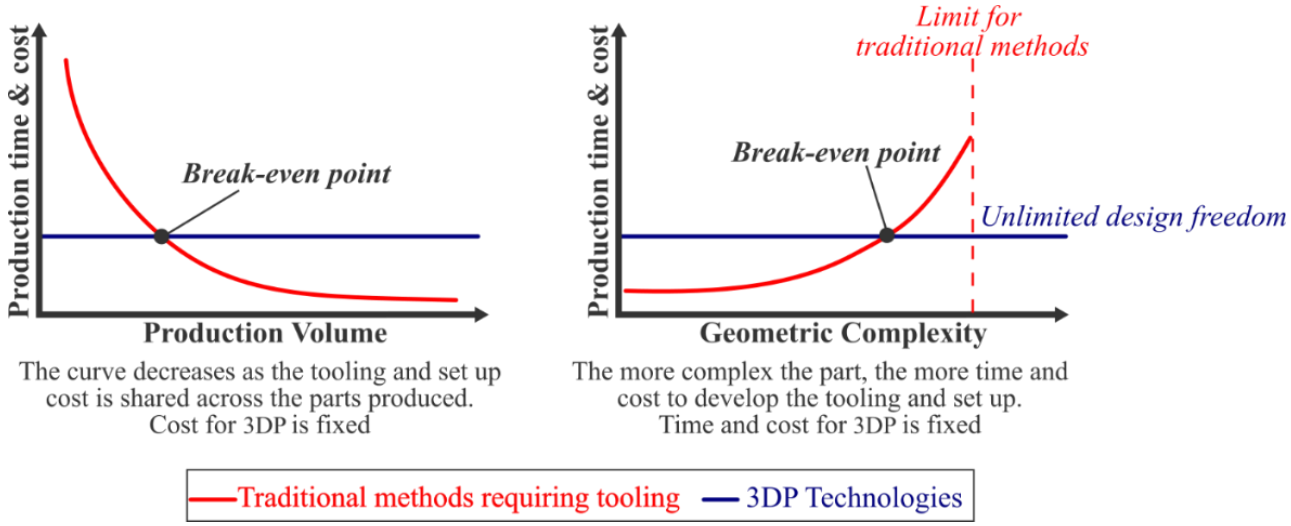

Figure 101: Production time and cost for 3DP versus traditional manufacturing processes

About their readiness and productivity level, applications of 3DP are positioned at different points on the so-called Hype Cycle (*Figure 102*). Industries seeking to directly or indirectly embrace 3DP to reform their products, services, business models, and supply networks *(Figure 103)* benefit from novel and sustainable features, adapting to Industry 4.0 trends. Granted the adoption of 3DP, the immediate likely developments and future scenarios for selected industries are shown in *Figure 104*.

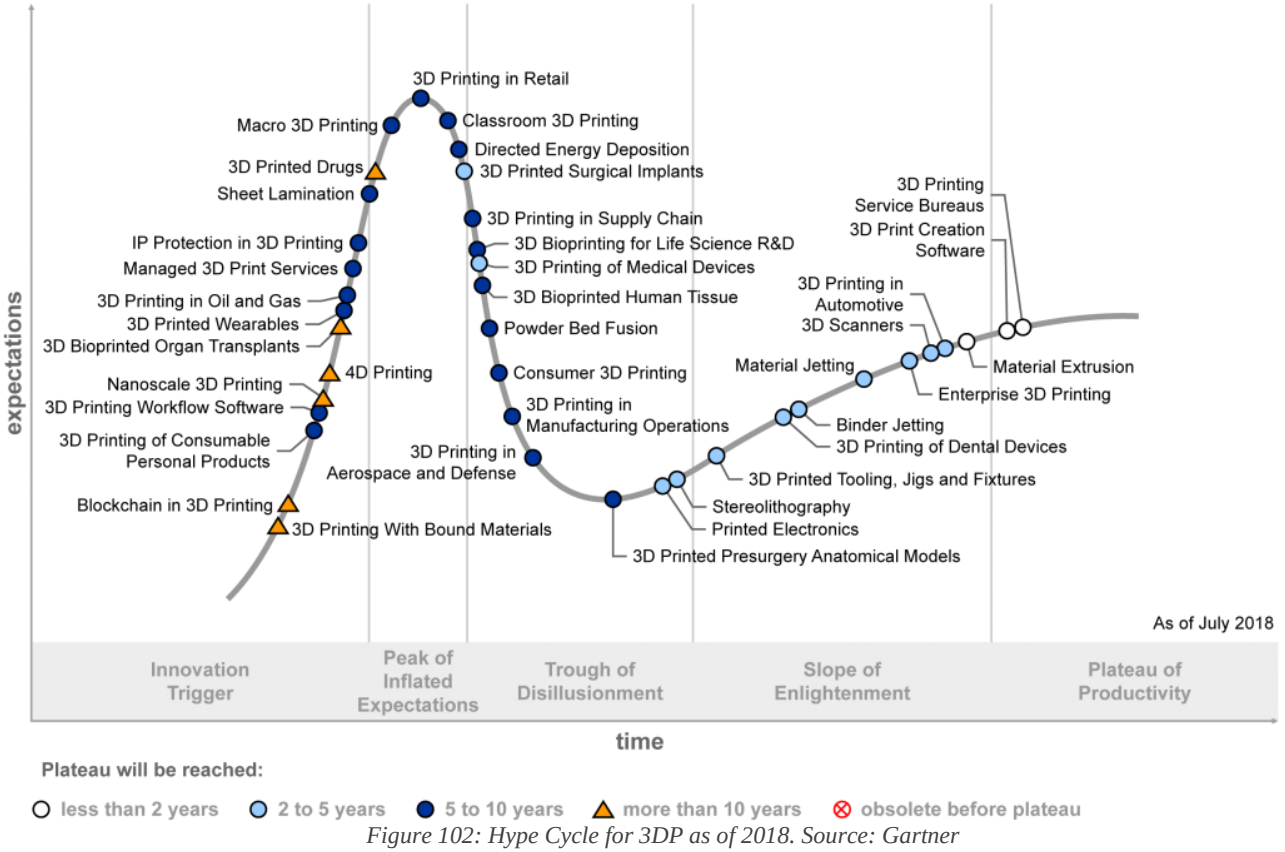

Figure 102: Hype Cycle for 3DP as of 2018. Source: Gartner

3D printer manufacturers, post-processing companies, raw materials suppliers, software vendors, and research institutes engaged in 3DP and product design market are shown in *Appendix I*.

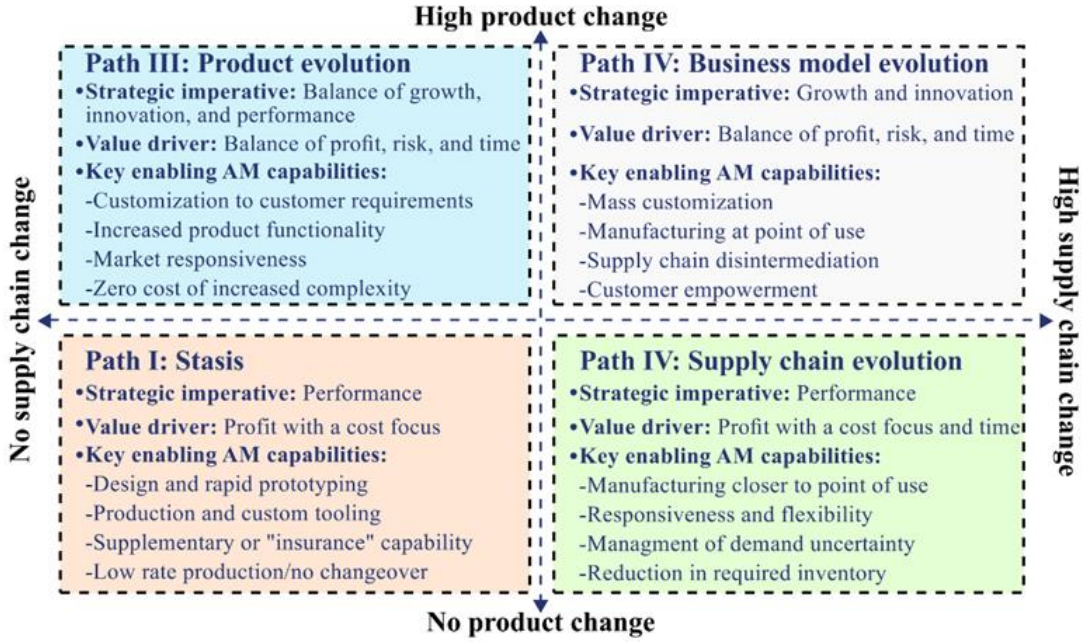

Figure 103: Potential impacts of 3DP on product offerings and supply chains. Source: Deloitte University Press

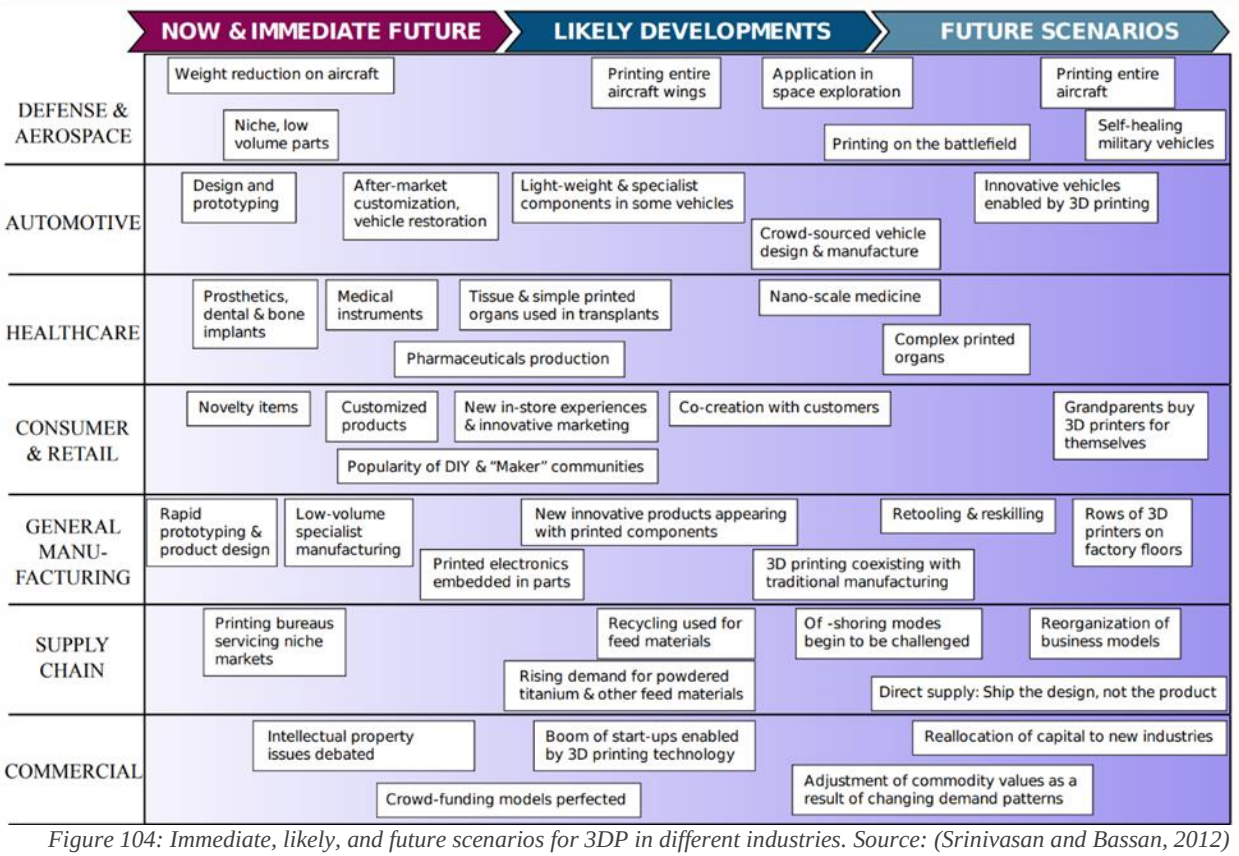

Figure 104: Immediate, likely, and future scenarios for 3DP in different industries. Source: (Srinivasan and Bassan, 2012)

65% of advanced manufacturing companies are using 3DP and most imagine owning their own 3D printer instead of outsourcing to service providers *(Jenner and Dharmani, 2021)*. In orthopaedics, which is the industry of interest in this Thesis, 3DP is the core technology that enables more sophisticated designs to be fabricated to serve improved individualized musculoskeletal rehabilitation. The production of specialized patient-specific parts can take place on-site or

outsourced near the PoC, without the need to hold any inventory and depend on fragile supply networks. Current non-technical challenges, limitations, and technical flaws that hold 3DP from springboarding will be addressed and 3DP will be further accelerated, as necessity is indeed the driver of invention.

3.4 About 3D Technologies in Orthopaedic Point-of-Care Units

The literature review is broken into this *Sub-section* regarding subjects on PoC 3D digital design and 3DP, a *Sub-section* about the uses of 3DP in orthopaedics, *Sub-sections* on orthopaedic products design optimization enabled by 3DP for superior biological and mechanical performance, and a *Sub-section* on xR applications in orthopaedics.

The majority of PoC manufacturers are universities and hospitals working together (62%) rather than individual hospitals with 3DP labs (38%) *(ASME, 2020)*. Even though 3DP proved to have the suitable characteristics and potential to enable decentralized manufacturing at the point-of-interest, technical, non-technical, and business-model-related frontiers are causing a hysteresis for the wide diffusion and adoption of 3DP in an orthopaedic PoC 3D Unit *(see Sub-section 1.4)*.

To design and manufacture patient-specific anatomical models (biomodels) for diagnostic, treatment, or educational purposes, instruments for intra-operation use, or implants and prostheses for osteosynthesis, bone reconstruction or substitution, the workflow shown in *Figure 106* is applied. The start line of any workflow requiring generation of the 3D digital anatomical model is the image data collection. Such data can be acquired using the 3D measurements methods shown in *Figure 105*. The most common categories in healthcare are internal scanning (tomography, e.g. CT, MRI, ultrasound imaging) or external 3D scanning (photogrammetry (passive stereo), structured light, time-of-flight) *(Bartol et al., 2021; Silva et al., 2023)* techniques. Applications, strengths and limitations of tomography and 3D scanning are shown in *Figure 107*.

3D scanners might be stationary or handheld with prices ranging from under 1k to several thousands, with structured light-based 3D scanners being the most accurate. Bartol et al. *(2021)* compared about 80 3D scanners from 50 manufacturers in terms of several characteristics, i.e. resolution, accuracy, dimensions, texture scanning, scanning time, and price.

Eley *(2017)* has bolded the usefulness of PoC 3DP applications in a medical setting within the National Health Service (NHS) in the UK and reported the requirements and challenges. Andrés-Cano et al. *(2021)* reviewed the applications of 3DP for biomodels, customized tools, implants, drugs, bioprinting, and orthotics, and mentioned the 3DP technologies and materials that are most frequently applied for each application *(Figure 108)*. They emphasized the importance of human (clinical coordinator, medical specialists in radiodiagnosis, radiodiagnostic technicians, bioengineers, medical specialists), technological (3D printers, post-processing tools, computer software), and

infrastructural resources to integrate design, validation, and manufacturing of orthopaedic products in the hospital itself, under the existing legislation and under the responsibility of medical specialist that delivers the treatment. Thus, costs and surgical time are reduced, whilst safety and patient-doctor satisfaction increases. Guidelines were also briefly provided on image acquisition specifications for bone (slice thickness <1 mm with <1 mm increment, Kernel filter for soft or moderate parts, collimation 1,25-1,5 mm), segmentation method (manual, automatic, semi-automatic techniques), surface mesh model export and processing (mesh correction, closing ends, internal structures optimization, smoothing, modifications, separations), and 3DP and post-processing.

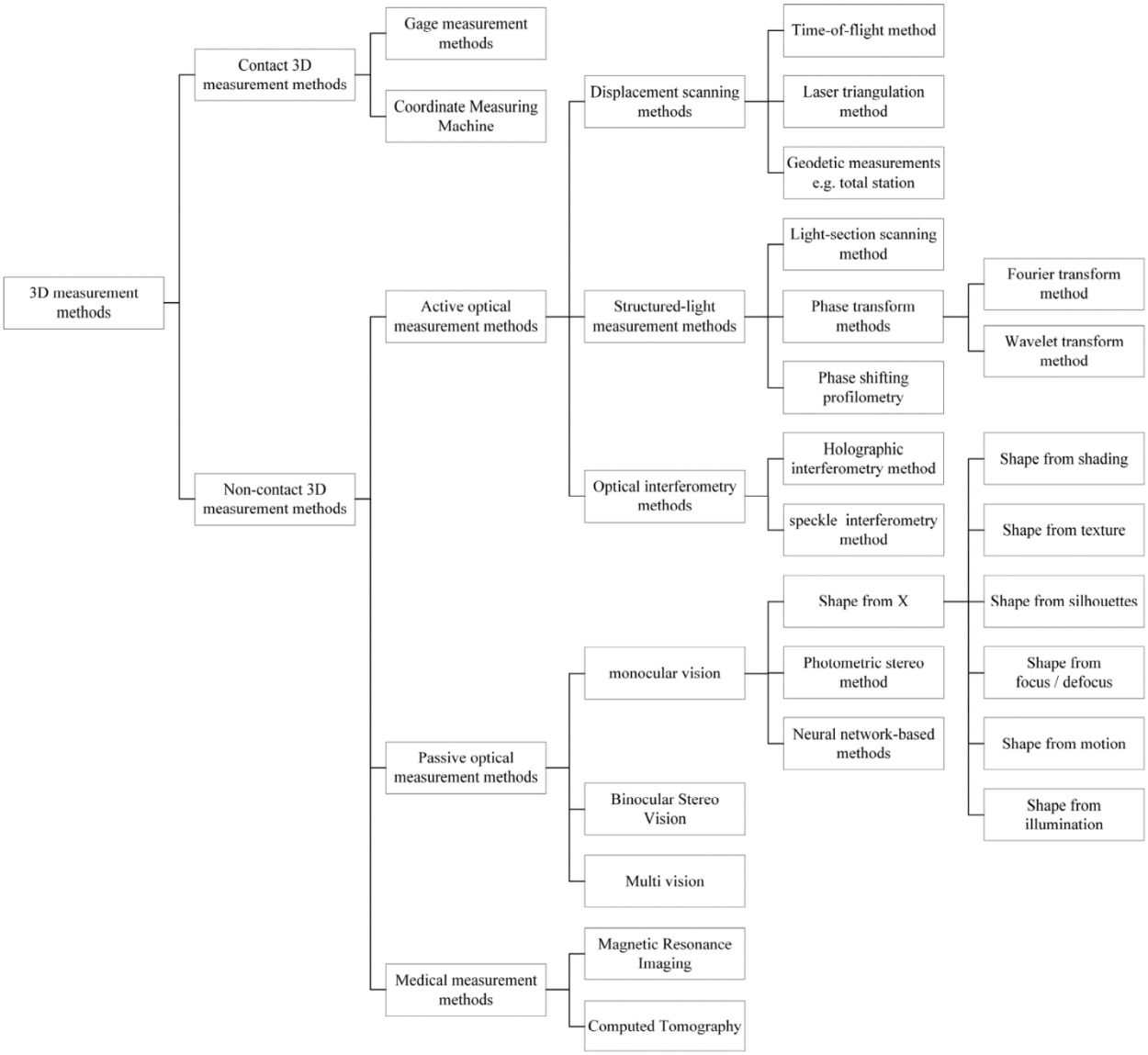

Figure 105: Measurement methods for 3D object reconstruction. Source: (Cui, Tao and Zhao, 2021)

Serrano et al. *(2020)* reviewed the associated costs (3D printers purchase and maintenance, staff, software, material, ancillary services, and components) and the economic impact of using 3DP in the clinic for orthopaedic surgical application and the potential savings. Similarly, Talanki et al. *(2021)* conducted an economic analysis of the time and cost savings occurring from utilizing 3DP for anatomical models and surgical guides in orthopaedic surgical applications. Frizziero et al. *(2019)*

carried out a case study (rigid flatfoot due to tarsal coalition) and adopted PoC 3DP workflow that reduces costs and time and improves orthopaedic procedures.

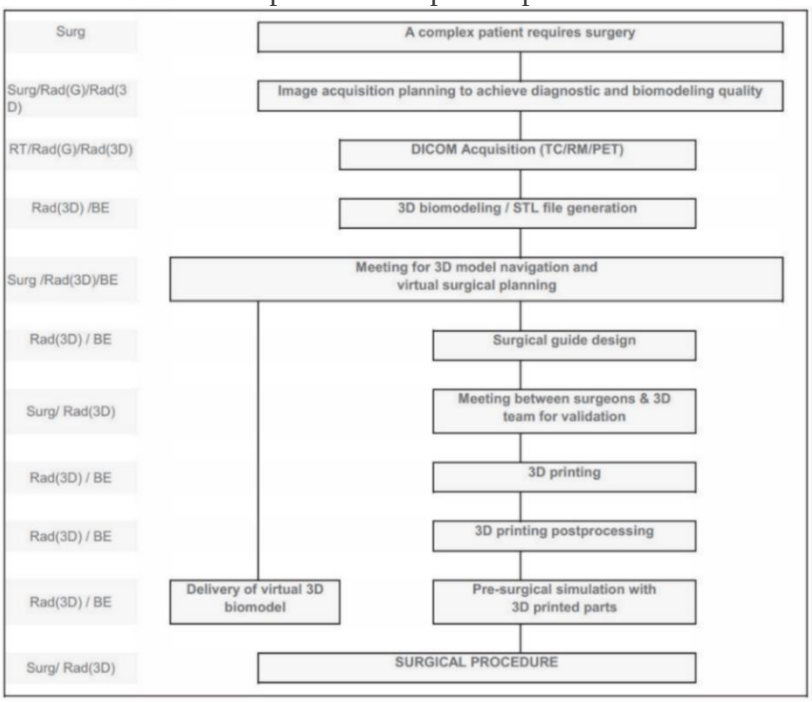

Figure 106: Workflow for patient-specific products 3DP. Source: (Travers, 2021)

Internal Body Scanner

Source: Siemens

VS

External Body Scanner

Source: ZG Technology

Technology	Strengths	Limitations	Applications
X-Rays	• X-rays pass through the non-metallic objects such as human organs and tissues • It is like a giant camera which helps for doctors without having to do surgery and provide information inside the patient's body • Soft tissues such as organs and skin cannot absorb high-energy rays and beam passed them, and dense material such as bones absorb these rays	• With prolonged use, there is some risk of cancer • Can change the DNA base causing a mutation • Causes cell damage • Not used in the scanning of skin and outer body	• Used to treat malign tumours • Helpful for radiologists to identify various cracks, injury, infections and abnormal bones • Helps to detect bone cancer
CT Scan	• A CT scan easily record an image of the bone, blood vessels and soft tissues • Without doing any invasive angiography, a cardiologist can view clear 3 D images	• Gives the patient a high dose of radiation which increases the risk of cancer	• Provides detailed internal information of the body which is helpful for the physician • Quite precise; doctors can get a clear picture where the problem is located and quickly undertake the surgery, radiation and various treatment in more precision way.
MRI Scan	• Magnetic and radio waves create images of organs, tissues and other internal structure of the body • Provides information about blood circulation in the body, and it detects problem-related the blood	• MRI is performed in an enclosed space & makes thus many patient face problem during MRI due to fear of this enclosed surface and loud noise. • While processing, it involves loud noise • MRI scan is expensive	• Detects abnormalities from the structure of the soft tissue in the body like cartilage tissues and soft organs such as heart and brain
Ultrasound	• Painless and safe which produces inside pictures of the body using sound waves • A small transducer (probe) of the ultrasound machine and gel are placed directly on the skin. High-frequency sound waves are transmitted, through the probe & the gel, these sound waves finally create the image of the internal part.	• Large images by ultrasound are difficult. • Creates difficulty in imaging of penetrating bone. It only sees the outer surface of the bony structure.	• Shows the movement of internal body's organs and blood flowing through blood vessels • It helps physicians to evaluate symptoms of pain, infection and swelling
3D Scanning	• 3D Scanning takes few seconds for a single scan • 3D Scanning measures and analysis quickly the part • Used to capture the design of medical implant with high accuracy and as per required dimensions • Safe to use on the human body	• Does not provide any information about the internal shape of the organ/body • Only includes measurement/ information about the upper surface of the body or objects.	• Used to capture the sizes of any physical objects • Ensures that parts will fit together for the first time

Figure 107: Strengths, limitations, and applications of medical imaging and 3D scanning. Source: (Haleem and Javaid, 2019)

Utility	Technology	Material
3D planning biomodel	FDM	PLA/ABS/TPU 95A
3D demonstration biomodel	MJ	Photopolymers
Patient-specific guide	SLA	Sterilisable resin
Orthesis	MJF	Nylon
Surgical instruments	DMLS	Stainless steel
Customised Implant	DMLS	Titanium (Ti-6Al-4V)

ABS: Acrylonitrile butadiene styrene; DMLS: Direct metal laser sintering; FDM: Fused deposition modelling; MJ: Material jetting or polyjet; MJF: Multijet fusion; PLA: Polylactic acid; SLA: Stereolithography; TPU 95A: Thermoplastic polyurethane.

Figure 108: Most frequently used technologies and materials for 3DP in orthopaedics. Source: (Andrés-Cano et al., 2021)

Pajot et al. *(2020)* discussed the implementation of a *"digital chain"* for the design and manufacture of customized surgical guides in a hospital setting, whereas Honigmann et al. *(2021)* harnessed a ME 3DP to fabricate an individualized proof-of-concept scaphoid PEEK implant within the hospital environment.

Teo et al. (*2021)* assessed the feasibility of 3DP custom stainless steel 316L proximal tibia locking plates and accompanying polymer surgical drill guides *(Figure 109)*. The 3DP implants were post-processed at a local center. The reported mean time consumed for each plate fabrication was approximately 24 hours starting from the image data acquisition completion. This means that customized orthopaedic implants can be produced in a PoC 3D Unit within clinically acceptable times as long as adequate manufacturing facilities and skilled personnel exist.

Keller et al. *(2021a)* overviewed applications of 3DP in hand surgery (splints, fracture models, surgical guides, endo-prostheses) and reported their practical experience and challenges for the implementation of 3DP into daily clinical routine. In another study, Keller et al. *(2021b)* proposed a multidisciplinary workflow for PoC 3DP of patient-specific hand and wrist orthotics *(Figure 110)* using a tablet connected to a structure sensor and VP and ME 3D printers. The 75%-circumferential forearm splint cost $6 using a ME-based 3DP and $20 using the VP-based technology.

Similar upper limb orthotics were 3DPed on-demand, just in time at the PoC 3D Unit by Popescu, Marinescu and Sandach *(2021)* and Blaya et al. *(2018).* They experienced improved quality for the patient at reduced development time with quicker turnaround but highlighted the reliance on skilled engineering staff, special equipment, and logistics.

Sanicola et al. (*2020)* were the first and only to provide forward-thinking guidelines for establishing a 3D biofabrication laboratory within a HCF aiming at engineering models and tissue constructs for therapeutic and non-therapeutic applications. They presented a hypothetical layout of the *"hospital of the future"(Figure 111)* and structured the guidelines in categories, i.e. site choice and regulations, facility requirements, 3DP and post-processing areas, power considerations, procedural safety, vibration isolation of the printers, ventilation requirements/considerations, laboratory space and storage, QMS, data ecosystem and cloud manufacturing, data protection, cloud security, and IoT regulations.

Figure 109: 3D Printed metal proximal tibia locking plate and polymer drill guide. Source: (Teo et al., 2021)

Figure 110: 3D Printed splints at the PoC. Source: (Keller et al., 2021b)

Daoud et al. *(2021)* reported the complex yet realistic process of in-house 3DP of medical devices: from materials and resources to digital workflow, regulations, and formation of multi-disciplinary teams. Their guidelines are summarized in *Figure 112*.

Calvo-Haro et al. *(2021)* dealt with the *"Do-it-yourself"* 3DP evolution identification in PoC 3D Units for manufacturing and co-design custom-made implants with external manufacturers. Their Department's experience in 623 custom 3D prints (product type, utility, time, materials used) from 2015 to 2020 in the fields of Traumatology, Reconstructive and Orthopaedic Oncology was reported. Lakshmi et al. *(2019)* supported the need to leverage the *"maker culture"* in PoC medical device making and stated that among the medical, engineering, administrative, and regulatory expertise, these *"expert amateurs"* could provide innovative input in patient care.

Beitler et al. *(2022)* outlined the importance of implementing quality management systems and regulations to which medical device manufacturers must adhere to, and PoC 3D Units should be mindful of when establishing their *"best practices"*: a) monitoring, maintenance protocols, control

of process parameters, b) image data acquisition, and c) physical device manufacturing: material characteristics, 3DP pre-processing, parameters of 3DP, post-processing, sterilization. After all, the medical specialist to attach the custom-manufactured orthopaedic part has full responsibility.

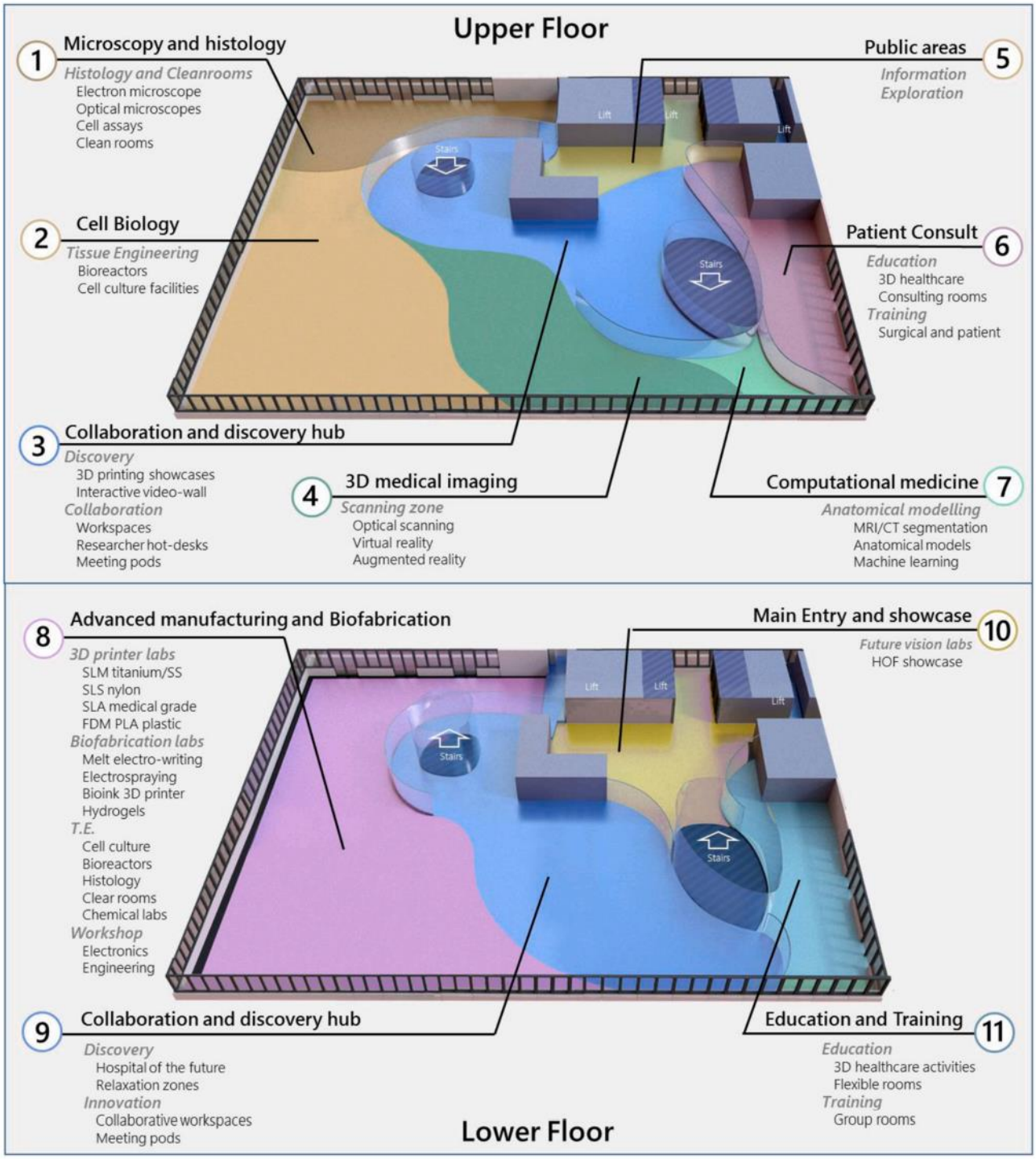

Figure 111: Floorplans of hypothetical PoC 3D Unit indicating the various zones. Source: (Sanicola et al., 2021)

Even individual owners of 3D printers could theoretically take over medical device fabrication from traditional manufacturers due to the rapid fabrication, customizability, and design freedom for unlimited geometric complexity offered by 3DP technologies. Although these *"makers"* and *"do-it-yourselfers"* input beneficially in the evolution of medical devices, the fact that current regulations

do not regulate such 3DPed devices, introduces considerable concerns about the quality control and assurance and post-processing such as cleaning and sterilization.

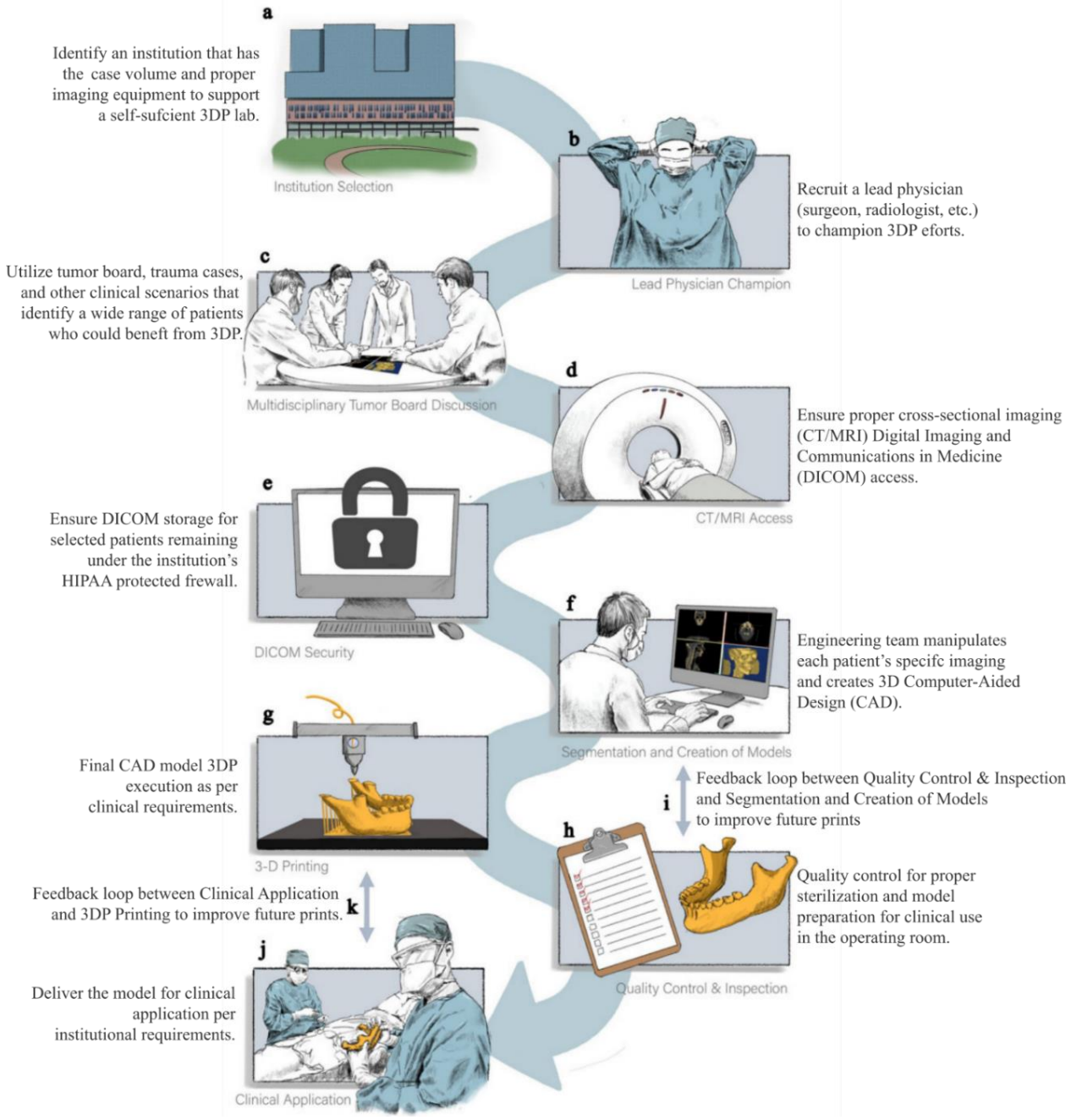

Figure 112: Steps in creating a PoC 3D Unit. Source: (Daoud et al., 2021)

Considerations and suitable frameworks to understand the paths and value of 3DP in designing and manufacturing medical devices under the existing regulatory perspective were described by Morrison et al. *(2015)* and Shamsi et al. *(2017)*, whereas Kirillova et al. *(2020)* pointed the bioethical and legal issues engaged with 3D (bio)printing of medical devices.

It is suggested that legislators and regulatory bodies adapt or enter new guidelines and regulations to guarantee maximum benefit to public health, whilst minimizing safety concerns. Although regulations on the design, manufacture, and quality control of medical devices around the world differ *(Bhat et al., 2019)*, the Personalized Medical Devices authoring group of the International

Medical Device Regulators Forum (IMDRF) *(2020)* seeks to provide regulatory pathways for custom-made, patient-matched and adaptable medical devices (*Figure 113*) and recommends three possible approaches that regulators might choose to implement for regulatory oversight of manufacturers of medical devices at the PoC. These are:

1. **Manufacturing under special arrangements:** healthcare institutions and professionals are recommended to be required to protect patient safety and ensure appropriate performance of the medical device, by meeting certain imposed requirements that include:
   i. manufacture and use of devices to be under an appropriate QMS.
   ii. have on file and provide information on the use of devices manufactured to the competent authority: justification of the indispensable clinical needs warranting manufacture of the device and details of manufacture, including appropriate quality management validation documentation, device designs or modifications, and the intended use.
   iii. make available to the patient receiving the device the name and address of the manufacturing healthcare institution or professional, the details necessary to identify the device, a declaration that the device meets general safety principles, and where applicable, information on which principles have not been fully met together with a reasoned justification thereof.
   iv. documentation of understanding of the manufacturing facility, the manufacturing process, and the design and data providing confidence that the device will function as intended, including the intended purpose, and that is sufficiently detailed to enable the regulatory authority to ascertain that the general safety and performance requirements have been met.
   v. to take all necessary measures to ensure that all devices it manufactures are manufactured in accordance with the documentation referred to previous point.
   vi. review experience gained from the clinical use of all devices it manufactures, report any adverse events to the regulatory authority, and take all necessary corrective and preventive actions.
   vii. the healthcare institution will allow the regulatory authority to inspect the manufacturing processes when appropriate.
2. **Medical Device Production Systems (MDPS):** a collection of raw materials, software and digital files, and main production and post-processing equipment intended to be used by a healthcare provider/facility to produce a specific type of medical device at the PoC, for treating their patients. The responsibilities placed upon the user of the MDPS will vary depending on the complexity and type of medical devices produced and may include:
   i. following the manufacturer's instructions for the use of the system, including using materials, components, software, or other equipment as specified by the manufacturer.

ii. keeping records.
iii. controlling the production environment (including contamination control).
iv. ensuring that infrastructure (including networks and cybersecurity) is in place as per the manufacturer's requirements.
v. completing post-processing activities, such as annealing and heat-treating operations.
vi. undertaking end-user verification and validation activities, including any associated testing, of the final medical device.
vii. cleaning.
viii. sterilizing.
ix. Reporting the performance of the MDPS to the manufacturer.
x. applying identification marking (e.g. labeling) to the final device for identification by the patient or user.
xi. post-market reporting as per jurisdictional requirements.
xii. making arrangements with the manufacturer of the MDPS with regard to adverse events, complaints, and investigations

3. **Fully regulated manufacturing:** treated as traditional manufacturers. There is a need to ensure correct classification according to risk level, following the usual regulatory requirements to obtain pre-market approval. Manufacturers are required to meet pre- and post-market regulatory requirements: implementation of appropriate QMS, generation of clinical evidence, compliance with safety and performance standards, design, testing, manufacturing standards, undertaking supplier control, provision of labels and information, registration, post-market surveillance, corrective action, adverse-event reporting.

Existing regulatory frameworks for medical devices do not specifically account for the differences between 3DP and conventional manufacturing. On the US market, the majority of 3DPed medical devices cleared are Class II, approved via the 510(k) pathway by the FDA. From April 2019 to March 2020, the FDA cleared approximately fifty 3DPed devices *(ASME, 2020)*. *Figure 114* shows the number of FDA-approved 3DPed medical device types from 2010 to 2020, the materials from which these devices are made of, and the 3DP technologies used for producing each type.

For emergency custom-made devices that are of interest to this Thesis, in the US, the FDA *(2014)* describes the exemption of non-trialing custom-made devices from regulatory control under certain circumstances involving life-threatening conditions and no alternative treatments, by allowing authorized healthcare professionals to provide design input and take responsibility for the quality assurance and control, safety, and performance of the customized medical devices.

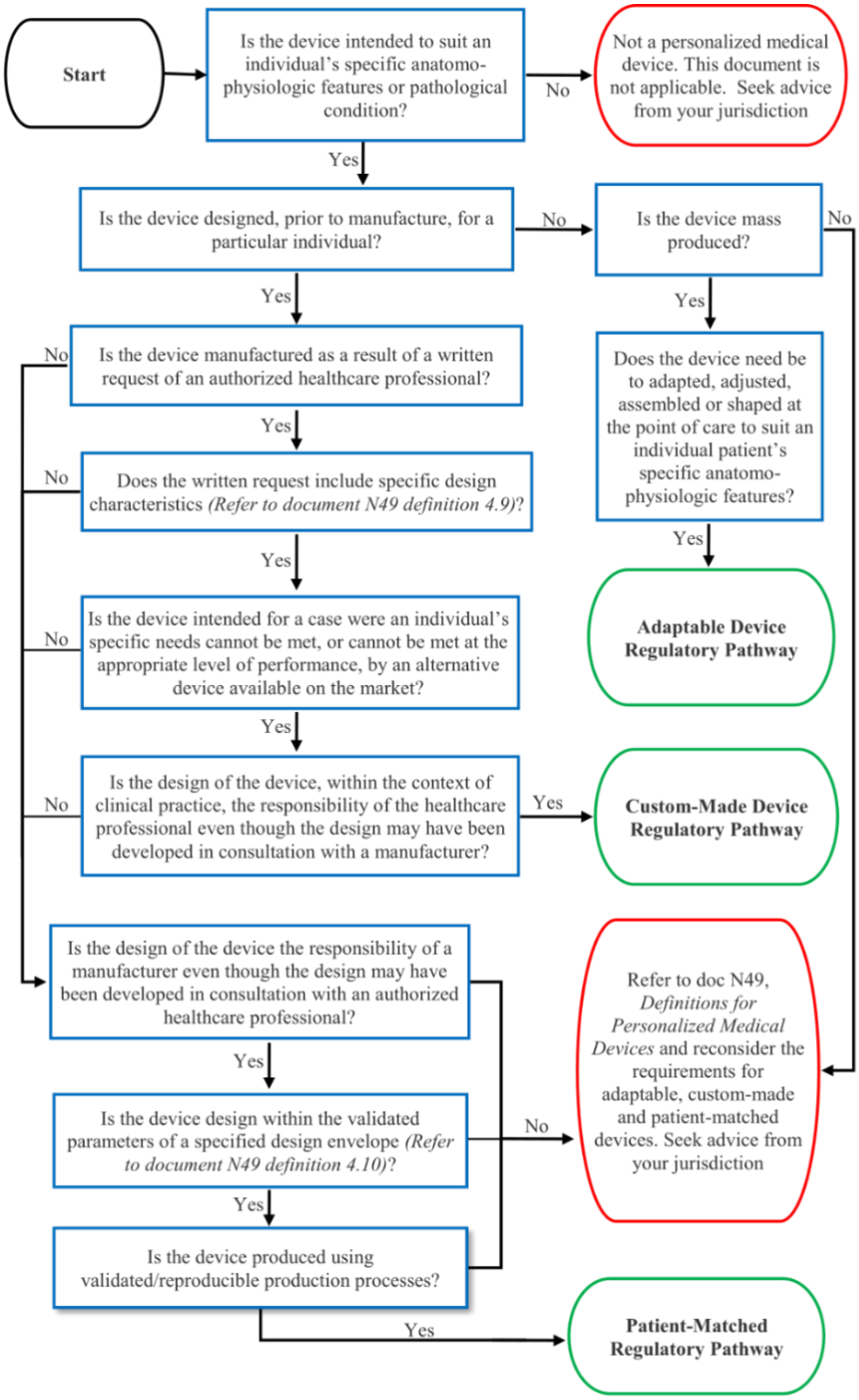

Manufacturer: *any natural or legal person4 with responsibility for design and/or manufacture of a medical device with the intention of making the medical device available for use, under his name; whether or not such a medical device is designed and/or manufactured by that person himself or on his behalf by another person(s).*
Custom-made device: *intended for the sole use of a particular individual and is specifically made in accordance with a written request of an authorized healthcare professional, which gives, under their responsibility, specific design characteristics even though the design may be developed in consultation with a manufacturer and is intended to address the specific anatomo-physiological features or pathological condition of the individual for whom it is intended.*
Patient-matches device: *matched to a patient's anatomy within a specified design envelope using techniques such as scaling of the device based on anatomic references, or by using the full anatomic features from patient imaging and it is typically produced in a batch through a process that is capable of being validated and reproduced and is designed and produced under the responsibility of a manufacturer even though the design may be developed in consultation with an authorized healthcare professional.*
Adaptable device: *it is mass-produced and adapted, adjusted, assembled or shaped at the point of care, in accordance with the manufacturer's validated instructions, to suit an individual patient's specific anatomo-physiologic features prior to use.*

Figure 113: Regulations tree for custom-made, patient-matched, and adaptable medical devices. Source: (IMDRF, 2020)

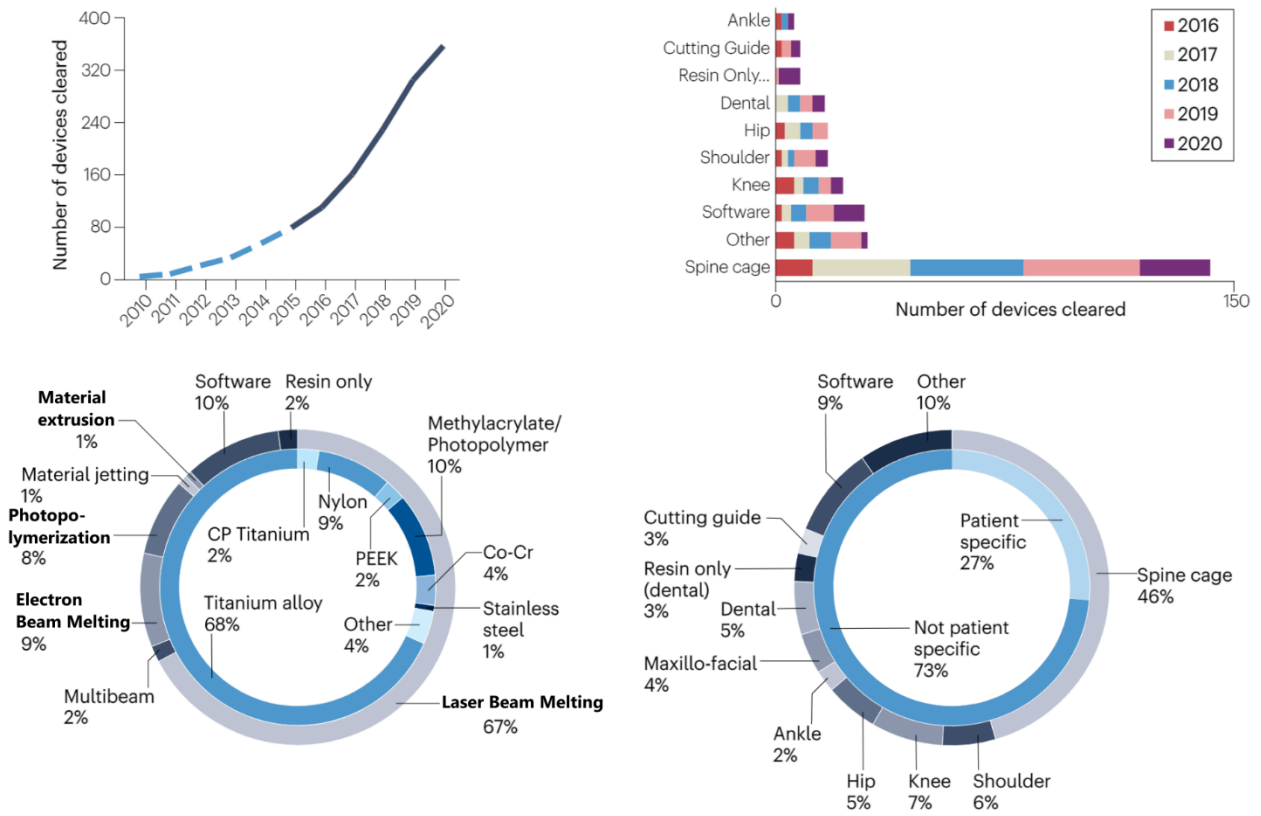

Figure 114: FDA-cleared 3DPed medical devices breakdown. Source: (Fogarasi, Snodderly and Di Prima, 2023).

In the EU, custom-made medical devices are regulated as per Annex XIII, and emergency medical devices developed within HCFs in the EU must conform to Article 5.5 of the MDR 2017/745 *(Official Journal of the EU, 2017)*.

FDA has mentioned technical considerations *(2017)* and five possible scenarios for a HCF to implement PoC design and 3DP *(2021)* as shown and described in *Figure 115*.

Scenario	Additional Details and Considerations
A healthcare facility prints and uses 3D-printed devices in a way that presents minimal risk in terms of patient safety and ability to print	• Should employ monitoring and risk mitigations strategies • Should leverage existing standards, certifications • Not intended for implants, life-supporting / life- sustaining devices or devices that present a serious health risk to patients
A device is designed by manufacturer to be printed by the healthcare facility where the post-processing steps are automatic or self-contained	• Uses a validated process that has been evaluated by FDA • Device use should be consistent with cleared indications and manufacturer instructions for use
A device is designed by manufacturer to be printed by the healthcare facility where there is more complex manufacturing and post-printing processes	• The healthcare facility would have to have appropriately trained personnel and proper equipment • May require labeling, training, instructions for calibration, or testing on-site in order to facilitate appropriate 3D printing by the healthcare facility
A manufacturer or contract manufacturer is co- located at the healthcare facility	• The healthcare facility doesn't intend to set up and manage their own 3D facility or the devices are not minimal risk • The healthcare facility is performed by a traditional manufacturer, contract manufacturer, or other 3rd party using their own equipment and personnel
A healthcare facility chooses to become a manufacturer (develop, test, print) and the devices are not minimal risk	• The healthcare facility desires to design and control their own 3D printing operations and the devices are not minimal risk • The healthcare facility is responsible for development/design, testing, and printing • The healthcare facility is responsible for all regulatory requirements

Figure 115: PoC design and 3DP scenarios mentioned by the FDA. Source: (Beitler et al., 2022) as per FDA (2021)

Regardless of the scenario to be implemented by a potential PoC 3D Unit, the approximate costs of 3D printers and materials that are most commonly used in orthopaedics are encapsulated in *Figure*

116. In contrast to PoC 3DP of metallic and polymer end-parts such as endo-prostheses and orthotic parts that require industrial grade machines, PoC 3DP polymer anatomical models, molds, and surgical guides are well-established and ready to be implemented in a healthcare setting at relatively low initial capital costs and maintenance costs due to less sophisticated infrastructures and simpler ancillary equipment. However, suitable sterilization methods should be implemented.

Printing Process	*Materials Used*	*Manufacturers*	*Common Applications*	*Estimated Cost of Machine (US$)*	*Material Cost (US$/Kg)*
VAT Photopolymerization (VP)	Varieties of resin (thermosetting plastics). Standard, engineering (ABS-like, PP-like, flexible, heat-resistant), castable, dental, and medical (biocompatible)	FormLabs, 3D Systems	Medical Models, Splints & prosthetics, Surgical guides	$3,000 (desktop)->$80,000 (industrial)	$149-$200/L of resins
Powder Bed Fusion	Engineering thermoplastics, such as nylon	FormLabs, 3D Systems	Medical devices and tools	$10,000 (desktop), $100,000 (industrial)	$100/Kg for nylon
Powder Bed Fusion	Metal Powders (Ti6Al4V, Co-Cr-Mo, Al2O3-ZrO2)	EOS Group, SLM-Solutions	Implants	>$350,000	>$300/Kg
Powder Bed Fusion	Metal Powders (Ti6Al4V, Co-Cr-Mo, Al2O3-ZrO2)	Arcam, GE Additive, Qbeam	Implants, Surgical instruments	>$250,000	>$300/Kg
Material Extrusion	Standard thermoplastics, such as ABS (Acrylonitrile Butadiene Styrene), PLA (Polylactic Acid), and their various blends	Stratasys, FormLabs	Medical Models, Splints & prosthetics, Surgical guides	$1,000->$15,000	$50-$150/Kg
Binder Jetting	Gypsum Based Powders (ZP150, ZP151), Metal powders	ExOne, Zcorp, 3D Systems, HP	Medical Models	$30,000 (desktop) - $450,000 (industrial)	-
Material Jetting	Liquid (VeroWhite, VeroClear, TangoPlus, Multi-material)	Stratasys, Projet, (3D Systems), Polaris	Medical Models (Combination of multiple colours and materials)	$10,000 – >$250,000	$300-$1000/Kg

Figure 116: Feedstock materials costs and 3D printers used in orthopaedics. Source: (Gandapur and Amin, 2022)

Once the orthopaedic device has been 3DPed and post-processed, before implantation, it has to be sterilized to prevent infection. Many sterilization methods exist, each having advantages and disadvantages *(Rutala and Weber, 2013; 2016; Govindaraj and Muthuraman, 2015) (see Figure 38)*, but the most suitable must be selected depending on the application and biomaterial(s) to be sterilized as toxic byproducts can be produced. Especially for the sterilization of 3DPed products, the following apply *(Garot, Bettega and Picart, 2021)*:

- Metals and ceramics can be sterilized by most methodologies and of course, autoclave steam techniques as these materials can withstand high temperatures.
- For polymers, the following were reported:
    a. Hydrogen peroxide plasma sterilization or Ethylene Oxide (EtO) sterilization is suggested due to their low temperature and gentleness. ABS and PLA materials 3DPed with ME were sterilized with ethylene oxide *(Aguado-Maestro et al., 2021; Toro et al., 2021)* and hydrogen peroxide plasma (*Oth et al., 2019*) with acceptable dimensional deformation.
    b. Frizziero et al. *(2021)* have steam-sterilized PLA parts with success. Surgical jigs 3DPed with photo-polymerization out of photocurable resins were found to be successfully sterilized with plasma sterilization and autoclave steam sterilization *(Marei et al., 2019; Török et al., 2020).*
    c. Electron-beam irradiation accelerates degradation rate, whereas autoclaving might impact their morphology and physical-chemical-mechanical properties. Davila et al. *(2021)* reviewed different sterilization techniques for 3DPed PLA parts and stated that the choice should be based on product type and application.
- For biodegradable polymers, UV exposure, γ-irradiation, and β-irradiation are recommended.

Out-of-healthcare-facility custom-made orthopaedic devices have been extensively 3DPed for over a decade for many simple to special cases. Hence, in the previous scenarios, the scenario of a PoC 3D Unit that designs (exclusively or in collaboration with external partners) but outsources the manufacturing (3DP, post-processing) has to be considered. Although HCFs are now shifting towards implementing in-house manufacturing, until recently, *"in-house design and outsourced manufacture"* approaches were mostly the de facto standard.

Such approaches were presented by Willemsen et al. *(2019)* who applied a workflow of design, production, and regulatory procedures *(Figure 117)* for two successful patient-specific spinal prostheses (*Figure 118*) development under the current EU regulations. Both implants and drill guides were 3DPed. The implants were designed with beam-based unit cells of 500-600 μm pore size with an overall porosity of 70% to facilitate bone ingrowth and evaluated by FEA analysis by engineers in close collaboration with the surgical team in-hospital, manufactured (3DP, hot isostatic pressing, polishing, screw holes finishing) by certified external partners (ISO 9001:2008, ISO 13485:2012), and sterilized in situ (manual cleaning, autoclave sterilization, sterile packaging) before implantation. Before 3DP the final metallic implants with PBF technology, they 3DPed plastic prototypes to check and ensure optimal fit.

Willemsen et al. *(2019)* prepared a technical file in accordance with the regulations of the EU MDR 2017/745 *(Official Journal of the EU, 2017)* containing the clinical substantiation, all technical and design considerations, the risk analysis *(Figure 119)*, manufacturing process, labeling, as well as

mechanical simulations with FEA, compression strength tests, and cadaveric experiments. They reported that for the second custom device, the team was better prepared and it was developed within weeks instead of months.

Thinking out of the box, the potential and feasibility of 3DP at the point of interest are best comprehended if we imagine the need for custom orthopaedic devices and instruments beyond Earth, for long-duration extraterrestrial missions. It was reported that 3DP is promising for making medical devices for operational orthopaedics in space *(Wong, 2016; Rajput, 2021; Navarro et al., 2021)*.

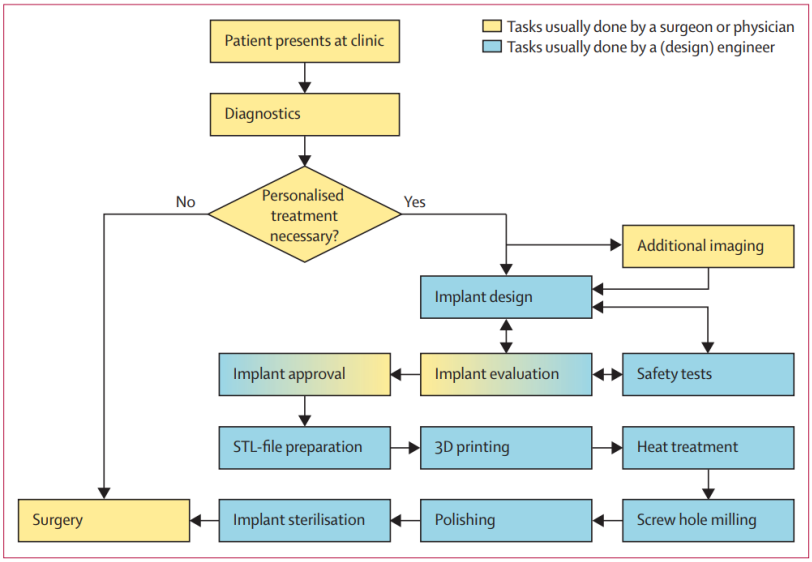

Figure 117: Workflow for patient-specific implants 3DP. Source: (Willemsen et al., 2019)

Custom 3DP Ti6Al4V ELI grade 23 prothesis to treat a 16-year-old boy with incomplete paralysis due to severe kyphotic deformity of the thoracic spine resulting from neurofibromatosis type 1

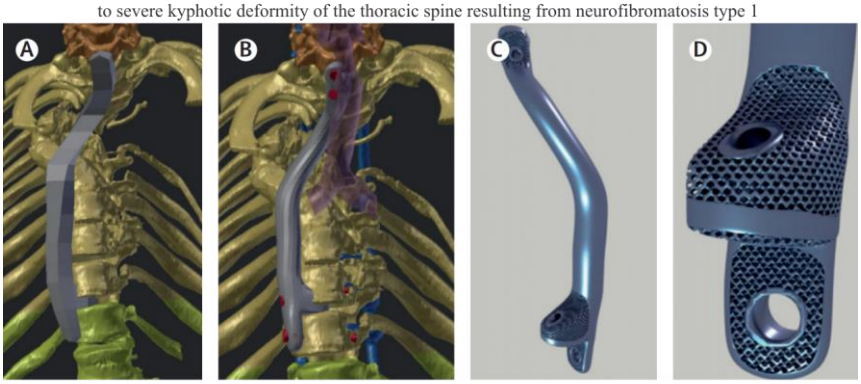

Custom 3DP Ti6Al4V ELI grade 23 prothesis and polyamide drill guides to treat a 68-year-old woman with progressive paralysis due to a severe cervicothoracic dissociation

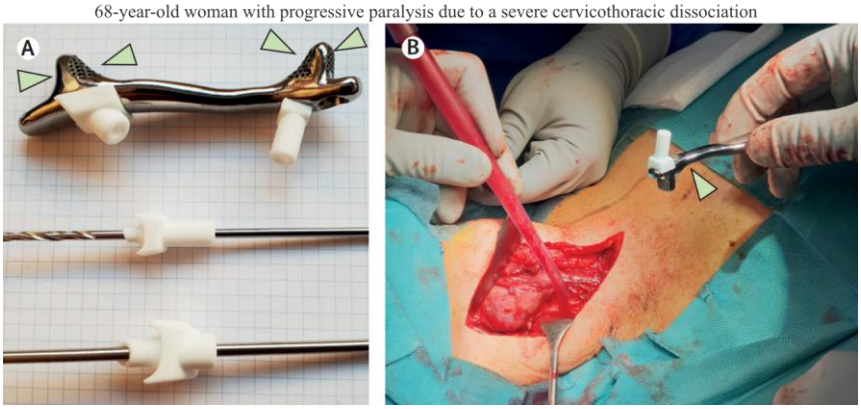

Figure 118: Custom 3D Printed spinal prostheses. Source: (Willemsen et al., 2019)

	Requirements	Variables	Justification
Surgical approach			
Anatomical positioning of the implant	Must not interfere with anatomical structures in the cervical and thoracic spine	Size of implant, thickness of implant	Cadaveric trial surgery before implantation, experience of the surgical team, literature
Anatomical free space	Must allow positioning without great difficulties in the surgical approach	Drill guides, fitting guides for optimal placement on desired position	Cadaveric trial surgery before implantation, experience of the surgical team, literature
Implant specifications			
Material properties	Must not cause adverse tissue reaction	Material, hot isostatic pressing (metal stress-relieving treatment)	Literature
Implant strength	Must provide support for lifetime of patient, must provide axial compressive mechanical support	Size of implant, thickness of implant, weight of patient	Finite-element analysis, biomechanical compression test
Optimisation of bone–implant interface	Should have porous interface with bone to facilitate ingrowth	Pore-sizes, porosity, unit-cell structure	Literature
Screws	Must allow compressive fixation to the spine and provide rotational stability	Quantity, lengths, thickness, type, and trajectories of screws	Computer-aided design and three-dimensional analysis, finite-element analysis, literature
Alternatives			
Off-the-shelf implant and fixation rods	Should not be an equal or better treatment option than the personalised treatment	Size of spinal rods, osteosynthesis material	Literature, experience of the surgical team, biomechanical compression test

Figure 119: Risk assessment for custom 3DPed spinal prostheses. Source: (Willemsen et al., 2019)

Before closing this *Section* on PoC design and 3DP, it is worth mentioning that it is a common practice that inventions and methods for designing and manufacturing standard or customized orthopaedic implants with special features are being protected by patents to enable corporations' sales to grow and prosper. However, in the current epoch of mass customization enabled by 3DP, as long as a digital design is readily available, medical device-making can easily take place at the point of interest. As manufacturing is being decentralized, intellectual property protection issues and patent infringement *(Mendis et al., 2020*) are among the main issues that shield innovation in 3DP and adoption from the healthcare industry *(ASME, 2020*). Especially in orthopaedics, surgeons and engineers could share their designs to receive credits and thus, develop community-based individualized healthcare that is both affordable and sustainable *(D'Urso, 2017).*

3.5 3D Printing Applications and Impacts on Orthopaedics

Depending on the case, orthopaedic products such as implants can be either geometrically simple (e.g. screws and plates for bone fixation), or complex when it comes to bone substitution. Standard and modular off-the-shelf parts cannot offer ideal outcomes as these are not tailored and optimized for a unique individual patient. Instead of using such and fitting the patient to the method, the method should be matched to the patient's morphology through customized design and production. This is essential, especially for critical reconstruction and oncological cases.

The process flow for individualized implant design and manufacturing was described back in the late 80s by Walker and Ewald *(1990)*: radiology is harnessed to generate the patient's anatomy, and granted the surgeon's instructions, computer software is utilized to design and fit the implant (CAD), and program the manufacturing operations (CAM).

Until recently, implants were shaped by traditional technologies (machining, casting, forging, molding, powder forming). An ideal alternative method for rapidly producing tailored one-off implants of high complexity is 3DP which can ensure unlimited geometrical design freedom, time and cost-effectiveness, efficiency, and flexibility through all stages of the product development: from the initial design (what to be made?) to final production (how to be made?). Nevertheless, the development process via 3DP will again involve several challenges *(Figure 120)*.

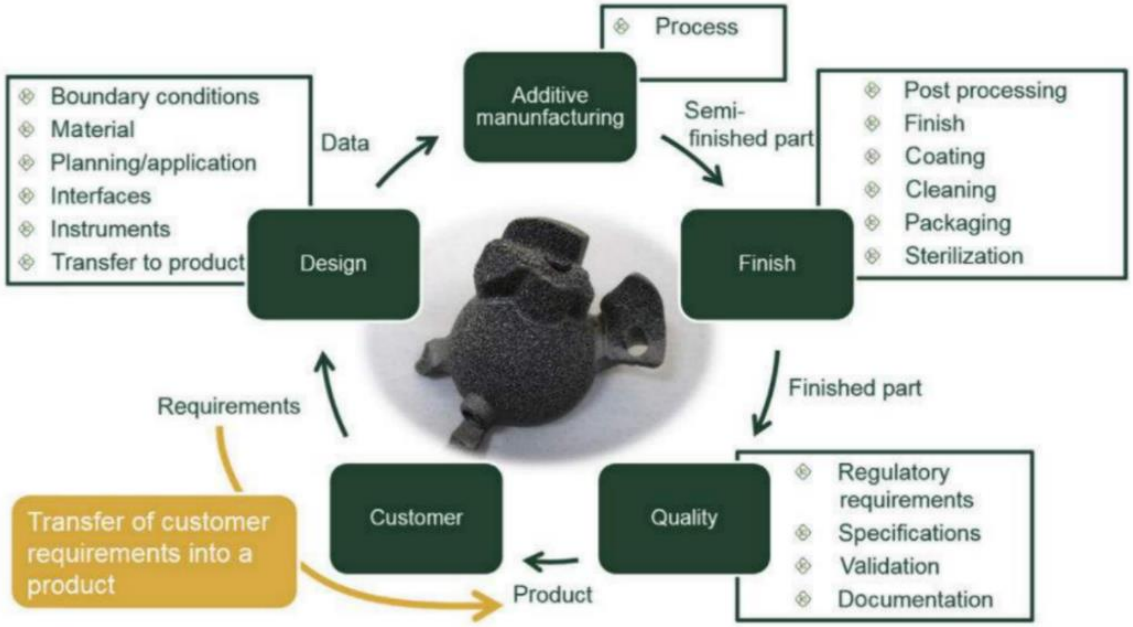

Figure 120: Process and challenges of custom implant 3DP. Source: (Munsch, 2019)

To sustainably achieve the required delivery times at low costs, 3DP is deployed both by the giants of the standard orthopaedic products market that are gradually shifting towards bespoke product design, and also by companies[54] with alternative business models that are focused exclusively on patient-specific services.

A summary of 3DP applications in medicine is pictured in *Figure 121*, whereas, regarding the usage of 3DP in orthopaedics, Charbonnier, Hadida and Marchat *(2020)* gave an extensive overview of musculoskeletal-related clinical applications and the ongoing research trends.

During the early 90's, 3DP was initially intended for rapid prototyping of anatomical models utilizing mostly VP techniques (SLA) *(Mankovich, Cheeseman and Stoker, 1990; Klein et al., 1992; Baker et al., 1993).* D'Urso et al. *(1999)* coined the terms *"biomodelling"* and *"real virtuality" (D'Urso, 2005)* to describe replicated morphologies of biological structures in solid material

[54] E.g. Implantcast (Implantcast Gmbh, Buxtehude, Germany), founded in 1988, Materialise (Materialise NV, Leuven, Belgium), founded in 1990, Anatomics (Anatomics Pty Ltd, Melbourne, Australia), founded in 1995, Ossis (Ossis Ltd, Christchurch, New Zealand), founded in 2007, Ortho Baltic Implants (Ortho Baltic Uab, Kaunas, Lithuania), founded in 2012, ATTRI (ATTRI Orthopaedics Pty Ltd, Cape Town, Africa), founded in 2012, Polygon Medical Engineering (Moscow, Russia), founded in 2016, 3D-Side (3D-Side SA, Mont-Saint-Guibert, Belgium), founded in 2018.

substances and use 3DP technologies in spine complex spine surgery cases *(Izatt et al., 2007)*. A 3DPed spinal biomodel is shown in *Figure 122*.

Shortly later, 3DP for customized implants to substitute and regenerate bones was proposed, and associated patents were issued *(Fink, DiNovo and Ward, 1994; L. Cima and M. Cima, 1996).*

3D technologies *(Papagelopoulos et al., 2018)* and 3DP are currently being used in basic to intricate surgical orthopaedic applications *(Ejnisman et al., 2020)*, to directly or indirectly reinstate musculoskeletal form and function by fabricating biomodels, Patient-Specific Instruments (PSIs) and molds, implants, (mega)endo-prostheses, orthotics and prosthetics, TE constructs, and drug delivery products *(Giannatsis and Dedoussis, 2009; Lunsford et al., 2016; Javaid and Haleem, 2018; Charbonnier, Hadida and Marchat, 2020; Salmi, 2021).*

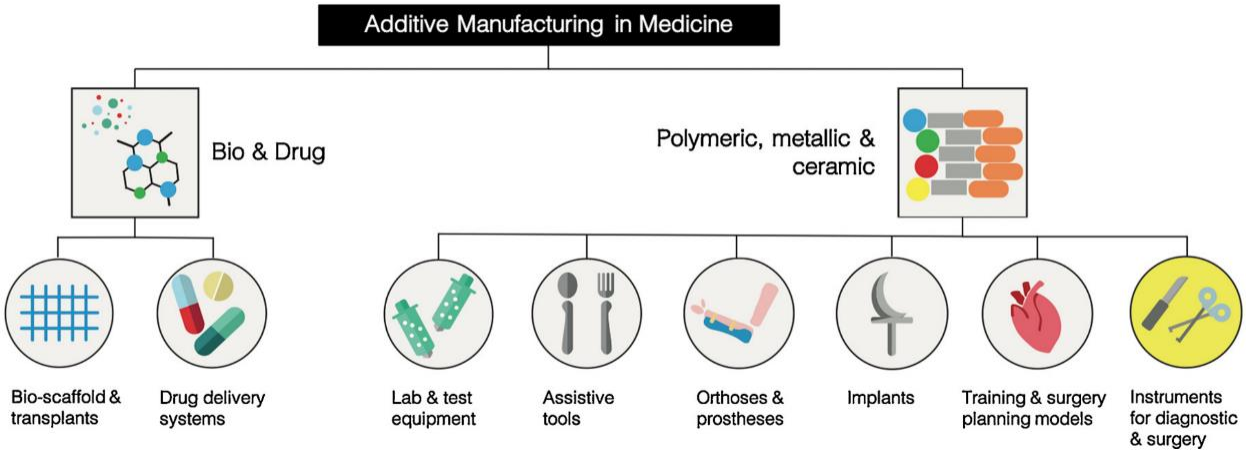

Figure 121: 3DP applications in medicine. Source: (Culmone, Smit and Breedveld, 2019)

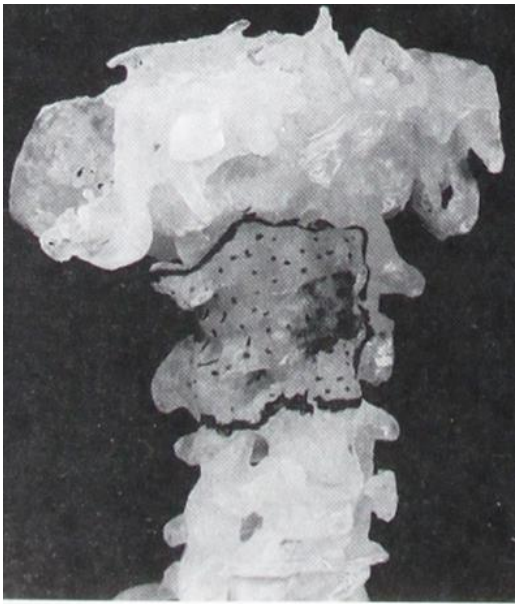

Figure 122: 3D Printed biomodel displaying osteoblastoma and planned resection margins. Source: (D'Urso et al., 1999)

3DP technologies are successfully being used for individualized rehabilitation in a plethora of cases in anatomical areas ranging from head to toe, most of them usually featuring interconnected porous architectures. For example.:

1. Primary arthroplasties, mainly in the hip and knee *(Robbins et al., 2020; Kumar et al., 2021).*

2. Fractures over the appendicular skeleton *(Morgan et al., 2020; Alonso et al., 2021; Yang, Li and Luo, 2021)*: upper and lower extremities surgeries trauma *(Figure 123) (Lal and Patralekh, 2018; Gomà et al., 2021; Foukas et al., 2024)*, pelvis *(Hill et al., 2020; Wu et al., 2020; Wang et al., 2020; Cao, Zhu and Gao, 2021)*, calcaneus *(Chung et al., 2014; Lee et al., 2019; Savvidou et al., 2020)*, and salvage of foot and ankle *(Hamid, Parekh and Adams, 2016; Kadakia et al., 2020a)*.

S No.	Anatomical Region	Applications of 3D Printing
Upper Limb		
1	Acromion	3D model used for plate pre-contouring[14]
2	Clavicle	3D model used for planning and plate pre-contouring[15,16]
3	Proximal Humerus	3D model used for planning[17]
4	Distal Humerus and elbow	3D-printed plates,[18] templates and guides[19–21], 3D model[22]
5	Distal radius	3D planned osteotomies[23]
6	Hand	3D model for planning thumb reconstruction,[24] vascularized bone flaps,[25] scaphoid plate- experimental[28]
Lower Limb		
7	Acetabulum	Several applications [see Table 2]
8	Pelvis	3D model used for planning[33–35]
9	Distal Femur	3D model used for planning[37]
10	ACL Reconstruction	Patient-specific, arthroscopic ACL femoral tunnel guide (MRI based)[41]
11	Proximal Tibia	3D model used for planning[6,42–44]
12	Tibial Pilon and Malleoli	3D model used for planning[46]
13	Talus	3D model used for planning safe zones for screws[47]
14	Calcaneum	3D model used for planning[48,49]
15	Ankle	Patient specific navigational template for ankle ligament reconstruction[50]
16	Bowed femora: atypical fractures	3D model used for planning nailing[51]

Anatomical Region	Clavicle	Glenoid	Shoulder joint	Proximal humerus	Distal humerus - elbow	Elbow	Distal radius	Metacarpal
Description	Proximal fracture with oblique fracture pattern	Post traumatic defect	Brachial plexus injury	Symptomatic nonunion with lateral cortex bone defect	Trochlear fracture malunion	Post traumatic, multidirectional instability	Distal radius post traumatic malunion	5th metacarpal post traumatic malunion
Treatment	Open reduction and internal fixation with a superior plate	Open glenoid reconstruction with iliac crest autograft	Shoulder arthrodesis with a precontoured tibia plate	Open reduction and internal fixation with a plate and frozen cadaveric bone allograft	Hardware removal, osteotomy of the fragment and correct reduction and fixation with the use screws	Reconstruction of lateral and medial elbow ligaments (Box-Loop technique).	Corrective osteotomy and internal fixation with volar plate	Corrective osteotomy and internal fixation with retrograde intramedullary screw
3D approach	• Virtual planning • Anatomical model	• Virtual planning • PSI	• Virtual planning • Anatomical model	• Anatomical model	• Virtual planning • Anatomical model • PSI	• Virtual planning • PSI	• Virtual planning • PSI	• Virtual planning • PSI
3D Advantages	• Pre-operative choice of implant • Preventing complications • Reduction of surgical time	• Pre-operative awareness of the problem • Design of the bone graft shape needed • Reduction of surgical time	• Improvement of patient's satisfaction • Pre-operative choice of implant • Reduction of surgical time	• Pre-operative knowledge of the defect • Pre-modelling the allograft • Reduction of surgical time	• Improvement of accuracy • Minimization of cartilage damage • Reduction of surgical time	• Improvement of accuracy • Reduction of surgical time	• Improvement of accuracy • Ensure the correct positioning through contralateral image (healthy)	• Improvement of accuracy • Ensure the correct positioning through contralateral image (healthy)

Figure 123:3DP applications in upper and lower extremity trauma. Source: (Lal and Patralekh, 2018; Gomà et al., 2021)

3. Revision arthroplasties and oncological cases for bone substitution and limb salvage *(Angelini et al., 2019; 2020; Park et al., 2020)*. For example, tumors of the clavicle, scapula and shoulder *(Fan et al., 2015; Savvidou et al., 2018; Deng et al., 2019)*, thorax chest wall, abdominal wall, sternum and adjacent ribs *(Turna et al., 2014; Aranda et al., 2015; Tran et al., 2018; Wu et al., 2018; Kamel et al., 2020; Vannucci et al., 2020; Wang et al., 2020; Danker et al., 2021; Alvarez et al., 2021; Nihum et al., 2022)*, radius, ulna and humerus *(Park et al., 2020; Savvidou et al., 2021; Jovičić et al. 2021)*, metacarpus *(Xu et al., 2021; Punyaratabandhu et al., 2021)* and finger phalanges *(Beltrami, 2018)*, pelvis *(Wong et al., 2015; Liang et al., 2017; Hennessy, Anderson and Lozano-Calderon, 2018; Han et al., 2019; Wang et al., 2019; Wang et al., 2020; Durand-*

Hill et al., 2020; Gruber et al., 2020; Ji et al., 2020; Geng et al., 2020; Chen et al., 2020; Peng et al., 2020; Cao, Zhu and Gao, 2021; Park et al., 2021; Yu et al., 2021; Döring et al., 2021; Xu et al., 2022; Hu et al., 2022; Broekhuis et al., 2022; Gortzak et al., 2022; Pu et al., 2022; Khal et al., 2023; Hu et al., 2023; Zoltan, Popescu and Sanei, 2023; Li et al., 2023; Lv et al., 2023b) and sacrum *(Wei et al., 2016; Kim et al., 2017; Peng et al., 2019; Chaptain an Finn, 2020; Shi et al., 2021; Lv et al., 2021; 2023a; Kotrych et al., 2023),* femur *(Zhang et al., 2020;l Ji, Wu and Li, 2021),* tibia and ankle *(Papagelopoulos and Savvidou, 2022a; Savvidou et al., 2022),* calcaneus *(Imanishi and Choong, 2015; Park et al., 2018; Papagelopoulos et al., 2019a)* and talus *(Fang et al., 2018; Papagelopoulos et al., 2019b; Papagelopoulos and Savvidou, 2022b; Yang et al., 2021; Huang et al. 2021a).*

4. Molds for making antibiotic-eluting cement spacers for permanent or temporary bone reconstruction in two-stage approaches in trauma and tumor surgeries for limb salvage *(Zhao et al., 2018; Yatkınlığı et al., 2018; Chiu and Wan, 2019; Broughton et al., 2021; Zhang et al., 2021; Liu et al. 2021).* Different mold designs for femoral, talar, humeral, and calcaneal spacers are shown in *Figure 124*.

Multi-part calcaneal and talar plastic molds

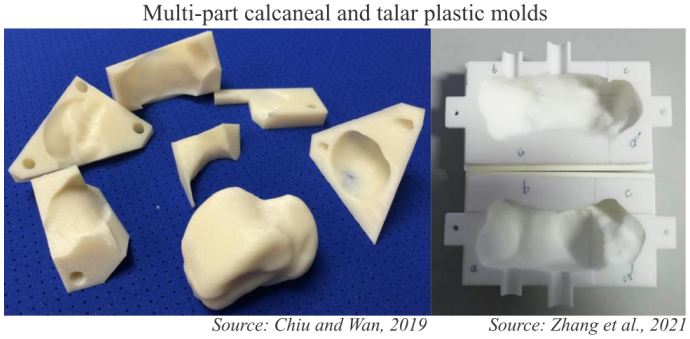

Source: Chiu and Wan, 2019 *Source: Zhang et al., 2021*

Two-part talar CoCr mold

Source: Broughton et al., 2021

Two-part humeral and femoral plastic molds

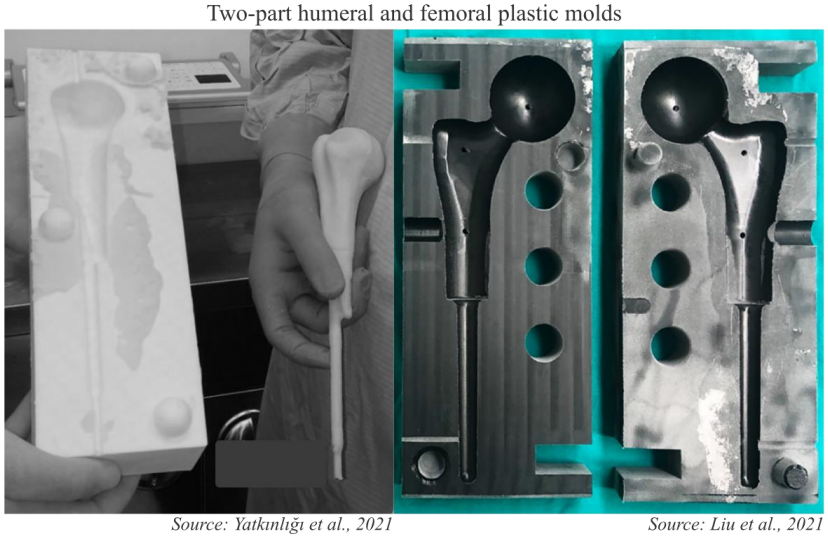

Source: Yatkınlığı et al., 2021 *Source: Liu et al., 2021*

Figure 124: 3D Printed molds for making antibiotic-eluting spacers

5. Chronic joint instabilities *(Luenam et al., 2018),* avascular necrosis *(Kadakia et al., 2020b),* and bone losses: pelvic losses *(Gruber et al., 2020)* and femoral losses *(Wangm, Xu and Zhang, 2020)* treated with 3DPed endo-prostheses.

6. Spine surgery *(Burnard et al., 2020; Wallace et al., 2020; Lador et al., 2020; Tong et al., 2020).*
7. 3DPed patient-specific jigs for implant and screw insertion guidance, bone resection, hole drilling for implant attachment, and corrective osteotomies *(Hoekstra et al., 2016; Popescu et al., 2018; Jones et al., 2018; Chen et al., 2019; Parrat and Liverneaux, 2019; Mishra et al., 2020; Marcoin et al., 2020; Pijpker et al., 2020; Raza, Murphy and Gelfer, 2021).* Such 3DPed instruments have been reported to have a short learning curve, decrease malpositioning and minimize tissue trauma and the risk of damaging nervous and vascular structures, be cost-effective and superior to conventional and freehand techniques, and achieve the same accuracy and precision with navigation systems but with decreased blood loss, exposure time and surgical time required *(MacDessi et al., 2014; Gouin et al., 2014; Wong et al., 2016; Ma et al., 2016; Jentzsch et al., 2016; Bosma et al., 2018; Pauzenberger et al., 2019; Inoue et al., 2020; Wu et al., 2021; Yam et al., 2021).* PSIs used for tibial osteotomies and pedicular sighting incorporating various features are shown in *Figure 125*.

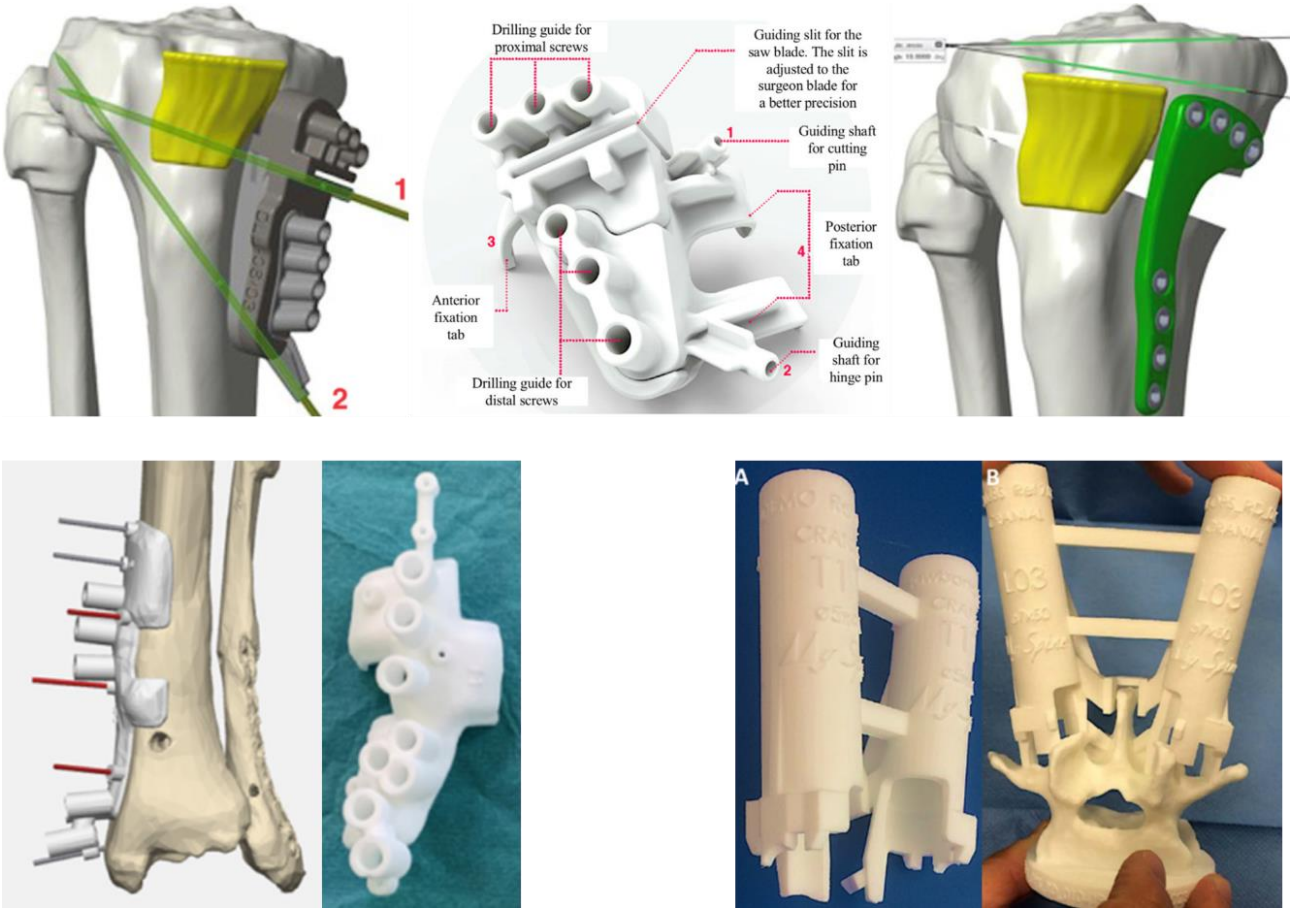

Figure 125: 3DPed PSI for tibia osteotomies and pedicular sighting. Source: (Gauci, 2022; D'Amelio et al., 2022)

In their book, the editors Özger et al. *(2022)* have collected oncological case studies on biological and 3DPed endo-prostheses used for reconstruction and limb-salvage: spine, sacrum, pelvis, femur, tibia, ankle, foot, shoulder, humerus, elbow, and hand.

The first five figures in *Appendix B* illustrate some custom-made 3DPed orthopaedic endo-prostheses and guides, and a series of cases on reconstructing osseous tissue utilizing 3DPed parts

taken from Anatomics (Anatomics Pty Ltd, Melbourne, Australia), Kang *(2021)* and Implantcast (Implantcast Gmbh, Buxtehude, Germany) *(2019)* are shown in *Appendix J*.

Wong et al. *(2015)* applied a complete process flow and showed how 3DP technologies can be used for one-step reconstruction after bone tumor resection *(Figure 127)*. They fabricated anatomical models, patient-specific cutting guides for tumor resection, patient-specific endo-prosthesis, and the accompanying patient-specific drilling guides. Pelvic resection and reconstruction with 3DPed endo-prostheses were followed by others, e.g. Han et al. *(2019)* and Yu et al. *(2021)*.

Similar workflows for developing and 3DP custom endo-prostheses were followed by Thayaparan et al. *(2019; 2020a)* for revision lumbar spine and occipitocervical fixation solutions *(Figure 126)*, and by Kadakia et al. *(2020a)* for navicular-talar foot reconstruction *(Figure 128)*.

Figure 126: Development process and 3DP patient-specific spine solutions. Source: (Thayaparan et al., 2019;2020a)

3DPed biomodels, guides, and implant prototypes are being extensively used for education and training, communication with patients, pre-operative planning and fit verification, and intra-operatively to assist surgical navigation and improve intra-operative metrics *(Jian et al., 2020)*. For example, biomodels can be used as templates for pre-contouring osteosynthesis plates for fractured bones *(Jouffroy and Riouallon, 2017; Marinescu, Popescu and Laptoiu, 2020)*. *Figure 129* shows two such examples with a fractured scapula and a healthy mirrored calcaneus. Certain SL, MJ, and BJ 3DP technologies are capable of producing impressive multi-color and multi-material demo biomodels including soft and hard tissue details as shown in *Figure 130*.

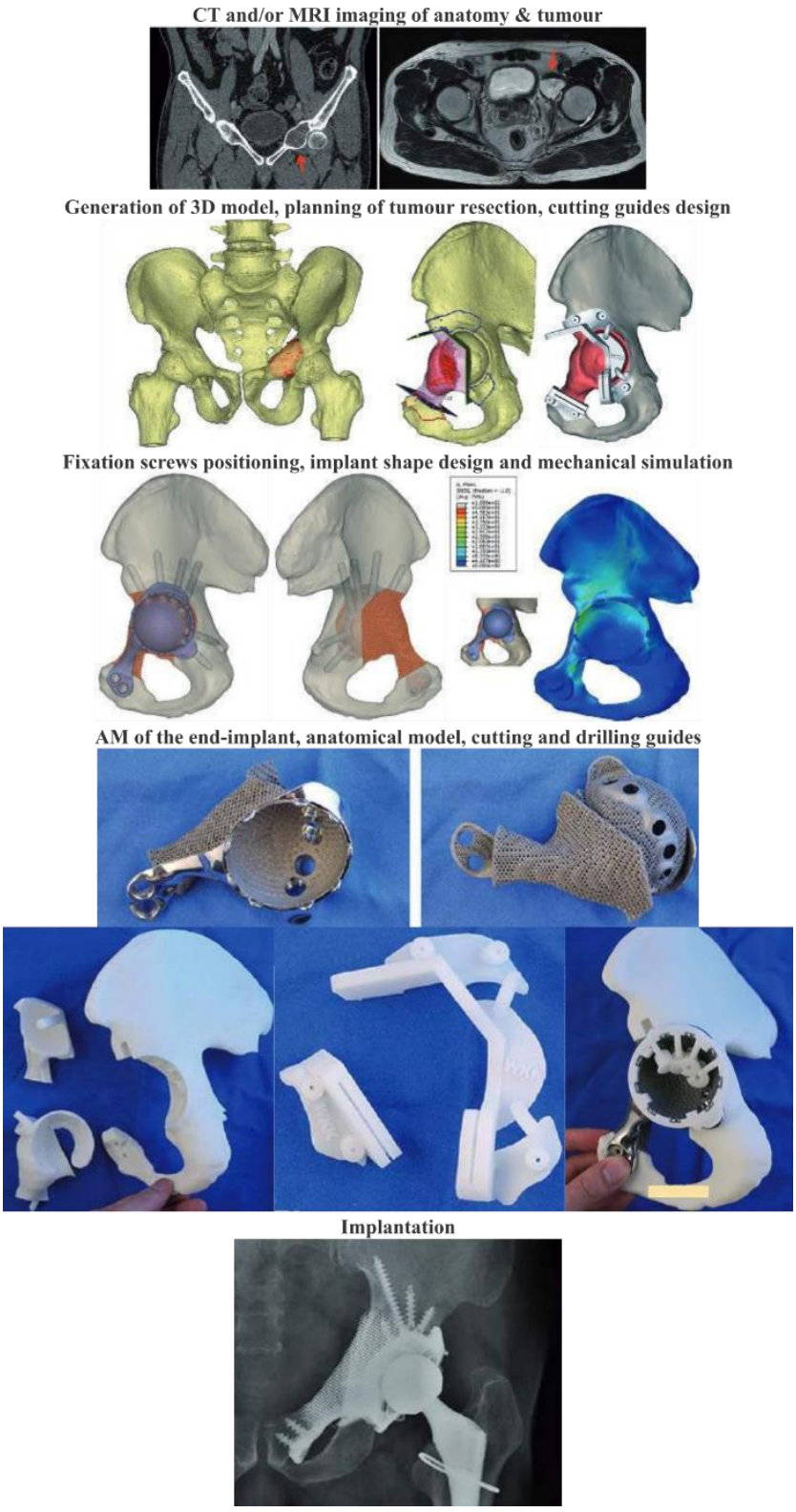

Figure 127: Process and 3DPed parts for one-step reconstruction after tumor resection. Source: (Wong et al., 2015)

PSIs (drilling, cutting, registration) for intra-operative minimally invasive *(Thayaparan et al., 2020b)* and open surgery are also being 3DPed *(Dahake et al., 2016)* either to be used for osteotomies or to accompany custom-made 3DPed fixation *(Wang et al., 2017)* and prosthetic implants *(Fukuda, 2015)* targeting joint, spine, pelvic and other locations. Such approaches were reported to have no complications and satisfactory outcomes *(Figure 131)*.

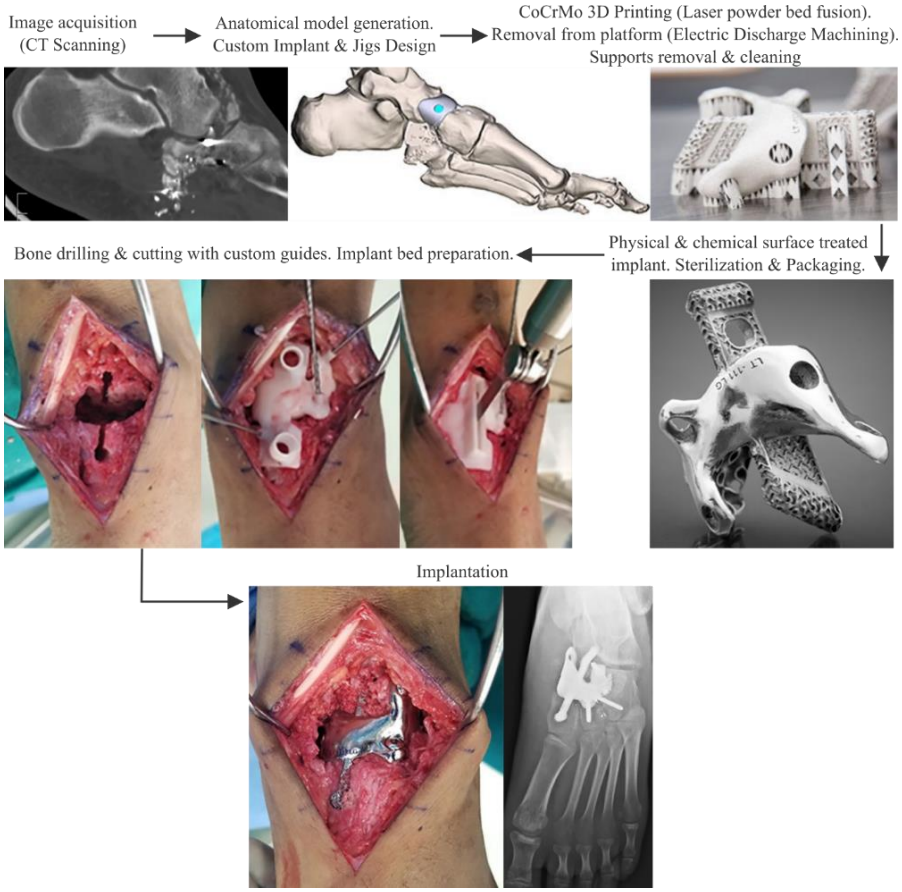

Figure 128: Foot bone reconstruction using 3D Printed jigs and endo-prosthesis. Source: (Kadakia et al., 2020a)

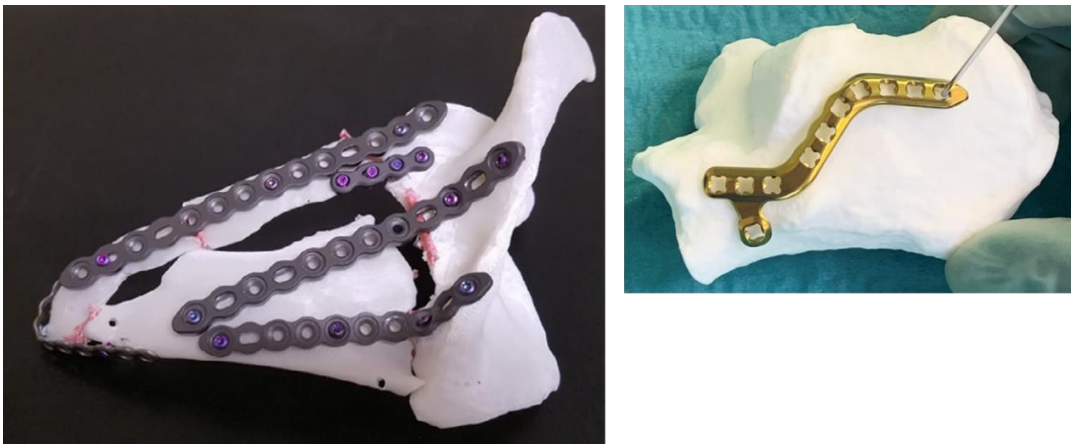

Figure 129: 3DPed scapula and calcaneus models for pre-operative plate preparation.

Source: (Thomas et al., 2021; D'Amelio et al., 2022)

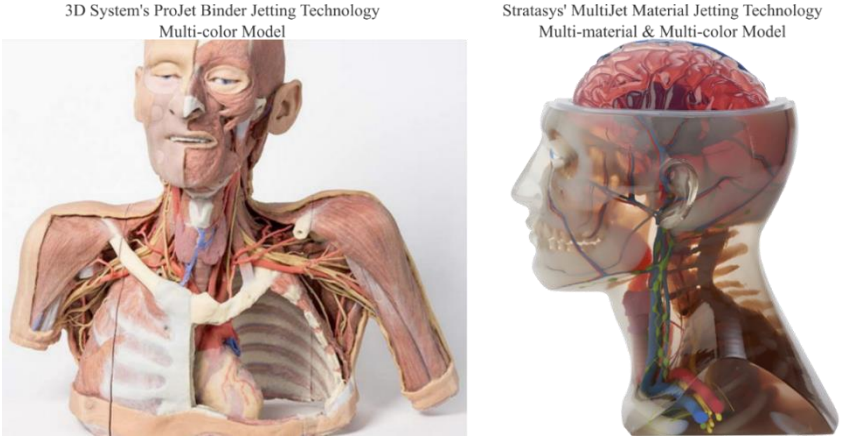

Figure 130: 3D Printed multi-color and multi-material anatomical models. Source: Stratasys and 3D Systems

Location	Disease characteristics	3DP implants	Design principles of implants	Outcomes
Joint	Glenoid defect, clavicle and scapular Ewing's sarcoma	Glenoid, clavicle, scapular	Porous structure reduces the modulus, small holes for adjacent structures fixed	No complications, achieved good functional and MSTS scores
	Distal radius giant cell tumor and posttraumatic bone defect	Semi and total wrist joint	Surface fitting, porous structure, suture grooves, bionic part, artificial deepen track	No complications, Good function recovery 9~12 month post-op
	Lunate bone collapse	Lunate	According to the variation of lunate functional anatomy and the Wolf Law	No complications, nearly full range of motion 12 months post-op
	Revision hip arthroplasty	Acetabular cages	Personalized design matched the bone defect perfectly, pore structure promoted bone ingrowth, stable support	Improved HHS scores, restoration of hip center, low complications
	Tibial plateau giant cell tumor	Tibia block	Precise matching of bone defect and the ligament firmly combining with grid	No complications, good functional and MSTS score at 7 months post-op
	Revision knee arthroplasty	Tibial and femoral blocks	Unique shape, high porosity, suitable mechanical strength, low elastic modulus	No complications, improved functional score 6 month post-op
	Calcaneus chondrosarcoma	Calcaneal	Polished the talocalcaneal and calcaneocuboidal joints, anchor points for soft tissue attachment	No complications, function was similar to the healthy side 5 months post-op
Spine	C2 Ewing sarcoma and T9 and C2–C4 tumor	Vertebral body	Optimized microstructure of the implant to acquire an ultrastructural balance, pre-angled screw holes assisting implantation	No complications, evidence of implant osseointegration 6 and 12 months post-op
	C1/2 chordoma and congenital L5 hemivertebra	Occipito-cervical fixation device and hemivertebra	Unique shape and microporous structure promoting fusion	No complications, successful fusion at 9 and 12 months
	Facet joint arthropathy	C1/2 posterior fixation device	Assisted with osseointegration around the device to encourage C1 and C2 arthrodesis	No complications, pain reduction, satisfactory imaging 6 months post-op
Pelvic	35 cases of pelvic tumor resection	Iliac, hemipelvic, screw-rod connected prosthesis	Pre-angled screw holes, modified the off-the-shelf modular prosthesis	Five died from metastatic disease, others obtained a good short-term functional outcome
	Pelvic chondrosarcoma	Iliac	Porous structure reduced modulus, cutting plane, implant position, and screw sites basing on surgical approach and exposure	No complications, satisfactory imaging showed good alignment 18 months post-op
	Sacral osteosarcoma and chordoma	Hemi sacrum and sacrum	Minimizing space between implant-bone, maximizing contact area for better stability	No complications, improved symptoms and satisfactory imaging post-op
	Complex pelvic fracture	Bone plate	Improved by modifying support parameters and heat treatment processin	Had good mechanical property, reduced operation time
Others	Distal intercondylar humeral fractures	Osteosynthesis plates	Pre-shaped, individual plates design	Shortened operative time, no significant improved elbow function
	Severe segmental defect	Truss	Mixed bone powder or antibiotics filling the bone defect for bone regeneration	No complications, promoted bone regeneration

Figure 131: 3DP applications in joint, spine, pelvis, and other areas. Source: (Li et al., 2018)

Figure 132 shows a tailored Ti acetabular implant and a matching polymer drilling guide fabricated by metal and polymer PBF 3DP.

Figure 132: 3D Printed custom Ti acetabular prosthesis and polymer drilling guide. Source: Implantcast

Compared to traditional instrumentation, PSIs for routine operations such as total knee arthroplasties are reduced and compact *(Figure 133)*. It was estimated that such PSI might result in 8-32 hours of operating room time corresponding to $1.500 savings per case, but to break even the higher cost of PSIs per se, 63 cases per year have to be carried out *(Ballard et al., 2020)*.

The conclusions found in the literature as to whether to use PSIs or not for routine operations are mixed. Beyer et al. *(2022)* anticipate that savings did not equal the costs for PSIs and that PSIs seem useful in special non-routine cases where conventional instrumentation is difficult or impossible, whereas Hafez and Moholkar *(2017)* stressed that PoC PSI development where transportation expenses and transferring management are eliminated and imaging, modeling, 3DP, sterilization, and surgery are controlled under the responsible surgeon, has more advantages.

Compared to freehand and conventional procedures, PSIs have the following advantages and disadvantages *(Gauci, 2022; Benady et al., 2022; D'Amelio et al., 2022)*:

- Advantages of PSIs:
  - Are accurate with low recurrence rates with excellent positioning and bone correction if planned and designed correctly.
  - Lead to reduced intraoperative radiation dose by a factor up to 6, which is important for the surgery team and critical for young scoliotic patients.
  - Help in blood sparing, though might be counter-balanced by the need to fully expose the bone.
  - Help in time savings during decision definition and procedures per se during surgery.
  - Have no risks for missing instruments and for defective sterilization as they are single-use.
  - There is a learning curve for positioning and exposure, but it is lower for the procedure itself.
  - Better functional outcome with lower possibility and cost for post-operative hospitalization.
- Disadvantages of PSIs:
  - No direct feedback on accuracy, but paramount to anatomical landmarks and design features of PSI per se, flexibility of K-wires, and material of PSI. For this reason, there is a need for high-quality and fidelity imaging which implies radiation for patients during CT scanning, and proper design for minimal soft tissue and periostal stripping and removal.
  - Regulatory burdens have to be considered and suitable sterilization has to be applied.
  - The lead time to develop and deliver the PSIs is higher but this is addressed if PSIs are developed at the PoC.
  - Each case requires a well-coordinated and synchronized inter-epistemic and multi-disciplinary team to produce the desired outcome, though this is addressed if PSIs are developed at the PoC.
  - The cost to develop a PSI is higher, compared to the conventional off-the-shelf counterpart (if a counterpart exists).

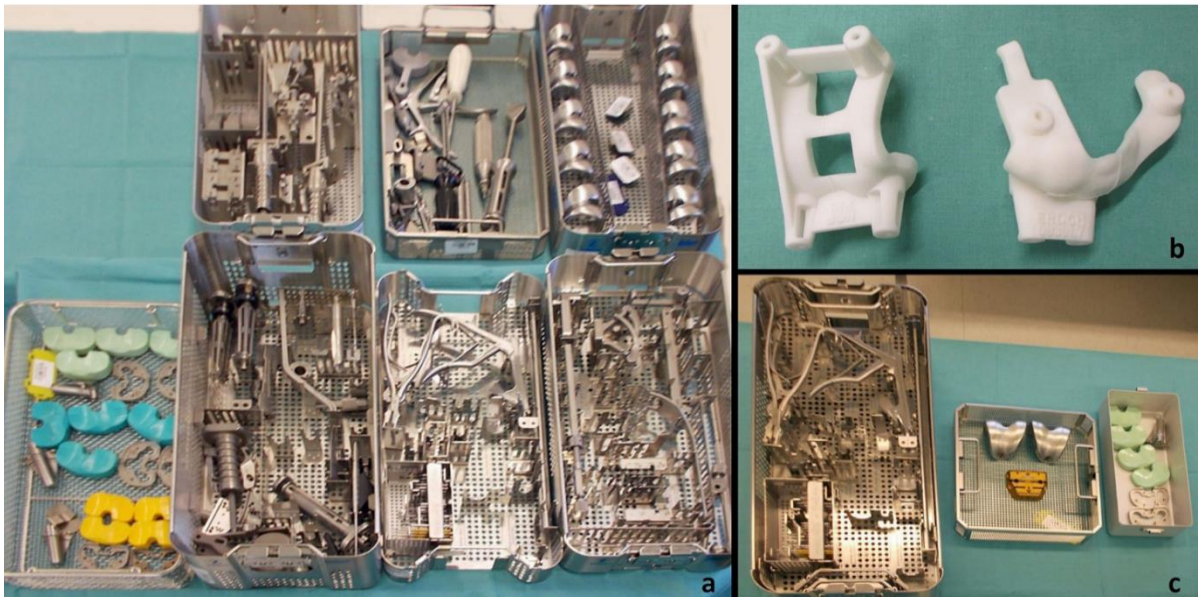

Figure 133: Conventional (a) and PSI (b and c) sets for total knee arthroplasty. Source: (Beyer et al., 2022)

3DP is being used by many disciplines of medicine for various purposes. Tack et al. *(2016)*, Chepelev et al. *(2017)*, and Kermavnar et al. *(2021)* conducted literature reviews and found that orthopaedics is the top user. In addition, Levesque et al. *(2020)* found the orthopaedic specialties that utilize 3DP the most and the materials that are mostly used. Such data is shown in *Figure 135*.

Table 7 summarizes books on medical applications of 3DP, whereas graphs in *Figure 134* show the exponentially increasing number of annually published papers on *"3D Printing"*, *"Additive Manufacturing"*, and *"Bioprinting"*, generally, and related to *"bone"* or *"orthopaedics"*.

Table 7: Book list on medical 3DP

Book Author/Editor & Year	Title
Chua and Yeong, 2015	Bioprinting: Principles and Applications.
Gibson, 2005	Advanced Manufacturing Technology for Medical Applications: Reverse Engineering.
Bartolo and Bidanda, 2008b; Bartolo, 2011	Biomaterials and Prototyping Applications in Medicine. Virtual Prototyping and Bio Manufacturing in Medical Applications.
Ringeisen, Spargo, and Wu, 2010	Cell and Organ Printing.
Liebschner, 2010	Computer-Aided Tissue Engineering.
Narayan, Boland, and Lee, 2010; Calvert and Narayan, 2011; Narayan, 2020 (First ed. 2013)	Printed Biomaterials: Novel Processing and Modeling Techniques for Medicine and Surgery. Computer Aided Biomanufacturing. Rapid Prototyping of Biomaterials.
Forgacs and Sun, 2013	Biofabrication: micro and nano fabrication, printing, patterning and assemblies.
Zhang, Fisher, and Leong, 2015	3D Bioprinting and Nanotechnology in Tissue Engineering and Regenerative Medicine.
Bibb, Eggbeer, and Paterson, 2015	Medical Modelling: The Application of Advanced Design and Rapid Prototyping Techniques in Medicine.
Atala and Yoo, 2015	Essentials of 3D Biofabrication and Translation.
Turksen, 2015	Bioprinting in Regenerative Medicine.
Cho, Jang, Lee, Park, and Pati, 2015	Organ Printing.

Ozbolat, 2016	3D Bioprinting: Fundamentals, Principles and Applications.
Deepak, 2017	3D Printing in Medicine.
Mitchell, 2017	Bioprinting.
Rybicki and Grant, 2017	3D Printing in Medicine: A Practical Guide for Medical Professionals.
Thomas, Jessop, and Whitaker, 2017	3D Bioprinting for Reconstructive Surgery.
Bhatia and Ramadurai, 2017	3D Printing and Bio-Based Materials in Global Health.
Basit and Gaisford, 2018	3D Printing of Pharmaceuticals.
Khademhosseini and Camci-Unal, 2018	3D Bioprinting in Regenerative Engineering: Principles and Applications.
Ovsianikov, Yoo, and Mironov, 2018	3D Printing and Biofabrication.
Dipaola and Wodajo, 2019	3D Printing in Orthopaedic Surgery.
Tsoulfas, Bangeas, and Suri, 2019	3D Printing: Applications in Medicine and Surgery.
Ahmad and Dutta, 2019	3D Printing Technology in Nanomedicine.
Kumar, Zindani, and Davim, 2020	Rapid Prototyping, Rapid Tooling and Reverse Engineering: From Biological Models to 3D Bioprinters.
Devine, 2019	Polymer-Based Additive Manufacturing: Biomedical Applications.
Guvendiren, 2019	3D Bioprinting in Medicine: Technologies, Bioinks, and Applications.
Cho, Kim, Jang, Gao, Han, and Singh, 2019	3D Bioprinting: Modeling In Vitro Tissues and Organs Using Tissue-Specific Bioinks.
Cho, 2019	Biofabrication and 3D Tissue Modeling.
Chen, 2019	Extrusion Bioprinting of Scaffolds for Tissue Engineering Applications.
Ouyang, 2019	Study on Microextrusion-based 3D Bioprinting and Bioink Crosslinking Mechanisms.
Singh, Prakash, and Singh, 2020	3D Printing in Biomedical Engineering.
Lamprou, 2020	3D Printing of Pharmaceuticals and Drug Delivery Devices.
Guvendiren and Serpooshan, 2020	3D Printing for Tissue Engineering and Regenerative Medicine.
Thomas and Singh, 2020	3D Printing in Medicine and Surgery.
Toit, Kumar, Choonara, and Pillay, 2020	Advanced 3D-Printed Systems and Nanosystems for Drug Delivery and Tissue Engineering.
Crook, 2020	3D Bioprinting: Principles and Protocols.
Suri, Tsioukas, and Papadopoulos, 2021	3D Printing: Applications in Medicine and Surgery Volume 2.
Wake, 2021	3D Printing for the Radiologist.
Kumar, Voicu, and Thakur, 2021	3D printable Gel-inks for Tissue Engineering.
Douglas, 2021	Bioprinting: To Make Ourselves Anew.
Sharma, Subburaj, Sandhu, and Sharma, 2021	Applications of 3D printing in Biomedical Engineering.
Kang, 2021	Clinical Atlas of 3D Printing Bone Reconstruction.
Kasper, Egger, and Lavrentieva, 2021	Basic Concepts on 3D Cell Culture.
Kalaskar, 2022	3D Printing in Medicine.
Zhang, Leong, and Fisher, 2022 (First ed. 2015)	3D Bioprinting and Nanotechnology in Tissue Engineering and Regenerative Medicine.
Conti and Marino, 2022	Bioprinting: From Multidisciplinary Design to Emerging Opportunities.
Salunkhe, Hussein and Davim, 2022	Applications of Artificial Intelligence in Additive Manufacturing.
Sandhu, Singh, Prakash, Sharma, and Subburaj, 2022	Emerging Applications of 3D Printing During Covid 19 Pandemic.
Canciglieri and Trajanovic, 2022	Personalized Orthopedics: Contributions and Applications of Biomedical Engineering

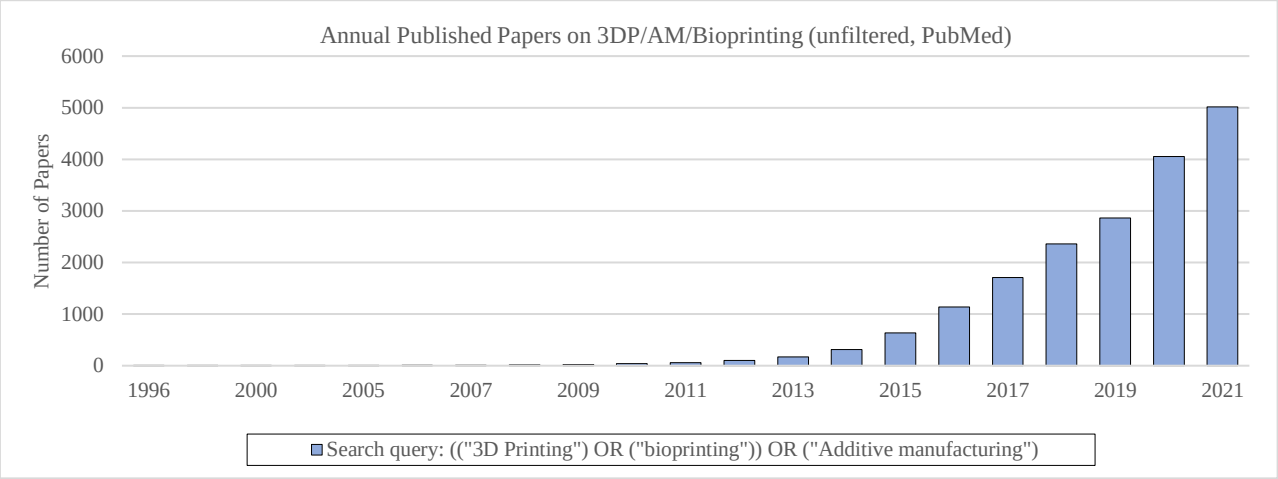

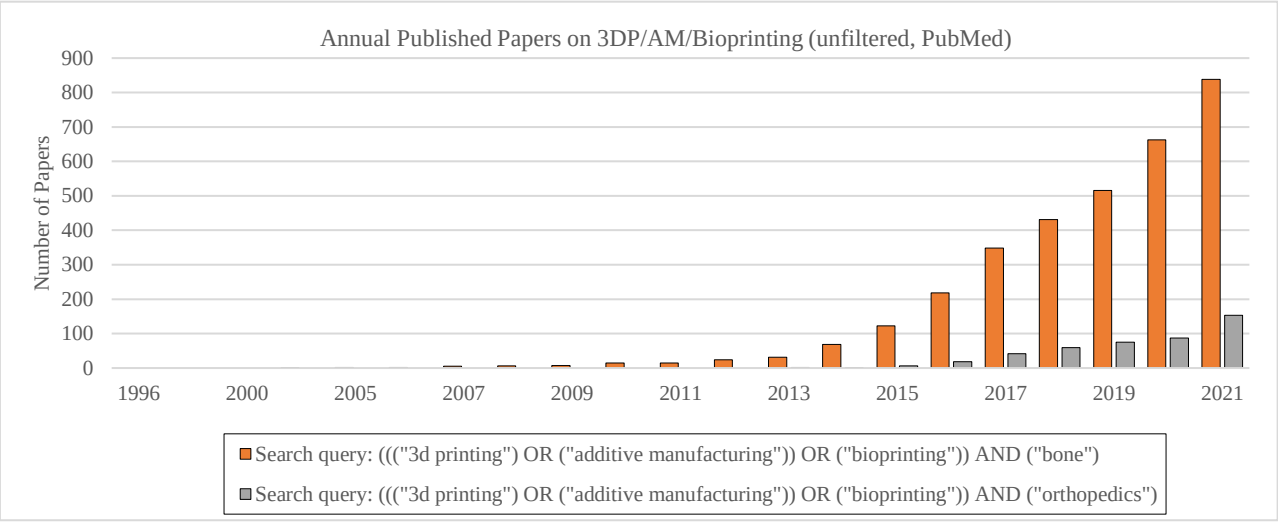

Figure 134: Published papers on 3DP/AM/Bioprinting listed on PubMed

3DPed endo-prostheses such as hemi-pelvic *(Ji et al., 2020)* for example, have been found to achieve high survival rates with acceptable functional outcomes, even though peri-acetabular tumors are associated with high rates of morbidity and mortality *(Kostakos et al., 2021)*.

The cost and development time for 3DPed custom orthopaedic surgical solutions depend on the case complexity. The cost for implants/endo-prostheses accompanied by patient-specific surgical guides might range from $4.750 to $20.000 and the total development time might range from hours to weeks *(Levesque et al., 2020)*.

Compared with classic manufacturing methods, 3DP of Ti femoral stems was found to be 35% more cost-effective than machining *(Cronskär, Bäckström, and Rännar, 2013)*, whereas compared to hot forging *(Fousová et al., 2015)* and casting *(Moiduddin et al., 2016)*, 3DPed metal biomaterials (e.g. Ti, CoCrMo, Stainless Steel 316L) were proved to have equivalent and even better mechanical performance, with higher strength, finer microstructure, and higher wear resistance *(Toh et al., 2016)*, making them ideal to be used in load-bearing and articulated orthopaedic implants.

Until now, classic manufacturing ways were the *"Achille's heel"* for many candidate biomaterials and super-alloys. With 3DP, forming of such is not the case *(Panwisawas, Tang and Reed, 2020)*.

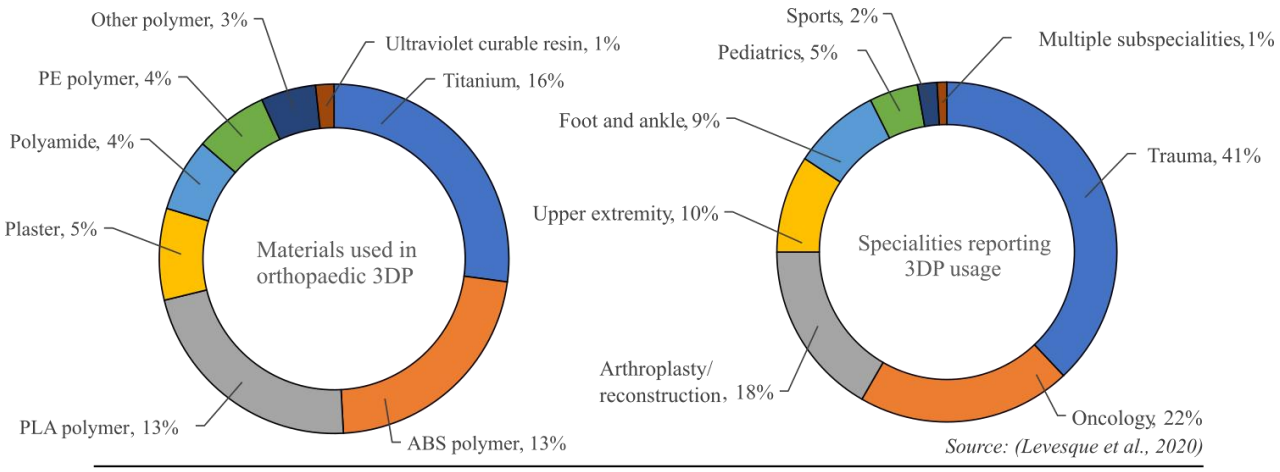

Source: (Levesque et al., 2020)

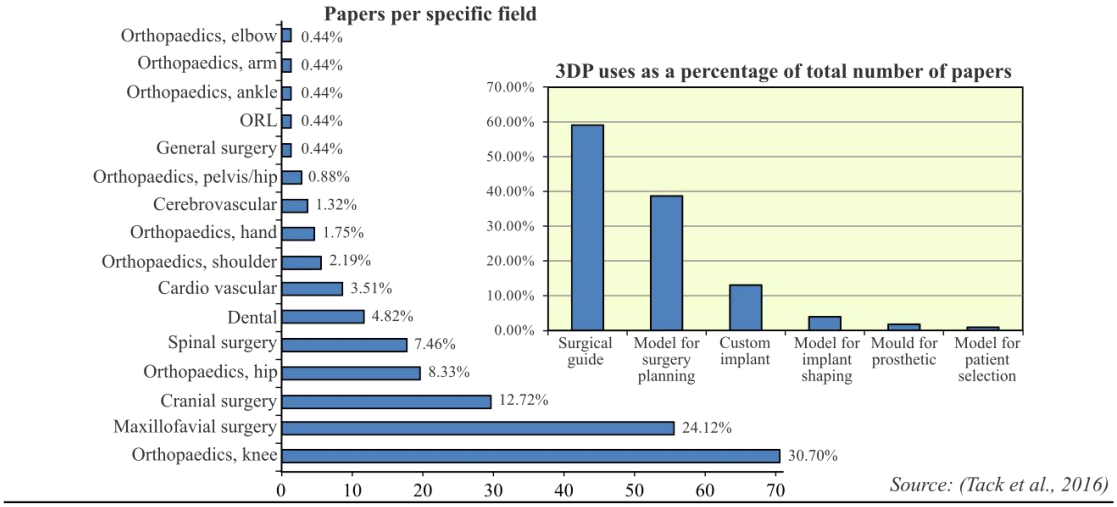

Source: (Tack et al., 2016)

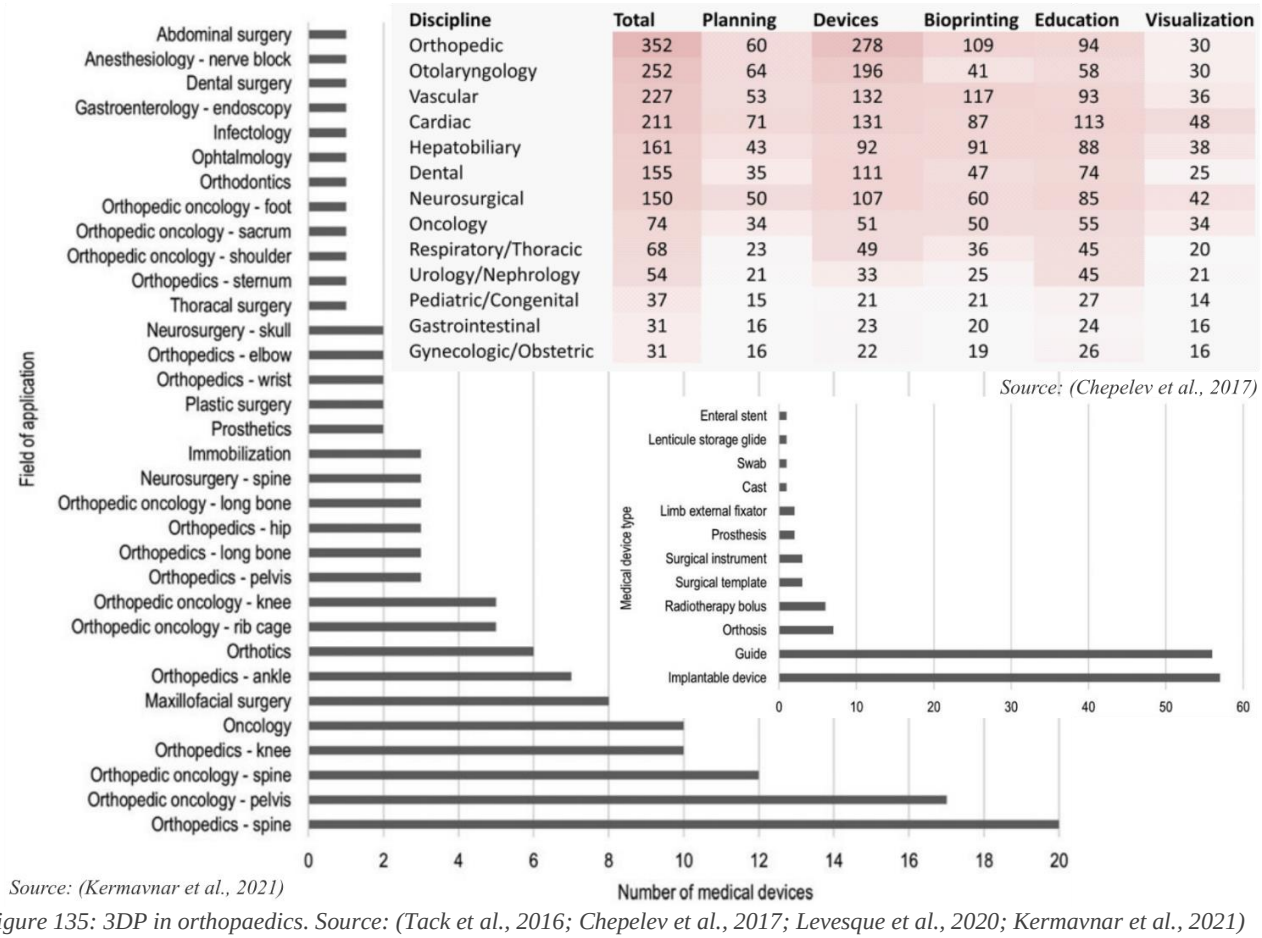

Discipline	Total	Planning	Devices	Bioprinting	Education	Visualization
Orthopedic	352	60	278	109	94	30
Otolaryngology	252	64	196	41	58	30
Vascular	227	53	132	117	93	36
Cardiac	211	71	131	87	113	48
Hepatobiliary	161	43	92	91	88	38
Dental	155	35	111	47	74	25
Neurosurgical	150	50	107	60	85	42
Oncology	74	34	51	50	55	34
Respiratory/Thoracic	68	23	49	36	45	20
Urology/Nephrology	54	21	33	25	45	21
Pediatric/Congenital	37	15	21	21	27	14
Gastrointestinal	31	16	23	20	24	16
Gynecologic/Obstetric	31	16	22	19	26	16

Source: (Chepelev et al., 2017)

Source: (Kermavnar et al., 2021)

Figure 135: 3DP in orthopaedics. Source: (Tack et al., 2016; Chepelev et al., 2017; Levesque et al., 2020; Kermavnar et al., 2021)

Although many technical and non-technical challenges still exist, many breakthroughs have been achieved in individualized orthopaedics owing to the utilization of custom 3D part modeling and 3DP technologies *(Martelli et al., 2016; Langridge et al., 2017; Javaid and Haleem, 2018; Levesque et al., 2020; Kumar, Haleem and Javaid, 2021)*, i.e.:

1. 3DPed biomodels aid in physical surgical simulations and pre-operative planning for direct visualization of malformation and better anatomic anticipation.
2. 3DPed biomodels and other devices can be used as teaching tools for studying and exercising on musculoskeletal fractures, pathologies, and anomalies, or as communication tools for improved transfer of information with the patients.
3. 3DPed biomodels and PSI assist in intra-operative navigation for improved guidance and positioning accuracy and precision.
4. 3DPed custom-made solutions (implants/endo-prostheses and instrumentation) with geometrical features and shapes tailored to the patient's anatomy facilitate:
    a. Decreasing operating time, and increasing the time-efficiency of surgical procedures.
    b. Decreasing surgical risks, errors, and incidence of post-operative complications and infections.
    c. Lowering blood loss and radiation exposure/fluoroscopy shots.
    d. Minimizing post-treatment discomfort, maximizing surgical (biomechanics and functions), and aesthetic results.
    e. Minimizing the cost and development time for one-off unique parts, compared to traditional manufacturing methods.
5. 3DP for fabricating custom solutions is easy to integrate in current classic workflows with fewer requirements for expertise for the surgeon, whilst facilitating better coordination of multi-disciplinary and inter-epistemic synergies.
6. 3DPed parts are easy to work with, possessing adequate mechanical properties. For example, 3DPed bone fixation plates have been found to reduce average varus collapse by 47,2% and the risk of screw cut-out by 14,6% when compared to conventional plate design *(Tilton et al., 2020a)*, whilst having comparable strength to conventionally made plates *(Tilton et al., 2020b)*.
7. Instead of coating the implants/endo-prostheses to gain spongy surfaces, the 3DPed counterparts can have integrated porosity. This implies an absence of interfacial layers, with greater structural solidity, eliminating delamination issues, shedding, and galvanic effects.
8. 3DPed can be weight, surface, and topology optimized. Totally or partially porous scaffold can be produced with tunable properties where desired along the monolithic part. This way, the bone-implant interface can be customized and the implant itself can be functionally adjusted and graded

to approach the mechanical behavior of the host tissue to reduce mechanical mismatches and minimize stress-shielding phenomena.

9. A library of worked cases can be created and replicated when similar cases emerge.
10. A do-it-yourself approach is enabled and novel out-of-the-box ideas are accelerated.
11. Design and/or manufacturing at the PoC just on time is empowered.

3DP is not necessarily used for custom-made parts, but can also be brought into play for mass-materialization of new innovative standard or modular parts that cannot or are extremely difficult to be made using traditional methodologies.

Additionally, non-surgical custom parts for external rehabilitation like orthotics *(Figure 136)* and prosthetics are also 3DPed successfully at low cost with short lead times *(Manero et al., 2019; Ribeiro et al., 2019; Choo, Boudier-Revéret and Chang, 2020; Piyush P. and Piyush G., 2022; Schwartz and Schofield, 2023).*

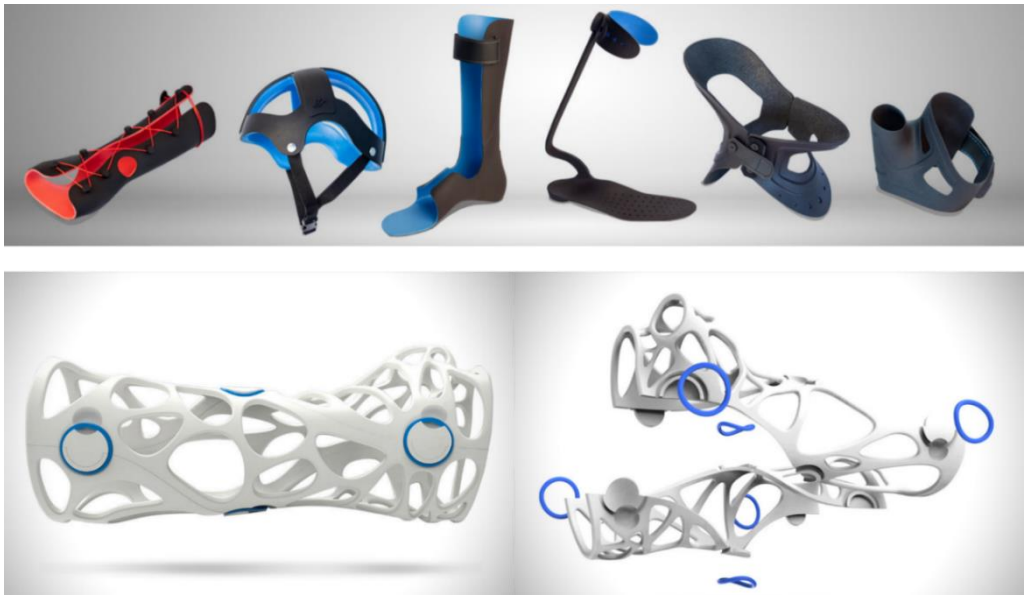

Figure 136: 3D Printed orthotics. Source: Crispin Orthotics (Up) and Xkelet (down)

The literature deals with the usage and characteristics of various biomaterials suitable for 3DP *(Poologasundarampillai and Nomm, 2017; Li et al., 2022)*; polymers *(Weems et al., 2021; Pugliese et al., 2021),* ceramics and bioglasses *(Wen et al., 2017; Zafar et al., 2019; Lim et al., 2020; Zhang et al., 2021),* composites *(Han et al., 2021; Long et al., 2021),* hydrogels *(Zhang et al., 2019a; Abdollahiyan et al., 2020; Nosrati et al., 2020)* and of course metals which are the most developed; stainless steel 316L *(Čapek, et al., 2016),* CoCr *(Furqan et al., 2016; Acharya et al., 2021),* Ti *(Sidambe, 2014; Jing et al., 2020)* and Ta *(Wauthle et al., 2015a; Han et al., 2019; Qian et al., 2021)* for 3DP of bone-inspiring implants with porous surfaces. Biodegradable metals such as Mg alloys *(Karunakaran et al., 2020; Dong et al., 2020; Telang et al.,2021),* shape memory alloys such as NiTi *(Elahinia et al., 2016; Zhang et al., 2021)* and new metallic biomaterial with antibacterial properties such as pure silver have also been 3DPed into interconnected pore scaffolds *(Arjunan et al., 2020).*

Coupled with 3DP, research and development of patient-specific orthopaedic devices are proliferated. Some fields where customized design and 3DP have promising potential are:

- 3DP of metallic, synthetic and natural polymers, ceramic, composite and hydrogel scaffolds or direct living cell bioprinting are of the last frontiers that are being tested to be used for fully functional hard or soft-TE *(see Sub-section 3.2)* to achieve *"autologous-like"* bone grafting *(Mok et al., 2016; Hagedorn, 2017; Mandrycky et al., 2016; Munaz et al., 2016; Haleem et al., 2020; Garot, Bettega and Picart, 2021; Poomathi et al., 2021).*
- Hybrid biological-artificial endo-prostheses, e.g. 3DPed endo-prostheses combined with bone grafts *(Figure 137) (Beltrami et al., 2021).*
- Multi-material 3DP where geometric freedom and materials functionality *"grow"* side-by-side, e.g. hard-soft composites *(Mirzaali et al., 2020),* Ti-, Mg-, and Fe-based biomaterials *(Putra et al., 2020),* PCL-PEGDA hydrogel *(Moura et al., 2020),* NiTi-Ti6Al4V structures *(Bartolomeu et al., 2020),* Ti-bioactive glass composites *(Mani et al., 2020).*

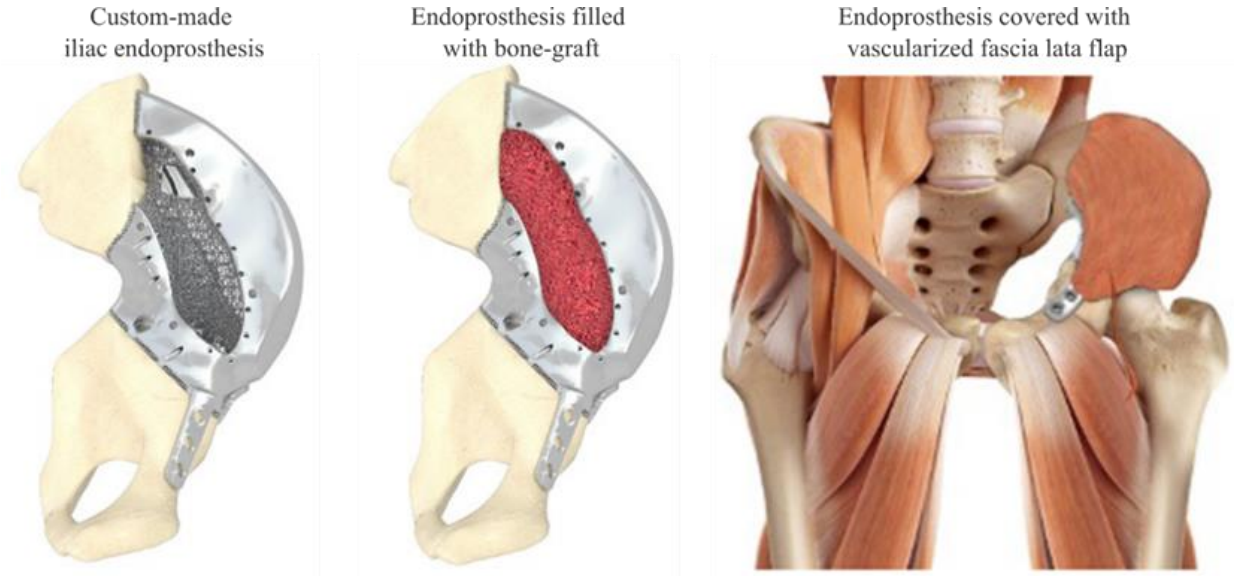

Figure 137: 3DPed endo-prosthesis filled with bone graft and covered with a vascularized flap. Source: (Beltrami et al., 2021)

- 4D (bio)printing for reconstructive and regenerative orthopaedic methodologies. The term *"4D printing"* was introduced by Tibbit et al. *(2014)* as a class of 3DP capable of producing highly accurate 3D structures that can undergo controlled changes over the fourth dimension (time). It is an approach to *"smartly"* use stimuli-responsive biomaterials to make structures capable of morphing (shape transformation over time) based on different stimuli such as temperature, humidity, electric/magnetic fields, light, acoustic, ion, pH, biological *(Rohit and Apurba, 2017; Li et al., 2017; Wan et al., 2020).* Shape memory alloys and polymers, smart inorganic polymers, electroactive polymers, electro-responsive polymers, temperature-responsive polymers, photo-responsive polymers, and smart hydrogels are being tested for making splints, stents, self-assembled orthopaedic implants, knee, spinal and acetabular prostheses, scaffolds for TE, and bone

grafts *(Javaid and Haleem, 2020)*. In *Figure 138*, the stent that morphs as per temperature changes presents the principle of 4D Printing.

Figure 138: 4D Printed stent shape morphing due to temperature change. Source: (Rohit and Apurba, 2017)

- 3DP drug delivery systems that elute under control *(Prasad and Smyth, 2016; Lim et al., 2018; Wang et al., 2021; Domsta and Seidlitz, 2021)*. 3DP applications range from oral formulations (tablets, capsules) to drug-eluting implants *(Willemen et al., 2021)*. Implantable drug delivery systems are excellent alternatives to traditional delivery as the drug is released accurately under control locally to the target tissue and toxic side-effects are avoided *(Quarterman, Geary and Salem, 2021)*: incorporating drugs/antibiotics into endo-prostheses could be used to combat associated infections and blends with HA could enhance osseointegration at the bone-implant interface. 3DPed implants with stimuli-triggered thermal effects and anti-cancer drug release can be used for local chemotherapy to kill tumor cells *(Li et al., 2021)*. For example, Bezuidenhout et al. *(2015)*, Cox et al. *(2016)* and Benmassaoud et al. *(2019)* studied drug/antibiotic eluting Ti6Al4V femoral design concepts with embedding reservoirs and microchannels that end up to the surface *(Figure 139)*, whereas Yavari et al. *(2016)* harnessed the possibility of 3DP to make fully interconnected porous Ti structures and biofunctionalized them by inserting nanotubes filled with silver for antibacterial mechanisms. 3DPed microfluidics are also capable of controllable drug release *(Amoyav et al., 2020)*. The drug release can be rate-programmed, activation-modulated, or feedback-regulated. Such stimuli-responsive components are in clinical trials and others are already commercialized *(Lorenzo and Concheiro, 2014)*.

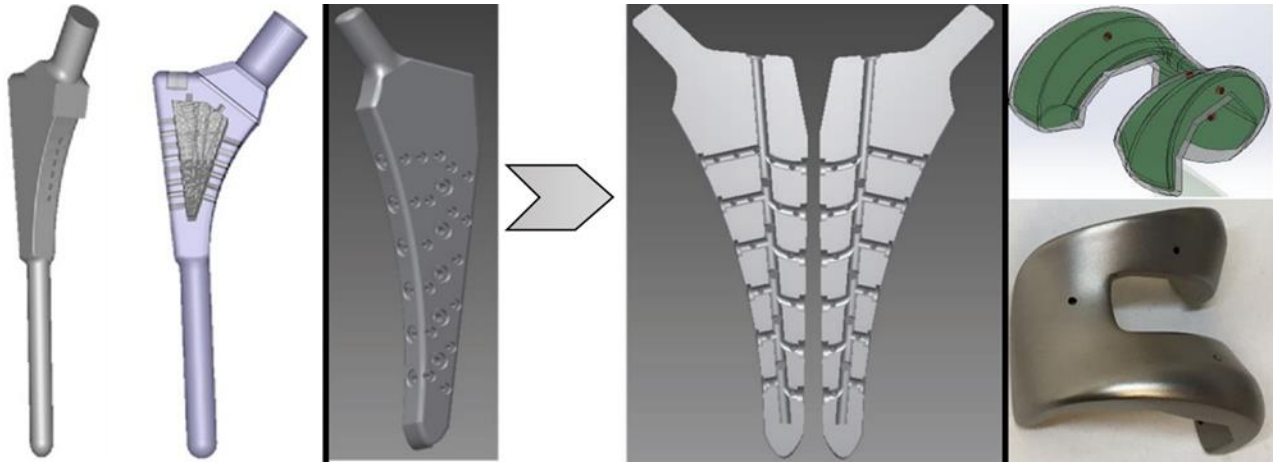

Figure 139: 3DPed drug eluting endo-prostheses. Source: (Bezuidenhout et al., 2015; Cox et al., 2016; Benmassaoud et al., 2019)

- 3DPed devices with features to house sensors and electronics for real-time implant condition monitoring and patient-data acquisition, hence setting evidence-based medicine to rise and ultimately improve the outcomes for the patient. Researchers have reviewed such *"instrumented"* endo-prostheses capable of measuring physical quantities (e.g. temperature, force, acceleration/vibration, strain) by embedding sensors and also technologies for wireless communications and telemetry *(Ledet et al., 2018; Karipott et al., 2018; Ramakrishna et al., 2020; Qiblawey et al., 2020; Nelson et al., 2020)*. Vickers et al. *(2021)* graphically presented how the post-implantation condition of hip arthroplasty can be monitored in vivo *(Figure 142)*, whereas Baumann et al. *(2021)* have mentioned the considerations and challenges (engineering and technology, clinical and patient, cybersecurity, regulatory) associated with orthopaedic sensing, measuring, and reporting. Bergmann et al. *(1988; 2012)* and Damm et al. *(2010)* showed that electronic components can be embedded within femoral stems *(Figure 140)*, whilst Gaalen et al. *(2016)* described how 3DP can be used to make similar *"smart"* femoral prostheses *(Figure 141)*. Interestingly, embedded electronic-mechanical micro-components within implants could also be utilized for the selective release of drugs and antibiotic compounds in times of need. Expandable endo-prostheses *(Dotan et al., 2010; Wong et al., 2010; Borkowski, Pawlikowski and Skalski, 2015; Savvidou et al., 2019)* with embedded electromechanical actuators for non-invasive actuation also fall under this category of devices, parts of which could be 3DPed *(Figure 144)*.

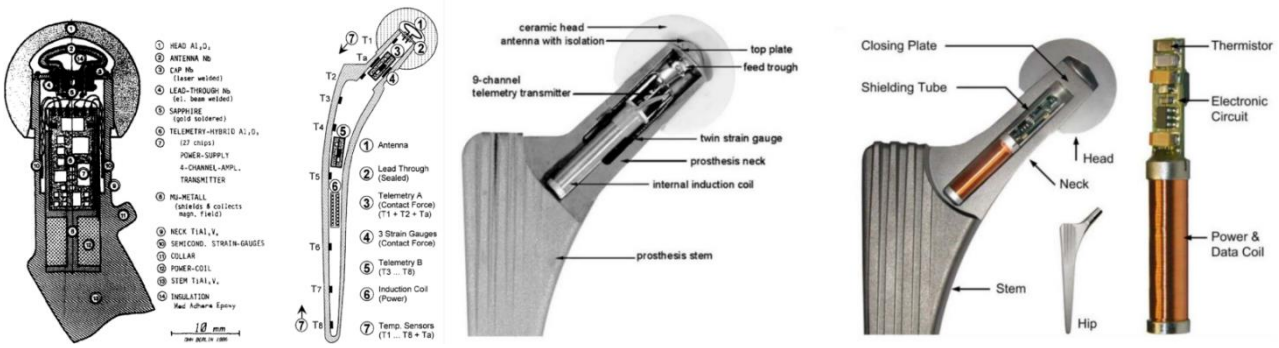

Figure 140: Femoral stems with embedded electronics. Source: (Bergmann et al., 1988; 2012; Damm et al., 2010)

Figure 141: 3D Printed femoral stems with embedded electronics. Source: Renishaw and (Gaalen et al., 2016)

3DP can help orthopaedic industry to shift towards a more sustainable and circular economy, especially when bioresorbable materials will go mainstream *(Yadav et al., 2020)*. Looking at the landscape of all possible applications of 3DP in fabricating a particular standard/modular/adaptable/personalized or customized orthopaedic device, the manufacturing

systems and business/supply models to be implemented will depend on the complexity, the level of customization and the production volume of this device *(Figure 143)*.

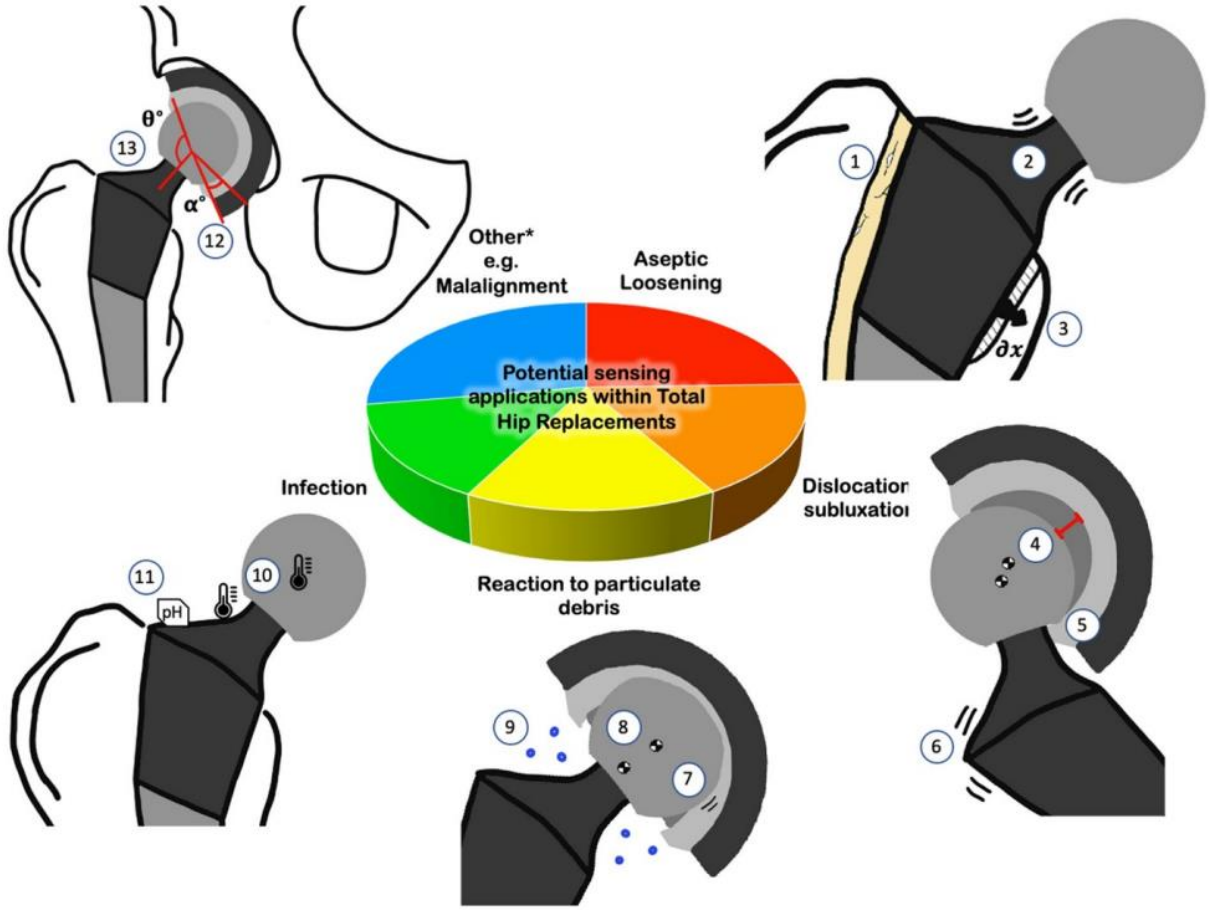

Aseptic Loosening	
1.	Acoustic Emission sensing to monitor the integrity of the bone cement
2.	Vibration sensing can be used to compare vibrational response of well fixed and loose implant – bone system
3.	Measuring the displacement of the implant components relative to the bone and so the magnitude of the Micromotions (dx)
Dislocation/Subluxation	
4.	Measuring relative displacement of components to show if bearing surfaces separate
5.	Force or pressure sensors at the cup's rim to sense force from femoral stem contact
6.	Vibration sensing could detect torque generated when components contact
Reaction to particulate debris	
7.	Vibration sensing could show changes in friction as bearing surfaces become worn/rough
8.	Measuring relative displacement of components to show if head position in cup has changed due to excessive wear
9.	Directly measure wear particle concentration at the implant sight or in patients' blood
Infection	
10.	Measuring the temperature of components or the tissue surrounding the components
11.	pH sensing the tissue surrounding the components
Malalignment	
12.	Measuring the relative angles of the components relative to the bones to show if they are positioned in "Gold Standard" range intra or post-op
13	Measuring the relative angles of the components to show if they are positioned in "Gold Standard" range intra or post-op

Figure 142: Condition monitoring after hip arthroplasty using embedded sensors. Source: (Vickers et al., 2021)

Most 3DP technologies are capable of materializing polymer orthopaedic devices, whereas directed energy deposition-based technologies are capable of metal forming, but PBF techniques are mostly used for high-end metallic parts *(Sing et al., 2015)*. After 3DP, post-processing methodologies such as surface treatments, heat treatments, and machining usually follow.

For load-bearing articulating implants, classically manufactured and 3DPed metallic parts such as Ti alloys are usually coated with TiN due to its excellent biocompatibility, increased wettability,

extremely high hardness, high wear resistance, reduced ion release, minimized polyethylene wear, chemical long-term stability *(Hove et al., 2015; Santecchia et al., 2015).*

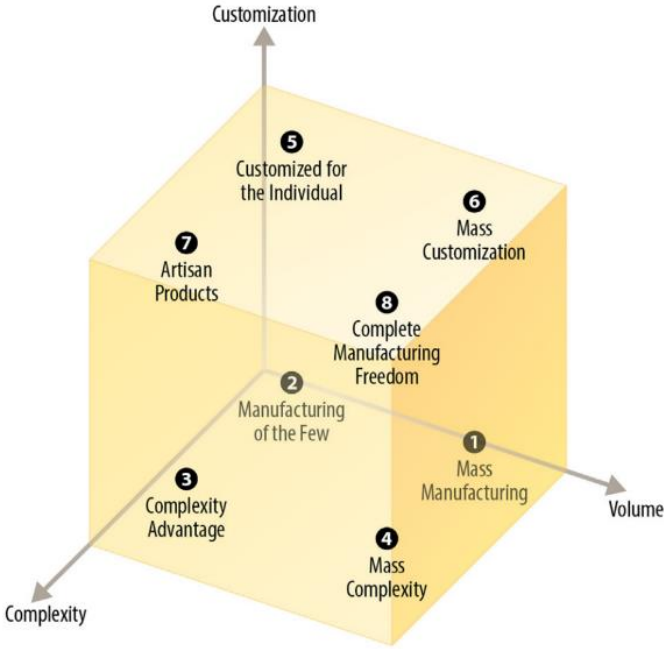

Figure 143: Three-axis model of manufactured products. Source: (Conner et al., 2014)

As justified in *Sub-section 3.1*, the implant's surface must be ultimately modified to be multifunctional with balanced osseointegrative and anti-bacterial properties. Surface-functionalization can be enabled by coatings targeting osseointegration boosting and infection prophylaxis and/or properly structuring the implant surface (roughness, micro and nano-topography, porosity, surface energy/wettability) for increased osteoconductivity and osteoinductivity to promote osteogenic differentiation of stem cells and bone formation onto and into the pores.

After 3DP, post-processing and coatings might be applied, and before implantation, the 3DPed device must be sterilized with the most suitable method *(see Sub-section 3.1)*, depending on the application and the biomaterial(s) that it is composed of.

It is known that the lifetime of an endo-prosthesis in vivo is limited by septic and aseptic loosening. Properly designed, optimized, and 3DPed spongy endo-prosthesis combined with suitable coatings could reach the maximum lifetime of the biomaterial. For example, 3DPed acetabular cups have shown favorable mid-term clinical outcomes with high survival rates, great clinical improvements and excellent initial biological fixation and performance *(Regis et al., 2015; Perticarini et al., 2015; Dall'Ava et al., 2019a; Geng et al., 2020; Huang et al., 2021b)*, whereas in a study *(Dall'Ava et al., 2021)* that involved retrieved 3DPed and conventionally made acetabular implants, greater bone ingrowth and osseointegration were verified for the 3DPed category. Analogously, excellent short-term and mid-term results have been reported in the majority of the published materials cited in this Thesis for other 3DPed implants, especially (mega)endo-prostheses used for limb-salvage.

Figure 144: Custom-made expandable endo-prostheses. Source: Implantcast

Wang et al. *(2019)* reported a 2,5 years follow-up of 13 patients treated with custom 3DPed Ti hemipelvic endo-prostheses that were designed by the clinical team at the PoC but manufacturing (metal 3DP by EBM PBF) and post-processing were outsourced. In all cases, stable fixation, well osseointegration, and good functional outcomes were observed, without severe complications (infection, dislocation, aseptic loosening, mechanical failure) occurrence: the extensive data is shown in *Figure 145*. The authors concluded that: a) porous structures with gradient porosities imitating cortex and trabecular bone could be better options, and b) finite element biomechanical analyses and in vitro tests should be conducted for different porous structures and different fixation methods. A similar study was published later *(Wang et al., 2020)*.

Implants incorporating accurately controlled interconnected open cellular architectures are very important for both mechanical and biological reasons, but making such geometrical features is difficult or impossible with traditional methods. 3DPed porous implants can be fabricated into lighter forms with adequate mechanical strength and higher permeability of bone ingrowth compared to their solid counterparts. Two custom 3DPed by EBM PBF Ti6Al4V hemi-pelvic endo-prostheses are shown in *Figure 146*: one natural-like and one low-profile featuring trabecular-like structures to allow the bone to grow within the pores (biological fixation) and holes for soft tissue re-attachment,

whereas the mechanical fixation is achieved with screws that are positioned as per the patient's anatomy and host bone quality.

P1: Ilium
P2: Acetabulum
P3: Pubis & Ischium

AO: Acetabular orientation

Vr: Volume of resected specimen
Ve: Volume of endoprosthesis
We: Weight of endoprosthesis
VPPS: Volume proportion of porous structure

Case	Age (years)	Gender	Resection classification	Diagnosis	Enneking staging	Follow-up (months)	Anatomical AO An (°)	AO I (°)	Tumor size (cm^3)	Sacroiliac joint	Pubic ramus RS	Pubic ramus RC	Ischium RS	Ischium RC	V_r (ml)	V_e (ml)	W_e (g)	VPPS (%)
1	46	F	P1+P2+P3	Parosteal osteosarcoma	III	29.0	21.0	44.5	12×18×13	N	Total	Stem	Total	N	732.8	266.1	394.5	73.7
2	37	F	P1+P2+P3	Chondrosarcoma	IIB	28.0	27.2	44.4	11×16×10	Y	Total	Stem	Total	N	543.8	137.8	289.5	58.2
3	48	M	P1+P2+P3	Chondrosarcoma	IIB	27.0	18.9	38.4	10×15×14	Y	Total	Stem	Total	N	709.7	163.3	377.0	53.0
4	65	F	P1+P2+P3	Fibrosarcoma	IIB	23.0	20.0	41.3	7×12×12	Y	Partial	Cap-like	Total	N	700.6	212.8	374.9	66.7
5	31	F	P1+P2+P3	Ewing's sarcoma	III	27.0	23.1	42.4	14×16×13	Y	Partial	Stem	Partial	Y	510.6	190.2	275.1	74.6
6	61	M	P1+P2	Solitary plasmacytoma	IIB	26.0	18.6	43.2	5×6×4	Y	N	N	N	N	186.7	96.7	102.1	84.4
7	40	M	P1+P2	Chondrosarcoma	IIB	25.0	18.8	45.8	7×11×7	Y	Partial	Stem	Partial	Y	697.2	164.2	370.5	54.3
8	40	M	P1+P2+P3	Chondrosarcoma	IIB	25.0	18.3	40.1	4×7×4	N	Partial	Cap-like	Partial	Y	494.8	128.4	263.6	59.4
9	46	F	P1+P2	Chondrosarcoma	IIB	24.0	21.5	38.8	6×6×4	N	N	N	N	N	202.9	75.6	109.4	74.6
10	66	M	P1+P2+P3	Fibrosarcoma	IIB	22.0	18.9	41.2	7×12×9	Y	Partial	Stem	Partial	Y	474.2	204.8	189.9	79.4
11	53	F	P1+P2+P3	Osteosarcoma	III	26.0	21.8	39.9	5×7×8	N	Total	Stem	Total	N	412.3	98.7	219.2	55.2
12	35	M	P1+P2+P3	Angiosarcoma	IIB	24.0	15.0	40.5	5×6×6	Y	N	N	N	N	203.2	112.4	111.5	86.0
13	65	F	P1+P2+P3	Chondrosarcoma	IIB	23.0	19.3	41.6	7×10×7	Y	Partial	Stem	Partial	Y	475.7	175.7	256.2	74.3
Mean	48.7	-	-	-	-	25.3	20.2	41.7	7.7×10.9×8.5	-	-	-	-	-	488.0	155.9	256.4	68.8

I/D: Inserted/Designed

AO: Acetabular orientation

MSTS: Musculoskeletal Tumor Society

ROM: Range of motion

Case	S_1 screw no. (I/D)	S_2 screw no. (I/D)	Iliac screw no. (I/D)	Pubic screw no. (I/D)	Ischial screw no. (I/D)	Intraoperative Time (min)	Intraoperative Blood loss(ml)	Postoperative AO A (°)	Postoperative AO I (°)	MSTS score Pain	Function	Emotional acceptance	Supports	Walking ability	Gait	Total	hip joint ROM (°)
1	3/4	1/1	0/0	1/1	0/0	420	8200	19.5	41.4	2.0	2.0	4.0	2.0	3.0	2.0	15 (50.0%)	100.0
2	4/4	1/1	0/0	1/1	0/0	260	2500	25.8	44.0	4.0	4.0	5.0	4.0	4.0	4.0	25 (83.3%)	130.0
3	5/5	1/1	0/0	1/1	0/0	230	4200	20.0	40.7	3.0	4.0	4.0	4.0	4.0	4.0	23 (76.7%)	120.0
4	5/5	2/2	0/0	2/2	0/0	255	2100	27.7	40.9	4.0	2.0	3.0	3.0	3.0	2.0	17 (56.7%)	105.0
5	4/5	1/1	0/0	1/1	1/2	390	5600	22.9	40.2	4.0	2.0	5.0	3.0	3.0	2.0	19 (63.3%)	110.0
6	3/4	1/1	0/0	1/1	1/2	220	900	24.0	44.6	3.0	4.0	4.0	3.0	4.0	3.0	21 (70.0%)	130.0
7	3/5	1/2	1/2	0/1	1/2	270	2600	24.5	45.8	4.0	4.0	4.0	5.0	5.0	4.0	26 (86.7%)	130.0
8	0/0	0/0	6/6	1/1	1/2	180	2300	22.8	45.0	5.0	4.0	5.0	4.0	5.0	4.0	27 (90.0%)	125.0
9	0/0	0/0	3/5	1/2	1/2	170	1700	23.5	43.0	4.0	4.0	5.0	5.0	5.0	4.0	27 (90.0%)	125.0
10	4/5	2/2	0/0	1/1	1/2	390	5100	18.2	37.3	3.0	3.0	3.0	2.0	3.0	2.0	16 (53.3%)	110.0
11	0/0	0/0	5/6	2/2	0/0	210	1900	25.0	48.1	4.0	4.0	5.0	5.0	5.0	4.0	27 (90.0%)	130.0
12	4/5	1/1	1/2	1/1	1/2	270	2600	29.8	42.3	4.0	4.0	4.0	4.0	4.0	4.0	24 (80.0%)	125.0
13	4/5	1/2	0/0	1/1	2/2	540	6300	28.4	44.4	4.0	3.0	4.0	3.0	3.0	3.0	20 (66.7%)	110.0
Mean	-	-	-	-	-	292.7	3538.5	24.0	42.9	3.7	3.4	4.2	3.6	3.9	3.2	22.1(73.6%)	119.2

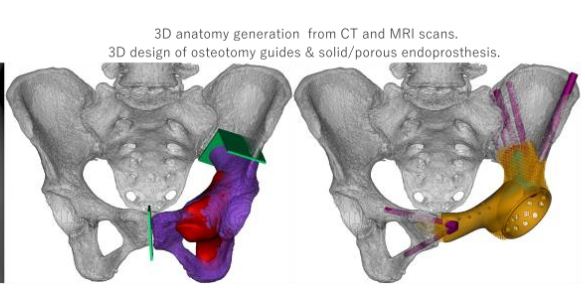

Orientation	Angles measured	
Anteversion	Anatomical	Designed
	20.2° ± 2.9°	23.2° ± 1.7°
	Designed	Postoperative
	23.2° ± 1.7°	24° ± 3.5°
Inclination	Anatomical	Designed
	41.8° ± 2.3°	42.4° ± 1.7°
	Designed	Postoperative
	42.4° ± 1.7°	42.9° ± 2.8°

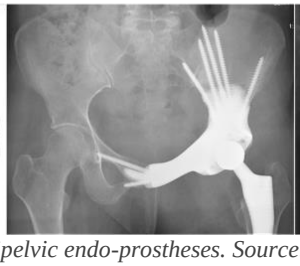

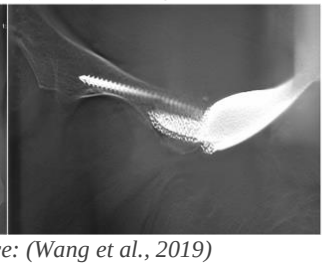

Figure 145: Cases treated with custom 3DPed hemipelvic endo-prostheses. Source: (Wang et al., 2019)

Figure 146: 3DPed custom Ti6Al4V hemi-pelvic endo-prostheses with porous features. Source: Ossis

As stated earlier in *Sub-section 3.3*, the selection of the most suitable manufacturing method depends on the application and the product's characteristics *(Figure 45)*. 3DP is not a panacea as it might or might not be opportunistic and the most effective manufacturing method, so its selection has to be weighted under time and cost criteria *(Figure 101)*. Once 3DP's potential and readiness will stop remaining under question, and the last frontiers are overcome, it will be widely adopted by the medical industry for developing orthopaedic devices in or out of the PoC.

Next, the 3DP-enabled design optimization of orthopaedic devices for mechanical and biological superiority based on biomimetic approaches is discussed in detail along with associated algorithms.

3.6 3D Printing of Optimized Designs: Biomimesis

"Biophysics" was coined by O. Schmitt in 1957 as *"not so much a subject matter as it is a point of view. It is an approach to problems of biological science utilizing the theory and technology of the physical sciences. Conversely, biophysics is also a biologist's approach to problems of physical science and engineering, although this aspect has largely been neglected".* Later (1969) he stated that he preferred the word *"Biomimetics"* over *"Bionics"*, whereas in 1974 the world *"Biomimetics"* appeared in Webster's Dictionary as *"the study of the formation, structure, or function of biologically produced substances and materials (as enzymes or silk) and biological mechanisms and processes (as protein synthesis or photosynthesis), especially for the purpose of synthesizing similar products by artificial mechanisms which mimic natural ones" (Vincent et al., 2006).*

Biomimesis (also known as Biomimicry) originates from the Greek words *"βίος"* (vίos; life) and *"μίμησης"* (mímesis; imitation), referring to methodologies that are used for implementing biological forms and functions into artificial products and processes.

Perricone et al. *(2021)* referred to biomimetics with the term organismal design to spotlight the development of novel designs inspired by nature and organisms.

There is no better mentor than nature to indicate how products should be designed efficiently bearing in mind optimization criteria and sustainability by economizing material and energy consumption. Natural forms are developed and adapted to perform their assigned functions optimally. Despite the fact that nature uses a limited palette of building blocks to form structures, their intelligent management and hierarchical arrangement give rise to striking efficiency with completely different end properties *(Fratzl and Weinkamer, 2007; Meyers et al., 2008; Chen, McKittrick, and Meyers, 2012).* Although natural materials are very light and 50% less dense than artificial engineering materials, they mechanically outperform them, e.g. woods have comparable strength (per unit weight) to the strongest steels, shells and bones have significantly greater toughness than engineering ceramics *(Oxman, 2011a).* Some examples of natural structures are pictured in *Figure 130.*

By nature's *"guidance"*, granted that natural forms and functions are adequately understood, product designs can be advanced *(Srinivasan, Haritos and Hedberg, 1991)* and enjoy high mechanical efficiency *(Wegst and Ashby, 2004).* Biomimetism can be used as a toolbox for the design of innovative materials and systems *(Sanchez, Arribart and Guille, 2005).* We should explore nature's secrets by trying to mimic anisotropic heterogeneous architectures with spatial variation in material composition and structure along their volume that result in corresponding property changes and optimize our designs accordingly to generate biologically-inspired products *(Oxman, Keating, and Tsai, 2011; Oxman, 2011a).*

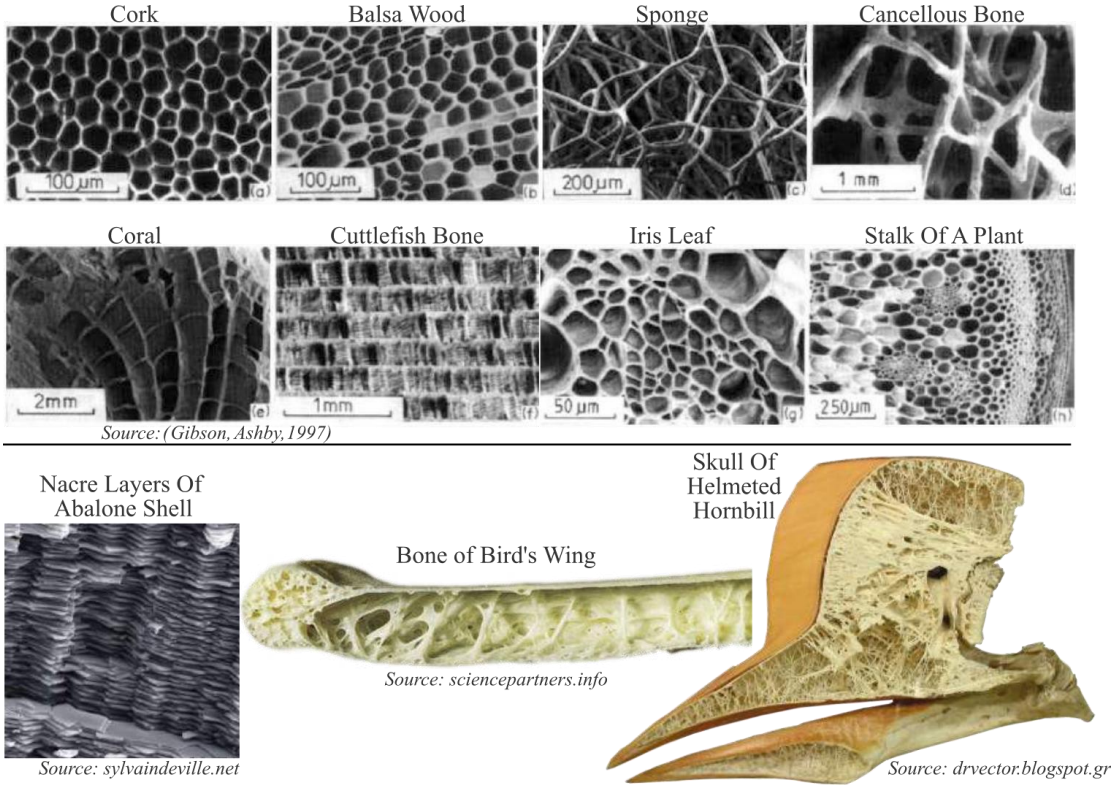

Figure 147: Examples of structures found in nature

Materials found in nature experience functional gradients. Functionally graded materials (FGMs) are an advanced category of heterogeneous materials with multifunctional characteristics on the same part by gradually changing composition or structure and are very suitable for engineering and medical applications requiring conflicting properties in a single component *(Saleh et al., 2020)*.

FGM can be considered *metamaterials*. The term *metamaterial* is derived from the Greek words *"μετά"* (metá; beyond) and *"material"*, denoting materials deriving their properties not from the properties and composition of their base material(s), but from their newly arranged structures. In short, metamaterials are governed by their design characteristics (material-by-design) rather than by their composition.

Manufacturing of components with complex organic-like architectures is challenging. Foam-like materials with open or closed cells can be made by various classic methods *(Ashby et al., 2000)*, but these have many limitations: cannot shape intricate freeform geometries, density variations and geometry of internal features cannot be accurately and selectively assigned under full topological control. On the other hand, accurate FGMs with complex internal and external topologies and topologically varying material distribution, geometry, and properties can be obtained by 3DP technologies as the building process is fully controllable during the variable single or multi-material addition *(Oxman, Keating, and Tsai, 2011; Oxman, 2011a)*. After all, natural forms emerge and grow in an additive/generative fashion as this allows micro, meso, to macro structural growth control, whilst consuming the minimum material and energy.

Figure 148: Examples of nature's "biological 3D printers"

Table 8 sums up the major bibliography (books) on designing and manufacturing biomimetic products and FGMs.

Table 8: Book list on biomimesis and Functionally Graded Materials

Author	Title
Thompson, 1917	On growth and form
Fraser, MacRaw and Rogers, 1972	Keratins: Their Composition, Structure, and Biosynthesis
Brown, 1975	Structural Materials in Animals
Wainwright et al., 1976	Mechanical Design in Organisms
Vincent and Currey, 1980	The Mechanical Properties of Biological Materials
Currey, 1984	The Mechanical Adaptations of Bones
Simkiss and Wilbur, 1989	Biomineralization: Cell Biology and Mineral Deposition
Lowenstam and Weiner, 1989	On Biomineralization
Fung, 1990	Biomechanics: Motion, Flow, Stress, Growth
Vincent, 1990	Structural Biomaterials
Byrom, 1991	Biomaterials: Novel Materials from Biological Sources
Fung, 1993	Biomechanics: Mechanical Properties of Living Tissues

Neville, 1993	Biology of Fibrous Composites
Fung, 1997	Biomechanics: Circulation
Feughelman, 1997	Mechanical Properties and Structure of a-Keratin Fibres
Gibson and Ashby, 1997; 1999 (2nd Edition)	Cellular Solids: Structure and Properties
Kaplan and McGrath, 1997	Protein-based Materials
Miyamoto et al., 1999	Functionally Graded Materials: Design, Processing and Applications
Elices, 2000	Structural Biological Materials: Design and Structure-Property Relationships
Mann, 2001	Biomineralization: Principles and Concepts in Bioinorganic Materials Chemistry
Currey, 2002	Bones: Structure and Mechanics
Ratner et al., 2005	Biomaterials Science: An Introduction to Materials in Medicine
Cohen, 2006	Biomimetics: Biologically Inspired Technologies
Forbes, 2007	The Gecko's Foot
Behrens and Bäuerlein, 2007	Handbook of Biomineralization: Biomimetic and Bioinspired Chemistry
Reis and Weiner, 2008	Learning from Nature How to Design New Implantable Biomaterials
National Research Council, 2008	Inspired by Biology: From Molecules to Materials to Machines
Gibson, Ashby and Harley, 2010	Cellular Materials in Nature and Medicine
Jiang and Feng, 2010	Bioinspired Intelligent Nanostructured Interfacial Materials
Mukherjee, 2010	Biomimetics: Learning from Nature
Zhang, 2010	Morphology Genetic Materials Templated from Nature Species
Kumar, 2010	Biomimetic and Bioinspired Nanomaterials
Altenbach and Öchsner, 2010	Cellular and Porous Materials in Structures and Processes
Gruber et al., 2011	Biomimetics: Materials, Structures and Processes
Mano, 2012	Biomimetic Approaches for Biomaterials Development
Lee and Henthorn, 2012	Materials in Biology and Medicine
Cohen, 2012	Biomimetics: Nature-Based Innovation
Bhushan, 2012	Biomimetics: Bioinspired Hierarchical-Structured Surfaces for Green Science and Technology
Ennos, 2012	Solid Biomechanics
Boal, 2012	Mechanics of the Cell
Nosonovsky and Rohatgi, 2012	Biomimetics in Materials Science: Self-Healing, Self-Lubricating, and Self-Cleaning Materials
Schmidt and Belegratis, 2013	Laser Technology in Biomimetics
Ruys, 2013	Biomimetic Biomaterials: Structure and Applications
Ramalingam, 2013	Biomimetics: Advancing Nanobiomaterials and Tissue Engineering
Lakhtakia and Palma, 2013	Engineered Biomimicry
Pompe et al., 2013	Bio-Nanomaterials: Designing Materials Inspired by Nature
Fratzl, Dunlop and Weinkamer, 2013	Materials Design Inspired by Nature: Function Through Inner Architecture
Brennan and Kirschner, 2014	Bio-inspired Materials for Biomedical Engineering
Jabbari et al., 2014	Handbook Of Biomimetics And Bioinspiration
Mallick, 2014	Bone Substitute Biomaterials
Meyers and Chen, 2014	Biological Materials Science: Biological Materials, Bioinspired Materials, and Biomaterials
Molina, Novio and Roscini, 2015	Bio- and Bioinspired Nanomaterials
Ngo, 2015	Biomimetic Technologies: Principles and Applications
Bououdina, 2016	Emerging Research on Bioinspired Materials Engineering
Tampieri and Sprio, 2016	Bio-Inspired Regenerative Medicine: Materials, Processes, and Clinical Applications
Luo and Ng, 2016	Bio-inspired Surfaces And Applications
Cohen and Reich, 2016	Biomimetic Design Method for Innovation and Sustainability
Xia, 2016	Biomimetic Principles and Design of Advanced Engineering Materials

Rodrigues and Mota, 2017	Bioinspired Materials for Medical Applications
Ito, Chen and Kang, 2017	Advances in Bioinspired and Biomedical Materials
Mahamood and Akinlabi, 2017	Functionally Graded Materials
Noh, 2018	Biomimetic Medical Materials: From Nanotechnology to 3D Bioprinting
Bezerra, Ferreira and Barbosa, 2019	Frontiers in Biomaterials: Bio-Inspired Materials
Estrin, Bréchet, Dunlop and Fratzl, 2019	Architectured Materials in Nature and Engineering
Ehrlich, 2019	Marine Biological Materials of Invertebrate Origin
Chun et al., 2020	Biomimicked Biomaterials: Advances in Tissue Engineering and Regenerative Medicine
Soboyejo and Daniel, 2020	Bioinspired Structures and Design
Pollini and Paladini, 2021	Bio-Inspired Materials for Biomedical Applications
Hisham, 2021	Inspiration and Design for Bio-Inspired Surfaces in Tribology
Wang and Packwood, 2021	Cell-Inspired Materials and Engineering
Nurunnabi, 2021	Bioinspired and Biomimetic Materials for Drug Delivery
Dash, 2022	Biomimetic Biomaterials for Tissue Regeneration and Drug Delivery
Pandey et al., 2022	Functionally Graded Materials (FGMs): Fabrication, Properties, Applications, and Advancements

The impressive inspiring characteristics and properties of the human bone are summarized in *Appendix E*. Bone is a hypodigmatic functionally-graded anisotropic tough-elastic composite material structurally supporting the human body *(Wang et al., 2018; Yang et al., 2019)*:

- A compact shell (cortical bone) that is almost solid to improve hardness and provide structural integrity, and an inner trabecular structure (cancellous bone) with 50-90% porosity comprised of a 3D network of interconnected osseous beams and surfaces. Trabecular bone is present at load-bearing sites including movement, and can absorb energy and withstand forces with different directions and magnitudes. The bone derives its fracture toughness from this bimodal form.
- An extracellular matrix composed of organic components (provide flexibility) and inorganic crystalline minerals (provide strength and toughness).
- "Living" hierarchical endo-structure, performing diverse mechanical, biological, and chemical functions at each level. This irregular endo-structure continuously undergoes a dynamic remodeling process: functional (structural and compositional) adaptation to maintain optimal mechanical performance at the lowest metabolic cost.
- Self-healing of cracks and non-critical size osseous losses.
- Mechanical properties vary with age, anatomical site, and bone quality.

Biological systems have excellent proficiency thanks to seven core properties *(Shi et al., 2021)*:

1. Self-assembly.
2. Multi-functionality.
3. Self-healing.
4. Hierarchy of structure.

5. Evolution against environmental constraint.
6. Synthesis under normal environmental conditions.
7. Hydration necessity.

Although artificially made products are comparatively amateur and have a long way to reach these properties, the implementation of such would make the ideal orthopaedic implantable device to substitute or regenerate osseous tissue. Nevertheless, 3DP is a promising manufacturing method that enables the materialization of biomimetic forms *(Figure 149)*. For example, *Figure 150* illustrates some biomimetically optimized 3DPed metallic and polymer replicas of the femoral head based on the biomechanical stress lines of the human femur.

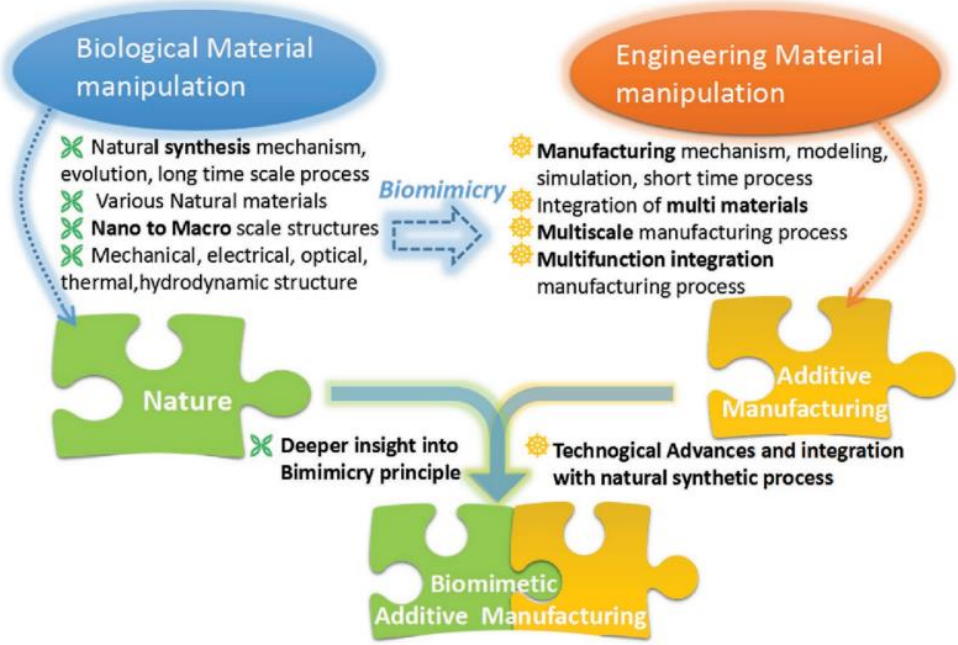

Figure 149: 3DP enables biomimetic forms fabrication. Source: (Yang et al., 2018)

Oxman *(2011b; 2012)* investigated novel design approaches for digital functional graded fabrication (gradient geometrical, structural, material anisotropy) and finite element synthesis to create new expressions in nature's dialect and program physical matter mimicking nature's strategies where form generation is driven by maximal performance with minimal resources through local material property variation. *Figure 151* shows two examples of custom 3DPed (Stratasys's photo-polymer jetting printer) multi-material multi-color products designed by Oxman:

1. Carpal skin: a wrist splint that protects against Carpal Tunnel Syndrome, featuring a patient-specific pain-profile map made of hard and soft materials with controlled stiffness variation.
2. Gravida: a comfortable pregnancy corset composed of an external armor shell and an internal soft membrane offering support as the female belly transforms.

A new paradigm shift is now being established in biomaterials. Holzapfel et al. *(2013)* dealt with the diachronic evolution of orthopaedic biomaterials (bioinert, biocompatible, bioactive, biodegradable, biomimetic), Jamróz et al. *(2018)* presented the role of 3DP in processing the classic

and biomimetic biomaterials, whereas Montoya et al. *(2021)* assumed that today's *"smart biomaterials"* (i.e. materials that respond to specific cellular signals) will be *"outsmarted"* by future innovations, for this reason, they classified such biomaterials as inert, active, responsive *(Figure 154)*, autonomous. All previous are graphically illustrated in *Figure 152*.

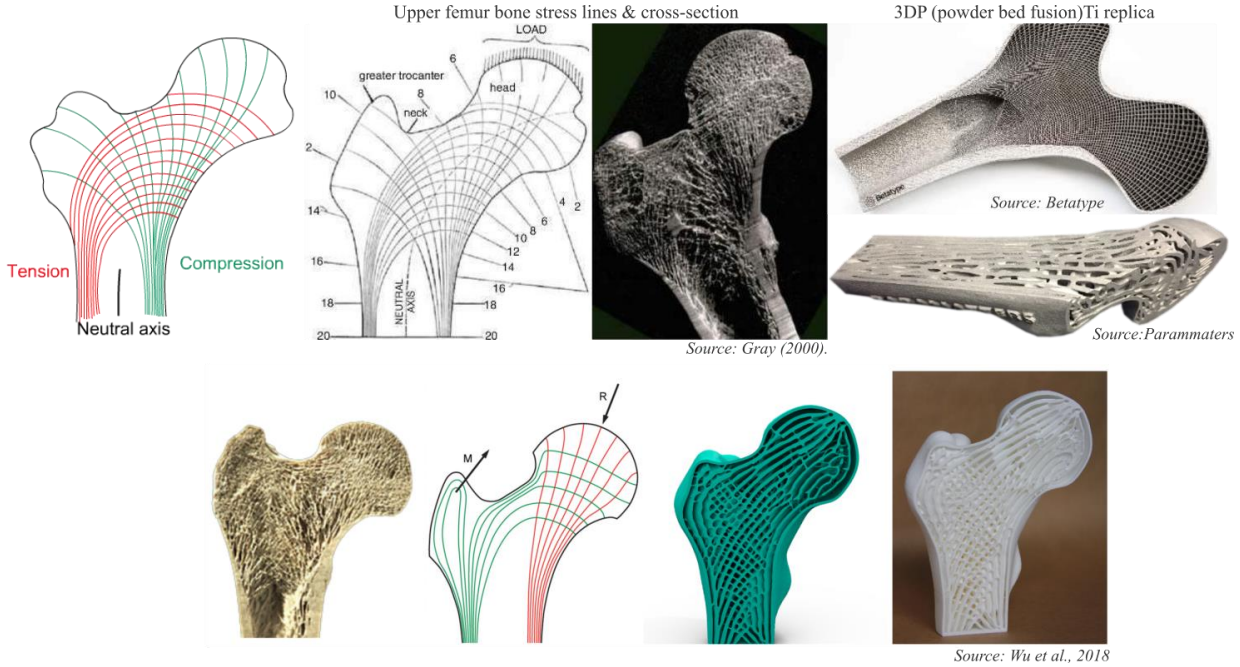

Figure 150: 3DPed femoral head replicas as per the natural stress distribution

Figure 151: Biomimetic 3DPed wrist splint and pregnancy corset by N. Oxman. Photos: (M. Siegel and Y. Reshef)

Biomimetic biomaterials and 3DP of such can be considered the protagonists in achieving TE's quest to regenerate tissue *(see Sub-section 3.2*) via endocultivation, in vivo or in vitro approaches *(Figure 153) (Holzapfel et al., 2016)*, though considerable barriers exist *(Qasim, Chae and Lee, 2019)*: biomimetic 3DPed constructs should be cost-effective, whilst also: a) being responsive to in-body stimuli around host tissue *(Figure 154)*, b) composed of porous biomaterials to allow proper vascularization and osteogenesis, c) having adequate and host tissue matching mechanical strength, d) biodegrade at matching rates with patient's host tissue healing and formation.

In academia, the research interest in regenerating tissue instead of replacing/reconstructing it with grafts and artificial endo-prostheses is considerably higher. As can be seen in *Figure 155*, the

published articles on tissue regeneration are rising exponentially, with most articles focusing on medical devices, TE, bioactive, and smart materials.

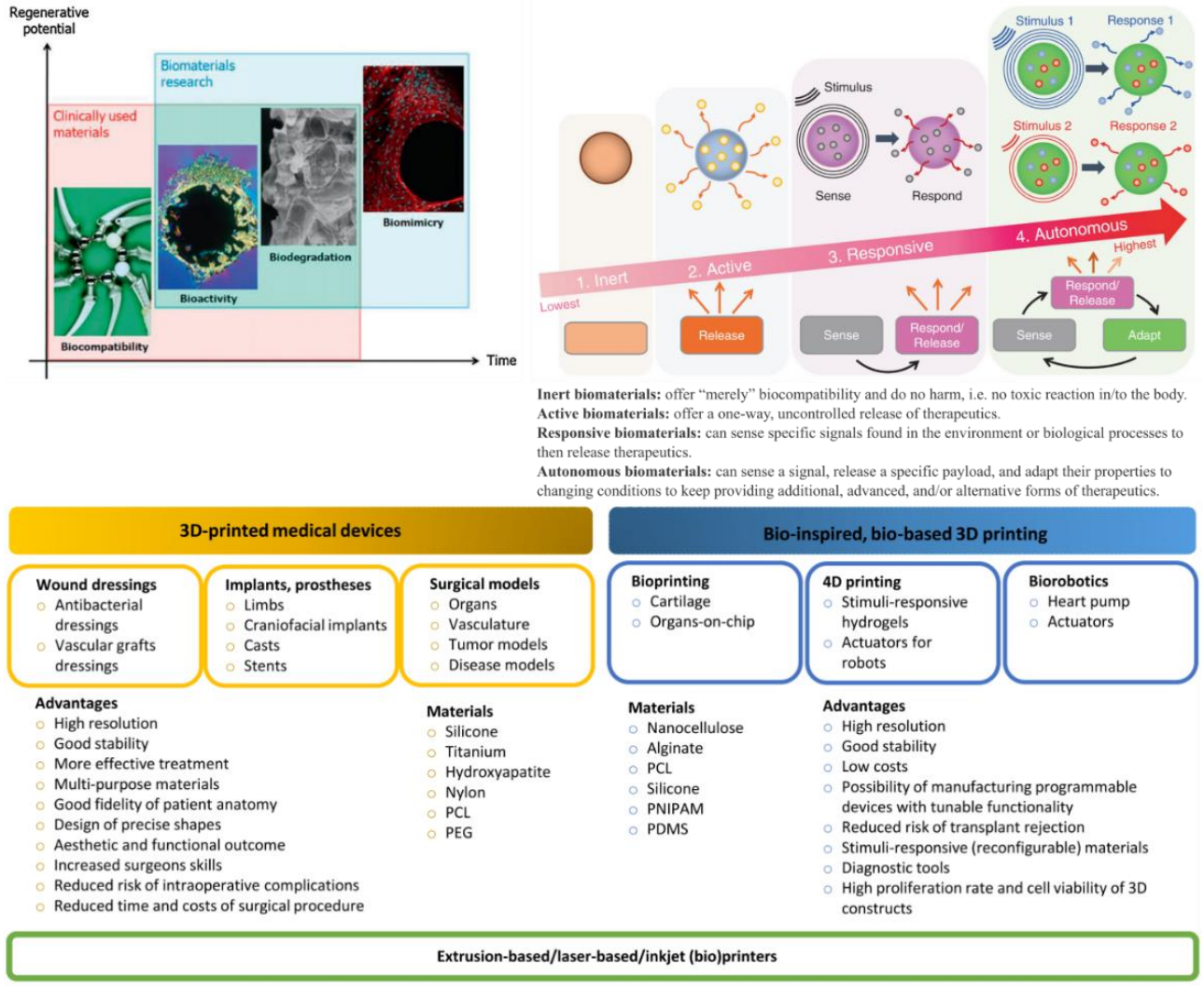

Figure 152: Evolution of biomaterials, smart biomaterials, and 3DP role. Source: (Holzapfel et al., 2013; Jamróz et al., 2018; Montoya et al., 2021)

Many MJ, BJ, ME, PBF, and VP-based 3DP technologies are being used for fabricating scaffolds and "living" constructs for TE applications as was described in *Sub-section 3.2*. For example, *Figure 157* shows the Envisiotec 3D-Bioplotter and some 3DPed scaffolds, whereas an interesting approach for 3DP bone mimicking mineralized constructs was proposed by Romanazzo et al. *(2021) (Figure 156)*: scaffolds are generated by 3D writing an apatite-transforming ink in a supportive microgel matrix with living cells at room temperature without requiring invasive chemicals, radiation, or post-processing steps. The cells showed robust adhesion and proliferation, with 95% viability after several weeks in culture and the 3DPed structure showed promising osteogenesis.

As the scope of this Thesis is the PoC design and 3DP of products to assist individualized reconstructive (not regenerative) orthopaedics, emphasis will be given to functionalizing artificial bone-replacing endo-prostheses by biomimetic design for mechanical and biological optimization.

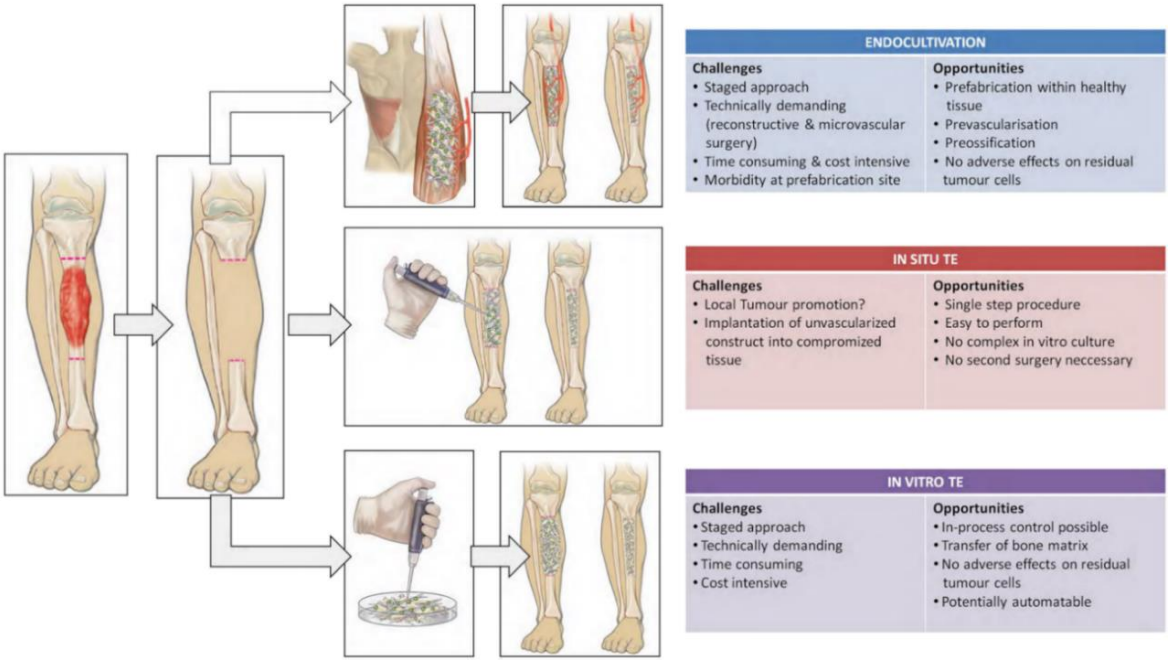

Figure 153: Endocultivation, in vivo, in vitro TE approaches. Source: (Holzapfel et al., 2018)

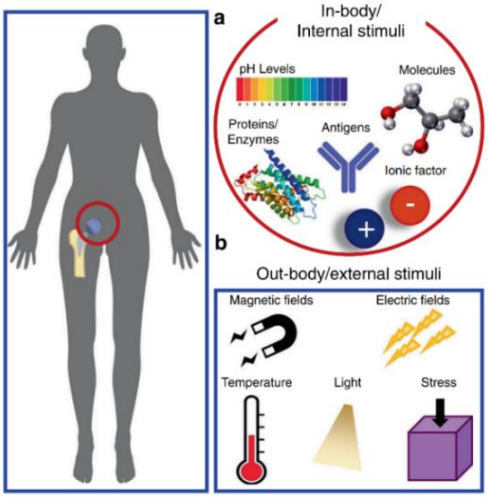

Figure 154: Internal and external stimuli used to enable biofunctionalities. Source: (Montoya et al., 2021)

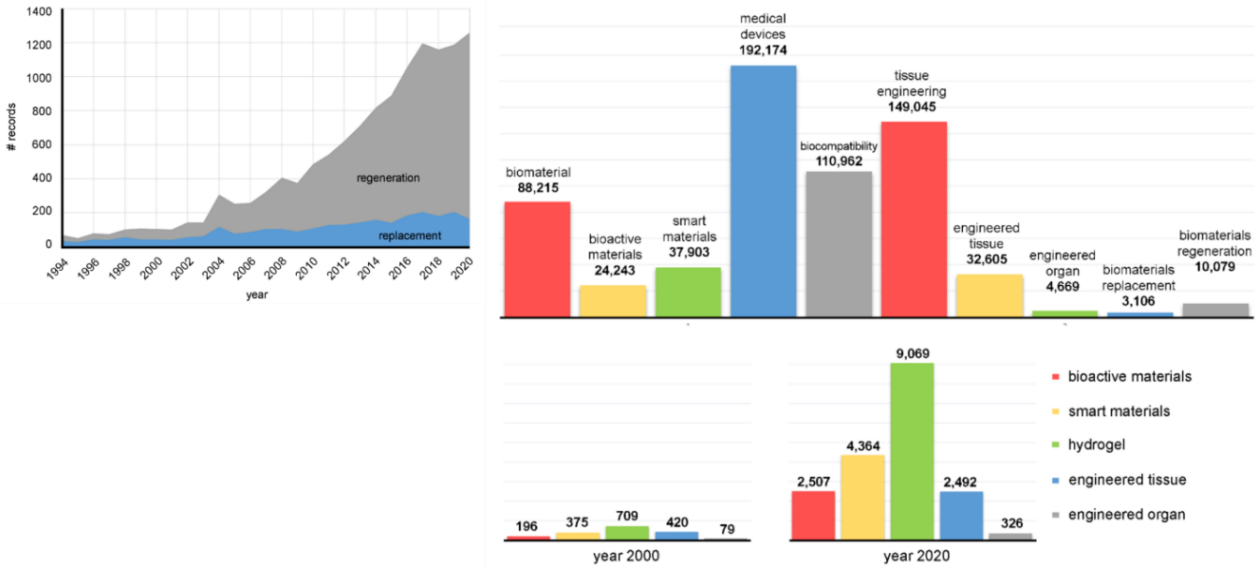

Figure 155: Published records on Scopus on tissue "regeneration" and "replacement"

Source: (Todros, Todesco and Bagno, 2021)

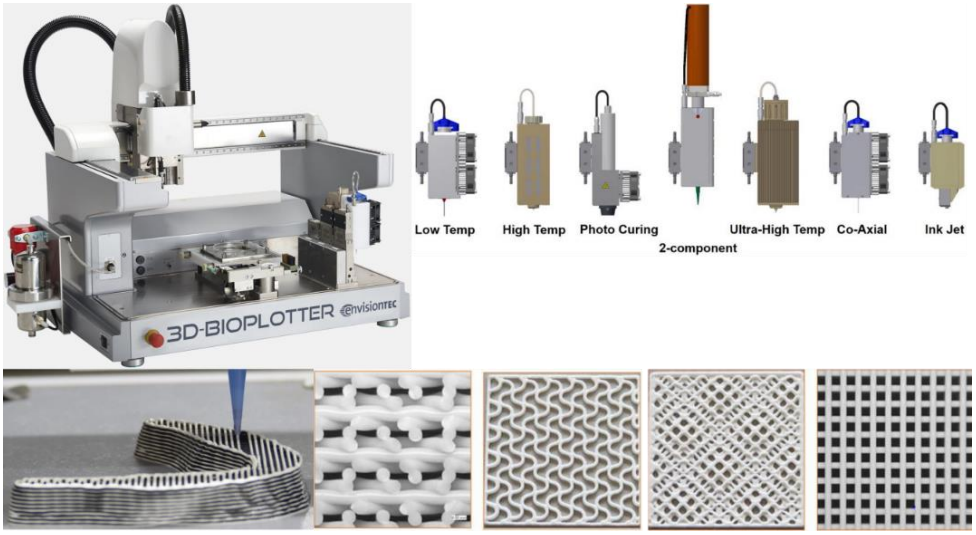

Figure 156: 3D-Bioplotter and bioconstructs. Source: Envisiotec

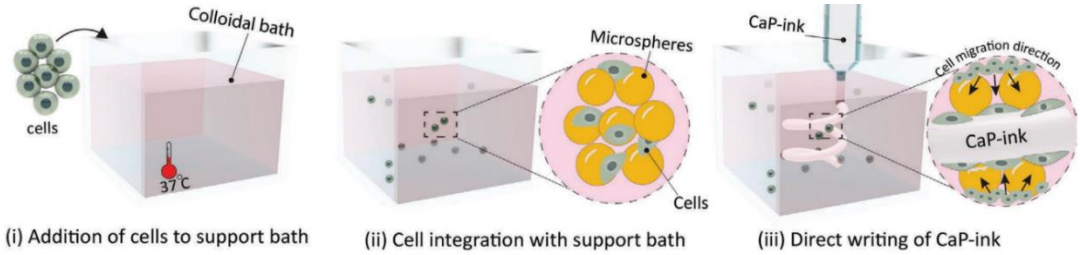

Figure 157: 3D ink (bio)printing within a supportive gel. Source: (Romanazzo et al., 2021)

3.6.1 Biomimetic Meta-Materials-by-Design: Cellular and Functionally-Graded-Materials

Cellular solids are metamaterials as they derive their unusual properties from their architected structures designed to perform particular functions. Although 3DP holds the key to creating such extraordinary paradigms, Askari et al. *(2020)* accentuated the research challenges and solution domains of metamaterials 3DP *(Figure 158)*.

	Solution Domain		
Research Challenge	Metamaterial Design/Modelling	AM Process Development	Materials Science
To enhance fidelity to design intent	X	X	X
To increase build rate		X	
To enhance resolution		X	X
To improve part integrity	X	X	X
To increase complexity of multi-material systems	X	X	X
To liberate more design freedom	X	X	X

Figure 158: Research challenges and solution domain of metamaterials 3DP. Source: (Askari et al., 2020)

A *"cell"* is a small compartment with enclosed space. Structures termed lattice, porous, spongy, trabecular/cancellous, foams, and scaffolds are all cellular designs, though a lattice is usually a reticulated cellular solid with a network of regular or variable unit cells, whereas a foam is a stochastic cellular solid with either a random, regular or variable pattern of interconnected beams. Gibson's and Ashby's *(1999)* fundamental book on cellular solids is the epitome of extensive analysis

of biomimetic structures featuring interconnected pores/voids. They defined a cellular solid as *"an interconnected network of solid struts or plates which form the edges and faces of cells"*, hence individual non-interconnected pores are not cellular solids but porous solids. They categorized cellular solids as:

- Two-dimensional polygon arrays packed to fill plane areas, e.g. hexagonal cells (honeycombs). Only 3 types of polygons can be interconnected and packed regularly without distortion to fill any 2D space as shown in *Figure 159*.
- Open-celled and closed-celled interconnected foams or lattices made of any cell geometry packed in a regular, variable, or random pattern in three dimensions to fill space. The elementary space-filling polyhedra cells that can be interconnected and packed regularly without distortion to fill any 3D space are the 5 shown in *Figure 159*. All lattice structures are based on these unit cells.

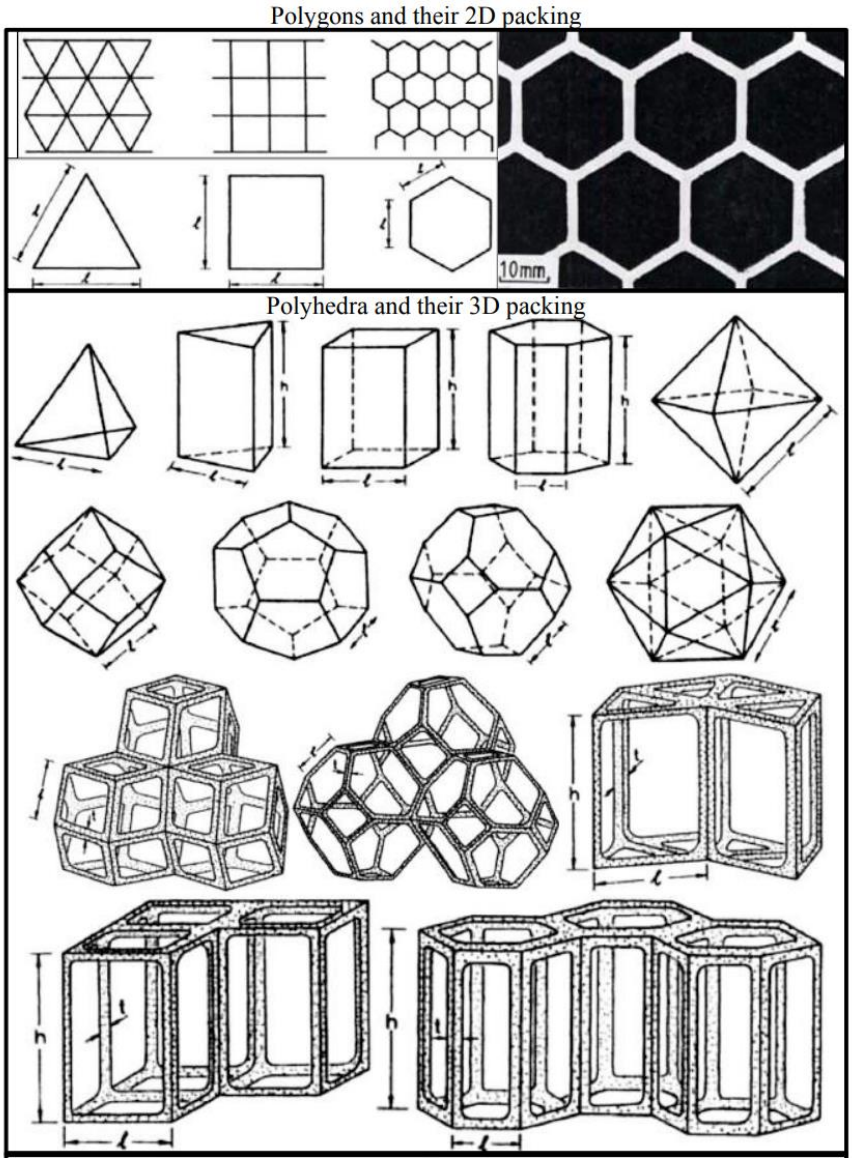

Figure 159: 3 2D polygons and 5 3D polyhedral that can fill space without distortion. Source: (Gibson and Ashby, 1999)

Cellular solids have high specific stiffness and high surface area, making them ideal for implantable or not orthopaedic devices. Although not orthopaedic devices, *Figure 161* shows two

examples of optimized products that enjoy energy absorption properties whilst being lightweight thanks to the implementation of cellular architectures: a helmet featuring hexagonal cells and a shoe sole with fixed-size bend-dominated unit cells.

A cellular solid can be categorized per its structural shape (form), cell topology, cell geometry, cell element dimension, and deformation behavior as shown in *Figure 160*.

Several approaches can be followed to design cellular structures. The most common modeling options used today are shown in *Figure 162*.

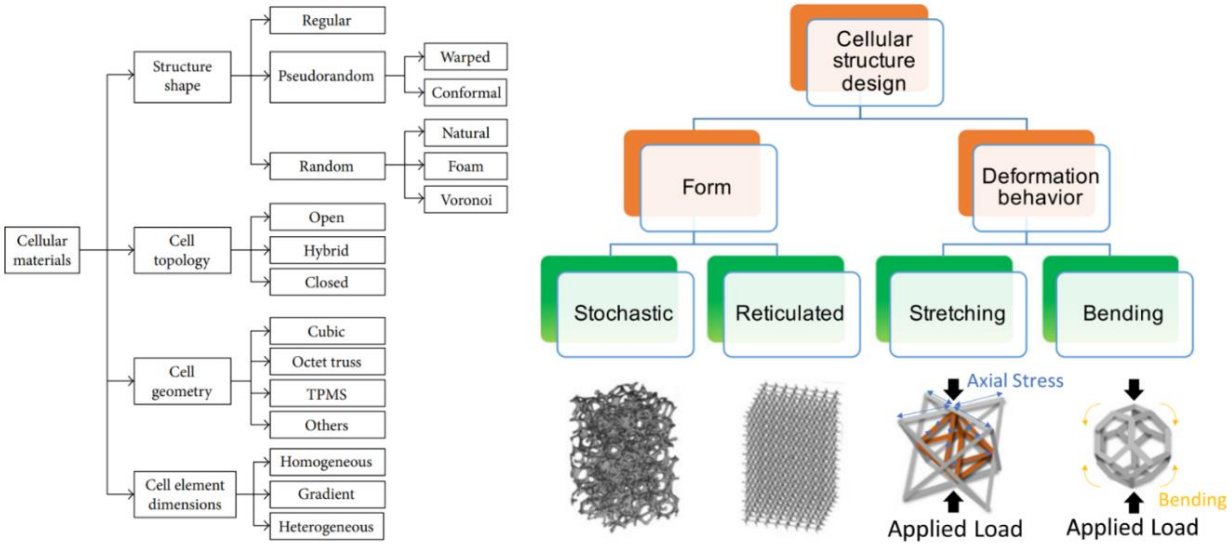

Figure 160: Classification of cellular materials. Source: (Tan et al., 2017; Savio et al., 2018)

Figure 161: Optimized helmet and shoe featuring cellular structures

The most characteristic property of a cellular structure is its porosity (φ) which is defined as:

$$\varphi = \left(1 - \frac{\rho_c}{\rho_d}\right) * 100 \text{ (percent), where:}$$

ρ_c and ρ_d are the densities of the cellular solid and fully dense solid respectively.

Cellular architectures are formed by periodic regular, graded, or random geometric arrangements of homogenous, heterogenous or gradient cells over a given space. As per their mechanical behavior under compression, cellular solids are either bend or stretch-dominated. *Figure 163* shows the characteristic stress-strain curves, photographs under compression, and the Maxwell number (derived from the number of beams and nodes) that defines a particular unit cell type.

Methods	Structures	Design principle	Advantages	Disadvantages
CAD method		Boolean operations between unit structures	• Low cost • High efficiency • Good permeability	• Poor controllability of parameters • Poor mechanical properties
TPMS method		Modeling of trigonometric function expression of minimal surface	• Smooth transition • Large specific surface area • Good controllability of parameters	• Small function coverage
Topology optimization method		According to requirements, optimized by finite element method	• Combine with multiple design methods • Good mechanical properties • Good permeability	• Variable and complex parameters
Voronoi tessellation method		Based on the seed point, surround the seed point to form a spatial polygon, and build a support based on the edge of the polygon	• Simulate the irregular porosity of natural bone • Good controllability of parameters	• Poor mechanical performance • Complex relationship between parameters and performance
CT imaging method		Extract the key shape features of the CT images and perform 3D reconstruction	• Internal structure closest to natural bone • Good permeability	• Complex data processing • High equipment requirements

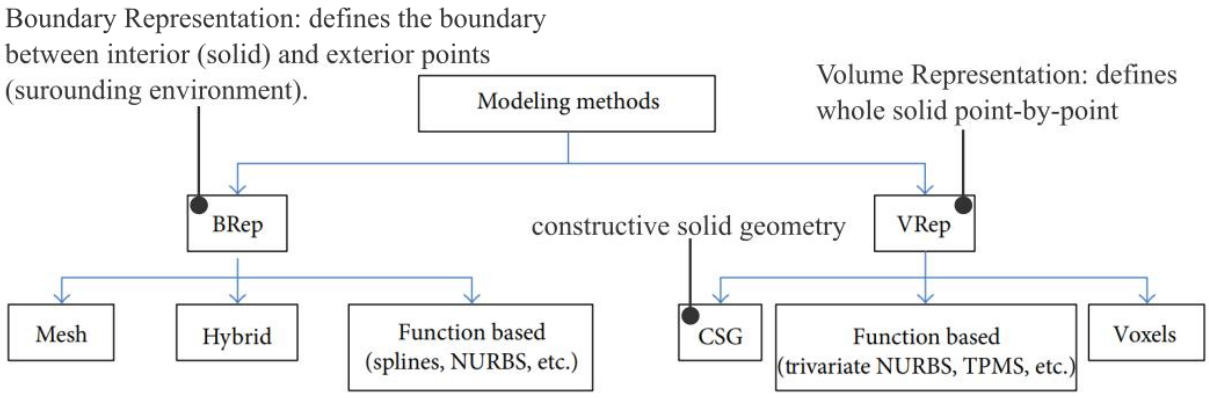

Figure 162: Modelling methods for cellular structures generation. Source: (Savio et al., 2018; Lv et al., 2021)

Cellular structures under compression undergo first linear elastic deformation, then plastic deformation, and then densification by three failure modes: successive cell collapse (due to buckling or crushing), crack propagation through the structure (initiates from pre-existing defects), and diagonal shear where the structure loses around 50% of its strength *(Maconachie et al., 2019)*.

Bend-dominated structures have low moduli of elasticity and strengths but high energy absorption, whereas stretch-dominated are stiffer and stronger. Gibson and Ashby *(1999)* gave the following equations for calculating the modulus of elasticity (E) and strength (σ) for a cellular solid:

$$E_c = E_s * C_1 * \left(\frac{\rho_p}{\rho_s}\right)^n$$

$$\sigma_c = \sigma_s * C_2 * \left(\frac{\rho_p}{\rho_s}\right)^m$$

where:

- E_c and E_s are the moduli of elasticity of the cellular and fully dense solids respectively.
- σ_c and σ_s are the strengths of cellular and fully dense solids respectively.
- The constants C_1, C_2, n, m depend on cell topology and characteristics. Usually $n=2$ and $m=\frac{3}{2}$ for bending-dominated structures and $n=1$ and $m=1$ for stretch -dominated structures.

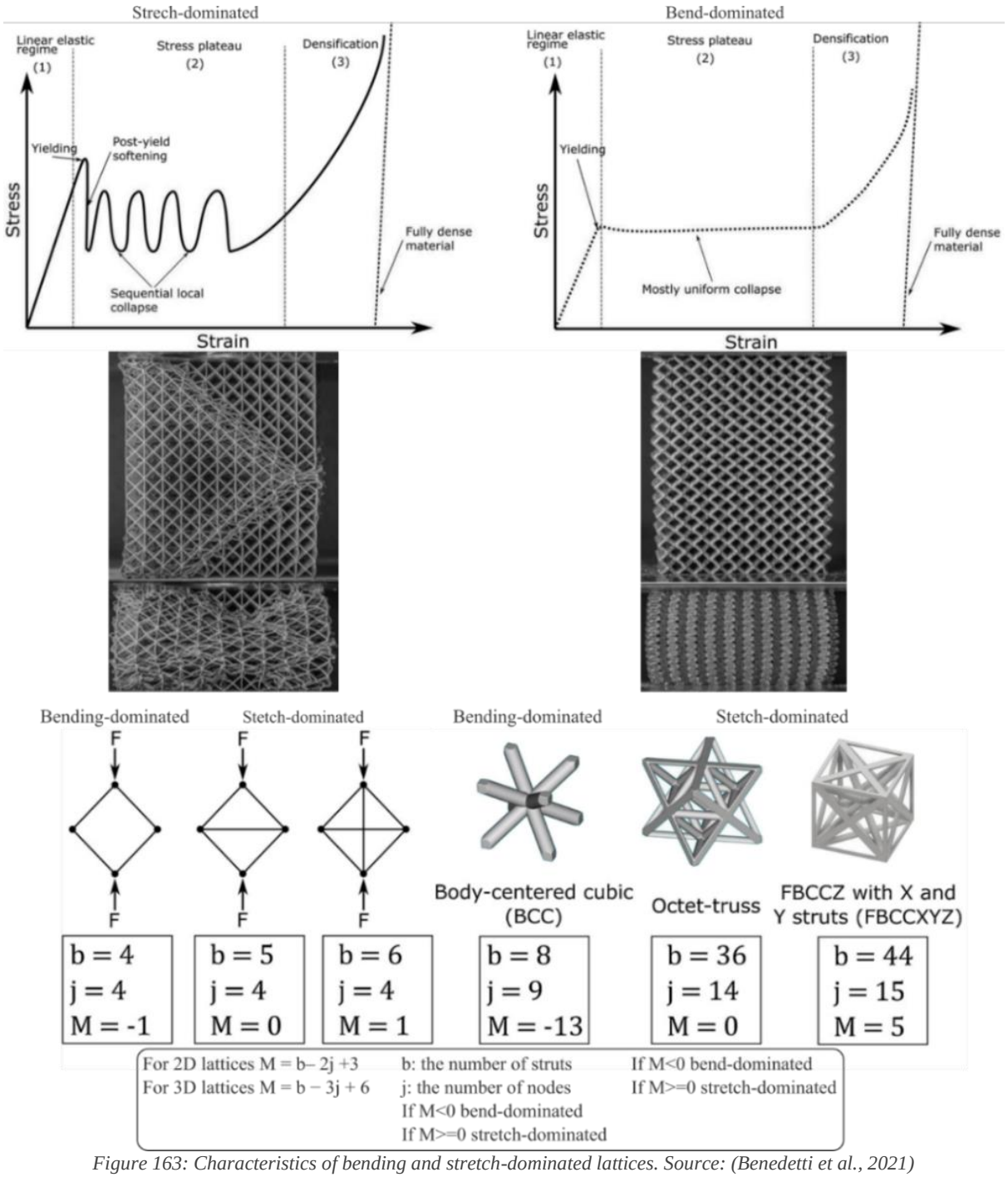

Figure 163: Characteristics of bending and stretch-dominated lattices. Source: (Benedetti et al., 2021)

McGregor et al. *(2021a)* reviewed the histomorphometric properties of trabecular bone at different anatomical sites of the human body *(Figure 164)* and collected data on artificial and natural parameters *(McGregor et al., 2021b)* to be used as a reference to design and 3DP cellular solids.

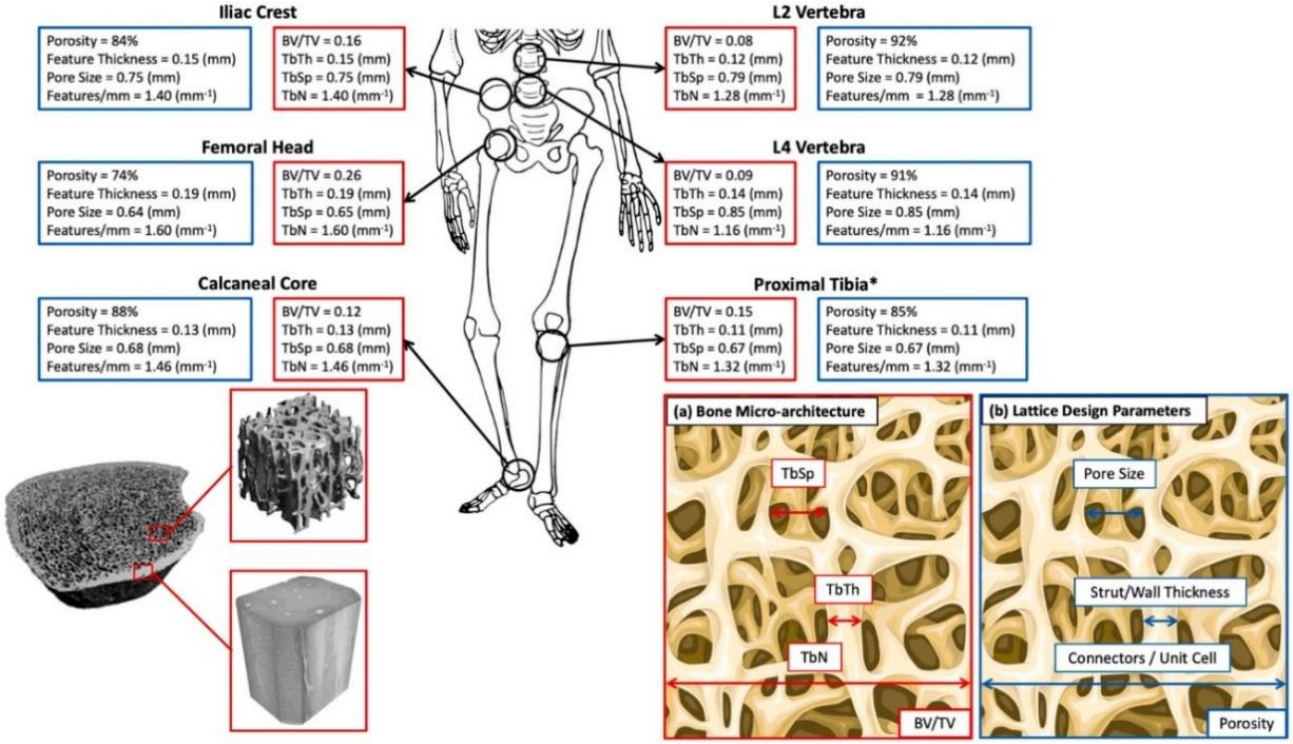

Figure 164: Trabecular bone as a reference to design cellular structures. Source: (McGregor et al., 2021a)

Introducing interconnected pores/cells and tweaking the structure selectively and topologically under control, its mechanical performance can be tuned to match the mechanical characteristics of bones to minimize the stress shielding effect that decreases bone mineral density and weakens the healthy tissue around the implant. Open-celled cellular solids can facilitate bone ingrowth and osseointegration, but pores that favor tissue ingrowth conflict with the need for strong load-bearing orthopaedic implants. It is therefore challenging to obtain bone-like mechanical properties (especially when these have to be customized as per the patient's host site characteristics) whilst retaining suitable pore morphology to allow bone tissue adsorption and regeneration within the porous architecture. To obtain this optimum bimodal performance, there is a need not only to design workflow to develop cellular structures characterization databases to guide selection *(Park, Min and Roh, 2021)* but also for software solutions powered by machine learning and AI algorithms to generate and assess cellular structures by sourcing from libraries of previous applications and cases.

Figure 33 and *Sub-section 3.1* reviewed the optimal trade-off between cell seeding and vascularization by defining porosity (around 70%) and pore size (0,3-0,6 mm) values to achieve osseointegration and osteogenesis within cellular structures of bone-contacting implantable devices. The interest of this Thesis is mainly in the beam-based Voronoi and in the Triply Periodic Minimal

Surface (TPMS)-based cellular solid architectures that are drawing research attention in literature for implementation into orthopaedic implants to create a better biomorphic environment, i.e.:

- **Voronoi:** the Voronoi diagram or tessellation was named after the mathematician G. Voronoy and is composed of finitely random or positioned points (seed points) in a plane for each of which there is a region that divides the plane called Voronoi cell which is formed by the nearest-neighbor principle, i.e. closer to that seed than any other seed *(Okabe et al., 1992).* Similarly, a given 3D space can be seeded with points and their Voronoi cells to be calculated. The borders/edges of the Voronoi cells can be then given a strut thickness as will be illustrated next. Examples of 2D and 3D Voronoi diagrams are shown in *Figure 165.* Voronoi foams exhibit bend-dominated deformation with approximately $C_1=1$, $C_2=1$, $n=2$, and $m=\frac{3}{2}$ in Gibson-Ashby equations for predicting the modulus of elasticity and strength of cellular solids *(Roberts and Garboczi, 2002; Benedetti et al., 2019; Mueller et al., 2019; Dewey et al., 2023).* In a randomized Voronoi, the pore size which is defined as the diameter of a sphere that can be inscribed within the Voronoi cell, cannot be fixed but has a range, hence the average pore size applies. Voronoi and Voronoi-like patterns are the most commonly used types of beam-based architectures for implants and endo-prostheses at the bone-contact regions (shown next).

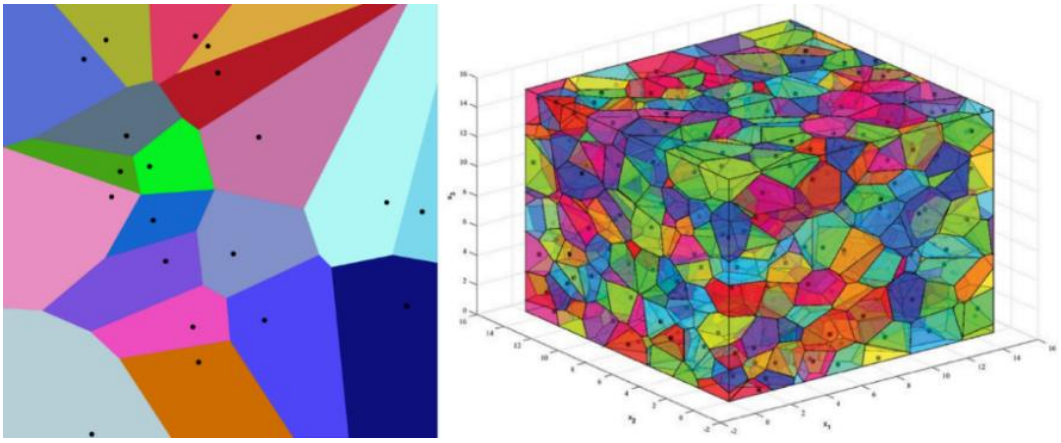

Figure 165: 2D and 3D Voronoi diagrams. Source: Left (Wikipedia: Balu Ertl), Right (Zhao et al., 2021)

- **Gyroid TPMS:** Triply Periodic Minimal Surfaces are naturally inspired continuous infinite non-self-intersecting surfaces with zero mean curvature at all locations of the 3D space. TPMSs *"possess locally minimized surface area that intertwines in 3D space and typically separate the finite bounding volume into closely entangled labyrinthine domains, that fill the volume without enfolded voids" (Yang et al., 2019).* TPMSs are implicit surfaces that can be expressed by algebraic equations, simplified as $f(x, y, z) = c$ with c being an iso-value constant parameter that defines the offset and can take positive and negative values. TPMS surfaces were described by Schwarz *(1933)* and Neovious *(1883)* in 1865 and 1883 respectively. Schoen introduced other examples of TPMS surfaces in 1970 *(1970)* including the Gyroid. The space of TPMS is divided into two parts: f(x, y,z) > c and f(x, y,z) < c.

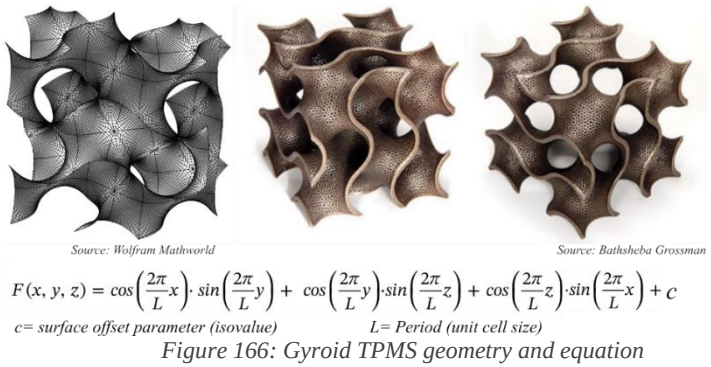

Figure 166: Gyroid TPMS geometry and equation

The Gyroid separates space into two oppositely congruent labyrinths of passages that gyrate down the channels that run through them. The Gyroid equation and its geometry are illustrated in *Figure 166*. Sheet-based TPMSs (two partitioned, unconnected void spaces) are generated by offsetting the surfaces and solidifying the space enclosed between these surfaces, and skeletal (network)-based TPMSs (solid structure with a single void domain) emerge by solidifying one of the two sub-spaces partitioned by the minimal surfaces *(Figure 167)*.

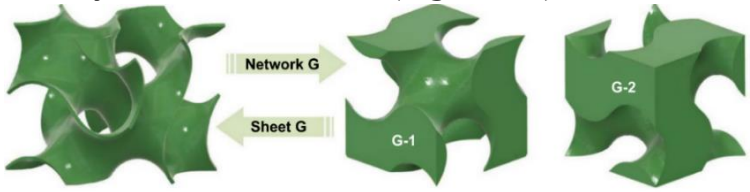

Figure 167: Sheet and skeletal Gyroid TPMS. Source: (Feng et al., 2022)

The surface area to volume for some sheet-TPMS and the volume fraction of some sheet and skeletal TPMSs as per the changes in parameter c is illustrated graphically in *Figure 168*, whereas in *Figure 169* the characteristics of a sheet-based and skeletal-based Gyroid unit cells that both achieve a relative density of 50% are shown.

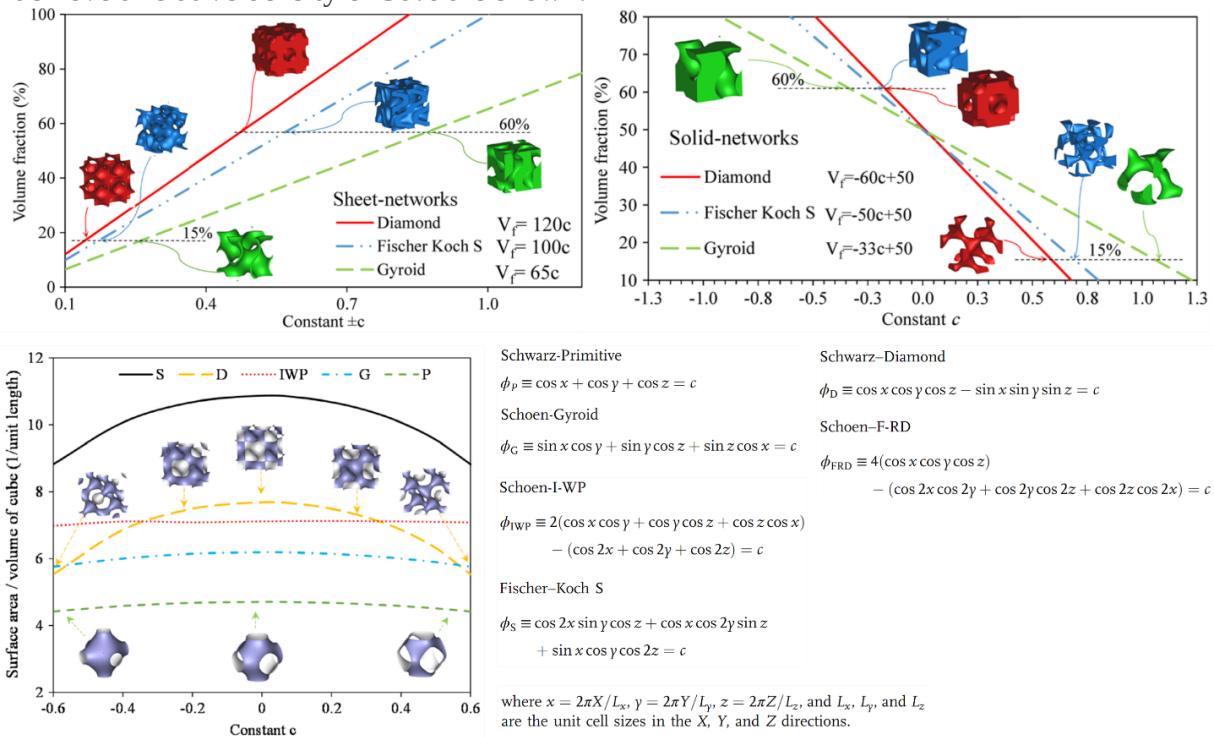

Figure 168: Volume fraction and surface-to-volume of TPMS as a function of c. Source: (Al-Ketan and Al-Rub, 2019)

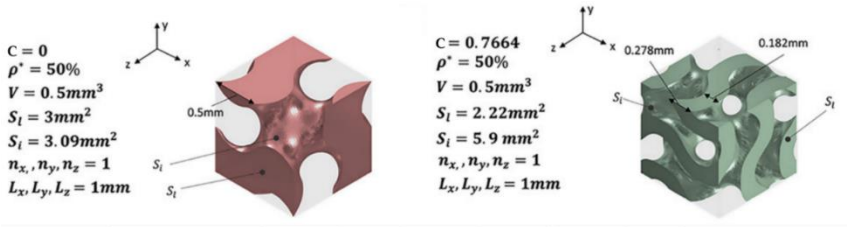

$$F_G(x,y,z) = \sin\left(2\pi n_x \frac{x}{L_x}\right)\cdot cos\left(2\pi n_y \frac{y}{L_y}\right) + sin\left(2\pi n_y \frac{y}{L_y}\right) \cdot cos\left(2\pi n_z \frac{z}{L_z}\right) + \sin\left(2\pi n_z \frac{z}{L_z}\right)\cdot cos\left(2\pi n_x \frac{x}{L_x}\right) = C$$

Figure 169: Sheet and skeletal-based Gyroid unit cells with 50% relative density. Source: (Pugliese and Graziosi, 2023)

The relation of pore size (inscribed sphere) and strut size (wall thickness) for the same unit cell size of the sheet and skeletal Gyroid TPMSs are shown in *Figure 170*.

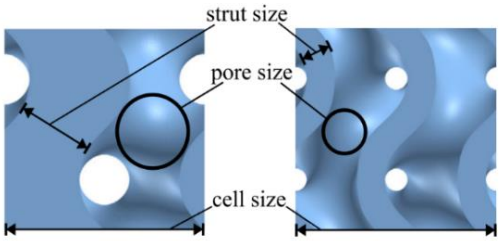

Property	Description
Cell size	Outer size of the unit cell
Pore size	Largest possible size of spherical particle that fits through the cell
Strut size	Smallest thickness of any feature in the cell surface area

Figure 170: Different strut and pore sizes of sheet and skeletal Gyroids of same cell size. Source: (Günther et al., 2022)

The reported C_1, C_2, n and m constants of Gibson-Ashby equations might differ considerably as will be shown next. Sheet-TPMS structures exhibit stretching-dominated elastic behavior for stiffness and bending-dominated plastic behavior for strength with superior mechanical properties compared to skeletal-TPMS that experience bending-dominated deformation thought can be altered to stretching-dominated depending on geometric topology *(Alketan et al., 2018a; 2018b; Abueidda et al., 2019; Abou-Ali et al., 2020; Abou-Ali, Lee and Abu Al-Rub, 2022)*. Sheet-TPMSs have higher surface area to volume ratio thus more exposure to and interaction with surrounding environment for vascularization and cell activities for bone ingrowth, but skeletal-TPMSs might have an advantage over sheet-TPMSs due to better pore interconnection. Transitions and gradients can be achieved by blending skeletal and/or sheet TPMSs topologically to imitate the bone structure and eliminate the disadvantages of each TPMS type *(Figure 171)*.

TPMSs have many application areas *(Feng et al., 2022)*, especially for biomimetic biomedical devices *(Pugliese and Graziosi, 2023)* due to their a) accurate control of pore and strut sizes, curvature and volume fraction, b) functional grading (cell size, volume fraction, cell type), c) high surface area at low volume fraction, d) high strength at low stiffness and low densities, e) good permeability, and f) high energy absorption *(Günther et al., 2022)*, making them ideal for orthopaedic implantable devices *(Maconachie et al., 2019)*.

To design a cellular solid any homogenous, heterogenous, or gradient cell can be arranged periodically with regular, random, or graded packing spacing by various modeling approaches. Beam and skeletal and sheet TPMS unit cells to make lattice structures are shown in *Figure 172*.

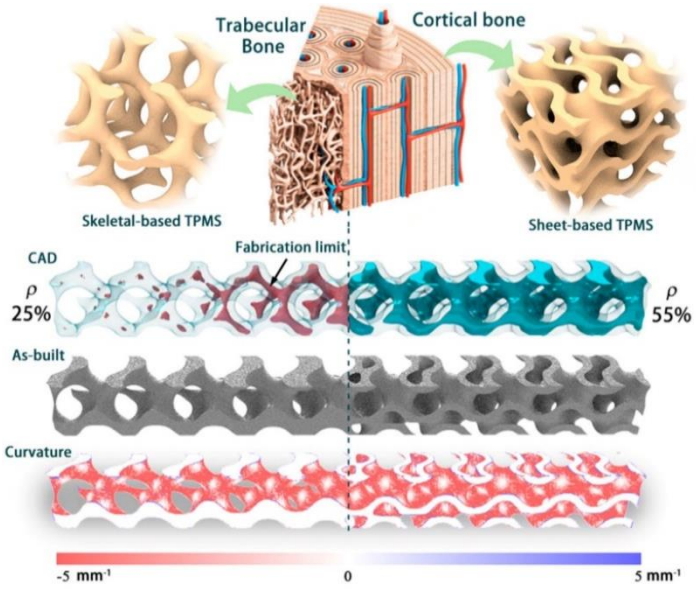

Figure 171: Sheet and skeletal Gyroid TPMS blending for bone imitation. Source: (Zhang et al., 2023)

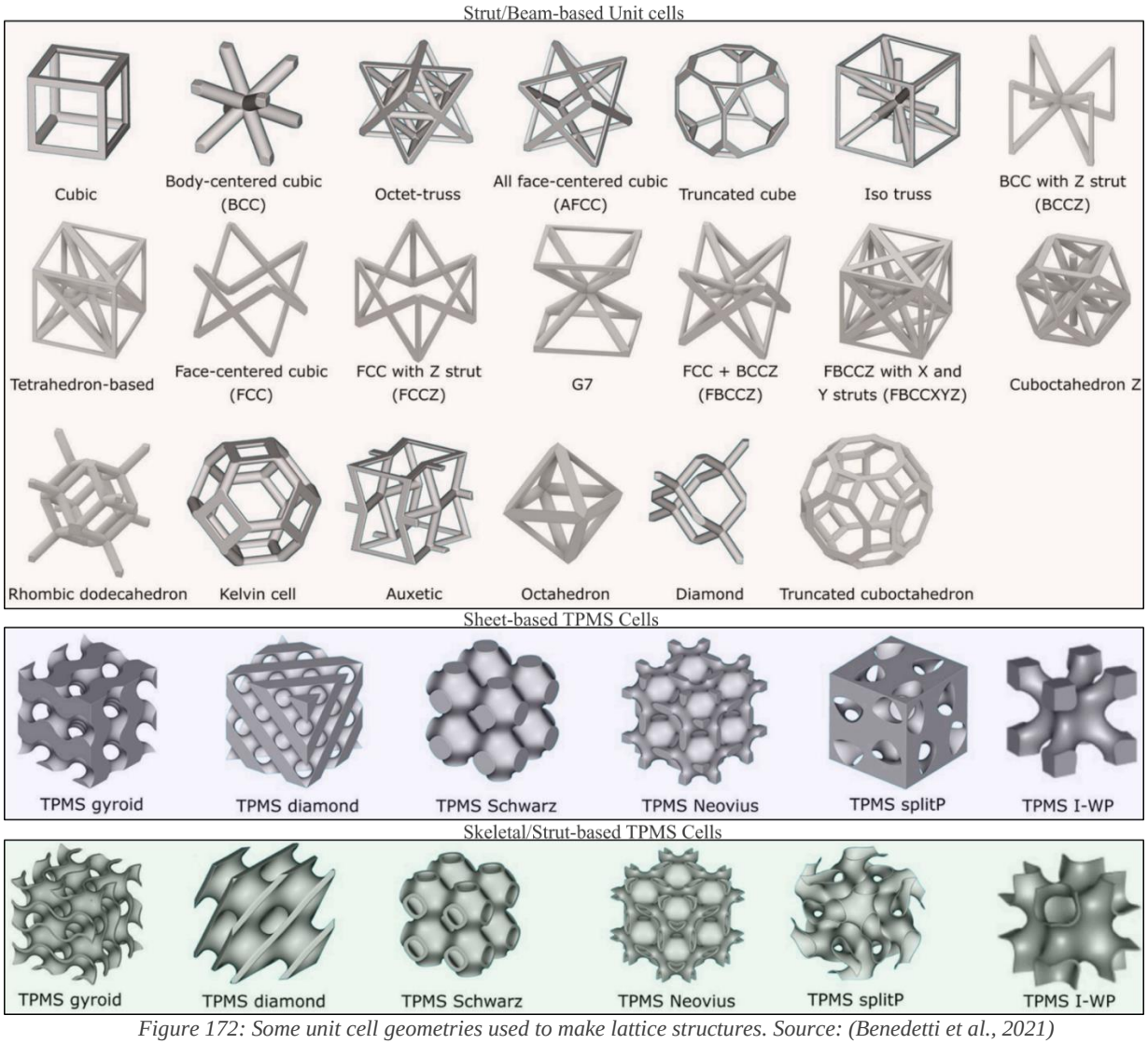

Figure 172: Some unit cell geometries used to make lattice structures. Source: (Benedetti et al., 2021)

Inspired by the histomorphometric indexes of trabecular bone, Gómez et al. *(2016)* implemented Voronoi tessellation to synthesize customized trabecular-like designs with gradient-controlled interconnected porosity, pore distribution, and shapes *(Figure 173)*. Similar approaches to mimic the

trabecular bone were followed by Wang et al. *(2018)* (compressive behavior of Voronoi-based scaffolds with functionally-graded porosity), Deering et al. *(2021)* (selective and isotropic Voronoi seeding with tunable strut architectures and increased anisotropy *(Figure 174)*), Chen et al. *(2021)* (Rhinoceros (Robert McNeel & Associates, Washington, US) modeling software with Grasshopper plug-in to model gradient irregular scaffolds *(Figure 175))*, Frayssinet, Colabella and Cisilino *(2022)* (Rhinoceros with Grasshopper plug-in to generate Voronoi-based microstructures comparable to micro-CT scanned bovine femoral head reference cuboids *(Figure 176))*.

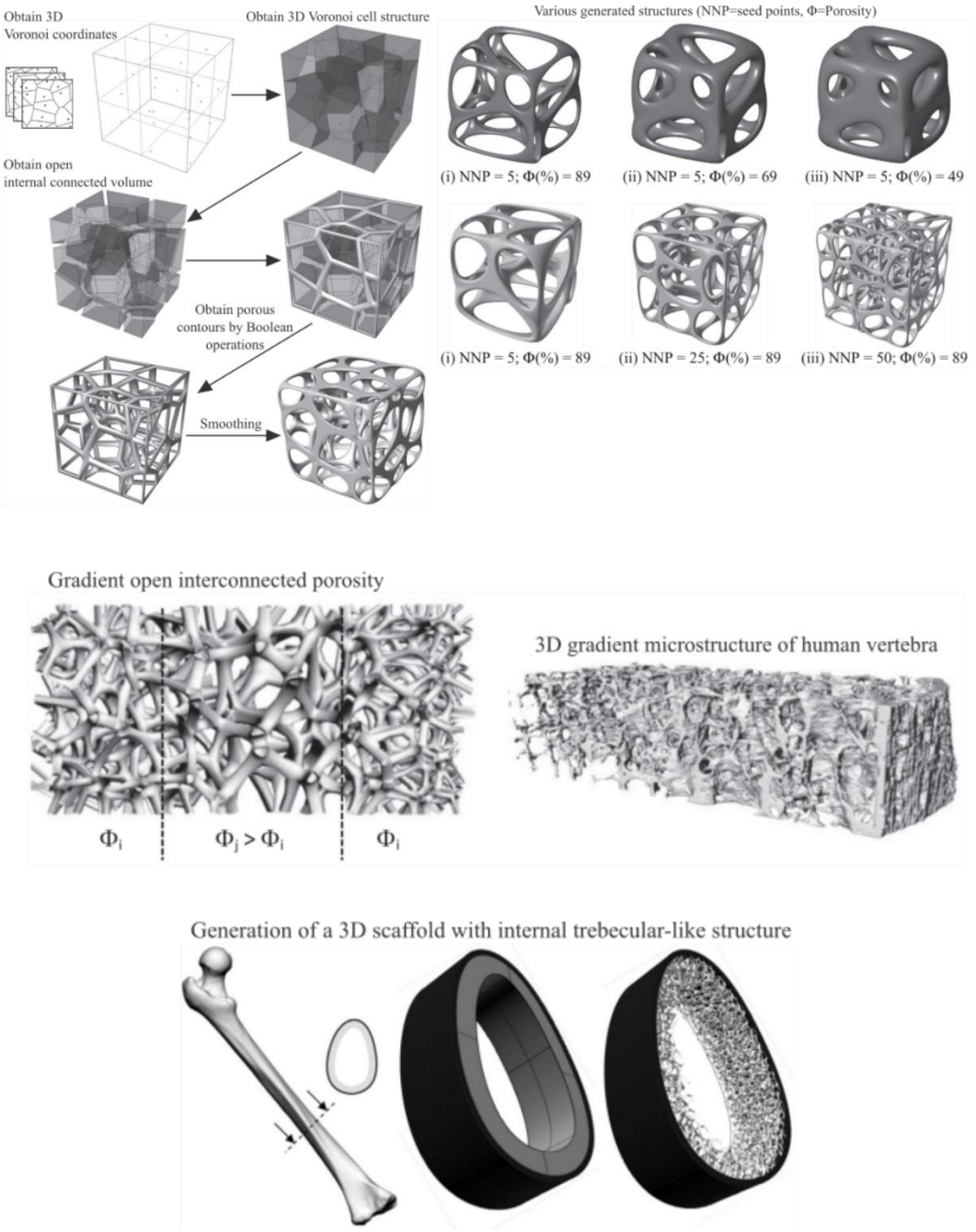

Figure 173: Voronoi tessellation for synthesizing trabecular-like designs. Source: (Gómez et al., 2016)

Wu et al. *(2018)* presented a method to generate bone-like porous structures as a lightweight infill during the process planning of 3DP utilizing a voxel-wise topology optimization *(Figure 177)*.

Ghouse et al. *(2019)* 3DPed stochastic porous scaffolds with topologically controlled stiffness by filling a volume (discretized into sections) with a random distribution of points and connecting these points with a desired connectivity for each section. The scaffold achieved bone-like mechanical behavior and facilitated 10,73% bone ingrowth after 6 weeks in the medial femoral condyle of ewes.

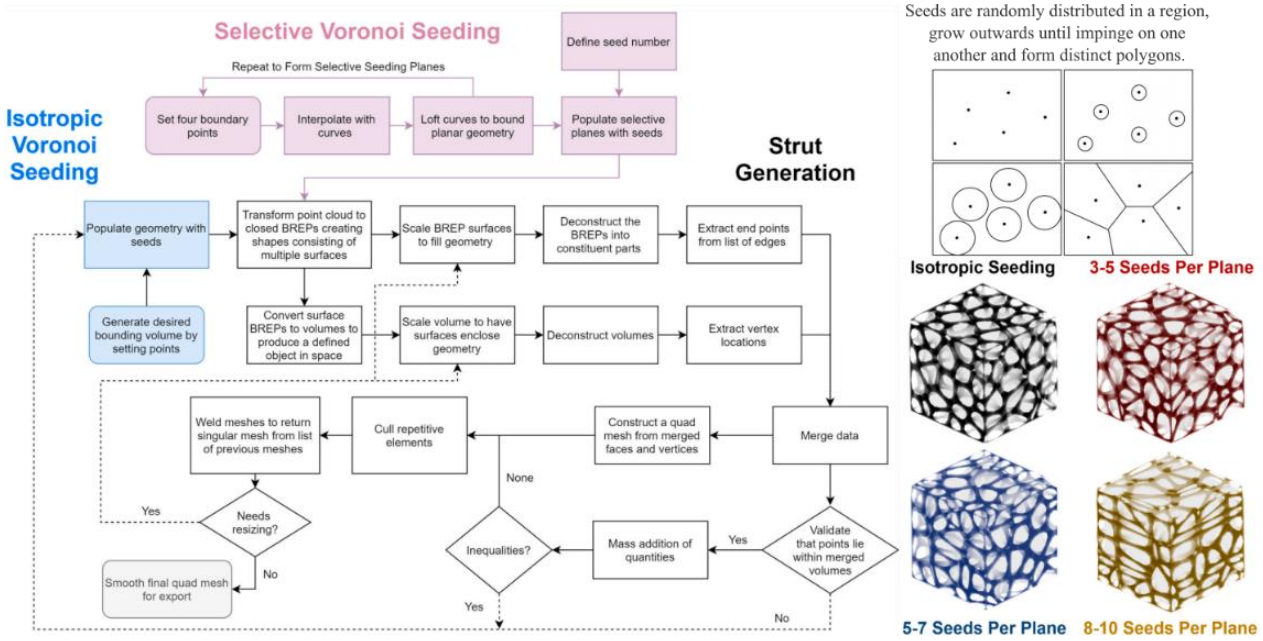

Figure 174: Selective and isotropic Voronoi tessellation. Source: (Deering et al., 2021)

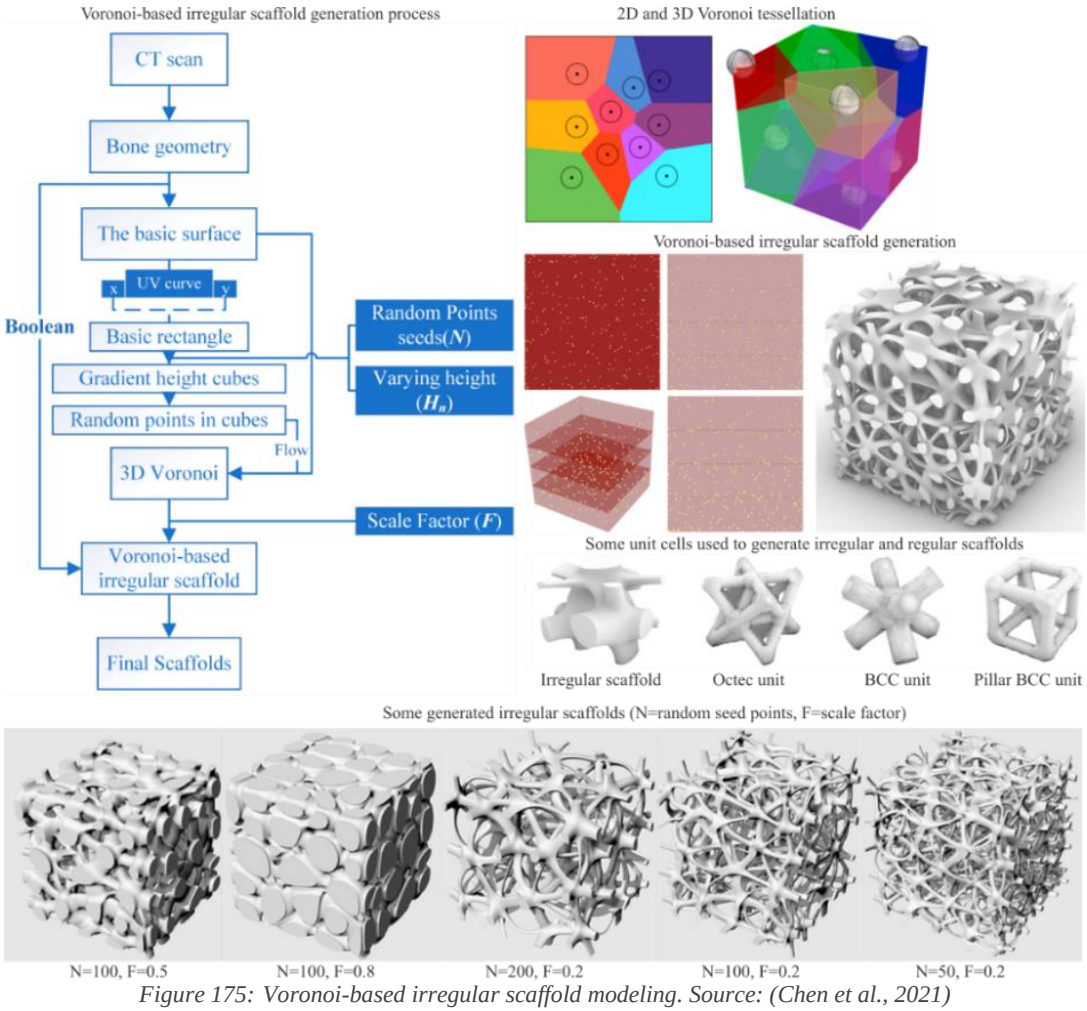

Figure 175: Voronoi-based irregular scaffold modeling. Source: (Chen et al., 2021)

Alsheghri et al. *(2021)* investigated the computational reproduction of the iterative process of network connectivity refinement occurring in trabecular bone using a heuristic structural network optimization algorithm *(Figure 178)* that is abstract and dimension-independent and can be subject to morphological refinements: adding anisotropy, stiffness gradients, combinations of materials.

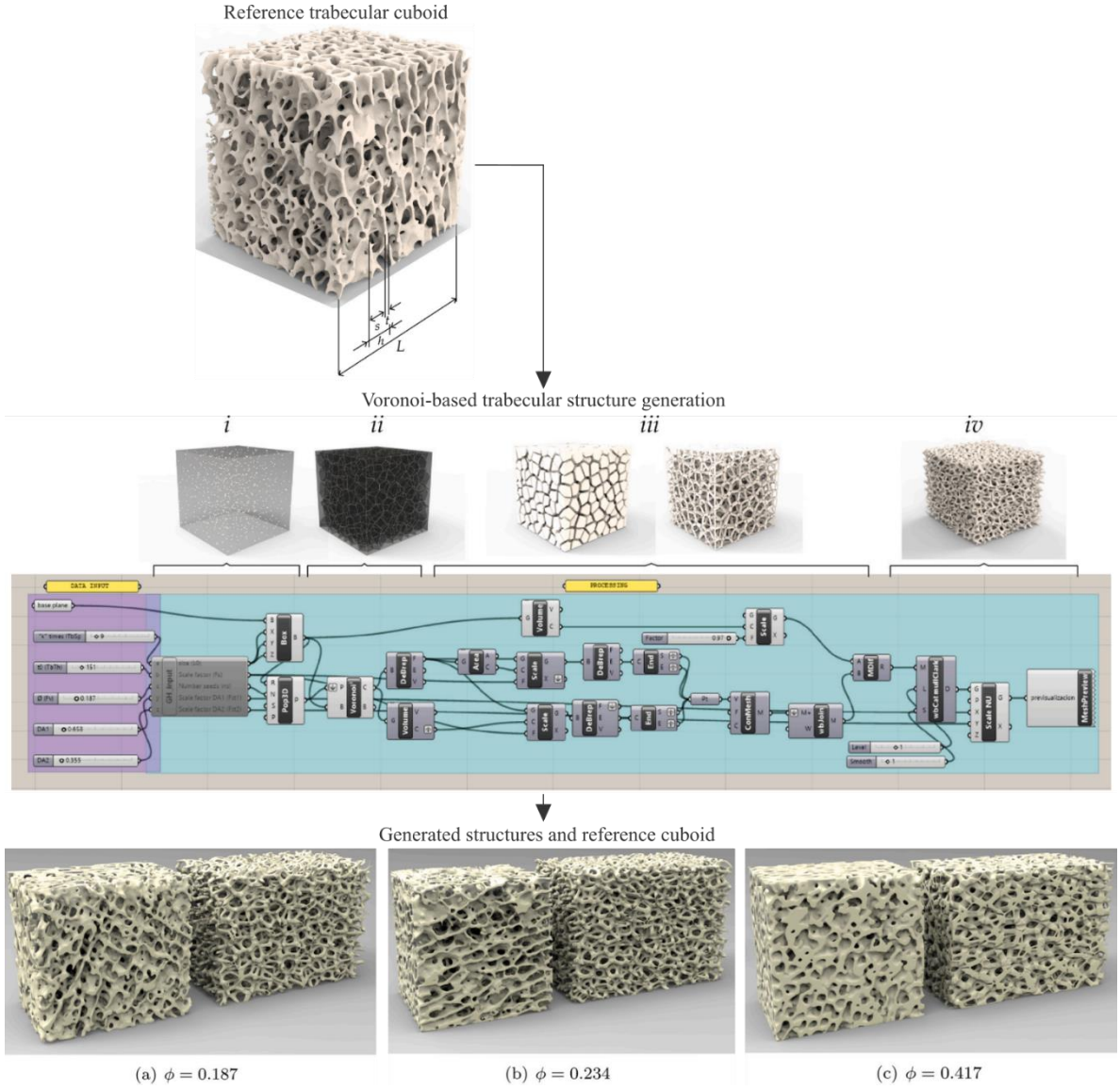

Figure 176: Voronoi designs compared to micro-CT scanned reference. Source: (Frayssinet, Colabella and Cisilino, 2022)

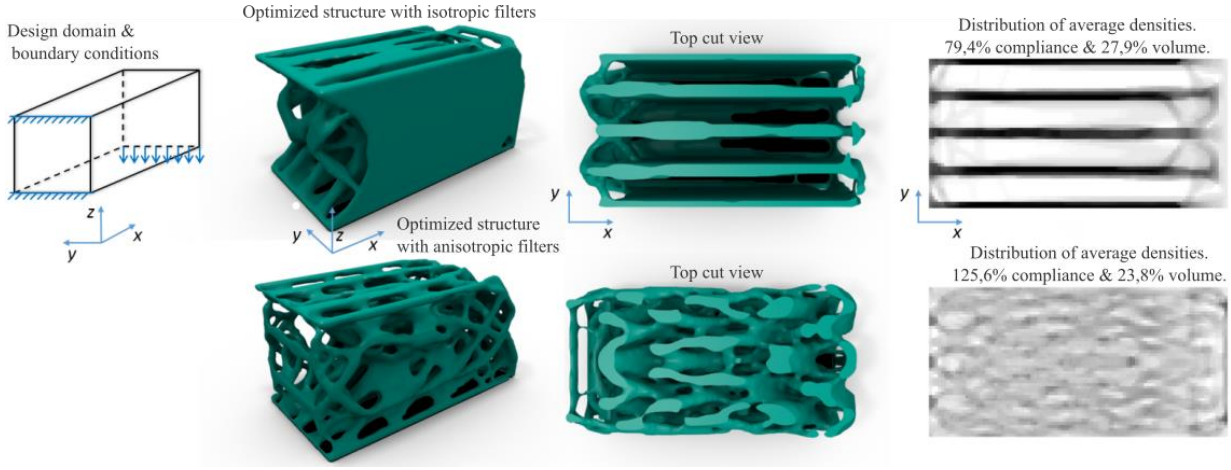

Figure 177: Infill geometries generated by voxel-wise topology optimization. Source: (Wu et al., 2021)

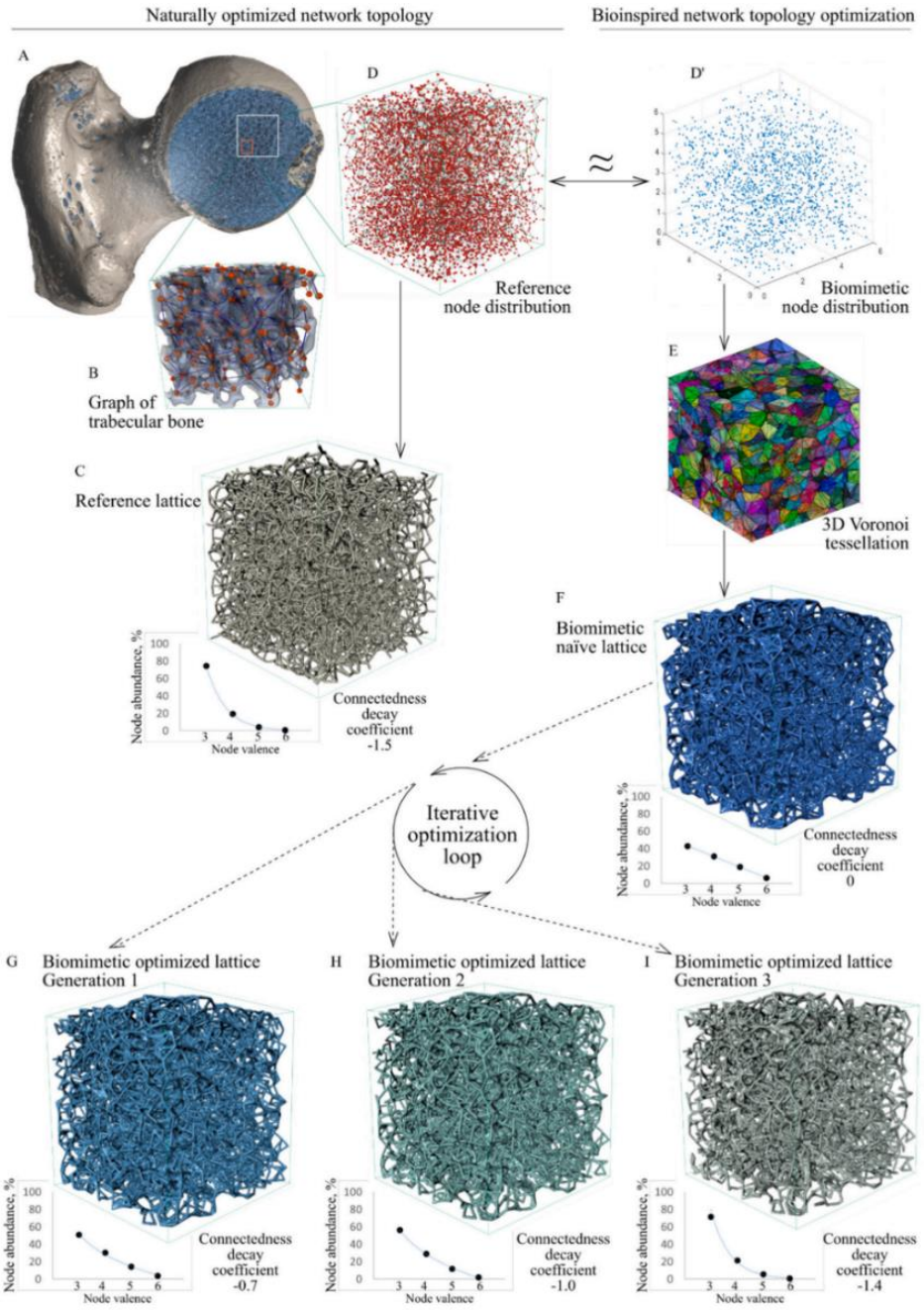

Figure 178: Biomimetic networks by iterative network topology optimization. Source: (Alsheghri et al., 2021)

White et al. *(2021)* introduced a concept of multi-body interpenetrating lattice metamaterials, where two or more lattices interlace through the same volume without any direct connection to each other, allowing control of energy and fluid transfer by surface interactions *(Figure 179)*.

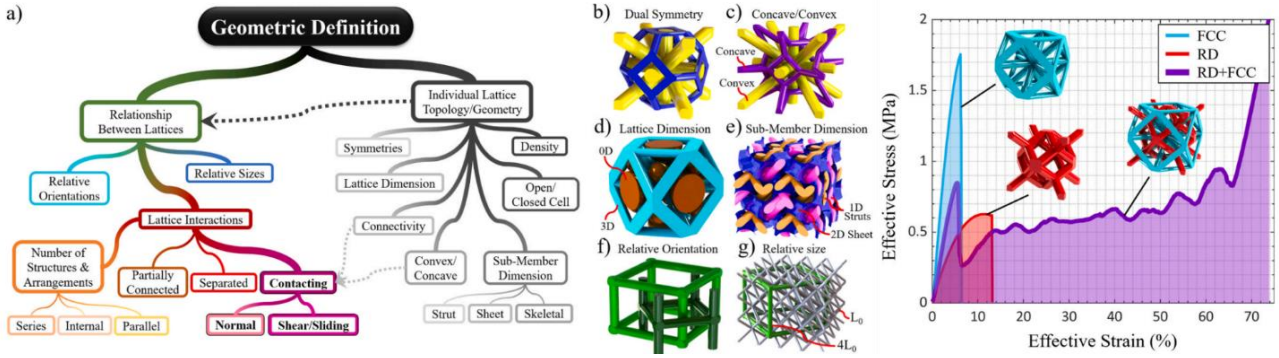

Figure 179: Multi-body interpenetrating lattices. Source: (White et al., 2021)

The ideal biomimetic implant design would be heterogeneous with density and composition gradients instead of being homogeneous with equally spaced fixed-size unit cells. For example, *Figure 180* shows a generatively designed tire concept with functionally gradient density distribution driven by the mechanical loads exerted.

Figure 180: A biomimetic functionally graded airless tyre design: Michellin's Vision Concept. Source: Michellin

FGMs are monolithic solids with spatially varying composition and density distribution. As described previously, 3DP technologies can fabricate functionally-graded structures under full control regardless of the geometric complexity. An FGM experiences functional deviations and has different properties topologically, i.e. it can be solid at its exterior and porous at its interior, thus having excellent strength-to-weight ratios. FGMs can be: a) single-material with modulated density and microstructure, or b) multi-material monoblock component with compositional gradients, whilst embedding the optimum properties of each base material. Although it is still difficult to fully utilize the potential of FGM as there are no design guidelines and software to design and simulate FGMs, Loh et al. *(2018)* presented the steps for 3DP FGMs *(Figure 181)*.

Step	Process	
Step 1: Design and modelling	Product concept generation Computer-aided design for manufacturing and simulation Topology and infill optimisation	The mechanical function of the part is defined by describing the fundamental attributes including the geometry and material composition. Some parts can be optimised by the lattice or cellular structure. Other important attributes include topology optimization, gradient dimension or vector, the geometric of equi-composition or equi-property surfaces, the material characteristics, and mechanical parameters before developing a modelling scheme [19].
Step 2.1: Materials description	Material selection and microstructure allocation Defining optimum material properties distribution Gradient classification Analysis of area void density	Material data that concerns the chemical composition and characteristics of the part is modelled. Digital simulation is used to represent the materials, formulate a matching epistemology for the material selection, gradient discretisation, volume of support, residual stresses, etc. [20]. The void density needs to be taken into account in the theoretical calculation.
Step 2.2: Product description	Classification of the part (geometry and material repartition) with mathematical data.	Mathematical data is used to identify an appropriate manufacturing strategy and process control.
Step 2.3: Manufacturing description	Classify information from step 2.2 into slices and build orientation	The manufacturing strategy is determined according to a triptych material-product-manufacturing. The mathematical data from product and material description are used to define the slicing orientation, categorised as planar or complex slices [16].
Step 3: Additive manufacturing	Manufacturing strategy and process plan determination. Paths classification NC Programming Process control and monitoring	This type of path strategy is defined and then evaluated according to the geometry and material repartition. Numerical Control (NC) programming involves the generation of paths and modification of process parameters using, but not limited to G-code programming language [15,21]. The file is sent to the AM machine for the production sequence to commence [16].
Step 4: Post-processing	Part removal Heat and pressure treatment Machining Surface treatment	Post-processing ensures that the quality aspects (e.g. surface characteristics, geometric accuracy, aesthetics, mechanical properties) of the printed part meets its design specifications. AM post-processing methods include, but not limited to, tumbling, machining, hand-finishing, micromachining, chemical post-processing, electroplating and laser micromachining [22].
Step 5: Final Product	Quality assurance Validation	Experimental analysis such as non-destructive testing, stress analysis or microscopic imaging is carried out to validate the final product and resultant part properties.

Figure 181: Steps for manufacturing FGMs. Source: (Loh et al., 2018)

Zhang et al. *(2019b),* Saleh et al. *(2020),* and Shi et al. *(2021)* reviewed the design criteria, structures, and types *(Figure 182)*, biomedical applications, challenges in production techniques, and 3DP of FGMs, whereas Hofman et al. *(2014)* illustrated multi-component phase diagrams that were developed by thermodynamic modeling as a guiding map for desired gradients *(Figure 183).*

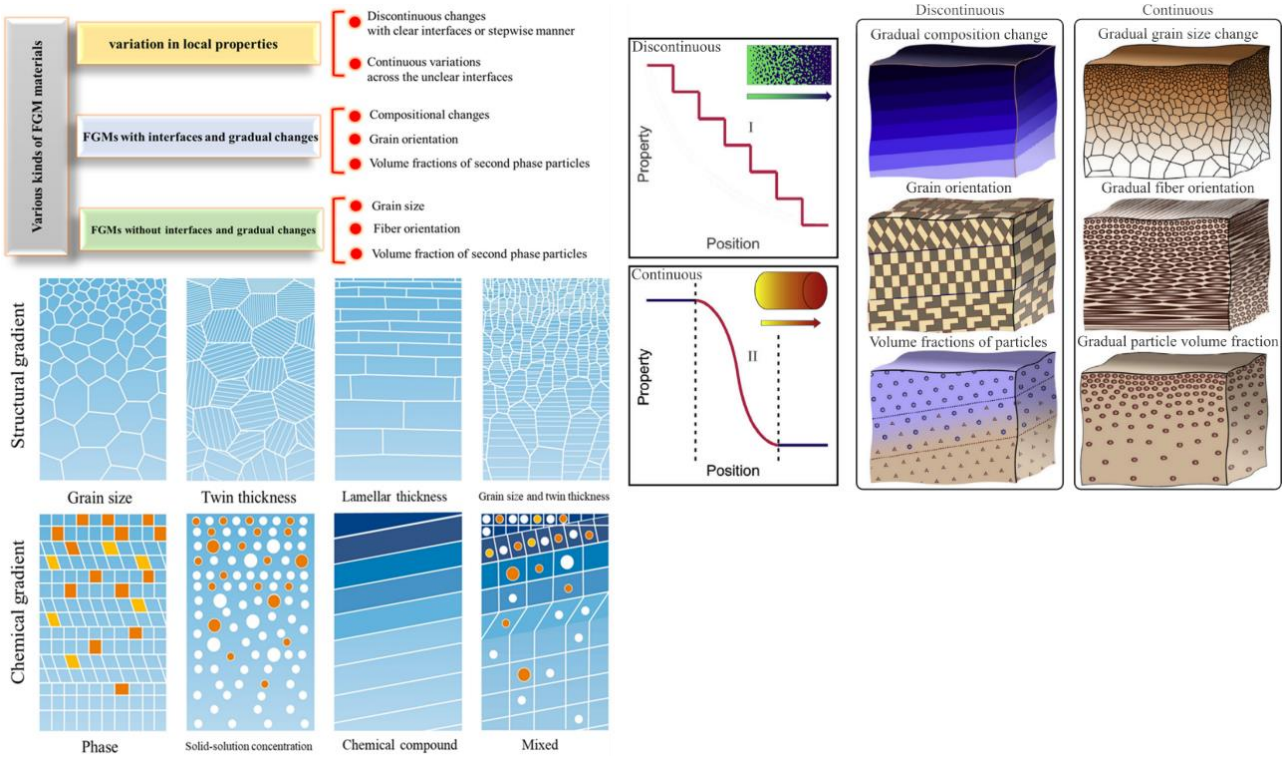

Figure 182: Structures and types of FGMs. Source: (Zhang et al., 2019b; Shi et al., 2021)

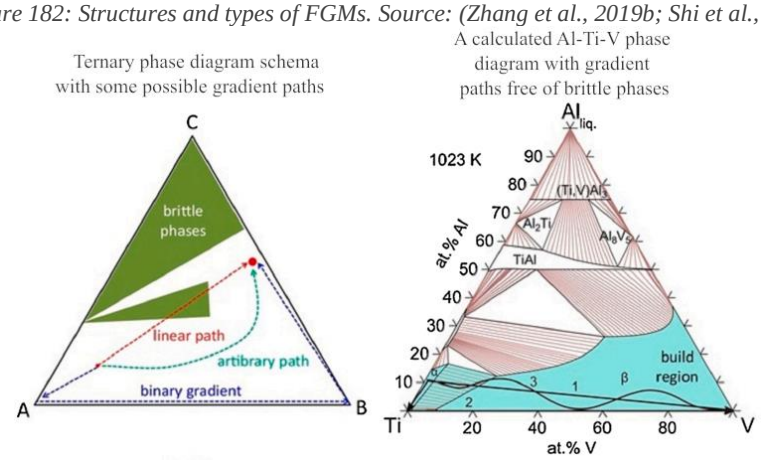

Figure 183: Multi-component phase diagrams for FGMs. Source: (Hofman et al., 2014)

3.6.1 Mechanical Performance Optimization

Mechanical optimization of cellular architectures pertains to matching the implant's material stiffness to that of the host bone to reduce the stress shielding phenomenon.

Murr et al. *(2011)* demonstrated some 3DPed open-celled reticulated mesh and stochastic foam specimens and incorporated such architectures into a knee implant *(Figure 184)*, whereas Harrysson et al. *(2008)* and Arabnejad et al. *(2016b)* 3DPed cellular femoral stems with bone-matching stiffness.

Cell morphology and orientation affect both mechanical properties and biological tissue fixation into high-strength spongy 3DPed biomaterials *(Weißmann et al., 2016; Zhao et al., 2016; Arabnejad*

et al., 2016a). However, post-implantationally, as tissue ingrowth progresses and the implant's voids are no longer empty, the mechanical characteristics and loading conditions change. Indeed, Hedayati et al. *(2017)* experimented with polymer filling of porous Ti structures and studied the differences in static and fatigue mechanical performance. They reported an increase in static and fatigue strength by a factor of 2-7, whilst the more porous the structure, the higher the increase.

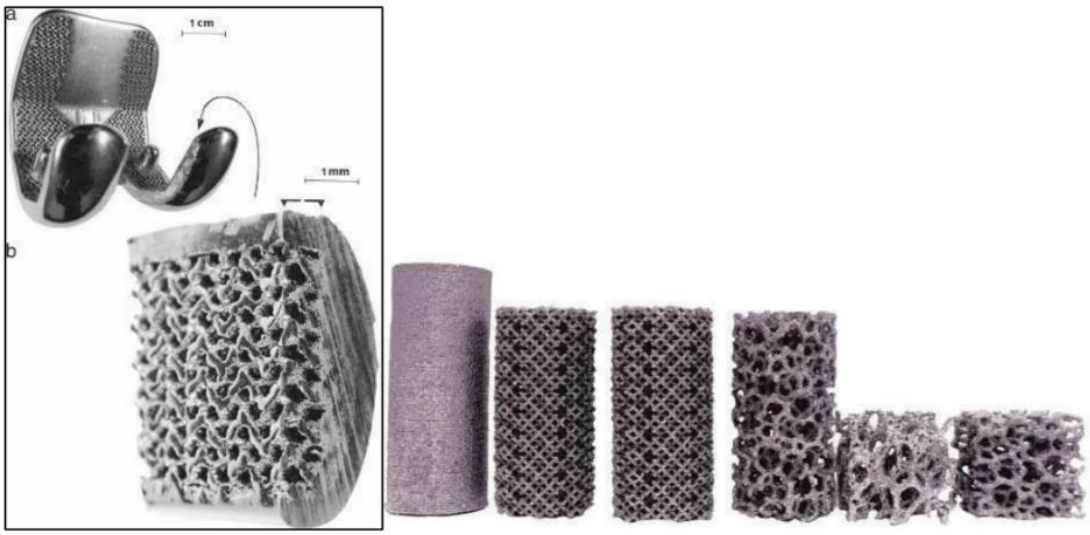

Figure 184: 3DPed porous specimens and knee implant. Source: (Murr et al., 2011)

Wang et al. *(2016)* reviewed the current status of topological design of porous metallic implants for mechanical and biological optimization and 3DP of such. They stated the need to establish a database with properties of human bones (different age, gender, locations) and topology optimization algorithms to deal with the selection of optimum porosity, pore size, and interconnectivity.

Sola, Bellucci and Cannillo *(2016)* focused on the mechanical superiority of FGM designs and their orthopaedic surgical applications *(Figure 185),* and their manufacturing methods (3DP).

Arabnejad et al. *(2016a)* assessed the interplay between cell morphology, mechanical properties (compression tests), bone ingrowth (canine in vivo model), and manufacturing constraints. The authors provided a graphical all-in-one scheme for two example unit cells (Tetrahedron, Octet truss) to select the most suitable unit cell size morphology from an admissible design space that emerges from pore size (50-800 μm, vertical red line), porosity (higher than 50%, inclined red line), and minimum strut thickness manufacturing constraints (200 μm, horizontal red line). Their workflow, the tested specimens, and the results of the moduli of elasticity are shown in *Figure 186.*

Arabnejad et al. *(2016b)* followed a systematic approach for 3DPed fully porous femoral stems that were fine-tuned to locally mimic the mechanical properties of bone tissue. Compared to fully solid implants, the amount of bone loss by stress shielding was reduced by 75% *(Figure 187).* Similar results (60% stress shielding reduction for porous stems) were reported by Naghavi et al. *(2023).*

Qin et al. *(2017)* combined bottom-up computational modeling with experiments based on 3DPed models to investigate the mechanics of porous Gyroid geometries. The authors verified that the

material architecture features, instead of the mechanics of its constituting materials, play the dominant role in governing their performance and scaling laws.

Application	FGM benefits	Approach	Comments
Knee			
Total knee replacement	Stress profile optimization (minimal stress shielding effect; maximum component resistance)	FE method and design of experiment	Combined design of geometry and FGM
Total knee replacement (tibia)	Stress profile optimization (minimal stress shielding effect)	2D axisymmetric FE model	
Total knee replacement (tibia)	Stress profile optimization (minimal stress shielding effect)	2D FE model	
Femur and hip			
Hip prosthesis, cementless (coating)	Stress profile optimization (minimal stress shielding effect; reduced shear stresses)	2D FE model and optimization technique	Systematic comparison of various 1D-FGMs and 2D-FGMs
Hip prosthesis, cementless/cemented (stem)	Stress profile optimization (minimal stress shielding effect; reduced shear stresses)	2D FE model and optimization technique	
Hip prosthesis, cemented (stem)	Stress profile optimization (minimal stress shielding effect; reduced shear stresses)	3D FE model	Length of the stem considered as an additional parameter
Hip prosthesis, cementless/cemented, nonbonded/bonded (femur)	Stress profile optimization (minimal stress shielding effect; reduced shear stresses)	3D FE model	Systematic comparison of various profiles and gradient indexes
Hip prosthesis, cemented (femur)	Stress profile optimization (minimal stress shielding effect; reduced shear stresses)	3D FE model	Various anchoring solutions and various loading conditions (walking, stair climbing)
Hip prosthesis, cementless (stem, proximal femur)	Stress profile optimization (minimal stress shielding effect; reduced shear stresses)	2D FE model	Bone remodeling theory implemented into the simulation
Hip prosthesis, cementless/cemented (acetabulum)	Stress profile optimization (minimal stress shielding effect; reduced shear stresses)	2D FE model and optimization technique	Costs/performance balance
Intervertebral disk			
Intervertebral disk (C6–C7 segment)	Optimization of stress distribution at the implant-bone interface	3D FE model	Experimental-computational approach. Additional information on strength and resistance of materials.
Orbit			
Inferior orbital wall	Stress profile optimization (minimal stress shielding effect; higher compressive stresses at the fracture surface)	3D FE model	FE model based on computed tomography scan images of a patient
Bone plates			
Bone-plates (contacted)	Stress profile optimization (minimal stress shielding effect)	Analytical equations; FE model	
Bone plates (non-contacted)	Stress profile optimization (minimal stress shielding effect)	3D FE model	
Porous devices			
Hip prosthesis, cementless/cemented (stem)	Weigth reduction and flexibility increase	CAD-based FE models	Experimental-computational approach. Additional information on flexibility of materials.
Hip prosthesis, cementless (stem, proximal femur)	Reduced bone resorption and reduced shear stresses under static load	2D FE model Multiscale homogeneization method (mechanics) Multi-objective optimization (porosity gradient)	Static load corresponding to stance phase of walking. AM prototype.
Hip prosthesis, cementless (stem, proximal femur)	Reduced bone resorption, reduced interface failure and increased life expectancy under cyclic load	2D FE model Multiscale homogeneization method (mechanics) Soderberg fatigue criterion	Cyclic dynamic forces associated to walking. EBM prototype
Hip prosthesis, cementless (acetabulum)	Increased stability	Analytical equations; CAD model	On-going AM prototyping
Graded porous structures for bone substitution	Increased strength	Microstructural shape design	Experimetal counterparts by rapid prototyping

Figure 185: Summary of orthopaedic surgical applications of FGMs. Source: (Sola, Bellucci and Cannillo, 2016)

Murr *(2017)* showed how to reduce the stiffness of fully dense 3DPed Ti6Al4V (110 GPa) and Co-Cr alloys (210 GPa) to approximate the highest stiffness of cortical bone (~20 GPa) *(Figure 188)*. For Ti6Al4V to reach 10 GPa and 20 GPa, a relative density of 56% (44% porosity) and 70% (30% porosity), and a mesh or foam with ~350 μm and ~270 μm pore size are required respectively. As bone ingrowth and osseointegration require larger pore size, and vascularization even larger *(Figure 33)*, the compressive strength and fatigue strength for the particular load-bearing application have to be assessed as these might be critically compromised. E.g. the compressive strength of cortical bone is ~100-230 MPa and the compressive strength of 44% porous Ti6Al4V achieves ~190 MPa at 10 GPa stiffness, whereas the fatigue strength of 44% porous Ti6Al4V is ~16 MPa at 10 GPa stiffness for ~1 million loading cycles/year (~1 Hz for normal human gait, ~2 million steps/year).

Zhang et al. *(2018)* identified and discussed the technical and clinical characteristics, as well as the challenges and research opportunities of PBF 3DPed Ti6Al4V lattices and Kolken et al. *(2018)* introduced 3DPed Ti femoral meta-implants with rationally distributed values of negative (auxetic) and positive Poisson's ratios *(Figure 189)* that always press onto the bone on both the medial and lateral sides, improving the implant-bone contact and implant longevity. Later, Kolken et al. *(2021)*,

investigated non-auxetic fixed-porosity and functionally-graded meta-biomaterials to 3DP Ti acetabular cups and proved that among diamond, body-centered cubic, and rhombic dodecahedron, the functionally-graded diamond infill exhibited the most promising behavior *(Figure 191)*.

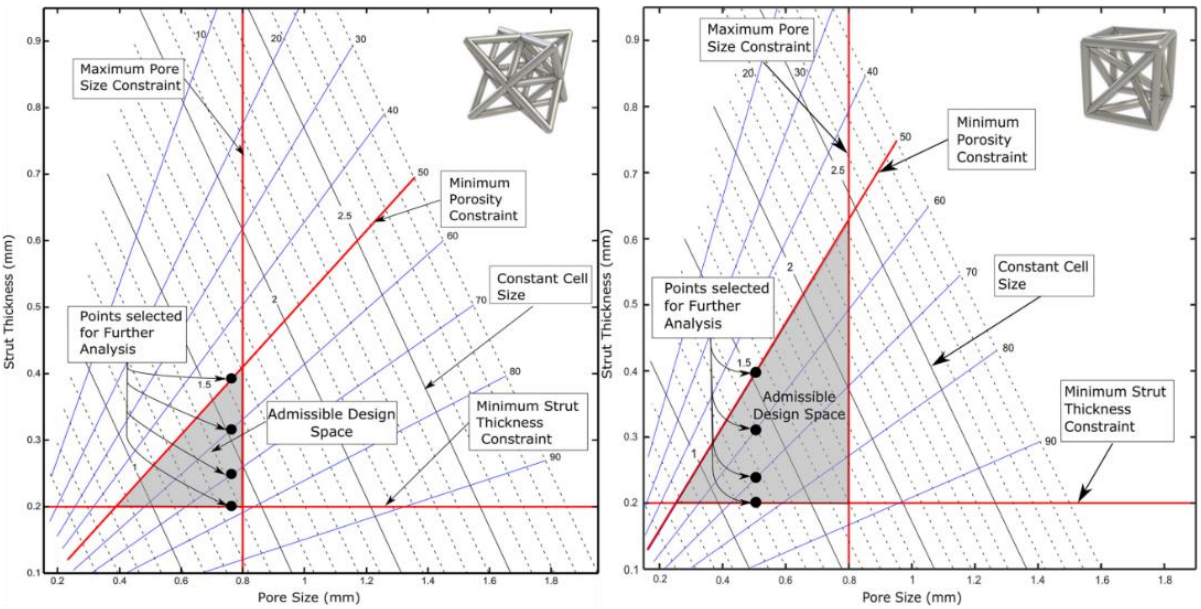

Unit cell	#	Porosity (%)	Strut thickness (mm)	Unit cell size (mm)	Pore size (mm)
Tetrahedron	1	50	0.39	1.52	0.5
	2	60	0.31	1.39	0.5
	3	70	0.24	1.27	0.5
	4	75	0.20	1.20	0.5
Octet truss	1	50	0.4	1.66	0.77
	2	60	0.32	1.54	0.77
	3	70	0.25	1.44	0.77
	4	75	0.20	1.37	0.77

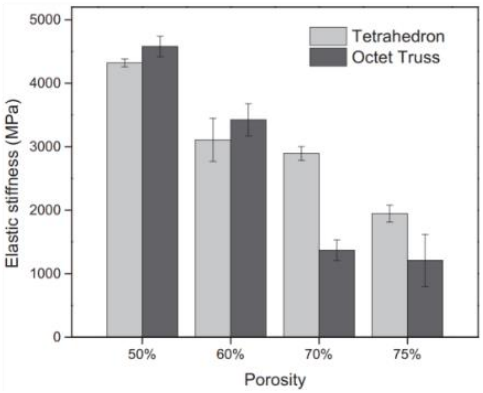

Figure 186: Admissible design space of unit cells for optimum parameters selection. Source: (Arabnejad et al., 2016a)

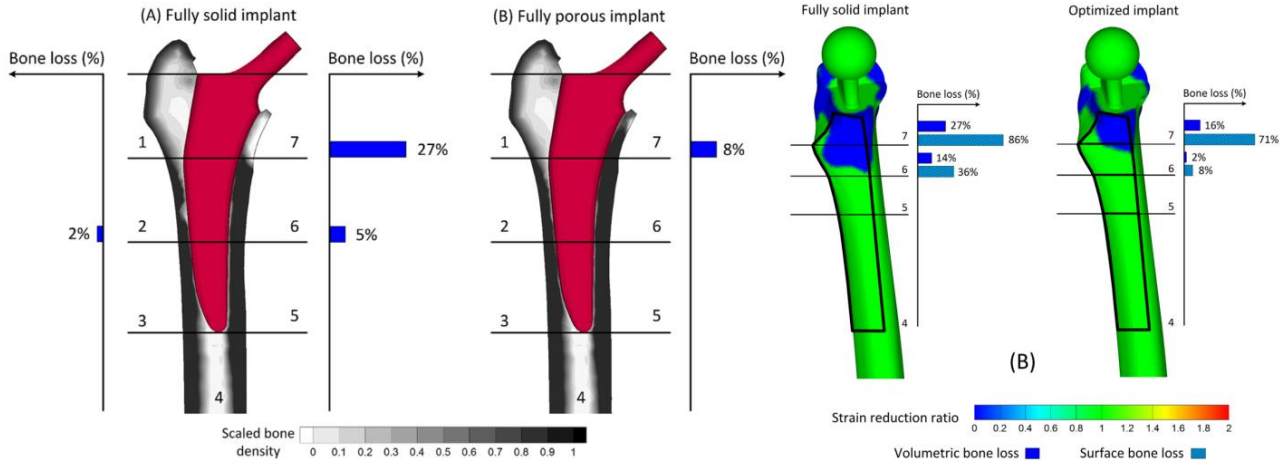

Figure 187: Bone loss by stress shielding for fully dense and fully porous femoral stems. Source: (Arabnejad et al., 2016b)

Liu et al. *(2018)* expressed the status, challenges, and future of topology optimization for 3DP, whereas Zhang et al. *(2018)* dealt with the biomimetic design and fabrication of diamond lattice implants by FEA analysis and 3DP and investigated the effect of pore size, porosity and strut thickness design on the mechanical and biological properties for optimum bone reconstruction.

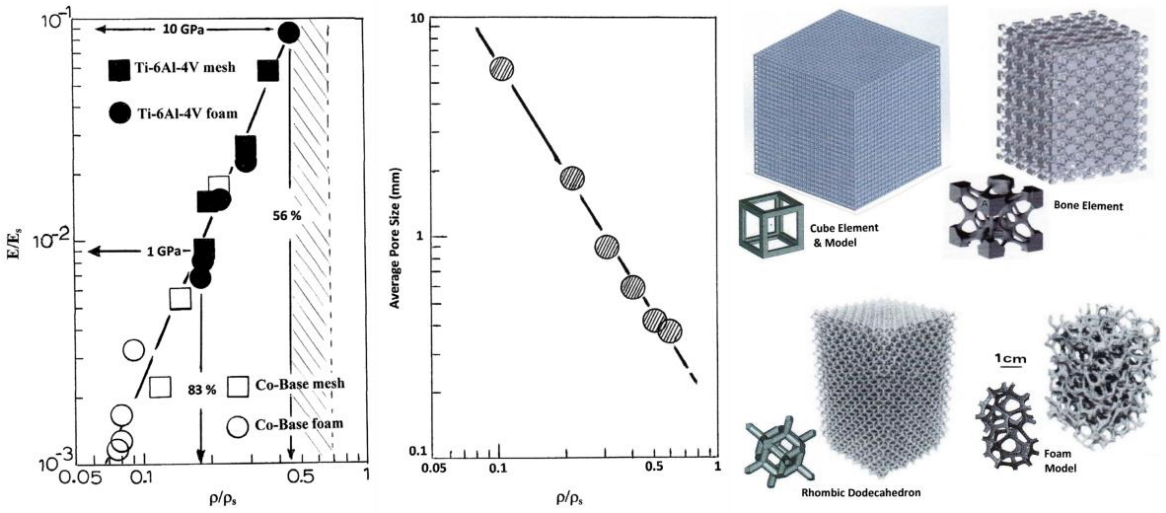

Figure 188: Relative density, modulus, and pore size for cellular Ti and Co-Cr alloys. Source: (Murr, 2018)

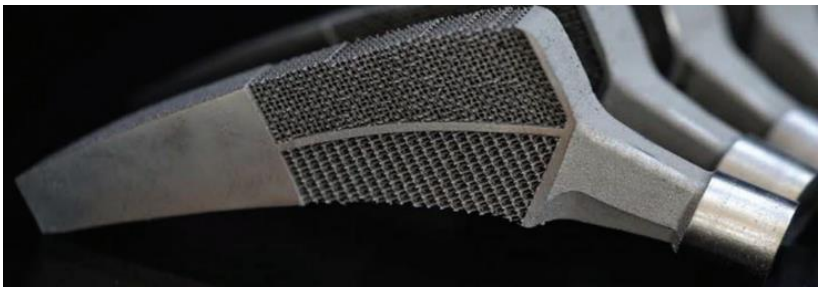

Figure 189: 3DPed Ti femoral meta-implant with negative and positive Poisson's ratios. Source: (Kolken et al., 2018)

Jetté et al. *(2018)* assessed the stiffness reduction, calculated the surface-to-volume (STVR) and the strength-to-stiffness (STSR) ratios, and compared them to human bone *(Figure 192)*.

Mueller et al. *(2019)* compared periodic (periodic Voronoi, body-centered cubic, octet, and Delaunay) and stochastic Voronoi (random) cellular solids for mechanical performance and energy absorption. Interestingly, cubic units which are defined as bending-dominated, experience stretch-dominated performance when loaded along horizontal and vertical directions. It was confirmed that the stochastic foams experience bending-dominated behavior and the relative density is the main tuning parameter. Although the energy absorption properties depend on the nodal connectivity, unit cell geometry, and load orientation, the periodic Voronoi and the stochastic foams had a consistent and best overall performance with minimum initial peak stresses as shown in *Figure 190*. The authors suggested optimizing the unit cells for performance maximization as per the application and combining periodic with stochastic structures to unlock great potential.

Raghavendra et al. *(2021)* reported C=0,5/0,69/1,06 and n=1/1,74/1,41 for regular cubic, C=0,9/0,85/1,61 and n=1,93/2,36/2,33 for irregular cubic, and C=0,67/0,79/1,07 and n=1,87/2,34/2,18 for trabecular-like foams, with C and n corresponding to values obtained by FEA of as-designed models, physically compression and tensile tested specimens respectively.

that the as-designed and as physically tested Gibson-Ashby coefficients greatly vary, i.e.

Zadpoor *(2019)* emphasized on 3DP and rational design techniques, including analytical and computational models, to enable the development of metallic meta-biomaterials (regular beam-based

lattice, sheet-based lattice, TPMS, graded designs) aimed at bone substitution, and mechanical testing under quasi-static and cyclic loading conditions.

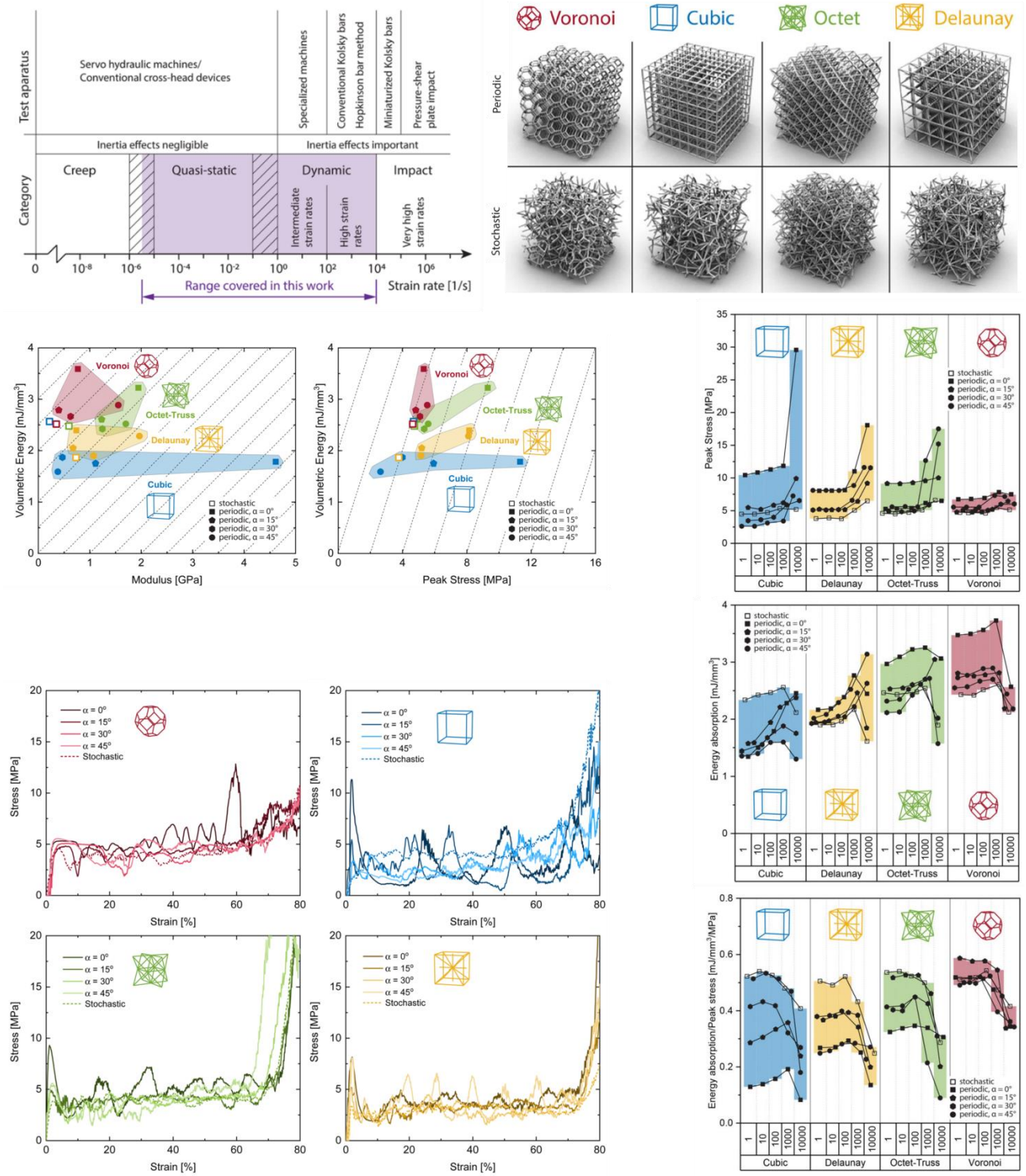

Figure 190: Mechanical properties and energy absorption of periodic and stochastic structures. Source: (Mueller et al., 2019)

Kelly et al. *(2019)* investigated the effect of construct design (solid, solid with surface porous layer, fully porous) and surface treatment (roto polishing and SILC cleaning) on tensile fatigue behavior of 3DPed Ti6Al4V under monotonic and cyclic loading profiles. Solid samples improved fatigue strength with a reduction in roughness. However, porous samples with reduced roughness after surface treatment caused no improvement in fatigue strength.

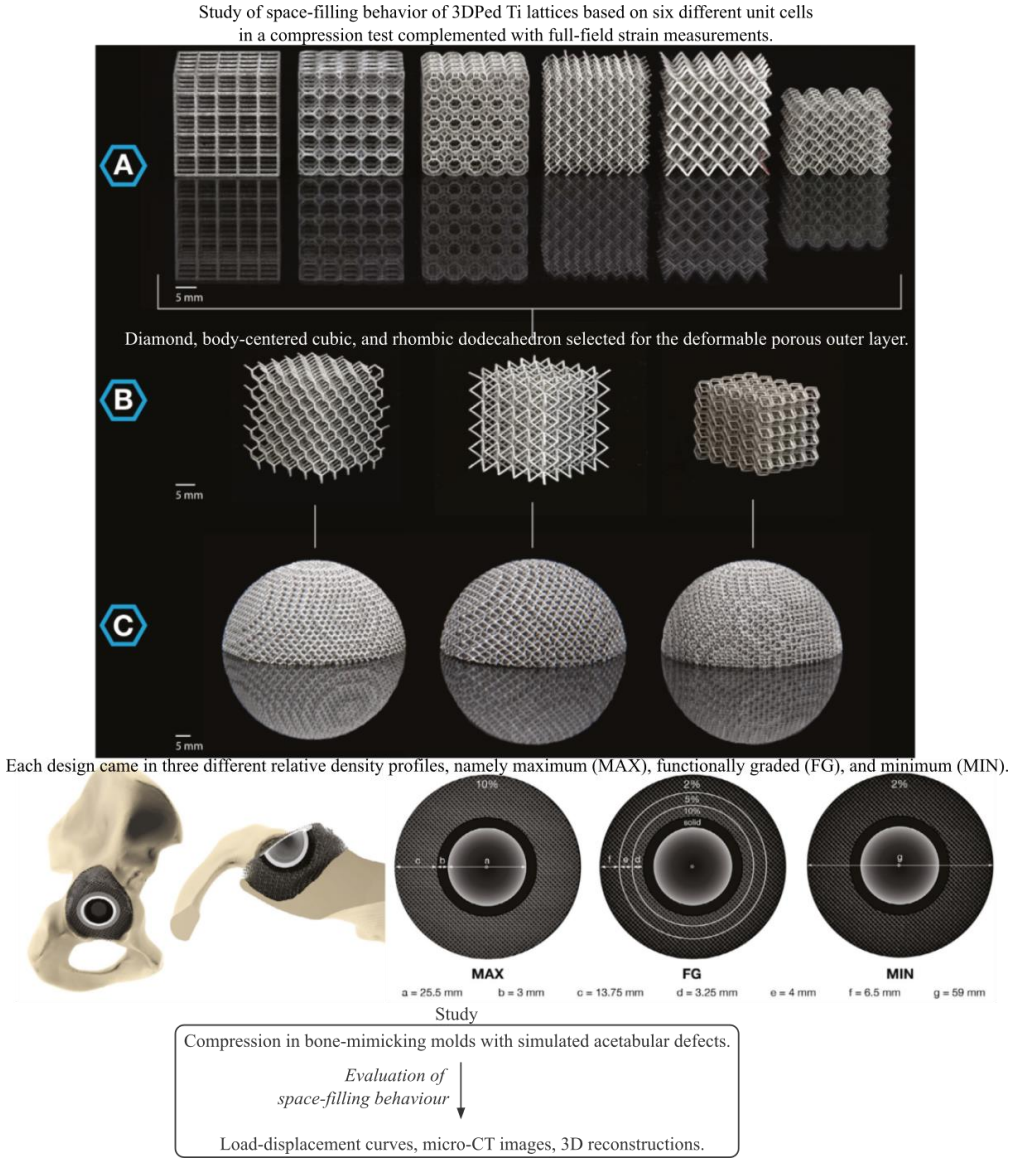

Figure 191: 3DPed non-auxetic fixed-porosity and functionally-graded Ti acetabular cups. Source: (Kolken et al., 2021)

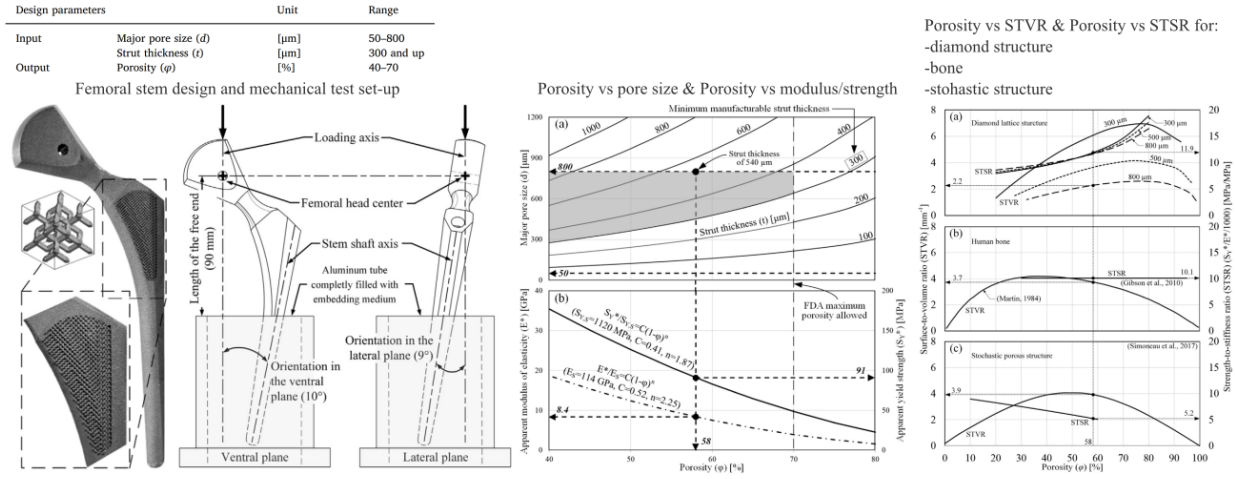

Figure 192: Mechanical performance of 3DPed porous Ti femoral stem. Source: (Jetté et al., 2018)

Maconachie et al. *(2019)* reported geometrical and mechanical data for 3DPed lattice structures made of different cell morphologies (*Figure 193*).

Yang et al. *(2019)* investigated the impact of 3DPed Ti TPMS Gyroid geometric parameters on the mechanical properties, structural behavior, and energy absorption, whilst replicating the

mechanical properties of cortical bone (16,81 GPa modulus of elasticity, 150,47 MPa yield stress, over 300 MPa ultimate compressive strength) by sheet-based Gyroids with 7 cells at each edge (7C), 40 mm cube bulk sizes, 0 iso-value, and 0,55 mm surface thickness *(Figure 194)*.

Topology	Material	Relative density (%)	Cell size (mm)	Strut diameter (mm)	Geometry (N = nominal, M = measured)	Compressive strength (MPa)	Modulus (MPa)
BCC	316L SS	3.5–13.8	1.25	0.19–0.22	N	0.36–5.89	17.89–378
BCC	316L SS	2.3–4.3	–	0.162–0.23	N	0.2–1	8.68–57.56
BCC, BCCZ	316L SS	5.3–16.6	1.5–2.5	0.25	N	0.92–15	50–2700
BCC, BCCZ	AlSi10Mg	0.7–22.2	10	1	N, M	0.46–4.36	21.71–490.22
BCC, BCCZ, FCC, FCCZ	Inconel 625	2.5–13.8	2–4	0.3	N, M	0.8–10.9	22.1–1246
BCC, BCCZ, FCC, FCCZ, FBCCZ, FBCCXYZ	Ti6Al4V, AlSi12Mg	7.5–39.7	2–7.5	0.3–1	N, M	4–124	110–2780
BCC, Octet-truss	SS 630 (17-4PH)	43	–	–	N, M	–	9710–13,960
Diamond	Ti6Al4V	3.6–26.5	–	–	N	8.2–99.64	370–4240
Dodecahedron	Ti6Al4V	15.78–314.55	–	–	N, M	19.4–117.2	550–3490
Gyroid	CP titanium	26.7–31.3	2–3	–	N	44.9–54.5	1465–2676
Gyroid, Schwartz diamond	Ti6Al4V	5–95	3–7	–	N	47–1559	120–17,190
Octet-truss, Rhombicuboctahedron	AlSi10Mg	10.4–14.7	–	–	N, M	4.7–9.1	690–1250
Schwartz primitive, cylinder grid	Ti6Al4V	70–90	1.5	0.37–0.58	N, M	–	920–2420
Simple cubic	Ti6Al4V	19.4–36.2	–	0.54–0.64	N, M	108–170	5360–8730
Truncated cuboctahedron, simple cubic, diamond	Ti6Al4V	20–34	–	–	N, M	31.7–112.6	2180–4578

Figure 193: Geometrical and mechanical data for different 3DPed cell morphologies. Source: (Maconachie et al., 2019)

Numerous studies on manufacturability, mechanical performance, generation of associated graphs for sheet and skeletal-TPMSs *(Figure 195)* have been published, but interestingly, the reported Gibson-Ashby constants for the same TPMSs vary strongly *(Maskery et al., 2017; Yang et al., 2018; Al-Ketan et al., 2018a; 2018b; Al-Ketan and Al-Rub, 2019; Abueidda et al., 2019; Li et al., 2019; Abou-Ali et al., 2020; Lu et al., 2020; Maskery and Ashcroft, 2020; Wang et al., 2020; Abou-Ali, Lee and Abu Al-Rub, 2022; Caiazzo et al., 2022).*

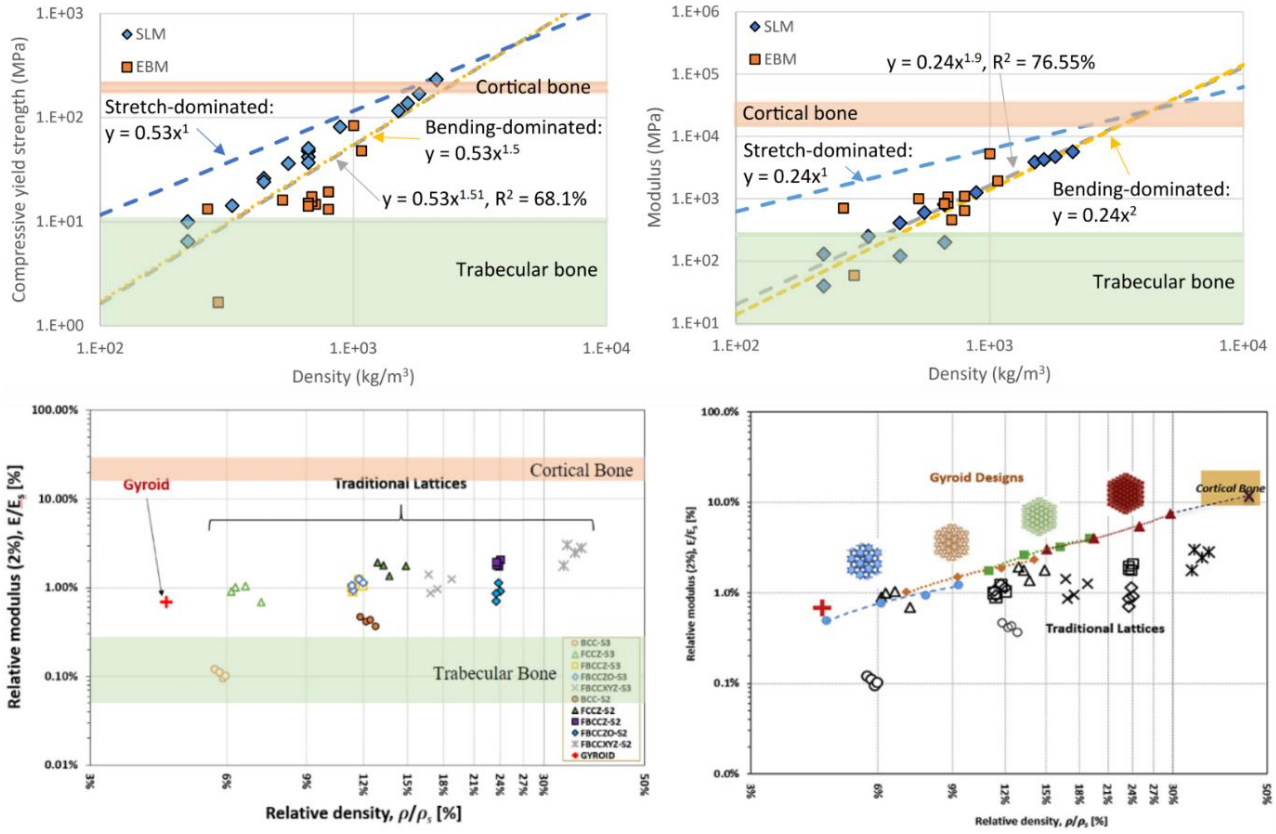

Figure 194: Gyroid designs that approximate mechanical properties of cortical bone. Source: (Yang et al., 2019)

Sheet /solid networks	Material	TPMS	Unit cell [mm]	Range of RD [%]	Young's modulus [GPa]		Max strength [MPa]		Yield strength [MPa]		Plateau strength [MPa]	
					C	N	C	n	C	n	C	n
Sheets	Maraging steel	Primitive	7	10.3–20.6	19.6	1.31	1419	1.77	–		1667	1.94
		Diamond		16.8–27.6	6.7	0.522	933	1.39			1112	1.53
		Gyroid		12.1–23.4	18.5	1.23	885	1.43			1402	1.76
		IWP		15.8–22.8	15.9	1.15	2354	2.13			1982	1.98
	Stainless steel	Primitive	4	10.4–18.2	106.4	1.89	–		–		1412	2.23
		Diamond		17.8–31.4	81.7	1.42					973	1.76
		Gyroid		14.1–24.4	216.6	2.23					1449	2.1
	Titanium	Primitive	1.5	29–50	12.2	1.12	–		1000.5	1.8	1042	1.81
		Diamond		40–55	9.9	0.79			480.7	1.3	351	0.67
		Gyroid		34–48	12.7	1.1			1059.5	2.1	1463	2.16
		IWP		36–55	11.5	1.03			903.8	1.9	1084	1.43
	Plastic	Primitive	15	4.8–23.5	0.672	1.52	53	1.75	–		–	
		IWP		8.1–25.6	0.836	1.18	64	1.65				
		Neovius		9.8–23.7	1.669	1.59	98	1.89				
solids	Maraging steel	IWP	7	8.9–20.9	34.6	2.01	1531	2.17	–		1389	2.13
		Diamond		12.3–26.1	62.5	2.22	4418	2.73			4566	3.28
		Gyroid		12.6–23.1	24.5	1.68	1189	1.86			1374	1.99
	Maraging steel	IWP	7	8.9–20.9	34.57	2.01	1531	2.17	1663.6	2.29	1389	2.13
		IWP Secondary		16.8–22.5	19.09	1.31	8575	2.94	2219.8	2.27	49385	4.58
	Aluminum	Gyroid	3–7.5 with 0.5 steps	5–20	13.7	2	283.92	1.5	–		–	
	Titanium	Gyroid	2–3	27.6–31.3	30.8	2			–		–	
		Diamond	–	20.5–33.9	88.58	2.67	2154.9	2.55	–		–	
		Diamond	3–7 with 0.5 steps	5–20	18.7	1.64	–		1723.6	2	–	
		Gyroid			20.9	1.71			1624.4	1.8		
		IWP Secondary	2	22–75	9.91	1.12	–		438.95	1.1	316	1.06
		FRD	2	30–56	14.73	1.86			561.7	1.8	440	1.79
		IWP	4	10–30	21.4	1.8017	–		1741.6	2.18	–	
	Stainless steel	Gyroid	1.25, 2.5, 5	6–15	11.9	2	219.3	1.5	–		–	
	Plastic	Diamond	5	10.3–25.1	0.864	2.24	91.1	2.49	55.1	2.48	1753.2	4.48

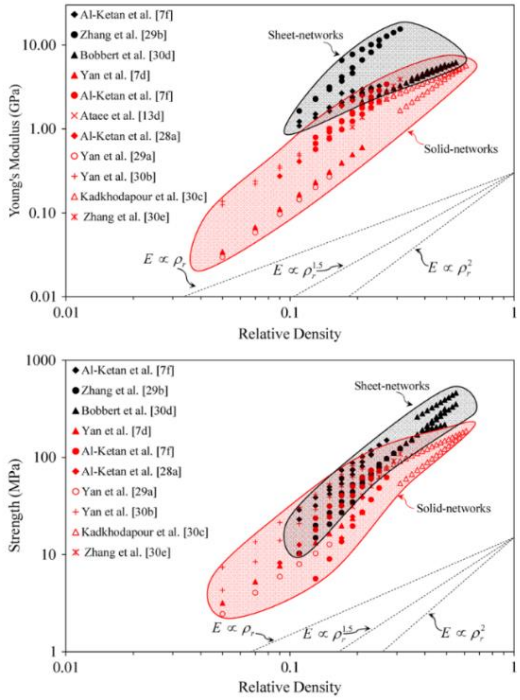

Figure 195: Modulus of elasticity and strength of sheet and skeletal TPMSs. Source: (Al-Ketan and Al-Rub, 2019)

Barba, Alabort and Reed *(2019)* studied the mechanical performance and (*Figure 196*) developed a unified graphical implant design framework to facilitate achieving 3DPed "synthetic bones" with superior biomechanical matching and osseointegration using TPMSs. The design criteria emphasized on interlinking manufacturability, mechanical properties, and osseointegration. Four skeletal-TPMS (Diamond, IWP, Neovius, and Gyroid) were selected, and the combination of material, lattice geometry, unit cell size, and porosities determined the design spaces *(Figure 198)*. For Ti6Al4V, Neovius presented the most flexibility, followed by Gyroid and Diamond. To relax manufacturability limitations and enlarge the design spaces, either less stiff materials can be selected or widen the elastic miss-match. They reported interesting approaches to mimic cortical and trabecular bone in terms of modulus of elasticity and mechanical anisotropy showing the uniform axisymmetric stiffness tensor of TPMSs (homogenization) (*Figure 197*).

In the absence of definite standards and guidelines, to facilitate optimal selection and acceleration of the translation process, Hanks et al. *(2020)* reported the mechanical properties of regular unit cell topologies for non-stochastic 3DPed lattice structures through analytical modeling, FEA analysis, and experimental testing, whereas Riva, Ginestra and Ceretti, *(2021)* collected parameters for the mechanical characterization (compression, tensile, bending, fatigue) of metallic lattice structures.

Cvrček, Denk and Čejka *(2020)* compared 3DP and plasma spraying to make Ti6Al4V trabecular structures, and confirmed that 3DP achieves a better and controlled reduction of the modulus of elasticity, reaching closer to host tissue, allowing bony ingrowth into the open-celled structure.

Poltue et al. *(2021)* focused on the controllable parameters of six TPMSs (Primitive, Gyroid, Diamond, Neovius, FRD, and IWP) that affect their physical characteristics (surface-to-volume ratio,

pore size, elastic properties, fluid behavior) and interconnected the mechanical properties and permeability, biological performances, and manufacturing limitations by analytical approach, FEA simulations, and Computational Fluid Dynamics (CFD). The authors presented design spaces as per the TPMS geometry, pore size, manufacturing limitations (3DP), elastic properties, and flow behaviors but found no optimal structure but the Gyroid, Diamond, and IWP as the most promising candidates due to their flexible design space, isotropic elastic property, adequately uniform Gaussian curvature and fluid-induced wall shear stress, and high permeability.

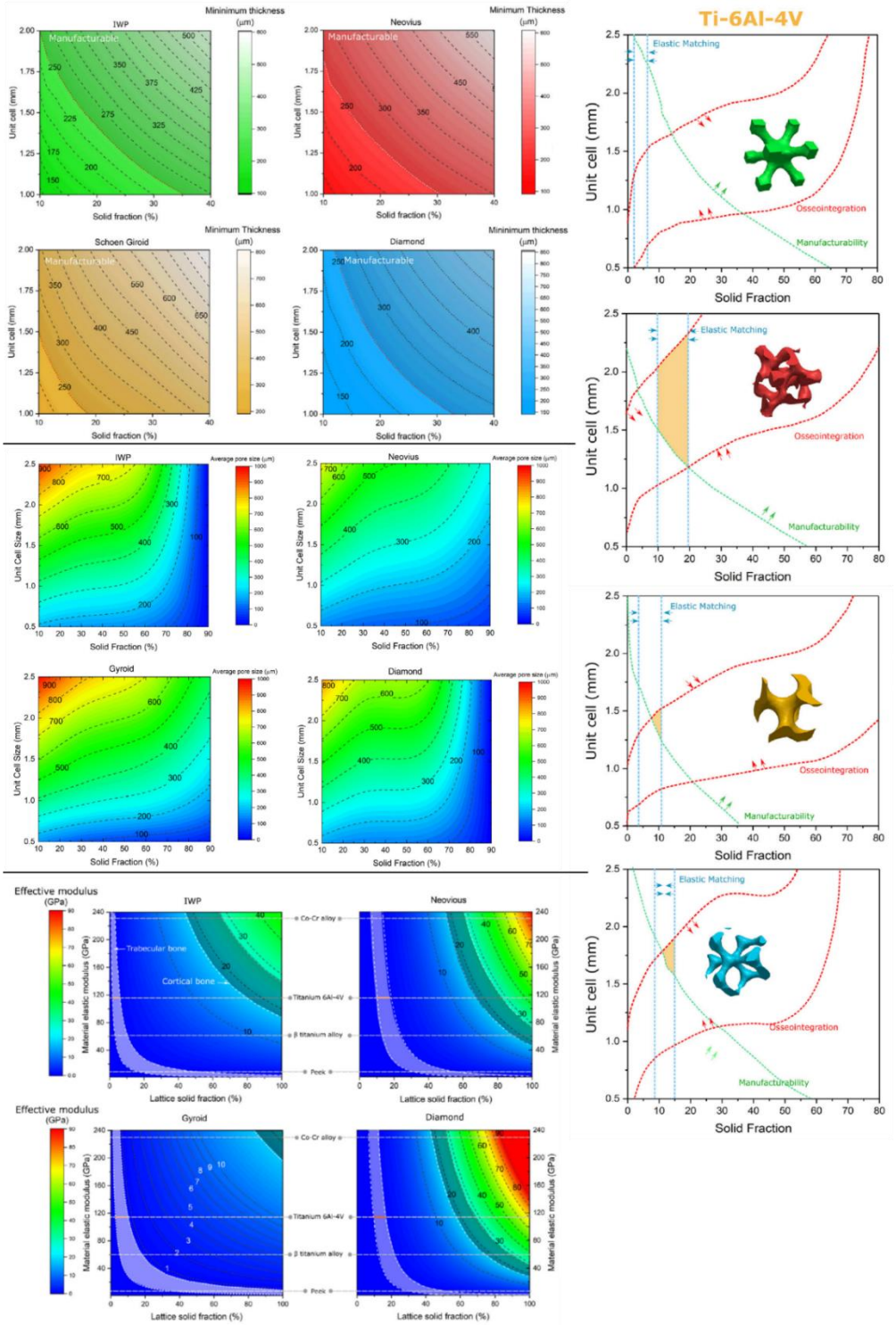

Figure 196: Mechanical performance of 3DPed TPMS to make "synthetic bone". Source: (Barba, Alabort and Reed, 2019)

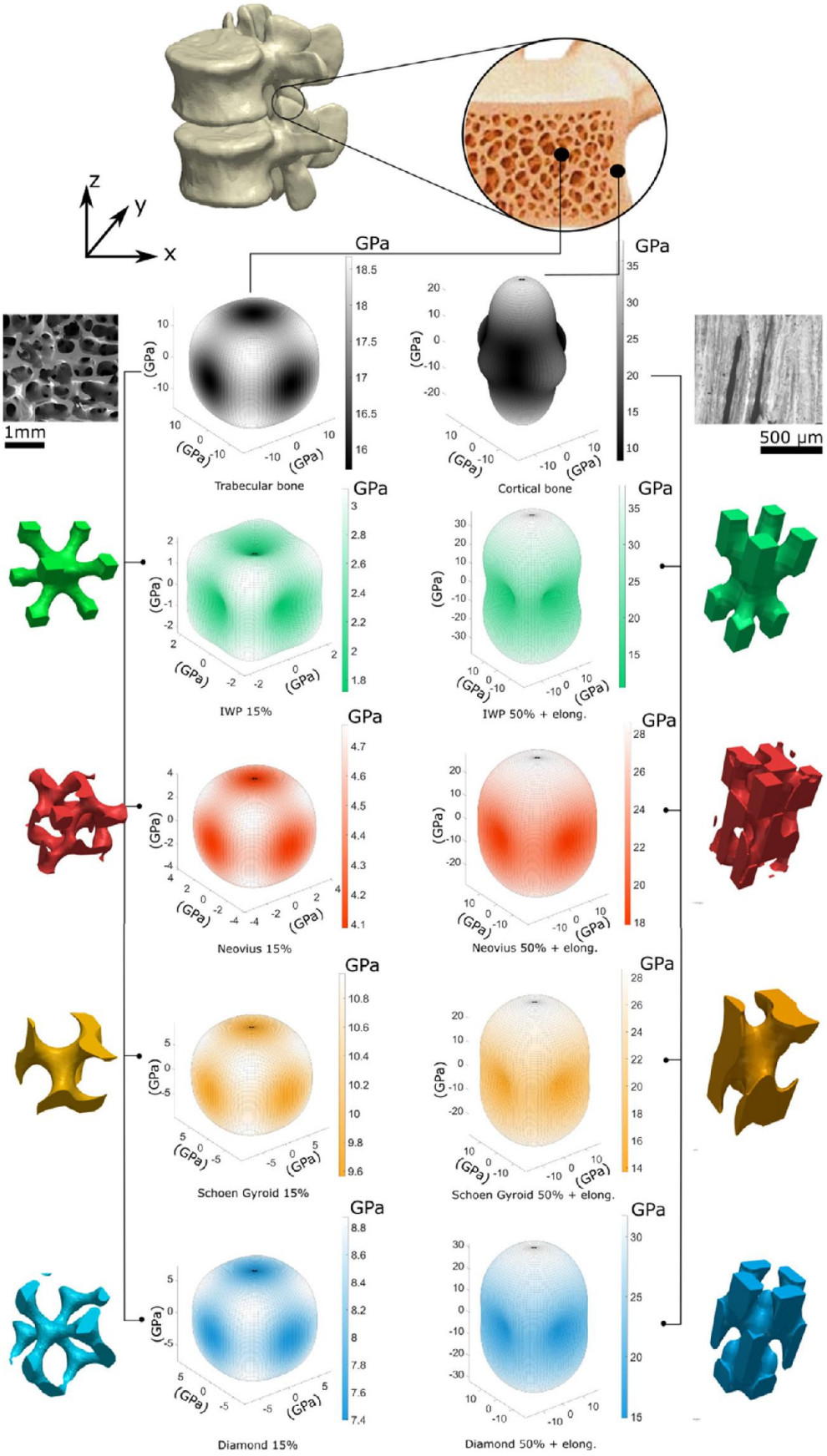

Figure 197: Mimicking bone's anisotropy by TPMS designs. Source: (Barba, Alabort and Reed, 2019)

Timercan, Sheremetyev and Brailovski *(2021)* have studied diamond and gyroid lattices for intervertebral disks with osseointegrative properties, with reduced stiffness (1,9-4,8 GPa) and greater

mechanical resistance (52-160 MPa) of the natural vertebra (3-6 MPa), but with fluid permeability and surface-to-volume ratio close to those of vertebrae.

Corona-Castuera et al. *(2021)* have designed sheet and skeletal Gyroid foams with such porosities, pore sizes, and thicknesses to be manufacturable and approached the elastic modulus of cortical and trabecular bone. The authors found that cell size impacts compression strength.

Günther et al. *(2022)* also approached the cortical and trabecular bone characteristics by defining numerically the admissible design space limited by pore and strut size, volume fraction, modulus of elasticity, cell size, and surface area (*Figure 199*). They assessed 6 sheet and skeletal (network) TPMSs (Primitive (P), Gyroid (G), Diamond (D), I-WP (I), Fischer Koch S (S) and F-RD (F)) to be 3DPed by a suitable PBF technology. It was found that the P sheet with 67,57 μm pore size, 0,54 volume fraction, and 18,76 GPa modulus was the best choice for the cortical bone and the G network with 401,39 μm pore size, 0,3 volume fraction and 4,68 GPa modulus was best for trabecular bone. The author used functional grading of such structures to obtain the optimal result by varying volume fraction, cell size, and TPMS type.

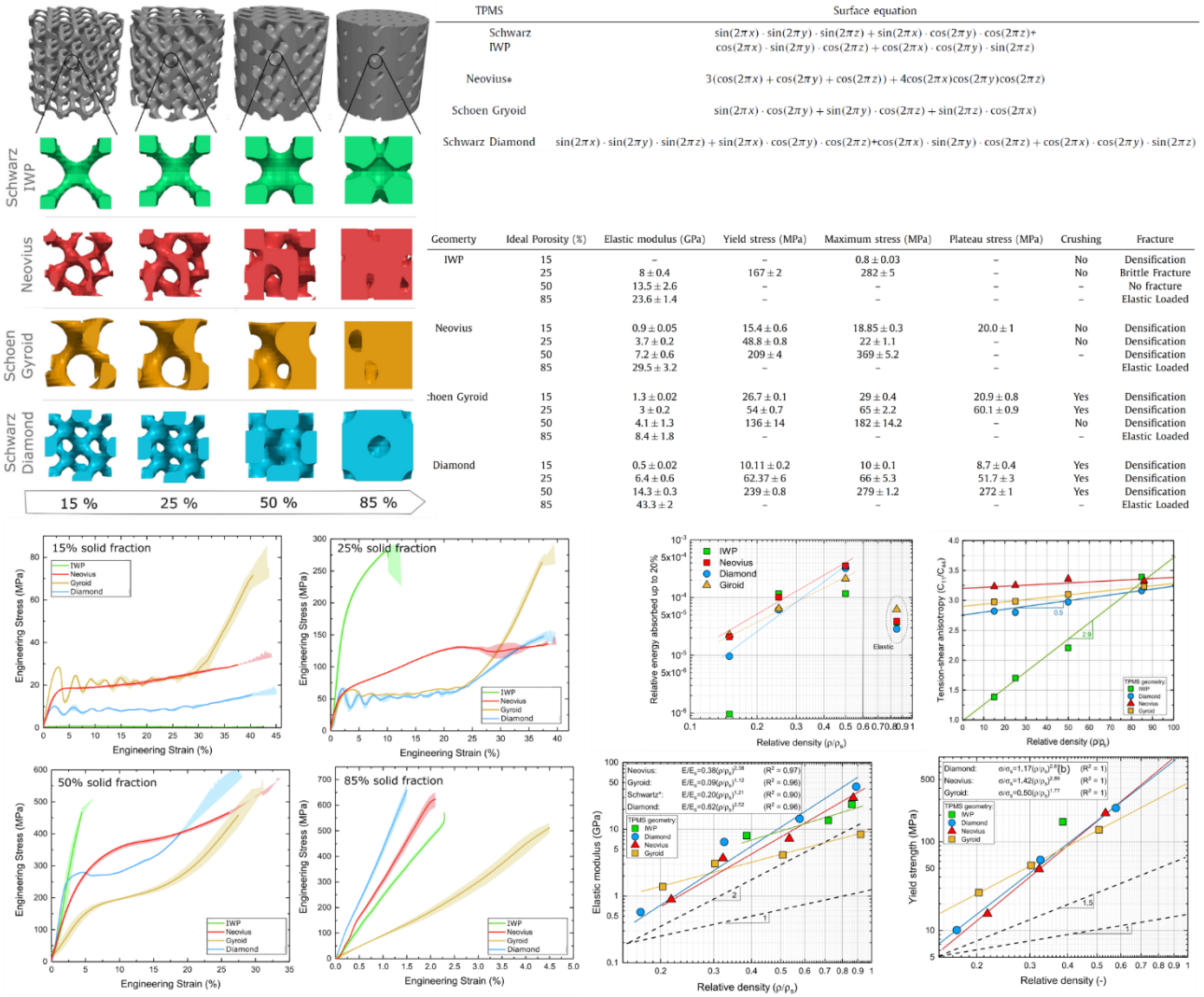

TPMS	Surface equation
Schwarz IWP	$\sin(2\pi x)\cdot\sin(2\pi y)\cdot\sin(2\pi z)+\sin(2\pi x)\cdot\cos(2\pi y)\cdot\cos(2\pi z)+\cos(2\pi x)\cdot\sin(2\pi y)\cdot\cos(2\pi z)+\cos(2\pi x)\cdot\cos(2\pi y)\cdot\sin(2\pi z)$
Neovius*	$3(\cos(2\pi x)+\cos(2\pi y)+\cos(2\pi z))+4\cos(2\pi x)\cos(2\pi y)\cos(2\pi z)$
Schoen Gyroid	$\sin(2\pi x)\cdot\cos(2\pi y)+\sin(2\pi y)\cdot\cos(2\pi z)+\sin(2\pi z)\cdot\cos(2\pi x)$
Schwarz Diamond	$\sin(2\pi x)\cdot\sin(2\pi y)\cdot\sin(2\pi z)+\sin(2\pi x)\cdot\cos(2\pi y)\cdot\cos(2\pi z)+\cos(2\pi x)\cdot\sin(2\pi y)\cdot\cos(2\pi z)+\cos(2\pi x)\cdot\cos(2\pi y)\cdot\sin(2\pi z)$

Geomerty	Ideal Porosity (%)	Elastic modulus (GPa)	Yield stress (MPa)	Maximum stress (MPa)	Plateau stress (MPa)	Crushing	Fracture
IWP	15	–	–	0.8 ± 0.03	–	No	Densification
	25	8 ± 0.4	167 ± 2	282 ± 5	–	No	Brittle Fracture
	50	13.5 ± 2.6	–	–	–	–	No fracture
	85	23.6 ± 1.4	–	–	–	–	Elastic Loaded
Neovius	15	0.9 ± 0.05	15.4 ± 0.6	18.85 ± 0.3	20.0 ± 1	No	Densification
	25	3.7 ± 0.2	48.8 ± 0.8	22 ± 1.1	–	No	Densification
	50	7.2 ± 0.6	209 ± 4	369 ± 5.2	–	–	Densification
	85	29.5 ± 3.2	–	–	–		Elastic Loaded
:hoen Gyroid	15	1.3 ± 0.02	26.7 ± 0.1	29 ± 0.4	20.9 ± 0.8	Yes	Densification
	25	3 ± 0.2	54 ± 0.7	65 ± 2.2	60.1 ± 0.9	Yes	Densification
	50	4.1 ± 1.3	136 ± 14	182 ± 14.2	–	No	Densification
	85	8.4 ± 1.8	–	–	–	–	Elastic Loaded
Diamond	15	0.5 ± 0.02	10.11 ± 0.2	10 ± 0.1	8.7 ± 0.4	Yes	Densification
	25	6.4 ± 0.6	62.37 ± 6	66 ± 5.3	51.7 ± 3	Yes	Densification
	50	14.3 ± 0.3	239 ± 0.8	279 ± 1.2	272 ± 1	Yes	Densification
	85	43.3 ± 2	–	–	–	–	Elastic Loaded

Figure 198: Optimal design spaces of 3DPed TPMS to make "synthetic bone". Source: (Barba, Alabort and Reed, 2019)

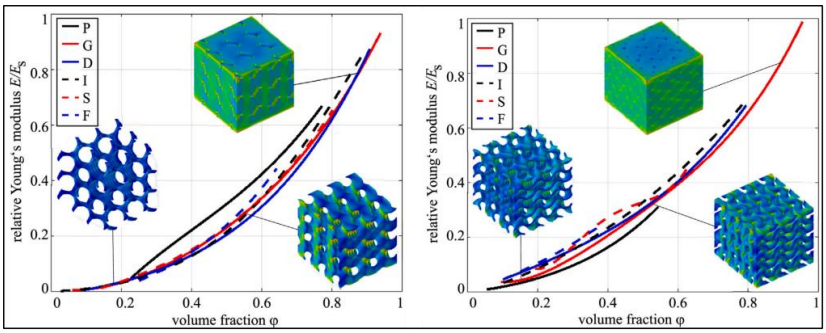

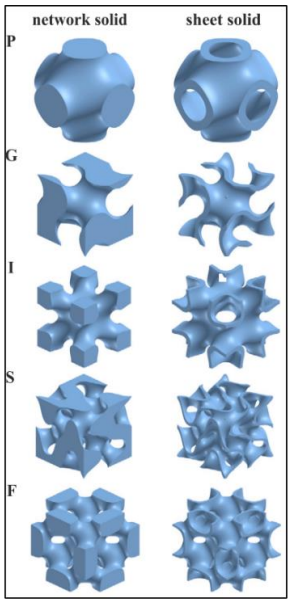

Property	Cortical bone	Trabecular bone	Addressed characteristic	Priority
Pore size (μm)	45–106	300–500	Optimal osseointegration	Primary
Strut size (μm)	≥ 200	≥ 200	Accurate LPBF processability	Primary
Volume fraction	≤ 0.95	≤ 0.3	Optimal osseointegration	Primary
Stiffness (GPa)	15–19	2–5	Avoiding of the stress shielding effect	Secondary
Cell size (μm)	5–500	450–1100	Optimal osseointegration	Secondary
Surface area	Maximal	Maximal	Optimal osseointegration	Secondary

Effective realizable geometric values for considered TPMS

Property	Cortical bone	Trabecular bone
Pore size (μm)	45–106	347–500
Volume fraction	0.51–0.95	0.23–0.3
Cell size (μm)	271–2633	620–1855

Data of optimal TPMS lattices for cortical and trabecular bone

Property	Cortical bone	Trabecular bone
TPMS solid	P sheet	G network
Pore size (μm)	67.572	401.39
Strut size (μm)	200	200
Volume fraction	0.5445	0.3
Cell size (μm)	671.9	620.4
Stiffness (GPa)	18.758	4.6835
Surface area (mm^2)	5.7218	4.5937

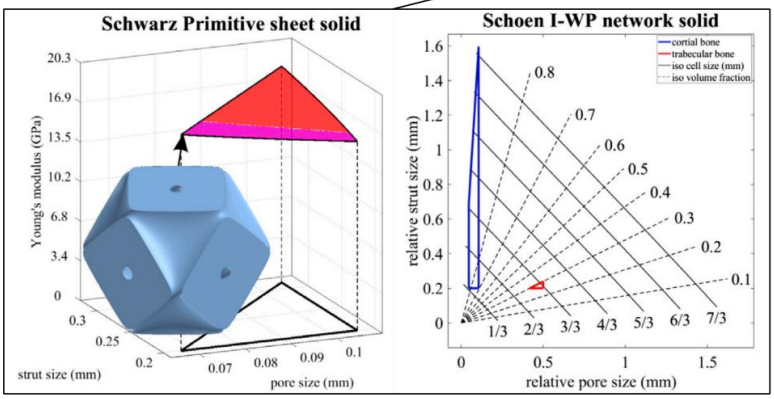

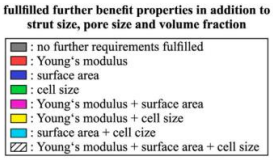

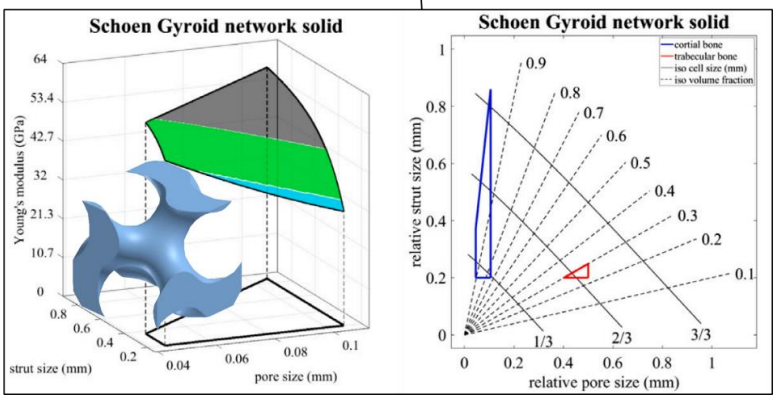

Figure 199: Mimicking cortical and trabecular bone by TPMS designs. Source: (Günther et al., 2022)

Moussa et al. *(2020)* presented a 3DPed topology-optimized acetabular cage concept consisting of a multifunctional graded porous layer with structural and bone ingrowth properties *(Figure 200)*. The implant could enhance bone ingrowth and achieve long-term stability as it resulted in a 21,4% reduction of maximum contact stress on the bone surface, and a 26% decrease of bone-implant interface peak micromotion.

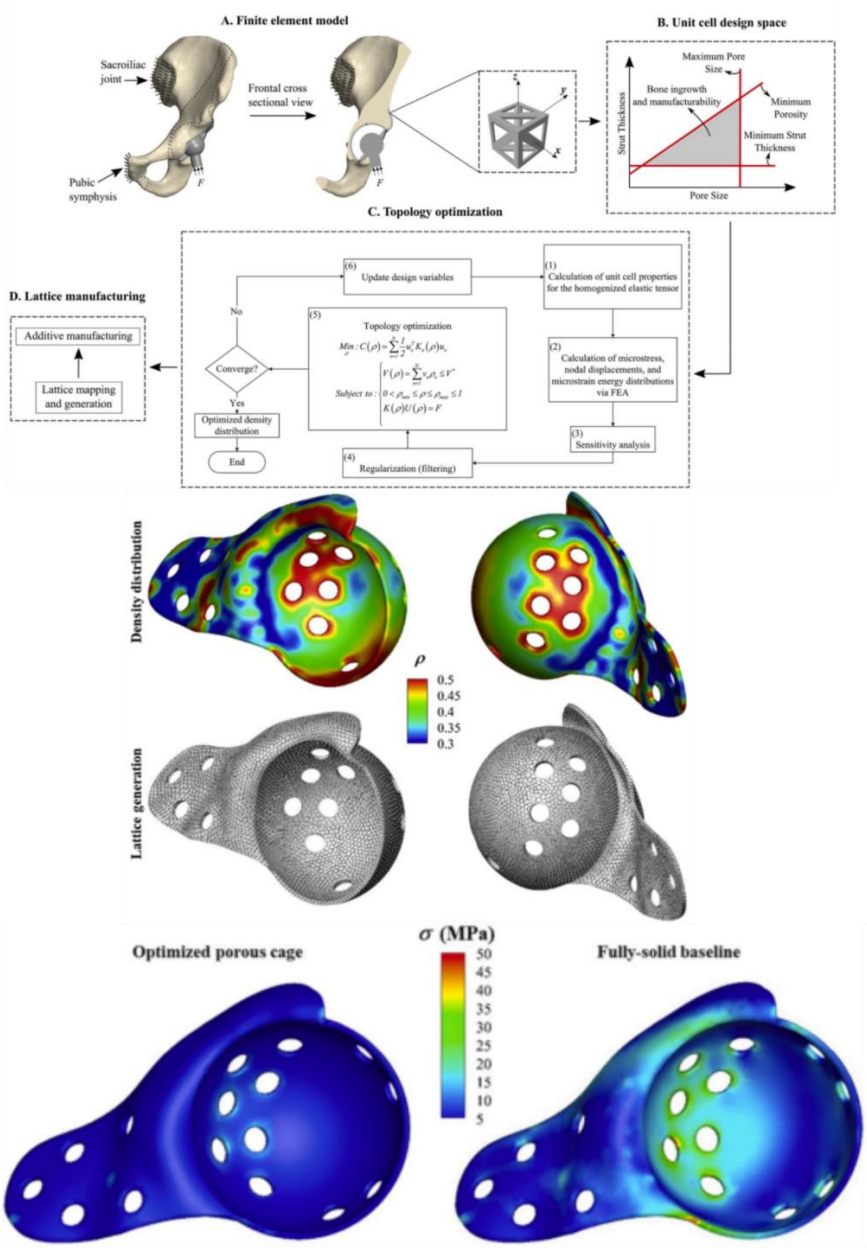

Figure 200: Topology-optimized 3DPed acetabular cage with graded porosity. Source: (Moussa et al., 2020)

Yang et al. *(2020)* 3DPed biomimetic Ta scaffolds with 70% open porosity, 542 μm average pore diameter, 929 μm largest pore diameter, 322 μm average strut diameter, 564 μm largest strut diameter, and 99,99% pore interconnectivity. The impact of porosity on the mechanical properties was investigated: decreasing the porosity from 70% to 60%, the compressive strength, compressive modulus, bending strength and shear modulus increased to 59,5 MPa, 3,3 GPa, 97 MPa, 6,8 GPa, 41 MPa respectively, whereas increasing the porosity from 70% to 80%, the values reduced to 14,2 MPa, 1,5 GPa, 23 MPa, 1,2 GPa, and 11,2 MPa respectively.

Zhang et al. *(2020)* designed and 3DPed five variations of functionally-graded Gyroid TPMS with bone-comparable properties by tuning the parameters of the TPMS equation (pore size, strut thickness, porosity). The morphology, permeability, 3DPability, and mechanical characteristics of each variation were studied *(Figure 201)*, as well as the effect of heat treatment.

Al-Ketan et al. *(2020)* focused on the compressive and deformation behavior of functionally-graded sheet-based Gyroid, and Diamond TPMS by implementing density grading, cell size grading, and morphology grading *(Figure 202)*. Each grading influences the mechanical performance and sheet-based exhibit higher moduli of elasticity compared to skeletal-based lattices.

Type	TPMS equations
T	$\phi_T = \alpha(x,y,z)(\cos(ax)\sin(ay) + \cos(ay)\sin(az) + \cos(az)\sin(ax) - 0.85) + (1-\alpha(x,y,z))(\cos(ax)\sin(ay) + \cos(ay)\sin(az) + \cos(az)\sin(ax) - 0.3) > 0$
Po	$\phi_{Po}=\cos(K_z(x,y,z)x)\sin(K_z(x,y,z)y) + \cos(K_z(x,y,z)y)\sin(K_z(x,y,z)z) + \cos(K_z(x,y,z)z)\sin(K_z(x,y,z)x) - 0.85 > 0$
	$K_z\left(x,y,z\right) = \left(1 - \frac{1}{1+e^{-0.5(x-7.5)}}\right) \times 1.33 + \frac{1}{1+e^{-0.5(x-7.5)}} \times 0.87$
S	$\phi_1=\cos(a(x-1.5\alpha(x,y,z)))\sin(ay) + \cos(ay)\sin(az) + \cos(az)\sin(a(x-1.5\alpha(x,y,z))) - 0.85 > 0$
	$\phi_2=\cos(ax)\sin(ay) + \cos(ay)\sin(az) + \cos(az)\sin(ax) - 0.85 > 0$
	$\phi_S = \phi_1 \cup \phi_2,$
P	$\phi_P = \cos(ax(1-0.23\alpha(x,y,z)))\sin(ay(1-0.23\alpha(x,y,z))) + \cos(ay(1-0.23\alpha(x,y,z)))\sin(az(1-0.23\alpha(x,y,z))) + \cos(az(1-0.23\alpha(x,y,z)))\sin(ax(1-0.23\alpha(x,y,z))) + 0.55\alpha(x,y,z) - 0.85 > 0$
Sh	$\phi_1 = \alpha(x,y,z)(\cos(ax)\sin(ay) + \cos(ay)\sin(az) + \cos(az)\sin(ax) + 0.5) + (1-\alpha(x,y,z))(\cos(ax)\sin(ay) + \cos(ay)\sin(az) + \cos(az)\sin(ax) - 0.85) > 0$
	$\phi_2 = \alpha(x,y,z)(\cos(ax)\sin(ay) + \cos(ay)\sin(az) + \cos(az)\sin(ax) - 0.73) + (1-\alpha(x,y,z))(\cos(ax)\sin(ay) + \cos(ay)\sin(az) + \cos(az)\sin(ax) - 1.5) > 0$
	$\phi_{Sh} = \phi_1 \setminus \phi_2$

Group	Strut thickness	Pore size	Porosity	CAD structure
T	Graded	Graded	Graded	
Po	Graded	Graded	Constant	
S	Constant	Graded	Graded	
P	Graded	Constant	Graded	
Sh	Graded	Graded	Graded	

Sample	E_s (GPa)	σ_s (MPa)	σ_{max} (MPa)	σ_{pl} (MPa)	ε_f (%)
P60	5.33 ± 0.22	188.67 ± 10.56	250.44 ± 10.20	275.33 ± 9.05	12.13 ± 0.54
P80	2.30 ± 0.10	76.03 ± 4.35	85.09 ± 7.68	90.34 ± 1.54	9.99 ± 0.09
T	2.04 ± 0.08	70.25 ± 3.52	93.68 ± 5.32	93.88 ± 1.65	12.23 ± 0.35
Po	1.11 ± 0.11	33.88 ± 5.66	43.75 ± 4.98	34.71 ± 7.15	7.60 ± 0.43
S	2.44 ± 0.05	75.25 ± 2.10	95.41 ± 6.67	97.85 ± 9.46	8.87 ± 0.12
P	2.22 ± 0.40	73.05 ± 5.55	94.44 ± 4.33	91.22 ± 6.74	11.41 ± 0.63
Sh	5.75 ± 0.21	198.19 ± 6.98	286.11 ± 16.98	338.68 ± 28.99	17.16 ± 0.56

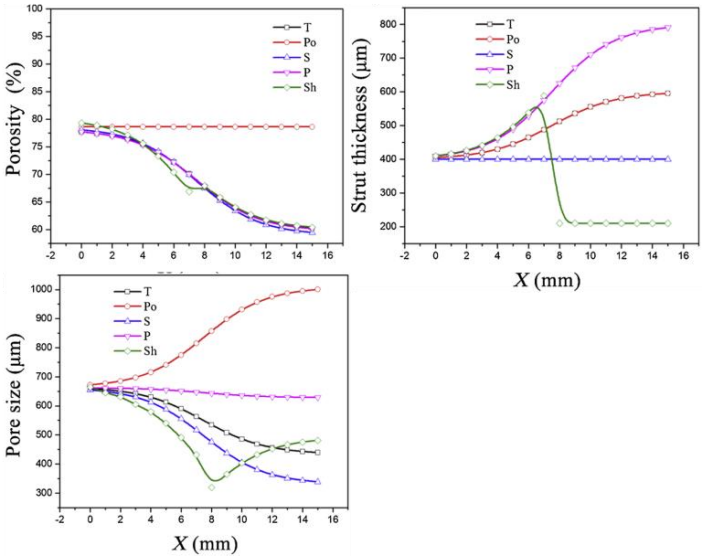

Figure 201: Five variations of functionally-graded Gyroid TPMS. Source: (Zhang et al., 2020)

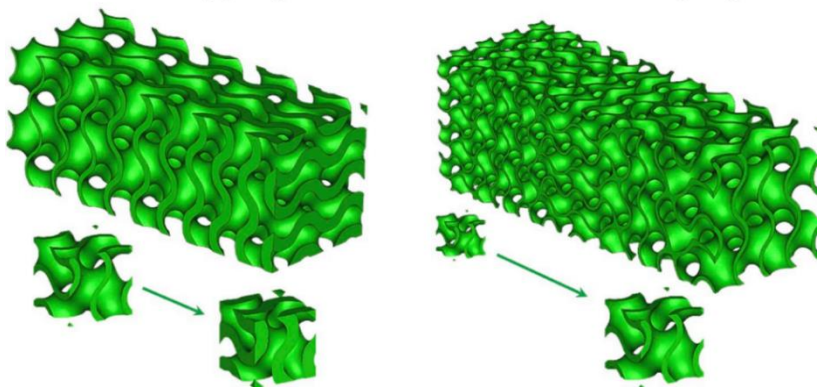

Figure 202: Density and cell grading for Gyroid and Diamond TPMS. Source: (Al-Ketan et al., 2020)

Ghaziani, Soheilifard and Kowsar *(2021)* addressed the advantages of Ti/HA FGM for trans-femoral fixations and studied the effect of gradation direction on the bone adaptation procedure. The

results showed that a radial FGM with low-stiffness material in the outer layer and less metal composition significantly improves the bone remodeling behavior *(Figure 203)*.

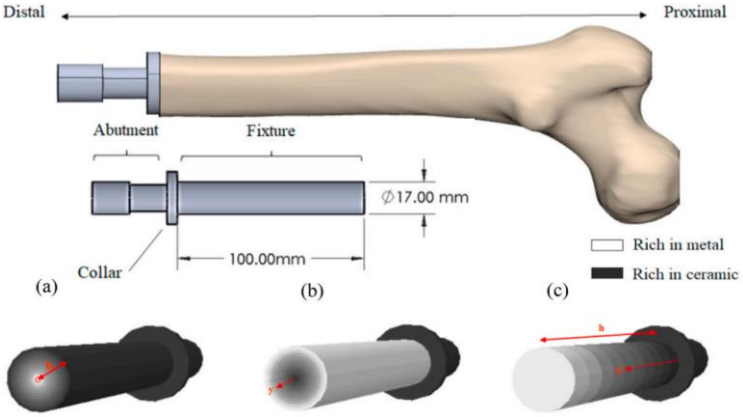

Figure 203: 3DPed Ti/HA FGM trans-femoral fixation. Source: (Ghaziani, Soheilifard and Kowsar, 2021)

Gao et al. *(2021)* overviewed the fabrication, structure, biological *(Figure 209)* and mechanical *(Figure 204)* properties, and orthopaedic applications of 3DPed Voronoi-like porous Ta scaffolds. The authors claimed that Ta scaffolds facilitated osseointegration, osteoconductivity, bone formation, and blood vessel formation, whilst being more promising than Ti. It was underlined that to achieve the superior combined performance of porous implants, the pore geometry, pore size, strut diameter, porosity, interconnectedness, and surface roughness have to be considered.

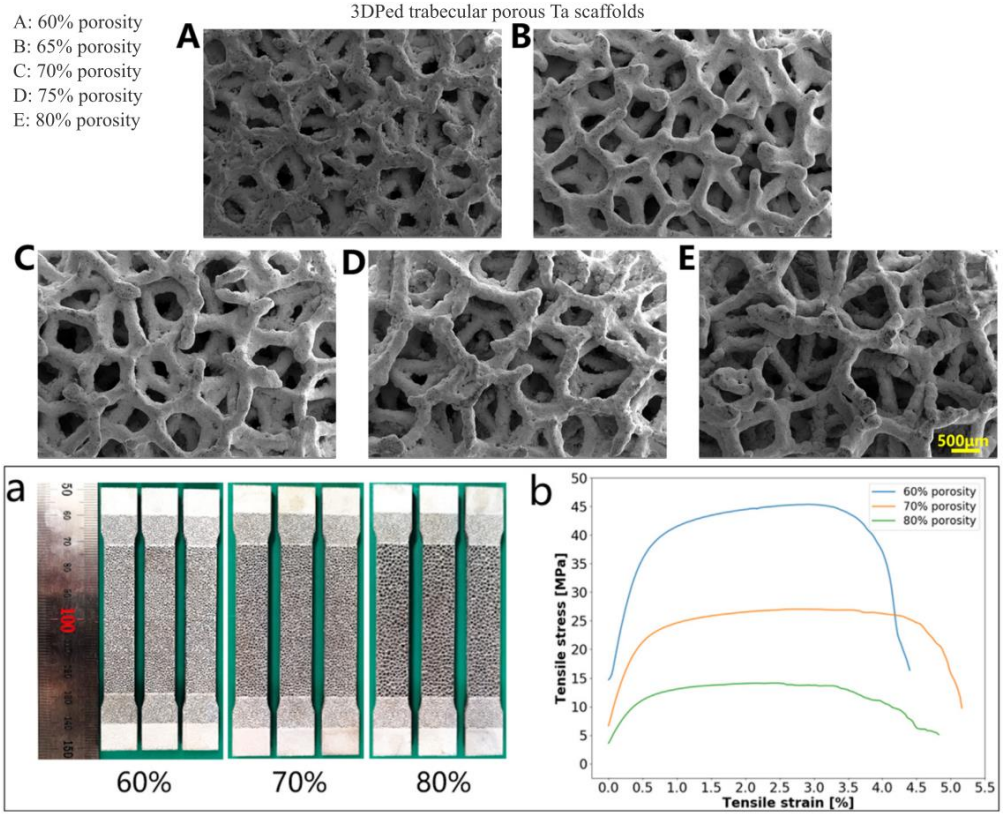

Figure 204: Tensile strength of 3DPed porous Ta with different porosities. Source: (Gao et al., 2021)

Hasanov et al. *(2021)* reviewed the latest developments, challenges, and potential applications of 3DPed multi-material components (thermoplastic and composites, metal-ceramics, metals and alloys) and concluded that further research and development is needed.

Liu et al. *(2021)* focused on a literature review and 3DP of femoral stems featuring cellular architectures and collected relative data *(Figure 205)* on porous structures and mechanical properties.

Chen et al. *(2021)* gave similar but more extensive and detailed data in tabulated forms *(Figure 206 and Figure 207)* for both standard and degradable biomaterials, and underlined the challenges for surface modifications of metallic lattice structures and the need for software to generate advanced functionally graded lattices.

Unit cell	Material	Porosity (%)	Unit cell size (mm)	Pore size (mm)	Strut thickness (mm)	Young's modulus (Gpa)	Yield strength (MPa)	Ultimate compressive strength (MPa)
Square unit cell	Ti6AL4V	57–64	-	0.6–3.24	1.1–3.08	9.27–4.74	134	-
	Ti6AL4V	57	-	0.6	1.1	9.27	197	-
	Ti6AL4V	89.6–21.6	4	-	0.3–0.9	4.86–71.36	-	-
	Ti6AL4V	10–100	1.36–1.8		0.07–0.1			
	Ti6AL4V	> 40	-	0.05–0.8	> 0.1	-	-	-
	CoCrMo	-	-	1.57–1.88	0.5–1.5	4.79–17.98	65.4–295.7	-
	CoCrMo	-	-	1.57–1.88	0.5–1.5	4.79–17.98	65.4–295.7	-
Body center cubic	Ti6AL4V	20–80%	4	-	1.25–0.51	8–70	-	-
	Ti6AL4V	78.7–29.3	4	-	0.3–0.9	18–79	188–839	-
	Ti6AL4V	90–18	-	-	0.33–1.25	2.8–76.7	37–760	-
Tetrahedral	Ti6AL4V	-	-	-	-	-	-	-
	Ti6AL4V	-	-	0.05–0.8	> 0.2	-	-	-
Diamond lattice	Ti6AL4V	89.4–21.5	4	-	0.3–0.9	0.55–54.18	-	-
	Ti6AL4V	58	-	0.8	0.54	8.4	91	-
	Ti6AL4V	60–40	-	0.05–0.8	> 0.3	7.3–12.1	136.7–274.5	-
Pillar octahedral unit	CoCrMo	67–14	-	-	-	2.33–5.26	36–299	113–916
Rhombic dodecahedron	Ti6AL4V	59–96	3–12	-	-	-	-	85.7–0.85
Vintile	Ti6AL4V	40–58.5	4–7	0.8–1.5	0.7–1.5	0.68–1.58		1,431–5,021
Re-entrant honeycomb	Ti6AL4V		-	-	0.35	34–43	-	≈2.4
Honeycomb	Ti6AL4V		-	-	0.35	38–50	-	≈2.4

Figure 205: Mechanical characteristics of different unit cells. Source: (Liu et al., 2021)

Material	Fabrication method	Porosity (%)	Unit cell	E (GPa)	σ_y (MPa)	σ_{max} (MPa)	H (HV)
Mg	SLM		Cubic	–	–	–	48.3
Mg-Ca	SLM	6~38	Cubic	–	–	112 ^{C}	60–68
WE43 Mg	SLM	76	Lattice	–	–	15 ^{C}	–
WE43 Mg	SLM	67	Diamond	0.8	23 ^{C}	27 ^{C}	–
Fe	SLM	67	Cubic	–	70 ± 4 ^{C}	135 ± 5 ^{C}	–
Fe	SLM	85	Diamond	1	11 ^{C}	–	–
Fe	SLM	70	Diamond	1	29 ^{C}	–	–
Fe	SLM	70	Diamond	2	31 ^{C}	–	–
Fe	SLM	59	Diamond	3	54 ^{C}	–	–
Fe	SLM	73	Diamond	1.6 – 1.8	24 ^{C}	40 ^{C}	–
Fe-Mn	BJ	39	–	–	228 ± 11 ^{T}	190 ± 26 ^{T}	39 ± 1
Fe+HA	DIW	–	Cubic	1.25	–	141 ^{C}	–
Zn	SLM	73	Diamond	0.4	4 ^{C}	–	–
Zn	SLM	69 ± 2	Diamond	0.5	6 ^{C}	–	–
Zn	SLM	62 ± 3	Diamond	0.8	11 ^{C}	–	–

Figure 206: Mechanical characteristics of biodegradable metallic cellular architectures

Source: (Chen et al., 2021)

Benedetti et al. *(2021)* extensively discussed the mechanical and fatigue performance of 3DPed metallic cellular structures by architecting only the geometrical features. The authors presented the graphs shown in *Figure 208* where the modulus of elasticity, yield strength, and fatigue strength concerning the relative density of each different unit cell are summarized.

Babamiri et al. *(2021)* introduced a design topology-microstructure-based optimization method that considers scale separation and size effects to control the deformation mechanisms of lattice structures and improve certain mechanical performance metrics: yield strength, plastic flow stress, and energy absorption capacity.

Material	Fabrication Method	Unit cell	Porosity (%)	E (GPa)	σ_y (MPa)	σ_{max} (MPa)
CP-Ti (Grade 1)	SLM	Dodecahedron	66–81	0.58–2.61	8.6–36.5	–
CP-Ti (Grade 1)	SLM	Gyroid	72.4	1.47–2.30	49.0–53.3	–
CP-Ti (Grade 2)	SLM	Cellular	37	13 ± 3	113 ± 0.3	–
Ti-6Al-4V	SLM	Cubic	72.8	12.6 ± 3.3	16.6 ± 0.5	–
Ti-6Al-4V	EBM	Cubic	80	1.6 ± 0.3	22.0 ± 1.1	29.3 ± 0.8
Ti-6Al-4V	EBM	Diamond	60–87	0.4–6.5	11.4–99.7	16.3–118.8
Ti-6Al-4V	SLM	Diamond	65	2.481	76.2	–
Ti-6Al-4V	SLM	Truncated cube	80–91	0.99–3.19	10–40	–
Ti-6Al-4V	SLM	Truncated cuboctahedron	64–81	2.37–4.62	25–100	–
Ti-6Al-4V	SLM	Rhombic dodecahedron	68–89	0.22–2.97	7–88	–
Ti-6Al-4V	EBM	Rhombic dodecahedron	62.7–83.8	–	–	20–90
Ti-6Al-4V	EBM	Rhombic dodecahedron	58–88	0.5–6.5	–	10–100
Ti-6Al-4V	SLM	Rhombic cuboctahedron	68–89	2.23–4.40	39–93	–
Ti-6Al-4V	SLM	Octet truss	50–75	1.2–4.6	34–172	–
Ti-6Al-4V	SLM	Tetrahedron	50–75	1.9–4.3	57–156	–
Ti-6Al-4V	EBM	Honeycomb	66	2.5 ± 0.5	–	116 ± 10
Ti-6Al-4V	SLM	Cuboctahedron	58	2.77	119.4	–
Ti-6Al-4V	SLM	Twist struts	55–61	3.4–26.3	103–402	–
Ti-6Al-4V	EBM	Hatched structure	60	12.9 ± 0.9	107.5 ± 3.6	148.4 ± 3.5
Ti-6Al-4V	EBM	G7	58–88	0.5–5	–	8–80
Ti-6Al-4V	SLM	F-RD	45	2.81	173.9	–
Ti-6Al-4V	SLM	I-WP	45	2.52	125	–
Ti-6Al-4V	SLM	Gyroid	80–95	0.13–1.25	6.5–81.3	–
Ti-6Al-4V	EBM	Gyroid	82	0.64 ± 0.05	13.16 ± 1.6	24.4 ± 2.4
Ti-6Al-4V	SLM	Diamond TPMS	80–95	0.12–1.25	4.7–69.2	–
Ti-6Al-4V	EBM	Solid cellular foam	55–82	0.75–9.97	–	–
Ti-6Al-4V	EBM	Hollow cellular foam	55–89	0.48–9.77	–	–
Ti-24Nb-4Zr-8Sn	SLM	Rhombic dodecahedron	75	0.95 ± 0.05	–	50 ± 0.9
Ti-24Nb-4Zr-8Sn	EBM	Rhombic dodecahedron	75	1.34 ± 0.04	–	45 ± 1.1
Ti-24Nb-4Zr-8Sn	EBM	G7	70	0.7 ± 0.1	–	35 ± 2
Ti-35Zr-28Nb	SLM	Face centered cubic	83	1.1 ± 0.1	–	–
Ti-35Zr-28Nb	SLM	Face and body centered cubic	50	1.3 ± 01	–	–
NiTi	SLM	Octahedron	79.3	–	21	–
NiTi	SLM	Gyroid	78.5	–	29	–
Ti-25Ta	SLM	Schwartz	25–64	14.3–36.1	86–319	–
Co-28Cr-6Mo	SLM	Cubic	81	7.18 ± 0.47	–	271.5 ± 20.9
Co-28Cr-6Mo	SLM	Face centered cubic	76	12.88 ± 0.64	–	501.7 ± 12.6
Co-28Cr-6Mo	SLM	Body centered cubic	77	11.81 ± 0.59	–	453.9 ± 28.4
Co-28Cr-6Mo	SLM	Spherical hollow cubic	77	8.79 ± 0.28	–	315.5 ± 17.6
316 L stainless steel	SLM	Cubic	87	0.15	3	–
316 L stainless steel	SLM	Gyroid	85	0.24–0.31	12.4–17.0	–
Ta	SLM	Dodecahedron	80	1.22 ± 0.07	12.7 ± 0.6	–
Ta	SLM	Diamond	70	3.10 ± 0.03	–	–

Figure 207: Mechanical characteristics of standard metallic cellular architectures. Source: (Chen et al., 2021)

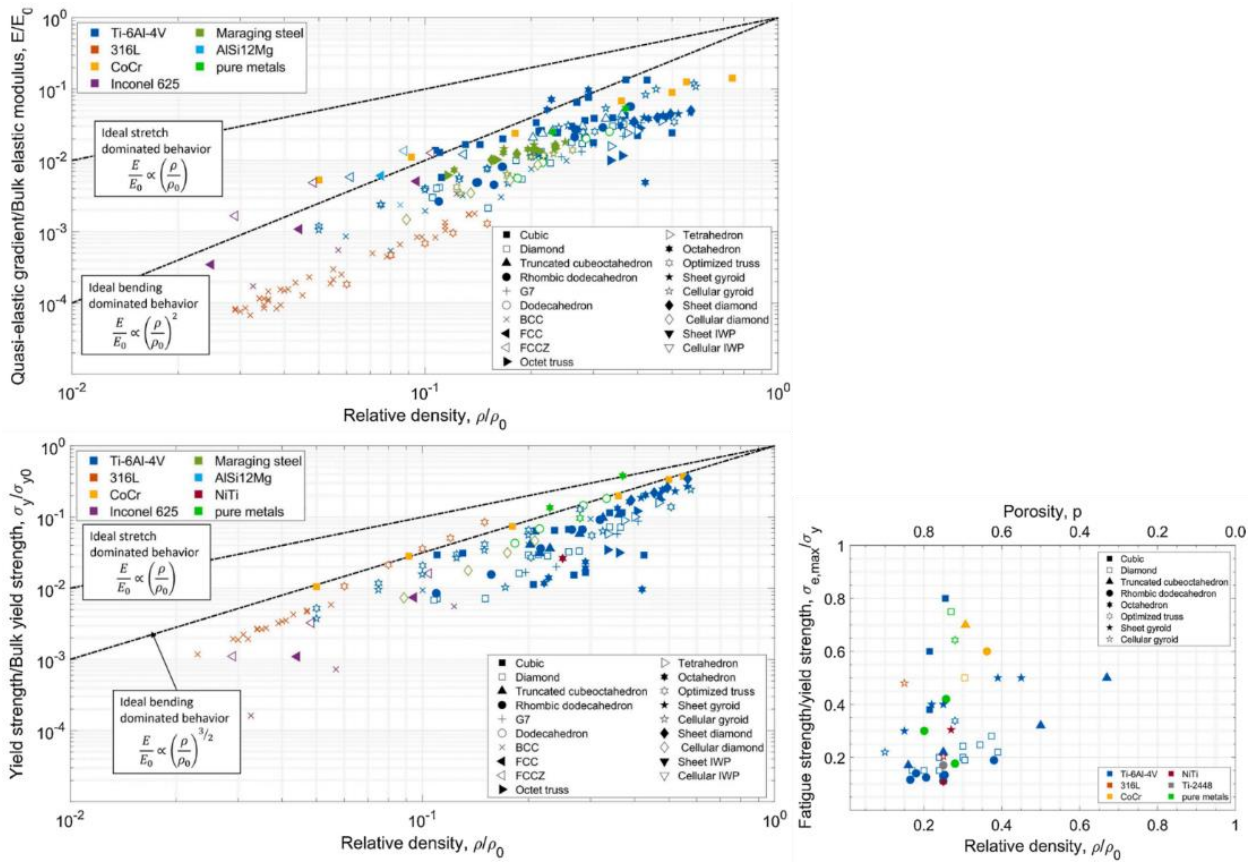

Figure 208: Modulus of elasticity, yield strength, and fatigue strength for different unit cells. Source: (Benedetti et al., 2021)

Implementing cellular structures into 3DPed biomaterials proved to be successful in approximating the mechanical properties of trabecular and cortical bone. As bone's characteristics vary with age, sex, health status, and anatomical site, all these should be considered during the customized endo-prostheses design where pore size, porosity, and unit cell have to be optimized not only for mechanical optimization but also for maximum permeability and osseointegration.

3.6.2 Biological Performance Optimization

Adopting porous elements into the implant enhances the transport of oxygen, nutrients, and bone formation inducing elements for cell migration and vascularization, allowing bone formation. Trabecular bone-imitating architectures with suitable pore size and porosity have to be selected as these have crucial impacts on the implant's performance regarding bone ingrowth and osseointegration *(Figure 209* and *Figure 210).* Cellular structures with 0,24 to 1,5 pore size and 60-88% porosity made by EBM and LBM showed beneficial biological responses with good tissue ingrowth *(Sing et al., 2015).* For orthopaedic implants, typical values usually suggested are trending at ~70% porosity with ~600 μm pore size *(see Figure 33 and Sub-section 3.1) (Karageorgiou and Kaplan, 2005; Palmquist et al., 2013; Regis et al., 2015; Taniguchi et al., 2016; Shah et al., 2016; Hara et al., 2016; Tan et al., 2017; Wild et al., 2018; Wang et al., 2019; Barba, Alabort and Reed, 2019).* Post-operative follow-ups of such porous morphologies implemented into endo-prostheses showed good short and mid-term outcomes *(Regis et al., 2015; Perticarini et al., 2015; Dall'Ava et al., 2019a; Geng et al., 2020; Huang et al., 2021b).*

Roy et al. *(2003)* studied (rabbit calvarial defect) the in vivo performance of 3DPed degradable composite (PLGA with 20% beta-TCP) bone implants and verified that customized macroscopic channels, controlled gradient porosity, and controlled pore size promoted greater bone ingrowth.

Numerous such 3DPed implantable devices featuring Voronoi-like cellular architectures have been researched, commercialized, and cleared by the FDA as shown in *Figure 211,* whereas there is a wide variability between manufacturers that 3D print porous orthopaedic implants as has been shown by morphometric analyses *(Hothi et al., 2022).* FDA-cleared 3DPed medical devices breakdown from 2010-2020 presented in *Figure 114* also include many such porous architectures.

Sidambe *(2014)* reviewed the capabilities of 3DP for biomedical implant applications emphasizing on surface finishes and porous structures, referencing published studies of in vitro and in vivo research on host tissue responses.

Amin Yavari et al. *(2014)* applied three surface biofunctionalizing treatments to PBF 3DPed Ti implants (acidealkali (AcAl), alkalieacide heat treatment (AlAcH), and anodizing-heat treatment (AnH)) and found that each has a considerable effect on apatite forming ability, cell attachment, cell proliferation, and bone ingrowth. AcAl showed higher apatite-forming ability but did not have any

positive effect on cell attachment, cell proliferation, and osteogenic gene expression. AnH had the exact vice versa results and AlAcH's performance was in between.

Technique	Pore geometry	Porosity (%)	Pore size (μm)	Strut diameter (μm)	Pore interconnectivity (%)	Conclusion
SLM	Diamond	58.5 ± 4.3	406.5 ± 34.1	483 ± 33.9	–	Ta scaffolds exhibited suitable mechanical compatibility and biocompatibility.
SLM	Dodecahedron	68.3 ± 1.1	334 ± 86	–	–	Ta scaffolds exhibited good biocompatibility, osteointegration, and osteogenesis.
Space-holder	Spongy	8–70.8	9–367	–	–	Ta scaffolds with 48–56% porosity exhibited desired mechanical and biological properties.
SEBM	Dodecahedron	75–85	–	386–540	–	The as-printed Ta samples exhibited excellent ductility and achieved satisfactory clinical performance.
PM	Spongy	66.7	300–600	–	–	The porous Ta scaffolds exhibited good mechanical compatibility and biocompatibility.
LENS™	Net-shape	27–55	200–2000	–	–	The laser-processed porous Ta exhibited good biocompatibility and bioactivity.
Space-holder	Spongy	60–80	40–120	–	–	Ta scaffolds with 70% porosity had elastic modulus similar to cancellous bone.
SLM	Dodecahedron	80	500	150	–	Ta scaffolds exhibited favorable biocompatibility, osteoconductivity, and osteointegration.
SLM	Trabecular	60–80	300–800	300–500	99.99	Ta scaffolds exhibit excellent ductility, reliability, and suitable mechanical strength.
PM	Trabecular	60–80	200–500	–	–	The novel porous Ta scaffolds exhibited good biocompatibility and osteoinductivity.
CVD	Trabecular	66–88	122–581	204–479	–	Ta scaffolds had fluid flow and mechanical characteristics very similar to natural bone.
CVD	Trabecular	75–85	400–600	–	–	Trabecular Metal (Zimmer) exhibited great biocompatibility, bioactivity, and osteogenesis.
CVD	Trabecular	75–85	400–600	–	–	Trabecular Metal (Zimmer) exhibited superior biocompatibility comparable to allograft and autograft.
CVD	Trabecular	75–85	350–450	–	–	Ta scaffolds exhibited greater biocompatibility and osteointegration compared with conventional titanium implants.
CVD	Trabecular	75–85	200–500	–	–	BMSC-load pTa combined with biomimetic 3D collagen-based scaffold has excellent potential in the repair of load-bearing areas of femoral heads.
LMLMC	Net-shape	35–50	300	–	–	The mechanical properties of as-prepared porous Ta scaffolds are very close to human spongy bone and compact bone.
Slip-casting	Spongy	65–80	400–600	100	–	Porous Ta combined with BMP-7 achieved excellent osteointegration with host bone.

Alloy	Pore Size Range (μm)	Tissue	Duration
Ti-6Al-4V	160 - 660	Goat - spinal cages	12 weeks
	200 - 700	Human osteoblasts	2 weeks
	500 - 1000	Human periosteum cells	2 weeks
	450 - 1200	Human osteoblasts	6 weeks
Commercially Pure Ti (cp-Ti)	100 - 800	Human osteoblasts	12 weeks
	300 - 900	Rabbit femoral condyle and tibia metaphysis	8 weeks
Tantalum	200 - 2000	Human osteoblasts	11 days

Figure 209: 3DPed porous implants with various architectures in literature. Source: (Lowther et al., 2019; Gao et al., 2021)

Wauthle et al. *(2015a)* studied (histological analysis, mechanical tests) in vivo (rat femur defect model) the bone regeneration performance of PBF 3DPed porous (dodecahedron structure, 500μm pore size, 80% porosity) Ta load-bearing implant with tuned mechanical properties close to cancellous bone (12,7 MPa yield strength, 1,22 GPa modulus of elasticity). After 12 weeks, good bone ingrowth, strong full-bridged regenerated bone, and functional implant-bone interface connection were observed.

Van der Stok et al. *(2015)* 3DPed load-bearing porous Ti implants filled with physiologically concentrated fibrin gel and loaded with bone morphogenetic protein-2 (BMP-2) to graft critical-sized segmental femoral bone defects in rats. Complete regeneration and bridging within 8 weeks, and

bone formation and remodeling after 12 weeks were observed (in vivo and ex-vivo micro-CT, histological analysis) as shown in *Figure 212*.

AM material	AM method	Feature[a]	Post treatment	Outcome[b]
Ti–6Al–4V	EBM	Diamond units with pore 500 (501), 640 (656), 800 (786), and 1000 (933) μm. Porosity 65, 70, 76 and 70%, elastic modulus 1.6, 1.2, 1.3 and 1.4 GPa	No	Implanted in rabbit distal femur 4 and 12 weeks. Similar bone ingrowth between 501, 656 and 786 μm; less bone ingrowth observed for 933 μm pores. Implant with 656 μm has comparable bone bonding with titanium fiber mesh controls.
Pure titanium	SLM	Diamond crystal lattice based plates and cylinders with pore size 300 (309), 600 (632) and 900 (956) μm, porosity 62, 66 and 64%, elastic modulus 0.56, 0.65 and 0.66 GPa.	Heat-treated at 1300 °C for 1 h	Plates in rabbit tibia showed 632 μm pore size implants have significantly higher bone-implant bonding at 2 weeks. Cylinders in the femur with 309 μm pores have significantly lower bone ingrowth at 4 weeks than 956 μm, 632 μm pore ones favor bone ingrowth at 2 and 4 weeks.
Ti–6Al–4V	SLM	Straightforward connected circular pore 500 (401), 700 (607) and 900 (801) μm sizes, porosity 45, 51 and 56%, elastic modulus 7.56, 5.97 and 5.04 GPa.	Alkali-acid-heat treatment	Small pores (401 μm) were beneficial for cell adhesion while large pores (801 μm) were conducive to proliferation. Implants in rabbit femoral epiphysis with pore size 607 μm were in favor of bone ingrowth, maturation and implant fixation.
Pure titanium	SLM	Diamond unit with pore 400 (395), 650 (650), 850 (845) and 1100 (1105) μm, porosity 66, 68, 70 and 72%.	Heat-treated at 800 °C for 2 h	*In vitro* DNA and Ca^{2+} contents of cultured cells and *in vivo* bone ingrowth followed the same trend: increased with pore size from 395 to 650 μm and decreased with further larger pore sizes.
Ti–6Al–4V	EBM	Wave structures with pore size 0.9 mm, porosity 49%; cubic structures with pore size 1.2 mm and porosities 77%.	Sandblasted with corundum	Implanted in goat femoral condyle illustrated that deeper bone ingrowth for cubic structure (1.2 mm) but significantly more bone was observed for wave structure (0. 9 mm).
Ti–6Al–4V	Laser sintering	Trabecular bone structures have pores 177, 383 and 653 μm, porosity 15, 38 and 70%, elastic modulus 3.7, 3.5 and 2.6 GPa.	Blasted with calcium phosphate and acid-etched	Largest pore size (653 μm) and corresponding highest porosity (70%) supported the greatest osteogenic differentiation and growth factor (BMP2 and VEGF) production.
Ti–6Al–4V	EBM	Hexagonal unit with pore size 640 (682) and 1200 (1266) μm, porosity 73 and 82%.	Powder blasting to remove loose particles	Scaffolds with smaller pores (682 μm) have lower inflammatory cytokines secretion, higher osteogenic differentiation and mineralization than 1266 μm.
Ti–6Al–4V	SLM	Scaffolds with unit: triangular, hexagonal and rectangular, size 500 and 1000 μm, porosity 42–83%, and elastic modulus 0.45–11.26 GPa.	Oxidized in 5 M NaOH solution	Significantly higher living cell density on the scaffolds with 1000 μm pores. Cells were able to differentiate in Ti–6Al–4V bone scaffolds with a 500 μm triangular pore without osteogenic differentiation inducers.

AM material	AM method	Feature	Outcome
Ti–6Al–4V	SLM	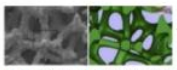 Voronoi-Tessellation principle used to design trabecular like scaffolds with irregularities 0.05–0.5 and porosities 48.83–74.28%.	Trabecular-like scaffolds with full irregularity (0.5) and higher porosity (74.28%) exhibited promotion to osteoblast proliferation and differentiation, significantly higher than flat control.
Ti–6Al–4V	SLM	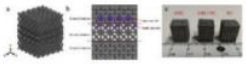 PFGs with octet truss cell (pore size 1042 μm and 75% porosity) as exterior and tetrahedron cell (pore size: 700 μm and porosity 80%) as internal. Elastic modulus 1 GPa.	Compared to the homogeneous structure, PFGs can improve the cell proliferation rate. Under the same mechanical properties, the cell proliferation rate of PFGS from day 4 to day 7 was 140% while the uniform structures were about 90%.
Ti–6Al–4V	EBM	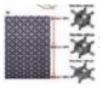 Dodecahedron units with pores 600, 400 and 200 μm (porosity 65%, strut size 500 μm).	Higher expression of actin and vinculin by osteoblasts on part of PFGs with smaller pore size (200 μm) than larger pore size (600 μm).
Ti–6Al–4V	SLM	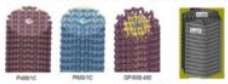 Dense core in the center and graded pore at outer layer. A 'spider web' design with 250 μm radial spokes used to form hexagonal prisms. Porosity ranging from 50-80%.	The young's moduli were higher for scaffolds with 'spider web' structure and 2 mm dense core constructs. Web structure with 70% porosity has similar mechanical properties with diamond unit structures (porosity 50%). Similar cell viability and cell mineralization observed.
Ti–6Al–4V	SLM	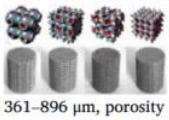 Primitive, I-WP, gyroid and diamond TPMS, pore 361–896 μm, porosity 35–71%, elastic modulus 3.2–6.4 GPa.	Similar morphology and permeability with trabecular bone. Low elastic modulus, high yield strength, and extremely high fatigue resistance achieved for some combined designs.
Ti–6Al–4V	SLM	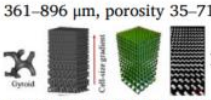 FGPs in patterns (density, hetero-structure and cell-size gradients) with Gyroid and Diamond units were designed based on TPMS.	Gyroid and Diamond structures possess modulus similar with bone. Porous surface area and pore size could be controlled by the cell-size gradient with consistent density and moduli, and continuous topology and interconnectivity.

Figure 210: 3DPed porous implants with various architectures in literature. Source: (Li et al., 2020)

In 3DPed Ti6Al4V bone-interfacing constructs, to enhance cellular response and implant osseointegration, it was found that osteoblasts prefer 3D architectures to 2D surfaces, whilst expressing sensitivity to the resolution of cell pore size and porosity *(Cheng et al., 2016).*

Anatomical Region	Product Type	Alloys In Use	Key Features and Clinical Benefits	Manufacturers	FDA Number
Foot & Ankle	Osteotomy truss	Ti-6Al-4V	Porous surface for osseointegration, reduced density for limited radiographic artefacts	4-Web Medical Inc.	K130185
				Additive Orthopaedics	K170214
Hip	Acetabular cup	Ti-6Al-4V	Porous surface for fixation and osseointegration	Lima Corporation	K141395
				Smith & Nephew	K150790
	Femoral stem			Theken	K161184
				Adler Ortho	K171768
Knee	Tibial cavity	Ti-6Al-4V	Porous surface for fixation and osseointegration	Medacta International	K170149
	Tibial baseplate			Stryker	K123486
Sacroiliac	Sacroiliac fusion	Ti-6Al-4V	Porous surface for fixation and osseointegration	SI-Bone Inc	K162733
Spinal	Interbody fusion	Ti-6Al-4V	Porous surface for fixation and osseointegration	Camber Spine Tech.	K172446
		Co-Cr-Mo		Medicrea Int. S.A	K163595
				4-Web Medical Inc.	K142112
				K2M	K163364
				EIT	K172888
				Stryker	K171496
				Nexxt Spine LLC	K171140
				NuVasive	K172676
				joimax GmbH	K151143
				HT Medical	K170318
				CoreLink, LLC	K162496

Implant/sample	Porosity (%)	Average strut spacing (μm)	Average strut thickness (μm)
Renovis, tesera (titanium)	64.37	607	277
Stryker, tritanium (Ti-6Al-4V)	60	616	–
Biomet, regenerex (Ti-6Al-4V)	67	300	–
Zimmer, trabecular metal (tantalum)	75–85	550	–
Smith and nephew, stiktite (titanium)	60	200	–
Fully porous human femoral trabecular scaffold (Ti-6Al-4V)	15	177	628
	38	383	454
	70	653	305
Fully porous human femoral trabecular scaffold (Ti-6Al-4V)	67	563	–
Fully porous dodecahedron unit cell scaffold (Ti-6Al-4V)	85 (88)	577 (500)	165 (120)
	89 (88)	596 (500)	160 (120)
	86 (88)	578 (500)	175 (120)
Fully porous dodecahedron unit cell scaffold (Ti-6Al-4V)	68	(490)	(230)
	88	(490)	(120)
Cylindrical interconnected channels (Ti-6Al-4V)	–	401 (500)	(300)
	–	607 (700)	(300)
	–	801 (900)	(300)
Fully porous diamond unit cell scaffold (Ti-6Al-4V)	45.5	305	175
Surface porous diamond unit cell scaffold (Ti-6Al-4V)	45.4	294	174

Company	Cup Brand	Porous Structure	Properties: Porosity; Pore Size
Adler Ortho (Milan, IT)	Agilis Ti-Por® *Custom* Fixa Ti-Por® Omnia Ti-Por® PolyMax Ti-Por®	Tri-Por™Cup	65%; 700 μm
Corin (Cirencester, UK)	Trinity™ Plus	Porous Layer Unique Structure (PLUS)	50–90%; 300–900 μm
Implantcast (Buxtehude, DE)	C-Fit 3D® (custom) EcoFit®	EPORE®	60%; 100–500 μm
Lima Corporate (Udine, IT)	Delta TT Delta ONE TT Delta Revision TT Promade (custom)	Trabecular Titanium (TT)	65%; 640 μm
Materialise (Leuven, BE)	aMace® (custom)	aMace®	70%; 720 μm
Medacta astel San Pietro, CH)	Mpact®	3D Metal™	~75%; 600–800 μm
Smith&Nephew (Memphis, USA)	Redapt	Conceloc Advanced Porous Titanium	~67%; 202–934μm
Stryker (Mahwah, USA)	Trident® II	Tritanium® AMagine™	55–65%; 100–700 μm
Zimmer Biomet (Warsaw, USA)	G7	OsseoTi™	~70%; 475 μm

Figure 211: Commercialized and under research 3DPed porous implants. Source: (Lowther et al., 2019; Kelly et al., 2019; Dall'Ava et al., 2019)

Shah et al. *(2016)* compared (Scanning Electron Microscope (SEM), histological analysis) 3DPed porous implants made of CoCr and Ti6Al4V in terms of osseointegration *(Figure 213)*. Although bone formation patterns around and inside were comparable for both materials, Ti6Al4V showed

higher bone-implant contact (39,2%) than CoCr (27%), but osteocyte density in the periphery of CoCr was higher.

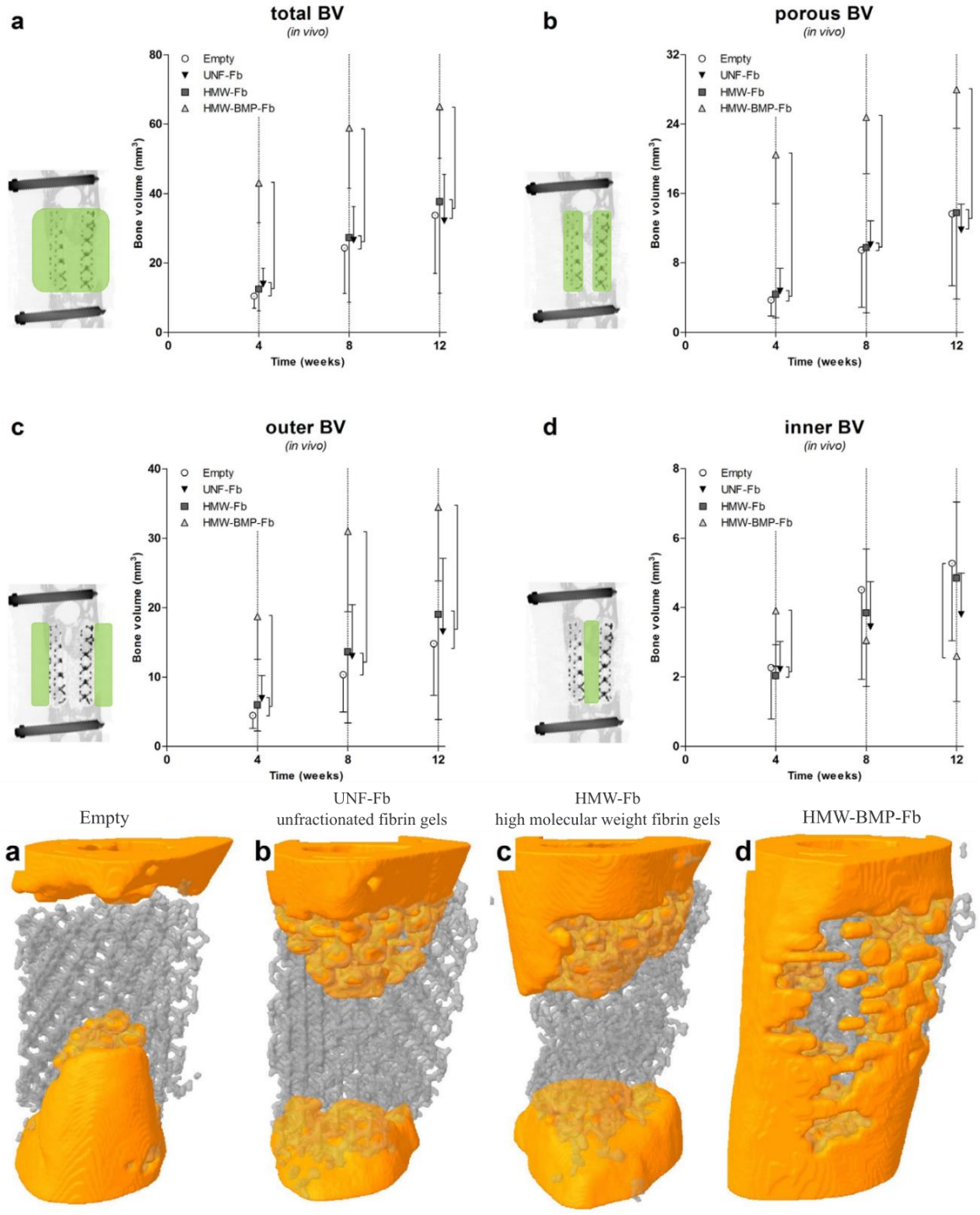

Figure 212: 3DPed porous Ti implants filled with fibrin gel and loaded with BMP-2. Source: (Van der Stok et al., 2015)

Arabnejad et al. *(2016a)* reviewed 3DPed tetrahedron and octet truss sample structures and reported 28,6% and 41,3% (tetrahedron), and 35,5% and 56,9% (octet truss) bone ingrowth after four and eight weeks respectively *(Figure 214)*.

Ran et al. *(2018)* investigated (SEM, micro-CT, compression tests) in vitro and in vivo the mechanical and biological performance of different Ti6Al4V scaffold pore sizes (500, 700, and 900

μm diameter), and found that the 700 μm sample was superior in favor of bone ingrowth, maturation and bone-implant fixation stability *(Figure 215).*

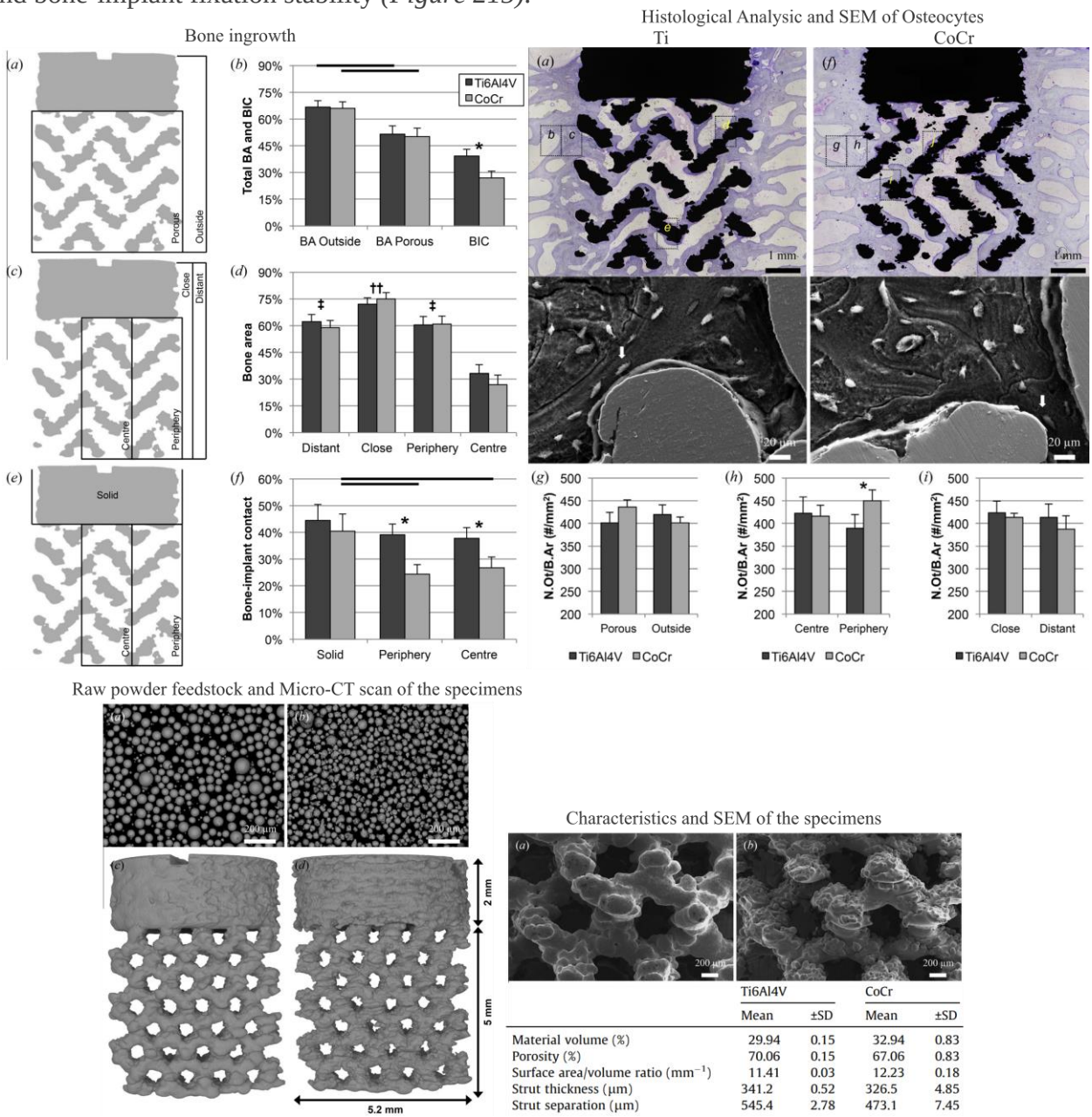

	Ti6Al4V		CoCr	
	Mean	±SD	Mean	±SD
Material volume (%)	29.94	0.15	32.94	0.83
Porosity (%)	70.06	0.15	67.06	0.83
Surface area/volume ratio (mm^{-1})	11.41	0.03	12.23	0.18
Strut thickness (μm)	341.2	0.52	326.5	4.85
Strut separation (μm)	545.4	2.78	473.1	7.45

Figure 213: Osseointegration of 3DPed porous Ti versus porous CoCr. Source: (Shah et al., 2016)

Unit cell	#	Porosity (%)	Strut thickness (mm)	Unit cell size (mm)	Pore size (mm)
Tetrahedron		60	0.31	1.39	0.5
		70	0.24	1.27	0.5
Octet truss		60	0.32	1.54	0.77
		70	0.25	1.44	0.77

Time period (weeks)	Topology	Porosity (%)	Bone ingrowth
4	Tetrahedron	55.5	28.6% ± 11.6%
	Octet truss	69.9	35.5% ± 1.9%
8	Tetrahedron	55.5	41.3% ± 4.3%
	Octet truss	69.9	56.9% ± 4.0%

Figure 214: Bone ingrowth in 3DPed tetrahedron and octet truss. Source: (Arabnejad et al., 2016)

Qin et al. *(2018)* 3DPed with laser-based PBF technology Ti6Al4V implants with a micro-structured surface followed by two extra surface modification steps to form titania nanotubes (TnT) (electrochemical anodization) and HA coating. Osseointegration was examined using human primary

osteoblasts and cell line models, and the results showed significant protein adsorption, osteoblast cell adhesion, spreading, and expression of certain genes for osteoblast differentiation and mineralization *(Figure 216)*. The authors mentioned the capability to load drugs into the titania nanotubes for additional therapeutic functions and bacterial prophylaxis.

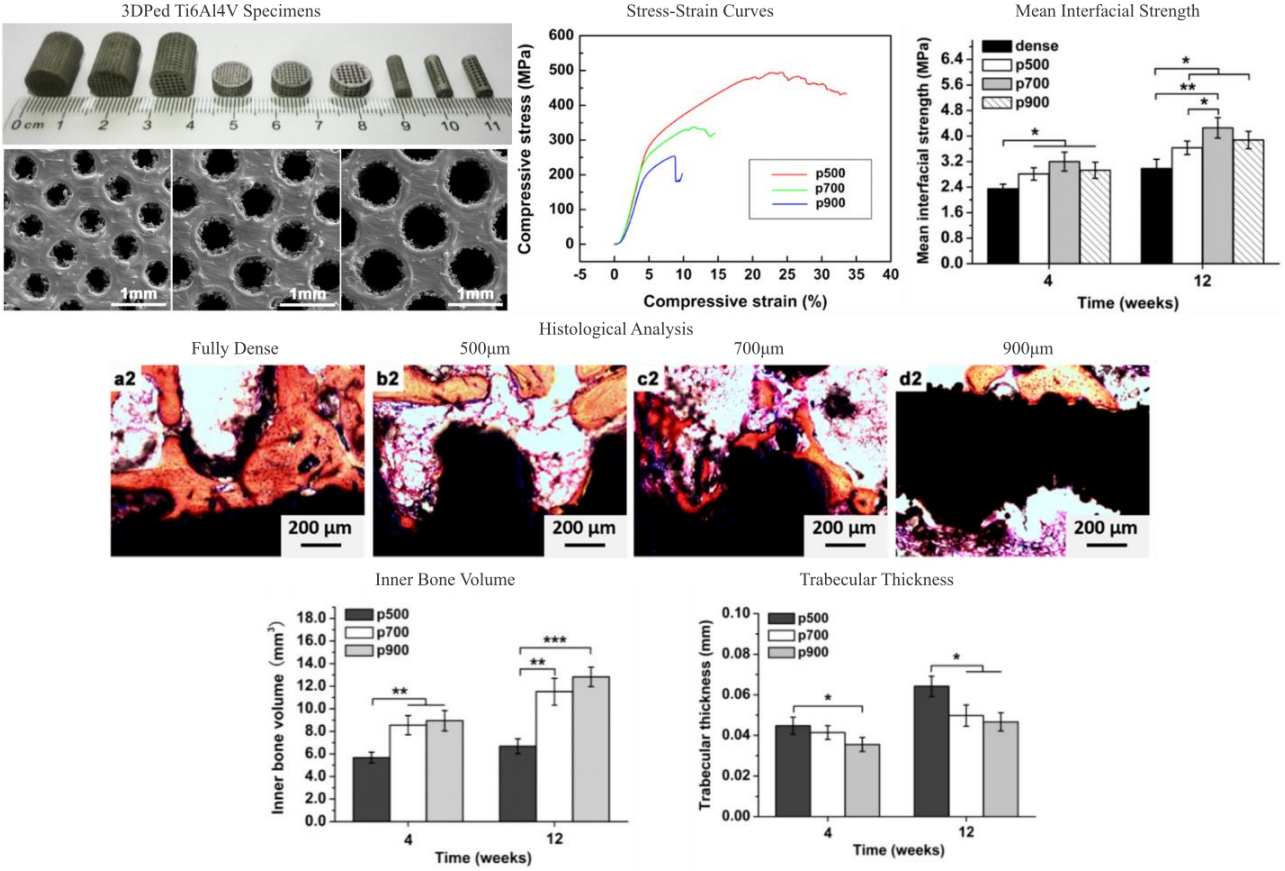

Figure 215: Mechanical-biological performance of 3DPed porous Ti with different pore sizes. Source: (Ren et al., 2018)

PBF 3DPed porous acetabular cups demonstrated favorable short to mid-term clinical outcomes (high survival rate, great clinical improvements, excellent biological fixation) in total hip arthroplasty patients (*Regis et al., 2015; Perticarini et al., 2015; Geng et al., 2020; Huang et al., 2021b; Dall'Ava et al., 2021)*. By 2017, it has been estimated that more than 60.000 acetabular cups have been produced by PBF 3DP *(Murr, 2018)*. Dall'Ava et al. *(2019)* provided information about post-operative results of commercially available 3DPed porous off-the-shelf and custom acetabular cups, with the majority showing encouraging clinical and radiographic short to mid-term results, higher survival rates, and lower incidence of aseptic loosening.

Wo et al. *(2020)* studied the effects of pore size and porosity distribution model on adhesion, proliferation, and differentiation of mouse embryonic osteoblast precursor (MC3T3-E1) cells on 3DPed porous Ti. High porosity (HP) and low porosity (LP) specimens with 300 μm, 500 μm, and 800 μm pore sizes (PS) were analyzed, but the PS800/HP displayed the highest cell proliferation.

Park et al. *(2020)* showed that minimizing the implant-host bone gap is essential for high osseointegration levels. They presented a limb-salvage case using custom 3DPed Ti6Al4V radius

and ulna endo-prostheses, and evaluated histologically that porous features enhanced bone ingrowth with the total tissue integration rate at the proximal and distal bone junctions reaching 46% and 15% respectively *(Figure 218)*.

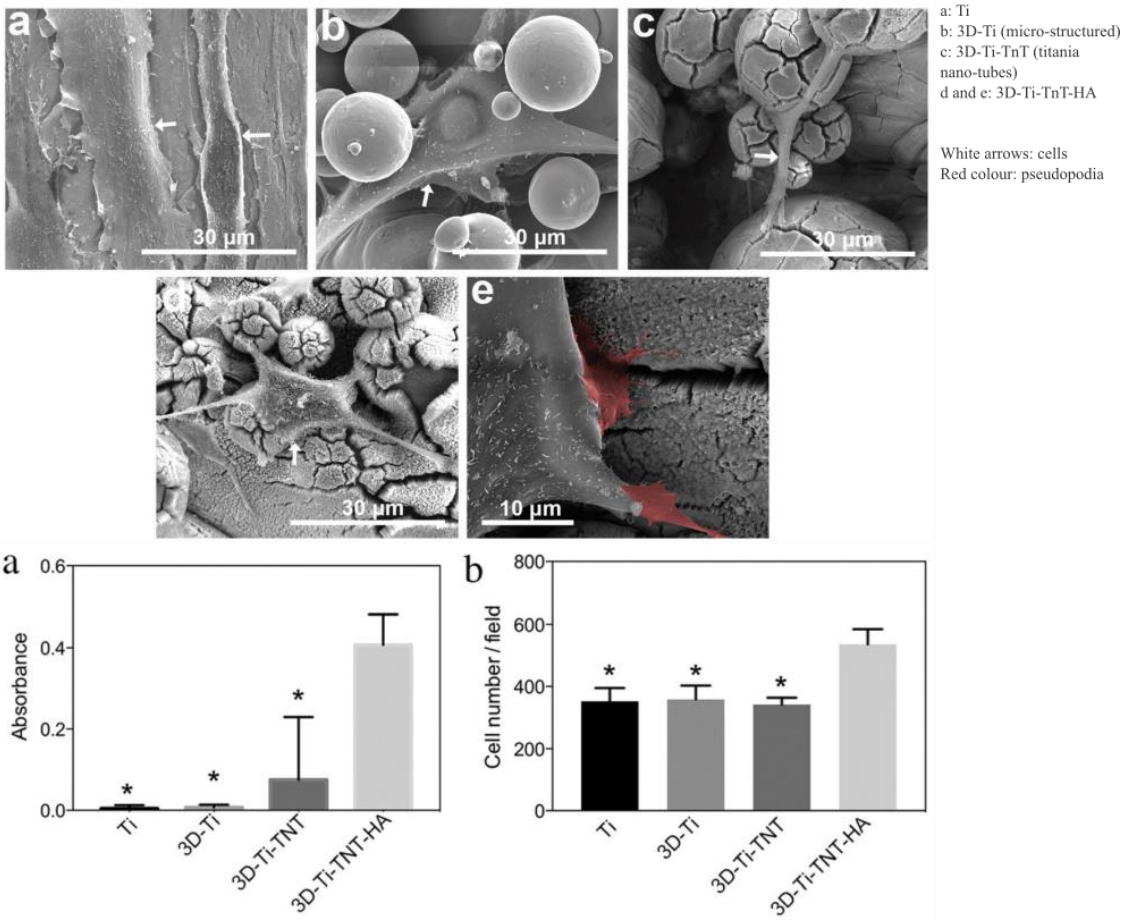

Figure 216: Biological performance of 3DPed porous specimens with TnT and HA coating. Source: (Qin et al., 2018)

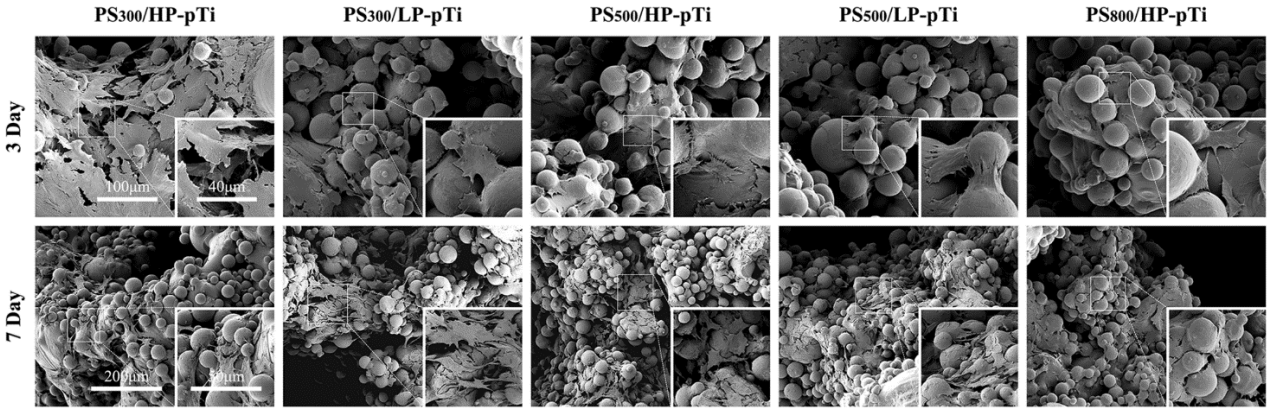

Figure 217: Biological performance of different 3DPed Ti porous scaffolds. Source: (Wo et al., 2020)

Van den Brink and Lamerigts *(2020)* described the histological findings of a retrieved 3DPed porous Ti cervical cage (EIT Cellular Titanium) explanted 2 years after insertion: complete osseointegration with mature lamellar bone and bone marrow, a pattern of trabecular bone, absence of stress-shielding, and physiological remodeling activity *(Figure 219)*.

Sarker, Leary and Fox *(2020)* reviewed PBF 3DP technologies for orthopaedic implants and discussed different surface modifications to improve bio-integration and protect against infections.

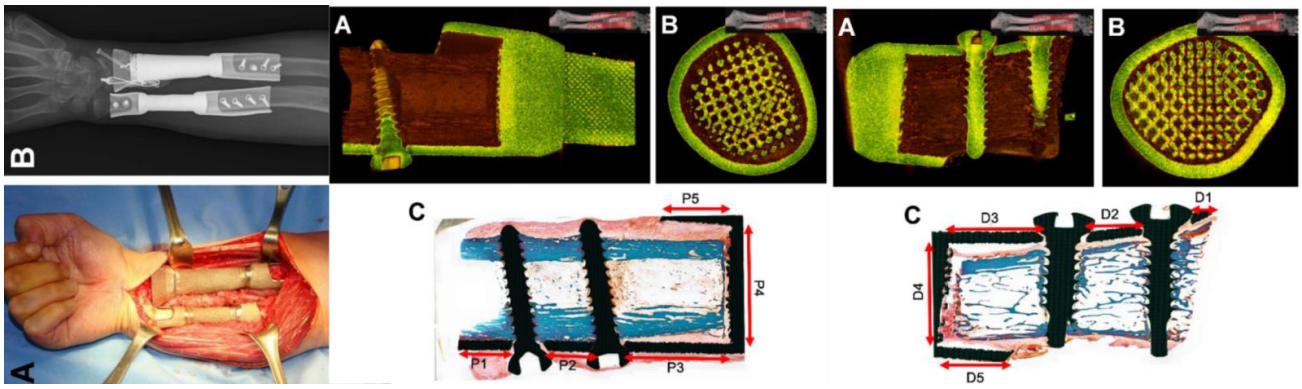

Figure 218: Osseointegration of radial and ulnar endo-prostheses. Source: (Park et al., 2020)

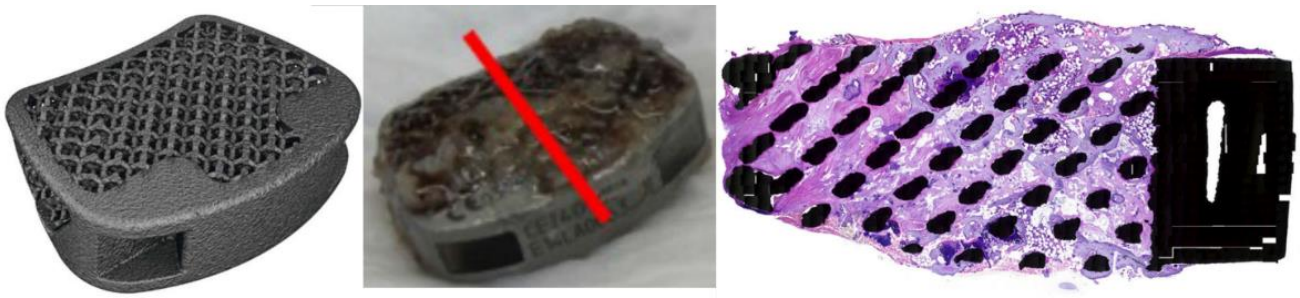

Figure 219: Osseointegrated 3DPed porous Ti cervical cage. Source: (Van den Brink and Lamerigts, 2020)

Li et al. *(2020)* summarized the current status of 3DPed bone-interfacing implants, focusing on the experimental outcomes of various factors that influence osseointegration, bone and vascular ingrowth as well as hybrid strategies to combat infection *(Figure 220)*: pore size and structure, porosity, surface modifications, incorporation of biological factors.

AM Material	AM method	Drug loading	Antibacterial	biocompatibility
Pure titanium	DMP	vancomycin and Ag^+-containing chitosan/gelatine were electrophoretic deposited	Ag^+ and vancomycin coated separately or together fully eradicated adherent and planktonic *S. aureus*	Ag^+ demonstrated moderate cytotoxicity to osteoblast which was not observed for vancomycin.
Pure titanium	DMP	Ag^+ and vancomycin-containing chitosan were electrophoretic deposited	The antibacterial effect observed *in vitro* but did not achieve *in vivo* infection prevention	Ag^+ negatively impacted bone response and the efficiency of bacterial uptake by innate immune cells.
Pure titanium	DMP	Anodized surface soaked in $AgNO_3$ solution	The Ag^+ was effective to prevent biofilm formation and kill planktonic bacteria.	Severe cytotoxicity to hMSC was observed for the high amount Ag^+ loading group.
Ti–6Al–4V	SLM	Ag nanoparticles were incorporated by electrolytic oxidation	Strong antimicrobial to methicillin-resistant *S. aureus in vitro* and *ex vivo*.	No toxicity observed for hMSC proliferation
Ti–6Al–4V	EBM	PDA coated MAO surface soaked in $AgNO_3$ solution	Active killed planktonic/adherent *S. aureus* and *E. coli* up to 12 weeks. Destroyed mature biofilm.	Hampered early MT-63 attachment, promoted cell proliferation and osteogenic differentiation.
Ti–6Al–4V	EBM	Ag^+ containing SF was immobilized by PDA, UV reduced to nanosilver	Maintained antibacterial to *S. aureus* up to 6 weeks. Destroyed mature biofilm.	Hampered MC3T3-E1 attachment, no harm for cell proliferation and osteogenic differentiation.
Pure titanium	LENS™	Anodized surface electrodeposited in $AgNO_3$.	_	Silver coating did not affect bone generation.

Figure 220: Bacterial protection of 3DPed Ti implants. Source: (Li et al., 2020)

Chen et al. *(2020)* referred to the pros and cons of biomaterials used for fabricating bone scaffolds *(Figure 221)* and provided a comprehensive overview of materials and techniques used in 3DP bone scaffolds as well as clinical applications and pre-clinical trials *(Figure 222* and *Figure 223)*.

Spece et al. *(2021)* reviewed the published research on pre-clinical animal trials on 3DPed porous Ti6Al4V implants for orthopaedic bone ingrowth, showing successful and quantifiable osseointegration across all 58 studies reviewed.

Type	Advantages	Disadvantages	Applications
Metal-based composite scaffolds	High mechanical strength and wear resistance, good biomechanical compatibility and cytocompatibility, controllable porosity, and pore size	Uncontrolled degradation rate and inadequate osteogenic activity	Bone implant prosthesis or cortical bone repair
Synthetic polymer -based scaffolds	High mechanical strength and easy processability, tunable degradation and mechanics, low cost	Highly hydrophobic and lack of cell recognition sites, poor osteoconductivity	Both cortical bone and cancellous bone
Hydrogel-based scaffolds	Good cell and tissue compatibility, high osteogenic activity, and easy processability	Low mechanical strength and fast degradation rate	Repair of cartilage or subchondral bone
Ceramic-based scaffolds	High mechanical strength and osteogenic activity	Limited machining accuracy and high brittleness	Both cortical bone and cancellous bone

Figure 221: Pros and cons of different materials used for bone scaffolds. Source: (Chen et al., 2020)

Type	Raw materials	Printing system	Enhanced properties	Application
Metal-based composite scaffolds	Fe/HA	EB	Improved ALP activity and osteogenic differentiation of rBMSCs on the scaffold	Function of cells cultured on scaffold surface in vitro[69]
	Ti6Al4V/HA	SLS	Increased protein adsorption, cell adhesion and cell spreading	Evaluation of interaction between scaffolds and cells[192]
	Titanium/SiO_2	SLS	Increased the compressive strength of scaffold to 142 MPa	Mechanical strength and biocompatibility of scaffold were studied[193]
	Titanium/PVA	3DP	Enhanced the porosity and fracture toughness of scaffolds	Effect of PVA ratio on physical and mechanical properties of composite stent were evaluated[194]
Polymer-based composite scaffolds	PCL/bioglass	EB,	Improved the biocompatibility and osteoconductive properties of composite scaffolds	The interaction between the composite scaffold and cells in vitro and the osteogenic activity of the scaffold in vivo were studied[195–198]
	PCL/HA	3DP, SLS	Enhanced the biocompatibility and osteoconductive properties of composite scaffolds	Evaluated the biocompatibility and osteogenic activity of scaffolds in a mouse or rabbit implant model[24,199]
	PLGA/nHA	3DP, SLS	Improved bone regeneration and angiogenesis in vivo, and also increased the compressive strength and modulus of scaffold	The mechanical strength and the osteogenic activity of composite scaffolds were studied[200,201]
	PLGA/TCP/Mg	EB	Enhanced mechanical properties, porosity rate and promoted new bone formation	Studied the osteogenic activity of the scaffold in a rabbit implant model[202]
	PLA/PDA/HA	SLA	Enhanced adhesion and differentiation of human mesenchymal stem cell	To evaluate the in vitro regulation of cell behavior by scaffolds[203]
	PEEK/HA	EB	Exhibited a good biocompatibility and cell attachment	The biocompatibility and cyclic compression of the scaffold were evaluated[204]
	PEEK/carbon fibers	FDM	Improved the biocompatibility, bending strength, and the tensile strength of scaffolds	The mechanical strength and biocompatibility of the scaffold were evaluated[83]
	PEEK/Ag	FDM	Composite scaffolds displayed significant antibacterial and higher osteogenic activity	Antibacterial property of the scaffold and its osteoblastic differentiation were studied[205]
Ceramic-based composite scaffolds	HA/PCL	SLS	Supporting cell adhesion and proliferation	Studied the bone regeneration ability of scaffolds in a rabbit osteochondral defect model[27]
	β-TCP/PCL	SLA	Increased the compressive strengths and toughness of composite scaffolds	The influence of the scaffold with gradient structure on its mechanical strength was studied[206]
	β-TCP/GRMA	EB	The cell proliferation, differentiation and mechanical strength of scaffolds were enhanced simultaneously	Studied the expression of bone-related genes and proteins in cells co-cultured with scaffolds[207]
	α-TCP/collagen	EB	Improved mechanical properties and enhanced cellular metabolic activity and mineralization	The osteogenic ability of the cells in theα-TCP/collagen scaffold was evaluated[208]

Figure 222: Composite 3DPed biomaterials for bone scaffolds. Source: (Chen et al., 2020)

Paxton et al. *(2021)* investigated (histological analysis, in vitro cell culture) the role of porosity and surface chemistry in optimizing of tissue ingrowth into porous high-density polyethylene (HDPE) scaffold implants. They used Anatomics' StarPore manufactured with traditional molding

and PBF 3DP, and Stryker's (Stryker Corp, Michigan, US) clinical gold-standard MEDOPOR. 3DPed StarPore scaffolds exhibited significantly higher tissue ingrowth without foreign body reactions *(Figure 224)*.

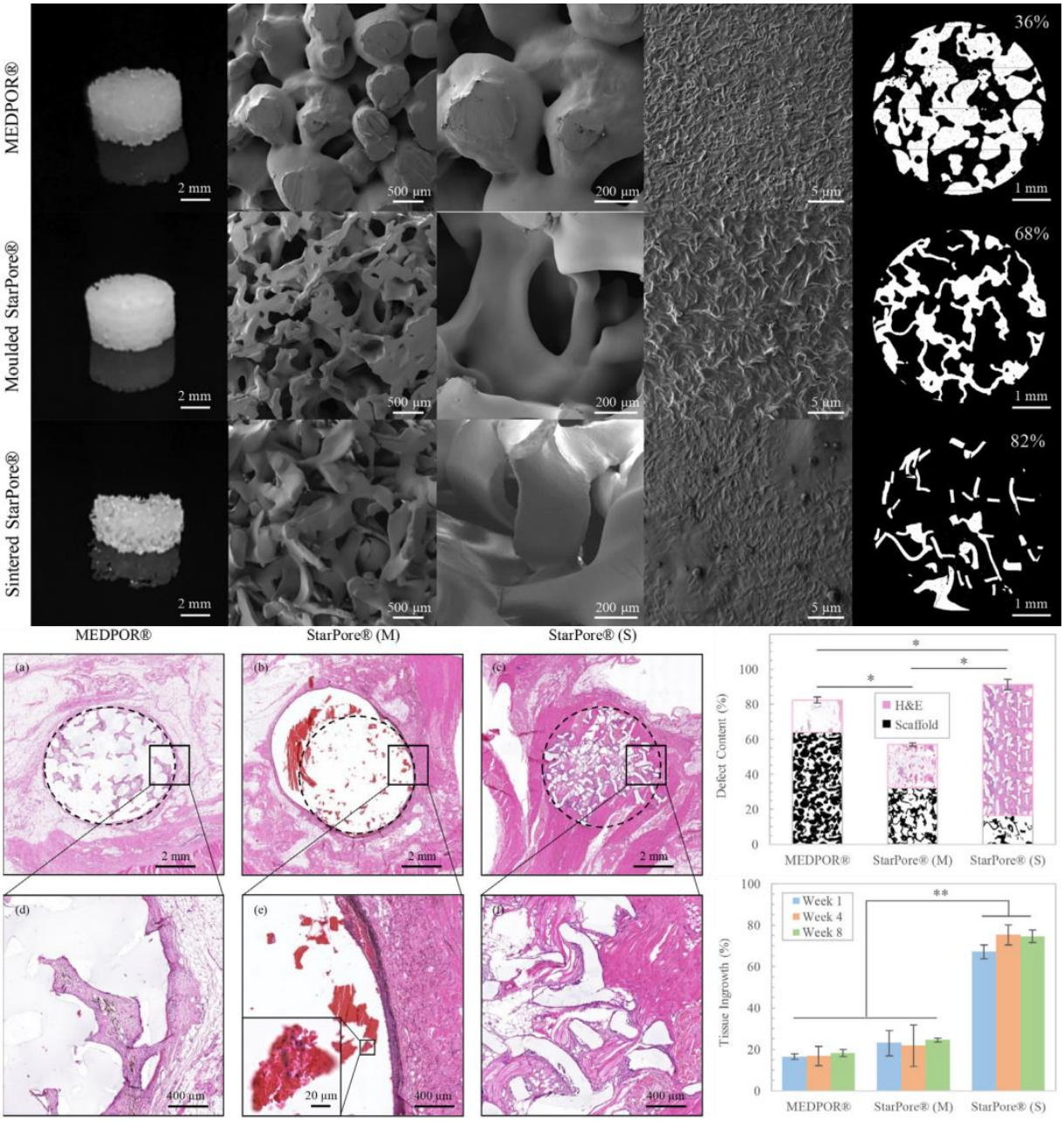

Figure 223: Metal, polymer, and ceramic 3DPed biomaterials for bone scaffolds. Source: (Chen et al., 2020)

Dall'Ava et al. *(2019b)* analyzed and compared different beam-based foam designs of 3DPed acetabular cups from multiple manufacturers (Delta TT, Trident II Tritanium, Mpact 3D Metal). Later, Dall'Ava et al. *(2020)* compared the performance and the porous structure morphologies (Coordinate-measuring machine (CMM), SEM, micro-CT) of 3DPed Ti acetabular cups with conventionally made ones. The median porosity, pore size, strut thickness, and thickness of the porous structure were 72,3%, 915 μm, 498 μm, and 1,287 mm respectively. The median bony attachment was 84,9% and 69,3% for 3DPed and conventional cups respectively. It should be noted that the authors were concerned about the presence of partially molten particles on the 3DPed cups.

Metal Materials	Particle size	Layer thickness	Laser power	Laser scanning speed	Printing system	Applications
Titanium (Ti)	<45 μm	100 μm	120 W	200 mm s^{-1}	SLM	Rabbits, bone[41]
Ti6Al4V	30 μm	≈100 μm	Not mentioned	Not mentioned	EB	Biomedical prototypes[42]
TiTa alloy	44 μm	50 μm	360 W	400 mm s^{-1}	SLM	Mechanical properties[43]
Nb coating Ti alloy	Nb 15–125 μm Ti grade 2	40 μm	160 W	200 mm s^{-1}	SLM	MC3T3-E1 cells[44]
CoCr alloy	Not mentioned	Not mentioned	Not mentioned	Not mentioned	SLM	Mouse 3T3 fibroblasts[45]
Zr doping CoCr alloys	25–150 μm	70 μm	Not mentioned	5.5 mm h^{-1} (building rate)	EB	Rabbits, bone[46]
Fe	3–27 μm	Not mentioned	Not mentioned		3DP	Mouse fibroblast 3T3 cells[47]
Fe–Mn alloy	<10 μm	100 μm	Cured at 230 °C for 3 h Sintered at 1200 °C for 3 h		3DP	MC3T3-E1 cells[48]
Fe–Mn–Ca alloys	5–30 μm	Not mentioned	Cured at 200 °C for 2 h Post heat treated at 430 °C for 0.5 h, 620 °C for 0.5 h, and 1200 °C for 3 h		3DP	MC3T3-E1 cells[49]
Mg–Zn–Zr alloys	60–70 μm	100 μm	Not mentioned		3DP	Mechanical properties[50]
Mg–Ti alloy	Not mentioned	100 μm	Cured at 150 °C for 2 h Post treated at 600 °C for 1 h and at 1200 °C for 2 h		3DP	Mechanical properties[51]

Polymer Materials	Layer thickness	Printing system	Raw materials/Printing parameters	Applications
PLA	100 μm	FDM	PLA filament Heating temperature near is 186 °C	Biocompatible with HBMSC[70]
PLA/polyethylene glycols (PEG)	N/A	3DP	PLA/PEG in chloroform solution. The syringe temperature was 40±5 °C	Modulating scaffold degradation and increasing surface wettability[71]
PDLLA	50 μm	SLA	Liquid PDDLA resins irradiated with 365 nm UV-light (intensity 3–4 mW cm^{-2}) for 15 min	Scaffolds improved the proliferation rates of MC3T3[72]
PDLLA-PEG-PDLLA	15 μm	SLA	Liquid DLLA-PEG resin Blue light (wavelength 400–550 nm, Light intensities of 20 mW cm^{-2}). Curing time was 32.5 s per 15 μm thick layer	Cultivation of hMSCs[73]
PCL	100 μm	SLS	PCL particle size of 10–100 mm Scanning the laser at 4.5 W power and 1.257 m s^{-1} scan speed	4 weeks post implanted in mice, new bone could be found in the scaffold pores.[74]
PLGA	N/A	3DP	Dispense pressure was ≈600 kPa and the speed was 80 mm min^{-1} at 135 °C	Rabbit rotator cuff repair[75]
PLGA/tetraglycol	200 μm	3DP	PLGA solution Flow rate was 0.05–0.12 μL s^{-1}	Both microporous and hollow fiber biocompatible scaffolds[76]
PEEK	200 μm	FDM	PEEK filament Nozzle temperature and extrusion rate were 400–430 °C and 2.2 mg s^{-1}, respectively.	Human bone structure[77]

CaP-based materials	Particle size [μm]	Binder type or curing method	Printing system	Post-treatment	Applications
α/β-TCP	20–30	5–30% H_3PO_4	3DP	Post-hardening 3 × 30 s in 20% H_3PO_4	56 weeks post implantation in femoral extensor muscles[114]
TTCP or HA	5–10	10% phosphoric acid and 1 M NaH_2PO_4	3DP	Stored in 10% H_3PO_4 for 30 s and immersed in 2.5% Na_2HPO_4 solution at 37 °C for 7 s	TTCP scaffolds had little tissue growth[115]
α-TCP	Not mentioned	8.75% H_3PO_4 + 0.25% Tween 80	3DP	Select scaffolds coated with PLGA	Scaffolds improve the outcomes of an implant-related bone infection in mouse[130]
Mixture of α-TCP and HA	30–150	10–20% H_3PO_4+0.25% Tween 80	3DP	Dipping in 0.1% H_3PO_4	Enable bone ingrowth in a critically sized murine femoral defect[131]
β-TCP	14–79	10% H_3PO_4	3DP	0.2 M Na_2HPO_4 solution was used for wetting ability	Not mentioned[99]
Mesoporous silica/ CPC/rhBMP-2	20–30	10wt% poly(vinyl) alcohol solution	EB	rhBMP-2 in acetic acid solution was dropped onto scaffold	Vessel and new bone formation of scaffolds in rabbit femoral defects[123]
Pasty CPC	Not mentioned	Water	EB	Post-hardening after 4–7 days of incubation at 37 °C	Cultivation of hMSCs on printed CPC scaffolds[124]
CPC	Not mentioned	Water	EB	In a humid atmosphere for 3 days	Scaffolds cytocompatible with hMSCs and maintenance of the bioactivity of VEGF[132]
TCP/HA	Not mentioned	$CaCl_2$ solution crosslinking	EB	Scaffold loaded BMP2 activity factor	Osteogenic differentiation and bone formation of scaffold after subcutaneous implantation in mice[133]
TTCP/β-TCP	<100	25% citric acid	3DP	1000–1400 °C, 6–24 h	MC3T3-E1 cells spread well on the scaffold and protein corrected AP-activity was low.[134]
HA/β-TCP	32–57	20% dextrin and 2.5% saccharose	3DP	1250 °C, 2 h	Osteoconductivity for enhanced bone healing[19]
α/β-TCP	30	5–30% H_3PO_4	3DP	1100–1300 °C, 5 h	High density and compressive strength of >40 MPa[135]
HA/β-TCP	Not mentioned	Acid-hydrolytic modified potato starch powder	SLS	1200 °C, 4 h	This scaffold yielded significant amounts of newly formed bone in heterotopic locations[136]

Figure 224: Biological comparison of 3DPed and traditionally made porous implants. Source: (Paxton et al., 2020)

Dall'Ava et al. *(2021)* investigated (macroscopic and histological analysis) the osseointegration (bone attachment, ingrowth, and bone-implant contact) in retrieved 3DPed and conventionally made acetabular implants with beam-based foam structures, and found greater bone ingrowth and osseointegration in the 3DPed group with 840 μm mean pore size 72,4% porosity *(Figure 225)*.

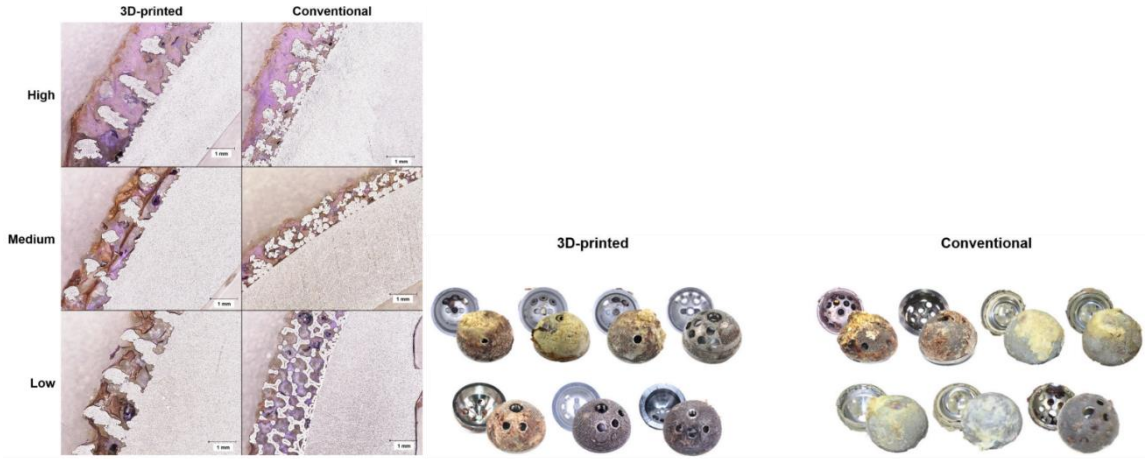

Variable	3D-printed	Conventional
Median age, yrs (IQR)	61.1 (48.4 to 70.9)	66.0 (56.9 to 68.9)
Sex, male, % (n)	29 (2)	57 (4)
Median time to revision, mths (IQR)	24.9 (20.5 to 45.6)	46.3 (34.7 to 49.1)
Median implant diameter, mm (IQR)	54 (50 to 58)	53 (50 to 56)
Median porosity, % (IQR)	72.4 (70.8 to 74.4)	59.6 (55.7 to 71.5)
Median pore size, mm (IQR)	0.84 (0.83 to 0.89)	0.36 (0.23 to 0.52)
Median thickness of porous layer, mm (IQR)	1.30 (1.23 to 1.38)	1.05 (0.95 to 1.63)

Figure 225: Biological comparison of 3DPed and traditionally made porous Ti cups. Source: (Dall'Ava et al., 2020)

Lim et al. *(2021)* studied (radiologically, histologically) differences in bone formation in different pore designs (Dode, Gyroid, Octadens, Solid) of 3DPed porous Ti scaffolds. 25% new bone formed within the pores but no differences among the studied pore designs were observed *(Figure 226)*.

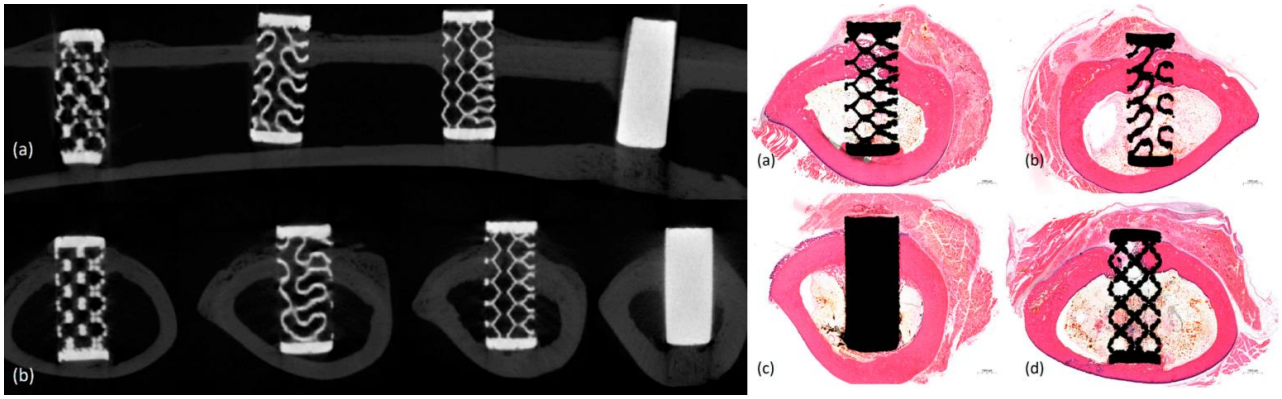

Figure 226: Radiological and histological evaluation of different 3DPed Ti pore architectures. Source: (Lim et al., 2021)

Yang et al. *(2021)* demonstrated that 3DPed rigid polymer/ceramic composite scaffolds with rhBMP-2-eluting collagen sponges can treat extremely large-scale segmental defects in sheep metatarsus fracture models stabilized with intramedullary nails. Bone regenerated after 24 weeks and load-bearing cortical bridging achieved in all animals.

Zhang et al. *(2021)* 3DPed individualized porous implants without any bone grafts, osteoinductive agents, or surface biofunctionalization to treat large bone defects, and systematically studied the long-term therapeutic effects and osseointegration characteristics as shown in *Figure 227*.

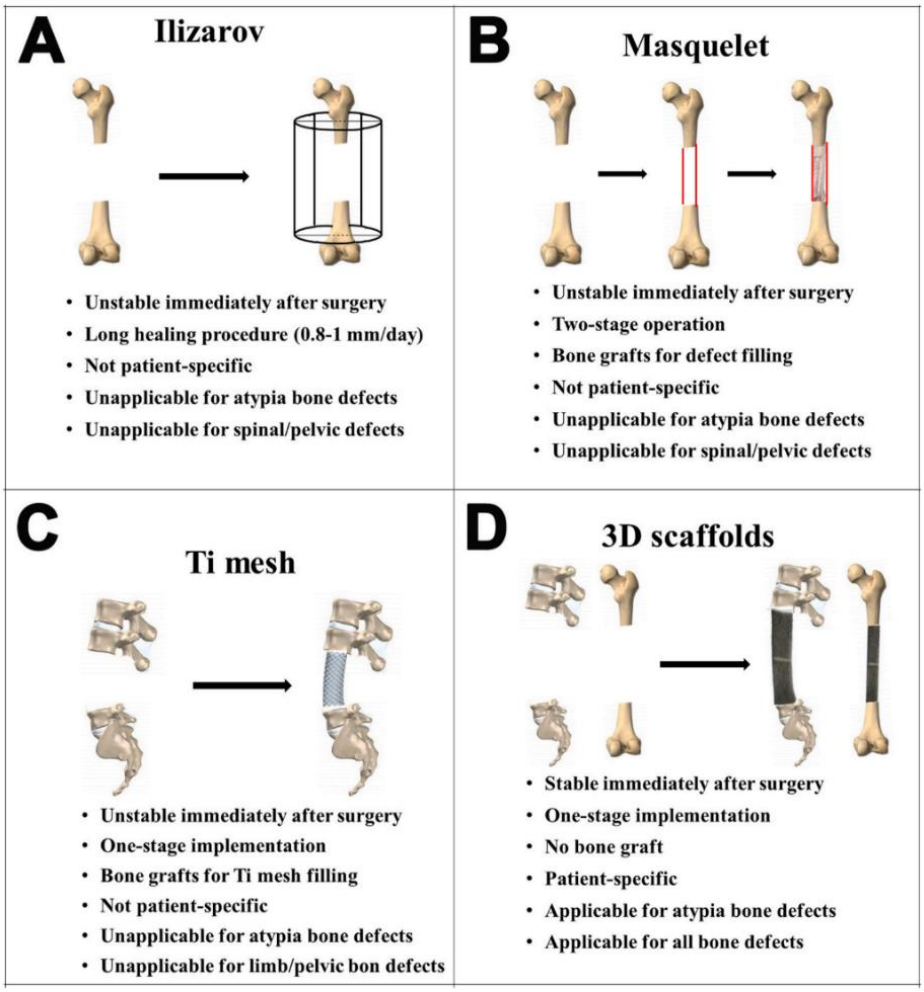

Figure 227: Advantages of 3DPed 3D scaffolds. Source: (Zhang et al., 2021)

Kelly et al. *(2021a)* tested (ovine cortical and trabecular model) osseointegration in 3DPed porous Gyroid Ti implants with 0-90% porosity. Bone formation and remodeling of woven bone within the pores were verified *(Figure 228)*. Regarding the mechanical properties, a linear relationship with porosity, and a non-linear relationship between porosity-interfacial shear strength were observed.

Kelly et al. *(2021b*) assessed Gyroid TPMS-based Ti scaffolds to repair femoral cortical bone defects in rats. Empty Gyroid with smaller pore sizes were shown to repair defects better with up to 38% torsional strength and 54% torsional stiffness of the intact control femur after 12 weeks, whereas the BMP-2 infused Gyroid proved to have better osseointegration with superior torsional strength and stiffness compared to the intact control femur *(Figure 229)*.

Zhao et al. *(2021)* 3DPed porous Gyroids with 90% porosity out of Ti-Ta alloys with a bone-like modulus of elasticity (1,8 GPa) and high compressive yield strength (55,5 MPa) with 3,03% elongation at break. These exhibited enhanced vinculin expression, early cell extension, nuclei density, cell proliferation, and osteogenesis.

Van Horn et al. *(2021)* used in vivo ovine models to assess (micro-CT, histological analysis) the osseointegration of lumbar interbody fusion devices made of Polyetheretherketone (PEEK), Ti and 3DPed porous Ti, and found that 3DPed porous Ti achieved higher bone ingrowth volume.

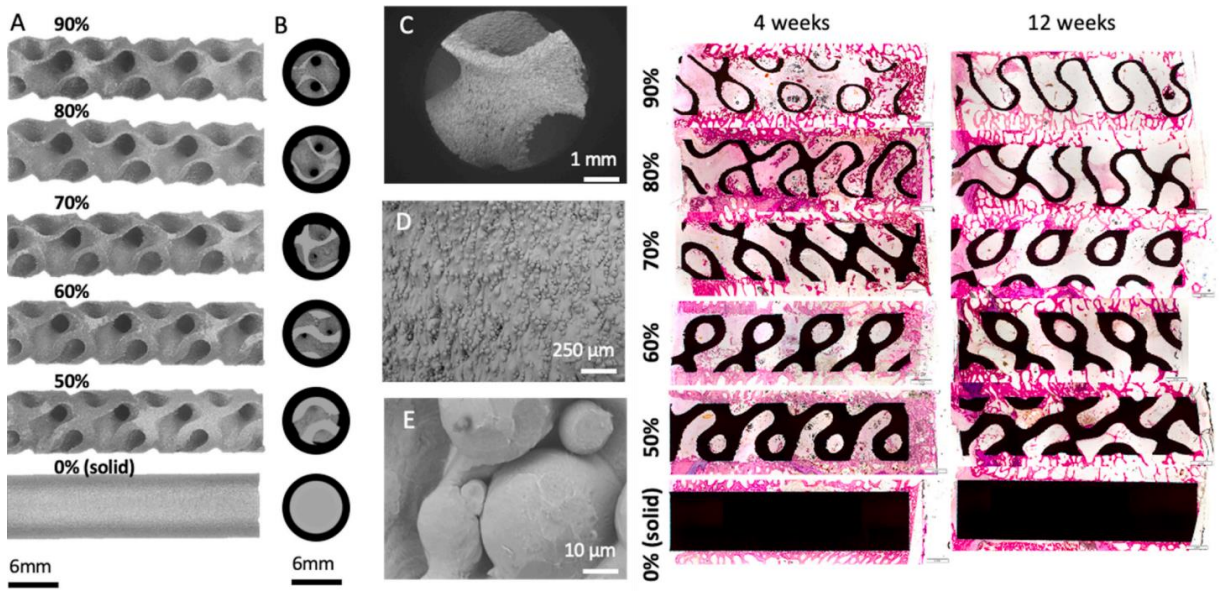

Figure 228: Osseointegration into 3DPed porous Ti with different porosities. Source: (Kelly et al., 2021a)

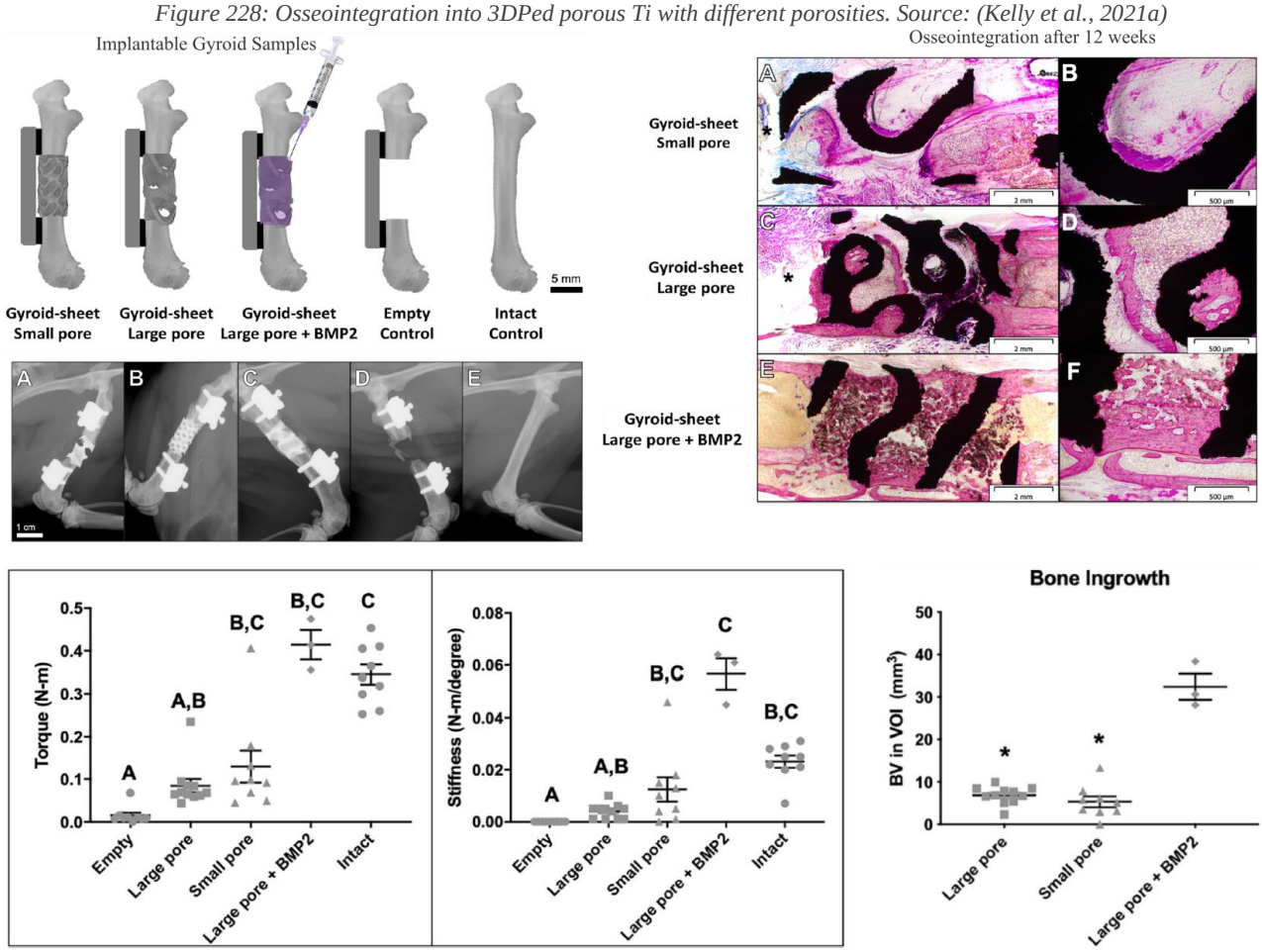

Figure 229: Mechanical and biological comparison of different Gyroid scaffolds. Source: (Kelly et al., 2021b)

Luo et al. *(2021)* confirmed by in vivo and in vitro studies that porous Ta with 400-600 µm pore size and 75% porosity is conducive to osteogenesis and bone integration.

Porous structures proved to be highly osteocompatible and at the same time susceptible to bacterial adhesion, proliferation, and periprosthetic infection. Diez-Escudero et al. *(2021)* experimented and found an optimum balance between osteocompatibility and antimicrobial effects by silver coating (7 at.% Ag, releasing 3,5 ppm in 28 days) porous 3DPed Ti implants (500-600 µm

pores size and 5-10 μm surface roughness). The authors stressed the need to coat the implants with higher silver contents to protect against fast-growing bacteria.

It is essential for a porous implant that fluids flow efficiently through its voids. Asbai-Ghoudan, Ruiz de Galarreta and Rodriguez-Florez *(2021)* developed an analytical framework to calculate the permeability of sheet-based TPMS structures using CFD, as per the architecture type (Fisher-Koch S (FKS), Gyroid (G) and Schwarz P (SP)), pore size (1, 3, 5, 7,5, 10 mm) and porosity (50%, 60%, 70%, 80%, 90%) *(Figure 230)*. The pore distribution and morphology have to be carefully selected as per the individual's requirements as permeability increases with porosity at different rates for each structure; increasing the porosity from 50% to 90%, led to increased permeability of 6,4, 4,3, and 6,2 times for FKS, G and SP respectively; SP was the most permeable in most cases, however, G was the most permeable for the 50% porosity models. Poltue et al. *(2021)* also conducted CFD analysis to assess the fluid behavior in addition to the other mechanical and biological properties tuning by controlling the geometric characteristics of six TPMSs (Primitive, Gyroid, Diamond, Neovius, FRD, and IWP) and found that the most promising candidates for bone substitution implants were the Gyroid, Diamond, and IWP due to their flexible design space, isotropic elastic property, adequately uniform Gaussian curvature, fluid-induced wall shear stress, and high permeability.

Wang et al. *(2021)* presented 3DPed Ti6Al4V implants with alkali-heat treatment and subsequent hydrothermal treatment to form hierarchical micro/nano surface topographies and studied the osseointegration performance in vivo and in vitro. The hydrophilicity was improved and the HA deposition and mineralization from bone marrow-derived mesenchymal stromal cells (BMSCs) was accelerated.

Ren et al. *(2021)* applied ultrasonic acid etching and anodization modifications on PBF 3DPed Ti6Al4V implants to create submicron grooves and nanotubes so that osteoblast responses are activated through certain signaling pathways. The obtained hierarchical micro/nano-structure improved hydrophilicity and biological activity. In vitro cell culture experiments showed increased conducive to cell adhesion and expansion, promoted cell proliferation, and enhanced cell differentiation. In vivo experiments in rats showed increased new bone formation and excellent direct bone connection. The authors underlined that physical morphology and surface chemistry are interdependent: altering the surface morphology will inevitably change chemical composition.

Liu et al. *(2022)* studied (X-ray, micro-CT, histological analysis) the osseointegration of PBF 3DPed Ti6Al4V cement-less tibial prostheses in sheep knee joints by modifying metal surfaces with a three-partition trabecular-like porous structure. Favorable pre-osteoblasts proliferation and differentiation, improved osseointegration, and strong biological fixation were observed.

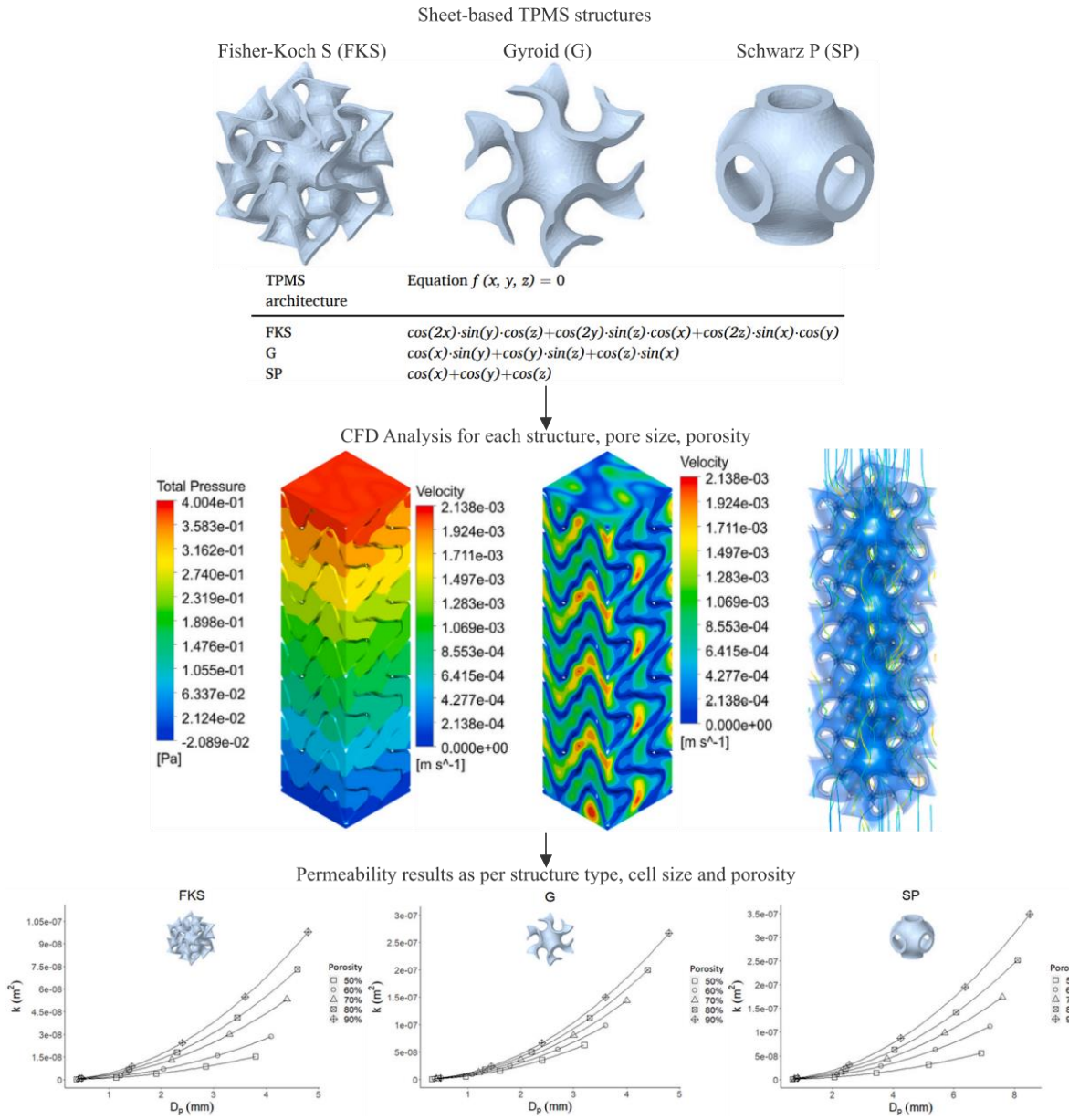

Figure 230: Permeability of different unit cells, pore size, and porosity

Source: (Asbai-Ghoudan, Ruiz de Galarreta and Rodriguez-Florez, 2021)

Gu et al. *(2022)* conducted a systematic review to evaluate the osteogenic potential of 3DPed Ti6Al4V scaffolds for repairing long animal bone defects. They found that 500-600 μm pore size and 60-70% porosity were the most ideal parameters, whereas both dodecahedron and diamond unit cells promoted osteogenesis.

Jia et al. *(2023)* implemented PEEK/Ta-15 Gyroid structures in cages with cervical vertebra-matching mechanical properties and microparticles to obtain biomimetic gradient porous micro-structures with high surface energy to guide biological activities and promote new bone formation and penetration for accelerated osseointegration.

Deering et al. *(2023)* assessed Ti6Al4V Gyroid structures in vitro for cytocompatibility and in vivo for osteogenesis. After 12 weeks, bone formed unidirectionally, and infiltration of bone marrow occurred.

High porosity provides sufficient space for cell migration and circulation of nutrients and oxygen which are essential for bone ingrowth, osseointegration, and new bone formation. On the other hand, mechanical properties and the load-bearing capability are lowered. This is not necessarily a drawback but rather an advantage as long as the obtained porous structure has mechanical performance close to the host bone. Therefore, porous structures should possess balanced structural and micro/nano architectural characteristics for optimal mechanical and biological performance, whilst being tailored to the anatomical area to be implanted and as per the individual patient's status. For this reason, workflows under appropriate frameworks conforming to harmonized standards, guidelines, and QMS should be established. Such workflows could be coupled with databases/libraries of worked cases and approved designs from which the most suitable could be sourced as a paradigmatic reference for each unique musculoskeletal case.

3.6.3 Challenges and Defects in 3D Printing Biomimetic Designs

As discussed in *Sub-section 1.4*, numerous frontiers hinder the wide adoption of PoC 3D digital design and 3DP. Although 3DP is the most promising method for materializing topologically optimized and customized complex structures such as cellular solids, 3DPed parts suffer from technical flaws that depend on many factors *(see Sub-section 3.3.6)*.

Not all cellular solids share the same mechanical and biological behavior *(see previous Sub-sections)*. For example, the strength and fatigue performance of a given porous form depends not only on the material's properties, porosity, pore size, beam thickness, and geometry of cells per se and geometric arrangement of cells but also on the staircase effect and other internal defects caused by 3DP *(Maconachie et al., 2019)*. However, by heat and hot isostatic post-treatments, the fatigue properties can be improved at the cost of increased brittleness *(Benedetti et al., 2021)*.

The characteristics of the designed porous architecture (porosity, pore size, strut thickness, geometric arrangement) have to satisfy optimal mechanical (implant-bone modulus of elasticity matching) and biological (osseointegration) specifications whilst conforming to the processability limitations of the available manufacturing equipment (3D printer). This mechanical-biological-manufacturing triad of constraints defines the allowable design space for cellular architectures which graphically emerges by a commonly shared area as shown in *Figure 231* and also shown in the previous *Figure 186* and *Figure 198*. *Figure 231* is qualitative as the mechanical properties for stiffness matching and the manufacturability (3DP) depend on the selected material and on the 3DP technology and post-processes to be applied which should take into consideration not only the minimum feature size but also the de-powdering of the non-sintered powder.

Various 3DP technologies are being deployed for orthopaedic device manufacturing but the protagonists for high-end (non)implantable parts *(see Sub-section 3.5 and Appendices B and J)* are

mainly based on metal PBF, e.g. Electron Beam Melting (EBM) and Laser Beam Melting (LBM). Herzog et al. *(2016)* have reviewed in detail the fine-grained microstructural and other resulting properties of metals made with PBF technologies, whereas Murr *(2015)* verified that the residual properties of powder-bed fused biomaterials are as good or even better than conventionally manufactured products.

On the other hand, PBF 3DP techniques have technical limitations regarding the lowest 3DPable limits such as minimum truss thickness and fillet radii, and these have to be considered during the design phase of cellular structures *(Benedetti et al., 2021)*. Each cell type *(Figure 172)* presents its own unique set of challenges for 3DP, e.g. stochastic foams such as Voronoi-generated have numerous overhanging beams that might be at non-self-supporting angles (*McGregor et al., 2021a*), whereas self-supporting lattice structures such as TPMS is of high interest compared to long slender beams that might cause manufacturing errors or require supports *(Benedetti et al., 2021)*.

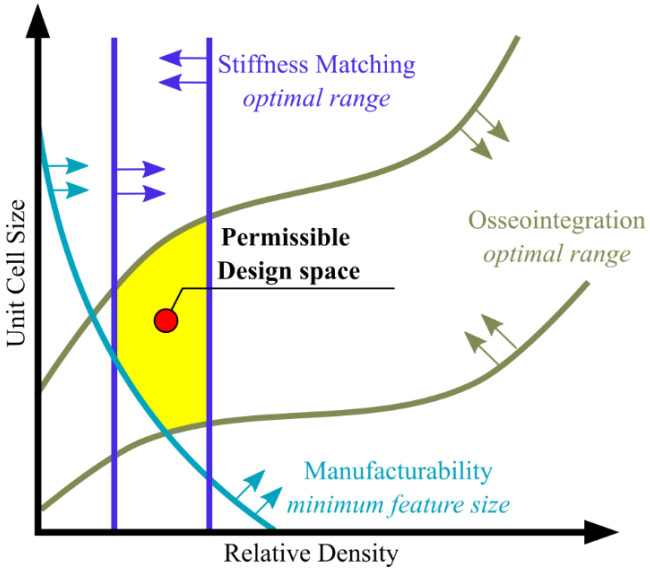

Figure 231: Permissible design space of cellular solids for 3DP

EBM and LBM are capable of producing cellular solids with 70% porosity and 0,3-0,6 mm pore size, with LBM being superior in terms of achievable details and less sintered unmelted powder particles attached to the cellular structure *(Gruber et al., 2020; Park et al., 2022). Figure 232* shows SEM views of the same lattice structure with a 2 mm unit cell size made by EBM and LBM where the sintered unmelted powder particles attached to the beams are shown. LBM can form Ti6Al4V into 0,1 mm thin walls, but overhang structures require a minimum thickness of 0,3 mm with low-power and low-speed parameters as increasing the inclination angles creates more defects *(Wu, Narra and Rollett, 2023)*.

It is worth mentioning that multi-scale, multi-physics phenomena occur during PBF 3DP as illustrated in *Figure 233*. During PBF of cellular solids, as grains are formed, trying to follow the beams at nodes, they intersect diagonal or horizontal edges, thus creating candidate crack initiation topologies with poor performance. In addition to the well-known poor dimensional accuracy and

surface roughness, and stair-stepping phenomenon of 3DPed products, selecting and applying sub-optimal processing parameters might lead to increased structural defects and have severe implications on the final properties and performance. It is therefore critical that process parameters are always optimized according to the scope of their application as they affect the final properties of powder-bed fused parts *(see Figure 88 and Sub-section 3.3.6) (Spierings, Herres and Levy, 2011; Hrabe and Quinn, 2013; Zhang et al., 2014b; Wauthle et al., 2015b; Cheng, Shrestha, and Chou, 2016; Maconachie et al., 2019; McGregor et al., 2021a, Chen et al., 2021)*, i.e.:

- Laser/electron beam parameters*:* spot size, power, pulse duration.
- Layer scanning strategy: scanning path (pattern, spacing), speed.
- Build orientation, layer thickness, and support structures.
- Build chamber temperature and temperature uniformity.
- Melt pool size, which is affected by the laser/electron beam power and scanning speed.
- The characteristics, mechanisms, performance, condition, and monitoring of the 3D Printer.
- Feedstock material: powder morphology, particle size and distribution, chemical composition, and quality that depend on powder production technique and influence flowability, packing density, and thermal conductivity.

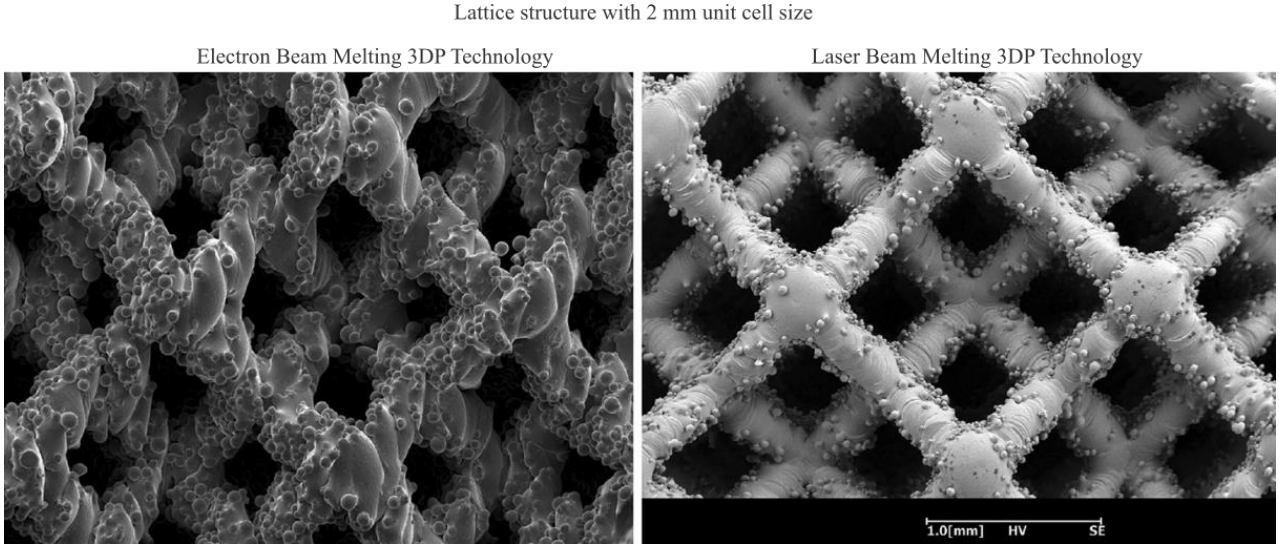

Figure 232: Sintered unmelted particles on lattice produced by EBM and LBM. Source: (Park et al., 2022)

Defects of 3DPed cellular solids can be categorized as *(Lowther et al., 2019; Echeta et al., 2020; McGregor et al., 2021a; Benedetti et al., 2021; Davoodi et al., 2022; Mostafaei et al., 2022)*:

- **Geometric:**
  - Dimensional inaccuracies:
    - On the unit cell's strut: waviness, thickness variations, varying cross-sectional shape, cross-section eccentricity, over/under-sized, missing strut.
    - On the unit cell's node: irregular geometry, parasitic mass, missing node.
  - Surface roughness:

- Raw powder particles (non-fused) on the boundary of beams. If unfused powder particles are released within the human body, infections might occur.
- Orientation based: stair-stepping effect.

- **Microstructural:**
  - Internal/external defects and pores:
    - Feedstock powder related: pores and trapped gas in feedstock powder, pores created due to feedstock contamination and oxidation, powder spreading dynamics, and anomalies.
    - Processing-induced pores: metallurgical pores, incomplete melting and lack of fusion, keyholing, spattering, balling, microstructural inhomogeneities and impurities, loss of allowing elements, and formation of columnar grains.
    - Post-processing defects: thermally induced porosity, chemically induced material loss.
  - Material property imperfection:
    - Deformation of strut or node: notches or distortions.
    - Residual stresses due to significant uncontrolled thermal gradients might lead to microstructure changes, cracks, and delamination.

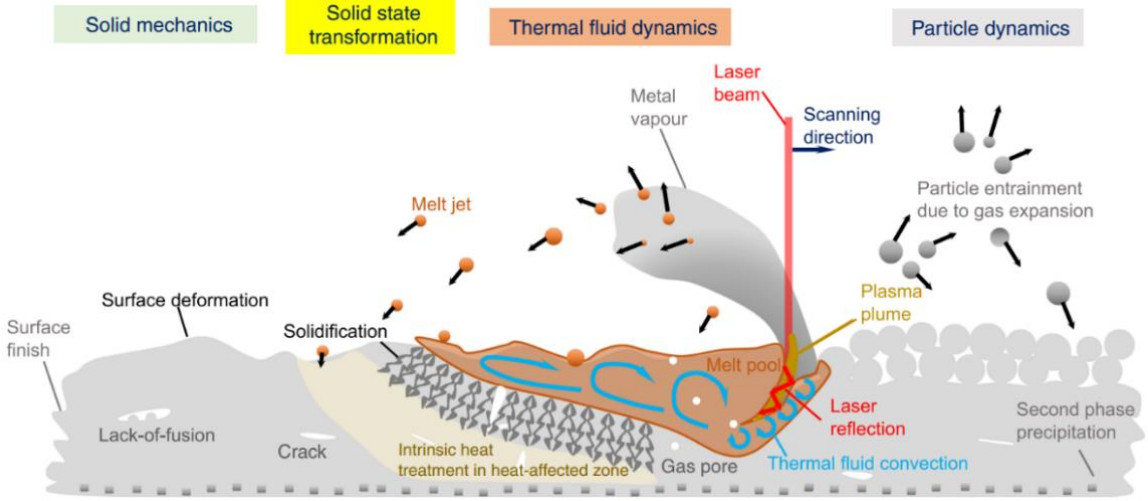

Figure 233: Multi-scale, multi-physics phenomena during PBF 3DP. Source: (Panwisawas et al., 2020)

Although structural micro-cavities within 3DPed acetabular cups have not been reported to cause failures, they are present in PBF 3DP technologies *(Hothi et al., 2019)*. Such and other common structural and geometrical defects that significantly degrade the structural integrity of metallic parts 3DPed by PBF technologies are illustrated in *Figure 234*.

Emphasizing on optimized porous biomaterials, Melancon et al. *(2017)* presented morphological and mechanical property maps (pore size, porosity, strut thickness, topology) to facilitate visualization and prediction of property shifts between as-designed and as-3DPed products. Barba, Alabort and Reed *(2019)* have shown the deviations between the as-built and as-designed TPMSs more than 0,1 mm as shown in *Figure 235*. Similar works were published by Naghavi et al. *(2022)* who studied the morphological deviations between as-designed and as-3DPed cellular parts and

reported that strut thickness was greater and pore size was less than the designed values respectively. The authors suggested developing design compensation strategies to compensate for such deviations.

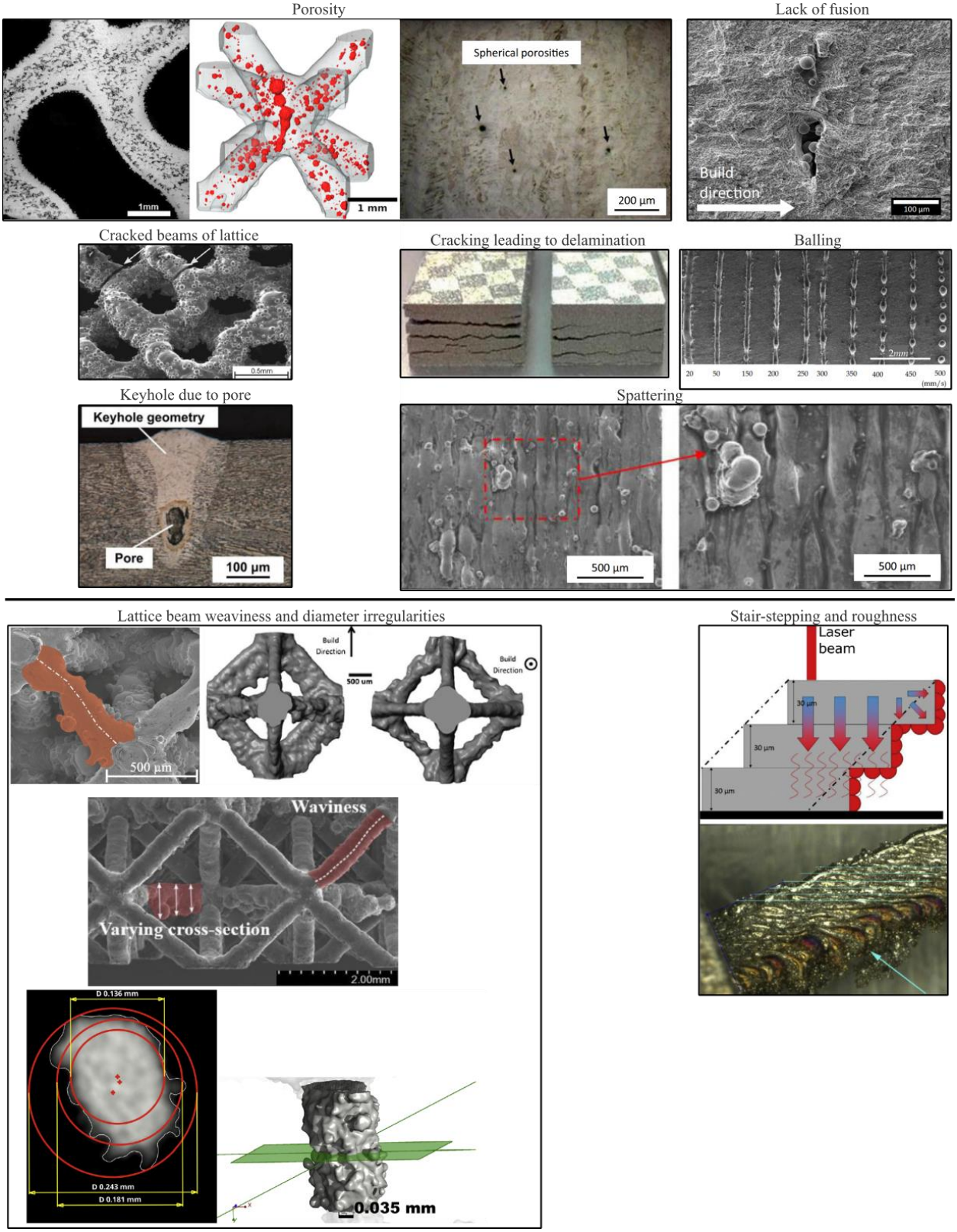

Figure 234: Structural and geometric defects of metallic parts 3D printed by PBF technologies. Source: (Benedetti et al. 2019, Kelly et al., 2019; Echeta et al., 2020)

Dallago et al. *(2019)* published an article on the effects of geometrical defects and residual stresses on the mechanical behavior of 3DPed porous (regular cubic cells) specimens: morphological

deviations had a complex influence on the modulus of elasticity, fatigue resistance was more sensitive to surface irregularities than internal porosity, but also affected by residual stresses, even after stress relief heat treatment.

Echeta et al. *(2019)* presented a review of design constraints, process parameters, post-processing, measurement methods, and defects in porous structures produced by PBF 3DP processes: dimensional inaccuracies, surface quality, and porosity.

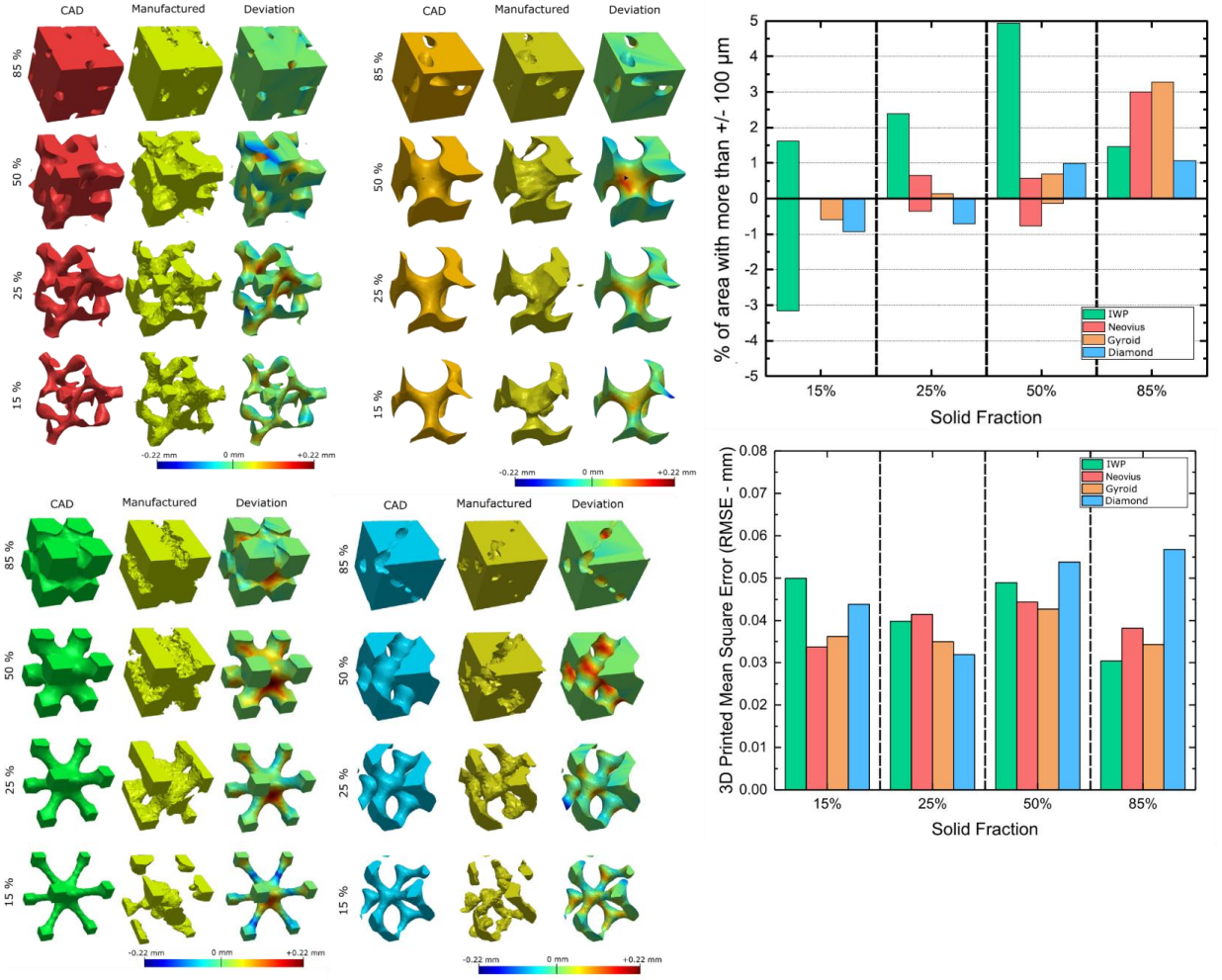

Figure 235: Geometric errors of as-built compared to as-designed TPMSs. Source: (Barba, Alabort and Reed, 2019)

Moussa et al. *(2021)* developed a general framework to assess the role of process-induced geometric defects and parameters that impact the mechanical properties and optimum design of 3DPed cellular solids. Defects can reduce the modulus of elasticity by as much as 25%.

As with fully dense 3DPed parts, cellular 3DPed parts also suffer from the anisotropic modulus of elasticity and strength that depends on build orientation. Munford et al. *(2020)* utilized a tensorial form of power-law relationships to predict the apparent modulus and strength, based on structure density and fabric. Their model was validated for stochastic foams and rhombic dodecahedron lattices against mechanical tests across many orientations *(Figure 236)*.

There are literature gaps on the suggested methods and analysis of entrapped powder that fills the voids within porous metallic parts 3DPed by Laser or Electron PBF technologies. Depending on the

powder morphology (particle size) and the 3DP technology used, as the pore size of the porous structure decreases and the channels get long and narrow, the removal of entrapped powder becomes more challenging. For EBM technologies the powder particle size used is larger than the size used in LBM technologies, plus the fact that during EBM the powder is pre-heated at high temperature, thus binding the particles to each other, making the removal more difficult. On the other, EBM prevents the formation of brittle martensite grain phases in metals and produces more ductile and more dense parts which is a plus compared to LBM technologies *(Khrapov et al., 2023).* Exit holes must be implemented to allow de-powdering. Possible techniques are brushing off, air-jetting and blasting with inert gas, bead blasting with various media, heat treatment for sintering the loose powder, Dry Ultrasonic Vibration (USV) or Wet-USV, Chemical Etching (CE), mechanical vibration *(Seiffert, Hopkins, and Sutcliffe, 2017).*

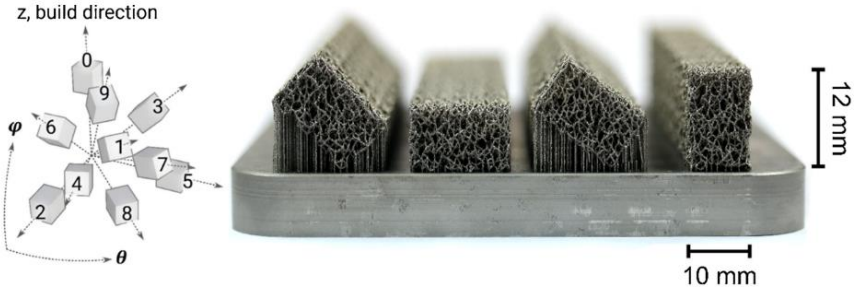

Figure 236: 3DPed cellular solids with different build orientations. Source: (Munford et al., 2020)

Khrapov et al. *(2023*) assessed the air jetting Powder Recovery System (PRS), USV, and CE techniques to remove residual powder from the pores of sheet-based TPMSs made by EMB (*Figure 237*) and evaluated their impacts on the end properties. They found that CE affected the wall thickness and etched away subsurface pores whilst deteriorating the mechanical properties, whereas USV achieved no accumulation of particles, accompanied by slight morphology and microstructural changes. The authors suggested the use of USV in combination with CE but noted carefulness with skeletal TPMSs or beam-based designs due to their lower mechanical integrity.

3DP is a primary forming manufacturing process, hence flaws such as the poor surface finish and dimensional inaccuracies, should not be considered necessarily drawbacks because usually finishing post-processing follows *(Longhitano et al., 2015; Wohlers Associates, 2021b)* to meet the final product's specifications, not to mention that surface roughness might be beneficial for orthopaedic implants. 3DPed implantable porous structures are usually post-processed and surface modified to improve the required bimodal function they have to perform: mechanical characteristics such as ductility and fatigue strength, and biological responses that occur at the bone-implant interface are strongly affected by the defects induced during the manufacturing process. Before any coating, the usual surface treatments for 3DPed implants include polishing to remove undesired as-fabricated roughness, sandblasting to construct micro-roughness, and (ultrasonic-assisted) acid etching to remove residual grits and further modify the roughness.

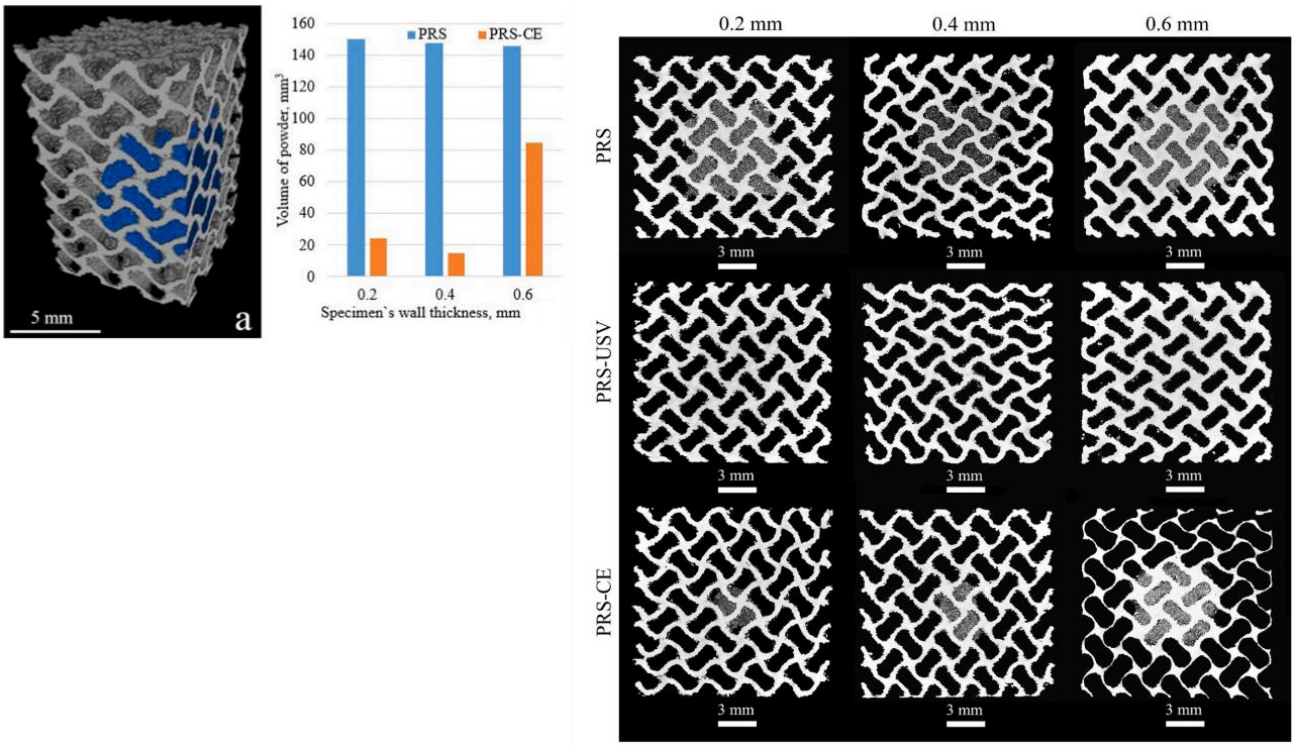

Figure 237: Powder removal from cellular solids 3DPed by EMB. Source: (Khrapov et al., 2023)

Biomimetic interconnected porous designs should be optimized by exploiting the full potential of 3DP utilizing the so-called Design with 3DP (Dw3DP) *(Floriane et al., 2016)*, and at the same time optimized for manufacturability as it is apparent that the development of optimized structures requires the adoption of design rules for ensuring manufacturability by specific 3DP process(es), i.e. design for 3DP (Df3DP) (*Kranz, Herzog and Emmelmann, 2014; Thompson et al., 2016; Schnabel, Oettel and Mueller, 2017; ISO/ASTM, 2018; Diegel, Nordin and Motte, 2019; Leary, 2019)*. Freeform shapes, topology optimization and generative design, internal channels, infill modifications, cellular structures, thin and small features, segmentation and part consolidation, non-assembly mechanisms, embedded components, surface texturing, material choices, and multi-material parts, have associated design parameters that affect *(Vaneker et al., 2020)*. 3DP is comprised of technologies that can fabricate any part with nearly unlimited design freedom but 3DP is not a panacea as it is prone to challenges, especially when cellular structures and fine details are involved. That is why Df3DP frameworks have to be implemented during the product development phases (product discovery, project planning, product definition, conceptual design, product development, and product support) *(Renjith, Park and Okudan, 2019)*.

To minimize technical flaws of PBF 3DP, several methods can be implemented *(Davoodi et al., 2022)*, for example:

- **Process parameters optimization:**
  - Scanning speed and path, remelting.
  - Laser power.

- Layer thickness, build orientation, and support structures.
- Powder morphology, particle size and distribution, composition.

- **Post-processing** *(see Figure 32)***:**
  - Material subtraction: mechanically, laser-based, chemically.
  - Without material removal: mechanically, laser-based, chemically.
  - Coatings, oxidation, anodizing.
  - Heat treatments.
  - Hot isostatic pressing: powerful thermo-mechanical treatment utilized to close internal pores and improve the microstructure.
- **Design strategies and defect simulations:**
  - Thickness compensation strategy.
  - Design constraints.
  - Overhang elimination.
- **In situ process optimization by monitoring and live correction**

Figure 238 illustrates some scan patterns during PBF 3DP and an example of the optimal selection of parameters (laser power and scan speed) for LBM technologies for defect-free product materialization, whereas *Figure 239* shows the beneficial effects of chemical etching, heat treatments, and HIP on the mechanical properties (fatigue strength) and porosity reduction.

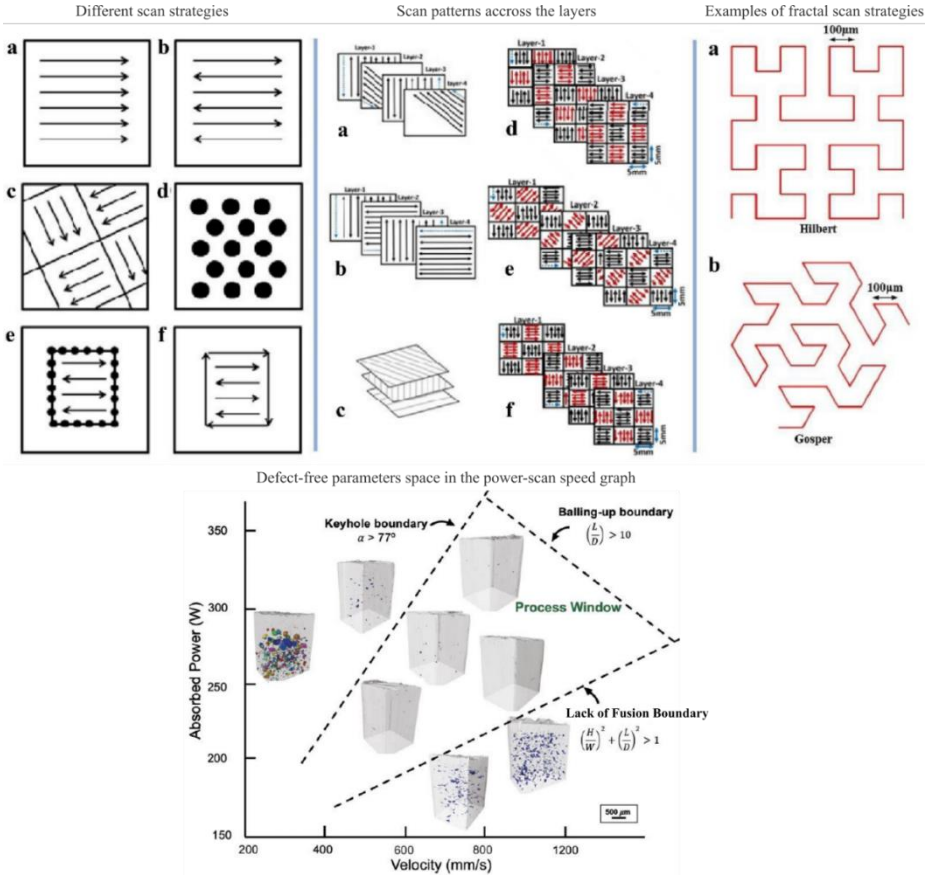

Figure 238: Scan strategies and optimal power-speed parameters for defect-free PBF 3DP. Source: (Mostafaei et al., 2022)

To improve technical flaws of 3DPed optimized components with cellular structures, it is crucial to mitigate manufacturing errors and imperfections. The 3DP process optimization cannot be generalized, as it is not simple to carry it out from one process to the other. Zhang et al. *(2019b)* proposed to implement AI techniques and associated databases with validated cases and worked applications to help in a) in situ design optimization of cellular microstructures and FGMs, and b) diagnostic techniques coupled with feedback control loops to maintain consistent process conditions. Algorithmically driven and machine-learning methods for optimizing geometrical design, process parameter configuration, and in situ anomaly detection will contribute to defect-free 3DP of complex biomimetic porous products *(Jin et al., 2020) (Figure 240)*.

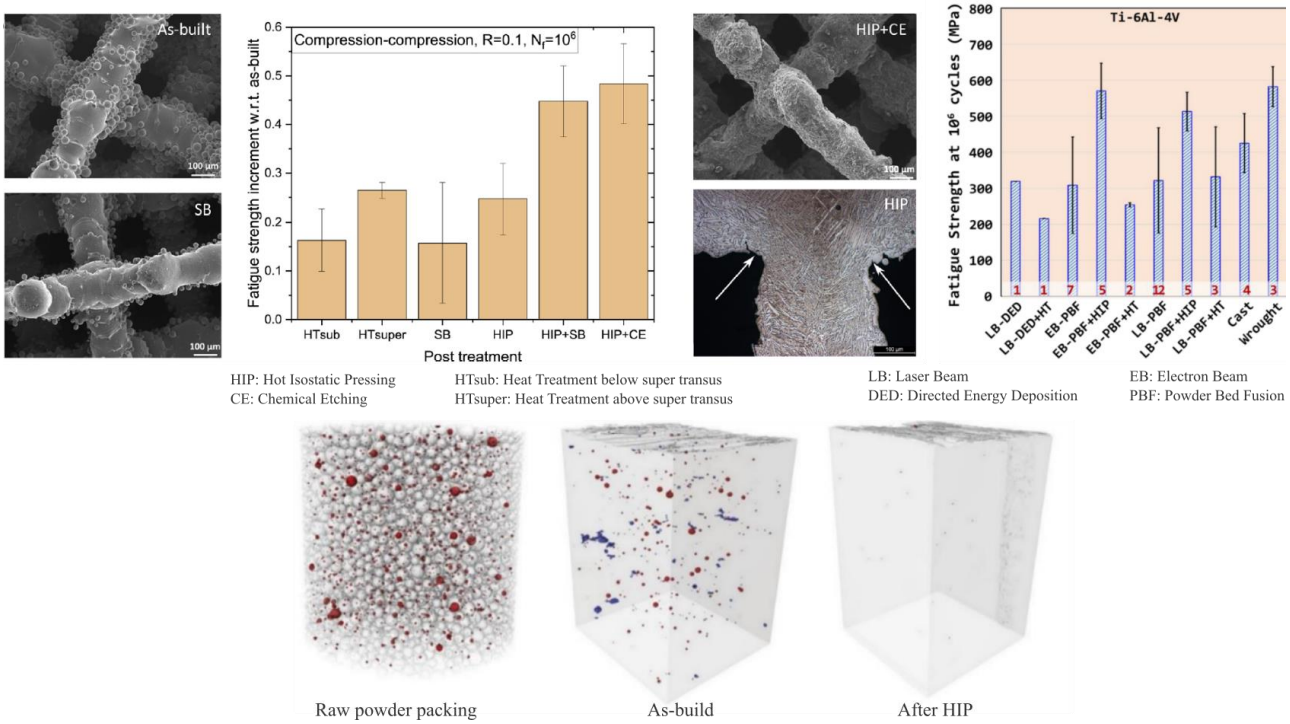

Figure 239: Effects of heat and chemical treatments on PBF 3DPed parts. Source: (Benedetti et al., 2019; Mostafaei et al., 2022)

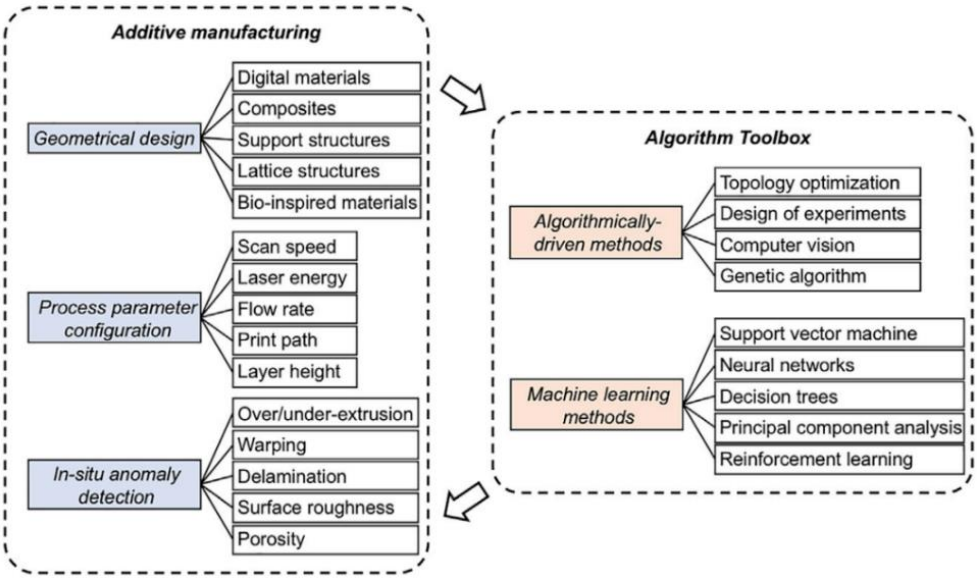

Figure 240: Algorithmically-driven methods and machine learning for 3DP. Source: (Jin et al., 2020)

3.7 xReality in Orthopaedics

Computer-assisted orthopaedic surgery is currently being clinically applied successfully *(Haaker and Konerman, 2013; Sugano, 2018)* thanks to advancements in computer graphics and medical imaging that in turn led to the introduction of Digital Surgery *(Atallah, 2021)* and Digital Anatomy *(Uhl et al., 2021)* to visualize and process the complex spatial relations of the human body in a computer-accessible digital format. This way, the patient's anatomy and artificial parts are generated with powerful new 3D tools that assist clinical diagnosis and better modeling, design, simulation, treatment, and guidance for more efficient rehabilitation strategies and tactics.

xR systems (Virtual Reality (VR), Augmented Reality (AR), Mixed Reality (MR)) are newly inserted tools into the modern cosmos of individualized intelligent digital orthopaedics:

1. **Virtual Reality (VR):** although VR might seem oxymoron due to the contradiction of the two words that synthesize the term, it refers to a completely immersive, interactive, multi-sensory, viewer-centered, three-dimensional real-time computer-generated environments and the combination of technologies required to build and explore these environments *(Cruz-Neira, 1993)*. The term was coined by Jaron Lanier in 1987 and expanded from the entertainment industry to other industries including clinical medicine. VR systems require real-time rendering, real space, and real interaction, and typically involve head-mounted displays (HMD) and audio devices, controllers with position trackers, and haptic feedback devices that stimulate the skin mechanoreceptors to create the sense of touch. The user experiences a feeling of actually being (virtual presence) part of the artificial world which is distinct from the actual physical reality. VR is used in simulation-based medical education and training and for pre-operative planning. Because the user loses sight of their real environment, VR is not applicable for intra-operative applications. VR is being used by the patients per se for pain management, treatments, entertainment, and physical fitness *(Figure 241)*. Example VR systems are shown in *Figure 242* and the immersive environment of a shoulder arthroplasty simulator is shown in *Figure 243*.

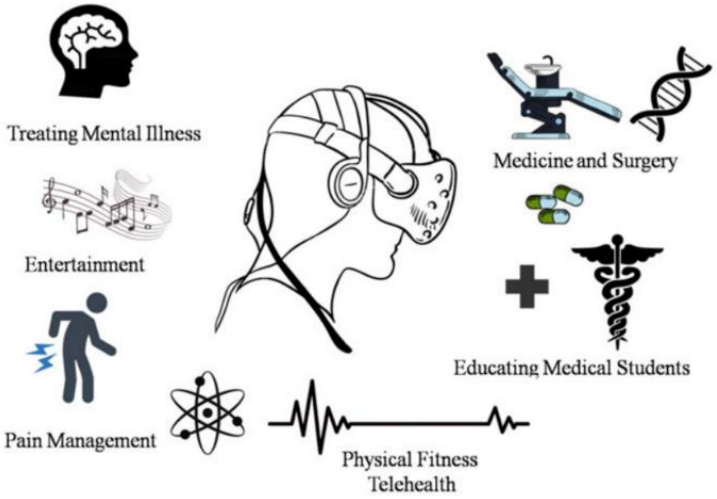

Figure 241: Applications of VR in healthcare. Source: (Gupta et al., 2020)

Figure 242: Example VR Systems

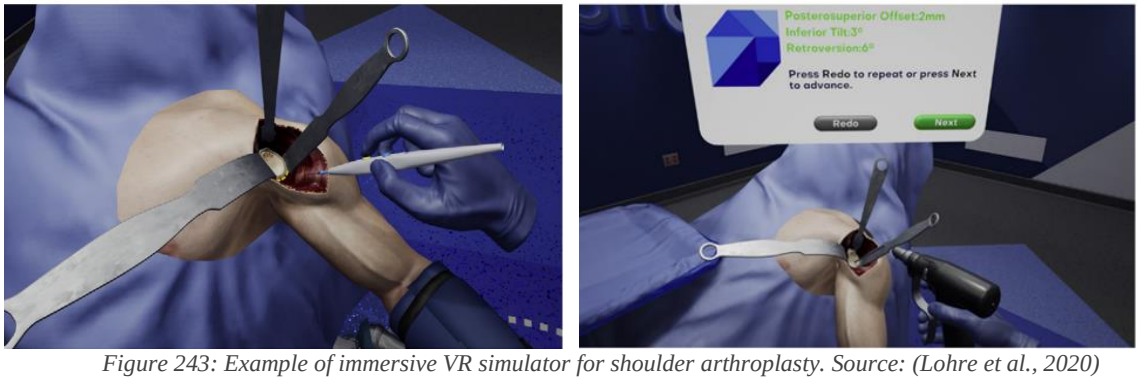

Figure 243: Example of immersive VR simulator for shoulder arthroplasty. Source: (Lohre et al., 2020)

2. **Augmented Reality (AR):** enhances in real-time the real world with virtual computer-generated sensory impressions that appear to coexist in the same space as the real world. It provides a semi-immersive experience by superimposing computer-generated content (text, images, animation) on the user's actual environment. AR systems can be monitor-based display systems, HMD see-through systems, or projection systems (*Figure 244*). AR is not only used in medical education, training, and surgical planning but also in intra-operative execution. In orthopaedic surgeries, a plethora of numeric and geometric parameters are required both pre- and intra-operatively. Using AR, such data can be superimposed on the real-life patient to aid navigation for screw or implant insertions, osteotomies, and correction of deformities. With HMD AR, the surgeon's cognitive load is minimized as the hands and eyes are focused on the operation without attention shifts and averting to ancillary screens that might potentially reduce efficiency and impact accuracy and precision creating a higher chance for surgical error.

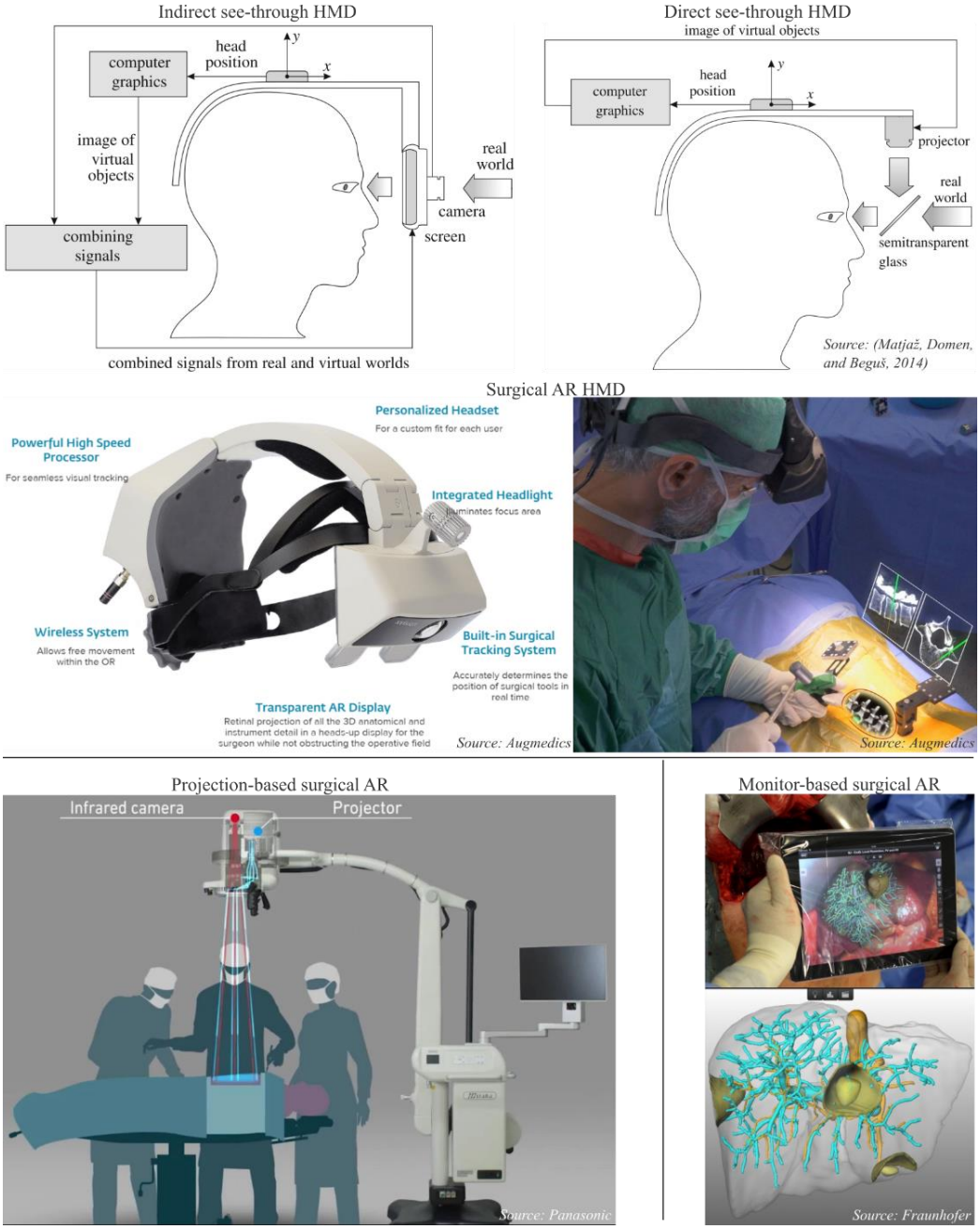

Figure 244: HMD, monitor and projection AR Systems

3. **Mixed Reality (MR):** a hybrid between VR-AR as it complements external reality, whilst adding virtual elements, allowing interaction between objects that coexist in physical and virtual worlds. The computational processing and level of interactivity are much more complex than AR or VR alone. MR equipment and applications are typically similar to AR. *Figure 245* pictures some application examples.

Figure 246 shows the position of VR, AR, and MR in the real physical world, whereas *Figure 247* shows the Reality-Virtuality continuum as described by Milgram and Kishino *(1994).*

In xR systems, there should be a continuous information flow and feedback loops between user-real world-virtual world as shown in *Figure 248*. For the user to experience a realistic (semi)immersive virtual presence, suitable visual, non-visual, or mechanical tracking methods

(Figure 249) have to be implemented, coupled with high-performance rendering of dynamically responsive environments. Marker-based visual tracking provides higher accuracy and precision levels with lower computational demands compared to marker-less tracking, however, the physical markers placement adds time to the workflow. Markers usually refer to spherical objects that actively emit or passively reflect IR light, or have a unique shape for easy registration.

Figure 245: MR applications examples

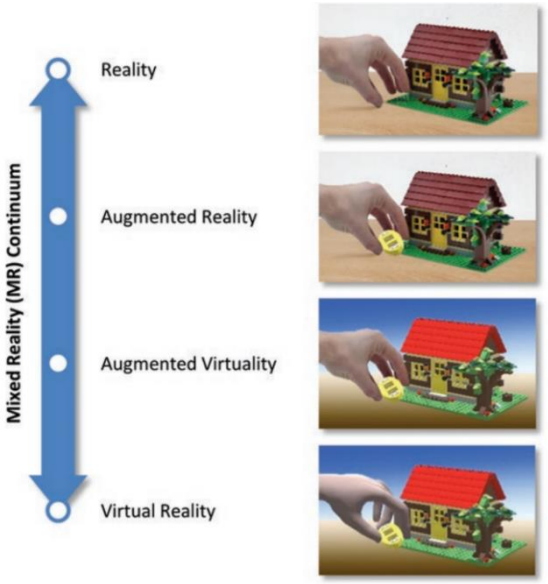

Figure 246: VR, AR, and MR about the physical world. Source: (Verma and Sudip, 2022)

Steinicke *(2016)* gave a historical background on the evolution of xR systems from the early 1940s to 2016, highlighting that the ideal virtual experience is still far but as technology advances,

unfulfilled past promises are being covered. As Sutherland *(1965)* stated: *"the ultimate display would, of course, be a room within which the computer can control the existence of matter. A chair displayed in such a room would be good enough to sit in. Handcuffs displayed in such a room would be confining, and a bullet displayed in such a room would be fatal. With appropriate programming such a display could literally be the Wonderland into which Alice walked".*

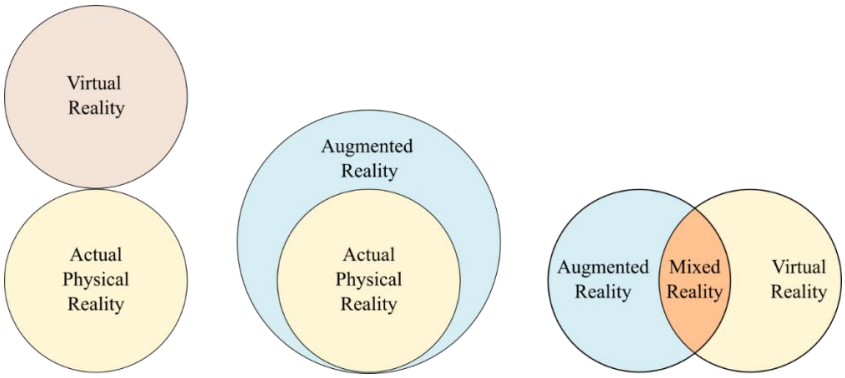

Figure 247: Reality-Virtuality continuum. Source: (Doerner, Broll, Grimm and Jung, 2022) after (Milgram and Kishino, 1994)

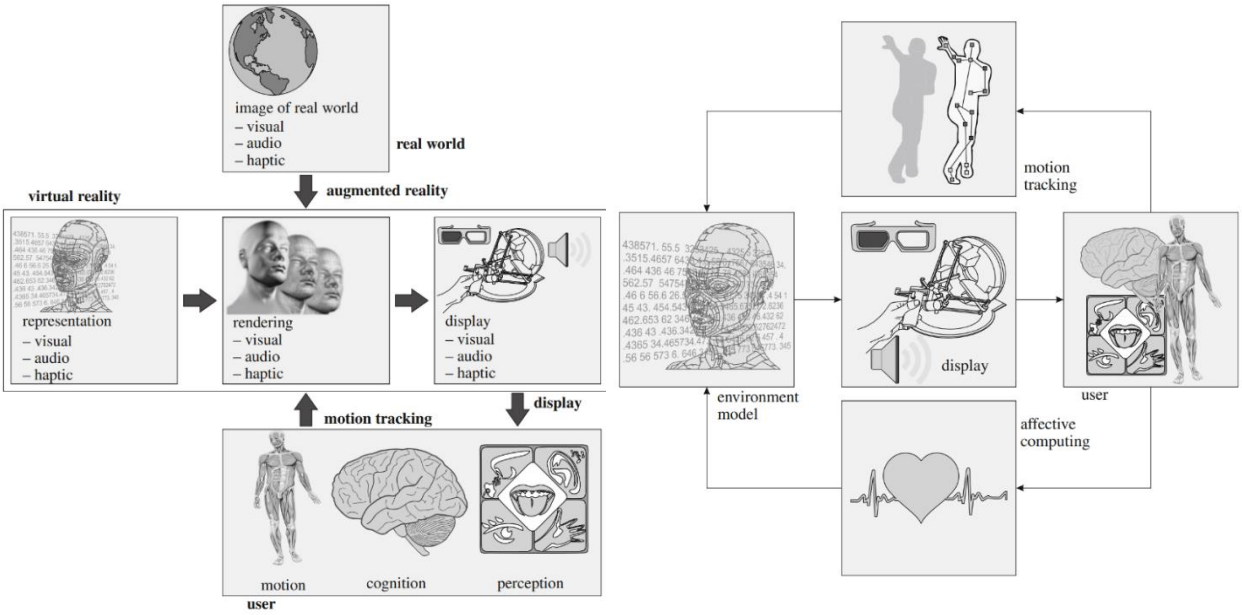

Figure 248: Information flow and feedback loop in xR systems. Source: (Matjaž, Domen, and Beguš, 2014)

Harnessing xR system to create a holographic healthcare metaverse for anatomical visualization, collaboration, and evidence-based insights are among the last frontiers in medical imaging and surgical navigation. Systems such as the *da Vinci Skills Simulator, dV-Trainer, Robotic Surgery Simulator, Robotix Mentor, SEP Robot,* and *Actaeon Robotic Surgery Training Console*, have been used as surgical simulators without offering the experience of the currently available HMD VR solutions where the user is completely immersed into the artificially generated environment, feeling as if actually being present there.

Condino et al. *(2018)* and Viglialoro et al. *(2021)* have presented multimodal medical simulation tools using 3DP and AR/MR to enrich the simulated scenario and guide the learner during the surgical procedure for an interactive and immersive experience.

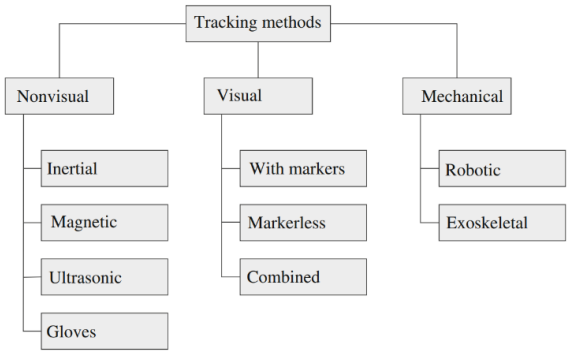

Figure 249: Tracking methods in xR systems. Source: (Matjaž, Domen, and Beguš, 2014)

As computer-assisted surgery methods advance, xR technologies for orthopaedic training, planning, and navigation will evolve hand-in-hand. The ability to visualize patient data in real-time, enhance pre-operative planning, and improve the accuracy and precision of interventions has been demonstrated to improve both treatment quality and patient outcomes *(Verhey et al., 2020).*

Some marketed VR solutions are offered by:

- **Medical Augmented Intelligence:** VR-based software solutions *(BodyMap, AcuMap, DigiTwin)* to transform the field of medical and patient education.
- **FundamentalVR:** created the Fundamental Surgery platform for medical education, skills acquisition, and practice. Delivers multimodal simulation using tethered and all-in-one VR.
- **Karuna Labs:** digital therapeutics programs (KVET Virtual Embodiment Training) to address chronic pain through a combination of physical and cognitive retraining.
- **OxfordVR:** evidence-based psychological treatments using immersive VR technology.
- **Health Scholars:** clinical competency and confidence with protocol-based VR simulation and competency assessment for high-risk care scenarios.
- **ImmersiveTouch:** offers FDA-cleared VR and MR platforms for enhanced surgical planning, training, and collaboration.
- **OSSO VR:** VR training and assessment platform to train on any procedure.
- **SyncThink:** delivers the FDA-approved SyncThink digital health platform for assessing brain health, managing recovery, and optimizing performance.
- **PresicionOS**: develops the FDA-cleared *InVisionOS* solution for immersive training and planning using the Oculus Quest 2.
- **EaseVRx:** an immersive VR system that uses cognitive behavioral therapy and other behavioral methods to help with pain reduction in patients with chronic lower back pain.

Similarly, some AR and MR systems available on the market are developed by:

- **Augmedics:** offers the FDA-cleared AR *Xvision Spine System (Figure 244)* composed of a wireless headset and markers. It allows surgeons to *"see-through"* the patient's anatomy like they had "x-ray vision," and accurately navigate during spine surgery.

- **Apoqlar:** develops the VSI *HoloMedicine* platform that leverages HoloLens 2 to transform medical images, clinical workflows, and medical education into an MR experience to revolutionize how medicine is practiced, experienced, learned, and shared globally (*Figure 245*).
- **MediView XR:** includes the MediView product series that combines AR, telecollaboration, and data-driven insights for diagnostic imaging and surgical navigation.
- **Medivis:** provides the FDA-cleared *SurgicalAR* using HoloLens 2. Medivis also offers *AnatomyX*, an AR anatomy lab and learning platform.
- **SentiAR:** developer of the FDA-cleared *CommandEP* AR system using HoloLens 2. It is a holographic cardiac guidance system used inter-operationally, enabling a real-time, interactive, 360-degree view of the delivered treatment.
- **Proximie:** uses AI and AR to allow multiple people in remote locations to virtually interact as if they are in the same operating room.
- **Proprio:** offers the *Adaptive Registration* technology that synthesizes AI, xR, and robotics for an algorithmic, real-time, multimodal image registration system to improve surgical navigation.
- **HoloAnatomy:** develops the *HoloAnatomy* software suite for students to experience 3D perspectives of every body part.
- **Surgical Theater:** maintains the FDA-approved *Precision MR* for evidence-based visualization to improve surgical planning and navigation.
- **Novarad:** maker of the FDA-approved *OpenSight* AR surgical navigation system.
- **Pixee medical:** FDA-cleared AR-assisted surgical navigation solutions to support total knee arthroplasty (*Figure 250*). The system includes AR glasses combined with reduced-size instrumentation equipped with markers.

The scientific interest in xR technologies has been growing exponentially as evidenced by the increasing annual number of published articles diachronically *(Figure 251)*. xR systems are excellent tools for accelerating and improving the way orthopaedic surgery is practiced today, as they are utilized as alternative tools for decision-making, which can improve both patients' healthcare outcomes and economic value *(Han et al., 2020)*. Indeed, researchers report that xR leads to improved healthcare education, training, and surgical skills acquisition, and outperforms traditional training approaches *(Pfandler et al., 2017; Hooper et al., 2019; Walbron et al., 2020; Gerup, Soerensen and Dieckmann, 2020; Capitani et al., 2021; Yamazaki et al., 2021; Tang et al., 2022)*, not to mention their applications in multidisciplinary and inter-epistemic team meetings for surgery planning *(Kumar et al., 2020)*.

Numerous advantages emerge when using xR training systems *(Figure 252):*

- Risk-free surgical environment with no patients or animals involved.

- Tracking all user actions in a fully-known simulated environment.
- Bench-station examination and objective structured assessment of technical skills forms.
- Students can practice, regardless of operating room or cadaver availability.
- A plethora of different anatomies and pathologies can be practiced in a short time.
- Training on rare and dangerous complications that trainees might not otherwise experience.
- Potential to save costs in education and training.

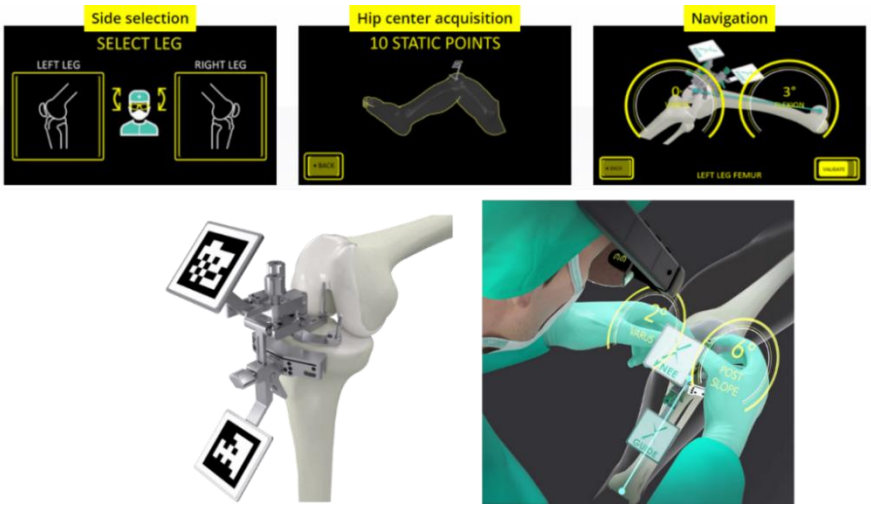

Figure 250: Knee+ AR knee arthroplasty navigation system. Source: Pixee Medical

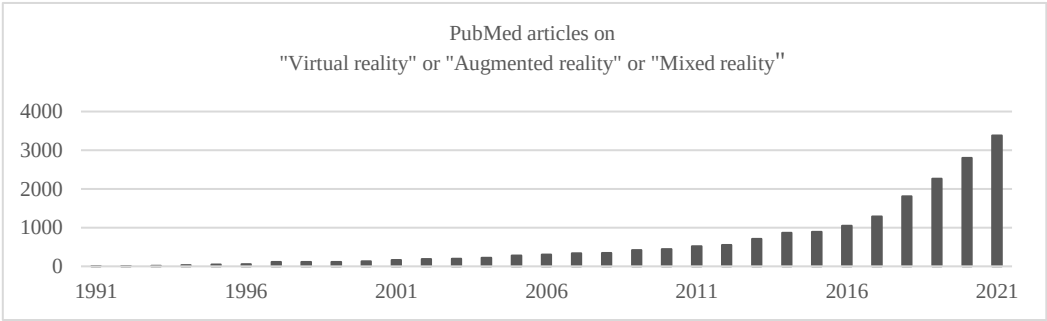

Figure 251: Annually published articles on virtual/augmented/mixed reality on PubMed

Researchers argue that xR technologies represent an exciting trend for a diversity of orthopaedic applications, and their widespread adoption and refinement for daily clinic practice will only accelerate *(Hersh et al., 2021)*. On the other hand, the equipment prices should not be prohibitive and data protection issues have to be addressed for greater penetration *(Verhey et al., 2020)*.

AR/MR technologies have been used on phantom models and cadavers and proved to reduce cognitive load, operative time, and radiation exposure while improving surgical accuracy and precision in challenging conditions. Early trials verified that AR/MR systems for intra-operative navigation and information visualization are promising in complex surgical procedures that require high precision and accuracy: arthroscopy, arthroplasty, osteotomies, orthopaedic trauma, oncology (tumor resection), and spine surgeries *(Jud et al., 2020; Sakai et al., 2020; Casari et al., 2021; Furman and Hsu, 2021)*.

Pratt et al. *(2018)* constructed 3D anatomical models from CT scans of the lower leg and used HoloLens (Microsoft Corp, Washington, US) MR to overlay the plan on patients in a series of reconstructive surgeries. MR proved to be more reliable and less time-consuming than audible Doppler ultrasound, reduced anesthesia time, improved training, and provided remote surgeon support. They stated the need to automate the data preparation and model registration, whilst being highly precise and accurate.

Paradigm	Pros	Cons
Training in operation room	Real behavior of patient, actual environment and tools	Risk to patient, subjective skill evaluation, additional operation-room time/cost, limited exposure to rare cases
Cadavers	Reduced time constraints, exact anatomy	Availability of cadavers, changed tissue behavior, no physiology, one-time use, special preparation required, inappropriate for MIS training
Animals	In-vivo physiology and anatomy	Prohibited in some countries, limited availability of animals, ethical concerns, limited similarity to human anatomy, specialized facilities required, high cost, one-time use
Mock-ups	Relatively inexpensive, usually allows repeated training, effective rehearsal of basic manipulative skills	Needs replacement of components after training, tactile and biomechanical properties of tissue incorrect, limited physiology, low immersion
Non-interactive, PC-based tools	Detailed 3D visualizations, intra-operative movies, self-paced learning, low hardware requirements, limited cost	No tactile information, very limited interactivity, no evaluation, no immersion

Figure 252: Advantages and disadvantages of non-VR training options. Source: (Riener and Harders, 2012)

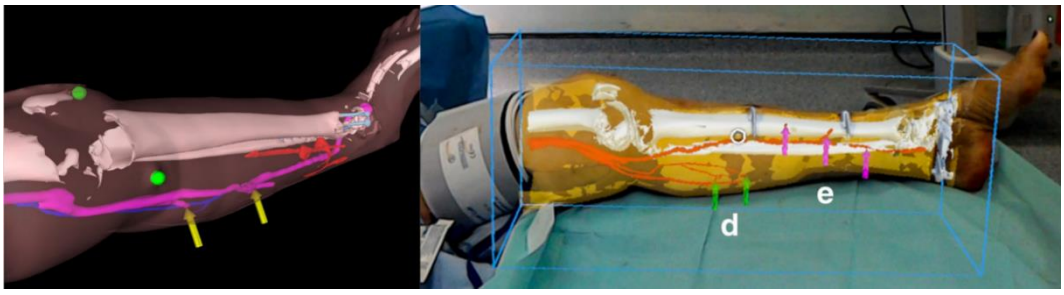

Figure 253: 3D lower leg rendering and AR overlay with arrows indicating perforators. Source: (Pratt et al., 2018)

Al Janabi et al. *(2019)* compared HoloLens MR to conventional endoscopic monitors, and stated that MR facilitated improved outcomes and was widely accepted as a surgical visual aid by the participants.

Peh et al. *(2020)* deployed an AR surgical navigation system composed of a flat panel detector c-arm with 3D imaging capabilities, and 4 integrated cameras, and optical markers on the patient's skin for tracking *(Figure 254)*. A comparison with standard fluoroscopy-guided surgery was conducted. AR proved to be feasible and as accurate (assessed by CT-scanning) as fluoroscopy without significant additional time consumption and without the use of any intra-operative X-ray imaging. The laboratory study focused on 136 minimally invasive thoracic and lumbar pedicle screws placement on 4 cadavers.

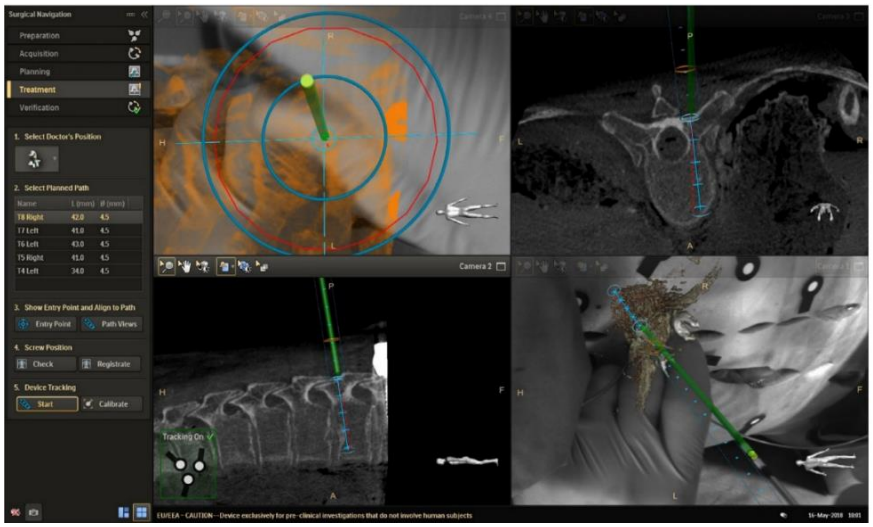

Figure 254: Intra-operative AR system for minimally invasive screws placement. Source: (Peh et al., 2020)

The same equipment was used by Elmi-Terander et al. *(2020)* to conduct a similar study to compare AR-assisted to fluoroscopy-assisted free-hand minimally invasive thoracic and lumbar pedicle screw placement in 40 patients. Although the operation time, hospital stay, and blood loss were the same, the AR placement accuracy was higher (93,9% and 86,9% respectively).

Teatini et al. *(2021)* developed a surgical tool integrating surgical instrument tracking and HMD AR with an average accuracy of 8 mm, whereas Moreta-Martinez et al. *(2021)* proposed a low-error (3 mm) surgical navigation workflow incorporating 3DPed registration guides, a 3DPed registration mark (cube), and a monitor-based AR system: a smartphone application for displaying the patient's anatomy and the tumor's location. Their system can be used for training, pre-operative planning, and patient communication.

Tanji et al. *(2022)* utilized AR and 3DP for humeral and ulnar component placement, leading to more accurate total elbow arthroplasty compared to conventional techniques.

Although xR systems are on the rise, many improvements have to be made to achieve clinically accepted precision and accuracy, whilst lowering the xR acquisition costs and the required set-up time. Only then xR systems could be routinely implemented into the daily orthopaedic practices for assisting in treating common and complex musculoskeletal disorders.

By harnessing 3DP to materialize the virtual/digital (real/material virtuality) and by utilizing xR systems to virtually realize the digital, the pre-, intra- and post-operative phases of a musculoskeletal rehabilitation workflow are better served. Implementing this duo at the PoC is truly beneficial to individually treat the patients.

The future holds individualized intelligent digital orthopaedic workflows where PoCs will incorporate xR systems coupled with advanced computer digital design and 3DP, powered by AI and robotics to facilitate orthopaedic education, training, pre-operative planning and decision making, intra-operative execution, and post-operative follow-up and monitoring.

SPECIFIC PART

4. Approach and Contribution

4.1 Rationale of Research

Digital design, Virtual/Augmented/Mixed Reality (VR/AR/MR (xR)), 3D Printing (3DP), and computer-guided approaches for visualizing the complex spatial relations of the human body and materializing custom rehabilitation solutions, have revolutionized healthcare practices. Such intelligent orthopaedic models for individualized treatments, assist in improved diagnosis of pathologies, pre-operative planning and simulation, and intra-operative procedures.

Orthopaedic surgeons can rehabilitate musculoskeletal anomalies by realizing individualized solutions together with the engineers, rapidly, and at the lowest cost. Surgical or not orthopaedic operations can be simplified by mitigating as much complexity possible from the operating room and transferring that at the planning phase by preparing suitable products for each unique patient at the right time, before operation, as per the orthopaedic surgeon's guidelines.

For custom-made orthopaedic devices, 3DP technologies are ideal as there are requirements for tailoring to each individual, short delivery times, reduced development and logistic costs, reduced material waste, reduced mass, consolidated parts, and functionally-graded (meta)biomaterials with high geometrical complexities and topology optimized features, e.g. cellular solids.

3DP is the key to unlocking unlimited creativity and design freedom. Indeed, anything that can be digitally designed can also be materialized on-demand, just in time using 3DP technologies. As long as suitable 3DPable biomaterials exist, manufacturability is almost taken for granted, whereas the complexity level for the product to be made is mitigated to the design phase: software capabilities, design engineer's skills, and expertise. This way, healthcare professionals and engineers can make use of full 3DP potential and think out-of-the-box on how to (re)design the next-generation implants out of advanced (meta)materials.

The 3DP market matures with numerous companies engaged pertaining to material supplies, 3D printer manufacturers, post-processing service providers, and software vendors for design and process optimization *(Appendix I)*.

Towards assisting individualized orthopaedic operations, as discussed in the previous critical literature review *Section 3*, research on the utilization of 3D digital design and 3DP of custom orthopaedic solutions is highly active *(Tack et al., 2016; Chepelev et al., 2017; Levesque et al., 2020; Kermavnar et al., 2021)*, with a plethora of successful applications being reported *(see also Appendices B and J)*, including the pelvic *(Wong et al., 2015; Liang et al., 2017; Hennessy, Anderson and Lozano-Calderon, 2018; Han et al., 2019; Wang et al., 2019; Wang et al., 2020; Durand-Hill et al., 2020; Gruber et al., 2020; Ji et al., 2020; Geng et al., 2020; Chen et al., 2020; Peng et al., 2020; Cao, Zhu and Gao, 2021; Park et al., 2021; Yu et al., 2021; Döring et al., 2021; Xu et al., 2022; Hu*

et al., 2022; Broekhuis et al., 2022; Gortzak et al., 2022; Pu et al., 2022; Khal et al., 2023; Hu et al., 2023; Zoltan, Popescu and Sanei, 2023; Li et al., 2023; Lv et al., 2023b) and sacrum areas *(Wei et al., 2016; Kim et al., 2017; Peng et al., 2019; Chaptain an Finn, 2020; Shi et al., 2021; Lv et al., 2021; 2023a; Kotrych et al., 2023)*. Most articles present custom 3DPed solutions that are optimized and better than traditionally made and off-the-shelf counterparts. However, innovation can still emerge by fully exploiting the potential of 3DP for mechanical and biological superiority. The fact that the literature lacks to a) holistically deal with the implementation of a de novo inter-epistemic synergy at the PoC, b) focus on the design and requirements of a PoC 3D Unit per se, and c) methodically present a holistic systematic end-to-end workflow for patient-tailored services and optimized products development and analyze each step applied whilst providing guidelines, offer the highly sought area for scientific contribution.

This Thesis will try to bridge these gaps, engaging simultaneously medical and engineering/manufacturing criteria, whilst investigating the hypothesis stated in *Section 2* and graphically impressed in *Figure 255*. Hence, the ultimate goals set to be achieved are epigrammatically:

1. Accent the inter-epistemic synergy for individualized orthopaedic services and optimized product development at the PoC under a de-novo holistic view.
2. Construct a systematic patient-specific design and manufacture methodology, and end-to-end guidelines, highlighting the critical parameters and challenges of each step of the workflow.
3. Set and present the characteristics of a small hypodigmatic 30 sqm pilot PoC 3D Unit in "Attikon" University General Hospital (equipment, organizational structure, framework, infrastructure and layout, costing) and review its performance and sustainability under its potential for decentralized manufacturing model, readiness for routine operation, challenges, and cost and time responsiveness *(Figure 255).*
4. Granted that bespoke digital, virtual, and physical solutions have been developed for some selected pragmatic pelvic and sacrum reconstruction case studies, novel, *"smart"* solutions and the need to shift from reconstructive to regenerative approaches will be discussed.

The etiology to establish a strong synergy between (bio)mechanical engineering and orthopaedics to enable optimum implant realization at reasonable costs and lead times, was given in *Sub-section 1.2*. Current technological tools (digital design, xR, 3DP, robotics, and imaging techniques that enable this synergy to emerge *(see Sub-section 1.3.)* are both facilitators of the inter-epistemic synergy, and barriers as they are associated with frontiers (*see Sub-section 1.4)* that hinder the uptake of PoC 3D Units. Establishing a PoC 3D Unit to support the distributed and localized manufacturing models for in situ production, and operate efficiently and effectively under a suitable inter-epistemic

and inter-disciplinary synergistic framework is considered intriguing and challenging from both engineering and medical/clinical perspectives.

Referring to the objectives mentioned in *Section 2*, the following first three were covered:

1. Review modern and 3DPable biomaterials used in individualized orthopaedic reconstruction.
2. Explore/exploit the full potential of digital design, xR, 3DP, and 3D scanning in individualized orthopaedics.
3. Review the requirements and characteristics of PoC 3D digital design, xR, 3DP, and 3D scanning.

In this *Section*, the rationale of the research and the methodology are unfolded and structured to cover the remaining three objectives, i.e.:

1. Carry out scenarios with pragmatic cases by applying digital design, xR, 3DP, and 3D scanning technologies in situ (PoC). Select orthopaedic oncology and orthosis cases and treat them as currently ongoing pragmatic cases to be carried out by a pilot PoC 3D Unit set at the First Department of Orthopaedic Surgery, School of Medicine, NKUA.
2. Apply advanced design techniques and optimization algorithms for the custom solutions to be developed, inspired from, and mimicking the cosmos of natural structures that are optimized for their assigned functions.
3. Evaluate and compare these technologies with traditional approaches based on mechanical and biological performance, and sustainability, and against technical, time, and economic criteria.

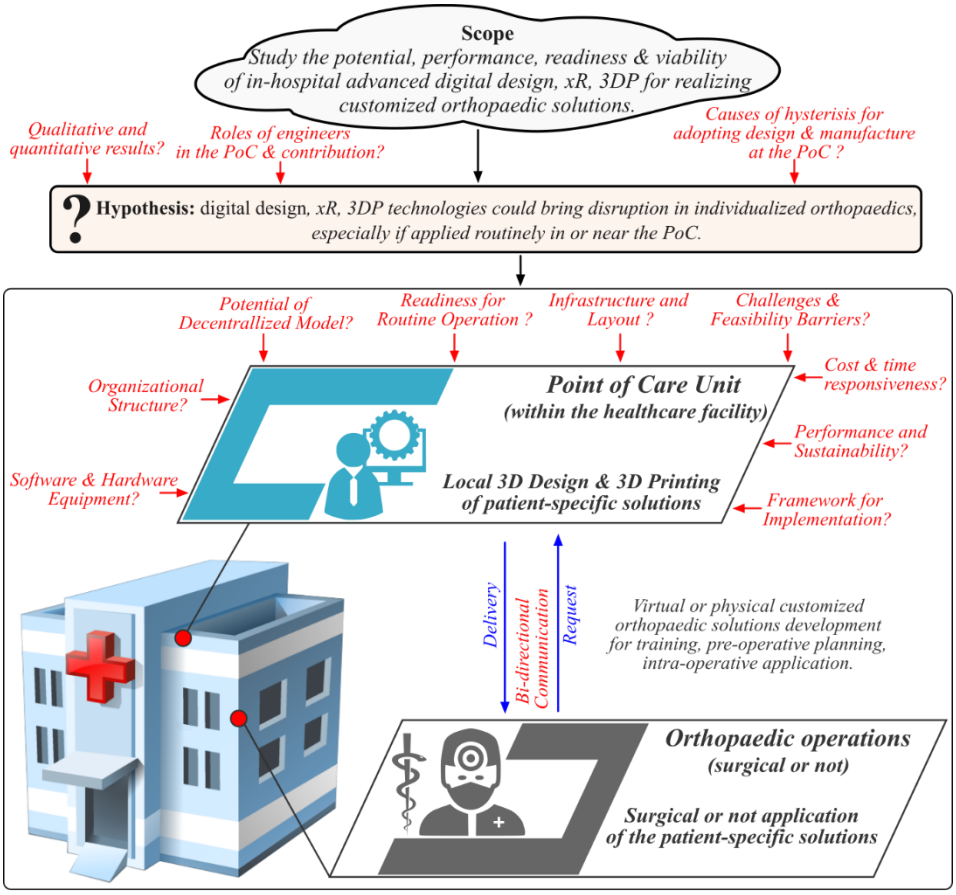

Figure 255: Thesis hypothesis

Current large bone reconstruction/regeneration strategies implemented within PoCs are standstill as they follow a top-down approach *(Figure 256)*, as a result, the final solution is adapted to the existing capacity of in-house expertise and equipment. It is known that needs drive innovation, hence it is more orthological for strategies to start fading over bottom-up approaches where clinical needs drive the development (collaboration and planning) for scientifically relevant custom solutions *(Figure 256)*. This way, clinical needs for bone reconstruction and regeneration can be met.

The Thesis scope revolves around unfolding an inter-epistemic workflow enriched with a combination of emblematic technologies for PoC rapid design and manufacture (3DP) of custom-made medical devices to enable the routine establishment of individualized reconstructive orthopaedics. Apart from materializing anatomical models, instruments, and orthotic parts, special focus is given to the capabilities of 3DP for making patient-specific orthopaedic endo-prostheses by forming biomaterials into interconnected pore architectures to functionalize-by-design a) the exo-structure (surface) to promote osseointegration and combat microbial activities, and b) the endo-structure so that the mechanical properties are tweaked to match the physical and mechanical properties of the host tissue and minimize stress-shielding phenomena. Functionally graded-(meta)biomaterials with heterogeneous structure and density variations are of high interest.

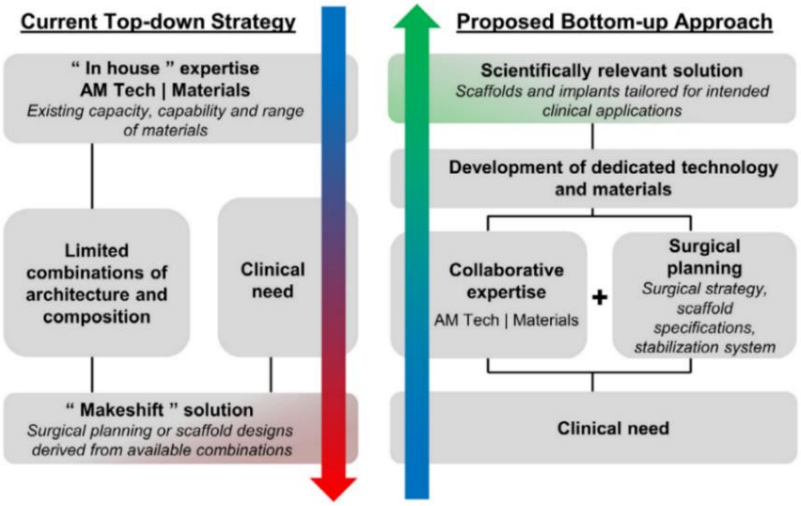

Figure 256: Bottom-up and top-down approaches for custom 3DPed solutions. Source: (Charbonnier, Hadida and Marchat, 2021)

Note: it should be underscored that due to the context of this Thesis that has an engineering-centered research character aiming to serve the orthopaedic surgeons, and considering that the solutions to be prototyped were not surgically applied to the patients studied, scenarios were established and hypotheses/assumptions were made. Additionally, due to budget and resources constraints, both top-down and bottom-up concepts were discussed.

4.2 Methodology

The Thesis approach is illustrated in *Figure 257*. The structure, specifications, functions, and equipment of a PoC 3D Unit will be presented first. Then, orthopaedic oncology cases on pelvic and sacrum reconstruction will be studied and custom solutions will be developed within the PoC under

an inter-epistemic custom orthopaedic products development methodology. The results and discussion, and conclusions and future work will follow.

To facilitate the development of physical patient-specific products that solve musculoskeletal problems, a suitable orthopaedic engineering design methodology should be adopted.

The *"iceberg"* model characterizes best the *"what"*, *"how"* and *"why"* dimensions of any physical product *(Figure 258)*. The user and anyone not engaged in its development, sees "what" was made, however, the reason "why" it was made that way and "how" it was made are not apparent. The "how" and "why" are fundamental parts of the product's design process.

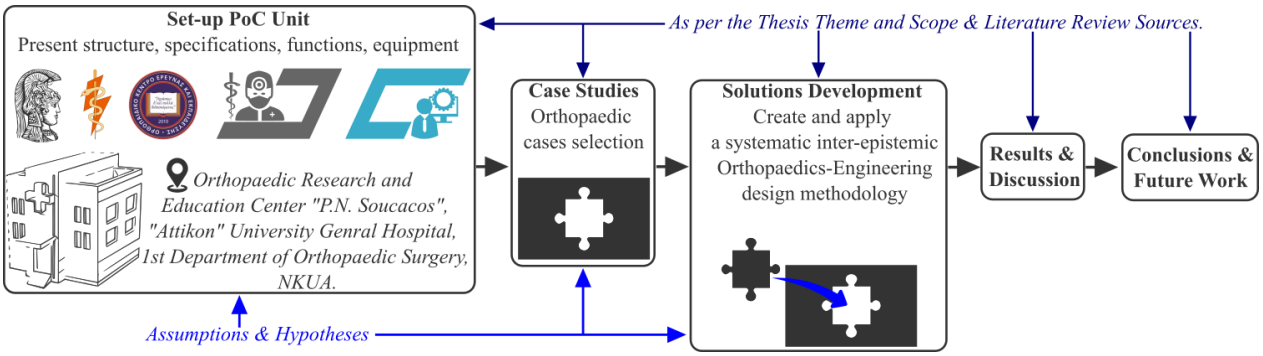

Figure 257: Thesis approach

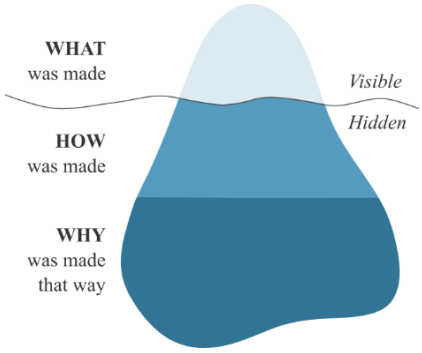

Figure 258: "Iceberg" model of physical product-making

More specifically, illustrates the inter-epistemic why-what-how process development of an orthopaedic product engaging orthopaedics and (bio)mechanical engineering.

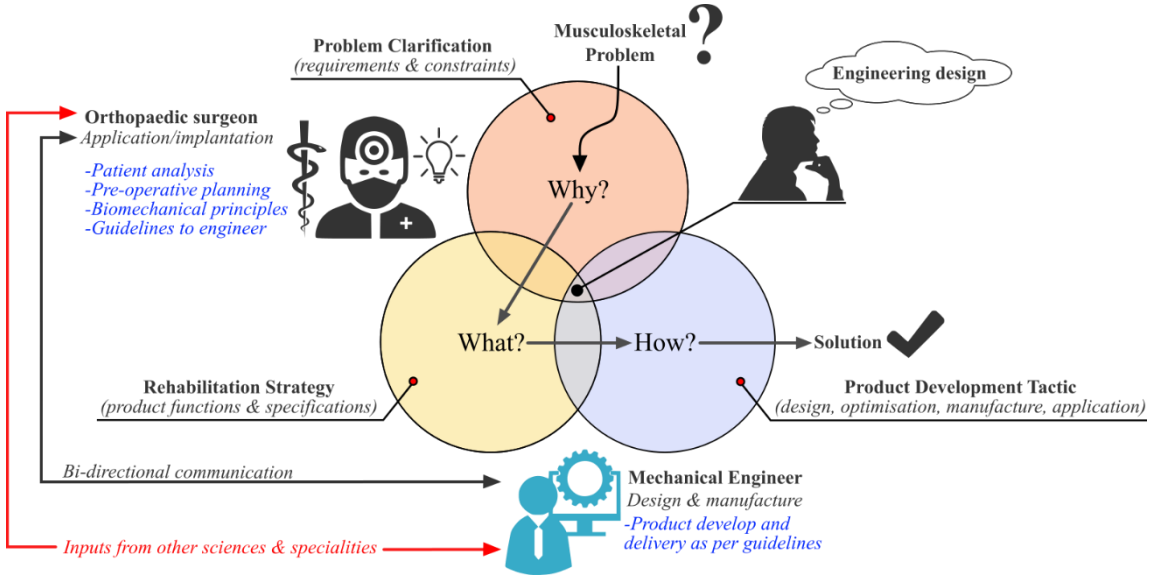

Figure 259: Inter-epistemic why-what-how orthopaedic product development process

The orthopaedic device development process includes several variables. A process chain for ideal customized implant design and production is shown in *Figure 260*. Once the implant's requirements are set, and its functions and environment identified, the design process commences. Shape and features are established, properties are defined, and the most suitable biomaterials are selected based on the other three interrelated phases. Under a suitable standardized QMS that ensures overall quality assurance and control, and granted regulatory approval, the optimal techniques are selected for production, and the implant is materialized, post-processed, sterilized, and delivered.

Any engineering design methodology is a problem-solving process, utilized to answer the "why", "what", and "how" questions. Many such have been developed *(Krishnan and Ulrich, 2001; Tomiyama et al., 2009)*, however, Pahl-Beitz's *(2007)* systematic approach to engineering design was selected as a reference as it is well-established and analytical. This systematic approach was then adjusted and seen in parallel with extra approaches *(Figure 263)* that helped in constructing the matching workflow at the end, i.e.:

1. Design for 3DP (Df3DP[55]) *(Kranz, Herzog and Emmelmann, 2014; Thompson et al., 2016; Schnabel, Oettel and Mueller, 2017; ISO/ASTM, 2018; Diegel, Nordin and Motte, 2019; Leary, 2019; Renjith, Park and Okudan, 2019; Vaneker et al., 2020)* and Design with 3DP (Dw3DP[56]) *(Floriane et al., 2016)* principles structured in divergent-convergent modes as per the Double Diamond design process model[57], though Df3DP span across both modes.
2. The biomimicry toolbox[58] (design spiral *(Figure 262)*) part of which is the biomimicry taxonomy of biological strategies *(Appendix O)* as presented by the Biomimicry Institute was also considered to facilitate the design of orthopaedic parts driven by biomimesis.

Figure 264 shows the de-novo, role-based, and end-to-end systematic inter-epistemic patient-specific orthopaedic product design methodology (workflow) that was set to be applied for each case study to be carried out *(Section 6)*. As the theme of this Thesis has 3D technologies (xR, 3D design,

[55] Design for X refers to techniques used to adapt a design to a given set of constraints and seen from a particular perspective indicated by X. Design for 3DP (Df3DP) includes practices for optimizing the fabrication process (e.g. selection of optimal built orientation, elimination of overhangs and support structures) and product designs by fully benefiting from the potential of 3DP (e.g. topology and shape optimization, part consolidation, embodiment of porous structures). Rosen and Kim *(2021)* defined Df3DP as *"synthesis of shapes, sizes, geometric mesostructures, and material compositions and microstructures to best utilize manufacturing process capabilities to achieve desired performance and other life-cycle objectives".*

[56] Instead of adapting a design to a specific purpose as Df3DP does, Design with 3DP (Dw3DP) uses a knowledge database to inspire and widen the conceptualization phase of the design with special attention to innovation and creativity.

[57] The Double Diamond design process model was popularized by the British Design Council *(2007)*, based on Banathy's *(1996)* divergence-convergence model. The process contains four phases to explore an issue widely or deeply (divergent thinking) to then take focused actions (convergent thinking). It contains four phases, i.e. discover, define, develop, and deliver.

[58] The biomimicry toolbox is a guide for applying nature's lessons to design challenges provided by the Biomimicry Institute. More info at https://toolbox.biomimicry.org/.

3DP) utilization in its core, to explore and exploit their capabilities, this workflow sourced its logic from the previous methodologies which were mixed and tweaked to match the needs and the inter-epistemic nature of the musculoskeletal disorder treatment process after careful critical thinking and filtering for applicability, efficiency, sustainability, and optimal involvement and engagement level of all required parties. This end-to-end inter-epistemic workflow must be accompanied by a suitable QMS and by a properly structured online platform (*SkeletoMy*) to offer continuous seamless data exchange between all parties involved and special request forms, guidelines and reports to promote efficient status tracking for each request as it progressively reaching the desired solution as per the exact needs and specifications list set by the orthopaedic surgeon. The application of this workflow is presented in *Section 6* to solve selected cases, whereas *SkeletoMy* is presented in the next *Section*

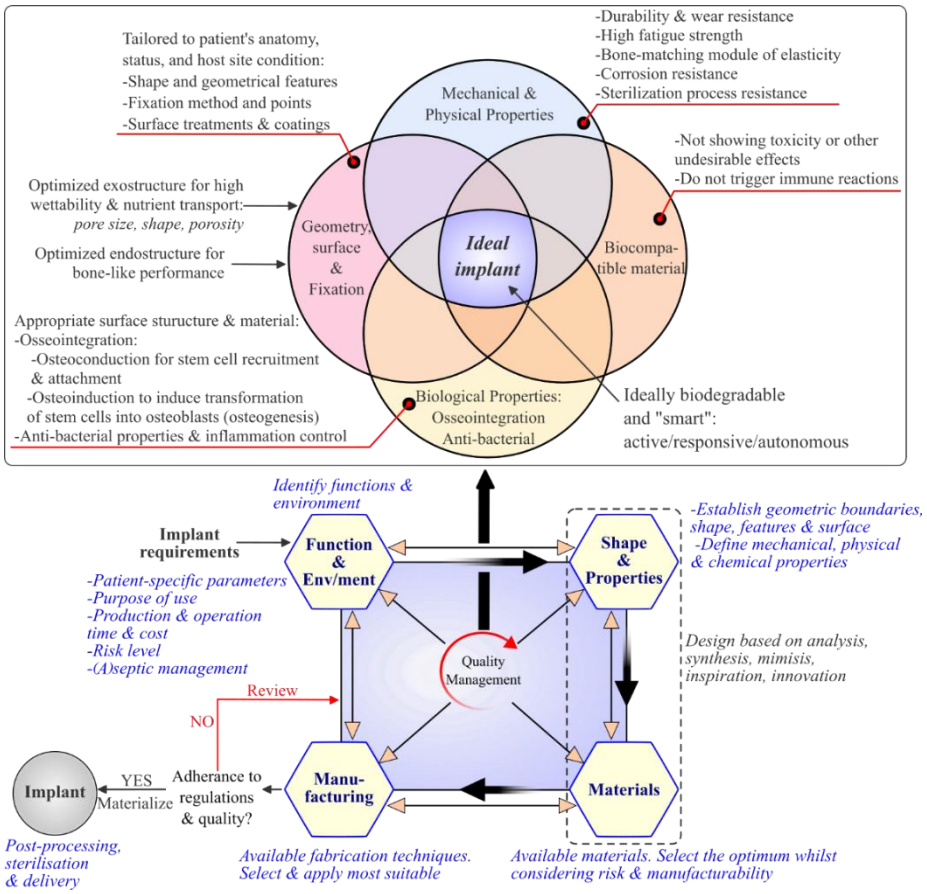

Figure 260: Ideal implant development process

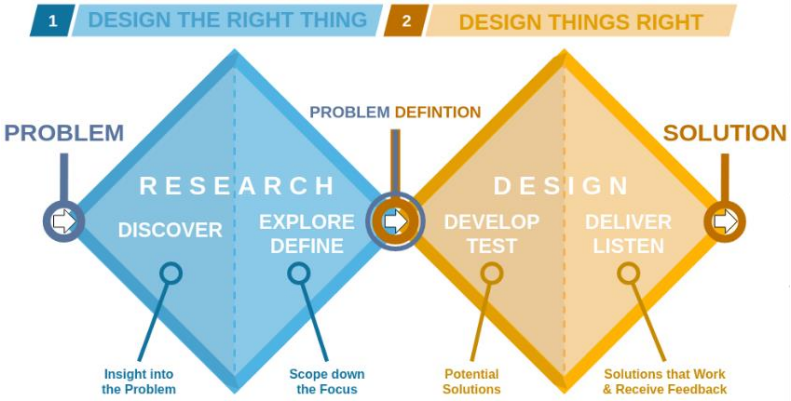

Figure 261: Double Diamond design process

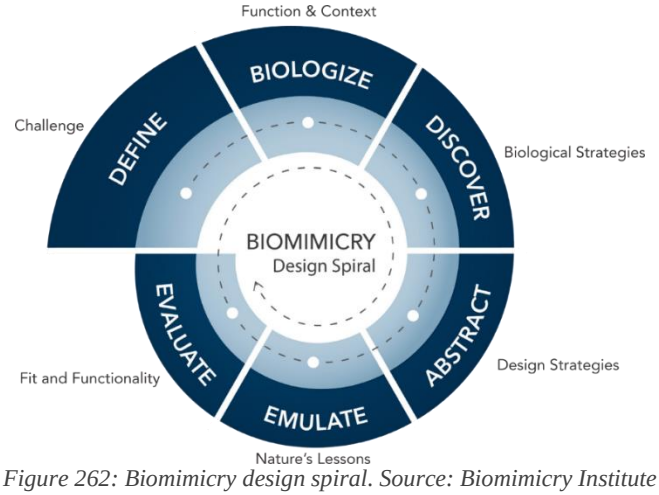

Figure 262: Biomimicry design spiral. Source: Biomimicry Institute

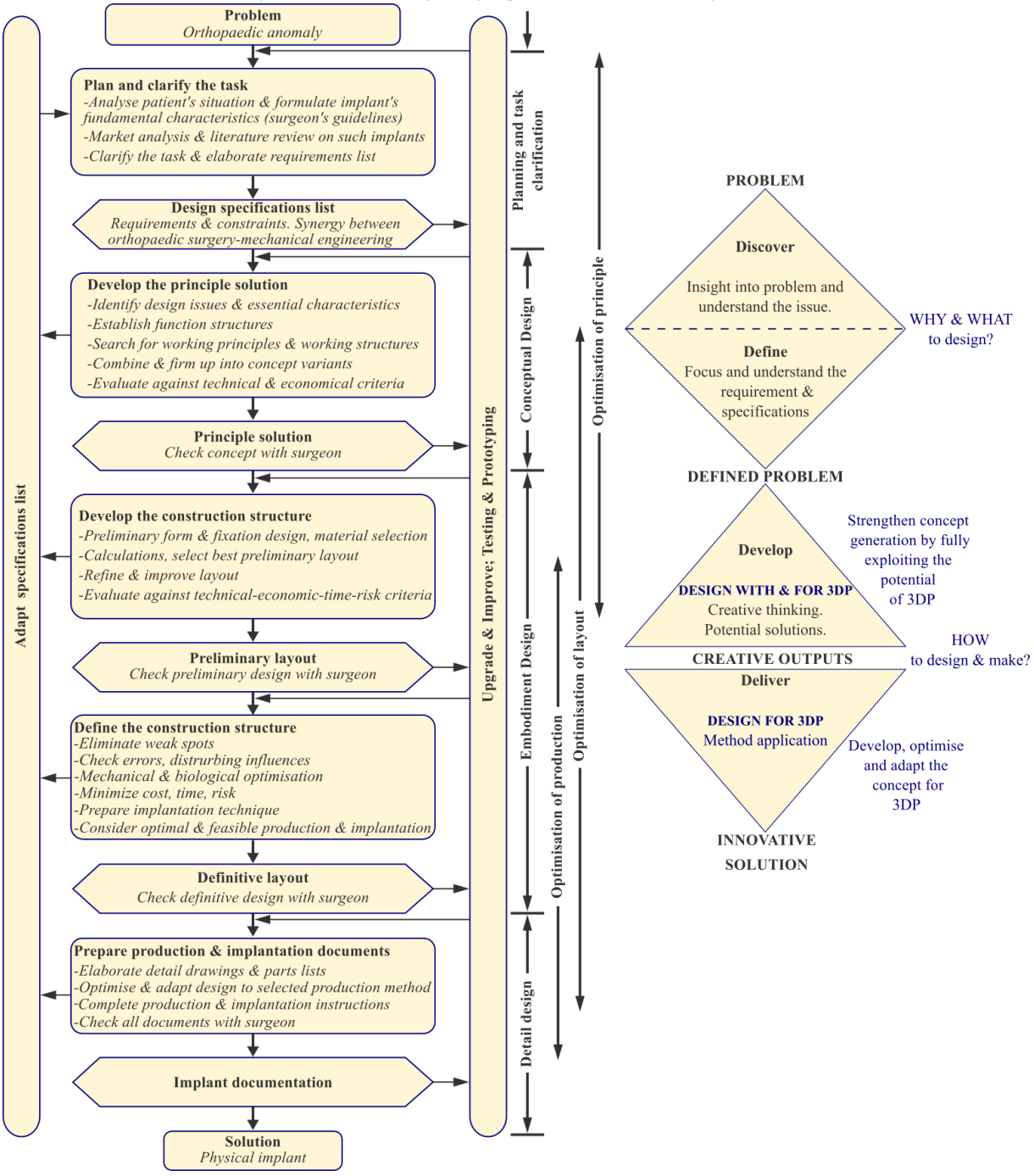

Figure 263: Systematic design, Double Diamond and Dw3DP-Df3DP. After (Pahl et al., 2007; British Design Council, 2007)

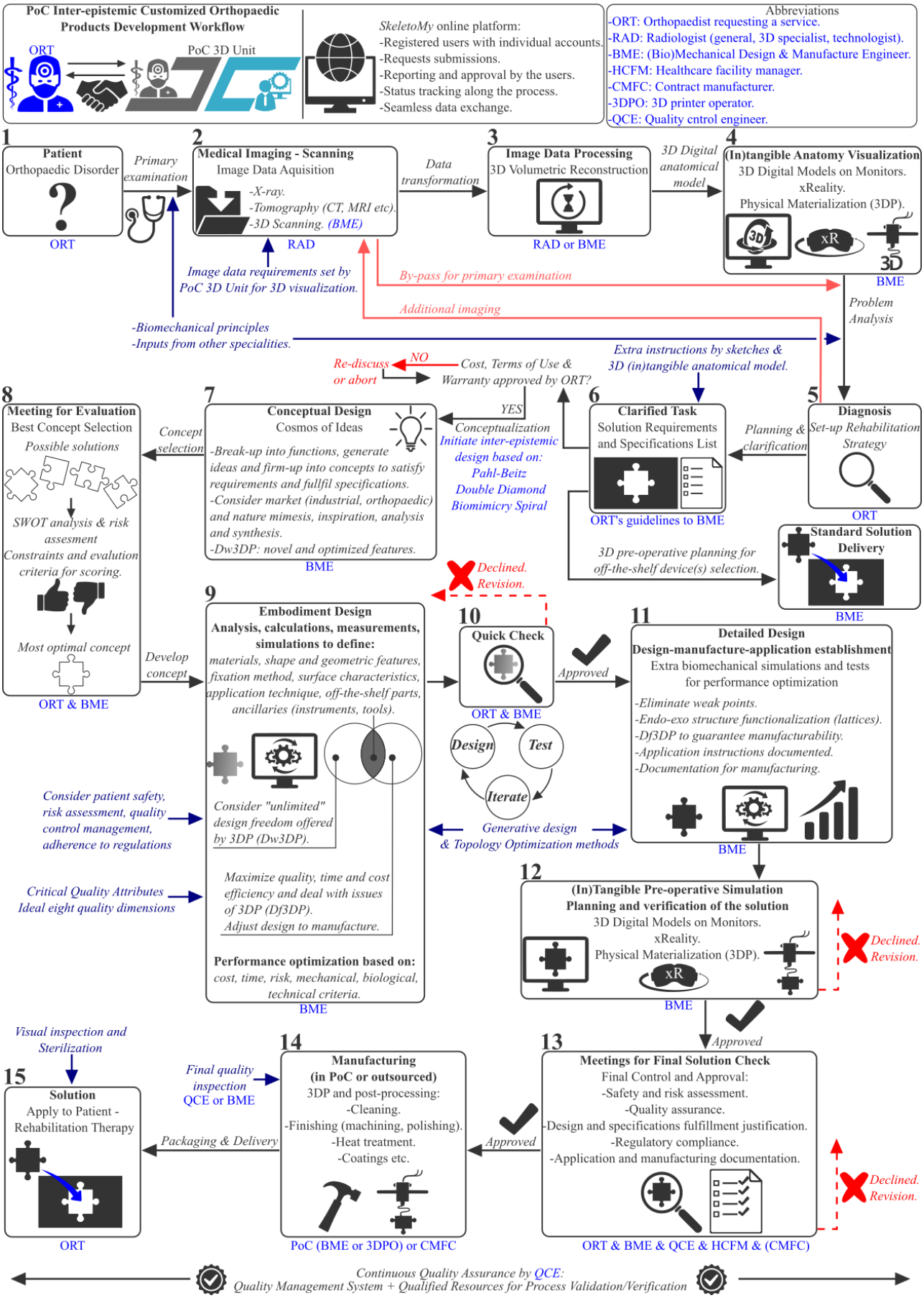

Figure 264: Thesis PoC inter-epistemic custom orthopaedic product development workflow

In summary, the methodology consists of 15 fundamental phases explained below:

1. **Patient:** the patient's orthopaedic disorder is examined by the orthopaedic surgeon whilst considering biomechanical principles and inputs from other specialties. At this Stage (or at Stage 5), the surgeon might contact the PoC 3D Unit and register the case via *SkeletoMy* platform so that the requirements for image data acquisition are set for 3D visualization.
2. **Medical imaging-scanning:** image data is acquired by the radiologist. X-Ray, or CT, MRI, or other tomographers for in-body anatomical imaging, or 3D scanners for surface imaging are utilized. Steps 3 and 4 might be bypassed for primary examination not requiring 3D model generation. Step 2 might be repeated for additional imaging during Step 5, e.g. a surgical operation might intervene, modifying the patient's anatomy, hence the post-operative image data has to be acquired again.
3. **Image data processing:** the image data is processed by the radiologist or the (bio)mechanical design engineer using suitable software for segmentation and reconstruction of the medical image data to generate the digital 3D model of the anatomical region of interest.
4. **(In)Tangible anatomy visualization:** the 3D anatomical model is prepared by the radiologist or the (bio)mechanical design engineer and delivered to the orthopaedic surgeon for visualization and manipulation. In this case, the term visualization might refer to a) digital 3D models viewed on computer, smartphone, or tablet screens, b) digital 3D models imported in xR environments for (semi) immersive experience and interaction, using special xR equipment, and c) physical anatomical models fabricated by 3DP techniques.
5. **Diagnosis:** the orthopaedic surgeon analyzes thoroughly the problem by diagnosing the pathology/disorder based on the primary examination and the 3D visualized anatomy, and the rehabilitation strategy is planned and clarified. Surgical or not operations might emerge during this Stage, and additional imaging might be required post-operatively, thus creating a loop in the methodology. At this Stage, the PoC 3D Unit is fully engaged and the process continues to Stage 6 to develop a customized solution, or if matching off-the-shelf products exist, the (bio)mechanical design engineer can help the orthopaedic surgeon select the most suitable device(s) by pre-operative planning in 2D/3D using digital design software.
6. **Clarified task:** the solution specifications list is set by the orthopaedic surgeon or collaboratively with the (bio)mechanical design engineer or more members. The surgeon might provide sketches, marked screenshots, or directly edit the 3D anatomical model, or even physically model with clay on the tangible 3DPed anatomical replica for extra design instructions. Granted that the cost, Terms of Use and Warranty Notes (agreement) are approved by the orthopaedic surgeon, from this Stage and on, the solution is being developed by the (bio)mechanical design engineer as per the specifications and instructions set by the orthopaedic surgeon.

7. **Conceptual design:** this phase is carried out by the (bio)mechanical design engineer or collaboratively with the orthopaedic surgeon. The product's requirements are broken up into functions, ideas are generated for each function and firmed up into concepts that accomplish the requirements and fulfill the specifications. Concepts are created by inspiring, mimicking, analyzing, and synthesizing ideas sourced from the cosmos of industrial and orthopaedic devices market, literature, and nature as per the biomimicry spiral design approach discussed before. As stated by Floriane et al. *(2016)*, design with 3DP (Dw3DP) can be harnessed as a toolbox to expand conceptualization toward new design spaces by inspiring from a knowledge database to boost creativity with emphasis on innovation.
8. **Meeting (face-to-face or remotely) for evaluation:** concepts are evaluated by SWOT (Strengths, Weaknesses, Opportunities, Threats) analysis and under any constraints and pre-defined weighted criteria. Risks are assessed, and the top-scored concept is selected for development. The meeting involves at least the surgeon and the (bio)mechanical design engineer.
9. **Embodiment design:** the selected concept is developed by the (bio)mechanical design engineer. Based on analysis, measurements, and calculations, the following are defined for the product per se and for any ancillaries: materials, shape and geometrical features, surface characteristics, fixation method, standard off-the-shelf components, and application technique. Biomechanical simulations to optimize performance are carried out based on several criteria (e.g. cost, time, risk, mechanical, biological, technical), whilst considering, patient safety, risk assessment, quality control management, and adherence to medical device regulations.

   Implemented features might introduce both issues and benefits. To balance such bimodal impacts, Dw3DP coupled with Df3DP toolboxes need to be harmonically combined to identify the most well-fitted 3DP technology and manufacturing flow to develop, optimize, and adapt the selected concept design for manufacture. During the embodiment, quick check, and detailed design phases the design-test-iterate loop is followed. Also, computational/generative design algorithms and/or topology optimization might be applied.

   The Critical Quality Attributes (dimensional, mechanical, biological, physiochemical, functional) and the ideal eight quality dimensions (product-based (performance, features, reliability), manufacturing-based (conformance, durability), user-based (serviceability, aesthetics, perceived quality)) *(Martinez-Marquez et al., 2018)* is suggested to be considered along with reviewing design and fabrication methods to ensure that products are designed and manufactured correctly.
10. **Quick check:** the orthopaedic surgeon receives all intangible content of the developed design and reviews it before approving or declining for revision. A meeting session with the PoC 3D Unit might be arranged. If the design is declined the process might return back to Step 7, 8 or 9.

11. **Detailed design:** granted approval, the (bio)mechanical design engineer establishes the final design, manufacture, and application. Extra biomechanical tests and simulations for performance optimization might be carried out. Any weak points are eliminated, the endo and exo structure are "biologized" and functionalized by introducing porous architectures, and Df3DP is applied to guarantee its manufacturability. Additionally, the application instructions are documented, the design is justified, and the manufacturing instructions are prepared.
12. **(In)tangible pre-operative simulation:** as in Step 4, digital, virtual, or physical prototyping of the anatomical replica and product(s) (e.g. implants, instruments, tools, orthotics) is deployed by the (bio)mechanical design engineer for the orthopaedic surgeon to pre-operatively simulate, plan and verify the solution. The solution is approved or declined (back to Step 7, 8 or 9).
13. **Meetings (face-to-face or remotely) for final solution check:** meeting sessions among all parties involved for final solution control and approval. Submitted documentation (a) final proposal check and specifications fulfillment justification report, b) safety, risk assessment and quality management report, c) application/implantation instructions, d) manufacturing instructions) and compliance with regulations are checked and reviewed. If the solution is declined the process might return back to Step 7, 8, 9 or 11.
14. **Manufacturing:** the approved solution is manufactured as per the instructions. Products are 3DPed and post-processing techniques follow: cleaning, finishing (machining, polishing, etc.), heat treatment, coatings, etc. Depending on the available resources, manufacturing takes place at the PoC (3D printer operator) or outsourced to a contract manufacturer. The (bio)mechanical design engineer or the quality control engineer is responsible for the final quality inspection.
15. **Solution:** the product is packaged and delivered to the HCF, where it is visually inspected before sterilization. The product-solution that conforms to the initially set rehabilitation strategy and fulfills the specifications set is applied to the patient by the orthopaedic surgeon.

The aforementioned methodology revolves around digital design, xR, and 3DP to explore and exploit the full potential, as well as deal with their limitations for quality control. It is suggested that a properly structured QMS and qualified resources are employed to address the applicable regulations and standards and assure quality in each phase for safe and reproducible results so that the whole process is verified or validated to meet the applicable specifications and high-quality output. For this purpose, a quality control engineer or the (bio)mechanical design engineer has to ensure that all activities, equipment used, and the product per se are quality assured under the QMS.

The methodology will be deployed for each orthopaedic case to be studied, to develop next-generation custom solutions. However, in cases where obstacles will be encountered, assumptions and hypotheses will be made.

Last but not least, it is important that for each patient-specific medical device to be 3DPed, all factors that contribute to lowering its quality from start to finish to be taken into consideration during its development workflow. The Ishigawa diagram shown in *Figure 265* summarizes the most crucial factors impacting the quality of a 3DPed individualized medical device: method, machine, personnel, and materials. Parameters affecting the end quality of a 3DPed part were discussed in *Sub-section 3.3.6* and graphically illustrated in *Figure 88* for metal PBF-based technologies.

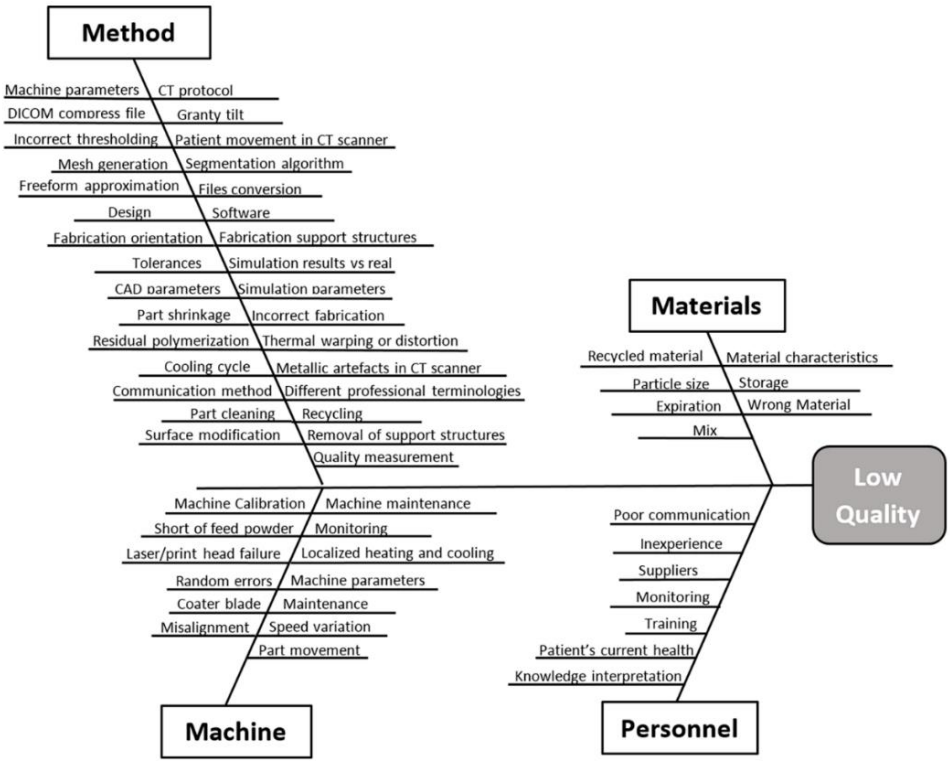

Figure 265: Ishigawa diagram for causes of low-quality 3D printed products. Source: (Martinez-Marquez et al., 2018)

5. Point-of-Care 3D Unit

5.1 Introduction

Localized 3D design and manufacturing of patient-specific solutions in PoC Units embedded within HCFs were discussed in the introductory *Section 1* and in the previous literature review *Sub-section 3.4* where it was stressed that few articles deal with guidelines for setting up a PoC 3D Unit *(Sanicola et al., 2020)*, though certain companies[59] are offering guidelines and certification programs for setting up validated PoC 3D Units.

Via PoC 3D Units, digital, virtual, and physical customized orthopaedic solutions can be delivered in a short-time to the orthopaedic surgeon for training, pre-operative planning, and intra-operative applications. The fact that the key enabling technologies are readily available in the market *(see Sub-section 1.3)* makes the realization of PoC 3D Units easier to set up now, aiming not only at special cases but also for routine applications.

[59] For example, Materialise offers the Mimics Certification Program to validate PoC 3D labs aiming at diagnostic usage. See https://www.materialise.com/en/healthcare/hcps/point-of-care-3d-printing/mimics-certification.

A PoC 3D Unit must define and manage a regulated and standardized workflow, capacity, and portfolio. The decision whether to develop in situ or outsource activities, or create a mixed process depends on complexity, lead time and cost, demand, and objectives *(García et al., 2022)*. For cost-effective integration and selection of optimal technologies, all parties involved must be qualified.

Any PoC 3D Unit establishment must be driven by the clinical needs of the HCF, so that the collaboratively developed solutions are clinically and scientifically relevant and ultimately beneficial for each unique patient. Hence, a bottom-up approach is ideally highly sought, compared to top-down approaches that adapt the solution development as per the existing capacity of PoC expertise and equipment *(see Figure 256)*.

Budget is not the only crucial parameter that affects the PoC 3D Unit's capacity and capabilities. Before investing in any strategy, a HCF should prioritize its needs and consider not only the costs of equipment acquisition and ownership (maintenance, operation), but also the ease of implementation and transition, sustainability, competitiveness, technologies selected, scale-up scenarios, and available space and resources. For example, it is suggested that a HCF initially invest in market-proven technologies with widespread adoption with larger lifecycles.

The FDA has given technical considerations *(2017)* and has mentioned five possible scenarios for a HCF to implement PoC design and 3DP *(2021)* as shown in the previous *Figure 115*. In this *Section*, two scenarios for PoC 3D Units set-ups are unfolded simultaneously:

1. **Scenario 1:** an ideal PoC 3D Unit where the HCF both designs and becomes the manufacturer of any polymer and metal product for reconstructive orthopaedics, including ceramic manufacturing and bioprinting of constructs for TE applications and research on regenerative orthopaedics. For this scenario, no budget, space, and resource restrictions were considered. A medium-scale design and production volume were assumed: such that can be carried out by a six-member PoC 3D Unit as described next. Apparently, to create a high-demand pool, more than one HCFs must be served by a suitable decentralized supply network.
2. **Scenario 2:** a more realistic PoC 3D Unit where design and polymer prototyping take place within the HCF. Metal and polymer manufacturing is outsourced to contract manufacturers, but there is an option to process small polymer biomaterials for end-parts production in-house. The minimum required hardware at the lowest possible budget was considered for this scenario. The lowest-scale design and production volume were assumed: such that can be carried out by a single-person PoC 3D Unit as described next. Hence, this Scenario best fits for serving locally exclusively one HCF.

It is more orthological for a HCF to commence with a small hypodigmatic pilot PoC 3D Unit that initially designs and prototypes parts without manufacturing in-house, and then, granted sufficient

demand to rationalize any investment, gradually expand and implement in situ manufacturing. As needs and budget drive the number and responsibilities of personnel, resources selection, specifications, and space layout of any PoC 3D Unit, these have to be arranged in a scalable manner in case capacity has to increase.

Including assumptions and extra resources limitations, a hypodigmatic small 30 sqm pilot PoC 3D Unit under Scenario 2 was taken as a reference to assess the Thesis hypothesis *(see Section 2 and Section 4).* The exact equipment to be employed in this Thesis is given in the software and hardware *Sub-section 5.4.1* and their usage is described in *Section 6* where cases are carried out. It was assumed that the PoC 3D Unit was set up by the First Department of Orthopaedic Surgery, National and Kapodistrian University of Athens, in a typical 30 sqm office housed at Orthopaedic Research and Education Center "Panayiotis N. Soucacos", "Attikon" University General Hospital. In this *Section*, the following are discussed: a) organizational structure and framework for implementation, b) hardware and software equipment, c) infrastructure and layout, d) costing, and e) distributed and localized manufacturing.

Granted that such a PoC 3D Unit is utilized to carry out the selected case studies shown in the next *Section 6* by applying the end-to-end workflow presented in the previous *Section 4*, the remaining aspects of the Thesis hypothesis are impressed in the results and discussion *Section 7*, i.e. a) roles of (bio)mechanical design engineers and their contribution, b) performance and qualitative and quantitative results, c) potential for decentralized manufacturing model, d) readiness for routine operation, and e) challenges and barriers, and causes for adoption hysteresis will be impressed.

5.2 Organizational Structure and Framework

A PoC 3D Unit should be structured with a lab-like character that operates under suitable procedures with matching hardware and software equipment for quality management, whilst being powered by scientific knowledge and orthopaedic experience and expertise, and penetrated by advanced (industrial) engineering methodologies and tools brought by skilled professional (bio)mechanical design and manufacture engineers. With this in mind, *Figure 266* shows the organizational structure tree for Scenario 1 and 2, each having the following discrete roles:

1. **Orthopaedic surgeon manager:** manages the operation and acts as a link among the HCF, the interested healthcare professionals/orthopaedic surgeons that request services, and the (bio)mechanical design and manufacture engineers of the PoC 3D Unit. Filters information entering and exiting the PoC 3D Unit and provides design input, orthopaedic expertise, and checks the solutions as they are being developed. Has the product owner role and shared responsibility for the quality, risk, and safety control. *Note: In this Thesis, where Scenario 2 is implemented, there are no active requests from interested users and no PoC 3D Unit officially*

established, the orthopaedic surgeon manager role cannot be justified. The interested orthopaedic surgeon requesting a service communicates directly with the (bio)mechanical design and manufacture engineer and has also the manager's role. Granted the establishment of a real PoC 3D Unit, to manage an adequate flow of requests and provide the required expertise and input, an orthopaedic surgeon manager would be required.

2. **(Bio)mechanical design and manufacture lead supervisor:** interacts with the orthopaedic manager and ensures tactic (daily) and strategic goals are on track, by supervising and leading the team ((bio)mechanical design and manufacturing engineers, quality management engineer, 3D printer operator-mechanic). Has product owner role and shared responsibility for quality, risk and safety control. Able to design, simulate, optimize, and manufacture planning of orthopaedic products, as well as able to set up xR sessions and operate 3D scanners and 3D printers, and post-process and package the final parts for delivery. For sustainability, ensures Unit's needs for resources are covered to deliver the requested services and products effectively and efficiently. *Note: In this Thesis, where Scenario 2 is implemented, there are no active requests from interested users and no PoC 3D Unit officially established. In this case, the "one-man show" role is assigned to a single person for localized development, i.e. biomechanical design, manufacture and quality management, and 3D printer operation. This is orthological for very low request flows that are a characteristic feature of initially small pilot PoC 3D Units that might or might not later expand into larger Units.*
3. **(Bio)mechanical design and manufacture engineers:** design, simulate, and optimize patient-specific orthopaedic products to meet the pre-set specifications. Additionally, able to plan 3DP processes, set up xR sessions, operate 3D scanners and 3D printers, and post-process and package the final parts for delivery.
4. **3D printer operator-mechanic:** responsible for manufacturing (3DP) planning (model and data preparation for 3DP), preparation, operation, and maintenance of 3D printers, cleaning, post-processing, and packaging the products for delivery. Also, responsible for production quality control, and managing the workshop areas and 3DP feedstock materials and ancillary supplies.
5. **Quality management engineer:** follows and ensures the development of medical devices is as per the pre-set specifications and is being developed and tested as per the established regulated and standardized quality management procedures. Acts as Scrum master[60], synchronizing

[60] Scrum is an agile project management framework that helps teams structure and manage their work through a set of values, principles, and practices. See https://www.scrum.org/resources/what-is-scrum and https://scrumguides.org/ for more details. Scrum masters are project facilitators whof ensure best practices are followed. Must be skilled at collaboration, conflict resolution and process improvement.

tactically and strategically the team to track the status of projects and indicate whether tasks are issue-free and within the deadlines. Supervises the quality, documentation preparation, and supplies ordering, as well as the packaging, labeling, sterilization, and delivery.

All team members should be self-managed, self-motivated, competent, certified, and/or qualified to conduct the assigned tasks using quality and (medically) approved tools.

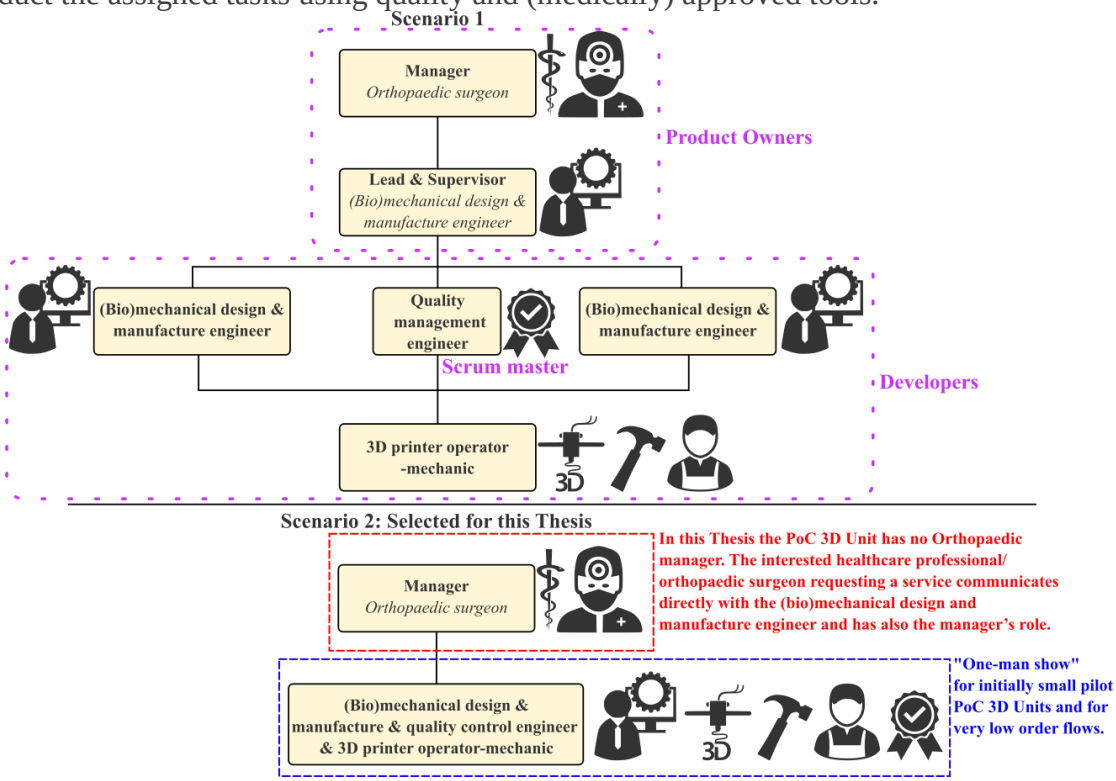

Figure 266: Organizational structure of the PoC 3D Unit

To deal with the workload and manage the projects, the scrum framework *(Figure 267)* can be established (daily 15-minute standup meetings, backlog list creation, sprint goals setting, sprint planning, review, and retrospective) to help the team a) communicate with the user who will be engaged actively in the scrum model, and b) to embrace an agile mindset and synchronize, plan out the work for the day, identify obstacles, inspect the progress toward the goals set, adapt the backlog respectively, and adjust the upcoming planned work. *Jira*[61] (Atlassian Corp, Sidney, Australia) is such software (free for up to 10 users) that serves the scrum approach for project management.

Graphic management tools such as *Miro*[62] (RealtimeBoard Inc., Nevada, US) (free/paid) are useful for collaboration. For remote meetings, *Teams*[63] (Microsoft Corp, Washington, US) (free/paid) or *Workspace*[64] (Google LLC, California, US) (free/paid) can be adopted.

[61] Jira is used for issue tracking and project management. For details, see https://www.atlassian.com/software/jira.

[62] Miro is a visual platform used by teams to connect, collaborate, and create for brainstorming, diagramming, meetings, scrum events, mapping, research and design, and strategic planning. For more, see https://miro.com.

[63] Microsoft Teams is used for online meetings, chat, and cloud storage. For details, see https://www.atlassian.com/software/jira.

[64] Google Workspace is composed of Meet (online video meetings), Drive (cloud storage), Chat (messaging), Docs (word processing, spreadsheets, presentations), Gmail (business email), and Calendar (shared calendars) services. See https://workspace.google.com/.

Figure 268 summarizes the interactions of the PoC 3D Unit with the healthcare professional that requests a service, their roles in the why?-what?-how? flow, and the services offered by the PoC 3D Unit by applying the inter-epistemic workflow shown in *Figure 264*. Any healthcare professional or orthopaedic surgeon *("user")* interested in any service provided by the PoC 3D Unit (3D anatomy reconstruction, 3D digital design, 3D scanning, xR experience set-up, manufacturing (3DP)) can contact or visit the Unit, or better register and login to submit requests via its online platform.

The characteristics of the PoC 3D Unit interactions are highlighted below:

- The user analyzes his patient, plans pre-operatively the approach whilst taking into account biomechanical principles and inputs from other specialties and departments of the HCF, and provides all available data, notes, and guidelines to the PoC 3D Unit as per the instruction during request submission to accompany the submitted request.
- As long as the collaboratively pre-defined specifications list is satisfied for the requested service or product, the user that contacted the PoC 3D Unit takes full responsibility for the developed solution, not the Unit. For this reason, before manufacturing a product or delivering a service, special reports and forms accompanied by all necessary materials are sent to the user for approval.
- The agreed service or product is delivered to the user within the shortest possible lead time thanks to continuous bi-directional interaction with the PoC 3D Unit.
- Requests, case submissions, and communications can, of course, be done via e-mails or by visiting the PoC 3D Unit, but would be better facilitated by a dedicated online platform. For this reason, the so-called *SkeletoMy* online platform was implemented, via which the following are offered:
    - User registration, and granted approval, credentials to login into the personal account.
    - Special submission forms, guidelines, and reports are exchanged with the user to ensure prerequisites fulfillment for delivering the requested services and products.
    - Constant tracking and updates of submitted request status. Especially for physical product development, the whole process is communicated step-by-step following the phases of the quality-assured inter-epistemic workflow shown before *(Figure 264)*.
    - 3D reconstructed anatomical models, 3D digital models, and other visual aids become available for download by the user via their accounts for viewing, manipulating, and editing.
    - Appointments for setting up xR experiences can be booked. However, as long as the user owns compatible xR devices, files for xR experience can be downloaded via the platform.
    - 3D scanning of body parts or any other objects can be arranged by appointment.
    - Physical 3DPed anatomical replicas and patient-specific products developed by the quality-assured inter-epistemic workflow *(Figure 264)* are packaged with all required

documentation and delivered clean but non-sterile, hence, sterilization is required before application. The packaged products can be picked up by or delivered to the user.

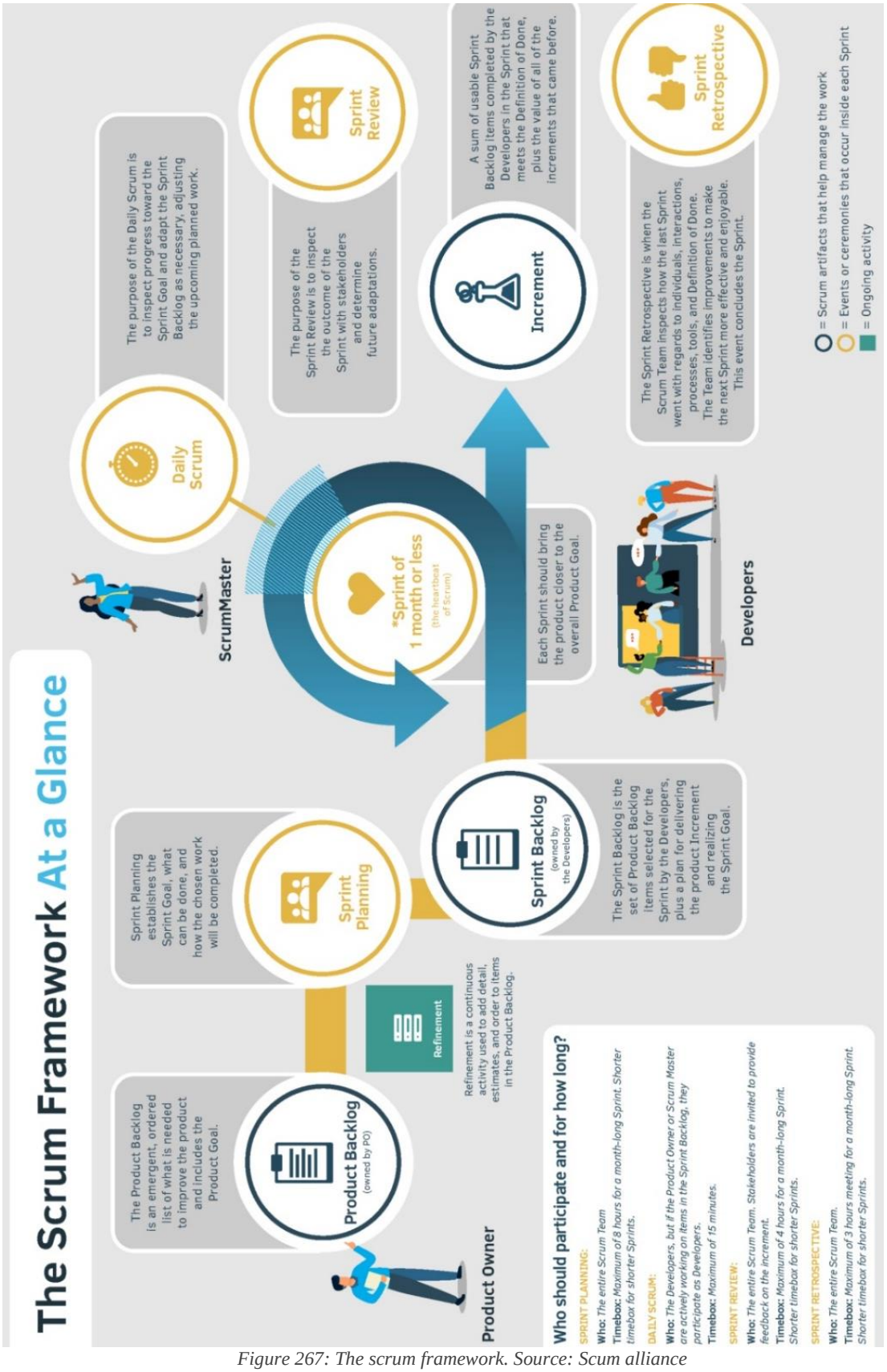

Figure 267: The scrum framework. Source: Scum alliance

The methodology employed and all documents and forms exchanged via the *SkeletoMy* platform between the user and the PoC 3D Unit are described next.

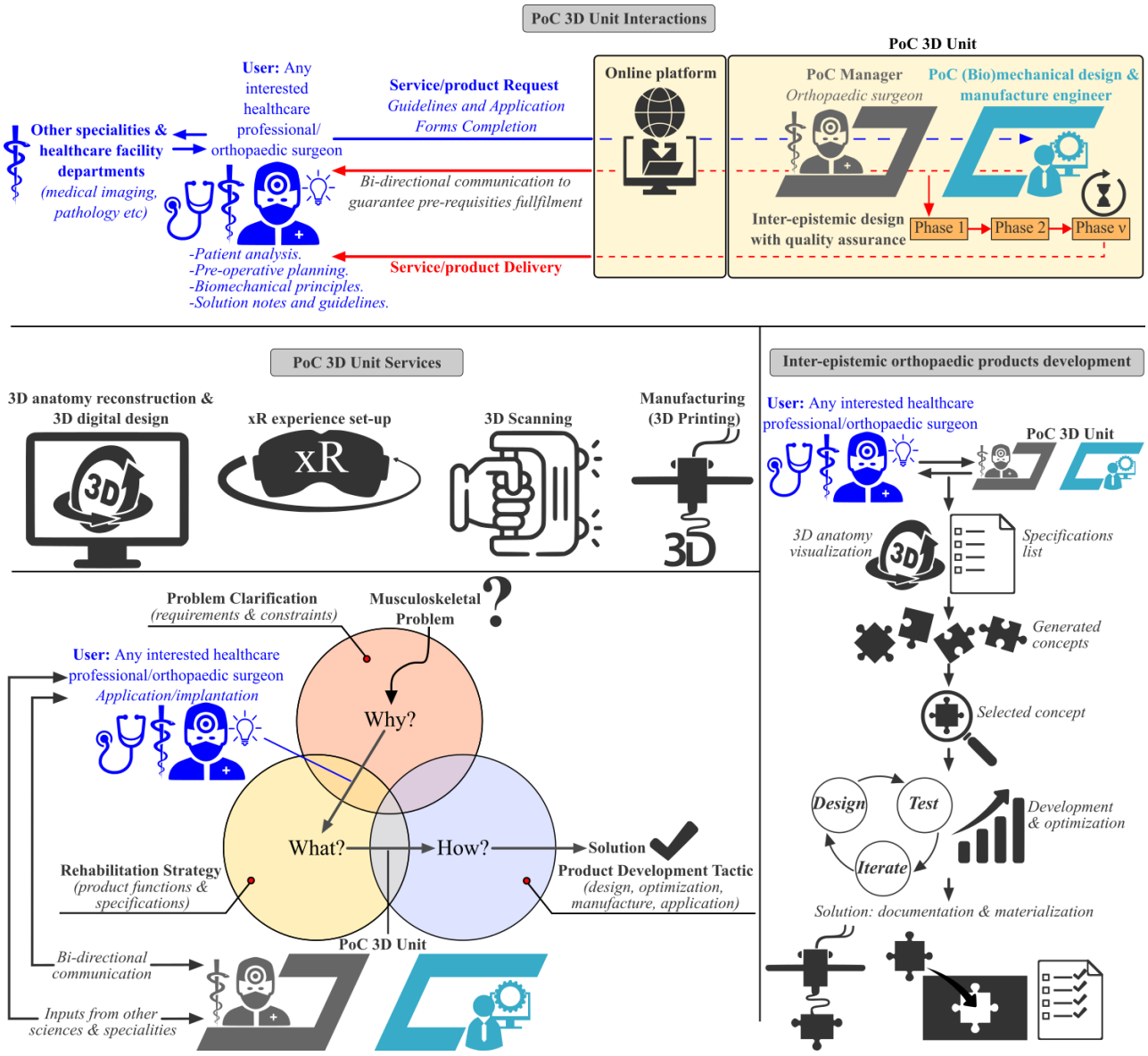

Figure 268: PoC 3D Unit interactions, services, and product development

5.2.1 SkeletoMy Online Platform

SkeletoMy's logo and its punch line are shown in *Figure 269* whereas the home page, login/registration, contact, privacy policy, and terms and conditions pages of the website are pictured in *Appendix M*. The skeletomy.com domain was bought and embedded with the free and open-source *WordPress*[65] which was loaded with all the necessary plug-ins to serve our needs.

Users can visit in person the PoC 3D Unit, or contact (call or e-mail (info@skeletomy.com)), or via the *SkeletoMy* website (https://www.skeletomy.com) where they can register and obtain personal accounts to submit and track their requests *(Figure 270)*. It is worth mentioning that users are defined as *"any interested healthcare professionals/orthopaedic surgeons registered to SkeletoMy platform*

[65] WordPress is a free open-source content management system (CMS) written in hypertext preprocessor language and paired with a MySQL or MariaDB database with supported HTTPS. Features include a plugin architecture and template system (themes). For details see https://wordpress.org/.

holding an active account with the ability to submit requests for services and/or products to use these as aids in diagnosing and/or treating his patient(s) for whom (patient(s)) he (user) is responsible for. Users a) provide design input, guidelines, notes, and instructions for the development and delivery of the services and/or products they request, b) approve in their whole the requested services and/or products before realization and delivery by SkeletoMy, and c) take full responsibility for their performance, usage, risk, and safety of the requested services and/or products".

Figure 269: SkeletoMy logo and punch line

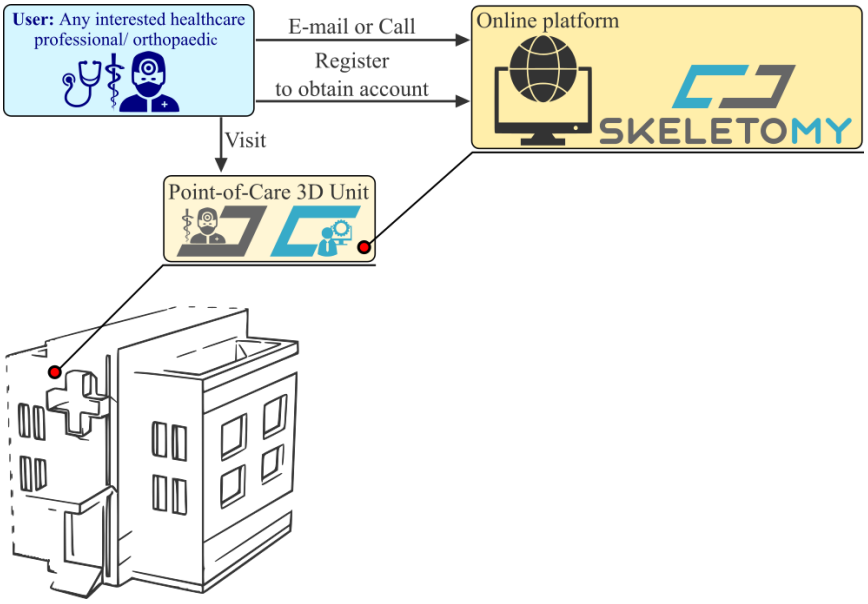

Figure 270: Options for users to communicate with the PoC 3D Unit

SkeletoMy was set up in such a manner, as if Scenario 1 was realized with an adequate flow of requests for localized or distributed manufacturing. The flow chart in *Figure 276* explains how users are served by the PoC 3D Unit via *SkeletoMy* online platform, i.e. *(see Appendix M for screenshots)*:

1. Interested potential users enter https://www.skeletomy.com and submit the registration form.
2. Granted administrator approval, users get an e-mail with activation instructions and obtain credentials to log into their accounts.
3. Registered users can request any of the available services: 3D Scanning, Virtual/Augmented/Mixed Reality, 3D reconstruction and 3DP of anatomical models, 3D design, and 3DP of customized products. To facilitate service request submission, the user is guided through application forms. For suitable patient medical image data acquisition and sharing, a document (scan protocol) containing instructions is made available to the users before service request submission *(Figure 271)*.

For patient privacy, it is necessary to anonymize all patient's data. To do so (anonymization), the free and open-source PixelMed Publishing's (Pennsylvania, US) *DicomClearner*[66] software was recommended *(Figure 272)*. For physical materials being delivered to the PoC 3D Unit, the patient data was recommended to be masked for privacy. A special code is assigned to submitted requests so that each case is addressed using this code.

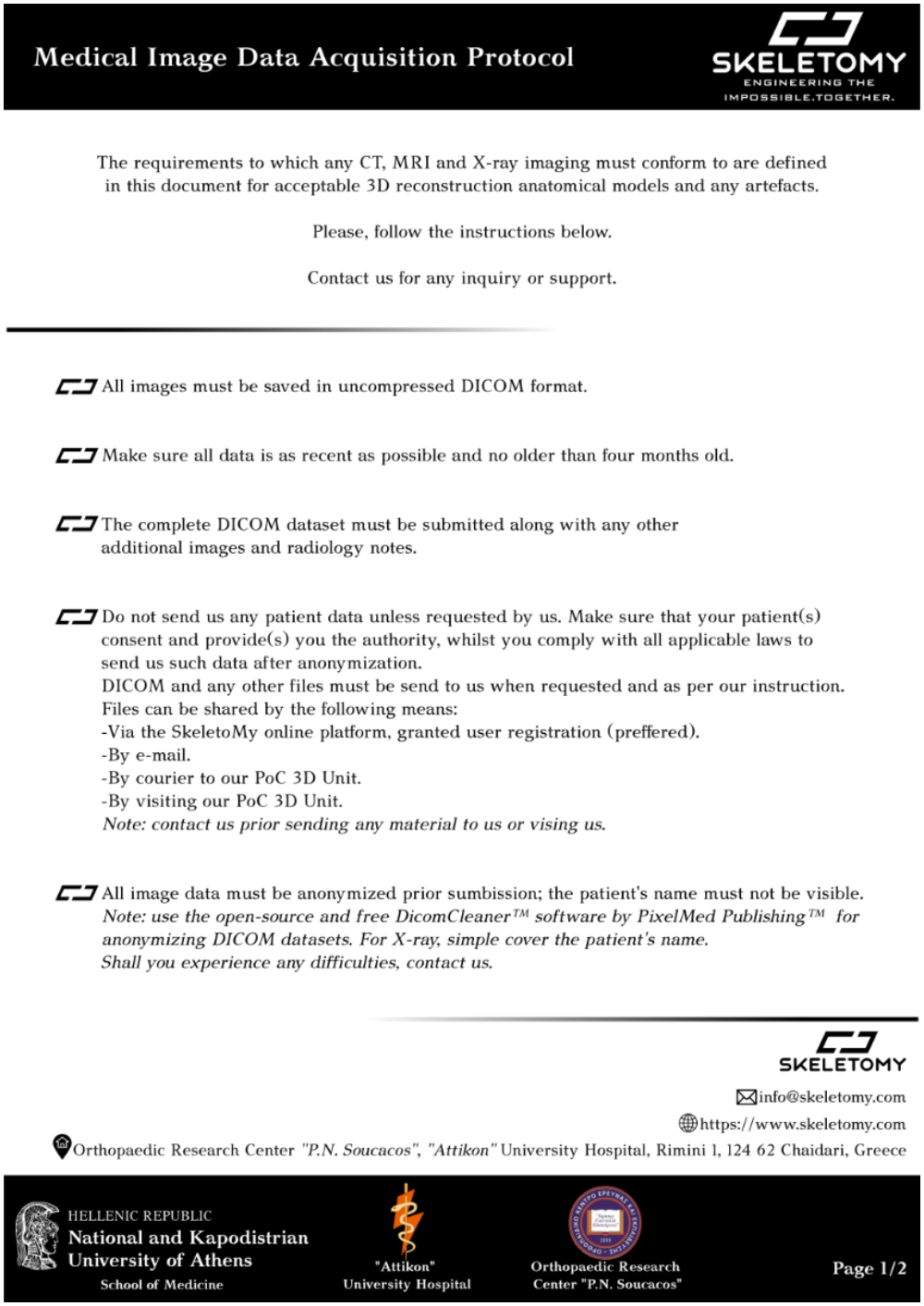

Medical Image Data Acquisition Protocol

SKELETOMY
ENGINEERING THE IMPOSSIBLE.TOGETHER.

The requirements to which any CT, MRI and X-ray imaging must conform to are defined in this document for acceptable 3D reconstruction anatomical models and any artefacts.

Please, follow the instructions below.

Contact us for any inquiry or support.

- All images must be saved in uncompressed DICOM format.
- Make sure all data is as recent as possible and no older than four months old.
- The complete DICOM dataset must be submitted along with any other additional images and radiology notes.
- Do not send us any patient data unless requested by us. Make sure that your patient(s) consent and provide(s) you the authority, whilst you comply with all applicable laws to send us such data after anonymization.
  DICOM and any other files must be send to us when requested and as per our instruction.
  Files can be shared by the following means:
  -Via the SkeletoMy online platform, granted user registration (preffered).
  -By e-mail.
  -By courier to our PoC 3D Unit.
  -By visiting our PoC 3D Unit.
  Note: contact us prior sending any material to us or vising us.
- All image data must be anonymized prior sumbission; the patient's name must not be visible.
  Note: use the open-source and free DicomCleaner™ software by PixelMed Publishing™ for anonymizing DICOM datasets. For X-ray, simple cover the patient's name.
  Shall you experience any difficulties, contact us.

SKELETOMY
info@skeletomy.com
https://www.skeletomy.com
Orthopaedic Research Center *"P.N. Soucacos"*, *"Attikon"* University Hospital, Rimini 1, 124 62 Chaidari, Greece

HELLENIC REPUBLIC
National and Kapodistrian University of Athens
School of Medicine
"Attikon" University Hospital
Orthopaedic Research Center "P.N. Soucacos"
Page 1/2

(continues)

[66] PixelMed Publishing's DicomClearner is a free and open-source tool with a user interface for importing, "cleaning" (removing and/or replacing information) and saving sets of DICOM instances (files). For more information visit http://www.dclunie.com/pixelmed/software/webstart/DicomCleanerUsage.html.

(continued)

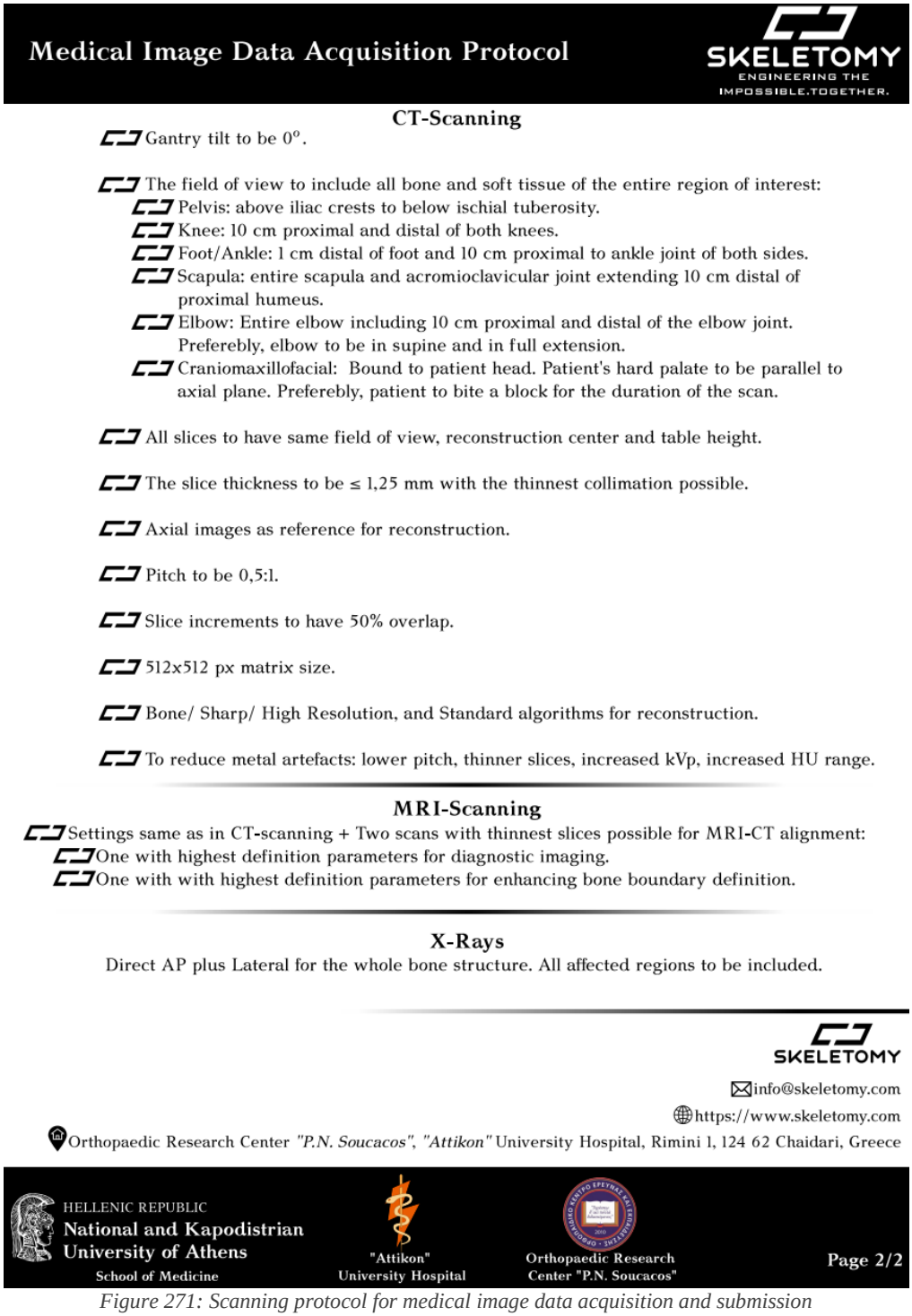

Figure 271: Scanning protocol for medical image data acquisition and submission

During service request submission, files less than 1 GB combined are shared directly via *SkeletoMy's* upload tab, and larger files via *WeTransfer*[67] (WeTransfer BV, Amsterdam, Netherlands) or *Google Drive*[68]. Supplementary or pending material can be shared later, both digitally or physically. For 3D scanning of a patient's body part or any other object, and for xR

[67] WeTransfer is a file transfer service, free up to 2 GB file size. For more visit https://wetransfer.com/.

[68] Google Drive is a file storage, synchronization, and file sharing service, free up to 15 GB. More details can be found at https://www.google.com/drive/.

experience (if the user does not own equipment), the user must book a time slot to arrange a visit to the PoC 3D Unit (or the PoC 3D Unit team to visit him). 3D visuals can be sent via *SkeletoMy* to the user and 3DPed objects are delivered to the user or picked up by the user.

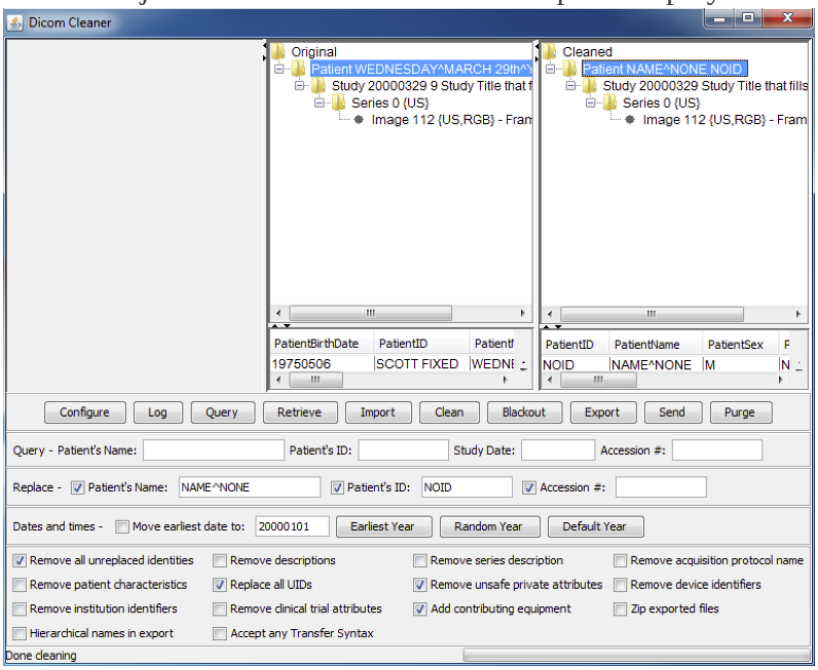

Figure 272: PixelMed Publishing's DicomCleaner interface

4. Granted all prerequisites have been covered for the requested service(s), an agreement document containing Terms of Use and Warranty Notes[69] (*Figure 273*), and the estimated cost are shared with the user for approval and sign off. This agreement document, as well as payment options, will not be analyzed in this Thesis.
5. Once the agreement document has been approved and signed off by the user, the process proceeds. A code is assigned to the request/case and a project is created and shared privately with the user. Projects are broken into tasks assigned to each party (user or PoC 3D Unit). Via their accounts, users can access their projects, track their progress, and see which task is assigned to each party. A project management system (Atlassian's Jira software) is adopted by the members of the PoC 3D Unit for the reasons mentioned before. Users can chat and exchange data under the corresponding project. Any 3D digital material is made available to the user for online interactive viewing via *SkeletoMy* (3D models are embedded using *Sketchfab*[70] (Sketchfab Inc., New York, US)) or any of the suggested online and offline viewer *(see next Sub-section 5.3).*

[69] Important information is included in the Terms of Use and Warranty Notes, e.g. sterilization notes, packing list, required tools, associated risks, indications, contraindications, warnings, precautions, and potential side effects (e.g. premature loss of fixation, wear, failure to abnormal activity and loadings, soft tissue irritation or damage, bone loss, loss of sensation and mobility, dislocations, pain, allergic reactions).

[70] Sketchfab is a platform used to upload and share 3D models to be interactively viewed on 3D in any computer or mobile device, or viewed in VR/AR mode. See https://sketchfab.com.

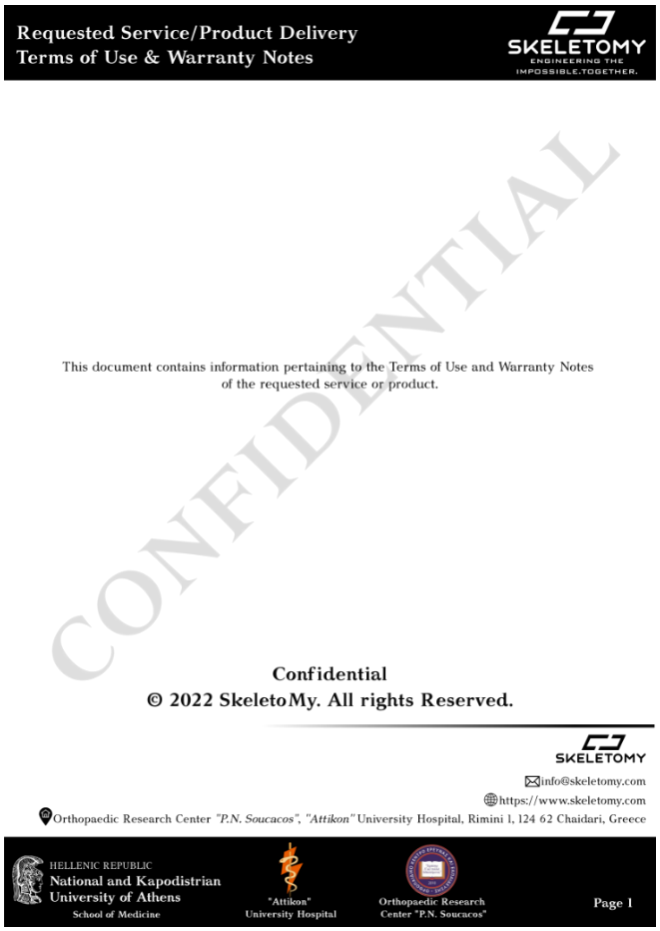

Figure 273: SkeletoMy's Terms of Use and Warranty Notes

6. As the user takes most, if not all, of the responsibility for the usage and performance of any service or product offered by the PoC 3D Unit, documentation is delivered to the user for approval and sign off. These reports are part of the technical folder justifying the need for a custom-made device and are used to gain the required approval by the HCF and adhere to applicable regulations. Especially for custom-made devices, the orthopaedic surgeon who tracks the progress step-by-step via the *SkeletoMy* platform and participates in the workflow must approve and sign off the following reports which are accompanied by extra materials *(Figure 275):*
    a. **Final proposal check and justification report:** workflow highlights and features of the final solution are graphically summarized. Materials selected and their usage and performance are justified. Custom manufacturing rather than sourcing off-the-shelf is rationalized. The adopted QMS ensures the reduction of errors and risks for high-quality consistency throughout all stages of the inter-epistemic workflow *(Figure 264)*.
    b. **Safety, risk assessment, and quality management report:** safety must be guaranteed by identifying and mitigating any associated risks to assure and control high-quality output by following standardized procedures using certified equipment and software by qualified personnel, whilst conforming to applicable national and international regulations as per the medical device category to be developed.

c. **Application/implantation instructions:** detailed illustrated step-by-step instructions to guide application/implantation must accompany the developed solution.
d. **Manufacturing instructions:** the end-to-end manufacturing processes of the selected materials to be applied and the end-result specifications are outlined.

The reports are confidential and must not redistributed, duplicated, or disclosed to others. The reports must be approved on their whole and signed-off to commence production and deliver the product to the user. Alternative proposals or approaches, or amendments and remarks must be noted for design revision and iteration.

7. Once all reports have been approved and signed-off, the product is prepared for the production of all (in)tangible deliverables, and delivered to the user as, when, and where agreed.
8. For business improvement (offered services and products, strategy and tactics) and the user experience, a feedback report is sent to the user after the successful application/implantation of the requested service/product *(Figure 274)*.

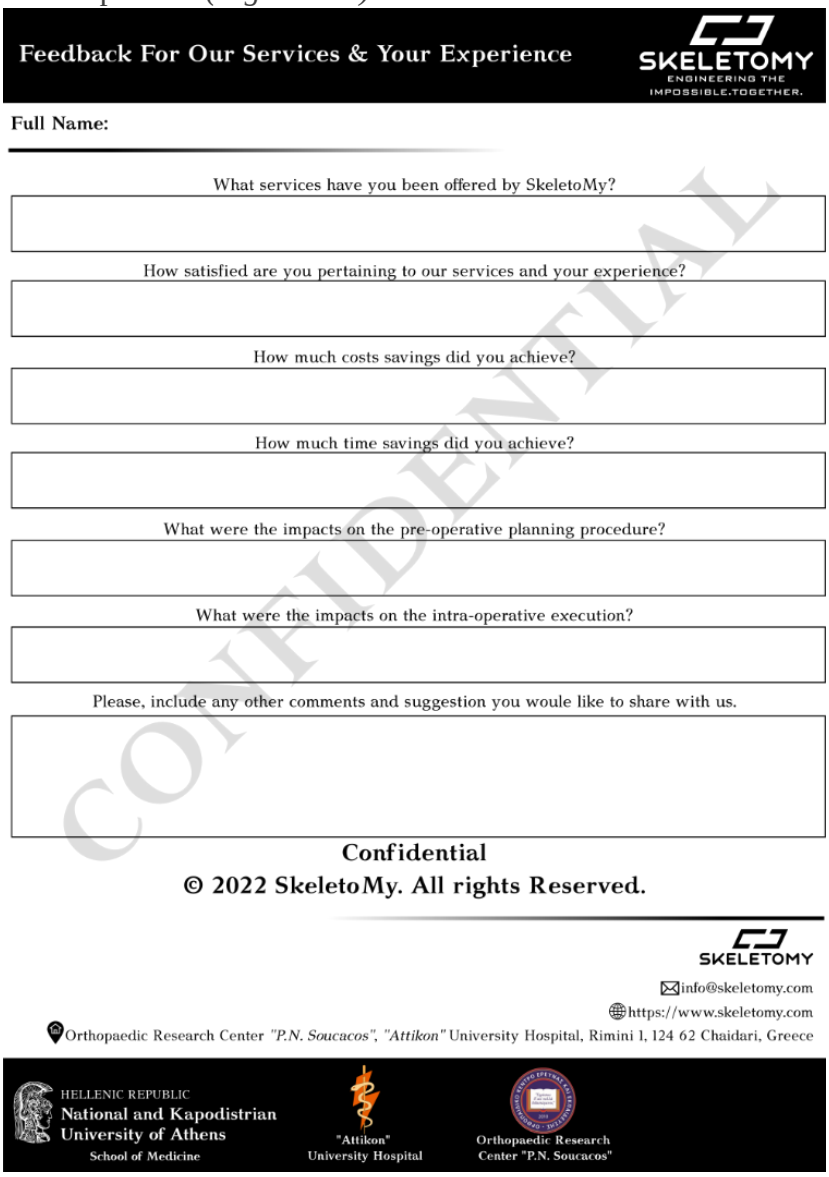
Feedback For Our Services & Your Experience

SKELETOMY
ENGINEERING THE IMPOSSIBLE.TOGETHER.

Full Name:

What services have you been offered by SkeletoMy?

How satisfied are you pertaining to our services and your experience?

How much costs savings did you achieve?

How much time savings did you achieve?

What were the impacts on the pre-operative planning procedure?

What were the impacts on the intra-operative execution?

Please, include any other comments and suggestion you woule like to share with us.

CONFIDENTIAL

Confidential
© 2022 SkeletoMy. All rights Reserved.

SKELETOMY
info@skeletomy.com
https://www.skeletomy.com
Orthopaedic Research Center *"P.N. Soucacos"*, *"Attikon"* University Hospital, Rimini 1, 124 62 Chaidari, Greece

HELLENIC REPUBLIC
National and Kapodistrian University of Athens
School of Medicine
"Attikon" University Hospital
Orthopaedic Research Center "P.N. Soucacos"

Figure 274: User feedback report for SkeletoMy improvement

Patient-specific Product
Final Proposal Check - Justification Report

SKELETOMY ENGINEERING THE IMPOSSIBLE.TOGETHER.

Case No.:
Submission Date:
Responsible Professional:

Case Description:

This report contains information pertaining to the proposed customized solution requested and satisfies the specifications list that was set collaboratively.

To facilitate the review, this report is accompanied by 3D digital and physical models (and optionally models for Virtual/Mixed Reality experience).

Please, approve or decline the proposed solution and provide any notes.

The Responsible Healthcare Professional:

I approve the solution in its whole: Yes ☐ No ☐

Signature: Date:

Please, also confirm receipt and approve by responding to the e-mail sent to you by SkeletoMy.

Confidential
© 2022 SkeletoMy. All rights Reserved.

SKELETOMY
info@skeletomy.com
https://www.skeletomy.com
Orthopaedic Research Center *"P.N. Soucacos"*, *"Attikon"* University Hospital, Rimini 1, 124 62 Chaidari, Greece

Patient-specific Product
Manufacturing Instructions

SKELETOMY ENGINEERING THE IMPOSSIBLE.TOGETHER.

Case No.:
Submission Date:
Responsible Professional:

Case Description:

This report contains information pertaining to the proposed customized solution requested.

Please, confirm receipt of this report and provide any notes.

The Responsible Healthcare Professional:

I approve the solution in its whole: Yes ☐ No ☐

Signature: Date:

Please, also confirm receipt and approve by responding to the e-mail sent to you by SkeletoMy.

Confidential
© 2022 SkeletoMy. All rights Reserved.

SKELETOMY
info@skeletomy.com
https://www.skeletomy.com
Orthopaedic Research Center *"P.N. Soucacos"*, *"Attikon"* University Hospital, Rimini 1, 124 62 Chaidari, Greece

Patient-specific Product
Application/Implantation Instructions

SKELETOMY ENGINEERING THE IMPOSSIBLE.TOGETHER.

Case No.:
Submission Date:
Responsible Professional:

Case Description:

This report contains information pertaining to the proposed customized solution requested.

This report is accompanied:

- 3D digital and physical models (and optionally models for Virtual/Mixed Reality experience).
- Final proposal check report.
- Manufacturing instructions.

Please, confirm receipt of this report and provide any notes.

The Responsible Healthcare Professional:

I approve the solution in its whole: Yes ☐ No ☐

Signature: Date:

Please, also confirm receipt and approve by responding to the e-mail sent to you by SkeletoMy.

Confidential
© 2022 SkeletoMy. All rights Reserved.

SKELETOMY
info@skeletomy.com
https://www.skeletomy.com
Orthopaedic Research Center *"P.N. Soucacos"*, *"Attikon"* University Hospital, Rimini 1, 124 62 Chaidari, Greece

Patient-specific Product Report
Safety-Risk Assesment-Quality Management

SKELETOMY ENGINEERING THE IMPOSSIBLE.TOGETHER.

Case No.:
Submission Date:
Responsible Professional:

Case Description:

This report contains information pertaining to the proposed customized solution requested.

This report is accompanied:

- 3D digital and physical models (and optionally models for Virtual/Mixed Reality experience).
- Final proposal check report.
- Manufacturing instructions.
- Application/implantation instruction.

Please, confirm receipt of this report and provide any notes.

The Responsible Healthcare Professional:

I approve the solution in its whole: Yes ☐ No ☐

Signature: Date:

Please, also confirm receipt and approve by responding to the e-mail sent to you by SkeletoMy.

Confidential
© 2022 SkeletoMy. All rights Reserved.

SKELETOMY
info@skeletomy.com
https://www.skeletomy.com
Orthopaedic Research Center *"P.N. Soucacos"*, *"Attikon"* University Hospital, Rimini 1, 124 62 Chaidari, Greece

Figure 275: Reports sent to the user for approval of patient-specific products

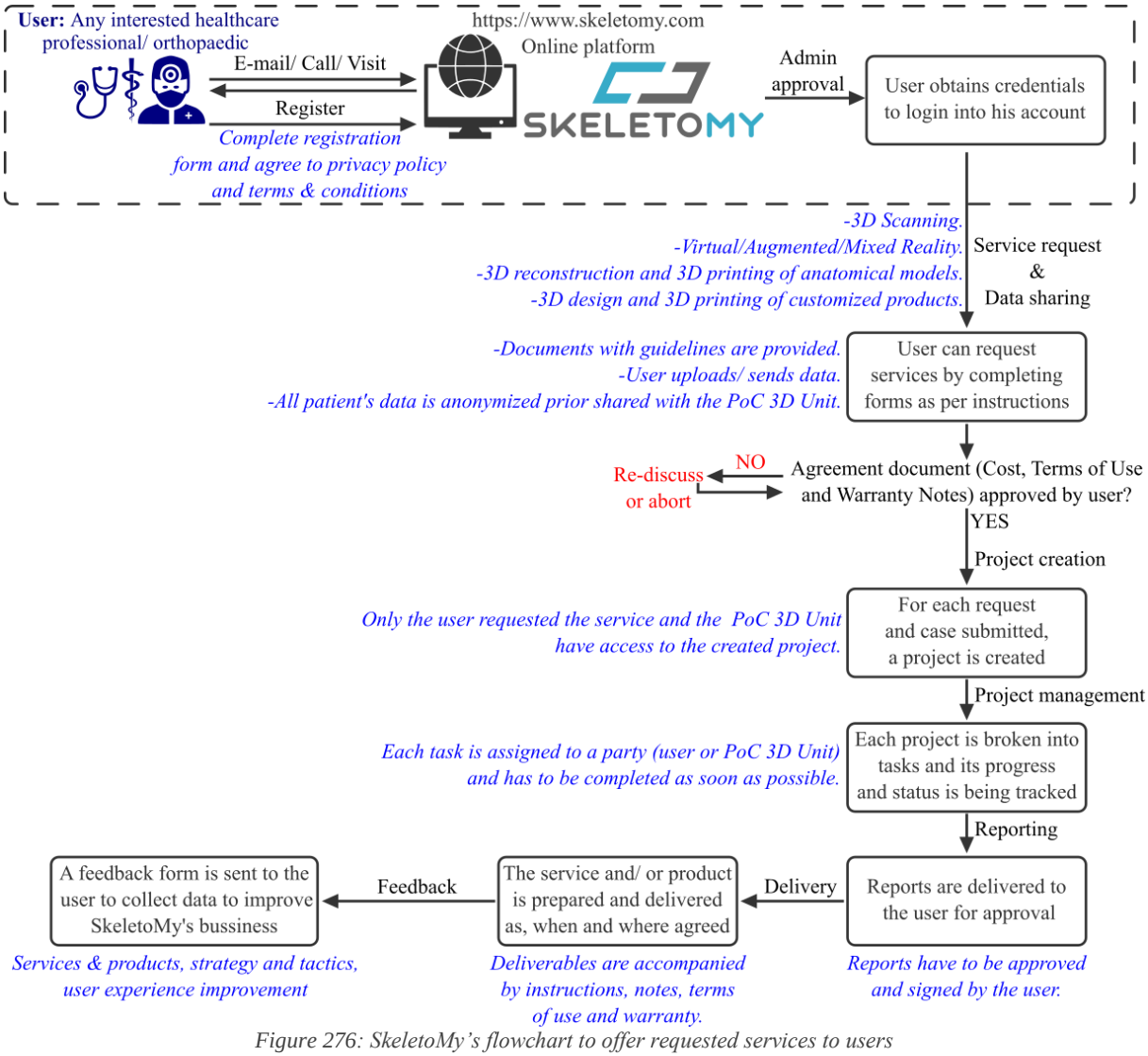

Figure 276: SkeletoMy's flowchart to offer requested services to users

5.2.2 Regulations and Quality Management

As per the EU's MDR 2017/745 *(Official Journal of the EU, 2017)*:

- A medical device is *"any instrument, apparatus, appliance, software, implant, reagent, material or other article intended by the manufacturer to be used, alone or in combination, for human beings for one or more of the following specific medical purposes:*
  - *diagnosis, prevention, monitoring, prediction, prognosis, treatment, or alleviation of disease.*
  - *diagnosis, monitoring, treatment, alleviation of, or compensation for, an injury or disability. investigation, replacement, or modification of the anatomy or of a physiological or pathological process or state.*
  - *providing information by means of in vitro examination of specimens derived from the human body, including organ, blood, and tissue donations,*

and which does not achieve its principal intended action by pharmacological, immunological, or metabolic means, in or on the human body, but which may be assisted in its function by such means. The following products shall also be deemed to be medical devices:

- *devices for the control or support of conception.*
- *products specifically intended for the cleaning, disinfection, or sterilization of devices."*

- A custom-made device is *"any device specifically made in accordance with a written prescription of any person authorized by national law by virtue of that person's professional qualifications which gives, under that person's responsibility, specific design characteristics, and is intended for the sole use of a particular patient exclusively to meet their individual conditions and needs. However, mass-produced devices that need to be adapted to meet the specific requirements of any professional user and devices that are mass-produced by means of industrial manufacturing processes in accordance with the written prescriptions of any authorized person shall not be considered to be custom-made devices".*

Regulations pertaining to custom-made orthopaedic devices were described in *Sub-section 3.4*. Regulations should be seen as encouragement for high-quality personalized techniques, rather than restrictions. To ensure that the specific needs of an individual patient are met, many jurisdictions involve special regulatory pathways that exempt emergency-use non-trialing custom-made medical devices: an authorized healthcare professional provides design input and takes some of the responsibility normally placed on manufacturers for the safety and performance of the finished medical devices.

ASME *(2020)* mentioned the barriers that impede PoC 3D Unit establishment, with the most important being regulatory compliance, lack of harmonized standards, and QMS. Custom-made medical devices in the EU are regulated by Annex XIII of the MDR 2017/745 *(Official Journal of the EU, 2017)*. The outlined requirements apply to the *"person responsible for regulatory compliance"* which must have a relevant degree or be technically competent with experience to carry out the requirements. In case such a person is not available, the entity can consult a third-party expert who has regulatory compliance or train an internal person. These regulations give enough flexibility to healthcare facilities to organize their own development process for custom orthopaedic devices as long as proper collaborations and an appropriate product QMS are maintained, loaded with processes to reduce risks, errors, and mistakes to ensure safety and high-quality consistency not only for the design and manufacture but also for increasing the creditability of the legal entity (PoC 3D Unit).

More specifically, in the MDR 2017/745, the following notes are given:

1. The manufacturer or its authorized representative draws up a statement containing:
    a. Manufacturer's name and address sites.

b. Authorized representative name and address (if applicable).
c. Data allowing identification of the device in question.
d. A statement that the device is intended for exclusive use by a particular patient or user, identified by name, an acronym, or a numerical code.
e. Name of the person who made out the prescription and who is authorized by national law by virtue of their professional qualifications to do so, and, where applicable, the name of the health institution concerned.
f. Specific characteristics of the product as indicated by the prescription.
g. Statement that the device in question conforms to the general safety and performance requirements set out in Annex I and, where applicable, indicating which general safety and performance requirements have not been fully met, together with the grounds.
h. Where applicable, an indication that the device contains or incorporates a medicinal substance, including a human blood or plasma derivative, or tissues or cells of human origin, or of animal origin as referred to in Regulation (EU) No 722/2012.

2. The manufacturer shall undertake to keep available for the competent national authority's documentation that indicates its manufacturing site or sites and allows an understanding to be formed of the design, manufacture, and performance of the device, including the expected performance, to allow assessment of conformity with the requirements of this Regulation.
3. The manufacturer shall take all measures necessary to ensure that the manufacturing process produces devices in accordance with the documentation referred to in Section 2 (i.e., 1) Device description and specification, 2) Information to be supplied by the manufacturer, 3) Design and manufacturing information, 4) General safety and performance requirements, 5) Benefit-risk analysis and risk management, 6) Product verification and validation).
4. The statement referred to in the introductory part of Section 1 shall be kept for at least 10 years after the device has been placed on the market. In the case of implantable devices, the period shall be at least 15 years. Section 8 of Annex IX shall apply.
5. The manufacturer shall review, and document experience gained in the post-production phase, including from post-market clinical follow-up (PMCF) as referred to in Part B of Annex XIV, and implement appropriate means to apply any necessary corrective action. In that context, it shall report in accordance with Article 87(1) to the competent authorities any serious incidents or field safety corrective actions or both as soon as it learns of them.

Especially for emergency medical devices developed and used within HCFs, such are exempted from the aforementioned regulations, but must conform to Article 5.5 of the MDR 2017/745 *(Official Journal of the EU, 2017)*. More specifically, for non-mass-produced devices, it is stated that *"With*

the exception of the relevant general safety and performance requirements set out in Annex I, the requirements of this Regulation shall not apply to devices, manufactured, and used only within health institutions established in the Union, provided that all of the following conditions are met:

a) The devices are not transferred to another legal entity.

b) The manufacture and use of the devices occur under appropriate quality management systems.

c) The health institution justifies in its documentation that the target patient group's specific needs cannot be met or cannot be met at the appropriate level of performance by an equivalent device available on the market.

d) The health institution provides information upon request on the use of such devices to its competent authority, which shall include a justification of their manufacturing, modification, and use.

e) The health institution draws up a declaration which it shall make publicly available, including:

- *The name and address of the manufacturing health institution.*
- *The details necessary to identify the devices.*
- *A declaration that the devices meet the general safety and performance requirements set out in Annex I to this Regulation.*
- *Where applicable, information on which requirements are not fully met with a reasoned justification, therefore.*

f) The health institution draws up documentation that makes it possible to understand the manufacturing facility, the manufacturing process, the design and performance data of the devices, including the intended purpose, and that is sufficiently detailed to enable the competent authority to ascertain that the general safety and performance requirements set out in Annex I to this Regulation are met.

g) The health institution takes all necessary measures to ensure that all devices are manufactured in accordance with the documentation referred to in point (f), and (h) the health institution reviews experience gained from the clinical use of the devices and takes all necessary corrective actions.

Member States may require that such health institutions submit to the competent authority any further relevant information about such devices that have been manufactured and used on their territory. Member States shall retain the right to restrict the manufacture and the use of any specific type of such devices and shall be permitted access to inspect the activities of the health institutions. This paragraph shall not apply to devices that are manufactured on an industrial scale".

In summary, Annex I includes notes under the following sections for a medical device:

- Safe and effective design, manufacture, and packaging to achieve intended performance by the manufacturer.
- Establishment, implementation, documentation, and maintenance of a risk management system by the manufacturer.
- Chemical, physical, and biological properties.
- Active or made of biological constructs or from materials that are absorbed after implantation.
- Protection from infection and microbial contamination.
- Labeling, packaging, and instructions for use.

The QMS is a coordinated customer (patient) focused management activity including continuous improvement and encloses both quality assurance and quality control and is a crucial part of the medical device development process. Quality control aims at meeting the established quality criteria, and quality assurance provides confidence that quality requirements are being met.

A QMS as per the American Society for Quality is defined as *"a formal system that documents the structure, processes, roles, responsibilities, and procedures required to achieve effective quality management".* Any PoC entity must implement a QMS to execute its business by adopting policies, procedures, forms, and work instructions with a defined sequence, interactions, and resources, with records being documented to demonstrate adherence to the corresponding established QMS. The contents of the QMS to be adopted should address all applicable national and international standards and regulatory requirements, depending on the types and applications of medical devices the PoC entity will develop.

A QMS must focus on a) documenting how activities must be performed to maintain consistent high-quality practices and outputs, b) analytically describing process validation, verification, qualification, and equipment usage and maintenance, c) controlling quality whilst ensuring regulatory compliance, d) qualification and certification of personnel, and e) updating. Quality documentation must include seamlessly interconnected files throughout the entire product lifecycle: product information, risk assessment, scientific literature, clinical use and tests of materials, and technical documentation and records that are being stored and updated.

All stages of the medical device development must be reviewed, i.e.:

1. Planning: design and development plan, product description and specifications, quality plan, regulatory plan, risk management plan.
2. User needs: requirements and risk analysis
3. Design input: product specifications and risk analysis (identification) and management (mitigation and minimization) plan.

4. Design output: product and process design outputs (drawings, instructions, studies, tests, medical device realization).

The design output must satisfy the design inputs and reviewed, verified, and validated (verification and validation reports, manufacturing plan, residual risk acceptance, risk control) in terms of fulfillment of the planning and user needs, and associated documents must accompany all stages. Validation, verification, as well as qualification and certification of both personnel and any equipment used, are important elements of a QMS. More specifically *(Formlabs, 2021; Schlagintweit, 2021)*:

- Validation: it is a confirmation that a product fulfills fully or partially the requirements at the end of the process, but these cannot be clearly determined, hence the process parameters are checked and maintained. Validation can be categorized into conceptional (process mapping, risk assessment, validation planning) and hands-on (installation qualification, operational qualification, and performance qualification).
- Verification: it is a confirmation that a product satisfies specified requirements at the end of the process by measuring specific properties, e.g., dimensions, and mechanical and physical properties.
- Qualification: it is proof that the physical device functions properly with the desired properties and form. It includes installation qualification (ensure machinery is installed correctly and operates correctly), process characterization (conduct experiments to understand input factors that affect the output of the manufacturing process), operational qualification (demonstrate that devices built at process extremes meet device requirements), and performance qualification (demonstrate that devices built at nominal process settings consistently meet device requirements). For installation qualification the following should be outlined: purpose of use, scope, description, supplier, components, utilities, and construction-installation requirements, along with supporting documentation, maintenance plans, list of spare parts, drawings, testing and acceptance criteria, discrepancies, summary and conclusions. For operational qualification, there is a need for test calibration and verification, standard operating procedures, alarm/control challenges, operating parameters, rationale and sampling locations, testing and acceptance criteria, and test result documentation.

ISO 13485:2016 is the most well-fitted standard for QMS of medical device development. The standard includes several sub-sections that are illustrated in *Figure 277*.

The applicable sections of ISO 13485 can be established for a company using 3D design and 3DP for a comprehensive and well-controlled QMS to address the associated challenges whilst meeting all regulatory requirements and specifications of the customized medical device. PoC Units must establish their best practices by implementing quality management systems whilst conforming to

applicable regulations and standards. However, because existing regulations and standards oversee the way medical devices are manufactured, 3DP needs further guidance to establish quality control measures as numerous parameters might lead to a low-quality 3DPed product, i.e., data preparation variables, design features, feedstock materials, process and 3D printer parameters, personnel, documentation, infrastructure, and post-processing. Therefore, appropriate QMS including strategies and processes for addressing errors and improving consistency are important to control and assure quality and safety. Otherwise, the uncontrolled rapid growth of 3D design and 3DP technologies and the increasing complexity might put patients at increased risk for potential errors, decreased quality, and sub-optimal performance of the solution.

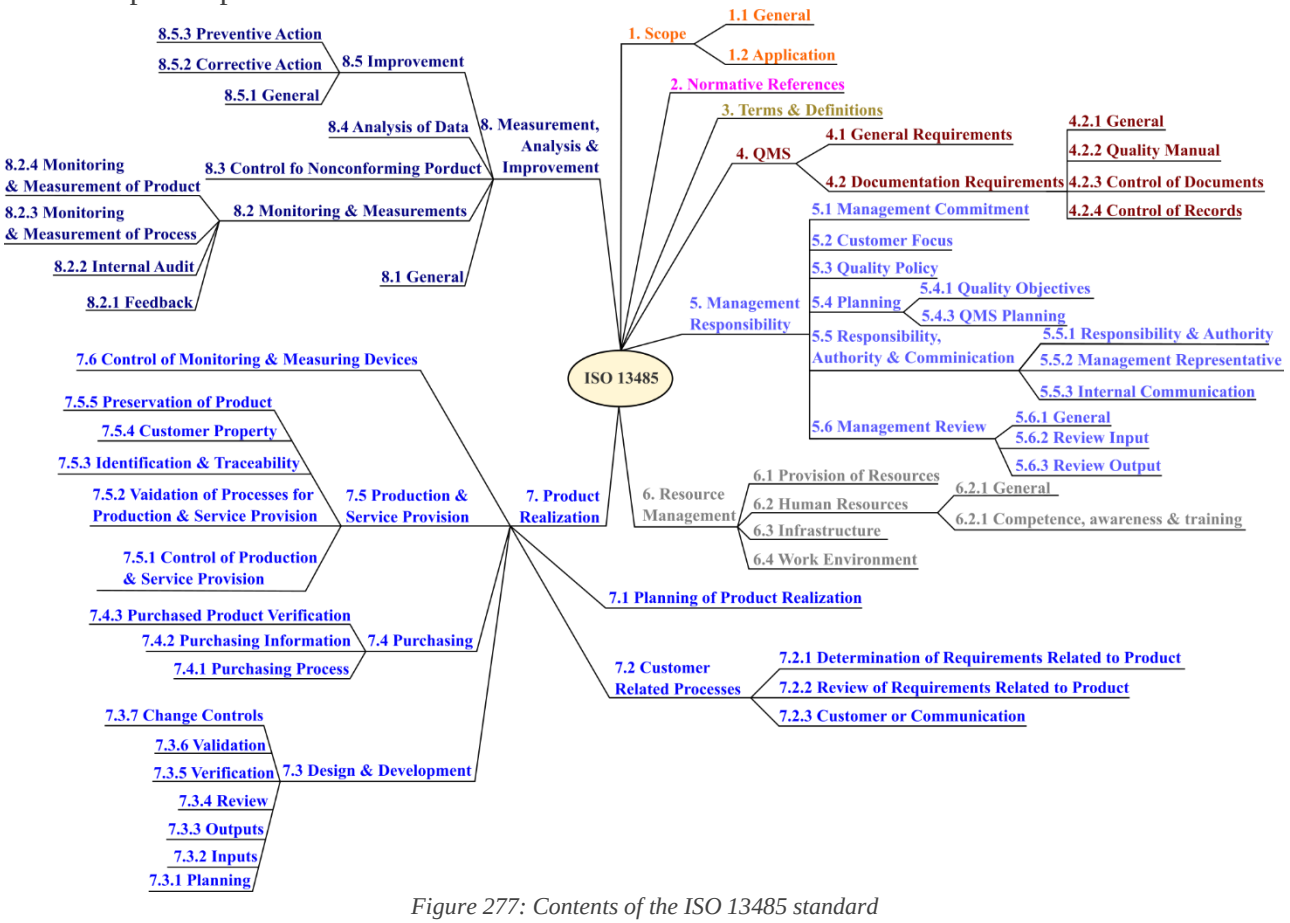

Figure 277: Contents of the ISO 13485 standard

Figure 278 shows a process mapping for 3DP of medical devices and an Ishigawa diagram with the parameters affecting the quality, time, compliance, and cost of the 3DPed part. 3DP processes can be broken chronologically into pre-process (verification of part requirements, data preparation, system set-up), in-process (verification/validation of 3DP equipment and feedstock), and post-processing techniques (e.g., surface treatments, cleaning, part property changing, assembly, packing, sterilization). Erroneous or inadequate cleaning, sterilization, and packaging can have serious consequences for the safety of a product. All these, plus documentation and qualified personnel have to be managed for quality management. Personnel should be competent (and this has to be maintained) to perform the required activities through education, training, skills, and experience.

Generic quality management standards cannot cover associated challenges, hence ISO/ASTM 3DP-specific standards *(see Table 9)* were established to serve as foundations for safety and non-safety critical parts development.

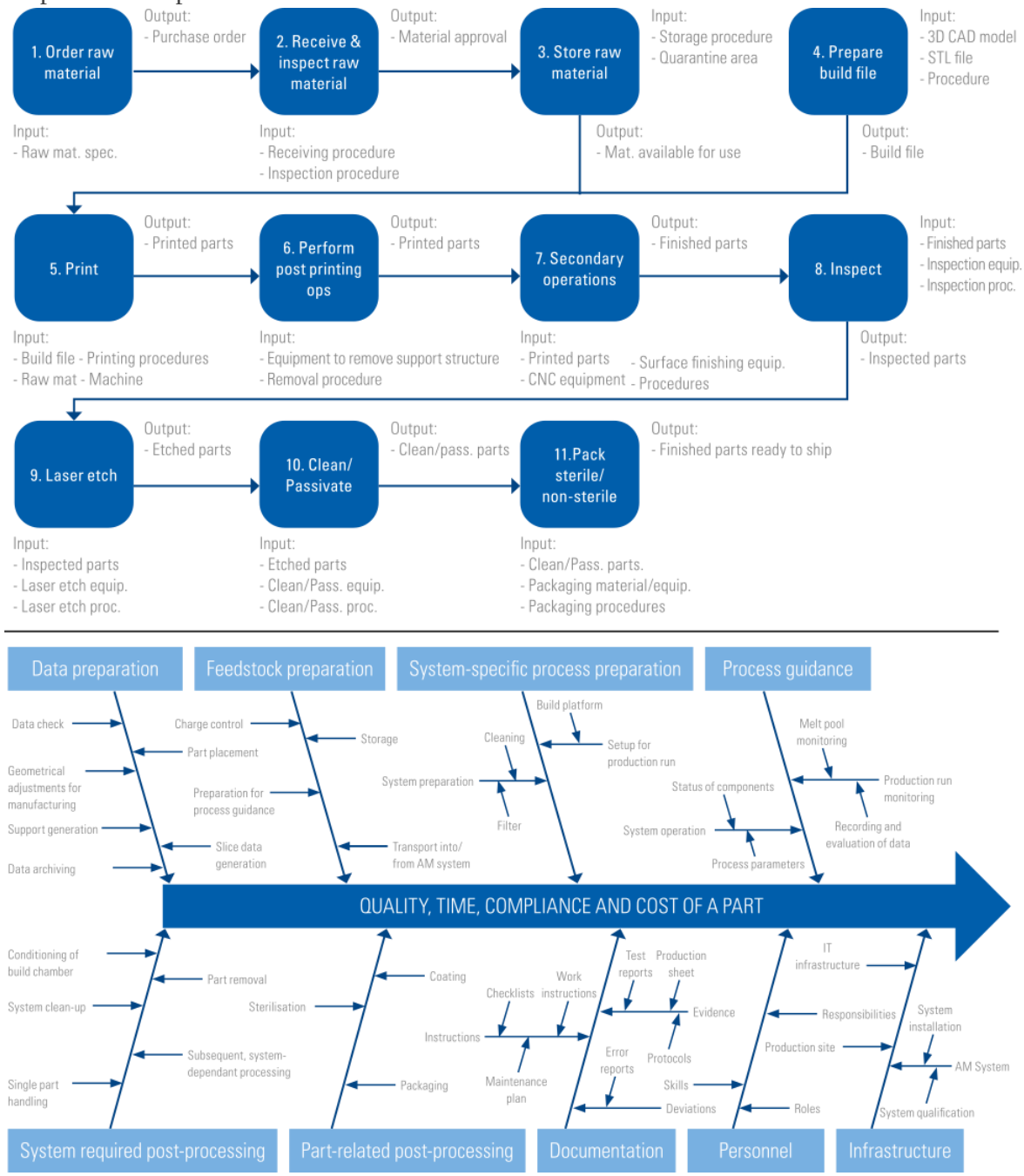

Figure 278: Process mapping for 3DP and parameters impacting the 3DPed product. Source: (Schlagintweit, 2021)

A technology-tailored and resources-specific QMS is necessary, as steps, processes, and testing requirements can vary depending on the device and application. For 3DPed devices, associated requirements and challenges must be clarified, e.g. compliant design, process parameters, checking dimensions and tolerances, and material properties.

In cases where contract manufacturers are employed, they must have the necessary competence and skills to deliver the requested product and/or service under a regulated and standardized scheme, which has to be checked via documentation, reports, and audits.

ISO 149671:2019 explains how to establish a risk management system that must accompany medical devices *(Figure 279)*. Harms occurrence probability and their severity help in defining a hierarchy of risks that should be identified, evaluated, analyzed, assessed, and mitigated. To ensure the biocompatibility of a medical device, a biological risk assessment should be carried out by evaluation as per ISO 10993-1:2018. Other applicable standards for medical devices and 3DP of such at by a manufacturer (PoC 3D Unit) are summarized in *Table 9*, and further considerations for PoC manufacturers of medical devices are summarized in *Appendix N*.

Table 9: List of standards on development, 3DP, and quality control of medical devices

Description	Standards
Quality management	EN ISO 13485:2016 (Medical devices – Quality management systems – Requirements for regulatory purposes). ISO 9001:2015 (Quality management systems – Requirements).
Biological evaluation	ISO 10993-1:2018 (Biological evaluation of medical devices – Part 1: Evaluation and testing within a risk management process).
Risk management	ISO 14971:2019 (Medical devices – Application of risk management to medical devices).
Packaging	Packaging for terminally sterilized medical devices, comprised of: ISO 11607-1:2019 (Part 1: Requirements for materials, sterile barrier systems and packaging systems). ISO 11607-2:2019 (Part 2: Validation requirements for forming, sealing and assembly processes).
Sterilization	EN 556-1:2001 (Sterilization of medical devices). Sterilization of health care products – Microbiological methods, comprised of: ISO 11737-1:2018 (Part 1: Determination of a population of microorganisms on products). ISO 11737-2:2019 (Part 2: Tests of sterility performed in the definition, validation and maintenance of a sterilization process). ISO 11737-3:2023 (Part 3: Bacterial endotoxin testing).
Labeling	ISO 15223-1:2021 (Medical devices – Symbols to be used with information to be supplied by the manufacturer – Part 1: General requirements). ISO 15223-2:2010 (Medical devices – Symbols to be used with medical device labels, labeling, and information to be supplied – Part 2: Symbol development, selection and validation).
On machinery	• Directive 2006/42/EC of the European Parliament and of the Council of 17 May 2006 on machinery, and amending Directive 95/16/EC (recast). Safety of machinery, e.g.: • EN ISO 12100:2010 (Safety of machinery – General principles for design – Risk assessment and risk reduction).

	• EN 60204-1:2018 (Safety of machinery – Electrical equipment of machines). • EN 13849-1:2015 (Safety of machinery – Safety-related parts of control systems). • EN 13850:2015 (Safety of machinery – Emergency stop function – Principles for design). • EN ISO 11553-1:2020 (Laser processing machines). • EN 1127-1:2019 (Explosive atmospheres – Explosion prevention and protection). • EN ISO 19353:2019 (Safety of machinery – Fire prevention and fire protection). • EN 60825-1:2014 (Safety of laser products – Part 1: Equipment classification and requirements). • EN 60825-4:2022 (Safety of laser products – Part 4: Laser guards).
ASTM's committee F42 and ISO's 261 technical committee on 3DP-related standards.	• ISO/ASTM 52920 (Additive manufacturing – Qualification principles – Quality assurance requirements for production). • ISO/ASTM 52904:2019 (Additive manufacturing – Process characteristics and performance: Practice for metal powder bed fusion process to meet critical applications). • ISO/ASTM TS 52930:2021 (Additive manufacturing – Qualification principles – Installation, operation and performance (IQ/OQ/PQ) of PBF-LB equipment). • ISO/ASTM 52950:2021 (Additive manufacturing – General principles – Overview of data processing). • ISO/ASTM 52936-1 (Additive manufacturing of polymers – Qualification principles – Part 1: General principles and preparation of test specimens for PBF-LB). • ISO/ASTM DIS 52935 (Additive manufacturing of metals – Qualification principles – Qualification of AM coordination personnel). • ISO/ASTM CD 52933 (Additive manufacturing – Environment, health and safety – Consideration for the reduction of hazardous substances emitted during the operation of the non-industrial ME type 3D printer in workplaces, and corresponding test method). • ISO/ASTM 52931 (Additive manufacturing of metals – Environment, health and safety – General principles for use of metallic materials). • ISO/ASTM DIS 52928 (Additive manufacturing of metals – Feedstock materials – Powder life cycle management). • ISO/ASTM DIS 52927 (Additive manufacturing – General principles – Main characteristics and corresponding test methods). • ISO/ASTM DIS 52926-1 (Additive Manufacturing of metals – Qualification principles – Part 1: General qualification of operators). • ISO/ASTM 52925:2022 (Additive manufacturing of polymers – Feedstock materials – Qualification of materials for laser-based powder bed fusion of parts). ISO/ASTM DIS 52924 (Additive manufacturing of polymers – Qualification principles – Classification of part properties).

	• ISO/ASTM CD TR 52918 (Additive manufacturing – Data formats – File format support, ecosystem and evolutions). • ISO/ASTM TR 52916:2022 (Additive manufacturing for medical – Data – Optimized medical image data). • ISO/ASTM 52915:2020 (Specification for additive manufacturing file format (AMF) Version 1.2). • ISO/ASTM DTR 52913-1 (Additive manufacturing – Feedstock materials – Part 1: Parameters for characterization of powder flow properties). • ISO/ASTM TR 52912:2020 (Additive manufacturing – Design – Functionally graded additive manufacturing). • ISO/ASTM FDIS 52911-3 (Additive manufacturing – Design – Part 3: PBF-EB of metallic materials). • ISO/ASTM 52911-2:2019 (Additive manufacturing – Design – Part 2: Laser-based powder bed fusion of polymers). • ISO/ASTM 52911-1:2019 (Additive manufacturing – Design – Part 1: Laser-based powder bed fusion of metals). • ISO/ASTM DIS 52910:2018 (Additive manufacturing – Design – Requirements, guidelines and recommendation). • ISO/ASTM 52910:2018 (Additive manufacturing – Design – Requirements, guidelines and recommendations). • ISO/ASTM 52909:2022 (Additive manufacturing of metals – Finished part properties – Orientation and location dependence of mechanical properties for metal powder bed fusion). • ISO/ASTM DIS 52908 (Additive manufacturing of metals – Finished Part properties – Post-processing, inspection and testing of parts produced by powder bed fusion). • ISO/ASTM 52907:2019 (Additive manufacturing – Feedstock materials – Methods to characterize metal powders). • ISO/ASTM TR 52906:2022 (Additive manufacturing – Non-destructive testing – Intentionally seeding flaws in metallic parts). • ISO/ASTM DTR 52905 (Additive manufacturing of metals – Non-destructive testing and evaluation – Defect detection in parts). • ISO/ASTM 52903-2:2020 (Additive manufacturing – Material extrusion-based additive manufacturing of plastic materials – Part 2: Process equipment). • SO/ASTM 52903-1:2020 (Additive manufacturing – Material extrusion-based additive manufacturing of plastic materials – Part 1: Feedstock materials).

	• ISO/ASTM 52902:2019 (Additive manufacturing – Test artifacts – Geometric capability assessment of additive manufacturing systems). • ISO/ASTM 52901:2017 (Additive manufacturing – General principles – Requirements for purchased AM parts). • ISO/ASTM 52900:2021 (Additive manufacturing – General principles – Fundamentals and vocabulary). • ISO/CD 27548 (Additive manufacturing of plastics – Environment, health and safety – Test method for determination of particle and chemical emission rates from desktop 3D printer material extrusion). • ISO/IEC 23510:2021 (Information technology – 3D printing and scanning – Framework for an Additive Manufacturing Service Platform (AMSP)). • ISO 17296-3:2014 (Additive manufacturing – General principles – Part 3: Main characteristics and corresponding test methods). • ISO 17296-2:2015 (Additive manufacturing – General principles – Part 2: Overview of process categories and feedstock). • ISO 17295:2023 (Additive manufacturing – General principles – Part positioning, coordinates and orientation). • ISO 14649-17:2020 (Industrial automation systems and integration – Physical device control – Data model for computerized numerical controllers – Part 17: Process data for additive manufacturing). • ISO/DIS 5425:2022 (Specifications for use of poly(lactic acid) based filament in additive manufacturing applications). • ISO/IEC DIS 3532-2 (Information technology – Medical image-based modelling for 3D printing – Part 2: Segmentation). • ISO/IEC FDIS 3532-1 (Information technology – Medical image-based modelling for 3D printing – Part 1: General requirements). • F2924-14:2021 (Standard Specification for Additive Manufacturing Titanium-6 Aluminum-4 Vanadium with Powder Bed Fusion). • F3001-14:2021 (Standard Specification for Additive Manufacturing Titanium-6 Aluminum-4 Vanadium ELI (Extra Low Interstitial) with Powder Bed Fusion). • F3091/F3091M-14:2021 (Standard Specification for Powder Bed Fusion of Plastic Materials). • F3122-14:2022 (Standard Guide for Evaluating Mechanical Properties of Metal Materials Made via Additive Manufacturing Processes). • ISO/ASTM CD 52926 (Qualification of machine operators for metallic parts production).

Any other safety and quality control standards on manufacturing and use of specific medical devices regardless of the production method used. For example, ISO's 11.040.40 standards catalog (https://www.iso.org/ics/11.040.40/x/), ASTM's standards under Jurisdiction F04 (https://www.astm.org/get-involved/technical-committees/committee-f04/subcommittee-f04) and FDA's guidance documents (https://www.fda.gov/regulatory-information/search-fda-guidance-documents) and recognized consensus standards to which FDA accept a declaration of conformity (https://www.accessdata.fda.gov/scripts/cdrh/cfdocs/cfStandards/search.cfm).

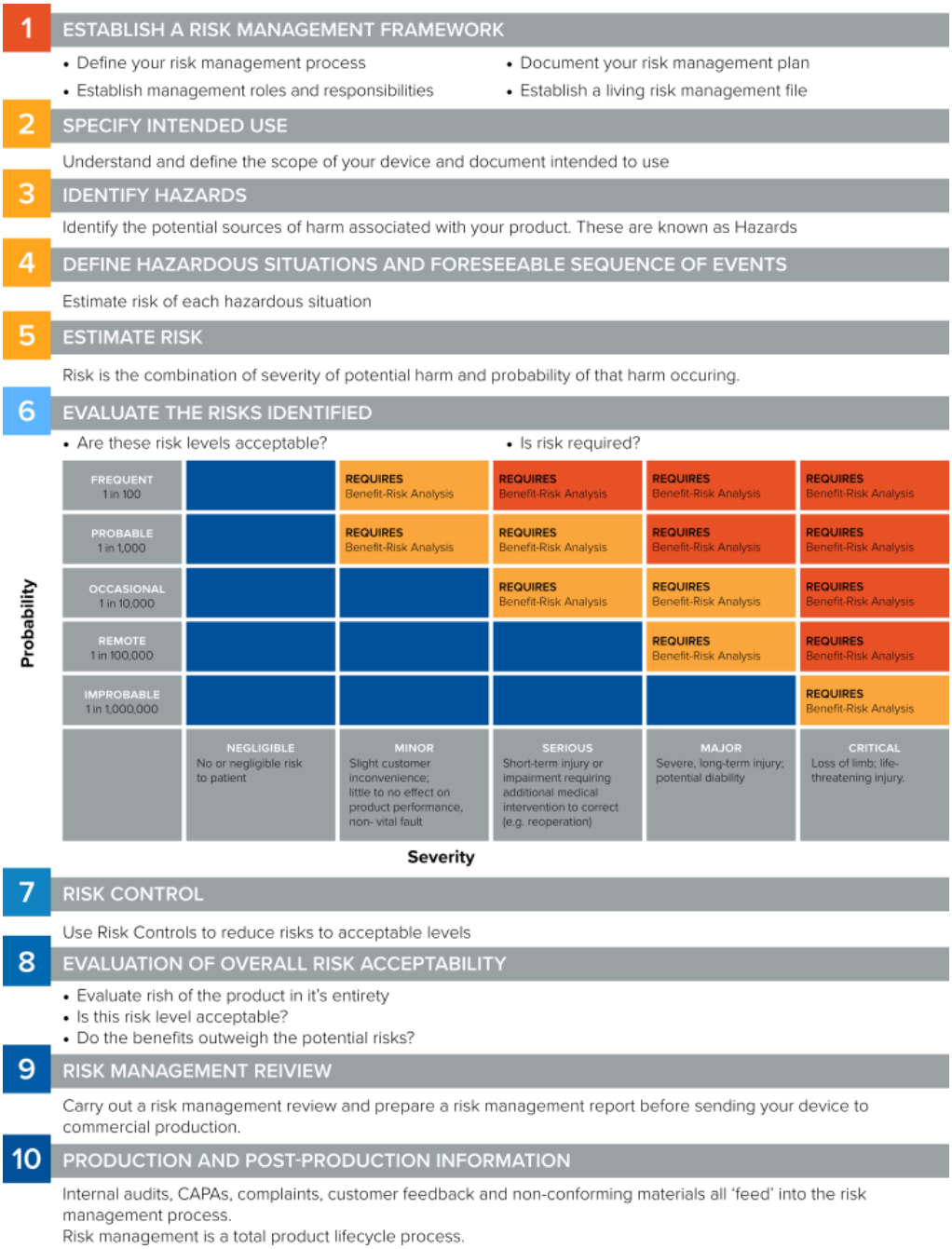

Figure 279: Risk management as per ISO 149671:2019. Source: (Formlabs, 2021)

5.3 Hardware and Software

3DP techniques of metallic, ceramic, polymer, and composites *(Appendix G)* are being used for numerous applications in medicine and orthopaedics *(see Sub-section 3.3, 3.4, 3.5, 3.6 and*

Appendices B and J) and a plethora of companies are engaged in the corresponding market *(Appendix I)* which is being expanded both technologically and economically *(Wohlers Associates, 2021a; Wohlers and Gornet, 2021).*

In this *Sub-section*, the hardware to equip an ideal high-end PoC 3D Unit with cutting-edge technologies that enable local design and end-parts manufacturing (metal, polymer, ceramic, and constructs for TE) is listed bearing in mind all necessary equipment, without considering cost and resources restrictions (Scenario 1). On the other hand, in reality, numerous trade-offs can be made depending on the needs and the selected format of PoC the 3D Unit (design-only, manufacture-only, or both). For this reason, in contrast to the unconstrained approach of Scenario 1, at the end of each of the following *Sub-sections*, the minimum required hardware at the lowest possible budget is given for a PoC 3D Unit where mainly design and prototyping takes place, and final manufacturing being outsourced, with optional equipment being suggested to be installed in-house for small polymer end-parts 3DP *(Scenario 2).*

In summary, the total hardware and software cost was budgeted at 3.440.150 € and 207.612 € for Scenario 1 and Scenario 2 respectively. Detailed listings are given next with the cost being broken down into 1) Computer and office equipment, 2) xR equipment, 3) 3D Scanners, 4) 3D Printers and materials, and 5) Software.

It should be underscored that for some software, the costs refer to 3-year license duration and extra costs would be required for renewal. Additionally, in either scenario, neither service nor feedstock materials costs for the 3D printers were considered. Also, extra costs emerge for outsourcing parts for post-processing, e.g. machining, hot-isostatic-pressing, polishing, coatings, etc.

5.3.1 Computer and Office Equipment

For the two (bio)mechanical design and manufacturing engineers, the quality control engineer, the (bio)mechanical design and manufacturing lead supervisor, and the orthopaedic surgeon manager (Scenario 1), it was decided that three desktop stations and three laptop computers were required, accompanied by various peripheral devices. These computers have to be powerful enough to process medical image data, run 3D digital modeling, simulation, and optimization software, as well as supporting 3D scanning and xR applications. More specifically, the components, characteristics, and total costs for the selected parts are described in *Table 10*.

Table 10: Computer equipment for the PoC 3D Unit

Category	Component	Description	Quantity (pcs)	€ with VAT
Desktop monitor	-	27" Dell S2721DGFA	6 (2 per station)	2.750
	Tower case	Corsair Crystal 570X RGB Midi	3	15.100
	Tower case fan	Corsair SP120 RGB Elite	3	

Desktop computer tower	Power Supply Unit (PSU)	Corsair HX Series 1000 W Platinum	3	
	Motherboard	Asus Z690 ProArt Creator Wifi (Z690/1700/DDR5)	3	
	Central Processing Unit (CPU)	Intel Core i9 12900K (1700/3.2 GHz/30 MB)	3	
	CPU cooler	Corsair CUE H100i Elite Capellix 240 mm Radiator	3	
	Random Access Memory (RAM)	Corsair Dominator Platinum RGB 64GB Kit 5200MHz DDR5	3	
	Graphics Processing Unit (GPU)	Nvidia GeForce RTX 3090 Ti Gaming X Trio 24 GB	3	
	Solid State Storage	Western Digital SN850 NVMe Heatsink 1TB Black	3	
Desktop computer peripherals	Mouse	Logitech MX Master 3s Graphite	3	3.050
	Keyboard	Logitech MX Keys Bluetooth	3	
	Headset	Corsair Virtuoso 7.1 Carbon Wireless	3	
	Speakers	Logitech Z200 Black	3	
	Web cam	Logitech C920S Pro	3	
	Spacemouse	3D Connexion Wireless	3	
	Digitizer	Wacom Intuos Medium Pen Black Bluetooth	3	
Laptop and accessories	Laptop	Dell G15 5511 Special Edition 15.6" Full HD (CPU Intel Core i7 11800H, RAM 32 GB, SSD 1 TB, GPU RTX 3060 6 GB, Windows 11 Pro)	3	8.400
	Laptop case	Thule 16" Hard Case	3	
	Mouse	Logitech MX Master 3s Graphite	3	
	Headset	Corsair Virtuoso 7.1 Carbon Wireless	3	
Basic Software	Operating software	Microsoft 11 Pro for desktops	3	645
	Office suite	Microsoft office 365 (5 seats)	1	
	Graphic design	Gimp and Inkscape	1	Free
Total cost				**29.945**

Extra essential office, power, network, and miscellaneous equipment had to be included. The cost of such equipment is mentioned in *Table 18*. Regarding the network server, the readily available infrastructure of the university was planned to be utilized.

All aforementioned equipment is illustrated in *Figure 280*.

Table 11: Office, power, networking and miscellaneous equipment for the PoC 3D Unit

Category	Component	Description	Quantity (pcs)	€ with VAT
Multifunctional printer	-	HP LaserJet Pro M183fw	1	400
Power, storage and networking	Uninterruptible Power Supply Unit	APC 3000 VA Double Conversion Online SRT3000XLI	1	6.100
	Network Attached Storage (NAS)	Synology NAS DS418	1	
	NAS Disks	Western Digital Red Plus HDD 12TB	4	
Digitizer monitor	Digitizer monitor	Samsung Digital Signage 55" Flip 2	1	2.070
	Stand	Samsung Flip 2 Stand	1	700
Miscellaneous	-	Cables, adapters, paper, toner, batteries, USB sticks, stationary, accessories etc.	-	1.500
Total cost				**10.770**

As this kind of equipment is fundamental, it was suggested to not economize on budget and minimize costs. For Scenario 1, the total sum is 40.715 €, whereas for Scenario 2, where only one (bio)mechanical design and manufacturing engineer and an orthopaedic surgeon manager are the personnel of the PoC 3D Unit, the total cost for the same equipment but in lower quantities (one desktop and one laptop computer), is 20.900 €.

Figure 280: Computers, peripherals, power, networking, and office equipment of PoC 3D Unit

5.3.2 xR Equipment

xR equipment was planned to be used exclusively for pre-operative planning and intra-operative information and 3D model visualization (not for navigation), product design, education, and training. The selected xR and haptic devices are shown in *Figure 281* and their costs are in *Table 19*.

Display: 2880x2720 px per eye @ 90 Hz.
Field of View: 115° horizontal, 90° vertical.
Weight: 944 gr with headstrap.
Tracking: Eye and hands.
Tracking method: 6 DoF marker-based.
Tracking frequency: 1000 Hz/ 100 Hz positional sensors.
Speackers and microphone: No, only audio jack.

Display: 2448x27448 px per eye @ 120 Hz.
Field of View: 116° horizontal, 96° vertical.
Weight: 850 gr with headstrap.
Tracking: Eye and hands.
Tracking method: 6 DoF marker-based.
Tracking frequency: 1000 Hz.
Speackers and microphone: Yes, removable.

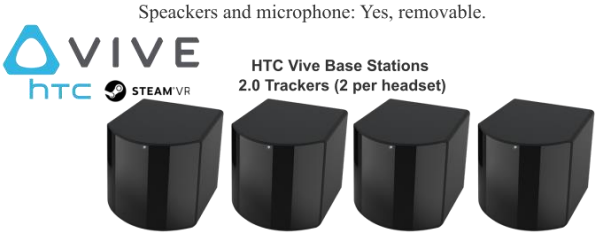

Type: PC-powered.
Passthrough: Via tracking cameras.
Resolution: 2880x2720 per-eye @ 90Hz.
Field of view: 115° horizontal and 90° vertical.
Weight: 980 gr with headstrap.
Tracking: eye and hand.
Tracking type: 6 DOF marker-based.
Tracking frequency: 1000 Hz / 100Hx positional sensors.
Speacker and microphone: No, just audio jack.

Type: Standalone (Qualcomm Snapdragon 850 chipset, Octa-core Kryo. 385 CPU, Adreno 630 GPU, 4GB RAM, 64GB storage).
Batterfy life: 3 hours.
Passthrough: Native passthrough, 8MP camera @ 30 fps.
Resolution: 1440x936 per-eye @ 60Hz.
Field of view: 43° horizontal and 29° vertical.
Weight: 556 gr with headstrap.
Tracking: eye and hand.
Tracking type: 6 DOF inside-out via 4 intergrated cameras.
Speacker and microphone: Yes.

3-DOF force feedback workspace: 160 x 120 x 120 dia. mm.
6-DOF position sensing: x, y, z at base and pitch, roll, yaw at stilus gimbal.
Positional resolution: 0.023 mm.
Max. exertable force: 7.9 N.
Continuous exertable force: >1.75 N.
Stiffness: 1.86 N (x-axis), 2.35 N (y-axis), 1.48 N (z-axis).
Inertia: 35 gr.
Footprint: 143 x 184 dia. mm.
Weight: 3.257 gr.

Figure 281: xR equipment of PoC 3D Unit

Table 12: xR equipment for the PoC 3D Unit

Category	Component	Description	Quantity (pcs)	€ with VAT
Virtual Reality (VR)	Virtual Reality Goggles	Varjo[71] VR-3	1	7.750
	Virtual Reality Goggles	HTC Vive[72] Pro 2	1	

[71] Varjo offers some of the highest-end VR and MR products and services for advanced users. See https://store.varjo.com/vr-3.

[72] Vive (HTC company) develops a series of VR headsets, trackers, controllers, and other accessories. For more information see https://www.vive.com/us/product/#pro%20series.

	Trackers	HTC Vive Base Stations	4 (2 per goggle)	
	Controllers	HTC Vive Blue Controller	4 (2 per goggle)	
Mixed Reality (MR)	Mixed Reality Goggles	Varjo XR-3 (trackers and controllers used from VR setup)	1	12.950
	Mixed Reality Goggles	Microsoft Hololens 2[73] Industrial Edition (tracker-less and controller-less)	1	
Haptics	-	3D Systems Geomagic Touch X[74]	1	14.000
Total cost				**34.700**

The cost for Scenario 1 is 34.700 €. For Scenario 2, the cost for xR equipment can be minimized to 7.460 € with the following sacrifices:

- VR experience: only one *Vive Pro 2* (HTC Corp, New Taipei City, Taiwan) with two *Vive Base Stations* and two *Vive Blue Controllers* can be utilized for VR applications.
- AR/MR experience: only the *Hololens 2* can be selected.
- Haptic device: although this offers force feedback for real-like sensations when designing products and for pre-operative surgery planning, education, and training, it can be ignored.

It should be highlighted that with only one xR headset, this has to be shared among users. Hence, simultaneous collaboration in xR would be impossible. However, users with no xR headsets can participate and communicate in sessions in non-xR mode via their computers or mobile devices.

5.3.3 3D Scanners

Portable 3D scanners are required when there is a need to acquire the external (surface) body morphology to design personalized rehabilitation products such as orthotics and prosthetics. In *Figure 282* the selected 3D scanners are illustrated, and their costs are summarized in *Table 13*.

Table 13: 3D Scanners for the PoC 3D Unit

Description	Quantity (pcs)	€ with VAT
Shining 3D[75] EinScan H	1	5.700
Shining 3D EinScan Pro HD+ Industrial Pack+Color Pack	1	10.700
+ Solid Edge Shining 3D Edition software is offered		
Total cost		**16.400**

To lower the required budget from 16.400 € (Scenario 1) to 5.700 € (Scenario 2), only one 3D *EinScan H* (Shining 3D Tech Co. Ltd, Hangzhou, China) can be purchased.

[73] Microsfot Hololens 2 is an ergonomic, untethered self-contained see-through holographic device. For more information see https://www.microsoft.com/en-us/hololens.

[74] 3D System's Geomagic Touch X is a precise haptic device with positioning input and high-fidelity, force-feedback output. Users feel 3D on-screen objects by force feedback on their hands, delivering true-to-life sensations. See https://www.3dsystems.com/haptics-devices/touch-x.

[75] Shining 3D develops 3D digitizing solution. More details at https://www.shining3d.com/3d-digitizing-solutions/.

5.3.4 3D Printers and Materials

For materializing anatomical models and any personalized or not orthopaedic products and ancillaries, various 3D printers and feedstock materials were specified. The selected 3D printers and materials as per the established needs are summarized in *Table 14* and graphically presented along with their specifications and capabilities in *Figure 283* to *Figure 290*.

Table 14: 3D Printers and materials for the PoC 3D Unit

Needs	Description	Characteristics and Materials	Quantity (pcs)	€ with VAT
High-temperature polymer (bio)materials extrusion, e.g. PEEK. For anatomical models, instruments, implants, orthotics-prosthetics, molds.	Intamsys[76] Funmat Pro 410 FFF and Nabertherm annealing furnace. Including start pack, and software for build preparation.	See *Figure 283*	1	30.000
Standard polymer (bio)materials extrusion. For anatomical models, instruments, orthotics-prosthetics, and molds.	• Zortrax[77] M300 Dual FFF. • Raise3D[78] Pro3 Plus FFF. Including start packs, and software for build preparation.	See *Figure 284*	1 each	10.850
Low-cost extrusion and photopolymerization of polymer (bio)materials for setting up a mini print farm. For anatomical models, instruments, orthotics-prosthetics, and molds.	• Creality[79] Sermoon D3 FFF. Including start pack and software for build preparation. • Phrozen Sonic Mighty 8K[80] screen-based VP. Including start pack, and software for build preparation.	See *Figure 285*	4 each	13.800
Transparent and opaque (bio)materials photo-polymerization. For high-end quality anatomical models, instruments, orthotics-prosthetics, and molds.	• Formlabs[81] Form 3Bl laser VP with Wash and Curing stations. • Formlabs Form 3B+ laser VP. Including start packs, and software.	See *Figure 286*	1 each	26.500
Photo-polymer multi-color and multi-(bio)materials jetting, including transparent. High-end anatomical models, instruments, orthotics-prosthetics, and molds.	Stratasys[82] J850 Digital Anatomy photo-polymer MJ. Including cleaning kit, start pack, installation, training, and software for build preparation.	See *Figure 287*	1	470.000

[76] Intamsys manufactures high-temp polymer ME 3D printers. More information at https://www.intamsys.com/.

[77] Zortrax's ME and VP 3D printers and materials can be found at https://zortrax.com/.

[78] See https://www.raise3d.com/ for Raise3D material extrusion 3D printers and materials.

[79] Creality is a Chinese company that produces 3D printers of ME and VP technologies. More details at https://www.creality.com/.

[80] Creality is a Chinese company that produces 3D printers of ME and VP technologies. More details at https://www.creality.com/.

[81] Formlabs develops laser VP and recently polymer PBF 3D printers. See https://formlabs.com/.

[82] Stratasys is a giant of the 3D printing industry with a large portfolio of 3D printing technologies and solutions. More at https://www.stratasys.com/.

Multi-color anatomical models at low cost with BJ technology.	3D Systems[83] CJP660 Pro BJ. Including start pack, installation, training, and software for build preparation.	See *Figure 288*	1	116.000
Polymer (bio)material PBF. For anatomical models, instruments, orthotics-prosthetics, and molds.	• Formlabs Fuse 1+ SLS with powder handling station. • HP[84] multi-jet fusion 5200 with powder handling station. Including start packs, installation, training, and software for build preparation.	See *Figure 289*	1 each	426.000
Metal (bio)materials PBF. For implants, and instruments.	• GE[85] Arcam Q10plus EBM with helium tank, water cooling system, powder handling station, vacuum cleaner, sieving station, filling station, lifters, and trolleys. • GE Concept Laser M2 DMLS with nitrogen, argon gas tanks, and air compressor. Including start packs, installation, qualification, training and certification for medical device manufacture. Including software for build preparation.	See *Figure 290*	1 each	1.625.000
Bioresorbable ceramic (bio)materials for implants.	Lithoz S65 medical photocuring system for ceramic-loaded photocurable slurries + Nabertherm furnace for de-bindering and sintering the ceramic parts. Including start pack, installation, training, and software for build preparation.	See *Figure 291* and *Figure 292*	1 each	500.000
Extrusion-based bioprinting of hydrogels, polymers, and ceramic slurries for TE applications.	Envisiontec 3D Bioplotter. Including start pack, installation, training, and software for build preparation.			
Note: Service costs and feedstock materials costs have not been included				
Total cost				**3.218.150**

The calculated total cost of 3.218.150 € for the 3D printers is the highest among all other cost categories and refers to Scenario 1 where the PoC 3D Unit designs and manufactures in-house any bespoke metal and polymer orthopaedic product, including ceramic parts and constructs for TE applications. By removing some 3D printers, the total cost can be reduced dramatically as various trade-offs can be made depending on the needs.

For Scenario 2 where the PoC 3D Unit mainly a) designs and prototypes orthopaedic solutions, b) outsources manufacturing to contract manufacturers, but can also c) 3DP in-house small polymer orthopaedic parts, is enabled by the following 3D printers the total cost of which is 78.900 €: *Pro3*

[83] 3D Systems is a pioneer of the 3D printing industry with a variety of 3D printing technologies and solutions. See https://www.3dsystems.com/.

[84] HP has entered the 3D printing market with its multi-jet fusion technology. More details at https://www.hp.com/us-en/printers/3d-printers/products/multi-jet-technology.html.

[85] GE has acquired Arcam and Concept Laser that develop EBM and DMLS technologies for metal PBF 3D printing. See https://www.ge.com/additive/.

Plus (Raise 3D Technologies Inc., California, US) and 2 pcs *Sermoon D3* (Shenzhen Creality 3D Technology Co. Ltd, Shenzhen, China) for PLA biomaterials, *Form 3Bl* (Formlabs Inc., Massachusetts, US) and 2 pcs *Sonic Mighty 8K* (Phrozen Technology, Hsinchu City, Taiwan) for photocurable resin biomaterials, accompanied by washing and curing stations, and *Formlabs Fuse 1+* for PA12 biomaterial, accompanied by all ancillary.

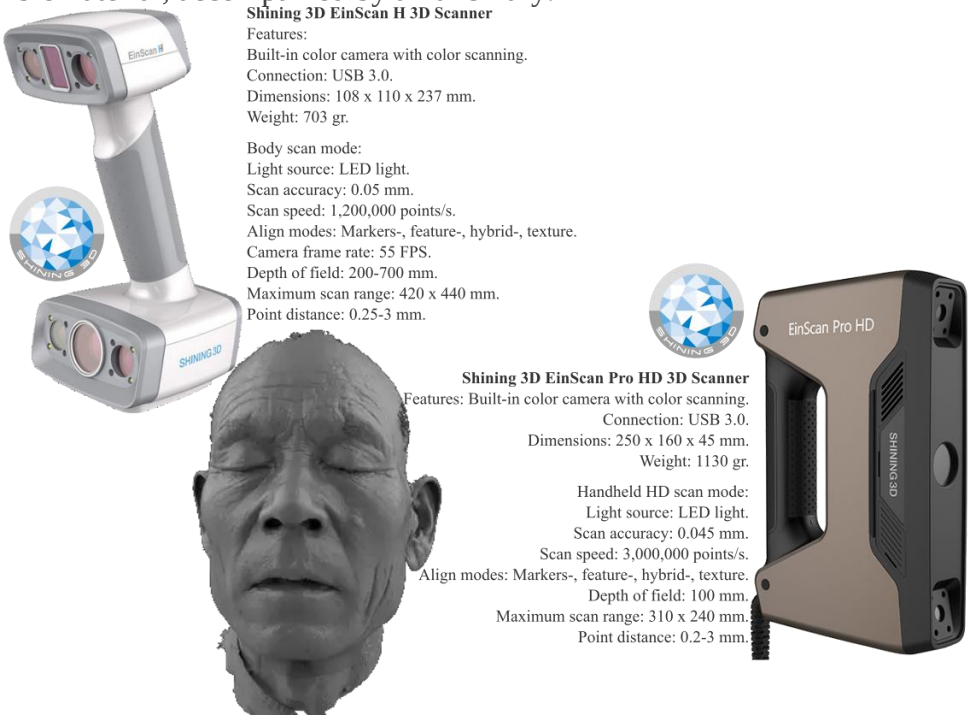

Figure 282: 3D Scanners of PoC 3D Unit

Figure 283: 3D Printers of PoC 3D Unit: high-temp ME

Zortrax M300 Plus Dual material extrusion 3D Printer

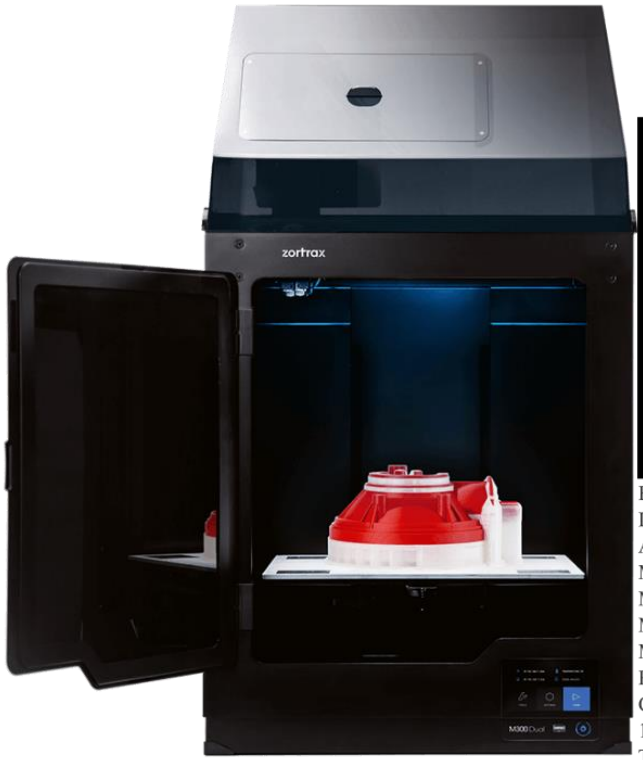

Build material spool

Support material spool

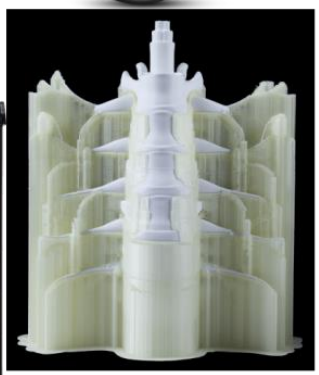

Build volume: 265 x 265 x 300 mm.
Dual extruder with typical nozzle diameter: 0.4 mm.
Automatic platform level measurement.
Min layer thickness: 0.15 mm.
Max print speed: 150 mm/s.
Max print temperature: 310° C.
Max platform temperature: 105° C.
Power consumption: 400 W.
Connectivity: Wi-fi, Ethernet and USB.
1.75mm filaments: PLA, ABS & ULTRAT, ASA, Z-ESD, HIPS, PC, TPU, NYLON, TPE, PETG, PP, GF/ CF reinforced, water-soluble.
Features: 4" 800x400 touchscreen, camera, HEPA filter.
Dimensions: 480 x 576 x 665 mm.
Weight: 41 Kg.

Raise3D Pro3 Plus Dual material extrusion 3D Printer

Build material spool

Support material spool

Build volume: 255 x 300 x 605 mm.
Dual extruder with typical nozzle diameter: 0.4 mm.
Automatic platform level measurement.
Min layer thickness: 0.10 mm.
Max print speed: 150 mm/s.
Max print temperature: 300° C.
Max platform temperature: 120° C.
Power consumption: 600 W.
Connectivity: Wi-fi, Ethernet and USB.
1.75mm filaments: PLA, ABS, ASA, HIPS, PC, TPU, NYLON, TPE, PETG, PP, GF/ CF reinforced, water-soluble.
Features: 7" 1024x600 touchscreen, camera, HEPA filter.
Dimensions: 620 x 626 x 1105 mm.
Weight: 49 Kg.

Figure 284: 3D Printers of PoC 3D Unit: ME

Figure 285: 3D Printers of PoC 3D Unit: low-cost ME and VP print farm

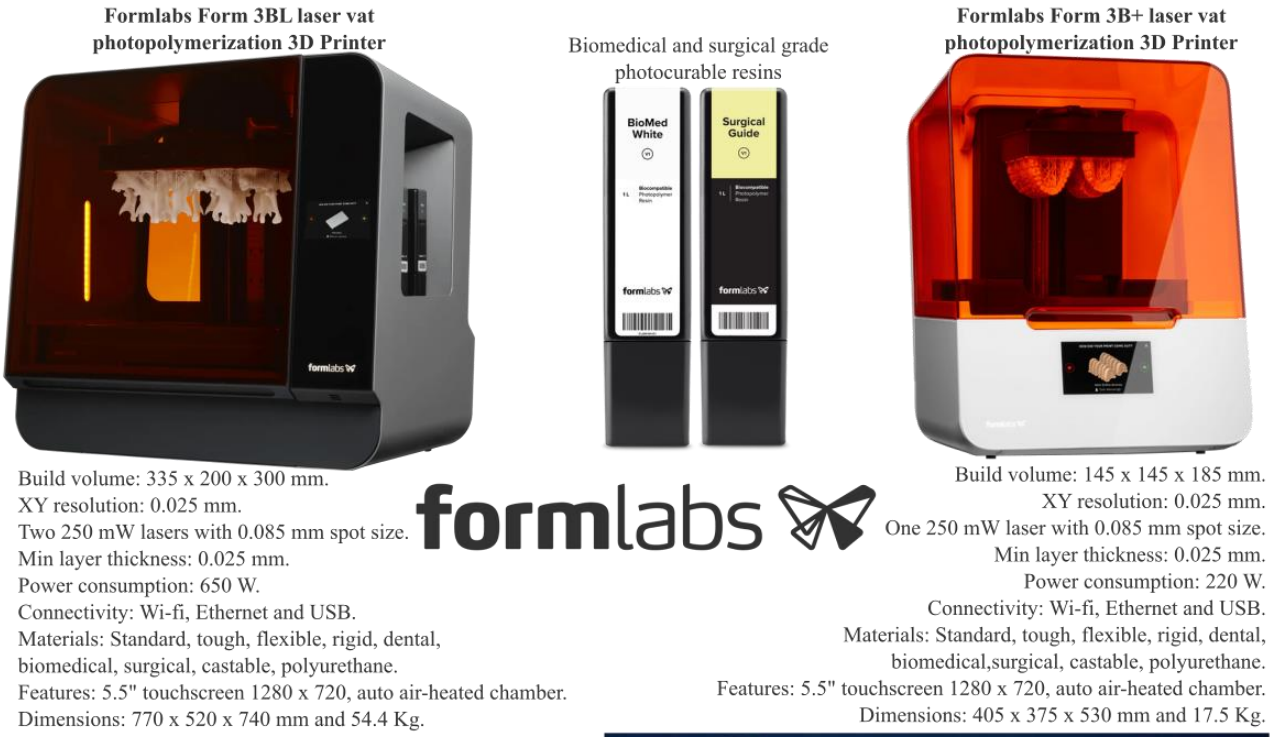

Figure 286: 3D Printers of PoC 3D Unit: VP

Figure 287: 3D Printers of PoC 3D Unit: (photo-polymer) MJ

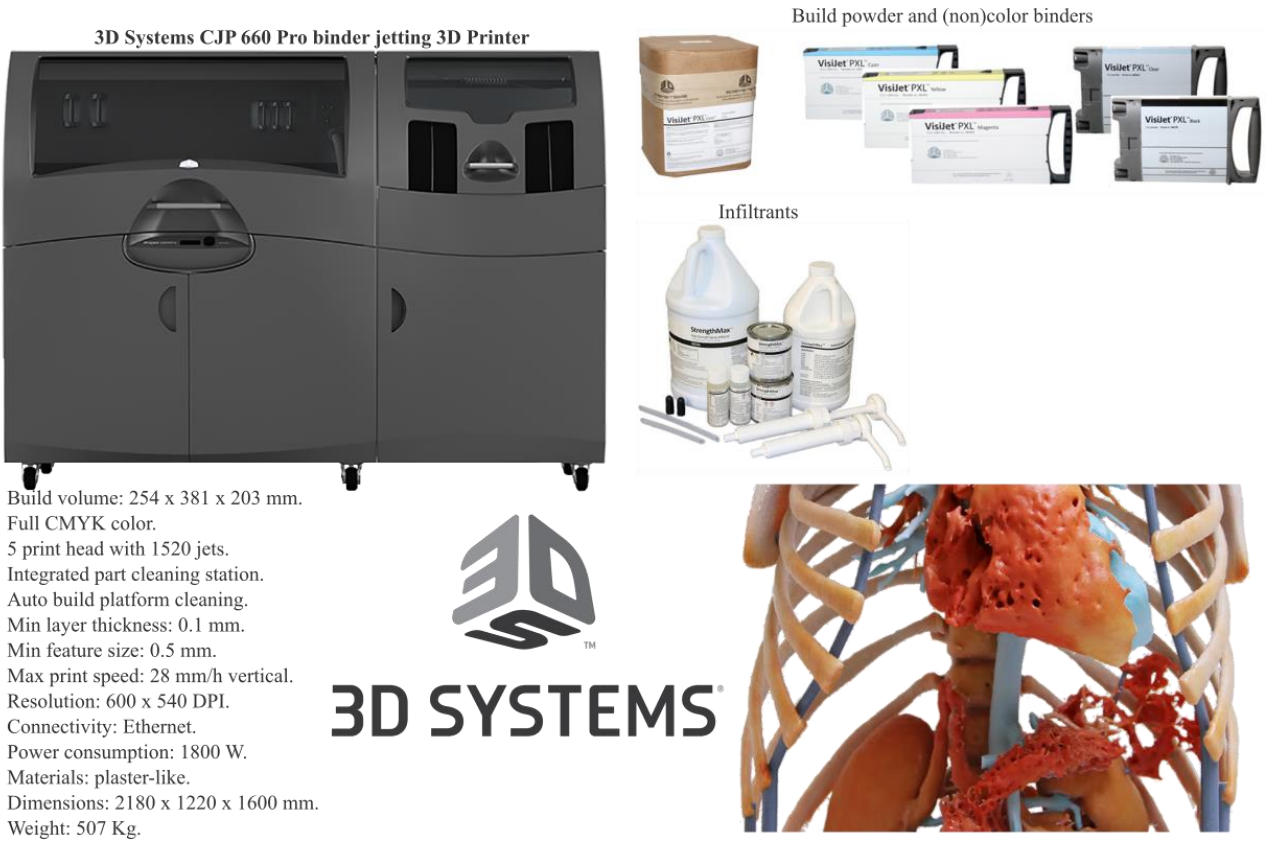

Figure 288: 3D Printers of PoC 3D Unit: BJ

Figure 289: 3D Printers of PoC 3D Unit: plastic PBF

GE Arcam M2 Q10plus EBM
Powder-bed fusion 3D Printer

Powder feedstock material

Build volume: 200 x 200 x 200 mm.
Min layer thickness: 0.07 mm.
Min part resolution: 0.75 mm.
Max beam travel speed: 8,000 m/s.
Single beam 3000W.
Does not require neither wire EDM machining to remove the part, nor themral stress-relief.
Parts are 99.9% solid. Hot-isostatic-pressing optional.
Thermal and build monitoring and control.
Water-cooled heat sink.
Beam spot size: 0.140 mm.
Power consumption: 7000 W.
Connectivity: Wi-fi, Ethernet and USB.
Requirements: Helium gas 1 lt/ h + 50-75 lt/ build.
Materials: Titanium Ti6Al4V Grade 5/ Grade 23, Titanium Grade 2, CoCr, Pure Copper.
Dimensions: 2060 x 1066 x 2608 mm.
Weight: 1681 Kg.

Helium tank, powder handling station, vacuum cleaner, sieving station, filling station, lifters and trolleys are required.

GE Concept Laser M2 DMLM
Powder-bed fusion 3D Printer

+ Nitrogen and argon gas tanks

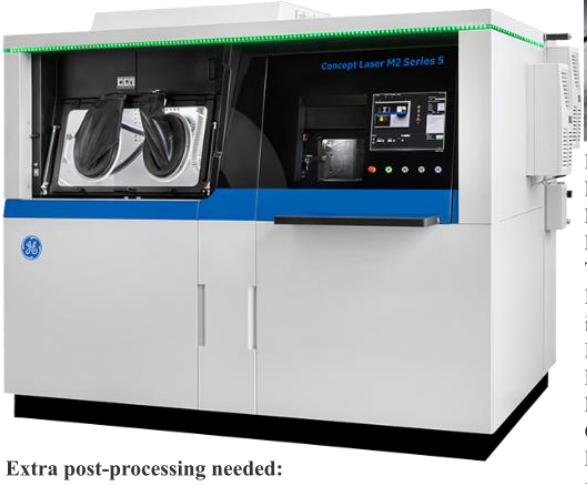

Extra post-processing needed:
-Wire EDM machining for product separation from platform.
-Furnace for thermal stress-relief.
-(Option) Hot-Isostatic-Pressing.

Powder feedstock material

Build volume: 245 x 324 x 350 mm.
Min layer thickness: 0.02 mm.
Max print speed: 2-35 q.cm/h.
Dual 400W fibre laser.
Thermal and build monitoring and control.
Integrated sieving and powder handling at inert atmosphere.
Integrated powder sieving & cleaning station.
Laser spot size: 0.070 mm.
Power consumption: 9000 W.
Connectivity: Wi-fi, Ethernet and USB.
Requirements: compressed air, nitrogen and argon gas tanks (depends on material).
Materials: Stainless steel 316L/ 17-4PH, Steel M300, Tool Steel H13, Aluminum AlSi10Mg/ AlSi7Mg/ A205, Nickel 718/ 625/ X, Titanium cp-Ti/ Ti6242/ Ti6Al4V Grade 3, CoCrW, CoCrMo.
Dimensions: 2695 x 1818 x 2185 mm.
Weight: 2500 Kg.

Figure 290: 3D Printers of PoC 3D Unit: metal PBF

Figure 291: 3D Printers of PoC 3D Unit: ceramic photocuring

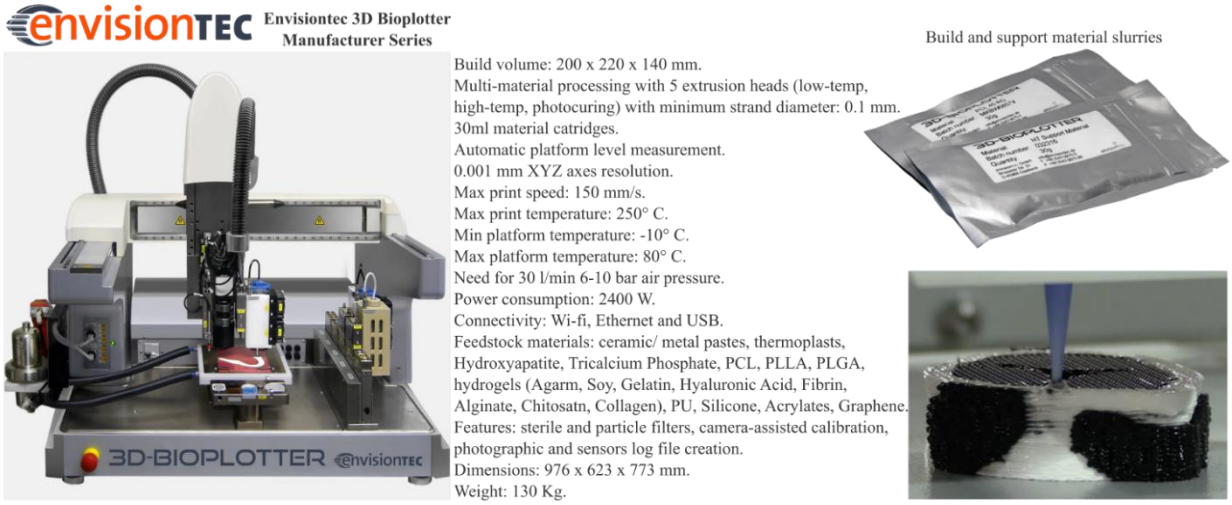

Figure 292: 3D Printers of PoC 3D Unit: extrusion bioprinter

5.3.5 Software

Table 15 and *Figure 293* summarize all necessary software to a) process medical image data (DICOM) originating from tomographers (internal scanning), b) reconstruct 3D scanned data (external scanning), b) edit 3D surface mesh models, c) view 3D models in desktop/mobile devices, d) photorealistic render 3D models, e) experience 3D digital models in xR, f) design, simulate and optimize orthopaedic products and ancillaries, and g) plan and simulate 3DP processes. Additionally, software for project management and meetings were also considered.

Apart from possible academic licenses that might be offered by some software vendors, the total cost can be reduced from 130.185 € (Scenario 1) to 94.652 € (Scenario 2) by excluding *Medical Imaging xR* (Medicalholodeck AG, Zurich, Switzerland), the *Discovery* or *Workbench* (Ansys Inc., Pennsylvania, US) and *Inspire* (Altair Engineering Inc., Michigan, US) software.

Table 15: Software used in PoC 3D unit

Category	Selected software	Needs	Alternatives	€ with VAT
Medical image data (DICOM) processing (tomographers)	Materialise Mimics Innovation Suite[86] (Paid)	DICOM data processing and 3D surface mesh models generation. MIMICS Innovation Suite also offers patient-specific product design and finite element meshing (3-matic), and 3DP planning.	• Numerous alternatives *(Presti et al. 2015; Haak, Page, and Deserno, 2016)*, e.g. 3D Slicer[87] (Free, open-source). • Oqton Dicom2Print[88] (Paid). • DICOM processors in 3D modeling software, e.g. Rhino3DMedical[89] (Paid) and OrtogOnblender[90] (Free).	20.000
Reconstruct 3D scanned data (3D scanners)	Siemens Solid Edge Shining 3D Edition (included in the cost of 3D Scanners listed previously)	3D reconstruction of point cloud data acquired by 3D scanners.	Oqton Geomagic Design X[91] (Paid)	-
3D surface mesh editors	Autodesk Meshmixer[92] (Free) Meshlab[93] (Free, open-source)	Surface mesh editing tools.	-	Free
3D model viewers for computers	Blender[94] (Free, open-source)	View and edit 3D surface meshes and solid models. Also model, sculpt, animate, render models.	• Microsoft 3D Builder & 3D Viewer[95] (Free). • 3D Slicer (Free, open-source). • Autodesk Meshmixer (Free). • Meshlab (Free, open-source). • Robert McNeel & Associates Rhinoceros[96] (Paid).	Free

[86] Mimics Innovation Suite is an FDA-approved software used for medical image data processing, 3D analysis, operation planning and simulation, custom product design, finite element meshing and 3D printing process planning. See https://www.materialise.com/en/medical/mimics-innovation-suite.1

[87] Although 3D Slicer is not yet FDA-approved, it is a free open-source, multi-platform software distributed under a BSD style license, widely used for medical, biomedical, and related image processing, visualization, and data analysis *(Fedorov et al., 2012).* 3D Slicer is being developed by a community of users, developers, contributors, and commercial partners around the world, with the US National Institutes of Health (NIH) being the major contributor. See at https://www.slicer.org/.

[88] An FDA-cleared software to create diagnostic-quality 3D models and preparation for 3D Printing. See https://oqton.com/d2p/.

[89] Developed by Mirrakoi based on Robert McNeel & Associates Rhinoceros. More at https://rhino3dmedical.com/.

[90] Add-on for Blender. See http://www.ciceromoraes.com.br/doc/pt_br/OrtogOnBlender/OrtogOnBlender_Como_Funciona.html.

[91] Characteristics of the Oqton's (a 3D Systems company) Geomagic Design X can be found at https://oqton.com/d2p/.

[92] Meshmixer is a free 3D surface (triangular) mesh processing, sculpting, and editing software. See https://www.meshmixer.com/.

[93] MeshLab is an open-source system for processing and editing 3D triangular meshes *(Cignoni et al., 2008)*. More at https://www.meshlab.net/.

[94] Blender is a free and open-source 3D creation suite, supporting modeling, rigging, animation, simulation, rendering, compositing, motion tracking, video editing, and game creation, whilst allowing scripting for customization. More at https://www.blender.org/.

[95] 3D Builder and 3D Viewer are free Microsoft Apps for viewing (screen or Mixed Reality), creating and 3D Printing 3D objects.

[96] Rhinoceros is used to create, edit, analyze, document, render, animate, and translate curves, surfaces and solids, point clouds, and polygon meshes. It includes the novel graphical algorithmic node editor named Grasshopper (See https://www.grasshopper3d.com/). More at https://www.rhino3d.com/.

			• Autodesk Fusion 360[97] (Paid). • Any online viewer.	
3D model viewers for smart mobile devices	Any free online or offline 3D viewer	View 3D surface meshes and solid models on mobile devices.	• STL Simple Viewer (iOS). • Fusion 360 (iOS/Android). • Fast STL Viewer (Android). • Exocad (Android). • Online 3D viewer[98].	Free
Photorealistic rendering	Luxion KeyShot[99] (Paid)	High-end realistic visuals.	• Robert McNeel & Associates Rhinoceros (Paid). • Blender (Free, open-source). • Autodesk Fusion 360 (Paid). • Rendering engines in 3D CAD software (Free and Paid).	3.385/ 3 years
Virtual Reality (VR)	Unity[100] (Free) Luxion KeyVR[103] plug-in for Keyshot (Paid) Medicalholodeck Medical Imaging xR[104] (Paid) Steam's VR App store (Free)	Immersive experience and interaction with 3D models for training, education, pre-operative planning.	• Specto Medical VR[101] (Free and Paid). • 3D Systems D2P (Paid). • SimLab-soft VR[102] (Free and Paid). • SlicerVirtualReality plug-in for 3D Slicer (Free, open source). • Plug-ins for Robert McNeel & Associates Rhinoceros and Blender (Free and Paid).	11.700/ 3 years
Augmented/Mixed Reality (AR/MR)	Unity (Free) Luxion KeyVR for Keyshot (Paid) Microsoft 3D Viewer (Free) Microsoft's App Store	xR experience and interaction with 3D models for training, education, pre-operative planning.	-	-
Computer-Aided Design (CAD)	Autodesk Fusion 360 + product design extension (Paid)	Edit 3D surface mesh anatomical models and model (non)organic	Any parametric or not CAD software (Paid), e.g. Siemens NX/Solid Edge[105], Dassault	15.900

[97] Fusion 360 is a cloud-based 3D modeling, CAD, CAM, and CAE software platform for product design and manufacturing developed by Autodesk. More at https://www.autodesk.com/.

[98] More details at https://3dviewer.net/.

[99] KeyShot is a powerful photorealistic rendering software developed by Luxion. More at https://www.keyshot.com/.

[100] Unity Technologies' Unity is a free cross-platform software engine used to create 3D content and interactive simulations and other custom real-time 3D experiences for xR, mobile, desktop, and web. See https://unity.com/ for more details.

[101] Specto is developed by Specto Medical (ex Diffuse) and focuses on advanced visualization of medical image datasets in 3D. See https://spectomedical.com/en/.

[102] Features of Simlab's VR Studio, VR Viewer, and VR Collaboration software can be found at https://www.simlab-soft.com/.

[103] See https://www.keyshot.com/keyvr/ for more details.

[104] Medicalholodeck's Medical Imaging xR is a platform for 3D surgical planning, education, and teamworking in VR. See https://www.medicalholodeck.com/en/.

[105] Siemens PLM Software offers the Solid Edge and the more comprehensive NX design software. See https://www.plm.automation.siemens.com/global/en/products/.

	Ansys Spaceclaim[109] (Paid) Oqton Geomagic Freeform[110] (Paid) Blender (Free, open source) Autodesk Meshmixer (Free) Robert McNeel & Associates Rhinoceros (Paid)	orthopaedic products to exactly fit into/onto the patient's anatomy.	Systemes Catia/Solidworks[106], PTC Creo[107], Autodesk Inventor[108].	(3.400/3 years for Fusion 360)
Computer-Aided Engineering (CAE) and design optimization	Simulation and Generative Design extensions for Autodesk Fusion 360 (Paid) Ansys[112] Discovery/Workbench (Paid) Altair SimSolid[113] (Paid) nTopology[114] (Paid) Altair Inspire[115] (Paid) Grasshoper for Robert McNeel & Associates Rhinoceros (Free) plus Intact Simulation plug-in[116]	• Mechanical simulations (FEA), generative design and optimization studies. • Functionally-graded materials-by-design. • Surface texturing. • Conformal cellular solids and lattice generation with density gradients. • Computational, algorithmic and graphic node modeling.	• CAE features in CAD/CAE/CAM software such as Dassault Systemes CATIA (Paid), Siemens NX (Paid), PTC Creo (Paid). • Carbon CogniCAD[111] (Paid).	79.200/3 years
Computer-aided Manufacturing (CAM)- 3DP	Materialise Magics[117] (included in previously listed costs) (Paid)	• Preparation for 3DP.	• Oqton Geomagic 3DXpert and Amphyon[118].	-

[109] Spaceclaim is a solid CAD software able to directly edit meshes. See https://www.ansys.com/products/3d-design/ansys-spaceclaim.

[106] Dassault Systemes develops the Solidworks and the more comprehensive CATIA design software. For more see https://www.3ds.com/products-services/.

[107] PTC Creo is a complete product development and experience software. More at https://www.ptc.com/en/products/creo.

[108] Features of Autodesk Inventor design software are listed at https://www.autodesk.com/products/inventor/overview.

[110] Oqton (a 3D Systems company) Geomagic Freeform includes toolsets to design and sculpt *"clay"* models into any form. See https://www.oqton.com/geomagic-freeform/.

[111] Cognicad is a generative design and topology optimization platform that also includes simulation of 3DP processes. See https://www.carbon3d.com/products/cognicad.

[112] Ansys (Discovery and workbench-based) is the leading engineering simulation software. See https://www.ansys.com/.

[113] Altair SimSolid performs structural analyses by eliminating geometry preparation and meshing. See https://altair.com/simsolid.

[114] nTopology is an engineering design software built for 3D printing, utilizing computational modeling to generate complex geometries not possible with traditional CAD. Materials can be architecture with cellular structures with targeted physical response, thus achieving enhanced performance. See https://ntopology.com/.

[115] Altair Inspire accelerates simulation-driven creation, optimization, and study of innovative, structurally efficient parts. See https://www.altair.com/inspire.

[116] Intact Solution's Simulation is a fast meshless mechanical simulation technology (Immersed Method of Moments™) based on the Kantorovich method which accepts any form of 3D volume or surface model. See https://www.intact-solutions.com/rev/.

[117] See https://www.materialise.com/en/industrial/software/magics-data-build-preparation.

[118] See https://oqton.com/3dxpert/ and https://oqton.com/amphyon/.

preparation and build simulation	PrusaSlicer[128] and Ultimaker Cura[129] slicers for ME 3D Printers (Free) 3D printer-specific software supplied with each 3D printer (Free)	• Simulation of 3DP processes. • Generation of 3D Printer-specific control code.	• AlphaStar Genoa 3DP[119]. • 3D Systems 3D Sprint[120]. • Altair Inspire Print3D[121]. • Hexagon Simufact Additive[122]. • Autodesk Netfabb[123]. • e-Xstream Digimat-AM[124]. • CAE platforms that offer 3DP process studies, e.g. Comsol Multiphysics[125], Ansys Additive Suite[126], Dassault Systemes Simulia[127].	
Project management	Atlassian Jira (free for 10 users)	Scrum-based project management.	-	3.456/3 years for 6 users
	Miro online whiteboard (Paid for Business version)	Graphical management tools.	-	
Online meetings	Google Workspace Business Standard (Paid)	Online meetings, messaging, cloud storage and other assistive services.	Microsoft Teams (Free and Paid)	2.592/3 years for 6 users
Total cost				**130.185**

Figure 293: Software for the PoC 3D Unit

[128] See https://www.prusa3d.com/page/prusaslicer_424/.

[129] See https://ultimaker.com/software/ultimaker-cura.

[119] See http://alphastarcorp.com/genoa-3dp-simulation/.

[120] See https://www.3dsystems.com/software/3d-sprint.

[121] See https://www.altair.com/inspire-print3d.

[122] See https://hexagon.com/products/simufact-additive.

[123] See https://www.autodesk.com/products/netfabb/overview.

[124] See https://www.e-xstream.com/product/digimat-am.

[125] See https://www.comsol.com/comsol-multiphysics.

[126] See https://www.ansys.com/products/additive/ansys-additive-suite.

[127] See https://www.3ds.com/products-services/simulia/.

5.4 Infrastructure and Layout

Many trade-offs can be made for a PoC 3D Unit about its infrastructure and layout. For Scenario 1, a new building addition near or within the HCF complex is required to house all necessary resources. Two such concepts for Scenario 1 can be seen in *Figure 294* and*Figure 295*.

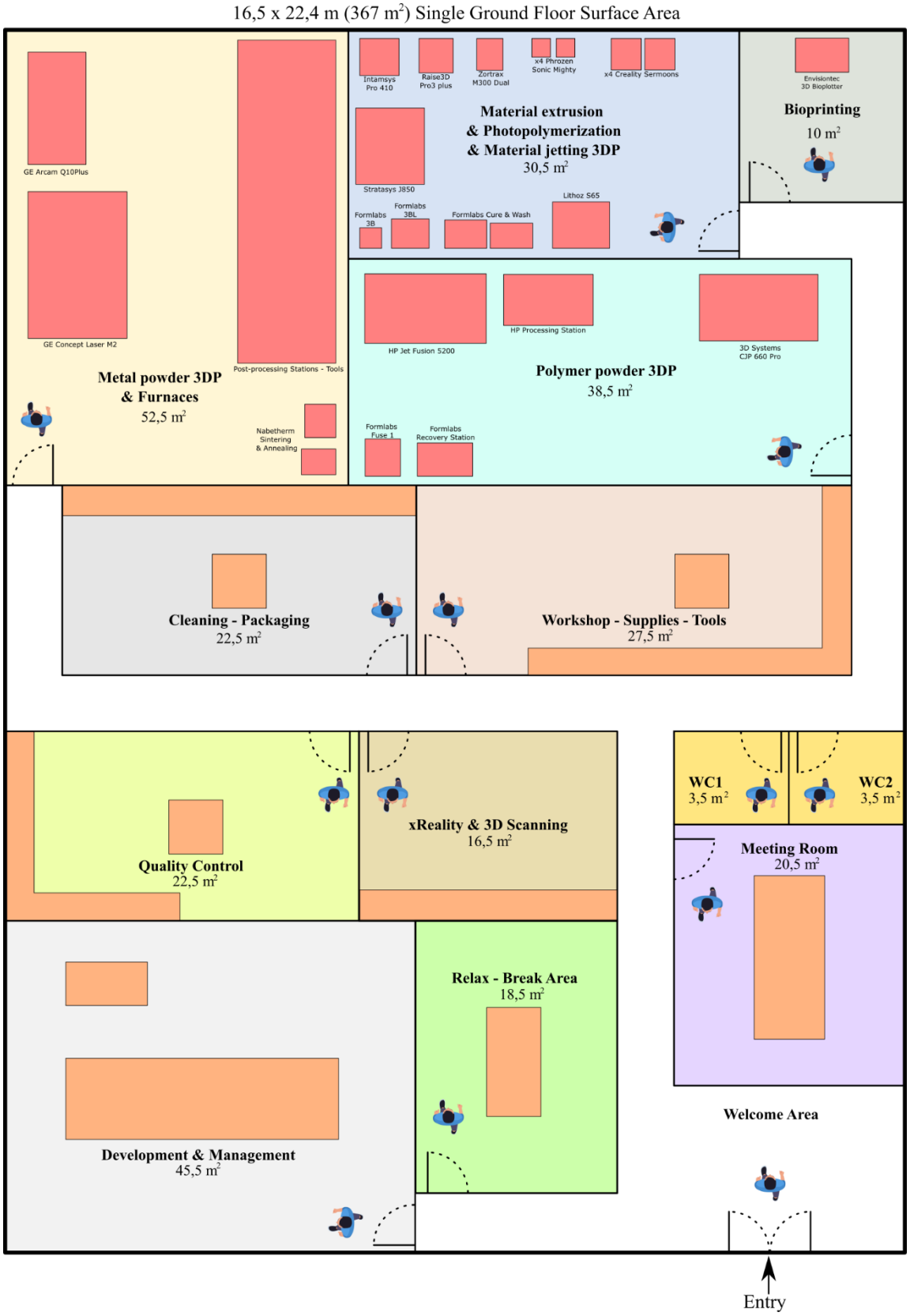

Figure 294: Single ground floor PoC layout concept for Scenario 1

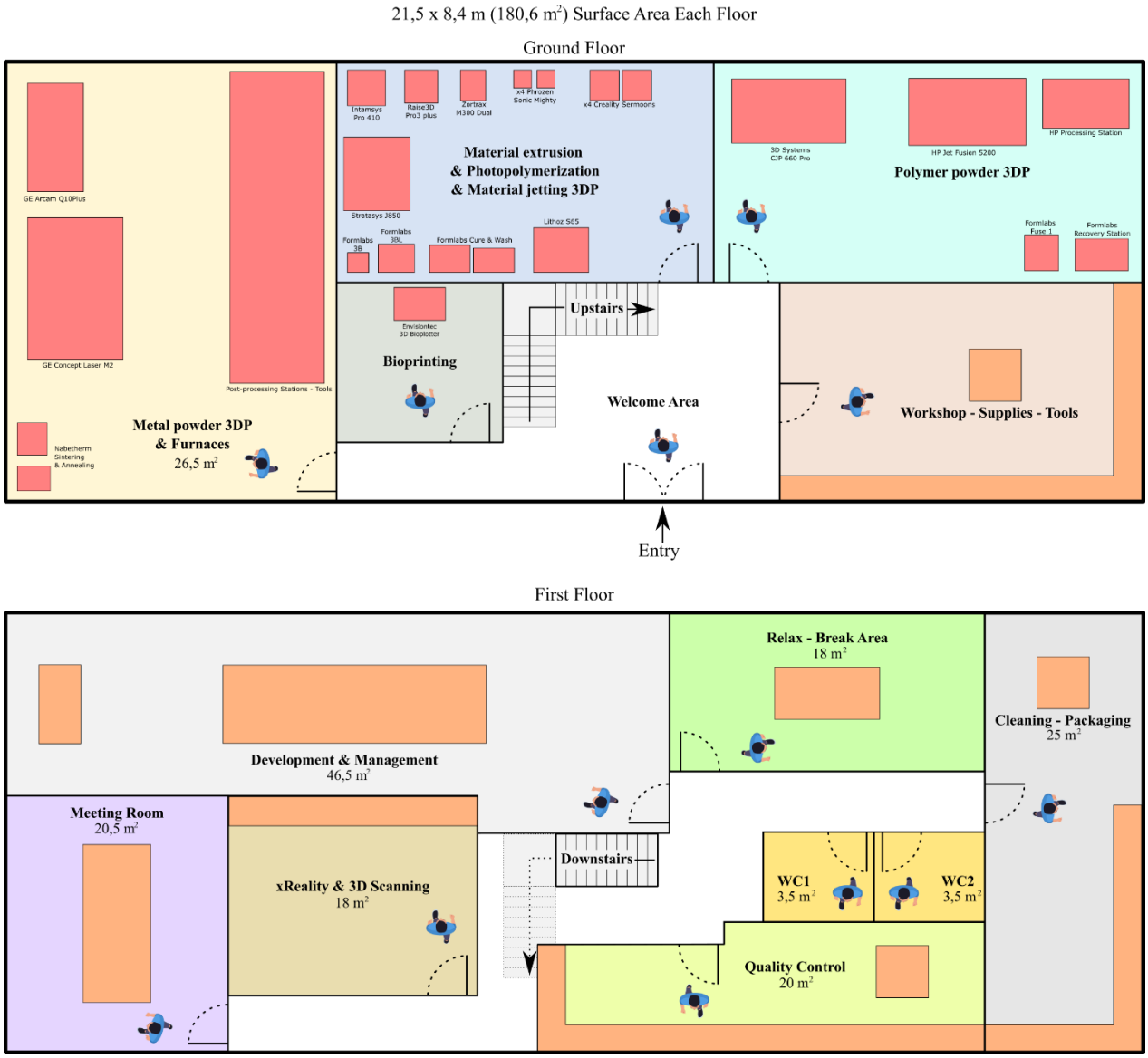

Figure 295: Two-floor PoC layout concept for Scenario 1

For the previous layouts for Scenario 1, the single ground floor concept has 367 square meters and the two-floor concept has 180,6 square meters of total surface area respectively. The following rooms-departments were included in both layouts:

1. Metal powder-based 3DP area for fabricating metal parts. Equipped with annealing and sintering furnaces. This area has to be air-filtered for the small metal powder particles and air-ventilated.
2. Material extrusion, photopolymerization, and materials jetting 3DP area where polymer and ceramic parts are being fabricated. Proper air filtration and ventilation are required.
3. Bioprinting area for producing constructs for TE. Clean-room specifications are required.
4. Polymer powder-based 3DP area for making of polymer parts. Proper air filtration and ventilation are required.
5. Cleaning and packaging area where each part is being cleaned, and packaged after its quality inspection.

6. Workshop area equipped with all necessary tools to support the 3D printers per se and other hands-on activities (assembly, post-processing). Supplies for 3D printers can be stored there as well. For example, *Figure 296* shows suitable workbenches, toolsets, and carriers for measuring instruments, hand and power tools, consumables, personal protective equipment, and other accessories for the workshop that approach a cost of 25.000 €.

Figure 296: Example of PoC workshop equipment for Scenario 1

7. Quality control area for the inspection of each part produced and quality tests. Clean-room specifications are required.
8. xReality and 3D scanning area. Used for VR, AR/MR for training, education, pre-operative planning and simulation, and collaboration. Also, 3D scanning of objects and body parts.
9. Development and management area where the medical devices are being developed (3D design), and management activities take place.
10. Meeting room used for patient consulting, training, education, and collaboration.
11. Relax and break area, a welcome area, and WCs.

The considerably high costs of civil works and building preparation as well as the required heating, ventilation, and air filtration and conditioning systems and other ancillary building works and furnishings have to be considered very carefully.

OpenAI's[130] DALL·E 3[131] was utilized to generate photorealistic concepts for Scenario 1. A modern building design concept with a great glass surface area for the two-floor layout of Scenario 1 is shown in *Figure 297*. *Figure 298* shows the glass-wall meeting room and the other departments of the PoC Unit being autonomous white pods with glass walls, the production areas being more industrial in style, and the development area (3D design) being more cozy and natural for boosting creativity and motivation.

Figure 297: Example of a two-floor PoC building concept for Scenario 1. Source: DALL·E 3

For Scenario 2, the PoC might be established near or within the HCF, as there is no need for a new building addition. *Figure 299* shows a single ground floor layout concept where 60 square meters of surface area are required to house a 30 square meters area for 3DP and workshop activities and a 30 square meters area for the design and management, meetings, and xR and 3D scanning tasks. *Figure 300* shows two photorealistic concepts of a single ground floor and a two-floor layout that can serve the needs of Scenario 2. A budget of 3.000 € for special and basic measurement and hand tools is enough for the workshop, whereas the high cost required for heating, ventilation, air filtration and conditioning systems and other ancillary building works and furnishings have to be considered very carefully.

[130] AI research organization consisting of the non-profit OpenAI Inc., based in San Francisco, California, US. See https://openai.com/.

[131] Text-to-image model developed by OpenAI using deep learning methodologies to generate digital images from natural language descriptions, called "prompts". See https://openai.com/dall-e-3.

Pods with glass walls for each room-department

Industrial design of production and workshop areas

Cosy and natural design of design office

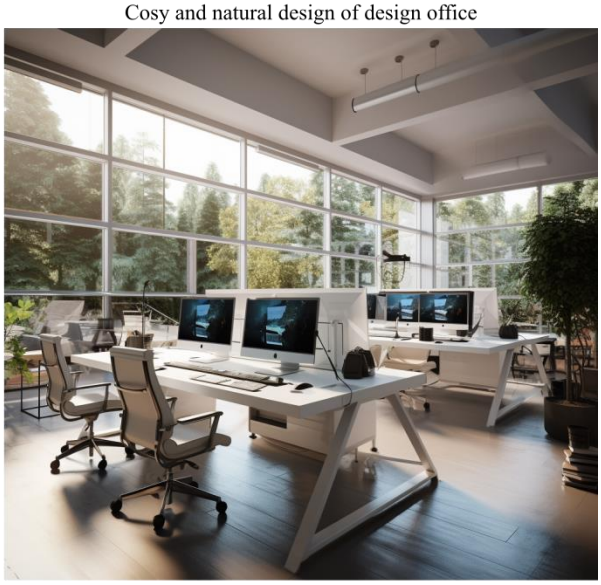

Meeting room

Figure 298: Example of departments and rooms of the two-floor PoC for Scenario 1. Source: DALL·E 3

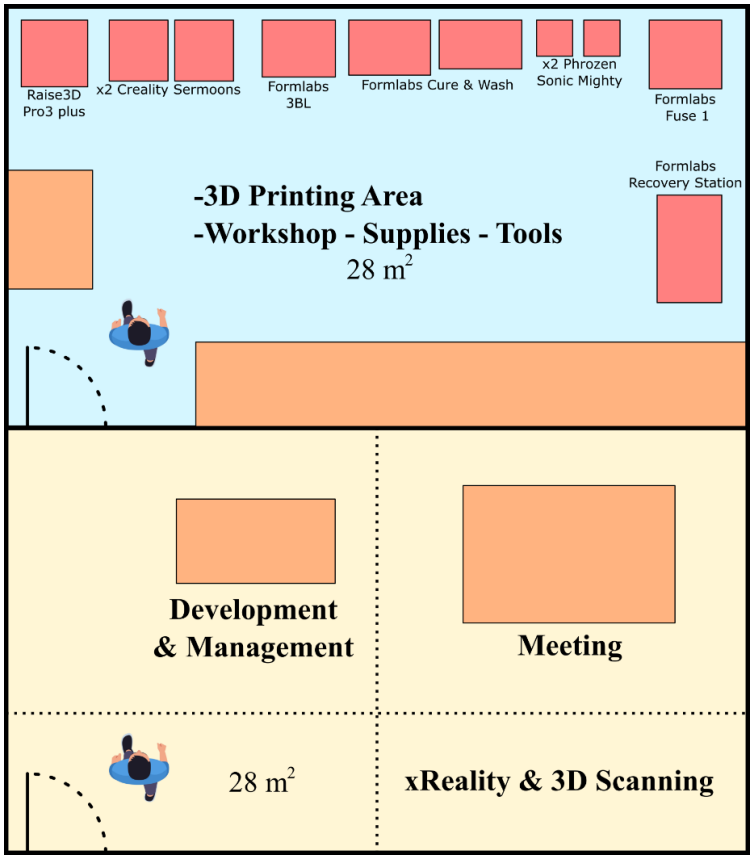

Figure 299: Single ground floor PoC layout concept for Scenario 2

Figure 300: Single ground floor and two-floor PoC concept for Scenario 2. Source: DALL·E 3

5.4.1 Thesis Available Resources – Constraints

For HCF interested in housing small PoC 3D Units within existing available office space up to 30 square meters, a layout similar to this shown in *Figure 301* can be established.

In this Thesis, a simple small hypodigmatic 30 square meters pilot PoC 3D Unit was set in Orthopaedic Research and Education Center "Panayiotis N. Soucacos", "Attikon" University General Hospital, First Department of Orthopaedic Surgery, School of Medicine, National and Kapodistrian University of Athens (*Figure 302*). The total budget required to equip the Unit was 6.000 €, including the following resources (*Figure 303*):

1. A workstation computer equipped with Intel Core i9-12900K 3.2GHz CPU, MSI GeForce RTX 3090 24GB GPU, 64 GB RAM, and 1 TB SSD NVMe storage, running Microsoft Windows 11 64-bit and loaded with all required software.
2. Oculus Rift S (Lenovo Group Ltd, Quarry Bay, Hong Kong, now owned by Meta Platforms Inc., California, US) headset for virtual reality applications.
3. Apple iPad Pro 2021 (Apple Inc., California, US) for screen-based Augmented Reality applications and LiDAR-based and TrueDepth camera-based 3D scanning.
4. Creality CR-10s (Shenzhen Creality 3D Technology Co. Ltd, Shenzhen, China) material extrusion 3D printer and ColorFabb (Colorfabb B.V., Belfeld, Netherlands) PLA/PHA feedstock materials.
5. Elegoo Saturn S (Elegoo Inc., Shenzhen, China) vat photopolymerization 3D printer with Elegoo Mercury XS washing and curing stations, and Elegoo plant-based photopolymer resins.

Figure 301: A small PoC Unit concept housed within an office of a HCF. Source: DALL·E 3

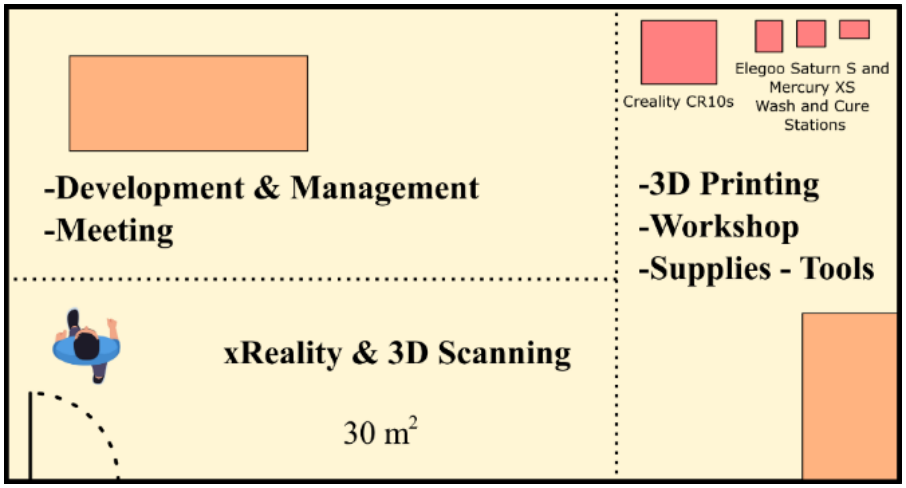

Figure 302: Pilot PoC 3D Unit used in this Thesis

Although the available resources are constraining the acquisition of the required space and equipment to apply Scenario 2, in this Thesis, the *SkeletoMy* platform will be utilized, as well as all required software (but not medically approved). However, the QMS will be left out of scope and will be researched in the future, and as stated in the previous *Sub-section 5.2*, a "one-man show" engineer will have the roles of (bio)mechanical design and manufacture engineer, quality control engineer and 3D printer operator-mechanic.

Figure 303: Equipment of pilot PoC 3D Unit used in this Thesis

5.5 Cost Analysis

Compared to traditional manufacturing methods requiring tooling (primary shaping like casting, forging, molding, and subtractive like CNC machining) in terms of time and cost, 3DP has unlimited design freedom and is effective for low to medium production volumes and/or fabrication of complex geometries. These trends were shown in the qualitative graphs pictured in *Figure 101* and also pictured in *Figure 304* published by Formlabs *(2021)* referring to plastic production, though metal production trends are similar. It should be noted that each 3DP technique has different graphic characteristics in terms of time and cost.

Different cost models have been proposed *(Hopkinson and Dickens, 2003; Ruffo et al., 2006; Costabile et al., 2017; Kadi, Yusof and Wahab, 2020)* to estimate the cost for 3DPed parted by considering several variables. 3DP enables novel product designs and redesign (optimization, consolidation) for 3DP for further cost and time savings, whilst offering superior performance *(Atzeni et al., 2010; 2012)*. On the other hand, possible failures have great levels of negative cost impacts (*Ding et al., 2021*). Cost models should be seen as a means to guide product design and manufacturing planning for further process improvement. For example, it is possible to increase time and cost-

effectiveness, by inserting multiple and different parts into the same built platform simultaneously in single print sessions *(Ruffo and Hague, 2007; Rickenbacher, Spierings and Wegener, 2013).*

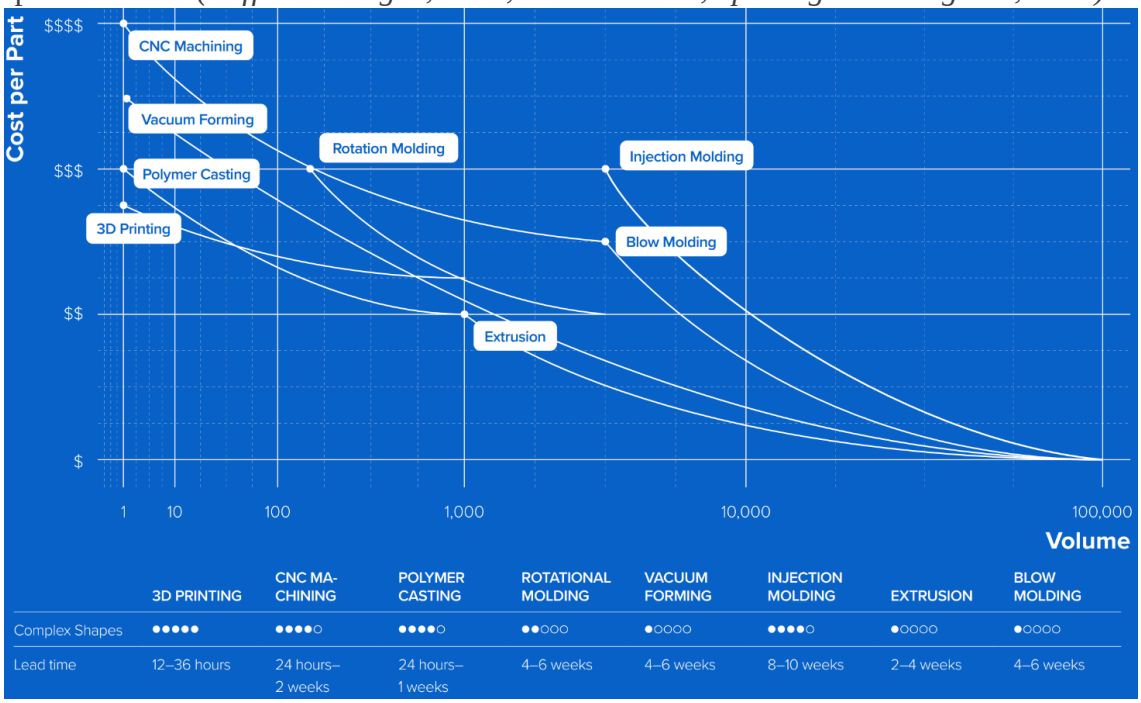

	3D PRINTING	CNC MACHINING	POLYMER CASTING	ROTATIONAL MOLDING	VACUUM FORMING	INJECTION MOLDING	EXTRUSION	BLOW MOLDING
Complex Shapes	●●●●●	●●●●○	●●●●○	●●○○○	●○○○○	●●●●○	●○○○○	●○○○○
Lead time	12–36 hours	24 hours–2 weeks	24 hours–1 weeks	4–6 weeks	4–6 weeks	8–10 weeks	2–4 weeks	4–6 weeks

Figure 304: Cost per part versus production volume for plastic manufacturing methods. Source: (Formlabs, 2021)

Kadi, Yusof and Wahab *(2020)* provided a review of 3DP cost estimation models developed over the past three decades using systematic classification *(Figure 305)*. They mentioned the three perspectives (finance and accounting, manufacturing, and management), broke the cost components into the lifecycle, total, and production costs, and classified the cost classification techniques into method- (intuitive, parametric, analogy, and analytical), task- and level-based *(Figure 305)*.

The total cost C_{total} for any service or product a PoC 3D Unit offers (3D anatomical reconstruction and 3DP, 3D digital design and 3DP of customized products, xR, and 3D scanning) can be estimated by a series of applicable cost factors creating the following task-based process-oriented formula *(see Figure 306 for cost per offered service)*:

$$C_{total} = O_{pre-process} * C_{pre-process} + O_{in-process} * C_{in-process} + O_{post-process} * C_{post-process}$$

- O are the coefficients for operational and extra overhead drivers for pre-process, in-process, and post-processing activities.
- $C_{pre-process}$ is the cost during pre-processing. For 3D anatomical model reconstruction and 3D design of medical devices for 3DP, it is the sum of:

$$C_{pre-process} = C_{preparation} + C_{CAD/CAE/CAM}$$

  - $C_{preparation}$ is the preparation cost, emerging from set up used and activities executed, e.g. image data processing software for 3D model generation. It can be fixed or calculated per hour by multiplying the total time consumed in hours ($t_{p\ labor}$) by the members involved.

- $C_{CAD/CAE/CAM}$ is the software cost for CAD, CAE, and CAM, including any modeling and optimization, and Design for 3DP (Df3DP). It can be fixed or calculated per hour by multiplying the total time consumed in hours ($t_{c\ labor}$) by the members involved in completing the CAD, CAE, and CAM activities.

- $C_{in-process}$ is the cost of the process per se. For 3DP services, it is the sum of:

$$C_{in-process} = C_{equipment} + C_{material} + C_{energy} + C_{auxiliaries} + C_{outsource}$$

  - $C_{equipment}$ is the cost to operate the hardware (and possibly software) equipment, which contains the cost spent for acquisition and maintenance, and it is formed by the capacity factor and desired investment pay-back period. It can be fixed or calculated per hour by multiplying the total time consumed in hours ($t_{e\ labor}$) by members involved in operating the equipment and conducting any other work.
  - $C_{material}$ is the cost per Kg of feedstock material (structural and support) used. This is usually estimated automatically during pre-processing by the process planning software.
  - C_{energy} is the cost of the total energy consumed.
  - $C_{auxiliaries}$ is the cost of any ancillary utilized.
  - $C_{outsource}$ is the cost of outsourcing to contract manufacturers the production of parts.

- $C_{post-process}$ is the cost of post-processing the developed product. For 3DPed parts, it is:

$$C_{post-process} = C_{handling} + C_{treatments} + C_{QA} + C_{deliver}$$

  - $C_{handling}$ is the cost to handle the feedstock material and clean the fabricated part per se. It can be fixed or calculated per hour by multiplying the total time consumed in hours ($t_{h\ labor}$) by members involved in handling.
  - $C_{treatments}$ is the cost for any post-treatments outsourced or conducted in-house. If conducted in-house, it can be fixed or calculated per hour by multiplying the total time consumed in hours ($t_{t\ labor}$) by members involved in all treatments executed.
  - C_{QA} is the cost for quality assurance and control by verification and validation. It can be fixed or calculated per hour by multiplying the total time consumed in hours ($t_{QA\ labor}$) by members involved in quality assurance and control.
  - $C_{delivery}$ is the cost for preparation, packaging, and delivery of the part. It can be fixed or calculated per hour by multiplying the total time consumed in hours ($t_{d\ labor}$) by members involved in preparation, packaging, and delivery.

The time spent by members involved in each activity, along with fixed and variable costs have to be carefully assigned to each factor to calculate the total cost, including operational and overhead.

Classification techniques		Definition
Method-based	Qualitative: Intuitive	Based on the experience of the estimator
	Qualitative: Analogy	Based on historical data. A comparison is often made between old parts and new parts during estimation
	Quantitative: Parametric	Based on statistical regression expression where variables are referred to as cost drivers
	Quantitative: Analytical	Based on product decomposition into units, operations, or activities that relate to how to manufacture the product
Task-based	Design-oriented	Based on design-related activities
	Process-oriented	Based on the process of commissioning the product development activities covering production-related and post-processing costs
Level-based	Process-level	Based on the production cost, which involves entire product development phases (pre-processing, production and post-processing)
	System-level	Based on product lifecycle that covers supply chain, operation management and system-level services

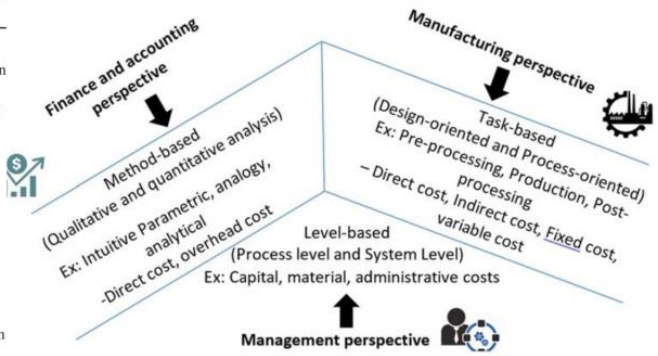

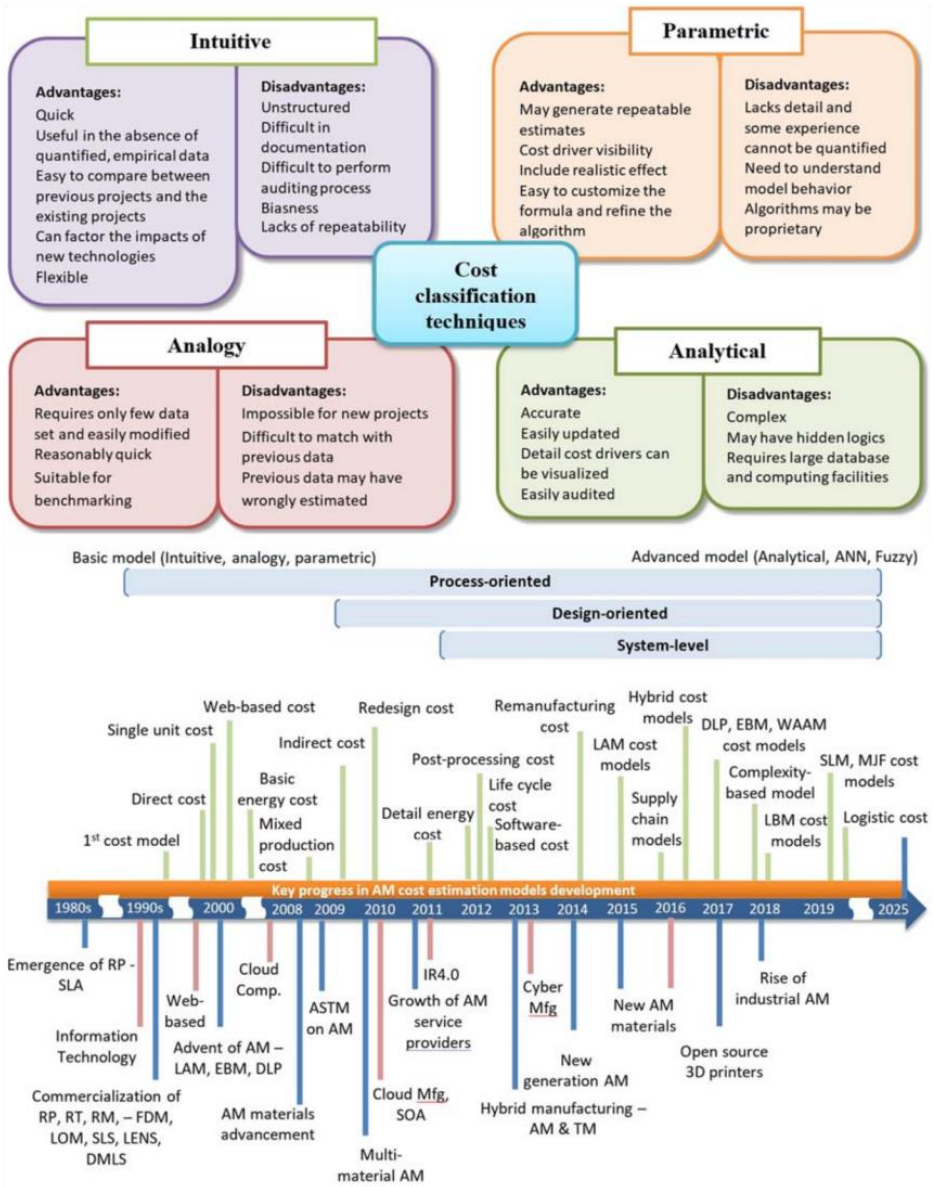

Figure 305: Evolution, classification, and perspectives of 3DP cost models. Source: (Kadi, Yusof and Wahab, 2020)

Post-treatments are usually implemented to improve the dimensional accuracy and surface quality of 3DPed parts *(Wohlers Associates, 2021b)*. Usually, post-treatments are outsourced to external partners as extra high-cost industrial systems are required. Post-treatments for medical devices refer to techniques used to modify their morphological, physicochemical, biochemical, and biological properties by conventional and non-conventional techniques *(see Sub-section 3.1 and Figure 32)*.

For example *(Kumbhar and Mulay, 2016; Liu et al., 2019; Florea et al. 2020; Maleki et al., 2021; Montoya et al., 2021; Ferraris and Spriano, 2021):*

1. Material removal by:
    a. Mechanical treatments:
        i. Machining.
        ii. Polishing.
        iii. Vibratory tribo-finishing.
    b. Laser-based treatments:
        i. Laser micro-machining.
        ii. Femtosecond laser micro-machining.
    c. Chemical treatments:
        i. Chemical etching.
        ii. Chemical polishing.
        iii. Electro-chemical polishing.
2. No material removal by:
    a. Mechanical treatments:
        i. Rolling.
        ii. Bead blasting.
        iii. Shot peening.
        iv. Cavitation peening.
        v. Ultrasonic modifications.
    b. Laser-based treatments:
        i. Laser shot peening.
        ii. Laser remelting.
        iii. Laser polishing.
    c. Chemical treatments:
        i. Alkali treatment.
    d. Thermal and thermomechanical treatments:
        i. Hot isostatic pressing.
        ii. Various heat treatments.
3. Coatings by:
    a. Electro spark deposition.
    b. Electrophoretic deposition.
    c. Physical or chemical vapor deposition.

d. Anodizing.
e. Plasma electrolytic oxidation.
f. Plasma spray.
g. Sol-gel.
h. Biological materials seeding.
i. Dip coating.

4. Hybrid techniques.

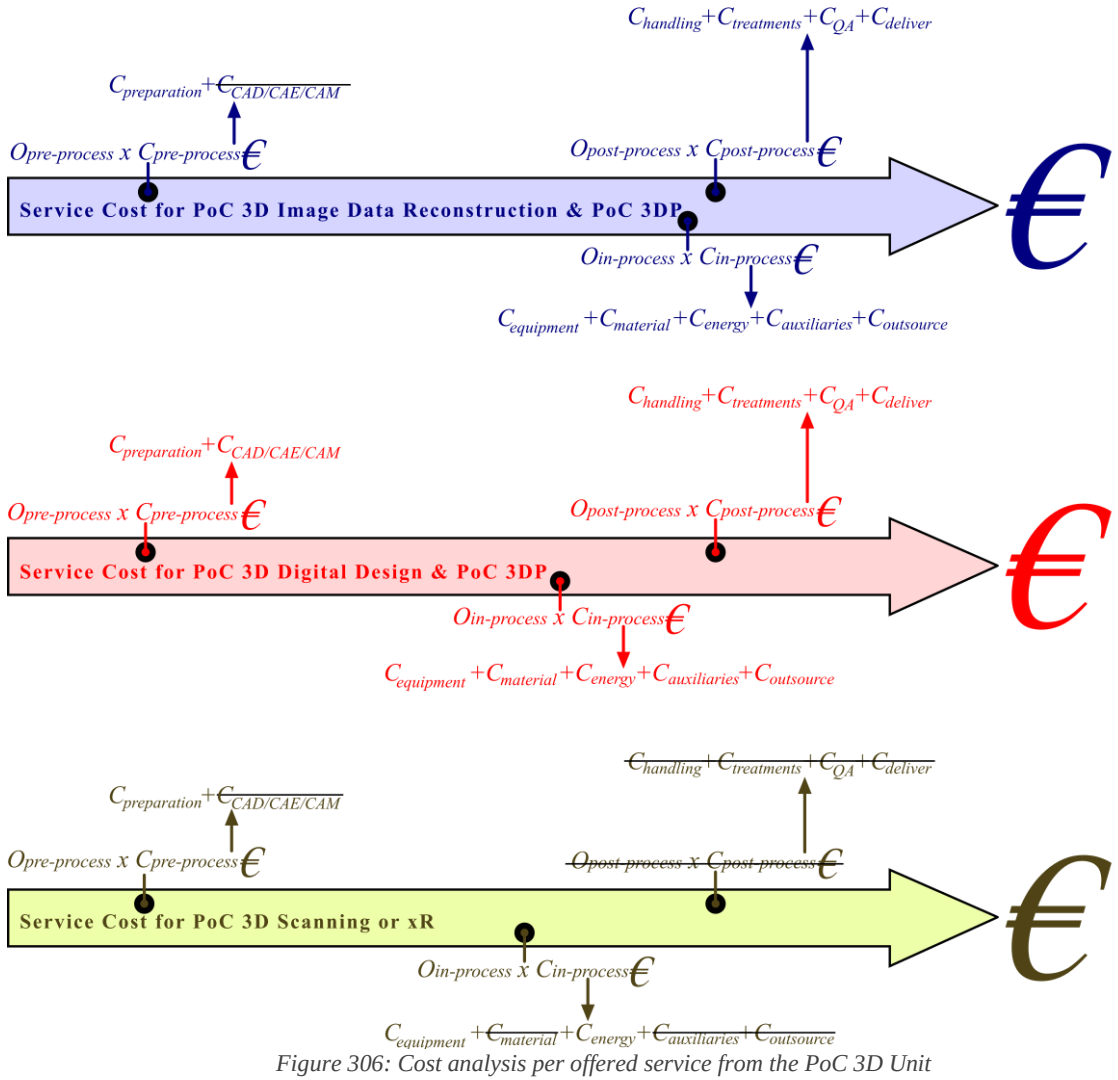

Figure 306: Cost analysis per offered service from the PoC 3D Unit

Post-processing techniques have pros and cons and their selection depends on the nature of the application, material type and properties, level of finish, product shape and geometrical complexity, initial surface roughness, and economic considerations *(Boban et al., 2022)*.

Based on the aforementioned formulas, *Figure 307* shows an internal report that can be used within the PoC 3D Unit to present the final cost (for the PoC 3D Unit) per requested service.

For Scenario 2 where final part materialization is outsourced to contract manufacturers, the cost per part would be higher compared to Scenario 1 where final part production takes place in-house. However, for sustainability, benefit, investment cost, and capacity warrant for Scenario 1, there

should be a reasonably high flow of requests that drive machine and all equipment utilization to be as high as possible. In other words, before investing in any strategy, PoC 3D Units should prioritize their needs first and then consider the costs for equipment acquisition and ownership based on the ease of implementation and transition, sustainability, competitiveness, technologies selected, scale-up scenarios, and available space and resources. A safe approach would be to initially invest in market proven technologies with widespread adoption with larger lifecycles.

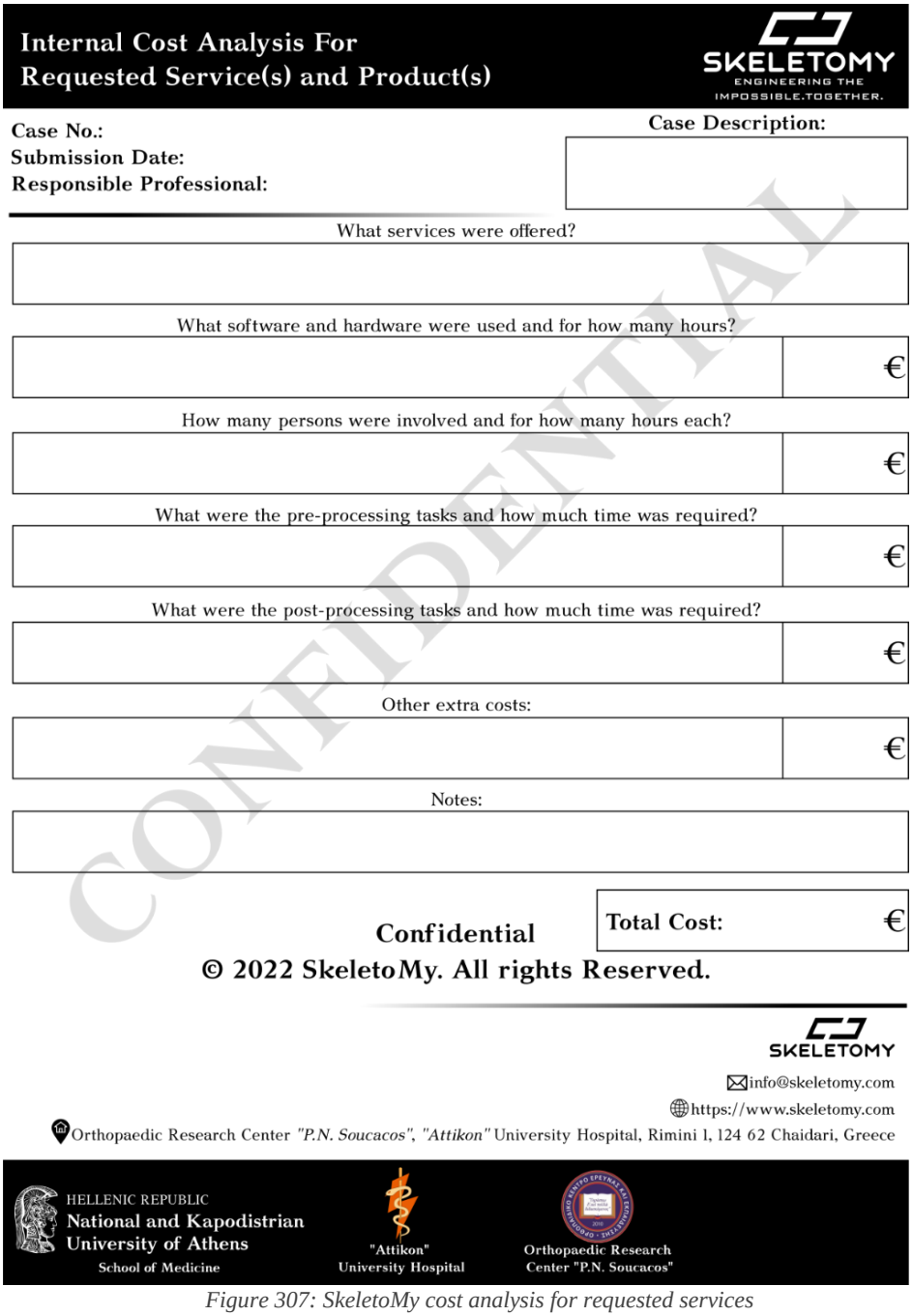
Internal Cost Analysis For
Requested Service(s) and Product(s)

SKELETOMY
ENGINEERING THE IMPOSSIBLE.TOGETHER.

Case No.:
Submission Date:
Responsible Professional:

Case Description:

What services were offered?

What software and hardware were used and for how many hours? €

How many persons were involved and for how many hours each? €

What were the pre-processing tasks and how much time was required? €

What were the post-processing tasks and how much time was required? €

Other extra costs: €

Notes:

Total Cost: €

Confidential

© 2022 SkeletoMy. All rights Reserved.

SKELETOMY
info@skeletomy.com
https://www.skeletomy.com
Orthopaedic Research Center "P.N. Soucacos", "Attikon" University Hospital, Rimini 1, 124 62 Chaidari, Greece

HELLENIC REPUBLIC
National and Kapodistrian University of Athens
School of Medicine
"Attikon" University Hospital
Orthopaedic Research Center "P.N. Soucacos"

CONFIDENTIAL

Figure 307: SkeletoMy cost analysis for requested services

5.6 Distributed and Localized Manufacturing

Manufacturing systems have been reorganized through the decades to adjust to the market trends. The behavior and performance of manufacturing systems are set by the main market trends. More specifically on manufacturing models *(Mourtzis and Doukas, 2012)*:

- Competitive priorities and production paradigms evolution: these have evolved from quality-cost only (craft production paradigm: exactly what the end-user wants), to quality-time-cost (mass production paradigm: large volumes at low cost, and lean manufacturing paradigm: waste reduction and value improvement), to quality-time-cost-flexibility (mass customization paradigm: high product variety and end-user involvement), to quality-time-cost-flexibility-innovation-adaptability (personalized production paradigm: unlimited product variety driven by the end-user).
- Manufacturing networks evolution: from centralized functional facilities to centralized segmented facilities, to decentralized strategic supply networks, to decentralized production clusters.
- Issues and challenges:
    - End-user demands: small batches, reduced life cycles, short delivery times, low cost, better service, high quality, high variety.
    - Constraints: employment, technology, environmental issues, social and political forces.
    - Manufacturing systems: development planning and management, implementation of new efficient and effective technologies, coordination, quality management, production and transportation cost, energy consumption, and raw materials.
- Enablers for evolution: information and communication technologies, resource planning, 3DP, digital design, and manufacturing planning (CAD-CAE-CAM), end-user relationship management, xR, life-cycle assessment, supply chain management. These provide flexibility, automation control, changeability, coordination, collaboration and intra-operability, sustainability and eco-friendliness, and decentralization for increased product modularity for heterogeneous end-user needs.

The advantages of 3DP versus classic manufacturing methods were discussed in *Sub-section 3.3.6*. 3DP changes how products are designed and manufactured (e.g. efficiency, mass customization, on-demand making, decentralized model, extreme complexity at low cost), impacting the humanitarian supply chain (short lead time, fast response to needs, reduced inventory and transportation costs, reduced waste, improved sustainability) with concerning networks, governance, processes, and products *(Attaran, 2017; Corsini, Aranda-Jan and Moultrie, 2020)*.

3DP is a main driver for sustainable (environmentally, societally, and economically) degrowth and localization of production, and can disrupt the structure and operations of businesses at international, national, and local levels *(Priavolou et al., 2022)*. Various key variables affect the localization of production: intellectual property, industrial standards, branding, aesthetics, authenticity, material, complexity, customization, size, logistical complexity, delivery timeliness, demand, access, and technical competence *(Hannibal and Knight, 2018)*.

The strategic potential of 3DP and other emerging digital technologies (e.g. automation, robotics, big data, IoT, cloud computing, mobile technologies, social networks, modular design) is embedded in the vision of Industry 4.0 which is defined as a *"paradigm shift from centralized to decentralized production made possible by technological advances which constitute a reversal of conventional production process logic" (Moreno and Charnley, 2016).* Industry 4.0 is foreseen to transform product life cycles and leverage mass customization by switching centralized models into decentralized models that have common drivers with the circular economy concept that is driven by resource constraints, technological development, and socio-economic opportunities. Localization of production, design customization, ownership, knowledge, and structure distribution are characteristic features of decentralized manufacturing *(Moreno and Charnley, 2016).*

Manufacturing network paradigms are shifting towards decentralization. Ryan et al. *(2017)* geographically categorized the manufacturing network models into personal (end-user point), local (closer to end-user by many distributed facilities), regional (close to end-user with fewer distributed facilities), national (single centralized facility), and mobile (portable manufacturing, taken to the point of use or make in transit). Compared to the traditional manufacturing network model, 3DP serves both centralized manufacturing, but better serves the decentralized and democratized characteristics of the distributed and localized models that have several advantages *(Ben-Ner and Siemsen, 2017).* Decentralized manufacturing network models reaching near or at the point-of-use, powered by 3DP, can materialize parts rapidly just in time, reduce resources and minimize waste, reduced transportation costs, and emissions from transportation.

Rauch, Unterhofer and Dallasega *(2018),* identified that medical and dental instruments and supplies are the top sectors for the integration and utilization of 3DP for distributed manufacturing. Indeed, this is especially useful for medical device manufacturing, where lead time reduction implies a decrease in surgery time and costs and ultimately better healthcare delivery and patient satisfaction. Patient-specific medical device development is engineered to order, and 3DP can be utilized for both engineer-to-order but also for device making of higher standardization levels *(Figure 308)*.

The COVID-19 pandemic outbreak dictated that supply networks of time-critical medical devices must be resilient and responsive. Despite some safety concerns and challenges *(Singh, Venkatesh and Deoghare, 2021),* decentralized local manufacturing (3DP) at the PoC, within the HCF, was proven to cope with the increased local demand for personal protective equipment and other medical devices (*Vakharia et al., 2021; Tareq et al., 2021; Sandhu et al., 2022).* 3DP is even capable of zero-waste 3DP by recycling the non-structural material used *(Kantaros et al., 2021),* thus showing its value on sustainability and circular economy.

Distributed and local manufacturing models encapsulate social, economic, and technological aspects. For such to be implemented, there is a need for *(Priavolou et al., 2022)*:

- transparency, accessibility, replicability, and openness (license and documentation) to distribute information.
- structural and organizational changes. Proper business strategies must be adopted as it is known that the market success of promising products can be undermined by poor business strategies.
- awareness of data exchange standards.
- local availability for human resources, physical infrastructure, information (data/digital) infrastructure, and scientific and technological infrastructure.
- a mixture of social and industrial policies, and adherence to local laws, standards, and regulations.

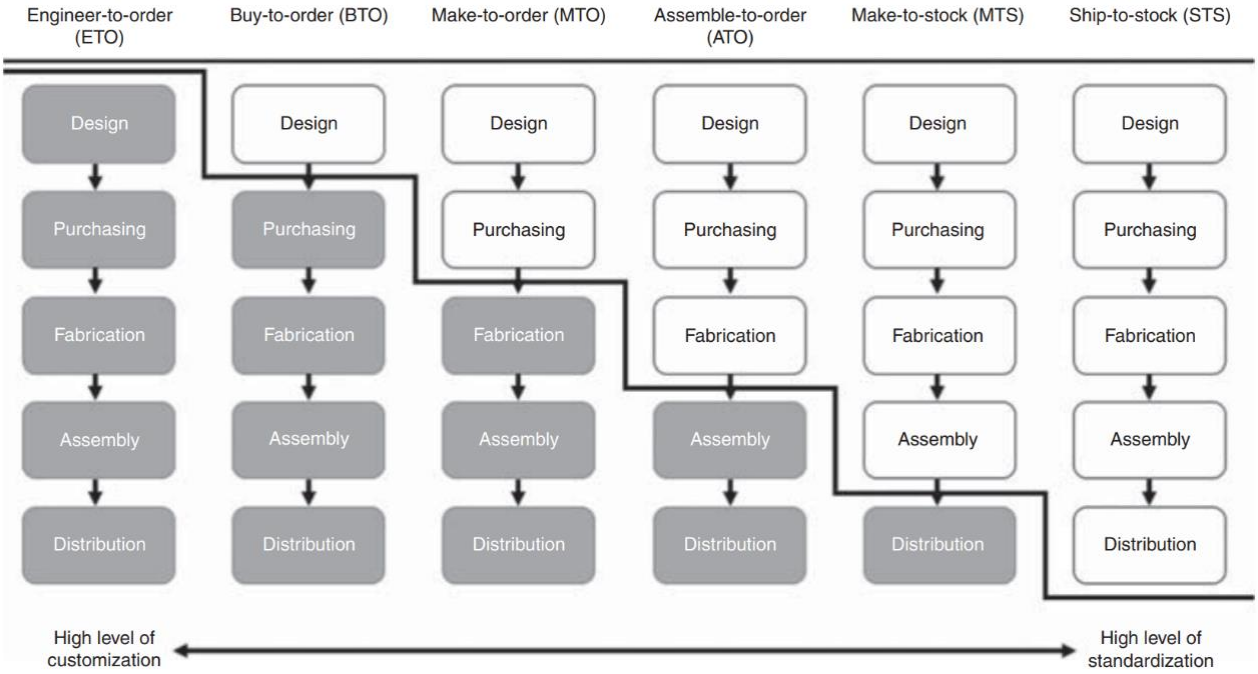

Figure 308: Business production strategies. Source: (Ryan et al., 2017)

Figure 309 illustrates the differences and *Table 16* summarizes the characteristics, advantages, and disadvantages of centralized and decentralized manufacturing networks.

Table 16: Characteristics of centralized and decentralized manufacturing networks.
Source: (Škulj et al., 2015; Srai et al., 2016; Rauch, Dallasega and Matt, 2017; Harrison et al., 2018; Pei et al., 2019; Meyer, Glas and Eßig, 2020; Zhang et al., 2020; Srai et al., 2020; Verboeket et al., 2021; Priavolou et al., 2022).

	Centralized	**Decentralized**
Characteristics	• Delivery of finished products is done by one or more centralized hubs to multiple end-users. • A traditional hub and spoke-like network. Spokes are fully dependent on their hubs. Hubs carry out both production and oversight	• Splitting production into various geographical locations with the ability to democratize and personalize production at multiple scales and locations with active user participation across design, fabrication, and supply. Composed of a set of technologies, systems, and strategies that change manufacturing economics and organization.

	(research, design, and overall control). • Usually implemented for mass production (for economies of scale) at sites established in low-cost regions.	• A hub and node-like network. Hubs might carry out oversight (research, design, overall control) and nodes are fabrication facilities. Nodes fabricate and deliver the finished products to the nearby end-users, whilst might be supported by a hub, though not dependent on the hubs. • Facilities can be a) standardized and replicable, b) modular and scalable, c) flexible and reconfigurable, or d) smart and agile.
Pros	• Mature classic networks with known issues, challenges, and advantages. There is expertise to run such networks. • Economies of scale apply. • Manufacturing costs are cheaper. • Administration, maintenance, quality control, and standardization are simpler.	• Cloud- manufacturing that can actively co-evolve with its environment. • Favors speed and democratize the supply network with high responsiveness. • Creates jobs without geographical restrictions. • Allows more flexible responses to external peaks of pressures and demands as the whole network is more resilient to disturbances. • Logistics are simpler and local needs are met easier. • Transportation costs and emissions are lower. • Material waste is less. • Sustainable network. • User per se or via third-party service provider can 3DP parts with data provided by designers (design global - manufacture local), though intellectual property licensing might be required. • Make or buy options are resurrected. • Engineered-to-order and just in time manufacturing without complex inventory management and stocks required. • Mass customization to end-user needs.
Cons	• Prone to disruption and disturbances, thus a risky choice for medical device production. • More complex logistics. • Point-to-point logistics are more challenging. • Hubs might be the single point of	• Quality control and standardization are more complex. • Manufacturing costs and overall network costs are higher. • Need for expertise and organizational reforms.

	failure for the whole network. • Delivery time is longer and the transportation emissions are higher. • More material waste.	

The dynamism and disruption brought by decentralized manufacturing for patient healthcare delivery can be understood if remote and difficult-to-reach locations are considered. Instead of waiting for the delivery of custom or standard parts from the traditional supply network of centralized manufacturers, parts can be materialized near or within the healthcare center, close to the patient. Thinking extra terrestrially is even more paradigmatic as surgical or non-surgical operations are indeed challenging due to minimum resources, nevertheless, individualized healthcare can be deployed in space via on-board fabricators (3D (bio)printers) for making on-the-go patient-specific or standard instrumentation and other critical parts *(Rajput, 2021; Navarro et al., 2021)*.

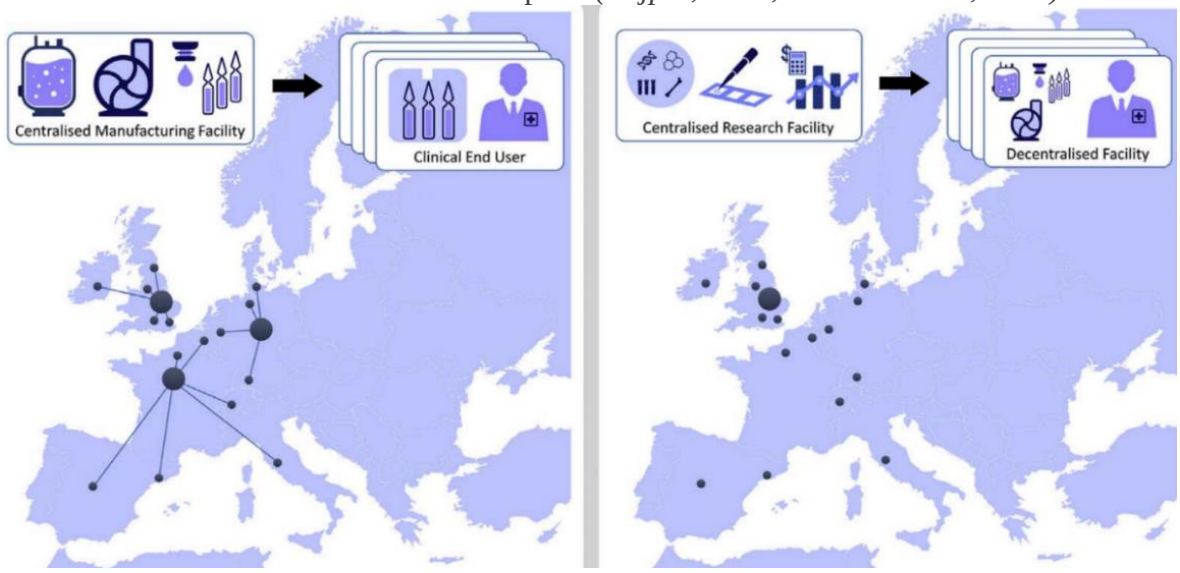

Figure 309: Centralized versus decentralized manufacturing network. Source: (Harrison et al., 2018)

Example cases on distributed manufacturing networks have been studied by:

- Emelogu et al. *(2016)*: a case study for centralized versus decentralized manufacturing (3DP) of medical devices (hip and knee implants, dental braces, stents) in the state of Mississippi, US (*Figure 310*). Identified that product lead time and demands affect 3DP economic feasibility.
- Bilalis et al. *(2022)*: a case study for decentralized 3DP of novel medical face masks in Greece using a p-median method, based on a weighted factor that was assigned to each healthcare center, to minimize distances by optimum geographical distribution *(Figure 269)*. Technical and economic feasibility was found by assuming a) even demand distribution across the whole period, b) masks are produced as fast as possible, c) 3D printers are at full capacity and installed within the HCFs (PoC 3D Units). They stated that trade-offs between manufacturing cost and speed/flexibility can be made depending on the strategic objectives.

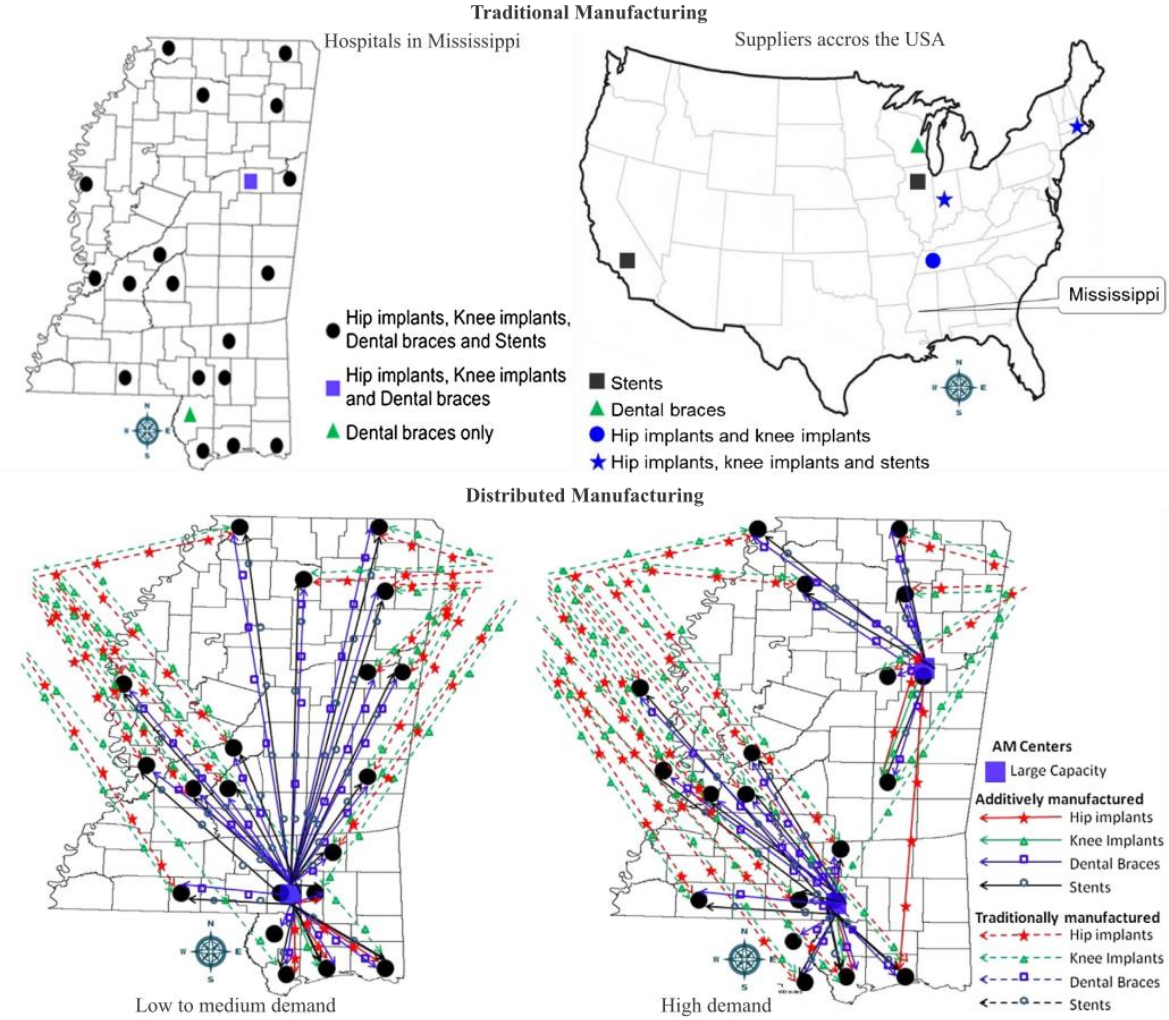

Figure 310: Centralized versus decentralized manufacturing example in the US. Source: (Emelogu et al., 2016)

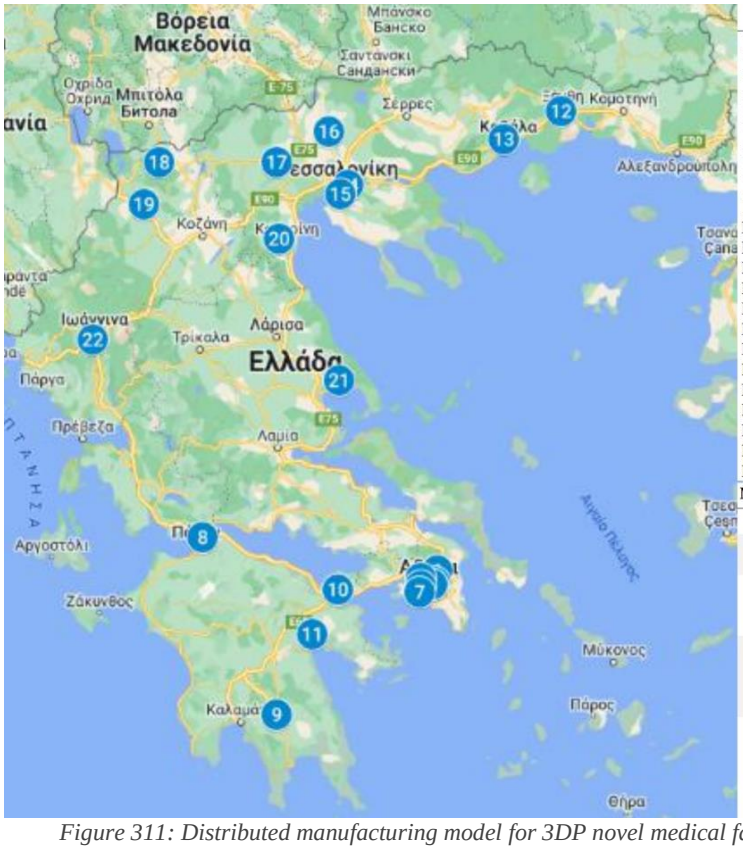

Hospital	Latitude	Longitude	Weighting Factor
Hospital 1	38.07	23.81	6.86
Hospital 2	38.00	23.78	8.35
Hospital 3	37.98	23.76	5.78
Hospital 4	37.98	23.76	4.84
Hospital 5	38.02	23.67	10.23
Hospital 6	37.97	23.66	7.12
Hospital 7	37.93	23.65	5.49
Hospital 8	38.30	21.79	9.65
Hospital 9	37.09	22.42	1.27
Hospital 10	37.94	22.95	2.14
Hospital 11	37.64	22.73	0.45
Hospital 12	41.12	24.87	2.18
Hospital 13	40.94	24.38	3.80
Hospital 14	40.64	23.04	5.52
Hospital 15	40.58	22.97	3.18
Hospital 16	40.99	22.87	1.82
Hospital 17	40.79	22.42	1.27
Hospital 18	40.79	21.41	1.53
Hospital 19	40.51	21.28	1.40
Hospital 20	40.29	22.45	2.34
Hospital 21	39.35	22.96	2.92
Hospital 22	39.62	20.84	11.86

Number of Facilities	Facility Location	Served Hospitals
1	Hospital 2	1–22
2	Hospital 2	1–11
	Hospital 16	12–22
3	Hospital 2	1–2, 5, 8
	Hospital 7	3–4, 6–7, 9–11
	Hospital 16	12–22
4	Hospital 5	1–2, 5
	Hospital 7	3–4, 6–7, 9–11
	Hospital 22	8, 22
	Hospital 16	1–4, 6, 9–20
5	Hospital 5	1–2, 5
	Hospital 7	3–4, 6–7, 9–11
	Hospital 8	8
	Hospital 16	12–21
	Hospital 22	22

Figure 311: Distributed manufacturing model for 3DP novel medical face masks. Source: (Bilalis et al., 2022)

The PoC 3D Unit of this Thesis is housed within the “Attikon” University General Hospital (at Orthopaedic Research and Education Center “Panayiotis N. Soucacos”) located at Rimini 1, 124 61 Chaidari, Attica region, Greece *(Figure 312)*. For medical devices making, both Scenario 1 (design and materialization of any end-parts in situ) where distributed manufacturing and more HCFs can be served, and Scenario 2 (design, prototyping, and some polymer end-parts production) where localized manufacturing or few HCFs can be served, can be deployed as the location of the “Attikon” hospital is benefited from various other agents co-located within a 50 Km radius circle, i.e. a) machine shops for post-processing the 3DPed parts or manufacturing of parts via machining or other classic processes, b) service providers for outsourcing the parts 3DP for Scenario 2 and after cost-benefit make-or-buy analysis for Scenario 1, c) standard medical device suppliers, d) healthcare centers and experts, and e) airport for fast transportation.

The interest of this Thesis is localized production of medical devices, and distributed manufacturing networks are out of the scope. Nevertheless, such cases are interesting to study: a regional or holistic national network for distributed manufacturing across the nation could be developed and simulated, and various trade-offs can be made as per the exact clinical needs to design a smart cloud-based distributed manufacturing network for establishing a sustainable supply of individualized medical devices to effectively and efficiently serve most HCFs.

Figure 312: Geographic location of the PoC 3D Unit

6. Case studies

6.1 Introduction and Assumptions

In this *Section*, the cases carried out within the PoC 3D Unit *(see Section 5)* are introduced, and solved under the inter-epistemic custom product development methodology shown in *Figure 264.*

All cases were treated as if they were currently ongoing pragmatic cases and as if the responsible surgeon required pragmatically the active engagement of the PoC 3D Unit. All patients presented to Prof. Panayiotis J. Papagelopoulos, Chairman of First Department of Orthopaedic Surgery, National and Kapodistrian University of Athens, "Attikon" University General Hospital, and all medical image data and patients' data were anonymized before being delivered to ensure patient privacy.

Note: within the context of this Thesis that has an engineering-centered research character aiming to serve the orthopaedic surgeons (see Sub-sections 4.1 and 4.2), the solutions prototyped (designed and manufactured) at the PoC 3D Unit were not implanted into the patients, whereas due to budget and resources constraints, both top-down and bottom-up approaches (Figure 256) were discussed, and scenarios and hypotheses/assumptions were made along the application of the inter-epistemic development process flow chain (Figure 264).

6.2 Bone Tumor Resection and Reconstruction

Orthopaedic oncology[132] deals with the study and treatment of *neoplasms*[133] in bone. Tumors are neoplasms that can be classified as:

1. Benign tumors that grow slowly, have smooth distinct boundaries, and neither invade nor grow into the surrounding tissue.
2. Malignant/cancerous tumors have the properties of quick anaplasia, and irregular boundaries, and tend to invade into and metastasize to surrounding tissue.

Primary malignant bone tumors (osteogenic[134]) are rare and among the most uncommon types of neoplasms as most emerge from other malignant tumors that tend to metastasize[135] to bone. Paget *(1889)* used the *"seed and soil"* metaphor to describe the metastasis mechanism which is achieved only when appropriate tumor cells (*"seeds")* separate, travel to distant sites, and favorably adhere to the micro-environment of suitable tissue regions (*"soil")* where they can grow *(Liu et al., 2017)*. Malignant cells spread hematogenously, via the lymphatic system, or by direct extension. To grow, they must survive the transit and develop their own blood supply. This is why most metastatic bone tumors occur in the spine and pelvis, where there is a lot of vascularized red marrow. Based on the

[132] From the Greek *"όγκος"* (ónkos; mass) + *"λόγος"* (lógos; root of logic), i.e. the study of masses.

[133] The term *"neoplasm"* has its roots in the Greek words *"νέος"* (neos; new) and *"πλάσμα" (plasma; formation), from "πλάσσω" (plásō; to form)*. Therefore, it refers to new formation of tissue that is usually characterized by progressive and uncontrolled growth.

[134] From the Greek *"οστό"* (ostó; bone) + *"γένεσις"* (génesis; origin), i.e. derived from bone.

[135] From the Greek *"μετά"* (metá; change) + *"στάσις"* (stásis; placement), i.e. transfer from one part of the body to another.

amount of bone resorption and formation, bone tumors can be categorized as lytic (resorption predominates), sclerotic (formation predominates), or mixed *(Wu and Hochman, 2012)*.

The bone tumors classification as per the World Health Organization *(Choi and Ro, 2021)* and the statistics of the most common bone tumor types are shown in *Appendix K*. The histologic forms and anatomical sites, as well as the radiologic images of the most common bone tumor types are shown in *Figure 313* and *Figure 314* respectively.

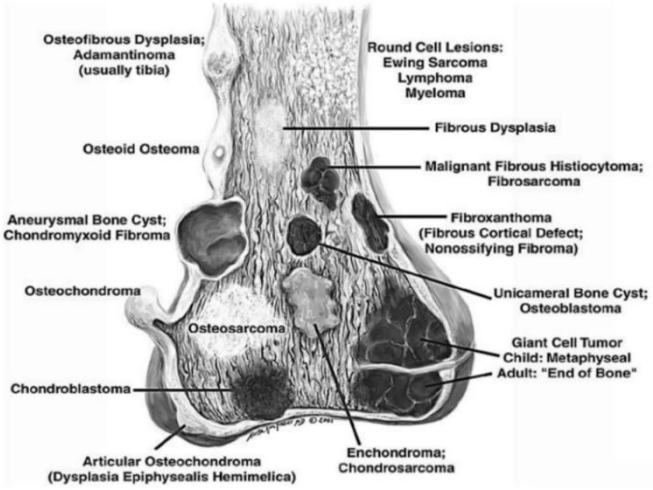

Figure 313: Histologic form and sites of common bone tumors. Source: (Kransdorf and Murphey, 2016)

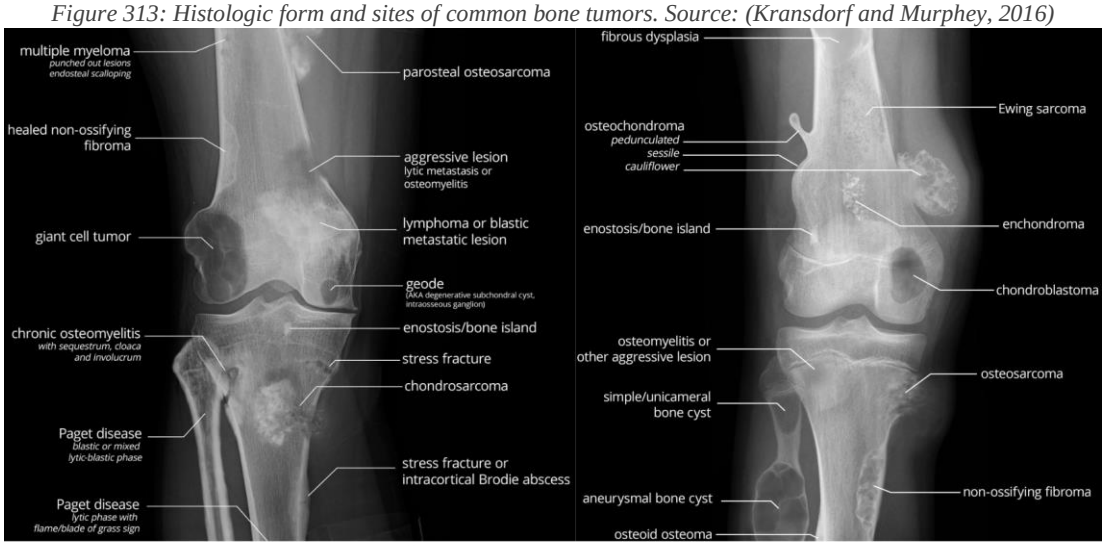

Skalski, M. Bone lesion differential diagnosis - illustrations. Case study, Radiopaedia.org.
Figure 314: X-ray images of common bone tumor types

The most common primary bone neoplasms are *(Murphey, 2006; Wu and Hochman, 2012)*:

1. For malignant tumors: plasma cell myeloma (in patients over 40 years of age), followed by malignancies of mesenchymal tissue, i.e. sarcomas: osteosarcoma (35%), chondrosarcoma (25%), Ewing sarcoma (16%), chordoma (8%), fibrous histiocytoma (5%). Primary bone sarcomas comprise 0,2% of all neoplasms, occurring at 1/10 the rate of soft tissue sarcomas. Osteosarcoma can be classified into many types as per histopathological and clinical criteria and is characterized by osteoblast-like tumor cells that generate a disorganized field of calcified tissue containing osteoid and bone *(Bronner and Farach-Carson, 2009)*. Most sarcomas occur in the extremities (mainly in the distal femur and pelvis) of children and young adults, with pain and an

enlarging mass being the most common symptoms. Before 5 years of age, destructive bone lesions are most common, above 5 years of age, it is often a primary bone sarcoma, and after 40 years of age, it tends to be metastasis or myeloma *(Mavrogenis et al., 2014)*.

2. For benign tumors: osteochondroma (35%), enchondroma (20%), giant cell tumor of bone (15%), osteoid osteoma (10%), and fibrous dysplasia (5%).

Medical history examination focuses on symptoms such as duration, intensity, and timing of complaints, pain, and fracture *(Mavrogenis et al., 2014)*. Lesions are identified using radiographic and clinical tools first, and only if it is necessary to conduct a biopsy[136] or resection. Standard radiographs in two planes are the first imaging examination, and if the malignancy cannot be excluded with certainty, an MRI of the whole compartment is performed, possibly accompanied by CT scanning to visualize clearly bone formation or destruction. Even though biopsy is a key practice to determine the tumor type through histological diagnosis of the acquired tumor tissue, this should always be the final step within the diagnostic process flow chain *(Figure 315 and Figure 316)*. Moreover, utilization of a tumor staging system such as the American Joint Committee on Cancer's (AJCC), Musculoskeletal Tumor Society's (MSTS), or Enneking's *(1985)*, are important tools that facilitate the surgical planning process. Enneking's staging system takes into account the histological grade (G1 = low grade; G2 = high grade), local anatomical tumor extension (T0 = confined within a real capsule; T1 = extracapsular extension but intra-compartmental; T2 = extra-compartmental), and the presence of metastasis (M0 = no metastasis; M1 = regional or distant metastasis). Stages I and II are based on tumor grade (stage I = low grade; stage II = high grade), with each stage being further divided into A and B subcategories based on local anatomical tumor extension (A = T1; B = T2), and stage III refers to any grade and any anatomical tumor extension with regional or distant metastasis.

The goals when treating musculoskeletal malignancies are prioritized and summarized as saving the patient's life, saving the limb, preserving the imb's function, achieving good cosmetic results, and align the treatment method to the psycho-socio-cultural status of the patient (*Özger et al., 2022)*.

Malignant bone tumors must be resected with marginal, wide or radical margins[137] as was described by Enneking *(1983)*. Resections are usually combined with neoadjuvant therapies (such as chemotherapy and radiation therapy) pre-operatively to treat potential micro-metastatic disease and shrink the tumor (reduce soft tissue around the mass and mature the mass), and post-operatively to destroy any remaining malignant cells and impede metastases *(Malawer and Sugarbaker, 2004)*.

[136] From the Greek *"βίος"* (vios; life) + *"όψη"* (ópsi; look), i.e. removal of tissue from a living organism for diagnosis.

[137] With marginal margins (<20-30 mm healthy tissue around the tumor), the tumor is removed around its *"reactive zone"*. With wide margins (20-30 mm healthy tissue around the tumor), the tumor is resected with healthy tissue around it. With radical margins, the tumor plus muscles and tissue in the compartment are resected.

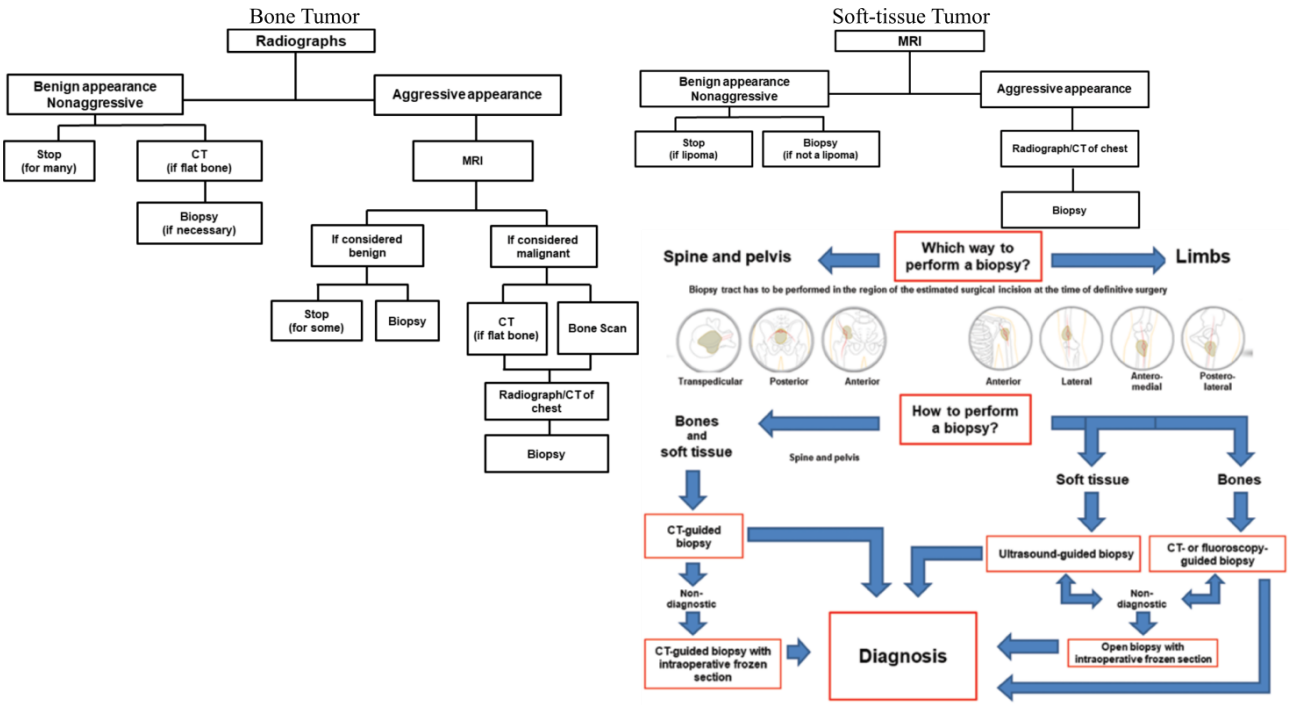

Figure 315: Bone and soft tissue tumor diagnosis and biopsy algorithm. Source: (Mavrogenis et al., 2017b)

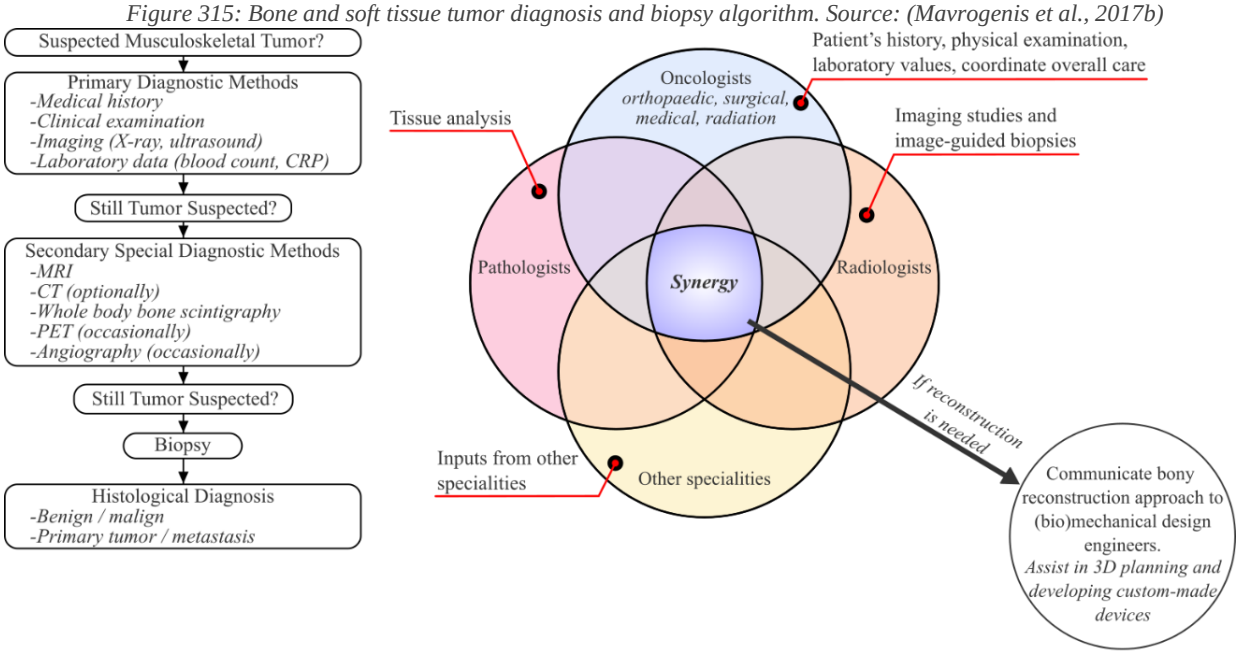

Figure 316: Tumor diagnosis process flow chain and synergy . Left image after (Tunn, 2009)

Resection can be conducted by free-hand, and/or using computer guidance, robotic navigation, or PSI. Although fraught with difficulties (soft tissue and organ injuries, extended bleeding, wound closure, infection, etc), rapid customized implant and instrument design and manufacturing techniques enable precise resection and reconstruction to take place not only in two-stage but also in a single-stage operation *(Wong et al., 2015)*.

Depending on the case, amputations can be avoided with surgical limb-salvage techniques where bone tumors are resected and reconstruction follows to reinstate the musculoskeletal functions. Many published studies showed that limb salvage can achieve as low risk of recurrence as amputation surgery without compromising the survival of the patients *(Mavrogenis et al., 2014)*. However,

critical structures such as muscles, ligaments, skin, nerves, vessels, and organs might be sacrificed. Reconstruction of bone defects must be considered case-by-case due to its complexity and lack of strong guidelines. Reconstructions provide better functional outcomes as limb functions are preserved, but at higher complication rates, hence reconstruction has both advantages and disadvantages *(Mavrogenis et al., 2021)*. The indications and contraindications for limb salvage surgery are summarized in *Table 17*.

Table 17: Indications and contraindications for limb salvage surgery. Source: (Mavrogenis et al., 2011)

Indications	Contraindications	Relative contraindications
1. Tumors of the extremities and/or axial skeleton. 2. Ability to achieve tumor-free resection margins: 3 cm of normal bone around a malignant bone tumor and 1 cm of normal soft tissue. 3. Local recurrence should be no greater and survival no worse than with amputation. 4. The procedure, or treatment of its complications, should not delay adjuvant therapy. 5. Reconstruction should be enduring and not associated with a large number of local complications requiring secondary procedures and frequent hospitalizations. 6. The function of the limb should approach that obtained by amputation.	1. Extensive local disease. 2. Limb salvage requires complex reconstructive procedures with prolonged rehabilitation. 3. Consequent morbidity threatens to compromise oncological treatment. 4. Extreme age groups. 5. Terminal appendage.	1. Major neurovascular structures encased by tumors when vascular bypass is not feasible. 2. Pathological fracture with hematoma violating compartment boundaries. 3. Inappropriately performed biopsy or biopsy-site complications. 4. Severe infection in the surgical field. 5. Immature skeletal age with predicted leg-length discrepancy >8 cm. 6. Extensive muscle or soft tissue involvement. 7. Poor response to pre-operative chemotherapy.

Osseous tissue can be substituted with a) biological auto/allo/xeno grafts, b) TE graft substitutes, or c) readily available or custom-made artificial endo-prostheses *(see Appendix K)*, all conforming to strict requirements *(Tunn, 2009; Ratner et al., 2013; Lewallen et al., 2015; Özger et al., 2022)*. However, a multi-disciplinary effort to manage (evaluation, diagnosis, treatment) musculoskeletal tumors is essential: contributions from orthopaedic, medical, and radiation oncologists (provide data on patient's history, physical examination, and laboratory values, and coordinate the patient's overall care), radiologists (perform imaging studies and image-guided biopsy), pathologists (provide tissue analysis), plastic surgeons, and other specialties based on tumor site *(Tunn, 2009)*. In case 3D planning and/or custom-made devices are to be developed to reconstruct resected tissue, (bio)mechanical design engineers are engaged in the synergistic treatment scheme *(Figure 316)*.

Selecting when and why to choose biological or artificial implant reconstruction involves several prognostic factors and parameters that have to be weighted *(Tunn, 2009; Özger et al., 2022)*; technical consideration, short-to-long-term advantages, and disadvantages, attempted functional and aesthetical outcome, surgical margins, response to neoadjuvant therapies, complication rates, risk,

and other parameters such as patient demographics (gender, age), tumor properties (type, site, amount), socioeconomic and psycho-socio-cultural factors, healthcare policies, capabilities of the medical institution, and surgeon's skills, knowledge, and experience. To further assist this multi-variable selection process, the orthopaedic oncologist can seek standardized approaches that evaluate the end results of different surgical alternatives for limb salvage *(Enneking et al., 1993)*. Although, overlapping indications might fall into a *"gray zone"*, biological and artificial reconstruction options have advantages and disadvantages *(see Table 18)* (*Özger et al., 2022)*, whereas it is not impossible to implement both reconstruction options. As shown in *(Figure 27)*, the ideal reconstruction would be a hybrid artificially-made biological construct.

Table 18: Advantages and disadvantages of biological and artificial reconstruction

Type	Advantages	Disadvantages
Biological Reconstruction	• The healing process is complete with implanted materials totally incorporated into the body, becoming eventually the patient's own, being able to remodel, self-heal, and hypertrophy. • More spared tissue and less morbid. • Biologically manageable complications: soft tissue (e.g. infected hematoma) and hard-tissue complications (fractures, non-unions) are effectively treated as in normal tissue. • Wound problems and secondary deep infections are less common. • Can be converted to artificial implant reconstruction in a worst-case scenario. • Economically more advantageous.	• Long recovery time: problem for lower extremities due to prolonged period of restricted weight-bearing. Hence, most suitable for patients with a high likelihood of survival, non-metastatic, showing good neoadjuvant treatment response, and not have large tumors and pathological fractures. • Quantities are not readily available. • Lack of perfectly matching shapes. • Require surgical skills, team, experience, infrastructure, and organization. • Patients might reject such options.
Artificial Reconstruction	• Precise fit. • Easy application with good function. • Adjustment of near-normal biomechanics. • Immediate or rapid recovery time with weight-bearing daily activities allowed. • Ideal for large tumors and pathological fractures.	• Loss of biological joint surfaces, physeal plates, and bone stock. • Long-term complications such as periprosthetic infections require an inevitable need for revision and further loss of bone stock. • Require surgical skills, team, experience, infrastructure, and organization.

Reconstruction operations require long surgery times with extensive exposures and are often combined with immunosuppression. Implant survival, limb function, and patient outcomes are challenged after reconstruction by stress shielding, (a)septic loosening, infection, non-union, and refracture that might lead to periprosthetic fractures *(Savvidou et al., 2017)*. Especially infections, which were always the nemesis of reconstruction options, these must be prevented, and if not, diagnosed promptly and treated appropriately (*Mavrogenis et al., 2011)*. Such microbial phenomena should be eliminated by proper sterilization procedures, antibiotic prophylaxis, aseptic management techniques, and the use of biomaterials coated with anti-bacterial layers or having anti-bacterial surfaces *(see Sub-section 3.1)*.

6.3 Pelvic Reconstruction

The pelvis is the lower part of the trunk between the abdomen and the thighs. It has an embedded skeleton (bony pelvis) within and on which a plethora of sensitive organs and soft tissue are being supported and attached to muscles, tendons, ligaments, nerve roots, and blood vessels. The bony pelvis is composed of three bone components (innominate bones and sacrum) which have no inherent stability: if all soft tissue are removed it would fall apart *(Figure 317)*. *Appendix L* shows analytically the anatomy of pelvic bones, the hip joint, and the muscles and neurovascular systems involved. The pelvis has the following characteristics *(Tortora and Derrickson, 2020)*:

- It has a deep basin-like structure made up of two hip (innominate) bones with three components each (superior ilium, inferior and anterior pubis, inferior and posterior ischium) that unite anteriorly at the pubic symphysis joint, and posteriorly through the sacrum at the sacroiliac joints. The pubic symphysis prevents the collapse of the pelvis, whereas the sacroiliac joints are the major stabilizing structures as the major weight-bearing forces are transmitted from the hip joint through the iliac bone, across the sacroiliac joint into the sacrum and up the spine *(Tile et al., 2015)*.
    - The ilium is the largest of the three components of the hip bone. It is composed of a superior ala (wing) and an inferior body. The superior border of the ilium is the iliac crest. Its spines (anterior superior iliac spine, anterior superior iliac spine, anterior inferior iliac spine, posterior superior iliac spine, posterior inferior iliac spine) serve as points of attachment for the tendons of the muscles of the trunk, hip, and thighs. The sciatic nerve (the longest nerve in the body) along with other nerves, blood vessels, and muscles pass through the greater sciatic notch. The iliacus muscle attaches to the iliac fossa and the sacroiliac ligament is attached posteriorly to the iliac tuberosity to form the sacroiliac joint on the auricular surface. Anteriorly and inferiorly from the auricular surface is a ridge called an arcuate line. On the lateral iliac surface, the gluteal muscles are attached.
    - The ischium is composed of a superior body and an inferior ramus. The ramus fuses with the pubis. The major anatomical landmarks are the prominent ischial spine, the lesser sciatic notch, the ischial tuberosity, and the obturator foramen which contains blood vessels and nerves enclosed by a fibrous sheath (obturator membrane).
    - The pubis is composed of a superior ramus, an inferior ramus, and a body between the rami. The pubic symphysis is the joint between the two pubes of the hip bones, consisting of a disc of fibrous cartilage. The anterior, superior border of the body is the pubic crest, and at its lateral end is the pecten pubis: a tubercle that is the beginning of the pectineal line extending superiorly and laterally along the superior ramus to merge with the arcuate line of the ilium.

- The sacrum is a triangular bone composed of five fused sacral vertebrae and positioned posteriorly of the pelvic cavity medial to the hip bones. It serves as a strong foundation for the pelvic girdle and allows the passage of nerves and blood vessels through its four pairs of anterior and superior foraminas. On both lateral surfaces, the sacrum has an ear-like auricular surface that articulates with the ilium of each hip bone, forming the sacroiliac joint. Posterior to the auricular surface is a roughened sacral tuberosity where ligaments are attached. The superior articular surface of the sacrum articulates with the inferior articular surface of the fifth lumbar vertebra and forms the lumbosacral joint. There, the sacral canal continues the vertebral canal that ends at the sacral hiatus, on either side of which is the sacral cornu that connects by ligaments to the coccyx: a triangular-like shape with four fused coccygeal vertebrae that articulates with the apex of the sacrum.

- It connects the lower limbs (through the femoral heads) with the axial skeleton through the acetabulum fossa (hip socket) (formed by the ilium, pubis, and ischium) creating the ball-and-socket joint that is surrounded and protected by muscles, tendons, and a ligamentous capsule. The acetabular notch (on the inferior side of the acetabulum) forms a foramen where ligaments of the femur are attached to and which blood vessels and nerves pass through.
- It provides strong support for the vertebral column, as well as for the pelvic and lower abdominal organs involved with bowel, bladder, and reproductive functions.
- It serves as a common attachment point for muscles of the lower extremity and the trunk. The majority of muscles moving the femur (thigh bone) are attached to the pelvic girdle.
- Numerous nerves pass through the pelvis: a) the roots of spinal nerves L1-L4 form the lumbar plexus and split into anterior and posterior divisions to supply the anterolateral abdominal wall, external genitals, and part of the lower limbs, b) the roots of spinal nerves L4-L5 and S1-S4 form the sacral plexus (with the largest nerve in the body (sciatic nerve) originating from sacral plexus) and supply the buttocks, perineum, and lower limbs, c) the roots of spinal nerves S4-S5 and the coccygeal nerves form a small coccygeal plexus that participate in the sensory innervation of the skin overlying the coccyx.
- Numerous blood vessels pass through the pelvis. The abdominal aorta ends by dividing into the right and left common iliac arteries, which are split into internal and external iliac arteries. External iliac arteries become femoral arteries in the thighs, popliteal arteries posterior to the knee, and anterior and posterior tibial arteries in the lower legs. Blood from lower limbs is drained by superficial and deep veins.
- It is able to withstand great forces. The bone provides the fundamental structure and enjoys stability thanks to the surrounding soft tissue, hence, stability and structure enable weight transference. The

pelvis transmits the weight of the upper body and trunk either to the ischial tuberosities (sitting) or to the lower extremities (standing, walking). The pelvis is subjected to mechanical stresses along multiple directions as forces are transferred from the upper to the lower skeleton and vice-versa, not to mention direct impacts. During weight bearing, forces flow through the vertebral column to the pelvis and are transmitted to the ground by the lower limbs. Forces generated from the ground during gait, are transferred to the pelvis through the femur which is the longest, heaviest, and strongest bone of the body. The pelvis withstands great stresses and absorbs shocks thanks to its spongy internal form and external geometry: the pelvic girdle serves as an energy absorber and guides forces to flow through closed-loop paths and to the ground.

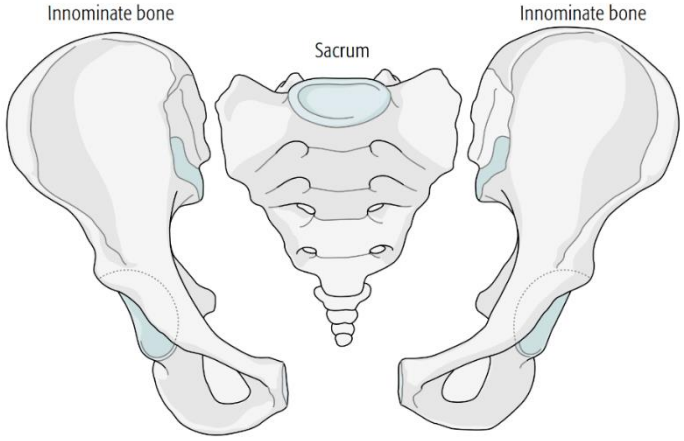

Figure 317: Three pelvic bone components. Source: (Tile et al., 2015)

The pelvis is a frequent site of metastatic malignancies due to the amount of vascularized red marrow, but primary pelvic tumors can also develop (*Wu and Hochman, 2012*). Of the total primary malignant bone tumors, 5-15% are located in the pelvis, and surgical treatment is challenging *(Mavrogenis et al., 2012; Han et al., 2019)*. Patients with high-grade and high-volume malignant pelvic tumors are at high risk as low survival and high recurrence rates occur. Pelvic tumors are among the most difficult in musculoskeletal oncology: they are often large, can invade other structures, and resections are intriguing due to the adjacent soft tissue involved *(Tunn, 2009)*. In such cases, patient survival is the primary objective, rather than function and cosmetic outcomes.

External pelvectomies (amputations) are often the only option due to associated complications such as infections and failures. The following situations might lead toward choosing the amputation approach: destroyed biomechanics, failed reconstruction, failed neoadjuvant therapy, severe deep infection, infiltration of sciatic nerves and femoral vessels, local tumor recurrence, life-saving and palliative procedures *(Wedemeyer and Kauther, 2011)*. Compared to reconstruction options, amputations have shorter surgical duration, are relatively easier procedures, have lower incidence of complications and risk for recurrence, and faster recovery time, however, leg-length discrepancy, impaired gait function, disabilities, and permanent loss of lower extremities impact the later quality of life and psychology of the patient *(Mavrogenis et al., 2012)*.

On the other hand, although challenging, reconstruction following pelvectomies is of great importance as healthy tissue and extremities are preserved. Reconstruction options were enabled and evolved thanks to multi-disciplinary and inter-epistemic synergies and technological tools *(see Sub-sections 1.2 and 1.3)*. The ability to obtain wide margins without compromising survival and function is the parameter that determines limb salvage over amputation *(Mavrogenis et al., 2012)*.

There are no standard procedures for pelvic reconstruction. Thus, treatments might refer to artificial endo-prosthetic implants, allografts, autografts, arthrodesis, and hip transposition, with each having its own advantages and disadvantages *(Ji and Guo, 2019; Fujiwara et al., 2021)*.

Artificial endo-prosthetic implants can be categorized as: a) off-the-shelf modular or fixed saddle, pedestal/stemmed (ice-cream) cone *(Barrientos-Ruiz, Ortiz-Cruz and Peleteiro-Pensado, 2017)*, flanged acetabular components, pedicle screw-rod systems *(Yu et al., 2021)*, and b) custom-made 3DPed. *Figure 318* illustrates the time when each pelvic reconstruction approach was introduced.

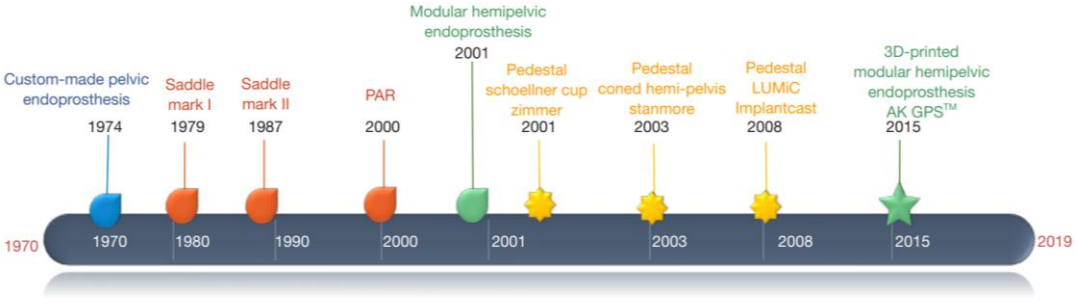

Design/ Structure	Geometrical restore	Loading axis	Loading axis	Loading axis	Ilium fixed	Ilium (posterior column	Ilium (posterior column	Ilium (posterior column	Iliosacral fixed with screws passing sacroiliac joint
Fixation	Screws extramedullar	Flail	Flail	Cross-locking bolt	Multi-axis screws Intra- and extramedullar	Cemented stem	Hybrid stem with additional screws	Cemented or uncemented stems	Multi-axis screws Intra- and extramedullar and osseointegration interface
Modularity	Monoblock	Monoblock	Modular	Modular	Modular	Monoblock	Monoblock	Modular	Modular
Cup Adjustability	N/A	N/A	N/A	N/A	Yes	Yes	Yes	Yes	Yes
Others	CAD							Silver-coating	Porous structure at implant-bone interface

Figure 318: Timeline of pelvic reconstruction approaches. Source: (Ji and Guo, 2019)

As modern endo-prostheses design and fabrication techniques have emerged, innovative reconstruction decisions with custom-made devices can be favored, backed by 3DP *(Park, Shah and Hornicek, 2021; Angelini et al., 2021)*. Numerous individualized 3DPed pelvic endo-prostheses are being reported in the literature with positive results *(Wong et al., 2015; Liang et al., 2017; Hennessy, Anderson and Lozano-Calderon, 2018; Han et al., 2019; Durand-Hill et al., 2020; Gruber et al., 2020; Ji et al., 2020; Chen et al., 2020; Peng et al., 2020; Cao, Zhu and Gao, 2021; Park et al., 2021; Yu et al., 2021; Döring et al., 2021; Xu et al., 2022; Hu et al., 2022; Broekhuis et al., 2022; Gortzak et al., 2022; Pu et al., 2022; Khal et al., 2023; Hu et al., 2023; Zoltan, Popescu and Sanei, 2023; Li et al., 2023; Lv et al., 2023b)*. The reported functional scores *(Fujiwara et al., 2021)* verified that the superior options following bony resection are custom-made endo-prostheses with accurate patient-matching geometries that fill the bone loss and optimized porous surface morphology.

Especially for tailored 3DPed pelvic endo-prostheses with porous morphologies, these were found to have good short and mid-term outcomes, i.e. initial stability, acceptable cosmesis, and rapid function restoration *(Regis et al., 2015; Perticarini et al., 2015; Dall'Ava et al., 2019a; Wang et al., 2019; Geng et al., 2020; Wang et al., 2020; Huang et al., 2021b).*

6.4 Case 1: Ilium and Hip Joint Reconstruction

Note: as this Thesis has an engineering-centered research character aiming to serve the surgeons, and to assess the initially set hypothesis (see Sub-sections 4.1 and 4.2), and due to budget and resources constraints, both top-down and bottom-up approaches (Figure 225) were discussed, and scenarios and hypotheses/assumptions were made along the application of the inter-epistemic development process flow chain (Figure 231). This case was treated as if it was a currently ongoing pragmatic case and as if the responsible surgeon required truly the active engagement of the PoC 3D Unit, as a result, the solution prototyped at the PoC 3D Unit was not implanted into the patient.

The adult male patient presented to First Department of Orthopaedic Surgery, National and Kapodistrian University of Athens, "Attikon" University General Hospital (Chairman: Prof. Panayiotis J. Papagelopoulos), examined, and diagnosed with pelvic osteosarcoma (tumor), the anatomic extent of which determined radiologically by X-ray, CT and MRI imaging *(Figure 319)*.

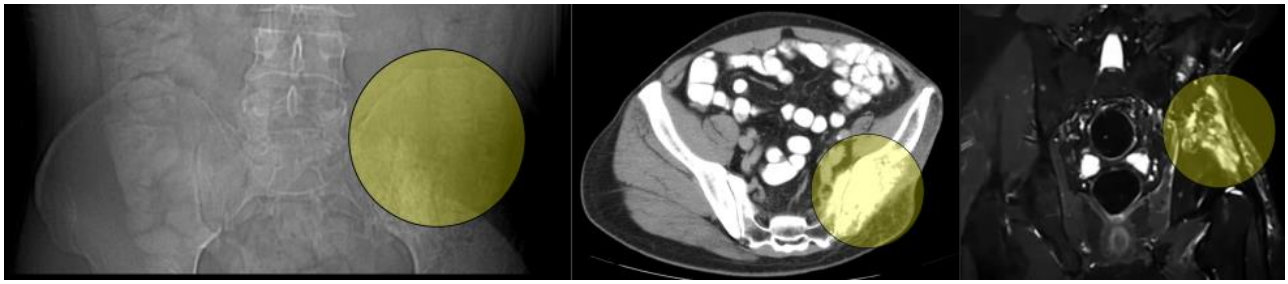

Figure 319: X-ray, CT, and MRI image of the pelvic osteosarcoma site

This case study reports a pelvic reconstruction workflow targeting an adult male patient diagnosed with pelvic osteosarcoma. The case was carried out within the PoC 3D Unit introduced previously, and an artificial 3DPed custom-made endo-prosthesis accompanied by PSIs was developed under the inter-epistemic custom product development methodology shown in *Figure 264*.

The stages of this methodology are unfolded along the next *Sub-sections*.

6.4.1 Medical Imaging, Processing, Visualization and Diagnosis

The PoC 3D Unit was instructed to reconstruct a 3D digital visualization of the pelvis from the CT-scanned data to aid in the diagnosis and pre-operative planning. To do so, the surgeon registered and gained credentials and an account on *SkeletoMy* platform with access to submit requests for services and products to be delivered by the PoC 3D Unit. The case was submitted by completing a request form and uploading the anonymized medical image data (DICOM) of the patient's pelvis on *SkeletoMy* platform *(see Section 5)* which was obtained by CT-scanning as per the suggested scan protocol *(see Section 5)* with 0,75 mm slice thickness by a *Somatom Definition Flash CT scanner*

(Siemens Healthcare Ltd, Erlangen, Germany) *(Figure 320)*. All details were checked to ensure that all prerequisites were fulfilled, and the case was created on *SkeletoMy* platform where both the surgeon and the PoC 3D Unit could exchange data, organize their tasks, communicate and track the status of the requested services and products to meet the agreed delivery deadline.

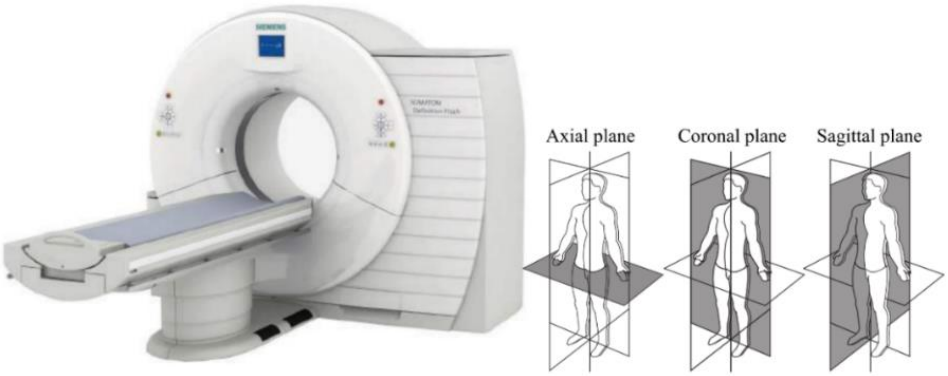

Figure 320: Siemens Somatom Definition Flash and scanning planes. Source: Siemens

Based on the uploaded anonymized image data, the (bio)mechanical design engineer downloaded and imported the data into the DICOM processing software to generate the anatomical 3D model in digital format in 3 minutes. *Figure 321* and *Figure 322* show views of the delivered 3D anatomical models, requiring 15 minutes for delivery. The software tools, the 3D reconstruction process, and delivery options are the same as the ones discussed in detail in the next post-tumor resection Stages.

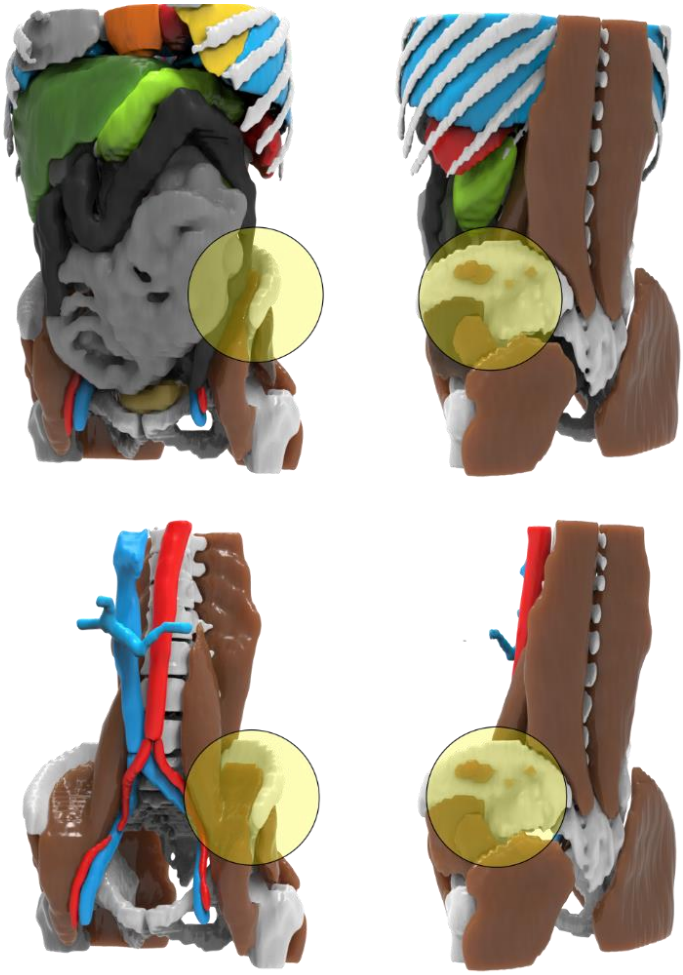

Figure 321: Pre-operative photorealistic views of 3D pelvic anatomy; hard and soft tissue

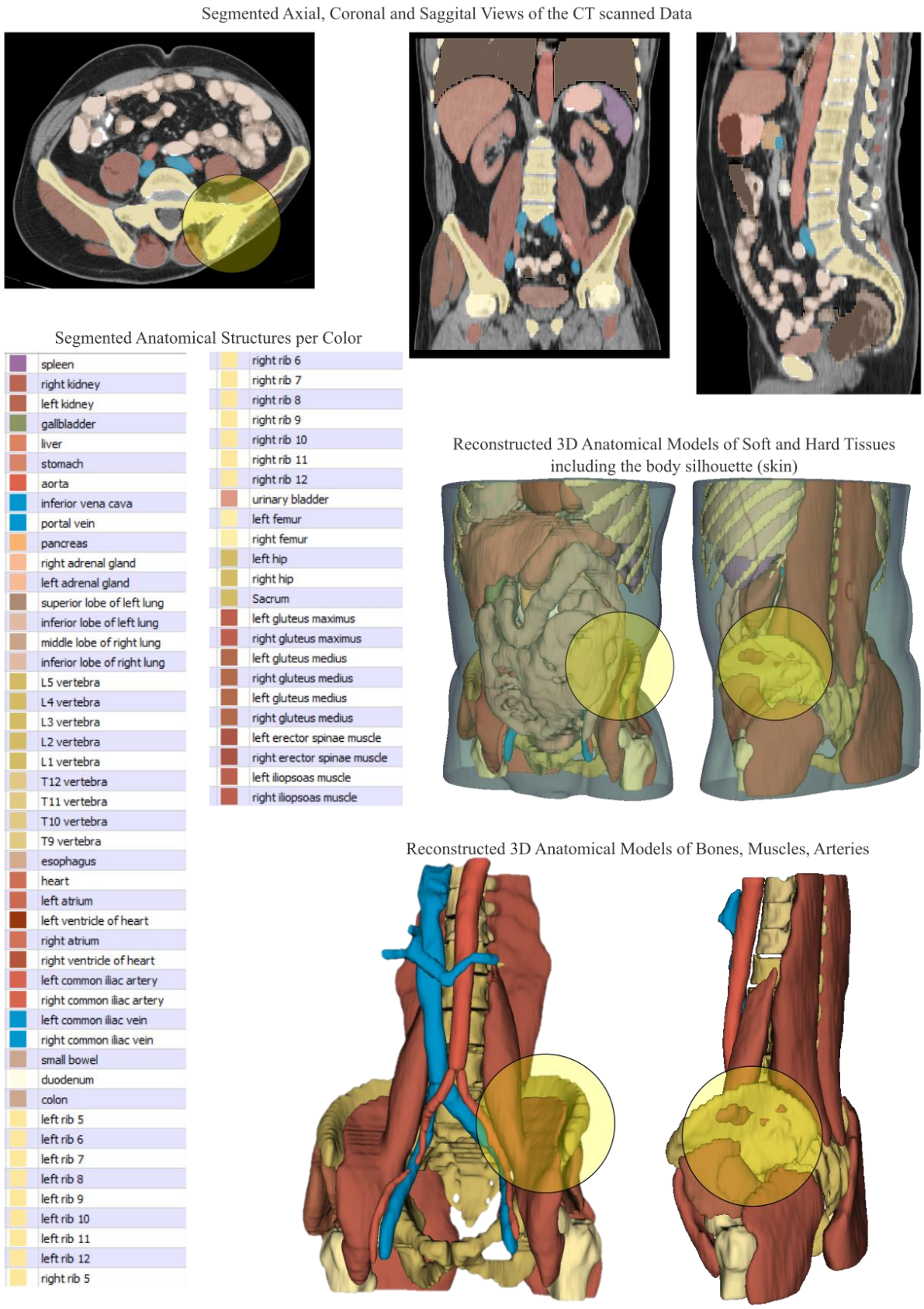

Figure 322: 3D digital pre-operative anatomical pelvic model generation

Before the surgical treatment, the patient underwent neoadjuvant therapy, and an oncologically acceptable resection level was planned as per the tumor stage and site and the prognostic factors and parameters. A two-stage limb-salvage operation was decided instead of a single-step operation with

immediate reconstruction following resection to a) verify that all tumor mass has been resected and b) minimize the extended time to develop and deliver the PSI and endo-prosthesis that would delay the operation whilst allowing oncological progression. Free-hand en bloc[138] tumor resection (without the need for PSIs which could have been developed by the PoC 3D Unit) and artificial patient-specific endo-prosthetic implant reconstruction substituting the resected bone tissue were chosen instead of other approaches such as wired arthrodesis and screw-rod systems augmented with bone grafts *(Zhou et al., 2016).*

The first stage included surgical tumor removal by Prof. Panayiotis J. Papagelopoulos who executed a challenging free-hand iliac plus sacroiliac joint plus part of the acetabulum en bloc resection (Type I plus partial IV plus partial II according to Enneking's classification *(Enneking and Dunham, 1978) (Figure 323)* with radical margins. Most of the compartmental hard and soft tissue was resected whilst preserving as much peripheral tissue stock as possible. T-shaped cylindrical metal bars were implanted (connecting medially the ischium bodies of left and right hip bones to the sacrum) to structurally stabilize the pelvis and hold the left femoral head in place.

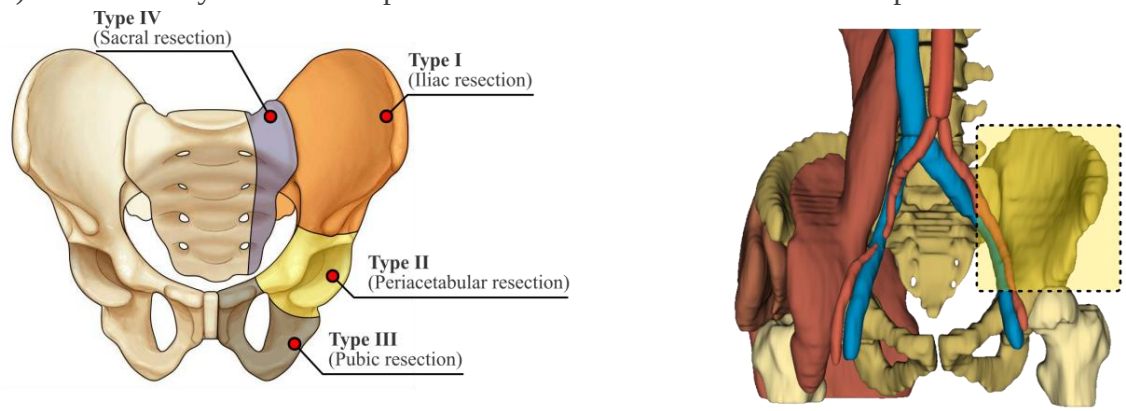

Figure 323: Enneking classification of pelvic tumor resections and planned resection

The patient had to undergo extra neoadjuvant therapy post-resectional whilst ensuring no metastases, and healthy status with the host site being ready to accept the endo-prosthesis. Following the free-hand tumor resection, only after tumor-free margins verification, stable and healthy patient status, as well as the definition of the exact amount of resected tissue and resultant anatomy as per extra imaging means, the development of custom bony substitution could be initiated.

Tumor-free margins were verified by the pathologist and the new arrangement of adjacent soft tissue and the resultant left post-resected hemipelvic bony anatomy was planned to be radiologically assessed. The patient's health status was being monitored (non-metastatic with positive response to neoadjuvant therapy) to verify readiness until the second-stage (reconstruction) time was reached.

Regarding the inter-epistemic custom product development methodology (*Figure 264*), it is apparent that Stages 1 to 5 were applied to diagnose and free-hand resect the tumor, but the process

[138] En bloc resection refers to removal of tumoral mass in its entirety (in one piece), surrounded by a continuous layer of healthy tissue.

had to return to Stage 2 as additional imaging was required to visualize the post-resected anatomy in 3D, thus engaging the PoC 3D Unit to visualize the resultant 3D anatomy and then to develop (design and 3DP) the tailored osseous substitution endo-prosthetic implant conforming to the rehabilitation strategy and notes set as initial reference by the surgeon on *SkeletoMy* platform.

6.4.2 Post-resection Medical Imaging

The post-resected pelvic anatomy was CT-scanned with the same equipment as before with the settings outlined on the CT-scan protocol *(see Section 5)*, and delivered by the surgeon to the PoC 3D Unit via the *SkeletoMy* platform after anonymization *(see Section 5)*.

6.4.3 Post-resection Image Data Processing

The received post-tumor resection anonymized DICOM data was processed within the PoC 3D Unit to reconstruct the digital 3D anatomical model. Presti et al. *(2015)* and Haak, Page, and Deserno *(2016)* have reviewed and compared the most widely used many DICOM viewers and processors. Although *Materialise Mimics* has become the industry's standard software, the equally powerful *3D Slicer (Fedorov et al., 2012) version 5.2.2* software was selected for all cases studied in this Thesis. illustrates its graphical user interface after loading the patient's post-resectional image data set and applying the default volume rendering of bony tissue. However, an actual 3D surface model had to be generated instead of the rendered volume, not only for viewing with little processing power requirements but also to export it for further processing and manipulation.

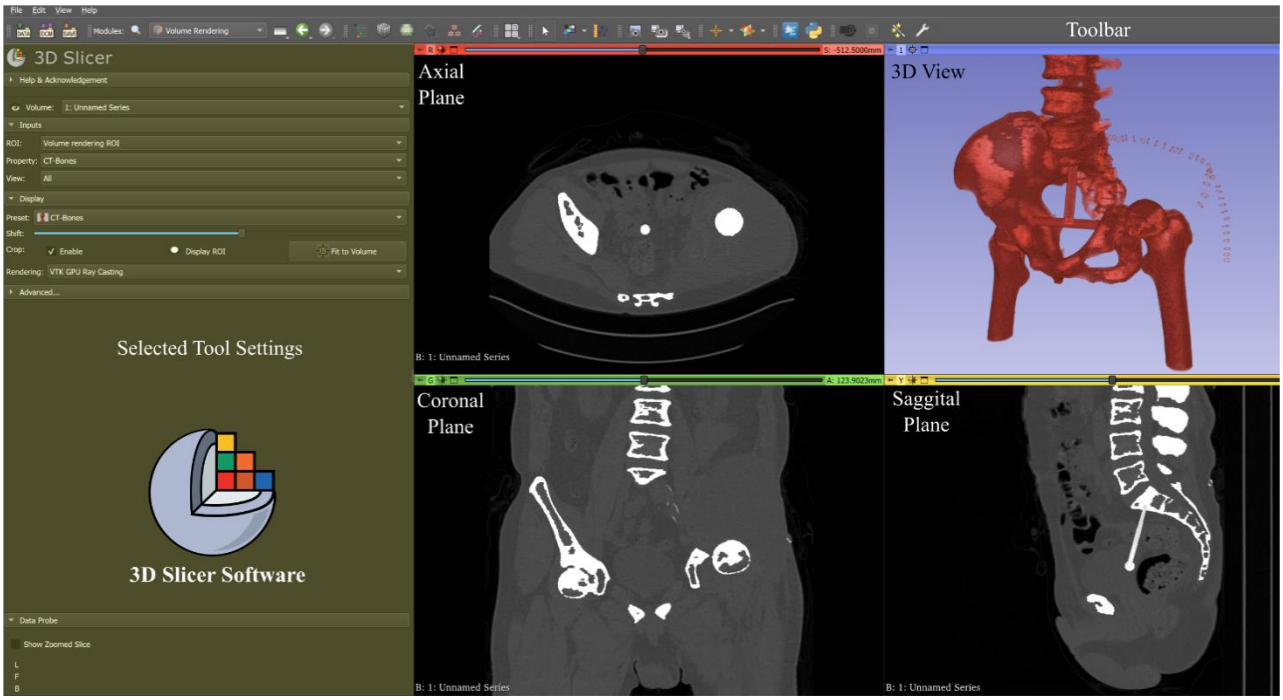

Figure 324: 3D Slicer graphical user interface

Two approaches were implemented and assessed for the anatomical structure segmentation[139]:

[139] Segmentation is a process used to reconstruct 3D forms where pixels (2D) are selected from the scanned slices along the axial, coronal, and saggital planes to create voxels (3D"pixels") that compose the final 3D form.

1. **Automatic soft and hard tissue segmentation:** the *Total Segmentator*[140] AI tool *(Wasserthal et al., 2023)* based on the self-configuring *nnU-Net*[141] *(Isensee et al., 2021)* method which is a deep learning biomedical image segmentation was used *(Figure 325)* to auto-segment soft and hard anatomical structures that are recognizable from trained data. *Figure 326* shows the 3D generated models within 3D Slicer (170 MB .stl file size). Although fast (approx. 3 minutes) and acceptable for visualization, to obtain the finest bony structures that are required for the endo-prosthesis and PSI fit, manual interventions were adopted as described in the next approach.

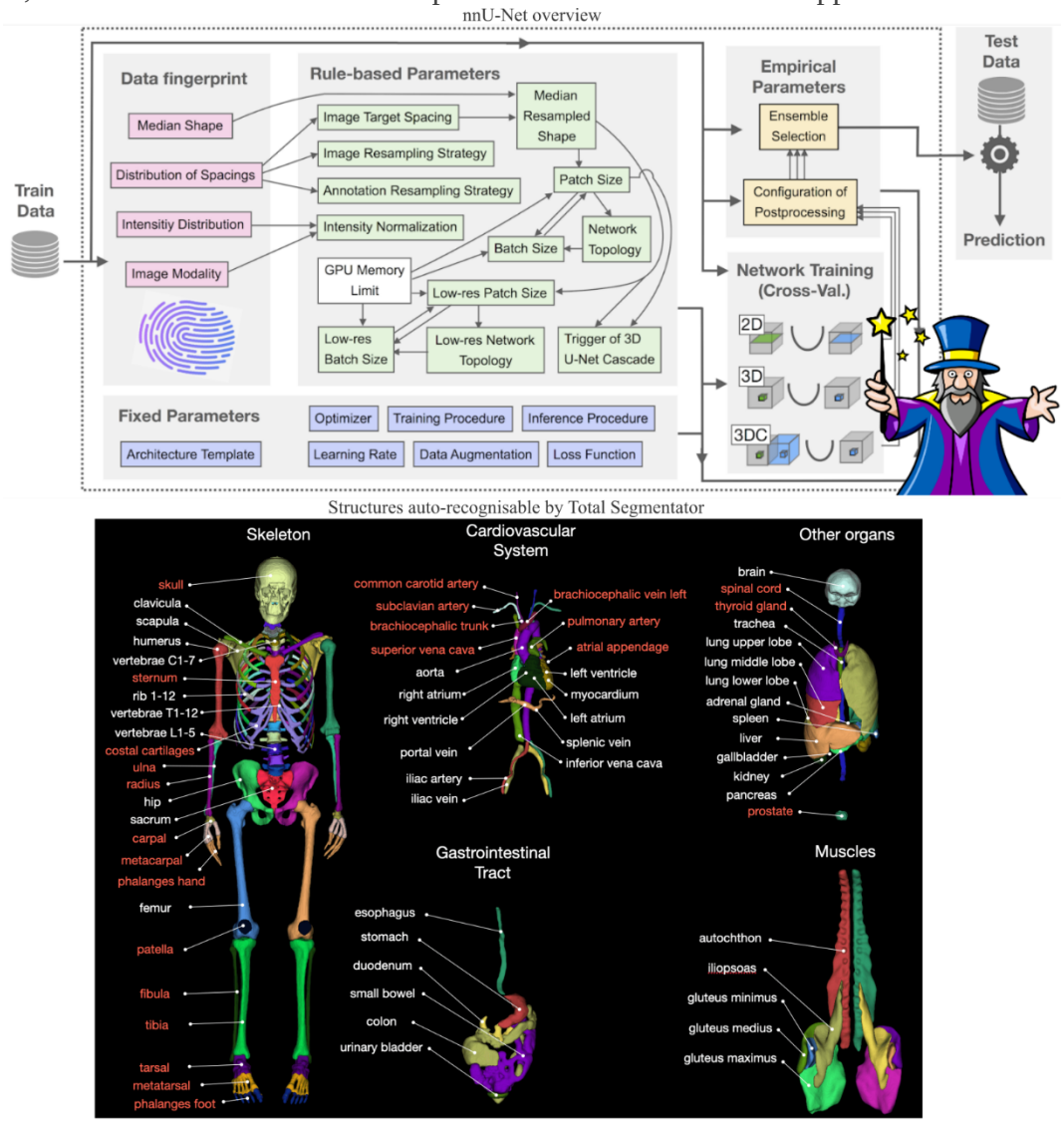

Figure 325: nnU-Net pipeline and structures recognized by Total Segmentator. Source: (Isensee et al., 2021; Wasserthal et al., 2023)

[140] The Total Segmentator tool is developed by the Department of Research and Analysis at University Hospital Basel. It is trained on a wide range of different CT images and can be manually trained further. The code is available at https://github.com/wasserth/TotalSegmentator. More info at https://totalsegmentator.com/.

[141] nnU-Net is a semantic segmentation method that automatically adapts to a given dataset. It analyzes the provided training cases and automatically configures a matching U-Net-based segmentation pipeline. It is developed by the Applied Computer Vision Lab (ACVL) of Helmholtz Imaging and the Division of Medical Image Computing at the German Cancer Research Center (DKFZ). The code is available at https://github.com/MIC-DKFZ/nnUNet.

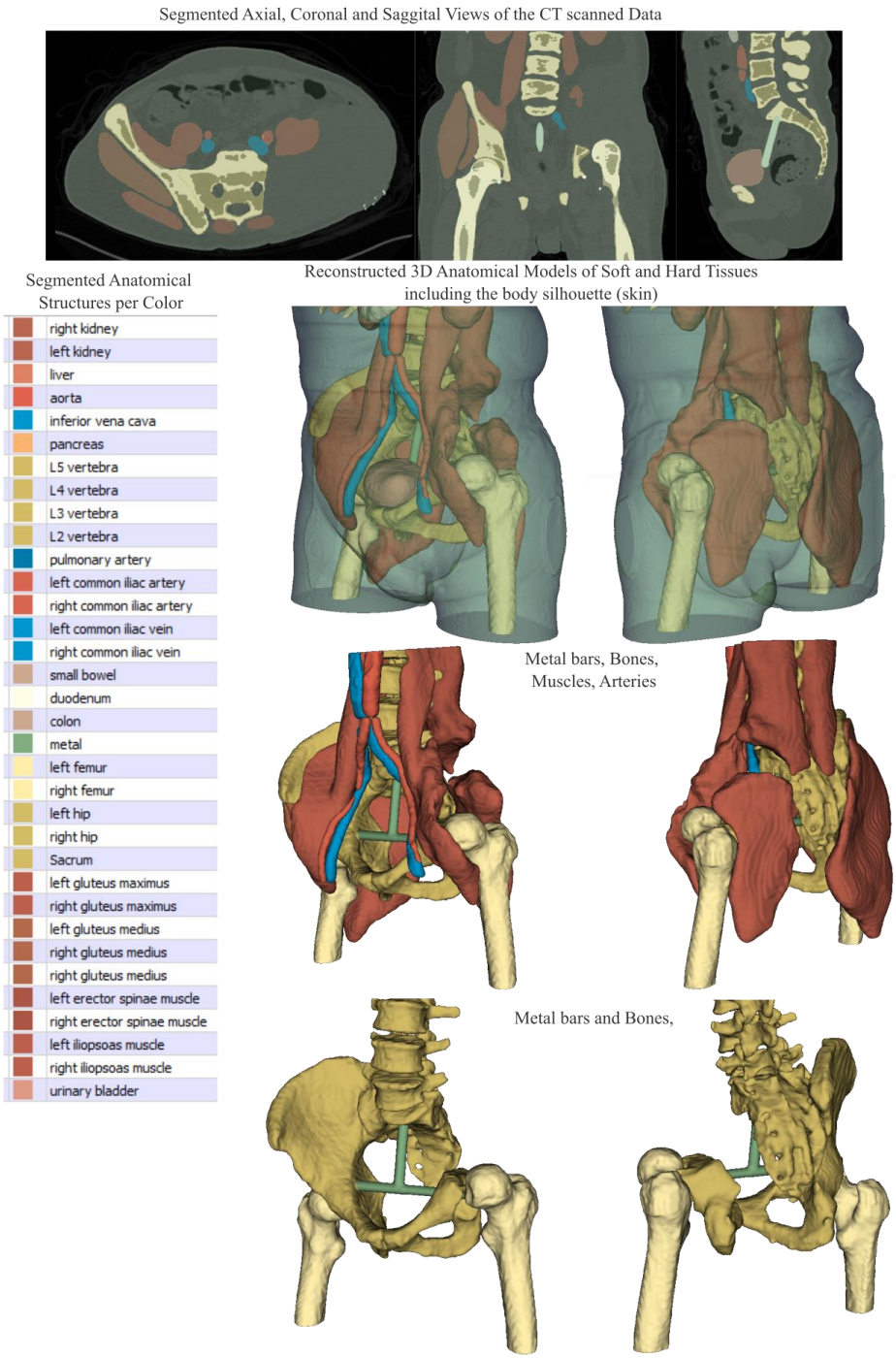

Figure 326: 3D digital post-resection anatomical pelvic model generation

2. **Semi-automatic and manual segmentation:** to obtain a clear and smooth surface mesh model, segmentation tools were used to capture the high-intensity hard tissue areas and filter out soft tissue and noise. The intensity threshold range tool was set to 300-3000 Housfield Units[142] (HU)

[142] The Hounsfield unit (HU) was named after Sir Godfrey Hounsfield (Nobel Prize in 1979, for his part in the invention of CT). It is a relative quantitative dimensionless measurement unit of radio density to interpret CT images. HU are obtained from a linear transformation of the measured absorption/attenuation coefficient of X-ray radiation within a tissue to produce a grayscale image. This transformation is based on the arbitrarily assigned densities of air (-1000 HU) and pure water (0 HU). The upper limits can reach up to 1000 for bones, 2000 for dense bones, and more than 3000 for metals. The denser the tissue, the brighter it appears, and vice versa. That is the reason why CT images are 12-bit; to store values between −1024 to 3071.

(Figure 327) for automatic bone tissue and metals selection. Then, noise and unnecessary regions were automatically removed using the *islands* tools by choosing to keep the biggest island. A surface facet (mesh) model was generated from the corresponding selected areas in all slices of axial, sagittal, and coronal planes *(Figure 328)*. The total elapsed time starting from importing the DICOM data to generate and export (model maker tool) the initial tessellated surface 3D model in .stl file format was only 4 minutes, and the exported file size measured 96 MB.

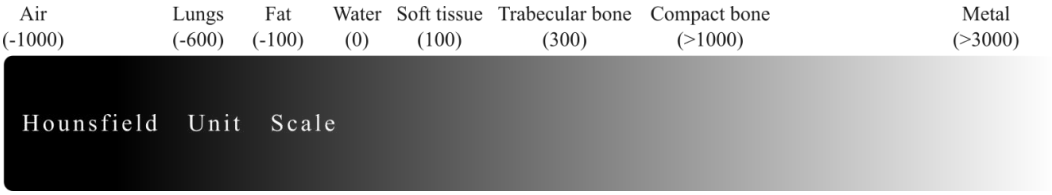

Figure 327: The Hounsfield unit scale

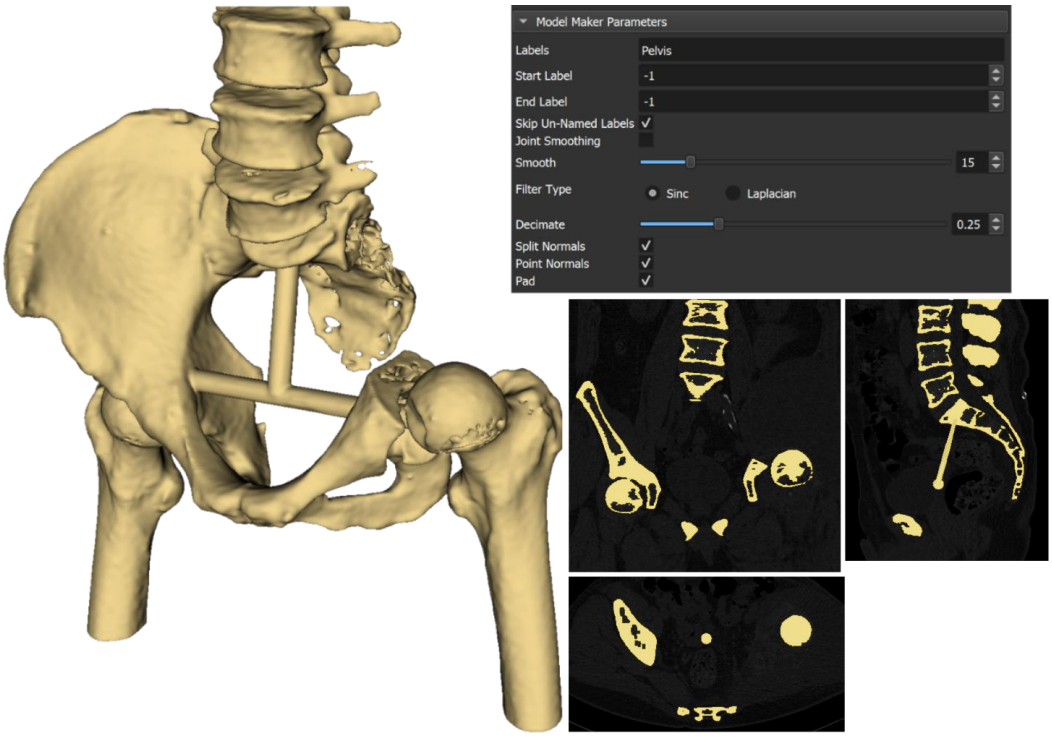

Figure 328: As-generated surface mesh model of the post-resected pelvis and export settings

It is worth mentioning that bones have a spongy endo-structure composed of trabeculae where red and yellow marrow are stored. Often, these porous structures lack adequate intensity and cannot be distinguished from soft tissue, thus leaving empty spaces within the generated 3D models. To accelerate the 3DP of the anatomical model, implant design, and mechanical simulations, all (micro)spaces and openings were closed in all slices of all planes *(Figure 329)* to obtain solid bones with error-free and smaller .stl file size as only the external surface is tessellated. At the same time, the pelvis was split from the femoral heads, the metal T-bar, and the vertebrae, with each one being segmented into separate layers. Both automatic *(grow from seeds, islands, smoothing (median, close holes, remove protrusions), wrap solidify)* and manual fine selection processes followed with *scissors*, *level tracing*, *paint*, and *eraser* tools. *Figure 330*

shows the complete post-resected 3D digital pelvic model in grey color, the femoral heads in yellow color, the vertebrae in red color, and the T-shaped metal bars in blue color, totaling 62 MB .stl file size. The total elapsed time to solid-fill all regions, split each anatomical segment, and generate the surface mesh models was approximately 170 minutes. Although the left hemipelvis is the region of interest, the whole 248x231x168 mm pelvis was isolated and exported for better visualization *(Figure 331)*. The exported .stl file size measured 33 MB.

Figure 329: Comparison of as-CT-scanned and solid-filled regions of the same slice

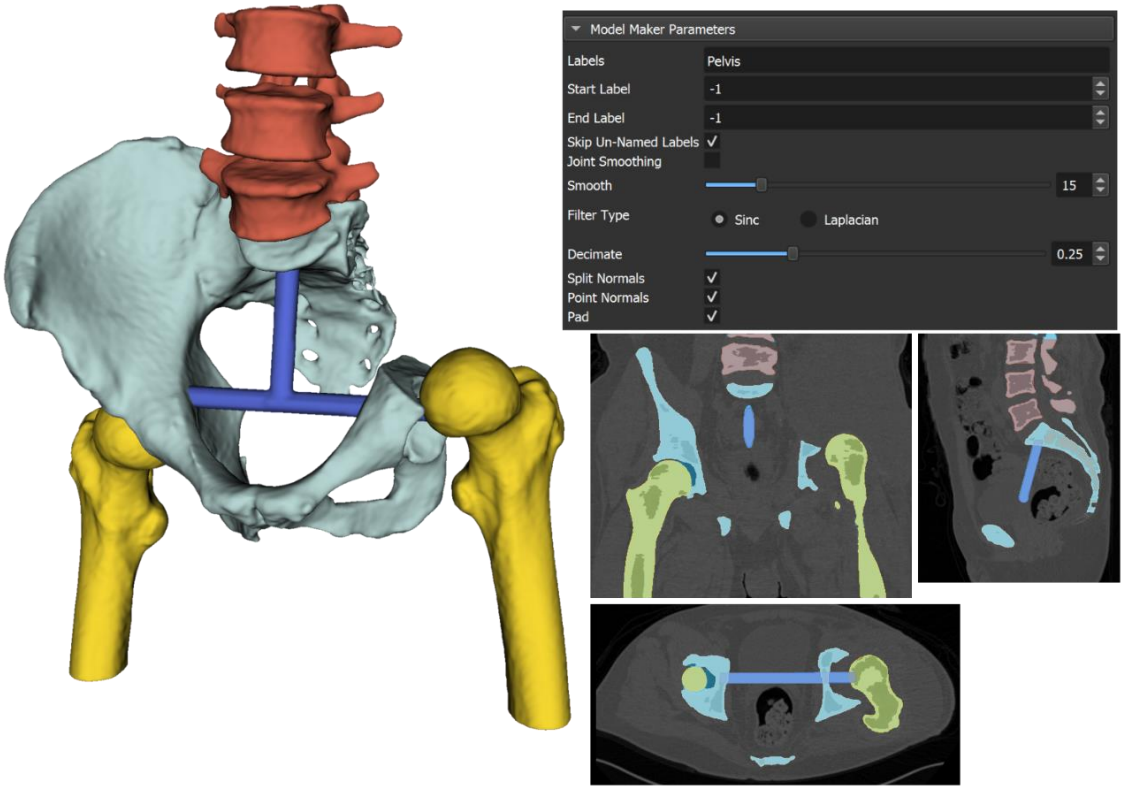

Figure 330: Solid-filled post-resected surface mesh models and export settings

Figure 333 shows the settings for remeshing and simplification used in the most well-known software for mesh processing: *Meshlab (Cignoni et al., 2008)* and *Meshmixer* (Autodesk Inc., California, US). For easy manipulation and lightweightness, the exported surface mesh model was simplified in Meshlab software *(Figure 332)* in under 1 minute and exported into a 20 MB .stl file size with 208.524 vertices and 417.120 triangles from initially 347.564 vertices and 695.200 triangles. Further processing of the simplified surface mesh model was conducted later, during the endo-prosthesis design stages.

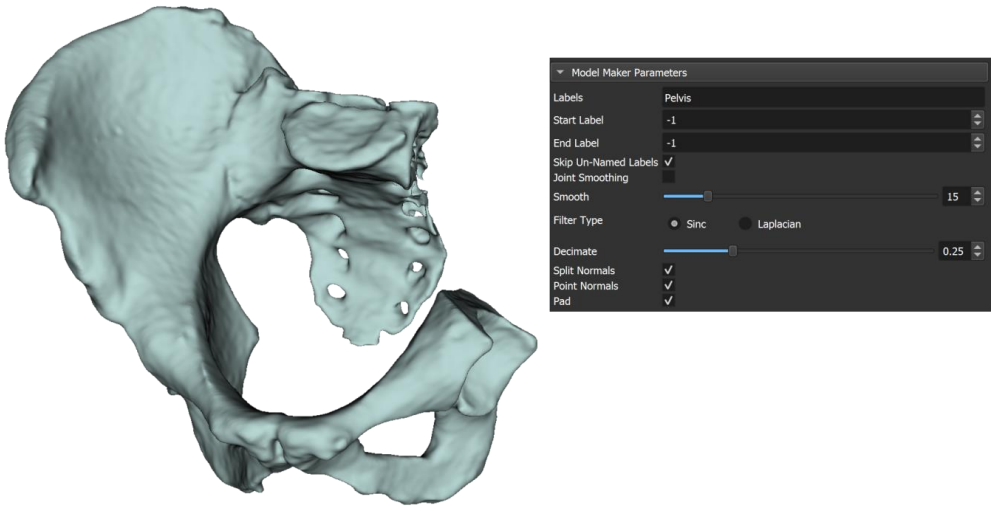

Figure 331: Isolated solid-filled surface mesh model of post-resected pelvis and export settings

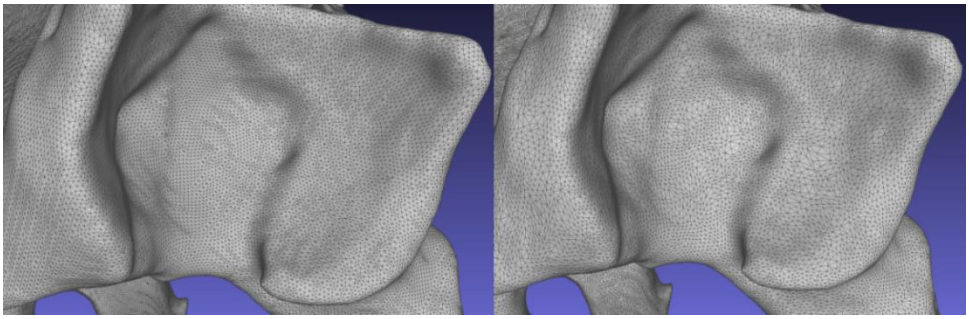

Figure 332: Initial (left) and simplified (right) mesh in Meshlab software

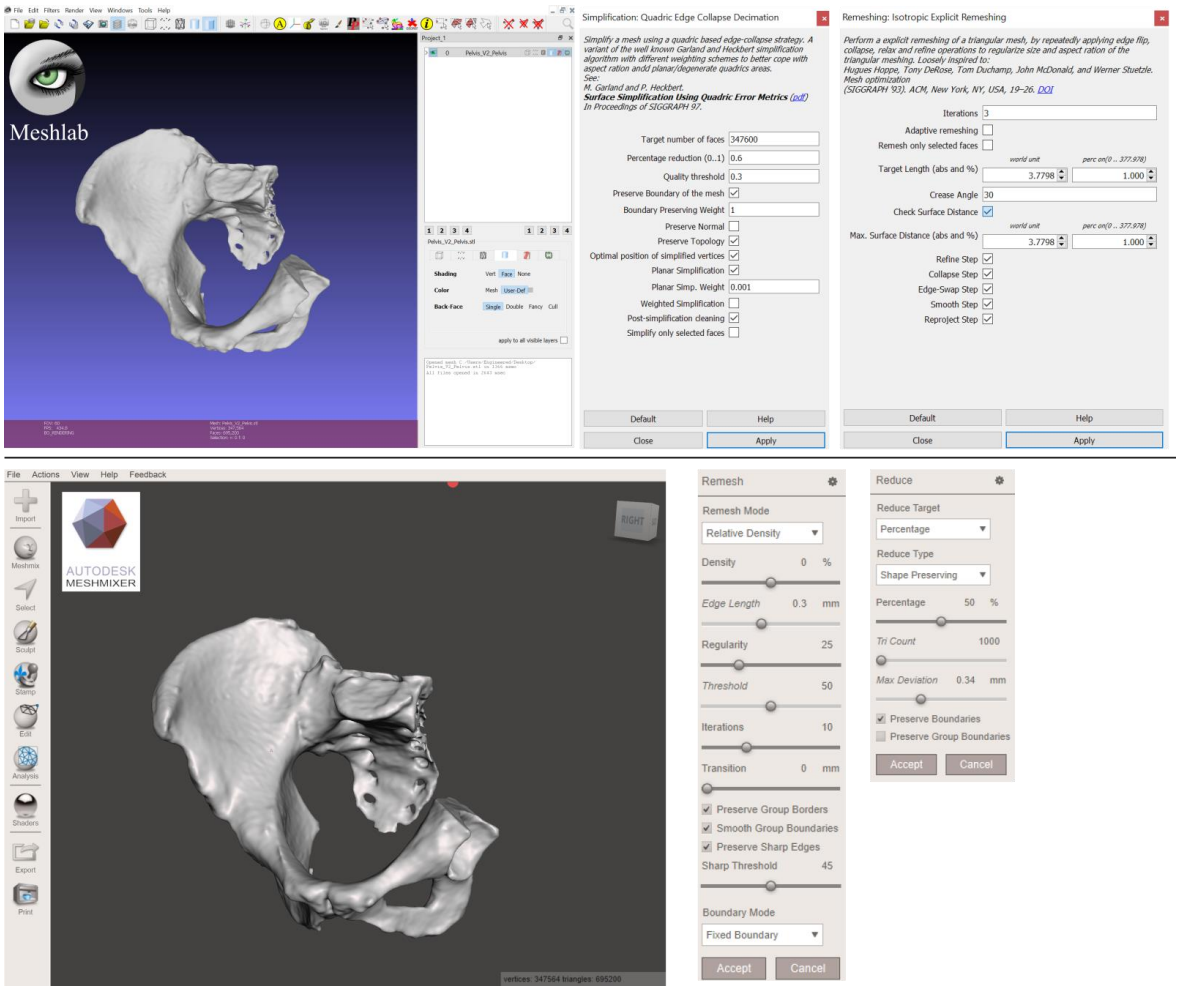

Figure 333: Remeshing and simplification settings in Meshmixer and Meshlab software

6.4.4 (In)Tangible Anatomy Visualization

The patient's post-resected pelvic anatomy (resected left ilium and part of the sacrum) was visualized both digitally, virtually, and physically. More specifically, the following were prepared by the (bio)mechanical design engineer (PoC 3D Unit) to be experienced by the orthopaedic surgeon at the PoC 3D Unit or his office as these were also delivered via the *SkeletoMy* platform:

1. **Digital visualization:**
   - **1.1. Static views:** photorealistic snapshots of the surface mesh model *(Figure 334)* were generated and delivered to the orthopaedic surgeon via the *SkeletoMy* platform for a quick clear initial assessment. Although rendering engines are available in many (non)free modeling software, *KeyShot* was chosen due to its out-of-the-box readiness, easy and intuitive user interface, and reduced time (1 minute in this case) to export high-end realistic visuals.

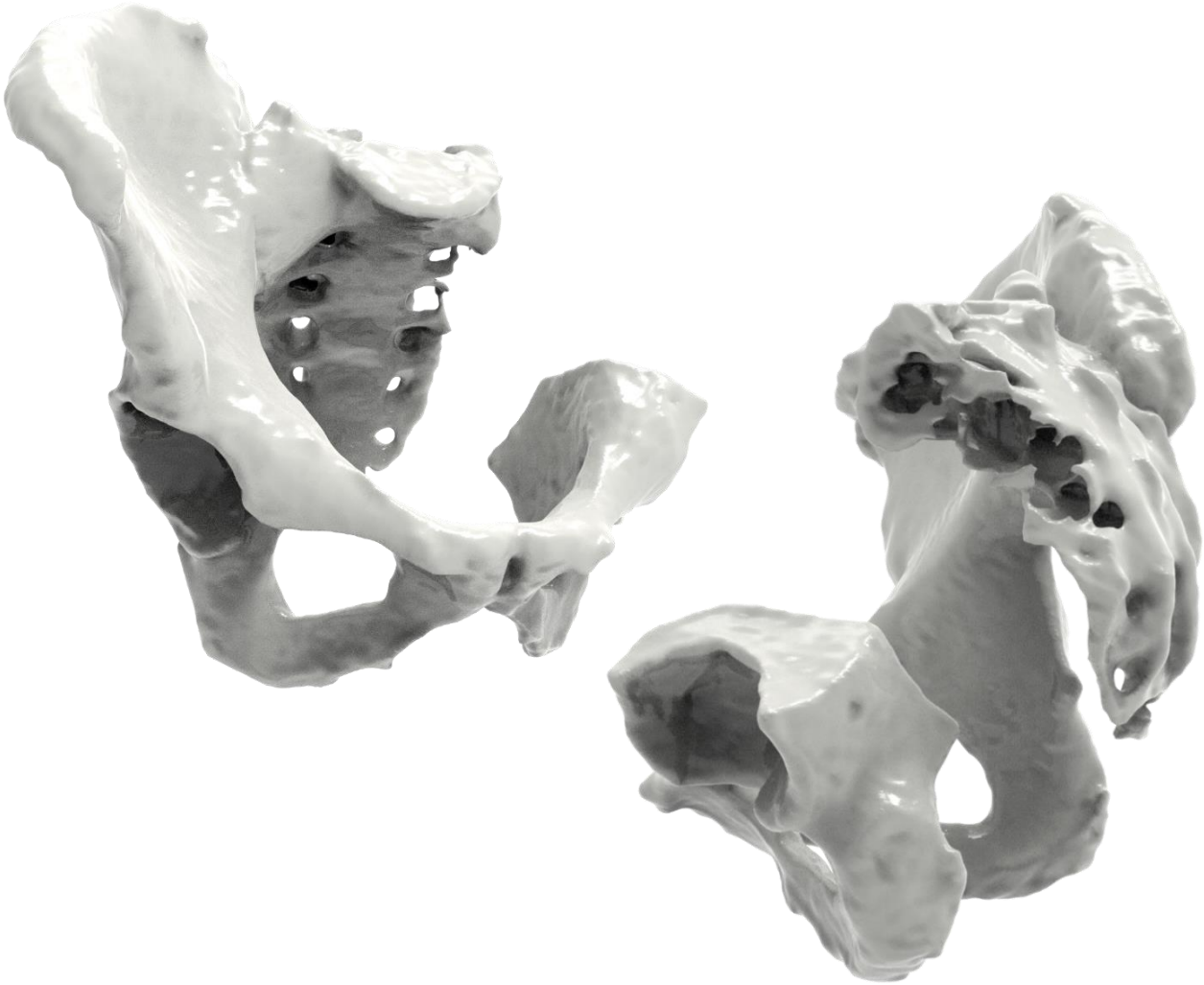

Figure 334: Photorealistic rendered views of post-resected pelvic anatomy

   - **1.2. Dynamic view:** an interactive photo-realistically rendered 3D representation (Keyshot) was uploaded to Sketchfab (Sketchfab Inc., New York, US) online viewer and the link was shared via the *SkeletoMy* platform to be viewed by the surgeon in 3D on any device. Additionally, the surface mesh model per se was also uploaded to *SkeletoMy* platform to be viewed in 3D, and

optionally marked/edited by the surgeon. Alternatively, there are numerous online and offline 3D viewers. The following options were recommended:

1.2.1. For desktop-based devices: any of the online mesh viewers (e.g. online 3D viewer) or simple offline viewers such as the free Microsoft's *3D Viewer* or *3D Builder* for Windows *(Figure 336)*, or the previously presented Meshlab or Meshmixer could have been used. Although not as light, and because such are used later for the endo-prosthesis design phases by the (bio)mechanical design engineer, the free open-source 3D Slicer DICOM processor (presented previously) *(Figure 335)* and *Blender (Figure 337)* modeling software were suggested to be used by the surgeon. In 3D Slicer, the surgeon can load both surface mesh models and the corresponding patient's DICOM data to analyze the anatomy and take measurements and notes, whereas in Blender, the surface mesh model can be viewed and edited using a plethora of tools. The non-free *Rhinoceros* (Robert McNeel & Associates, Washington, US), *Fusion 360* (Autodesk Inc., California, US), *Geomagic Freeform* (Oqton Inc., Ghent, Belgium), and *Spaceclaim* (Ansys Inc., Pennsylvania, US) *(Figure 337)* are some of the many (non-free) modeling software alternatives to Blender that are used by the PoC 3D Unit. The surgeon must be shortly trained to use the aforementioned software for viewing or basic marking and editing, and even fundamental modeling if desired.

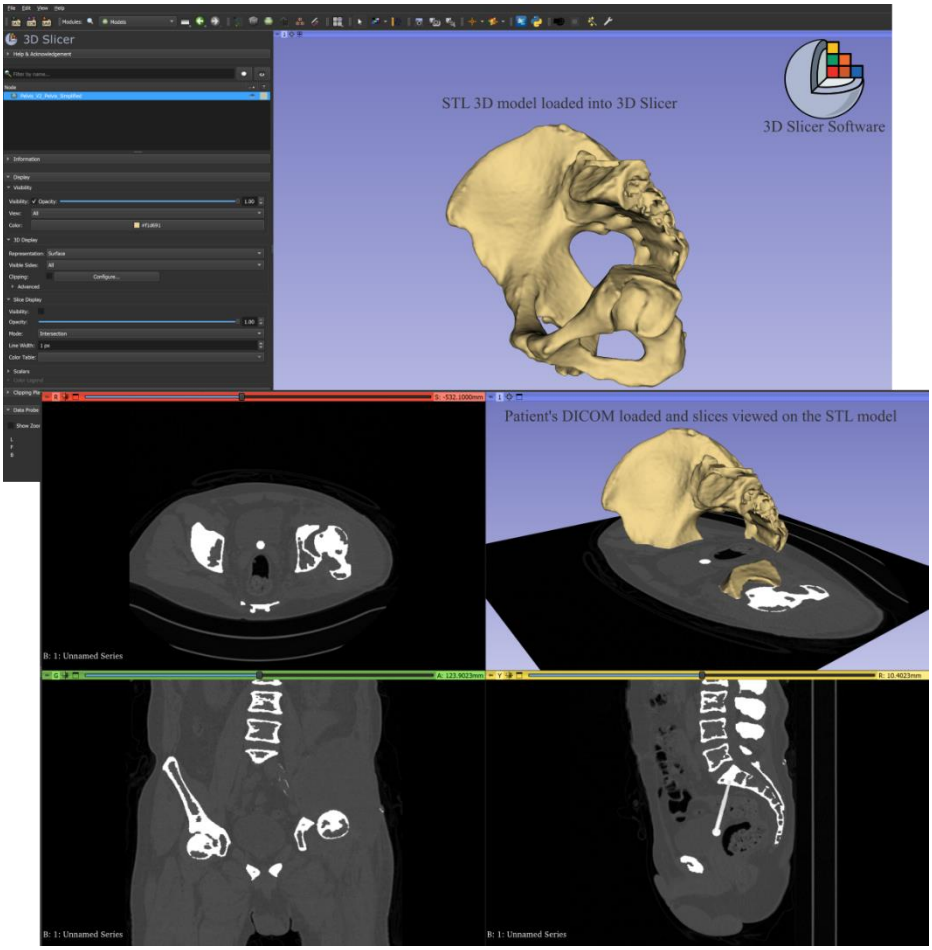

Figure 335: Post-resected mesh model and DICOM data loaded in 3D Slicer

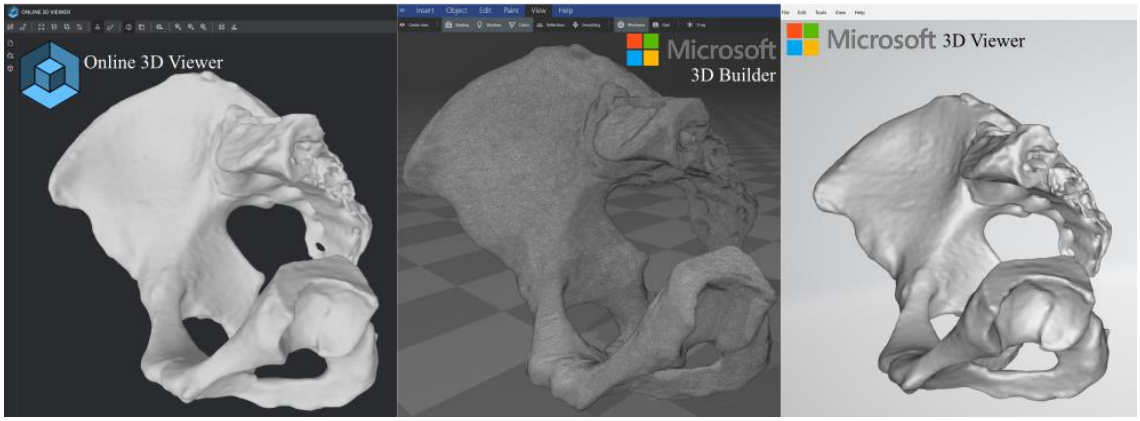

Figure 336: Online and offline 3D surface mesh viewers

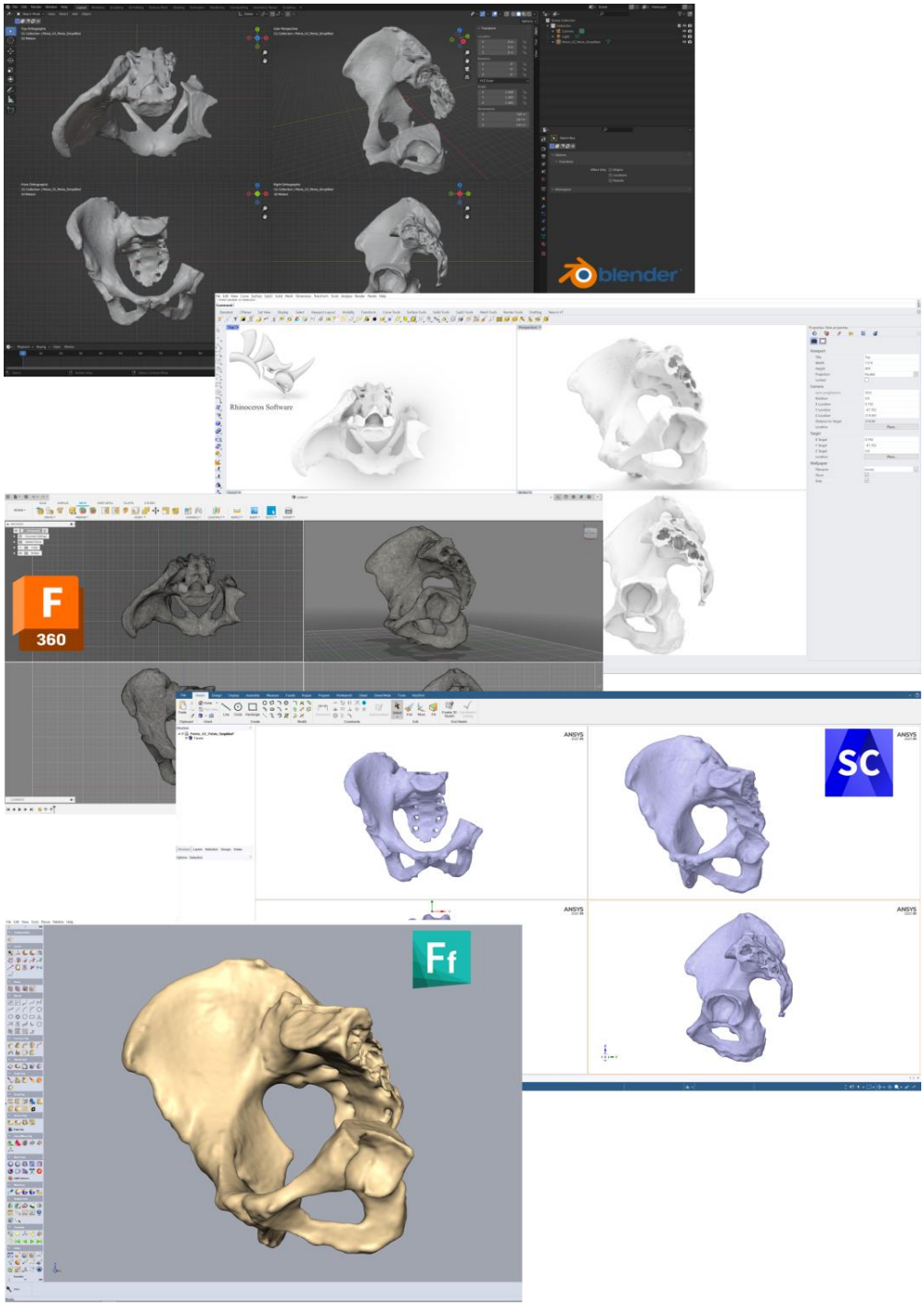

Figure 337: Blender, Rhinoceros, Fusion 360, Spaceclaim, Freeform interfaces

1.2.2. Smart mobile devices: the free STL *Simple Viewer* (developed by Victor Bovio), Fusion 360 for iOS-based and the free *Fast STL Viewer*, Fusion 360, *Exocad* (Exocad Gmbh, Darmstadt, Germany) applications for Android-based devices were suggested *(Figure 338)* for viewing the surface mesh model locally on mobile devices.

Figure 338: Post-resected pelvic mesh loaded into some viewers of mobile-based devices

2. **Virtual visualization:** the 3D anatomical model was prepared to be (semi)immersively viewed by the orthopaedic surgeon in xR, i.e.:

2.1. Virtual Reality (VR): of the numerous VR headsets available in the market the *Oculus Rift S* was selected due to cost constraints. *Figure 339* compares the Rift S with one of the highest-end VR systems, the *VR-3* (Varjo Technologies Oy, Helsinki, Finland).

Figure 339: The high-end Varjo VR-3 and the Oculus Rift S VR headsets. Source: Varjio and Oculus

A PC with demanding specifications is required to be able to support tethered VR platforms. A Windows 11 64-bit loaded PC was used, equipped with Intel Core i9-12900K 3.2GHz CPU, MSI GeForce RTX 3090 24GB GPU, 64 GB RAM, and 1 TB SSD NVMe storage.

Regarding the software for viewing the 3D anatomy in VR, two approaches were explored:

2.1.1. Using VR software to import the medical image dataset to generate the 3D anatomy in situ: in this approach, the as-CT-scanned slices of axial, coronal, and sagittal planes can be viewed along with the generated 3D volume. This approach, compared to the next one, requires much more processing power as the 3D model is generated and manipulated live simultaneously. *SlicerVirtualReality (Pinter et al., 2020)* plug-in for 3D Slicer (unfortunately did not perform well with Rift S), *Specto* (Diffuse (now Specto Medical), Basel, Switzerland) and the non-free *Medical Imaging xR* (Medicalholodeck AG, Zurich, Switzerland) are such examples. *Figure 340* illustrates the VR environment in Specto and Medicalholodeck software and *Figure 341* shows a photograph of the user immersed in these environments using the Rift S equipment.

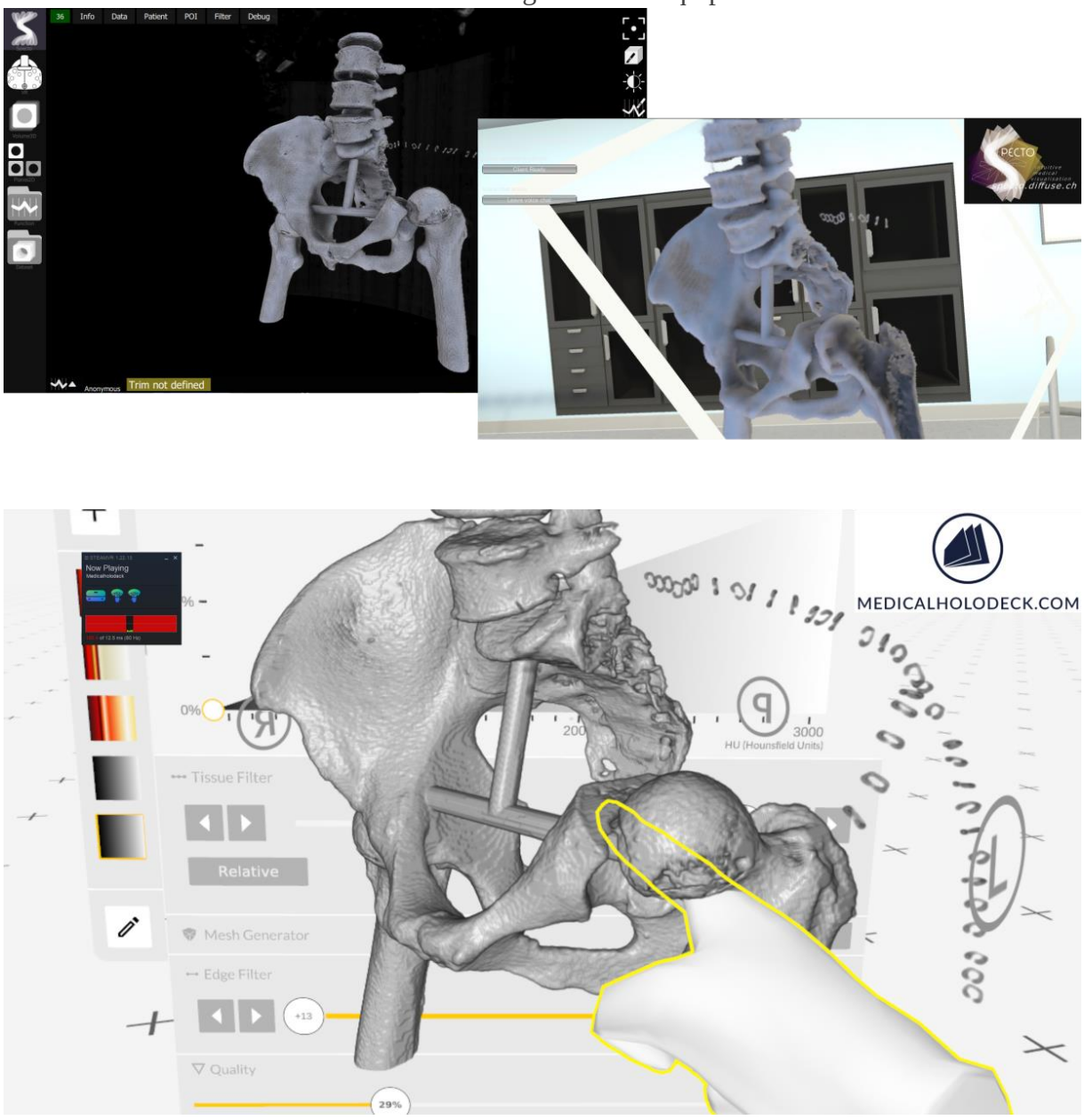

Figure 340: Post-resected pelvis as seen in Specto and Medical Imaging xR environments

Figure 341: User with Rift S equipment immersed in VR environment

2.1.2. Using any software capable of viewing surface mesh models in VR: the required processing power is much less as only the mesh model is imported and viewed, however, the as-CT-scanned medical images might not be available. Fortunately, both 3D Slicer and Medical Imaging xR are capable of both generating and importing mesh models instead of real-time generated volumes. *Figure 342* shows the post-resected 3D mesh model as generated from the medical image data and the as-loaded aforementioned isolated and simplified pelvic model in Medical Imaging xR. Additionally, the interactive rendered model uploaded on *SkeletoMy* (generated by KeyShot and uploaded to Sketchfab) could also be viewed in VR and AR/MR using the Steam VR software.

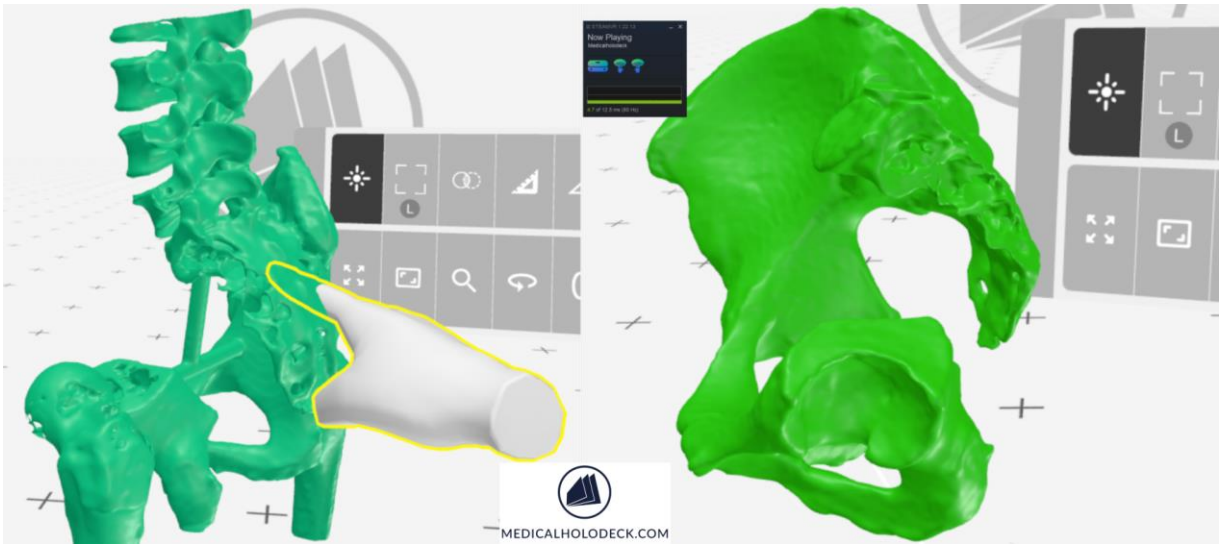

Figure 342: Post-resected mesh model as-generated and as-loaded in Medical Imaging xR

2.2. Augmented/Mixed Reality: due to budget limitations, an *iPad 2021 Pro* was used to augment the post-resected surface mesh model instead of a headset such as the *Hololens 2* (Microsoft, Washington, US) or the *XR-3* (Varjo Technologies Oy, Helsinki, Finland)

(Figure 343). Figure 344 shows the iPad's screen running the non-free *AR Viewer* (Augment Sas, Paris, France), used to load and track in space the 3D surface mesh model, and the non-free *Medical Imaging xR*, used to load the DICOM data and track in space the 3D rendered volumetric model as-generated from the CT-scanned slices.

Figure 343: Microsoft Hololens 2 and Varjo XR-3 MR headsets. Source: Varjo and Microsoft

Figure 344: Post-resected mesh model in AR Viewer and DICOM data in Medical Imaging xR

In xR (e.g. Medical Imaging xR), more than one user can participate and be present in the same environment thus team working with multiple users (interacting with a common model), even remotely, can take place.

3. **Physical visualization:** refers to materialization of the post-resected 3D anatomical model in a 1:1 scale physical replica. The process flow followed is summarized below:

3.1. Although VP, PBF, or MJ 3DP technologies can be used for high-end cosmetic results, a ME-based 3DP technology (Fused Filament Fabrication (FFF)) and Polylactic Acid (PLA) feedstock material (filament) were selected as the most cost-effective combination for fabricating the 248x231x168 mm object in a single monolithic piece with adequate results out of a functional-grade material. Specifically, the entry-level low-cost *Creality CR-10s* 3D printer and *colorFabb*[143] (Colorfabb BV, Belfeld, Netherlands) ivory color PLA/PHA filament were used *(Figure 345)*.

Type: Fused filament fabrication (Material extrusion)
Printable object dimensions: 300 x 300 x 400 mm
Default nozzle diameter: 0.4 mm
Default filament diameter: 1.75 mm
Z axis print resolution: 100 µm
Positioning accuracy: ± 0.1 mm
Build platform: heated bed with glass
Max heatbed temperature: 100 °C
Max nozzle temperature: 260 °C
Max print speed: 180 mm/s
Max power consumption: 350 W
Interface: LCD screen and knob
Print mode: SD card
Overall dimensions: 550 x 490 x 650 mm
Machine weight: 14 Kg
Power: 220V @ 50 Hz

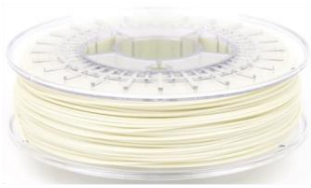

colorFabb

TYPICAL MATERIAL PROPERTIES			
Physical properties	**Unit**	**Value**	**Method**
Density	g/cm3	1,24	ISO 1183
Modulus of elasticity	MPa	2960	ISO 527
Tensile strength	MPa	61,5	ISO 527
Tensile strain at tensile strength	%	5,3	ISO 527
Tensile stress at break	MPa	38	ISO 527
Tensile strain at break	%	10,5	ISO 527
Flexural modulus	MPa	3295	ISO 178
Flexural strain at break	%	NB	ISO 178
Flexural stress at 3.5% strain	MPa	88,8	ISO 178
Notched impact strength (Charpy), RT	kJ/m²	2,8	ISO 179-1/1 eA
Impact strength (Charpy), RT	kJ/m²	30,8	ISO 179-1/1 eU
Melting temperature	ºC	>155	ISO 3146-C

FILAMENT SPECIFICATION		
Nominal diameter:	**Diameter tolerance**	**Ovality**
1,75 mm	± 0,05	≥ 95%

Figure 345: Creality CR-10s 3D printer and ColorFabb PLA/PHA filament properties. Source: Creality and Colorfabb

3.2. The surface mesh model was imported into a process planning software to select the fabrication parameters, slice the model, and generate the machine-specific code (G-code). Of the numerous such software, the free universal open-source *PrusaSlicer* 2.4.2 was selected. *Figure 346* shows the surface mesh model loaded into PrusaSlicer, its orientation, the most important settings chosen, the 3D extrusion paths of the structural and support materials, and the report of material consumption and required build time per operation. The model was optimally oriented for the best adhesion to the build platform and minimum support structure requirements. The total material consumed was 663 gr and the total 3DP

[143] ColorFabb is a polymer filament manufacturer aiming at Fused Filament Fabrication (material extrusion) based 3D printers. More information at https://colorfabb.com/.

time was 3 days and 13 hours. Given that each Kg of filament spool costs approximately 35 €, the material consumed cost 23,2 €.

3.3. The G-code file generated by PrusaSlicer was loaded into an SD card and fed into the CR-10s control box's slot. First, it was verified that the build platform was level by running the semi-automatic bed leveling algorithm: calibrating the nozzle-to-platform clearance using a 0,05 mm thick feeler by adjusting the thumb nuts at the bottom of the platform's four corners. Then, the 3D printer was prepared: a) by applying a layer of solvent-free UHU stick glue on the cleaned glass surface of the heated platform to ensure strong adhesion and avoid possible warping issues due to temperature gradients, b) an adequate amount of PLA/PHA filament (1.000 gr filament spool) was placed on the spool holder and the filament was inserted into the extruder that guides it to the heated nozzle. The preparation took 15 minutes.

Mesh model as-imported into Prusa Slicer

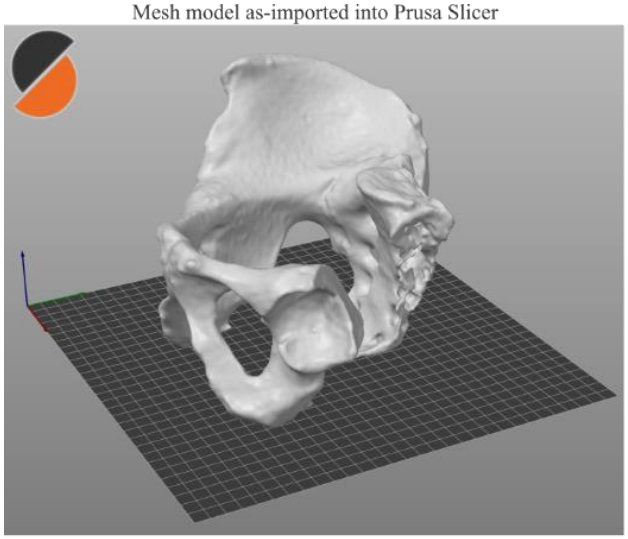

Structural and support material extrusion paths shown in 3D

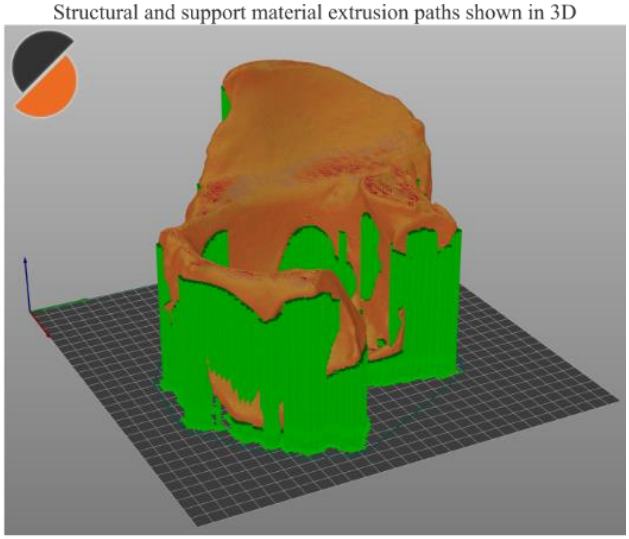

Report

Feature type	Time	Percentage	Used filament	
Perimeter	1h59m	2.3%	15.62 m	46.60 g
External perimeter	5h29m	6.5%	15.45 m	46.10 g
Overhang perimeter	9m	0.2%	0.63 m	1.87 g
Internal infill	11h9m	13.1%	63.42 m	189.15 g
Solid infill	7h4m	8.3%	13.40 m	39.97 g
Top solid infill	1h35m	1.9%	3.80 m	11.34 g
Bridge infill	49m	1.0%	2.61 m	7.78 g
Gap fill	2m	0.0%	0.01 m	0.02 g
Skirt/Brim	1m	0.0%	0.09 m	0.27 g
Support material	2d1h35m	58.4%	99.01 m	295.31 g
Support material interface	6h53m	8.1%	8.05 m	24.01 g
Custom	48s	0.0%	0.02 m	0.06 g

Estimated printing times:
First layer: 37m
Total: 3d12h52m

3DP major settings:
-Material: 1.75 mm diamater white PLA filament
-Nozzle diameter: 0.4 mm
-Layer height: 0.28 mm
-Perimeters: 2
-Solid layers: 3 top and 3 bottom
-Infill: 20% grid
-Speed: 20 mm/s solid infill/external perimeters/first layer,
60 mm/s perimeters/supports, 80 mm/s infill, 100 mm/s travel
-Skirt and Brim: Yes
-Temperature: nozzle @ 210 °C, heatbed @ 60 °C
-Supports: Yes
-Supports threshold: 45°
-Supports geometry: grid with 2 mm pattern spacing

Figure 346: Report, settings, and 3D paths for the post-resected model in Prusa Slicer

3.4. Once the heated platform and the nozzle reached the target temperatures, the layer-by-layer object building commenced. The process finished and the platform was left to cool down to air temperature (25 °C) before the part was carefully removed using a scraper, isolated from the support structures using a blade knife and a small slotted flat blade screwdriver, and cleaned with alcohol. The total post-processing procedure totaled 20 minutes with no extra sanding and filing being necessary. *Figure 347* shows photographs of the end result.

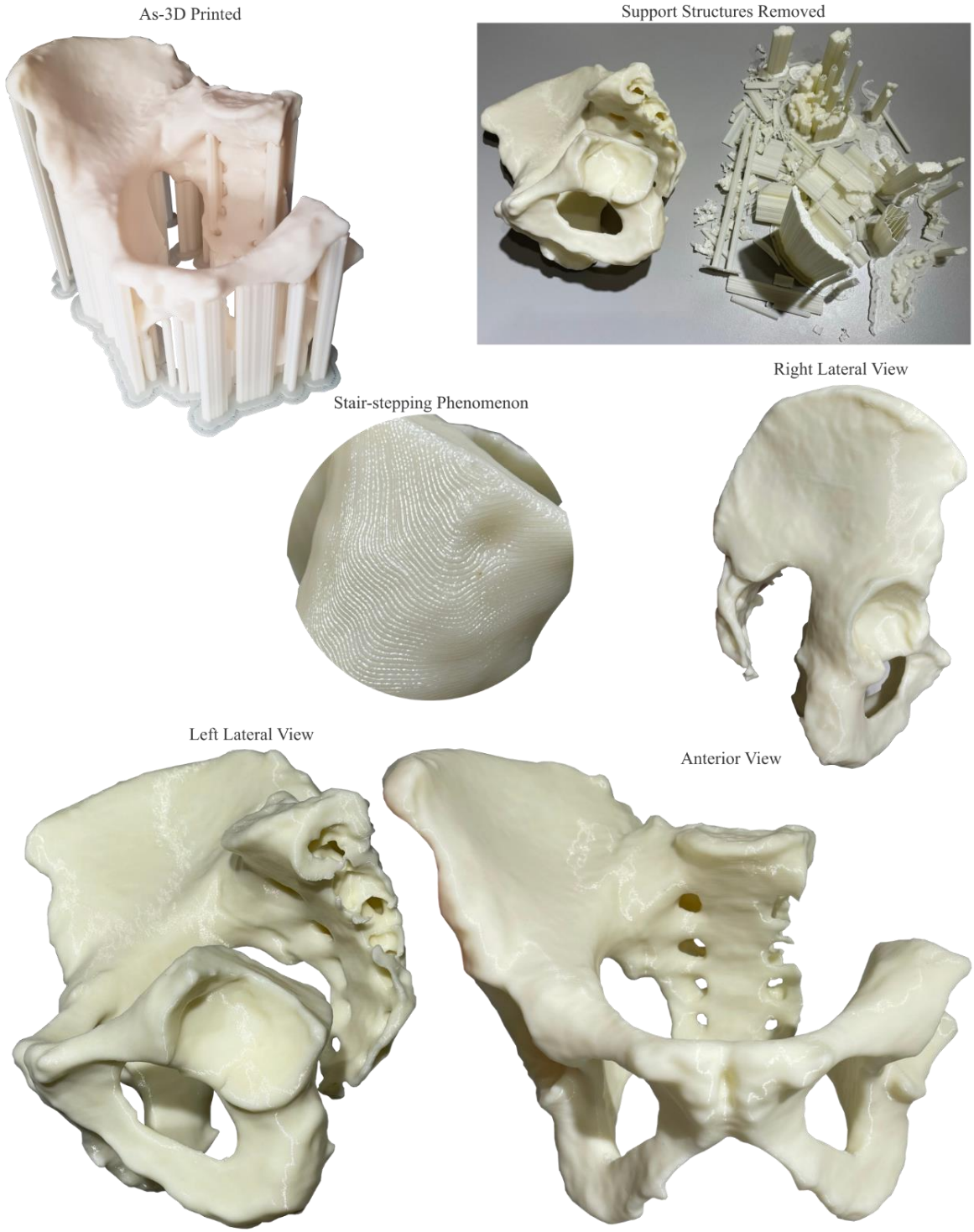

Figure 347: Post-resected 3DPed pelvic model

Although it was obvious that the 3DPed model suffered from the stair-stepping phenomenon due to its laserwire production, the result was more than acceptable per se *(Figure 347)*. Nevertheless, this could have been overcome by reducing the layer thickness (but the total build time would increase) and/or applying post-processing techniques for smoothing the surface by sanding and filing, chemical treatment, and/or spray coatings. For example, *Figure 348* shows the post-resected acetabulum section as-3DPed by the Morpheas 3D printer *(Mavrodontis, 2015) (see Figure 85)* out of ABS filament in blue color, and the obtained injection molded-like look after the treatments.

Dimensional inaccuracies caused by each phase of the process flow (image data acquisition, segmentation, surface mesh model generation (triangulation), fabrication (3DP), post-processing) always exist and impact the end anatomical product. Studies have shown that such errors are clinically acceptable *(Fitzwater et al., 2011; Huotilainen et al., 2014; Ogden et al., 2015)*, though triangulation resolution and segmentation threshold are the most critical factors, with errors concentrating at regions with high curvatures *(Pinto et al., 2015)*. The physical model was compared to the digital one by measuring various pre-defined landmark points using a calibrated digital caliper *(Figure 349)*. Deviations were satisfactorily under 0,3 mm, however, a coordinate measuring machine is needed for detailed analysis of such freeform geometries.

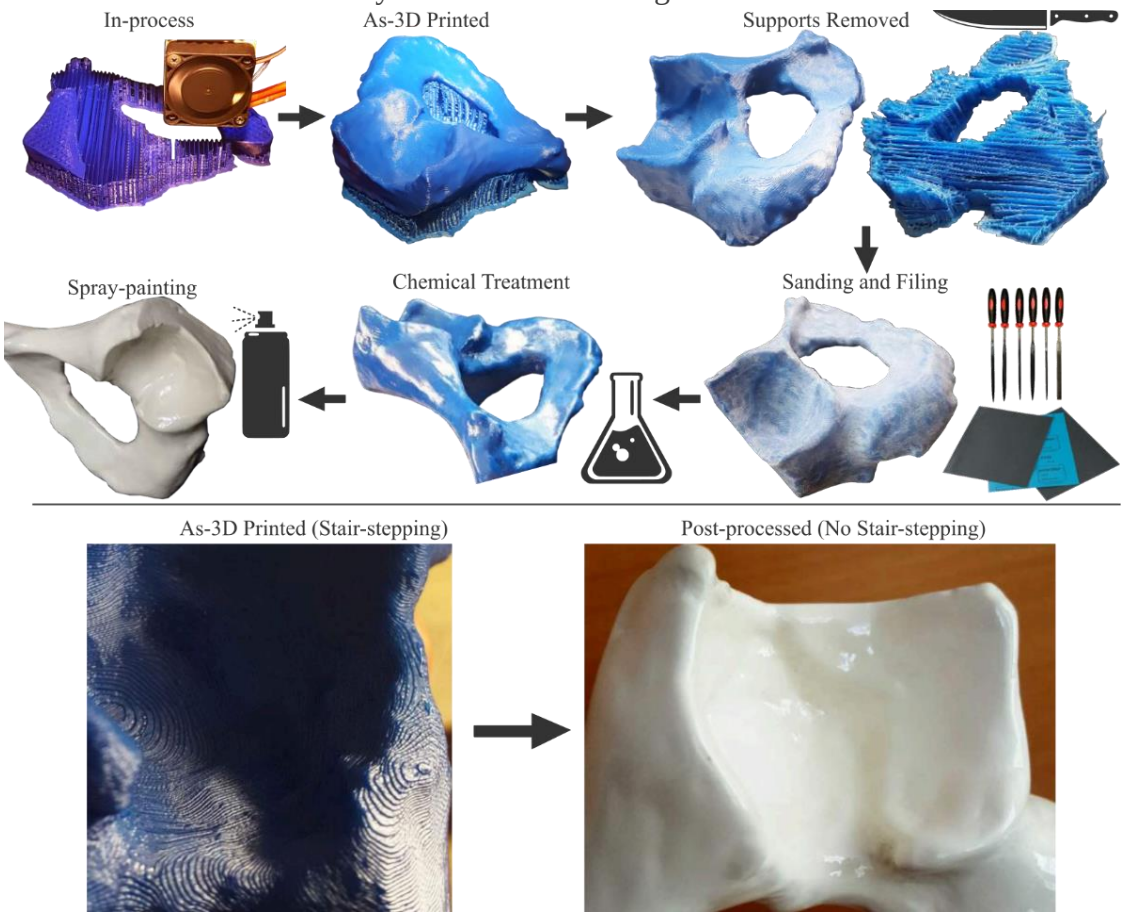

Figure 348: Post-processing example for surface quality enhancement

For 3D printers having smaller build volumes (e.g. max 200x200x200 mm) that are incapable of fabricating larger objects, and at the same time to address the fact that the total required time to print the monolithic pelvic model was considerably high, there are alternative options, e.g. a) 3DP only the tumor affected site and not the whole pelvis, or b) instead of 3DP the model as a monoblock piece, it can be split into sections and assembled. For example, *Figure 351* shows the splitting, 3DP, post-processing, and assembling of the pelvic anatomical model as carried out by Mavrodontis *(2017)*. The sections can be 3DPed either on the same 3D printer's platform by minimizing the support structures, or even simultaneously in multiple 3D printers, thus utilizing the concept of the so-called *3D printing farm*. Of course, such approaches requiring careful assembly will consume

extra effort both for pre- and post-processing, however, comparatively, the total elapsed time will be considerably lower. Although if properly designed and assembled, deviations induced by the assembling process of the parts should be negligible, though must be checked.

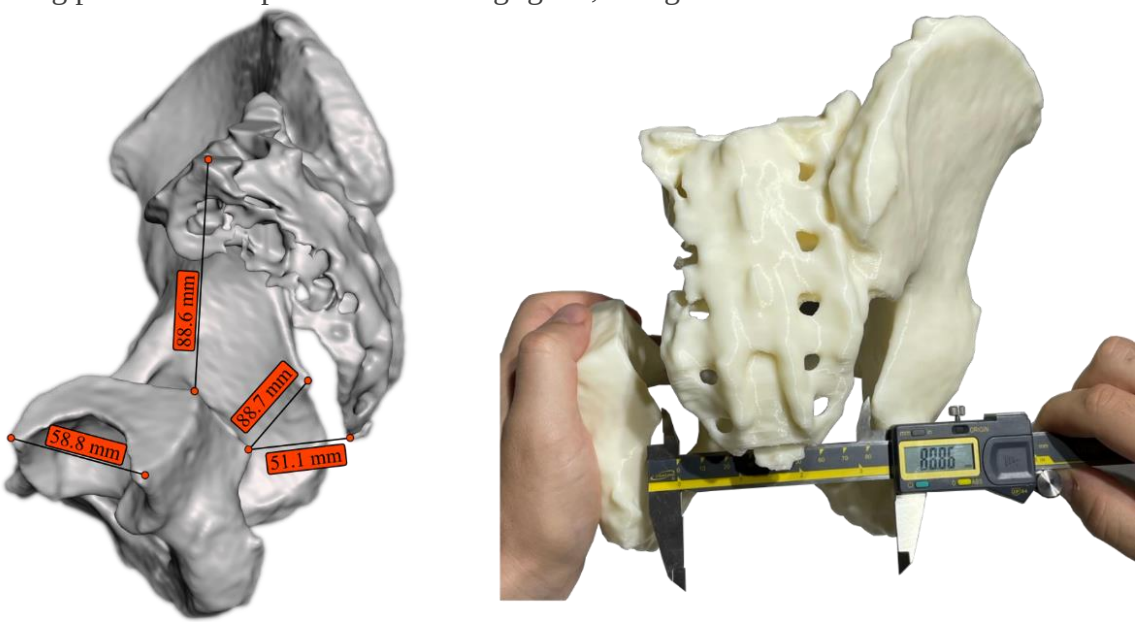

Figure 349: Measurement comparison between the 3DPed and digital post-resected model

Regarding the sectioning of the pelvic surface mesh model:

- In Fusion 360, plane cuts were used to split it into 4 components: sacrum, right ilium, left pubis and ischium, and right pubis and ischium. This anatomical logic of separating the model with 3 plane cuts created 6 flat surfaces to be joined, two of which were not touching the flat build platform which is ideal to guarantee flatness. Hence, another option was proposed with 3 plane cuts and 6 flat surfaces to be joined, with only one surface not touching the build platform. *Figure 352* and *Figure 353* show for both options the exploded sections in solid and *"X-ray"* representations. Instead of integrating pins on each section, it was found better to implement exclusively pin holes (two 5 mm diameter 20 mm long pin holes in each face) and standard off-the-shelf metal pins to facilitate easy and precise position registration, and application of cyanoacrylate-based glue to permanently join the parts just before assembling. Magnets instead of glue, or snap-fits *(Klahn, Singer and Meboldt, 2016)* instead of pins are also interesting alternatives.
- *Figure 354* and *Figure 355* show the total material consumption and required time to 3DP the sections in one, two, and four CR-10 3D printers with exactly the same settings as before *(Figure 345)*. Using four 3D printers the total material consumption dropped from 663 gr to 540 gr (470 gr for the alternative splitting option), and the total print time can be reduced from 3 days and 13 hours to 18 hours (14,5 hours for the alternative splitting option), however, the extra splitting, 3DP process planning, the preparation time of each 3D printer, extra post-processing and assembly time have to be considered and managed efficiently.

The speed settings selected for the Creality CR10s *(Figure 346)* are slow compared to currently available faster low-cost material extrusion 3D printers *(Figure 350)* that could drop the aforementioned 3DP time down four to five times, leading to a total 3DP time of 17 hours for the single monolithic piece, whereas, for the split model approach, the incorporation of more such high-speed 3D printers (print farm) would lead to even more time compression.

Type: Fused filament fabrication (Material extrusion)
Printable object dimensions: 300 x 300 x 400 mm
Default nozzle diameter: 0.4 mm
Default filament diameter: 1.75 mm
Z axis print resolution: 100 μm
Positioning accuracy: ± 0.1 mm
Build platform: heated bed with glass
Max heatbed temperature: 100 °C
Max nozzle temperature: 260 °C
Max print speed: 180 mm/s
Max power consumption: 350 W
Interface: LCD screen and knob
Features: filament sensor
Print mode: SD card
Overall dimensions: 550 x 490 x 650 mm
Machine weight: 14 Kg
Power: 220V @ 50 Hz

VS

Type: Fused filament fabrication (Material extrusion)
Printable object dimensions: 256 x 256 x 256 mm
Default nozzle diameter: 0.4 mm
Default filament diameter: 1.75 mm
Z axis print resolution: 7 μm
Product accuracy: ± 0.1 mm
Build platform: heated bed with flexible steel plate
Max heatbed temperature: 110 °C
Max nozzle temperature: 300 °C
Max print speed: 500 mm/s
Max power consumption: 350 W
Interface: Touchscreen
Features: Lidar-auto bed leveling, filament and door sensors, camera, power loss recovery, activated carbon air filter, vibration compensation, AI-powered live monitoring
Print mode: SD card, cloud-based
Overall dimensions: 389 x 389 x 457 mm
Machine weight: 14 Kg
Power: 220V @ 50 Hz

Figure 350: Creality CR-10s versus the Bambu Lab X1 Carbon 3D printer. Source: Creality and Bambu Lab

It should be noted that depending on geometry and selected 3DP technology, the splitting, and the process planning variables have to be optimized as per the desired parameters, e.g. time compression, minimum support structures, and maximum surface quality. In case of multiple

simultaneous 3DP sessions, the printing order has to be programmed starting from the one taking the longer so that the preparation time and post-processing time for the other sessions are not delayed and do not impact the overall process.

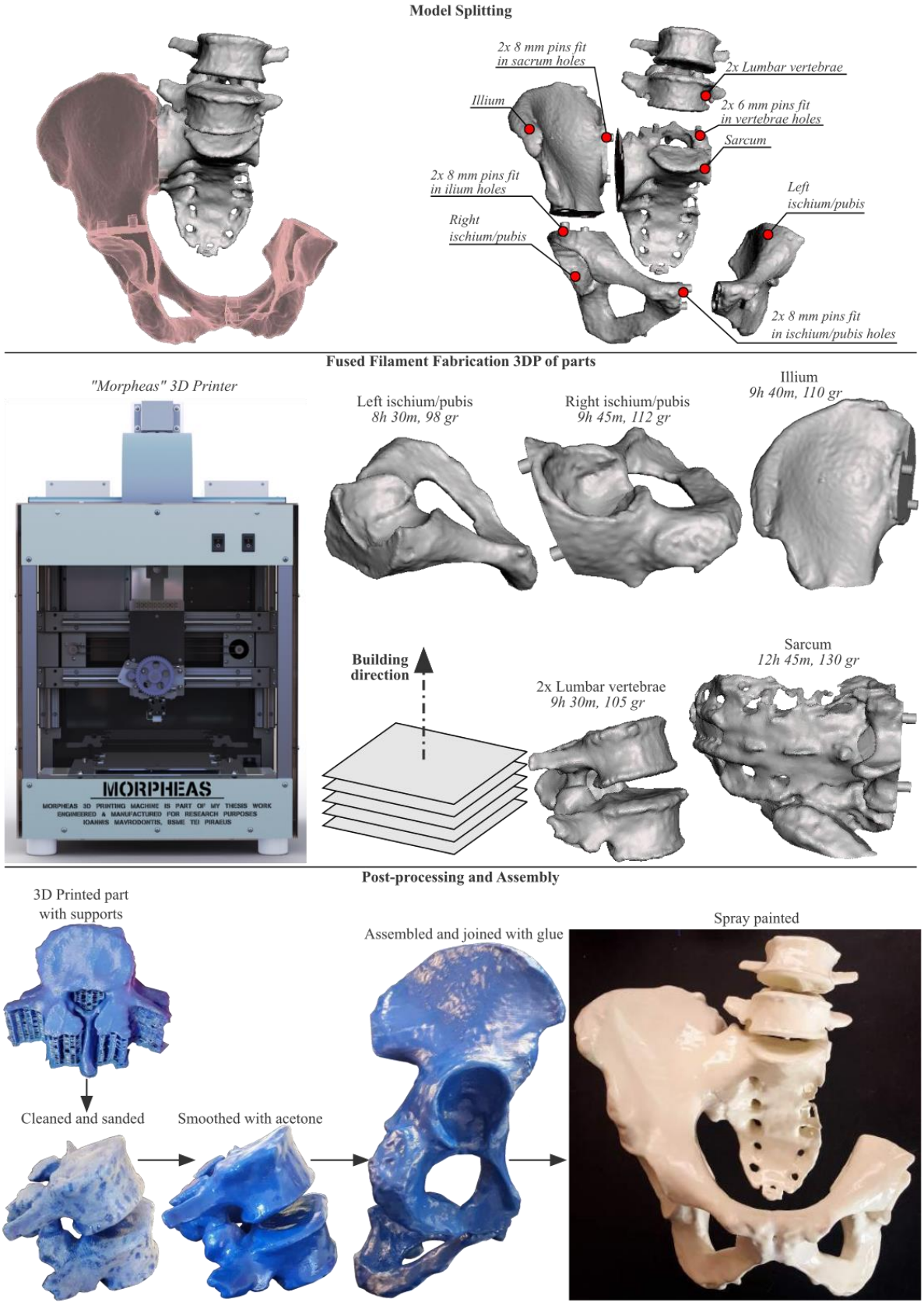

Figure 351: Splitting, 3DP, post-processing and assembling the pelvic model. Source: (Mavrodontis, 2017)

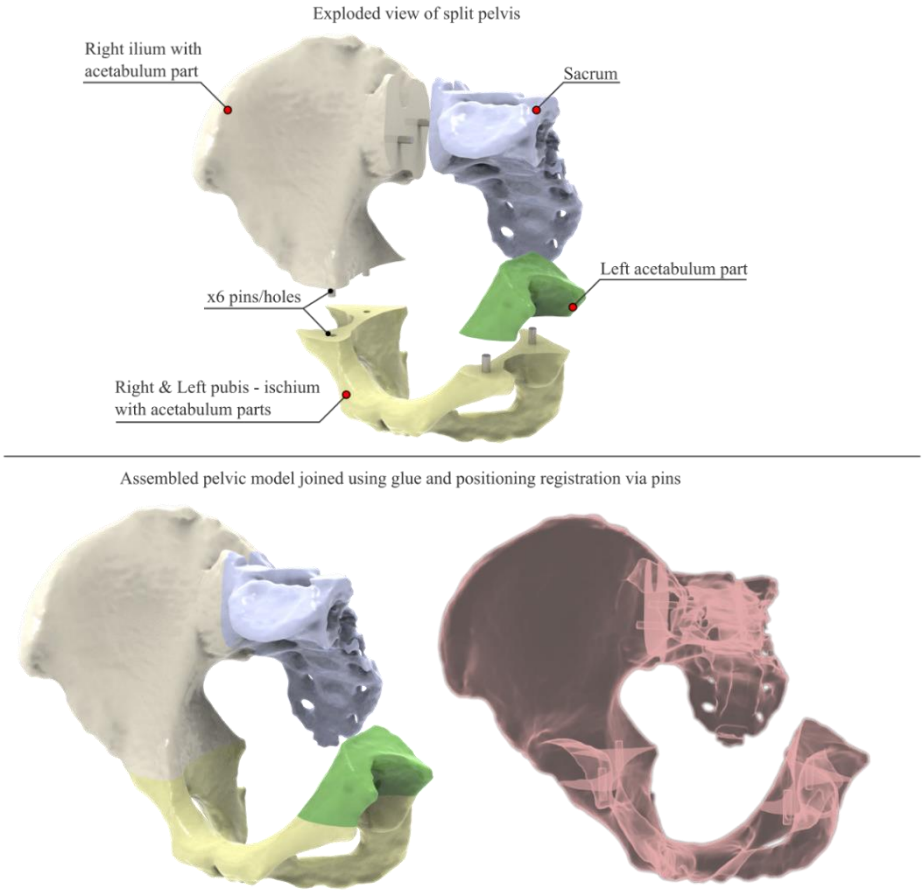

Figure 352: Post-resected pelvic model anatomically split into 4 sections

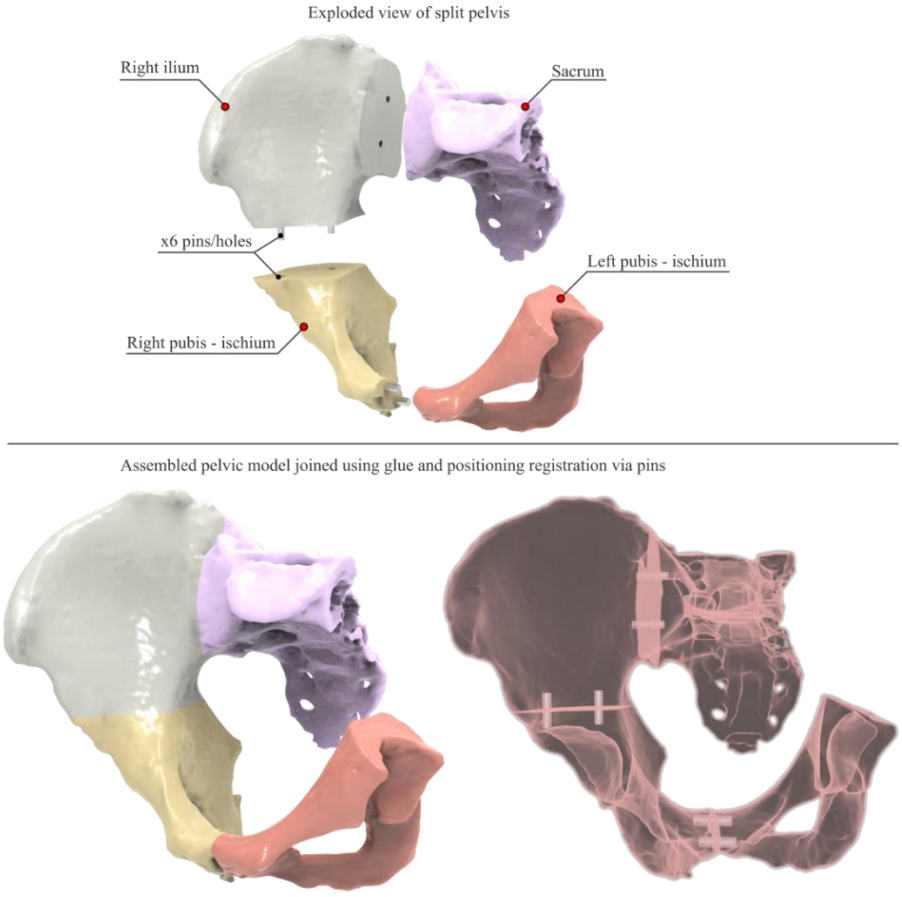

Figure 353: Alternative option for splitting the post-resected pelvic model split into 4 sections

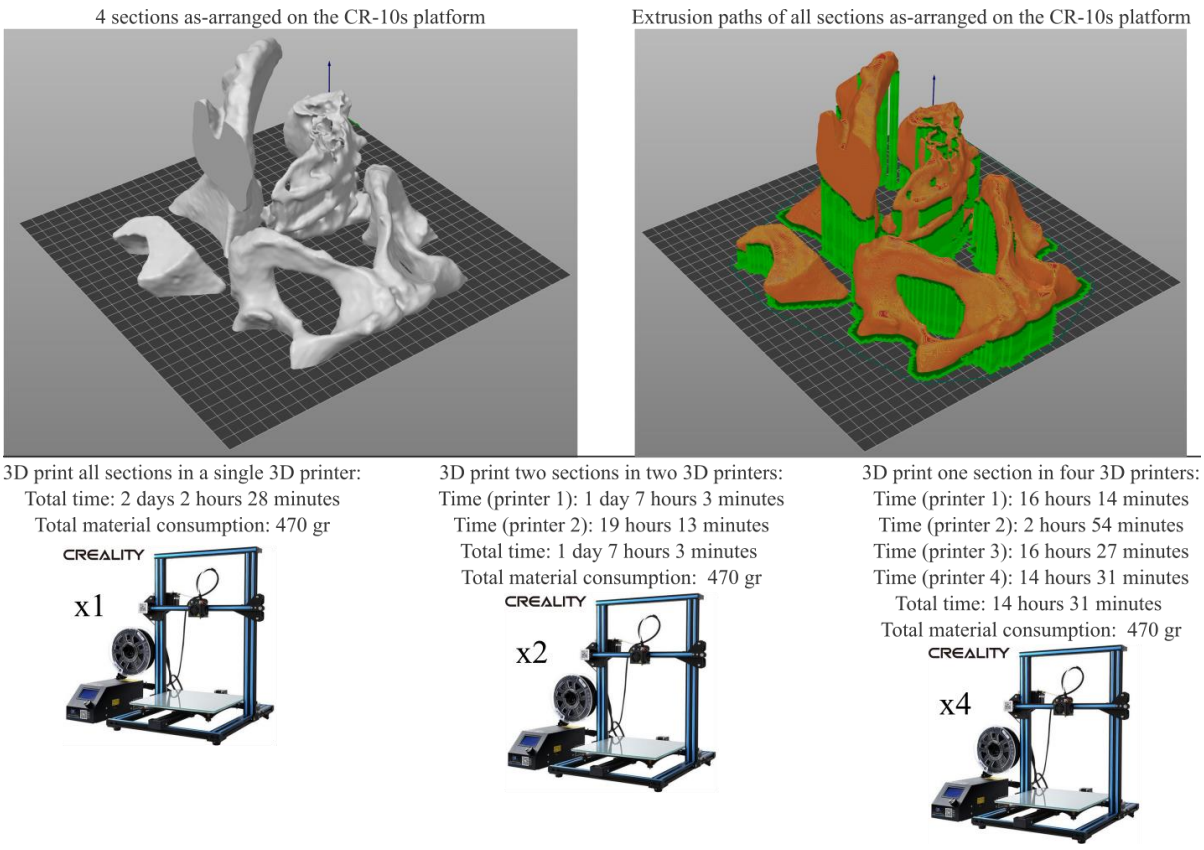

Figure 354: Multiple 3DP of the post-resected pelvic model anatomically split

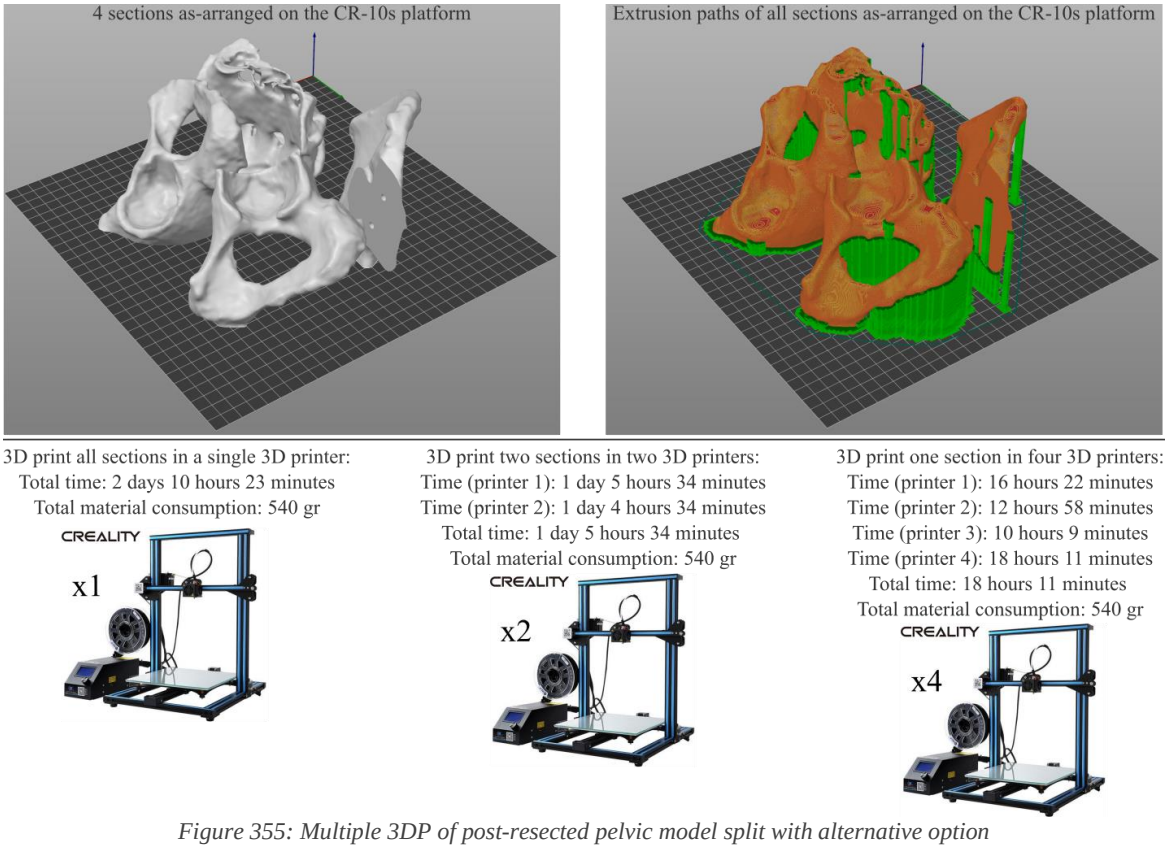

Figure 355: Multiple 3DP of post-resected pelvic model split with alternative option

As long as suitable medical image data readily exists, any of the aforementioned technologies per se or in combination can be implemented in the pre-operative planning workflow in a short time and at a low cost *(see Section 5)* regardless of the complexity and type of the case.

The surgeon can a) access the 3D digital model, the immersive experience in xR, and examine the 3DPed object either by visiting the PoC 3D Unit, along with the (bio)mechanical design engineers, to view digitally, virtually, and physically the anatomical model, or b) the digital 3D and the xR (granted that the surgeon owns xR equipment) files to be downloaded from the *SkeletoMy* platform and viewed/experienced individually using the options described previously, whereas the physical model can be packed and delivered to the surgeon's office.

The 3D digital visualization of the 3D anatomical model, the interaction with it in xR environments, and holding in hands the 3DPed true scale anatomical replica aided the surgeon in examining the post-operative results of the tumor resection and planning the second stage (reconstruction) of the operation. Thus, the rehabilitation strategy and the task to be carried out by the PoC 3D Unit could be clarified more efficiently and effectively in more detail.

6.4.5 Rehabilitation Strategy and Task Clarification

At the time of case submission as part of the request of services and products on *SkeletoMy* platform, all anonymized data provided by the surgeon were accompanied by initial specifications of the solutions and other notes. By examining the patient's pre and post-resected DICOM data, the 3D digital models, the virtual model, and the physical 3DPed model, the surgeon could set the rehabilitation strategy and clarify the task by setting the specifications and requirements of the solution to be developed by the PoC 3D Unit in detail.

The ultimate quest was to preserve the patient's limb and retain favorable functions in the long term by re-establishing the continuity of the pelvic girdle to prevent subsequent collapses and deformations of the residual bony tissue under load-bearing activities. Standard endo-prosthetic solutions to preserve the hip joint such as saddle, pedestal/stemmed (ice-cream) cone, and pedicle rod-screw systems are not suitable in this case as there is no iliac bone stock. Hence, following the conducted level of oncological en bloc resection, and serving total hip joint arthroplasty, a patient-specific iliac endo-prosthesis to precisely fit into the remnant of the pelvis and support any soft tissue had to be designed and manufactured. As the surgical implantation of pelvic endo-prostheses after wide and radical en bloc resections is fraught with difficulties and complications such as infections, loosening, and breakage *(see Sub-sections 3.1, 3.5, and 3.6)*, the developed solution should mitigate as much complexity from the operating room.

The surgeon outlined the need for a non-bulky low-profile endo-prosthesis conforming to the inner form of the resected bone tissue. The surgeon together with the PoC 3D Unit defined the specifications list based on a) the previously generated visual aids, b) the patient's CT-scan data, c) anatomical and biomechanical considerations, and general implant requirements for the pelvis. A modified version of Pugh's product design specification elements *(1991)* was utilized by considering

the applicable that the endo-prosthesis should adhere to *(Figure 357)*. The specifications were filled collaboratively within a 1-hour meeting session using sticky notes on *Miro* online whiteboard platform (link issued in *SkeletoMy* platform *(see Section 5)*) and a 24-hour window was left for amendments. The final specifications are summarized in *Table 19*.

Table 19: Specifications list for the pelvic endo-prosthesis and PSI

Element	Specifications
Environment	• The endo-prosthesis should withstand the aggressive environment within the human body that might lead to corrosion mechanisms: highly oxygenated saline electrolyte at 7,4 pH and 37°C *(Hansen, 2008)*. • None of the peripheral soft tissue must be disturbed, irritated, and damaged.
Testing	• The fit of the endo-prosthesis and any PSI must be verified digitally and/or virtually, and physically by a polymer prototype along with the anatomical model of the patient, before final manufacturing. • Mechanical evaluation by FEA simulations under realistic loading scenarios. • After primary shaping and post-processing of the final products, they must be visually inspected, and if possible, using non-destructive inspection techniques before packaging and sterilization. Also, before implantation and application, all products must be inspected again visually.
Safety	Maximum safety must be guaranteed, risks mitigated and future complications minimized (bone resorption by stress-shielding, peri-prosthetic fractures, (a)septic loosening, infections) by: • Geometrical features and fixation that facilitate and speed up implantation. • Surface characteristics that inhibit bacterial colonization and promote osseointegration. • Choosing biocompatible biomaterials with composition and properties that do not trigger reactions. • Protect and support surrounding soft tissue and organs.
Legal, Standards, Politics	• All custom-made and off-the-shelf products have to conform to all corresponding relevant national and international safety and quality management standards[144] and regulations[145]. • Especially for 3DPed *"emergency"* custom-made orthopaedic devices that are exempted from standard regulations *(FDA, 2014)*, not only the EU's MDR (EU) 2017/745 *(Official Journal of the EU, 2017)*, but also the FDA's technical notes *(FDA, 2017)* and the discussion papers on 3DP (e.g. the *"3D Printing Medical Devices at the Point of Care" (FDA, 2021))* are suggested to be considered (more at http://www.fda.gov/3DPrinting).
Documentation	• Risk assessment (could be based on ISO 14971:2019) and justification report on the mechanical and biological performance of the solution. • Manufacturing instructions and drawings. • Analytical implantation (surgical technique) instructions with descriptive illustrations.
Quantity	Unique one-off patient-specific solution.
Life Span, Service Life, Maintenance	Lifetime solution with maintenance-free operation.
Materials	• For the endo-prosthesis: biocompatible metals with high corrosion resistance, without showing toxicity or other undesirable effects, and without triggering immune reactions.

[144] Such as the ISO's 11.040.40 standards catalogue (see https://www.iso.org/ics/11.040.40/x/) and ASTM's standards under Juridiction F04 (see https://www.astm.org/get-involved/technical-committees/committee-f04/subcommittee-f04). See also *Table 9*.

[145] Such as the EU's MDR (EU) 2017/745 *(Official Journal of the EU, 2017)* or the FDA's guidance documents (see https://www.fda.gov/regulatory-information/search-fda-guidance-documents), or the recognized consensus standards to which FDA accepts conformity (see https://www.accessdata.fda.gov/scripts/cdrh/cfdocs/cfStandards/search.cfm). See also *Table 9*.

	• For the PSI: biocompatible metals and polymers. • For the anatomical model: any biocompatible polymer. • Selected biomaterials to be readily available in powder states to be used in PBF 3DP technologies. • Standard off-the-shelf materials for the total hip arthroplasty components: liner, stem, head.
Ergonomics and Aesthetics	Maximize aesthetical outcome by reinstating the initial form and ergonomics, without hindering functionality.
Implantation	• The T-shaped metal bars have to be removed and the endo-prosthesis has to be precisely fitted to substitute the left iliac bone loss and support the remnant soft tissue. • Facilitate surgical technique (lateral approach): easy and quick instruments and endo-prosthesis positioning and fixation with features as per patient's anatomy. • Guide the surgeon by providing instructions (surgical technique) in an intuitive style. • Reinstate biomechanical functions: pelvic girdle reconstruction (ilium plus part of acetabulum and sacrum), acetabulum preparation for standard total hip-joint arthroplasty, reinstate the center of mass. • Guarantee symmetry between right and left hip bones and avoid limb length discrepancy. • Fixation points and screw diameter and length based on the patient's host site morphology, bone stock amount, and quality, whilst avoiding soft tissue, neurovascular, and organ injury and damage. • Due to the en bloc wide resection, a low-profile non-bulky design is required. It should follow the symmetrical (mirrored) inner wall anatomy of the right healthy counterpart.
Performance	• Anti-bacterial surface characteristics to fight infections. • Do not irritate and disturb the peripheral soft tissue. • Cement-less bone-implant contact to allow interfacial phenomena to occur. *"Bioactivity"* to be enabled by interconnected porous surface functionalization to allow bone ingrowth and boost osseointegration, whilst avoiding aseptic loosening. • Shape and topologically optimized features. • Maximum fixation stability to maintain the pelvic girdle closed without micro-motions concerning the host tissue during gait and more intense activities. • Biomimetic internal architecture resembling trabecular bone, adjusted to approach bone-like modulus of elasticity and deformation, minimizing stress-shielding, bone resorption, and peri-prosthetic fractures. • Adequate durability for full weight-bearing operation and withstand direct impacts. • Wear resistance at the femoral stem head-acetabulum cup interface.
Cost and Timescale	• Cost performance and lead time for 3DP geometrically complex and one-off parts such as this endo-prosthesis and the PSIs are superior to conventional technologies. • Options to minimize the costs and lead time without compromising performance to be explored. • The design and prototyping of the final solution to be completed within two weeks.
Patient	• Endo-prosthesis and instruments to be customized as per the patient's status, anatomy, and host site condition. • The patient's pain must be relieved and mobilization recovered as quickly as possible. • Bone loss to be substituted with metal endo-prosthesis and acetabulum to be prepared for standard total hip-joint arthroplasty.
Processes	• Any matching 3DP technology to fabricate the anatomical models out of a polymer biomaterial. • Any matching 3DP technology to fabricate the trial endo-prosthesis prototype and the trial and final surgical instruments out of any biocompatible polymer materials. • PBF-based 3DP technology for high-quality primary shaping of the end endo-prosthesis. • Cleaning, post-processing (machining and surface treatments), packaging and sterilization. • Optionally, non-destructive inspection of the final parts before packaging and sterilization.

	• Visual inspection before packaging and sterilization, and before implantation/application.
Size and Weight	• Patient's morphology-tailored geometry and fixation. • Low-profile endo-prosthesis with similar weight as the resected hard tissue.
Packaging, Storage, Shipping	• All parts to be delivered to the surgeon to be cleaned, post-processed, packaged, and sterilized with material-matching and certified techniques. Standards must be applied for labeling (ISO 15223-1:2021 and ISO 15223-2:2010), sterilization (ISO 11737-1:2018, ISO 11737-2:2019, ISO 11737-3:2023), and packaging (ISO 11607-1:2019 and ISO 11607-2:2019) of medical devices. • The package to be stored in a clean, cool, and dry place before handed over to the surgeon and before being opened for inspection and implantation.
Constraints	• Design, analysis, prototyping, and delivery of the final solution to be completed within two weeks. This case had already received surgical treatment in the past. It is being treated as if it is a currently ongoing pragmatic case. Due to the research character of this thesis, both top-down and bottom-up approaches *(Figure 256)* will be discussed, and scenarios and hypotheses/ assumptions will be made along the application of the inter-epistemic development workflow *(Figure 264)*. Within the context of this thesis, the following constraints exist: • There are budget and resource constraints. However, there are readily available resources for software to design, simulate, and optimize the solution. • The solution will not be implanted into the patient. • There are limited resources to fabricate the end endo-prosthesis out of metal. Hence, it will be prototyped out of a polymer biomaterial.
Disposal	All remaining unnecessary materials can be recycled.
Manufacturing Facility	• The anatomical models and the trial endo-prosthesis to be 3DPed at the PoC. The trial and final surgical instruments could be 3DPed at the PoC. • 3DP and post-processing of final endo-prosthesis and final PSIs to be outsourced to a contract manufacturer as the PoC lacks high-end powder-based polymer and metal 3D printers. • The final parts can be packaged, stored, and sterilized at the PoC.
Market and Competition	• The characteristics of the solution can be inspired by other designs and methodologies found in the literature, in the orthopaedic devices market, or in nature.
Quality and Reliability	• Quality management standards for medical device development such as ISO 13485 and the generic ISO 9001:2015 must be applied. • The implant design, manufacturing, and surgical application should revolve around certifications and qualifications by validation or verification with the highest quality techniques, equipment, and materials. • All applicable standards, directives, and guidelines of *Table 1* and *Table 9* to be applied, especially for 3DP. • Quality and reliability to be assured for zero defects by conforming to the previously noted specifications under the a) Legal, Standards, Politics, b) Testing, and c) Documentation Elements.
Patents	The developed solution should not clash over any active intellectual property rights.

Although the anatomical model and the specifications list were enough for the PoC 3D Unit to develop the solution, the following options were offered to the surgeon for extra design instructions:

1. Sketch-friendly views *(Figure 358)* of the post-resected pelvis uploaded to *SkeletoMy* so that the surgeon can sketch and mark, before uploading back the edited picture(s) to *SkeletoMy*.
2. Marking or modeling screw placement points or basic forms on the digital 3D model using 3D Slicer, Autodesk Meshmixer, Meshlab, or any modeling software mentioned earlier, and upload back to *SkeletoMy* the edited model or screenshots accompanied by instructions.

3. 3D mark and sketch the digital 3D model in a VR environment using the Medicalholodeck VR software *(Figure 359)* and upload screenshots to *SkeletoMy*.
4. Modeling the solution on the physical 3DPed anatomical model using modeling clay, and sending back photographs to *SkeletoMy* or the physical parts per se to the PoC 3D Unit. An example of the physical modeling approach is presented at the end of the next *Sub-section*.

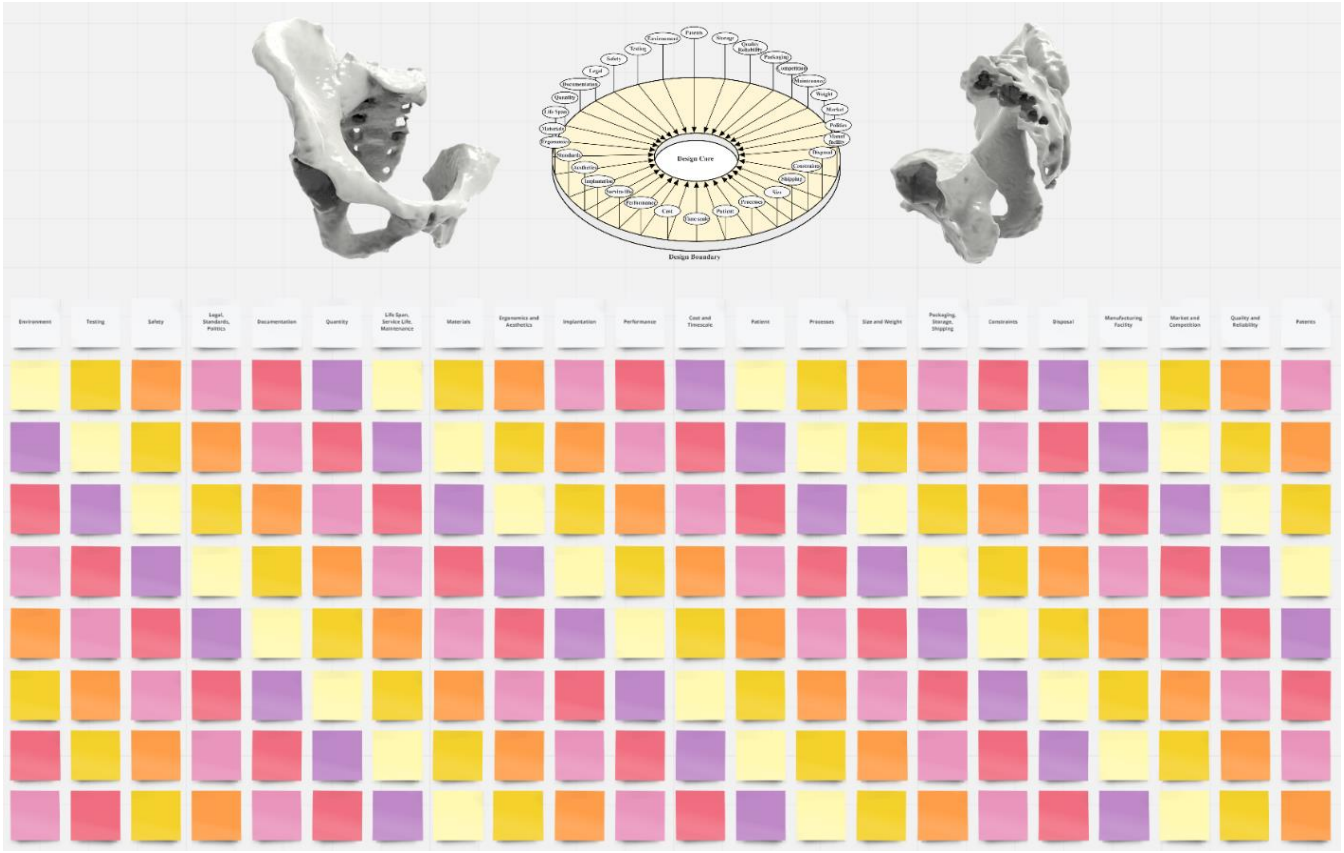

Figure 356: Screenshot of Miro whiteboard used to define specifications on sticky notes

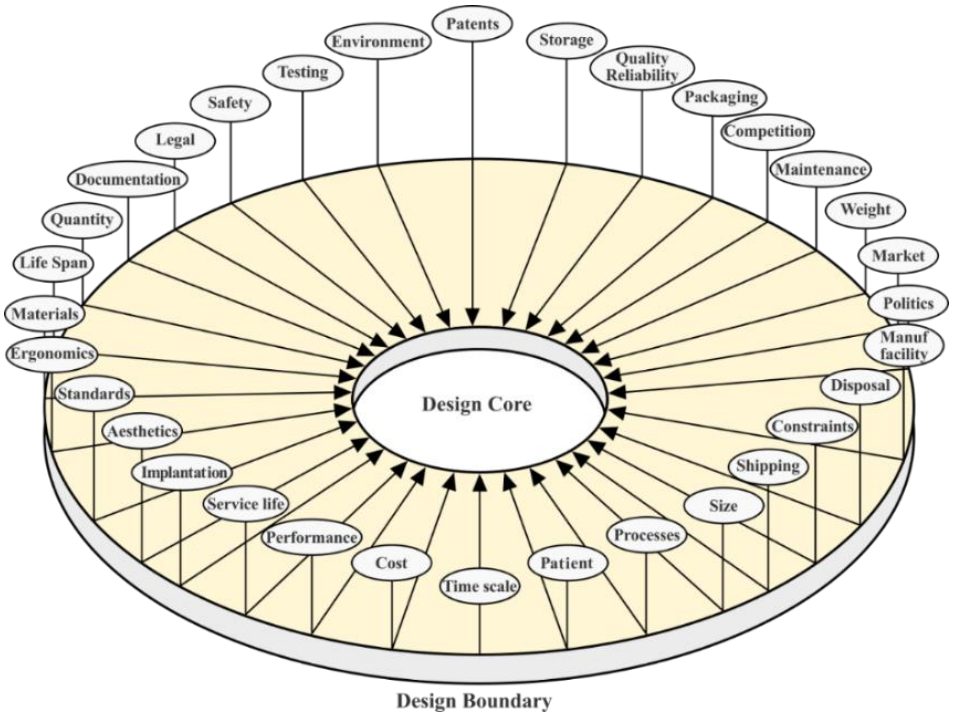

Figure 357: Elements of Pugh's product design specifications. Source: after Pugh (1991)

Once the specifications list was defined and granted that the PoC 3D Unit had all the data to commence developing the solution, the process moved to Stage 6, and the inter-epistemic engineering design of the endo-prosthesis and PSIs was initiated.

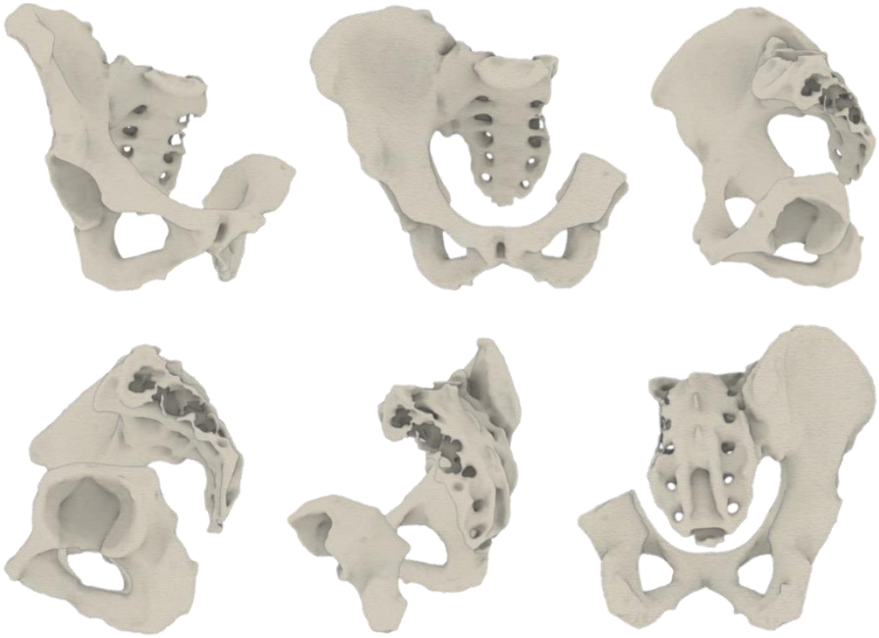

Figure 358: Views of the post-resected pelvis in sketch-friendly format

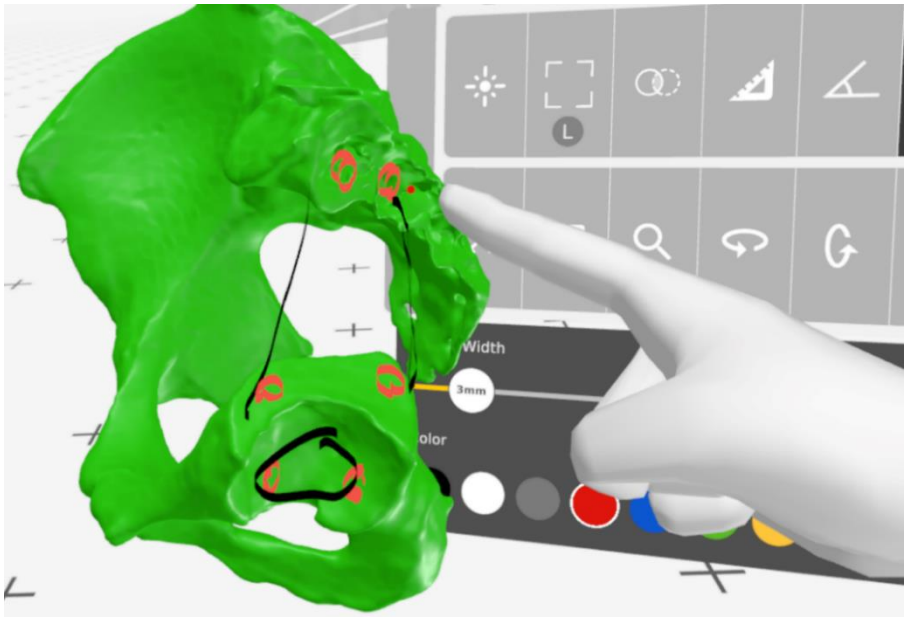

Figure 359: Drawing and marking the digital model in Medicalholodeck VR

6.4.6 Conceptual Design and Evaluation

The previous task clarification Stage answered the *"why?"* question of the iceberg model of physical product making *(Figure 258)* which was better illustrated in *Figure 259* with emphasis on orthopaedic products development process. During the conceptual design the *"what?"* to be made was defined before the *"how?"* to be made was solved during the next embodiment and detailed design Stages. Of course, to develop the ideal orthopaedic implant *(Figure 260)*, and granted that no resources constraints are encountered, a bottom-up approach has to be followed, driven by the exact needs of the patient *(Figure 256) (Charbonnier, Hadida and Marchat, 2021)*.

As was explained in the literature review *(Section 3),* 3DP technologies have lifted the manufacturing barriers so that any desired form regardless of its geometrical complexity can be rapidly materialized. This *"whatever can be designed can be manufactured"* fact has made manufacturing easier than designing, and new design spaces were opened to be explored.

Although the application of computational and generative design algorithms falls under the embodiment and detailed design phases, it is important to consider that ultimately as generation of extremely intricate simulation-driven topologically and shape-optimized constructs is highly sought. For this reason, to fully explore and exploit the capabilities of 3DP, Dw3DP *(Floriane et al., 2016)* should be harnessed as a toolbox to expand conceptualization by inspiring from a knowledge database with novel 3DPable features.

During the conceptual design phase, working principles and ideas were explored by searching in a knowledge database with inputs being sourced from:

1. Any industrial sector, and especially in the orthopaedic devices market.
2. Literature, where similar applications and devices are being reported.
3. Nature: musculoskeletal system and any (non)living system. For this reason, the biomimicry taxonomy (part of the biomimicry toolbox (design spiral *(Figure 237)*)) of biological strategies *(Appendix O)* was followed to aid in biomimesis.

For this particular case, knowledge obtained from the extensive literature review *(Section 3* on 3DP principles and characteristics, biomaterials and requirements for orthopaedic devices, biomimesis, mechanical and biological optimization) and similar components found in *Appendices B and J* were used as input to establish the database. Matching products, forms, functions, and principles were captured as hypodigms for inspiration and mimesis to compose working ideas after analysis and synthesis.

To maintain creativity boosted and motivation level high with an emphasis on innovation, it was suggested that before firmed-up into working concepts, ideas for each function of the product to be developed were generated unrestricted (without taking into consideration the constraints imposed by the elements of the product design specifications), and then, the functions to be synthesized into working concepts by filtering, revising and adapting the concepts to the specifications list and design instructions set previously.

Brainstorming could have been conducted in one or more sessions with many participants including the surgeon, physically or remotely, by adopting various techniques. In this case, it was conducted by the (bio)mechanical design engineer and the surgeon. First, ten functions of the endo-prosthesis were defined, and then ideas were written for each one. *Figure 366* shows a screenshot of

the Miro online whiteboard platform where the mind map of concepts was impressed within 1 hour and a 24-hour window was left for amendments before commencing the evaluation.

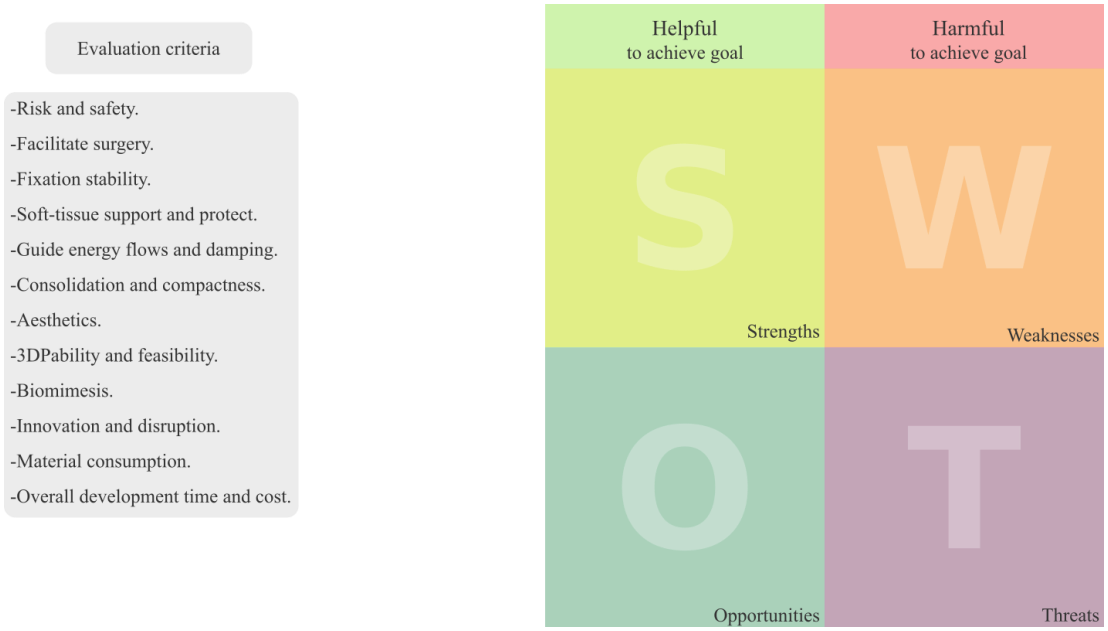

Figure 360: Evaluation criteria and SWOT analysis for each concept

For each function, the most suitable ideas were selected and firmed up into concepts satisfying the specifications list *(Table 19)*. Under SWOT analysis, from which threats were considered for risk assessment *(see Section 5)*, the generated concepts were evaluated collaboratively with the surgeon, based on pre-set constraints and weighted (1 to 5) criteria *(Figure 360)*. The concept achieving the best score was selected for development. The meeting took place remotely and the link to the shared Miro document for the evaluation was sent to the surgeon via the *SkeletoMy* platform. The meeting lasted 1 hour and the selected features of the solution to be developed are summarized below:

1. **External shape (silhouette):** the endo-prosthesis will have a non-bulky low-profile anatomically-conforming silhouette following the natural free-form inner wall of the symmetrical (mirrored) right healthy pelvic tissue *(Figure 361)*. The surrounding soft tissue and organs must be protected and supported. However, due to the amount of en bloc resected hard and soft tissue, it would add no value to exactly replicate the whole bulky right iliac tissue, as well as implementing re-attachment features, though such will be presented. A thin solid outer shell (to avoid soft tissue entrapment and infection risk) with interconnected cellular structure infill was selected, but optimized organic shapes will also be explored. For the total hip arthroplasty, standard components will be used.
2. **Integration and customization level:** the pelvic girdle will be reconstructed with a custom-made endo-prosthesis featuring an integrated acetabular shell. Regarding the other total hip arthroplasty components, there is no need for customized design as it would not be wise to increase the total cost and time: there are multifarious readily available off-the-shelf mass-produced femoral stems, heads, and liners in the orthopaedic devices market. An endo-prosthesis that does not integrate

the acetabular shell *(Figure 362)* would result in more parts and would make surgery more complex in terms of a) alignment of the endo-prosthesis with the remaining of biological acetabulum, b) reaming of the biological acetabulum, and b) fixation, that has to be achieved among three components: biological acetabulum, cup, endo-prosthesis.

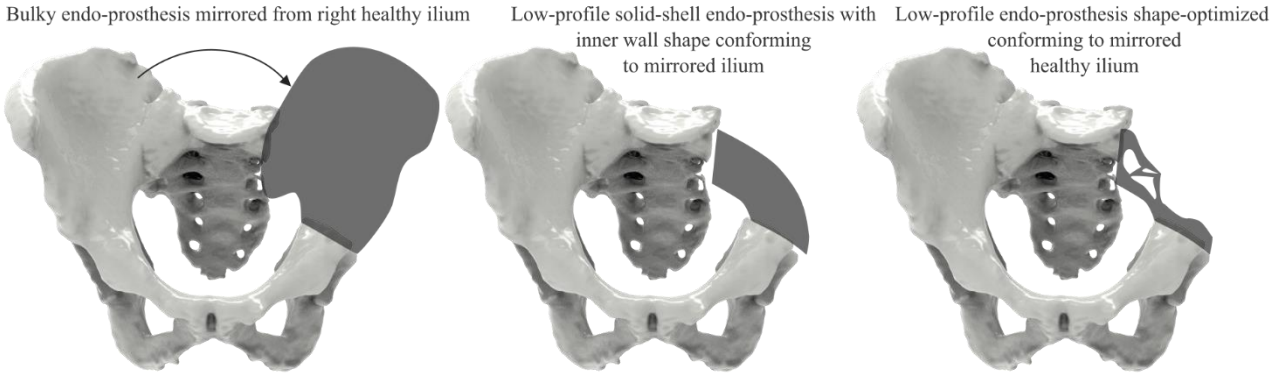

Figure 361: Bulky natural-like and low-profile design concepts

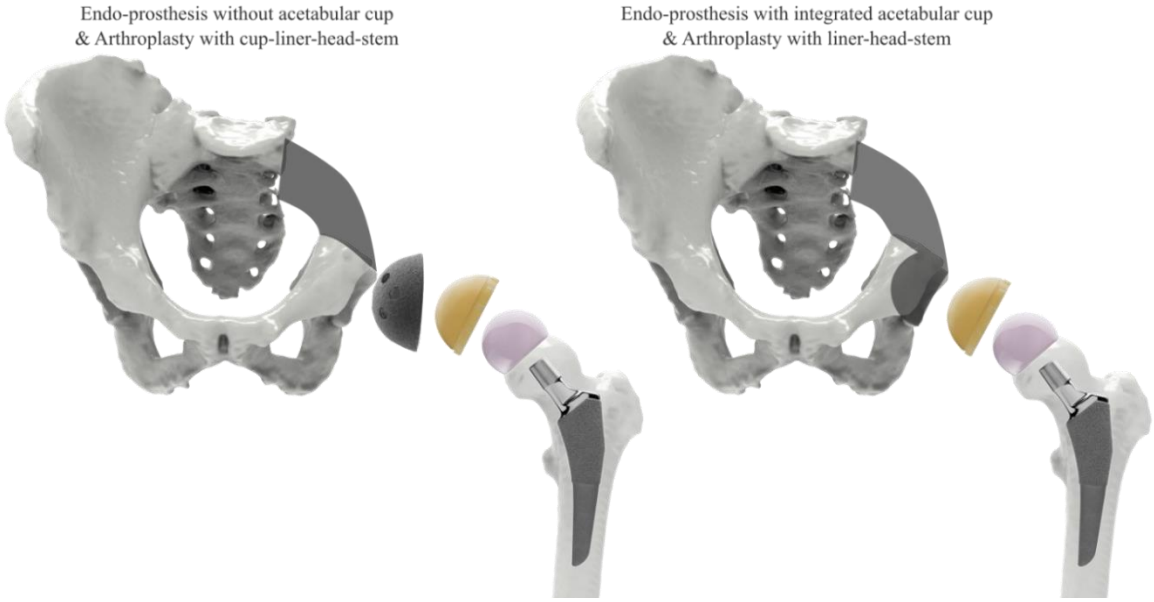

Figure 362: Endo-prosthesis with and without integrated acetabular shell

3. **Fixation:** the endo-prosthesis will be cement-less fixed by considering neurovascular tissue and maximum stability using bone screws inserted as per the patient's anatomy and bone quality. Optionally, porous stems, pedicle screw-rod systems for spondylodesis, and hook features will be explored. PSIs must facilitate the surgical technique by easy registration, positioning, drilling, and placement. The cup or liner will be locked in place within the acetabular shell of the endo-prosthesis using cement or other locking mechanisms. The femoral stem will be inserted in the femoral canal using standard tools and fixed cement-less. Risks of mechanical failure and aseptic loosening must be mitigated. All bone-implant interfaces must have porous structures for bone ingrowth to ultimately achieve biological fixation (osseointegration).
4. **Bony host site preparation:** the acetabulum will be reamed before implantation of the endo-prosthesis. Based on the CT scan, the exact geometric boundaries and the existence of extra bone tissue with lower densities (trabecular) were uncertain. Hence, the roof of the resected acetabulum

and the side of the resected sacrum have to be cut flat for perfect fit. Alternatively, the endo-prosthesis could be tailored to fit into the remnant bone stock, however, the fitting per se and any free-hand interventions might be of concern *(Figure 363)*. The left femoral head and neck will be cut and the femoral canal reamed to accept the femoral stem and head.

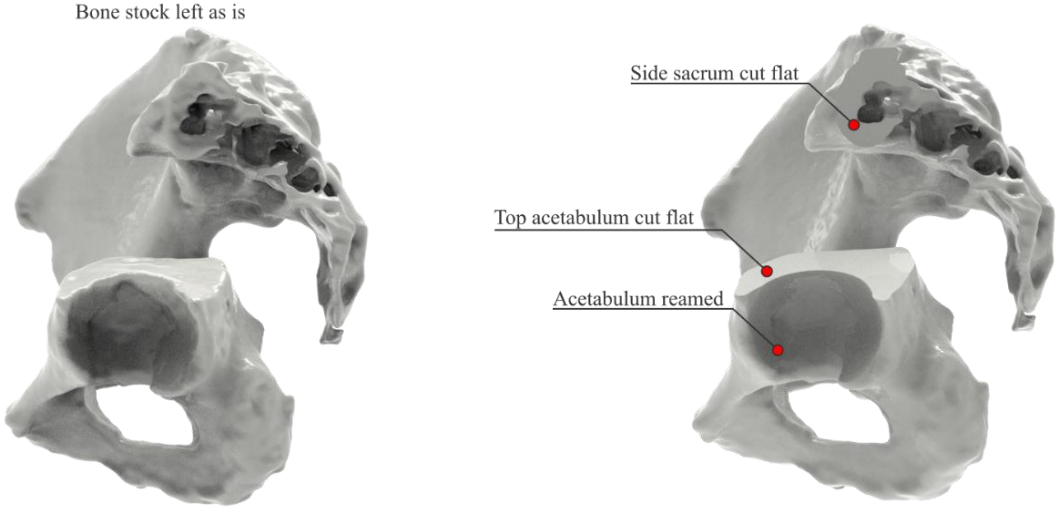

Figure 363: No-cutting and fine flat-cutting and reaming for perfect endo-prosthesis fit

5. **Surface characteristics:** the metal endo-prosthesis will feature a thin solid satin-finish outer shell to inhibit bacterial colonization, facilitate coatings, and not irritate soft tissue. Polishing Ti implants has been found to have little effect on bacterial adhesion and biofilm formation, whereas at the same time having a fully cellular structure without a solid shell can irritate tissue and affect soft tissue adherence, wound dehiscence, and healing, leading to infection *(Sarfraz et al., 2022)*. Holes and optionally porous features by integrated porosity or via coatings where soft tissue re-attachment might be possibly desired could have been explored, though there is little amount of remnant soft tissue in the corresponding compartment. Cellular structures will be implemented at all bone-contacting areas for a higher coefficient of friction to restrict micro-motions and allow biological fixation to be induced by bone ingrowth (osseointegration).
6. **Endo-structure:** the endo-prosthesis will have a thin solid shell and a bone-like spongy inner structure with topologically varying characteristics, whilst exhibiting adequate mechanical strength. The inter-connected porous endo-structure will end at the porous surfaces that touch the host bone and serve a bimodal function: a) allow vascular, oxygen, nutrients, and bone formation inducing elements invasion and circulation, and b) lower the stiffness to better match the properties of host tissue and minimize stress-shielding phenomena. Functionally graded-(meta)biomaterials with heterogeneous structure and density variations are of high interest. The fully solid option will have a high mass, whereas the fully porous (with no solid shell) might irritate soft tissue, and attract bacteria, and cleaning/coating will be challenging.
7. **Surgical technique:** the surgical incision (anterior/posterior with possible lateral ancillary) and approach will expose the bony pelvis was completely defined and planned by the surgeon and his

team. To facilitate bone preparation and implantation of the endo-prosthesis and the arthroplasty components, both custom and standard tools will be utilized. Anatomically tailored features should be implemented into the endo-prosthesis for easy registration and positioning. Neither robotic nor intra-surgical navigation systems will be used, hence no registration marks and tracking components are required to be established.

8. **Biomaterials:** as there are no readily available (bio)ceramics, composites, and natural materials to be processed by 3DP technologies into large intricate forms, whilst being able for load-bearing, the endo-prosthesis will be 3DPed out of metal alloys and any accompanying instrumentation manufactured out of biocompatible polymers and/or metal alloys. For the total hip arthroplasty, standard off-the-shelf components (liner, femoral head, and stem) will be selected from established companies in the orthopaedic devices market that offer certified biomaterials and tested implantable devices with successful records.
9. **Coatings:** coatings targeting enhanced biocompatibility (osseointegration-boosting) at the bone-contact areas and antimicrobial activity (infection prevention) topologically or universally can be applied. Also, coatings as an alternative to integrated porosity at the surface where soft tissue re-attachment might have been desired. There is no need to increase the hardness by hard coatings (e.g. TiN) due to the absence of direct tribological phenomena of the endo-prosthesis.
10. **Disruption:** due to the en bloc resection, a low-profile endo-prosthesis was required to substitute the iliac bone loss and support the remnant soft tissue. As multi-material 3DP, biodegradable materials, tissue-engineered grafting, and 4D printing of responsive and autonomous construct are in their infancy for load-bearing applications, disruption could only emerge by implementing electronics and drug elution systems within the endo-prosthesis and by hybrid biological-artificial reconstruction techniques. The aforementioned were left for future research.

Figure 364: Physical clay modeling of the agreed endo-prosthesis concept

After meeting completion, the deliverables were hand sketches (30 minutes required) *(Figure 365)* containing the main agreed features and a corresponding tangible red modeling clay replica of the concept attached and formed (40 minutes required) on the 3DPed anatomical model *(Figure 364)*.

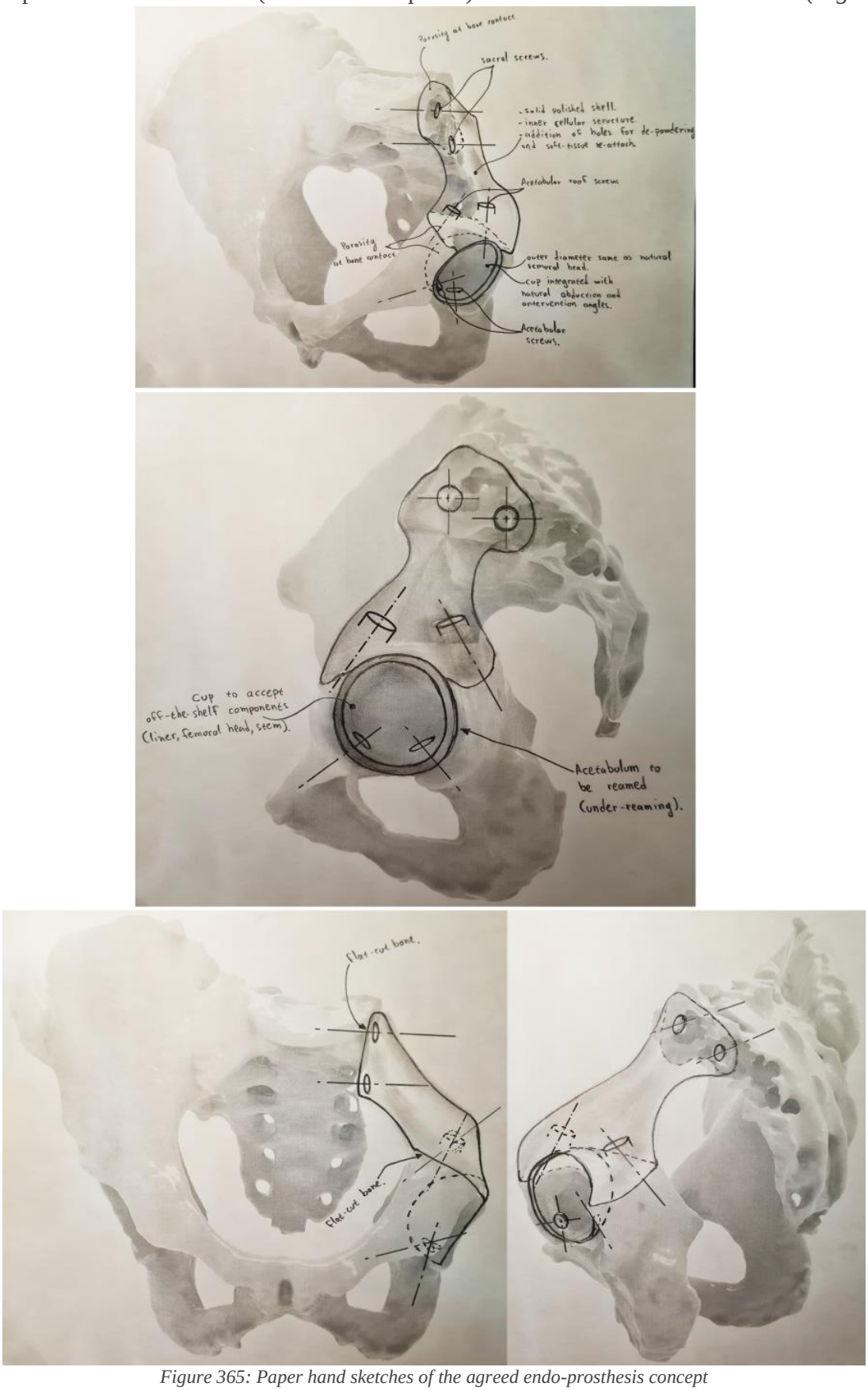

Figure 365: Paper hand sketches of the agreed endo-prosthesis concept

Figure 366: Screenshot of Miro whiteboard used to generate the mind map of concepts

6.4.7 Embodiment Design

The embodiment design links the previous conceptual design Stage (selected concept) with the next detailed design Stage *(Figure 367)*. In this Section, the transition towards the detailed solution will be shown by preliminarily defining fundamental elements: materials, shape and geometrical features, fixation method, surface characteristics, and application technique for the endo-prosthesis, as well as for any ancillaries such as standard or PSI.

To facilitate designing and measuring, the segmented and isolated pelvic facet model (surface mesh in .stl file format) had first to be aligned to the three axes of the cartesian space based on

anatomical landmarks. To do so, although all of the aforementioned mesh manipulation and modeling software were capable, Spaceclaim was selected as was proved to be the fastest and most convenient.

The translations along and rotations around all axes were saved so that the model could return manually to its exact initial position, being perfectly aligned with the origin of CT-scanned images. Alternatively, the Interactive Closest Point (ICP) algorithm *(Besl and McKay, 1991; Zhang, Yao and Deng, 2022)* which is also included in Meshlab software *(Cignoni et al., 2008)* can be used to re-align the translated model to the initial model by distance minimization between selected points.

Figure 368 shows the steps followed, i.e.:

- The projection of the line created by connecting the pubic tubercle with the anterior superior iliac spine was aligned parallel and set coincident with Z-axis. The ZY plane became the sagittal plane.
- The projection of the bi-ischial line (the line connecting the ischial tuberosities) was aligned parallel and set coincident with X-axis. The XZ plane became the coronal plane. The bi-ischial and the line connecting the teardrops of the acetabula were found to be almost parallel. The center of the pubic symphysis was set as a symmetry line coincident with Z-axis.
- The projection of the line created by connecting the pubic tubercle with the anterior superior iliac spine was aligned parallel and set coincident with X-axis. XY plane became the axial plane.

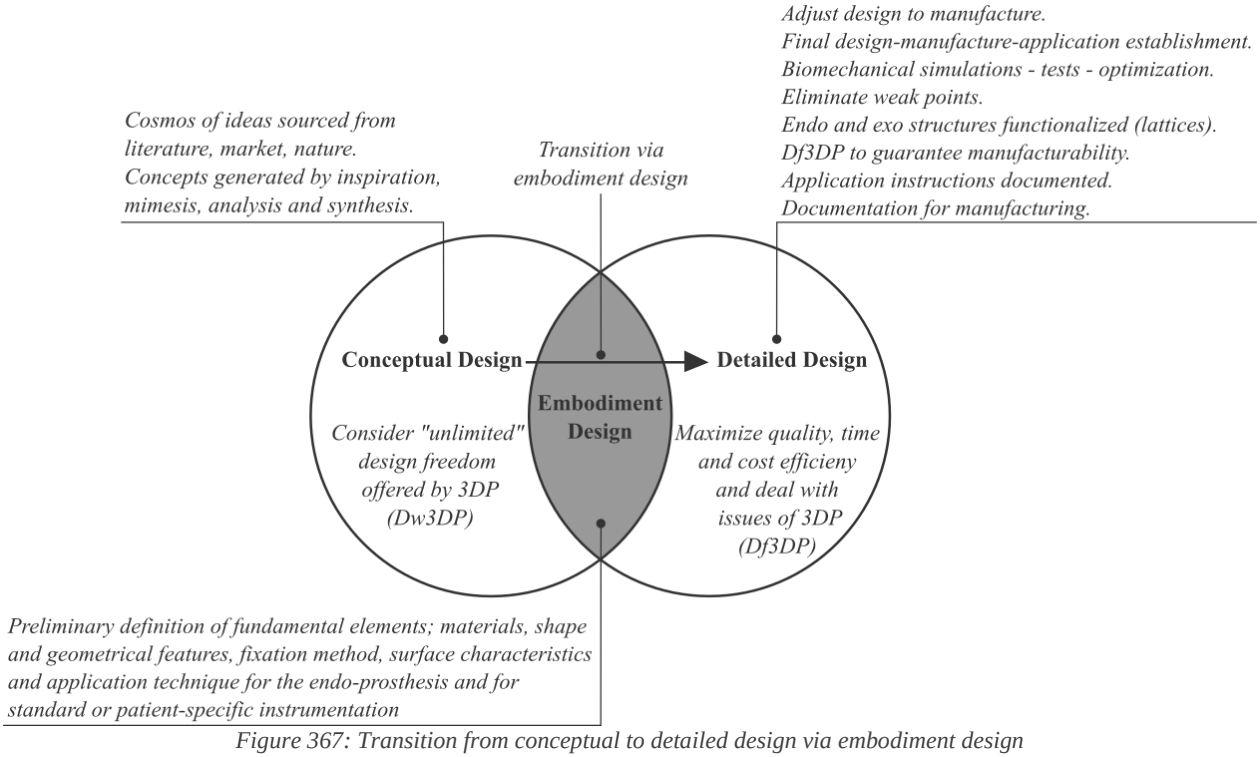

Figure 367: Transition from conceptual to detailed design via embodiment design

Due to the iliac plus sacroiliac joint plus part of acetabulum resection, and regardless of the T-shaped bar installed, it is apparent that the pelvic geometry is deformed. Characteristically, the sacrum can be seen as slightly skewed, whereas offsets greater than 2,5 mm were measured between the acetabula with respect to the cartesian system established before, based on the bi-ischial line and the pubic-tubercle-anterior superior iliac spine line. The offset was measured as follows:

- The faces of each acetabulum were selected and automatically best-fitted with a primitive sphere shape. The calculated diameter was 43 mm.
- A plane parallel to the coronal plane was created coincident with the center of the right acetabulum sphere. A sketch with a line parallel to the axial plane (X-axis) was created and the distal offset of the left acetabulum measured was 2,67 mm.
- A plane parallel to the axial plane was created coincident with the center of the right acetabulum sphere. A sketch with a line parallel to the coronal plane (X-axis) was created, and the medial (1,42 mm) and anterior offset (2,85 mm) of the left acetabulum were measured. The measured distance between the acetabulum spheres was 162,81 mm.

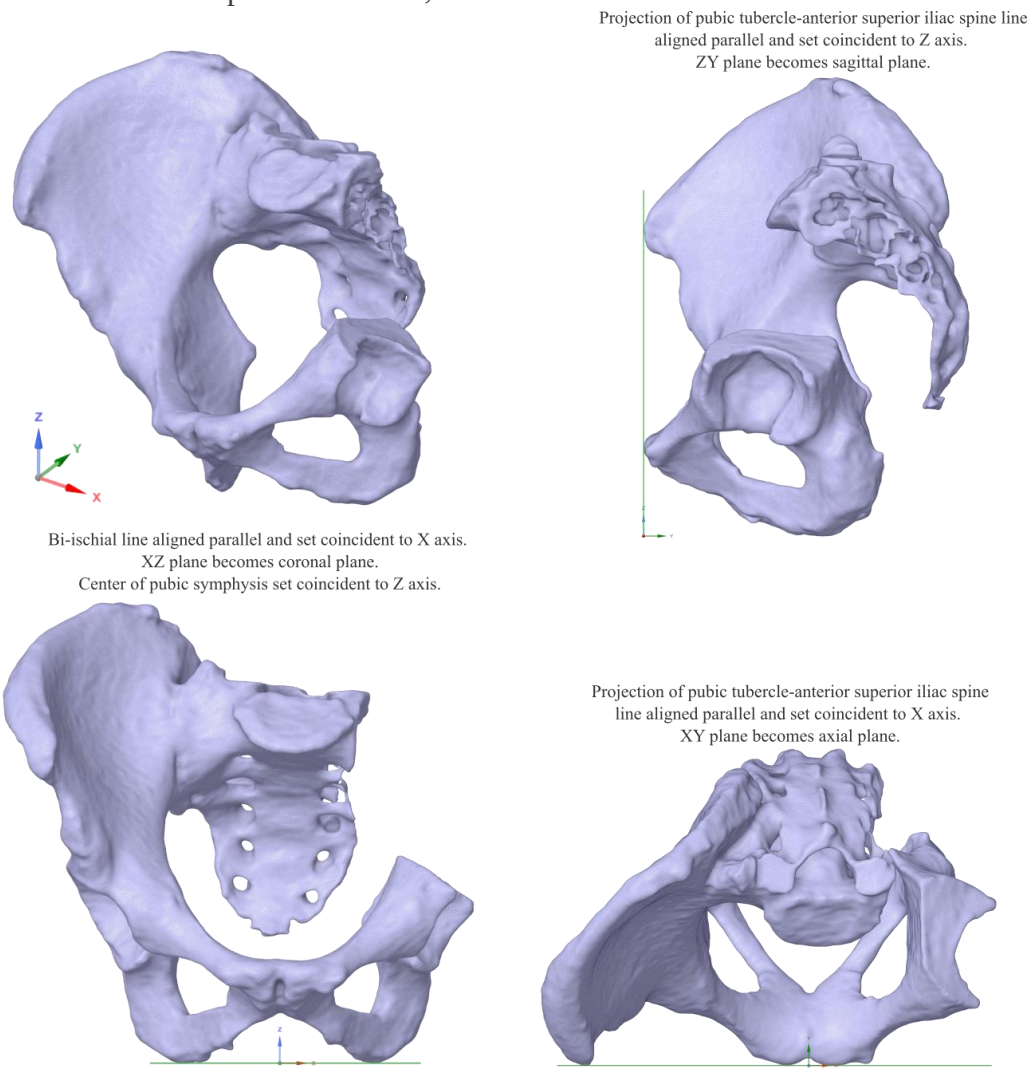

Figure 368: Anatomically alignment of post-resected pelvic mesh model to cartesian space

Asymmetry and offsets might have existed before the tumor resection but emerged mainly due to deformations caused after resection. To address these offsets, it is possible to use the centerline connecting the acetabula as a reference to align the pelvis to the cartesian coordinate system (override the classic anatomical landmarks of the pelvis used before) and transpose these misalignments. However, it was decided to keep the original alignment approach as a standard and align the left femoral head to establish a symmetrical result.

The endo-prosthesis must have shape and features conforming to the morphology of the patient's anatomy, however, as the resection was conducted by free-hand, and as only the hardest of the bone tissue was clearly visible in the CT-scan data, the exact amount and geometry of the less dense bony tissue at the resected surfaces were of concern. Hence, as was specified in the list previously, the roof of the left resected acetabulum and the side of the resected sacrum that serves as the endo-prosthesis bed had to be flat cut using personalized instrumentation to guarantee a precise fit. *Figure 370* presents the cut planes and the resultant flat surfaces. The maximum bone stock was planned to be preserved whilst ensuring sufficient flat surface area.

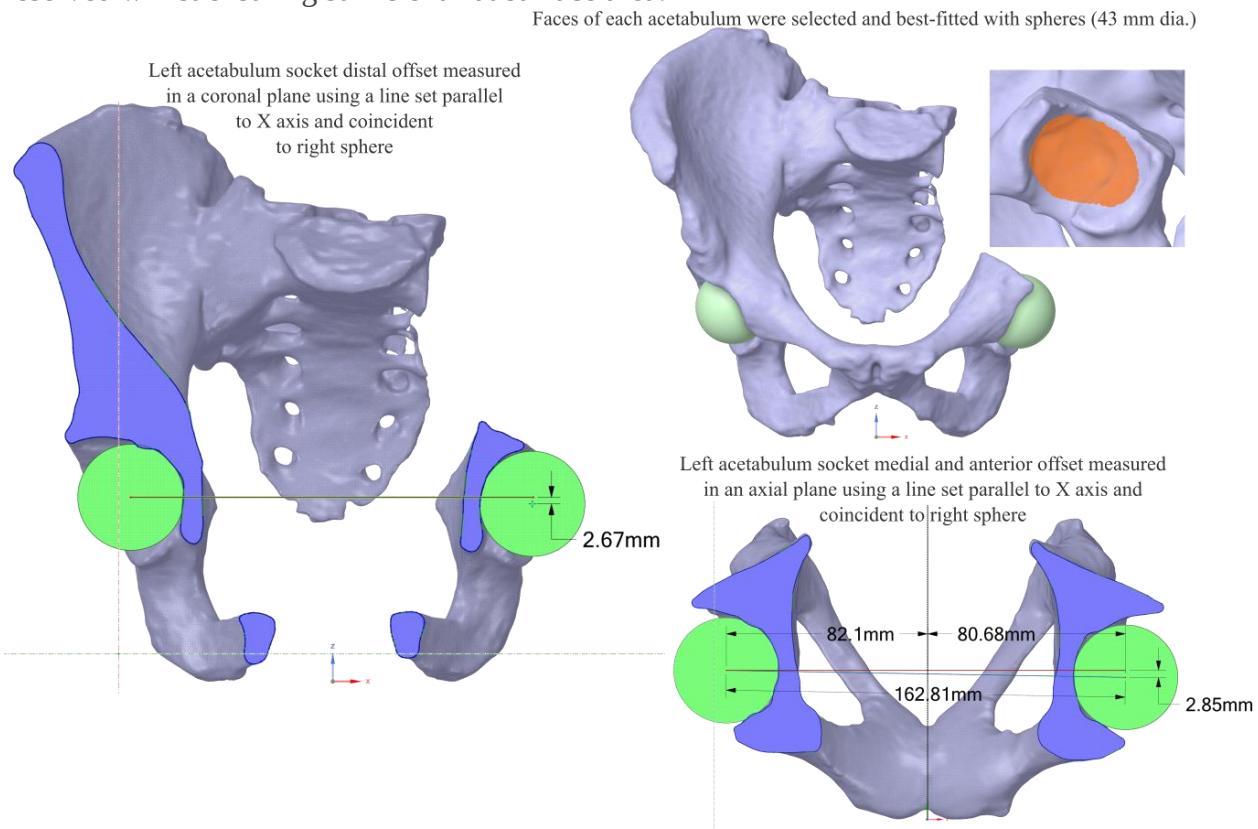

Figure 369: Measured offset between acetabula

It was decided that the components for the total left hip arthroplasty had first to be defined before the endo-prosthesis design. Total hip arthroplasty is among the most successful and popular operations thanks to decades of surgical and technological evolution *(Markatos et al., 2020)*. There are numerous materials developed to withstand mechanical loadings, minimize non-favorable biological phenomena, and minimize the wear between the components under tribological activities *(Merola and Affatato, 2019)*. The metallic acetabular shell to house the liner was integrated into the endo-prosthesis and was custom-made. Although many designs and inspirations exist *(see Sub-section 3.6)* to develop innovative and optimized custom-made femoral stems *(Guo et al., 2022)*, the femoral stem (and head) was selected off-the-shelf as there was no reason for customization due to increased manufacturing time and cost, not to mention certification and legislation issues as these were not emergency-use medical devices. Also, although various locking mechanisms exist *(Jaeger*

et al., 2020), the selected off-the-shelf liner was planned to be attached with bone cement into the acetabular shell for simplicity, and lower manufacturing cost and time for the endo-prosthesis.

For the acetabular shell to be positioned and placed within the left acetabulum, the required anteversion[146] and abduction[147] angles had to be established. Although the 2D slices of the CT-scanned data could have been used to measure these values, the 3D model was used instead. The method used to measure these angles is shown in *Figure 371*. The measured anteversion angle was 17,3° and 13,3° for the right and left acetabulum respectively, whereas the abduction angle for the right acetabulum was 39,8°. The values were rounded to 15° of anteversion and 40° of abduction angle, which were found to agree with and be within the *"safe zone"* for acetabular shell positioning as reported in the literature *(Figure 372) (Ha et al., 2012; Harrison et al., 2014; Snijders et al., 2018)*.

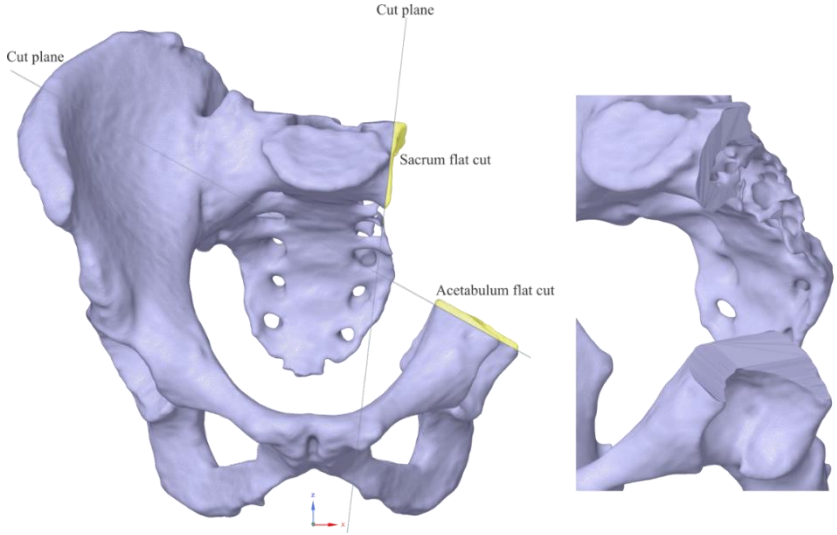

Figure 370: Cut planes and resultant flat surfaces on acetabulum rooftop and sacrum side

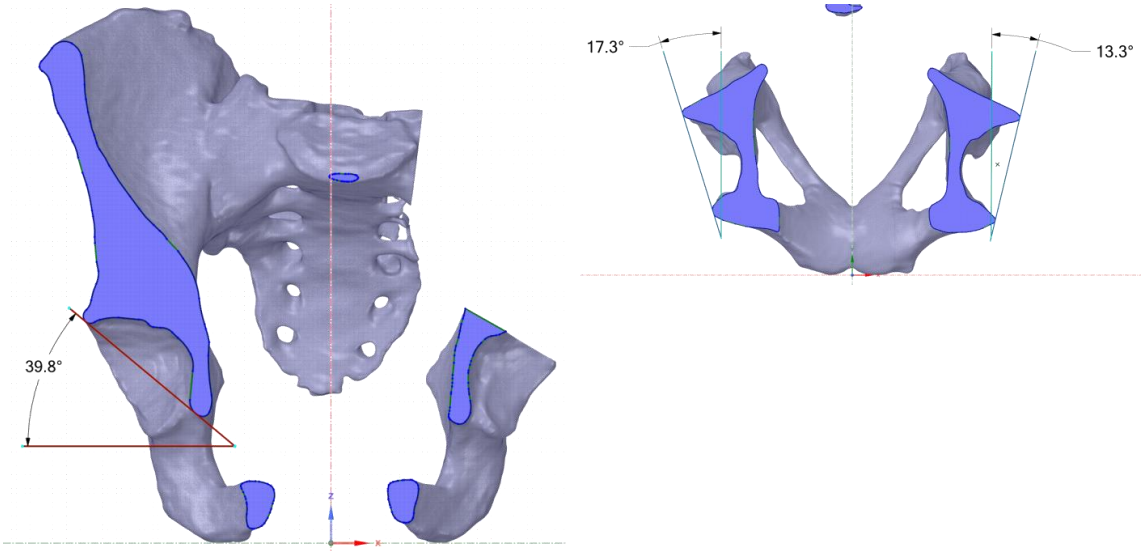

Figure 371: Measured anteversion and abduction angles for acetabular shell placement

[146] The acetabular anteversion angle is measured between the line connecting the anterior and posterior acetabular ridge and a reference line perpendicular to the line tangent to the anterior points of the pubic tubercles.

[147] The acetabular abduction angle is measured between the line connecting the acetabular teardrop to the lateral acetabular margin and the horizontal line connecting the ischial tuberosities (bi-ischial line).

However, it should be noted that these typical values of cup orientation "safe-zone" mentioned by Lewinnek et al. *(1978)*, have been found to differ significantly in some cases, hence patient-specific metrics are now suggested to be adopted *(Tezuka et al., 2019; Sharma et al., 2021)*.

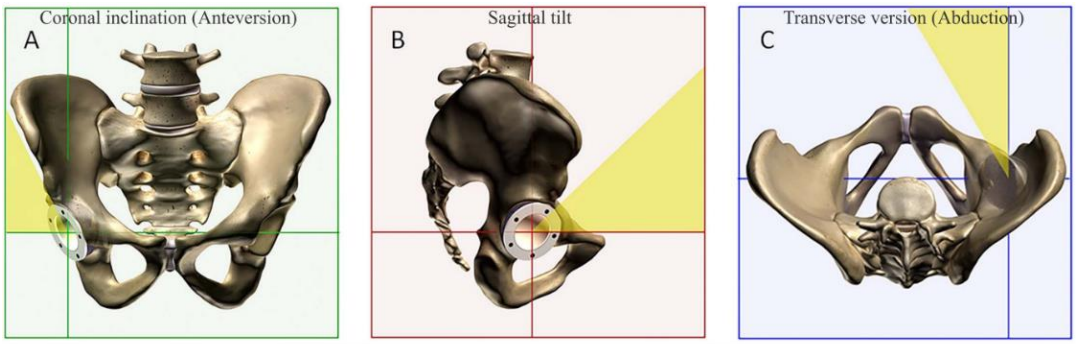

Three-dimensional surface diagram demonstrating the mathematical interrelation between coronal inclination, sagittal tilt, and transverse version. The blue area demonstrates the *"safe zone"* of Lewinnek.

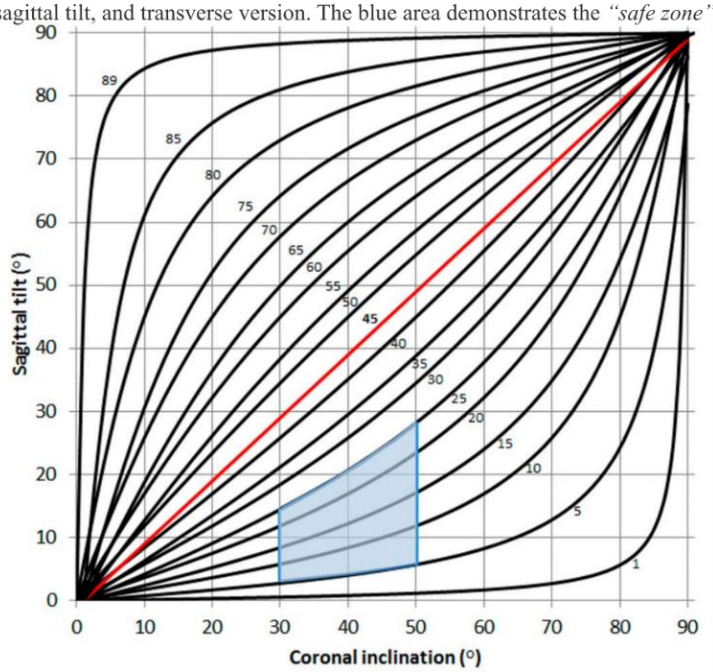

Figure 372: Safe zone of anteversion and abduction angles for acetabular shell placement. Source: (Snijders et al., 2018)

Figure 373 shows how the natural femoral head diameters were measured in 2D from CT-scanned slices and in 3D by fitting primitive spheres. The natural head diameters for both left and right femurs were 52 mm and this value was set as an initial reference for the outer diameter of the left acetabular shell to be integrated into the endo-prosthesis.

Then, the left femur was repositioned symmetrically to the right as follows *(Figure 374)*:

2. First, the right femur was rotated around its head center to achieve the standard 15° femur anteversion. This way, looking perpendicular to the coronal plane (anteroposterior), both lesser and greater trochanters are exposed. The long axis of the right femur was set parallel to the pelvic axis of symmetry (ZY sagittal plane). A normal 130° neck-shaft angle was measured.
3. The left femur was repositioned symmetrically with a) no lateral offset (92,2 mm from the pelvic axis of symmetry), b) no leg-length discrepancy, c) the long-axis set parallel to the pelvic axis of symmetry, and d) 2,43 mm anterior offset. A normal 130° neck-shaft angle was measured.

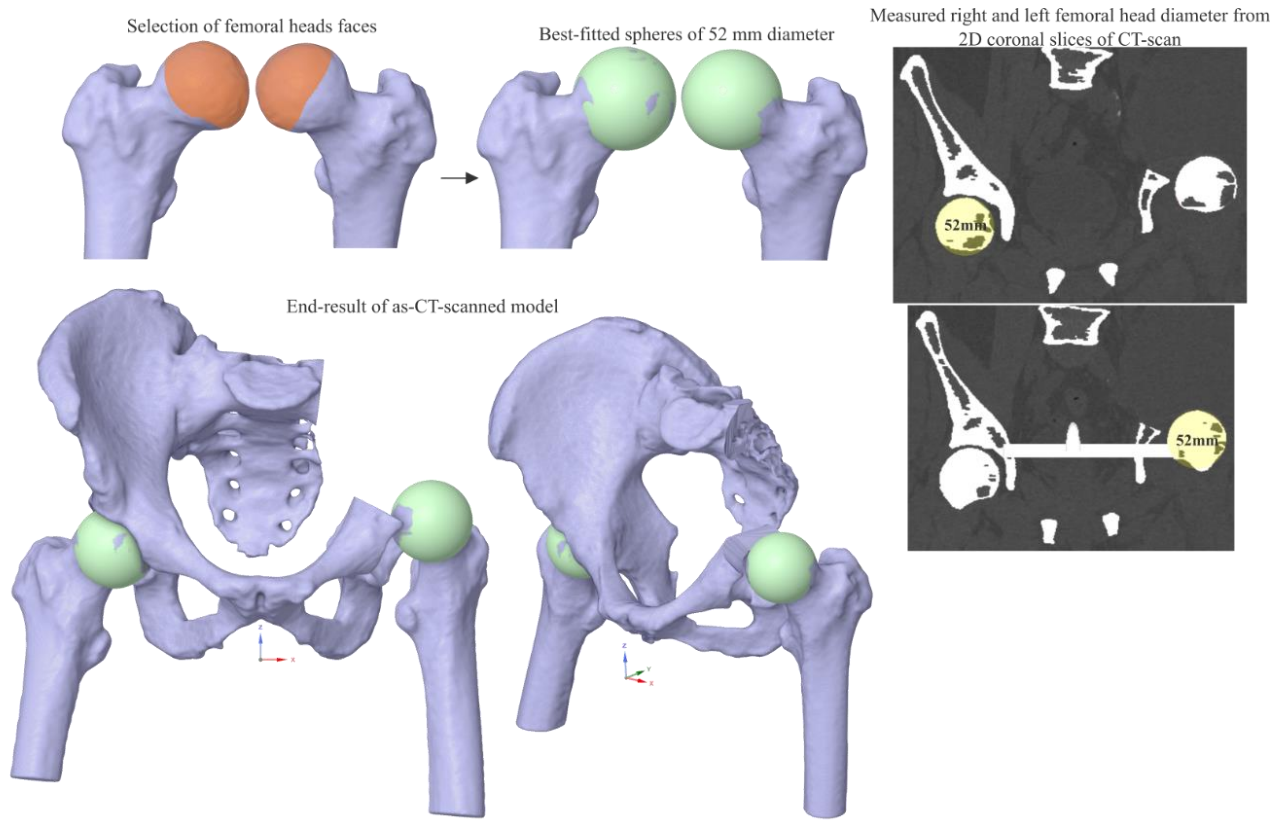

Figure 373: Femoral head diameter measurement

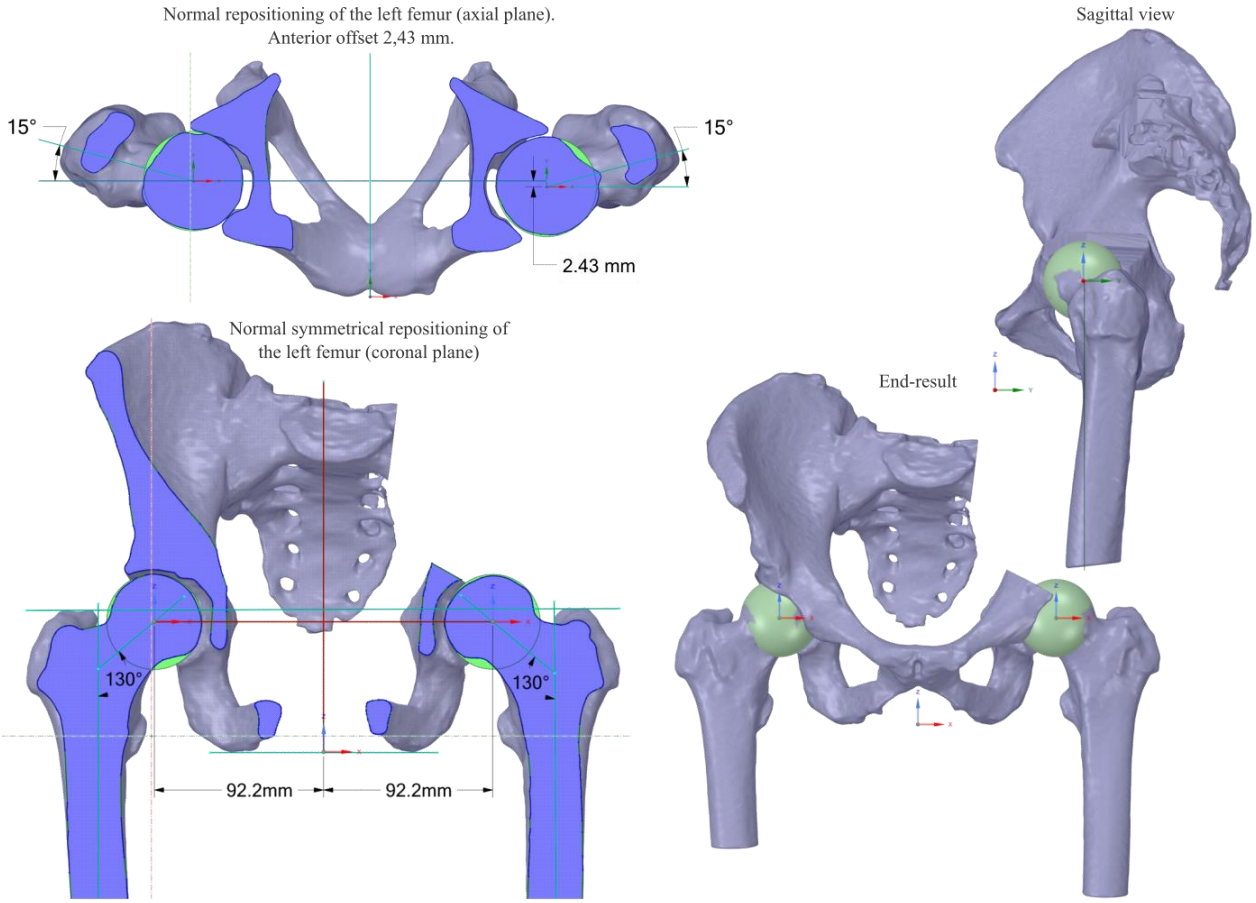

Figure 374: Normal repositioning of the left femur

Next, the femoral head size had to be defined by simultaneously considering the acetabular shell and liner thicknesses. The following notes were stressed:

- The tribological behavior and wear mechanisms of different femoral head-liner material combinations vary *(Knahr, 2013; Affatato, 2014)*. Metal on Ultra High Molecular Weight Polyethylene (UHMWPE) polymer combinations are the most common but ceramic on ceramic offers superior properties (low wear rate due to low coefficient of friction), however, their cost is considerably higher, audible squeaking is of concern, insertion of the liner is difficult, and fractures are common because of the increased stiffness *(Hu et al., 2015)*.
- The contact pressure changes as a function of the contact area. Thus, different head sizes affect not only stability and dislocation risk, but also wear, impingement, range of motion, and biomechanics *(Girard, 2015)*. The smaller the head size, the higher the revision risk due to dislocation and the higher the linear wear in metal-polymer combinations, whereas the larger the head size, the higher the volumetric wear *(Knahr, 2013)*.

For the highest possible stability and best hip function with the lowest possible wear to increase total hip arthroplasty longevity, Tsikandylakis et al. *(2018)* suggested the use of 32 mm head diameter for metal on UHMWPE combinations. Regarding the minimum recommended gold standard safe thickness for a UHMWPE liner, this was found to be is around 6 mm *(Girard, 2015)*, whereas thicknesses of standard acetabular cups in the orthopaedic devices industry are around 3-4 mm.

The acetabular shell of the endo-prosthesis could have been shaped with suitable features (similar to standard or dual mobility cups of the industry) to directly per se accept matching off-the-shelf liners that lock in place without cement *(Jaeger et al., 2020) (Figure 375)*. These options were declined given the fact that such features would require extra post-processing steps (machining and polishing) that would increase the total manufacturing time and cost. Hence, cementing a liner or a cup-liner combination was preferred.

Considering the previous, two options with off-the-shelf parts were explored *(Figure 376)*:

1. **32 mm femoral head diameter:** a 32/44 mm liner (Mueller II cup type) cemented (plus 1 mm clearance for bone cement) directly into the 46/54 mm acetabular shell of the endo-prosthesis.
2. **22 mm femoral head diameter:** a combination of a 22/38 mm mobile liner within a dual mobility[148] 38/44 (or 45) mm acetabular cup cemented (plus 0,5-1 mm clearance for bone cement) into the 46/54 mm acetabular shell of the endo-prosthesis. Dual mobility cups have cylindrical extensions (approximately 3 mm) that increase the jump distance[149] even further compared to hemispherical systems.

[148] A dual mobility cup consists of a "mobile liner" that has a dual articulation; femoral head-liner and liner-cup. These two distinct articulations achieve a greater range of motion before femoral neck impingement in a stable environment.

[149] It is the distance that the femoral head must travel to dislocate. The greater the jump distance, the greater the hip stability. It depends on the combination of femoral head size, cup depth, and inclination.

Figure 375: Taper-lock and anti-rotation features of standard and dual mobility cups. Source: DePuy Synthes

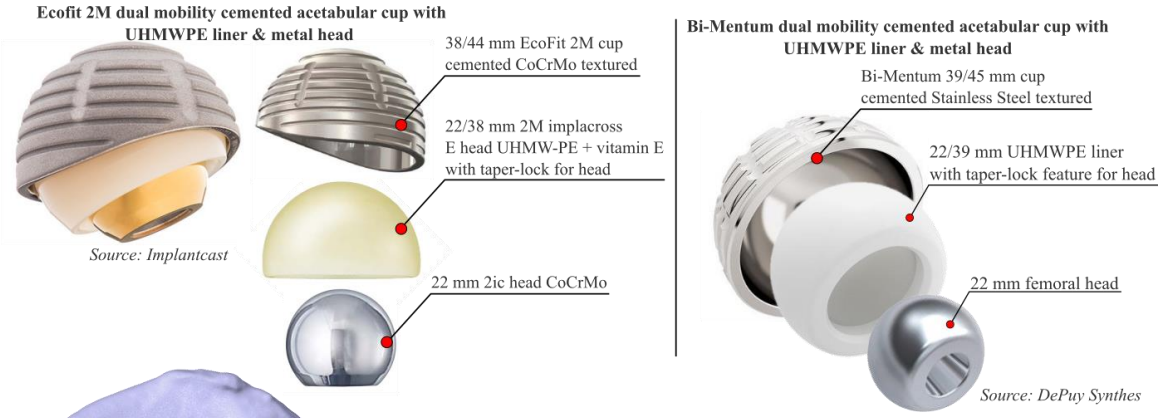

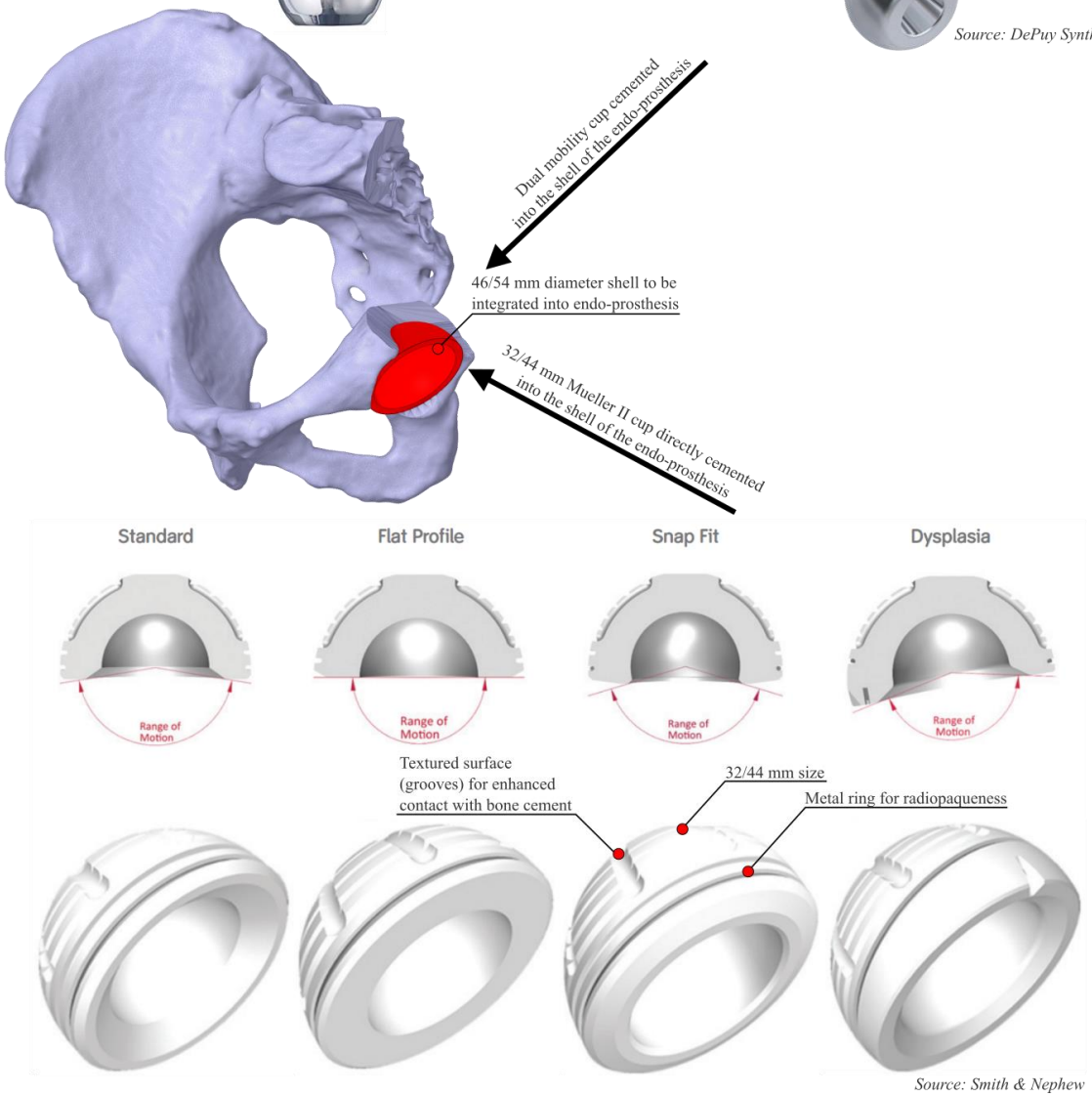

Figure 376: Cemented liner and cemented cup-liner combination options

Due to the en bloc resection of the iliac bone and the minimum remnant compartmental soft tissue including the abductor and gluteus muscles, to minimize the dislocation risk, the Mueller II snap-fit cup could have been used but a dual mobility cup was chosen; dual mobility systems have been found to improve the jump distance and so the dislocation risk, especially in patients at a high risk of instability (e.g. older, neuromuscular deficit) *(Martino et al., 2014; Ko and Hozack, 2016; Moon et al., 2022)*. In a ten-year follow-up of patients who received cement-less dual mobility cups, no aseptic loosening, dislocation, or intra-prosthetic dislocation was reported *(Laurendon et al., 2018)*. The use of dual mobility cups is being suggested and encouraged in the literature *(Neri et al., 2020)*, not only for patients at dislocation risks but even for everyone *(Blakeney, Epinette and Vendittoli, 2019; Aguado-Maestro et al., 2022)*.

According to the previous, the Bi-Mentum (DePuy Synthes, a company of Johnson & Johnson Services Inc., New Jersey, US) dual mobility cemented acetabular cup system for a 22 mm femoral head size was selected, so a matching stem had to be chosen.

Figure 377 shows the new center of rotation of the left hip socket. A 54 mm diameter sphere was set concentric with the previously fitted 43 mm sphere in the left acetabulum and translated along a direction perpendicular to a 15° anteversion and 40° abduction plane so that as much subchondral bone stock is preserved whilst achieving a clear true hemispherical reaming. Hence, the new acetabulum sphere center of rotation had 8,80 mm medial and 0,82 mm distal offset from the center of the natural femoral head, whereas the anterior offset of the left from the right femoral head was increased to 3,04 mm as it was aligned to the center of the acetabulum sphere.

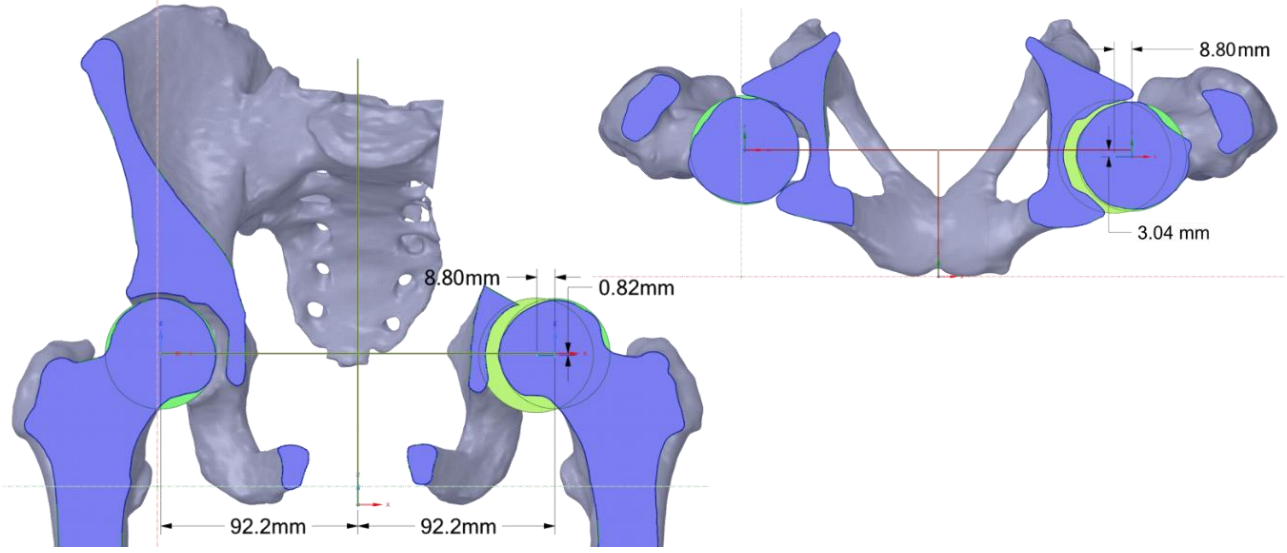

Figure 377: New left acetabulum center of rotation

The medial and distal offsets had to be addressed a) by developing a custom or choosing an off-the-shelf femoral stem, or b) by offsetting the acetabular center of rotation by adding material to the shell or by using a cup/liner with an offset center. As most compartmental soft tissue was resected, to minimize the hip joint reaction force and the dislocation risk, although higher stresses would

emerge within the femoral canal, it was decided to search for a suitable off-the-shelf femoral stem that would maintain the femoral bone in the natural position as much possible whilst approaching the new medially offset center of rotation. *Figure 378* illustrates the 54 mm diameter 4 mm thick shell within the reamed acetabulum with a 3 mm extension to house the selected dual mobility cup.

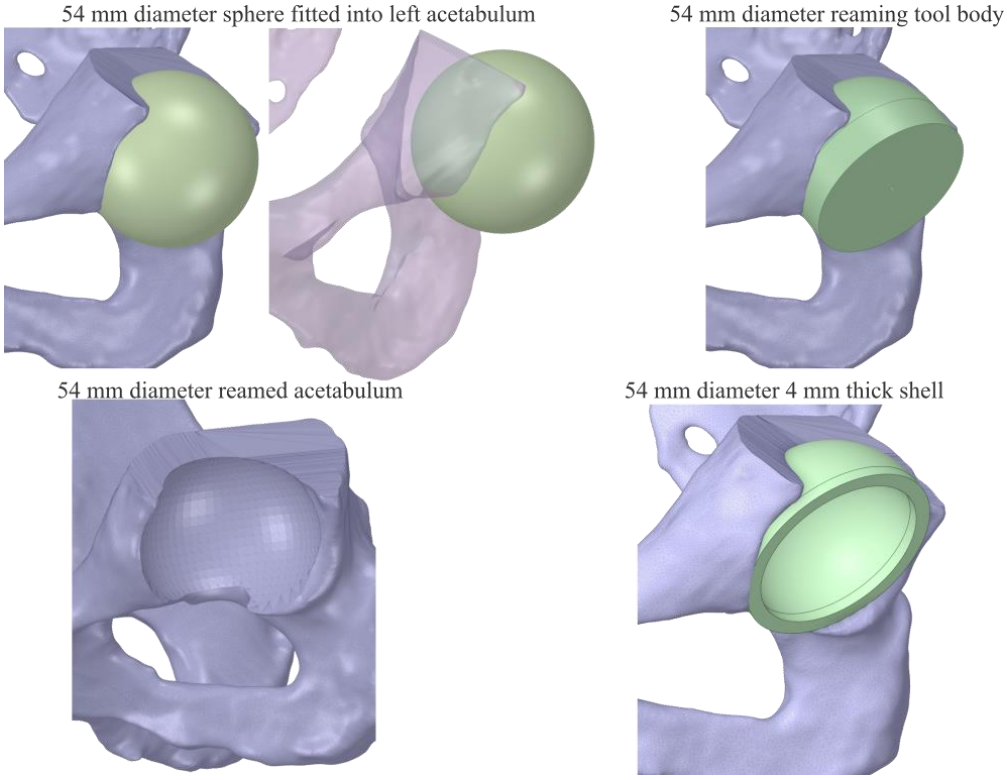

Figure 378: Endo-prosthesis acetabular shell part in the left reamed acetabulum

Figure 379 shows the process for selecting the off-the-shelf femoral stem to match the needs: maintain as much symmetry and eliminate leg-length discrepancy. The femoral head was rotated to 0° anteversion to facilitate measurements and templating from the coronal plane. The selected femoral stem was the Tri-lock Ti alloy stem with Ti coating (63% microtextured porosity with 300 μm pore size) with reduced distal medial-to-lateral width and narrow anterior-to-posterior width, coupled with a matching 22 mm diameter metal (CoCrMo) head. The 6 high-offset +1,5 mm stem size was found to be the most suitable from the catalog, resulting in a 3 mm medial offset of the femur bone and an 8,8 mm medial offset of the natural head center from the new acetabular center of rotation. The 6 high-offset +5 mm size maintained the femur bones symmetrical with an 8,8 mm medial offset of the natural head center from the new acetabular center of rotation, but the stem would exceed the safe margins by almost consuming the compact shell of the femoral neck section.

Figure 380 illustrates the dual mobility system components placed within the left acetabulum and the cut femoral neck with the stem inserted into the canal, i.e. 46/54 mm shell, 39/45 textured cemented cup, 39/22 mm mobile liner, 22 mm femoral head size and 6 high-offset +5 mm stem.

Figure 381 shows the final measurements of the arthroplasty components with the left center of rotation being 3,04 mm anteriorly offset and 8,8 mm medially offset with no leg length discrepancy.

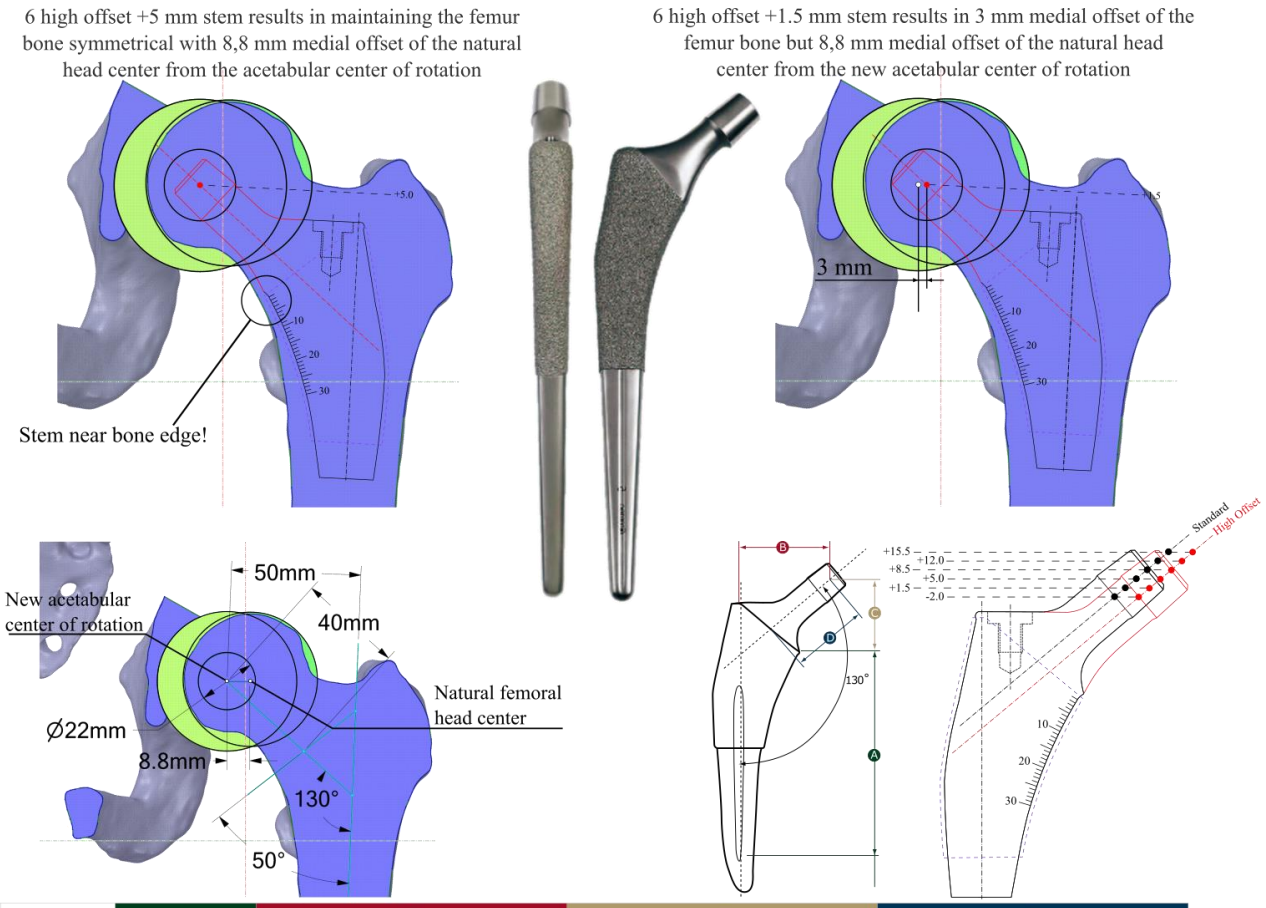

Size	A Stem Length (mm)	B Offset with Head (mm)						C Leg Adjustment Length with Head (mm)						D Neck Length with Head (mm)					
		-2	+1.5	+5	+8.5	+12	+15.5	-2	+1.5	+5	+8.5	+12	+15.5	-2	+1.5	+5	+8.5	+12	+15.5
6 Standard	107	36	39	42	44	47	50	28	30	32	34	37	39	28	32	35	39	42	46
6 High	107	44	47	50	52	55	58	28	30	32	34	37	39	33	37	40	44	47	51

Figure 379: Selected femoral stem: DePuy Synthes' Tri-lock

Next, the number and positions of fixation points and their orientation were determined. There are different types of bone screws in various diameters, and lengths *(Figure 383)*. Selection of optimal bone screw includes several variables: fixation site, bone quality (density) and morphology, anatomical constraints, attempted fixation strength and performance (mechanical, biological), and geometrical characteristics and function of the endo-prosthetic implant to be fixed.

It is true that to establish precisely the screws positions, orientation, diameters, and lengths for a unique patient, multi-modal CT, MRI, Computed Tomography Angiography (CTA), neurography imaging, and personalized anthropometric data are required *(Park et al., 2021)*. *Figure 382* shows an example with a customized endo-prosthesis attached to the bony pelvis (CT) with bone screws whilst accounting for neurovascular tissue (CTA, MRI) and aligned/registered with suitable algorithms *(Yu et al., 2021)*, though more detail would be needed for precision. A similar 3D model was generated for this purpose for this particular case as shown previously (*Figure 326*) using the automatic soft and hard tissue segmentation methodology (Total Segmentator) which can segment vascular tissue (arteries and veins) from CT scans.

The pullout strength of a bone screw is affected by the material (biocompatibility), surface and type of screw used, diameter of pilot hole (for non-self-drilling), tapping (for non-self-tapping), pitch and depth of thread, length of thread engaged, core diameter, insertional torque, and mainly by tissue density and strength *(Chapman et al., 1996; Steeves et al., 2005; Azwan and Rahim, 2011)*.

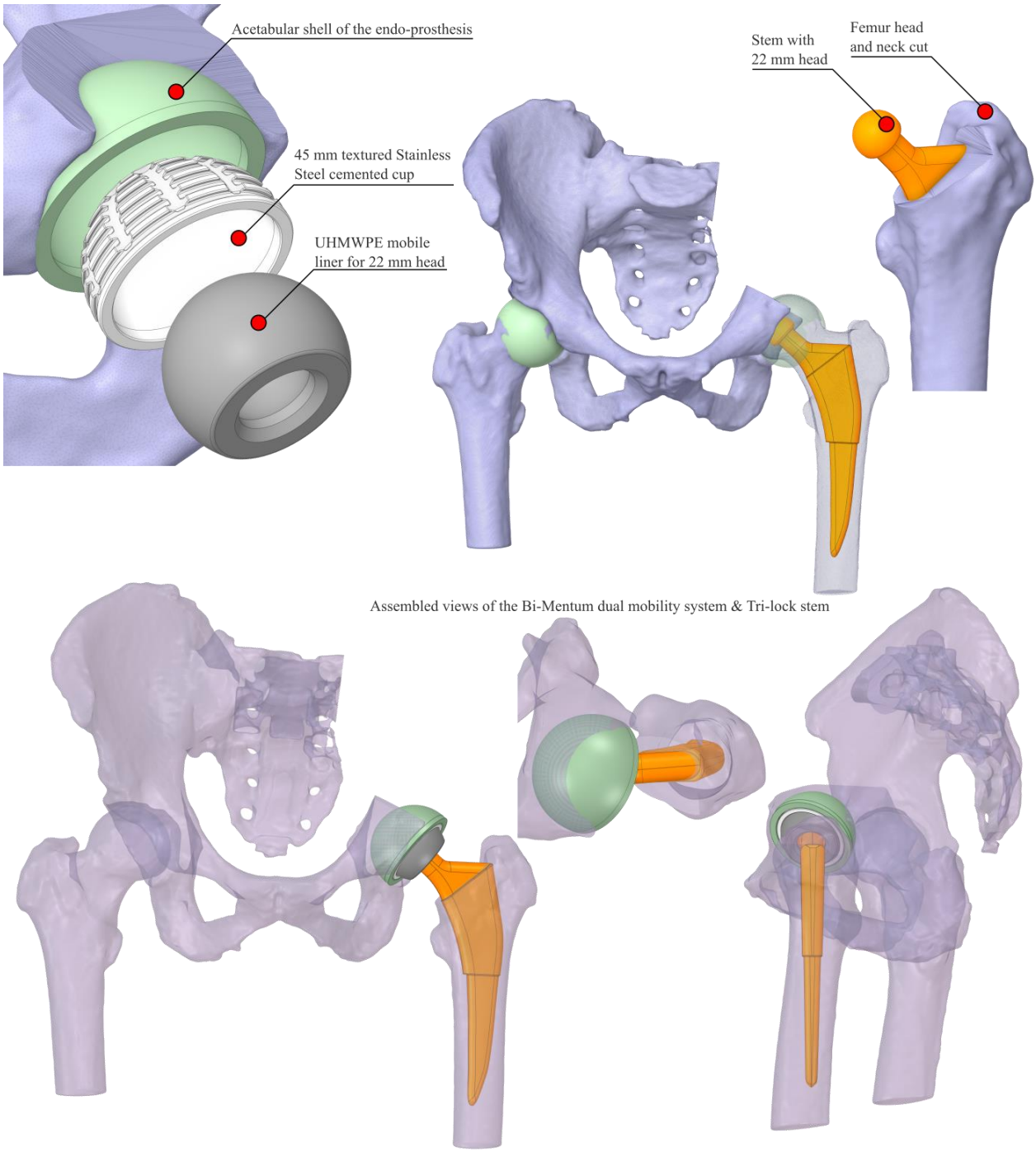

Figure 380: Femoral neck cut and views of the stem inserted in the femoral canal

During bone drilling and screw insertion, many different phenomena occur and have to be considered, e.g. thermal bone necrosis due to excessive heat generated *(Pandey and Panda, 2013; Jamil et al., 2020)*. When screws are inserted within the bone, they not only affect its blood supply but also act as mechanical reinforcements changing its mechanical performance. The more and the larger (diameter, length) the bone screws inserted, the more problematic the bone healing due to the

amount of damaged tissue, and bone remodeling due to the dissimilar amount of material. On the other hand, the more screws and length engaged into the bone, the better the anchorage.

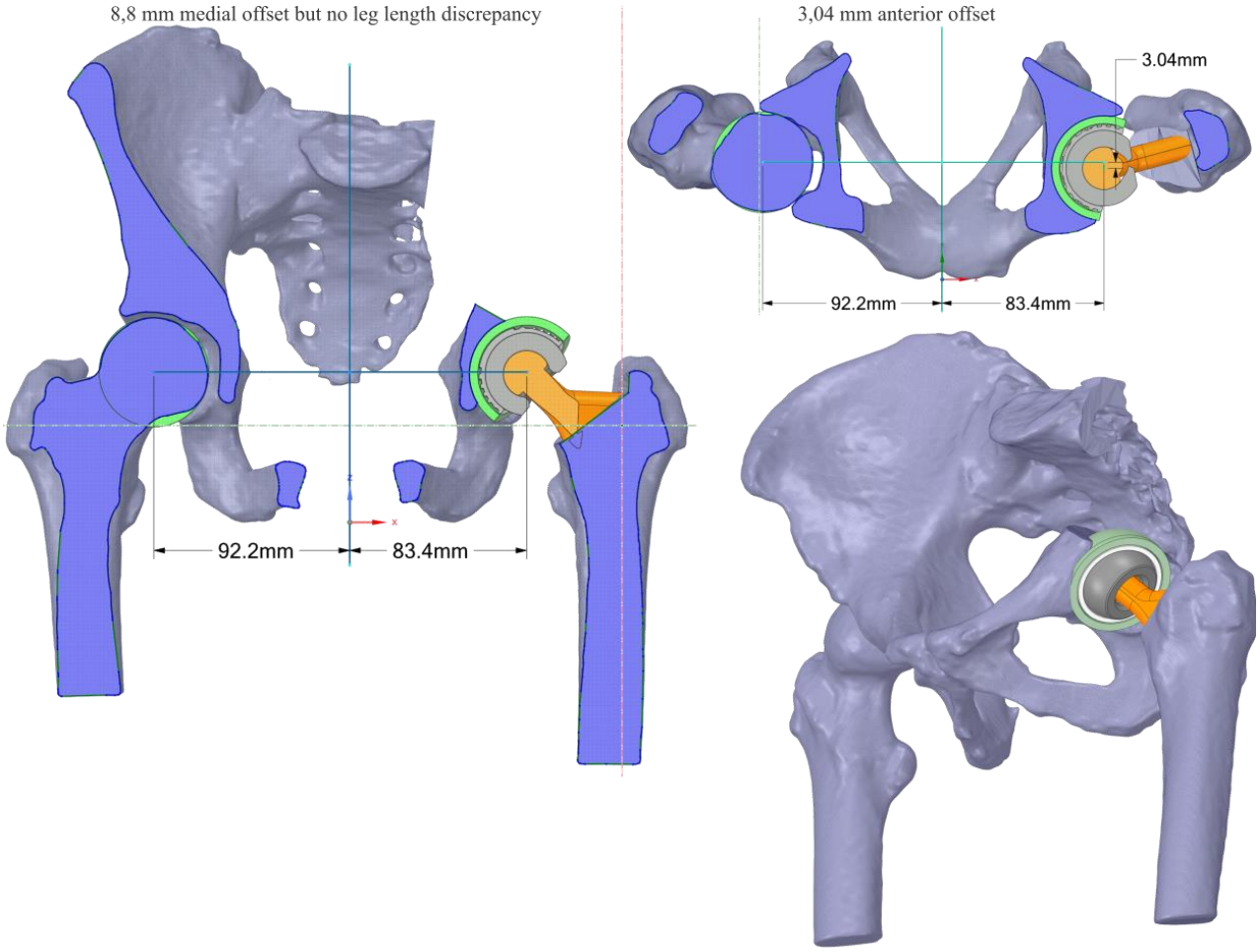

Figure 381: Components of total left hip arthroplasty

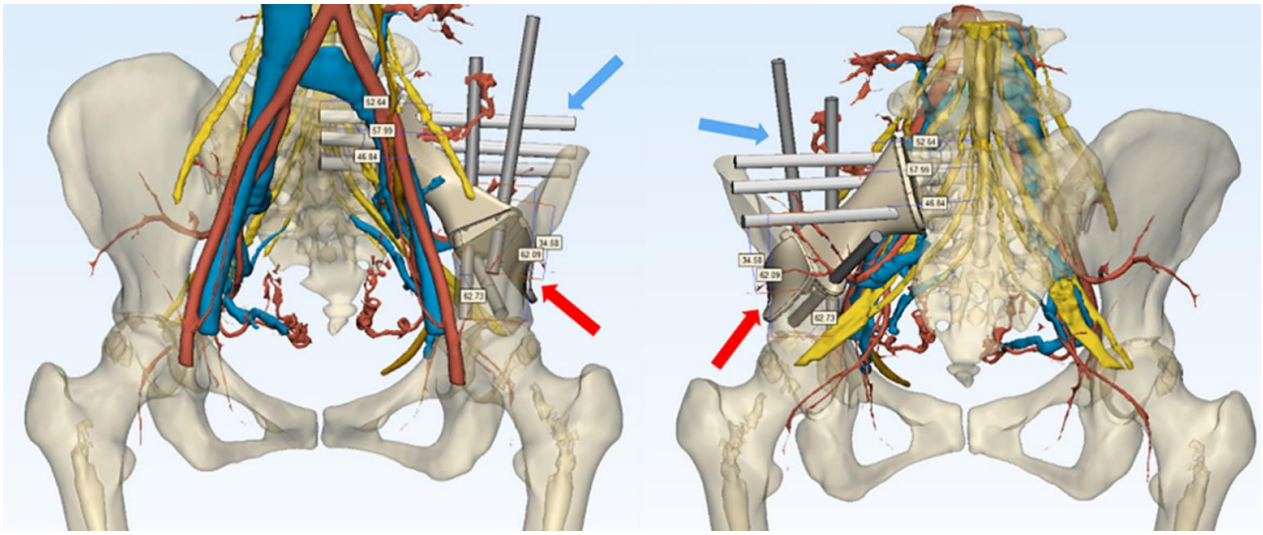

Figure 382: Multi-modal 3D digital model of the pelvis and reconstructive endo-prosthesis. Source: (Yu et al., 2021)

Porous cylindrical fixation stems and bone screws with roughened-by-coatings or with integrated porosity, experience enhanced pullout and biological performance: greater friction increases pullout strength and open pores allow biological fixation through bone ingrowth. Also, 3DP methods have been successfully used to make porous bone screws with positive clinical outcomes *(Yang et al.*,

2014). Such custom bone screws or stems with any desired diameter and length, head, surface, and thread characteristics could have been designed and employed to be 3DPed out of metal biomaterial, for example, *Figure 384* shows custom bone screws 3DPed using Ti alloy powder. It is worth mentioning that bone screws made of biodegradable materials *(Pina and Ferreira, 2012a; Pina and Ferreira, 2012b)* are promising future options as these have the potential to minimize heterogeneity and reduce impacts on bone's mechanical and biological functions, however, these have not been yet clinically approved to be routinely used. Stem and hook options will be shown at the end of the embodiment design section, but it was decided to apply exclusively standard off-the-shelf solid Ti cancellous bone screws for the fixation of the endo-prosthesis.

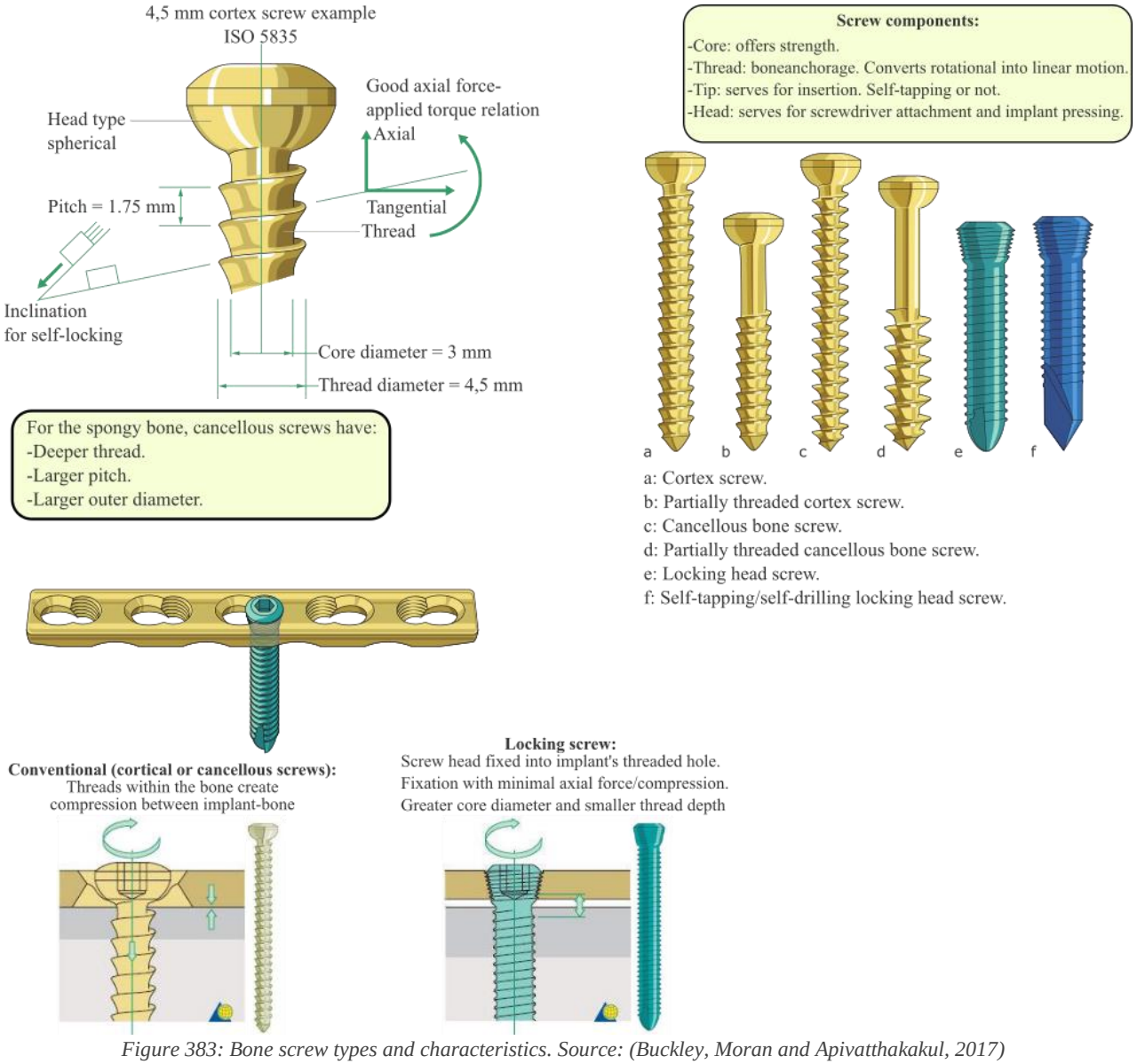

Figure 383: Bone screw types and characteristics. Source: (Buckley, Moran and Apivatthakakul, 2017)

Six bone screws were positioned and oriented as per the bone morphology, surrounding soft tissue *(see Figure 326)*, and bone quality as seen from the CT-scanned images. The goal was to obtain adequate initial stability by mechanical fixation. All screws were examined along their entire length using slices perpendicular to their axes. More specifically *(Figure 385)*:

1. Two 4 mm diameter cancellous screws were inserted 25 mm into the pubis and the ischium. These will push the shell towards the acetabulum. The length was determined based on the quadrant system as described by Wasielewski et al. *(1990)* which is a reference that guides safe screw placement within the acetabulum by dividing the acetabulum from the anterior-superior iliac spine caudally and then bisecting the acetabulum into four quadrants as shown *Figure 386*.
2. Two 6,5 mm diameter cancellous screws were inserted 30 mm from the acetabulum rooftop.
3. Two 6,5 mm diameter cancellous screws were inserted 50 mm within the sacrum. Most males and females can accommodate up to 8 mm diameter screws in S1 and S2, with the optimal safe entry point of the transverse screw being in the first 1/3 of the cancellous corridor for S1 and the center of the cancellous corridor for S2 as seen from the standard lateral perspective *(Figure 387) (König et al., 2015; Wu et al., 2020).*

Figure 384: Custom porous bone screws 3DPed out of Ti alloy powder. Source: nTopology

The selected number, diameter, and length of bone screws were the minimum to guarantee adequate fixation, avoiding loosening, dislocations, and mechanical failures. All selected bone screws are off-the-shelf components and are cancellous (to be inserted into the spongy bone (trabecular)), self-tapping (requiring only pilot hole pre-drilling), made out of Ti, and fully threaded. Locking head cancellous screws could be optionally placed, with extra post-machining time and cost for threading the screw holes. Alternatively, long porous stems or 8 mm cancellous screws could have been employed optionally.

Granted that the fixation screws were defined, the healthy right ilium was mirrored using the ZY sagittal plane *(Figure 388),* and all components (anatomical model with flat cut surfaces and reamed acetabulum, mirrored ilium, screws, shell, stem, dual mobility system) were exported *(Figure 389)* to be imported into Fusion 360 to model the endo-prosthesis.

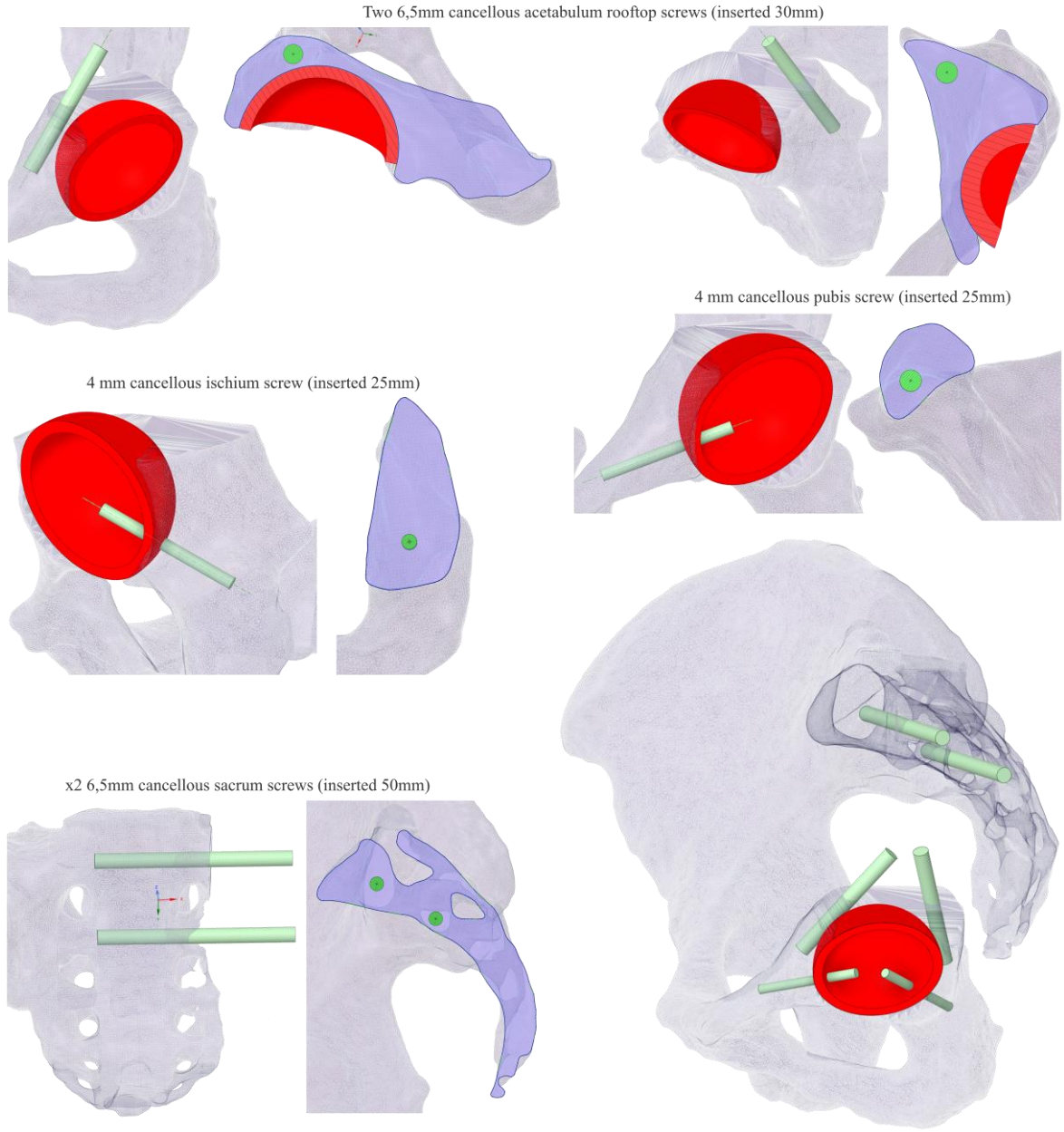

Figure 385: Points and orientation for screws insertion

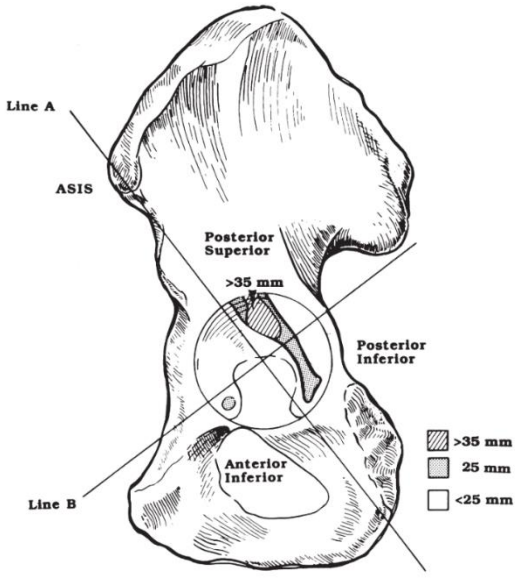

Figure 386: Optimal and safe insertion points and lengths of acetabular screws. Source: (Wasielewski et al., 1990)

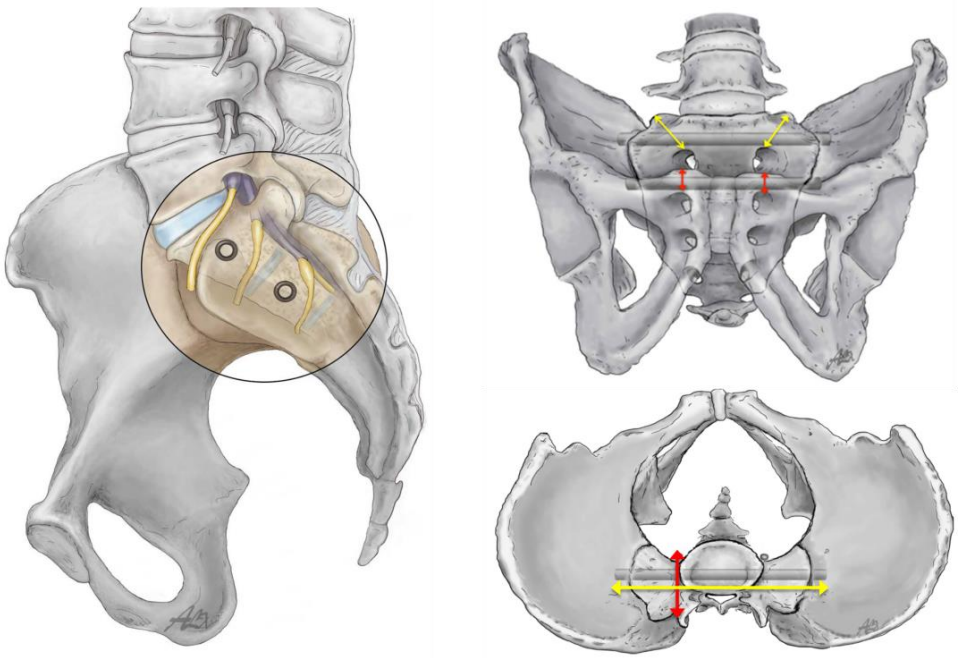

Figure 387: Optimal insertion points of sacral screws. Source: (König et al., 2015)

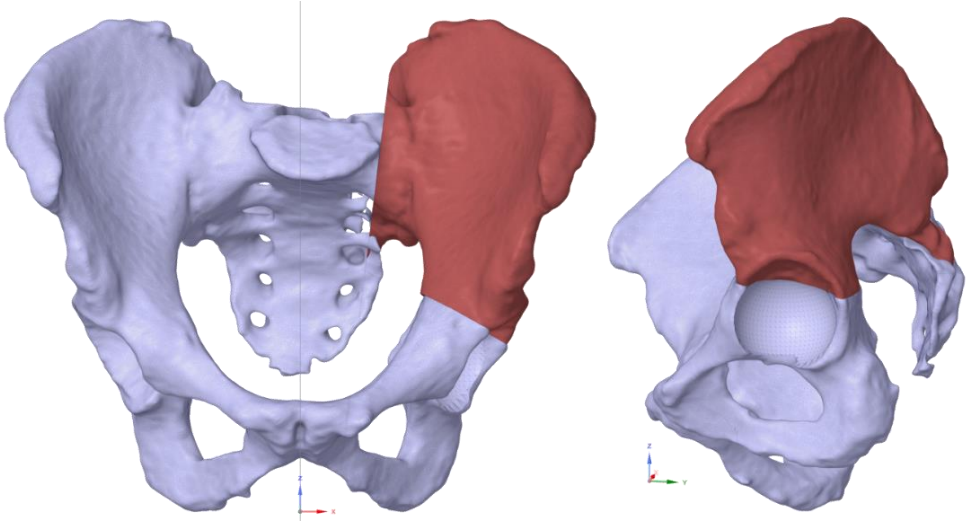

Figure 388: Healthy right ilium mirrored

The endo-prosthesis design followed to reconstruct the iliac bone loss and reinstate full weight bearing. After the en bloc resection, minimum soft tissue remained to account for porous surfaces and holes for re-attachment and suturing of remnant soft tissue, however, four holes were opened to allow de-powdering of the endo-prosthesis after its 3DP and for possible suturing.

Theoretically, uncemented elliptic cups would achieve greater strains at their periphery with less impaction force, however, they were found to be associated with more complications and fractures, and exhibit worse overall implant stability compared to hemispherical cups *(Hasegawa et al., 2017; Brown et al., 2017; Patsiogiannis, Kanakaris and Giannoudis, 2021).*

For cement-less porous acetabular cups, studies have shown that *(Hsu et al., 2007)* a) bone properties (mostly) and friction coefficient affect the stability, b) to achieve osseointegration, it is necessary to minimize micro-gaps not only at the central area but also at the rim edge, c) screws reduce the relative micromotion locally and favor osseointegration at these locations, d) it is

unnecessary to insert several screws closely together, e) the subchondral bone provides biomechanical advantage due to its high stiffness but reaming until well-vascularization and well-bleeding facilitates osseointegration.

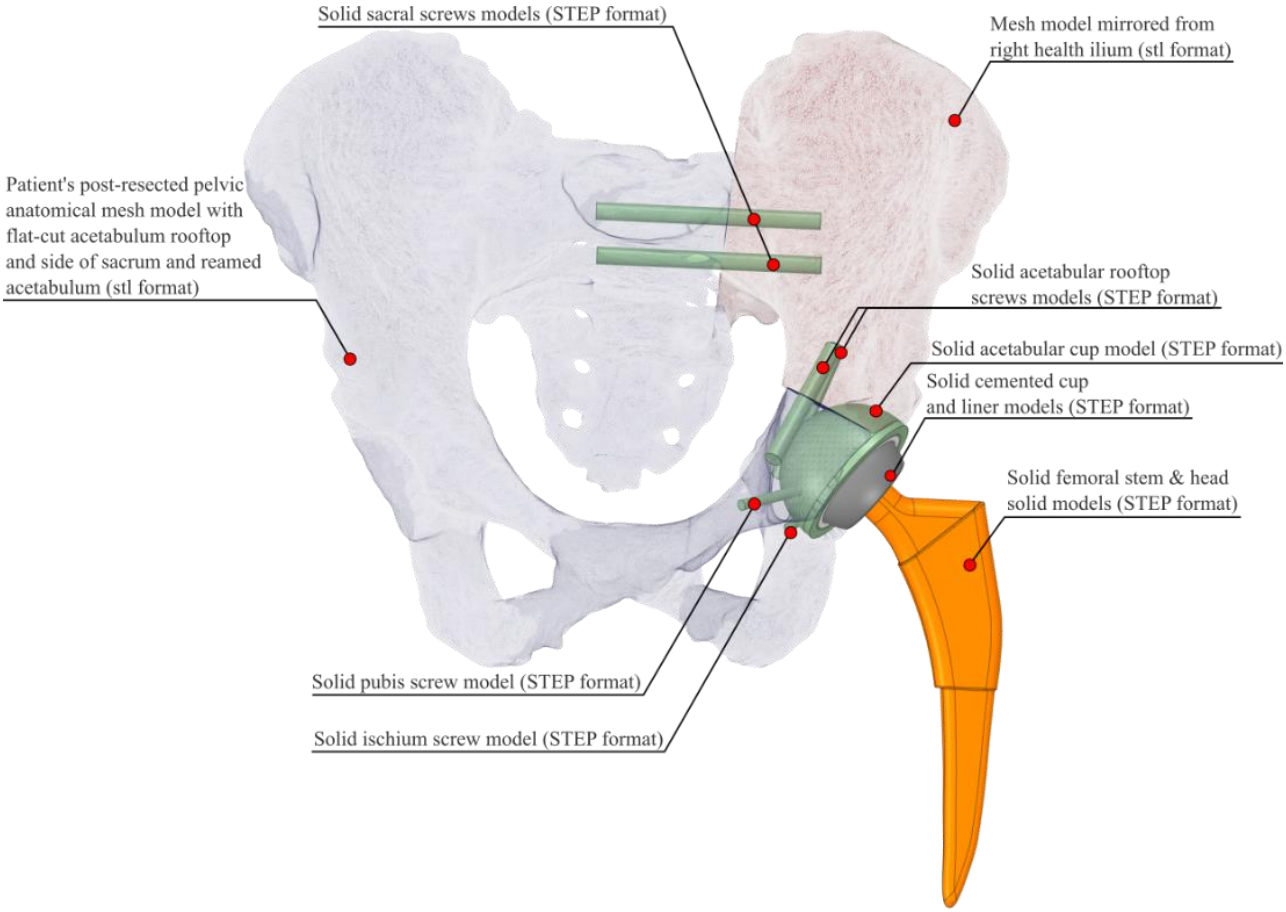

Figure 389: Exported components to model the endo-prosthesis

In this particular case, over-impaction and high-energy impacts on the acetabulum could generate great hoop stresses and damage the pelvic bone *(Ruhr, Baetz, Pueschel and Morlock, 2021)*. Press-fitting the endo-prosthesis into the acetabulum might result in adjustment difficulties intra-operatively, which of course can be addressed by reaming the acetabulum with a larger reamer. The designed 54 mm diameter 4 mm thick hemispherical acetabular shell was planned to be fixed with two 4 mm cancellous screws into the acetabulum after it was fitted into the under or exactly reamed acetabulum (52-54 mm diameter, to be decided intra-operatively) and its overall fit has been verified. The sclerotic subchondral bone was planned to be reamed truly hemispherical whilst simultaneously obtaining a well-vascularization and well-bleeding bone, and also preserving as much tissue.

Before commencing the modeling of the endo-prosthesis, it was decided to convert the triangular .stl format faced anatomical model to a solid body so that it would serve the later design and simulation needs. The following options were explored:

1. In Fusion 360, facet .stl models can be converted into solid bodies by choosing a facet, prismatic, or organic approach. First, the mesh body was directly converted into a solid body with each

unique triangle corresponding to a surface, resulting in a 441 MB STEP[150] file size which was hard to work with. For this reason, the organic option was selected which resulted in a T-Spline[151] model which in turn was converted into a Boundary Representation (B-Rep[152]) model, and exported to a 60,2 MB STEP file. *Figure 390* shows the outputs of these two approaches.

2. The .stl mesh was converted into a quadrilateral mesh which is friendlier for design and simulation software compared to triangular meshes. There are numerous tri-to-quad conversion methods *(Bommes et al., 2013)*. The original triangular mesh with 201.084 vertices, 402.240 triangles, and 19,6 MB .stl file size was first remeshed into 26.8752 vertices, 53.785 faces, and 4,6 MB quadrilateral mesh .obj file using the Quad Remesh tool in Rhinoceros, and then converted into two types of solid models *(Figure 393)*:
    a. In Rhinoceros, the quad mesh was converted into a Non-uniform Rational Basis Spline (NURBS[153]) solid with 26400 surfaces and exported to a 40,9 MB STEP file.
    b. In Fusion 360: the quad mesh was converted into a T-Spline model with the Quad-to-T-Spline tool (precise) and then converted into a B-Rep solid before exported to a 49,6 MB STEP file. Also, another less precise but more lightweight B-Rep model (24,1 MB STEP file) was generated using the organic conversion tool with the high accuracy option selected.

Figure 393 and *Figure 394* show the conversions and the comparison among the solid models and meshes. Although not as smooth, the NURBS solid was preferred as it was found to be the most accurate conversion from the quadrilateral mesh. Hence, the triangular surface mesh model or the NURBS solid was used as per the design and simulation needs *(Figure 391)*.

It was decided first to complete modeling the acetabular shell *(Figure 392)*. In Fusion 360, the as-imported shell was textured with spheroids that were cut (0,5 mm of material removed) by 3 mm diameter spheres populated on the internal surface of the shell for better anchorage of the bone cement that will fix in place the cemented shell and two screw holes for 4 mm cancellous bone screws were added to the textured shell (as per pre-defined orientations and points) to fully house their heads *(Figure 392)*. All cancellous bone screws were modeled in Fusion 360 as per ISO 5835 *(Figure 395)*.

[150] A STEP file is a widely used data exchange form that stands for "Standard for the Exchange of Product model data". It is based on ISO 10303 which represents 3D objects in CAD and provides related information.

[151] T-spline is a mathematical model for defining freeform surfaces defined by a network of control points. T-splines can be converted into NURBS surfaces and vice versa.

[152] Boundary Representation (B-rep) is a method for representing a 3D shape as a collection of connected surface elements, defining the boundary between interior and exterior points (limits of its volume).

[153] Non-uniform rational basis spline (NURBS) is a mathematical model of basis splines (B-splines) representing curves and surfaces. NURBS model curves in contrast to polygonal modeling or digital sculpting and is part of industry-wide standards, e.g. IGES, STEP.

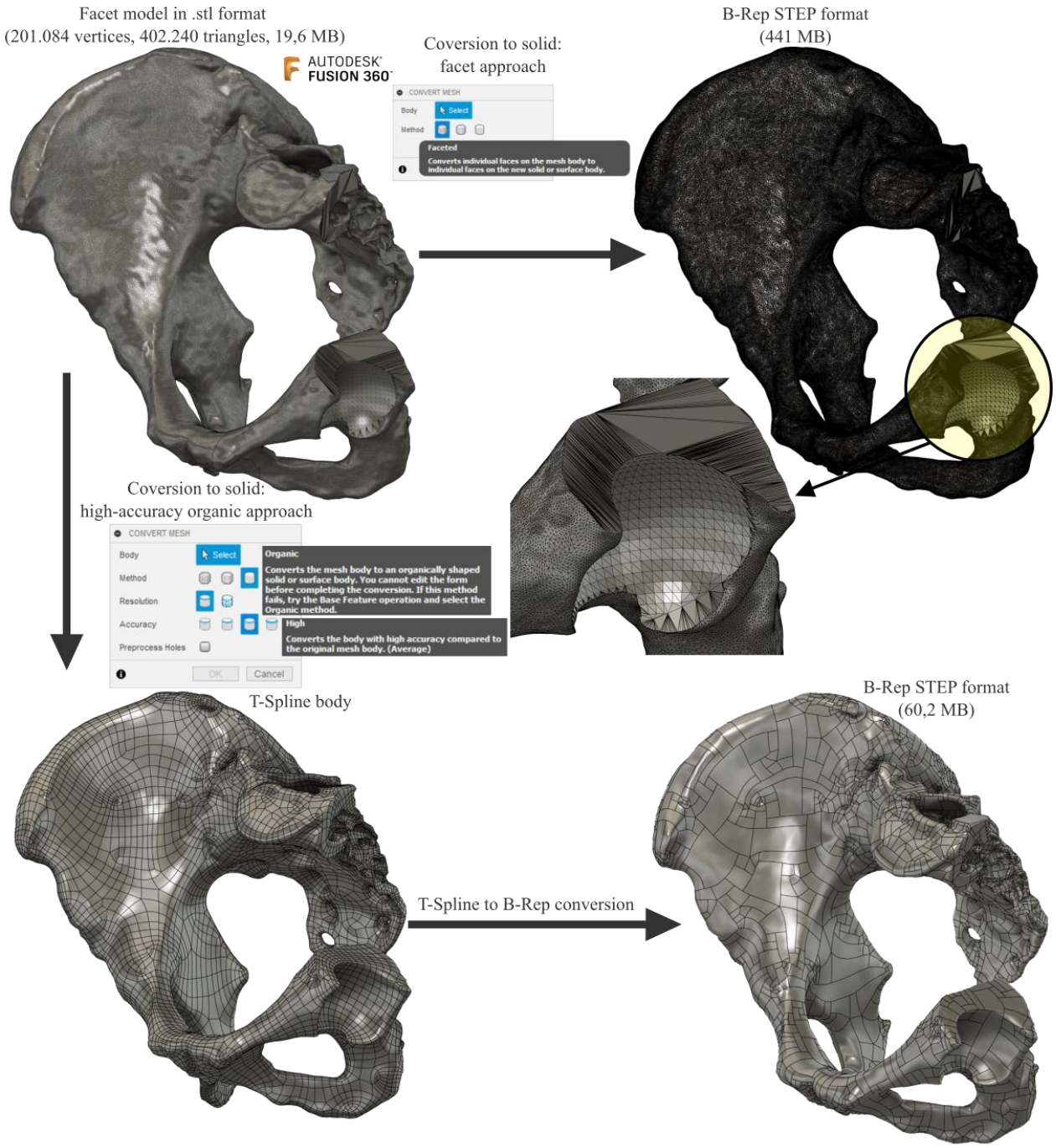

Figure 390: Conversion of triangular mesh model into solids

The modeling of the endo-prosthesis main body that was combined with the acetabular shell was conducted in Fusion 360 as follows *(Figure 396)*:

1. A plane on the flat-cut acetabulum rooftop and a plane on the flat-cut side sacrum were created.
2. A T-spline body conforming to the form of the healthy mirrored ilium was shaped starting from the flat acetabulum rooftop and reaching to the flat sacrum side. The body was modeled to be in contact with the full surface area of the acetabulum rooftop, and contact with the sacrum side with adequate surface area for fixation.
3. The T-spline body was converted into a solid B-Rep body and combined with the acetabular shell, thus consolidated into a single part.

4. Unnecessary material was removed and four 2,5 mm holes were added; two for de-powdering (trapped powder after the 3DP process) and two for possible soft tissue suturing.
5. Two sacral and two acetabular rooftop screw holes for 6,5 mm cancellous bone screws were added as per the pre-defined orientations and points. The holes were designed to fully house the screw heads which were seated at such distances that resulted in pressing approximately 10 mm of endo-prosthesis material towards the sacral and acetabular rooftop osseous tissue.
6. All features were blended for a smooth geometric result with no sharp edges, and the endo-structure was planned to be optimized during the detailed design phase.

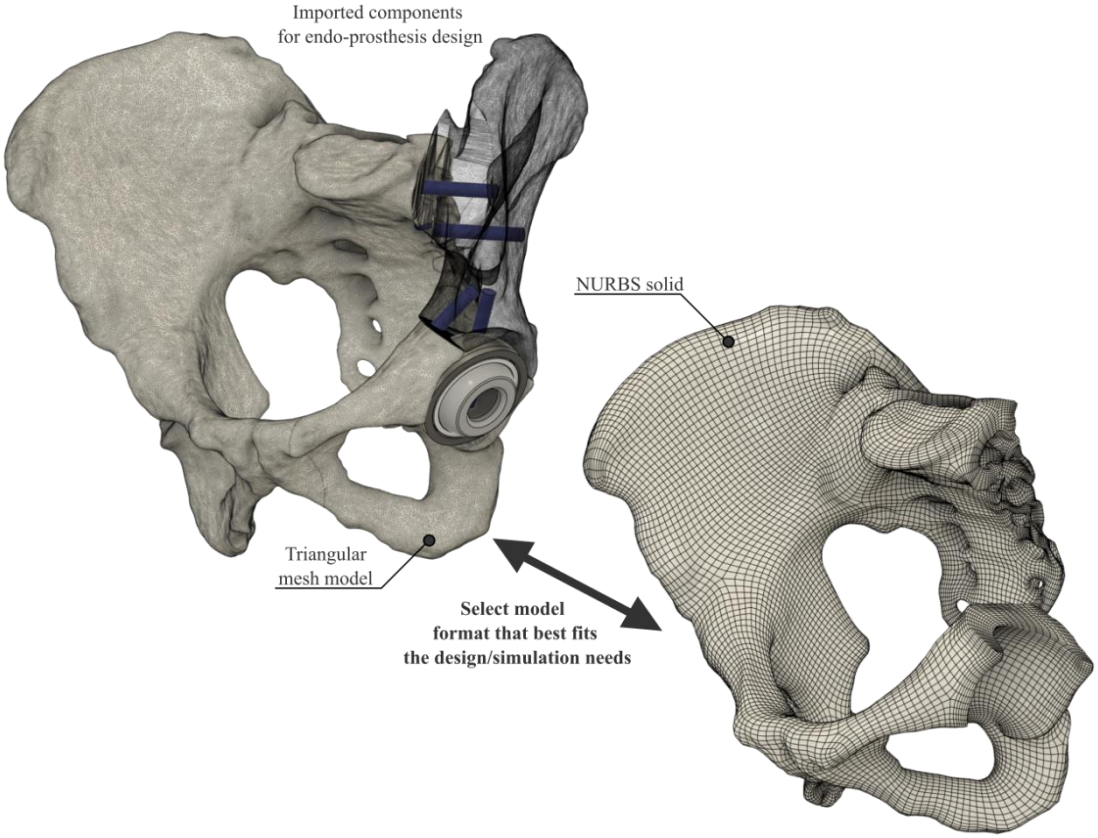

Figure 391: Models to design and simulate the custom solution

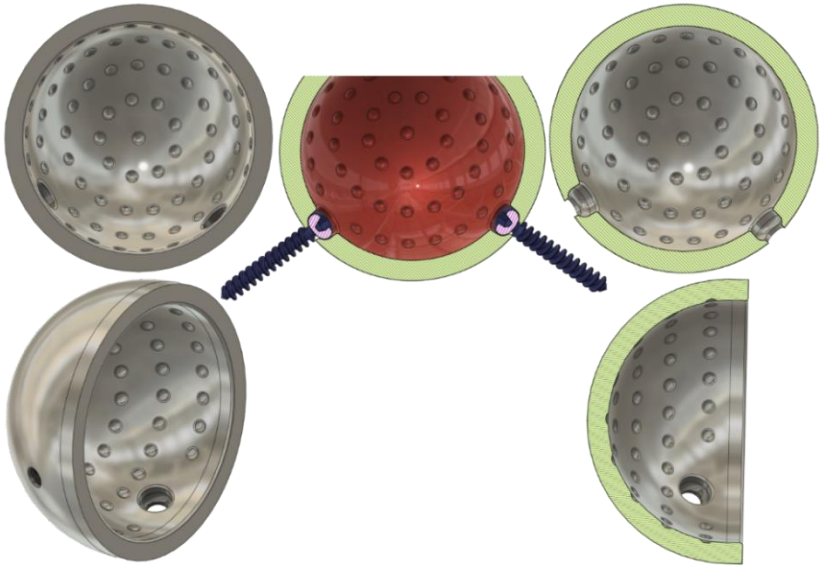

Figure 392: Textured acetabular shell with two 4 mm cancellous screws holes

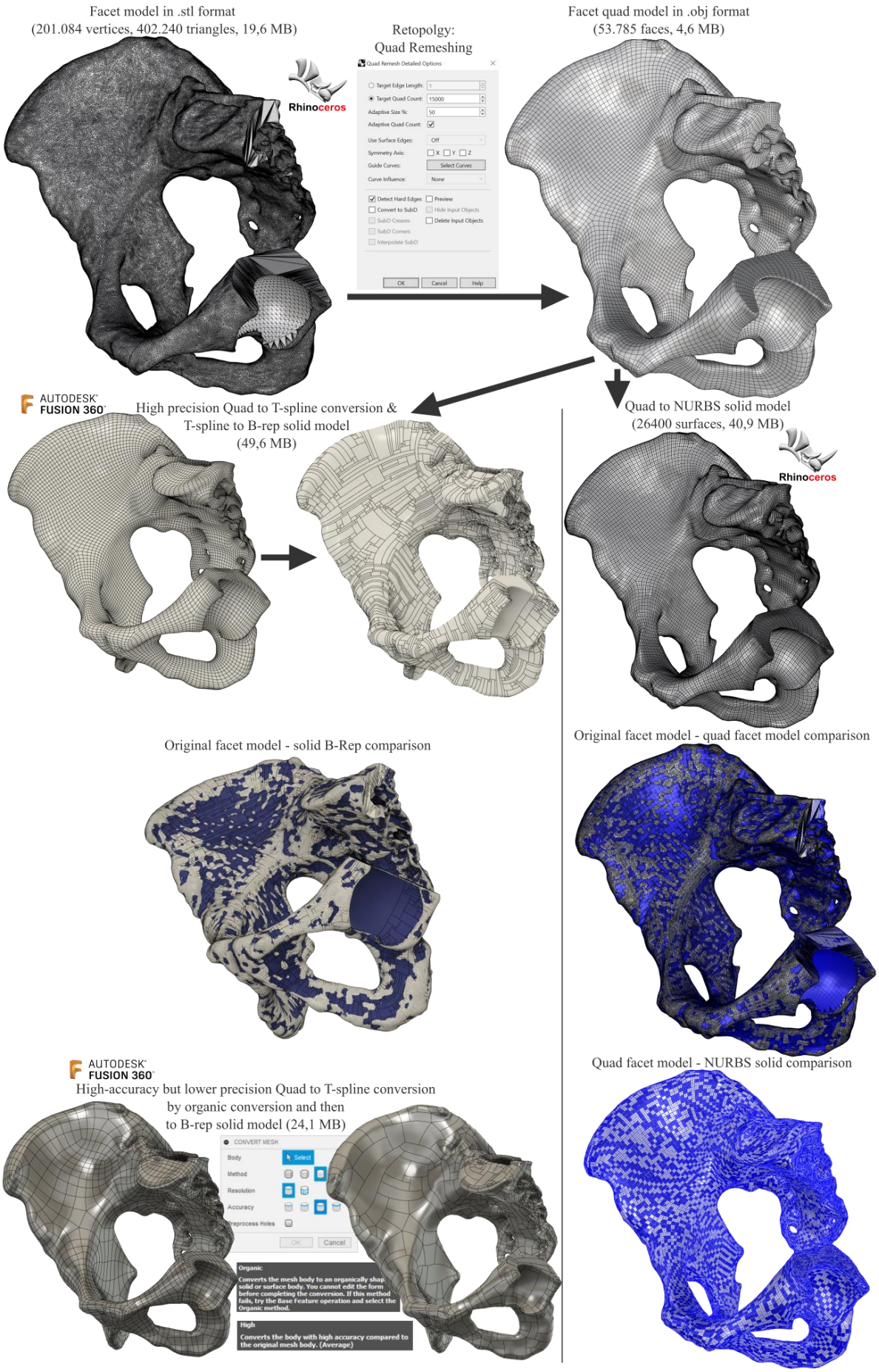

Figure 393: Conversion of quadrilateral mesh model into a solid model

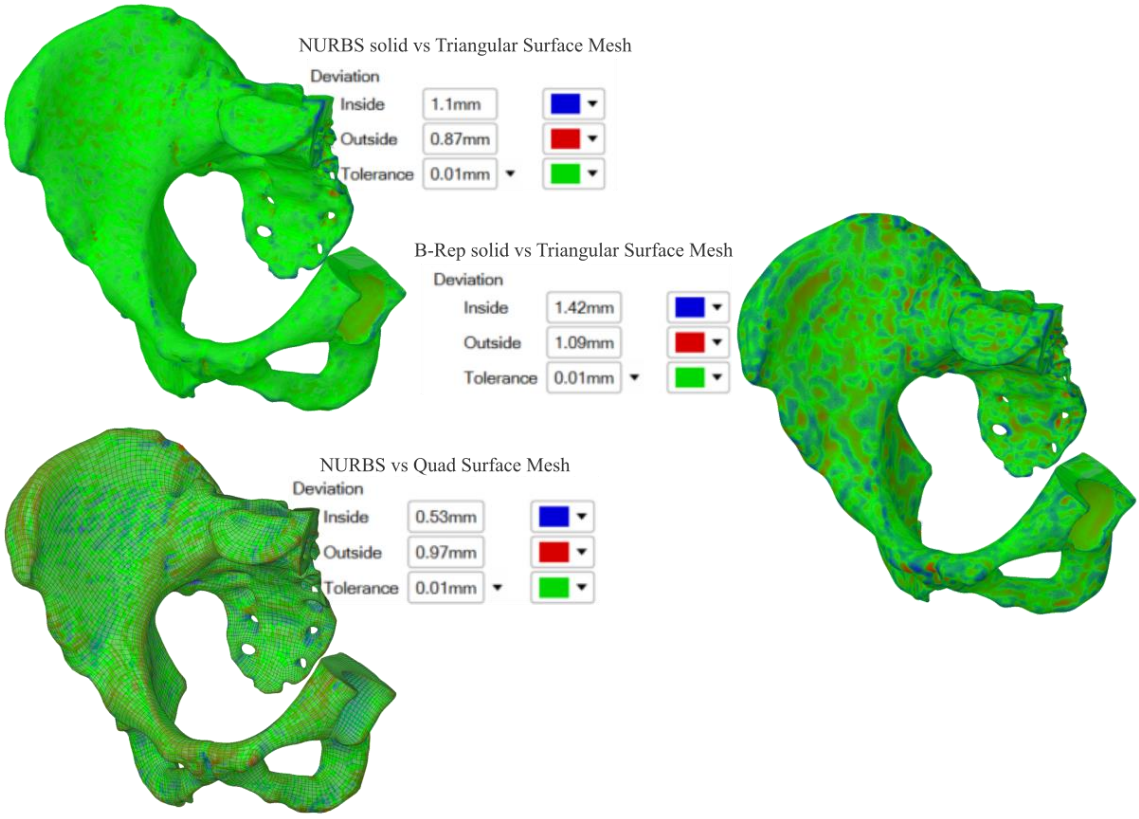

Figure 394: Comparison of quadrilateral, triangular mesh, and solid models

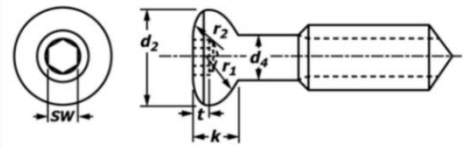

Screw Type and Size	Head Diameter, d_2		Shaft Diameter, d_4		Head Height, k	Bottom Head Radius, r_1		Top Head Radius, r_2	Screwdriver Size[A]
HB 4.0	6.00	+0.00 −0.15	2.40	+0.00 −0.15	2.9	3.250	+0.000 −0.075	2.5	2.5
HB 6.5	8.00	+0.00 −0.15	4.50	+0.00 −0.15	4.6	4.250	+0.000 −0.075	2.5	3.5

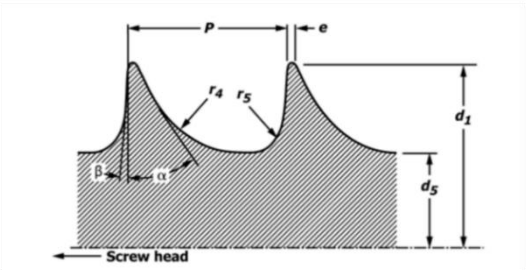

Screw Type and Size	Thread Diameter, d_1		Core Diameter, d_5		Crest Width, e	Thread Pitch, P	Leading Edge Radius, r_4	Trailing Edge Radius, r_5	Leading Edge Angle, α	Trailing Edge Angle, β
HB 4.0	4.00	+0.00 −0.15	1.90	+0.00 −0.15	0.1	1.75	0.8	0.3	25	5
HB 6.5	6.50	+0.00 −0.15	3.00	+0.00 −0.15	0.2	2.75	1.2	0.8	25	5

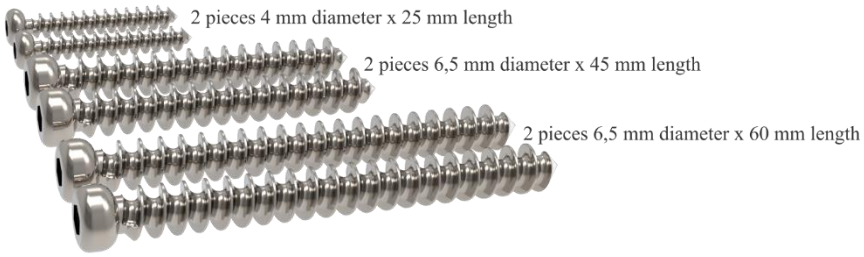

Figure 395: Cancellous bone screws modeled as per ISO 5835

The endo-prosthesis was planned to be fixed on the patient's anatomy with the selected six cancellous bone screws (2 pieces 4 mm diameter 25 mm long for shell, 2 pieces 6,5 mm diameter 45 mm long for acetabular rooftop, and 2 pieces 6,5 mm diameter for sacrum) is pictured in *Figure 397* as modeled in Fusion 360, whereas the photorealistic rendered outputs of Keyshot for the endo-prosthesis and the arthroplasty components (stainless steel AISI 316L cemented cup, UHMWPE liner, CoCrMo femoral head and Ti alloy femoral stem) shown in *Figure 398* and *Figure 400*.

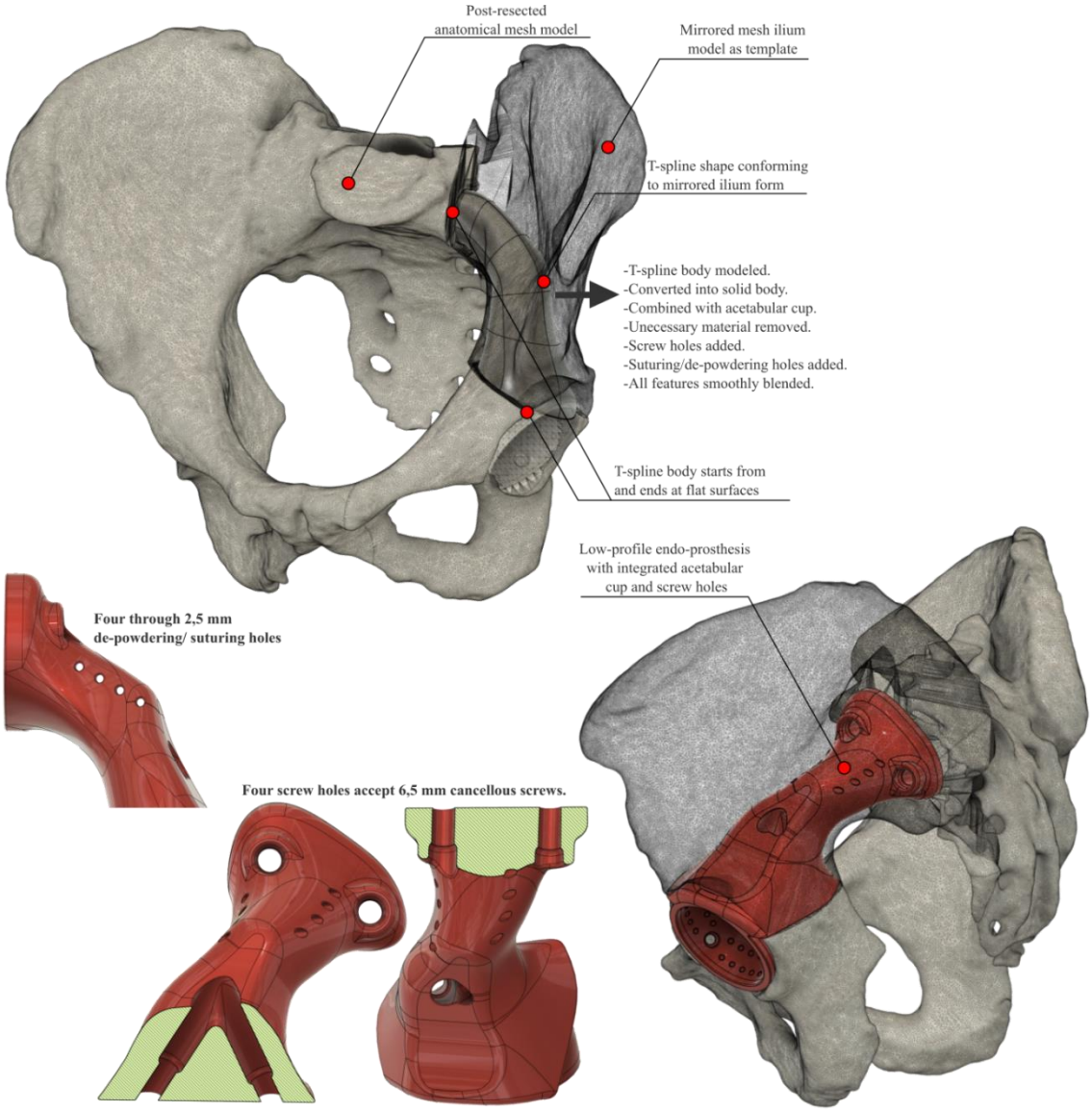

Figure 396: Endo-prosthesis modeling

If adequate soft tissue and muscles were available after resection, then an ilium-like form might be required instead of a low profile. *Figure 399* shows such an endo-prosthesis concept designed as per the mirrored healthy ilium that features an integrated acetabular cup that accepts a locking-by-snapping liner instead of cemented. In this version, porous surface areas and suturing holes could be added to support the soft tissue and muscles.

Granted that the preliminary design of the endo-prosthesis has been completed, the patient-specific bone screws pilot hole drilling instrument and a trial endo-prosthesis replica for intra-

operative usage before the final endo-prosthesis implantation had to be modeled. For this reason, a bi-modal polymer drilling jig-trial endo-prosthesis instrument was modeled in Fusion 360 *(Figure 401)*. First, the solid B-Rep model of the endo-prosthesis was duplicated and edited: texturing from the shell area and all bone screw holes were removed. Then, to avoid debris during drilling directly through the polymer jig, special features to accept stainless steel (AISI 316L) pilot hole drilling bushings by press-fitting were implemented. For the two 4 mm diameter cancellous bone screws, two 8/2,1 mm (for 1,9 drill bit) 15 mm length bushings were added, whereas for the remaining four 6,5 mm diameter cancellous bone screws, four 10/3,2 mm (for 3 drill bit) diameter 15 mm length bushing were inserted. These features were integrated into the solid body and smoothly blended.

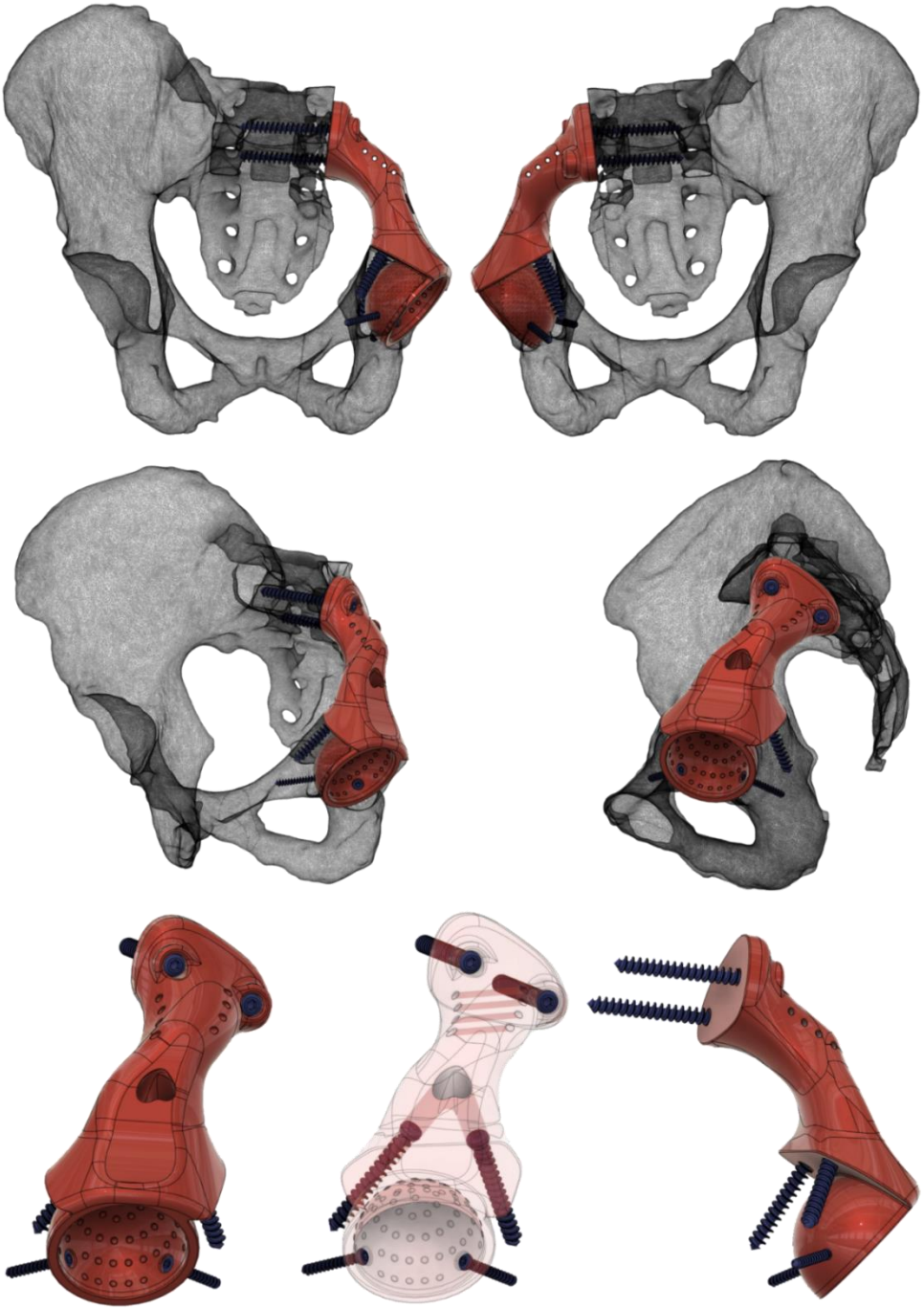

Figure 397: Endo-prosthesis fixed with bone screws

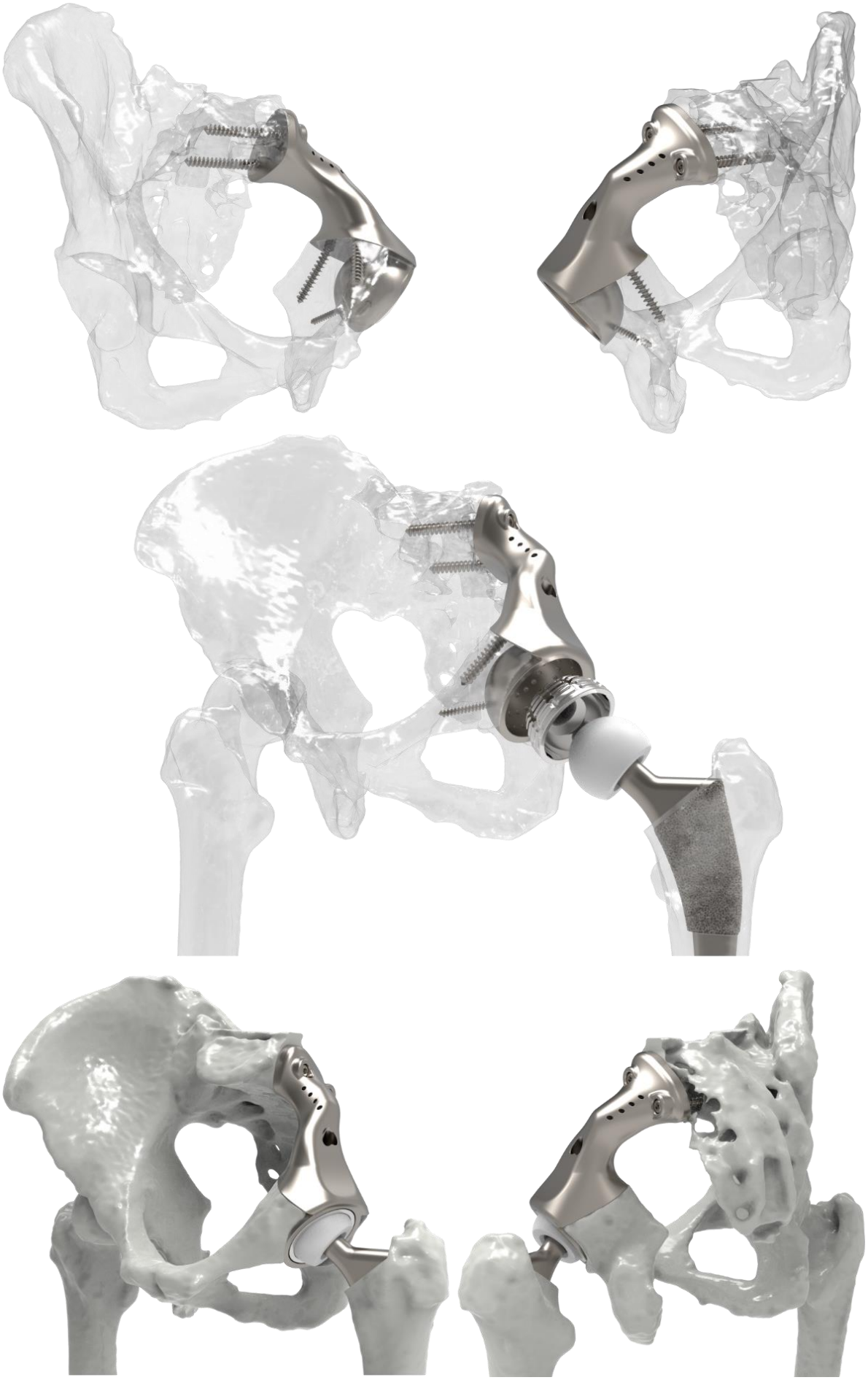

Figure 398: Photorealistic view of the implanted solution: endo-prosthesis and arthroplasty

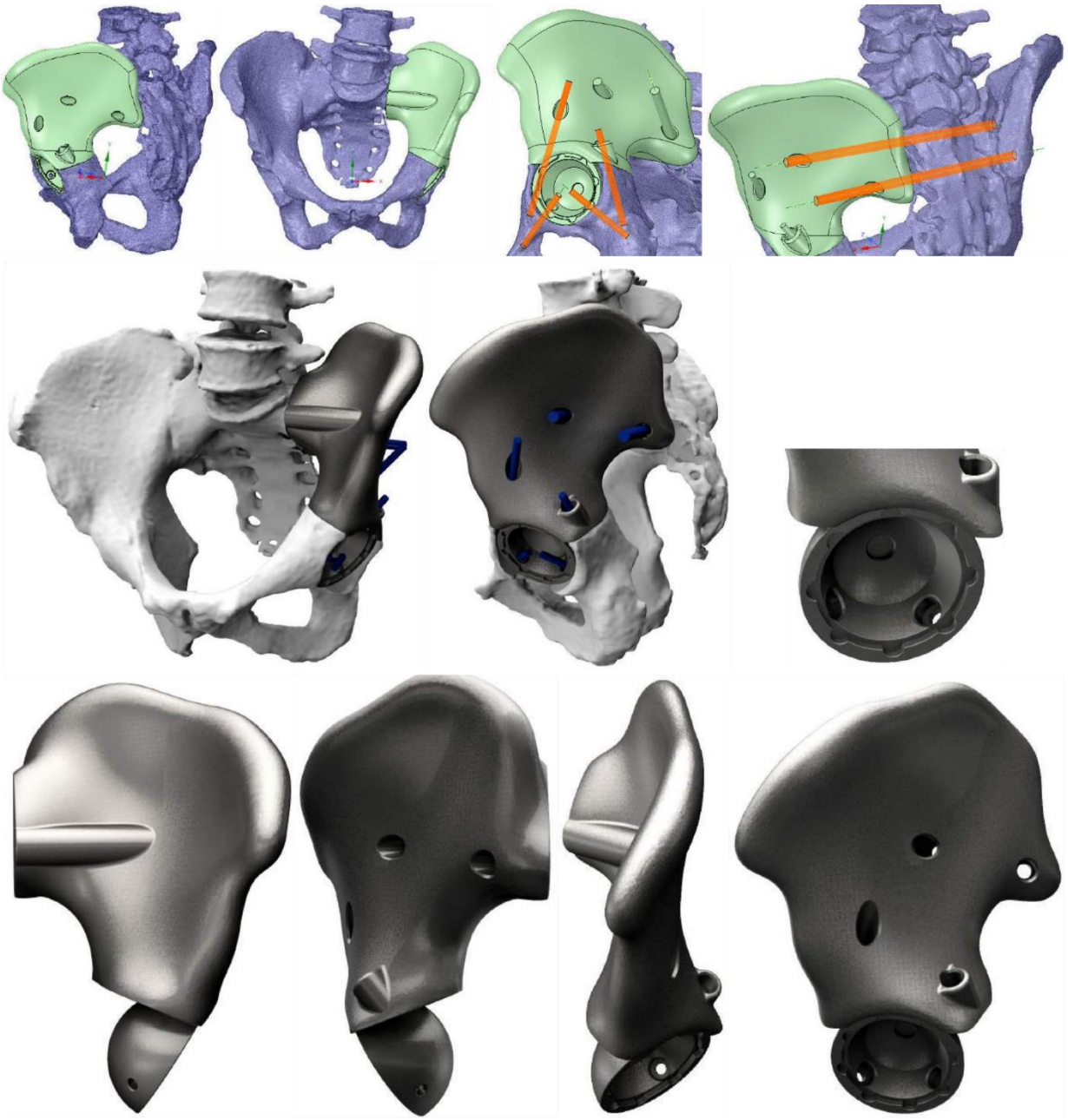

Figure 399: Ilium-like endo-prosthesis concept

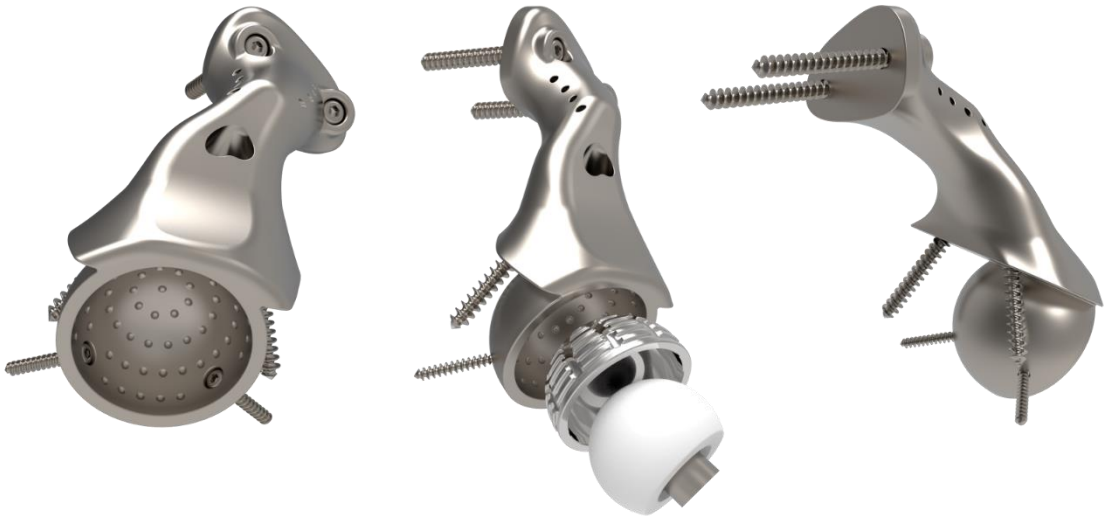

Figure 400: Photorealistic rendering of the endo-prosthesis and arthroplasty components

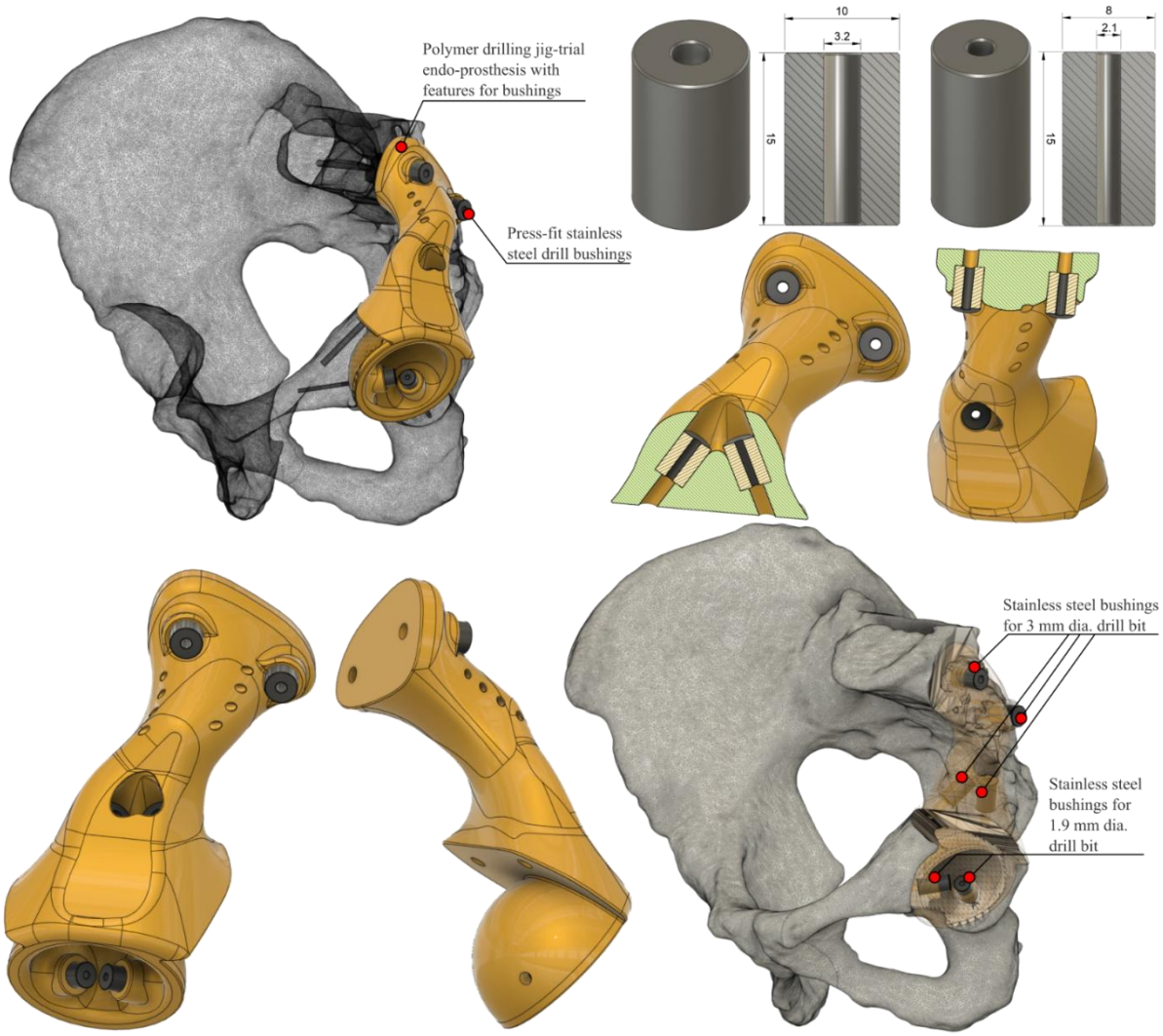

Figure 401: Drilling jig-trial endo-prosthesis instrument modeling

The photorealistic rendered model of the polymer pilot hole drilling jig-trial endo-prosthesis instrument with the press-fit stainless steel (AISI 316L) bushings is illustrated in *Figure 402*.

Figure 402: Photorealistic rendering of the drilling jig-trial endo-prosthesis instrument

Granted the completion of the endo-prosthesis and the drilling jig-trial instrument design, the remaining patient-specific tools had to be designed:

1. **Acetabulum reaming check tool:** the progressive reaming operation was planned to be checked by reaming check tool until it is fully inserted within the acetabulum and its side brackets touch the acetabular rim. The NURBS solid was used to cut the side brackets of the reaming check tool and an extra 0,3 mm offset was given to guarantee that the tool would not be materialized under-sized. *Figure 403* shows the modelled tool and *Figure 404* illustrates the photorealistic views.

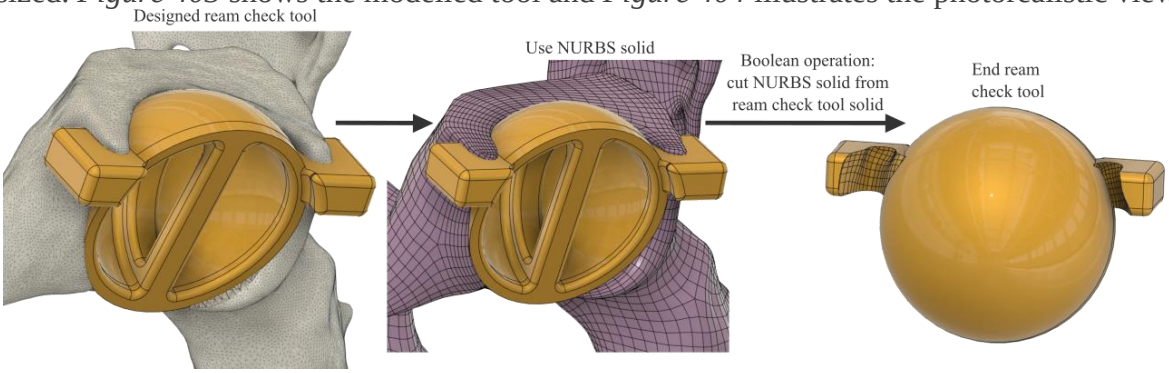

Figure 403: Reaming check tool modeling

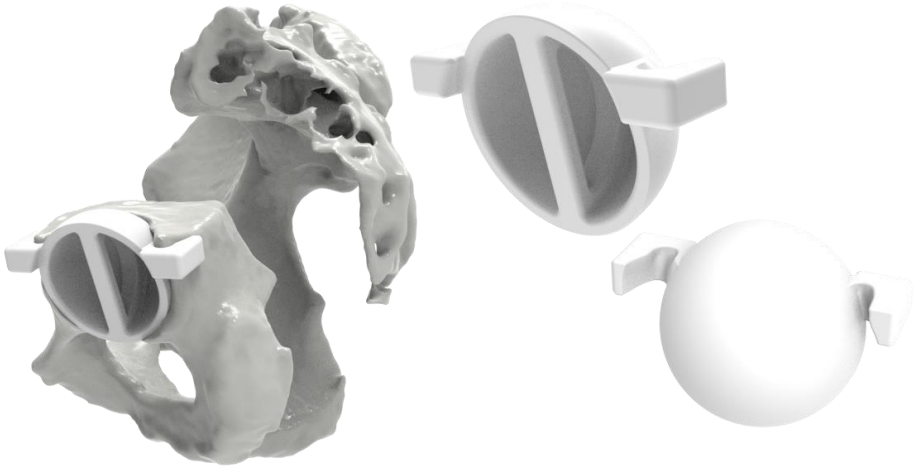

Figure 404: Photorealistic views of the reaming check tool

2. **Acetabulum rooftop and sacrum side flat cutting jig:** with the margins pre-defined in *Figure 283* (plus 0,2 mm offset), a single polymer cutting instrument was modeled as shown in *Figure 405*. The jig features one slot per cutting region. To avoid debris generated during bone sawing directly through the polymer slots, 1,5 mm thick stainless steel sheet (AISI 316L) inserts were designed to be fixed within the slots using M 2,5 size stainless steel (AISI 316L) countersunk screws (DIN 965H). The slots had 2,5 mm clearance so that 1-2 mm thick saw blades could be used. The jig is uniquely placed by inserting it into the properly reamed acetabulum and its sides touching the acetabular rim. Two optional holes (adequately far from the endo-prosthesis screw holes) accept 2 mm K-wires within the acetabulum for temporary fixation. The NURBS solid was used to cut the sides of the jig and an extra 0,3 mm offset was added to avoid under-sizing *(Figure 406). Figure 407* pictures photorealistic views of the cutting jig.

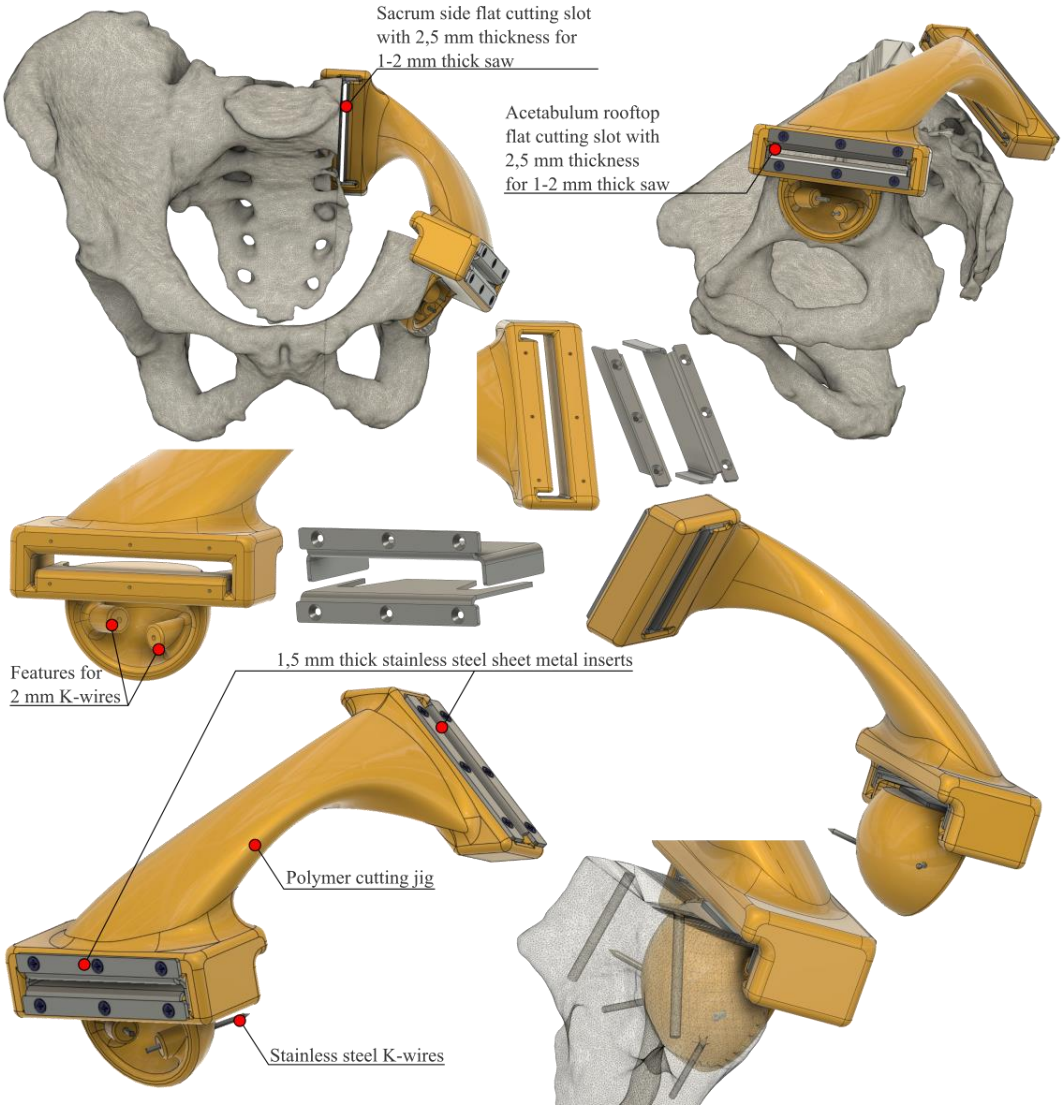

Figure 405: Cutting jig and insert modeling

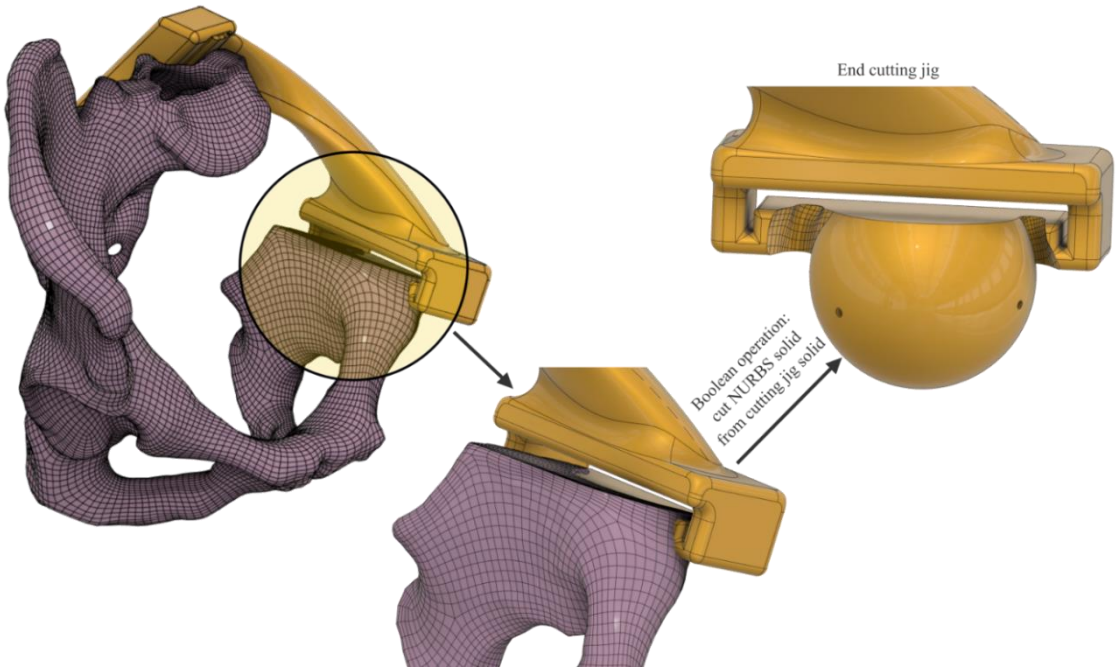

Figure 406: Features cut for the unique fit of cutting jig on anatomy

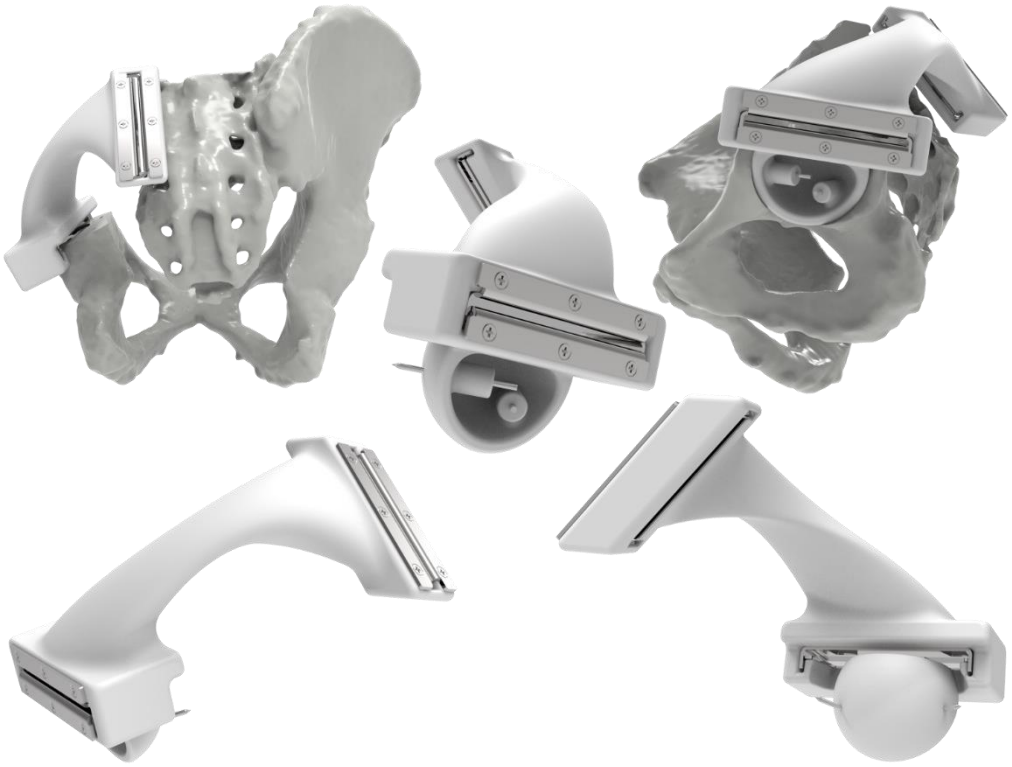

Figure 407: Photorealistic rendered views of the cutting jig

3. **Femoral head-cutting jig:** the modeled jig is shown in *Figure 408* and the photorealistic views in *Figure 409*. The jig is fitted on the femoral head-neck and fixed with two 2 mm K-wires. To avoid debris from the polymer jig during cutting, a 1,5 mm stainless steel (AISI 316L) sheet metal was inserted at the bottom surface where the saw blade will be touching. The mesh surface model of the femur was converted into a NURBS solid and then it was used to cut the jig (extra 0,3 mm offset was added) so that the resultant imprint could be used for unique registration.

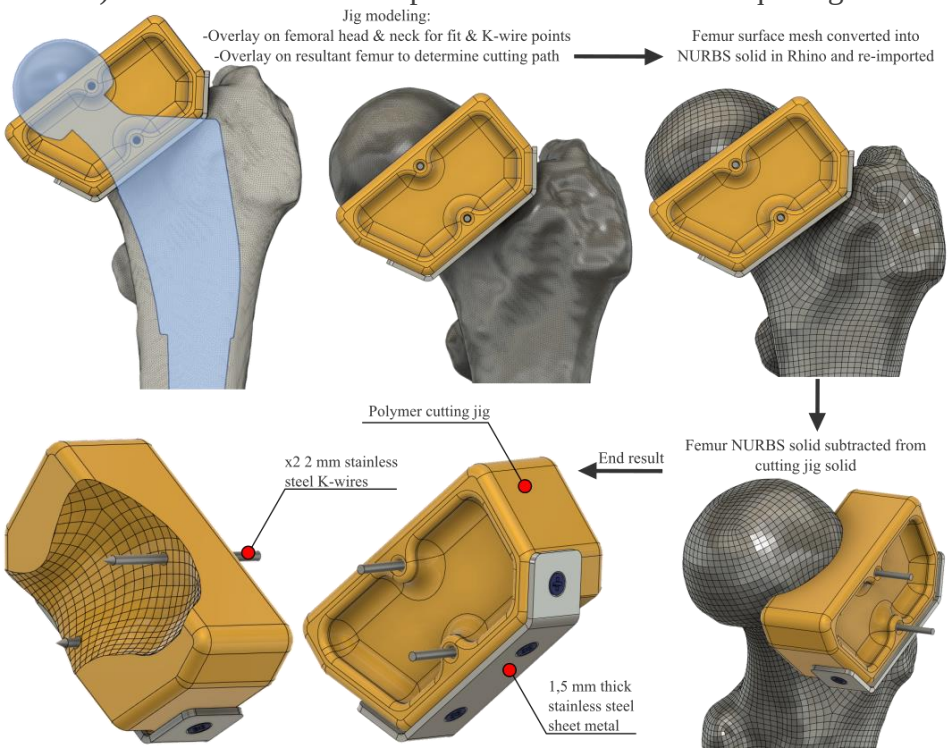

Figure 408: Femoral head-cutting jig modeling

Figure 409: Photorealistic views of the femoral head cutting jig

The next step was to evaluate the endo-prosthesis from a biomechanical point of view. For this purpose, the loads acting on the patient's acetabulum post-implantationally during routine activities had to be calculated. The human body is a well-engineered structure where bone and soft tissue interact in both static and dynamic situations to maintain balance and generate movement. The hip joint allows walking and a plethora of other activities, thanks to its six degrees of kinematic freedom (abduction/adduction, extension/flexion, lateral/medial rotation) the ranges of which are shown in *Figure 410*. Kinesiologically, during walking, a single gait cycle (heel strike-to-heel strike of the same foot) has a stance and swing phases *(Figure 411)*, with the hip abduction/adduction and extension/flexion being altered as per the graphics shown in *Figure 412*.

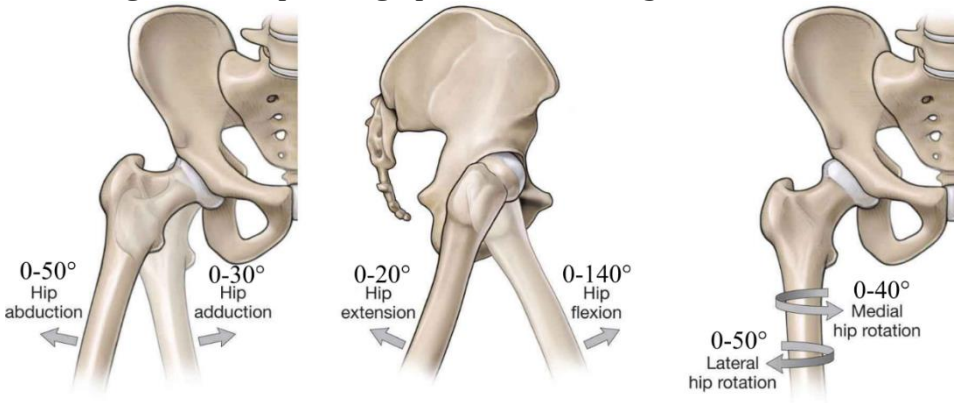

Figure 410: Hip joint range of motion. Graphics: (Morton, Foreman and Albertine, 2019), Values: (Cheng and Woo, 2020)

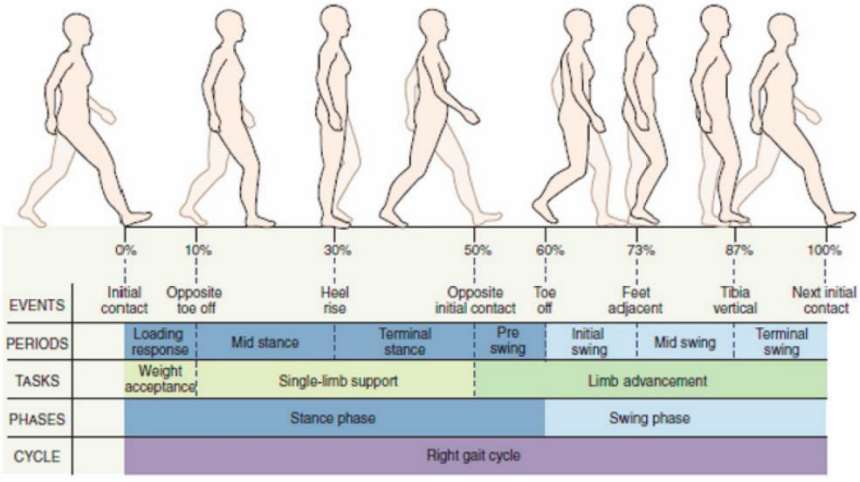

Figure 411: Kinesiology phases of walking. Source: (Simoneau, 2010)

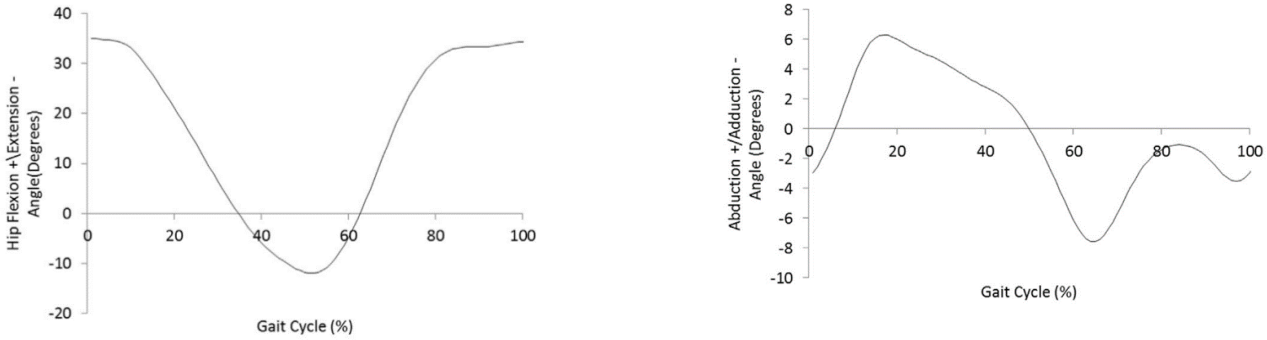

Figure 412: Hip range of motion pattern during walking. Source: (Lunn, Lampropoulos and Stewart, 2016)

The range of motion and active muscles during each period of a gait cycle and values of hip joint motion in the three planes for a variety of activities are shown in *Figure 413*.

Phase of Gait	Hip Position	Active Muscles	Occurrence During Cycle (%)
Stance			
Initial contact	30 degrees of flexion	Hamstrings and gluteus maximus	0-2
Loading response	30 degrees of flexion 5 to 10 degrees of adduction 5 to 10 degrees internal rotation	Hamstrings and gluteus maximus	0-10
Mid-stance	0 degrees of flexion-extension Neutral abduction-adduction	Gluteus medius, gluteus minimus, and tensor fascia lata	10-30
Terminal stance	10 degrees of extension	Iliacus	30-50
Pre-swing	0 degrees of flexion-extension	Iliacus and adductor longus	50-60
Swing			
Initial swing	20 degrees of flexion 5 degrees of abduction	iliopsoas, rectus femoris, gracilis, and sartorius	60-73
Midswing	20 to 30 degrees of flexion	iliopsoas, gracilis, and sartorius	73-87
Terminal swing	30 degrees of flexion	Hamstrings and gluteus maximus	87-100

Activity	Plane of Motion	Recorded Value (Degrees)
Tying shoe with foot on floor	Sagittal	124
	Frontal	19
	Transverse	15
Tying shoe with foot across opposite thigh	Sagittal	110
	Frontal	23
	Transverse	33
Sitting down on chair rising from sitting	Sagittal	104
	Frontal	20
	Transverse	17
Stooping to obtain object from floor	Sagittal	117
	Frontal	21
	Transverse	18
Squatting	Sagittal	122
	Frontal	28
	Transverse	26
Ascending stairs	Sagittal	67
	Frontal	16
	Transverse	18
Descending stairs	Sagittal	36

Figure 413: Active muscles during walking and hip joint motion during activities. Source: (Polkowski and Clohisy, 2010)

Four ligaments, three extracapsular ligaments (iliofemoral ligament, ischiofemoral ligament, and pubofemoral ligament), and one intracapsular ligament (ligamentum teres femoris) provide stability, restriction of excessive range of motion, reduction of muscle energy amount and strength of the hip joint. Regarding the hip muscles *(see Appendix L)* that provide movement force and stability for all six degrees of freedom, these are *(Cheng and Woo, 2020)*:

1. **Main flexor muscles:** iliopsoas muscles assisted by rectus femoris, sartorius, and tensor fasciae latae muscles. Adductor longus, brevis, and gracilis muscles also play a role in flexing.
2. **Main extensor muscles:** gluteus maximus as the largest muscle in the body, assisted by biceps femoris, semimembranosus, and semitendinosus muscles.

3. **Main abductor muscles:** gluteus medius, gluteus minimus, and tensor fascia latae muscles assisted by piriformis and sartorius muscles.
4. **Main adduction muscles:** adductor longus, brevis, and magnus muscles assisted by gracilis and pectineus muscles. The obturator externus muscle plays a role in adduction.
5. **Main external rotation muscles:** obturator externus, quadratus femoris, and gemelli muscles assisted by gluteus maximus, sartorius, and piriformis muscles. Adductor magnus and pectineus muscles also contribute.
6. **Main internal rotation muscles:** tensor fascia latae, anterior fibers of the gluteus medius, and minimus muscles.

Muscles are the main hip contact force contributors with gravitational and centrifugal forces totaling less than 5%. Gluteus medius and maximus, iliopsoas, and hamstrings contribute the most, along with the non-hip vasti, soleus, and gastrocnemius muscles *(Correa et al., 2010) (Figure 414)*.

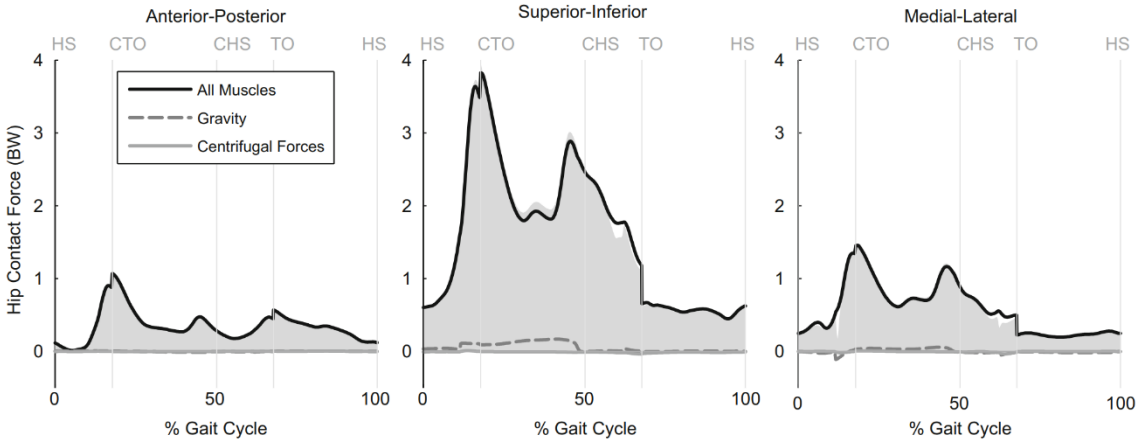

Figure 414: Muscles contribution on hip contact force during walking. Source: (Correa et al., 2010)

Simplified models can be used to estimate the magnitude of the hip joint contact force in two dimensions from the frontal view of the pelvis or in three dimensions *(Eschweiler et al., 2012)*. If all peripheral muscle (except abductor muscles) and ligament forces are ignored, the resultant left hip joint reaction force during dual and single-leg stance for the 90 Kg patient post-implantationally can be calculated as follows *(see applied forces in Figure 415)*:

- **Dual-leg stance:**
  - Constants:
    - Total patient's weight $W_T = 90\ Kg * 9{,}8\ \frac{m}{s^2} = 882\ N$
    - Upper body weight $W_B = \frac{2}{3} * W_T = \frac{2}{3} * 882\ N = 588\ N$
    - Left hip joint distance from the axis of symmetry $X_l = 83{,}4\ mm$ $(See\ Figure\ 381)$
    - Right hip joint distance from the axis of symmetry $X_r = 92{,}2\ mm$ $(See\ Figure\ 381)$
  - Assumptions:
    - Abductor muscles are not required to maintain balance.

▪ The center of gravity is at the pelvis' axis of symmetry as seen from the frontal plane.

Normally, the body weight and any extra weight force acting along the axis of symmetry are distributed equally on each hip joint. However, as the patient's left hip center of rotation was planned to be medially offset, the resultant hip joint reaction force R_l emerges as follows:

For static equilibrium, the sum of forces (F) and moments (M) in all axes (x, y, z) must be zero:

$$\sum F_{x,y,z} = 0 \ and \ \sum M_{x,y,z} = 0 \, , hence$$

$$\sum F_y = 0 \leftrightarrow W_B = R_l + R_r \ (1), and$$

$$\sum M_{y \ (at \ \ point \ P_d)} = 0 \leftrightarrow R_r * X_r = R_l * X_l = (W_B - R_r) * X_l = W_B * X_l - R_r * X_l \leftrightarrow$$

$$R_r = \frac{W_B * X_l}{(X_r + X_l)} = \frac{588 \ N * 83{,}4 \ mm}{92{,}2 \ mm + 83{,}4 \ mm} = 279 \ N, so \ from \ (1)$$

$$\boldsymbol{R_l = W_B - R_r = 309 \ N}$$

- **Single-leg stance**:
  - Constants:
    - Typically, the ratio $\frac{X_l}{Xa}$ is around 2-2,5. $\frac{X_{l+B}}{Xa_x}$ was set as 2,5.
    - Lower extremities weight $W_e = \frac{1}{3} * W_T$.
    - Upper body and left extremity weight $W_{b+re} = \left(\frac{2}{3} + \frac{\frac{1}{3}}{2}\right) * W_T = \frac{5}{6} * W_T$.
    - 30° is assigned to the angle α as a typical value.
  - Assumptions:
    - The patient's abductor mechanism muscles were not resected and will be re-attached.
    - The new center of gravity is translated by B distance away from the hip joint of the touching leg as the weight of the non-touching leg contributes. However, it is assumed that the new center of gravity is still at the pelvis' axis of symmetry as seen from the frontal plane, so the left hip joint distance from the axis of symmetry is $X_{l+B} = X_l$.
    - As the vertical R_y component of the force vector contributes the most to the resultant hip joint reaction force *(Bergmann et al., 2016)*, R_x and R_z can be ignored.

The resultant hip joint reaction force *R* would be:

$$\sum F_x = 0 \leftrightarrow R_x = A_x$$

$$\sum F_y = 0 \leftrightarrow R_y = A_y + W_{b+re}$$

$$\sum M_{y(at\ point\ P_s)} = 0 \leftrightarrow A_y * Xa_x = X_{l+B} * W_{b+re} \leftrightarrow$$

$$A_y = \frac{X_{l+B} * W_{b+re}}{Xa_x} = \frac{X_{l+B} * \frac{5}{6} * W_T}{Xa_x} = 2{,}5 * \frac{5}{6} * W_T \ (2)$$

$$R_y = 2{,}5 * \frac{5}{6} * W_T + \frac{5}{6} * W_T = 3{,}5 * \frac{5}{6} * W_T = 2{,}9 * W_T$$

If the three R_x, R_y, R_z force components are known, the resultant force *R* is given by:

$$R = \sqrt{{R_x}^2 + {R_y}^2 + {R_z}^2}$$

However, as the vertical R_y component of the force vector contributes the most (R_x and R_z assumed to be zero), the resultant *R* is given by:

$$\boldsymbol{R = \frac{R_y}{cos\alpha} = \frac{2{,}9 * W_T}{cos30^\circ} = 3{,}3 * W_T = 3{,}3 * 90\ Kg * 9{,}8 \frac{m}{s^2} = 2943\ N} \ (3)$$

Alternatively, *R* can be calculated trigonometrically by the force vectors as shown in *Figure 415* using the sine and cosine laws, i.e.:

$$R = \sqrt{A^2 + {W_{b+re}}^2 - 2 * A * W_{b+re} * cos\varphi,} \qquad and \qquad \frac{R}{sin\varphi} = \frac{A}{sin\alpha} = \frac{W_{b+re}}{sin\theta}$$

From *(2)*, it is implied that the point where the center of gravity is translated (distance X_{l+B}), and consequently the ratio $\frac{X_{l+B}}{A_x}$ determines significantly the amount of hip joint force during single-leg stance.

As the new left hip joint center of rotation was planned to be medially offset by 8,8 mm (*Figure 381*) using the total hip arthroplasty components shown previously, from a biomechanical point of view, the decreased body weight lever arm would in reality favor not only the lower muscle forces but also the lower hip joint reaction force *(Rüdiger et al., 2017).*

The previous calculation dismisses contributions of muscle, ligament, and tendon activities. The loads (contact force, bending moment, and torsional moment) acting on the femur *(Figure 416)* and consequently on the hip joint are influenced by the anatomical and physical characteristics of each individual, and even by the footwear that tends to increase the loads *(Palmowski et al., 2021)*. Such parameters and measured hip joint forces data must be taken into consideration and extrapolated to individually study each unique patient treated with artificial endo-prostheses.

On the other hand, all real forces acting on the hip joint can be measured in vivo by various instrumented hip implants *(Brinckmann et al., 2002),* though researchers have tried to develop load profiles to better simulate the in vivo loading conditions of total hip replacement by considering the interdependence of muscle and joint forces *(Heller et al., 2005).*

Hip joint forces are activity-dependent, the daily frequency of which varies for each individual *(Morloc et al., 2001)*. Bergmann et al. *(2001)* implanted instrumented prostheses to measure peak contact forces and directions, and torsional moments for various activities, with stair climbing activity reaching 330% of the body weight. Similarly, later, Bergmann et al. *(2016)* captured in vivo the profiles and peaks of hip joint forces and moments during different activities to be used in endo-prosthetic implant mechanical simulations *(Figure 417).*

Interestingly, for non-sport activities where hip joint forces are considerably higher, peak forces higher than eight times the body weight have been recorded in extreme events such as stumbling *(Bergmann, Graichen, and Rohlmann, 2004).*

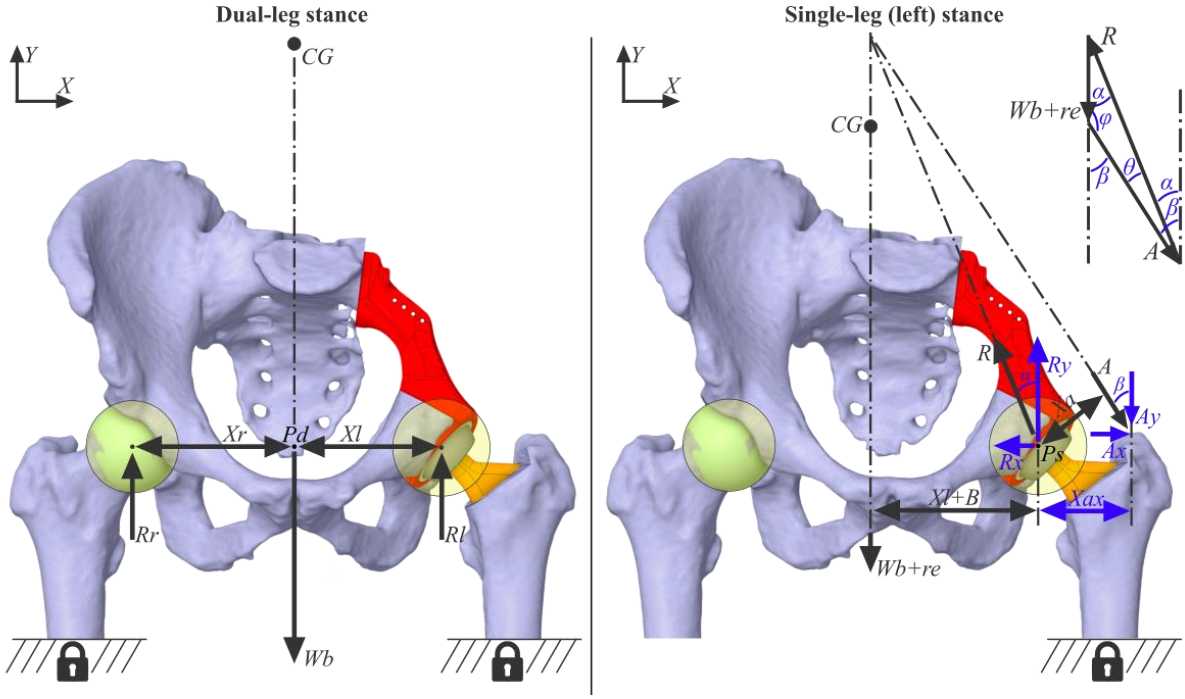

Figure 415: Loads acting on left acetabulum during dual and single-leg stance

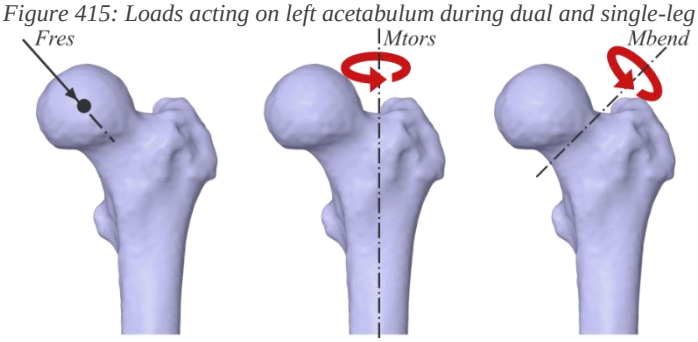

Figure 416: Loads acting on the femur

In reality, cortical and cancellous bone have anisotropic and inhomogeneous material properties *(see Appendix E)*. The local bone's apparent density and modulus of elasticity can be obtained by the

HU values of CT scan data and calibrated using equations *(Schileo et al., 2008; Helgason et al., 2008; Vivanco et al., 2014).* Inhomogeneous material properties can be automatically mapped onto a volumetric model using software algorithms and strategies that read an initial single-material volumetric mesh model, and based on its parent CT scan data, assign density and average modulus of elasticity for each mesh element, thus generating a multi-material volumetric mesh *(Schileo et al., 2007)*. *BoneMat*[154] is such a software *(Zannoni, Mantovani, and Viceconti, 1998; Taddei, Pancanti, and Viceconti, 2004; Taddei et al., 2007)* that could be used for this case along with *Ansys Workbech* to execute the static structural simulation *(Figure 418)*.

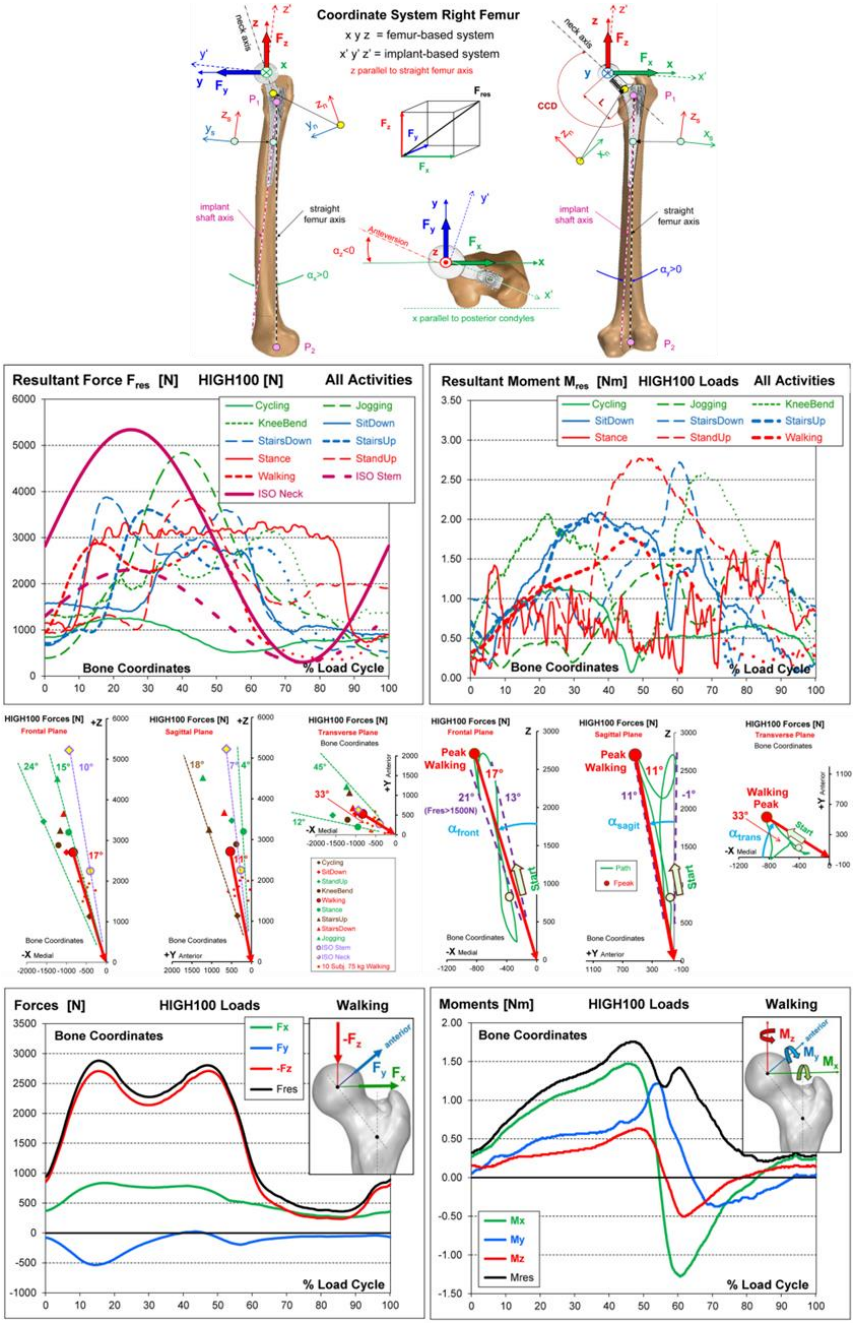

Figure 417: Resultant hip joint force and moment profiles for different activities. Source: (Bergmann et al., 2016)

[154] Bonemat is a free software used to map on a volumetric mesh, bone elastic properties derived from CT scan images. It is developed at Istituto Ortopedico Rizzoli in Bologna, Italy, with the active collaboration of other researchers. See http://www.bonemat.org/.

On the other hand, as the global load distribution was the scope, for simplification, and also to conduct the simulation on the same software where it was designed, the properties of cortical and cancellous bone were not distinguished, and the pelvic bones were assumed to behave as a single homogeneous, linear isotropic, elastic material with an averaged modulus of elasticity of E=7 GPa and a Poisson's ratio of ν=0,3 *(Ravera et al., 2015; Ricci et al., 2018).* Alternatively, the cortical layer could have been modelled as a solid body with a constant thickness by offsetting the outer surface inwards *(Maslov et al., 2021).*

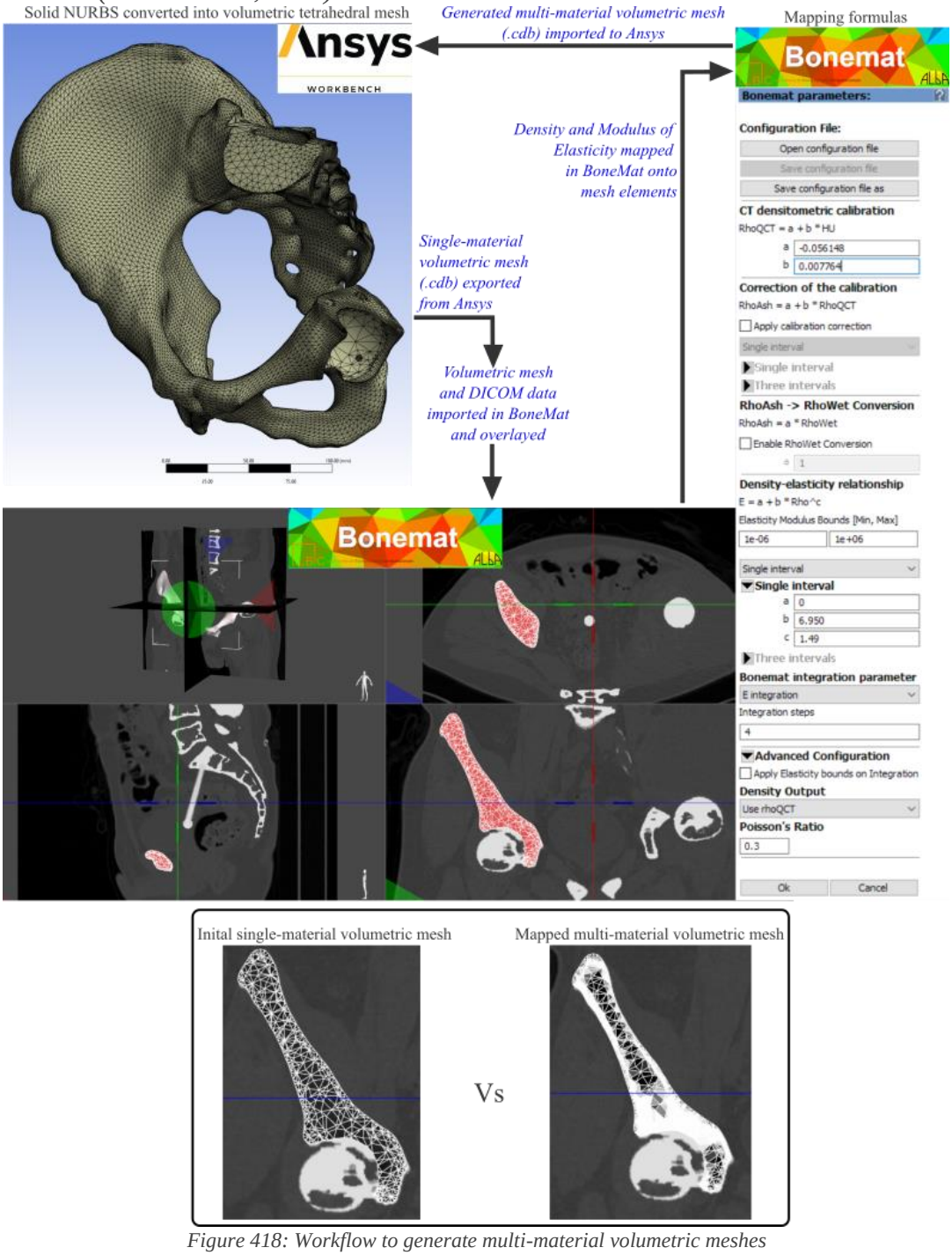

Figure 418: Workflow to generate multi-material volumetric meshes

For each hip, an FEA simulation (mechanical static stress) was set up in Fusion 360 (Nastran) to assess the mechanical performance of the endo-prosthesis as follows *(Figure 419)*:

2. **Material assignment:** Ti6Al4V material properties were assigned to the bone screws and the endo-prosthesis, and an averaged modulus of elasticity of E=7 GPa and a Poisson's ratio of ν=0,3 for all pelvic bones for the reasons justified earlier.
3. **Boundary conditions:** the top of the sacrum was fully fixed by constraining the top surfaces in all degrees of freedom.
4. **Loads**: a force four times the body weight (walking and stair descending activities *(Figure 417)*) was applied at the left hip joint ($4 * W_{b+re} = 2943$ N, set as 3000 N) at an α= 30° angle and perpendicular to the acetabular shell face as seen from the transverse plane. The same magnitude of force and direction was applied for each case study (right and left hip joint). The effects of all surrounding muscles, ligaments, and cartilage, as well as the threads of the bone screws and their tightening and reaction forces, were ignored.
5. **Meshing**: a volumetric mesh with tetrahedral elements and nodes was generated.
6. **Solution**: the Von Misses stresses and displacement results were locally analyzed on each component and animations were generated.

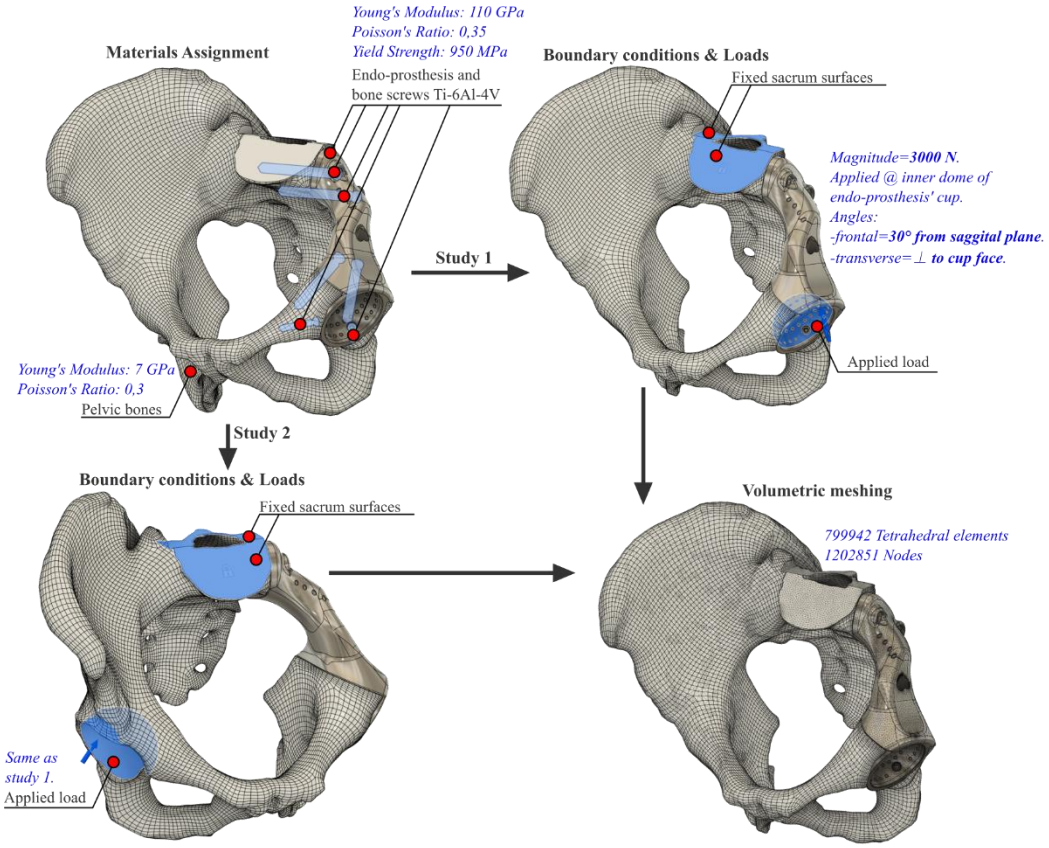

Figure 419: Set-up for the two mechanical simulation studies

The stress distribution and displacement of the pelvic bones, endo-prosthesis, and bone screws differed considerably in right and left hip socket loading scenarios. The results of the simulation studies for the applied peak contact forces on the left and right hip sockets are summarized below:

- **Pelvic bones and sacrum:**

- **Stresses** *(Figure 420 and Figure 421)*: the generated stresses by the exerted force at the right hip socket were higher along the pelvis compared to those generated at the left hip socket (endo-prosthesis shell) by the same symmetrical force. Stresses on the sacrum and acetabulum screw holes were higher for the right hip socket loading case, but stresses at the acetabulum rooftop were higher for the left hip socket loading case. Stresses on the pelvis and sacrum reached values below 10 MPa and 15 MPa for the left and right hip socket loading cases respectively. Values over 10 MPa and 12 MPa respectively, and peaks of 30 MPa were found on the sacrum-endo-prosthesis interface. These peaks of stresses are explained by a) the absence of soft cartilage layers and muscle/ligament forces, and b) the fixed (constrained in all degrees of freedom) top of the sacrum that made it virtually rigid, but in reality also translates, rotates and deforms, hence these peaks might be neglected. Additionally, the higher endo-prosthesis modulus of elasticity (Ti6Al4V) that makes it considerably stiffer compared to the pelvic bone causes stress shielding. All these make it apparent that the boundary and connect conditions have protagonistic impacts on FEA results *(Hu et al., 2017)*.

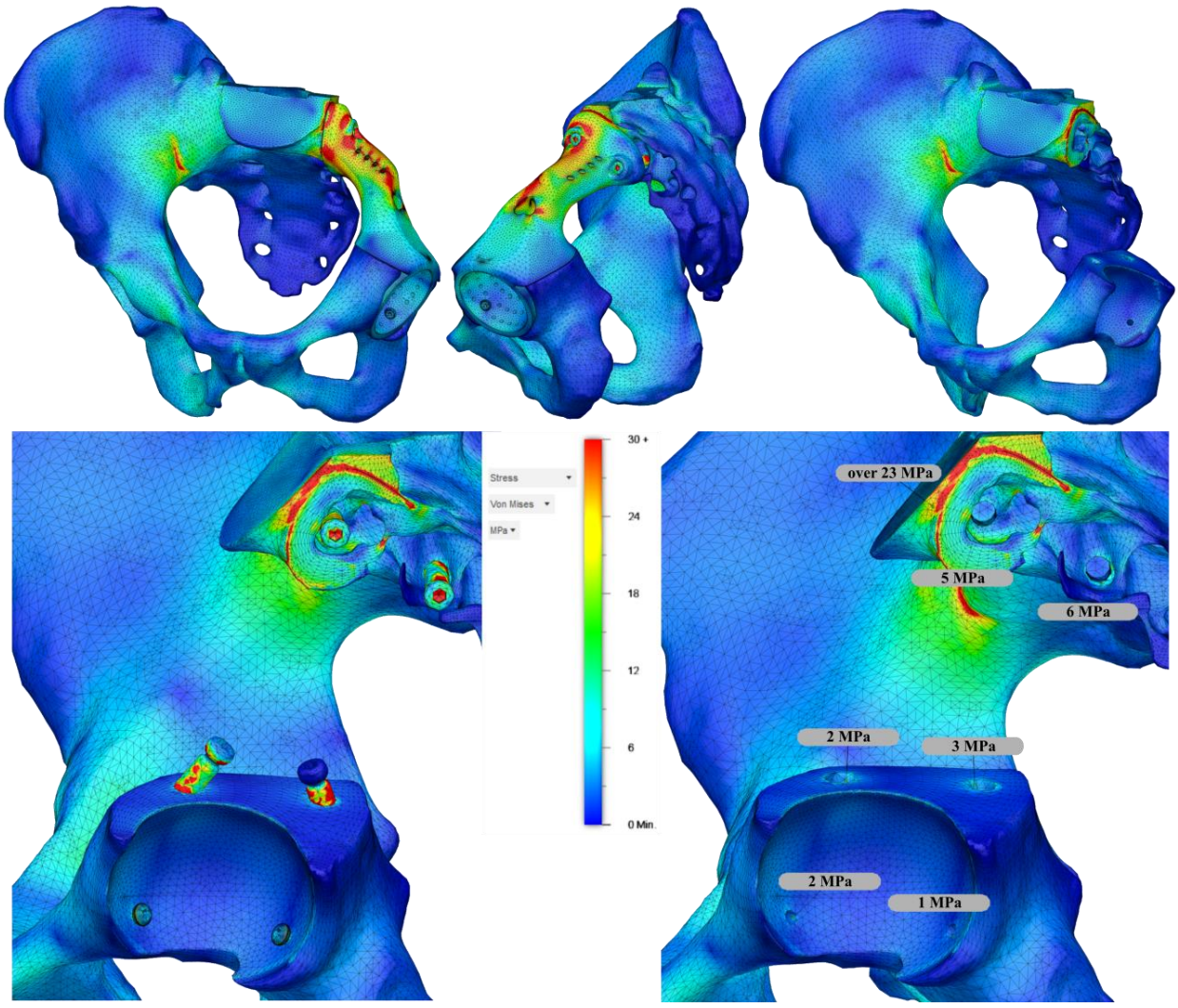

Figure 420: Von Mises Stresses on pelvis induced by right hip load

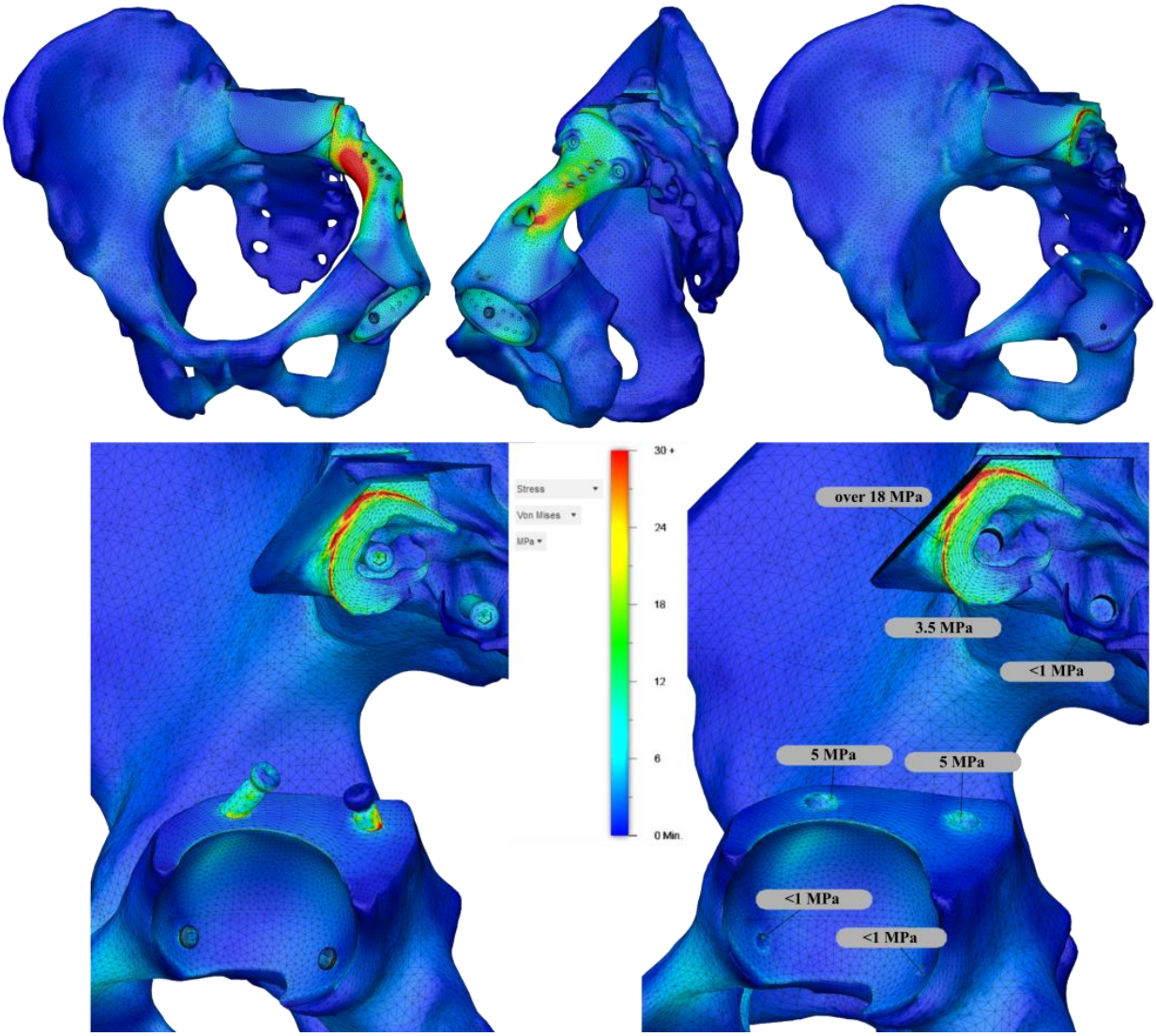

Figure 421: Von Mises Stresses on pelvis induced by left hip load

- **Displacements** *(Figure 422 and Figure 423)*: the maximum displacements for the right and left hip socket loading cases were 0,72 mm and 0,22 mm respectively, and recorded at the right and left pubic bones, close to the pubic symphysis.

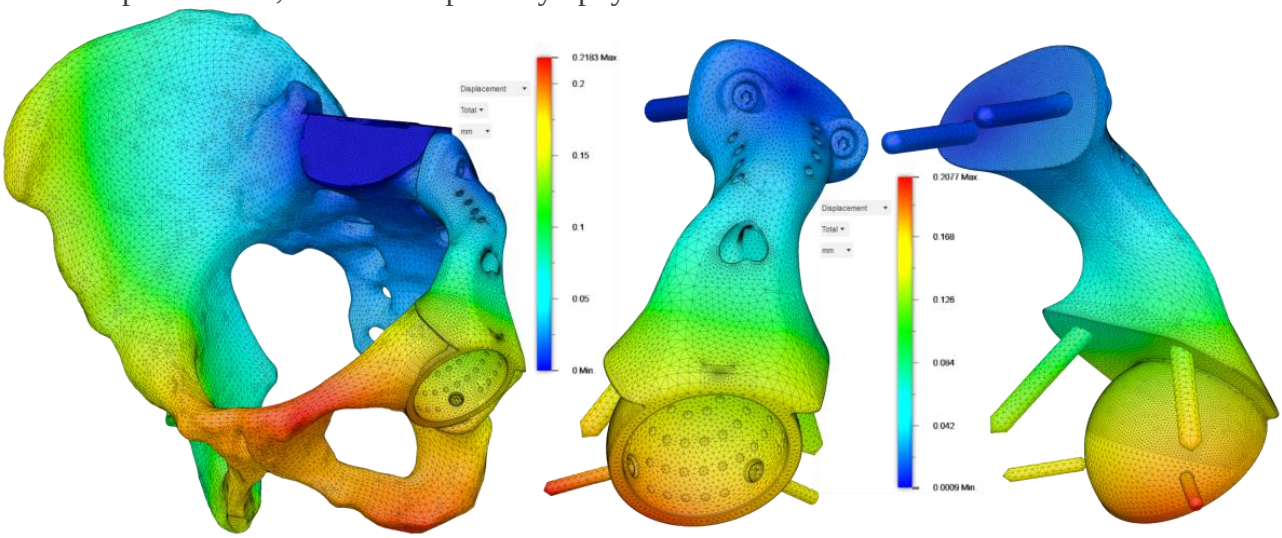

Figure 422: Pelvis, endo-prosthesis, and bone screws displacements induced by left hip load

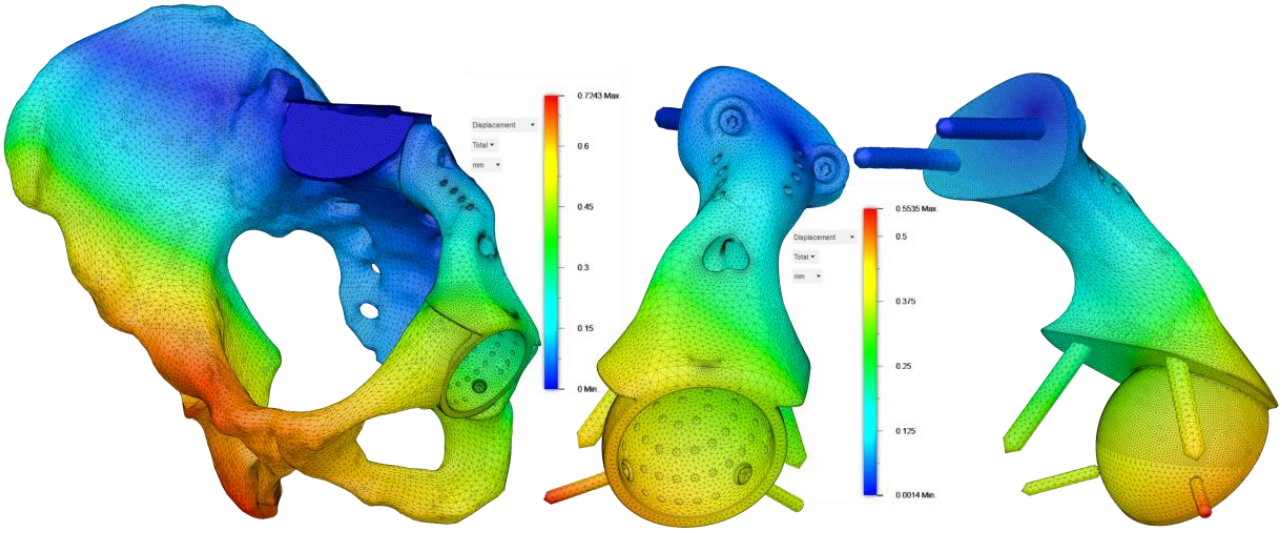

Figure 423: Pelvis, endo-prosthesis, and bone screws displacements induced by right hip load

- **Endo-prosthesis and bone screws:**
  - **Stresses** *(Figure 424 and Figure 425)*: higher stresses were generated at the superior part of the endo-prosthesis in both cases, with more uniform distribution during right hip socket loading, whereas for the left loading case, stresses were concentrated at the inner (pelvic) wall. The anterior sacrum and anterior acetabulum rooftop screw holes reached the highest stress values in both loading cases. Stresses on the bone screws were higher for the right hip socket loading case, compared to the left hip socket loading case.

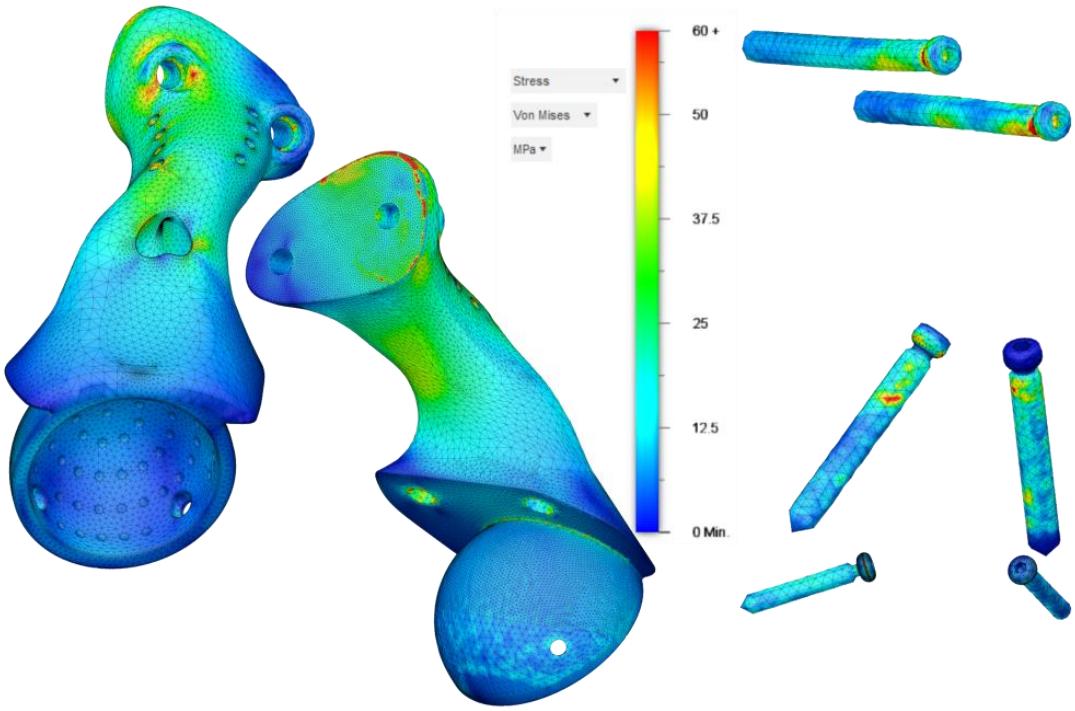

Figure 424: Von Mises stresses on endo-prosthesis and bone screws induced by right hip load

  - **Displacements** *(Figure 422 and Figure 423)*: the maximum displacement of the endo-prosthesis and bone screws were 0,21 mm and 0,55 mm for the left and right hip socket loading cases respectively, occurring around the anterior acetabular shell bone screw.

To simulate the pelvis loading during standing up *(Figure 417)* whilst both legs are on the ground (dual-leg stance scenario), both hip sockets were simultaneously loaded with a force four times the body weight ($4 * W_B = 2352$ N, set as 2400 N). *Figure 426* shows the stresses and displacements generated. The right hemipelvis recorded the highest stresses, with the lower part of the right ischium reaching the maximum displacement (0,78 mm). The sacrum-endo-prosthesis interface reached high peaks over 40 MPa for the same reasons as in the previous individual studies, and the stresses around the screw holes were increased by 1 MPa (except the acetabulum). The endo-prosthesis and the bone screws easily withstand the loads which were still lower than 60 MPa (excluding the peaks at the sacrum interface which are not realistic).

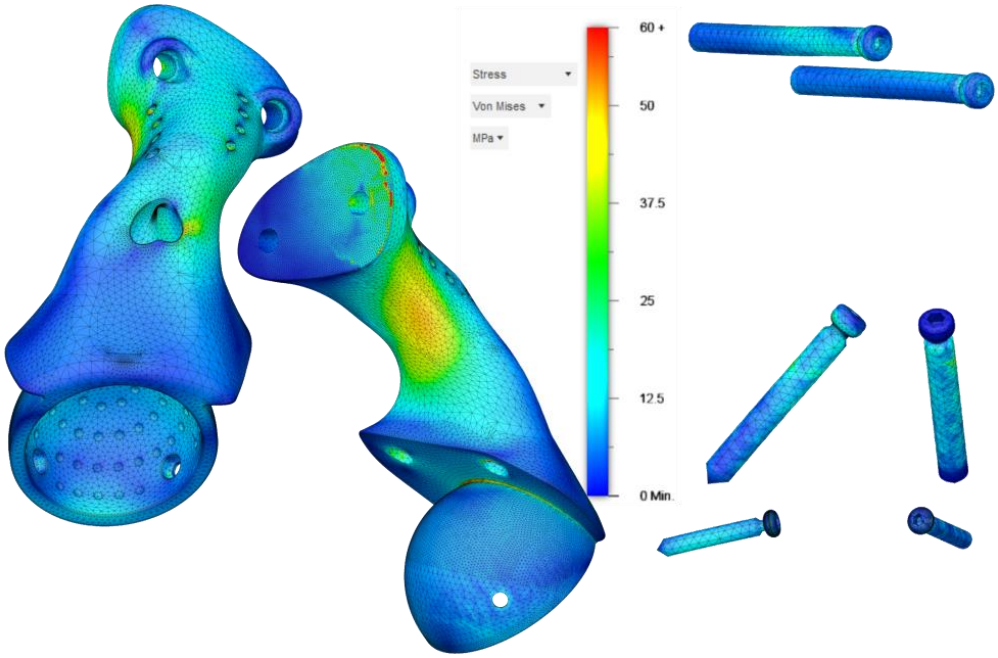

Figure 425: Von Mises stresses on endo-prosthesis and bone screws induced by left hip load

In all the previous scenarios, the peak stresses were considerably (16 times) lower (<60 MPa) than the yield stress of the endo-prosthesis and bone screws (950 MPa for Ti6Al4V). As the relationship between load and stress is linear, a force eight times the body weight (extreme event of stumbling) could have also been borne easily by the endo-prosthesis and bone screws materials, but the stresses (doubled) along the pelvis and sacrum would have been critically high.

For all simulations, it should be underscored that several assumptions were made:

- The top of the sacrum was fully constrained in all degrees of freedom, resulting in a fixed rigid and incompressible solid which is not realistic.
- The effects of all surrounding muscles, ligaments, and cartilage were ignored. In reality, these would assist in bearing and distributing greater loads. Sophisticated models or assisted by other software that simulates soft and hard tissue during routine activities could have been employed.
- No threads were considered in bone screw holes in the pelvic and sacrum bones, and also no screw tightening and reaction forces were modeled. Stress distribution in reconstructed pelvis under

different screw tensioning torque varies and should be optimal per each unique case *(Dong et al., 2018; Maslov et al., 2021).*

- The pelvic and sacrum bones were assumed to be solid with global homogeneous properties. As discussed previously, multi-material properties could have been assigned.
- The right hip socket was assumed to be spherical. However, the true anatomical femoral head, including the cartilage layer, leads to more accurate results *(Ghosh et al., 2013).*

Extra static or dynamic fatigue simulations could have been executed by taking (or not) into account the femur and the selected stem. Also, other loading scenarios could have been considered, e.g. direct impact by sideways fall *(Khakpour et al., 2021).*

The fixation of the endo-prosthesis could have been enhanced by either:

1. Integration of hook features under the sacrum promontory and the acetabulum for weight transferring to the remnant bone stock *(see Figure 428 and Figure 429).*
2. As the pullout strength of a bone screw is affected by: a) bone density and strength, b) bone screw material and type, c) pilot hole diameter, d) thread pitch and depth, e) engaged thread, f) core diameter, and g) insertional torque *(Chapman et al., 1996; Steeves et al., 2005; Azwan and Rahim, 2011),* the 6 mm cancellous bone screws of the sacrum and/or acetabulum rooftop could have been replaced with larger off-the-shelf or custom-made (3DP) cancellous bone screws or locking screws *(see Figure 384),* or with custom 8 mm diameter stems with integrated scaffold structures to enable osseointegration *(see Figure 428 and Figure 429).*
3. 7 mm diameter pedicle screws inserted into vertebrae, coupled with 6 mm diameter rods to further stabilize the endo-prosthesis by spondylodesis *(see Figure 428 and Figure 429).* Of course, PSIs for screw insertion will have to be developed.

however, such options were not found to be necessary mainly due to the number and orientation of the bone screws and due to the locking of the spherical acetabular cup into the spherical acetabulum.

Figure 427 shows the iliac bone plus sacroiliac joint as mirrored from the healthy right hemipelvis. The mirrored model has a volume of 318.963 mm^3, so assuming that the bone density distribution is uniform across the resected tissue and ignoring the resected soft tissue, with a typical bone density 1,9 $\frac{gr}{cm^3}$ the resected iliac bony tissue mass is estimated at 606 gr if considered fully solid, or 121 gr if considered with 84% porosity *(McGregor et al., 2021a) (see Figure 164),* whereas the mass of the solid endo-prosthesis is 416 gr. The new center of mass following reconstruction has a 12 mm medial, 2 mm posterior, and 36 mm inferior offset.

At this point, the embodiment design was completed. The total time to complete the embodiment design of the solution was 2 days. Further emphasis on the endo-structure and external surface functionalization was given during the next detailed design phase.

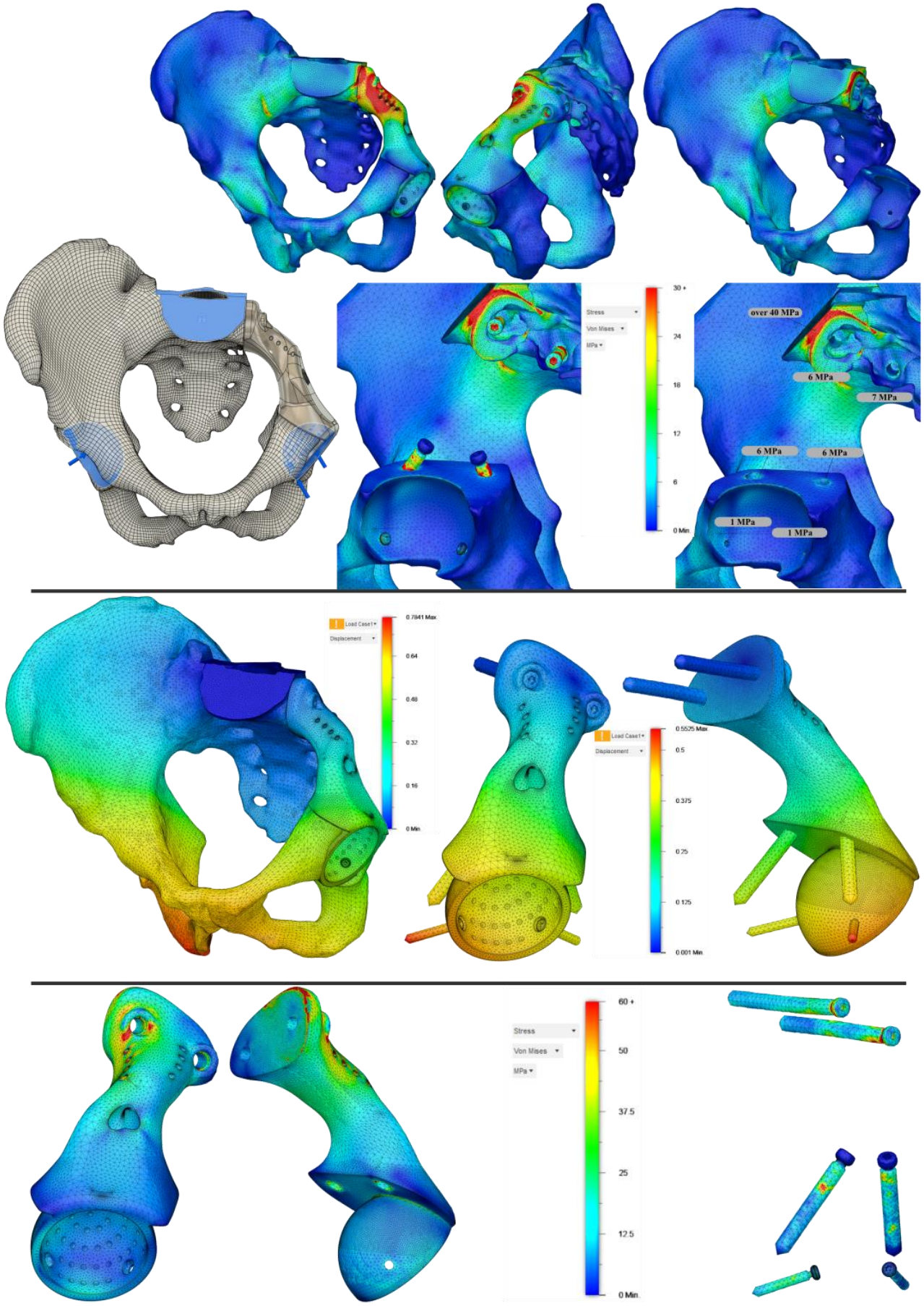

Figure 426: Pelvis, endo-prosthesis, and screw displacements-stresses by combined loading

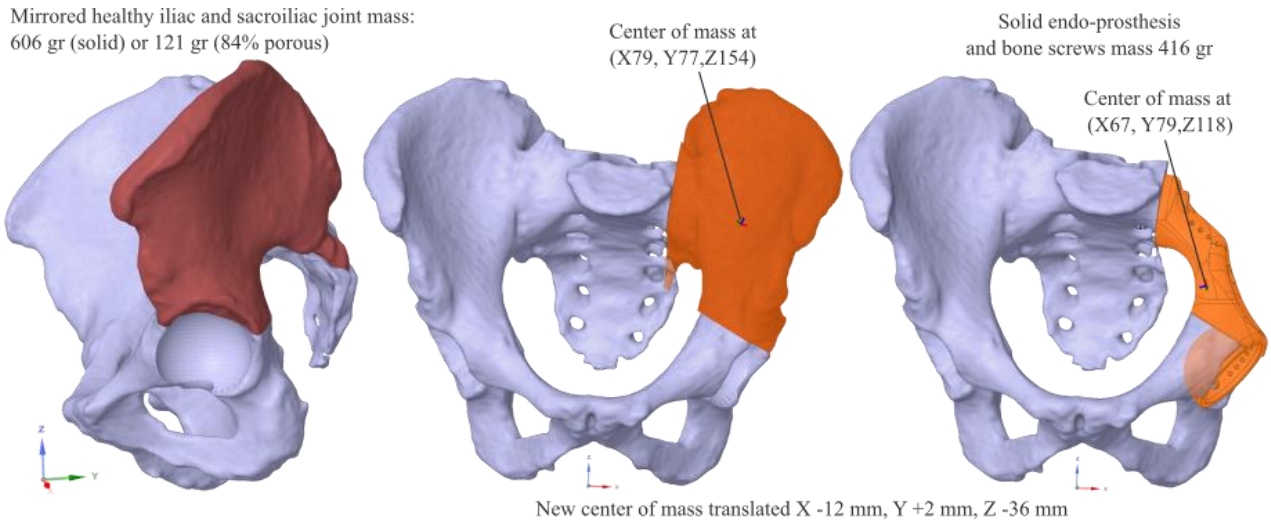

Figure 427: Resected mass and center of mass

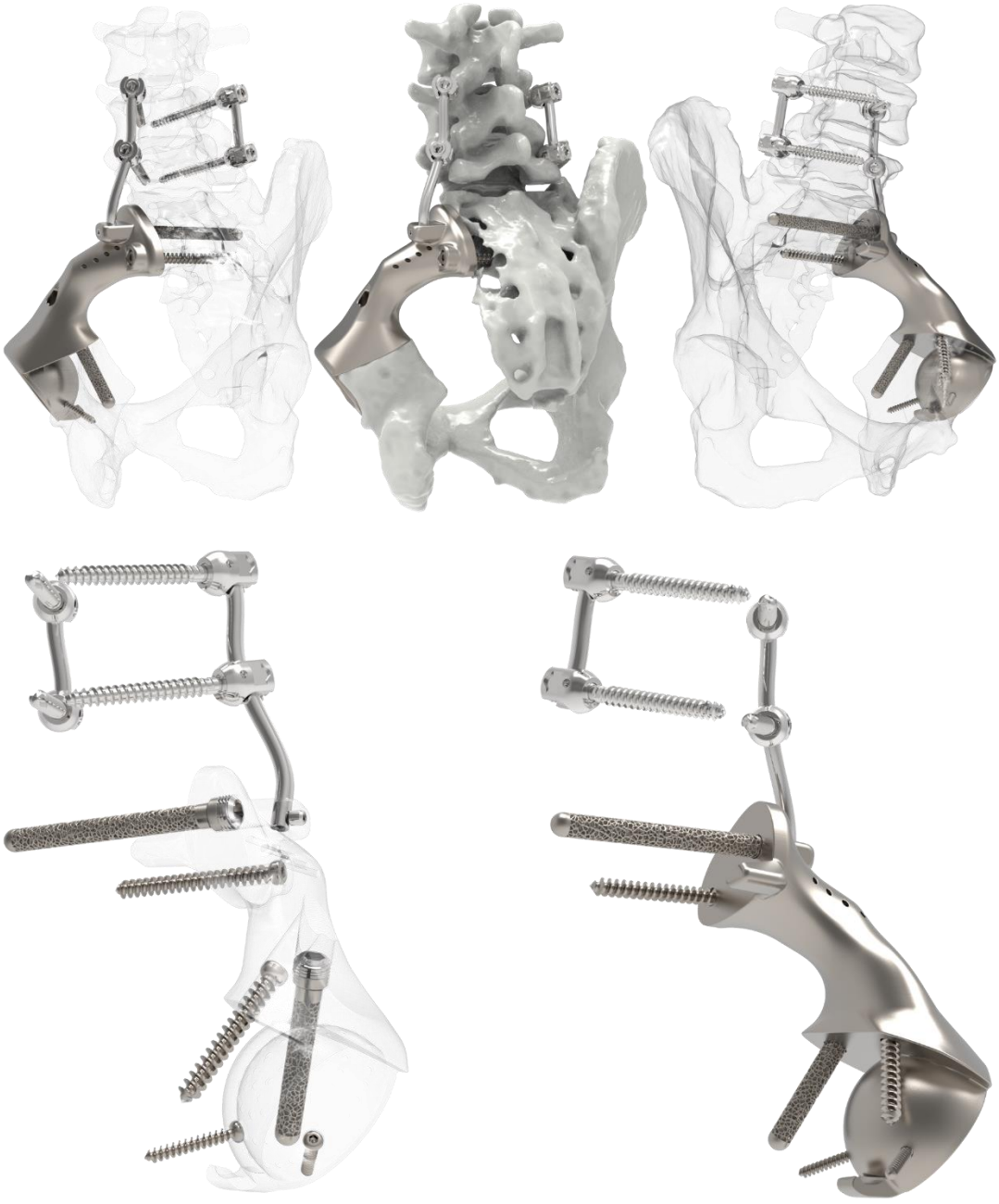

Figure 428: Photorealistic views of extra stabilization options for the pelvic endo-prosthesis

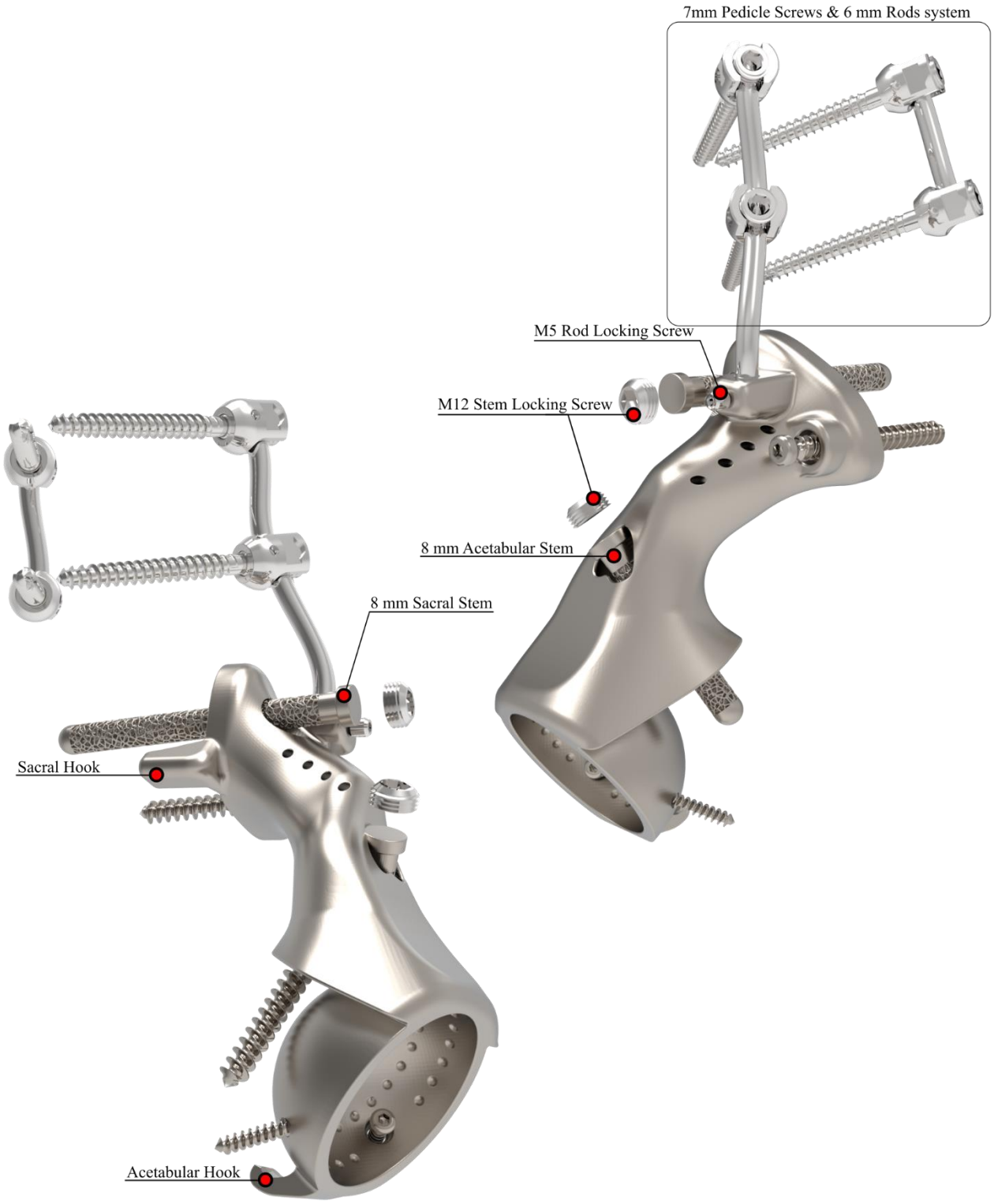

Figure 429: Views and details of the extra stabilization options for the pelvic endo-prosthesis

6.4.8 Design Check

As per the inter-epistemic workflow shown in *Figure 264*, following the embodiment design, the process enters the design-test-iterate loop until the developed design is fully approved by the surgeon, and only then, does the detailed design phase commence. The design was carefully checked by the surgeon based on the digital 3D static and dynamic visualizations of soft and hard tissue anatomy *(see Figure 430 and previous photorealistic figures).*

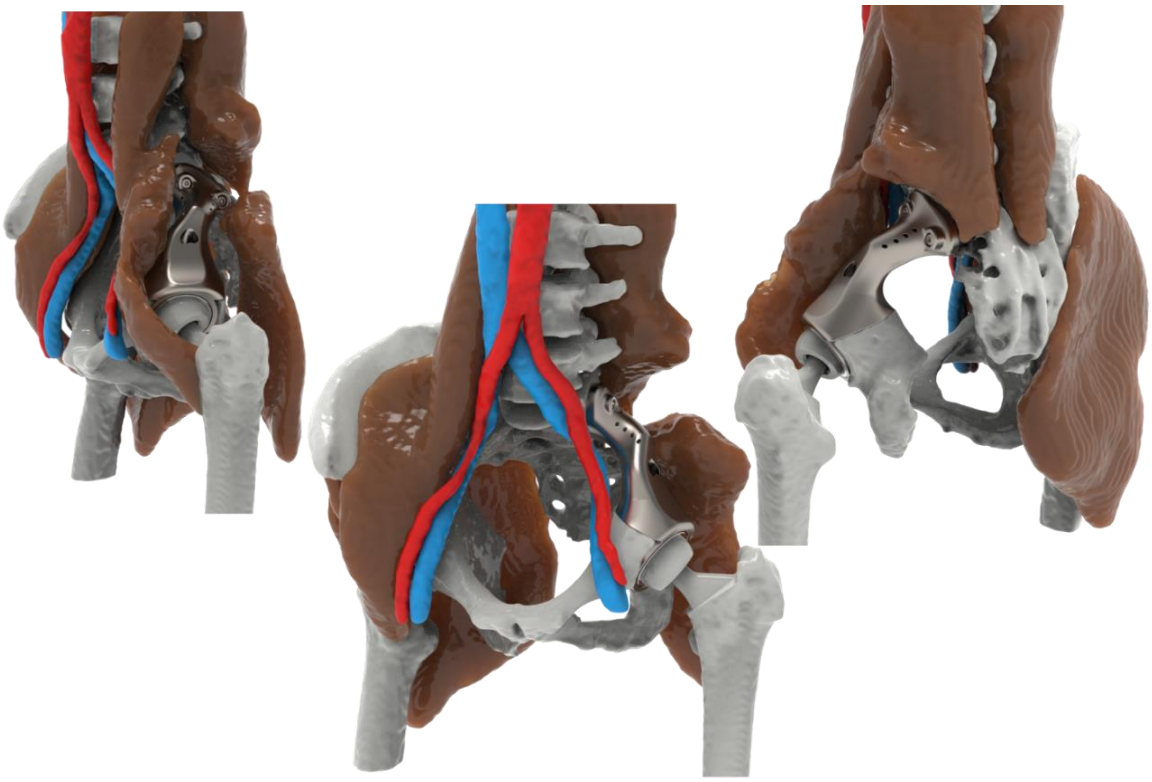

Figure 430: Photorealistic views of preliminary solution featuring soft and hard tissue

All intangible content about the endo-prosthesis and all ancillaries, along with the interactive 3D models per se, including the animated mechanical simulations were uploaded to *SkeletoMy* to be assessed by the surgeon for review. Also, the .stl models of all devices (endo-prosthesis, cemented cup acetabulum reaming check tool, acetabulum rooftop and sacrum side flat-cutting jig, femoral head-cutting jig, and left aligned femur with the stem inserted) were delivered to be imported into the 3D Slicer DICOM processing software by the surgeon to analytically view in 2D slices *(Figure 431)* and 3D *(Figure 432)* the fit of all parts and the fixation points, orientation and lengths. The design was approved and the workflow continued to the detailed design phase.

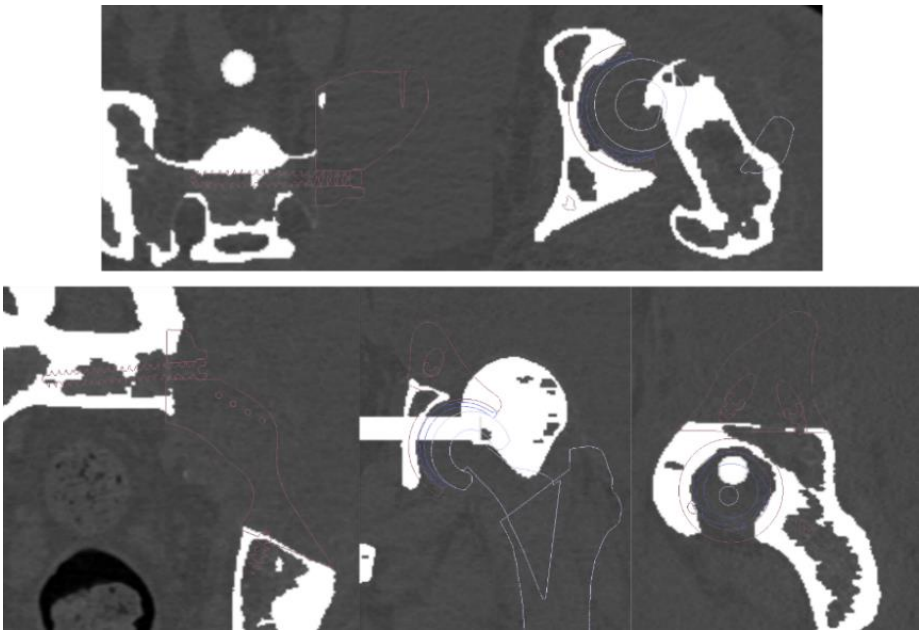

Figure 431: 2D slices of the preliminary solution in 3D Slicer

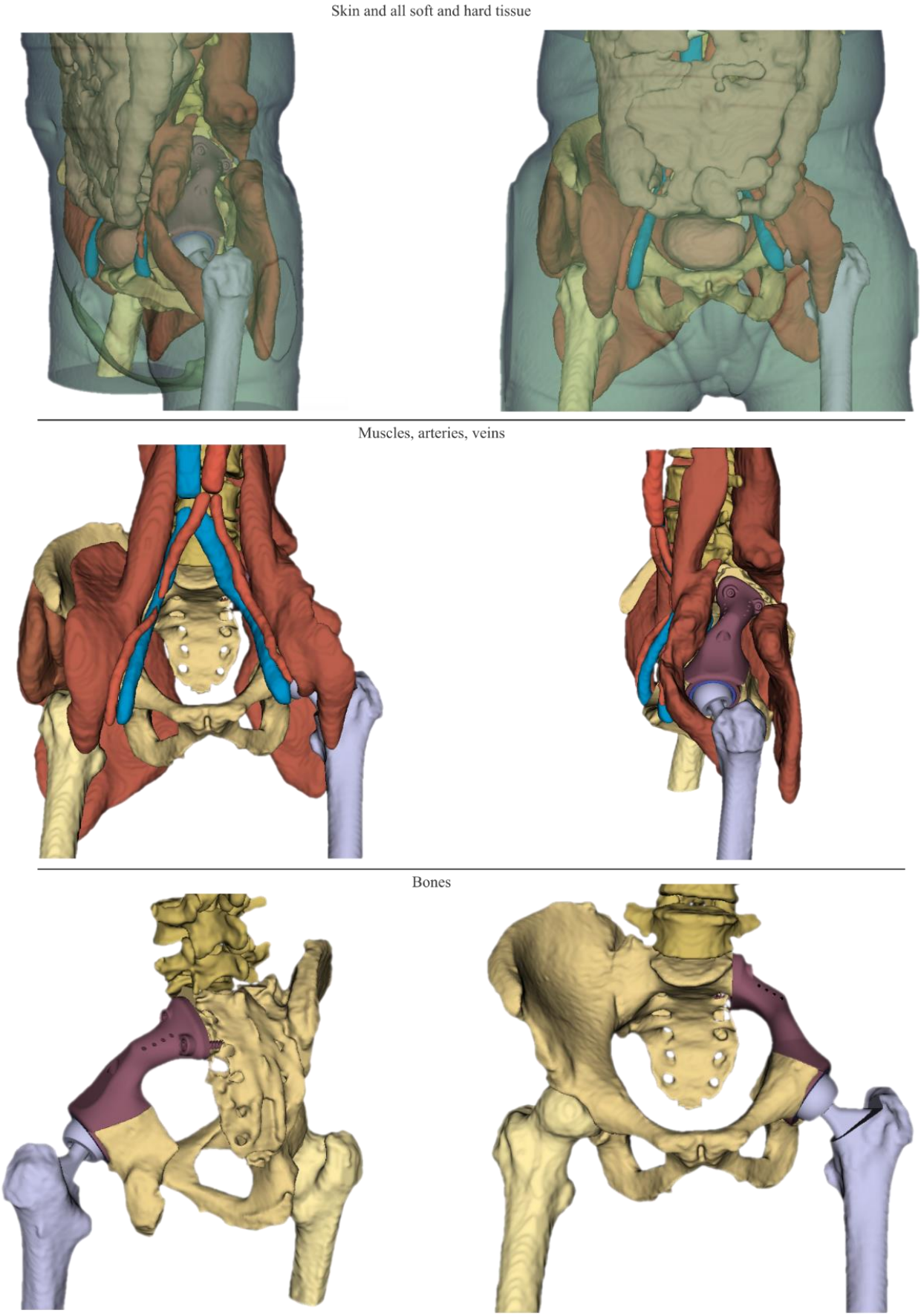

Figure 432: 3D views of the preliminary solution in 3D Slicer

6.4.9 Detailed Design

The detailed design is the last step of the development workflow and includes geometrical and functional fine-tuning interventions for making the materialization feasible and optimal. In this section, the design will be adjusted and optimized based on the pre-set specification list and the selected 3DP techniques and biomaterials.

The selected final biomaterials for each part of the solution to be used in the operating room are:

- **Endo-prosthesis:** Ti6Al4V Grade 3 (also known as Extra Low Interstitial (ELI)) as per ASTM F136 will be used which is very similar to Ti6Al4V but with improved ductility and fracture toughness due to the reduced contents of oxygen, nitrogen, carbon, and iron. *Figure 433* shows the composition of Ti6Al4V Grade 3 powder and the groups of different particle size ranges as emerged by the plasma atomization process.

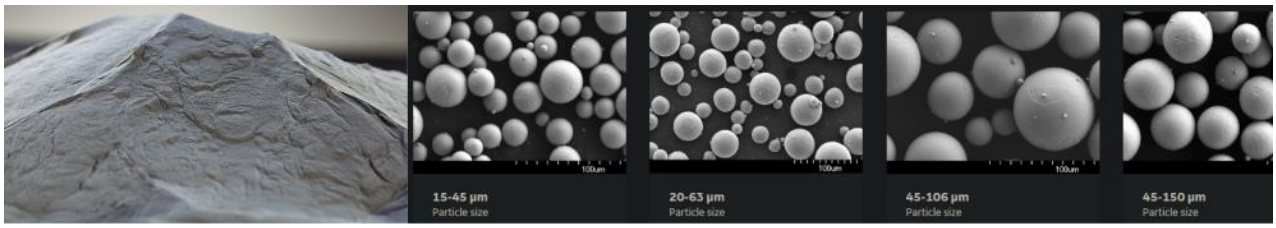

Element	ASTM F3001 requirement [wt.%]	Typical composition of solid material [wt.%]
Aluminum	5.50 – 6.50	6.15
Vanadium	3.50 – 4.50	3.99
Iron	Max 0.25	0.19
Oxygen	Max 0.13	0.12
Carbon	Max 0.08	0016
Nitrogen	Max 0.05	0.015
Hydrogen	Max 0.012	<0.001
Yttrium	Max 0.005	<0.001
Other elements, each	Max 0.10	-
Other elements, total	Max 0.40	-
Titanium	Balance	Balance

Figure 433: Ti6Al4V Grade 3 powder characteristics. Source: General Electric

- **Ancillary instruments:** all these will temporarily come in contact with hard and soft tissue during operation. Polyamide 12 (PA 12) group of polymers which are of high strength and chemical resistance are selected. *Figure 434* shows the properties of PA 2201 Medical-Grade powder which has been tested as per ISO 10993 for cytotoxicity, sensitization, irritation, acute systemic toxicity, and material-mediated pyrogenicity.

The 3DP techniques to be applied for materializing the required components out of the aforementioned biomaterials are powder-bed fusion-based which is the industry standard for producing high-end biomedical products with superior properties and fine geometrical features *(Sing et al., 2015).* Various standards *(see Table 9)* have been established about the specifications for pre-processing, in-processing and post-processing, materials characterization, and design and quality management of metallic parts fabricated by powder-bed fusion technologies.

MEASUREMENT	VALUE	UNIT	STANDARD
Density	0,93	g/cm³	N/A
Tensile Strength	48	MPa	DIN EN ISO 527
Tensile Modulus	1700	MPa	DIN EN ISO 527
Flexural Strength	58	MPa	DIN EN ISO 178
Flexural Modulus	1500	MPa	DIN EN ISO 178
Impact Strength	4,4	kJ/m^2	DIN EN ISO 180 (Notched, Izod)
Elongation at Break	15	%	DIN EN ISO 527
Hardness	75	Shore D	DIN EN ISO 868
Heat Deflection Temperature 1	70	°C	ASTM D648 (@1.81 MPa)
Heat Deflection Temperature 2	154	°C	ASTM D648 (@0.45 MPa)
Vicat A Softening Temperature	181	°C	DIN EN ISO 306 (10N)
Melting Temperature	176	°C	DIN EN ISO 11357 (20°C/min)

Figure 434: PA 2201 Medical-Grade powder characteristics. Source: Materialise

Kruth et al. *(2005)* have analyzed and classified the binding mechanisms of powder grains into four teams, namely solid-state sintering, chemically induced binding, liquid phase sintering (partial melting), and full melting (*Figure 435*).

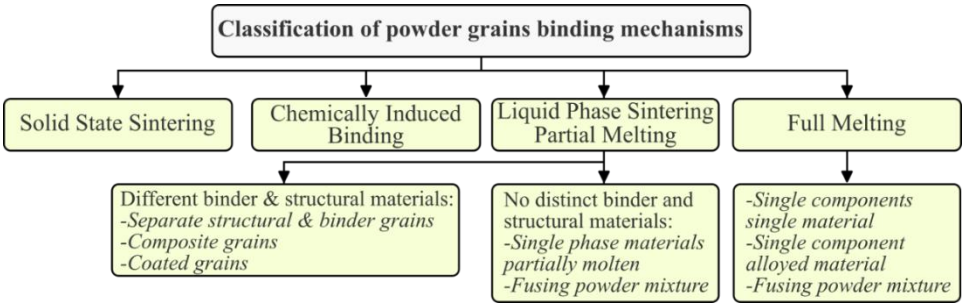

Figure 435: Powder grains binding mechanisms. Source: (Kruth et al., 2005)

Solid-state sintering will be used for the Polyamide 12 biomaterials. For example, Polyamide 12 biomaterials can be formed by 3D printers shown in *Figure 436*.

Fully melting will be used for the Ti6Al4V Grade 3 biomaterial. Nearly fully dense metal end-parts with outstanding properties better than conventionally manufactured products can be formed by fully melting the powder grains either by Electron Beam Melting (EBM) or Laser Beam Melting (LBM) *(Murr, 2015; Herzog et al., 2016)*. The comparative characteristics of EBM and LBM are listed in *Table 20*, the properties of Ti6Al4V Grade 3 products per technology are shown in *Figure 437*, whereas two such machines capable of shaping Ti6Al4V Grade 3 are shown in *Figure 438*.

Figure 436: Powder-bed fusion-based 3D printers for polymer parts. Source: Formlabs, HP, EOS

There are no special requirements for the PA 2201 ancillary instruments as these will be cleaned after 3DP, and then steam sterilized (autoclave) before application.

On the other hand, granted the successful 3DP of the Ti6Al4V Grade 3 endo-prosthesis and before its steam sterilization (autoclave) before implantation, it must be post-processed and then inspected for quality assurance and control, i.e.:

- Removal of the remnant entrapped powder particles by suitable techniques such as brushing off, blasting with inert gas, bead blasting, heat treatment for sintering the loose powder, ultrasonication in water, acid etching, high-intensity sound, mechanical vibration *(Seiffert, Hopkins and Sutcliffe, 2017).*
- Supports removal (if any) and part removal from build plate by hand or (if LBM) by machining, EDM wire cutting, or spark erosion.

- Heat treatment for stress relief (if LBM) and optionally Hot Isostatic Pressing (HIP) to increase the densification level, and improve the part's fatigue properties and ductility, though the tensile strength and hardness will be slightly lowered *(Bartolomeu et al., 2022).*
- The selection of surface post-treatments to improve the morphological, physicochemical, biochemical, and biological properties *(see Sub-section 3.1 and Figure 32)* depends on the nature of application, material type and properties, level of finish, part geometry and complexity, initial surface roughness, and economical considerations *(Boban et al., 2022).* As polishing Ti has been found to have little effect on bacterial adhesion and biofilm formation *(Sarfraz et al., 2022),* in this case, blasting with Al oxide abrasive followed by glass bead blasting will be used to obtain a satin surface finish at all non-bone contact areas.
- Bacteria-combat and osseointegration-boosting substances such as Ag coatings might be applied.

Table 20: Comparison of EBM versus LBM

Features	EBM	LBM
Beam type	Electron beam of high energy (4-5 kW) magnetically driven (high speed)	One or more laser (up to 1 kW each) beams driven by galvanometers (lower speed)
Chamber	Vacuum via helium and temperatures of 400-1000 °C.	Argon or Nitrogen and temperatures of 100-200 °C.
Powder pre-heating	Pre-heat scanning at 700-1000 °C	Platform pre-heat with resistances or infrared at 100-200 °C
Powder particle size	Larger (40-150 μm)	Smaller (10-45 μm)
Stress relief	No in most cases as temperature gradients are low	Yes in most cases as temperature gradients are high
Beam diameter	Larger (100 μm)	Smaller (50 μm)
Materials	Only conductive materials	Metals
Surface finish	Worse (25-35 Ra)	Better (4-11 Ra)
Scan speed	Faster (up to 8000 m/s)	Slower (up to 1250 mm/s)
Melt pool	Larger (0,2-1,2 mm)	Smaller (0,1-0,5 mm)
Supports	No need most of the time	Need supports
Layer thickness	Thicker (50-200 μm)	Thinner (15-150 μm)
Orientation	Up skins are smoother and vertical/down skins rougher	Up skins/verticals are smoother and down skins rougher
Support angle	Bottom edge and horizontals or areas vulnerable to over-melting	Bottom edge and surfaces over 45° or less from the platform need support
Wall thickness	Thicker (0,6-1,0 μm)	Thinner (0,2-0,5 μm)
Details	Coarser (0,6 minimum typically). Oriented upwards to avoid the need for supports and rougher textures	Finer (0,25-0,4 mm minimum typically). Oriented upwards to avoid the need for supports and rougher textures
Holes and tubes	0,5mm dia. vertical and < 8 mm dia. horizontal without support. Entrapped powder removal must be considered	0,5-2,0mm dia. horizontal holes need supports. Entrapped powder removal must be considered
Machining stock	0,5-2,0 mm extra for machining	0,1-0,5mm extra for machining
Hollowing	0,6-1,0mm min wall thickness. Removal of caked powder must be considered. Entrapped powder removal must be considered	0,2-0,5mm min wall thickness. Entrapped powder removal must be considered.
Screw Threads	Must be machined	Should be built vertically and must be machined
Cool-down	More time is needed until the part reaches room temperature	Less time is needed until the part reaches room temperature
Extra equipment	Powder handling and recovery systems, excess powder removal, blasting cabinet, unpacking and powder sieving and mixing stations, chiller unit, steady gas supply, build performance monitoring, and other post-processing operations.	

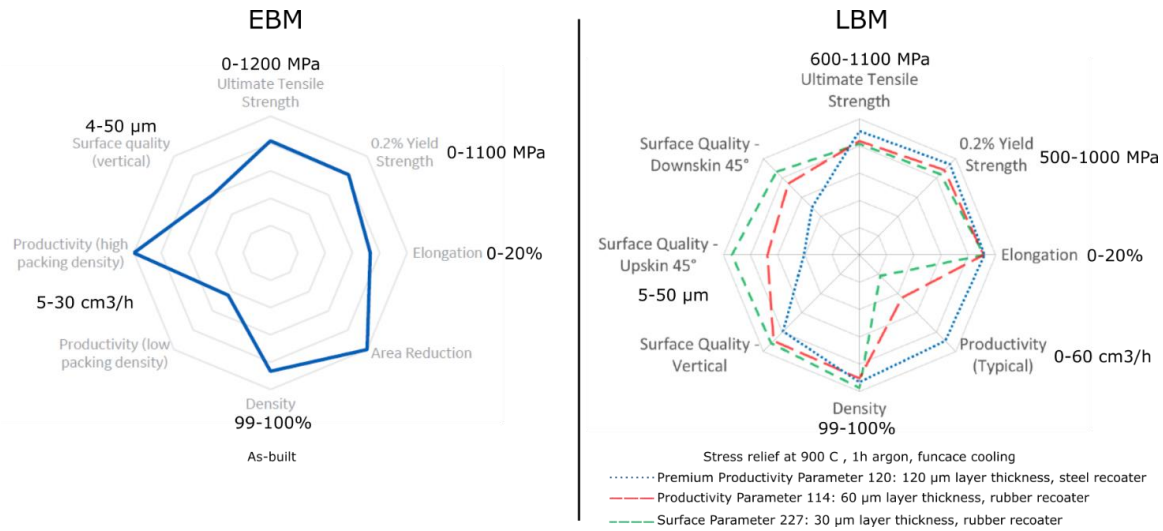

Figure 437: Properties of parts 3D printed by EBM versus LBM technologies. Source: General Electric)

GE Arcam M2 Q10plus EBM
Powder-bed fusion 3D Printer

Build volume: 200 x 200 x 200 mm.
Min layer thickness: 0.07 mm.
Min part resolution: 0.75 mm.
Max beam travel speed: 8,000 m/s.
Single beam 3000W.
Does not require neither wire EDM machining to remove the part, nor themral stress-relief.
Parts are 99.9% solid. Hot-isostatic-pressing optional.
Thermal and build monitoring and control.
Water-cooled heat sink.
Beam spot size: 0.140 mm.
Power consumption: 7000 W.
Connectivity: Wi-fi, Ethernet and USB.
Requirements: Helium gas 1 lt/ h + 50-75 lt/ build.
Materials: Titanium Ti6Al4V Grade 5/ Grade 23, Titanium Grade 2, CoCr, Pure Copper.
Dimensions: 2060 x 1066 x 2608 mm.
Weight: 1681 Kg.

Build volume: 245 x 324 x 350 mm.
Min layer thickness: 0.02 mm.
Max print speed: 2-35 q.cm/h.
Dual 400W fibre laser.
Thermal and build monitoring and control.
Integrated sieving and powder handling at inert atmosphere.
Integrated powder sieving & cleaning station.
Laser spot size: 0.070 mm.
Power consumption: 9000 W.
Connectivity: Wi-fi, Ethernet and USB.
Requirements: compressed air, nitrogen and argon gas tanks (depends on material).
Materials: Stainless steel 316L/ 17-4PH, Steel M300, Tool Steel H13, Aluminum AlSi10Mg/ AlSi7Mg/ A205, Nickel 718/ 625/ X, Titanium cp-Ti/ Ti6242/ Ti6Al4V Grade 3, CoCrW, CoCrMo.
Dimensions: 2695 x 1818 x 2185 mm.
Weight: 2500 Kg.

GE Concept Laser M2 DMLM
Powder-bed fusion 3D Printer

Figure 438: EBM and LBM powder-bed fusion-based 3D printers. Source: General Electric

Multi-scale, multi-physics phenomena occur during powder-bed fusion 3DP (*Figure 233)*, thus the process parameters (beam, layer scanning strategy, build orientation, layer thickness, support structures, build chamber environment, and feedstock and 3D printer per se) have to be optimized for the endo-prosthesis 3DP to avoid defects accordingly as per its geometrical features and application *(see Figure 88 and Sub-section 3.3.6 and Sub-section 3.6.3).* Selecting and applying sub-

optimal processing parameters not only during in-process but also during pre-processing and post-processing might lead to increased structural defects (geometric and micro-structural) that have implications on the final properties and quality of the 3DPed product. Additionally, the designed endo-prosthesis must not exceed the processability of the manufacturing equipment but conform to its manufacturability (design for manufacturing principles). Hence, it is apparent that Df3DP guidelines about design interventions and 3DP process planning have to be adopted targeting specific 3DP technology to maximize product performance and life-cycle objectives through synthesis of shapes, sizes, hierarchical structures, and material compositions for parts that can exhibit shape, material and functional complexities (*Kranz, Herzog and Emmelmann, 2014; Thompson et al., 2016; Schnabel, Oettel and Mueller, 2017; ISO/ASTM, 2018; Diegel, Nordin and Motte, 2019; Leary, 2019*; *Renjith, Park and Okudan, 2019; Vaneker et al., 2020).* By proper geometrical design, 3DP process simulation, suitable process parameter configuration, in situ monitoring and anomaly detection, and post-processing, defects can be minimized and performance maximized.

For endo-prostheses targeting osseous reconstruction, it is necessary that their surface is suitably architected to allow both hard tissue ingrowth and soft tissue re-attachment (if applicable) and their stiffness is tuned to comply with the loading conditions of the anatomical area where they are about to be applied. The stiffness of rigid metallic biomaterials such as Ti6Al4V can be tailored by computational modeling approaches generating meta(bio)materials-by-design. The ideal scenario would be to create smart degradable meta(bio)materials capable of morphing their geometrical features and dynamically altering their stiffness imitating the natural remodeling process of the bone as per the mechanobiological stimuli, but unfortunately, the materialization of such biomaterials capable of fully weight-bearing is not yet available.

The stiffer endo-prosthesis compared to the substituted bone tissue and the surrounding host pelvic bone could potentially cause stress shielding phenomena that decrease bone mineral density and weaken the healthy tissue around the implant. Therefore, it would be beneficial to reduce the stiffness by stress-driven mass reduction and implementation of suitable geometrical features. Towards this direction, topology optimization and generative design can be employed to light-weight the initially fully solid 416 gr endo-prosthesis by stress-driven mass reduction. Knowing, the fixation points of the endo-prosthesis, a generative design study was executed just to explore shape-optimized options. The generatively emerged solid-strut organic form selected in Fusion 360 is illustrated in *Figure 440*. The workflow applied is described below and shown in *Figure 439*:

1. **Preserved and obstacle regions definition:** the NURBS anatomical model and the screw insertion trajectories were set as obstacles to avoid, and the acetabular shell and screw beds (with 15 mm length) were set as preserved geometries.

2. **Material assignment:** Ti6Al4V with a modulus of elasticity of E=110 GPa, Poisson's ratio of ν=0,3, and 950 MPa yield strength.
3. **Boundary conditions and loads:** the sacrum screw seats were assumed to be fully fixed (constrained in all degrees of freedom) from the surface that touches the sacrum in all degrees of freedom and a 3000 N force (a force four times the body weight, explained next) was applied at the inner dome of the acetabular shell with a direction 30° as seen from the frontal plane and perpendicular to the acetabular shell face as seen from the transverse plane.
4. **Objectives:** mass minimization with a factor of safety of three, and no manufacturing constraints.
5. **Generated design selection:** the selected design had a mass of 179 gr, a factor of safety of 6,5, and reached a maximum von Mises stress of 136 MPa.

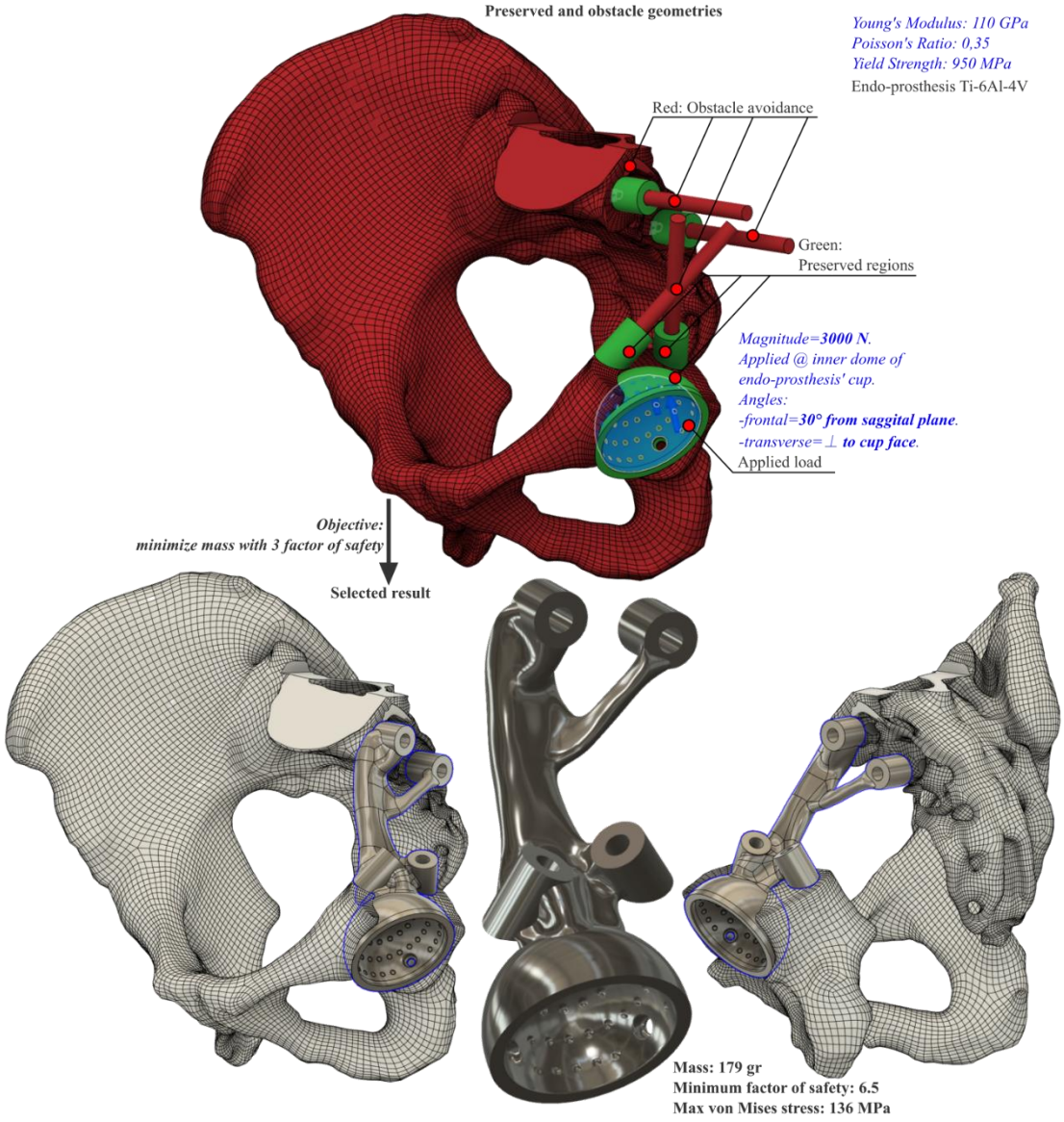

Figure 439: Generative design of endo-prosthesis

Although fascinating, shape-optimized endo-prostheses should indeed be carefully studied under all possible loading scenarios (magnitude, application points, directions) and under as realistic conditions as possible for maximum safety. Unfortunately, the simulation of the right hip socket

forces was not able to be generated as the anatomical model served as an obstacle object. Hence, the generated design did not consider stresses that emerged in cases when the right hip socket is loaded. The generated concept had a mass of 179 gr. *Figure 440* shows the final result as-modeled in Fusion 360 and as-rendered in KeyShot with screw head seats and flat surfaces to touch the side sacral and acetabulum rooftop bone that once implemented with porosity would allow bone ingrowth.

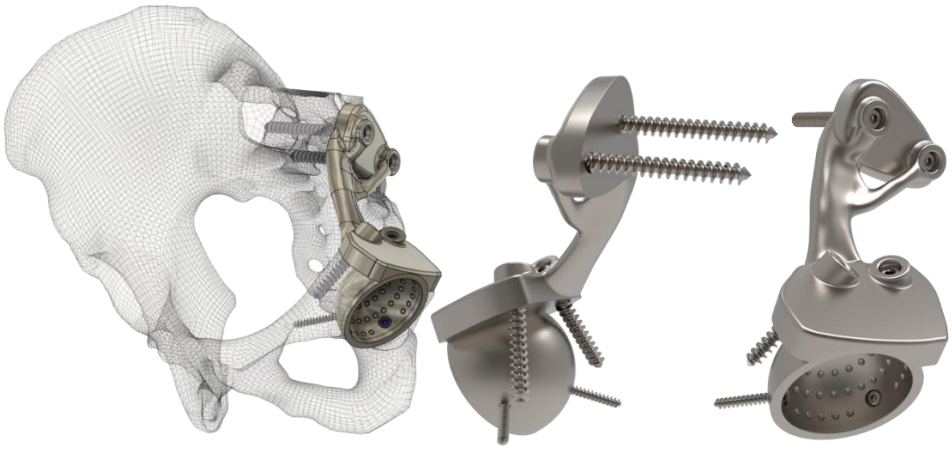

Figure 440: Final generatively designed and shape-optimized endo-prosthesis

Topology-optimized endo-prostheses can be weight-reduced whilst being stiffer than traditional ones *(Iqbal et al., 2019)*. Such approaches with stress maps were explored as a reference to drive optimal the later modeling of cellular architectures. *Figure 441* shows the topology optimization set-up workflow conducted in Fusion 360 (preserved regions, boundary conditions, applied loads, meshing) for three studies (similar to the previously mentioned, i.e. left, right, and combined hip socket loading scenarios) with the objectives of reducing the total mass by 30% (292 gr) and 40% (250 gr). *Figure 442* and *Figure 443* illustrate the stress-driven material removal results.

As per the pre-set specifications list, a mechanical/functional (instead of anatomical) restoration was selected using a low-profile endo-prosthesis with a solid-shell silhouette (instead of an organic strut-like shape-optimized) that conforms to the healthy mirrored ilium. Hence, it was decided to keep a solid outer shell as is and architect the endo-prosthesis suitably with cellular architectures within and at the bone-interfacing areas to imitate the structure of natural bone (cortical and trabecular).

With 3DP, optimized implants with accurately controlled interconnected open and closed cellular architectures mimicking trabecular-like spongy complexes can be formed. Such can achieve a bimodal superiority compared to the fully solid counterpart in mechanical (lower stiffness and stress-shielding, thus decreased risk of aseptic loosening and peri-prosthetic fracture) and biological (bone ingrowth and osseointegration) dimensions. It is true that the mechanical and biological properties are correlated with the structure of a material at the nano, micro, and meso levels which affect its macro properties such as the mechanical stiffness and stem cell adhesion, proliferation, and differentiation. Cellular structures have a higher friction coefficient compared to their fully solid

counterparts and traditionally coated material *(Hsu et al., 2007)*, thus supporting better fixation at bone-touching areas without allowing micro-motions leading to avoidance of aseptic loosening and bone resorption, good initial stability and successful and fast tissue ingrowth. At the same time, cellular spongy endo-structures can act as energy absorbers during impacts by elastic deformations, transmitting more efficient energy flows, though such performances have to be assessed by mechanical simulations and any weak points eliminated by varying the geometry: spacing, element size, thickness, orientation, node sharpness.

Focusing on the quest to reverse engineer the bone structure, various unit cell geometries can be selected to create regular, gradient, or random cellular complexes *(see Sub-section 3.6)*. See *Figure 33* and *Sub-section 3.1* for the justification of the optimal values of suggested 0,3-0,6 mm pore size and ~70% porosity for cellular structures, though these depend on cell and cellular characteristics in addition to biomaterial selected and the characteristics of the region to be applied *(Karageorgiou and Kaplan, 2005; Palmquist et al., 2013; Shah et al., 2016; Hara et al., 2016; Taniguchi et al., 2016; Tan et al., 2017; Wild et al., 2018; Wang et al., 2019; Barba, Alabort and Reed, 2019)*.

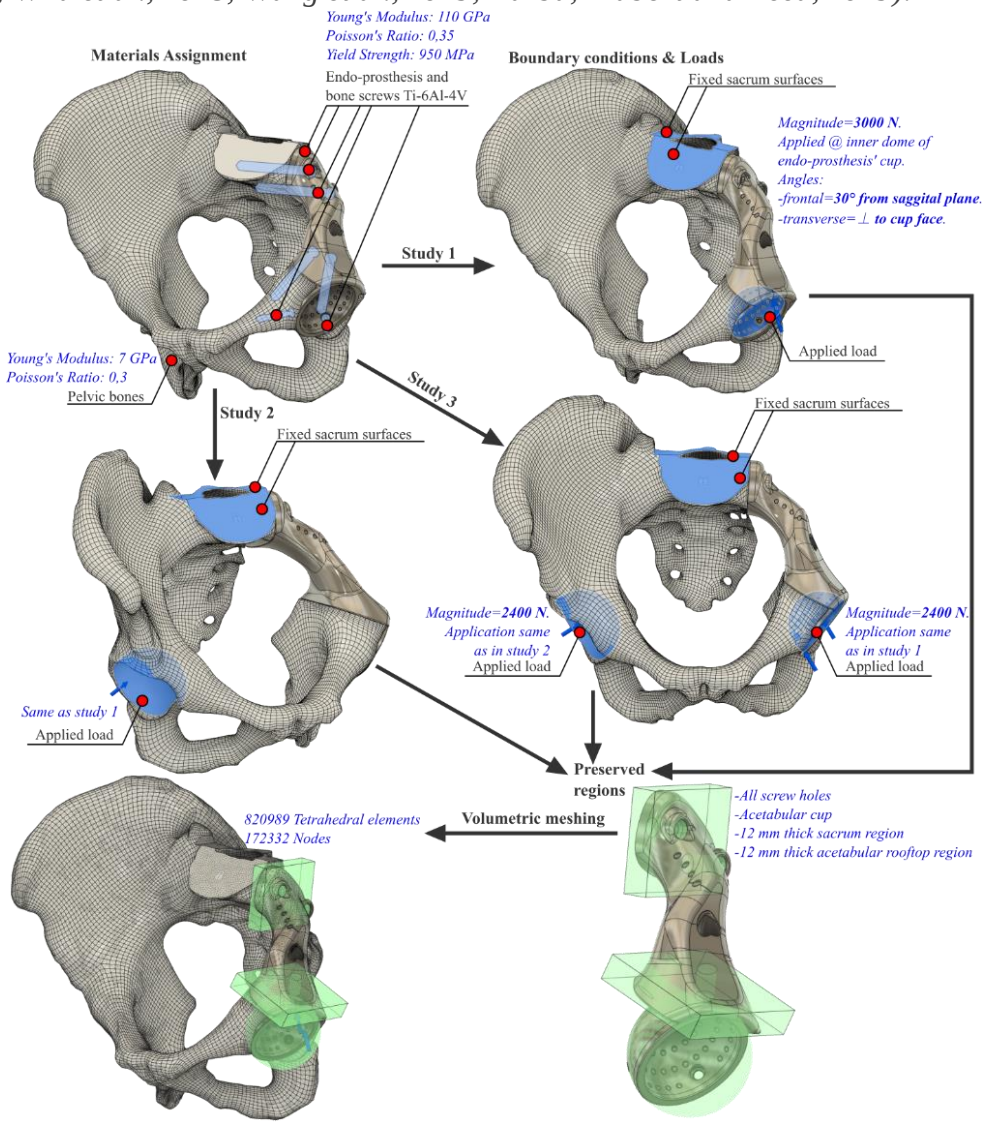

Figure 441: Topology optimization setup

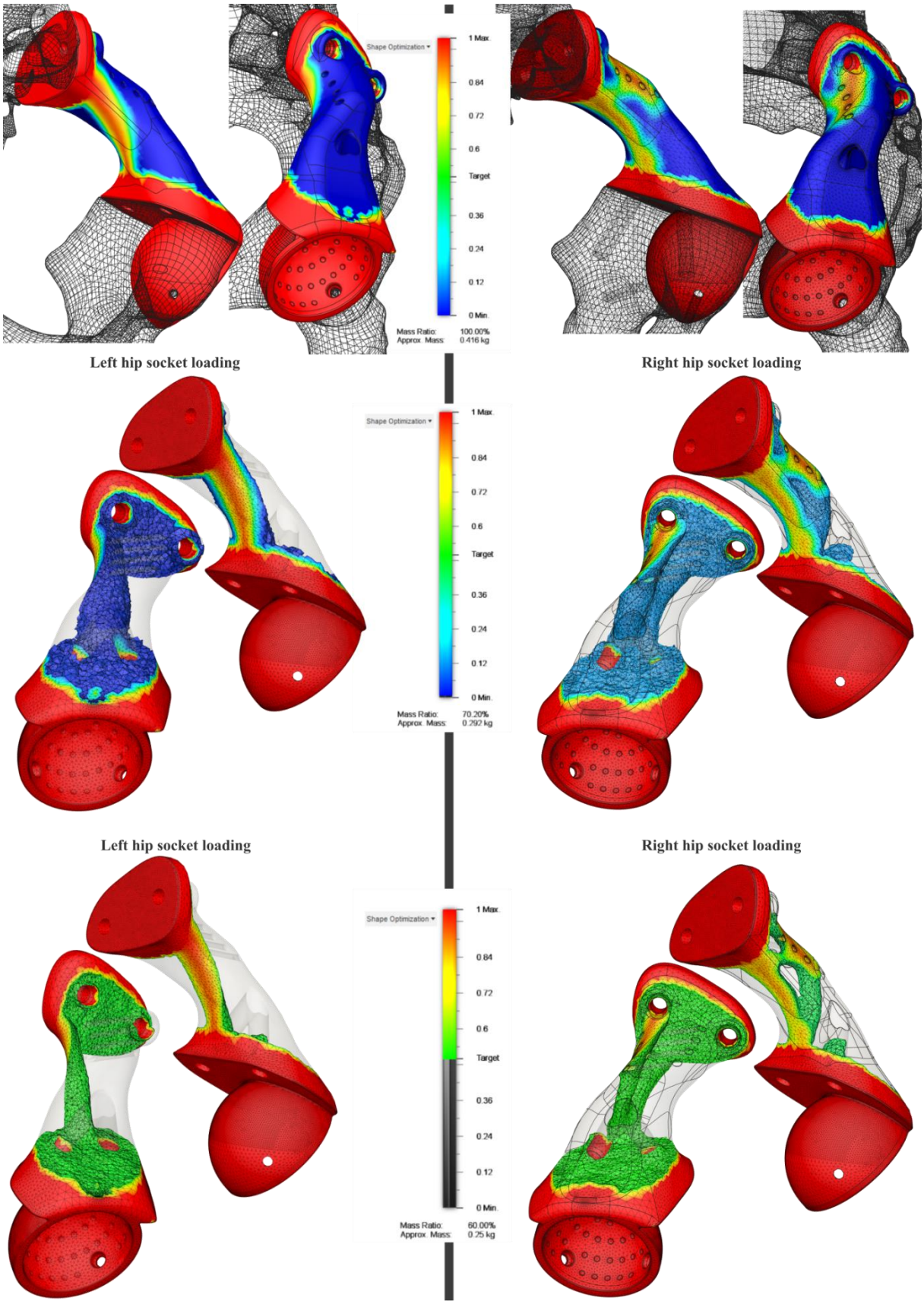

Figure 442: Topology-optimized endo-prosthesis for left and right hip loading cases

By addressing the ranges of good cell colonization, permeability for vascularization, and mechanical integrity, the optimal pore size was justified at 0,3-0,6 mm *(Tan et al., 2017; Barba, Alabort and Reed, 2019),* with supra-cellular architectures with large pores facilitating

vascularization and smaller pores promoting tissue maturation and formation being presented as possible alternatives *(Karageorgiou and Kaplan, 2005; Charbonnier, Hadida and Marchat, 2021).* Inspired by histomorphometric indexes of trabecular bone, many researchers have implemented sheet and skeletal-based TPMSs such as Gyroids and also stochastic (random distribution and pattern) Voronoi-generated elements to synthesize customized trabecular-like designs with constant and gradient-controlled interconnected porosity, pore distribution, and shapes *(see Sub-section 3.6)*.

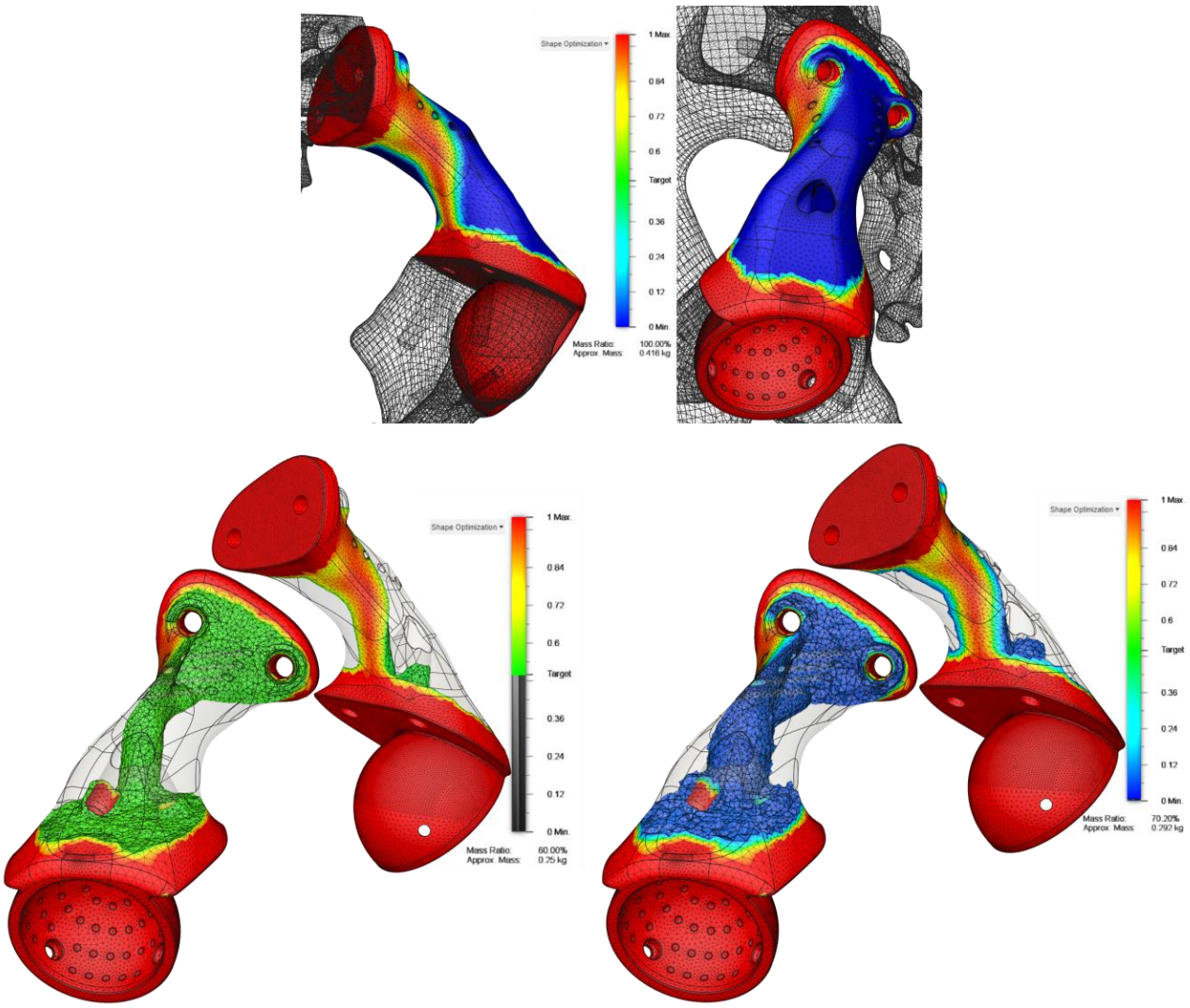

Figure 443: Topology-optimized endo-prosthesis for combined left-right hip loading

The characteristic parameters of a unit cell which can be arranged and interconnected with other cells to compose a cellular structure are shown in *Figure 444*. The cellular structure and properties of the external surfaces that touch the host bone had to adhere to the values reported in the literature *(see Sub-sections 3.1 and 3.6)*, however, the internal endo-structure further away from the bone-touching regions could be more relaxed and feature larger pore sizes and thicker strut thicknesses. Histomorphometric properties of trabecular bone at different anatomical sites can be used as a reference for artificial porous patterns *(McGregor et al., 2021a; 2021b)*. The histomorphometric properties of trabecular bone at the iliac crest (approximately 84% porosity, 0,15 mm feature

thickness, and 0,75 mm pore size) can be taken as a reference that would be then constrained by the mechanical-biological-manufacturing triad of limitations that define the allowable design space for cellular architectures.

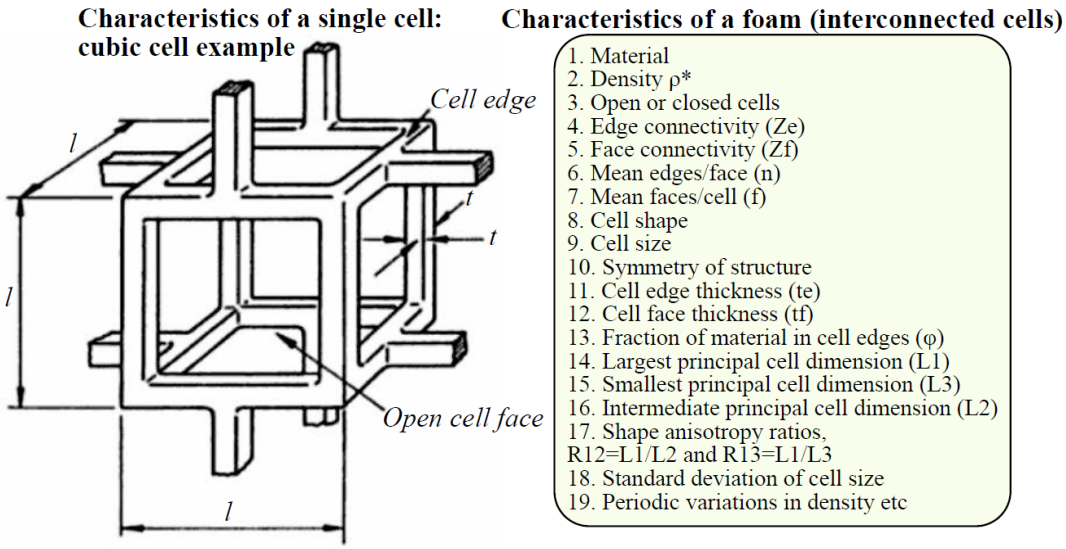

Figure 444: Unit cell and foam characteristics. Source: (Gibson and Ashby, 1999)

To *"biologize"* the internal form and external surfaces that touch the host bone and obtain optimal bimodal performance within a suitable design space, it was decided to explore two types of foams to mimic the spongy complex of the natural bone by considering a) optimal pore size of 0,3-0,6 mm as the best trade-off for good cell colonization, permeability for vascularization and mechanical integrity, b) the minimum allowable feature size for Ti6Al4V manufacturability (laser and electron beam PBF 3DP). The two structure types used to create meta-(bio)materials-by-design were:

1. **Stochastic beams:** randomized interconnected cells generated by Voronoi tessellation with both constant and graded seed point spacing and border thickness (strut/beam thickness).
2. **TPMS surfaces:** sheet and skeletal Gyroid TPMSs were selected to be explored and choose one to compose lattice structures with constant and graded cells and thicknesses.

LBM 3DP technology was considered as the best option for the beam-based Voronoi, and either LBM or EBM 3DP for the sheet or skeletal Gyroid structure, constraining thus their design process for manufacturability as per the limitations of each technology, e.g. minimum manufacturable feature and thickness and de-powdering requirements.

These types of cellular solids were presented with their characteristics in *Sub-section 3.6*. Sheet Gyroids have a stretching-dominated behavior, whereas stochastic Voronoi structures and skeletal Gyroids have a bending-dominated behavior, and their modulus of elasticity and strength are estimated by the Gibson-Ashby *(Gibson and Ashby, 1999)* formulas shown in *Figure 445*. Such can be assigned both internally and at the bone-contact surfaces with constant periodic/randomization or graded spacing and beam/wall thickness as per the topological mechanical and biological needs and constrained by the manufacturing limitations.

To design a cellular complex there are several approaches *(see Figure 162)*. Classic Boundary Representation (B-rep) parametric 3D modeling methods based on functions (NURBS, splines, etc.) and meshes/polygons/wireframes have limitations as such geometrical features are computationally intensive and might lead to failed boolean (union, subtraction) operations. Volume Representations (V-Rep) such as Constructive Solid Geometry (CSG) and especially voxel-based design, implicit/procedural modeling (algorithmic, math-driven computational design) and generative design approaches (iterative design process where the designer defines a computational model and design goals) are more suitable. For example, some software capable of architecting cellular solids by volumetric infill are *(Figure 446)*:

- **nTop** (nTopology Inc., New York, US): computational-based 3D modeling approach to generate extremely complex functional-graded surface or volume cellular solid geometries (sourced from libraries or custom-designed) not possible with traditional CAD methods. The implicit modeling platform combines B-rep, meshes, and simulation data to generate detailed models for manufacturing.
- **McNeel Rhino:** especially via the **Grasshoper** visual programming tool for generative design, assisted by many plug-ins for making any type of constant and gradient lattice and foams on surfaces and volumes.
- **Autodesk Fusion 360:** Gyroid, cross, x-cell, 1.5D-cell, Schwarz P, Schwarz D, and custom unit cells for uniform or gradient architecture generation of any cell size, strut thickness, porosity, and blend via the implicit volumetric lattice tool.
- **Ansys Spaceclaim:** extrusions (square, triangle, hex, 3D hex), lattices (cube-based, pyramid, diamond, octahedral, tetrahedral), TPMSs (Gyroid, Schwarz P, Schwarz D, Neovius, Lidinoid) and custom unit cells are for infilling bodies with regular periodic or graded lattices.
- **Autodesk Meshmixer:** processing, sculpting, and editing of 3D surface (triangular) meshes, capable of surface and volume periodic and gradient lattice and stochastic foam generation.
- **Autodesk Netfabb and Materialise Magics**: 3DP process preparation and simulation, supports generation and surface and volume lattice and stochastic structures generation software.
- **Materialise Mimics Innovation Suite**: using the 3-matic software to generate random, regular, or graded surface and volume cellular structures using the library or custom unit cells.
- **Blender:** many plug-ins to generate lattice and stochastic foams on surfaces and volumes, boosted by the geometry nodes design methodology (procedural).
- **Oqton Geomagic Freeform:** includes toolsets to design and clay-sculpt models into any form, capable of generating surface and volume lattice structures.

- **Altair Inspire:** to generate surface or volume regular, graded and random cellular solids (library of stochastic, TPMSs, 2D plate-based, and beam-based unit cells and option for custom) assess their mechanical performance through simulations, and analyze their geometrical characteristics.
- **Traditional parametric CAD platforms**: that are shifting towards implementing such design optimizations, e.g. 1) Siemens NX (Siemens Digital Industries Software Inc., Texas, US) especially with its new algorithmic-based approach and implicit modeling capabilities of surface or volume cellular structures, 2) DS Catia (Dassault Systèmes SE, Vélizy-Villacoublay, France) with its lattice designer tool and visual scripting approach to 3D modelling, and 3) PTC Creo (PTC Inc., Massachusetts, US) with the lattice generation tool.

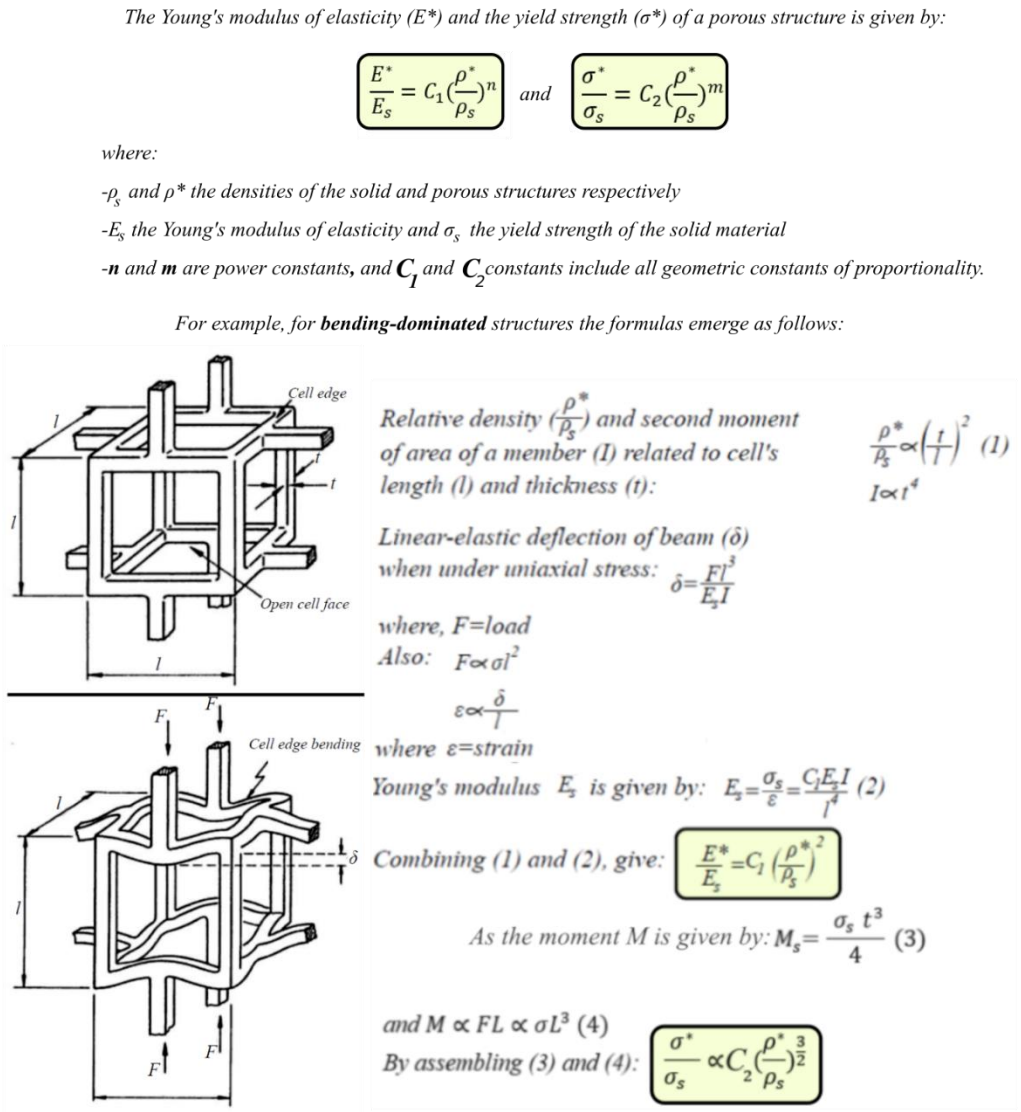

Figure 445: Formulas for relative modulus and strength cellular solids. Source: (Gibson and Ashby, 1999)

From the aforementioned software, nTop was selected to generate implicit models of complex cellular architectures. *Figure 447* and *Figure 448* show nTop's libraries to generate regular, gradient, or randomized (non)conformal cellular structures (Beam-based, stochastic, 2D plates, skeletal and sheet TPMS), though custom cells and stochastic patterns can be created. *Figure 449* shows two examples of cellular solids made by nTop: 1) a skeletal gyroid that transitions into sheet-like form

towards the left side and into beam-like forms towards the right side, and 2) a transition of a Gyroid into a Lidinoid TPMS from the center to the outer of a sphere.

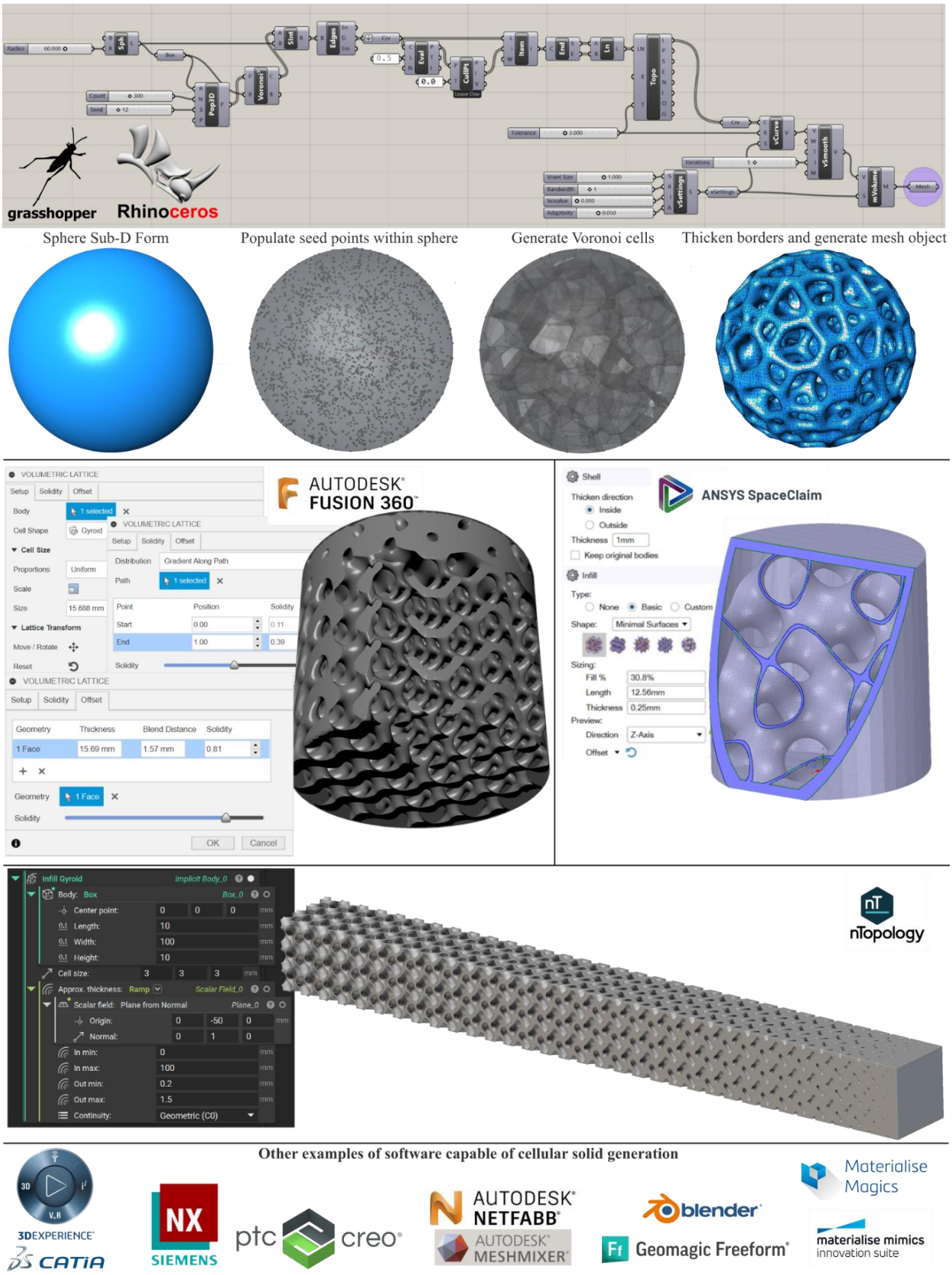

Figure 446: Examples of software capable of cellular structure 3D modeling

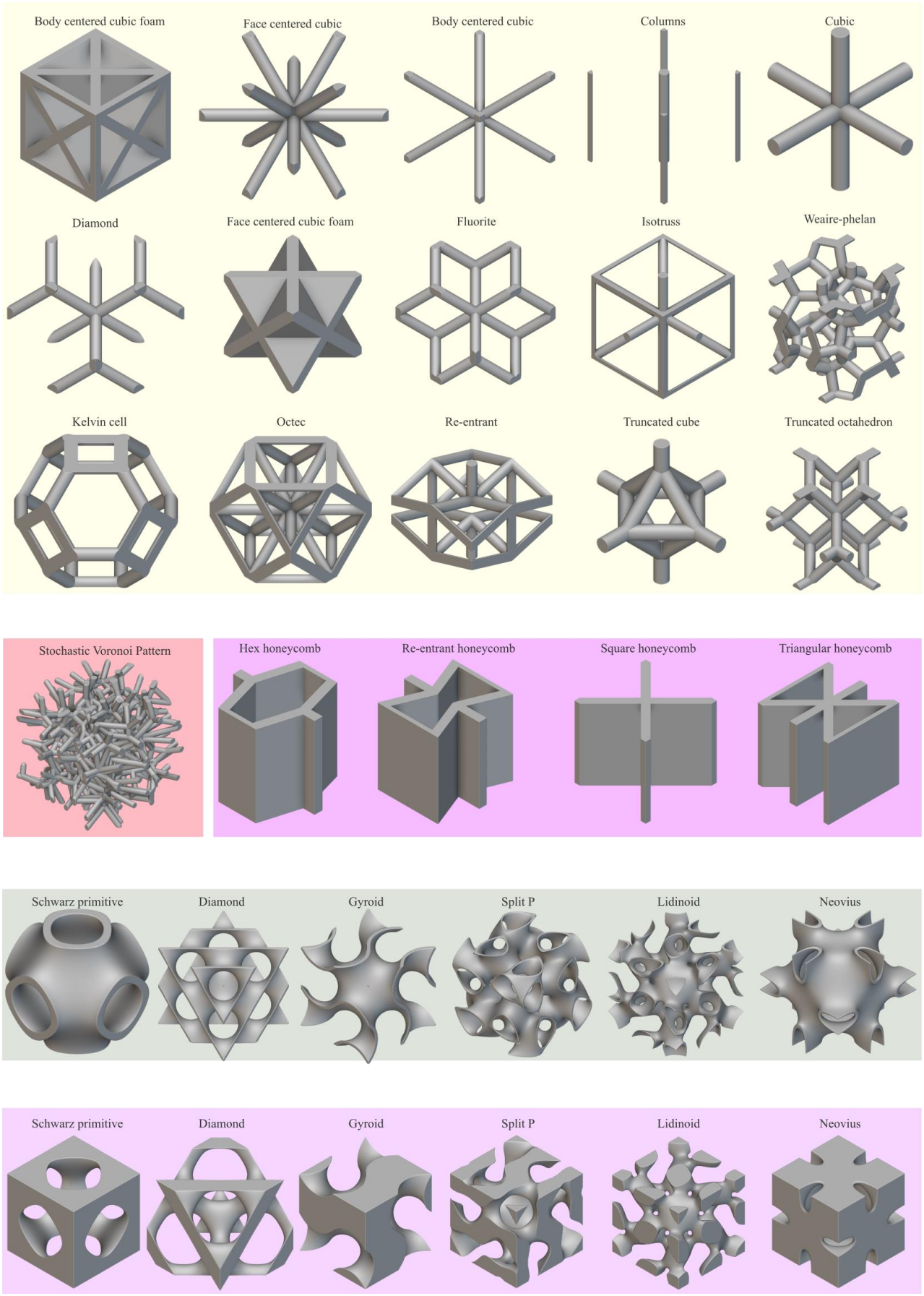

Figure 447: Beam-based, stochastic, 2D plates, skeletal, and sheet TPMS libraries in nTop

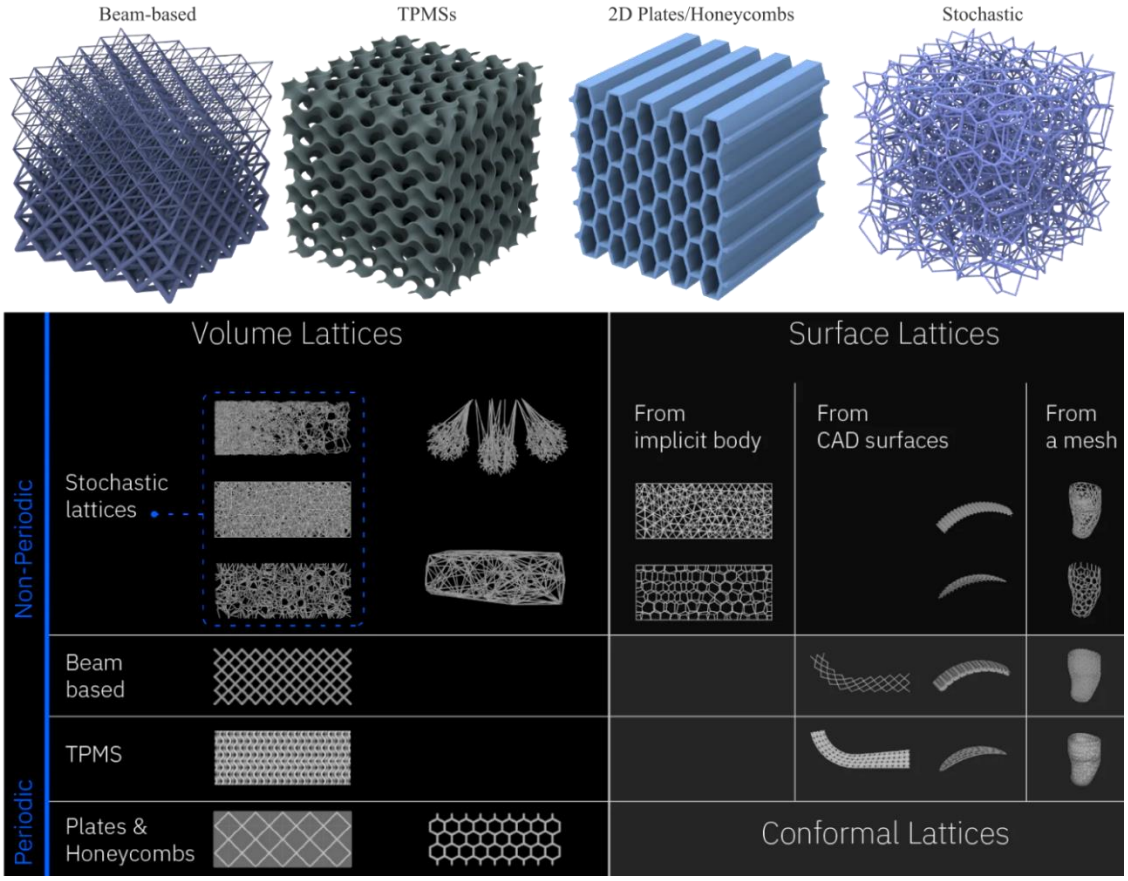

Figure 448: Types of cellular solids in nTop

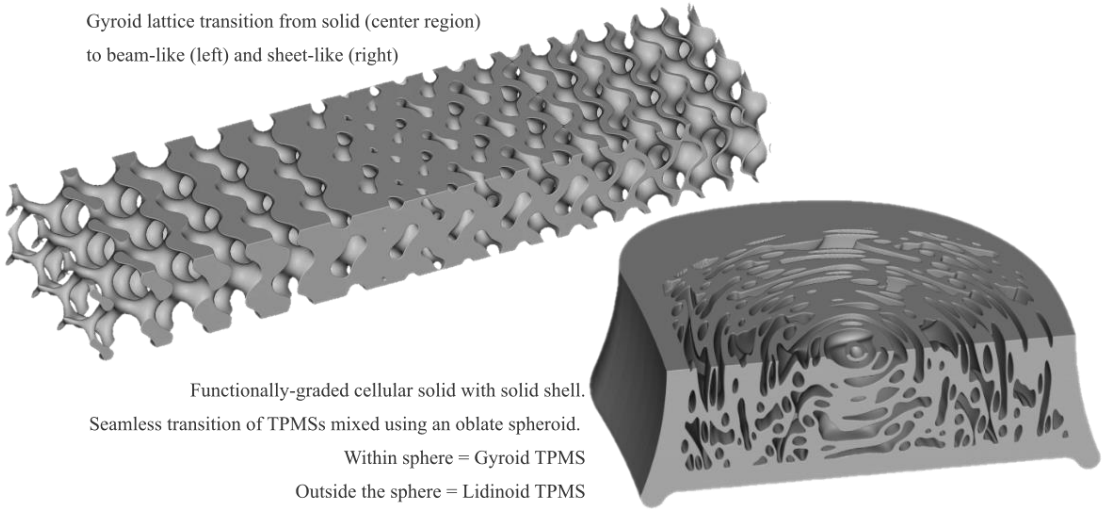

Figure 449: Examples of cellular structures generated by nTop

The initial stochastic Voronoi beam pattern architecting workflow concept of the endo-prosthesis is illustrated in *Figure 450.* More specifically:

1. First, the 3D solid STEP model (1,7 MB file size) of the endo-prosthesis was processed in Spaceclaim. The cup was left with a 1 mm wall thickness and the main body was hollowed with a 1 mm wall thickness (minimum required wall thickness for EBM 3DP technology) and the two faces touching the host bone were removed. as well. Walls 1 mm thick around all screw holes were set. The 1 mm thick hollowed main body and the 1 mm thick cup shell were combined into a single Ti6Al4V body which totaled a mass of 105 gr and a STEP file size of 9,5 MB. Two of the

four holes on the main body were set to be used for de-powdering after PBF 3DP in addition to the open faces of the main body that are enough, though extra holes can be opened if necessary. The remaining two holes were set to be used for optional soft tissue suturing. The regions where these holes were added did not suffer from high stresses.

2. A gradient stochastic Voronoi beam pattern with 0,6 mm average pore size and 60% porosity (0,45 mm and 1,35 mm beam thickness and 1,5 mm and 4,5 mm seed point spacing at the bone-contact areas and further away respectively) was architected selectively and topologically in nTop 4.0.5. The 3D solid STEP of the hollow shell model was imported and converted into an implicit model and the internal volume of the main body and the external surface of the cup were filled with a 3D stochastic Voronoi pattern. The total mass of the Ti6Al4V stochastic foam was 151 gr.
    a. The methodology followed to define the beam thickness parameters and the seed point spacing to achieve a 0,6 mm pore size (inscribed spheroid diameter within the voids) in a 15x15x15 mm reference cube is shown in *Figure 451* where spheres are fitted within the Voronoi cells and their diameters are averaged. 0,45 mm beam thickness and 1,5 mm random seed point spacing were selected, though by LBM details of 0,25-0,4 mm can be materialized.
    b. The most characteristic property of a porous structure is its porosity (φ) which is defined as $\varphi = \left(1 - \frac{\rho^*}{\rho_d}\right) * 100$ (percent), where ρ^* and ρ_d are the density of the cellular solid and fully dense solid respectively. The relative density $\frac{\rho^*}{\rho_d}$ was defined by dividing the volume of the cellular solid by the volume of the fully dense solid.
    c. Voronoi cells were infilled to fit and conform to the main body boundaries with its beam elements maintained intact without cutting off arbitrarily the beams' ends (no trimming) which could lead to edge effects. See *Figure 452* where boundary trimming and conforming with beam trimming and without beam trimming are shown for a reference cube body.
    d. As the regions further away from the bone-contacting areas which are pore size-constrained can be relaxed as there are no osseointegration requirements, the materialization of thicker beams would be more reliable and so would the powder removal after LBM 3DP. Thus, a gradient beam thickness and seed point spacing were assigned and created using an implicit model *(Figure 453)* with boundaries starting from and reaching 10 mm away from the bone-interfacing faces. The gradient was achieved by setting a ramp from the center of the main body towards the ends of the main body. The types of ramps supported by nTop are illustrated on a cube shown in *Figure 454*.
3. The cellular parts and the solid body shell and solid cup were combined and blended into a single Ti6Al4V body with a mass of 256 gr, converted into a surface mesh, and exported into a 2000 MB .stl file size. To obtain improved union, a blend radius of 1 mm was used, thus creating a solid

shell of 1,5 mm thickness. *Figure 455* shows the difference in implementing a blend radius to unite a shell with an infill cellular structure. Pertaining to the tolerance used for the surface mesh model generation, a 0,2 mm tolerance was used as acceptable compensation for the beams by triangular tessellation. *Figure 456* shows trade-offs between quality and file size differences for 0,1 mm, 0,2 mm, and 0,5 mm tolerance outputs.

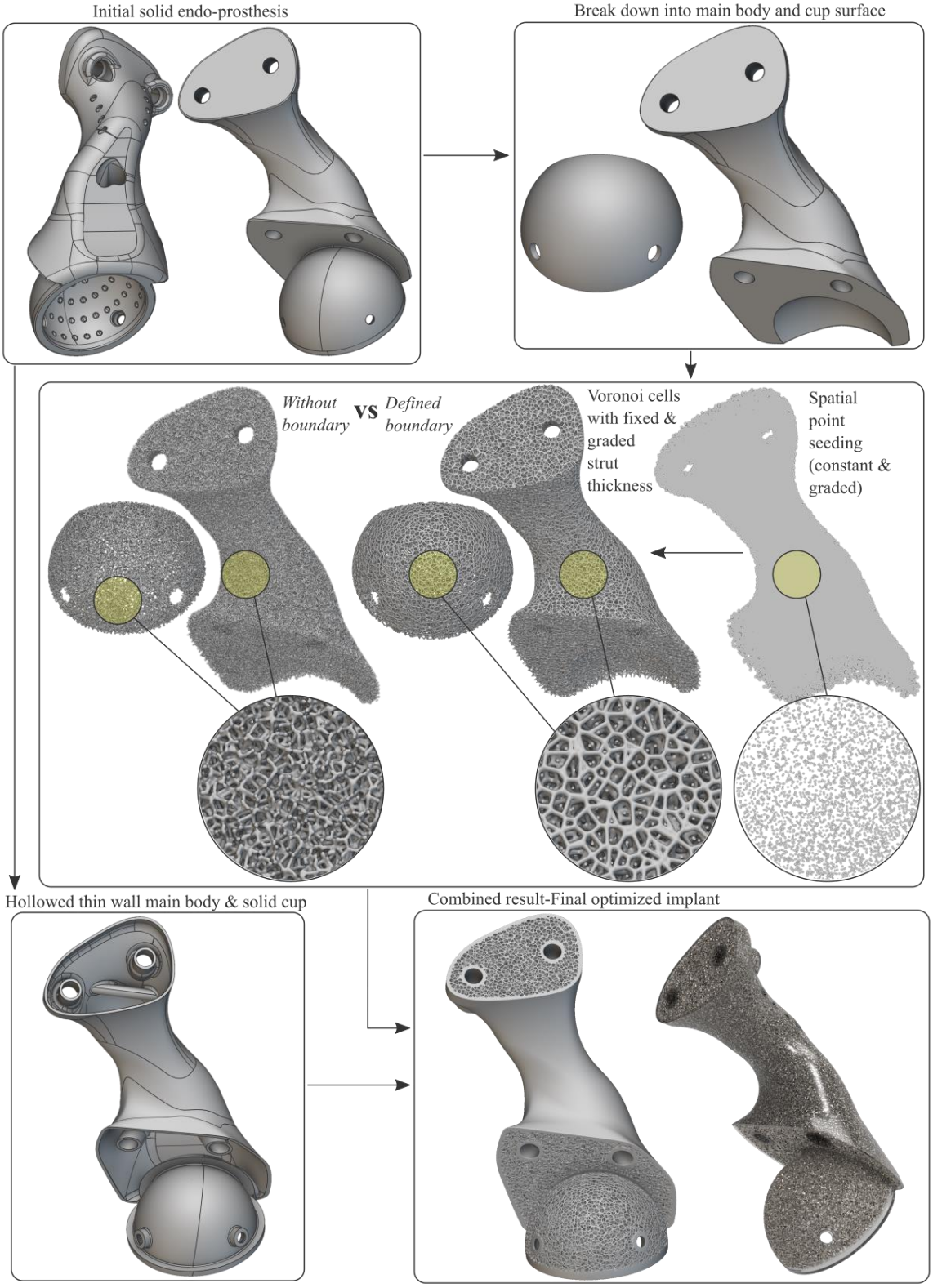

Figure 450: Endo-prosthesis porous optimization workflow

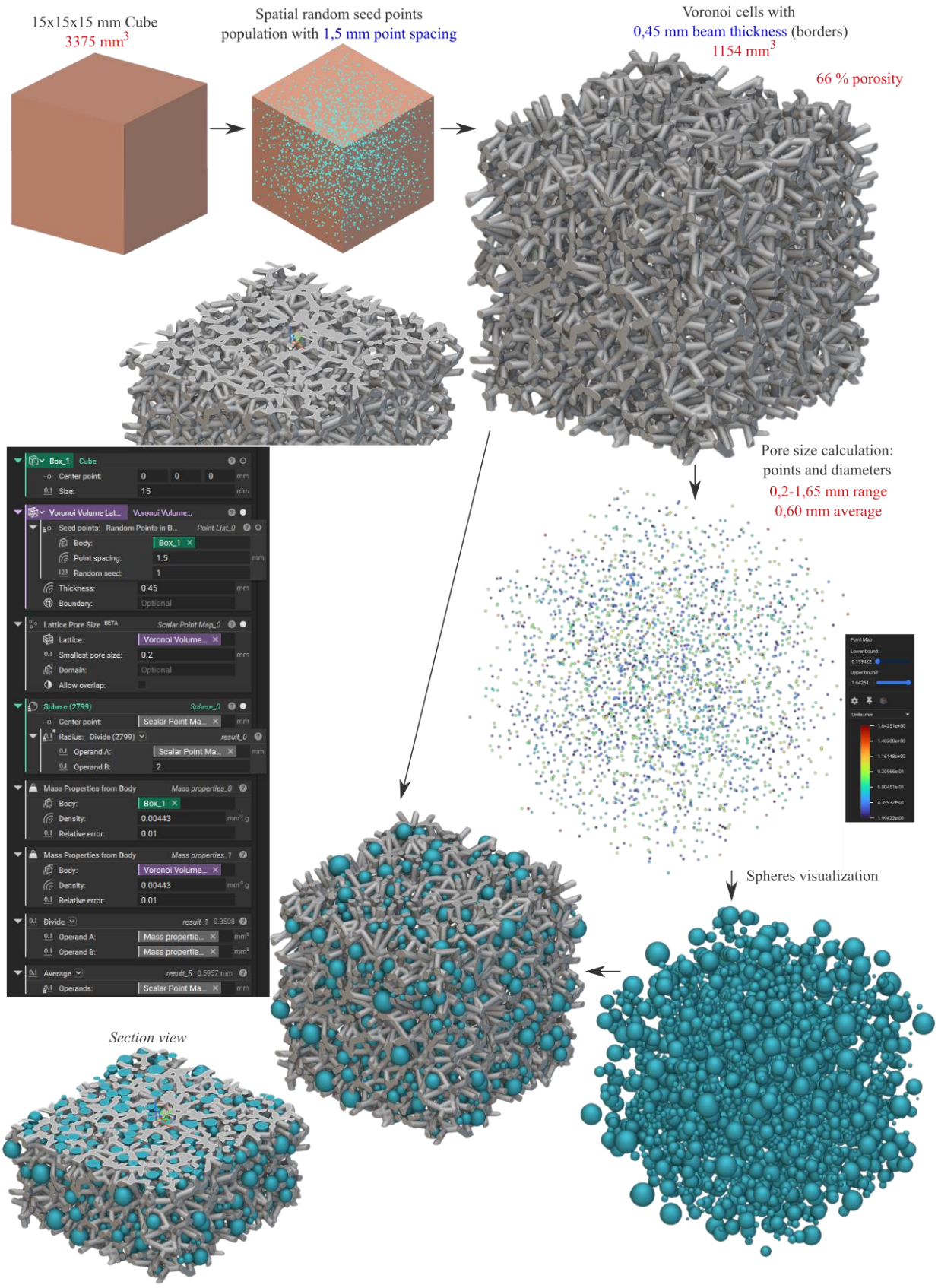

Figure 451: Voronoi complex pore size calculation workflow

Figure 457 shows the workflow used in nTop to generate the functionally-grade meta-(bio)material-by-design based on Voronoi cellular endo-structure, whereas *Figure 458* and *Figure 459* show characteristics, photo-realistic and detailed views of the final optimized endo-prosthesis.

In contrast to stretch-dominated cells that are stiffer and stronger, bend-dominated structures such as randomized interconnected Voronoi cells are ideal options due to their low modulus of elasticity and strength in tandem with high energy absorption properties *(see Sub-section 3.6)*. From the Gibson-Ashby equations shown in *Figure 445* for calculating the modulus of elasticity (E^*) and strength (σ^*) for cellular solids, Voronoi-based foams with open cells and high porosities can be considered ideal bending-dominated structures, and constants can take the values $C_1=1$, $C_2=1$, $n=2$ and $m=\frac{3}{2}$ *(Roberts and Garboczi, 2002; Benedetti et al., 2019; Mueller et al., 2019; Dewey et al., 2023*. Thus, the modulus of elasticity and strength of the generated Voronoi structure would be:

$E^* = 110\ GPa * (0{,}4)^2 = 17{,}6\ GPa$, close to the modulus of elasticity of cortical bone *(Appendix E)*

$$\sigma^* = 950\ MPa * (0{,}4)^{\frac{3}{2}} = 240{,}3\ MPa$$

Stochastic Voronoi structures are isotropic and homogeneous in terms of elastic properties along any loading direction as a result of their randomized cell orientation *(Mueller et al., 2019)*.

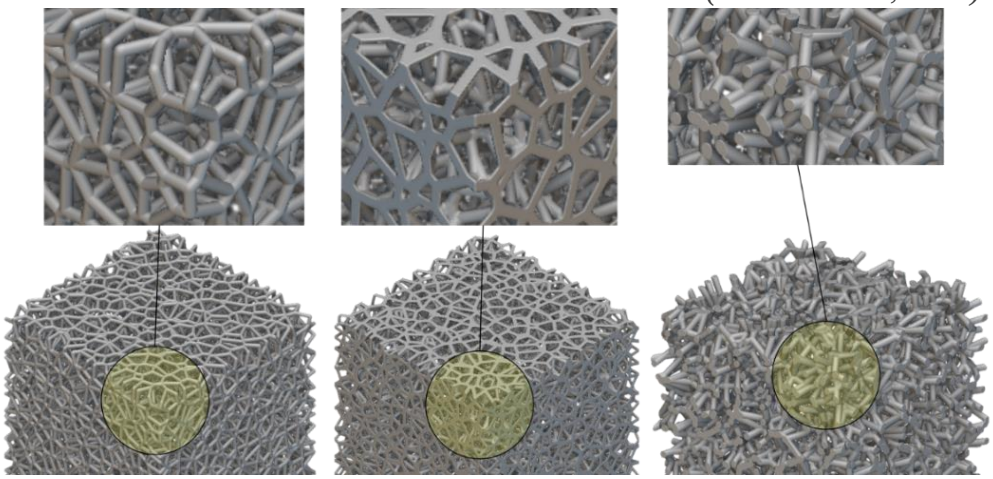

Figure 452: Examples of Voronoi pattern with and without defined boundary limits to conform

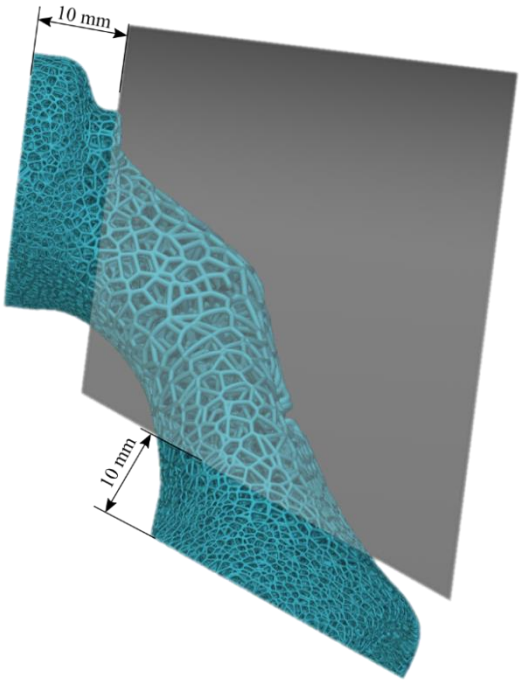

Figure 453: Gradient region for the Voronoi pattern

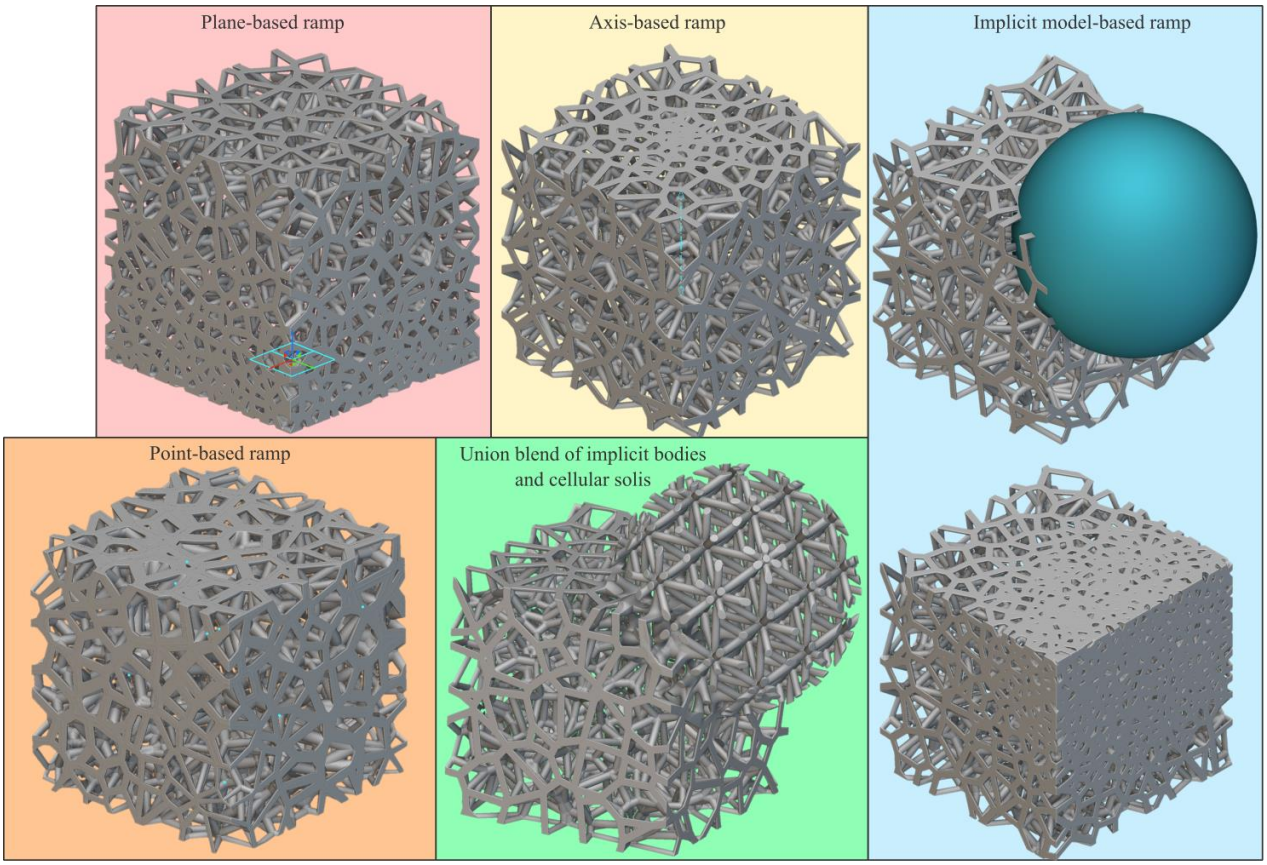

Figure 454: Ramp options to create point spacing and beam thickness gradients in nTop

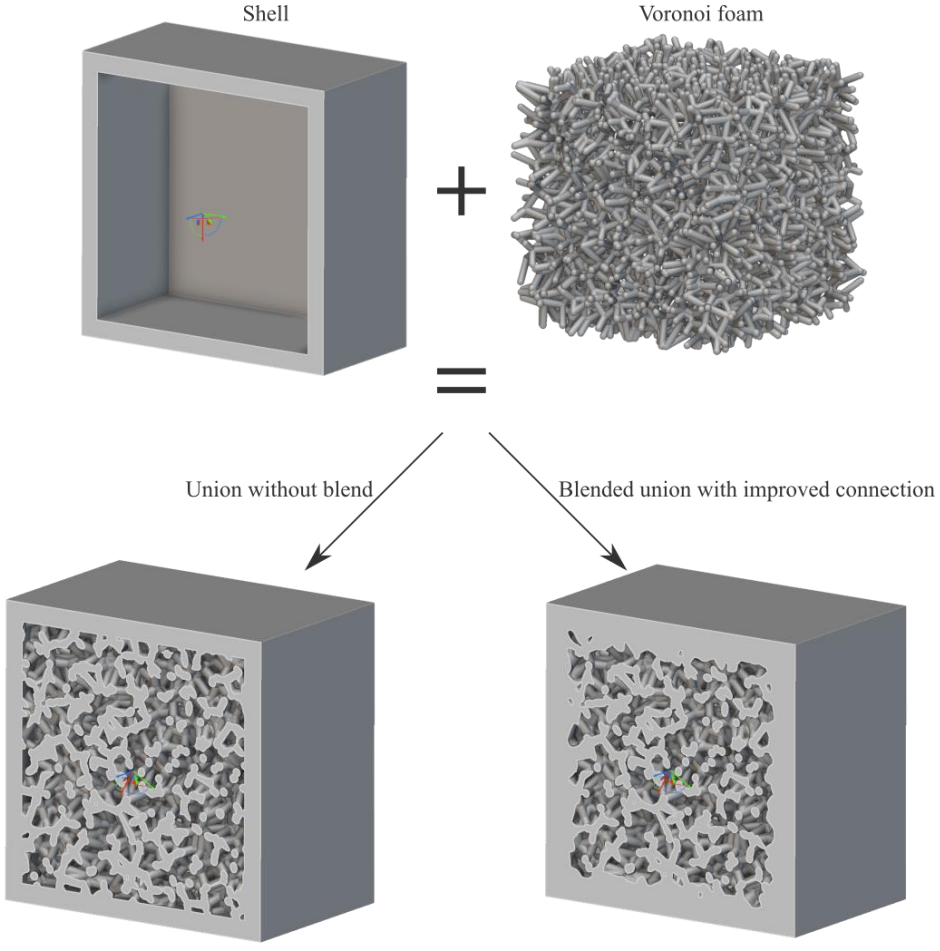

Figure 455: Examples of cellular infill-solid shell union with and without blending radius

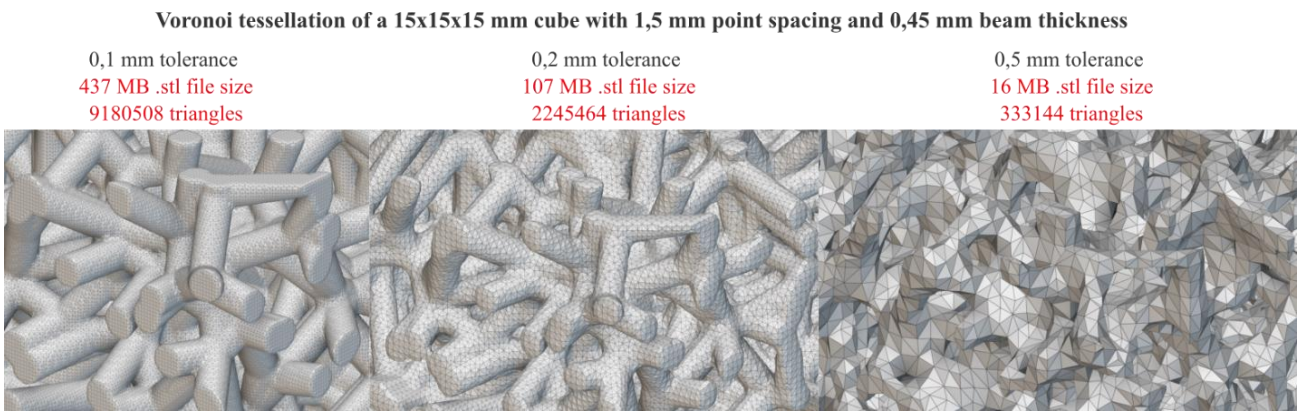

Figure 456: Tolerance and file size of facet meshes (.stl) output from nTop

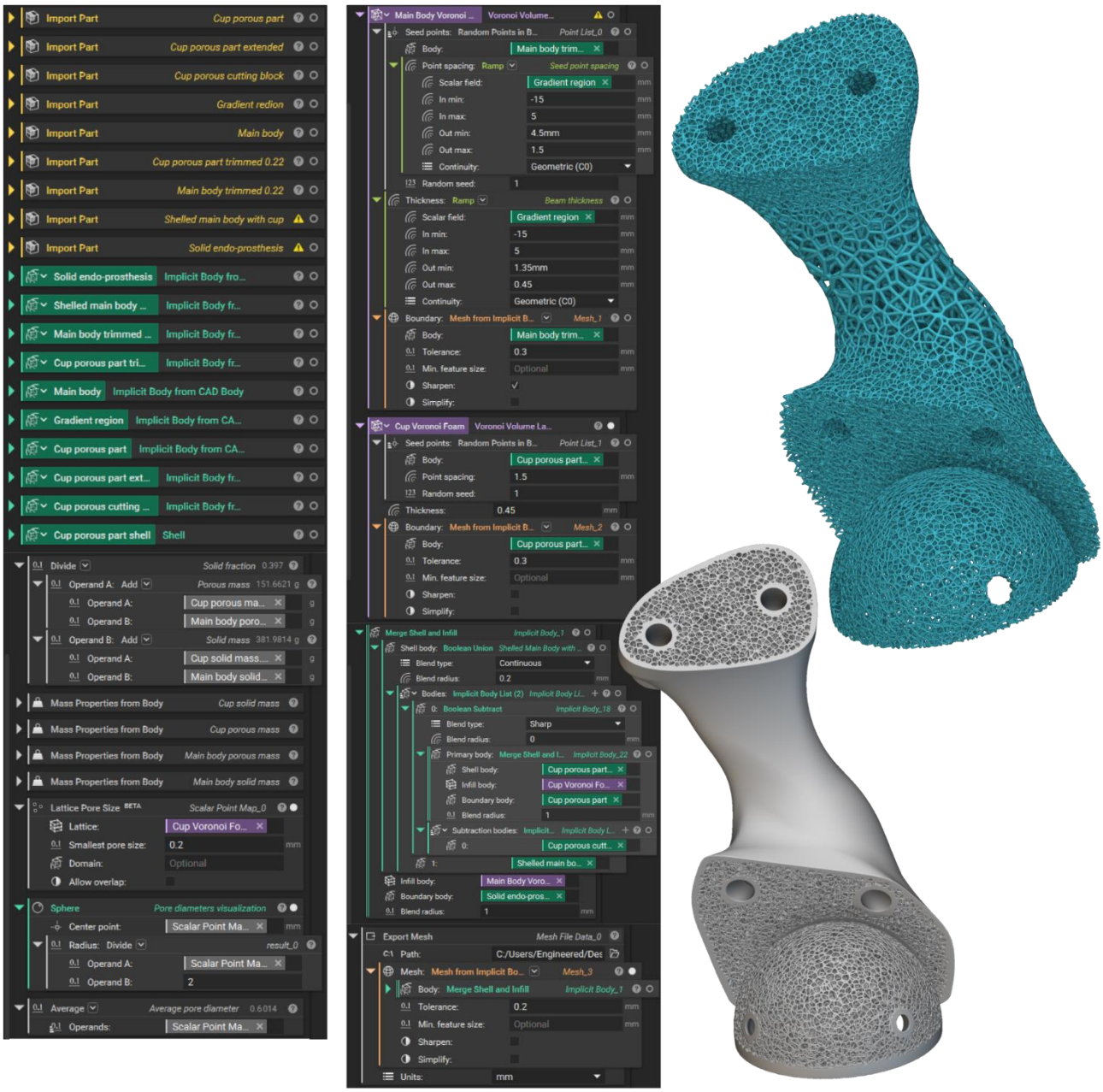

Figure 457: Endo-prosthesis optimization with Voronoi complexes workflow in nTop

The final optimized endo-prosthesis falls within the design space that satisfies the desired osseointegration potential, manufacturability for LBM (not for EBM as thicker (0,6 mm minimum) strut thickness would be required), and bone-matching stiffness. The aforementioned modulus of

elasticity and strength approach the properties of cortical bone *(Appendix E)*. It would be of concern to approach the trabecular bone properties by enlarging the pore size and/or lowering the thickness of the beams, as osseointegration requirements would have been sacrificed and the materialization risk would be significantly higher and manufacturability limit closer, whilst the sum of challenges encountered and their possibilities to emerge when 3DP cellular solids of high porosities would be more and higher *(see Sub-section 3.6.3)*.

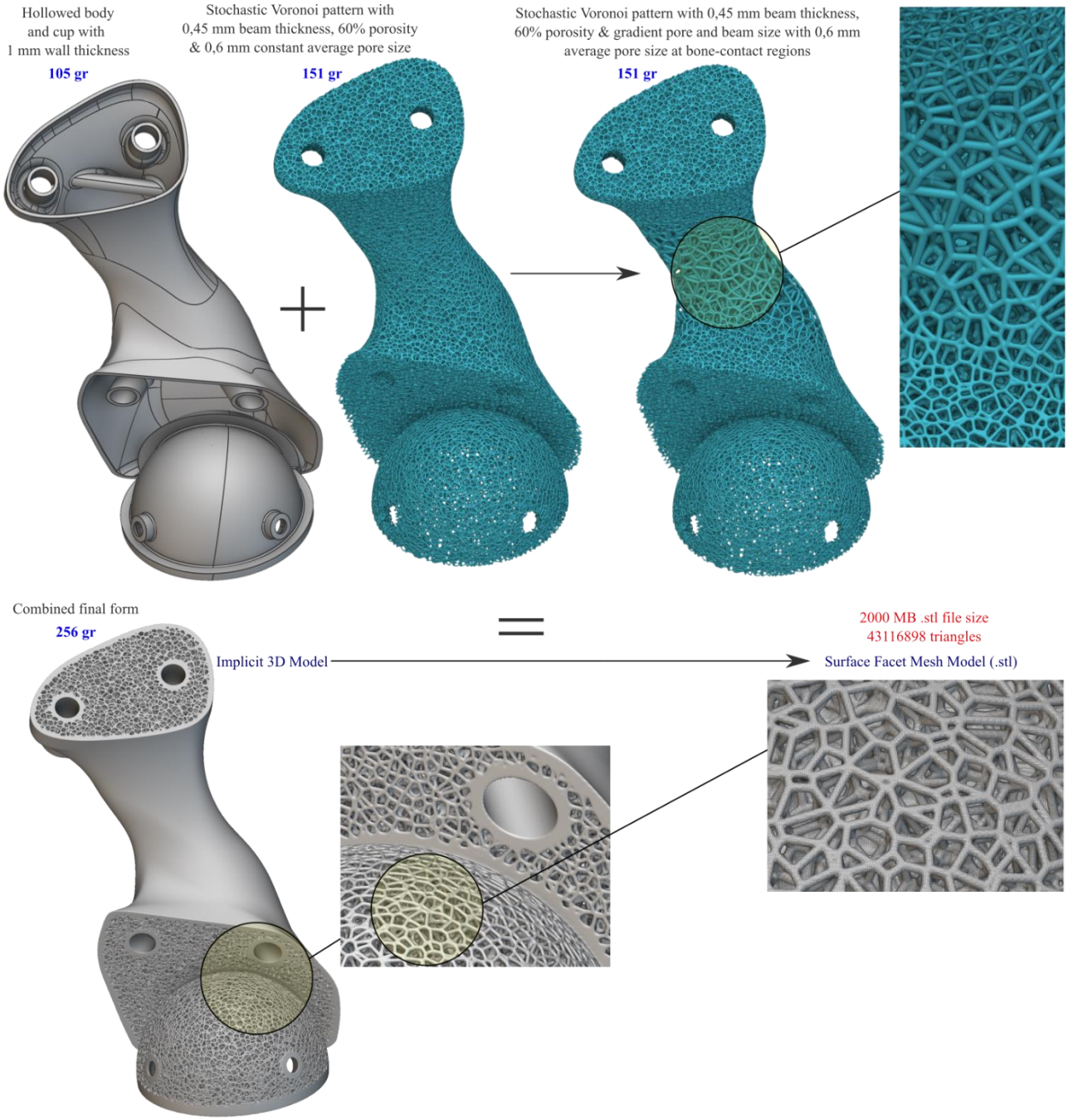

Figure 458: Mass, characteristics, and file size of the Voronoi-optimized endo-prosthesis

Facet meshes such as .stl files are prone to errors and are computationally costly to process large files such as the generated cellular structure in this case. Large .stl files emerge due to the tolerance required to approximate curves with flat triangles. Even in this case with 0,2 mm tolerance it is visible

that the beam is approximated by flat triangles, but as the tolerance is reduced the resultant .stl file size greatly increases. nTop includes tools to overcome surface meshing issues and export curved features to 3DP process planning software, these are: 1) exporting the implicit model per se without surface meshing it and importing the implicit model file into the process planning software, 2) slicing the part within nTop and exporting the slices and/or the toolpath for the desired manufacturing format to be imported into the process planning software. For example, *Figure 461* illustrates the slices of the final optimized endo-prosthesis.

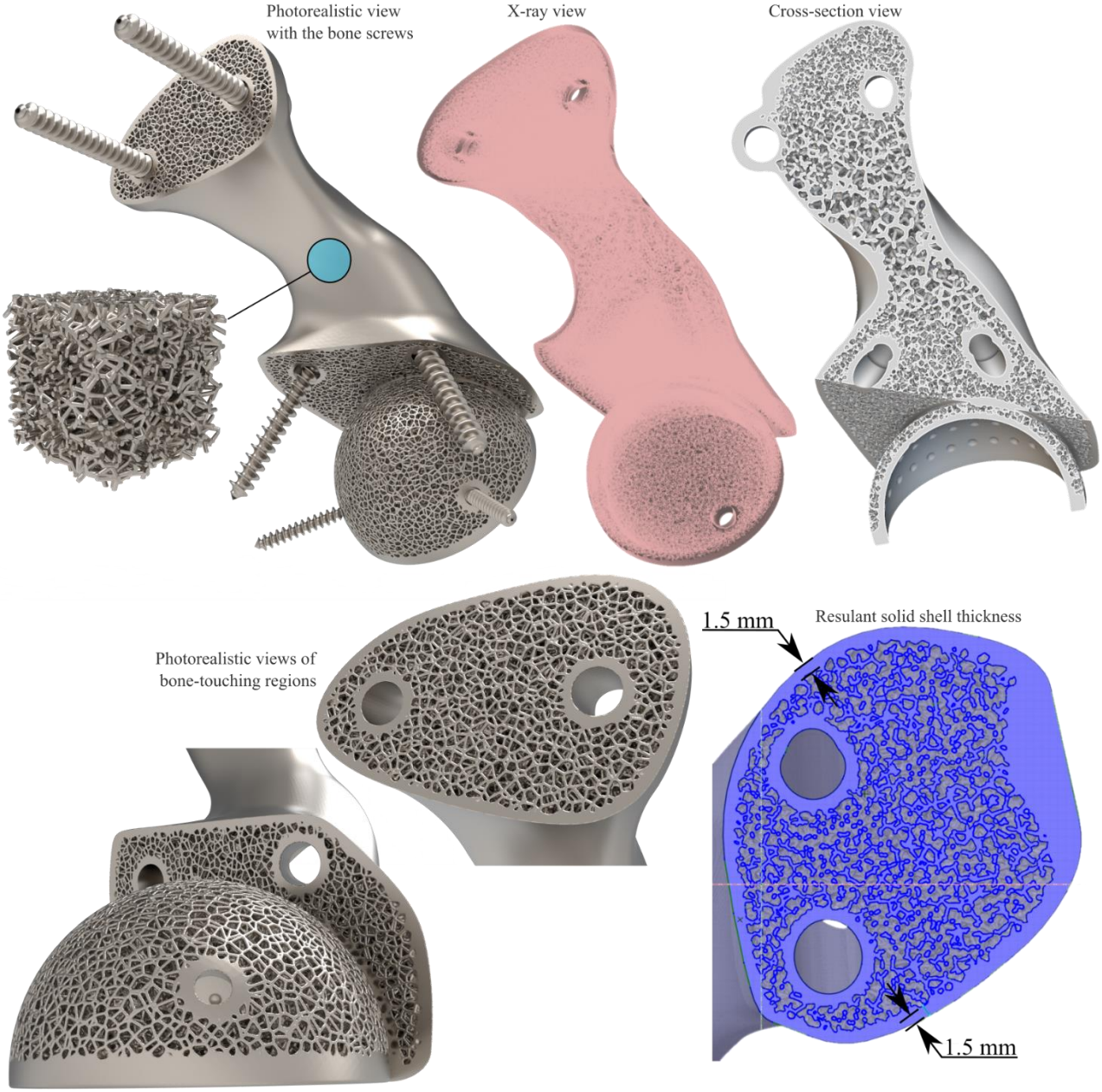

Figure 459: Voronoi-optimized endo-prosthesis photo-realistic, details, x-ray and section views

If EBM instead of LBM 3DP was selected for the Voronoi structure, then the minimum beam thickness had to be 0,6 mm, hence to achieve an average pore size of 0,6 mm, the porosity would be considerably lower. *Figure 460* compares the two types of Voronoi complexes for EBM and LBM.

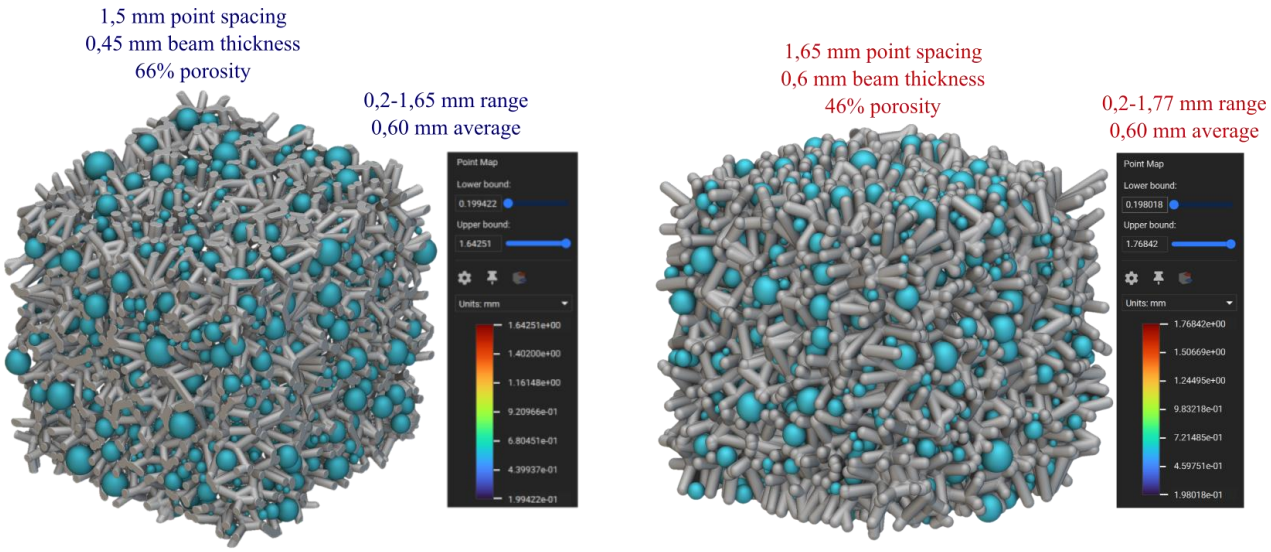

Figure 460: Stochastic Voronoi complexes designed for LBM and EBM 3DP technologies

As an alternative to the stochastic Voronoi scaffold used to be 3DP by LBM technology, sheet and skeletal Gyroid TPMSs were selected to be 3DP by EBM technology, though other types of foams and lattices with beam-based or sheet-based or skeletal-based interconnected cells could have been utilized and arranged periodically with fixed packing spacings, randomly, or with gradients *(see Sub-section 3.6)*. The Gibson-Ashby coefficients for Ti6Al4V Gyroids are *(Lu et al., 2020; Guariento, 2021)* C_1=0,95 and n=2,27 for skeletal and C_1=0,61 and n=1,27 for sheet-based respectively. A porosity level of 40% was maintained similar to the previous Voronoi pattern, giving a resultant moduli of elasticity of:

$$E^* = 0{,}95 * 110\ GPa * (0{,}4)^{2{,}27} = 13{,}06\ GPa \text{ for skeletal Gyroid}$$

$$E^* = 0{,}61 * 110\ GPa * (0{,}4)^{1{,}27} = 20{,}96\ GPa \text{ for sheet Gyroid}$$

The resultant skeletal Gyroid has a lower but the sheet Gyroid a higher modulus of elasticity than the Voronoi's. The skeletal modulus is a little less than that of the cortical bone *(Appendix E)* but it was decided to keep the relative density as is.

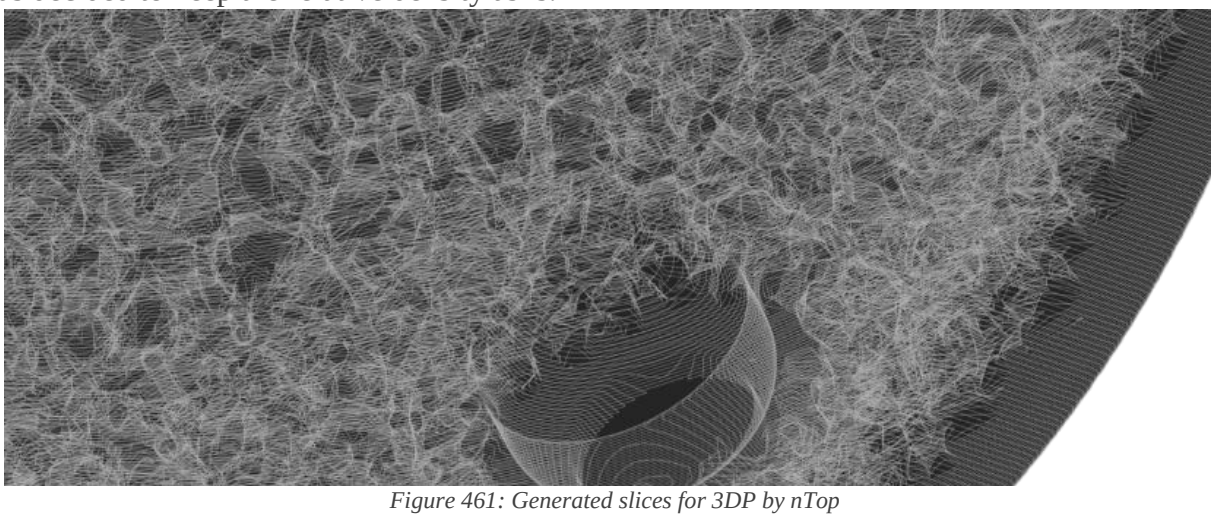

Figure 461: Generated slices for 3DP by nTop

The skeletal, sheet, and mixed (sheet with solid-filled regions) Gyroid unit cells and their arrays are illustrated in *Figure 463* where the following can be highlighted:

1. The effect of under-thickening of skeletal Gyroids might lead to loss of pore interconnection.
2. The effects of over-thickening of the skeletal and sheet Gyroids lead to loss of pore interconnection and the creation of separated voids, i.e. porous solid instead of cellular solid.
3. The mixed Gyroid approach features sheet and beam-like characteristics, with both small and bigger pore sizes. Tuning suitably the parameters of the beam and wall thicknesses, and approaching over-thickening might lead to a cellular solid which favors both vascularization (bigger pore size) and bone ingrowth (smaller pore size).

Sheet Gyroids have superior mechanical properties and strength whilst showing stretching-dominated behavior *(see Sub-section 3.6)* and greater surface area to volume ratio which of course is more area for cell seeding, though skeletal Gyroids have bending-dominated behavior and better pore interconnection with a connectivity of three struts per node.

Combinations of large and smaller pores to favor both vascularization and cell colonization by blending suitable geometries or implementing gradients *(Karageorgiou and Kaplan, 2005; Charbonnier, Hadida and Marchat, 2021)* such as the mixed unit cell Gyroid illustrated in *Figure 463* and similar TPMSs such as the Neovius, Split T and Lidinoid present interesting multi-pore approaches which will be assessed in the future. However, it can be claimed that both the previously shown randomized Voronoi architecture and the sheet and skeletal Gyroids feature different spacings where pore sizes of multiple diameters are created.

Both sheet and skeletal Gyroids are nearly isotropic in terms of their elastic properties when loaded along any direction. For example, the skeletal Gyroid unit cell homogenization graph (40% relative density, Ti6Al4V material) as generated by nTop is displayed in *Figure 462*.

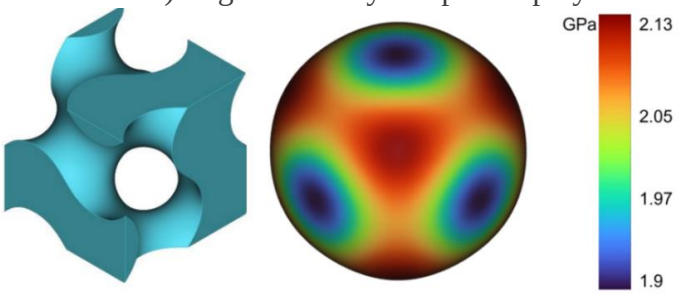

Figure 462: Ti6Al4V skeletal Gyroid unit cell (40% relative density) homogenization graph

In the previous Voronoi pattern designed to be manufactured by LBM 3DP technology, there were no similar unit cells due to the randomization tessellation approach, thus the design constraints were defined by the minimum achievable beam thickness for the selected materialization technology (LBM 3DP), and the required optimal pore size for osseointegration. However, in this case, the skeletal and sheet Gyroids can be sized by a unified conceptual design workflow *(Al-Ketan and Al-Rub, 2019; Barba, Alabort and Reed, 2019; Poltue et al. 2021)*, i.e. geometrical properties graphs were used to identify the admissible design space for the Gyroids unit cells by defining the offset parameter *c*, unit cell size, pore size and manufacturable beam/wall thicknesses for LBM and EBM

3DP. It is apparent that for LBM, the minimum achievable beam/wall thicknesses is lower (0,25 mm), shifting the manufacturability curve to the left, and expanding the design space *(Figure 464)*. The design space would be expanded towards the right if another material with a modulus of elasticity lower than Ti6Al4V would have been selected or if the relative density is shifted to the right.

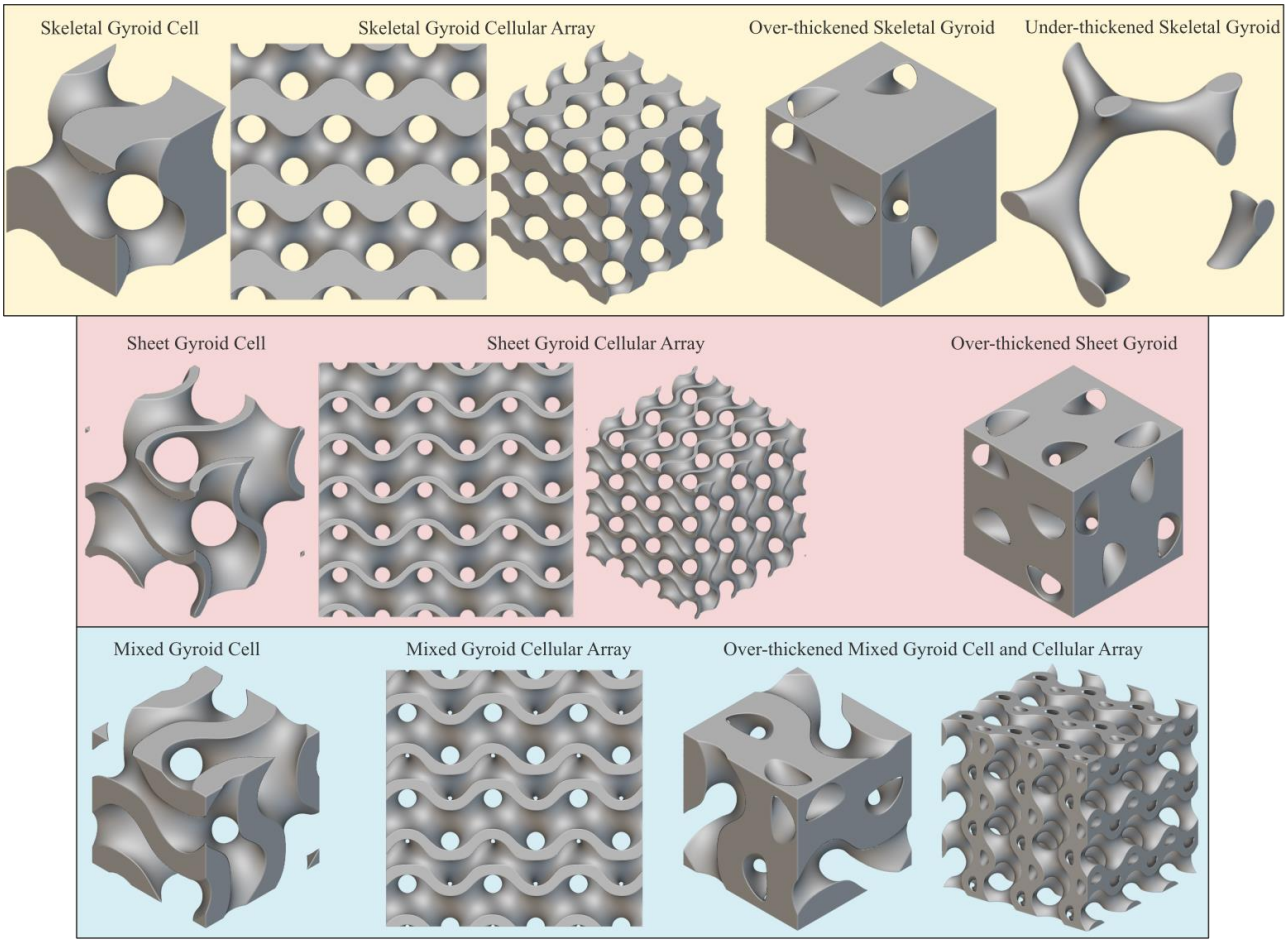

Figure 463: Characteristics of the skeletal, sheet, and mixed Gyroids

The workflow used to size the skeletal Gyroid unit cell for EBM and LBM is shown in *Figure 464*. A corresponding skeletal Gyroid unit cell was generated in nTop for verification. As the shape of labyrinths and the cross-sections of the beams change from elliptical (near the Plateau border) to circular at the midspan, the following can be mentioned for the pore size and beam thickness:

1. From the workflow shown in *Figure 465*, the pore size (0,55 mm) was defined as the sphere that fits in the circular voids as shown from the side orthographic view. However, the sphere diameter that can fit between the beams is larger (0,8 mm). It is more orthological to sacrifice the porosity and raise the modulus of elasticity by suitably changing the *c* parameter of the skeletal Gyroid unit cell to fit the sphere between the beams, i.e. 1,45 mm unit cell size, with 0,6 mm beam thickness and 0,6 mm pore size measured between the beams, 56% porosity, and 16,21 GPa modulus of elasticity *(Figure 465)*.
2. The beam thickness of the skeletal Gyroid was defined as the minimum beam thickness as shown from the side orthographic view *(Figure 465)*. However, this thickness is not fixed but

gets larger along the beam. The minimum beam thickness was measured from the side view to be 0,7 mm instead of 0,75 mm as was sized from the graphs shown in *Figure 464*. However, for the redesigned unit cell, the new minimum beam thickness was established at 0,6 mm.

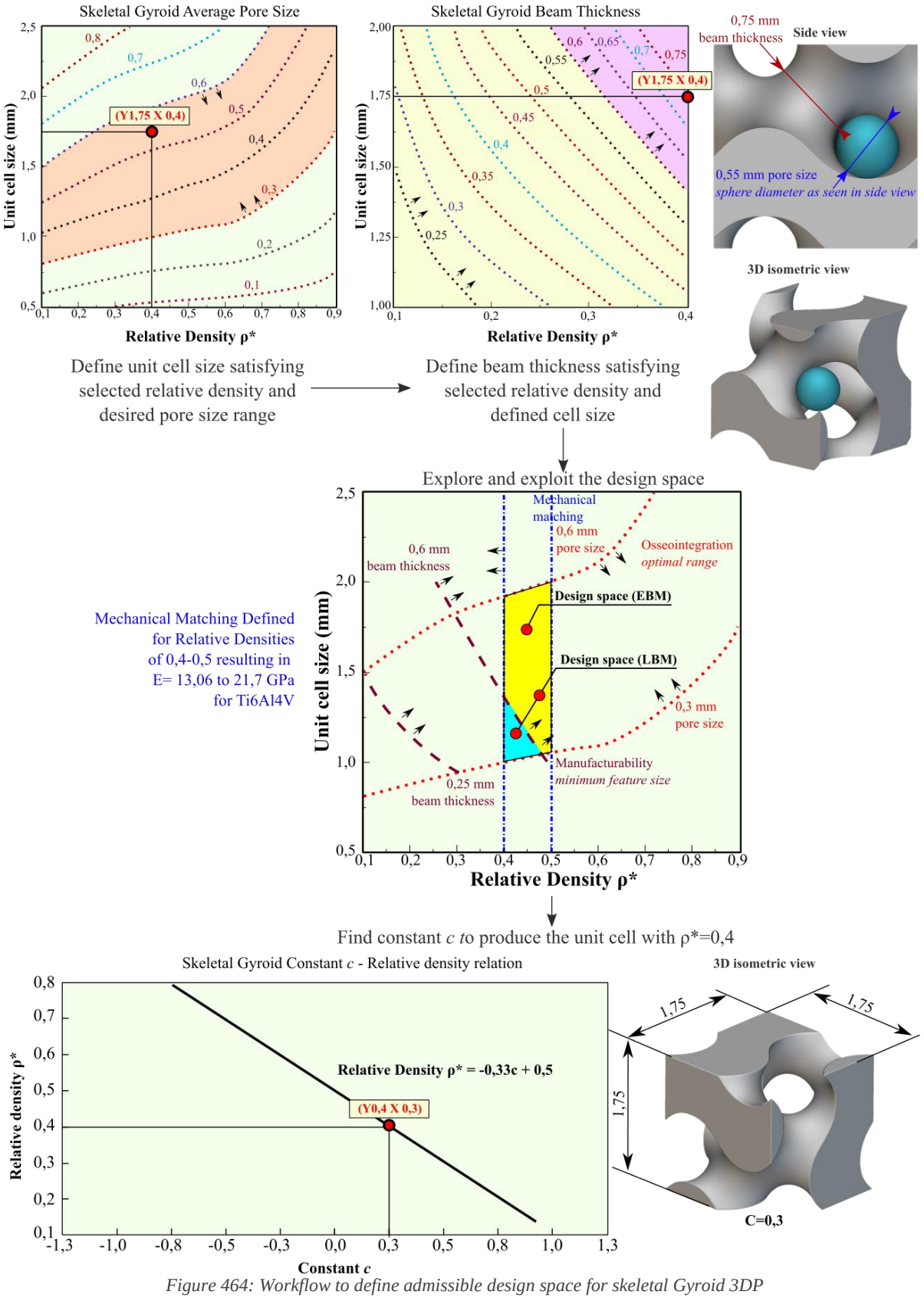

Figure 464: Workflow to define admissible design space for skeletal Gyroid 3DP

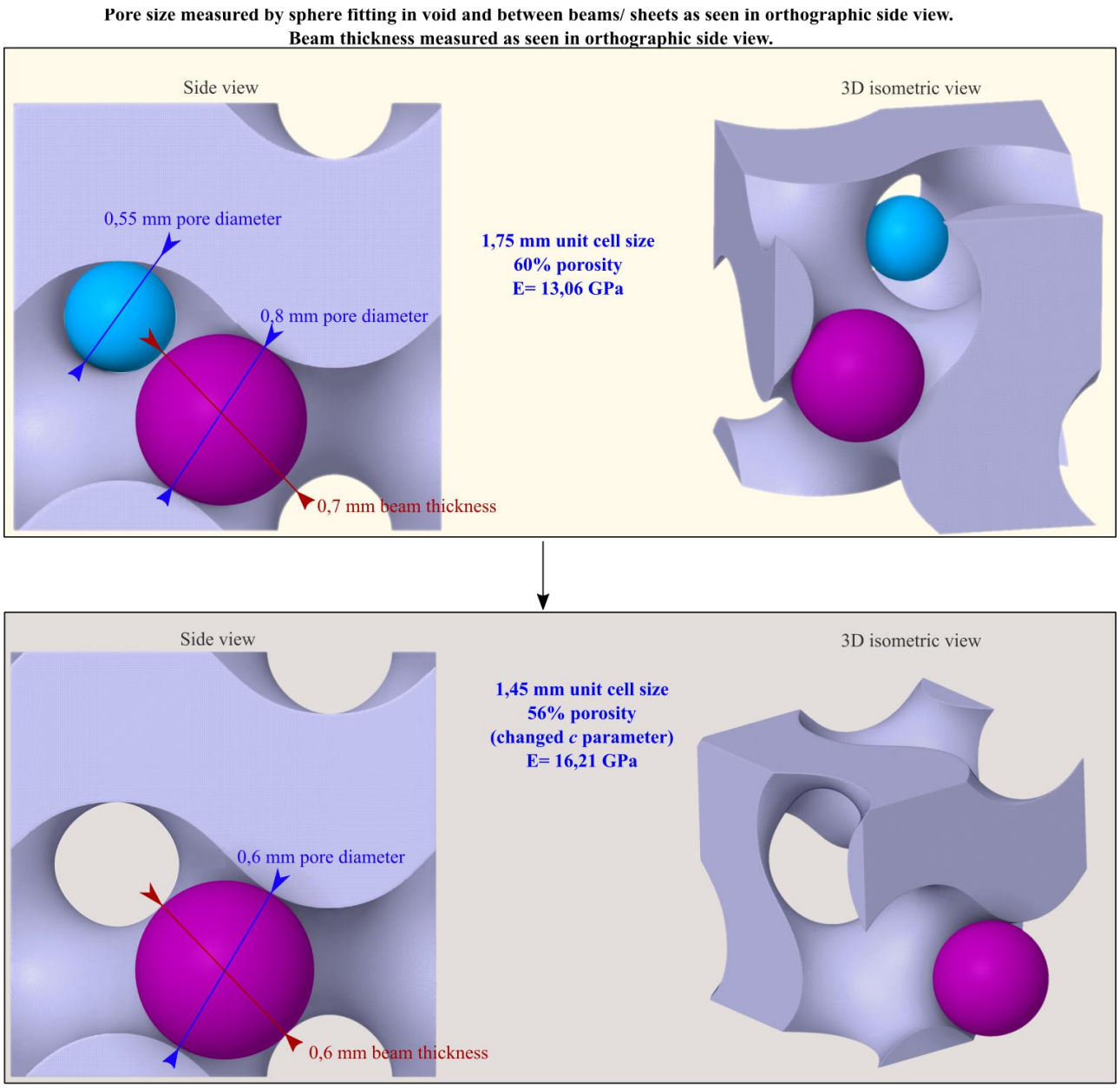

Figure 465: Redefined, more suitable parameters of the skeletal Gyroid unit cell

The sheet Gyroid was constructed in nTop by measuring the wall thickness, the pore size, and the porosity in situ by tweaking the unit cell size and the wall thickness. The parameters of the generated unit cell that was adjusted to be 3DPable by both EBM and LBM are shown in *Figure 466*.

The characteristics of Voronoi and Gyroids cellular architectures (porosity, pore size, beam/wall thicknesses) and the homogeneity of moduli of elasticity which are free of geometric arrangements, satisfy the mechanical-biological-manufacturing triad of constraints; optimal mechanical (bone-like modulus of elasticity) and biological (osseointegration) specifications whilst conforming to the processability limitations of the manufacturing equipment (LBM and EBM 3D printers). LBM 3DP allows the production of finer details in cellular structures to obtain closer to cortical bone properties.

The higher the manufacturability, the higher the as-designed output and the resultant performance. This is the reason why LBM was selected for the randomized Voronoi structure (finer

feature manufacture, finer powder particle, easier de-powdering), and EBM for the sheet or skeletal Gyroids (self-supporting structure with smooth paths for ease entrapped powder removal), though LBM could be also used for both types.

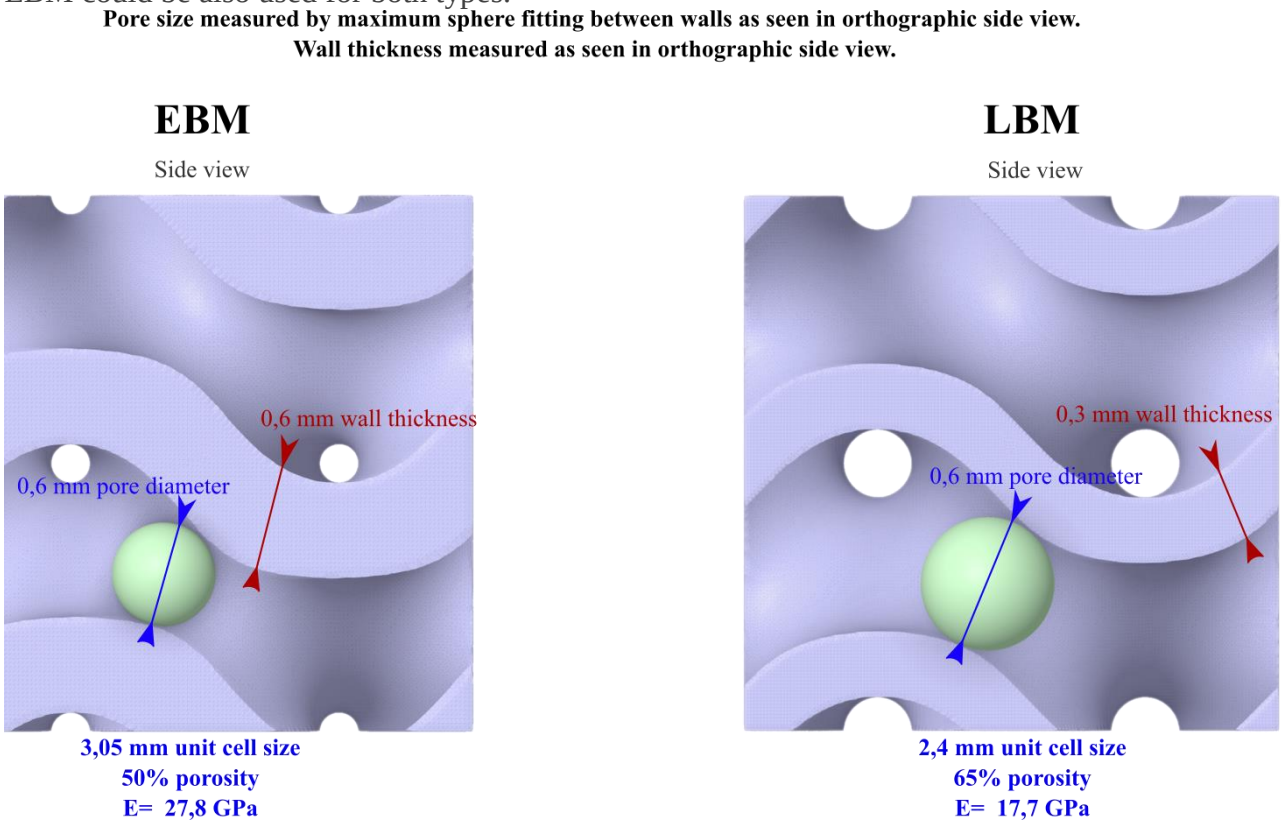

Figure 466: Parameters of the sheet Gyroid unit cell

The sheet Gyroid was found more to be more suitable and easier to implement. Similarly to the previous Voronoi architected structure, a similar workflow was followed in nTop to generate the areas functionally-graded sheet Gyroid cellular endo-structure. *Figure 467* and *Figure 468* show the characteristics, photo-realistic views, detail views, X-ray, and section cut views of the final optimized endo-prosthesis. A 0,6 mm pore size, 0,6 mm wall thick, and 50% porosity assigned at the bone contact and far from the bone interfaces, the structure features 60% porosity, 7 mm cell size, 1,8 mm pore size, and a 1 mm wall thickness. The total resultant mass of the meta-(bio)material is 313 gr. The final model was converted into a surface mesh and exported into an 1850 MB .stl file size.

The 1-1,5 mm thick solid shell that encloses the cellular structure had to be mechanically simulated under realistic loadings to verify that it would withstand the stresses. Simulation-based verification workflows of cellular solids are more complex than dealing with fully solid forms. There are various methodologies to deal with such:

1. **Classic FEA simulation:** volume-meshing the solid model after selecting the materials, setting the boundary conditions, and applying the loads. However, dealing with surface meshes containing large numbers of polygons as in this case where the complex porous structures are surface-meshed with triangles, requires time-consuming pre-processing and high computational

power to both a) convert the surface mesh model into a solid model, and b) to volume-mesh the solid model and generate the results.

2. **Representative volume element:** small representative volume elements to reduce the complexity and big enough to compensate or extrapolate the behavior of the total architecture can be obtained for classic FEA simulations. For example, for periodic lattices, the unit cell (or some interconnected unit cells) is/are the representative volume element(s), but for random foams such as the stochastic Voronoi structures larger samples would be required.
3. **Solid model of porous structures:** the cellular part can be simplified and treated as a homogeneous solid model with properties set equivalent to that of the porous structure *(Liu et al., 2021)*. However, local stresses and deformations on nodes and beams cannot be evaluated.
4. **Volume meshing-free simulation:** approaches emerged to solve mechanical simulation without the geometry pre-processing and meshing bottlenecks of classic FEA approaches. For example:
    a. **nTop**: includes Beam Elements and Homogenization options in addition to the classic solid element FEA analysis. *Figure 469* shows the advantages and disadvantages of each option. Even for the classic FEA analysis, in nTop, the implicit model can be volume-meshed directly bypassing the surface meshing step.
    b. **Intact Solutions' Simulation**[155] (plug-in for McNeel Rhino's Grasshopper available): meshless technology called Immersed Method of Moments (based on Kantorovich method) where instead of discretizing geometry per se, the space is made of discrete cells (elements), modifying the quadrature rule of standard FE elements. The generated .stl surface mesh model from nTop is supported by the software.
    c. **Altair Simsolid**[156]**:** fast and efficient analysis of large assemblies and complex parts using multi-pass adaptive analysis, difficult to analyze with traditional FEA techniques. The generated .stl surface mesh model from nTop is supported by the software.
5. **Simulation-driven cellular structures generation:** using the classic FEA or meshing-free approaches to design-iterate-redesign the implicit model of the cellular structure as soon as it is optimized as per the material selected, the pre-set boundary conditions loadings, and desired goals (e.g. mass reduction percentage). For example, nTop now includes a generative multi-objective and multi-scale design tool called *field optimization* tool that accounts for spatially varied design parameters, i.e. spatial cell size, beam/wall thickness, and shell thickness variations *(Figure 470)*.

Cellular structures must be simulation-optimized by studying the whole porous structure under loading, whilst investigating the local stress concentrations, contact phenomena, and deformation

[155] See https://www.intact-solutions.com/rev/.

[156] See https://altair.com/simsolid.

levels on the nodes and beams to ensure that these can withstand without failure the exerted loads. In cellular solids, loads are transmitted through the beams to and through the nodes, with local defects acting as stress raisers and potential locations for crack initiation. Of course, the presence of filleted connections and nodes as in these cases, increases the stiffness of the structure and affects the orthotropic elastic constants.

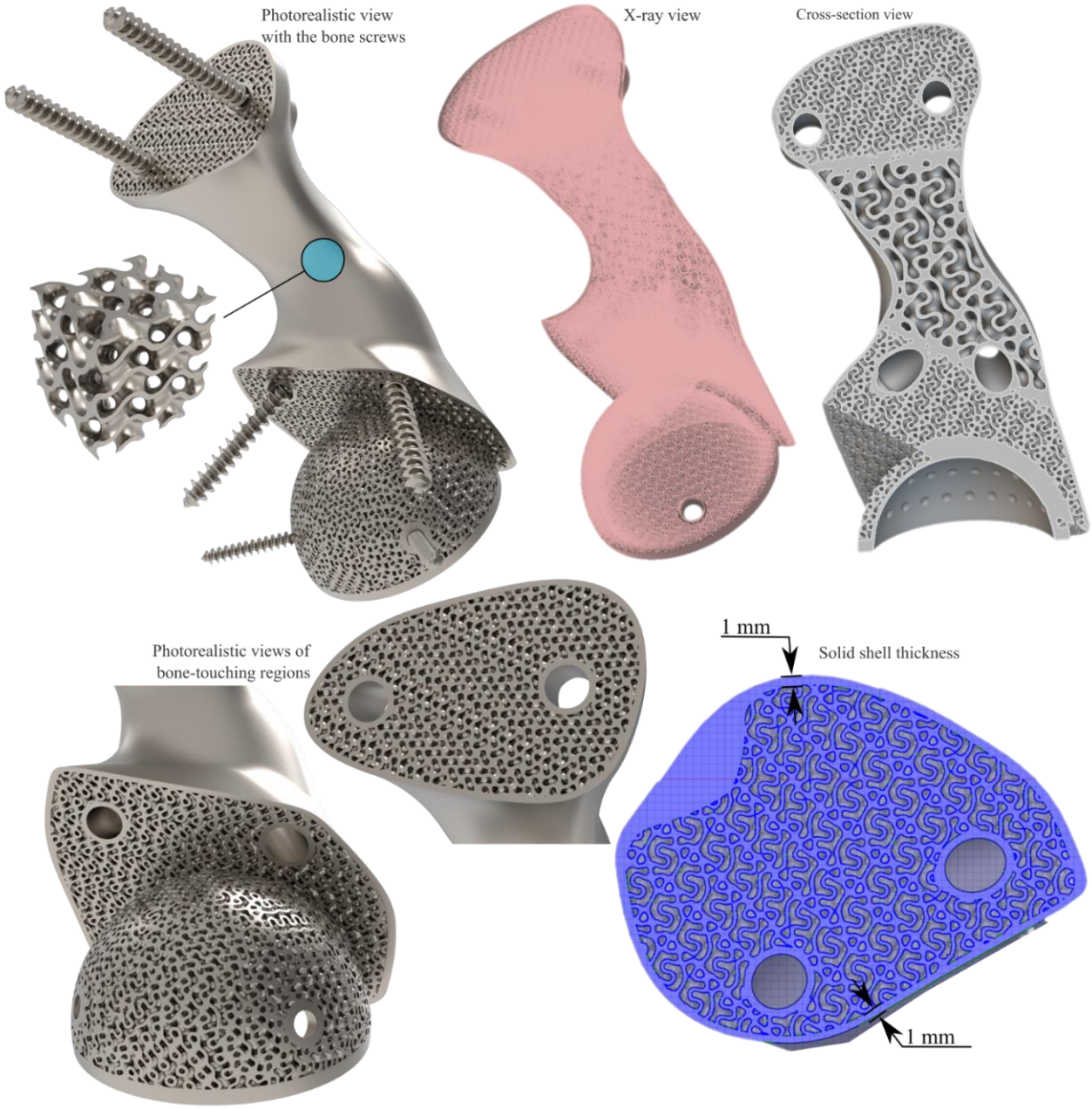

Figure 467: Sheet Gyroid-optimized endo-prosthesis views and details

Nevertheless, it was decided to follow an alternative approach. The 1,5 mm thick hollow shell body without the cellular structure infill was used to conduct static mechanical simulations in Fusion 360. As shown in *Figure 472-Figure 474*, the hollowed body withstood the same loads as exerted previously on the fully solid endo-prosthesis, but in this case, under greater (three-fold) stresses and displacements. At the same time, the pelvic bones were subjected to critically high stresses and strains as these were transferred through the less stiff hollow endo-prosthesis.

It is orthological to assume that introducing the aforementioned stochastic Voronoi and especially the Gyroid (reduced stress concertation due to smooth sharp-free interconnected beams) patterns would not compromise the mechanical performance of the solid shell and would not lead to mechanical failure as plastic deformation, crack propagation and ultimately densification *(Figure 471)* of the cellular structure is unlikely, though this claim should have been verified by suitable extra simulations. In other words, the cellular structure with the low modulus of elasticity is being stiffened by the solid shell and vice versa, whereas it is apparent that the solid shell could have been studied to become even thinner universally, or gradiently as per the generated stresses.

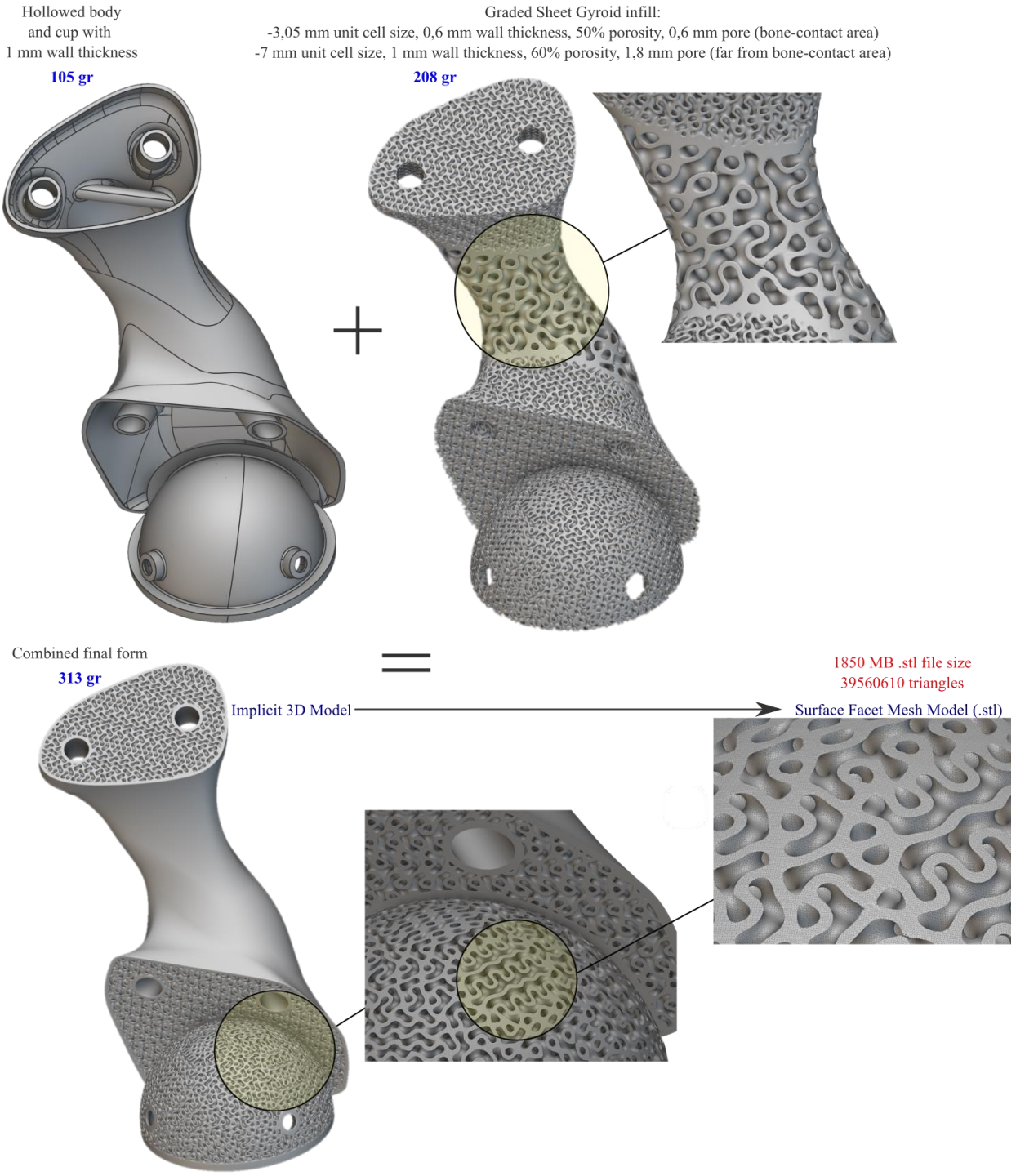

Figure 468: Mass, characteristics, and file size of the sheet Gyroid-optimized endo-prosthesis

Alternative options for the endo-prosthesis endo-structure could have been to have a thinner or variable shell thickness or keep the inner space that is away from the bone-touching areas hollow. The four holes initially planned for de-powdering and soft tissue suturing could be used exclusively for either purpose or even add additional holes. Surface roughness at the areas where soft tissue might be possibly sutured could have been implemented optionally. Additionally, electronic devices in the form of a cassette and drug reservoirs for controlled elution by active systems or by free flow could have been also considered as novel options, such could have been added within the endo-prostheses far away from the bone-interfacing areas and at the regions were there is low-stress concentration.

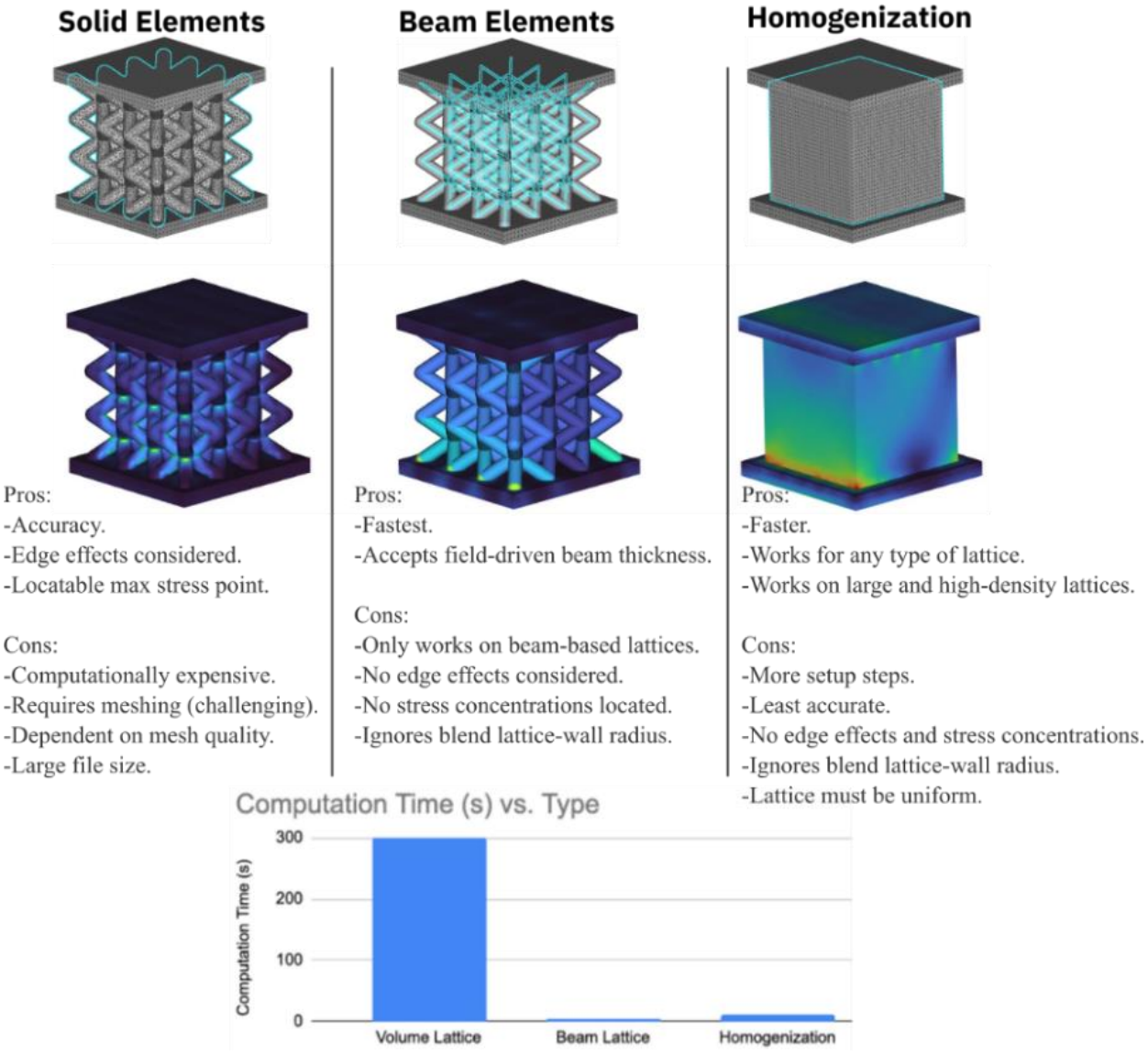

Figure 469: Different approaches to mechanical simulation of cellular solids in nTop. Source: nTopology

Last but not least, the following can be noted for the coatings and post-processing of the two types of optimized biomimetic endo-prosthesis designs:

- **Support structures removal:** the endo-prosthesis must be oriented on the platform of the 3D printer optimally to obtain a good surface finish without defects, i.e. minimization of thermal gradients and heat build-up to avoid stress concentrations that lead to geometric deformations,

pores, and cracks. For defect-free results, the ultimate goal in PBF-based metal 3DP is to minimize both the support structures by obtaining as much self-supporting surfaces as possible, and at the same time minimize the surface area of the part's cross-sections (average) so that the heat input into each layer of the part is also minimized during scanning and fusion of the metal particles by the electron or laser beam. For EBM, usually supports to lift the part a few millimeters from the build plate are used to facilitate easier part removal from the build plate. For LBM support structures are necessary not only to avoid geometric deformations but also for heat dissipation, whilst the sites and amount of support structures depend on the selected part orientation on the build plate. Once the process is finished, the part with its supports must be removed from the build plate using a cutting saw or Wire Electrical Discharge Machining, and the support structures and their anchoring points that protrude must be removed using hand and abrasive tools.

- **Unmelted powder removal:** the unmelted particles must be removed as there is a risk of entering the patient's body. The openings on the two bone-touching faces and the extra two 2,5 mm diameter de-powdering holes are enough for de-powdering the residual particles from the cellular solid. The Voronoi foam with thinner beams was designed to be 3DPed by LBM PBF technology, whereas the Gyroid was designed with thicker beams to be 3DPed by EBM or LBM PBF technology. The Gyroid features smoother paths to allow de-powdering the unmelted particles which are more in EBM technology. It should be noted that although the sintered particles on the beams and nodes could compromise fatigue strength (geometrical imperfections and notches), the created micro-roughness could be beneficial for cell seeding. The most common de-powdering techniques are brushing off, air-jetting and blasting with inert gas, bead blasting with various media, heat treatment for sintering the loose powder, dry or wet ultrasonic vibration, chemical etching, and mechanical vibration *(Seiffert, Hopkins, and Sutcliffe, 2017)*, though the most successful for cellular structures is air-jetting followed by dry ultrasonic vibration and chemical etching *(Khrapov et al., 2023) (see Sub-section 3.6.3).*
- **Post-processing:** as there is no direct tribological connection between the endo-prosthesis and other parts, the solid shell surface is left with a satin finish as polishing of Ti implants has been found to have little effect on bacterial adhesion and biofilm formation *(Sarfraz et al., 2022).* For the LBF technique, heat treatment for stress relief is required, whereas, for both LBF or EBM, HIP is optional but could be beneficial for removing any possible pores.
- **Coatings:** the solid shell can be coated with bacterial-fighting materials, whereas bone-inducing and anti-infection elements can be introduced onto and into the open-cellular foams of the endo-prosthesis at the bone-touching areas for anti-infection and bone formation boosting activities with any desired matching substances. For example, among others, coatings can be antibiotics,

antimicrobial Ag, HA/TCP, or even BMP-2. Coatings to roughen the surface instead of implementing integrated porosity could have been also opted in case soft tissue re-attachment was desired. As there is no direct tribological phenomena between the endo-prosthesis and other parts, there is no need for hard coatings (e.g. TiN) to increase the hardness.

The total time to complete the detailed design of the solution was 1 day.

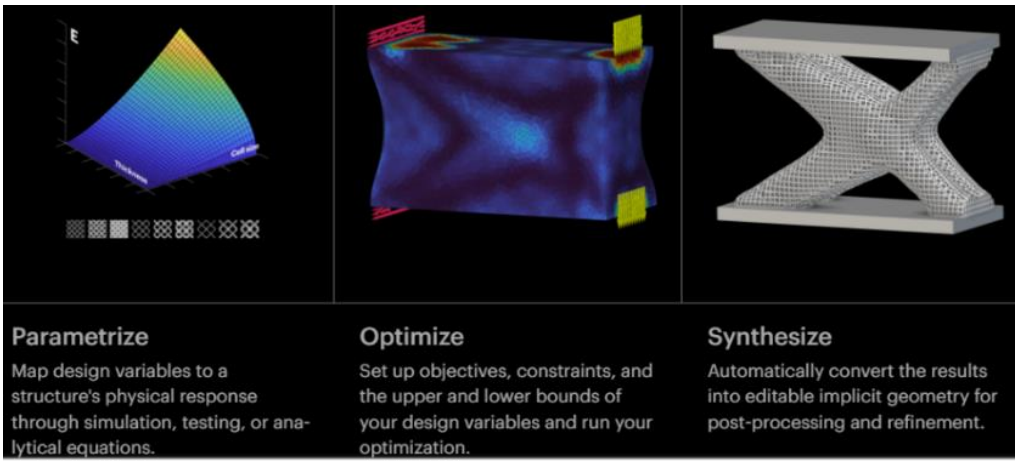

Figure 470: Characteristics of the field optimization design tool in nTop. Source: nTopology

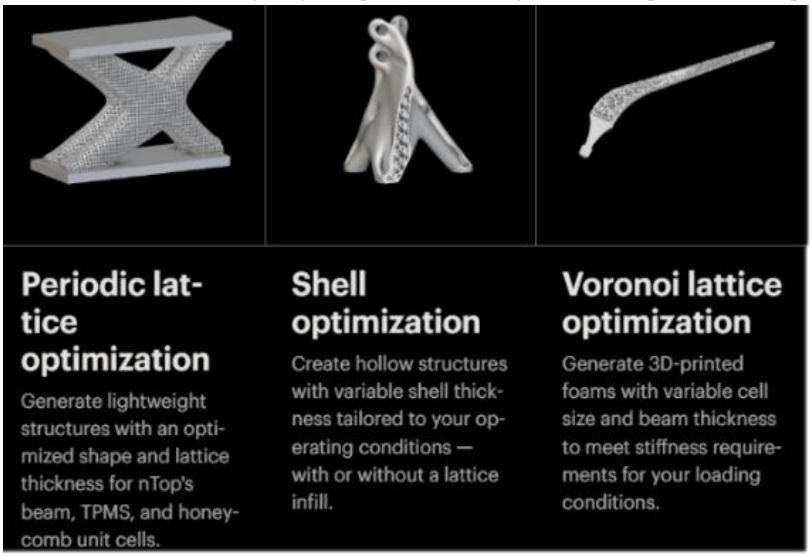

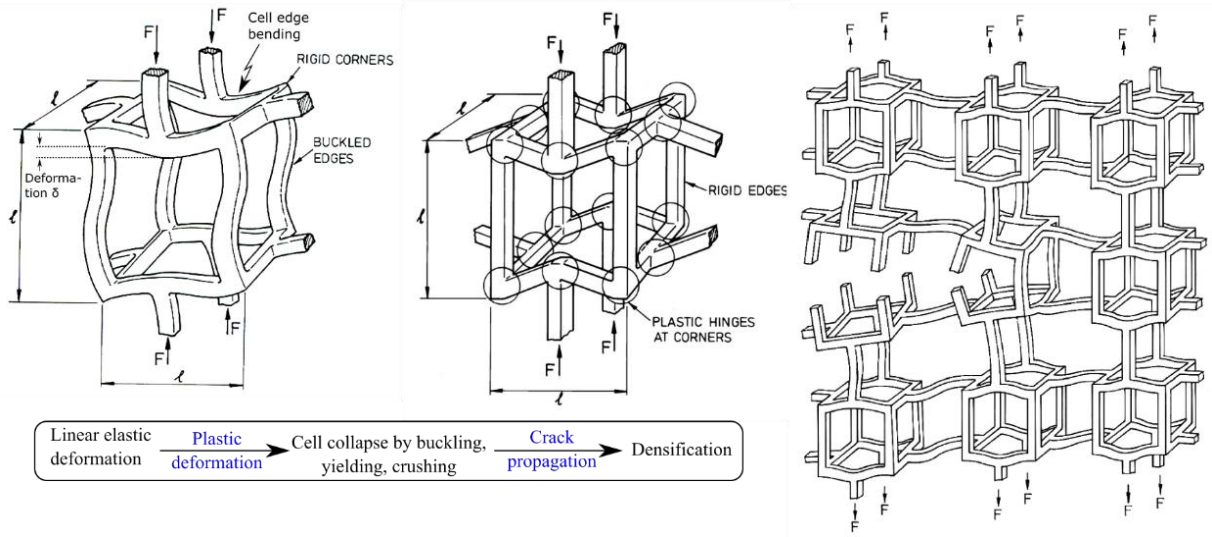

Figure 471: Elastic deformation and failure mechanisms of cellular solids. Source: (Gibson and Ashby, 1999)

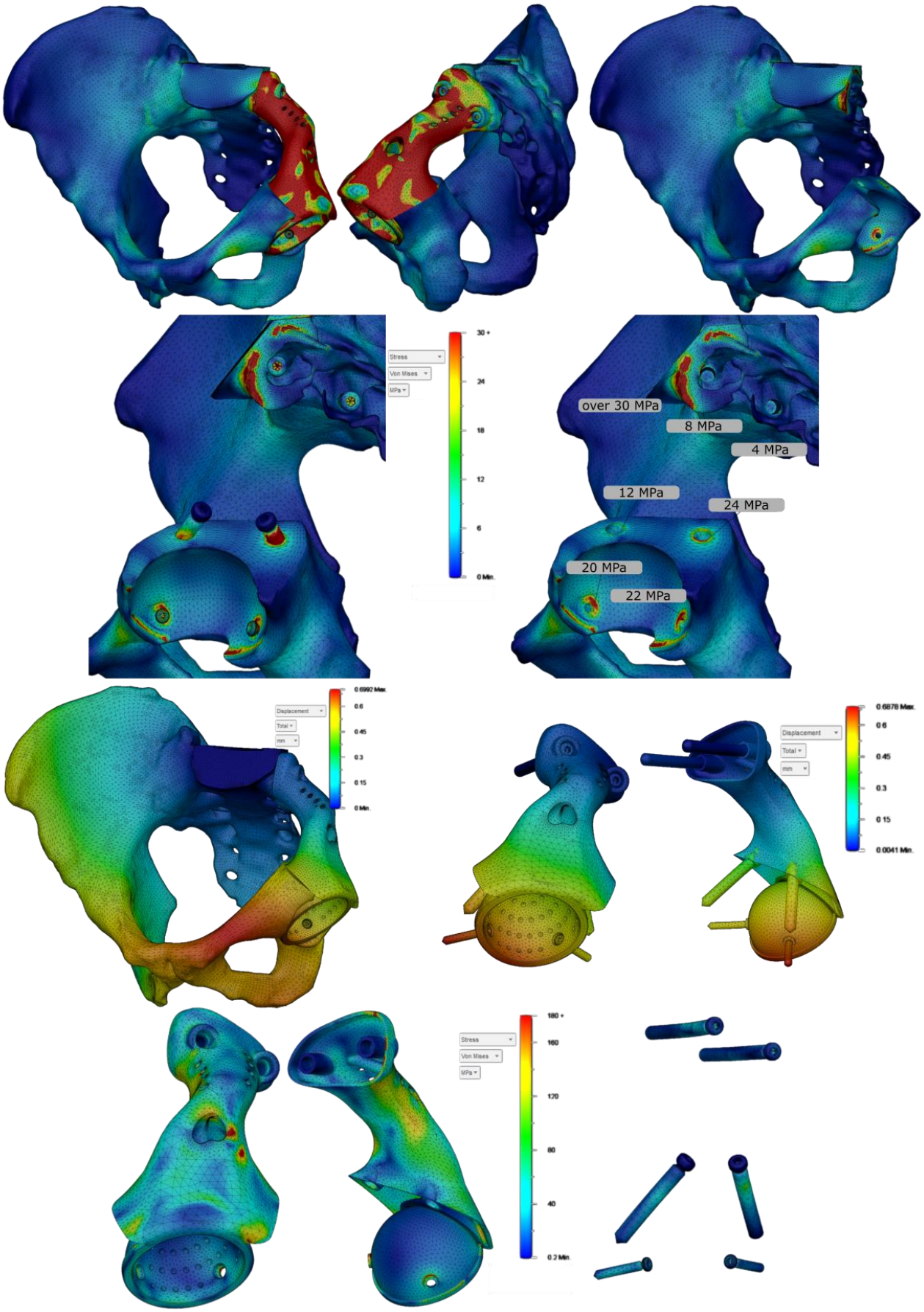

Figure 472: Results of hollow body mechanical simulation by loading the left hip socket

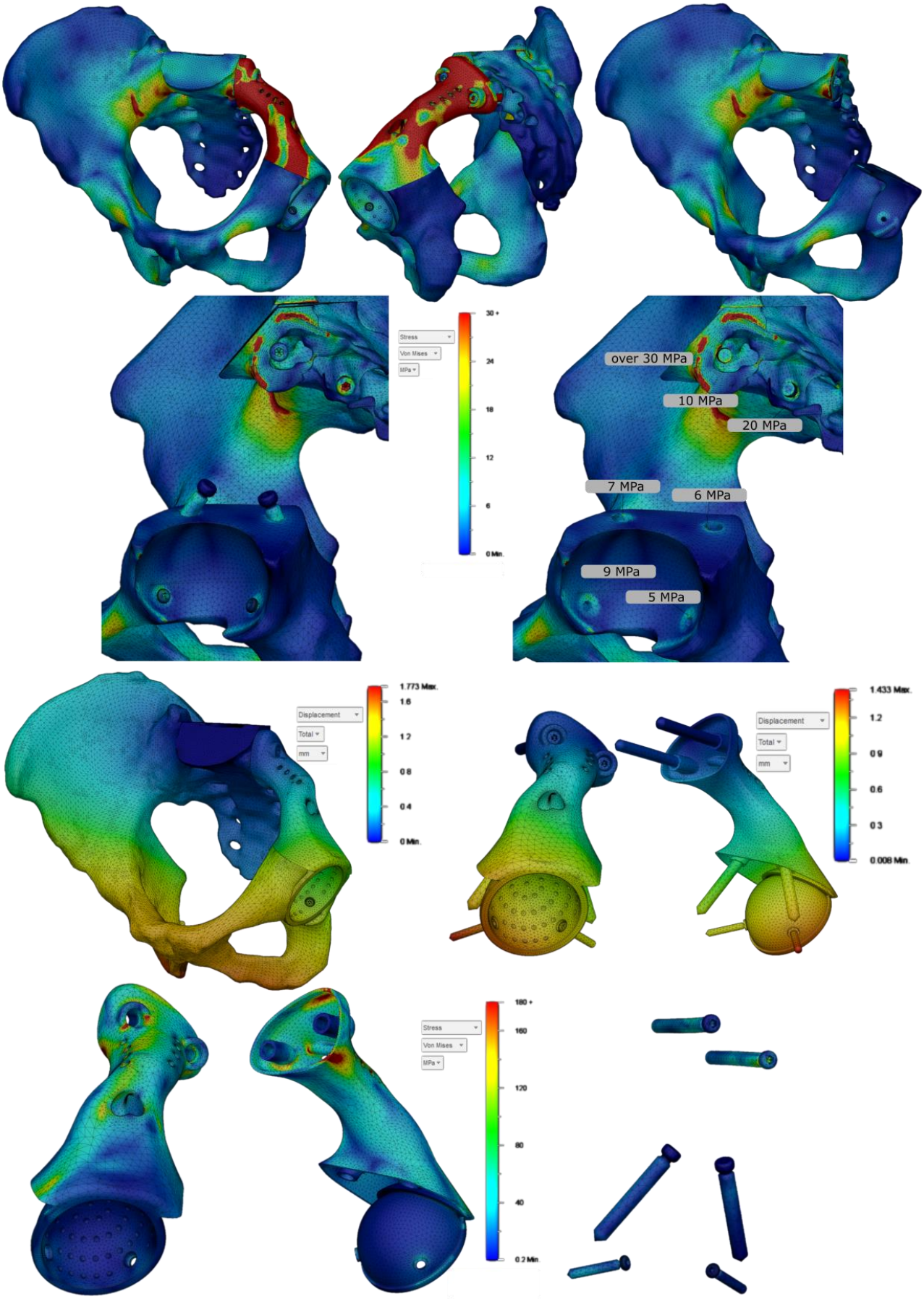

Figure 473: Results of hollow body mechanical simulation by loading the right hip socket

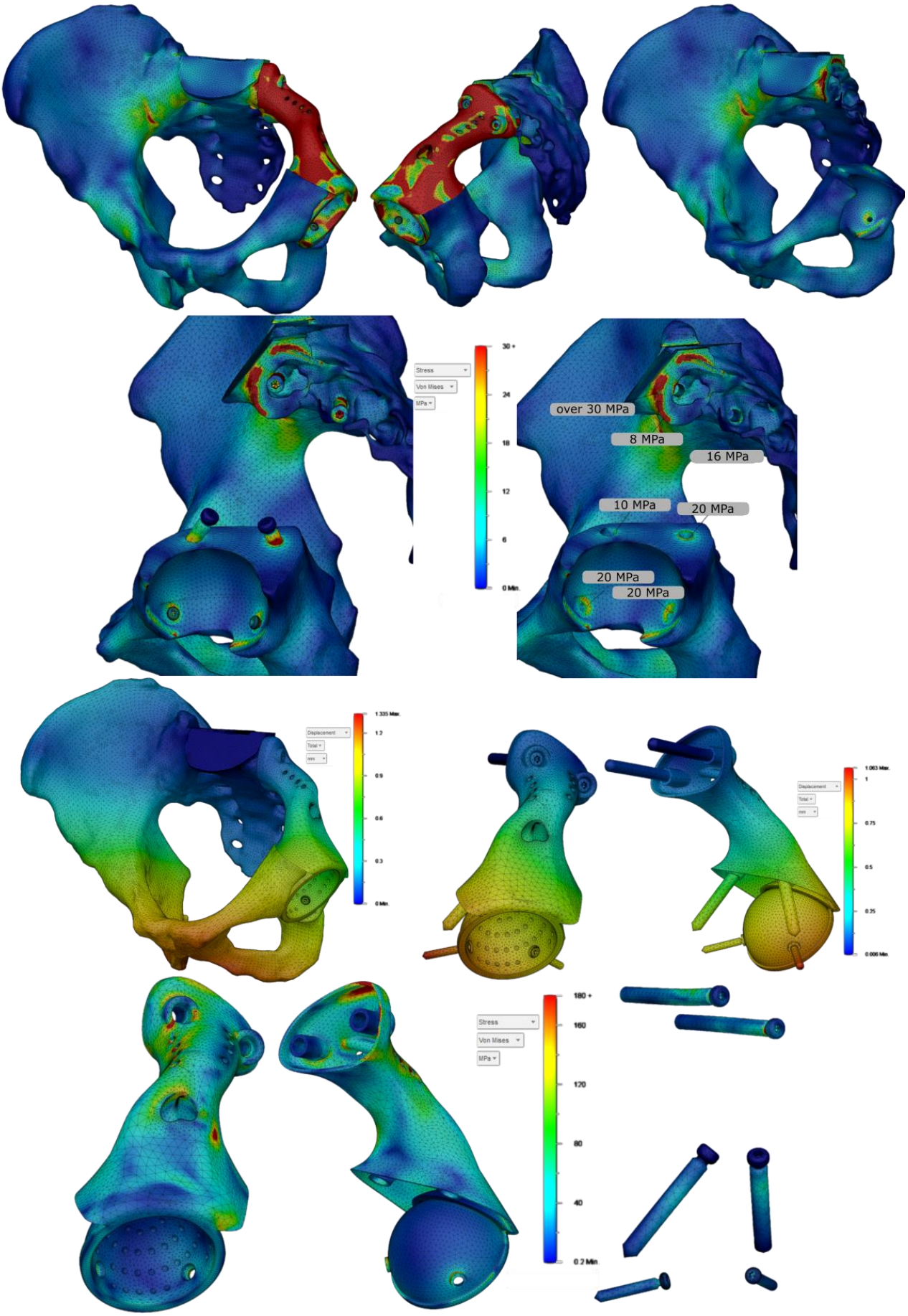

Figure 474: Results of hollow body mechanical simulation by loading both hip sockets

6.4.10 Pre-operative Simulation

Digital, virtual, and physical visualization was conducted for verification pertaining to all components of the solution. Physical parts were handed over to the surgeon. Digital visualization shared via *SkeletoMy* and virtual xR sessions were arranged to be carried out within the PoC Unit.

The anatomical model with reamed acetabulum and flat-cut surfaces, the femoral head, the femoral head with the femoral stem and head inserted, the cemented cup, and the prototypes of the cutting jig, reaming check tool, femoral head-cutting jig, drilling jig-trial endo-prosthesis instrument, and the endo-prosthesis were 3D printed in three sessions using the Creality CR-10s 3D printer in 3 days and 13 hours, 2 days and 4 hours, and 22 hours consuming 663 gr (Ivory, 23,2 €), 370 gr (Grey, 13 €) and 280 gr (Black, 10 €) ColorFabb PLA/PHA material respectively *(Figure 475)*. The total pre-processing in PrusaSlicer and the post-processing took 20 and 30 minutes respectively.

To illustrate better the details of the optimized endo-prosthesis *(Figure 483)*, the Elegoo (Elegoo Inc., Shenzhen, China) Saturn S vat photopolymerization 3D printer and a clear plant-based photocurable resin were used, coupled with the Elegoo Mercury X washing and curing post-processing stations *(Figure 476)*. Chitubox Basic (Chuangbide Technologies Co. Ltd, Shenzhen, China) was used to plan the process which took 6 hours, consuming 55 ml (3 €) of resin *(Figure 476)*.

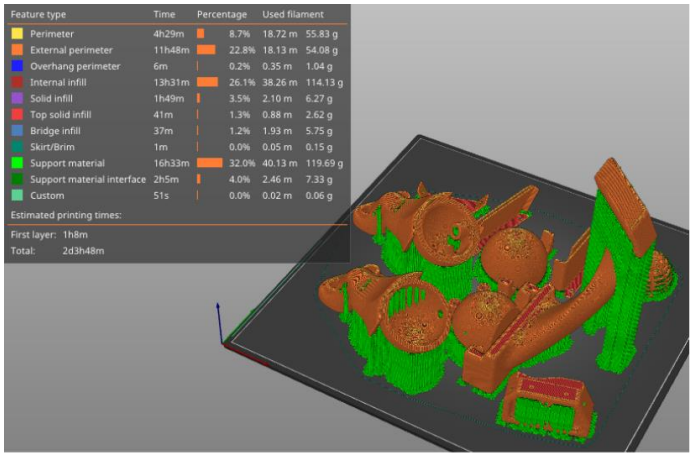

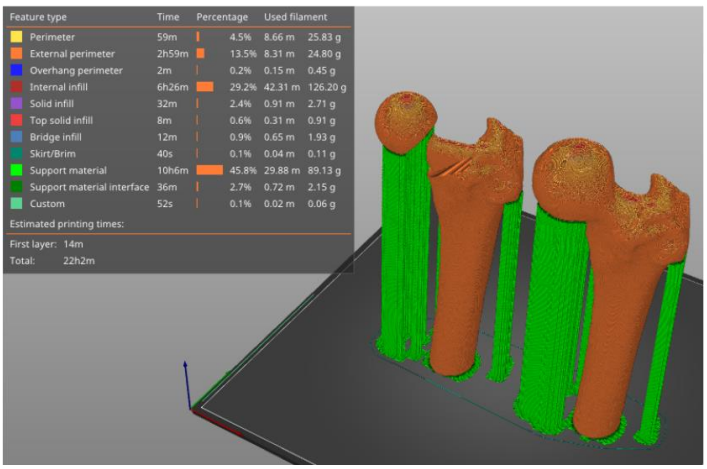

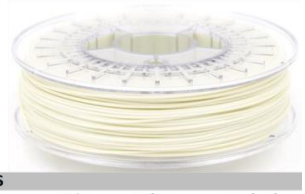

colorFabb

TYPICAL MATERIAL PROPERTIES			
Physical properties	**Unit**	**Value**	**Method**
Density	g/cm3	1,24	ISO 1183
Modulus of elasticity	MPa	2960	ISO 527
Tensile strength	MPa	61,5	ISO 527
Tensile strain at tensile strength	%	5,3	ISO 527
Tensile stress at break	MPa	38	ISO 527
Tensile strain at break	%	10,5	ISO 527
Flexural modulus	MPa	3295	ISO 178
Flexural strain at break	%	NB	ISO 178
Flexural stress at 3.5% strain	MPa	88,8	ISO 178
Notched impact strength (Charpy), RT	kJ/m²	2,8	ISO 179-1/1 eA
Impact strength (Charpy), RT	kJ/m²	30,8	ISO 179-1/1 eU
Melting temperature	ºC	>155	ISO 3146-C

FILAMENT SPECIFICATION		
Nominal diameter:	**Diameter tolerance**	**Ovality**
1,75 mm	± 0,05	≥ 95%

Figure 475: Material Extrusion 3DP for pre-operative simulation and verification

Figure 476: Vat Photopolymerization 3DP of optimized endo-prosthesis in transparent material

Figure 477 to *Figure 484* show all 3D printed parts that were used by the surgeon to approve the solution and verify the fit between all parts so that the workflow can move to the next step.

Figure 477: 3DPed components of the final solution

Figure 478: 3DPed reamed, flat-cut, and drilled anatomical model

Figure 479: 3DPed reaming check tool

Figure 480: 3DPed flat-cutting instrument

Figure 481: 3DPed drilling jig-trial endo-prosthesis instrument

Figure 482: 3DPed femur, femoral head cutting jig and stem with head

Figure 483: 3DPed endo-prosthesis out of clear resin photopolymer

Figure 484: 3DPed endo-prosthesis, cemented, and final assembled solution

6.4.11 Final Check, Manufacturing, and Delivery

A final meeting with all required parties had to be arranged for final approval as per the applicable legal and standard procedures. The off-the-shelf total hip arthroplasty components were readily available in the market for purchase, whereas custom parts were sent to a contract manufacturer, i.e.:

i. The cutting jig and drilling jig-trial endo-prosthesis instrument with all AISI 316 stainless steel metal inserts and sheet metals, reaming check tool, and femoral head-cutting jig were ordered to be 3D printed out of surgical-grade PA12 by a suitable laser-based powder-bed fusion technology. The total cost was 380 € for 6 working days delivery.
ii. The endo-prosthesis was ordered to be 3D printed out of surgical-grade Ti6Al4V by a suitable laser-based powder-bed fusion technology, followed by glass bead blasting for satin surface finish. The total cost was 1800 € for 6 working days delivery.

The extra costs of the off-the-shelf components (bone screws, cemented acetabular cup, femoral stem and head components, and K-wires) were not considered as these could be sourced by the

surgeon. Also, post-processing and surface coatings were not applied.

The documentation mentioned in *Figure 273* (terms of use and warranty notes) and *Figure 275* (proposal check-justification report, manufacturing instructions, application/implantation instructions, safety-risk assessment-quality management report) was sent to the surgeon for final approval and sign off to enable the beginning of patient-specific solution materialization.

The following notes should be mentioned:

1. Labels can be embossed on the surface of each unique part to comply with the labeling requirements of medical devices as per ISO 15223-1:2021 and ISO 15223-2:2010.
2. Data preparation and pre-processing, part design features (Df3DP), feedstock materials, process, system and 3DP machine, personnel, documentation, infrastructure, and post-processing might lead to low-quality products, see *Figure 88*, *Figure 265*, and *Figure 278* for associated Ishigawa diagrams. For this reason, quality assurance and control methodologies must be applied by incorporating a suitable QMS system based on ISO 13485 and the generic ISO 9001:2015 with all roles, techniques, equipment, infrastructure, and materials being certified and/or qualified by validation or verification must be applied to guarantee that that the developed endo-prosthesis and all PSIs are developed following good design, manufacturing, and management practices.
3. After post-processing and coating (if applicable), once all parts received, and before application, these have to be non-destructively inspected, cleaned, and sterilized within clean rooms to prevent contamination and infection by applying the most suitable method carefully. Erroneous or inadequate cleaning, post-processing, sterilization, and packaging can have serious performance and safety consequences. See *Sub-section 5.2.2*. All parts must be cleaned, and sterilized (autoclave steam, γ-irradiation, EtO or H2O2 plasma for metals, EtO or H2O2 plasma for polymers) as per ISO 11737-1:2018/-2:2019/-3:2023 and then packaged as per ISO 11607-1:2019/-2:2019. The package should be stored in a clean, cool, and dry place before surgery.

6.5 Case 2: Ilium-Acetabular and Hip Joint Reconstruction

Note: as this Thesis has an engineering-centered research character aiming to serve the surgeons, and to assess the initially set hypothesis (see Sub-sections 4.1 and 4.2), and due to budget and resources constraints, both top-down and bottom-up approaches (Figure 225) were discussed, and scenarios and hypotheses/assumptions were made along the application of the inter-epistemic development process flow chain (Figure 231). This case was treated as if it was a currently ongoing pragmatic case and as if the responsible surgeon required truly the active engagement of the PoC 3D Unit, as a result, the solution prototyped at the PoC 3D Unit was not implanted into the patient.

The adult male patient presented to the First Department of Orthopaedic Surgery, National and Kapodistrian University of Athens, “Attikon” University General Hospital (Chairman: Prof.

Panayiotis J. Papagelopoulos), examined, and diagnosed with pelvic tumor, the anatomic extent of which was determined radiologically. The CT scan indicating the tumor site is shown in *Figure 485*. All data was anonymized before sharing.

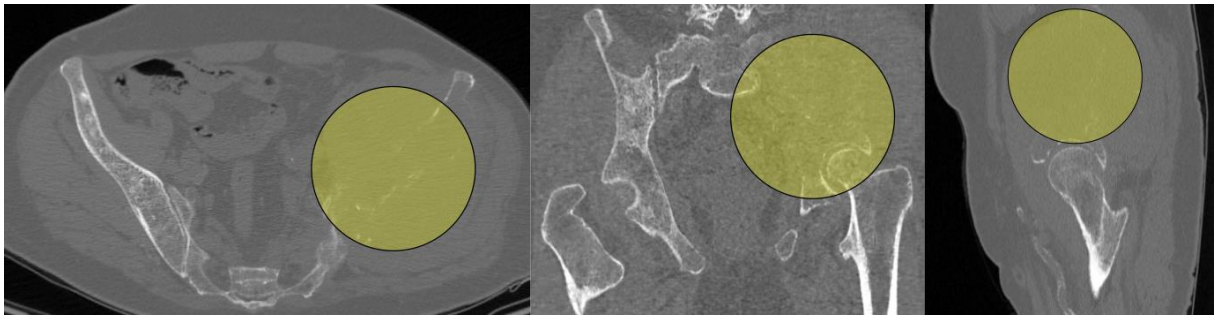

Figure 485: CT scan indicating the tumor site

The case was carried out in the pilot PoC 3D Unit introduced previously, and single-step en bloc tumor resection with wide margins and reconstruction was decided with artificial 3DPed custom-made endo-prosthesis accompanied by PSIs developed under the inter-epistemic methodology shown in *Figure 264*. In contrast to the first case study where the methodology was unfolded analytically, for this case, only the developed solution is presented. The pre-resected anatomy was visualized only intangibly (Step 4) by digital (interactive models and pictures) and virtual (xR) means, but the surgical simulation was visualized digitally, virtually, and physically (Step 12).

Figure 486 shows the automatically segmented and generated soft and hard anatomical structures from the CT scan data in 3D Slicer using the Total Segmentator AI tool *(Wasserthal et al., 2023)*. To obtain a finer bony structure required for the endo-prosthesis and PSI fit and resection planning, a more detailed anatomical model of the pelvis was generated using (semi)automatic tools in 3D Slicer. The planned resection (Type II and Type I plus sacroiliac joint) is shown in *Figure 487* and the photorealistic views of the pelvic model with peripheral hard and soft tissue is shown in *Figure 488*.

The 3D pre-operative planning including the a) resected tissue, b) positions and orientation of the four 6,5 mm cancellous bone screws and three 5 mm locking cortical screws, c) placement of femoral components, and d) orientation of the acetabular cup to be integrated into the endo-prosthesis per se, is illustrated in *Figure 489*. Stems as alternative options to bone screws were also explored.

The patient-specific bone tumor and femoral head-cutting instruments are illustrated in *Figure 490*. The instruments are registered on the bear bone uniquely thanks to the anatomically conforming shape of the polymer parts (to be 3DPed in PA12) held in place using 2 mm diameter K-wires, whilst AISI 316 stainless steel sheet metals are attached on the polymer parts by counter-suck screws to serve as contacting surface for the cutting saw.

Figure 491 pictures the patient-specific endo-prosthesis trial and bone drilling instrument to be 3DPed in PA12. For each bone screw, a 3 mm internal diameter AISI 316 cylinder is inserted into the housings of the instrument to guide the drill bit and protect the plastic from debris during drilling.

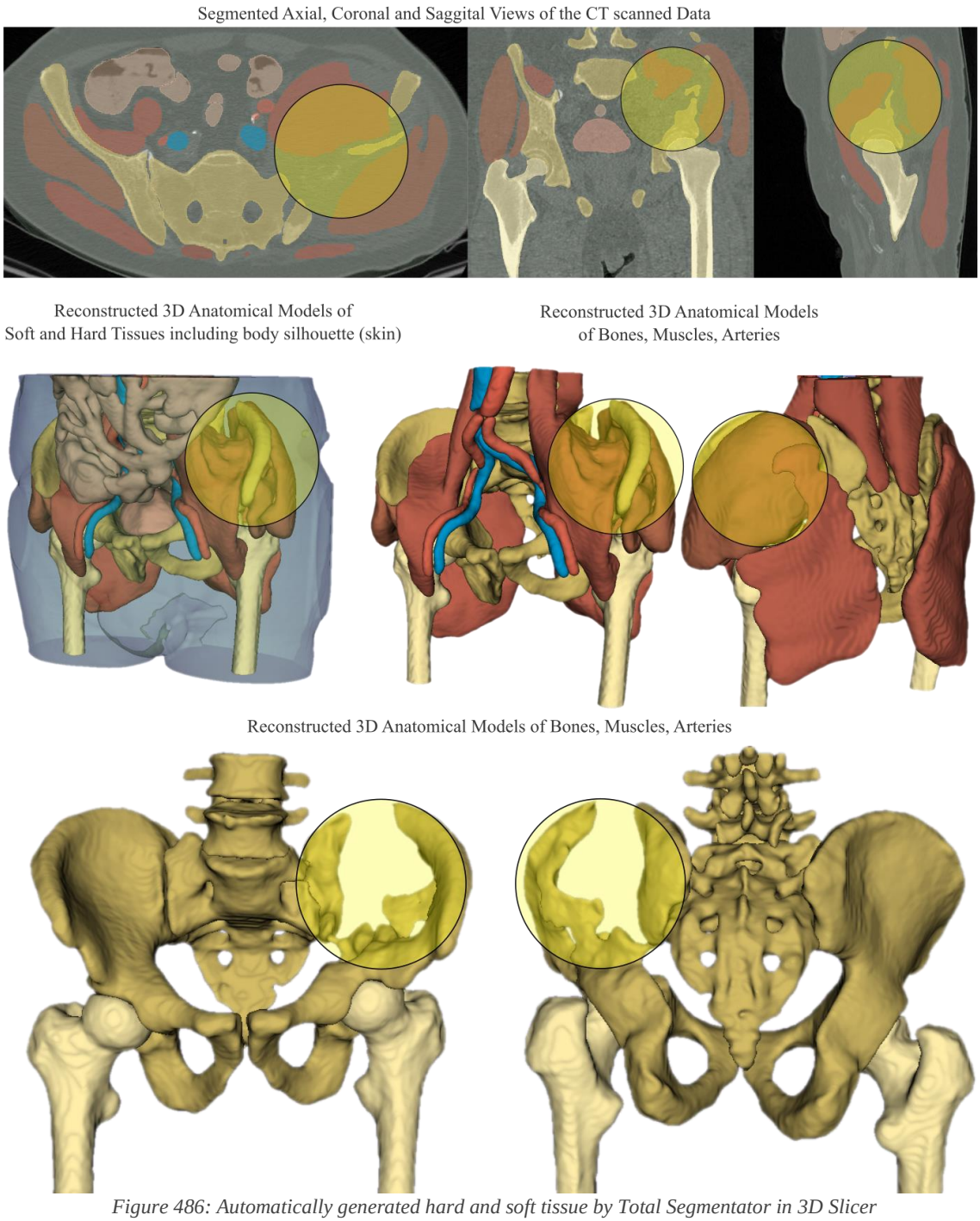

Figure 486: Automatically generated hard and soft tissue by Total Segmentator in 3D Slicer

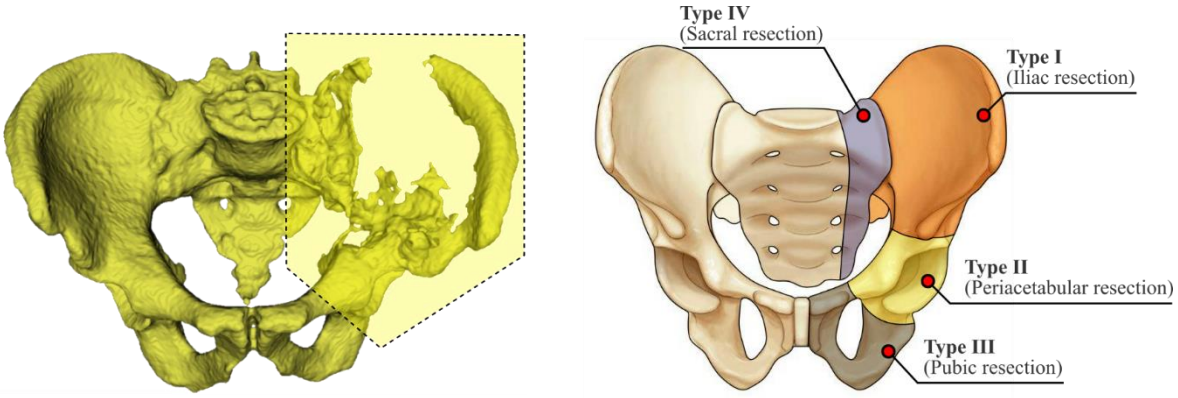

Figure 487: Planned resection and Enneking's classification

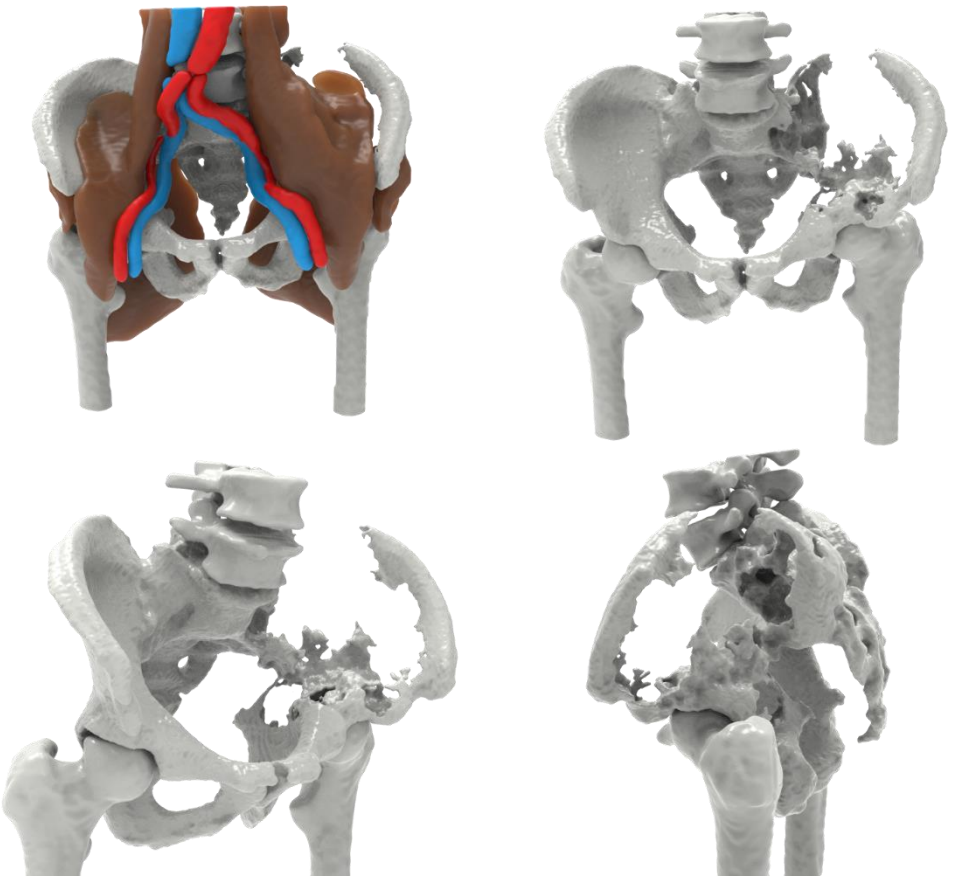

Figure 488: Photorealistic views of pelvic model and peripheral hard and soft tissue

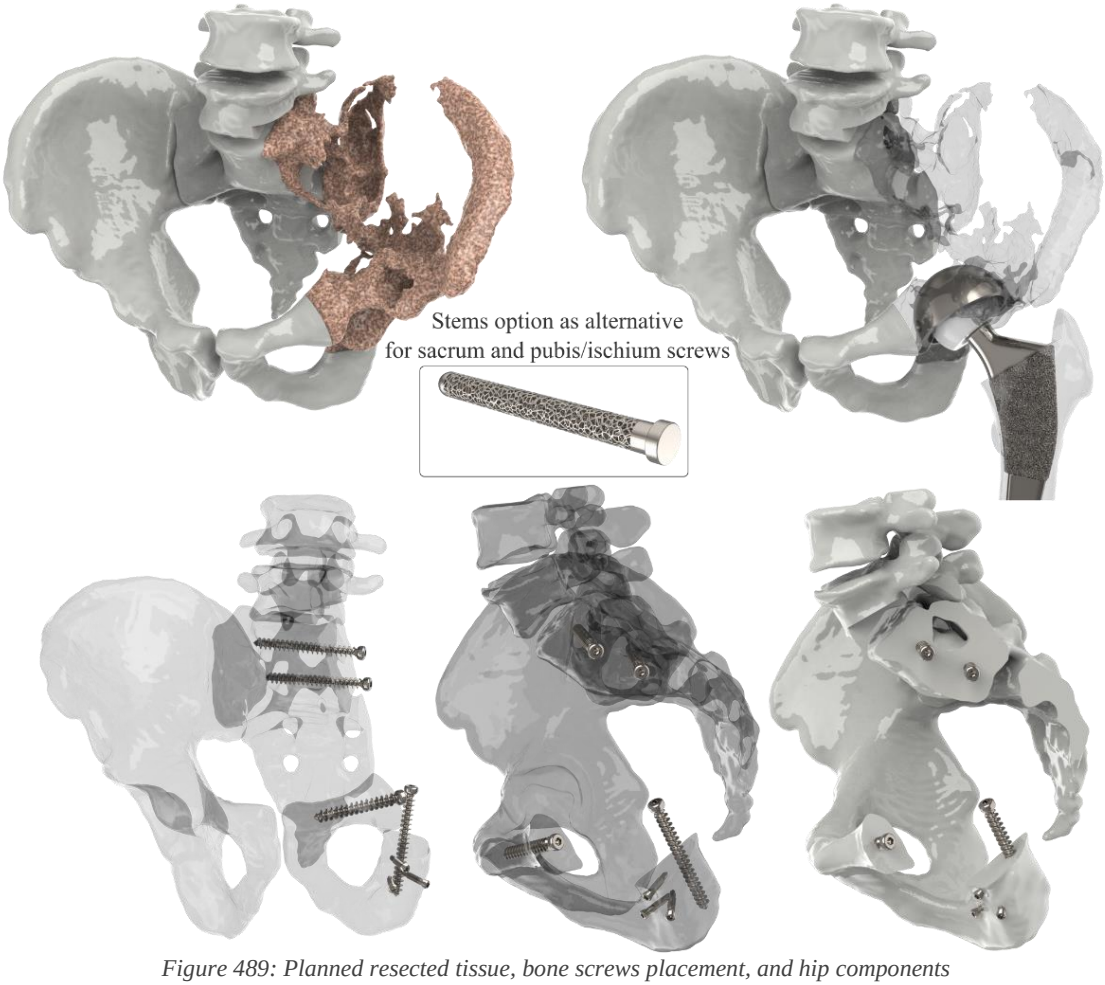

Figure 489: Planned resected tissue, bone screws placement, and hip components

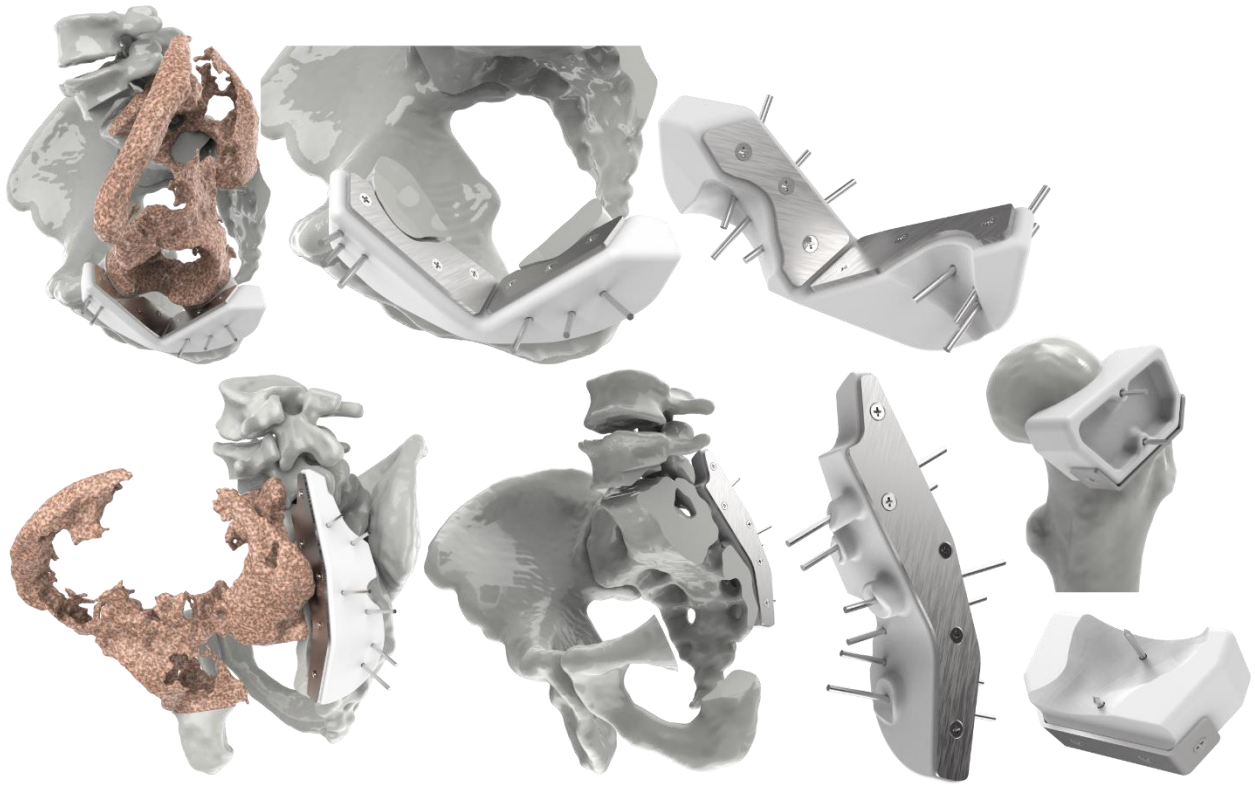

Figure 490: Patient-specific bone tumor and femoral head-cutting instruments

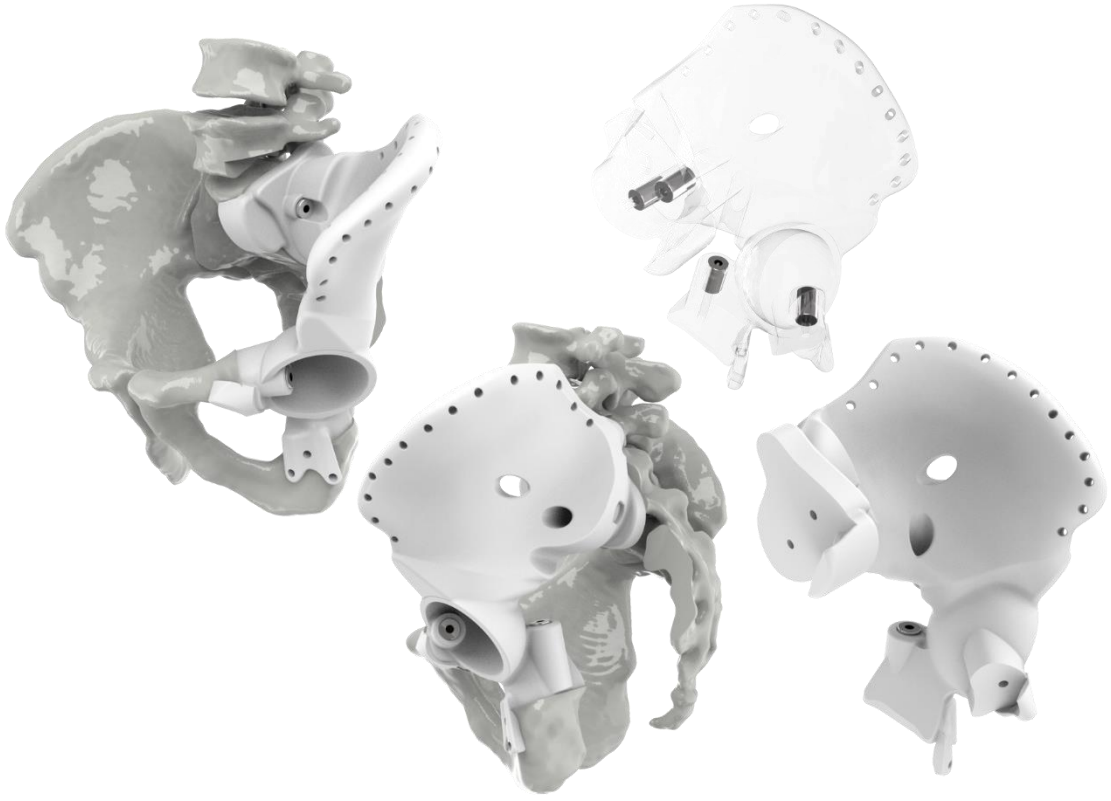

Figure 491: Patient-specific endo-prosthesis trial and bone drilling instrument

Photorealistic views of the solution with the off-the-shelf total hip arthroplasty components (dual mobility cup, liner, femoral stem and head), the individualized endo-prosthesis, and the bone screws are shown in *Figure 492*. Options for rod-pedicle screw system spondylodesis and rod attachment on the endo-prosthesis were also offered by implementing detachable fixators for a 6 mm rod.

The endo-prosthesis maintained a solid outer shell of 1 mm thickness and was architected with an inter-connected stochastic Voronoi complex at the surfaces that touch the bone and internally to achieve optimization for a bi-modal superiority in biological and mechanical dimensions by a) allowing bone ingrowth to reach biological fixation and osseointegration, and b) reducing the mass and the modulus of elasticity to approach the bone. *Figure 493* displays the views of the optimized endo-prosthesis.

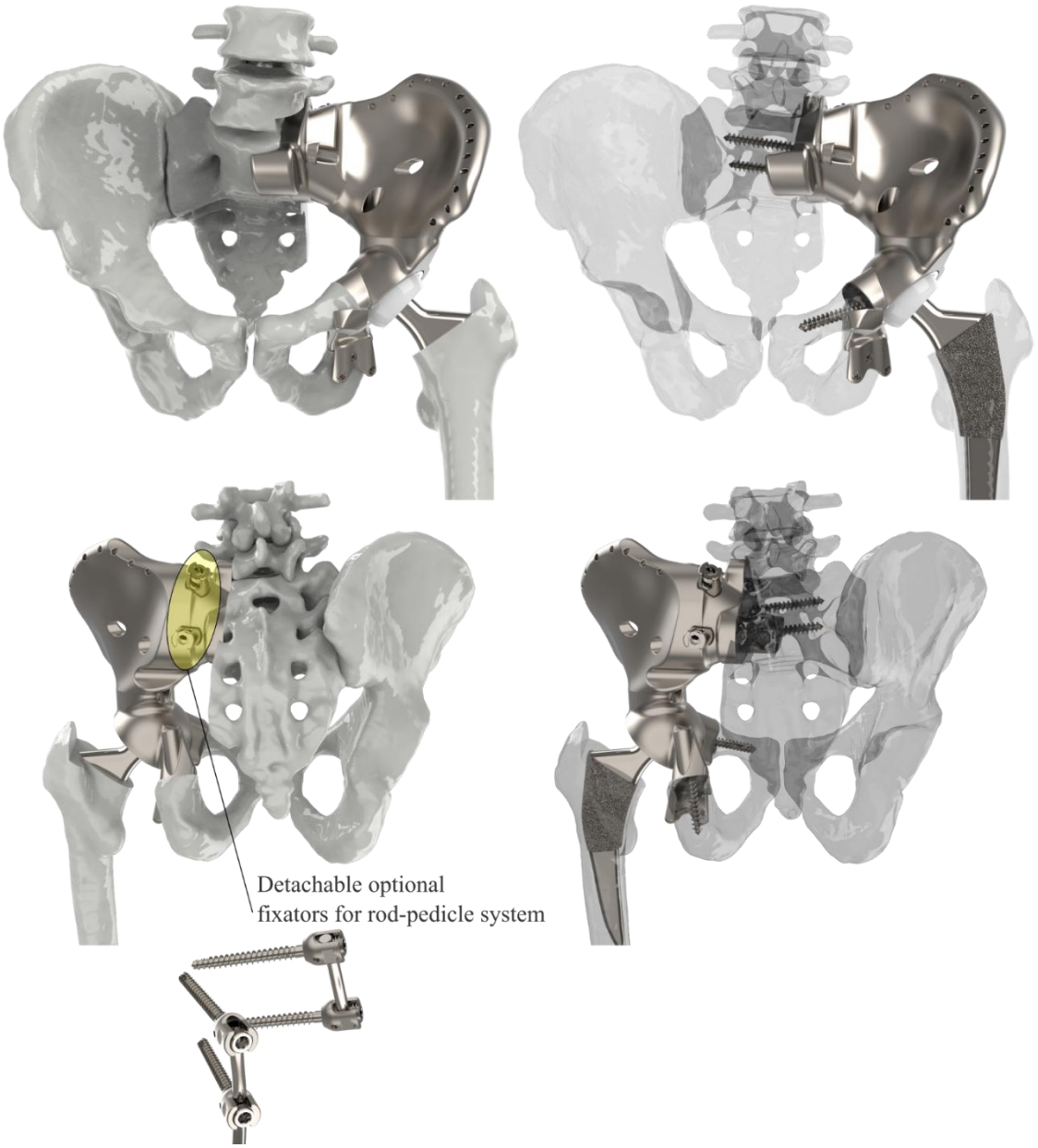

Figure 492: Solution with all components fixed on the anatomical model

The region of interest of the as-planned resected anatomical model, the resected tumor mass and the femur with and without the stem and head/liner, the cemented cup, the bone-cutting instruments, the endo-prosthesis trial and bone drilling instrument, and the endo-prosthesis were 3DPed out of colorFabb PLA/PHA filament using the low-cost 3D printer (Creality CR-10s) of the pilot PoC 3D Unit for physical simulation of the surgery (*Figure 494)*. The total material consumption, material

cost and total time required to 3DP all these prototype models in two sessions were 1.210 gr, 42,4 €, and 6 days 15 hours respectively. The overall development time of the solution was less than the first case because a) in Stage 4 only digital and virtual visualization of the anatomy took place, and b) in Stage 12 time was saved by 3DP only the anatomical regions of interest and not the whole anatomy.

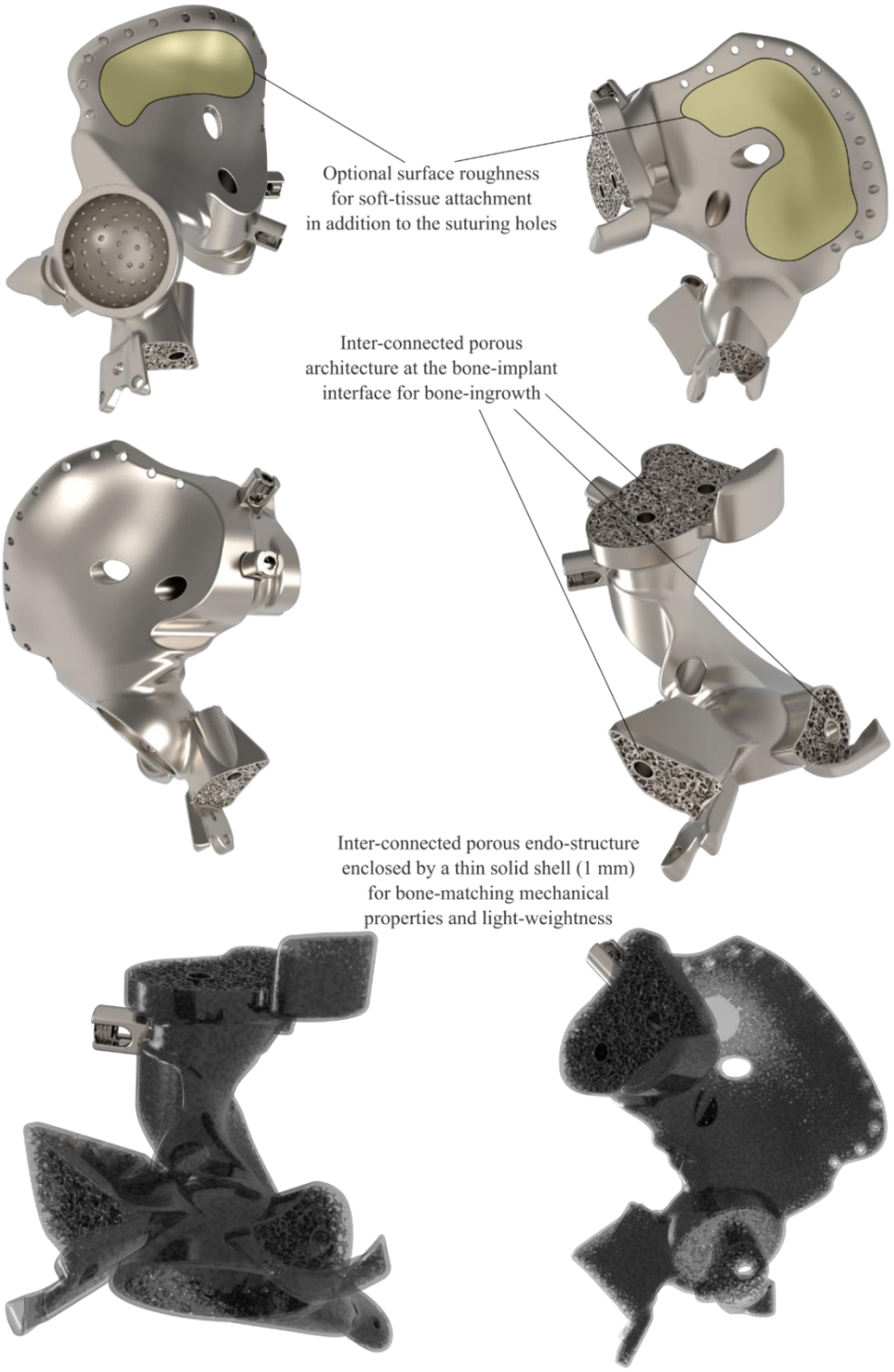

Figure 493: Optimized endo-prosthesis with inter-connected porous architectures

The documentation *(Figure 273 and Figure 275)* was sent to the surgeon for final approval and sign off to enable the beginning of patient-specific solution materialization. Once approved by the

surgeon and all required parties, the manufacturing of all parts to be used in the operating room was outsourced to a contract manufacturer. More specifically:

- All 3DPed (laser-based powder-bed fusion technology) surgical-grade PA12 ancillary instruments and the AISI 316 stainless steel inserts and sheet metals cost 530 € for a 6 working days delivery.
- The 3DP (laser-based powder-bed fusion technology) of the surgical-grade Ti6Al4V endo-prosthesis plus de-powdering and glass bead blasting for satin surface finish cost 3100 € for a 6 working days delivery.

The extra costs of the off-the-shelf components (bone screws, cemented acetabular cup, femoral stem and head components, and K-wires) were not considered as these were readily available in the market for purchase. Also, further post-processing and surface coatings were not considered.

Figure 494: 3DPed prototype parts for physical surgery simulation

6.6 Case 3: Acetabular and Hip Joint Reconstruction

Note: as this Thesis has an engineering-centered research character aiming to serve the surgeons, and to assess the initially set hypothesis (see Sub-sections 4.1 and 4.2), and due to budget and resources constraints, both top-down and bottom-up approaches (Figure 225) were discussed, and scenarios and hypotheses/assumptions were made along the application of the inter-epistemic development process flow chain (Figure 231). This case was treated as if it was a currently ongoing pragmatic case and as if the responsible surgeon required truly the active engagement of the PoC 3D Unit, as a result, the solution prototyped at the PoC 3D Unit was not implanted into the patient.

The adult female patient presented to the First Department of Orthopaedic Surgery, National and Kapodistrian University of Athens, "Attikon" University General Hospital (Chairman: Prof. Panayiotis J. Papagelopoulos), examined, and diagnosed with pelvic tumor, the anatomic extent of which was determined radiologically. The CT and MRI scans indicating the tumor site are shown in *Figure 495*. All data was anonymized before sharing.

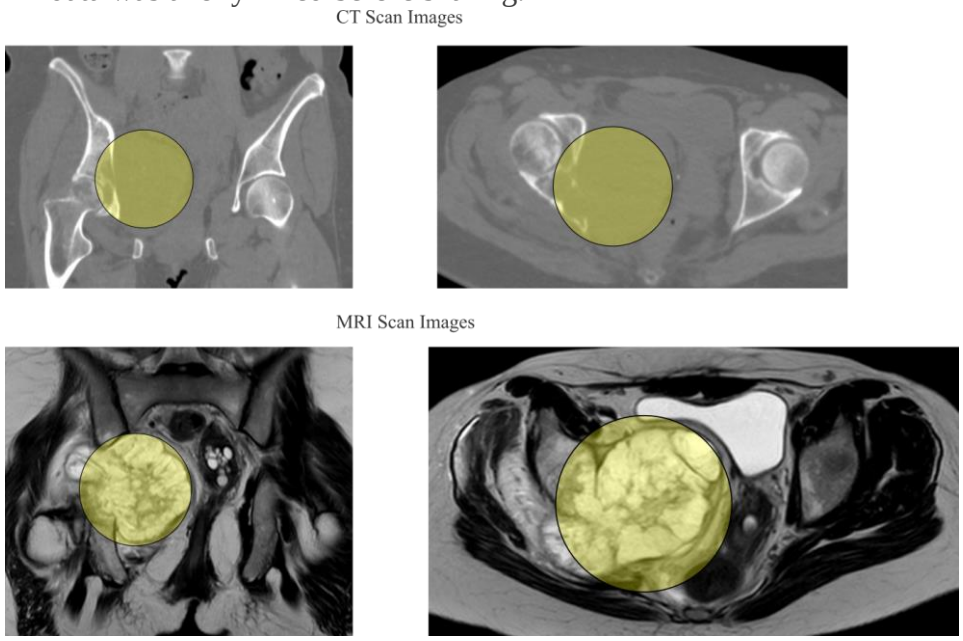

Figure 495: CT and MRI scans indicating the tumor site

The case was carried out in the pilot PoC 3D Unit introduced previously, and single-step en bloc tumor resection with wide margins and reconstruction was decided with artificial 3DPed custom-made endo-prosthesis accompanied by PSIs developed under the inter-epistemic methodology shown in *Figure 264*. In contrast to the first case study where the methodology was unfolded analytically, for this case, only the developed solution is presented. The pre-resected anatomy was visualized only intangibly (Step 4) by digital (interactive models and pictures) and virtual (xR) means, but the surgical simulation was visualized digitally, virtually, and physically (Step 12).

Figure 497 shows:

1. The automatically segmented and generated soft and hard anatomical structures from the CT scan data in 3D Slicer using the Total Segmentator AI tool *(Wasserthal et al., 2023)*. Also, a finer

bony structure was obtained using (semi)automatic tools in 3D Slicer as this was required for the endo-prosthesis and PSI fit.

2. The models of the tumor, arteries, and pelvic bones for registration purposes as obtained by the MRI scan in 3D Slicer using (semi)automatic tools.
3. The combined 3D model emerged from the multi-modal image alignment (CT and MRI scans). The alignment of the models was achieved using the Interactive Closest Point (ICP) algorithm *(Besl and McKay, 1991; Zhang, Yao and Deng, 2022)* in Meshlab software *(Cignoni et al., 2008) (Figure 496)*. Alternatively, although found to be more time-consuming, the CT and MRI scans and 3D models could have been aligned in 3D Slicer using the (semi)automatic or manual registration tools offered by the corresponding modules.

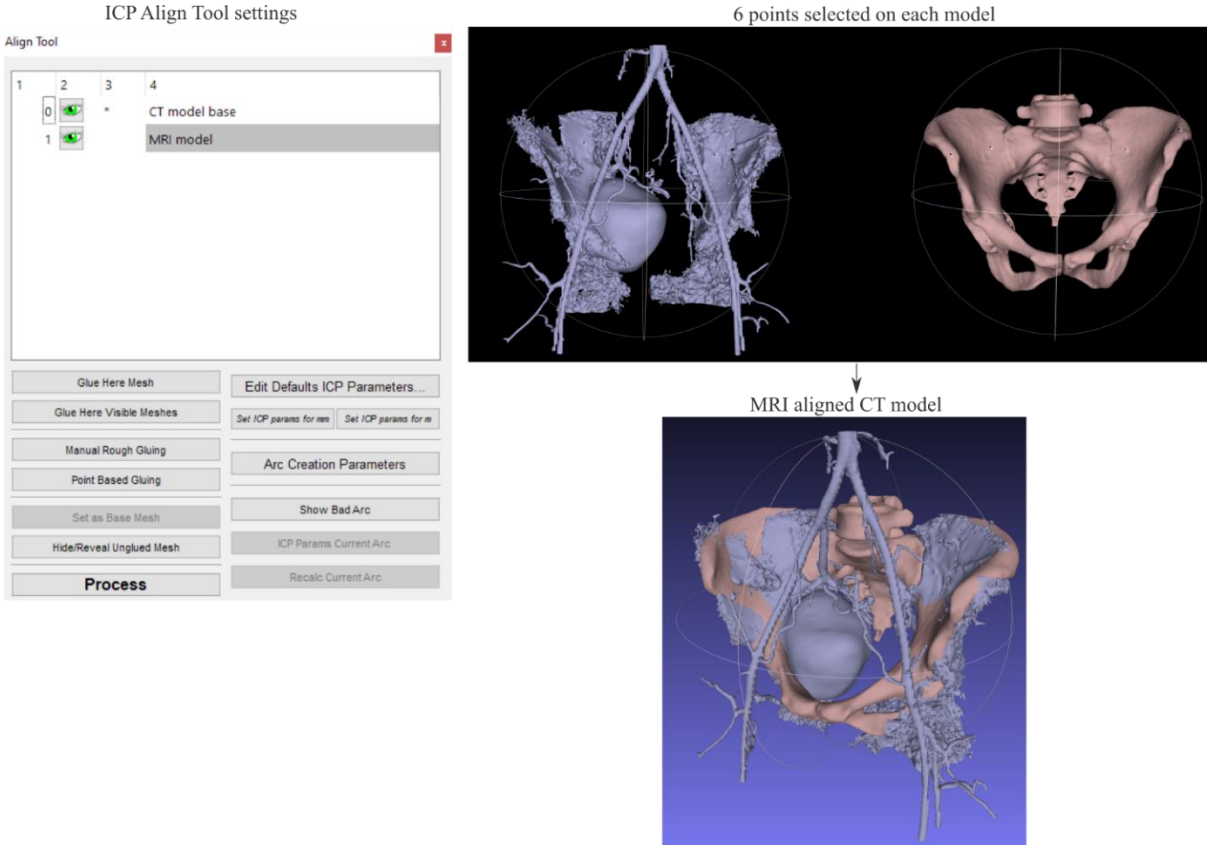

Figure 496: ICP alignment of CT and MRI-generated models

The photorealistic views of the pelvic model and peripheral hard and soft tissue are shown in *Figure 498* whereas the planned resection (Type II plus partial Type I) is illustrated in *Figure 499*.

The 3D pre-operative planning including the a) resected tissue, b) positions and orientation of the five 6,5 mm cancellous bone screws and a porous 8 mm stem, c) placement of femoral components, and d) orientation of the acetabular cup to be integrated into the endo-prosthesis per se, is illustrated in *Figure 500*. Six 5 mm locking cortical screws were also explored for optional flanges addition.

The patient-specific bone tumor and femoral head-cutting instruments are illustrated in *Figure 501*. The instruments are registered on the bear bone uniquely thanks to the anatomically conforming shape of the polymer parts (to be 3DPed in PA12) held in place using 2 mm diameter K-wires, whilst

AISI 316 stainless steel sheet metals are attached on the polymer parts by counter-suck screws to serve as contacting surface for the cutting saw.

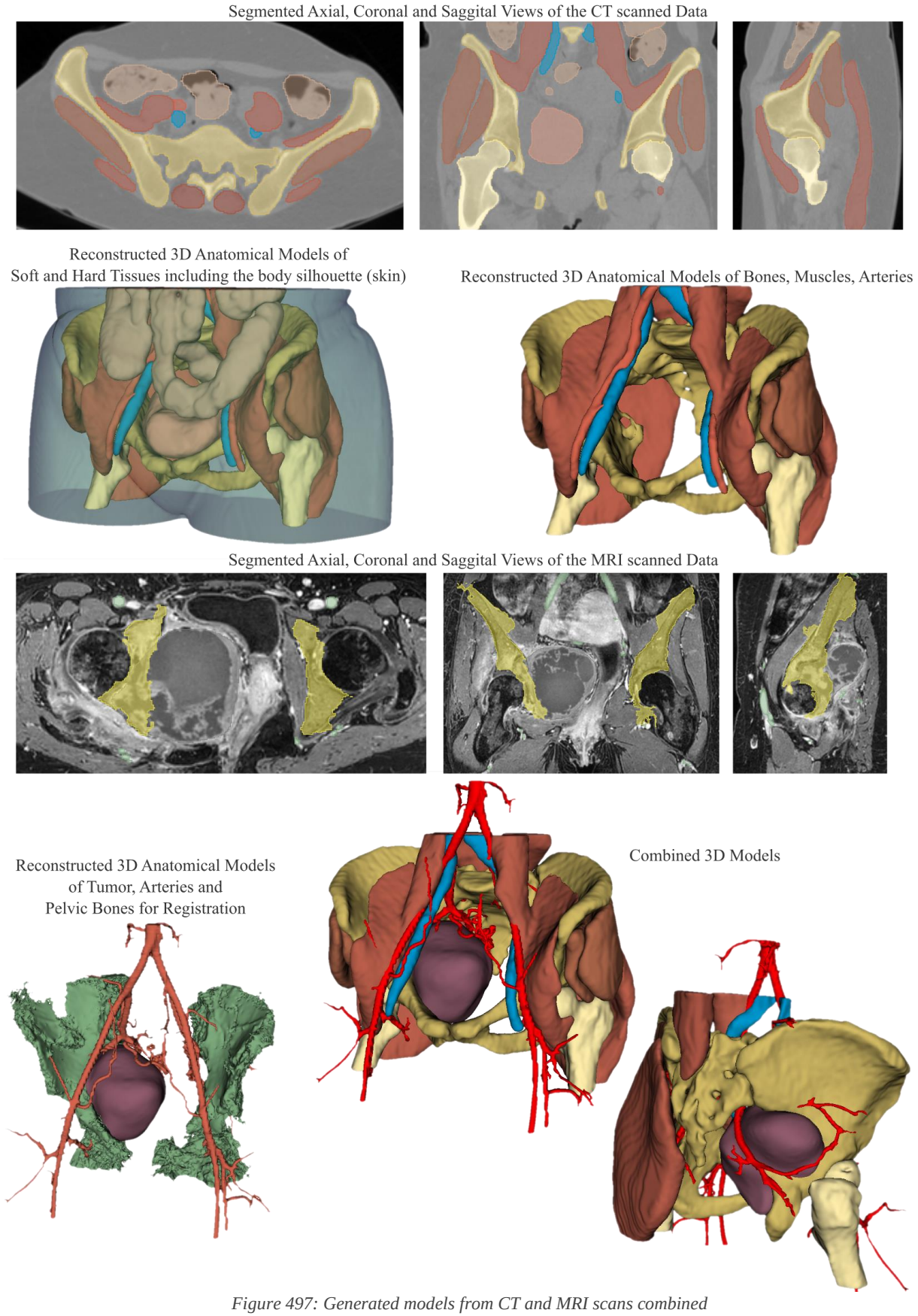

Figure 497: Generated models from CT and MRI scans combined

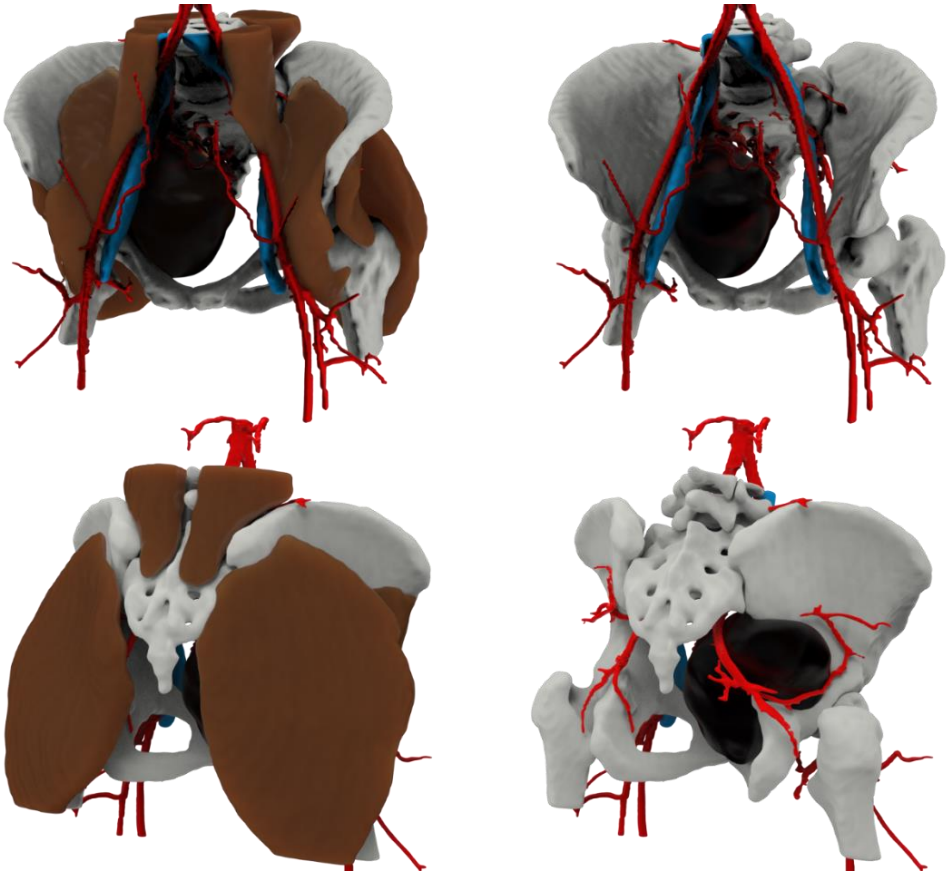

Figure 498: Photorealistic combined model

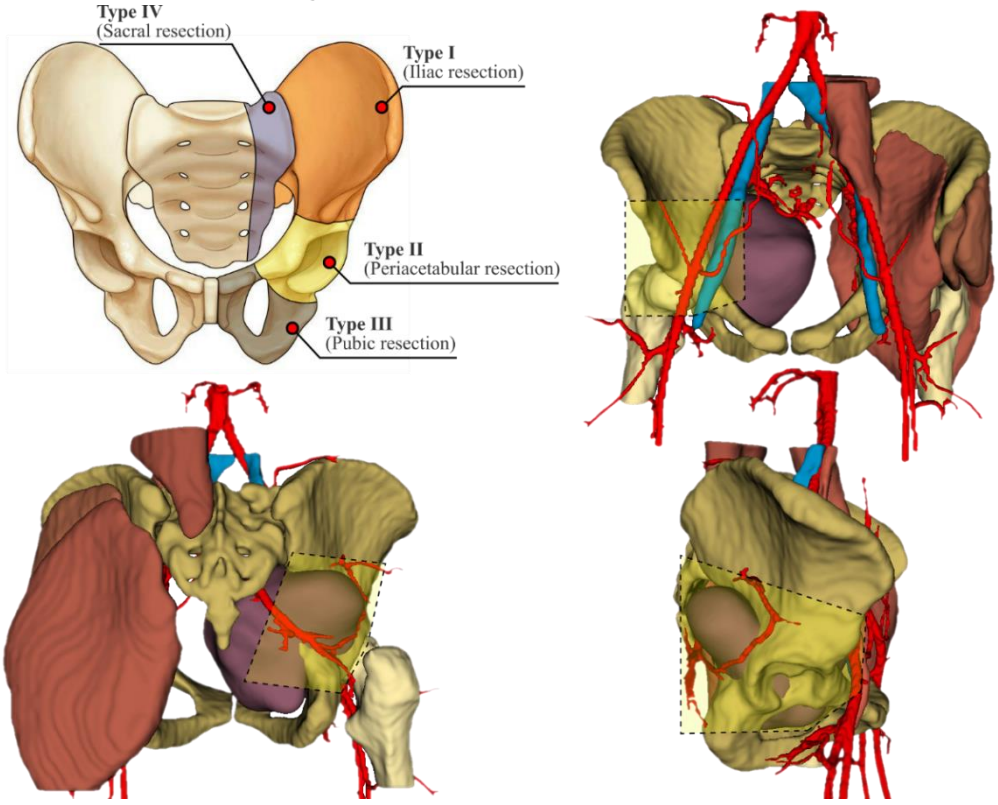

Figure 499: Planned bone resection and Enneking's classification

Figure 502 pictures the patient-specific endo-prosthesis trial and bone drilling instrument to be 3DPed in PA12. For each bone screw, a 3 mm internal diameter AISI 316 cylinder is inserted into the housings of the instrument to guide the drill bit and protect the plastic from debris during drilling.

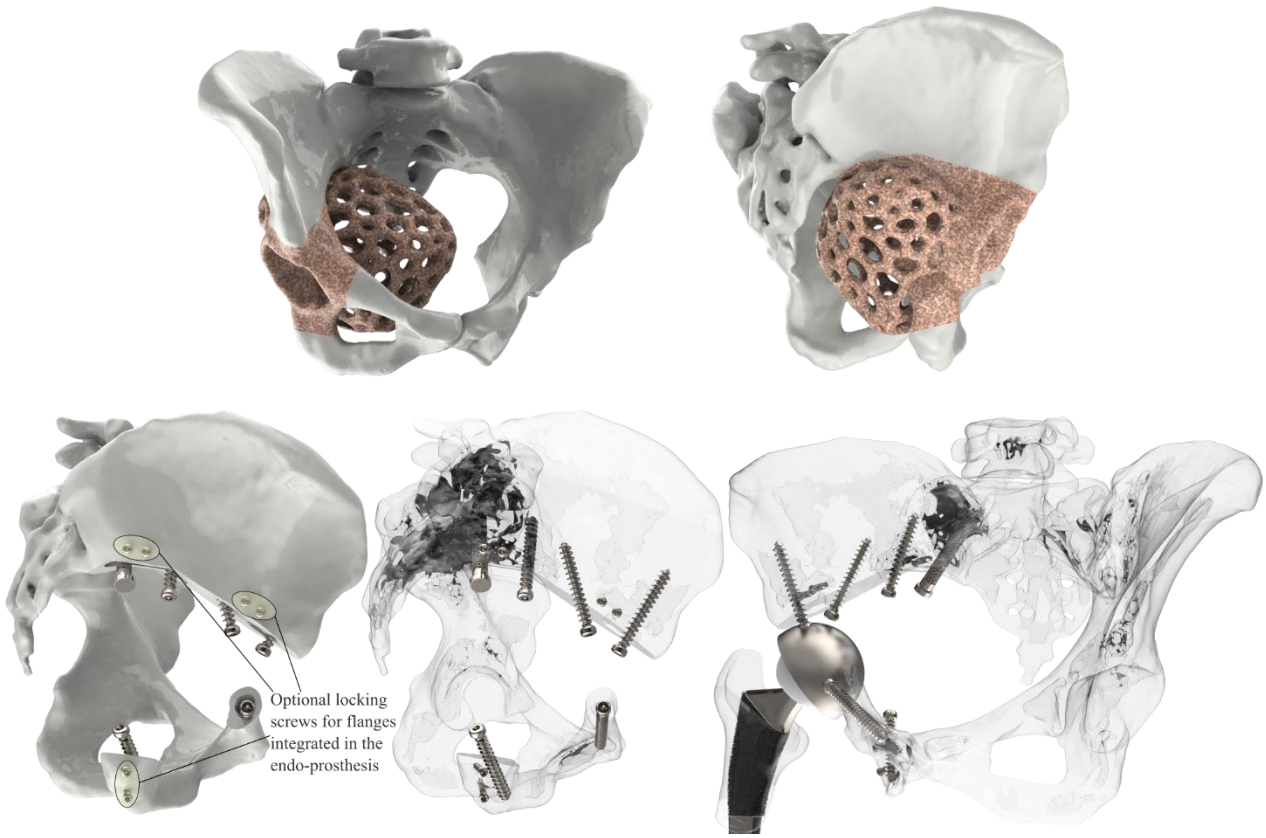

Figure 500: Planned resected tissue, bone screws placement, and hip components

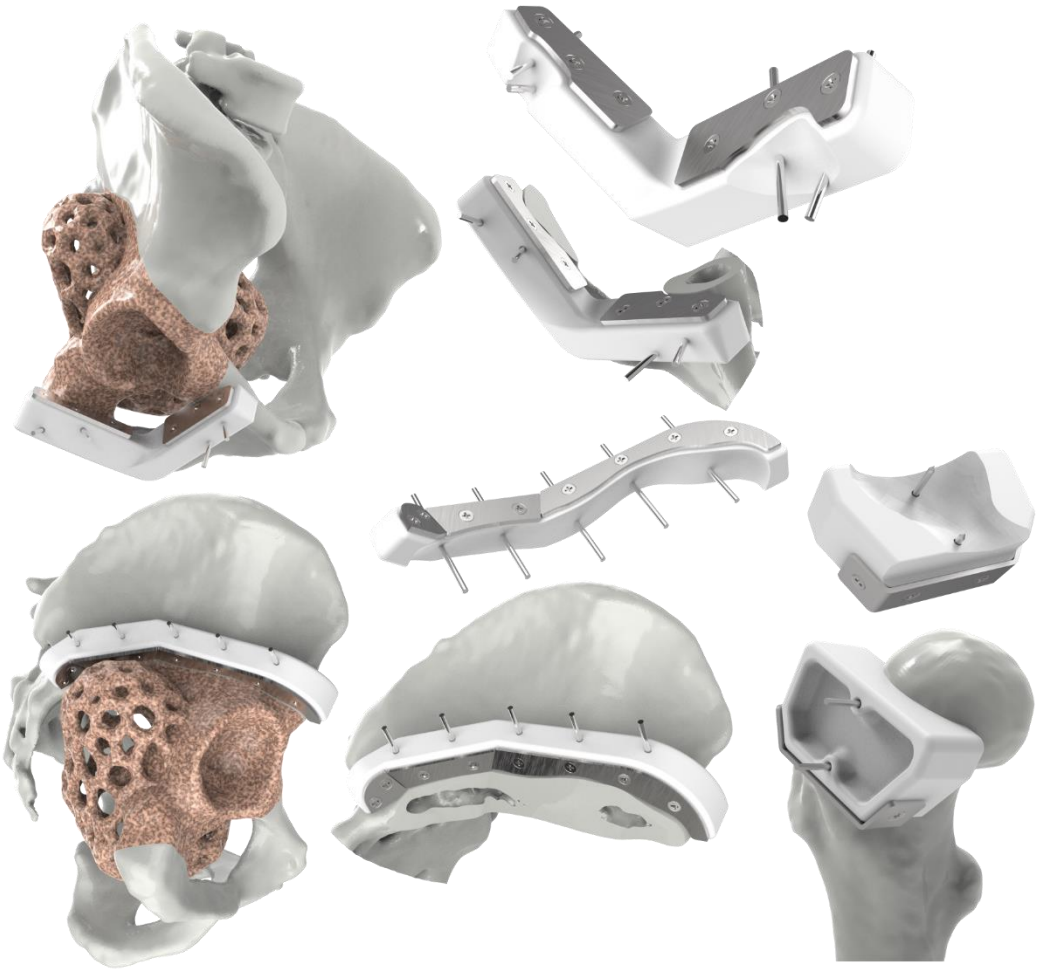

Figure 501: Patient-specific bone tumor and femoral head-cutting instruments

Figure 502: Patient-specific endo-prosthesis trial and bone drilling instrument

Photorealistic views of the solution with the off-the-shelf total hip arthroplasty components (dual mobility cup, liner, femoral stem and head), the individualized endo-prosthesis, the bone screws, and the custom-made stem are shown in *Figure 503*.

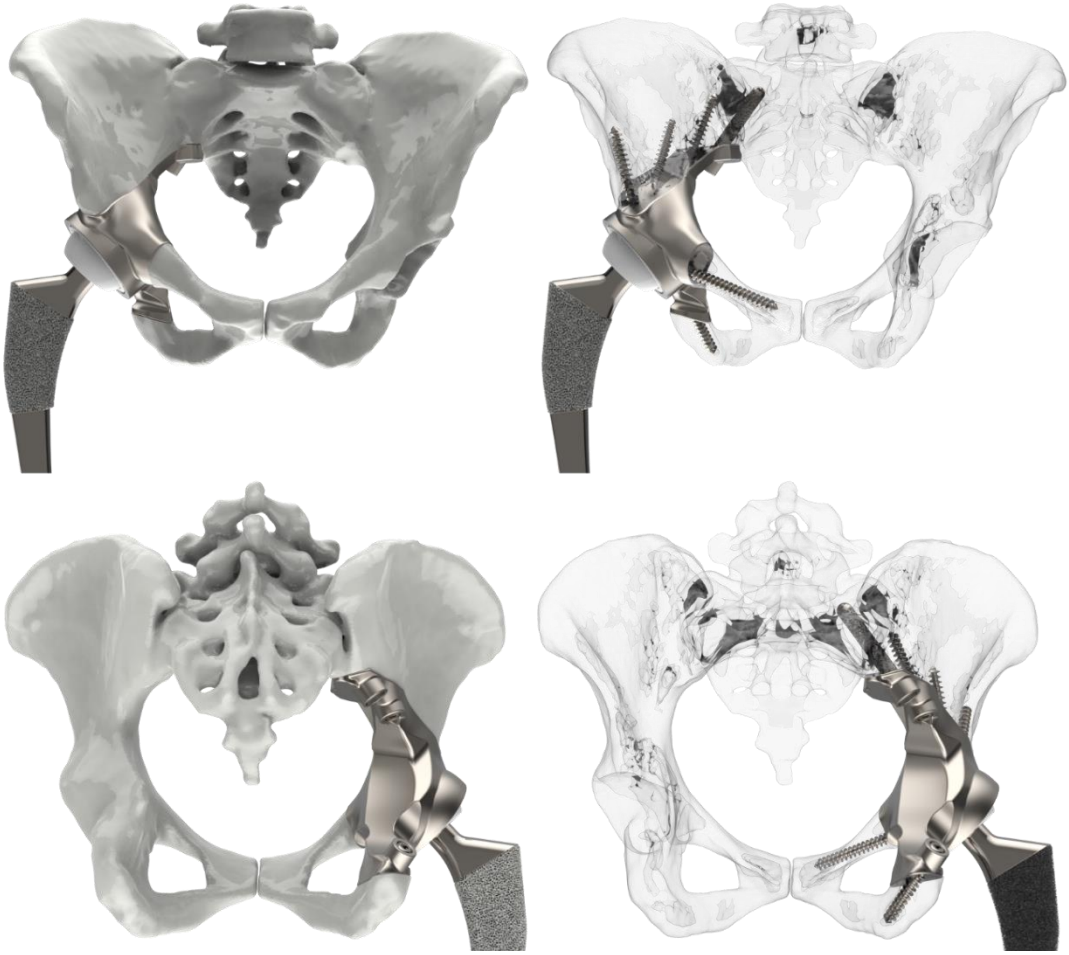

Figure 503: Solution with all components fixed on the anatomical model

The endo-prosthesis maintained a solid outer shell of 1 mm thickness and was architected with an inter-connected stochastic Voronoi complex at the surfaces that touch the bone and internally to achieve optimization for a bi-modal superiority in biological and mechanical dimensions by a) allowing bone ingrowth to reach biological fixation and osseointegration, and b) reducing the mass and the modulus of elasticity to approach the bone. *Figure 504* displays the views of the optimized endo-prosthesis.

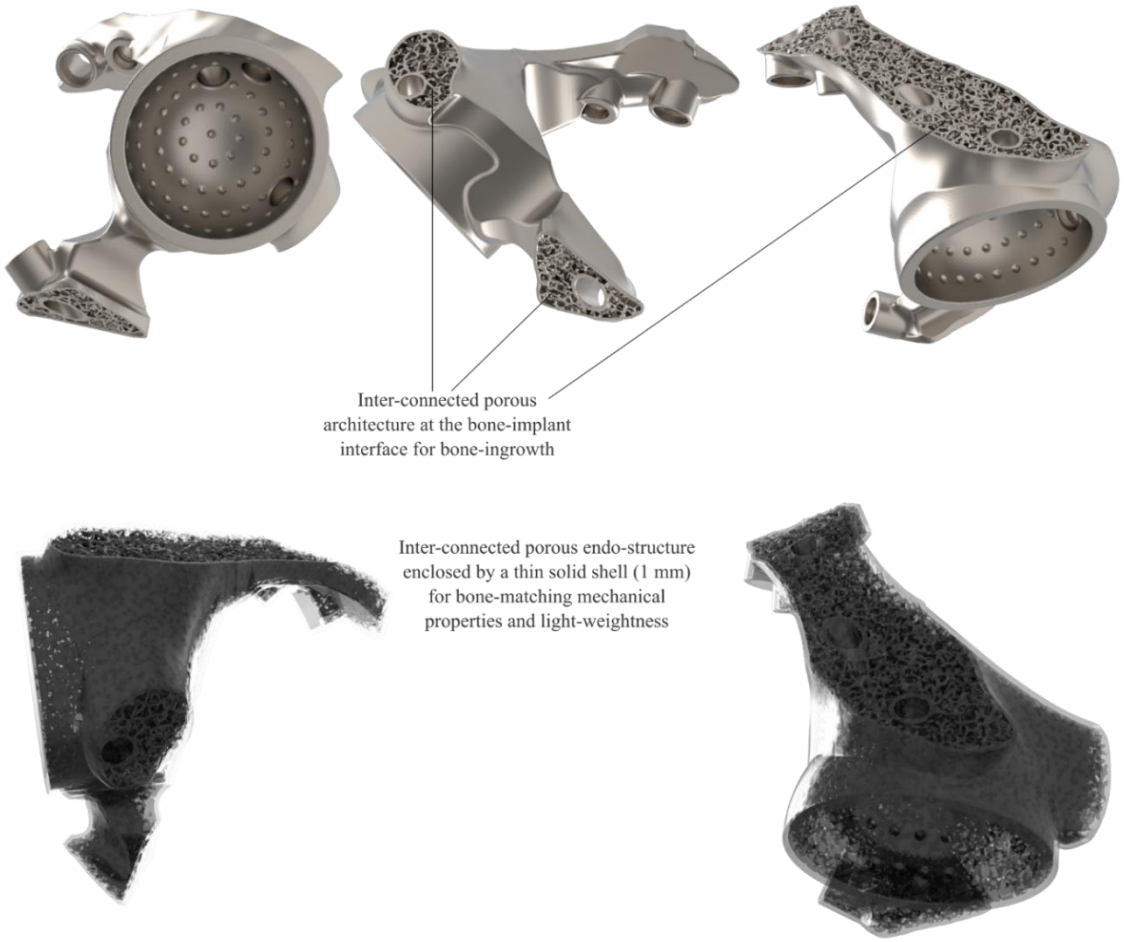

Figure 504: Optimized endo-prosthesis with inter-connected porous architectures

The region of interest of the as-planned resected anatomical model, the resected tumor mass and the femur with and without the stem and head/liner, the cemented cup, the bone-cutting instruments, the endo-prosthesis trial and bone drilling instrument, and the endo-prosthesis were 3DPed out of colorFabb PLA/PHA filament using the low-cost 3D printer (Creality CR-10s) of the pilot PoC 3D Unit for physical simulation of the surgery *(Figure 505)*. The total material consumption, material cost and total time required to 3DP all these prototype models in one session were 1000 gr, 35 €, and 5 days 7 hours respectively. The overall development time of the solution was less than the first case because a) in Stage 4 only digital and virtual visualization of the anatomy took place, and b) in Stage 12 time was saved by 3DP only the anatomical regions of interest and not the whole anatomy.

The documentation *(Figure 273 and Figure 275)* was sent to the surgeon for final approval and sign off to enable the beginning of patient-specific solution materialization. Once approved by the

surgeon and all required parties, the manufacturing of all parts to be used in the operating room was outsourced to a contract manufacturer. More specifically:

- All 3DPed (laser-based powder-bed fusion technology) surgical-grade PA12 ancillary instruments and the AISI 316 stainless steel inserts and sheet metals cost 380 € for a 6 working days delivery.
- The 3DP (laser-based powder-bed fusion technology) of the surgical-grade Ti6Al4V endo-prosthesis and the custom 8 mm porous stem plus de-powdering and glass bead blasting for satin surface finish cost 1800 € for a 6 working days delivery.

The extra costs of the off-the-shelf components (bone screws, cemented acetabular cup, femoral stem and head components, and K-wires) were not considered as these were readily available in the market for purchase. Also, further post-processing and surface coatings were not considered.

Figure 505: 3DPed prototype parts for physical surgery simulation

6.7 Case 4: Sacrum Reconstruction

Note: as this Thesis has an engineering-centered research character aiming to serve the surgeons, and to assess the initially set hypothesis (see Sub-sections 4.1 and 4.2), and due to budget and resources constraints, both top-down and bottom-up approaches (Figure 225) were discussed, and scenarios and hypotheses/assumptions were made along the application of the inter-epistemic development process flow chain (Figure 231). This case was treated as if it was a currently ongoing pragmatic case and as if the responsible surgeon required truly the active engagement of the PoC 3D Unit, as a result, the solution prototyped at the PoC 3D Unit was not implanted into the patient.

The adult female patient presented to the First Department of Orthopaedic Surgery, National and Kapodistrian University of Athens, "Attikon" University General Hospital (Chairman: Prof. Panayiotis J. Papagelopoulos), examined, and diagnosed with sacral tumor, the anatomic extent of which was determined radiologically. The CT and MRI scans indicating the tumor site are shown in *Figure 506*. All data was anonymized before sharing.

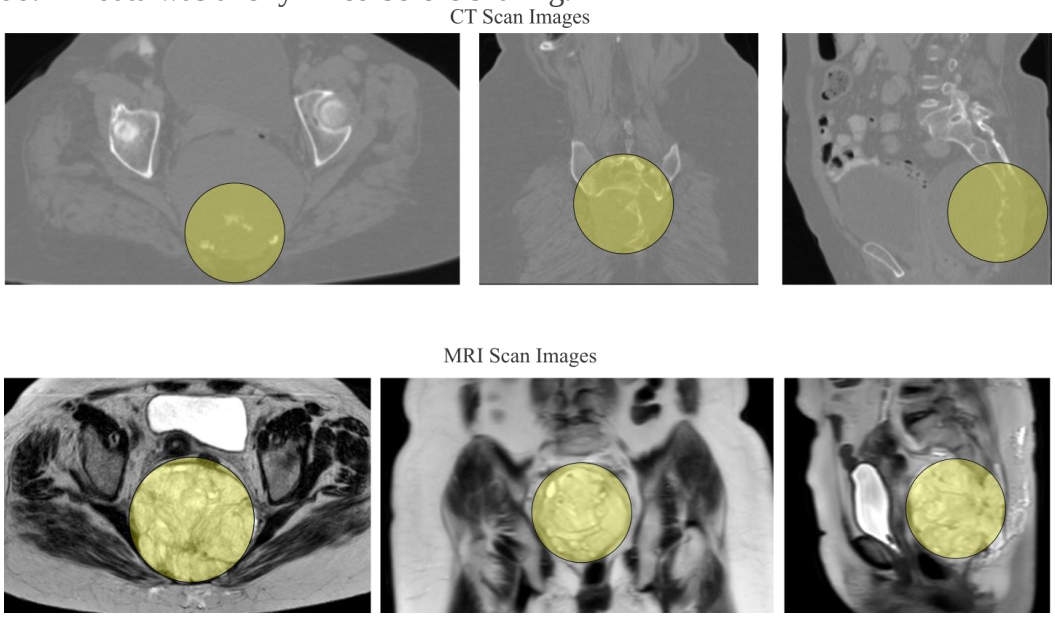

Figure 506: CT and MRI scans indicating the tumor site

The case was carried out in the pilot PoC 3D Unit, and single-step en bloc tumor resection with wide margins and reconstruction was decided under the inter-epistemic methodology shown in *Figure 264*. In contrast to the first case study where the methodology was unfolded analytically, for this case, only the developed solution is presented. The pre-resected anatomy was visualized only intangibly (Step 4) by digital (interactive models and pictures) and virtual (xR) means, but the surgical simulation was visualized digitally, virtually, and physically (Step 12).

Figure 507 shows the automatically segmented and generated soft and hard anatomical structures from the CT scan data in 3D Slicer using the Total Segmentator AI tool *(Wasserthal et al., 2023)*. Also, a finer bony structure was obtained using (semi)automatic tools in 3D Slicer as this was required for the endo-prosthesis and PSI fit. *Figure 508* illustrates the models of the tumor and pelvic

bones for registration purposes as obtained by the MRI scan in 3D Slicer using (semi)automatic tools, and the combined 3D model as emerged by the multi-modal image alignment (CT and MRI scans). The alignment of the models was achieved using the Interactive Closest Point (ICP) algorithm *(Besl and McKay, 1991; Zhang, Yao and Deng, 2022)* in Meshlab software *(Cignoni et al., 2008) (Figure 509)*. Alternatively, although found to be more time-consuming, the CT and MRI scans and 3D models could have been aligned in 3D Slicer using the (semi)automatic or manual registration tools offered by the corresponding modules.

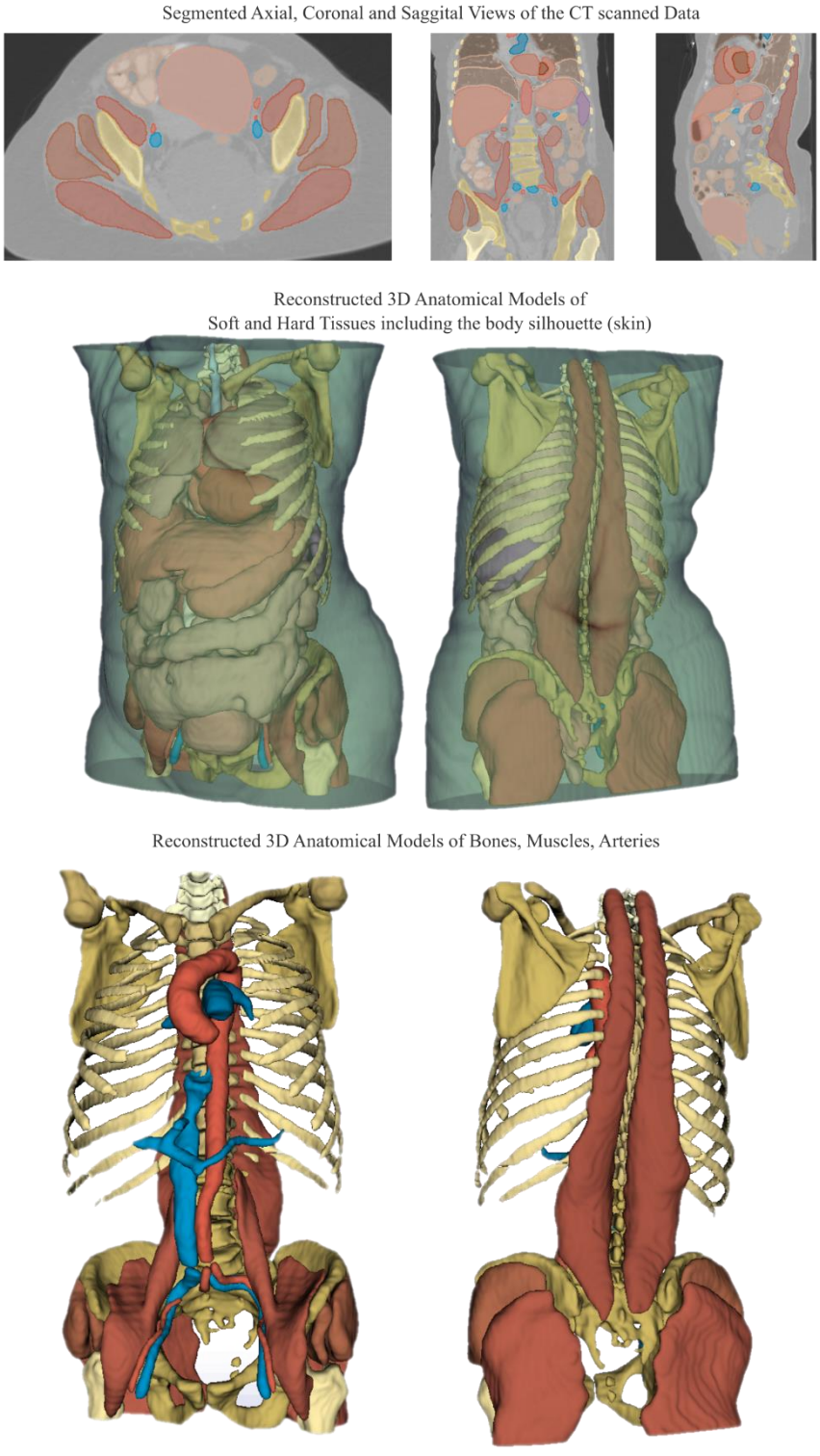

Figure 507: Generated models from CT scan

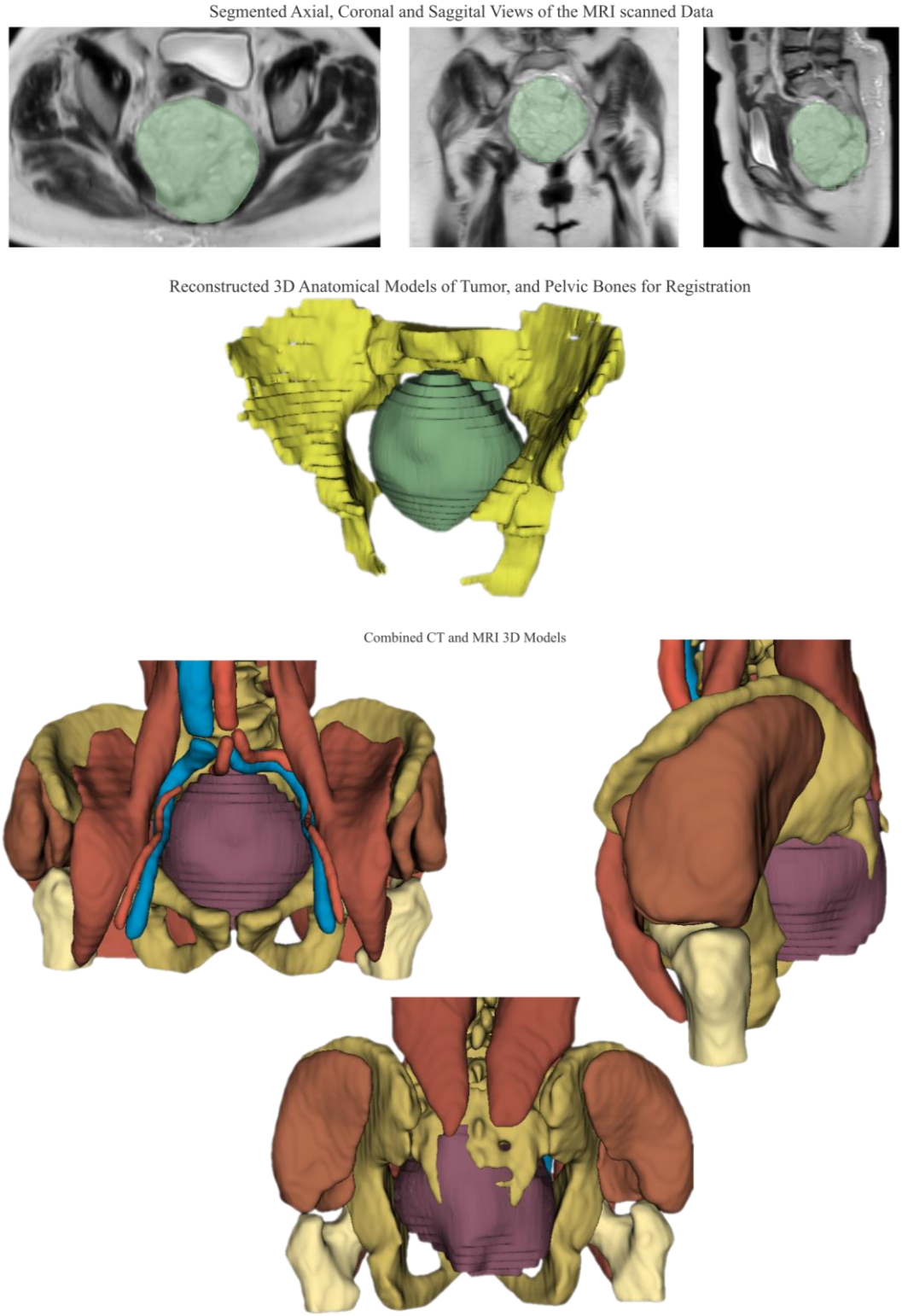

Figure 508: Generated models from MRI scan and combined model

The photorealistic views of the pelvic model and peripheral hard and soft tissue are shown in *Figure 510* whereas the en bloc tissue to be resected with wide margins is shown in *Figure 511* along with Mayo Clinic's classification of sacral tumor resection and reconstruction approaches. As more than 50% of the sacroiliac joint was planned to be resected, type B is applicable, though type A could also apply. The type B approach with reconstruction using pedicle screws-rods and bone grafts is

being described along with graphics by AO as can be seen in *Figure 514*. For this case, both the pedicle screw-rod system and custom-made artificial 3DPed endo-prosthesis reconstruction will be shown, though endo-prosthetic sacrum reconstruction offers superior biomechanical performance with more uniform stress distribution, lower peak stresses, and better stability *(Huang, Ji and Guo, 2019; Morales-Codina and Martin-Benlloch, 2022)*.

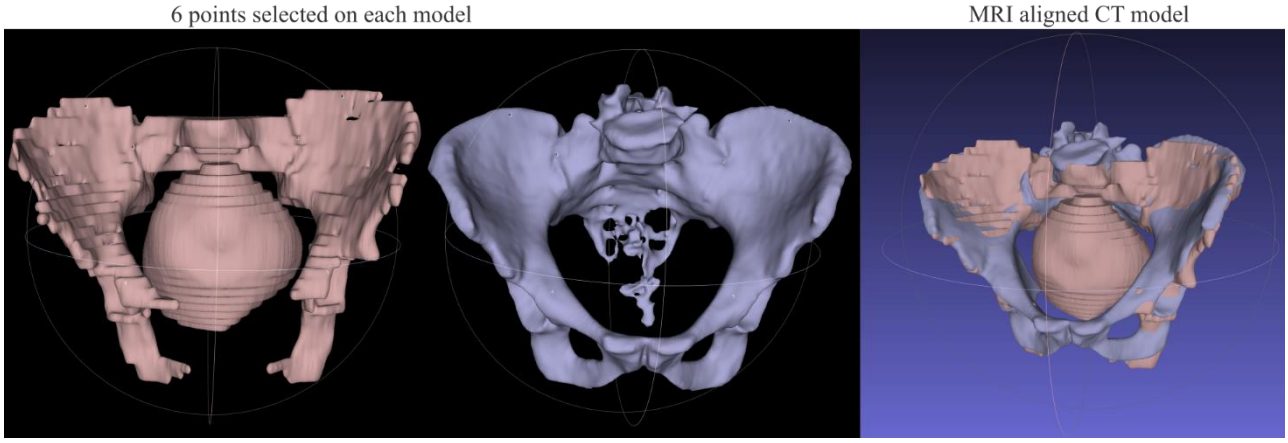

Figure 509: ICP alignment of CT and MRI-generated models

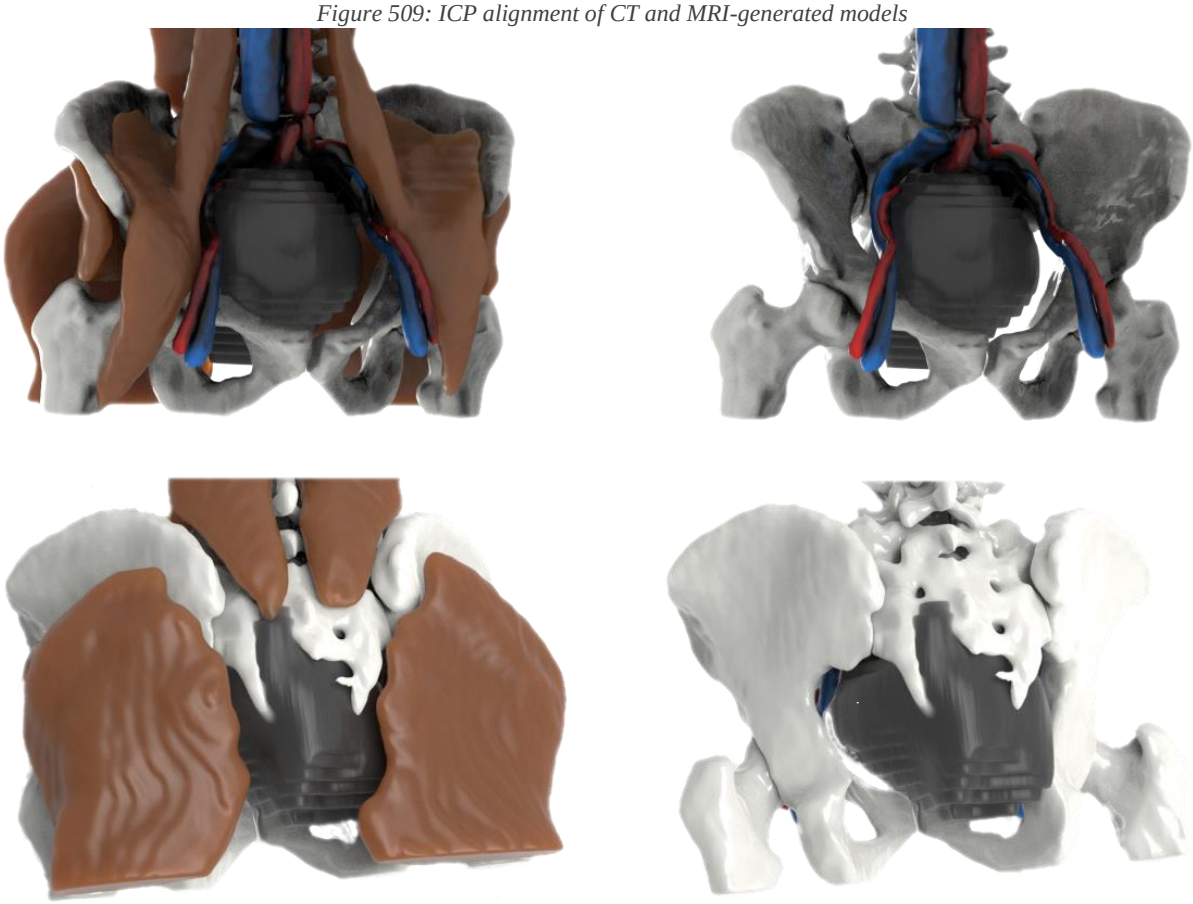

Figure 510: Photorealistic combined model

The patient-specific bone tumor-cutting instrument is illustrated in *Figure 513*. The instrument is registered on the bear bone uniquely thanks to the anatomically conforming shape of the polymer part (to be 3DPed in PA12) held in place using 2 mm diameter K-wires, whilst AISI 316 stainless steel sheet metals are attached on the polymer part by counter-suck screws to serve as contacting surface for the cutting saw.

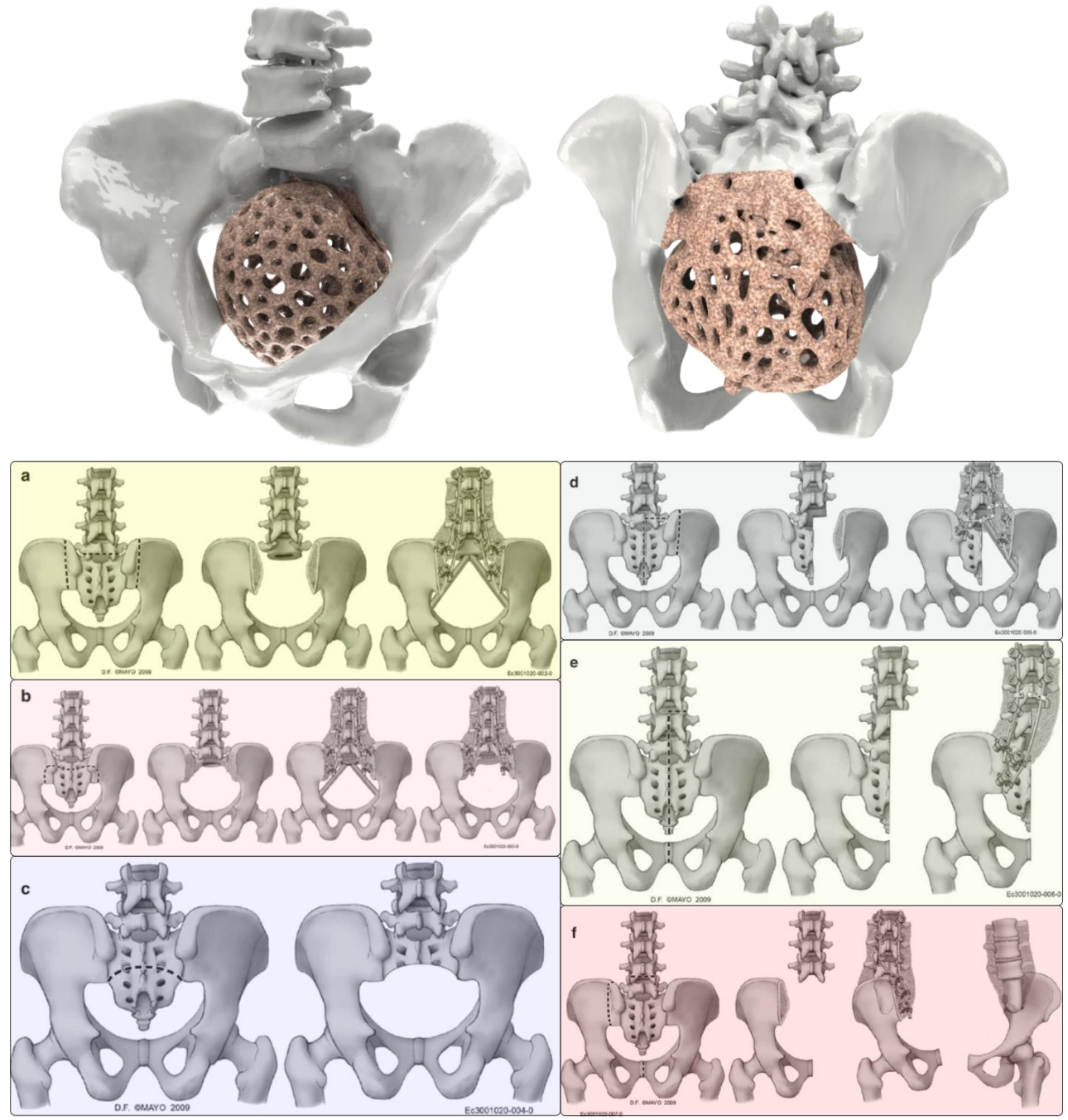

Figure 511: Planned resected tissue and Mayo Clinic's classification of sacral resections

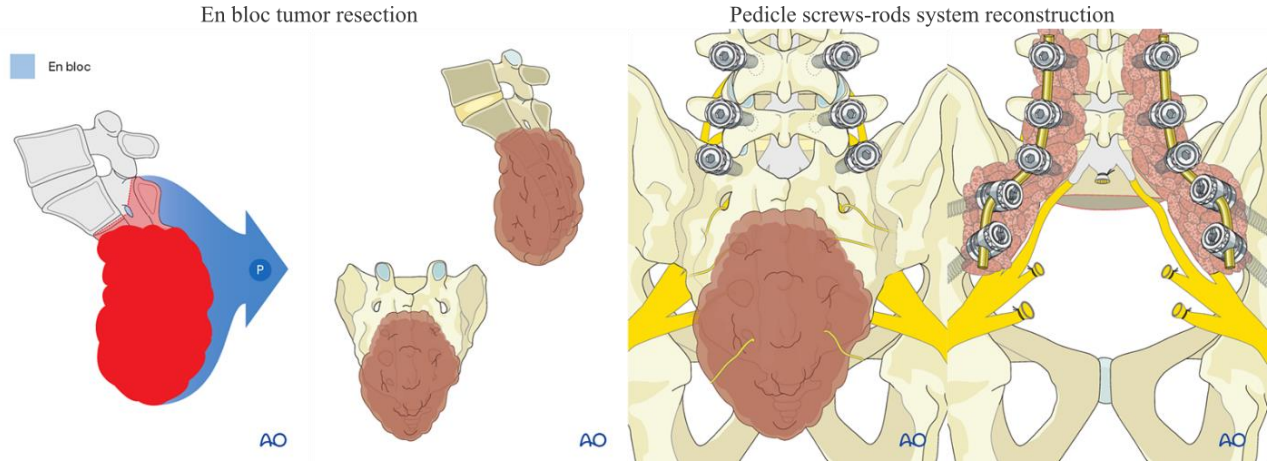

Figure 512: En bloc sacral tumor resection and reconstruction with pedicle screw-rod system. Source: AO

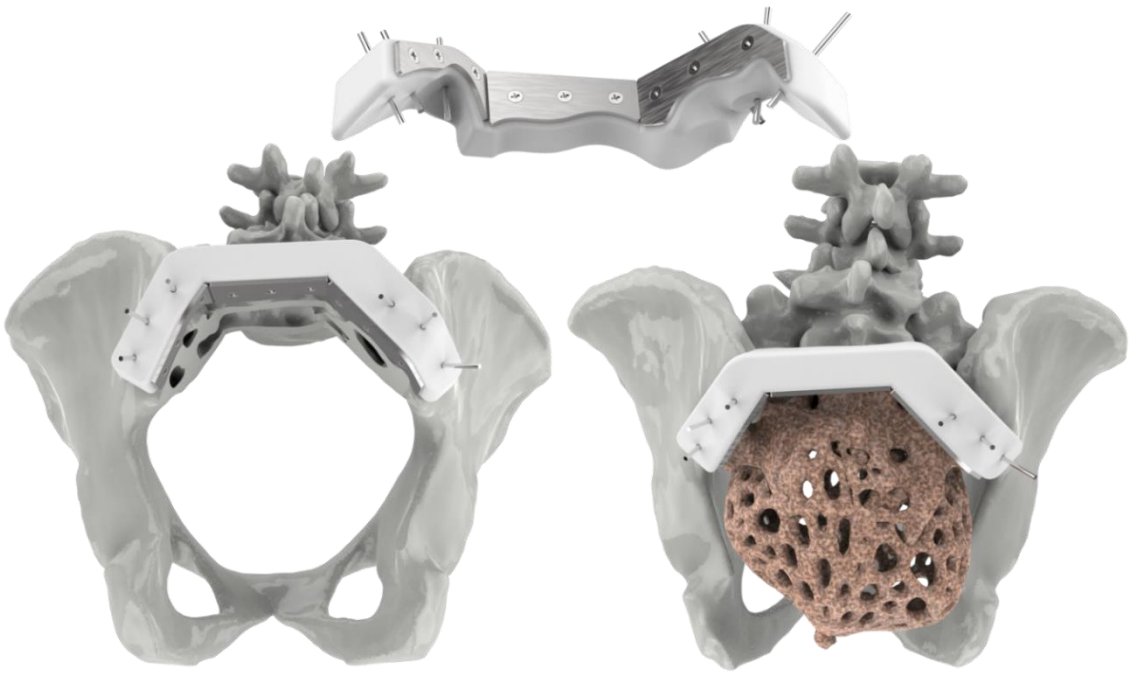

Figure 513: Patient-specific bone tumor-cutting instruments

The aforementioned pedicle screw-rod system reconstruction is shown in *Figure 514*. This solution could have been accompanied by PSI for the pedicle screw placement guidance, or alternatively, a patient-specific rod-like implant could have been developed similar to the one applied by Thayaparan et al. *(2019)* and shown in *Figure 126*.

Figure 514: Pedicle screw-rod system reconstruction

For the endo-prosthesis reconstruction, four 6,5 mm cancellous bone screws and two porous 8 mm stems were positioned and oriented as shown in *Figure 515*, whilst the patient-specific endo-prosthesis trial and bone drilling instrument to be 3DPed in PA12 is shown in *Figure 516*. For each bone screw, a 3 mm internal diameter AISI 316 cylinder is inserted into the housings of the instrument to guide the drill bit and protect the plastic from debris during drilling.

Photorealistic views of the solution are shown in *Figure 517*. The endo-prosthesis maintained a solid outer shell of 1 mm thickness and was architected with an inter-connected stochastic Voronoi

complex at the surfaces that touch the bone and internally to achieve optimization for a bi-modal superiority in biological and mechanical dimensions by a) allowing bone ingrowth to reach biological fixation and osseointegration, and b) reducing the mass and the modulus of elasticity to approach the bone. *Figure 518* displays the views of the optimized endo-prosthesis. An anatomical-like endo-prosthesis could have been developed but a non-bulky low-profile was chosen.

Figure 515: Planned placement of bone screws for artificial endo-prosthesis reconstruction

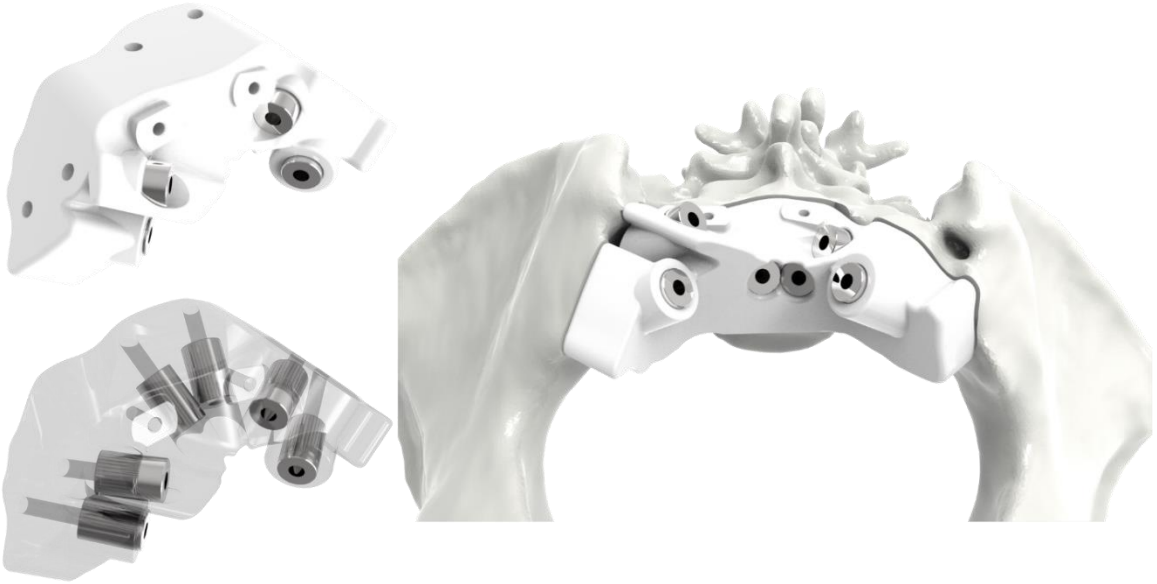

Figure 516: Patient-specific endo-prosthesis trial and bone drilling instrument

The region of interest of the as-planned resected anatomical model, the resected tumor mass, the bone-cutting instrument, the endo-prosthesis trial and bone drilling instrument, and the endo-prosthesis were 3DPed out of colorFabb PLA/PHA filament using the low-cost 3D printer (Creality CR-10s) of the pilot PoC 3D Unit for physical simulation of the surgery *(Figure 519).* The total material consumption, material cost and total time required to 3DP all these prototype models in one session were 900 gr, 31,5 €, and 5 days 8 hours respectively. The overall development time of the solution was less than the first case because a) in Stage 4 only digital and virtual visualization of the

anatomy took place, and b) in Stage 12 time was saved by 3DP only the anatomical regions of interest and not the whole anatomy.

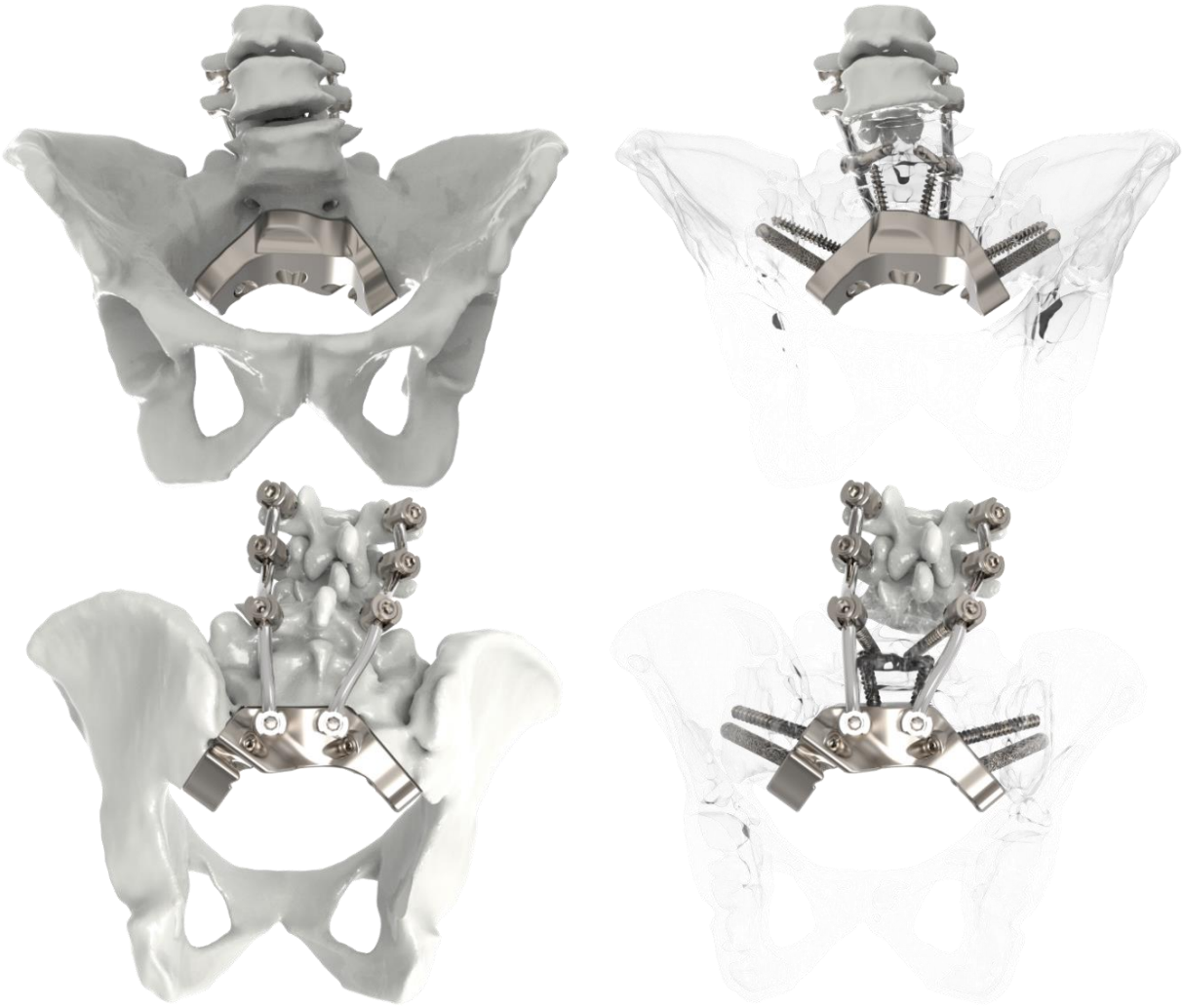

Figure 517: Solution with all components fixed on the anatomical model

The documentation *(Figure 273 and Figure 275)* was sent to the surgeon for final approval and sign off to enable the beginning of patient-specific solution materialization. Once approved by the surgeon and all required parties, the manufacturing of all parts to be used in the operating room was outsourced to a contract manufacturer. More specifically:

- All 3DPed (laser-based powder-bed fusion technology) surgical-grade PA12 ancillary instruments and the AISI 316 stainless steel inserts and sheet metals cost 280 € (90 € for the cutting jig only) for a 6 working days delivery.
- The 3DP (laser-based powder-bed fusion technology) of the surgical-grade Ti6Al4V endo-prosthesis and the custom 8 mm porous stems plus de-powdering and glass bead blasting for satin surface finish cost 1700 € for a 6 working days delivery.

The extra costs of the off-the-shelf components (bone screws, cemented acetabular cup, femoral stem and head components, and K-wires) were not considered as these were readily available in the market for purchase. Also, further post-processing and surface coatings were not considered.

Figure 518: Optimized endo-prosthesis with inter-connected porous architectures

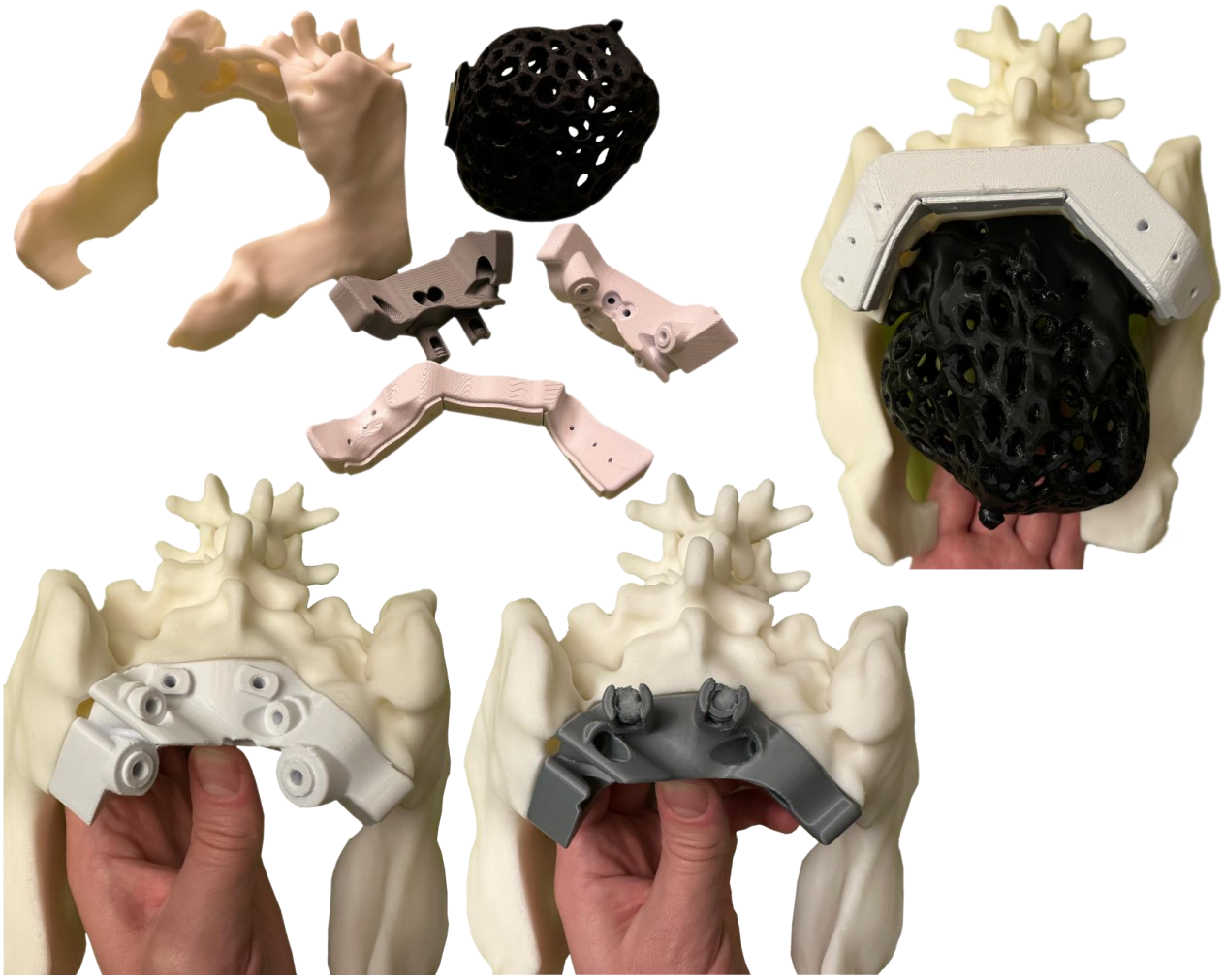

Figure 519: 3DPed prototype parts for physical surgery simulation

6.8 Sacral Tumor Resection

Note: as this Thesis has an engineering-centered research character aiming to serve the surgeons, and to assess the initially set hypothesis (see Sub-sections 4.1 and 4.2), and due to budget and resources constraints, both top-down and bottom-up approaches (Figure 225) were discussed, and scenarios and hypotheses/assumptions were made along the application of the inter-epistemic development process flow chain (Figure 231). This case was treated as if it was a currently ongoing pragmatic case and as if the responsible surgeon required truly the active engagement of the PoC 3D Unit, as a result, the solution prototyped at the PoC 3D Unit was not implanted into the patient.

The adult male patient presented to the First Department of Orthopaedic Surgery, National and Kapodistrian University of Athens, "Attikon" University General Hospital (Chairman: Prof. Panayiotis J. Papagelopoulos), examined, and diagnosed with sacral tumor, the anatomic extent of which was determined radiologically. The CT and MRI scans indicating the tumor site are shown in *Figure 520*. All data was anonymized before sharing.

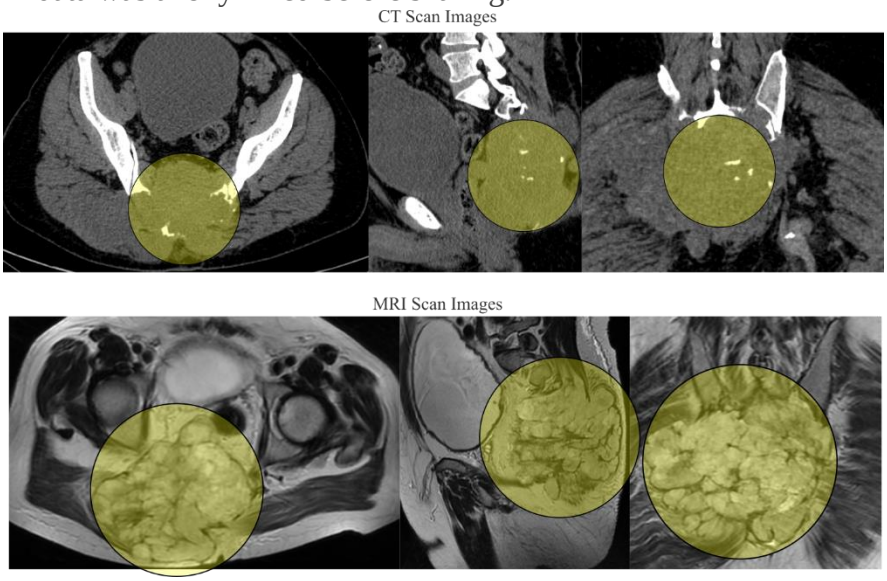

Figure 520: CT and MRI scans indicating the tumor site

The case was carried out in the pilot PoC 3D Unit, and single-step en bloc tumor resection with wide margins was decided under the inter-epistemic methodology shown in *Figure 264*. In contrast to the first case study where the methodology was unfolded analytically, for this case, only the developed solution is presented. The pre-resected anatomy was visualized only intangibly (Step 4) by digital (interactive models and pictures) and virtual (xR) means, but the surgical simulation was visualized digitally, virtually, and physically (Step 12).

Figure 521 shows the automatically segmented and generated soft and hard anatomical structures from the CT scan data in 3D Slicer using the Total Segmentator AI tool *(Wasserthal et al., 2023)*. Also, a finer bony structure was obtained using (semi)automatic tools in 3D Slicer as this was required for the endo-prosthesis and PSI fit. *Figure 522* illustrates the models of the tumor and pelvic bones for registration purposes as obtained by the MRI scan in 3D Slicer using (semi)automatic tools,

and the combined 3D model as emerged by the multi-modal image alignment (CT and MRI scans). The alignment of the models was achieved using the Interactive Closest Point (ICP) algorithm *(Besl and McKay, 1991; Zhang, Yao and Deng, 2022)* in Meshlab software *(Cignoni et al., 2008)*. Alternatively, although found to be more time-consuming, the CT and MRI scans and 3D models could have been aligned in 3D Slicer using the (semi)automatic or manual registration tools offered by the corresponding modules.

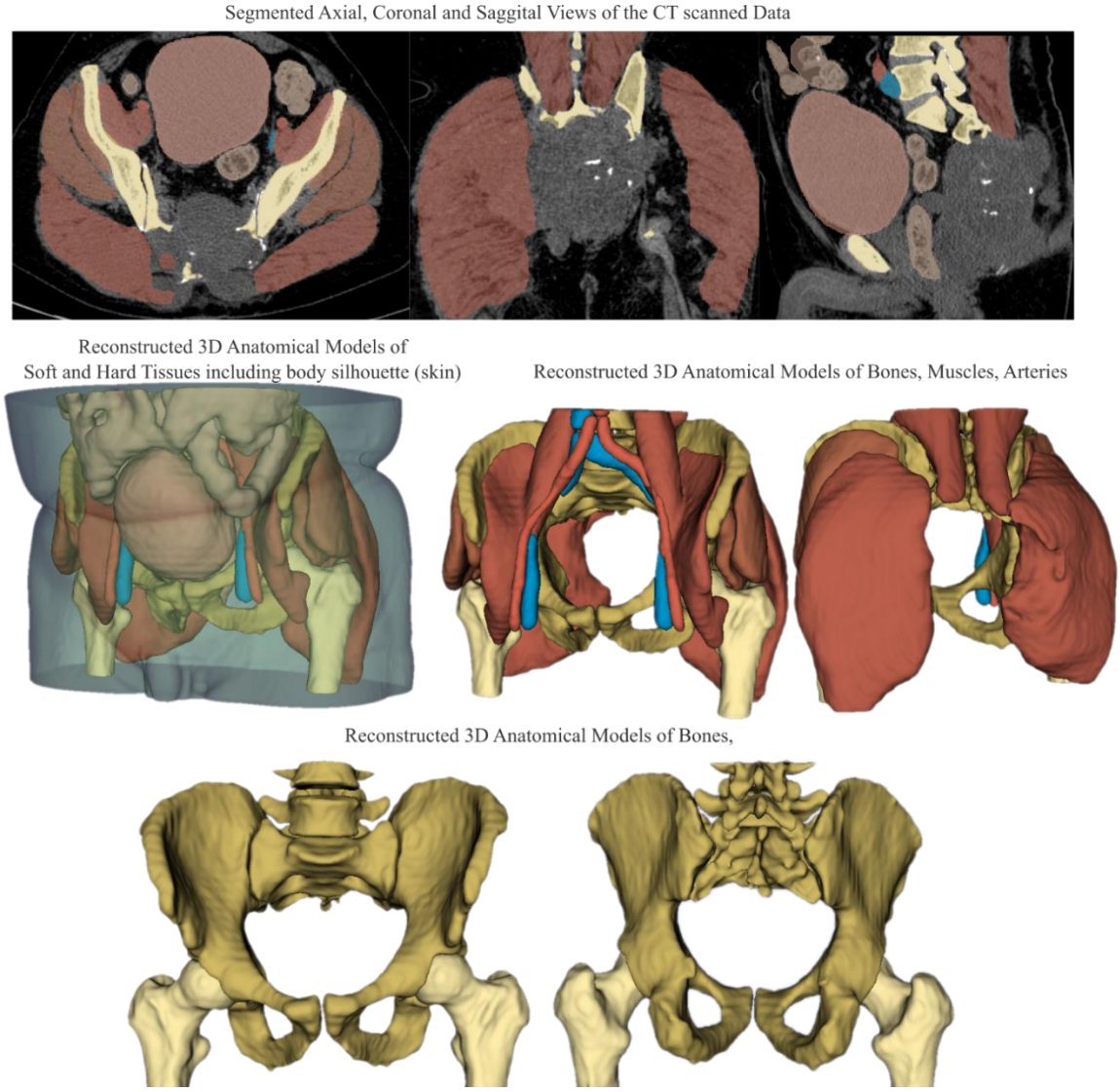

Figure 521: Generated models from CT scan

The tissue to be resected is shown in *Figure 523* along with Mayo Clinic's classification of sacral tumor resection and reconstruction approaches. As less than 50% of the sacroiliac joint was planned to be resected, type C is applicable, i.e. resection with no reconstruction.

The patient-specific bone tumor-cutting instrument is illustrated in *Figure 524*. The instrument is registered on the bear bone uniquely thanks to the anatomically conforming shape of the polymer part (to be 3DPed in PA12) held in place using 2 mm diameter K-wires, whilst AISI 316 stainless steel sheet metals are attached on the polymer part by counter-suck screws to serve as contacting surface for the cutting saw.

The region of interest of the as-planned resected anatomical model, the resected tumor mass, and the bone-cutting instrument, were 3DPed out of colorFabb PLA/PHA filament using the low-cost 3D printer (Creality CR-10s) of the pilot PoC 3D Unit for physical simulation of the surgery *(Figure 525)*. The total material consumption, material cost and total time required to 3DP all these prototype models in two sessions were 830 gr, 29 €, and 4 days 18 hours respectively. The overall development time of the solution was less than the first case because a) in Stage 4 only digital and virtual visualization of the anatomy took place, and b) in Stage 12 time was saved by 3DP only the anatomical regions of interest and not the whole anatomy.

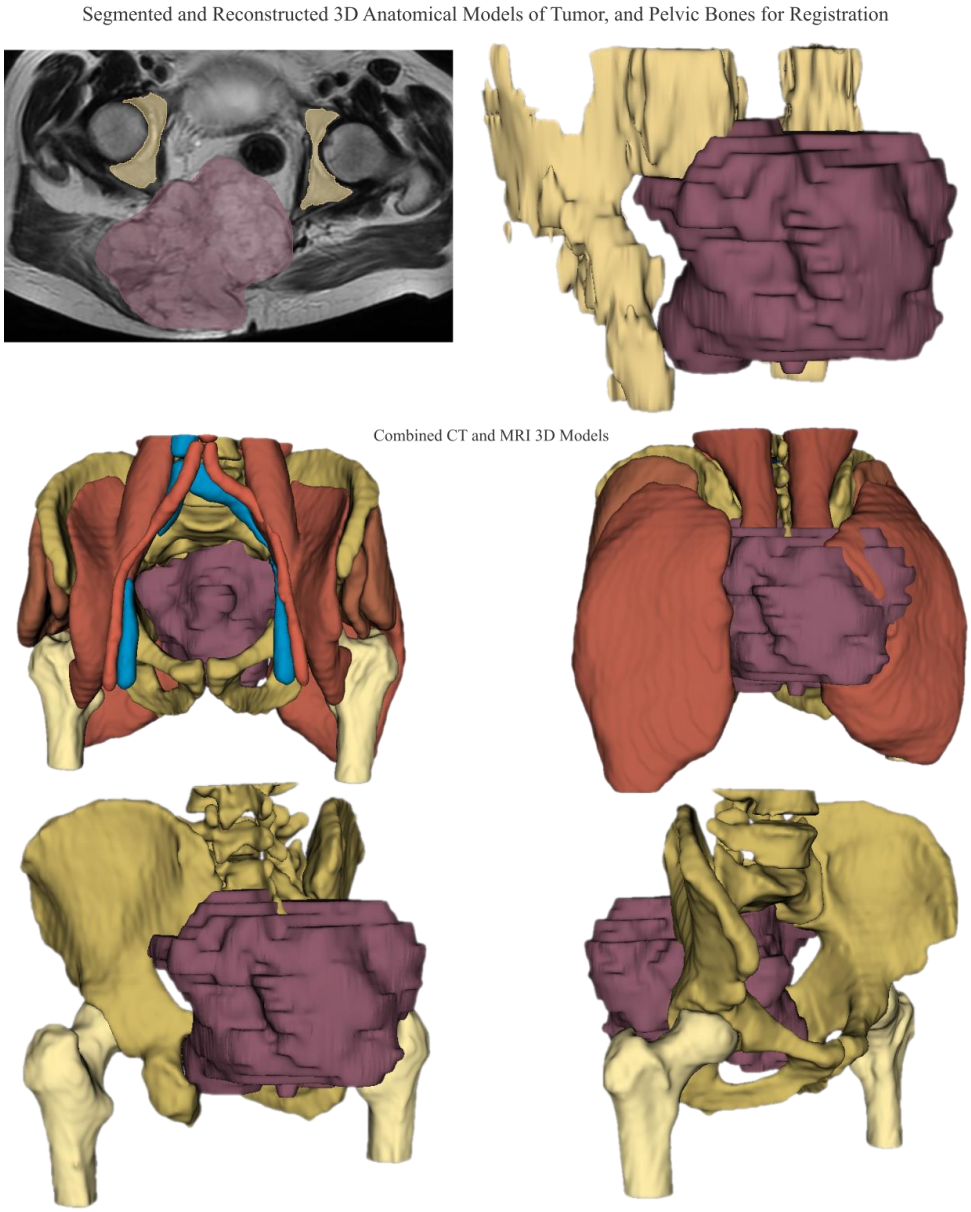

Figure 522: Generated models from MRI scan and combined model

The documentation *(Figure 273 and Figure 275)* was sent to the surgeon for final approval and sign off to enable the beginning of patient-specific solution materialization. Once approved by the surgeon and all required parties, the manufacturing of the surgical-grade PA12 cutting bone instrument (with the AISI 316 stainless steel sheet metals) to be used in the operating room was

outsourced to a contract manufacturer (laser-based powder-bed fusion technology 3DP) and cost 95 € for a 6 working days delivery.

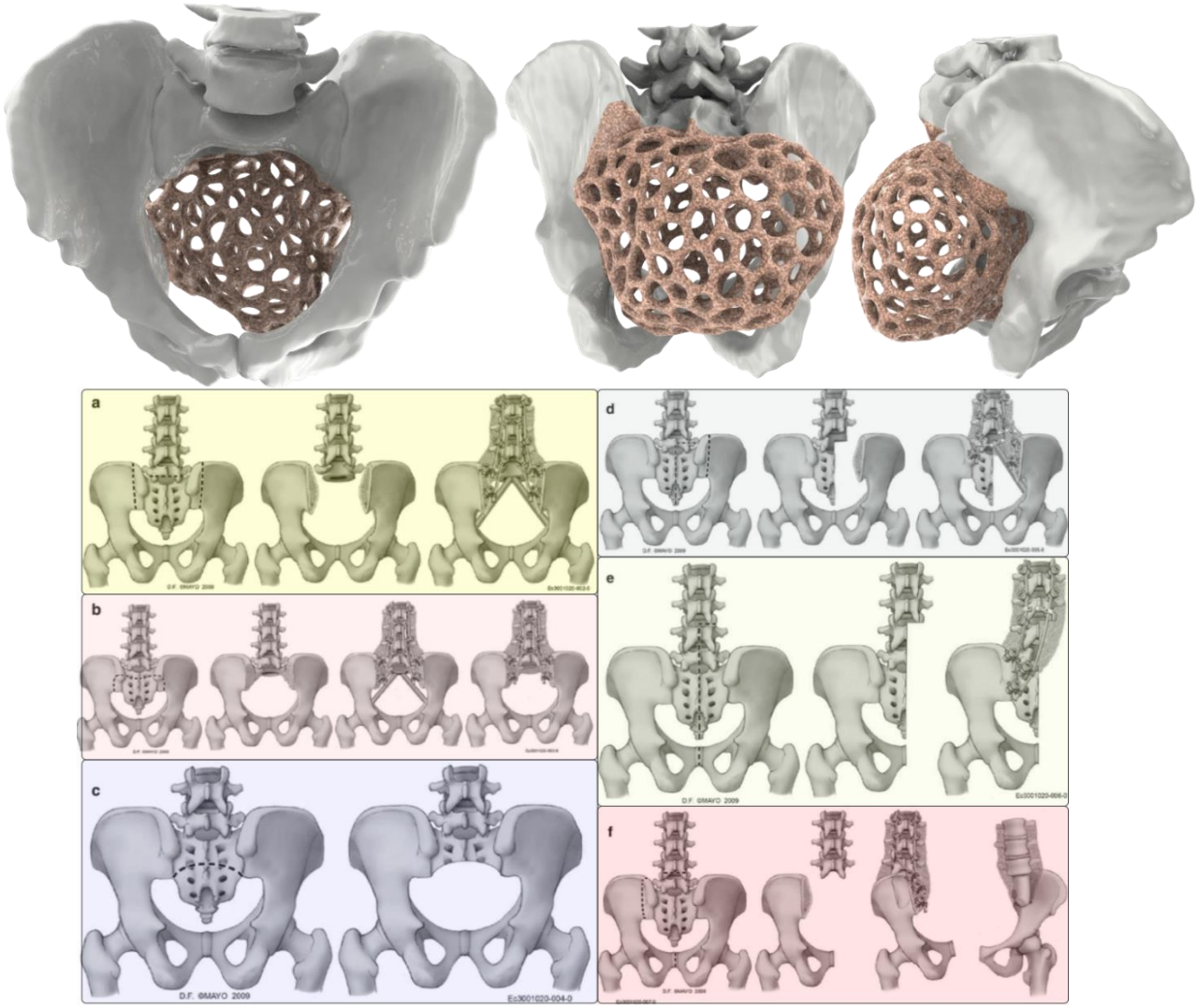

Figure 523: Planned resected tissue and Mayo Clinic's classification

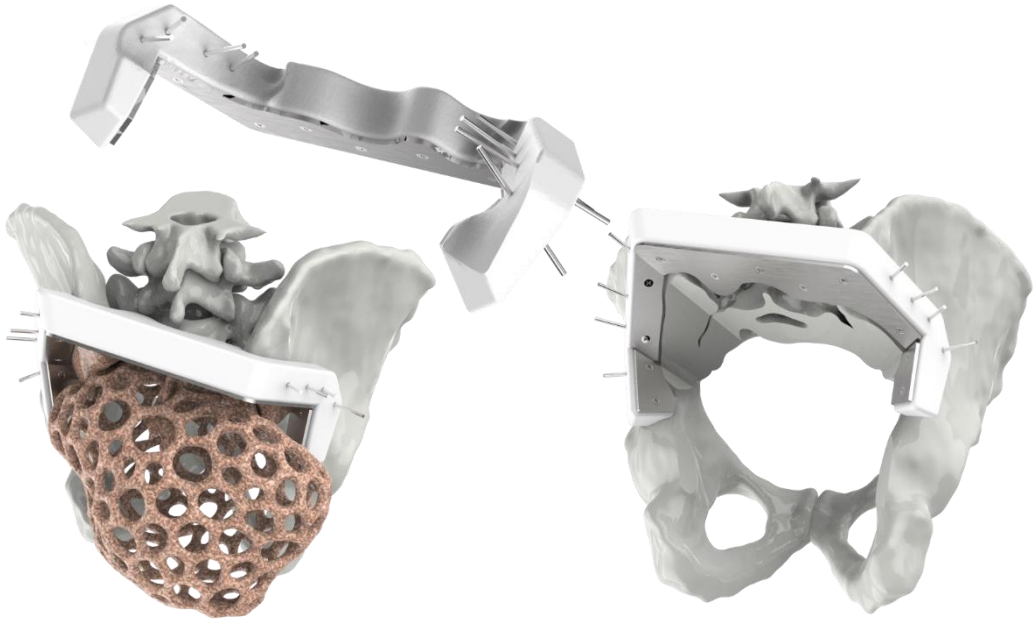

Figure 524: Patient-specific bone tumor-cutting instruments

Figure 525: 3DPed prototype parts for physical surgery simulation

6.9 Case 5: Orthotic Device: Hand Splint

For this case study, a healthy hand was assumed to require a custom-made anatomically matching polymer orthotic splint. The 3D digital anatomical model of the hand had to be acquired by a suitable image data collection method. Acquisition methods were summarized in *Figure 105*.

For external shape 3D scanning, the most common categories are photogrammetry, structured light, and time-of-flight. *Bartol et al., 2021; Silva et al., 2023).* Handheld structured light 3D scanning devices are mostly used *(see Table 13 and Figure 282)* for custom-made orthotics and prosthetics devices development, the 3DP of such is being applied successfully *(Manero et al., 2019; Ribeiro et al., 2019; Choo, Boudier-Revéret and Chang, 2020; Piyush P. and Piyush G., 2022; Schwartz and Schofield, 2023)*.

For 3D scanning of body parts, it is necessary to 3D scan the region of interest fast with the best possible accuracy, this is the reason why photogrammetry was not chosen as simultaneous photography by numerous cameras was not accessible and it is difficult when using only one device to take a series of pictures. On the other hand, structure light and time-of-flight techniques can perform better.

Modern smart mobile devices such as the Apple iPhone Pro and iPad Pro are now equipped with LiDAR (light detection and ranging) sensors next to the rear camera and TrueDepth front cameras. More specifically *(Vogt, Rips and Emmelmann, 2021)*:

1. A LiDAR is a time-of-flight sensor emitting pulses or modulated light signals. Distance is measured by calculating the time difference in the returning wavefront.

2. TrueDepth uses vertical-cavity surface-emitting laser technology and consists of a) a camera, b) an infrared camera, c) a proximity sensor, and d) a dot projector and flood illuminator. Hence, depth maps are created by software. In iPad Pro devices, the currently used TrueDepth sensor results in finer 3D models compared to the LiDAR-generated models as a result of the denser sampling. Hence, although it is ergonomically difficult to scan one's hand using the front-facing TrueDepth, it is more suitable compared to LiDAR for scanning small objects.

The 3D scanning of the hand's external shape was achieved utilizing the built-in front TrueDepth camera of an Apple iPad Pro 2021 as shown in *Figure 526*. The "patient" tried to maintain his hand as immobilized as possible, and the user 3D scanned his hand in a room with plenty of lighting, by rotating around the region of interest (hand) whilst trying to maintain the same distance throughout the process. The Scandy Pro app was used to capture the point cloud and reconstruct the 3D model before exporting it into a surface mesh file format (.stl) to be imported into Autodesk Meshmixer for editing (mesh cleaning, remeshing, reducing, and smoothing).

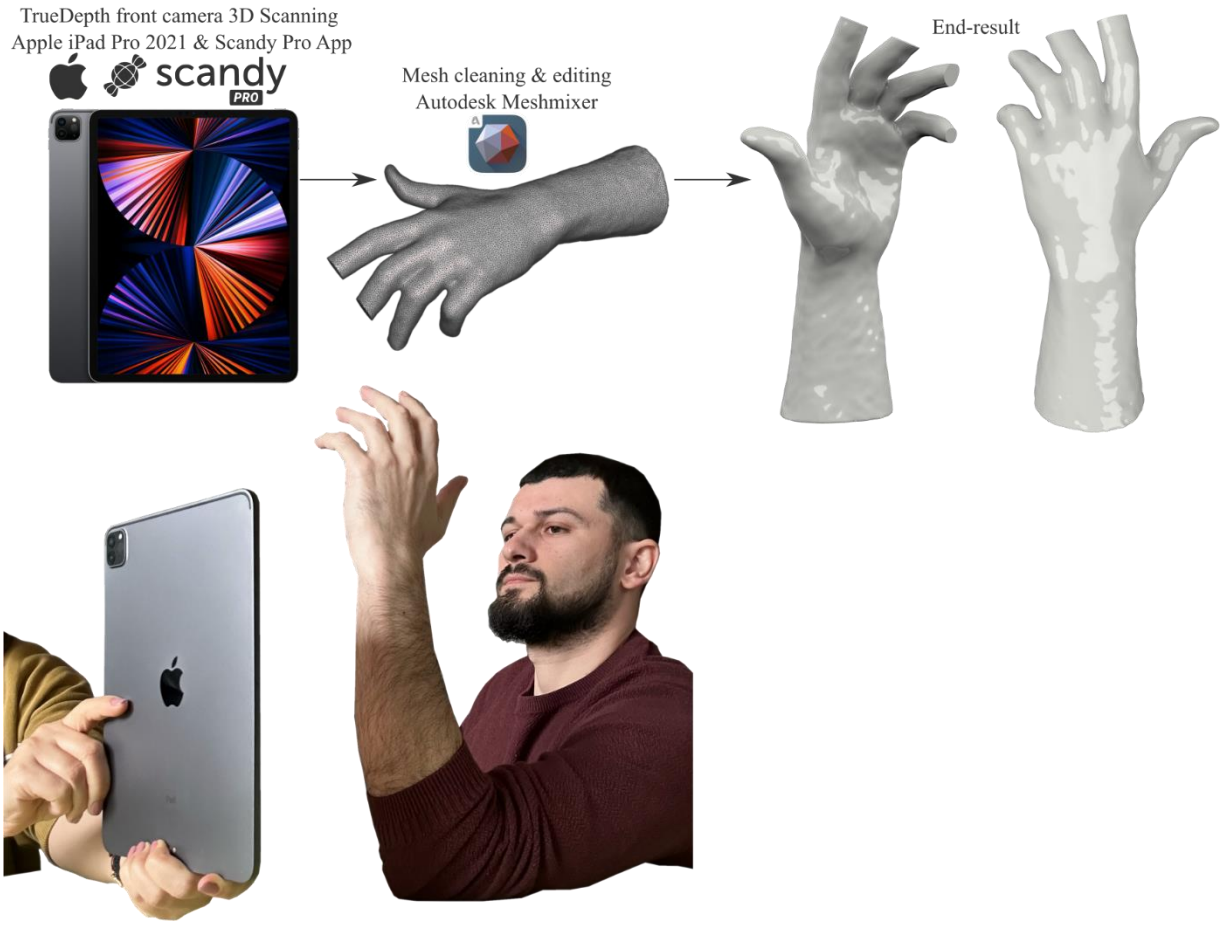

Figure 526: 3D hand scanning workflow

The workflow for the patient-specific hand splint design was as follows *(Figure 527)*:

1. The surface of the splint was selected, extracted, and offset in Meshmixer.
2. The surface was split into parts to be kept solid and a part to be turned into a Voronoi pattern in Ansys Spaceclaim.

3. In nTopology, the part to be turned into Voronoi was given a thickness of 5 mm. Both regular and randomized patterns were explored, but the regular was chosen. Also, the parts to be kept solid were thickened to 5 mm and all were united into a single part before exported into a surface mesh model.
4. In Spaceclaim, the model was split into two parts, and features for inserting and fastening eight 3x10 mm plastic screws were added. Alternatively, snap-fits, rubber rings or straps could have been used instead of screws.

Figure 527: Individualized hand splint design flow

70 minutes were required to develop the hand splint, starting from 3D scanning to completion.

The hand splint was 3DPed out of colorFabb PLA/PHA filament using the low-cost 3D printer (Creality CR-10s) of the pilot PoC 3D Unit. The total material consumption, material cost and total time required to 3DP the two parts in one session were 330 gr, 11,6 €, and 2 days 9 hours respectively. Alternatively, the cost for out-sourcing the two parts to be 3DPed out of PA12 powder material was 300 € for a 2 working days delivery.

Figure 528: 3DPed hand splint

7. Results and Discussion

Mass customization enabled by tailored 3D design and 3DP is embedded in the vision of Industry 4.0 for a new paradigm shift of manufacturing and supply models to adjust to the needs of society and market trends, assisting in decentralization for localized production, disrupting the structure and operations of businesses at international, national and local levels, thus changing how products are designed, manufactured and delivered. Patient-specific medical device development can be characterized as engineered-to-order and is among the most well-matched sectors to be served by decentralized manufacturing network models reaching near or at the point of use.

The COVID-19 pandemic outbreak dictated that the supply of time-critical medical devices must be resilient and responsive, while catalyzing the need to adopt a new model that embraces digital health tools *(Bini et al., 2020),* including xR devices, 3D design software, and 3DP. As the weaknesses of modern healthcare systems were revealed and their capacity, supply, and workforce were challenged, 3DP proved to have suitable characteristics and potential, giving a glimpse into the future of healthcare, by enabling decentralized (localized) manufacturing of personal protective equipment *(Figure 529)* and other critical parts at the PoC *(Vakharia et al., 2021)* despite some safety concerns and challenges *(Singh et al., 2021)*. Similarly, patient-specific medical devices can be designed and/or manufactured just in time at the PoC at affordable costs and short lead times, provided that suitable resources exist *(Teo et al., 2021).*

Figure 529: Two single-piece face shield designs for 3DP

3D technologies are now easily accessible, though their usage requires training and there is a considerable learning curve. 3DP technologies have great potential not only for intricate and unique medical devices but also for novel standard and modular parts that cannot or are extremely difficult to make using traditional methodologies. Among all disciplines of medicine, orthopaedics is the top user of 3DP where 3DP technologies are successfully being used for individualized rehabilitation in a plethora of cases *(Tack et al., 2016; Chepelev et al., 2017; Levesque et al., 2020; Kermavnar et al., 2021)* in anatomical areas ranging from head to toes *(Kang, 2021; Özger et al., 2022) (Appendix B and Appendix J).* Surgical instruments and implants/(mega)endo-prostheses are being 3DPed for a)

primary and revision arthoplasties, b) treating fractures, c) bone substitution and limb salvage, d) molds for making antibiotic-eluting cement spacers for permanent or temporary bone reconstruction, e) joint instabilities, avascular necrosis, and bone losses, f) spine surgeries, g) jigs for implant and screw insertion guidance, bone resection, hole drilling for implant attachment, and corrective osteotomies, and h) external rehabilitation devices such as orthotics and prosthetics. Also, tissue engineering constructs and drug delivery are reported in the literature.

Numerous 3DPed medical devices and endo-prostheses with interconnected porous patterns (cellular) featuring cellular architectures have been researched, commercialized, and cleared by the FDA, with post-operative follow-ups showing good bone ingrowth and osseointegration, favorable mid-term clinical results with high survival rates, good functional outcomes with stable initial fixation and without severe complications, and great performance. Such patterns have been implemented in many pelvic *(Wong et al., 2015; Liang et al., 2017; Hennessy, Anderson and Lozano-Calderon, 2018; Han et al., 2019; Wang et al., 2019; Wang et al., 2020; Durand-Hill et al., 2020; Gruber et al., 2020; Ji et al., 2020; Geng et al., 2020; Chen et al., 2020; Peng et al., 2020; Cao, Zhu and Gao, 2021; Park et al., 2021; Yu et al., 2021; Döring et al., 2021; Xu et al., 2022; Hu et al., 2022; Broekhuis et al., 2022; Gortzak et al., 2022; Pu et al., 2022; Khal et al., 2023; Hu et al., 2023; Zoltan, Popescu and Sanei, 2023; Li et al., 2023; Lv et al., 2023b)* and sacrum *(Wei et al., 2016; Kim et al., 2017; Peng et al., 2019; Chaptain an Finn, 2020; Shi et al., 2021; Lv et al., 2021; 2023a; Kotrych et al., 2023)* reconstruction case studies. Although a plethora of 3DPed individualized and optimized implantable orthopaedic solutions are being reported in the literature, this Thesis covered the lack to a) holistically deal with the implementation of a de novo inter-epistemic synergy at the PoC, b) focus on the design and requirements of a PoC 3D Unit per se, and c) methodically present a holistic and systematic end-to-end workflow for patient-tailored services and optimized products development and analyze each step applied whilst providing guidelines.

3D technologies favor the choice of limb-sparing surgery instead of amputation, however, the goal of adequate tumor resection to eliminate the possibility of recurrence must not be jeopardized. Towards this direction, custom reconstruction solutions were developed and prototyped at the PoC for three pelvic and two sacral oncological cases, i.e.:

1. First pelvic case: a two-stage ilium-partial periacetabular-sacroiliac joint resection and reconstruction was applied. Functional (mechanical) reconstruction of the pelvic grindle was achieved by a low-profile endo-prosthesis without the iliac wing and crest forms. Standard cancellous bone screws and off-the-shelf components for the total hip arthroplasty were chosen.
2. Second pelvic case: a single-stage ilium-partial periacetabular-sacroiliac joint resection and reconstruction was applied. Anatomical reconstruction of the pelvic grindle with iliac wing and

crest was achieved by a biological-like form which included holes for soft tissue re-attachment and optional features for extra spondylodesis with a pedicle screws-rods system. Standard cancellous bone screws and off-the-shelf components for the total hip arthroplasty were chosen.

3. Third pelvic case: a single-stage ilium resection and reconstruction was applied. An anatomical reconstruction of the pelvic grindle was achieved by a biological-like form. A custom-made porous stem was developed, and standard cancellous bone screws and off-the-shelf components for the total hip arthroplasty were chosen.
4. First sacral case: a single-stage sacrum resection and reconstruction was applied. Both pedicle screws-rods system and artificial endo-prosthesis reconstructions were explored. Two custom-made porous stems were developed, and standard cancellous bone screws and off-the-shelf components for pedicle screws and rods were chosen.
5. Second sacral case: a resection guide was developed with no reconstruction needed.

Additionally, a case on orthotic device development was studied. A custom-made hand splint was designed and materialized successfully based on a 3D-scanned hand by a smart mobile device.

For all oncological cases, patient-specific instruments were developed as part of the final solution. To avoid placement errors of the instruments that were designed to be placed on bone surface, any soft tissue had to be completely removed as these were not considered as extra layers.

The mechanical performance of all endo-prostheses was assessed by mechanical simulations based on FEA. All endo-prostheses were light-weighted and optimized by maintaining a thin 1 mm thickness solid shell infilled by an interconnected porous architecture. Both stochastic (randomized) Voronoi and TPMS (gyroid) unit cells were explored, and biological, mechanical, and manufacturability requirements were considered for the sizing of porosity, pore size, and thickness of the porous structures. Hence, these types of interconnected porous patterns were given suitable pore size and thickness gradients, thus obtaining the so-called meta-(bio)materials-by-design with properties tuned selectively and topologically across the monolithic part per se. was i.e.:

1. Biological optimization (exo-structure): the bone-touching interfaces were functionalized with an interconnected porous pattern of approximately 60% porosity and a mean pore size of 0,6 mm which is optimal as reported in the literature to allow vascular, oxygen, nutrients, and bone formation inducing elements invasion and circulation to facilitate bone ingrowth.
2. Mechanical optimization (endo-structure): away from the bone-touching regions (>10 mm), the architecture was graded by increasing the pore size and strut thickness, whilst maintaining the same porosity level. This way a) the mismatch between the endo-prosthesis and bone's moduli of elasticity was reduced to minimize stress-shielding phenomena, and b) de-powdering of unmelted trapped powder particles after 3DP was better facilitated.

To achieve custom materialization of as-designed optimized and biomimetic medical devices without errors and defects, it is necessary to employ algorithmically driven and machine-learning methodologies powered by trained datasets and sourcing from libraries of previous cases with emphasis on design and manufacturing(3DP)-specific process optimization for supreme mechanical and biological performance. As image data acquisition and processing, and design and manufacturing techniques are streamlined in tandem with AI methods for decision-making and automating processes, the range of applications will widen, lead times and costs will drop, and reliance on large centralized manufacturing plants and maintenance of expensive supply networks might be reduced.

Most of the time, unique patient-centric interventions in healthcare generate improved outcomes but result in higher costs *(Frizziero et al., 2019)*. To maintain improved outcomes at lower overall costs (direct intra-operative, operative theatre, and outpatient costs), custom 3D design, and 3DP must be implemented under suitable schemes and at lower costs. Foukas et al. *(2024)* have successfully implanted a patient-specific 3DPed porous (stochastic pattern with 0,1-0,5 mm pore size) Ti6AlV4 load-bearing endo-prosthesis filled with autologous bone graft to treat a 9-cm femoral segmental bone defect, which was osseointegrated within three months. Although resulted in a great outcome, the authors reported the overall cost for the series of operations required, with the most expensive part being the 3DPed endo-prosthesis. For cases where no alternative options are available and custom solutions must be developed, 3DP is opportunistic in terms of time and costs. Even if standard modular endo-prostheses along with off-the-shelf standard rods, pedicle/polyaxial bone screws, and plates can be used as possible solutions (though not perfectly conforming to the unique patient's anatomy), 3DPed endo-prostheses might still be more economical *(Yu et al., 2021)*.

By bringing the 3D design and/or 3DP of custom medical devices in-house, the time and costs can be further reduced. Towards this direction, in this Thesis, an inter-epistemic end-to-end workflow that revolves around 3D technologies was proposed *(Sub-section 4.2)* to study selected cases *(Section 6)* at the PoC, aiming at developing orthopaedic devices for pre-operative planning, education and training, intra-operative non-navigation usage, bone reconstruction/substitution, and orthosis. Granted that suitable (medical) image data exists, the proposed workflow can be deployed regardless of the case complexity. Viewing 3D digital models, interaction with such in (semi)immersive xR environments, and hands-on examination of the corresponding true scale physical 3DPed objects were enabled and verified. Being assisted by (bio)mechanical engineers, surgeons could collaboratively develop patient-specific devices within acceptable lead times and costs.

Healthcare facilities seeking to reduce the development time and cost of high-quality and safe patient-matched solutions targeting emergency or routine use can explore various scenarios for PoC utilization of 3D technologies. As many scenarios can be made about the format, structure, and

resources of a PoC, design, prototyping, and/or end-manufacturing can take place in situ. A plethora of trade-offs can be made in terms of software and hardware equipment, infrastructure and layout, organizational structure, and personnel.

Regarding the applied inter-epistemic synergy *(Sub-section 4.2)* used to solve selected cases *(Section 6)* and the PoC establishment, potential, specifications, and performance *(Section 5)*, after investigating the Thesis hypothesis outlined in *Section 2* and *Section 4* under specific assumptions and constraints, several results were generated:

1. Two Scenarios were explored in terms of organizational structure and framework, hardware and software equipment, infrastructure and layout, cost analysis, and decentralized manufacturing. Scenario 2 was taken as a reference to assess the Thesis hypothesis. Thus, the pilot PoC 3D Unit was set up and operated within a small office under assumptions and constrained by the available resources with a sub-6.000 € budget *(Sub-section 5.4.1)*. The two Scenarios presented were:
   a. Scenario 1: ideal PoC 3D Unit that both designs and becomes a manufacturer of any polymer, metal, and ceramic products, including bioprinting constructs for TE applications and research on regenerative orthopaedics. No budget, space, and resources limitations were considered, and medium to high-scale design and production volume were assumed to be carried out by a six-member team: an orthopaedic surgeon manager, a (bio)mechanical design and manufacture engineer lead supervisor, two (bio)mechanical design and manufacture engineers, a 3D printer operator-mechanic, and a quality control engineer. Many HCFs must be served by a suitable decentralized supply network to create a demand pool that justifies its existence.
   b. Scenario 2: a more realistic PoC 3D Unit where design and polymer prototyping take place within the HCF. The final metal and polymer manufacturing is outsourced to contract manufacturers, but there is an option to process polymer biomaterials for end-parts production in-house. The minimum required hardware at the lowest possible budget was considered, and the lowest-scale design and production volume was assumed to be carried out by a single person (“one-man show”). This Scenario best fits for serving locally exclusively one HCF.
2. The small hypodigmatic pilot PoC 3D Unit was housed within the Orthopaedic Research and Education Center “Panayiotis N. Soucacos” in “Attikon” University General Hospital, First Department of Orthopaedic Surgeon (Chairman: Prof. Panayiotis Papagelopoulos) School of Medicine, National and Kapodistrian University of Athens, located at Rimini 1, 124 61 Chaidari, Attica region, Greece. The PoC 3D Unit benefits from various agents and partners co-located within a 50 Km radius circle: a) machine shops for post-processing the 3DPed parts or manufacturing of parts via machining or other classic processes, b) service providers for outsourcing 3DP for Scenario 2, and even for Scenario 1 after cost-benefit make-or-buy analysis,

c) standard medical device suppliers, d) healthcare centers and experts, and e) airports and courier centers for fast transportation.

3. A "one-man show" fits Scenario 2 where the lowest flow of demand exists. For increased demand, more self-motivated and self-managed team members are required, with different responsibilities. The team members must embrace an agile mindset and suitable management tools to synchronize, plan out the work for the day, identify obstacles, inspect the progress toward the goals set, adapt the backlog respectively, and adjust the upcoming planned work.
4. The inter-epistemic workflow *(Sub-section 5.4.1)* was successfully applied at the PoC 3D Unit. The emblematic synergy-enabling tools (3D digital design, 3DP, xR) that are being sourced from industries where professional engineers have been traditionally harnessing them are now entering the home of orthopaedics with the potential to "make orthopaedic surgeons the designers" granted that they are assisted by skilled professional engineers. This way, orthopaedic surgeons can analyze musculoskeletal mechanics and participate in the development process of optimized medical devices actively by providing inputs on design principles, concepts, and specifications.
5. The *SkeletoMy* online platform serves the PoC 3D Unit and couples 3D digital design, xR, 3DP, and 3D scanning into a single website for seamless data exchange. It was proven an essential tool that can be tweaked as desired to facilitate the management of services and product requests, case submissions, and all communications among the users and the PoC 3D Unit. The image data acquisition protocol shared was highly useful to guide interested users in collecting the best image quality for 3D reconstruction and model generation. The a) final proposal check and justification report, b) safety, risk assessment, and quality management report, c) application/implantation instructions, and d) manufacturing instructions shared with the user for approval and sign off, ensured that all characteristics of the solution are understood by the surgeon and all specifications are met. The feedback report can improve the user experience, the offered services and products, as well as the operations of the PoC 3D Unit.
6. The hardware and software equipment of the PoC 3D Unit required to realize the inter-epistemic synergy for customized (in)tangible solutions development is readily available in the market. The required equipment was analytically listed and broken into a) computer, network, and office, b) xR, c) 3D scanners, d) 3D printers and materials, and e) software. The equipment characteristics and costs for both Scenario 1 and 2 were identified. The total cost for the aforementioned equipment, excluding the costs required for feedstock materials, tools, infrastructure, building works, furnishings and ancillary for Scenario 1 and 2 reached 3.440.150 € and 207.612 € respectively. Costs for Scenario 1 can be reduced by more orthological interventions, as this was

unconstrained and assumed that the PoC 3D Unit is an ideal manufacturing facility capable of polymer, metal, ceramic, and biological constructs making.

7. The equipment layout and infrastructure of the PoC 3D Unit depend on the available space, resources, and selected scenario. Nevertheless, possible layouts and infrastructure concepts for both Scenario 1 and 2 were given. The layout of the established small hypodigmatic 30 sqm pilot PoC 3D Unit based on a constrained Scenario 2 due to budget limitations was also given.
8. The lead time and economics for the offered services by the PoC 3D Unit are among the most important indicators of performance *(Sub-section 5.5)*. Parameters and variables affecting the cost per service offered by the PoC 3D Unit were explained. These can be used to calculate whether in-house or outsourcing is more beneficial.
9. Medical device making within the PoC or near the HCF is well served by decentralized manufacturing for localized (Scenario 2) and for distributed manufacturing serving other HCFs (Scenario 1). The benefits of decentralized manufacturing were explored and their potential was highlighted. Instead of shipping the physical parts per se, design files of any medical device accompanied by documentation can be shared with the user who can hand them over to any manufacturing facility or the PoC per se for materialization if these facilities are regulated under a proper QMS and conformed to standardized processes. Hence, via manufacturing decentralization, access to any suitable manufacturing facility implies democratization of production and just in time fabrication and delivery of products regardless of their complexity.
10. PoC 3D Unit operations involve the intersection of healthcare providers, regulatory groups, engineers, and manufacturers who contribute to a common goal of providing high-quality and safe solutions to each unique patient. In the quest to establish PoC 3D Units, non-technical challenges, and technical limitations hold 3D technologies from springboarding and should be addressed *(ASME, 2020)*. It was made apparent that in addition to intellectual property and digital security issues, the main causes of hysteresis for the wide settlement of PoC 3D Units are regulatory compliance, lack of harmonized standards and QMSs, further reduction in development time and cost, and the need for skilled personnel. EU's Medical Devices Regulation (MDR) 2017/745 and FDA's regulations on emergency custom-made device manufacturing *(FDA, 2014)*, along with the FDA's discussion paper on PoC scenarios *(FDA, 2021)* and guidance on technical considerations for 3DP of medical devices *(FDA, 2017)* should be taken into consideration. Additionally, special focus should be given to both generic standards on quality management, biological evaluation, risk management, packaging, and sterilization, as well as on the standards published by the ASTM F42 and ISO's 261 committees on 3DP-oriented topics for producing safely high-quality parts *(Sub-section 5.2.2)*.

11. PoC 3D Units must establish their best practices by implementing QMSs whilst conforming to applicable regulations and standards. In the USA and the EU, custom-made emergency devices can be exempted from regulatory control by allowing authorized healthcare professionals to provide design input and take responsibility for the safety and performance of the customized medical devices. However, because existing regulations and standards oversee the way medical devices are manufactured, 3D technologies need further guidance to establish quality control measures as numerous parameters might lead to a low-quality 3D-printed product, i.e. data preparation variables, design features, feed-stock materials, process and 3D printer parameters, personnel, documentation, infra-structure, and post-processing. Therefore, appropriate QMSs including strategies and processes for addressing errors and improving consistency are important to control and assure quality and safety. Otherwise, the uncontrolled rapid growth of 3D technologies and the increasing complexity might put patients at increased risk for potential errors, decreased quality, and sub-optimal performance of the solution. Ultimately, the evolution and synthesis of regulations, QMSs, and accessibility to 3D technologies will define the maturation of PoC patient-specific device development. As necessity drives invention and innovation, once the readiness of 3D technologies stops remaining under question, data protection issues are addressed, and costs in tandem with the medical device development time are further reduced, their PoC incorporation will accelerate healthcare into intelligent formats capable of unlocking mass-customization with high-quality end-results and increased patient satisfaction.
12. PoC 3D Units can be either design-centric (outsourcing manufacturing), manufacturing-centric (outsourcing design), or both. The capacity (required lead time and cost, and demand flow), personnel and their expertise, equipment, and portfolio (product and process complexity and manufacturability) of a PoC 3D Unit should adapted to the characteristics of the HCF and any investments should be rationalized by the exact clinical needs, so that the collaboratively developed solutions are clinically and scientifically relevant and ultimately beneficial for each unique patient. These attributes must be weighed before deciding to integrate, outsource activities, or create mixed processes, as well as arrange in a scalable manner in case capacity must increase. Before investing in any strategy, an HCF should prioritize its needs and consider not only the budget to acquire, maintain and operate equipment, but also the ease of implementation and transition, ecological sustainability, cost-effectiveness and efficiency (economical sustainability), competitiveness, technologies selected, scale-up scenarios, and available space and resources. PoC fabrication of end parts could eliminate reliance on external partners, potentially reducing costs, however, it is recommended to commence with in-house 3D design and 3DP for prototyping and outsourcing the end parts. Only if sufficient demand exists, it is

orthological to increase capacity and implement in situ final manufacturing. Low-risk medical devices (anatomical models and prototypes) or even medium-risk devices (patient-specific instruments and orthotic parts) can be fabricated in-house easier, but high-risk devices such as implant and (mega)endo-prostheses require more complex QMS, regulatory pathways, and adherence to applicable associated standards.

13. PoC 3D Units can become separate autonomous departments per se within HCFs. Hence, all required services can be housed within the same HCF. Especially for urgent cases, face-to-face meetings among all parties involved are enabled for fast solutions development.
14. It is truly beneficial to harness the triad of 3D design, xR, and 3DP to better serve workflows emphasizing individual healthcare delivery. The developed patient-specific solutions were successfully prototyped at the PoC within acceptable clinical time and cost frames. The end polymer and metallic parts that required high-cost industrial-grade systems were outsourced to external partners. Consequently, it can be highlighted that:
    a. 3D design of any model and the optimization of such,
    b. xR systems for pre-operative planning and intra-operatively (non-navigation) purposes, and
    c. 3DP of polymer anatomical models, PSIs, and implant/endo-prostheses prototyping.

    can be implemented at relatively low initial capital investments, as well as low operating and maintenance costs. Polymer 3DP is easier for immediate deployment but metal, ceramic, composite, and biological fabrication is more intricate, requiring more investments in industrial-grade machines and ancillary, whilst extra post-processing and strict QMSs are needed. If external partners are engaged, these must deliver the products/services under a regulated, qualified, verified, and/or validated scheme, checked by documentation, reports, and audits.

The time and material cost required for each stage of the inter-epistemic synergy applied for the first case study, excluding overhead and human-hours costs and costs for maintenance and operation of equipment, is given below and presented graphically in *Figure 530*:

1. Pre-resectionally, the soft and hard tissue anatomy was visualized only digitally for diagnosis in only 15 minutes using the automatic Total Segmentator AI tool *(Wasserthal et al., 2023)* in 3D Slicer. On the other hand, post-resectionally, the anatomy was visualized in both intangible and physical formats, i.e.:
    a. Digitally for viewing in computer or smart device monitors: 175 minutes were required to generate the fine-model of the bony pelvis using semi-automatic tools, and deliver the photorealistic and interactive 3D views to the surgeon.
    b. Virtually for (semi)immersive experience: under 10 minutes were required to set up the VR and AR sessions for the surgeon.

c. Physically: 3 days and 14 hours were required to 3DP the whole resected bony pelvis anatomy. The PLA material used cost 23,2 €. Alternatives for delivering the 3DPed anatomical model in less time were proposed.

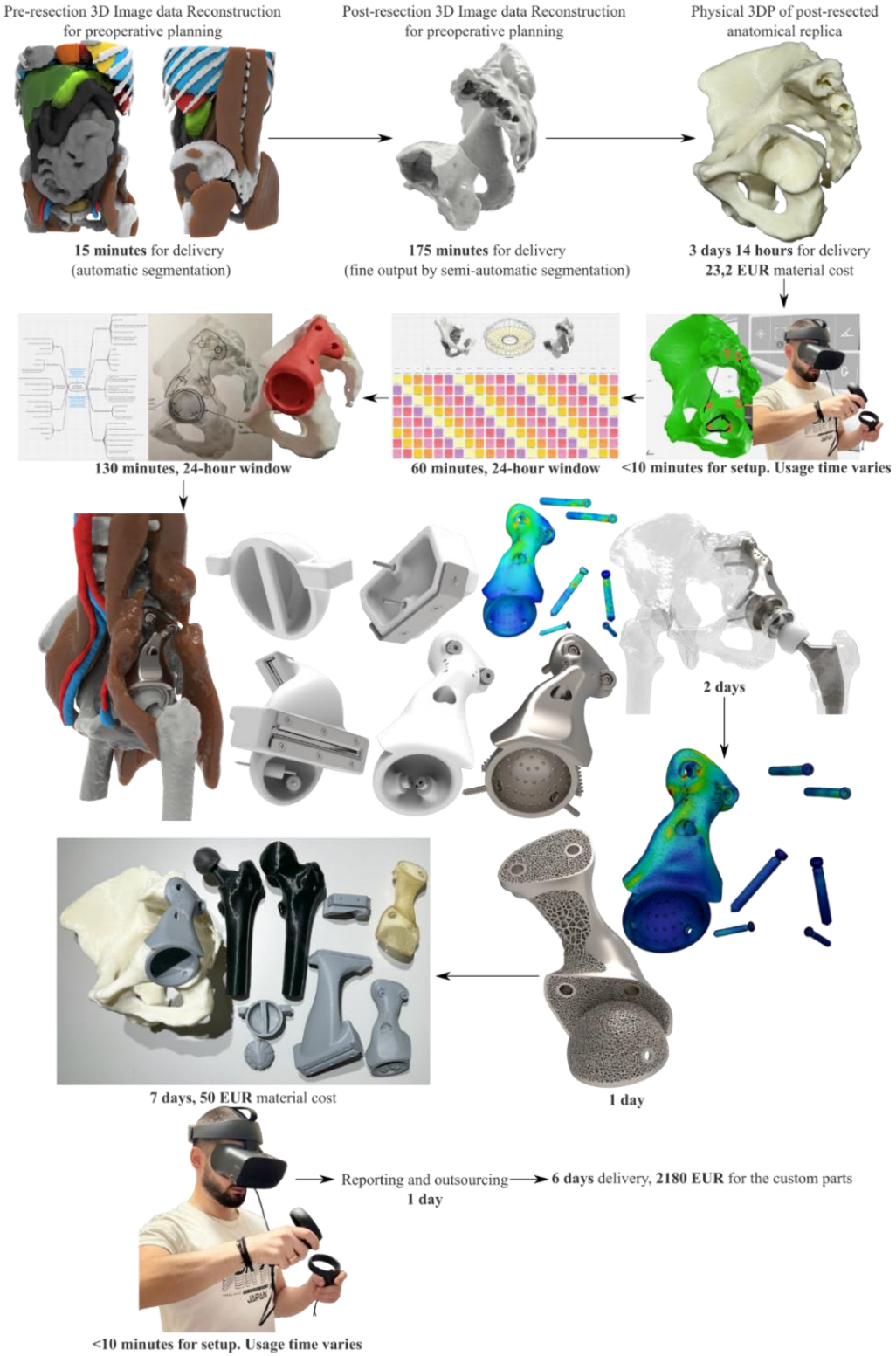

Figure 530: Time and cost per stage of the inter-epistemic workflow

2. The specifications list was established within an hour and an extra 24-hour window was agreed for possible changes. The deliverables were screenshots from the VR session and the specification list. Hand sketches and clay models could have been delivered also at this stage.

3. The conceptual design was completed within 130 minutes and an extra 24-hour window was agreed for possible changes, after which the optimal concept was selected. Hand sketches and a clay model on the 3DPed anatomical model were the deliverables.
4. The selected concept was developed during the embodiment design within two days. The off-the-shelf components for the total hip arthroplasty were selected, the endo-prosthesis geometry and fixation were designed and simulated mechanically, and all ancillary instruments were developed. Extra alternatives were explored. During a short meeting, the solution was approved.
5. During the detailed design, all final details were established and the endo-prosthesis was optimized internally and externally at the bone-contacting areas, to obtain a bi-modal superiority in biological (allow bone ingrowth) and mechanical (reduce the modulus of elasticity) dimensions by implementing inter-connected porous architectures. This stage took one day to complete.
6. The final pre-operative simulation was achieved by digital, virtual, and physical visualization of the solution. More specifically:
    a. The photorealistic and interactive 3D views were sent to the surgeon and were readily available.
    b. The VR and AR sessions were set up within 10 minutes.
    c. The 3DP of all models required 7 days and the PLA material cost 50 €. To illustrate the porous endo and exo architecture, the endo-prosthesis was also 3DPed with a transparent resin material using a vat photopolymerization 3DP technology.
7. The required documentation was prepared within a day, including the request and the receipt of the quotation for outsourcing the manufacturing of all custom-made parts. 6 working days and 2180 € were required for the delivery of the solution. All off-the-shelf parts were not considered as these could be sourced by the surgeon.

As the most time-consuming tasks were found to be the 3DP of the anatomical models and all prototype parts of the solution, for the other case studies, for the anatomy visualization (Stage 4), only digital and virtual visualization was applied and for the surgical simulation (Stage 12) only the region of interest of the anatomical model was 3DPed in such a way so that both the tumor and the patient-specific solution can be fitted precisely. It was suggested to use faster low-cost material extrusion 3D printers as shown in *Figure 350* to drop the 3DP time down 4-5 times, and even use more than one simultaneously (print farm) for even further time compression.

It is worth mentioning that the inter-epistemic workflow is tweakable as per the available surgeon's spare time and the urgency of the case, so that his/her engagement can be minimized, and some stages eliminated to speed up the development.

The inter-epistemic workflow served well the Thesis scope and hypothesis, verifying that the role of the (bio)mechanical engineer is useful for assisting surgeons in delivering tailored solutions utilizing (in)tangible tools. Granted that surgeons have clarified "why?" (diagnosis) and "what?" (treatment and solution specifications) to develop for an individual, (bio)mechanical engineers can answer "how?" (design and manufacture) to develop this particular solution. Granted that a scientifically amalgamated scheme is formed, the inter-epistemic methodology is easy to be integrated into the current classic orthopaedic surgery workflows.

Thanks to custom 3D design and 3DP, xR and 3D Scanning, many benefits are unlocked:

1. Pre-operative planning using 3DPed anatomical models for achieving better diagnosis and better anatomic anticipation of the malformations, defects, anomalies, and pathologies. This way, the complexity of the surgery and the need for a surgeon with high expertise and skills can be relaxed. For fractures in trauma cases, osteosynthesis plates can be pre-contoured and bone screws placement can be defined on the anatomical model pre-operatively, whereas in more complex cases such as tumor resection and reconstruction, the anatomical model can contribute greatly in planning the operation flow and deciding the form, fixation, and characteristics of the solution.
2. Teaching, training, and patient communications are empowered by 3DPed anatomical models, implants, endo-prosthesis, and patient-specific instruments. Also, better multi-disciplinary and inter-epistemic coordination is facilitated. For example, *Figure 531* illustrates an educational ilium anatomy 3DPed for educational purposes; tumor ablation demonstration by inserting needles through the holes that end up in a porous region.

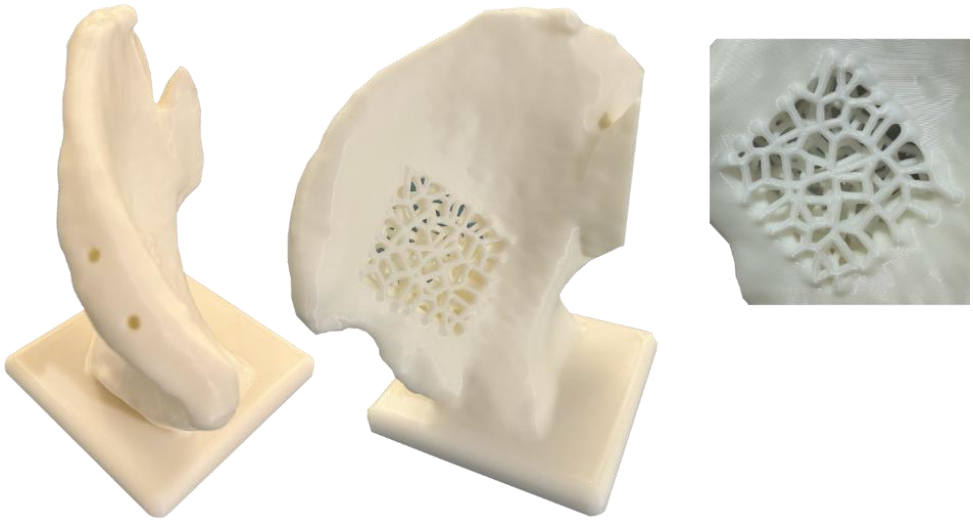

Figure 531: Pelvic tumor ablation education demo model

3. Design and/or manufacturing at the PoC is enabled. Hence, assisted by (bio)mechanical engineers, surgeons can be the "designers" and novel ideas can emerge.
4. Custom-made 3DPed solutions can directly decrease the operating time, blood loss and radiation exposure/fluoroscopy shots, risks, errors, and post-operative complications. Thus, the post-

treatment discomfort can be minimized whilst the intra-operative navigation and positioning accuracy and precision are improved, maximizing the functional and aesthetic results.

5. Oncological cases can be treated by two-stage (resection and reconstruction in two separate operations) and single-stage (one operation with reconstruction following resection) approaches. For two-stage approaches, 3DP can be utilized to make molds for producing PMMA spacers with antibiotics, until the reconstruction time is reached.
6. Compared to traditionally made solid parts, the 3DPed counterparts are superior in terms of geometry (any shape can be formed), mechanical properties (closer to bone, reducing stress-shielding), and surface characteristics for achieving better bone ingrowth and osseointegration. 3DPed parts can be surface and topology optimized (tunable different properties across the same part) and be internally porous or hollow, achieving less mass. Also, instead of coating the part to gain a spongy surface layer, 3DPed parts can have this architecture integrated at the surface of the same monolithic part per se, acting as weight-bearing scaffolds due to their high pore interconnectivity. This absence of extra layers leads to better structural bonding, eliminating delamination risks, shedding, and galvanic effects. Thus, peri-prosthetic fractures due to aseptic loosening, non-union, and stress-shielding can be reduced. However, to combat bacteria colonization and infections, coatings must still be applied to the 3DPed part.
7. xR is ready for utilization for pre-operative planning, training, and education. However, for intra-operative usage, if not medically approved all-in-one solutions are acquired, they must be only used for diagnostic and image information. Navigating by custom AR/MR set-ups contains increased risks as accuracy, precision, and repeatability of image registration and tracking are of concern. In this Thesis, xR equipment was utilized to be used exclusively for pre-operative planning and product design, but it could also be used for education and training, and possibly intra-operatively for information and 3D model visualization, not for navigation.
8. Low-cost 3D scanning using smart mobile devices can be used to successfully develop tailored orthotic devices. Orthotic devices such as splints and braces are suitable to be 3DPed but time-critical orthotic parts such as casts for immediate use are not due to the extended time required to materialize such. However, handheld 3D scanning devices are recommended.
9. A database of worked cases for which custom solutions were applied can be created and used as references when similar cases emerge.

On the other hand, 3DP is not a panacea and should be utilized when it is opportunistic for producing quality products within competitive time and cost. As with every manufacturing process, 3DP technologies have limitations. The characteristics, advantages, and disadvantages of 3DP technologies were described in *Sub-section 3.3.6*. For example, for parts that have non-intricate

geometries and are made of easy-to-machine (bio)materials, machining operations such as turning or milling for one-off or low-to-medium production volumes might be preferable. Compared to machining, 3DPed parts have poorer dimensional accuracy, rougher surface finish, might include internal pores and defects, and experience anisotropic mechanical properties depending on the build orientation of the part. As the required production volume rises, 3DP becomes more and more uncompetitive. For example, the face shields shown in *Figure 529* were designed to be 3DPed in as much volume as possible to protect the users from the SARS-CoV-2 virus during the pandemic, with each shield requiring 3 hours to be 3DPed out of 43 gr (1,5 €) of PLA material. For mass production, this is not beneficial either in terms of time and cost or in terms of safety as sterilization and disinfection are problematic due to the hard-to-reach areas between the layers of the laminated (3DPed) part. For this reason, the design can be adapted appropriately to be injection molded as shown in *Figure 532*, leading to approximately 0,2 € cost and 15 s production time per part, of course, there are extra costs and time for the metal mold manufacturing which is considerable, reaching approximately 9.000 € and 15 days respectively.

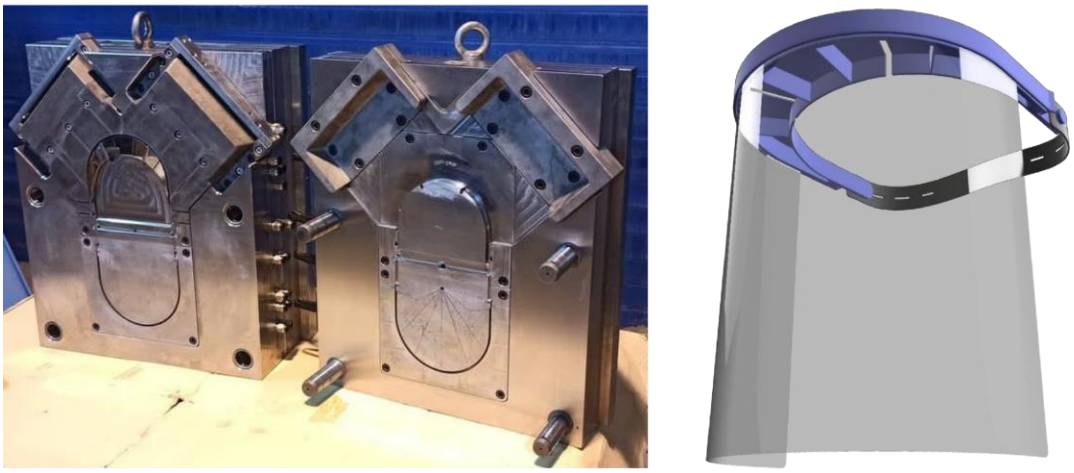

Figure 532: Two-part mold used for the injection molding of a two-piece face shield

The First Department of Orthopaedic Surgery (Chairman: Panayiotis Papagelopoulos) at Attikon University General Hospital, School of Medicine, National and Kapodistrian University of Athens, among other fields, focuses on bone tumor resection and reconstruction for limb salvage *(Mavrogenis et al., 2011a; 2012; 2014; 2017a; 2017b; 2021)*, as well as on the osseointegration, performance and infection prevention of tumor (mega)endo-prostheses *(Mavrogenis et al., 2009; 2011b; 2015; Savvidou et al., 2017; 2020; Lex et al., 2022)*. 3D technologies are being used by the Department *(Papagelopoulos et al., 2018)* to reconstruct with artificial endo-prostheses different anatomical regions, i.e. tibial and ankle *(Papagelopoulos and Savvidou, 2022a; Savvidou et al., 2022)*, *foot (Papagelopoulos and Savvidou, 2022b)*, calcaneus *(Papagelopoulos et al., 2019a; Savvidou et al., 2020)*, talus *(Papagelopoulos et al., 2019b)*, shoulder *(Savvidou et al., 2018; Trikoupis et al., 2024)*, radius *(Savvidou et al., 2021)*, and expandable endo-prostheses in children *(Savvidou et al., 2019)*.

Selected cases on pelvic, foot and lower limbs, and upper limb reconstructions using custom-made endo-prostheses are shown in *Figure 533* to *Figure 536*.

Until now, the Department has been outsourcing the development (3D design and manufacturing) of all cases to external partners. However, a shift towards bringing PoC 3D design, xR, and 3DP of such custom solutions is now being explored *(Mavrodontis et al., 2024)*. This way, the time and cost can drop considerably, by either 3D designing and prototyping the solutions before outsourcing the final manufacturing (3DP) or by 3D designing and manufacturing in-house. Under this approach, as per the scenarios presented by the *FDA (2021) (see Figure 115)* granted a suitable inter-epistemic synergy and methodology is formed and a suitable PoC 3D Unit is established, the following options are enabled for the HCF:

1. PoC development: the HCF designs, prototypes, and manufactures medical devices.
2. Outsourced development: the design and manufacturing of medical devices is outsourced.
3. Hybrid development: either the HCF designs and prototypes medical devices at the PoC 3D Unit and the final manufacturing is outsourced, or the design is outsourced and the HCF manufactures the medical devices.

Although will be researched in the future, the major limitations of this research were:

1. The developed endo-prostheses and instruments were not 3DPed in metal and end-polymer biomaterials, nor implanted into the patient.
2. More focus should have been given to the construction, details, and step-by-step application guidelines of a suitable QMS that must accompany the proposed workflow as per the applicable regulations and standards. inter-epistemic medical device development involves not only the design and manufacturing of products, but also refers to cleaning, post-processing, packaging, and sterilization which have serious consequences on product safety of a product. Hence, applicable national and international standards and regulatory requirements must be addressed by a QMS that governs the whole process for quality assurance and control, minimum risks, maximum safety, and high-quality results by adopting policies, procedures, forms, and work instructions with a defined sequence, interactions, resources, and documented records that are being updated and stored with interconnected files throughout the entire product lifecycle. The quality, development time, compliance with regulations and standards, and final cost of 3DPed parts are interconnected. From raw material to end-part collection, to cleaning, inspection, and approval, to sterilization and application, the adopted QMS should enclose qualified and if possible certified workforce conducting validated and/or verified pre-process (image data acquisition and processing to generate 3D models, part's geometry and preparation, 3DP process planning and settings, software used), in-process (machine and process-specific parameters and mechanisms, errors, feedstock

material properties and handling, process monitoring, and maintenance) and post-process (de-powdering and cleaning, machining, polishing, coatings, and other treatments) activities.

3. More research is required for the de-powdering, cleaning, sterilization, and non-destructive inspection of the 3DPed parts to be implanted.
4. To better define the endo-prosthesis form and its fixation points, directions, and lengths, multi-modal CT, MRI, Magnetic resonance neurography (MRN), and Computed Tomography Angiography (CTA) imaging are required to account for neurovascular tissue.
5. Extra mechanical simulations considering the anisotropic and inhomogeneous bone tissue properties, surrounding soft tissue (cartilage, muscles, tendons), threads of bone screws and their tightening reaction forces, and dynamic fatigue analyses should have been executed by considering more loading scenarios such as direct impacts by sideways falls.
6. Regarding the mechanical performance of the spongy architectures, alternative functionally graded structures could have been explored and simulated, whilst investigating local stress concentrations, contact phenomena, and deformation levels on the nodes and beams to ensure that these can withstand the exerted loads without failure. Ideally, cellular structures should be generated by simulation-driven multi-objective and multi-scale tools that account for spatial variations of parameters across the part per se. Although randomized Voronoi architectures and sheet and skeletal Gyroids featured different pore sizes, mixed unit cell Gyroid illustrated in *Figure 463* and similar TPMSs present interesting multi-pore potential; large and smaller pores favor both vascularization and cell colonization by blending suitable geometries or implementing gradients *(Karageorgiou and Kaplan, 2005; Charbonnier, Hadida and Marchat, 2021)*.
7. To improve possible technical flaws and defects of 3DPed optimized components with cellular structures, manufacturing errors, and imperfections should be mitigated by running manufacturing-specific process simulations.
8. Research on coatings substances that can be applied on the porous surface for bacterial-fighting and osseointegration-boosting activities must be addressed.
9. More case studies should be conducted to enrich the portfolio, and follow-ups after implantation must be reported.
10. For 3D scanning, a handheld device would be more suitable to be used instead of the LiDAR and TrueDepth sensors of smart mobile devices.
11. A realistic cost analysis including overhead and human-hour costs must be conducted. Also, a cost-benefit analysis for whether outsourcing or in-house manufacturing must be carried out.
12. Analytical documentation and associated templates must be constructed for all reports (final proposal check and justification, safety, risk assessment, and quality management,

application/implantation instructions, manufacturing instructions). Also, the terms of use and warranty notes must be defined.

13. The pilot PoC 3D Unit was constrained by the available resources. A properly structured adequately equipped Unit must be established.

The conclusions and suggested future research are mentioned in the next and last section.

Figure 533: Pelvic reconstructions using 3DPed endo-prostheses

Figure 534: Foot reconstructions using 3DPed endo-prostheses

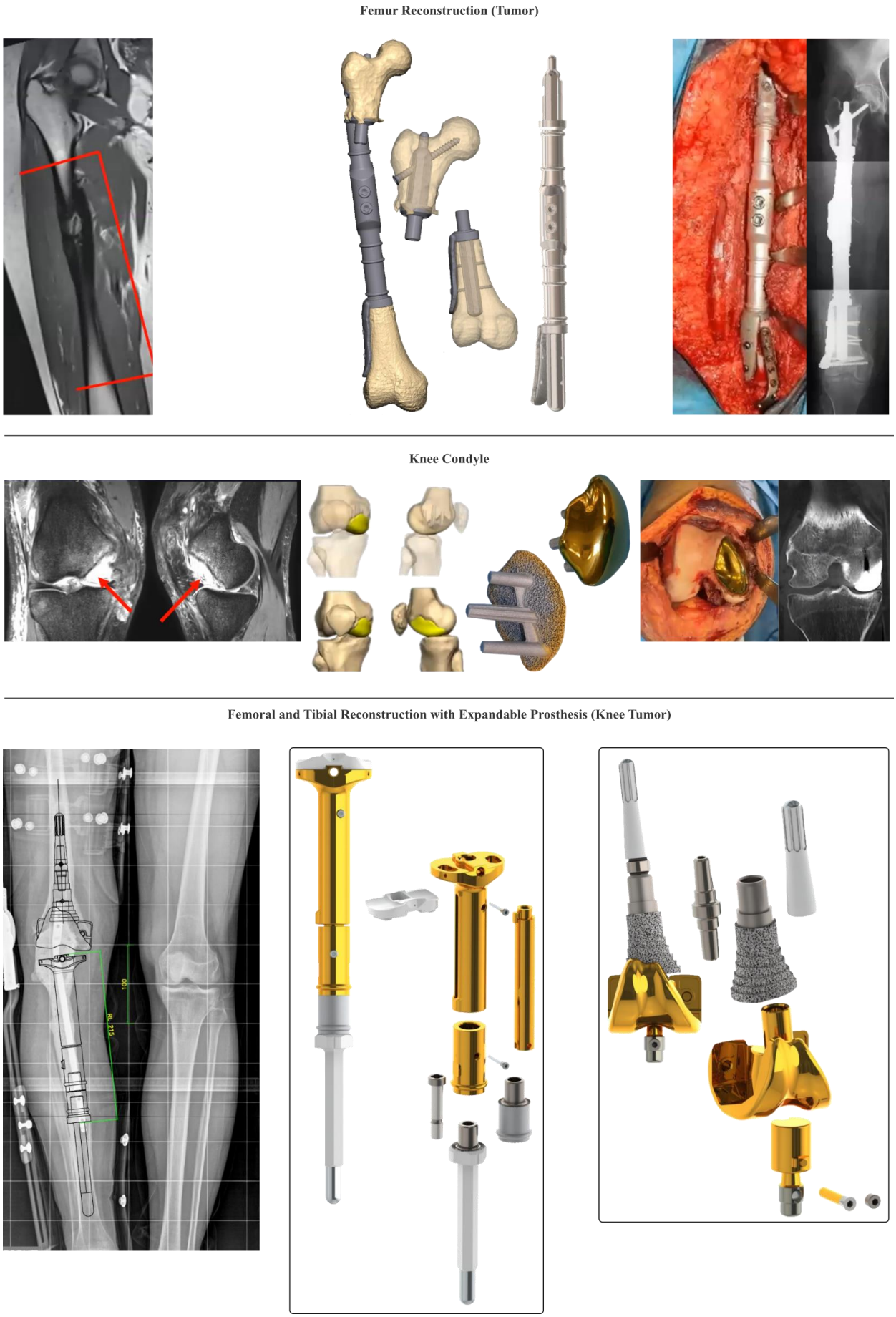

Figure 535: Lower-limb reconstructions using 3DPed endo-prostheses

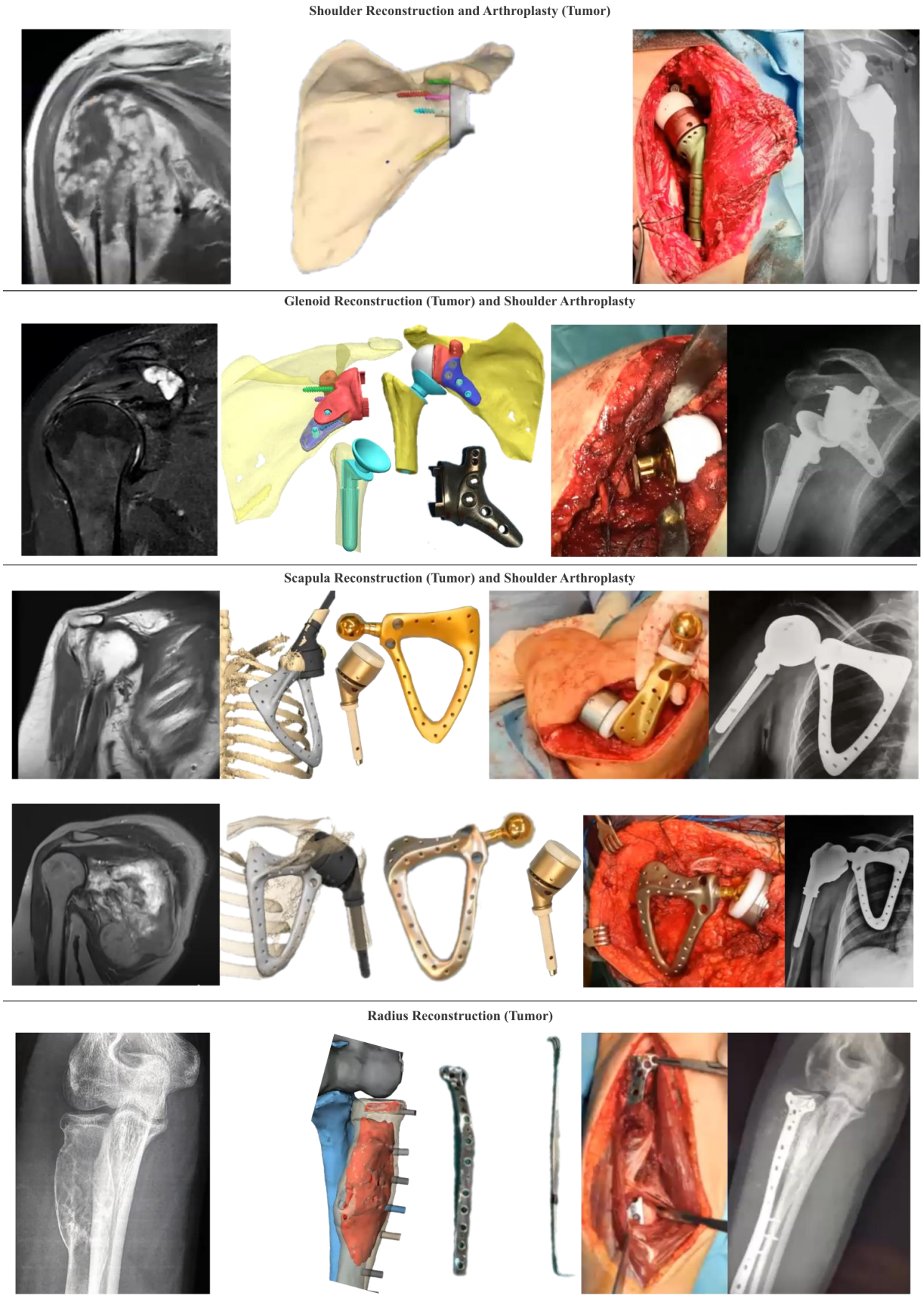

Figure 536: Upper-limb reconstructions using 3DPed endo-prostheses

8. Conclusions and Future Research

This Thesis deals with the individualization of orthopaedic rehabilitation by fitting the method to the patient's needs through customized design and production, instead of fitting the patient to the method. This is essential, especially for critical reconstruction and oncological cases.

The hypothesis that inter-epistemic workflows involving 3D technologies (3D design, 3DP, xR, 3D scanning) could be disruptive for individualized orthopaedics (especially if routinely applied at or near the PoC) was investigated, and the qualitative and quantitative results were explored. The roles of (bio)mechanical engineers in a PoC 3D Unit and their contribution to orthopaedic operations, the causes of hysteresis for adopting (bio)mechanical engineering design and manufacturing at the PoC, and topics related to the establishment of PoC 3D Units were addressed. The initially set objectives were followed to achieve the goals and contribute by covering the literature gaps, *Table 2* summarizes the objectives, goals, and gaps covered.

The state of the art was introduced, the theme, scope, and approach of the Thesis were presented, and an extensive critical literature review was carried out about a) orthopaedic biomaterials for reconstruction and regeneration, b) 3D design and 3DP characteristics, potential and applications on orthopaedics, especially for making biomimetic optimized products, and associated challenges were explored, c) the usage of 3DP, xR and 3D scanning for PoC utilization. The methodology and rationale of the research were established and a pilot PoC 3D Unit was set up after presenting two Scenarios. For the PoC 3D Unit the following were covered: organizational structure, framework for implementation, equipment, infrastructure and layout, cost per product/ service offered, and distributed and localized manufacturing. Five oncological and one orthosis cases were studied within the pilot PoC 3D Unit and the results were discussed.

Healthcare has traditionally been a non-engineering design and non-manufacturing sector, as neither design nor manufacturing usually takes place in situ. The entrance of 3D design and manufacturing technologies is transforming healthcare facilities into decentralized design and/or manufacturing sites. PoC 3D Units aiming at medical device development should be established accordingly to facilitate the symbiosis of healthcare professionals with skilled (bio)mechanical engineers to develop patient-specific devices at the PoC within acceptable lead times and costs.

A suitably established and regulated PoC 3D Unit has the potential to become an autonomous separate department within the HCF where design and/or manufacture can take place without sending sensitive patient data to external partners. Such a PoC 3D Unit can serve any other department, and all required services can be housed within the same HCF. This is important, especially for urgent cases, where face-to-face meetings among all parties involved are enabled for fast solutions development.

Table 21: Objectives followed to achieve the goals and cover the literature gaps

Objectives	Goals	Literature gaps covered
1. Review modern and 3DPable biomaterials used in individualized orthopaedic reconstruction. 2. Explore/ exploit the full potential of digital design, xR, 3DP, and 3D scanning in individualized orthopaedics. 3. Review requirements and characteristics of PoC 3D digital design, xR, 3DP, and 3D scanning. 4. Carry out scenarios with pragmatic cases (under hypotheses and assumptions and based on available budget and resources) by applying digital design, xR, 3DP, and 3D scanning technologies in situ, within the hospital environment. Select orthopaedic oncology and an orthosis case and treat them as currently ongoing pragmatic cases to be carried out by a pilot PoC 3D Unit set at the First Department of Orthopaedic Surgery, School of Medicine, NKUA. 5. Apply advanced design techniques and optimization algorithms for the custom solutions, inspired from and mimicking the cosmos of natural structures that are optimized for their assigned functions: biomimetic morphologies with heterogeneous architectures and topologically variable material density with gradient porous elements. Products incorporating biologically-inspired spongy endo- and exo-structures could reach superior mechanical and biological performance and minimize complications. 6. Evaluate and compare these technologies with traditional approaches based on mechanical and biological performance, and sustainability, and against technical, time, and economic criteria.	1. Accent inter-epistemic synergy for individualized orthopaedic services and optimized product development at the PoC 3D Unit under a holistic view. 2. Construct a systematic patient-specific design and manufacture methodology, and end-to-end guidelines, highlighting the critical parameters and challenges of each step of the workflow. 3. Set and present the characteristics of a hypodigmatic small 30 sqm pilot PoC 3D Unit in "Attikon" University General Hospital: organizational structure, framework for implementation, equipment, infrastructure and layout, and cost. Review PoC Unit's performance and sustainability under its potential for a decentralized manufacturing model, readiness for routine operation, challenges, and cost and time responsiveness. 4. Granted that bespoke digital, virtual, and physical solutions have been developed for some selected pragmatic pelvic and sacrum reconstruction case studies, novel, "smart" solutions and the need to shift from reconstructive to regenerative approaches will be discussed.	The literature is highly active and reports a plethora of novel topics on the design, manufacture (3DP), and performance of patient-specific orthopaedic parts. However, there were gaps in: 1. Holistically dealing with the implementation of a de novo inter-epistemic synergy at the PoC. 2. Focusing on the set-up requirements and assessment of a PoC 3D Unit per se. 3. Methodically presenting a systematic end-to-end workflow for patient-tailored services and optimized product development and analyzing each step applied whilst providing guidelines.

PoC 3D Units can design any medical device of any risk level, but manufacturing might be problematic due to regulatory, quality management, and standards being involved. For interested HCFs, it is suggested to initially commence with PoC 3D Units for prototyping low-risk (and optionally manufacture medium-risk) medical devices and outsourcing the medium-risk (instruments) and high-risk (implants and endo-prostheses) medical devices to external partners for the final manufacturing. In the future, granted that sufficient demand exists, production-class 3D printers and equipment for making the end medical devices and post-processing them in situ can be implemented to speed up the delivery time and lower the costs.

In this Thesis, individualized orthopaedic solutions development at the PoC is explored for which there are regulatory pathways that describe the exemption from strict regulatory control under certain circumstances involving life-threatening conditions with no alternative treatments available by allowing authorized healthcare professionals to provide design input and take responsibility for the safety and performance of the customized medical devices. For producing standard or modular or even custom orthopaedic medical devices for which alternative medically cleared options are readily available in the market, the applicable regulations differ considerably.

The de-novo 15-step role-based end-to-end systematic inter-epistemic patient-specific orthopaedic product design methodology (workflow) was successfully applied for each case study to synergistically develop tailored solutions. However, the surgeon must know how to provide instructions and guidelines so that the engineer can understand them clearly, and the engineers need to know about musculoskeletal anatomy, surgical approaches, and biomaterials and components used by surgeons. It is worth highlighting that the workflow steps and the engagement of the surgeon can be adjusted as per the surgeon's spare time and the urgency of the case.

Although numerous issues, barriers, and challenges exist, the proposed PoC 3D Unit format and the proposed inter-epistemic workflow can be readily deployed in an HCF without disturbing its normal daily operations. Thus, the benefits are:

1. The patient: satisfaction by better understanding of the surgery preoperatively, reduced surgery time, improved functional and aesthetic results, and reduced length of hospital stay.
2. The surgical procedure: decreased operating time, blood loss and radiation exposure/ fluoroscopy shots, risks, errors, and post-operative complications. Thus, post-treatment discomfort is minimized whilst intra-operative navigation and positioning accuracy and precision are improved, maximizing the functional and aesthetic results.
3. The HCF: trust, reputation, and consequently revenue streams might be increased due to the usage of cutting-edge technologies, reduced expenditure if external partners are replaced by in-house 3D design and/or 3DP, sensitive patient data is protected, the staff knowledge is extended, and their skills enriched with new technological tools.

It would be beneficial if as many HCFs as possible establish PoC 3D Units which 3D design and manufacture to increase the:

1. Number of innovators and participants.
2. The trend to shift towards bottom-up approaches in contrast to the top-down approach used today *(Figure 256).*
3. Applications.
4. Knowledge and database of case studies with useful information and post-operative follow-ups.

5. Employment of personnel.
6. Need for the establishment of a suitable distributed or localized manufacturing network that could contribute to the local economy.
7. Competition.
8. Pressure for regulatory reforms and the creation of associated standards and guidelines.
9. Safety of intellectual property and patient privacy.
10. Collaboration of clinicians with engineers for faster, cheaper, and automated solutions development.
11. Cost performance and acceleration for faster, cheaper, better, and automated healthcare delivery for each individual and society.

The Thesis dealt with the quest to develop safe and high-quality endo-prostheses to reconstruct osseous tissue, whilst trying to mimic the characteristics of biological bone. The pelvic and sacrum reconstruction procedure and considerations were analytically discussed from a (bio)mechanical engineering point of view, but orthopaedic and medical aspects were also engaged, whilst the reader is presented with numerous graphic materials regarding the solution development. However, in addition to the limitations of this research that were given in the previous Section, many extra future research topics were identified:

1. Shift from reconstructive to regenerative approaches: there is a need to shift from the current approaches where artificial bioinert load-bearing biomaterials (mostly Ti alloys) feature scaffolds with or without extra grafts or bone formation inducing materials that allow some level of bioactivity (osseointegration by bone ingrowth), to new orthopaedic biomaterials; from bioinert, to bioactive, to biodegradable, and ideally to autonomous biomimetic not only in terms of form and hierarchy but also in functions, thus fully reverse engineering the bone. The osseointegration phenomenon is a biological indication that proves the regenative potential of bone which can regenerate as long as there is a suitable construct to “guide” the human organism to build tissue. Towards this direction, bone Tissue Engineering is a very promising field that could ultimately allow bone tissue regeneration, though suitable biodegradable biomaterials with adequate structural integrity and mechanical properties have to be processed. Hence, scaffold-based or scaffold-free 3D (bio)printing for bone grafting can be researched; metallic, synthetic, and natural polymers, ceramic, composite, and hydrogel scaffolds or direct living cell bioprinting are the last frontiers that are being tested to be used for fully functional hard or soft Tissue Engineering to achieve “autologous-like” bone grafting.
2. Multi-material 3DP of hard-soft composites, where geometric freedom and materials functionality “grow” side-by-side.

3. Hybrids 3DPed endo-prostheses combined with biological constructs and grafts.
4. Drug delivery systems and carriers that elute under control. Drug-eluting endo-prostheses can be realized by implementing reservoirs containing drugs and microchannels that guide the drug to the desired areas. The drug release can be achieved by passive or active triggering based on different stimuli.
5. "Instrumented" endo-prostheses capable of sensing, measuring, and reporting real-time physical quantities. Aseptic loosening, dislocation, misalignment, infection, and reaction to debris can be sensed by suitable sensors (temperature, force, acceleration/ vibration, position, sound, strain).
6. 4D (bio)printing of stimuli-responsive materials that can undergo controlled changes over the fourth dimension (time). Stimuli-responsive biomaterials such as shape memory alloys, polymers, and hydrogels can morph based on different stimuli such as temperature, humidity, electric/ magnetic fields, light, acoustic, ion, pH, and biological.
7. Development of microfluidics (lab on chip) for orthopaedic applications (mechanical stimulation, culturing and bone tissue manufacturing, diagnosis, and treatment).
8. Custom 3DPed fixation devices and stems with anchors and porous features.
9. Prosthetic devices development and other types of orthotic devices.
10. Bacteria-fighting and osseointegration-boosting coating materials.
11. More research on interconnected porous architectures is required. It is interesting that such architectures can produce meta-(bio)materials-by-design the properties of which are mostly governed by their geometry rather than by the base material characteristics.
12. The design of bone-like architectures requires a database of bone properties for different age and gender groups at different locations as not all humans are anatomically and compositionally the same (age, sex, health, and bone condition), and not all bones are the same; bone quality and composition change along the skeleton (location). Ideally, micro-CT imaging of the patient's bone is required as bone remodels and adapts to the mechanical stimuli, whilst experiencing anisotropy.
13. Conduct physical mechanical tests and biological experiments on optimized biomimetic samples.
14. Carry out mechanical simulations on the endo-prostheses whilst considering all peripheral soft tissue and all interactions.
15. As the bottleneck of optimized biomimetic devices is the design and not their fabrication (thanks to 3DP), the value is no longer in the physical item, but in its digital model. Alternative software solutions or modeling and optimizing orthopaedic devices have to be explored. The following are highly sought: a) development of automated workflows powered by AI for the selection of optimum reconstruction approach for each patient, and automatic generation of optimized 3D

designs suitable for 3DP, and b) creation of open-source libraries with worked cases and guidelines, including the 3D models of all components used in each solution.

16. It is necessary to set up custom scenes in alternative free and open-source software for xR applications such as Unity Technologies' Unity which contains a plethora of tools. AR/MR can be combined with suitably prepared 3DPed models (registration marks) for projecting soft tissue, preoperative plans, etc.
17. Decentralized (distributed and localized) supply networks with highly flexible and smart manufacturing centers near/in HCF making bespoke orthopaedic devices manufacturing networks can be modeled and assessed in terms of performance and cost.
18. 3DP can help orthopaedic industry to shift towards a more sustainable and circular economy. 3DP ensures low cost and rapidness for one-off and complex implants. However, the impacts on the supply networks and the life-cycle of the individualized devices have to be exploited for a complete picture.

We are passing through an eon of emblematic technologies the advent of which has inaugurated a new era for patient-specific treatments that have groundbreaking potential. Three-dimensional technologies are newly inserted tools into the modern digital cosmos of individualized healthcare delivery and introduce advanced abilities for delivering medical devices at the PoC with greater customization, innovation in design, cost-effectiveness, and high quality. Digital design, xR, 3DP, and 3D imaging technologies streamlined with robotics and AI lead towards the realization of Industry 4.0 and transforming orthopaedics into digital and intelligent. As HCFs have no design and manufacturing experience, even though related pitfalls might be known to engineers, an increased awareness is suggested to explore and exploit the full potential of the 3D design–3DP–xR triad in realizing medical devices at the PoC under suitable QMSs and as per the applicable regulations and standards.

9. References

Abbott, A., 1972. *Laminated plastic propeller*. US Patent No. 3706511.

Abdollahiyan, P., Oroojalian, F., Mokhtarzadeh, A. and Guardia, M., 2020. Hydrogel-Based 3D Bioprinting for Bone and Cartilage Tissue Engineering. *Biotechnology Journal*, 15(12).

Abou-Ali, A., Alketan, O., Lee, D., Rowshan, R., Abu Al-Rub, R., 2020. Mechanical behavior of polymeric selective laser sintered ligament and sheet based lattices of triply periodic minimal surface architectures. *Materials and Design*, 196.

Abou-Ali, A., Lee, D. and Abu Al-Rub, R., 2022. On the Effect of Lattice Topology on Mechanical Properties of SLS Additively Manufactured Sheet-, Ligament-, and Strut-Based Polymeric Metamaterials. *Polymers*, 14 (21).

Acharya, S., Soni, R., Suwas, S. and Chatterjee, K., 2021. Additive manufacturing of Co–Cr alloys for biomedical applications: A concise review. *Journal of Materials Research*, 36(19), pp.3746-3760.

Adamson, A., 1977. *Method and apparatus for generating three-dimensional patterns*. US Patent No. 3609706.

Affatato, S., 2014. *Perspectives in Total Hip Arthroplasty*. New York: Woodhead Publishing.

Agrawal, R., 2022. Sustainable design guidelines for additive manufacturing applications. *Rapid Prototyping Journal*, 28(7), pp.1221-1240.

Aguado-Maestro, I., De Frutos-Serna, M., González-Nava, A., Merino-De Santos, A. and García-Alonso, M., 2021. Are the common sterilization methods completely effective for our in-house 3D printed biomodels and surgical guides?. *Injury*, 52(6), pp.1341-1345.

Ahart, J., 1951. *Apparatus for building concrete walls*. US Patent No. 2562403.

Ahn, D., Kim, H. and Lee, S., 2007. Fabrication direction optimization to minimize post-machining in layered manufacturing. *International Journal of Machine Tools and Manufacture*, 47(3-4), pp.593-606.

Abueidda, D., Elhebeary, M., Shiang, A., Pang, S., Abu Al-Rub, R., and Jasiuk, I., 2019. Mechanical properties of 3D printed polymeric Gyroid cellular structures: Experimental and finite element study. *Materials and Design*, 165.

Albrektsson, T. and Albrektsson, B., 1987. Osseointegration of bone implants: A review of an alternative mode of fixation. *Acta Orthopaedica Scandinavica*, 58(5), pp.567-577.

Al Janabi, H., Aydin, A., Palaneer, S., Macchione, N., Al-Jabir, A., Khan, M., Dasgupta, P. and Ahmed, K., 2019. Effectiveness of the HoloLens mixed-reality headset in minimally invasive surgery: a simulation-based feasibility study. *Surgical Endoscopy*, 34(3), pp.1143-1149.

Al-Ketan, O., Rezgui, R., Rowshan, R., Du, H., Fang, N. and Abu Al-Rub, R., 2018a. Microarchitected Stretching-Dominated Mechanical Metamaterials with Minimal Surface Topologies. *Advanced Engineering Materials*, 20.

Al-Ketan, O., Rowshan, R. and Abu Al-Rub, R., 2018b. Topology-Mechanical Property Relationship of 3D Printed Strut, Skeletal, and Sheet Based Periodic Metallic Cellular Materials. *Additive Manufacturing*, 19, pp.167-183.

Al-Ketan, O., Abu Al-Rub, R., 2019. Multifunctional mechanical-metamaterials based on triply periodic minimal surface lattices: A review. *Advanced Engineering Materials*, 21.

Al-Ketan, O., Lee, D., Rowshan, R. and Abu Al-Rub, R., 2020. Functionally graded and multi-morphology sheet TPMS lattices: Design, manufacturing, and mechanical properties. *Journal of the Mechanical Behavior of Biomedical Materials*, 102.

Allanic, A., Medard, C. and Schaeffer, P., 1992. Stereophotolithography: A Brand New Machinery. In: *Solid Freeform Fabrication Symposium Proceedings*.

Alsheghri, A., Reznikov, N., Piché, N., McKee, M., Tamimi, F. and Song, J., 2021. Optimization of 3D network topology for bioinspired design of stiff and lightweight bone-like structures. *Materials Science and Engineering: C*, 123.

Alvarez, K. and Nakajima, H., 2009. Metallic Scaffolds for Bone Regeneration. *Materials*, 2(3), pp.790-832.

Alvarez-Lorenzo, C. and Concheiro, A., 2014. ChemInform Abstract: Smart Drug Delivery Systems: From Fundamentals to the Clinic. *ChemInform*, 45(35).

Amin Yavari, S., van der Stok, J., Chai, Y., Wauthle, R., Tahmasebi Birgani, Z., Habibovic, P., Mulier, M., Schrooten, J., Weinans, H. and Zadpoor, A., 2014. Bone regeneration performance of surface-treated porous titanium. *Biomaterials*, 35(24), pp.6172-6181.

Amoyav, B., Goldstein, Y., Steinberg, E. and Benny, O., 2020. 3D Printed Microfluidic Devices for Drug Release Assays. *Pharmaceutics*, 13(1).

Andre, J., Le Mehaute, A. and De Witte, O., 1984. *Dispositif pour realiser un modele de piece industrielle*. FR Patent No. 8411241.

Andrés-Cano, P., Calvo-Haro, J., Fillat-Gomà, F., Andrés-Cano, I. and Perez-Mañanes, R., 2021. Role of the orthopaedic surgeon in 3D printing: current applications and legal issues for a personalized medicine. *Revista Española de Cirugía Ortopédica y Traumatología (English Edition)*, 65(2), pp.138-151.

Angelini, A., Trovarelli, G., Berizzi, A., Pala, E., Breda, A. and Ruggieri, P., 2018. Three-dimension-printed custom-made prosthetic reconstructions: from revision surgery to oncologic reconstructions. *International Orthopaedics*, 43(1), pp.123-132.

Angelini, A., Kotrych, D., Trovarelli, G., Szafrański, A., Bohatyrewicz, A. and Ruggieri, P., 2020. Analysis of principles inspiring design of three-dimensional-printed custom-made prostheses in two referral centres. *International Orthopaedics*, 44(5), pp.829-837.

Angelini, A., Kotrych, D., Szafrański, A. and Ruggieri, P., 2021. 3D Printed Reconstructions. In: *Surgery of Pelvic Bone Tumors*. Ed. by Ruggieri, P. and Angelini, A. Cham: Springer, pp.191-201.

Aguado-Maestro, I., de Blas-Sanz, I., Sanz-Peñas, A., Campesino-Nieto, S., Diez-Rodríguez, J., Valle-López, S., Espinel-Riol, A., Fernández-Díez, D. and García-Alonso, M., 2022. Dual Mobility Cups as the Routine Choice in Total Hip Arthroplasty. *Medicina*, 58(4).

Arabnejad, S., Burnett Johnston, R., Pura, J., Singh, B., Tanzer, M. and Pasini, D., 2016a. High-strength porous biomaterials for bone replacement: A strategy to assess the interplay between cell morphology, mechanical properties, bone ingrowth and manufacturing constraints. *Acta Biomaterialia*, 30, pp.345-356.

Arabnejad, S., Johnston, B., Tanzer, M. and Pasini, D., 2016b. Fully porous 3D printed titanium femoral stem to reduce stress-shielding following total hip arthroplasty. *Journal of Orthopaedic Research*, 35(8), pp.1774-1783.

Aranda, J. and Espiago, A., 2019. Custom-made prosthesis in thoracic surgery. *Precision Cancer Medicine*, 2, pp.15-15.

Arjunan, A., Robinson, J., Al Ani, E., Heaselgrave, W., Baroutaji, A. and Wang, C., 2020. Mechanical performance of additively manufactured pure silver antibacterial bone scaffolds. *Journal of the Mechanical Behavior of Biomedical Materials*, 112.

Asbai-Ghoudan, R., Ruiz de Galarreta, S. and Rodriguez-Florez, N., 2021. Analytical model for the prediction of permeability of triply periodic minimal surfaces. *Journal of the Mechanical Behavior of Biomedical Materials*, 124.

Ashby, M., Evans, A., Fleck, N., Gibson, L., Hutchinson, J. and Wadley, H., 2000. *Metal foams: A Design Guide*. Boston: Butterworth-Heinemann.

Ashby, M., 2016. *Materials Selection in Mechanical Design*. 5th ed. Oxford: Butterworth-Heinemann.

Ashby, M., Shercliff, H. and Cebon, D., 2018. *Materials: Engineering, Science, Processing and Design*. Oxford: Butterworth-Heinemann.

Askari, M., Hutchins, D., Thomas, P., Astolfi, L., Watson, R., Abdi, M., Ricci, M., Laureti, S., Nie, L., Freear, S., Wildman, R., Tuck, C., Clarke, M., Woods, E. and Clare, A., 2020. Additive manufacturing of metamaterials: A review. *Additive Manufacturing*, 36.

ASME, 2020. *Medical Additive Manufacturing/3D Printing: Year in Review 2019-20*. ASME. [Online] Available at: https://resources.asme.org/hubfs/AM%20Summit/Medical%20AM3DP%20Year%20In%20Review%2019-20.pdf?hsLang=en-us [Accessed 9 March 2022].

Atallah, S., 2021. *Digital Surgery*. Cham: Springer.

Attaran, M., 2017. The rise of 3-D printing: The advantages of additive manufacturing over traditional manufacturing. *Business Horizons*, 60(5), pp.677-688.

Atzeni, E. and Salmi, A., 2012. Economics of additive manufacturing for end-usable metal parts. *The International Journal of Advanced Manufacturing Technology*, 62(9-12), pp.1147-1155.

Atzeni, E., Iuliano, L., Minetola, P. and Salmi, A., 2010. Redesign and cost estimation of rapid manufactured plastic parts. *Rapid Prototyping Journal*, 16(5), pp.308-317.

Azwan, M. and Rahim, I., 2011. Recent studies on the pullout strength behavior of spinal fixation. *Journal of Developmental Biology and Tissue Engineering*, 3(4), pp.48-54.

Babamiri, B., Barnes, B., Soltani-Tehrani, A., Shamsaei, N. and Hazeli, K., 2021. Designing additively manufactured lattice structures based on deformation mechanisms. *Additive Manufacturing*, 46.

Baese, C., 1904. *Photographic Process for the Reproduction of Plastic Objects*. US Patent No. 774549.

Baker, R., 1925. *Method of making decorative articles*. US Patent No. 1533300.

Baker, R., 2007. The history of gait analysis before the advent of modern computers. *Gait & Posture*, 26(3), pp.331-342.

Baker, T., Earwaker, W., Frost, N. and Wakeley, G., 1993. Integration of 3-D medical imaging and rapid prototyping to create stereolithographic models. In: *Australasian Physical and Engineering Science in Medicine*, 16(2), pp.79-85.

Ballard, H., Mills, P., Duszak, R., Weisman, A., Rybicki, J. and Woodard, K., 2020. Medical 3D Printing Cost-Savings in Orthopedic and Maxillofacial Surgery: Cost Analysis of Operating Room Time Saved with 3D Printed Anatomic Models and Surgical Guides. *Academic radiology*, 27(8), 1103–1113.

Banathy, B., 1996. *Designing Social Systems in a Changing World*. New York: Springer.

Barba, D., Alabort, E. and Reed, R., 2019. Synthetic bone: Design by additive manufacturing. *Acta Biomaterialia*, 97, pp.637-656.

Barrientos-Ruiz, I., Ortiz-Cruz, E. and Peleteiro-Pensado, M., 2017. Reconstruction After Hemipelvectomy With the Ice-Cream Cone Prosthesis: What Are the Short-term Clinical Results?. *Clinical Orthopaedics and Related Research*, 475(3), pp.735-741.

Bartl, R. and Bartl, C., 2019. *The Osteoporosis Manual*. Cham: Springer.

Bartol, K., Bojanić, D., Petković, T. and Pribanic, T., 2021. A Review of Body Measurement Using 3D Scanning. *IEEE Access*, 9.

Bartolomeu, F., Costa, M., Alves, N., Miranda, G. and Silva, F., 2020. Additive manufacturing of NiTi-Ti6Al4V multi-material cellular structures targeting orthopedic implants. *Optics and Lasers in Engineering*, 134.

Bartolomeu, F., Gasik, M., Silva, F.S. and Miranda, G., 2022. Mechanical Properties of Ti6Al4V Fabricated by Laser Powder Bed Fusion: A Review Focused on the Processing and Microstructural Parameters Influence on the Final Properties. *Metals*, 12 (6).

Baumann, A., O'Neill, C., Owens, M., Weber, S., Sivan, S., D'Amico, R., Carmody, S., Bini, S., Sawyer, A., Lotz, J., Goel, V. and Dmitriev, A., 2020. FDA public workshop: Orthopaedic sensing, measuring, and advanced reporting technology (SMART) devices. *Journal of Orthopaedic Research*, 39(1), pp.22-29.

Beitler, B., Abraham, P., Glennon, A., Tommasini, S., Lattanza, L., Morris, J. and Wiznia, D., 2022. Interpretation of regulatory factors for 3D printing at hospitals and medical centers, or at the point of care. *3D Printing in Medicine*, 8(1).

Beltrami, G., 2018. Custom 3D-printed finger proximal phalanx as salvage of limb function after aggressive recurrence of giant cell tumour. *BMJ Case Reports*.

Beltrami, G., Ristori, G., Galeotti, A., Scoccianti, G., Tamburini, A., Campanacci, D., Capanna, R. and Innocenti, M., 2021. A hollow, custom-made prosthesis combined with a vascularized flap and bone graft for skeletal reconstruction after bone tumour resection. *Surgical Oncology*, 36, pp.56-60.

Ben-Ner, A. and Siemsen, E., 2017. Decentralization and localization of production: The Organizational and Economic Consequences of Additive Manufacturing (3D Printing). *California Management Review*, 59(2), pp.5-23.

Benady, A., Yair, G., Summer, S., Yuval, R., Netta, R., Avital, E., Ben, E., Eran, G., Ortal, S., Omri, M., Amir, S. and Solomon, D., 2022. Internal hemipelvectomy for primary bone sarcomas using intraoperative patient specific instruments- the next step in limb salvage concept. *BMC Musculoskeletal Disorders*, 23(1).

Benedetti, M., Klarin, J., Johansson, F., Fontanari, V., Luchin, V., Zappini, G. and Molinari, A., 2019. Study of the Compression Behaviour of Ti6Al4V Trabecular Structures Produced by Additive Laser Manufacturing. Materials, 12(9).

Benedetti, M., du Plessis, A., Ritchie, R., Dallago, M., Razavi, S. and Berto, F., 2021. Architected cellular materials: A review on their mechanical properties towards fatigue-tolerant design and fabrication. *Materials Science and Engineering Reports*, 144.

Benmassaoud, M., Kohama, C., Kim, T., Kadlowec, J., Foltiny, B., Mercurio, T. and Ranganathan, S., 2019. Efficacy of eluted antibiotics through 3D printed femoral implants. *Biomedical Microdevices*, 21(3).

Bergmann, G., Graichen, F., Siraky, J., Jendrzynski, H. and Rohlmann, A., 1988. Multichannel strain gauge telemetry for orthopaedic implants. *Journal of Biomechanics*, 21(2), pp.169-176.

Bergmann, G., Deuretzbacher, G., Heller, M., Graichen, F., Rohlmann, A., Strauss, J. and Duda, N., 2001. Hip contact forces and gait patterns from routine activities. *Journal of Biomechanics*, 34(7), pp.859-871.

Bergmann, G., Graichen, F. and Rohlmann, A., 2004. Hip joint contact forces during stumbling. *Langenbeck's Archives of Surgery*, 389(1), pp.53-59.

Bergmann, G., Graichen, F., Dymke, J., Rohlmann, A., Duda, G. and Damm, P., 2012. High-Tech Hip Implant for Wireless Temperature Measurements In Vivo. *PLoS ONE*, 7(8).

Bergmann, G., Bender, A., Dymke, J., Duda, G. and Damm, P., 2016. Standardized loads acting in hip implants. *PLOS ONE*, 11(5).

Besl, P. and McKay, H.D., 1992. A method for registration of 3-D shapes. *IEEE Transactions on Pattern Analysis and Machine Intelligence*, 14 (2), pp.239-256.

Beyer, F., Lützner, C., Stalp, M., Köster, G. and Lützner, J., 2022. Does the use of patient-specific instrumentation improve resource use in the operating room and outcome after total knee arthroplasty?–a multicenter study. *PLOS ONE*, 17(11).

Bezuidenhout, M., Dimitrov, D., van Staden, A., Oosthuizen, G. and Dicks, L., 2015. Titanium-Based Hip Stems with Drug Delivery Functionality through Additive Manufacturing. *BioMed Research International*, 2015, pp.1-11.

Bhat, S., Venkatesh, M., Balamuralidhara, V., Kumar, T., 2019. Comparison of 3D Printing in USA, Europe and Australia. *Journal of Pharmaceutical Sciences and Research*, 11(7), pp.2515-2520.

Bilalis, L., Canellidis, V., Papatheodorou, T. and Giannatsi, J., 2022. Direct Digital Manufacturing of a customized face mask. *Journal of Manufacturing and Materials Processing*, 6(5).

Bini, S., Schilling, P., Patel, S., Kalore, N., Ast, M., Maratt, J., Schuett, D., Lawrie, C., Chung, C. and Steele, G., 2020. Digital Orthopaedics: A Glimpse Into the Future in the Midst of a Pandemic. *The Journal of Arthroplasty*, 35(7), pp.68-73.

Blakeney, W., Epinette, J. and Vendittoli, P., 2019. Dual mobility total hip arthroplasty: should everyone get one?. *EFORT Open Reviews*, 4(9), pp.541-547.

Blanther, J., 1892. *Manufacture of Contour Relief Maps*. US Patent No. 473901.

Blaya, F., Pedro, P., Silva, J., D'Amato, R., Heras, E. and Juanes, J., 2018. Design of an Orthopedic Product by Using Additive Manufacturing Technology: The Arm Splint. *Journal of Medical Systems*, 42(3).

Boban, J., Ahmed, A., Jithinraj, E. K., Rahman, M. A. and Rahman, M., 2022. Polishing of additive manufactured metallic components: Retrospect on existing methods and future prospects. *The International Journal of Advanced Manufacturing Technology*, 121(1-2), pp.83-125.

Böllinghaus, T., et al., 2009. Manufacturing Engineering. In: *Springer Handbook of Mechanical Engineering*. Ed. by Grote, K. and Antonsson, E. Berlin: Springer, pp.523-785.

Bommes, D., Lévy, B., Pietroni, N., Puppo, E., Silva, C., Tarini, M. and Zorin, D., 2013. Quad-Mesh Generation and Processing: A Survey. *Computer Graphics Forum*, 32(6), pp.51-76.

Borkowski, P., Pawlikowski, M. and Skalski, K., 2005. Expandable Non-invasive Prostheses - an Alternative to Pediatric Patients with Bone Sarcoma. *Conference proceedings: Annual International Conference of the IEEE Engineering in Medicine and Biology Society.* IEEE Engineering in Medicine and Biology Society. Annual Conference, pp.4056-4059.

Bose, S. and Bandyopadhyay, A., 2016. *Materials and devices for bone disorders*. Cambridge: Academic Press.

Bosma, S., Wong, K., Paul, L., Gerbers, J. and Jutte, P., 2018. A Cadaveric Comparative Study on the Surgical Accuracy of Freehand, Computer Navigation, and Patient-Specific Instruments in Joint-Preserving Bone Tumor Resections. *Sarcoma*, 2018, pp.1-9.

Bourell, D., Kruth, J., Leu, M., Levy, G., Rosen, D., Beese, A. and Clare, A., 2017. Materials for additive manufacturing. *CIRP Annals*, 66(2), pp.659-681.

Brånemark, P., 1985. Introduction to osseointegration. In: *Tissue-integrated prostheses: Osseointegration in clinical dentistry*. Ed. by P. Branemark, G. Zarb and T. Albrektsson. Chicago: Quintessence Publishing.

Brinckmann, P., Frobin, W. and Leivseth, G., 2002. *Musculoskeletal Biomechanics*. New York: Thieme.

British Design Council, 2007. *Eleven lessons. A study of the design process*. [Online] Available at:https://www.designcouncil.org.uk/fileadmin/uploads/dc/Documents/ElevenLessons_Design_Council%2520%25282%2529.pdf [Accessed 9 March 2022].

Brogini, S., Sartori, M., Giavaresi, G., Cremascoli, P., Alemani, F., Bellini, D., Martini, L., Maglio, M., Pagani, S. and Fini, M., 2021. Osseointegration of additive manufacturing Ti–6Al–4V and Co–Cr–Mo alloys, with and without surface functionalization with hydroxyapatite and type I collagen. *Journal of the Mechanical Behavior of Biomedical Materials*, 115.

Broekhuis, D., Boyle, R., Karunaratne, S., Chua, A. and Stalley, P., 2022. Custom designed and 3D-printed titanium pelvic implants for acetabular reconstruction after tumour resection. *HIP International*, 33.

Bronner, F. and Farach-Carson, M, 2009. *Bone and cancer*. London: Springer.

Bronowski, H., 1986. *Device for building up a workpiece by deposit welding*. US Patent No. 4621762.

Broughton, K., Chien, B., Stenquist, D., Williams, C., Miller, C. and Kwon, J., 2021. 3-D generated anatomic custom talar cement spacers: case reports, technical tips and literature review. *3D Printing in Medicine*, 7(1).

Brown, C., Breinan, E. and Kear, B., 1982. *Method for fabricating articles by sequential layer deposition*. US Patent No. 4323756.

Brown, M., Borchard, S., Robbins, E., Ward, M., Talmo, T. and Bono, V., 2017. Management and Prevention of Intraoperative Acetabular Fracture in Primary Total Hip Arthroplasty. *American journal of orthopedics*, 46(5), 232-237.

Buckley, R., Moran, C. and Apivatthakakul, T., 2017. *AO principles of fracture management*. 3rd ed. Davos Platz, Switzerland: AO Foundation.

Burnard, J., Parr, W., Choy, W., Walsh, W. and Mobbs, R., 2019. 3D-printed spine surgery implants: a systematic review of the efficacy and clinical safety profile of patient-specific and off-the-shelf devices. *European Spine Journal*, 29(6), pp.1248-1260.

Caiazzo, F., Alfieri, V., Guillen, D. and Fabbricatore, A., 2022. Metal functionally graded gyroids: additive manufacturing, mechanical properties, and simulation. *The International Journal of Advanced Manufacturing Technology*, 123, pp.1-18.

Callister, W. and Rethwisch, D., 2018. *Materials science and engineering*. 10th ed. New Jersey: Wiley.

Calvo-Haro, J., Pascau, J., Asencio-Pascual, J., Calvo-Manuel, F., Cancho-Gil, M., Del Cañizo López, J., Fanjul-Gómez, M., García-Leal, R., González-Casaurrán, G., González-Leyte, M., León-Luis, J., Mediavilla-Santos, L., Ochandiano-Caicoya, S., Pérez-Caballero, R., Ribed-Sánchez, A., Río-Gómez, J., Sánchez-Pérez, E., Serrano-Andreu, J., Tousidonis-Rial, M., Vaquero-Martín, J., García San José, S. and Perez-Mañanes, R., 2021. Point-of-care manufacturing: a single University General Hospital's initial experience. *3D Printing in Medicine*, 7(1).

Canale, S., Azar, F. and Beaty, J., 2020. *Campbell's Operative Orthopaedics*. 14th ed. Philadelphia: Elsevier.

Canciglieri, O. and Trajanovic, M., 2022. *Personalized orthopedics*. Cham, Switzerland: Springer.

Cao, J., Zhu, H. and Gao, C., 2021. A Systematic Review and Meta-Analysis of 3D Printing Technology for the Treatment of Acetabular Fractures. *BioMed Research International*, 2021, pp.1-15.

Casari, F., Navab, N., Hruby, L., Kriechling, P., Nakamura, R., Tori, R., de Lourdes dos Santos Nunes, F., Queiroz, M., Fürnstahl, P. and Farshad, M., 2021. Augmented Reality in Orthopedic Surgery Is Emerging from Proof of Concept Towards Clinical Studies: a Literature Review Explaining the Technology and Current State of the Art. *Current Reviews in Musculoskeletal Medicine*, 14(2), pp.192-203.

Čapek, J., Machová, M., Fousová, M., Kubásek, J., Vojtěch, D., Fojt, J., Jablonská, E., Lipov, J. and Ruml, T., 2016. Highly porous, low elastic modulus 316L stainless steel scaffold prepared by selective laser melting. *Materials Science and Engineering: C*, 69, pp.631-639.

Capitani, P., Zampogna, B., Monaco, E., Frizziero, A., Moretti, L., Losco, M. and Papalia, R., 2021. The role of virtual reality in knee arthroscopic simulation: a systematic review. *Musculoskeletal Surgery*.

Chapman, J., Harrington, R., Lee, K., Anderson, P., Tencer, A. and Kowalski, D., 1996. Factors Affecting the Pullout Strength of Cancellous Bone Screws. *Journal of Biomechanical Engineering*, 118(3), pp.391-398.

Chatain, G. and Finn, M., 2020. Compassionate use of a custom 3D-printed sacral implant for revision of failing sacrectomy: case report. *Journal of Neurosurgery: Spine*, 33(4), pp.1-6.

Charbonnier, B., Hadida, M. and Marchat, D., 2021. Additive manufacturing pertaining to bone: Hopes, reality and future challenges for clinical applications. *Acta Biomaterialia*, 121, pp.1-28.

Chen, P., McKittrick, J. and Meyers, M., 2012. Biological materials: Functional adaptations and bioinspired designs. *Progress in Materials Science*, 57(8), pp.1492-1704.

Chen, G., Han, Q., Liu, H., Zhang, H., Jiang, Z., Feng, N. and Chang, F., 2019. Accurate Osteotomy for the Treatment of a Rare Case of Postaxial Polydactyly of the Foot That Originated From a Deformed Calcaneus Using a 3D-Printed Guiding Plate. *The Journal of Foot and Ankle Surgery*, 58(1), pp.171-175.

Chen, G., Muheremu, A., Yang, L., Wu, X., He, P., Fan, H., Liu, J., Chen, C., Li, Z. and Wang, F., 2020. Three-dimensional printed implant for reconstruction of pelvic bone after removal of giant chondrosarcoma: a case report. *Journal of International Medical Research*, 48(4).

Chen, Y., Li, W., Zhang, C., Wu, Z. and Liu, J., 2020. Recent Developments of Biomaterials for Additive Manufacturing of Bone Scaffolds. *Advanced Healthcare Materials*, 9(23).

Chen, L., Liang, S., Liu, Y. and Zhang, L., 2021. Additive manufacturing of metallic lattice structures: Unconstrained design, accurate fabrication, fascinated performances, and challenges. *Materials Science and Engineering Reports*, 146.

Chen, H., Liu, Y., Wang, C., Zhang, A., Chen, B., Han, Q. and Wang, J., 2021. Design and properties of biomimetic irregular scaffolds for bone tissue engineering. *Computers in Biology and Medicine*, 130.

Cheng, B., Shrestha, S. and Chou, K., 2016. Stress and deformation evaluations of scanning strategy effect in selective laser melting. *Additive Manufacturing*, 12, pp.240-251.

Cheng, A., Humayun, A., Boyan, B. and Schwartz, Z., 2016. Enhanced Osteoblast Response to Porosity and Resolution of Additively Manufactured Ti-6Al-4V Constructs with Trabeculae-Inspired Porosity. *3D Printing and Additive Manufacturing*, 3(1), pp.10-21.

Cheng, C., K. and Woo, S., Y., 2020. *Frontiers in orthopaedic biomechanics*. Singapore: Springer.

Chepelev, L., Giannopoulos, A., Tang, A., Mitsouras, D. and Rybicki, F., 2017. Medical 3D printing: methods to standardize terminology and report trends. *3D Printing in Medicine*, 3(1).

Chiu, S. and Wan, K., 2019. Use of Three-Dimensional Printing Techniques in the Management of a Patient Suffering From Traumatic Loss of the Talus. *The Journal of Foot and Ankle Surgery*, 58(1), pp.176-183.

Christodoulou, N., 2017. The unknown Greek roots of the term OrthopEdics/OrthopAEdics. It is time to establish a universally acceptable and unique writing only with an E. *Acta Orthopaedica Et Traumatologica Hellenica*, 68(4), pp.114-115.

Choi, J. and Ro, J., 2021. The 2020 WHO Classification of Tumors of Bone: An Updated Review. *Advances in Anatomic Pathology*, 28(3), pp.119-138.

Choo, Y.J., Boudier-Revéret, M. and Chang, M.C., 2020. 3D printing technology applied to orthosis manufacturing: narrative review. *Annals of palliative medicine*, 9(6), pp.4262-4270.

Chung, K., Hong, D., Kim, Y., Yang, I., Park, Y. and Kim, H., 2014. Preshaping Plates for Minimally Invasive Fixation of Calcaneal Fractures Using a Real-Size 3D-Printed Model as a Preoperative and Intraoperative Tool. *Foot & Ankle International*, 35(11), pp.1231-1236.

Cieza, A., Causey, K., Kamenov, K., Hanson, S., Chatterji, S. and Vos, T., 2020. Global estimates of the need for rehabilitation based on the Global Burden of Disease study 2019: a systematic analysis for the Global Burden of Disease Study 2019. *The Lancet*, 396(10267), pp.2006-2017.

Cignoni, P., Callieri, M., Corsini, M., Dellepiane, M., Ganovelli, F. and Ranzuglia, G., 2008. MeshLab: an Open-Source Mesh Processing Tool. *Sixth Eurographics Italian Chapter Conference*, pp.129-136.

Cima, L. and Cima, M., 1996. *Preparation of medical devices by solid free-form fabrication methods*. US Patent No. 5490962.

Ciraud, P., 1973. *Verfahren und vorrichtung zur herstellung beliebiger gegenstaende aus beliebigem schmelzbarem material*. DE Patent No. 2263777.

Cloake T, Jeys L., 2016. How important are surgical margins in Osteosarcoma?. *Journal of Bone and Soft Tissue Tumors*, 2(1), pp.22-26.

Condino, S., Turini, G., Parchi, P., Viglialoro, R., Piolanti, N., Gesi, M., Ferrari, M. and Ferrari, V., 2018. How to Build a Patient-Specific Hybrid Simulator for Orthopaedic Open Surgery: Benefits and Limits of Mixed-Reality Using the Microsoft HoloLens. *Journal of Healthcare Engineering*, 2018, pp.1-12.

Conner, B., Manogharan, G., Martof, A., Rodomsky, L., Rodomsky, C., Jordan, D. and Limperos, J., 2014. Making sense of 3-D printing: Creating a map of additive manufacturing products and services. *Additive Manufacturing*, 1-4, pp.64-76.

Corona-Castuera, J., Rodriguez-Delgado, D., Henao, J., Castro-Sandoval, J.C. and Poblano-Salas, C.A., 2021. Design and fabrication of a customized partial hip prosthesis employing CT-scan data and lattice porous structures. *ACS Omega*, 6(10), pp.6902-6913.

Corsini, L., Aranda-Jan, C.B. and Moultrie, J., 2020. The impact of 3D printing on the Humanitarian Supply Chain. *Production Planning & Control*, 33(6-7), pp.692-704.

Correa, A., Crossley, M., Kim, J. and Pandy, G., 2010. Contributions of individual muscles to hip joint contact force in normal walking. *Journal of Biomechanics*, 43(8), pp.1618-1622.

Costabile, G., Ferab, M., Fruggieroc, F., Lambiasea, A. and Pham, D., 2017. Cost models of Additive Manufacturing: A literature review. *International Journal of Industrial Engineering Computations*, pp.263-283.

Cox, S., Jamshidi, P., Eisenstein, N., Webber, M., Hassanin, H., Attallah, M., Shepherd, D., Addison, O. and Grover, L., 2016. Adding functionality with additive manufacturing: Fabrication of titanium-based antibiotic eluting implants. *Materials Science and Engineering: C*, 64, pp.407-415.

Cronskär, M., Bäckström, M. and Rännar, L., 2013. Production of customized hip stem prostheses – a comparison between conventional machining and electron beam melting (EBM). *Rapid Prototyping Journal*, 19(5), pp.365-372.

Crump, S., 1992. *Apparatus and method for creating three-dimensional object*. US Patent No. 5121329.

Cruz-Neira, C., 1993. Virtual reality overview. *SIGGRAPH 93 Course Notes 2First International Conference on Computer Graphics and Interactive Techniques, Orange County Convention Center*, Orlando, FL.

Cui, B., Tao, W. and Zhao, H., 2021. High-Precision 3D Reconstruction for Small-to-Medium-Sized Objects Utilizing Line-Structured Light Scanning: A Review. *Remote Sensing*, 13(21).

Culmone, C., Smit, G. and Breedveld, P., 2019. Additive manufacturing of medical instruments: A state-of-the-art review. *Additive Manufacturing*, 27, pp.461-473.

Cvrček, L., Denk, F. and Čejka, Z., 2020. Comparison of 3D printed trabecular structure with porous plasma spray: A method based on mapping the local modulus of elasticity. *Materials Research Express*, 7(7).

D'Amelio, A., Van Lieshout, E., Wakker, M., Verhofstad, J. and Van Vledder, G., 2022. 3D-printed patient specific instruments for corrective osteotomies of the lower extremity. *Injury*, 53.

D'Urso, P., 2005. Real virtuality: Beyond the image. In: *Virtual Modelling and Rapid Manufacturing: Advanced Research in Virtual and Rapid Prototyping.* Ed. By Bartolo, P., et al. London: Taylor and Francis.

D'Urso, P., 2017. Is patenting medical devices still viable?. *MedCrave Online Journal of Surgery*. 4(2).

D'Urso, P., Thompson, R. and Earwaker, W., 2000. Stereolithographic (SL) biomodelling in palaeontology: a technical note. *Rapid Prototyping Journal*, 6(3), pp.212-216.

Dahake, S., Kuthe, A., Mawale, M. and Bagde, A., 2016. Applications of medical rapid prototyping assisted customized surgical guides in complex surgeries. *Rapid Prototyping Journal*, 22(6), pp.934-946.

Dallago, M., Winiarski, B., Zanini, F., Carmignato, S. and Benedetti, M., 2019. On the effect of geometrical imperfections and defects on the fatigue strength of cellular lattice structures additively manufactured via Selective Laser Melting. *International Journal of Fatigue*, 124, pp.348-360.

Dall'Ava, L., Hothi, H., Henckel, J., Hart, A., 2019a. 3D Printed Acetabular Cups for Total Hip Arthroplasty: A Review Article. *Metals*, 9(7).

Dall'Ava, L., Hothi, H., Henckel, J., Di Laura, A., Shearing, P. and Hart, A., 2019b. Comparative analysis of current 3D printed acetabular titanium implants. *3D Printing in Medicine*, 5(1).

Dall'Ava, L., Hothi, H., Henckel, J., Di Laura, A., Shearing, P. and Hart, A., 2020. Characterization of dimensional, morphological and morphometric features of retrieved 3D-printed acetabular cups for hip arthroplasty. *Journal of Orthopaedic Surgery and Research*, 15(1).

Dall'Ava, L., Hothi, H., Henckel, J., Di Laura, A., Tirabosco, R., Eskelinen, A., Skinner, J. and Hart, A., 2021. Osseointegration of retrieved 3D-printed, off-the-shelf acetabular implants. *Bone & Joint Research*, 10(7), pp.388-400.

Damm, P., Graichen, F., Rohlmann, A., Bender, A. and Bergmann, G., 2010. Total hip joint prosthesis for in vivo measurement of forces and moments. *Medical Engineering & Physics*, 32(1), pp.95-100.

Danker, S., Mericli, A., Rice, D., Santos, D. and Butler, C., 2021. Custom 3D-printed Titanium Implant for Reconstruction of a Composite Chest and Abdominal Wall Defect. *Plastic and Reconstructive Surgery - Global Open*, 9(11).

Daoud, G., Pezzutti, D., Dolatowski, C., Carrau, R., Pancake, M., Herderick, E. and VanKoevering, K., 2021. Establishing a point-of-care additive manufacturing workflow for clinical use. *Journal of Materials Research*, 36(19), pp.3761-3780.

Davila, S., Rodríguez, L., Chiussi, S., Serra, J. and González, P., 2021. How to Sterilize Polylactic Acid Based Medical Devices?. *Polymers*, 13(13).

Davoodi, E., Montazerian, H., Mirhakimi, A., Zhianmanesh, M., Ibhadode, O., Shahabad, S., Esmaeilizadeh, R., Sarikhani, E., Toorandaz, S., Sarabi, S., Nasiri, R., Zhu, Y., Kadkhodapouri, J., Li, B., Khademhosseini, A. and Toyserkani, E., 2022. Additively manufactured metallic biomaterials. *Bioactive Materials*, 15, pp.214-249.

Deckard, C., 1989. *Method and apparatus for producing parts by selective sintering*. US Patent No. 4863538.

Deering, J., Dowling, K., DiCecco, L., McLean, G., Yu, B. and Grandfield, K., 2021. Selective Voronoi tessellation as a method to design anisotropic and biomimetic implants. *Journal of the Mechanical Behavior of Biomedical Materials*, 116.

Deering, J., Mahmoud, D., Rier, E., Lin, Y., do Nascimento Pereira, A., Titotto, S., Fang, Q., Wohl, G., Deng, F., Grandfield, K., Elbestawi, M. and Chen, J., 2023. *Osseointegration of functionally-graded ti6al4v porous implants: Histology of the pore network* [Preprint].

de Kater, E., Sakes, A., Edström, E., Elmi-Terander, A., Kraan, G. and Breedveld, P., 2022. Beyond the pedicle screw–a patent review. *European Spine Journal*, 31, pp.1553-1565.

De Martino, I., De Santis, V., Sculco, P., D'Apolito, R., Poultsides, L. and Gasparini, G., 2016. Long-Term Clinical and Radiographic Outcomes of Porous Tantalum Monoblock Acetabular Component in Primary Hip Arthroplasty: A Minimum of 15-Year Follow-Up. *The Journal of Arthroplasty*, 31(9), pp.110-114.

Deng, L., Zhao, X., Wei, C., Qu, W., Yu, L. and Zhu, S., 2019. Application of a three-dimensional printed segmental scapula prosthesis in the treatment of scapula tumors. *Journal of International Medical Research*, 47(11), pp.5873-5882.

Dewey, M.J., Chang, R.S.H., Nosatov, A.V., Janssen, K., Crotts, S.J., Hollister, S.J. and Harley, B.A.C., 2023. Generative design approach to combine architected Voronoi foams with porous collagen scaffolds to create a tunable composite biomaterial. bioRxiv [Preprint].

Di Prima, M., Coburn, J., Hwang, D., Kelly, J., Khairuzzaman, A. and Ricles, L., 2016. Additively manufactured medical products – the FDA perspective. *3D Printing in Medicine*, 2(1).

Diegel, O., Nordin, A. and Motte, D., 2019. *A practical guide to design for additive manufacturing*. Singapore: Springer.

Diez-Escudero, A., Andersson, B., Carlsson, E., Recker, B., Link, H., Järhult, J. and Hailer, N., 2021. 3D-printed porous Ti6Al4V alloys with silver coating combine osteocompatibility and antimicrobial properties. *Materials Science and Engineering: C*.

DiMatteo, P., 1976. *Method of Generating and Constructing Three-Dimensional Bodies*. US Patent No. 3932923.

DIN, 2003. *Manufacturing processes: Terms and definitions, division*. DIN 8580.

Ding, J., Baumers, M., Clark A.E., Wildman R.D., 2021. The economics of Additive Manufacturing: Towards a general cost model including process failure. *International Journal of Production Economics*, 237.

Doerner, R., Broll, W., Grimm, P. and Jung, B., 2022. *Virtual and Augmented Reality (VR/AR)*. Cham: Springer International Publishing.

Dohan Ehrenfest, D., Coelho, P., Kang, B., Sul, Y. and Albrektsson, T., 2010. Classification of osseointegrated implant surfaces: materials, chemistry and topography. *Trends in Biotechnology*, 28(4), pp.198-206.

Domsta, V. and Seidlitz, A., 2021. 3D-Printing of Drug-Eluting Implants: An Overview of the Current Developments Described in the Literature. *Molecules*, 26(13).

Donati, F., Di Giacomo, G., D'Adamio, S., Ziranu, A., Careri, S., Rosa, M. and Maccauro, G., 2016. Silver-Coated Hip Megaprosthesis in Oncological Limb Savage Surgery. *BioMed Research International*, 2016, pp.1-6.

Dong, E., Wang, L., Iqbal, T., Li, D., Liu, Y., He, J., Zhao, B. and Li, Y., 2018. Finite Element Analysis of the Pelvis after Customized Prosthesis Reconstruction. *Journal of Bionic Engineering*, 15, pp.443-451.

Dong, J., Li, Y., Lin, P., Leeflang, M., van Asperen, S., Yu, K., Tümer, N., Norder, B., Zadpoor, A. and Zhou, J., 2020. Solvent-cast 3D printing of magnesium scaffolds. *Acta Biomaterialia*, 114, pp.497-514.

Döring, K., Staats, K., Puchner, S. and Windhager, R., 2021. Patient-Specific Implants for Pelvic Tumor Resections. *Journal of Personalized Medicine*, 11(8).

Dotan, A., Dadia, S., Bickels, J., Nirkin, A., Flusser, G., Issakov, J., Neumann, Y., Cohen, I., Ben-Arush, M., Kollender, Y. and Meller, I., 2010. Expandable endoprosthesis for limb-sparing surgery in children: Long-term results. *Journal of Children's Orthopaedics*, 4(5), pp.391-400.

Durand-Hill, M., Henckel, J., Di Laura, A. and Hart, A., 2020. Can custom 3D printed implants successfully reconstruct massive acetabular defects? A 3D-CT assessment. *Journal of Orthopaedic Research*, 38(12), pp.2640-2648.

Echeta, I., Feng, X., Dutton, B., Leach, R. and Piano, S., 2019. Review of defects in lattice structures manufactured by powder-bed fusion. *The International Journal of Advanced Manufacturing Technology*, 106(5-6), pp.2649-2668.

Edmonds, D. and McAninch, M., 1988. *Method and apparatus for building a workpiece by deposit welding*. US Patent No. 4775092.

Ejnisman, L., Gobbato, B., de França Camargo, A. and Zancul, E., 2021. Three-Dimensional Printing in Orthopedics: from the Basics to Surgical Applications. *Current Reviews in Musculoskeletal Medicine*, 14(1), pp.1-8.

El Nihum, L., Shariff, M., Hosseini, M., Gibreel, W., Mardini, S., Morris, J., Pochettino, A. and Blackmon, S., 2022. Sternectomy Replacement with Three-Dimensional Printed Composite Porous High-Density Polyethylene. *The Annals of Thoracic Surgery*.

Elahinia, M., Shayesteh Moghaddam, N., Taheri Andani, M., Amerinatanzi, A., Bimber, B. and Hamilton, R., 2016. Fabrication of NiTi through additive manufacturing: A review. *Progress in Materials Science*, 83, pp.630-663.

Eley, K.A., 2017. Centralised 3D printing in the NHS: A Radiological Review. *Clinical Radiology*, 72(4), pp.269-275.

Elmi-Terander, A., Burström, G., Nachabé, R., Fagerlund, M., Ståhl, F., Charalampidis, A., Edström, E. and Gerdhem, P., 2020. Augmented reality navigation with intraoperative 3D imaging vs fluoroscopy-assisted free-hand surgery for spine fixation surgery: a matched-control study comparing accuracy. *Scientific Reports*, 10(1).

Emelogu, A., Marufuzzaman, M., Thompson, S., Shamsaei, N. and Bian, L., 2016. Additive manufacturing of biomedical implants: A feasibility assessment via supply-chain cost analysis. *Additive Manufacturing*, 11, pp.97-113.

Enneking, W. and Dunham, W., 1978. Resection and reconstruction for primary neoplasms involving the innominate bone. *The Journal of Bone & Joint Surgery*, 60(6), pp.731-746.

Enneking, W., 1983. *Musculoskeletal Tumor Surgery*. New York: Churchill Livingstone.

Enneking, W., 1985. Staging of musculoskeletal neoplasms. *Skeletal Radiology*, 13(3), pp.183-194.

Enneking, W., Dunham, W., Gebhardt, M., Malawar, M. and Pritchard, D., 1993. A System for the Functional Evaluation of Reconstructive Procedures After Surgical Treatment of Tumors of the Musculoskeletal System. *Clinical Orthopaedics And Related Research, 286*, pp.241-246.

Erikainen, S. and Chan, S., 2019. Contested futures: envisioning "Personalized," "Stratified," and "Precision" medicine. *New Genetics and Society*, 38(3), pp.308-330.

Ernst Eder, W., 2010. Engineering design science and theory of technical systems: legacy of Vladimir Hubka. *Journal of Engineering Design*, 22(5), pp.361-385.

Eschweiler, J., Fieten, L., Dell'Anna, J., Kabir, K., Gravius, S., Tingart, M. and Radermacher, K., 2012. Application and evaluation of biomechanical models and scores for the planning of total hip arthroplasty. *Proceedings of the Institution of Mechanical Engineers, Part H: Journal of Engineering in Medicine*, 226(12), pp.955-967.

Esmaeilian, B., Behdad, S. and Wang, B., 2016. The evolution and future of manufacturing: A review. *Journal of Manufacturing Systems*, 39, pp.79-100.

Espalin, D., Muse, D., MacDonald, E. and Wicker, R., 2014. 3D Printing multifunctionality: structures with electronics. *The International Journal of Advanced Manufacturing Technology*, 72(5-8), pp.963-978.

Fan, H., Fu, J., Li, X., Pei, Y., Li, X., Pei, G. and Guo, Z., 2015. Implantation of customized 3-D printed titanium prosthesis in limb salvage surgery: a case series and review of the literature. *World Journal of Surgical Oncology*, 13(1).

Fang, X., Liu, H., Xiong, Y., Zhang, W., Luo, Y., Wu, F., Zhou, Y., Song, L., Yu, Z., Tu, C. and Duan, H., 2018. Total talar replacement with a novel 3D printed modular prosthesis for tumors. *Therapeutics and Clinical Risk Management*, Volume 14, pp.1897-1905.

FDA, 2014. *Custom Device Exemption*. [Online] Available at: https://www.fda.gov/media/89897/download [Accessed 9 March 2022].

FDA, 2017. *Technical Considerations for Additive Manufactured Medical Devices*. [Online] Available at: https://www.fda.gov/media/97633/download [Accessed 9 March 2022].

FDA, 2021. *3D Printing Medical Devices at the Point of Care: Discussion Paper*. [Online] Available at: https://www.fda.gov/medical-devices/3d-printing-medical-devices/3d-printing-medical-devices-point-care-discussion-paper [Accessed 9 March 2022].

Fedorov, A., Beichel, R., Kalpathy-Cramer, J., Finet, J., Fillion-Robin, J. C., Pujol, S., Bauer, C., Jennings, D., Fennessy, F., Sonka, M., Buatti, J., Aylward, S., Miller, J. V., Pieper, S. and Kikinis, R., 2012. 3D Slicer as an Image Computing Platform for the Quantitative Imaging Network. *Magnetic Resonance Imaging*, 30(9), pp.1323–1341.

Feng, J., Fu , J., Yao, X. and He, Y., 2022. Triply periodic minimal surface (TPMS) porous structures: from multi-scale design, precise additive manufacturing to multidisciplinary applications. *International Journal of Extreme Manufacturing*, 4(2).

Ferraris, S., Spriano, S., 2021. Porous Titanium by Additive Manufacturing: A Focus on Surfaces for Bone Integration. *Metals*, 11.

Feygin, M., Gilad, S., Dollberg, Y., Ben-Ezra, B., Sheinman, Y., Barequet, G., Nagler, M., Bieber, A. and Katz, M., 1988. *Apparatus and method for forming an integral object from laminations*. US Patent No. 4752352.

Fillat-Gomà, F., Marcano-Fernández, F., Coderch-Navarro, S., Martínez-Carreres, L. and Berenguer, A., 2021. 3D printing innovation: New insights into upper extremity surgery planning. *Injury*, 52, pp.117-124.

Fink, J., DiNovo, S., Ward, T., 1994. *Rapid, customised bone prosthesis*. US Patent No. 5370692.

Florea, D., Albuleț, D., Grumezescu, A. and Andronescu, E., 2020. Surface modification – A step forward to overcome the current challenges in orthopedic industry and to obtain an improved osseointegration and antimicrobial properties. *Materials Chemistry and Physics*, 243.

Fitzwater, K., Marcellin-Little, D., Harrysson, O., Osborne, J. and Poindexter, E., 2011. Evaluation of the effect of computed tomography scan protocols and freeform fabrication methods on bone biomodel accuracy. *American Journal of Veterinary Research*, 72(9), pp.1178-1185.

Floriane, L., Frédéric, S., Gianluca, D. and Marc, L., 2016. Enriching design with X through tailored additive manufacturing knowledge: a methodological proposal. *International Journal on Interactive Design and Manufacturing (IJIDeM)*, 11(2), pp.279-288.

Flynn, J., Shokrani, A., Newman, S. and Dhokia, V., 2016. Hybrid additive and subtractive machine tools – Research and industrial developments. *International Journal of Machine Tools and Manufacture*, 101, pp.79-101.

Fogarasi, M., Snodderly, K.L. and Di Prima, M.A., 2023. A survey of additive manufacturing trends for FDA-cleared Medical Devices. *Nature Reviews Bioengineering* [Preprint].

Formlabs, 2021. *The Ultimate Guide to Quality Assurance and Regulatory Affairs in Medical 3D printing*. Available at: https://3d.formlabs.com/white-paper-the-ultimate-guide-to-quality-assurance-and-regulatory-affairs-in-medical-3d-printing/ [Accessed 9 March 2022].

Ford, S. and Despeisse, M., 2016. Additive manufacturing and sustainability: an exploratory study of the advantages and challenges. *Journal of Cleaner Production*, 137, pp.1573-1587.

Foukas, A., Hadjimichael, A., Nicolaou, C., Savvidou, O. and Papagelopoulos, P., 2024. A 3D-printed load sharing implant achieved union of a 9-cm femoral segmental bone defect within three months using a hybrid Masquelet induction membrane technique. A case-report. *Trauma Case Reports*, 49(1).

Fousová, M., Vojtěch, D., Kubásek, J., Dvorský, D. and Machová, M., 2015. 3D Printing as an Alternative to Casting, Forging and Machining Technologies? *Manufacturing Technology*, 15(5), pp.809-814.

Fratzl, P. and Weinkamer, R., 2007. Nature's hierarchical materials. *Progress in Materials Science*, 52(8), pp.1263-1334.

Frayssinet, E., Colabella, L. and Cisilino, A., 2022. Design and assessment of the biomimetic capabilities of a Voronoi-based cancellous microstructure. *Journal of the Mechanical Behavior of Biomedical Materials*, 130.

Frizziero, L., Santi, G., Liverani, A., Giuseppetti, V., Trisolino, G., Maredi, E. and Stilli, S., 2019. Paediatric Orthopaedic Surgery with 3D Printing: Improvements and Cost Reduction. *Symmetry*, 11(10).

Frizziero, L., Santi, G., Leon-Cardenas, C., Ferretti, P., Sali, M., Gianese, F., Crescentini, N., Donnici, G., Liverani, A., Trisolino, G., Zarantonello, P., Stallone, S. and Di Gennaro, G., 2021. Heat Sterilization Effects on Polymeric, FDM-Optimized Orthopedic Cutting Guide for Surgical Procedures. *Journal of Functional Biomaterials*, 12(4).

Frontera, E., 1967. *Sculpturing of art figures*. US Patent No. 3301725.

Fudim, E., 1988. *Method and apparatus for production of three-dimensional objects by photosolidification*. US Patent No. 475249.

Fujiwara, T., Ogura, K., Christ, A., Bartelstein, M., Kenan, S., Fabbri, N. and Healey, J., 2021. Periacetabular reconstruction following limb-salvage surgery for pelvic sarcomas. *Journal of Bone Oncology*, 31.

Fukuda, H., 2015. Additive Manufacturing Technology for Orthopedic Implants. In: *Advances in Metallic Biomaterials: Processing and Applications*. Ed. by Niinomi, M., Narushima, T. and Nakai, M. Berlin: Springer.

Furlong, R. and Osborn, J., 1991. Fixation of hip prostheses by hydroxyapatite ceramic coatings. *The Journal of Bone and Joint Surgery. British volume*, 73-B(5), pp.741-745.

Furman, A. and Hsu, W., 2021. Augmented Reality (AR) in Orthopedics: Current Applications and Future Directions. *Current Reviews in Musculoskeletal Medicine*, 14(6), pp.397-405.

Furqan, S., Omar, O., Felicia, S., Anders, S., Lena, E., Birgitta, N., Jukka, L., Peter, T. and Anders, P., 2016. Long-term osseointegration of 3D printed CoCr implants with an interconnected open-pore architecture. *Frontiers in Bioengineering and Biotechnology*, 4.

Gaalen, J., Trejos, A., Nikolov, H., Ivanov, T., Pollman, S. and Holdsworth, D., 2016. Versatile smart hip implant technology using 3D metal printing. *2016 IEEE International Symposium on Circuits and Systems (ISCAS)*, pp.2731-2734.

Galois, L. and Mainard, D., 2004. Bone ingrowth into two porous ceramics with different pore sizes: An experimental study. *Acta Orthopaedica Belgica*, 70, pp.598-603.

Gallo, J., Holinka, M. and Moucha, C., 2014. Antibacterial Surface Treatment for Orthopaedic Implants. *International Journal of Molecular Sciences*, 15(8), pp.13849-13880.

Gao, W., Zhang, Y., Ramanujan, D., Ramani, K., Chen, Y., Williams, C., Wang, C., Shin, Y., Zhang, S. and Zavattieri, P., 2015. The status, challenges, and future of additive manufacturing in engineering. *Computer-Aided Design*, 69, pp.65-89.

Gao, H., Yang, J., Jin, X., Qu, X., Zhang, F., Zhang, D., Chen, H., Wei, H., Zhang, S., Jia, W., Yue, B. and Li, X., 2021. Porous tantalum scaffolds: Fabrication, structure, properties, and orthopedic applications. *Materials & Design*, 210.

Garot, C., Bettega, G. and Picart, C., 2021. Additive Manufacturing of Material Scaffolds for Bone Regeneration: Toward Application in the Clinics. *Advanced Functional Materials*, 31(5).

García, R.I., Jauregui, I., Del Amo, C., Gandiaga, A., Rodriguez, O., Margallo, L., Voces, R., Martin, N., Gallego, I., Minguez, R. and Eguiraun, H., 2022. Implementation of an in-house 3D manufacturing unit in a public hospital's Radiology Department. *Healthcare*, 10(9).

Gaskin, T., 1973. *Earth Science Teaching Device*. US Patent No. 3751827.

Gauci, M., 2022. Patient-specific guides in orthopedic surgery. *Orthopaedics & Traumatology: Surgery & Research*, 108(1).

Gastaldi, G., Asti, A., Scaffino, M., Visai, L., Saino, E., Cometa, A. and Benazzo, F., 2010. Human adipose-derived stem cells (hASCs) proliferate and differentiate in osteoblast-like cells on trabecular titanium scaffolds. *Journal of Biomedical Materials Research Part A*.

Gebhardt, A. and Hötter, J., 2016. *Additive Manufacturing: 3D Printing for Prototyping and Manufacturing*. München: Hanser.

Gemalmaz, H., Sarıyılmaz, K., Ozkunt, K., Sungur, M., Kaya, I. and Dikici, F., 2018. A Novel 3D Printed Custom Antibiotic Spacer Mold for Osteomyelitis Cases which are Prone to Instability. *Gazi Medical Journal*, 29(3).

Geng, X., Li, Y., Li, F., Wang, X., Zhang, K., Liu, Z. and Tian, H., 2020. A new 3D printing porous trabecular titanium metal acetabular cup for primary total hip arthroplasty: a minimum 2-year follow-up of 92 consecutive patients. *Journal of Orthopaedic Surgery and Research*, 15(1).

Ghaziani, A., Soheilifard, R. and Kowsar, S., 2021. The effect of functionally graded materials on bone remodeling around osseointegrated trans-femoral prostheses. *Journal of the Mechanical Behavior of Biomedical Materials*, 118.

Ghosh, R., Pal, B., Ghosh, D. and Gupta, S., 2013. Finite Element Analysis of a hemi-pelvis: The effect of inclusion of cartilage layer on acetabular stresses and strain. *Computer Methods in Biomechanics and Biomedical Engineering*, 18(7), pp.697-710.

Ghouse, S., Reznikov, N., Boughton, O., Babu, S., Ng, K., Blunn, G., Cobb, J., Stevens, M. and Jeffers, J., 2019. The design and in vivo testing of a locally stiffness-matched porous scaffold. *Applied Materials Today*, 15, pp.377-388.

Giannatsis, J. and Dedoussis, V., 2007. Additive fabrication technologies applied to medicine and health care: a review. *The International Journal of Advanced Manufacturing Technology*, 40(1-2), pp.116-127.

Gibson, L. and Ashby, M., 1999. *Cellular solids*. 2nd ed. Cambridge: Cambridge University Press.

Gibson, L., Ashby, M. and Harley, B., 2010. *Cellular materials in nature and medicine*. Cambridge: Cambridge University Press.

Gibson, I., Rosen, D., Stucker, B. and Khorasani, M., 2021. *Additive manufacturing technologies*. 3rd ed. Cham: Springer.

Girard, J., 2015. Femoral head diameter considerations for primary total hip arthroplasty. *Orthopaedics and Traumatology: Surgery and Research*, 101(1), pp.S25-S29.

Gómez, S., Vlad, M., López, J. and Fernández, E., 2016. Design and properties of 3D scaffolds for bone tissue engineering. *Acta Biomaterialia*, 42, pp.341-350.

Gonzalez Alvarez, A., Evans, P., Dovgalski, L. and Goldsmith, I., 2021. Design, additive manufacture and clinical application of a patient-specific titanium implant to anatomically reconstruct a large chest wall defect. *Rapid Prototyping Journal*, 27(2), pp.304-310.

González-Alonso, M., Hermida-Sánchez, M., Martínez-Seijas, P. and Ruano-Ravina, A., 2020. Application of 3D printing in the treatment of appendicular skeleton fractures: Systematic review and meta-analysis. *Journal of Orthopaedic Research*, 39(10), pp.2083-2092.

Goodman, S., Yao, Z., Keeney, M. and Yang, F., 2013. The future of biologic coatings for orthopaedic implants. *Biomaterials*, 34(13), pp.3174-3183.

Gortzak, Y., Sofer, S., Ran, Y., Rumack, N., Elias, A., Efrima, B., Golden, E., Segal, O., Merose, O., Sternheim, A. and Dadia, S., 2022. Internal Hemipelvectomy for primary bone sarcomas using intraoperative patient specific instruments- the next step in limb salvage concept. *BMC Musculoskeletal Disorders*, 23(1).

Gouin, F., Paul, L., Odri, G. and Cartiaux, O., 2014. Computer-Assisted Planning and Patient-Specific Instruments for Bone Tumor Resection within the Pelvis: A Series of 11 Patients. *Sarcoma*, 2014, pp.1-9.

Govindaraj, S. and Muthuraman, M., 2015. Systematic Review on Sterilization Methods of Implants and Medical Devices. *International Journal of ChemTech Research*, 8(2), pp.897-911.

Gray, H., 2000. Anatomy of the human body. New York: Bartleby.com. [Online] Available at: https://www.bartleby.com/107/ [Accessed 9 March 2022].

Gerscovich, D., Schwing, C. and Unger, A., 2017. Long-term results of a porous tantalum monoblock tibia component: clinical and radiographic results at follow-up of 10 years. *Arthroplasty Today*, 3(3), pp.192-196.

Gerup, J., Soerensen, C. and Dieckmann, P., 2020. Augmented reality and mixed reality for healthcare education beyond surgery: an integrative review. *International Journal of Medical Education*, 11, pp.1-18.

Gridlogics Technologies, 2014. *3D Printing: Technology Insight Report*.

Gristina, A., 1987. Biomaterial-Centered Infection: Microbial Adhesion Versus Tissue Integration. *Science*, 237(4822), pp.1588-1595.

Gruber, M., Jesenko, M., Burghuber, J., Hochreiter, J., Ritschl, P. and Ortmaier, R., 2020. Functional and radiological outcomes after treatment with custom-made acetabular components in patients with Paprosky type 3 acetabular defects: short-term results. *BMC Musculoskeletal Disorders*, 21(1).

Gruber, S., Grunert, C., Mirko, R., Lopez, E., Marquardt, A., Brueckner, F. and Leyens, C., 2020. Comparison of dimensional accuracy and tolerances of powder bed based and nozzle based additive manufacturing processes. *Journal of Laser Applications*, 32.

Grynol, B., 2015. Disruptive manufacturing: The effects of 3D printing. *Deloitte*. [Online] Available at: https://www2.deloitte.com/content/dam/Deloitte/ca/Documents/insights-and-issues/ca-en-insights-issues-disruptive-manufacturing.pdf [Accessed 9 March 2022].

Gu, Y., Sun, Y., Shujaat, S., Braem, A., Politis, C. and Jacobs, R., 2022. 3D-printed porous Ti6Al4V scaffolds for long bone repair in animal models: a systematic review. *Journal of Orthopaedic Surgery and Research*, 17(1).

Guariento, L., 2021. *Design automation of lattice-based customized orthopedic for load-bearing implants* (doctoral thesis). Università degli Studi di Firenze – School of Engineering.

Günther, F., Wagner, M., Pilz, S., Gebert, A. and Zimmermann, M., 2021. Design procedure for triply periodic minimal surface based biomimetic scaffolds. *Journal of the Mechanical Behavior of Biomedical Materials*, 126.

Guo, L., Ataollah Naghavi, S., Wang, Z., Nath Varma, S., Han, Z., Yao, Z., Wang, L., Wang, L. and Liu, C., 2022. On the design evolution of hip implants: A review. *Materials and Design*, 216.

Gupta, D., Hassanien, A. and Khanna, A., 2020. *Advanced computational intelligence techniques for virtual reality in healthcare*. Cham: Springer.

Ha, Y., Yoo, J., Lee, Y., Kim, J. and Koo, K., 2012. Acetabular Component Positioning Using Anatomic Landmarks of the Acetabulum. *Clinical Orthopaedics and Related Research*, 470(12), pp.3515-3523.

Haak, D., Page, C. and Deserno, T., 2016. A Survey of DICOM Viewer Software to Integrate Clinical Research and Medical Imaging. *Journal of Digital Imaging*, 29(2), pp.206-215.

Haaker, R. and Konermann, W., 2013. *Computer and Template Assisted Orthopedic Surgery*. Berlin: Springer.

Hafez, M. and Moholkar, K., 2017. Patient-specific instruments: advantages and pitfalls, *SICOT-J*, *3*.

Hagedorn, Y., 2017. Laser additive manufacturing of ceramic components: Materials, processes, and mechanisms. In: *Laser Additive Manufacturing*. Ed. by Brandt, M. Woodhead Publishing Series in Electronic and Optical Materials. New York: Woodhead Publishing, pp.163-180.

Haleem, A., Javaid, M., Khan, R. and Suman, R., 2020. 3D printing applications in bone tissue engineering. *Journal of Clinical Orthopaedics and Trauma*, 11, pp.118-124.

Haleem, A. and Javaid, M., 2019. 3D Scanning Applications in Medical field: A Literature-based Review. *Clinical Epidemiology and Global Health 7*.

Hamid, K., Parekh, S. and Adams, S., 2016. Salvage of Severe Foot and Ankle Trauma With a 3D Printed Scaffold. *Foot & Ankle International*, 37(4), pp.433-439.

Han, Q., Wang, C., Chen, H., Zhao, X. and Wang, J., 2019. Porous Tantalum and Titanium in Orthopedics: A Review. *ACS Biomaterials Science & Engineering*, 5(11), pp.5798-5824.

Han, Q., Zhang, K., Zhang, Y., Wang, C., Yang, K., Zou, Y., Chen, B. and Wang, J., 2019. Individual resection and reconstruction of pelvic tumor with three-dimensional printed customized hemi-pelvic prosthesis. *Medicine*, 98(36).

Han, J., Kang, H., Kim, M. and Kwon, G., 2020. Mapping the intellectual structure of research on surgery with mixed reality: Bibliometric network analysis (2000–2019). *Journal of Biomedical Informatics*, 109.

Han, Y., Wei, Q., Chang, P., Hu, K., Okoro, O., Shavandi, A. and Nie, L., 2021. Three-Dimensional Printing of Hydroxyapatite Composites for Biomedical Application. *Crystals*, 11(4).

Hannibal, M. and Knight, G., 2018. Additive Manufacturing and the global factory: Disruptive Technologies and the location of International Business. *International Business Review*, 27(6), pp.1116-1127.

Hanks, B., Berthel, J., Frecker, M. and Simpson, T., 2020. Mechanical properties of additively manufactured metal lattice structures: Data review and design interface. *Additive Manufacturing*, 35.

Hansen, D., 2008. Metal Corrosion in the Human Body: The Ultimate Bio-Corrosion Scenario. *The Electrochemical Society Interface*, 17(2), pp.31-34.

Hara, D., Nakashima, Y., Sato, T., Hirata, M., Kanazawa, M., Kohno, Y., Yoshimoto, K., Yoshihara, Y., Nakamura, A., Nakao, Y., 2016. Bone bonding strength of diamond-structured porous titanium-alloy implants manufactured using the electron beam-melting technique. *Materials Science and Engineering C: Materials for Biological Applications*. 59, pp.1047-1052.

Harrison, C., Thomson, A., Cutts, S., Rowe, P. and Riches, P., 2014. Research Synthesis of Recommended Acetabular Cup Orientations for Total Hip Arthroplasty. *The Journal of Arthroplasty*, 29(2), pp.377-382.

Harrison, R.P., Rucka, S., Rafiqb, Q.A. and Medcalf, N., 2018. Decentralised manufacturing of cell and gene therapy products: Learning from other healthcare sectors. *Biotechnology Advances*, 36(2), pp.345-357.

Harrysson, O., Cansizoglu, O., Marcellin-Little, D., Cormier, D. and West, H., 2008. Direct metal fabrication of titanium implants with tailored materials and mechanical properties using electron beam melting technology. *Materials Science and Engineering: C*, 28(3), pp.366-373.

Hasanov, S., Alkunte, S., Rajeshirke, M., Gupta, A., Huseynov, O., Fidan, I., Alifui-Segbaya, F. and Rennie, A., 2021. Review on Additive Manufacturing of Multi-Material Parts: Progress and Challenges. *Journal of Manufacturing and Materials Processing*, 6(1).

Hasegawa, K., Kabata, T., Kajino, Y., Inoue, D. and Tsuchiya, H., 2017. Periprosthetic Occult Fractures of the Acetabulum Occur Frequently During Primary THA. *Clinical Orthopaedics and Related Research*, 475(2), pp.484-494.

Hedayati, R., Janbaz, S., Sadighi, M., Mohammadi-Aghdam, M. and Zadpoor, A., 2017. How does tissue regeneration influence the mechanical behavior of additively manufactured porous biomaterials?. *Journal of the Mechanical Behavior of Biomedical Materials*, 65, pp.831-841.

Heise, W., 1925. *Process for the production of sculptures*. US Patent No. 1527733.

Helgason, B., Perilli, E., Schileo, E., Taddei, F., Brynjólfsson, S. and Viceconti, M., 2008. Mathematical relationships between bone density and mechanical properties: A literature review. *Clinical Biomechanics*, 23(2), pp.135-146.

Heller, O., Bergmann, G., Kassi, P., Claes, L., Haas, P. and Duda, N., 2005. Determination of muscle loading at the hip joint for use in pre-clinical testing. *Journal of Biomechanics*, 38(5), pp.1155-1163.

Hennessy, D., Anderson, M. and Lozano-Calderon, S., 2018. Complex Pelvic Reconstruction using Patient-Specific Instrumentation and a 3D-Printed Custom Implant following Tumor Resection. *The Journal of Hip Surgery*, 2(2), pp.61-67.

Herbert, A., 1982. Solid Object Generation. *Journal of Applied Photographic Engineering*, 8(4), pp.185-188.

Herbert, A., 1989. A Review of 3D Solid Object Generation. *Journal of Imaging Technology*, 15, pp.186-190.

Hersh, A., Mahapatra, S., Weber-Levine, C., Awosika, T., Theodore, J.N., Zakaria, H.M., Liu, A., Witham, T.F. and Theodore, N., 2021. Augmented Reality in Spine Surgery: A Narrative Review. *HSS journal: the musculoskeletal journal of Hospital for Special Surgery*, 17(3), pp.351-358.

Herzog, D., Seyda, V., Wycisk, E. and Emmelmann, C., 2016. Additive manufacturing of metals. *Acta Materialia*, 117, pp.371-392.

Himmer, T., Nakagawa, T. and Anzai, M.,1999. *Lamination of metal sheets*. Computers in Industry, 39(1), pp.27-33.

Hoekstra, H., Rosseels, W., Sermon, A. and Nijs, S., 2016. Corrective limb osteotomy using patient specific 3D-printed guides: A technical note. *Injury*, 47(10), pp.2375-2380.

Hofmann, D., Kolodziejska, J., Roberts, S., Otis, R., Dillon, R., Suh, J., Liu, Z. and Borgonia, J., 2014. Compositionally graded metals: A new frontier of additive manufacturing. *Journal of Materials Research*, 29(17), pp.1899-1910.

Holzapfel, B., Reichert, J., Schantz, J., Gbureck, U., Rackwitz, L., Nöth, U., Jakob, F., Rudert, M., Groll, J. and Hutmacher, D., 2013. How smart do biomaterials need to be? A translational science and clinical point of view. *Advanced Drug Delivery Reviews*, 65(4), pp.581-603.

Holzapfel, M., Wagner, F., Martine, C., Reppenhagen, S., Rudert, M., Schuetz, M., Denham, J., Schantz, T. and Hutmacher, W., 2016. Tissue engineering and regenerative medicine in musculoskeletal oncology. *Cancer metastasis reviews*, *35*(3), pp.475-487.

Honigmann, P., Sharma, N., Schumacher, R., Rueegg, J., Haefeli, M. and Thieringer, F., 2021. In-Hospital 3D Printed Scaphoid Prosthesis Using Medical-Grade Polyetheretherketone (PEEK) Biomaterial. *BioMed Research International*, pp.1-7.

Hooper, J., Tsiridis, E., Feng, J., Schwarzkopf, R., Waren, D., Long, W., Poultsides, L., Macaulay, W., Papagiannakis, G., Kenanidis, E., Rodriguez, E., Slover, J., Egol, K., Phillips, D., Friedlander,

S. and Collins, M., 2019. Virtual Reality Simulation Facilitates Resident Training in Total Hip Arthroplasty: A Randomized Controlled Trial. *The Journal of Arthroplasty*, 34(10), pp.2278-2283.

Hopkinson, N. and Dicknes, P., 2003. Analysis of rapid manufacturing—using layer manufacturing processes for production. *Proceedings of the Institution of Mechanical Engineers, Part C: Journal of Mechanical Engineering Science*, 217(1), pp.31-39.

Horst, A. and McDonald, F., 2020. Uncertain But Not Unregulated: Medical Product Regulation in the Light of Three-Dimensional Printed Medical Products. *3D Printing and Additive Manufacturing*, 7(5), pp.248-257.

Hothi, H., Dall'Ava, L., Henckel, J., Di Laura, A., Iacoviello, F., Shearing, P. and Hart, A., 2019. Evidence of structural cavities in 3D printed acetabular cups for total hip arthroplasty. *Journal of Biomedical Materials Research Part B: Applied Biomaterials*, 108(5), pp.1779-1789.

Hothi, H., Henckel, J., Bergiers, S., Di Laura, A., Schlueter-Brust, K. and Hart, A., 2022. Morphometric analysis of patient-specifc 3D-printed acetabular cups: a comparative study of commercially available implants from 6 manufacturers. *3D Printing in Medicine*, 8(33).

Housholder, R., 1981. *Molding Process*. US Patent No. 4247508.

Hove, R., Sierevelt, I., van Royen, B. and Nolte, P., 2015. Titanium-Nitride Coating of Orthopaedic Implants: A Review of the Literature. *BioMed Research International*, 2015, pp.1-9.

Hrabe, N. and Quinn, T., 2013. Effects of processing on microstructure and mechanical properties of a titanium alloy (Ti–6Al–4V) fabricated using electron beam melting (EBM), Part 2: Energy input, orientation, and location. *Materials Science and Engineering: A*, 573, pp.271-277.

Hsu, T., Chang, H., Huang, L., Zobitz, E., Chen, P., Lai, A. and An, N., 2007. The number of screws, bone quality, and friction coefficient affect acetabular cup stability. *Medical Engineering and Physics*, 29(10), pp.1089-1095.

Hu, D., Tie, K., Yang, X., Tan, Y., Alaidaros, M. and Chen, L., 2015. Comparison of ceramic-on-ceramic to metal-on-polyethylene bearing surfaces in total hip arthroplasty: a meta-analysis of randomized controlled trials. *Journal of Orthopaedic Surgery and Research*, 10(1).

Hu, P., Wu, T., Wang, Z., Qi, Z., Yao, J., Cheng, D., Chen, W., Zhang, Z., 2017. Influence of Different Boundary Conditions in Finite Element Analysis on Pelvic Biomechanical Load Transmission. *Orthopaedic Surgery*, 9(1), pp.115-122.

Hu, X., Chen, Y., Cai, W., Cheng, M., Yan, W. and Huang, W., 2022. Computer-Aided Design and 3D Printing of Hemipelvic Endoprosthesis for Personalized Limb-Salvage Reconstruction after Periacetabular Tumor Resection. *Bioengineering*, 9(8).

Hu, X., Lu, M., Zhang, Y., Li, Z., Wang, J., Wang, Y., Xing, Z., Yang, X., Tu, C. and Min, L., 2023. Pelvic-girdle reconstruction with three-dimensional-printed endoprostheses after limb-salvage surgery for pelvic sarcomas: current landscape. *British Journal of Surgery*, 110(12), pp.1712-1722.

Huang, S., Ji, T. and Guo, W., 2019. Biomechanical comparison of a 3D-printed sacrum prosthesis versus rod-screw systems for reconstruction after total sacrectomy: A finite element analysis. *Clinical Biomechanics*, 70, pp.203-208.

Huang, J., Xie, F., Tan, X., Xing, W., Zheng, Y. and Zeng, C., 2021a. Treatment of Osteosarcoma of the Talus With a 3D-Printed Talar Prosthesis. *The Journal of Foot and Ankle Surgery*, 60(1), pp.194-198.

Huang, Y., Zhou, Y., Tian, H., Wang, J., Liu, W. and Li, H., 2021b. Minimum 7-year Follow-up of A Porous Coated Trabecular Titanium Cup Manufactured with Electron Beam Melting Technique in Primary Total Hip Arthroplasty. *Orthopaedic Surgery*, 13(3), pp.817-824.

Hubka, V. and Eder, W., 1988. *Theory of technical systems*. Berlin: Springer.

Hull, C. and Lewis, C., 1991. *Methods and apparatus for production of three-dimensional objects by stereolithography*. US Patent No. 4999143.

Hull, C., 1986. *Apparatus for production of three-dimensional objects by stereolithography*. US Patent No. 4575330.

Hung, B., Naved, B., Nyberg, E., Dias, M., Holmes, C., Elisseeff, J., Dorafshar, A. and Grayson, W., 2016. Three-Dimensional Printing of Bone Extracellular Matrix for Craniofacial Regeneration. *ACS Biomaterials Science & Engineering*, 2(10), pp.1806-1816.

Huotilainen, E., Jaanimets, R., Valášek, J., Marcián, P., Salmi, M., Tuomi, J., Mäkitie, A. and Wolff, J., 2014. Inaccuracies in additive manufactured medical skull models caused by the DICOM to STL conversion process. *Journal of Cranio-Maxillofacial Surgery*, 42(5), pp.259-265.

IDA Science and Technology Policy Institute Report, 2014. *The Role of the National Science Foundation in the Origin and Evolution of Additive Manufacturing in the United States*.

Imanishi, J. and Choong, P., 2015. Three-dimensional printed calcaneal prosthesis following total calcanectomy. *International Journal of Surgery Case Reports*, 10, pp.83-87.

IMDRF, 2020. Personalized Medical Devices - Regulatory Pathways. [Online] Available at: https://www.imdrf.org/sites/default/files/docs/imdrf/final/technical/imdrf-tech-200318-pmd-rp-n58.pdf [Accessed 9 March 2022].

Implantcast, 2019. *Case studies 2019: Tumour and revision cases*. [Online] Available at: http://oncotransfer.pl/wp-content/uploads/2021/05/C-Fit-3DR-Case-studies.pdf [Accessed 9 March 2022].

Inoue, D., Kabata, T., Kimura, H. and Tsuchiya, H., 2018. A prospective clinical trial to assess the accuracy of an MRI-based patient-specific acetabular instrument guide in total hip arthroplasty. *European Journal of Orthopaedic Surgery & Traumatology*, 29(1), pp.65-71.

Iqbal, T., Wang, L., Dong, E., Fan, H., Fu, J. and Hu, C., 2019. A general multi-objective topology optimization methodology developed for customized design of pelvic prostheses. *Medical Engineering and Physics*, 69, pp.8-16.

Iriart J., 2019. Precision medicine/personalized medicine: a critical analysis of movements in the transformation of biomedicine in the early 2First century. *Cadernos de saude publica*, *35*(3).

Isensee, F., Jaeger, P.F., Kohl, S.A., Petersen, J. and Maier-Hein, K.H., 2021. nnU-Net: a self-configuring method for deep learning-based biomedical image segmentation. *Nature methods*, 18(2), 203-211.

ISO/ASTM, 2018. *Standard Guidelines for Design for Additive Manufacturing*. ISO/ASTM52910-18.

ISO/ASTM, 2020. *Specification for additive manufacturing file format (AMF) Version 1.2*. ISO/ASTM 52915:2020.

ISO/ASTM, 2021. *Standard Terminology for Additive Manufacturing: General Principles-Terminology*. ISO/ASTM 52900:2021.

Ivanova, O., Williams, C. and Campbell, T., 2013. Additive manufacturing (AM) and nanotechnology: promises and challenges. *Rapid Prototyping Journal*, 19(5), pp.353-364.

Izatt, M., Thorpe, P., Thompson, R., D'Urso, P., Adam, C., Earwaker, J., Labrom, R. and Askin, G., 2007. The use of physical biomodelling in complex spinal surgery. *European Spine Journal*, 16(9), pp.1507-1518.

Jacofsky, D. and Allen, M., 2016. Robotics in Arthroplasty: A Comprehensive Review. *The Journal of Arthroplasty*, 31(10), pp.2353-2363.

Jaeger, S., Uhler, M., Schroeder, S., Beckmann, N. and Braun, S., 2020. Comparison of Different Locking Mechanisms in Total Hip Arthroplasty: Relative Motion between Cup and Inlay. *Materials*, 13(6).

Jahanmard, F., Dijkmans, F., Majed, A., Vogely, H., van der Wal, B., Stapels, D., Ahmadi, S., Vermonden, T. and Amin Yavari, S., 2020. Toward Antibacterial Coatings for Personalized Implants. *ACS Biomaterials Science & Engineering*, 6(10), pp.5486-5492.

Jakus, A., Rutz, A., Jordan, S., Kannan, A., Mitchell, S., Yun, C., Koube, K., Yoo, S., Whiteley, H., Richter, C., Galiano, R., Hsu, W., Stock, S., Hsu, E. and Shah, R., 2016. Hyperelastic "bone": A

highly versatile, growth factor–free, osteoregenerative, scalable, and surgically friendly biomaterial. *Science Translational Medicine*, 8(358).

Jamil, M., Rafique, S., Khan, A., Hegab, H., Mia, M., Gupta, M. and Song, Q., 2020. Comprehensive analysis on orthopedic drilling: A state-of-the-art review. *Proceedings of the Institution of Mechanical Engineers, Part H: Journal of Engineering in Medicine*, 234(6), pp.537-561.

Jamróz, W., Szafraniec, J., Kurek, M. and Jachowicz, R., 2018. 3D Printing in Pharmaceutical and Medical Applications – Recent Achievements and Challenges. *Pharmaceutical Research*, 35(9).

Javaid, M. and Haleem, A., 2018. Additive manufacturing applications in orthopaedics: A review. *Journal of Clinical Orthopaedics and Trauma*, 9(3), pp.202-206.

Javaid, M. and Haleem, A., 2020. Impact of industry 4.0 to create advancements in orthopaedics. *Journal of Clinical Orthopaedics and Trauma*, 11, pp.491-499.

Javaid, M. and Haleem, A., 2020. Significant advancements of 4D printing in the field of orthopaedics. *Journal of Clinical Orthopaedics and Trauma*, 11, pp.485-490.

Jenner, F. and Dharmani, S., 2020. *Is 3D printing's potential almost fully formed*? Ernst & Young Global Limited. [Online] Available at: https://assets.ey.com/content/dam/ey-sites/ey-com/en_gl/topics/manufacturing/ey-is-3d-printings-potential-almost-fully-formed.pdf?download [Accessed 9 March 2022].

Jentzsch, T., Vlachopoulos, L., Fürnstahl, P., Müller, D. and Fuchs, B., 2016. Tumor resection at the pelvis using three-dimensional planning and patient-specific instruments: a case series. *World Journal of Surgical Oncology*, 14(1).

Jetté, B., Brailovski, V., Dumas, M., Simoneau, C. and Terriault, P., 2018. Femoral stem incorporating a diamond cubic lattice structure: Design, manufacture and testing. *Journal of the Mechanical Behavior of Biomedical Materials*, 77, pp.58-72.

Ji, T. and Guo, W., 2019. The evolution of pelvic endoprosthetic reconstruction after tumor resection. *Annals of Joint*, 4.

Ji, T., Yang, Y., Tang, X., Liang, H., Yan, T., Yang, R. and Guo, W., 2020. 3D-Printed Modular Hemipelvic Endoprosthetic Reconstruction Following Periacetabular Tumor Resection. *Journal of Bone and Joint Surgery*, 102(17), pp.1530-1541.

Ji, Y., Wu, Y. and Li, J., 2021. Use of three-dimensional–printed custom-made prosthesis to treat unicondylar femoral defect secondary to pathological fracture caused by giant cell tumor. *Journal of International Medical Research*, 49(7).

Jia, C.Q., Zhang, Z., Cao, S.Q., Wang, T.J., Yu, H.C., Wang, W.X., Guo, B.M., Qiu, X.Y., You, Y.G., Hu, F.Q., Zhao, J. and Zhang, X.S., 2023. A biomimetic gradient porous cage with a micro-structure for enhancing mechanical properties and accelerating osseointegration in Spinal Fusion. *Bioactive Materials*, 16 (23), pp.234-246.

Jiang, M., Chen, G., Coles-Black, J., Chuen, J. and Hardidge, A., 2019. Three-dimensional printing in orthopaedic preoperative planning improves intraoperative metrics: a systematic review. *ANZ Journal of Surgery*, 90(3), pp.243-250.

Jin, Z., Zhang, Z., Demir, K. and Gu, G., 2020. Machine Learning for Advanced Additive Manufacturing. *Matter*, 3(5), pp.1541-1556.

Jing, Z., Zhang, T., Xiu, P., Cai, H., Wei, Q., Fan, D., Lin, X., Song, C. and Liu, Z., 2020. Functionalization of 3D-printed titanium alloy orthopedic implants: a literature review. *Biomedical Materials*, 15(5).

Jones, G., Jaere, M., Clarke, S. and Cobb, J., 2018. 3D printing and high tibial osteotomy. *EFORT Open Reviews*, 3(5), pp.254-259.

Jovičić, M., Vuletić, F., Ribičić, T., Šimunić, S., Petrović, T. and Kolundžić, R., 2020. Implementation of the three-dimensional printing technology in treatment of bone tumours: a case series. *International Orthopaedics*, 45(4), pp.1079-1085.

Jud, L., Fotouhi, J., Andronic, O., Aichmair, A., Osgood, G., Navab, N. and Farshad, M., 2020. Applicability of augmented reality in orthopedic surgery – A systematic review. *BMC Musculoskeletal Disorders*, 21(1).

Kadakia, R., Akoh, C., Chen, J., Sharma, A. and Parekh, S., 2020. 3D Printed Total Talus Replacement for Avascular Necrosis of the Talus. *Foot & Ankle International*, 41(12), pp.1529-1536.

Kalpakjian, S. and Schmid, S., 2017. *Manufacturing Engineering and Technology*. 8th ed. New Jersey: Pearson.

Kadir, A.Z., Yusof, Y. and Wahab, M.S., 2020. Additive Manufacturing Cost Estimation Models—A classification review. *The International Journal of Advanced Manufacturing Technology*, 107(9-10), pp.4033-4053.

Kamel, M., Cheng, A., Vaughan, B., Stiles, B., Altorki, N., Spector, J. and Port, J., 2020. Sternal Reconstruction Using Customized 3D-Printed Titanium Implants. *The Annals of Thoracic Surgery*, 109(6), pp.411-414.

Kantaros, A., Laskaris, N., Piromalis, D. and Ganetsos, T., 2021. Manufacturing Zero-waste covid-19 personal protection equipment: A case study of utilizing 3D printing while employing waste material recycling. *Circular Economy and Sustainability*, 1(3), pp.851-869.

Karageorgiou, V., Kaplan, D., 2005. Porosity of 3D biomaterial scaffolds and osteogenesis. *Biomaterials*. 26(27), pp.5474-5491.

Karipott, S., Nelson, B., Guldberg, R. and Ong, K., 2018. Clinical potential of implantable wireless sensors for orthopedic treatments. *Expert Review of Medical Devices*, 15(4), pp.255-264.

Karunakaran, R., Ortgies, S., Tamayol, A., Bobaru, F. and Sealy, M., 2020. Additive manufacturing of magnesium alloys. *Bioactive Materials*, 5(1), pp.44-54.

Kay, B., 1924. *Apparatus for building structures*. US Patent No. 1518149.

Keller, M., Guebeli, A., Thieringer, F. and Honigmann, P., 2021a. In-hospital professional production of patient-specific 3D-printed devices for hand and wrist rehabilitation. *Hand Surgery and Rehabilitation*, 40(2), pp.126-133.

Keller, M., Guebeli, A., Thieringer, F. and Honigmann, P., 2021b. Overview of In-Hospital 3D Printing and Practical Applications in Hand Surgery. *BioMed Research International*, pp.1-14.

Kelly, C., Evans, N., Irvin, C., Chapman, S., Gall, K. and Safranski, D., 2019. The effect of surface topography and porosity on the tensile fatigue of 3D printed Ti-6Al-4V fabricated by selective laser melting. *Materials Science and Engineering: C*, 98, pp.726-736.

Kelly, C., Wang, T., Crowley, J., Wills, D., Pelletier, M., Westrick, E., Adams, S., Gall, K. and Walsh, W., 2021a. High-strength, porous additively manufactured implants with optimized mechanical osseointegration. *Biomaterials*, 279.

Kelly, C., Lin, A., Leguineche, K., Shekhar, S., Walsh, W., Guldberg, R. and Gall, K., 2021b. Functional repair of critically sized femoral defects treated with bioinspired titanium gyroid-sheet scaffolds. *Journal of the Mechanical Behavior of Biomedical Materials*, 116.

Kermavnar, T., Shannon, A., O'Sullivan, K., McCarthy, C., Dunne, C. and O'Sullivan, L., 2021. Three-Dimensional Printing of Medical Devices Used Directly to Treat Patients: A Systematic Review. *3D Printing and Additive Manufacturing*, 8(6), pp.366-408.

Khakpour, S., Tanska, P., Esrafilian, A., Mononen, M., Saarakkala, S., Korhonen, R. and Jämsä, T., 2021. Effect of impact velocity, flooring material, and trochanteric soft tissue quality on acetabular fracture during a sideways fall: A parametric finite element approach. *Applied Sciences*, 11(1).

Khal, A.A, Apostu, D., Schiau, C., Bejinariu, N., Pesenti, S., Jouve, J.L., 2023. Custom-Made 3D-Printed Prosthesis after Resection of a Voluminous Giant Cell Tumour Recurrence in Pelvis. *Diagnostics*, 13(3).

Khrapov, D., Paveleva, A., Kozadayeva, M., Evsevleev, S., Mishurova, T., Bruno, G., Surmenev, R., Koptyug, A. and Surmeneva, M., 2023. Trapped powder removal from sheet-based porous structures based on triply periodic minimal surfaces fabricated by electron beam powder bed fusion. *Materials Science and Engineering: A*. 862.

Khoo, Z., Teoh, J., Liu, Y., Chua, C., Yang, S., An, J., Leong, K. and Yeong, W., 2015. 3D printing of smart materials: A review on recent progresses in 4D printing. *Virtual and Physical Prototyping*, 10(3), pp.103-122.

Kim, D., Lim, J., Shim, K., Han, J., Yi, S., Yoon, D., Kim, K., Ha, Y., Ji, G. and Shin, D., 2017. Sacral Reconstruction with a 3D-Printed Implant after Hemisacrectomy in a Patient with Sacral Osteosarcoma: 1-Year Follow-Up Result. *Yonsei Medical Journal*, 58(2).

Kirillova, A., Bushev, S., Abubakirov, A. and Sukikh, G., 2020. Bioethical and Legal Issues in 3D Bioprinting. *International Journal of Bioprinting*, 6(3).

Kirk, J. and Kirk, L., 1976. *Paper art process*. US Patent No. 3941631.

Klahn, C., Singer, D. and Meboldt, M., 2016. Design Guidelines for Additive Manufactured Snap-Fit Joints. *Procedia CIRP*, 50, pp.264-269.

Klein, H., Schneider, W., Alzen, G., Voy, E. and Günther, R., 1992. Pediatric craniofacial surgery: comparison of milling and stereolithography for 3D model manufacturing. *Pediatric Radiology*. 22, pp.458-460.

Klenerman, L., 2002. *The evolution of orthopaedic surgery*. London: Royal Society of Medicine Press.

Klette, R. and Tee, G., 2008. Understanding Human Motion: A Historic Review. In: *Human Motion: Understanding, Modelling, capture, and Animation*. Ed. by B. Rosenhahn, R. Klette and D. Metaxas. Dordrecht: Springer, pp.1-22.

Knahr, K., 2013. *Total hip arthroplasty*. Berlin: Springer.

Ko, L. and Hozack, W., 2016. The dual mobility cup. *The Bone and Joint Journal*, 98-B(1_Supple_A), pp.60-63.

Kodama, H., 1980. *Stereoscopic Figure Drawing Device*. JP Patent No. S56144478.

Kodama, H., 1981. Automatic Method for Fabricating a Three-Dimensional Plastic Model With Photo- Hardening Polymer. *Review of Scientific Instruments*, 52(11), pp.1770-1773.

Kojima, S., 1959. *Method of making laminated furniture or part*. US Patent No. 2903390.

König, M., Sundaram, R., Saville, P., Jehan, S. and Boszczyk, B., 2015. Anatomical considerations for percutaneous trans ilio-sacroiliac S1 and S2 screw placement. *European Spine Journal*, 25(6), pp.1800-1805.

Kolaitis, M., 1964. Engineer-Engineering, *Η τεχνική ανά την Υφήλιον*, 245, pp.55-58. [online] Available at: http://library.tee.gr/digital/techr/1964/techr_1964_245_55.pdf [Accessed 9 March 2022].

Kolken, H., Janbaz, S., Leeflang, S., Lietaert, K., Weinans, H. and Zadpoor, A., 2018. Rationally designed meta-implants: a combination of auxetic and conventional meta-biomaterials. *Materials Horizons*, 5(1), pp.28-35.

Kolken, H., de Jonge, C., van der Sloten, T., Garcia, A., Pouran, B., Willemsen, K., Weinans, H. and Zadpoor, A., 2021. Additively manufactured space-filling meta-implants. *Acta Biomaterialia*, 125, pp.345-357.

Kostakos, T., Nayar, S., Alcock, H., Savvidou, O., Vlasis, K. and Papagelopoulos, P., 2021. Acetabular reconstruction in oncological surgery: A systematic review and meta-analysis of implant survivorship and patient outcomes. *Surgical Oncology*, 38.

Kotlinski, J., 2014. Mechanical properties of commercial rapid prototyping materials. *Rapid Prototyping Journal*, 20(6), pp.499-510.

Kotrych, D., Angelini, A., Bohatyrewicz, A. and Ruggieri, P., 2023. 3D printing for patient-specific implants in musculoskeletal oncology. *EFORT open reviews*. 8(5), pp.331-339.

Kranz, J., Herzog, D. and Emmelmann, C., 2015. Design guidelines for laser additive manufacturing of lightweight structures in TiAl6V4. *Journal of Laser Applications*, 27(1).

Kransdorf, M. and Murphey, M., 2016. Imaging of Soft tissue Musculoskeletal Masses: Fundamental Concepts. *RadioGraphics*, 36(6), pp.1931-1948.

Krishnan, V. and Ulrich, K., 2001. Product Development Decisions: A Review of the Literature. *Management Science*, 47(1), pp.1-21.

Kruth, J., 1991. Material Incress Manufacturing by Rapid Prototyping Techniques. *CIRP Annals*, 40(2), pp.603-614.

Kulkarni, P., Marsan, A. and Dutta, D., 2000. A review of process planning techniques in layered manufacturing. *Rapid Prototyping Journal*, 6(1), pp.18-35.

Kumar, R., Pelanis, E., Bugge, R., Brun, H., Palomar, R., Aghayan, D., Fretland, Å., Edwin, B. and Elle, O., 2020. Use of mixed reality for surgery planning: Assessment and development workflow. *Journal of Biomedical Informatics*, 112.

Kumar, P., Vatsya, P., Rajnish, R., Hooda, A. and Dhillon, M., 2020. Application of 3D Printing in Hip and Knee Arthroplasty: A Narrative Review. *Indian Journal of Orthopaedics*, 55(S1), pp.14-26.

Kumar, L., Haleem, A. and Javaid, M., 2021. Impact of three dimensional printing in orthopedics. *Global Health Journal*, 5(4), pp.178-182.

Kumar, S. and Kruth, J., 2010. Composites by rapid prototyping technology. *Materials & Design*, 31(2), pp.850-856.

Kumbhar, N.N. and Mulay, A.V., 2016. Post processing methods used to improve surface finish of products which are manufactured by Additive Manufacturing Technologies: A Review. *Journal of The Institution of Engineers (India): Series C*, 99(4), pp.481-487.

Kunčická, L., Kocich, R. and Lowe, T., 2017. Advances in metals and alloys for joint replacement. *Progress in Materials Science*, 88, pp.232-280.

Lador, R., Regev, G., Salame, K., Khashan, M. and Lidar, Z., 2020. Use of 3-Dimensional Printing Technology in Complex Spine Surgeries. *World Neurosurgery*, 133, pp.327-341.

Lakshmi, U., Hofmann, M., Valencia, S., Wilcox, L., Mankoff, J. and Arriaga, R., 2019. Point-of-Care Manufacturing. *Proceedings of the ACM on Human-Computer Interaction*, 3(CSCW), pp.1-23.

Lal, H. and Patralekh, M., 2018. 3D printing and its applications in orthopaedic trauma: A technological marvel. *Journal of Clinical Orthopaedics and Trauma*, 9(3), pp.260-268.

Langer, R. and Vacanti, J., 1993. Tissue engineering. *Science*, 260(5110), pp.920-926.

Langridge, B., Momin, S., Coumbe, B., Woin, E., Griffin, M. and Butler, P., 2018. Systematic Review of the Use of 3-Dimensional Printing in Surgical Teaching and Assessment. *Journal of Surgical Education*, 75(1), pp.209-221.

Lanza, R., Langer, R., Vacanti, J., Atala, A., 2020. *Principles of Tissue Engineering*. 5th ed. Boston: Academic Press.

Laurendon, L., Philippot, R., Boyer, B., Neri, T. and Farizon, F., 2018. Ten-Year Clinical and Radiological Outcomes of 100 Total Hip Arthroplasty Cases with a Modern Cementless Dual Mobility Cup. *Surgical Technology International*, 32, pp.331-336.

Le Vay, D., 1990. *The history of orthopaedics*. New Jersey: The Parthenon Publishing Group.

Leary, M., 2020. Design for Additive Manufacturing. Oxford: Elsevier.

Ledet, E., Liddle, B., Kradinova, K. and Harper, S., 2018. Smart implants in orthopedic surgery, improving patient outcomes: a review. *Innovation and Entrepreneurship in Health*, Volume 5, pp.41-51.

Lee, H., Kim, W., Park, E., Kim, J., Kim, Y. and Lee, Y., 2019. Mid-term follow-up results of calcaneal reconstruction for calcaneal malunion. *BMC Musculoskeletal Disorders*, 20(1).

Lehmhus, D., Aumund-Kopp, C., Petzoldt, F., Godlinski, D., Haberkorn, A., Zöllmer, V. and Busse, M., 2016. Customized Smartness: A Survey on Links between Additive Manufacturing and Sensor Integration. *Procedia Technology*, 26, pp.284-301.

Levesque, J., Shah, A., Ekhtiari, S., Yan, J., Thornley, P. and Williams, D., 2020. Three-dimensional printing in orthopaedic surgery: a scoping review. *EFORT Open Reviews*, 5(7), pp.430-441.

Lewallen, E., Riester, S., Bonin, C., Kremers, H., Dudakovic, A., Kakar, S., Cohen, R., Westendorf, J., Lewallen, D. and van Wijnen, A., 2015. Biological Strategies for Improved Osseointegration and Osteoinduction of Porous Metal Orthopedic Implants. *Tissue Engineering Part B: Reviews*, 21(2), pp.218-230.

Lewinnek, G.E., Lewis, J.L., Tarr, R., Compere, C.L. and Zimmerman, J.R., 1978. Dislocations after total hip-replacement arthroplasties. *Journal of Bone and Joint Surgery*, 60(20), pp.217-2020.

Lex, J., Koucheki, R., Stavropoulos, N., Di Michele, J., Toor, J., Tsoi, K., Ferguson, P., Turcotte, R. and Papagelopoulos, P., 2022. Megaprosthesis Anti-Bacterial Coatings: A Comprehensive Translational Review. *Acta Biomaterialia*, 140(1), pp.136-148.

Li, X., Feng, Y., Wang, C., Li, G., Lei, W., Zhang, Z. and Wang, L., 2012. Evaluation of Biological Properties of Electron Beam Melted Ti6Al4V Implant with Biomimetic Coating In Vitro and In Vivo. *PLoS ONE*, 7(12).

Li, Y., Zhang, Y., Akpek, A., Shin, S. and Khademhosseini, A., 2016. 4D bioprinting: the next-generation technology for biofabrication enabled by stimuli-responsive materials. *Biofabrication*, 9(1).

Li, Q. and Mai, Y., 2017. *Biomaterials for Implants and Scaffolds*. Berlin: Springer.

Li, Z., Wang, C., Li, C., Wang, Z., Yang, F., Liu, H., Qin, Y. and Wang, J., 2018. What we have achieved in the design of 3D printed metal implants for application in orthopedics? Personal experience and review. *Rapid Prototyping Journal*, 24(8), pp.1365-1379.

Li, J. and Tanaka, H., 2018. Rapid customization system for 3D-printed splint using programmable modeling technique – a practical approach. *3D Printing in Medicine*, 4(1).

Li, D., Liao, W., Dai, N. and Xie, Y., 2019. Comparison of Mechanical Properties and Energy Absorption of Sheet-Based and Strut-Based Gyroid Cellular Structures with Graded Densities. *Materials*, 12(13).

Li, J., Cui, X., Hooper, G., Lim, K. and Woodfield, T., 2020. Rational design, bio-functionalization and biological performance of hybrid additive manufactured titanium implants for orthopaedic applications: A review. *Journal of the Mechanical Behavior of Biomedical Materials*, 105.

Li, R., Ting, Y., Youssef, S., Song, Y. and Garg, S., 2021. Three-Dimensional Printing for Cancer Applications: Research Landscape and Technologies. *Pharmaceuticals*, 14(8).

Li, B., Zhang, M., Lu, Q., Zhang, B., Miao, Z., Li, L., Zheng, T. and Liu, P., 2022. Application and Development of Modern 3D Printing Technology in the Field of Orthopedics. Applications of 3D Printing Technology in Orthopedic Treatment 2021. *BioMed Research International*, pp.1-15.

Li, Z., Lu, M., Min, L., Luo, Y., and Tu, C., 2023. Treatment of pelvic giant cell tumor by wide resection with patient-specific bone-cutting guide and reconstruction with 3D-printed personalized implant. *Journal of Orthopaedic Surgery and Research*. 18(1).

Liang, H., Ji, T., Zhang, Y., Wang, Y. and Guo, W., 2017. Reconstruction with 3D-printed pelvic endoprostheses after resection of a pelvic tumour. *The Bone & Joint Journal*, 99-B(2), pp.267-275.

Lim, S., Kathuria, H., Tan, J. and Kang, L., 2018. 3D printed drug delivery and testing systems — a passing fad or the future?. *Advanced Drug Delivery Reviews*, 132, pp.139-168.

Lim, H., Hong, S., Byeon, S., Chung, S., On, S., Yang, B., Lee, J. and Byun, S., 2020. 3D-Printed Ceramic Bone Scaffolds with Variable Pore Architectures. *International Journal of Molecular Sciences*, 21(18).

Lim, H., Ryu, M., Woo, S., Song, I., Choi, Y. and Lee, U., 2021. Bone Conduction Capacity of Highly Porous 3D-Printed Titanium Scaffolds Based on Different Pore Designs. *Materials*, 14(14).

Liu, Q., Zhang, H., Jiang, X., Qian, C., Liu, Z. and Luo, D., 2017. Factors involved in cancer metastasis: a better understanding to “seed and soil” hypothesis. *Molecular Cancer*, 16(1).

Liu, J., Gaynor, A., Chen, S., Kang, Z., Suresh, K., Takezawa, A., Li, L., Kato, J., Tang, J., Wang, C., Cheng, L., Liang, X. and To, A., 2018. Current and future trends in topology optimization for additive manufacturing. *Structural and Multidisciplinary Optimization*, 57(6), pp.2457-2483.

Liu, Y., Rath, B., Tingart, M. and Eschweiler, J., 2019. Role of implants surface modification in osseointegration: A systematic review. *Journal of Biomedical Materials Research Part A*, 108(3), pp.470-484.

Liu, Y., Pan, H., Chen, L., Ye, H., Wu, C., Wu, P. and Chen, L., 2021. Total hip revision with custom-made spacer and prosthesis: A case report. *World Journal of Clinical Cases*, 9(25), pp.7605-7613.

Liu, B., Wang, H., Zhang, N., Zhang, M. and Cheng, C., 2021. Femoral Stems With Porous Lattice Structures: A Review. *Frontiers in Bioengineering and Biotechnology*, 9.

Liu, H., Shi, W., Li, B., Cao, Y., Yin, F., Liu, R., Liu, L., Zhang, X., Li, J. and Liu, J., 2022. Enhanced osseointegration of 3D-printed cementless tibial prostheses with trabecular metal surfaces in a novel three-partition design. *Materials Today Communications*, 30.

Logo, J. and Ismail, H., 2020. Milestones in the 150-Year History of Topology Optimization: A Review. *Computer Assisted Methods in Engineering and Science*, 27(2-3), pp.97-132.

Loh, G., Pei, E., Harrison, D. and Monzón, M., 2018. An overview of functionally graded additive manufacturing. *Additive Manufacturing*, 23, pp.34-44.

Lohre, R., Warner, J., Athwal, G. and Goel, D., 2020. The evolution of virtual reality in shoulder and elbow surgery. *JSES International*, 4(2), pp.215-223.

Long, J., Zhang, W., Chen, Y., Teng, B., Liu, B., Li, H., Yao, Z., Wang, D., Li, L., Yu, X., Qin, L. and Lai, Y., 2021. Multifunctional magnesium incorporated scaffolds by 3D-Printing for comprehensive postsurgical management of osteosarcoma. *Biomaterials*, 275.

Lowther, M., Louth, S., Davey, A., Hussain, A., Ginestra, P., Carter, L., Eisenstein, N., Grover, L. and Cox, S., 2019. Clinical, industrial, and research perspectives on powder-bed fusion additively manufactured metal implants. *Additive Manufacturing*, 28, pp.565-584.

Lu, Y., Cheng, L., Yang, Z., Li, J. and Zhu, H., 2020. Relationship between the morphological, mechanical and permeability properties of porous bone scaffolds and the underlying microstructure. *PLOS ONE*, 15(9).

Luenam, S., Kosiyatrakul, A., Hansudewechakul, C., Phakdeewisetkul, K., Lohwongwatana, B. and Puncreobutr, C., 2018. The Patient-Specific Implant Created with 3D Printing Technology in Treatment of the Irreparable Radial Head in Chronic Persistent Elbow Instability. *Case Reports in Orthopedics*, 2018, pp.1-6.

Lunn, D.E., Lampropoulos, A. and Stewart, T.D., 2016. Basic biomechanics of the hip. *Orthopaedics and Trauma*, 30(3), pp.239-246.

Lunsford, C., Grindle, G., Salatin, B. and Dicianno, B., 2016. Innovations With 3-Dimensional Printing in Physical Medicine and Rehabilitation: A Review of the Literature. *PM&R*, 8(12), pp.1201-1212.

Luo, C., Wang, C., Wu, X., Xie, X., Wang, C., Zhao, C., Zou, C., Lv, F., Huang, W. and Liao, J., 2021. Influence of porous tantalum scaffold pore size on osteogenesis and osteointegration: A comprehensive study based on 3D-printing technology. *Materials Science and Engineering: C*, 129.

Lv, Z., Li, Z., Yang, Z., Li, X., Yang, Q., Li, K. and Li, J., 2019. One-Step Reconstruction with a Novel Suspended, Modular, and 3D-Printed Total Sacral Implant Resection of Sacral Giant Cell Tumor with Preservation of Bilateral S 1–3 Nerve Roots via a Posterior-Only Approach. *Orthopaedic Surgery*, 12(1), pp.58-66.

Lv, Y., Wang, B., Liu, G., Tang, Y., Lu, E., Xie, K., Lan, C., Liu, J., Qin, Z. and Wang, L., 2021. Metal Material, Properties and Design Methods of Porous Biomedical Scaffolds for Additive Manufacturing: A Review. *Frontiers in Bioengineering and Biotechnology*, 9.

Lv, Z., Li, J., Yang, Z., Li, X., Yang, Q., and Li, Z., 2023a. A novel three dimensional-printed biomechanically evaluated patient-specific sacral implant in spinopelvic reconstruction after total en bloc sacrectomy. *Frontiers in bioengineering and biotechnology*, 11.

Lv, Z., Li, Z., Yang, Q. and Li, J., 2023b. A 3D-printed patient-specific modular implants for pelvic reconstruction of bone tumors involving the sacroiliac joint. *Frontiers in Bioengineering and Biotechnology*. 11.

Ma, L., Zhou, Y., Zhu, Y., Lin, Z., Wang, Y., Zhang, Y., Xia, H. and Mao, C., 2016. 3D-printed guiding templates for improved osteosarcoma resection. *Scientific Reports*, 6(1).

MacDessi, S., Jang, B., Harris, I., Wheatley, E., Bryant, C. and Chen, D., 2014. A comparison of alignment using patient specific guides, computer navigation and conventional instrumentation in total knee arthroplasty. *The Knee*, 21(2), pp.406-409.

Maconachie, T., Leary, M., Lozanovski, B., Zhang, X., Qian, M., Faruque, O. and Brandt, M., 2019. SLM lattice structures: Properties, performance, applications and challenges. *Materials & Design*, 183.

Malawer, M. and Sugarbaker, P., 2004). *Musculoskeletal Cancer Surgery*. New York: Kluwer Academic Publishers.

Maleki, E., Bagherifard, S., Bandini, M. and Guagliano, M., 2021. Surface post-treatments for metal additive manufacturing: Progress, challenges, and opportunities. *Additive Manufacturing*, 37.

Malham, M. and Wells-Quinn, T., 2019. What should my hospital buy next?-Guidelines for the acquisition and application of imaging, navigation, and robotics for spine surgery. *Journal of spine surgery (Hong Kong)*, *5*(1), pp.155-165.

Mandrycky, C., Wang, Z., Kim, K. and Kim, D., 2016. 3D bioprinting for engineering complex tissues. *Biotechnology Advances*, 34(4), pp.422-434.

Manero, A., Smith, P., Sparkman, J., Dombrowski, M., Courbin, D., Kester, A., Womack, I., and Chi, A., 2019. Implementation of 3D Printing Technology in the Field of Prosthetics: Past, Present, and Future. *International Journal of Environmental Research and Public Health*, 16(9).

Mani, N., Sola, A., Trinchi, A. and Fox, K., 2020. Is there a future for additive manufactured titanium bioglass composites in biomedical application? A perspective. *Biointerphases*, 15(6).

Mankovich, N., Cheeseman, A. and Stoker N., 1990. The display of three-dimensional anatomy with stereolithographic models. *Journal of Digital Imaging*, 3(3), pp.200-203.

Manyika, J., Chui, M., Bughin, J., Dobbs, R., Bisson, P. and Marrs, A., 2013. Disruptive technologies: Advances that will transform life, business, and the global economy. *McKinsey*. [Online] Available at: https://www.mckinsey.com/~/media/mckinsey/business%20functions/mckinsey%20digital/our%20insights/disruptive%20technologies/mgi_disruptive_technologies_full_report_may2013.pdf [Accessed 9 March 2022].

Mao, Z., Agyei, O., Khan, A., Hess, M., Jowdy, K., Mullin, P. and Pollina, J., 2021. Technologic Evolution of Navigation and Robotics in Spine Surgery: A Historical Perspective. *World neurosurgery*, *145*, pp.159-167

Marcoin, A., Nerot, C., Lestra, T., Blasco, L., Ferrier, A., Siboni, R. and Ohl, X., 2020. The precision of patient-specific instrumentation guides for the positioning of the glenoid component in total reverse shoulder arthroplasty: an in vivo scanographic study. *International Orthopaedics*, 44(9), pp.1761-1766.

Marei, H., Alshaia, A., Alarifi, S., Almasoud, N. and Abdelhady, A., 2019. Effect of Steam Heat Sterilization on the Accuracy of 3D Printed Surgical Guides. *Implant Dentistry*, 28(4), pp.372-377.

Marinescu, R., Popescu, D. and Laptoiu, D., 2020. A Review on 3D-Printed Templates for Precontouring Fixation Plates in Orthopedic Surgery. *Journal of Clinical Medicine*, 9(9), p.2908.

Markatos, K., Savvidou, O., Foteinou, A., Kosmadaki, S., Trikoupis, I., Goumenos, S. and Papagelopoulos, P., 2020. Hallmarks in the History and Development of Total Hip Arthroplasty. *Surgical Innovation*, 27(6), pp.691-694.

Markillie, P., 2012. Manufacturing and Innovation: A Third Industrial Revolution. *The Economist*, Special Report.

Marro, A., Bandukwala, T. and Mak, W., 2016. Three-Dimensional Printing and Medical Imaging: A Review of the Methods and Applications. *Current Problems in Diagnostic Radiology*, 45(1), pp.2-9.

Martelli, N., Serrano, C., van den Brink, H., Pineau, J., Prognon, P., Borget, I. and El Batti, S., 2016. Advantages and disadvantages of 3-dimensional printing in surgery: A systematic review. *Surgery*, 159(6), pp.1485-1500.

Martinez-Marquez, D., Mirnajafizadeh, A., Carty, C. and Stewart, R., 2018. Application of quality by design for 3D printed bone prostheses and scaffolds. *PLOS ONE*, 13(4).

Martino, I., Triantafyllopoulos, G., Sculco, P. and Sculco, T., 2014. Dual mobility cups in total hip arthroplasty. *World Journal of Orthopedics*, 5(3).

Marutani, Y., 1985. *Optical shaping method*. JP Patent No. 60247515.

Marutani, Y., 1990. Production of 3-D plastic models with a UV laser. *The Review of Laser Engineering*, 18(7), pp.448-455.

Maskery, I., Sturm, L., Aremu, A., Panesar, A., Williams, C., Tuck, C., Wildman, R., Ashcroft, I. and Hague, R., 2017. Insights into the mechanical properties of several triply periodic minimal surface lattice structures made by polymer additive manufacturing. *Polymer*, 152(12), pp.62-71.

Maskery, I. and Ashcroft, I., 2020. The deformation and elastic anisotropy of a new gyroid-based honeycomb made by laser sintering. *Additive Manufacturing*, 36.

Maslov, L., Borovkov, A., Maslova, I., Soloviev, D., Zhmaylo, M. and Tarasenko, F., 2021. Finite Element Analysis of customized acetabular implant and bone after pelvic tumour resection throughout the gait cycle. *Materials*, 14(22).

Masters, W., 1987. *Computer automated manufacturing process and system*. US Patent No. 4665492.

Matjaž, M., Domen, N. and Beguš, S., 2014. *Virtual Reality Technology and Applications.* Dordrecht: Springer.

Matsubara, K., 1974. *Molding Method of Casting Using Photocurable Substance*. Japanese Kokai Patent, Sho 51 [1976]-10813.

Matter-Parrat, V. and Liverneaux, P., 2019. 3D printing in hand surgery. *Hand Surgery and Rehabilitation*, 38(6), pp.338-347.

Mavrodontis, I., 2015. *Additive Manufacturing Technologies: Design, Manufacture and Operation of a Material Extrusion Machine (BSc dissertation)*. Department of Mechanical Engineering, University of West Attica (ex-Piraeus University of Applied Sciences).

Mavrodontis, I., 2017. *Optimised Additive Manufacturing of Biomimetic Orthopaedic Implants (MSc dissertation)*. Department of Design Manufacture and Engineering Management, University of Strathclyde.

Mavrodontis, I.I., Trikoupis, I.G., Kontogeorgakos, V.A., Savvidou, O.D. and Papagelopoulos, P.J., 2024. Point-of-Care Orthopedic Oncology Device Development. *Current Oncology*, 31 (1), pp.211-228.

Mavrogenis, A., Dimitriou, R., Parvizi, J. and Babis, G., 2009. Biology of implant osseointegration. *Journal of Musculoskeletal and Neuronal Interactions*, 9(2), pp.61-71.

Mavrogenis, A., Coll-Mesa, L., Gonzalez-Gaitano, M., Ucelay-Gomez, R., Fabri, N., Ruggieri, P. and Papagelopoulos, P., 2011a. Criteria and outcome of limb salvage surgery. *Journal of BUON*, 16, pp.617-626.

Mavrogenis, A., Papagelopoulos, P., Coll-Mesa, L., Pala, E., Guerra, G. and Ruggieri, P., 2011b. Infected Tumor Prostheses. *Orthopedics*, 34(12), pp.991-998.

Mavrogenis, A., Soultanis, K., Patapis, P., Guerra, G., Fabbri, N., Ruggieri, P. and Papagelopoulos, P., 2012. Pelvic Resections. *Orthopedics*, 35(2).

Mavrogenis, A., Pala, E., Angelini, A., Calabro, T., Romagnoli, C., Romantini, M., Drago, G. and Ruggieri, P., 2015. Infected Prostheses after Lower-Extremity Bone Tumor Resection: Clinical Outcomes of 100 Patients. *Surgical Infections*, 16(3), pp.267-275.

Mavrogenis, A., Angelini, A., Vottis, C., Palmerini, E., Rimondi, E., Rossi, G., Papagelopoulos, P. and Ruggieri, P., 2014. State-of-the-art approach for bone sarcomas. *European Journal of Orthopaedic Surgery & Traumatology*, 25(1), pp.5-15.

Mavrogenis, A., Megaloikonomos, P., Panagopoulos, G. and Maffulli, N., 2017a. Biomechanics in Orthopaedics. *Journal of Biomedicine*, 2(2), pp.89-93.

Mavrogenis, A., Megalooikonomos, P., Vottis, C., Igoumenou, V., Galanopoulos, I., Panagopoulos, G. and Papagelopoulos, P., 2017b. Diagnosis and treatment of bone sarcomas. *Acta Orthopaedica et Traumatologica Hellenica*, 68(3), pp.95-108.

Mavrogenis, A.F., Papadopoulos, D., Tsantes, A.G., Angelini, A., Papagelopoulos, P.J. and Ruggieri, P., 2021. Reconstruction vs. No Reconstruction for Pelvic Resections. In: *Surgery of Pelvic Bone Tumors*. Ed. by Ruggieri, P. and Angelini, A. Cham: Springer, pp.165-183.

McEntire, B., Bal, B., Rahaman, M., Chevalier, J. and Pezzotti, G., 2015. Ceramics and ceramic coatings in orthopaedics. *Journal of the European Ceramic Society*, 35(16), pp.4327-4369.

McGregor, M., Patel, S., McLachlin, S. and Vlasea, M., 2021a. Architectural bone parameters and the relationship to titanium lattice design for powder-bed fusion additive manufacturing. *Additive Manufacturing*, 47.

McGregor, M., Patel, S., McLachlin, S. and Vlasea, M., 2021b. Data related to architectural bone parameters and the relationship to Ti lattice design for powder-bed fusion additive manufacturing. *Data in Brief*, 39.

Megaloikonomos, P., Savvidou, O., Vlachaki, A., Igoumenou, V., Vlasis, K. and Papagelopoulos, P., 2021. The Evolution of Orthopaedics in Greece: From Ancient Heritage to Modern Times. *Surgical Innovation*, 28(6), pp.780-793.

Mendis, D., Nordemann, J., Ballardini, R., Brorsen, H., Moreno, M., Robson, J. and Dickens, P., 2020. *The Intellectual Property Implications of the Development of Industrial 3D Printing. European Commission*. [Online] Available at: https://op.europa.eu/en/publication-detail/-/publication/e193a586-7f8c-11ea-aea8-01aa75ed71a1
[Accessed 9 March 2022].

Melancon, D., Bagheri, Z., Johnston, R., Liu, L., Tanzer, M. and Pasini, D., 2017. Mechanical characterization of structurally porous biomaterials built via additive manufacturing: experiments, predictive models, and design maps for load-bearing bone replacement implants. *Acta Biomaterialia*, 63, pp.350-368.

Menhennett, H. and Brown, R., 1996. *Apparatus and method for making three-dimensional articles using bursts of droplets*. US Patent No. 5555176.

Merola, M. and Affatato, S., 2019. Materials for Hip Prostheses: A Review of Wear and Loading Considerations. *Materials*, 12(3).

Meyer, M.M., Glas, A.H. and Eßig, M., 2020. Systematic review of sourcing and 3D printing: Make-or-buy decisions in industrial buyer–supplier relationships. *Management Review Quarterly*, 71(4), pp.723-752.

Meyers, M., Chen, P., Lin, A. and Seki, Y., 2008. Biological materials: Structure and mechanical properties. *Progress in Materials Science*, 53(1), pp.1-206.

Michael, W., Ghayor, C., Zimmermann, S., Rüegg, J., Nicholls, F., Schuler, F., Chen, T. and Weber, F., 2019. Osteoconductive Lattice Microarchitecture for Optimized Bone Regeneration. *3D Printing and Additive Manufacturing*, *6 (1), pp.40-49*.

Milgram P. and Kishino, F., 1994. A taxonomy of mixed reality visual displays. *IEICE Transactions on Information Systems*, E77–D(12), pp.1321-1329.

Mirzaali, Nava, Gunashekar, Nouri-Goushki, Doubrovski and Zadpoor, 2019. Fracture Behavior of Bio-Inspired Functionally Graded Soft–Hard Composites Made by Multi-Material 3D Printing: The Case of Colinear Cracks. *Materials*, 12(17).

Mishra, A., Verma, T., Rajkumar, Agarwal, G., Sharma, A. and Maini, L., 2020. 3D Printed Patient-Specific Acetabular Jig for Cup Placement in Total Hip Arthroplasty. *Indian Journal of Orthopaedics*, 54(2), pp.174-180.

Mohan Pandey, P., Venkata Reddy, N. and Dhande, S., 2003. Slicing procedures in layered manufacturing: a review. *Rapid Prototyping Journal*, 9(5), pp.274-288.

Moiduddin, K., Al-Ahmari, A., Nasr, E., Al Kindi, M. and Hamid, M., 2016. Evaluation of titanium alloy fabricated using electron beam melting and traditional casting technique. *Biomedical Research*, Special Issue, pp.68-74.

Mok, S., Nizak, R., Fu, S., Ho, K., Qin, L., Saris, D., Chan, K. and Malda, J., 2016. From the printer: Potential of three-dimensional printing for orthopaedic applications. *Journal of Orthopaedic Translation*, 6, pp.42-49.

Momeni, F., M.Mehdi Hassani.N, S., Liu, X. and Ni, J., 2017. A review of 4D printing. *Materials & Design*, 122, pp.42-79.

Monteath, F., 1924. *Photochemical Process for Producing BASReliefs*. US Patent No. 1516199.

Montoya, C., Du, Y., Gianforcaro, A., Orrego, S., Yang, M. and Lelkes, P., 2021. On the road to smart biomaterials for bone research: definitions, concepts, advances, and outlook. *Bone Research*, 9(1).

Moon, N., Do, M., Kim, J., Seo, J. and Shin, W., 2022. The usefulness of dual mobility cups in primary total hip arthroplasty patients at a risk of dislocation. *Scientific Reports*, 12(1).

Morales-Codina, A. and Martin-Benlloch, J, 2022. Sacral Prosthesis Substitution as a System of Spinopelvic Reconstruction After Total Sacrectomy: Assessment Using the Finite Element Method. *International Journal of Spine Surgery*, 16(3).

Moreno, M. and Charnley, F., 2016. Can re-distributed manufacturing and digital intelligence enable a regenerative economy? an integrative literature review. *Sustainable Design and Manufacturing 2016*, pp.563-575.

Moreta-Martinez, R., Pose-Díez-de-la-Lastra, A., Calvo-Haro, J., Mediavilla-Santos, L., Pérez-Mañanes, R. and Pascau, J., 2021. Combining Augmented Reality and 3D Printing to Improve Surgical Workflows in Orthopedic Oncology: Smartphone Application and Clinical Evaluation. *Sensors*, 21(4).

Morgan, C., Khatri, C., Hanna, S., Ashrafian, H. and Sarraf, K., 2019. Use of three-dimensional printing in preoperative planning in orthopaedic trauma surgery: A systematic review and meta-analysis. *World Journal of Orthopedics*, 11(1), pp.57-67.

Morioka, I., 1929. *Photographic method of reproducing original objects*. US Patent No. 1719483.

Morlock, M., Schneider, E., Bluhm, A., Vollmer, M., Bergmann, G., Müller, V. and Honl, M., 2001. Duration and frequency of every day activities in total hip patients. *Journal of Biomechanics*, 34(7).

Morrison, R., Kashlan, K., Flanangan, C., Wright, J., Green, G., Hollister, S. and Weatherwax, K., 2015. Regulatory Considerations in the Design and Manufacturing of Implantable 3D-Printed Medical Devices. *Clinical and Translational Science*, 8(5), pp.594-600.

Morton, D.A., Foreman, K.B. and Albertine, K.H., 2019. Gluteal Region and Hip. In: *The big picture: Gross anatomy*. New York: McGraw-Hill Education.

Mostafaei, A., Zhao, C., He, Y., Ghiaasiaan, R., Shi, B., Shao, S., Shamsaei, N., Wu, Z., Kouraytem, N., Sun, T., Pauza, J., Gordon, J., Webler, B., Parab, N., Asherloo, M., Guo, Q., Chen, L. and Rollett, A., 2022. Defects and anomalies in powder bed fusion metal additive manufacturing. *Current Opinion in Solid State and Materials Science*, 26 (2).

Moura, C., Trindade, D., Vieira, M., Francisco, L., Ângelo, D. and Alves, N., 2020. Multi-Material Implants for Temporomandibular Joint Disc Repair: Tailored Additive Manufacturing Production. *Frontiers in Bioengineering and Biotechnology*, 8.

Mourtzis, D. and Doukas, M., 2012. Decentralized Manufacturing Systems Review: Challenges and outlook. *Lecture Notes in Production Engineering*, pp.355-369.

Moussa, A., Rahman, S., Xu, M., Tanzer, M. and Pasini, D., 2020. Topology optimization of 3D-printed structurally porous cage for acetabular reinforcement in total hip arthroplasty. *Journal of the Mechanical Behavior of Biomedical Materials*, 105.

Moussa, A., Melancon, D., El Elmi, A. and Pasini, D., 2021. Topology optimization of imperfect lattice materials built with process-induced defects via Powder-bed Fusion. *Additive Manufacturing*, 37.

Mow, V. and Huiskes, R., 2005. *Basic Orthopaedic Biomechanics and Mechano-Biology*. 3rd ed. Philadelphia: Lippincott Williams & Wilkins.

Mueller, J., Matlack, K., Shea, K. and Daraio, C., 2019. Energy Absorption Properties of Periodic and Stochastic 3D Lattice Materials. *Advanced Theory and Simulations*, 2.

Munaz, A., Vadivelu, R., St. John, J., Barton, M., Kamble, H. and Nguyen, N., 2016. Three-dimensional printing of biological matters. *Journal of Science: Advanced Materials and Devices*, 1(1), pp.1-17.

Munford, M., Hossain, U., Ghouse, S. and Jeffers, J., 2020. Prediction of anisotropic mechanical properties for lattice structures. *Additive Manufacturing*, 32.

Munsch, M., 2017. Laser additive manufacturing of customized prosthetics and implants for biomedical applications. In: *Laser Additive Manufacturing*. Ed. by Brandt, M. Woodhead Publishing Series in Electronic and Optical Materials. New York: Woodhead Publishing, pp.399-420.

Munz, O., 1956. *Photo-Glyph Recording*. US Patent No. 2775758.

Munz, O., 1968. *Method for three-dimensional imprinting a thermoplastic object*. US Patent No. 340521.

Murphey, M., 2006. *Musculoskeletal Neoplasms: Fundamental Concepts. Radiologic Pathology*. 2nd ed.

Murr, L., Amato, K., Li, S., Tian, Y., Cheng, X., Gaytan, S., Martinez, E., Shindo, P., Medina, F. and Wicker, R., 2011. Microstructure and mechanical properties of open-cellular biomaterials prototypes for total knee replacement implants fabricated by electron beam melting. *Journal of the Mechanical Behavior of Biomedical Materials*, 4(7), pp.1396-1411.

Murr, L., 2015. Metallurgy of additive manufacturing: Examples from electron beam melting. *Additive Manufacturing*, 5, pp.40-53.

Murr, L., 2017. Additive manufacturing of biomedical devices: an overview. *Materials Technology*, 33(1), pp.57-70.

Muthaiah, V., Indrakumar, S., Suwas, S. and Chatterjee, K., 2022. Surface engineering of additively manufactured titanium alloys for enhanced clinical performance of biomedical implants: A review of recent developments. *Bioprinting*, 25.

Naghavi, S.A., Wang, H., Varma, S.N., Tamaddon, M., Marghoub, A., Galbraith, R., Galbraith, J., Moazen, M., Hua, J., Xu, W. and Liu, C., 2022. On the morphological deviation in additive manufacturing of porous ti6al4v scaffold: A design consideration. *Materials*, 15(14).

Naghavi, A., Tamaddon, M., Garcia-Souto, P., Moazen, M., Taylor, S., Hua, J. and Liu, C., 2023. A novel hybrid design and modelling of a customised graded ti-6al-4v porous hip implant to reduce stress-shielding: An experimental and numerical analysis. Frontiers in Bioengineering and Biotechnology, 11.

Nakagawa, T., 1976. Blanking Tool by Stacked Bainite Steel Plates. *Press Technique*, pp.93-101.

Nakai, T. and Marutani, Y., 1986. Shaping 3-D solid objects using a UV laser and photopolymer. In: *Conference on Lasers and Electro-Optics*, Bjorklund, G., Hinkley, E., Moulton, P. and Pinnow, D., OSA Technical Digest (Optica Publishing Group, 1986), paper ME2.

Navarro, M., Michiardi, A., Castaño, O. and Planell, J., 2008. Biomaterials in orthopaedics. *Journal of The Royal Society Interface*, 5(27), pp.1137-1158.

Navarro, S., Shaikh, H., Klop-Packel, N., Jethwani, H., Wu, J. and Sutton, J., 2021. The Impact of Additive Manufacturing for Medical Care Delivery in Space: A Systematic Review. *Advanced Materials Technologies*.

Nelson, B., Karipott, S., Wang, Y. and Ong, K., 2020. Wireless Technologies for Implantable Devices. *Sensors*, 20(16).

Neovius, E.R., 1883. Bestimrnung Zweier Speciellen Periodischen Minimalflachen. *Helsingfors*.

Neri, T., Boyer, B., Batailler, C., Klasan, A., Lustig, S., Philippot, R. and Farizon, F., 2020. Dual mobility cups for total hip arthroplasty: tips and tricks. *SICOT-J*, 6.

Nosrati, H., Sarraf Mamoory, R., Svend Le, D. and Bünger, C., 2020. Fabrication of gelatin/hydroxyapatite/3D-graphene scaffolds by a hydrogel 3D-printing method. *Materials Chemistry and Physics*, 239.

Nukavarapu, S., Freeman, J. and Laurencin, C., 2015. *Regenerative Engineering of Musculoskeletal Tissues and Interfaces*. New York: Woodhead Publishing.

Ødegaard, K., Torgersen, J. and Elverum, C., 2020. Structural and Biomedical Properties of Common Additively Manufactured Biomaterials: A Concise Review. *Metals*, 10(12).

Official Journal of the EU (2017). *Regulation (EU) 2017/745 Of The EU Parliament and The Council On Medical Devices*. [Online] Available at: http://eur-lex.europa.eu/legal-content/EN/TXT/PDF/?uri=OJ:L:2017:117:FULL&from=EN [Accessed on 9 March 2022].

Ogden, K., Aslan, C., Ordway, N., Diallo, D., Tillapaugh-Fay, G. and Soman, P., 2015. Factors Affecting Dimensional Accuracy of 3-D Printed Anatomical Structures Derived from CT Data. *Journal of Digital Imaging*, 28(6), pp.654-663.

Okabe, A., Boots, B., Sugihara, K., Nok Chiu, S., 1992. *Spatial Tessellations: Concepts and Applications of Voronoi Diagrams*. 2nd ed. Chichester: Wiley.

Orthoworld, 2022. *The Orthopaedic Industry Annual Report 2020*. [online] Available at: https://www.orthoworld.com/the-orthopaedic-industry-annual-report/ [Accessed 9 February 2023].

Oth, O., Dauchot, C., Orellana, M. and Glineur, R., 2019. How to Sterilize 3D Printed Objects for Surgical Use? An Evaluation of the Volumetric Deformation of 3D-Printed Genioplasty Guide in PLA and PETG after Sterilization by Low-Temperature Hydrogen Peroxide Gas Plasma. *The Open Dentistry Journal*, 13(1), pp.410-417.

Oxman, N., 2011a. Variable property rapid prototyping. *Virtual and Physical Prototyping*, 6(1), pp.3-31.

Oxman, N., 201b. Finite Element Synthesis, *Taylor & Francis*. [Online] Available at: https://neri.media.mit.edu/publications/article/finite-element-synthesis.html [Accessed 9 March 2022].

Oxman, N., Keating, S. and Tsai, E., 2011. Functionally Graded Rapid Prototyping. *Proceedings of VRAP: Advanced Research in Virtual and Rapid Prototyping*, pp.483-489.

Oxman, N., 2012. Programming Matter. *Architectural Design, Special Issue: Material Computation: Higher Integration in Mophogenetic Design*, 82 (2), pp.88-95

Ozbolat, I., Moncal, K. and Gudapati, H., 2017. Evaluation of bioprinter technologies. *Additive Manufacturing*, 13, pp.179-200.

Özel, T., Bártolo, P., Ceretti, E., Gay, J., Rodriguez, C. and Da Silva, V., 2016. *Biomedical devices: Design, Prototyping, and Manufacturing*. New Jersey: Wiley.

Özger, H., Sim, F., Puri, A. and Eralp, L., 2022. *Orthopedic surgical oncology for bone tumors: A Case Study Atlas*. Cham: Springer.

Paget, S., 1889. The distribution of secondary growths in cancer of the breast. *The Lancet*, 133(3421), pp.571-573.

Pahl, G., Beitz, W., Feldhusen, J. and Grote, K., 2007. *Engineering design*. 3rd ed. London: Springer.

Pajot, T., Benichou, L., Moreau, E., Tallon, V., Meningaud, J., Khonsari, R. and Ketoff, S., 2020. Implementation of a digital chain for the design and manufacture of implant-based surgical guides in a hospital setting. *Journal of Stomatology, Oral and Maxillofacial Surgery*, 121(4), pp.347-351.

Pal, S., 2014. *Design of artificial human joints & organs*. Boston: Springer.

Pala, E., Mavrogenis, A., Angelini, A., Henderson, E., Letson, G. and Ruggieri, P., 2013. Cemented versus cementless endoprostheses for lower limb salvage surgery. *Journal of B.U.ON.: official journal of the Balkan Union of Oncology*, *18*(2), pp.496-503.

Palais, H., 1932. *Method of making toys and the like and step product*. US Patent No. 1839889.

Pallua, N. and Suschek, C., 2011. *Tissue Engineering: From Lab to Clinic*. Berlin: Springer.

Palmowski, Y., Popović, S., Kosack, D. and Damm, P., 2021. Analysis of hip joint loading during walking with different shoe types using instrumented total hip prostheses. *Scientific Reports*, 11(1).

Palmquist, A., Snis, A., Emanuelsson, L., Browne, M., Thomsen, P., 2013. Long-term biocompatibility and osseointegration of electron beam melted, free-form-fabricated solid and porous titanium alloy: experimental studies in sheep. *Journal of Biomaterials Applications*, 27(8), pp.1003-1016.

Pandey, R. and Panda, S., 2013. Drilling of bone: A comprehensive review. *Journal of Clinical Orthopaedics and Trauma*, 4(1), pp.15-30.

Panesar, A., Brackett, D., Ashcroft, I., Wildman, R. and Hague, R., 2015. Design Framework for Multifunctional Additive Manufacturing: Placement and Routing of Three-Dimensional Printed Circuit Volumes. *Journal of Mechanical Design*, 137(11).

Panwisawas, C., Tang, Y. and Reed, R., 2020. Metal 3D printing as a disruptive technology for superalloys. *Nature Communications*, 11(1).

Papagelopoulos, P., Savvidou, O., Koutsouradis, P., Chloros, G., Bolia, I., Sakellariou, V., Kontogeorgakos, V., Mavrodontis, I., Mavrogenis, A. and Diamantopoulos, P., 2018. Three-dimensional Technologies in Orthopedics. *Orthopedics*, 41(1), pp.12-20.

Papagelopoulos, P., Sarlikiotis, T., Vottis, C., Agrogiannis, G., Kontogeorgakos, V. and Savvidou, O., 2019a. Total Talectomy and Reconstruction Using a 3-dimensional Printed Talus Prosthesis for Ewing's Sarcoma: A 3.5-Year Follow-up. *Orthopedics*, 42(4).

Papagelopoulos, P., Megaloikonomos, P., Korkolopoulou, P., Vottis, C., Kontogeorgakos, V. and Savvidou, O., 2019b. Total Calcaneus Resection and Reconstruction Using a 3-dimensional Printed Implant. *Orthopedics*, 42(2).

Papagelopoulos, P. and Savvidou, O., 2022a. Implant Reconstruction of the Tibial Diaphysis and Ankle: 3D-Printed Custom-Made Prosthesis. In: *Orthopedic Surgical Oncology For Bone Tumors: A Case Study Atlas*. Ed. By Özger, H., Sim, F., Puri, A. and Levent E. Cham: Springer.

Papagelopoulos, P. and Savvidou, O., 2022b. Implant Reconstruction of the Foot 3D-Printed Custom-Made Prosthesis. In: *Orthopedic Surgical Oncology For Bone Tumors: A Case Study Atlas*. Ed. By Özger, H., Sim, F., Puri, A. and Levent E. Cham: Springer.

Park, J., Kang, H., Lim, K., Kim, J. and Kim, H., 2018. Three-Dimensionally Printed Personalized Implant Design and Reconstructive Surgery for a Bone Tumor of the Calcaneus. *JBJS Case Connector*, 8(2), pp.25-25.

Park, J., Kang, H., Kim, J. and Kim, H., 2020a. New 3-dimensional implant application as an alternative to allograft in limb salvage surgery: a technical note on 10 cases. *Acta Orthopaedica*, 91(4), pp.489-496.

Park, J., Song, C., Kang, H., Kim, J., Lim, K. and Kim, H., 2020b. Integration of a Three-Dimensional-Printed Titanium Implant in Human Tissues: Case Study. *Applied Sciences*, 10(2).

Park, J., Kang, H., Kim, J. and Kim, H., 2021. The application of 3D-printing technology in pelvic bone tumor surgery. *Journal of Orthopaedic Science*, 26(2), pp.276-283.

Park, K., Min, K. and Roh, Y., 2021. Design optimization of lattice structures under compression: Study of unit cell types and cell arrangements. *Materials*, 15(1), 97.

Park, J., Kwon, H., Lee, W., Yang, I. and Park, K., 2021. Anthropometric Measurement About the Safe Zone for Transacetabular Screw Placement in Total Hip Arthroplasty in Asian Middle-Aged Women: In Vivo Three-Dimensional Model Analysis. *The Journal of Arthroplasty*, 36(2), pp.744-751.

Park, H., Shah, A.A. and Hornicek, F.J., 2021. Innovative Techniques in Pelvic Reconstructions. In: *Surgery of Pelvic Bone Tumors*. Ed. by Ruggieri, P. and Angelini, A. Cham: Springer, pp.123-134.

Park, J., Park, H., Kim, J., Kim, H., Yoo, C. and Kang, H., 2022. Fabrication of a lattice structure with periodic open pores through three-dimensional printing for bone ingrowth. *Scientific Reports*, 12(1).

Patsiogiannis, N., Kanakaris, N. and Giannoudis, P., 2021. Periprosthetic hip fractures: an update into their management and clinical outcomes. *EFORT Open Reviews*, 6(1), pp.75-92.

Paul, S., Riffat, M., Yasir, A., Mahim, M., Sharnali, B., Naheen, I., Rahman, A. and Kulkarni, A., 2021. Industry 4.0 Applications for Medical/Healthcare Services. *Journal of Sensor and Actuator Networks*, 10(3).

Pauzenberger, L., Munz, M., Brandl, G., Frank, J., Heuberer, P., Laky, B., Schwameis, E. and Anderl, W., 2019. Patient-specific instrumentation improved three-dimensional accuracy in total knee arthroplasty: a comparative radiographic analysis of 1257 total knee arthroplasties. *Journal of Orthopaedic Surgery and Research*, 14(1).

Paxton, N., Dinoro, J., Ren, J., Ross, M., Daley, R., Zhou, R., Bazaka, K., Thompson, R., Yue, Z., Beirne, S., Harkin, D., Allenby, M., Wong, C., Wallace, G. and Woodruff, M., 2021. Additive manufacturing enables personalised porous high-density polyethylene surgical implant manufacturing with improved tissue and vascular ingrowth. *Applied Materials Today*, 22.

Peacock, G., 1899. *Horseshoe*. US Patent No. 632423.

Peh, S., Chatterjea, A., Pfarr, J., Schäfer, J., Weuster, M., Klüter, T., Seekamp, A. and Lippross, S., 2020. Accuracy of augmented reality surgical navigation for minimally invasive pedicle screw insertion in the thoracic and lumbar spine with a new tracking device. *The Spine Journal*, 20(4), pp.629-637.

Pei, G., 2018. *Digital Orthopedics*. Dordrecht: Springer.

Pei, E., Ressin, M., Campbell, R.I., Eynard, B. and Xiao, J., 2019. Investigating the impact of additive manufacturing data exchange standards for re-distributed manufacturing. *Progress in Additive Manufacturing*, 4(3), pp.331-344.

Peltier, L., 1993. *Orthopedics: A History and Iconography*. San Francisco: Norman publishing.

Peng, L., Wang, P., Jiang, W., Cheng, C., Zuo, W., Qu, Y. and Li, W., 2019. Reconstruction with a 3D-printed Prosthesis and Internal Fixation with Novel Four-Rod Technique After En Bloc Resection of Meningiomas in the Lumbosacral Region (L5-S3) without Rectum/Bladder Function Sacrifice: Technical Case Report. *Turkish Neurosurgery*, 30(4).

Peng, W., Zheng, R., Wang, H. and Huang, X., 2020. Reconstruction of Bony Defects after Tumor Resection with 3D-Printed Anatomically Conforming Pelvic Prostheses through a Novel Treatment Strategy. *BioMed Research International*, 2020, pp.1-16.

Perera, B., 1940. *Process of Making Relief Maps*. US Patent No. 2189592.

Perricone, V., Santulli, C., Rendina, F. and Langella, C., 2021. Organismal Design and Biomimetics: A Problem of Scale. *Biomimetics*, 6(4).

Perticarini, L., Zanon, G., Rossi, S. and Benazzo, F., 2015. Clinical and radiographic outcomes of a trabecular titanium™ acetabular component in hip arthroplasty: results at minimum 5 years follow-up. *BMC Musculoskeletal Disorders*, 16(1).

Petrovic, V., Vicente Haro Gonzalez, J., Jordá Ferrando, O., Delgado Gordillo, J., Ramón Blasco Puchades, J. and Portolés Griñan, L., 2010. Additive layered manufacturing: sectors of industrial application shown through case studies. *International Journal of Production Research*, 49(4), pp.1061-1079.

Pfandler, M., Lazarovici, M., Stefan, P., Wucherer, P. and Weigl, M., 2017. Virtual reality-based simulators for spine surgery: a systematic review. *The Spine Journal*, 17(9), pp.1352-1363.

Pijpker, P., Kraeima, J., Witjes, M., Oterdoom, D., Vergeer, R., Coppes, M., Groen, R. and Kuijlen, J., 2020. Accuracy of Patient-Specific 3D-Printed Drill Guides for Pedicle and Lateral Mass Screw Insertion. *Spine*, 46(3), pp.160-168.

Pina, S. and Ferreira, J., 2012a. Biomechanical Properties of a Novel Biodegradable Magnesium Based Interference Screw. *Journal of Healthcare Engineering*, 3(2), pp.71-74.

Pina, S. and Ferreira, J., 2012b. Bioresorbable Plates and Screws for Clinical Applications: A Review. *Journal of Healthcare Engineering*, 3(2), pp.71-74.

Pinter, C., Lasso, A., Choueib, S., Asselin, M., Fillion-Robin, J. C., Vimort, J. B., Martin, K., Jolley, M. A. and Fichtinger, G., 2020. SlicerVR for Medical Intervention Training and Planning in Immersive Virtual Reality. *IEEE Transactions on Medical Robotics and Bionics*, 2 (2), pp.108-117.

Pinto, J., Arrieta, C., Andia, M., Uribe, S., Ramos-Grez, J., Vargas, A., Irarrazaval, P. and Tejos, C., 2015. Sensitivity analysis of geometric errors in additive manufacturing medical models. *Medical Engineering and Physics*, 37(3), pp.328-334.

Piyush, P. and Piyush, G., 2022. Custom orthotics development process based on additive manufacturing. *Materials Today: Proceedings*, 59(3), pp. 52-63

Poitout, D., 2016. *Biomechanics and biomaterials in orthopedics*. 2nd ed. London: Springer.

Poltue, T., Karuna, C., Khrueaduangkham, S., Seehanam, S. and Promoppatum, P., 2021. Design Exploration of 3D-Printed Triply Periodic Minimal Surface Scaffolds for Bone Implants. *International Journal of Mechanical Sciences*. 211.

Pomerantz, I., 1990. *Three dimensional modelling apparatus*. US Patent No. 4961154.

Poologasundarampillai, G. and Nomm, A., 2017. Materials for 3D printing in medicine: Metals, polymers, ceramics, hydrogels. In: *3D Printing in Medicine*. Ed. by Kalaskar, D. New York: Woodhead Publishing, pp.43-71.

Poomathi, N., Singh, S., Prakash, C., Subramanian, A., Sahay, R., Cinappan, A. and Ramakrishna, S., 2020. 3D printing in tissue engineering: a state of the art review of technologies and biomaterials. *Rapid Prototyping Journal*, 26(7), pp.1313-1334.

Popescu, D., Laptoiu, D., Marinescu, R. and Botezatu, I., 2018. Design and 3D printing customized guides for orthopaedic surgery – lessons learned. *Rapid Prototyping Journal*, 24(5), pp.901-913.

Popescu, D., Marinescu, R. and Sandache, O., 2021. Upper Limbs Orthoses Production in 3D Printing Points-of-Care. *2021 International Conference on e-Health and Bioengineering (EHB)*, pp.1-4.

Prasad, L. and Smyth, H., 2016. 3D Printing technologies for drug delivery: a review. *Drug Development and Industrial Pharmacy*, 42(7), pp.1019-1031.

Pratt, P., Ives, M., Lawton, G., Simmons, J., Radev, N., Spyropoulou, L. and Amiras, D., 2018. Through the HoloLens™ looking glass: augmented reality for extremity reconstruction surgery using 3D vascular models with perforating vessels. *European Radiology Experimental*, 2(1).

Presti, G., Carbone, M., Ciriaci, D., Aramini, D., Ferrari, M. and Ferrari, V., 2015. Assessment of DICOM Viewers Capable of Loading Patient-specific 3D Models Obtained by Different Segmentation Platforms in the Operating Room. *Journal of Digital Imaging*, 28(5), pp.518-527.

Priavolou, C., Troullaki, K., Tsiouris, N., Giotitsas, C. and Kostakis, V., 2022. Tracing sustainable production from a degrowth and localisation perspective: A case of 3D printers. *Journal of Cleaner Production*, 376.

Pu, F., Liu, J., Shi, D., Huang, X., Zhang, J., Wang, B., Wu, Q., Zhang, Z. and Shao, Z., 2022. Reconstruction With 3D-Printed Prostheses After Sacroiliac Joint Tumor Resection: A Retrospective Case-Control Study. *Frontiers in Oncology*, 11.

Pugliese, R. and Graziosi, S., 2023. Biomimetic scaffolds using triply periodic minimal surface-based porous structures for biomedical applications, *SLAS Technology*, 28, pp.165-182.

Puchner, S., Funovics, P., Böhler, C., Kaider, A., Stihsen, C., Hobusch, G., Panotopoulos, J. and Windhager, R., 2017. Oncological and surgical outcome after treatment of pelvic sarcomas. *PLOS ONE*, 12(2).

Pugh, S., 1991. *Total design: Integrated methods for successful product engineering*. Harlow: Prentice-Hall.

Pugliese, R., Beltrami, B., Regondi, S. and Lunetta, C., 2021. Polymeric biomaterials for 3D printing in medicine: An overview. *Annals of 3D Printed Medicine*, 2.

Punyaratabandhu, T., Lohwongwatana, B., Puncreobutr, C., Kosiyatrakul, A., Veerapan, P. and Luenam, S., 2017. A Patient-Matched Entire First Metacarpal Prosthesis in Treatment of Giant Cell Tumor of Bone. *Case Reports in Orthopedics*, 2017, pp.1-6.

Putra, N., Mirzaali, M., Apachitei, I., Zhou, J. and Zadpoor, A., 2020. Multi-material additive manufacturing technologies for Ti-, Mg-, and Fe-based biomaterials for bone substitution. *Acta Biomaterialia*, 109, pp.1-20.

Qasim, M., Chae, D. and Lee, N., 2019. Advancements and frontiers in nano-based 3D and 4D scaffolds for bone and cartilage tissue engineering. *International Journal of Nanomedicine*, Volume 14, pp.4333-4351.

Qian, H., Lei, T., Lei, P. and Hu, Y., 2021. Additively Manufactured Tantalum Implants for Repairing Bone Defects: A Systematic Review. *Tissue Engineering Part B: Reviews*, 27(2), pp.166-180.

Qiblawey, Y., Chowdhury, M., Musharavati, F., Zalnezhad, E., Khandakar, A. and Islam, M., 2021. Instrumented Hip Implant: A Review. *IEEE Sensors Journal*, 21(6), pp.7179-7194.

Qin, Z., Jung, G., Kang, M. and Buehler, M., 2017. The mechanics and design of a lightweight three-dimensional graphene assembly. *Science Advances*, 3(1).

Qin, J., Yang, D., Maher, S., Lima-Marques, L., Zhou, Y., Chen, Y., Atkins, G. and Losic, D., 2018. Micro- and nano-structured 3D printed titanium implants with a hydroxyapatite coating for improved osseointegration. *Journal of Materials Chemistry B*, 6(19), pp.3136-3144.

Quarterman, J., Geary, S. and Salem, A., 2021. Evolution of drug-eluting biomedical implants for sustained drug delivery. *European Journal of Pharmaceutics and Biopharmaceutics*, 159, pp.21-35.
Raja, V. and Fernandes, K., 2008. *Reverse engineering*. London: Springer.

Raghavendra, S., Molinari, A., Zappini, G. and Benedetti, M., 2021. Correlation between as-designed and as-built Young's modulus of cubic regular, cubic irregular, and trabecular cellular materials. *Material Design & Processing Communications*, 3(5).

Rajput, S., 2021. A review of space surgery - What have we achieved, current challenges, and future prospects. *Acta Astronautica*, 188, pp.18-24.

Ramakrishna, V., Chamoli, U., Rajan, G., Mukhopadhyay, S., Prusty, B. and Diwan, A., 2020. Smart orthopaedic implants: A targeted approach for continuous postoperative evaluation in the spine. *Journal of Biomechanics*, 104.

Ran, Q., Yang, W., Hu, Y., Shen, X., Yu, Y., Xiang, Y. and Cai, K., 2018. Osteogenesis of 3D printed porous Ti6Al4V implants with different pore sizes. *Journal of the Mechanical Behavior of Biomedical Materials*, 84, pp.1-11.

Raphel, J., Holodniy, M., Goodman, S. and Heilshorn, S., 2016. Multifunctional coatings to simultaneously promote osseointegration and prevent infection of orthopaedic implants. *Biomaterials*, 84, pp.301-314.

Rauch, E., Dallasega, P. and Matt, D.T., 2017. Distributed Manufacturing Network models of smart and agile mini-factories. *International Journal of Agile Systems and Management*, 10(3/4).

Rauch, E., Unterhofer, M. and Dallasega, P., 2018. Industry Sector Analysis for the application of additive manufacturing in smart and Distributed Manufacturing Systems. *Manufacturing Letters*, 15, pp.126-131.

Ravera, P., Crespo, J., Guarnieri, A. and Braidot, A., 2015. Stress in human pelvis throughout the gait cycle: Development, evaluation and sensitivity studies of a finite element model. *IFMBE Proceedings*, pp.246-249.

Ratner, B., Schoen, F., Hoffman, A. and Lemons, J., 2013. *Biomaterials Science: An Introduction to Materials in Medicine*. 3rd ed. London: Academic Press.

Raza, M., Murphy, D. and Gelfer, Y., 2021. The effect of three-dimensional (3D) printing on quantitative and qualitative outcomes in paediatric orthopaedic osteotomies: a systematic review. *EFORT Open Reviews*, 6(2), pp.130-138.

Reed, R., 1958. *Apparatus for building circular structures*. US Patent No. 283791.

Regis, M., Marin, E., Fedrizzi, L. and Pressacco, M., 2015. Additive manufacturing of Trabecular Titanium orthopedic implants. *MRS Bulletin*, 40(2), pp.137-144.

Ren, B., Wan, Y., Liu, C., Wang, H., Yu, M., Zhang, X. and Huang, Y., 2021. Improved osseointegration of 3D printed Ti-6Al-4V implant with a hierarchical micro/nano surface topography: An in vitro and in vivo study. *Materials Science and Engineering: C*, 118.

Ren, B., Wan, Y., Liu, C., Wang, H., Yu, M., Zhang, X. and Huang, Y., 2021. Improved osseointegration of 3D printed Ti-6Al-4V implant with a hierarchical micro/nano surface topography: An in vitro and in vivo study. *Materials Science and Engineering: C*, 118.

Renjith, S.C., Park, K. and Okudan Kremer, G.E., 2019. A design framework for Additive Manufacturing: Integration of additive manufacturing capabilities in the early design process. *International Journal of Precision Engineering and Manufacturing*, 21(2), pp.329-345.

Ribeiro, D., Cimino, S.R., Mayo, A.L., Ratto, M and Hitzig, S.L., 2021. 3D printing and amputation: a scoping review. *Disability and rehabilitation. Assistive technology*, 16(2), pp.221-240.

Rickenbacher, L., Spierings, A. and Wegener, K., 2013. An integrated cost-model for selective laser melting (SLM). *Rapid Prototyping Journal*, 19(3), pp.208-214.

Ricci, P. L., Maas, S., Kelm, J. and Gerich, T., 2018. Finite element analysis of the pelvis including gait muscle forces: An investigation into the effect of Rami fractures on load transmission. *Journal of Experimental Orthopaedics*, 5(1).

Ridzwan, M., Shuib, S., Hassan, A., Shokri, A. and Mohamad Ib, M., 2007. Problem of Stress Shielding and Improvement to the Hip Implant Designs: A Review. *Journal of Medical Sciences*, 7(3), pp.460-467.

Riener, R. and Harders, M., 2012. *Virtual Reality in Medicine.* London: Springer.

Riva, L., Ginestra, P. and Ceretti, E., 2021. Mechanical characterization and properties of laser-based powder-bed–fused lattice structures: a review. *The International Journal of Advanced Manufacturing Technology*, 113(3-4), pp.649-671.

Robbins, A., Maden, C., Volpin, A. and Konan, S., 2020. A systematic review of three dimensional (3-D) printing applications in hip and knee arthroplasty. *Acta Orthopaedica Belgica*, 86(2), pp.165-177.

Roberts, A.P. and Garboczi, E.J., 2002. Elastic properties of model random three-dimensional open-cell solids. *Journal of the Mechanics and Physics of Solids*, 50(1), pp.33-55.

Rodríguez-Contreras, A., Torres, D., Guillem-Marti, J., Sereno, P., Ginebra, M., Calero, J., Manero, J. and Rupérez, E., 2020. Development of novel dual-action coatings with osteoinductive and antibacterial properties for 3D-printed titanium implants. *Surface and Coatings Technology*, 403.

Rohit, J. and Apurba, D., 2017. Four dimensional printing in healthcare. In: *3D Printing in Medicine*. Ed. by Kalaskar, D. New York: Woodhead Publishing, pp.207-218.

Romanazzo, S., Molley, T., Nemec, S., Lin, K., Sheikh, R., Gooding, J., Wan, B., Li, Q., Kilian, K. and Roohani, I., 2021. Synthetic Bone-Like Structures Through Omnidirectional Ceramic Bioprinting in Cell Suspensions. *Advanced Functional Materials*, 31(13).

Romanò, C., Scarponi, S., Gallazzi, E., Romanò, D. and Drago, L., 2015. Antibacterial coating of implants in orthopaedics and trauma: a classification proposal in an evolving panorama. *Journal of Orthopaedic Surgery and Research*, 10(157).

Rosen, D. and Kim, S., 2021. Design and Manufacturing Implications of Additive Manufacturing. *Journal of Materials Engineering and Performance*, 30(9), pp.6426-6438.

Rosso, S., Uriati, F., Grigolato, L., Meneghello, R., Concheri, G. and Savio, G., 2021. An optimization workflow in design for Additive Manufacturing. *Applied Sciences*, 11(6).

Roy, T., Simon, J., Ricci, J., Rekow, E., Thompson, V. and Parsons, J., 2003. Performance of degradable composite bone repair products made via three-dimensional fabrication techniques. *Journal of Biomedical Materials Research*, 66A(2), pp.283-291.

Rüdiger, A., Guillemin, M., Latypova, A. and Terrier, A., 2017. Effect of changes of femoral offset on abductor and joint reaction forces in total hip arthroplasty. *Archives of Orthopaedic and Trauma Surgery*, 137(11), pp.1579-1585.

Ruffo, M. and Hague, R., 2007. Cost estimation for rapid manufacturing: simultaneous production of mixed components using laser sintering. *Proceedings of the Institution of Mechanical Engineers, Part B: Journal of Engineering Manufacture*, 221(11), pp.1585-1591.

Ruffo, M., Tuck, C. and Hague, R., 2006. Cost estimation for rapid manufacturing - laser sintering production for low to medium volumes. *Proceedings of the Institution of Mechanical Engineers, Part B: Journal of Engineering Manufacture*, 220(9), pp.1417-1427.

Ruhr, M., Baetz, J., Pueschel, K. and Morlock, M., 2021. Influence of acetabular cup thickness on seating and primary stability in total hip arthroplasty. *Journal of Orthopaedic Research*, 40(9), pp.2139-2146.

Rutala, W. and Weber, D., 2013. Disinfection and sterilization: An overview. *American Journal of Infection Control*, 41(5), pp.2-5.

Rutala, W. and Weber, D., 2016. Disinfection, sterilization, and antisepsis: An overview. *American Journal of Infection Control*, 44(5), pp.1-6.

Ryan, M.J., Eyers, D.R., Potter, A.T., Purvis, L. and Gosling, J., 2017. 3D printing the future: Scenarios for Supply Chains reviewed. *International Journal of Physical Distribution & Logistics Management*, 47(10), pp.992-1014.

Sacco, E. and Moon, S., 2019. Additive manufacturing for space: status and promises. *The International Journal of Advanced Manufacturing Technology*, 105(10), pp.4123-4146.

Sachs, E., Haggerty, J. Cima, M. and Williams P., 1993. *Three-dimensional printing techniques*. US Patent No. 5204055.

Sakai, D., Joyce, K., Sugimoto, M., Horikita, N., Hiyama, A., Sato, M., Devitt, A. and Watanabe, M., 2020. Augmented, virtual and mixed reality in spinal surgery: A real-world experience. *Journal of Orthopaedic Surgery*, 28(3).

Saleh, B., Jiang, J., Fathi, R., Al-hababi, T., Xu, Q., Wang, L., Song, D. and Ma, A., 2020. 30 Years of functionally graded materials: An overview of manufacturing methods, Applications and Future Challenges. *Composites Part B: Engineering*, 201.

Salmi, M., 2021. Additive Manufacturing Processes in Medical Applications. *Materials*, 14(1).

Sanchez, C., Arribart, H. and Giraud Guille, M., 2005. Biomimetism and bioinspiration as tools for the design of innovative materials and systems. *Nature Materials*, 4(4), pp.277-288.

Sandhu, K., Singh, S., Prakash, C., Sharma, N.R. and Subbura, K., 2022. *Emerging applications of 3D printing during covid 19 pandemic*. Singapore: Springer.

Sanicola, H., Stewart, C., Mueller, M., Ahmadi, F., Wang, D., Powell, S., Sarkar, K., Cutbush, K., Woodruff, M. and Brafman, D., 2020. Guidelines for establishing a 3-D printing biofabrication laboratory. *Biotechnology Advances*, 45.

Santecchia, E., Hamouda, A., Musharavati, F., Zalnezhad, E., Cabibbo, M. and Spigarelli, S., 2015. Wear resistance investigation of titanium nitride-based coatings. *Ceramics International*, 41(9), pp.10349-10379.

Santos-Coquillat, A., Martínez-Campos, E., Mora Sánchez, H., Moreno, L., Arrabal, R., Mohedano, M., Gallardo, A., Rodríguez-Hernández, J. and Matykina, E., 2021. Hybrid functionalized coatings on Metallic Biomaterials for Tissue Engineering. *Surface and Coatings Technology*, 422.

Sarfraz, S., Mäntynen, P., Laurila, M., Suojanen, J., Saarnio, J., Rossi, S., Horelli, J., Kaakinen, M., Leikola, J. and Reunanen, J., 2022. Effect of surface tooling techniques of medical titanium implants on bacterial biofilm formation in vitro. *Materials*, 15(9).

Sarker, A., Leary, M. and Fox, K., 2020. Metallic additive manufacturing for bone-interfacing implants. *Biointerphases*, 15(5).

Savio, G., Rosso, S., Meneghello, R. and Concheri, G., 2018. Geometric Modeling of Cellular Materials for Additive Manufacturing in Biomedical Field: A Review. *Applied Bionics and Biomechanics*, 2018, pp.1-14.

Savvidou, O., Sakellariou, V., Megaloikonomos, P., Mavrogenis, A. and Papagelopoulos, P., 2017. Periprosthetic Fractures in Megaprostheses: Algorithmic Approach to Treatment. *Orthopedics*, 40(3).

Savvidou, O., Zampeli, F., Georgopoulos, G., Dimopoulos, L., Antoniadou, T., Papanastassiou, I. and Papagelopoulos, P., 2018. Total Scapulectomy and Shoulder Reconstruction Using a Scapular Prosthesis and Constrained Reverse Shoulder Arthroplasty. *Orthopedics*, 41(6).

Savvidou, O., Kaspiris, A., Dimopoulos, L., Georgopoulos, G., Goumenos, S., Papadakis, V. and Papagelopoulos, P., 2019. Functional and Surgical Outcomes After Endoprosthetic Reconstruction With Expandable Prostheses in Children: A Systematic Review. *Orthopedics*, 42(4), pp.184-190.

Savvidou, O., Kaspiris, A., Trikoupis, I., Kakouratos, G., Goumenos, S., Melissaridou, D. and Papagelopoulos, P., 2020. Efficacy of antimicrobial coated orthopaedic implants on the prevention

of periprosthetic infections: a systematic review and meta-analysis. *Journal of Bone and Joint Infection*, 5(4), pp.212-222.

Savvidou, O., Zafiris, I., Goumenos, S., Melissaridou, D., Karampikas, V., Zikopoulos, A. and Papagelopoulos, P., 2020. Three-Dimensional Printed Calcaneus Implant for Open Calcaneal Fracture with Extensive Bone Loss: A Case Report and Literature Review. *Journal of Long-Term Effects of Medical Implants*, 30(4), pp.267-273.

Savvidou, O., Melissaridou, N., Bekyras, D., Georgoulis, J., Melissaridou, D., Koulouvaris, P. and Papagelopoulos, P., 2021. Three-Dimensional-Printed Proximal Radial Plate for Radial Reconstruction after Tumor Resection: Case Report and Literature Review. *Journal of Long-Term Effects of Medical Implants*, 31(2), pp.31-38.

Savvidou, O., Gavriil, P., Trikoupis, I., Kaspiris, A., Melissaridou, D., Papakonstantinou, O., Korkolopoulou, P. and Papagelopoulos, P., 2022. Three-dimensional Printed Endoprosthesis for Reconstruction of the Distal Tibia and Ankle Joint After Tumor Resection. *Orthopedics*, 45 (3), pp.1-5.

Schileo, E., Taddei, F., Malandrino, A., Cristofolini, L. and Viceconti, M., 2007. Subject-specific finite element models can accurately predict strain levels in long bones. *Journal of Biomechanics*, 40(13), pp.2982-2989.

Schileo, E., Dall'ara, E., Taddei, F., Malandrino, A., Schotkamp, T., Baleani, M. and Viceconti, M., 2008. An accurate estimation of bone density improves the accuracy of subject-specific finite element models. *Journal of Biomechanics*, 41(11), pp.2483-2491.

Schenk, R. and Buser, D., 1998. Osseointegration: a reality. *Periodontology 2000*, 17(1), pp.22-35.

Schwartz, D.A. and Schofield, K.A., 2023. Utilization of 3D printed orthoses for musculoskeletal conditions of the upper extremity: A systematic review. *Journal of hand therapy : official journal of the American Society of Hand Therapists*, 36(1), pp.166–178.

Schwerzel, R., Wood, V., McGinniss, V. and Veber, C., 1984. Three-Dimensional Photochemical Machining With Lasers. *Proceedings of the SPIE* 458, pp.90-97.

Schlagintweit, S., 2021. *Validating additive manufacturing processes to meet medical regulations: Ensure safe and reproducible manufacturing results*. TÜV SÜD.

Schnabel, T., Oettel, M. and Mueller, B., 2017. *Design For Additive Manufacturing: Guidelines and Case Studies for Metal Applications.* Fraunhofer IWU. [Online] Available at: https://publica-rest.fraunhofer.de/server/api/core/bitstreams/10ce4113-4285-48b2-bec4-67c229f8e411/content [Accessed 9 March 2022].

Schoen, A., 1970. Infinite periodic minimal surfaces without self-intersections. *NASA Technical Note TN D-5541***.**

Schwarz, H.A., 1933. Gesammelte Mathematische Abhandlungen, Berlin:Springer.

Seiffert, G., Hopkins, C. and Sutcliffe, C., 2017. Comparison of high-intensity sound and mechanical vibration for cleaning porous titanium cylinders fabricated using selective laser melting. *Journal of Biomedical Materials Research Part B: Applied Biomaterials*, 105(1), pp.117-123.

Sekar, M., Budharaju, H., Zennifer, A., Sethuraman, S., Vermeulen, N., Sundaramurthi, D. and Kalaskar, D., 2021. Current standards and ethical landscape of engineered tissues—3D bioprinting perspective. *Journal of Tissue Engineering*, Series in Electronic and Optical Materials. New York: Woodhead Publishing, pp.399-420.

Serrano, C., Fontenay, S., van den Brink, H., Pineau, J., Prognon, P. and Martelli, N., 2020. Evaluation of 3D printing costs in surgery: a systematic review. *International Journal of Technology Assessment in Health Care*, 36(4), pp.349-355.

Shaffer, V., Kutnick, D., Basiliere, P., Stevens, A. and Burton, J., 2015. Predicts 2016: 3D Printing Disrupts Healthcare and Manufacturing. *Gartner*. [Online] Available at: https://www.gartner.com/en/documents/3171223/predicts-2016-3d-printing-disrupts-healthcare-and-manufa [Accessed 9 March 2022].

Shah, F., Omar, O., Suska, F., Snis, A., Matic, A., Emanuelsson, L., Norlindh, B., Lausmaa, J., Thomsen, P. and Palmquist, A., 2016. Long-term osseointegration of 3D printed CoCr constructs

with an interconnected open-pore architecture prepared by electron beam melting. *Acta Biomaterialia*, 36, pp.296-309.

Shamsi, M., Huynh, C., Gordon, J. and Patloori, S., 2017. 3D opportunity for health care: Demystifying FDA regulations for medical devices. *Deloitte*. [Online] Available at: https://www2.deloitte.com/content/dam/insights/us/articles/3257_Demystifying-FDA-regulations-for-medical-devices/3257_Demystifying-FDA-regulations-for-medical-devices.pdf [Accessed 9 March 2022].

Sharma, A.K., Cizmic, Z., Dennis, D.A., Kreuzer, S.W., Miranda, M.A. and Vigdorchik, J.M., 2021. Low dislocation rates with the use of patient specific "Safe zones" in total hip arthroplasty. *Journal of Orthopaedics*, 21(27), pp.41-48.

Shi, H., Zhou, P., Li, J., Liu, C. and Wang, L., 2021. Functional Gradient Metallic Biomaterials: Techniques, Current Scenery, and Future Prospects in the Biomedical Field. *Frontiers in Bioengineering and Biotechnology*, 8.

Shi, Q., Ji, T., Huang, S., Tang, X., Yang, R. and Guo, W., 2021. Use of a 3D-Printed Patient-Specific Surgical Jig and Ready-Made Total Sacral Endoprosthesis for Total Sacrectomy and Reconstruction. *BioMed Research International*. 2021, pp.1-9.

Sidambe, A., 2014. Biocompatibility of Advanced Manufactured Titanium Implants—A Review. *Materials*, 7(12), pp.8168-8188.

Škulj, G., Vrabič, R., Butala, P. and Sluga, A., 2015. Decentralised Network Architecture for Cloud Manufacturing. *International Journal of Computer Integrated Manufacturing*, pp.1-14.

Silva, R., Silva, B., Fernandes, C., Morouço, P., Alves, N. and Veloso, A., 2023. A Review on 3D Scanners Studies for Producing Customized Orthoses, *10.20944/preprints202311.1915.v1*.

Simoneau, G., 2002. Kinesiology of Walking. In: *Kinesiology of the musculoskeletal system: Foundations for physical rehabilitation*. 2nd ed. Ed. By A. Neumann. Missouri: Mosby, pp.627-681.

Sing, S.L., An, J., Yeong, W.Y. and Wiria, F.E., 2015. Laser and electron-beam powder-bed additive manufacturing of metallic implants: A review on processes, materials and designs. *Journal of Orthopaedic Research*, 34(3), pp.369-385.

Singh, S.N., Venkatesh, V.S. and Deoghare, A.B., 2021. A review on the role of 3D printing in the fight against covid-19: Safety and challenges. *Rapid Prototyping Journal*, 27(2), pp.407-420.

Smith, J., 1908. *Method of reproducing objects*. US Patent No. 891013.

Snijders, T., Schlösser, T., van Gaalen, S., Castelein, R., Weinans, H. and de Gast, A., 2018. Trigonometric Algorithm Defining the True Three-Dimensional Acetabular Cup Orientation. *JBJS Open Access*, 3(3).

Snyder, G., Cotteleer, M. and Kotek, B., 2014. 3D opportunity in medical technology. *Deloitte*. [Online] Available at: https://www2.deloitte.com/content/dam/insights/us/articles/additive-manufacturing-3d-opportunity-in-medtech/DUP_709-3D-Opportunity-MedTech_MASTER.pdf [Accessed 9 March 2022].

Srinivasan, V. and Bassan, J., 2012. *3D Printing and the Future of Manufacturing*. Computer Sciences Corporation.

Sola, A., Bellucci, D. and Cannillo, V., 2016. Functionally graded materials for orthopedic applications – an update on design and manufacturing. *Biotechnology Advances*, 34(5), pp.504-531.

Spece, H., Basgul, C., Andrews, E., MacDonald, W., Taheri, L., Kurtz, M., 2021. A systematic review of preclinical in vivo testing of 3D printed porous Ti6Al4V for orthopedic applications, part I: Animal models and bone ingrowth outcome measures. *Journal of Biomedical Materials Research – Part B: Applied Biomaterials*, 109(10), pp.1436-1454.

Spierings, A., Herres, N. and Levy, G., 2011. Influence of the particle size distribution on surface quality and mechanical properties in AM steel parts. *Rapid Prototyping Journal*, 17(3), pp.195-202.

Srai, J.S., Kumar, M., Graham, G., Phillips,W., Tooze, J., Ford, S., Beecher, P., Raj, B., Gregory, M., Kumar, M.T., Ravi, B., Neely, A., Shankar, R., Charnley, F. and Tiwari, A., 2016. Distributed manufacturing: Scope, challenges and opportunities. *International Journal of Production Research*, 54(23), pp.6917-6935.

Srai, J.S., Graham, G., Hennelly, P., Phillips, W., Kapletia, D. and Lorentz, H., 2020. Distributed manufacturing: A new form of localised production?. *International Journal of Operations & Production Management*, 40(6), pp.697-727.

Srinivasan, A., Haritos, G. and Hedberg, F., 1991. Biomimetics: Advancing Man-Made Materials Through Guidance From Nature. *Applied Mechanics Reviews,* 44(11), pp.463-482.

Steeves, M., Stone, C., Mogaard, J. and Byrne, S., 2005. How pilot-hole size affects bone-screw pullout strength in human cadaveric cancellous bone. *Canadian Journal of Surgery,* 48(3), pp.207-212.

Steinhoff, G., 2016. *Regenerative Medicine: From Protocol to Patient*. 3rd ed. Cham: Springer.

Steinicke, F., 2016. *Being Really Virtual*. Cham: Springer.

Sugano, N., 2018. *Computer assisted orthopaedic surgery for hip and knee*. Singapore: Springer.

Sutherland, I., 1965. The Ultimate Display. *Information Processing Techniques Office*, ARPA, OSD.

Swainson, W., 1971. *Method, Medium and Apparatus for Producing Three-Dimensional Figure Product*. US Patent No. 4041476.

Swarup, I. and O'Donnell, J., 2016. An Overview of the History of Orthopedic Surgery. *American Journal of Orthopaedics*, 45(7), pp.434-438.

Tack, P., Victor, J., Gemmel, P. and Annemans, L., 2016. 3D-printing techniques in a medical setting: a systematic literature review. *BioMedical Engineering OnLine*, 15(1).

Taddei, F., Pancanti, A. and Viceconti, M., 2004. An improved method for the automatic mapping of computed tomography numbers onto finite element models. *Medical Engineering and Physics*, 26(1), pp.61-69.

Taddei, F., Schileo, E., Helgason, B., Cristofolini, L. and Viceconti, M., 2007. The material mapping strategy influences the accuracy of CT-based finite element models of Bones: An Evaluation Against Experimental Measurements. *Medical Engineering and Physics*, 29(9), pp.973-979.

Talanki, V., Peng, Q., Shamir, S., Baete, S., Duong, T. and Wake, N., 2021. Three - Dimensional Printed Anatomic Models Derived From Magnetic Resonance Imaging Data: Current State and Image Acquisition Recommendations for Appropriate Clinical Scenarios. *Journal of Magnetic Resonance Imaging*.

Tan, X., Tan, Y., Chow, C., Tor, S. and Yeong, W., 2017. Metallic powder-bed based 3D printing of cellular scaffolds for orthopaedic implants: A state-of-the-art review on manufacturing, topological design, mechanical properties and biocompatibility. *Materials Science and Engineering: C*, 76, pp.1328-1343.

Tang, Y., Chau, K., Kwok, A., Zhu, T. and Ma, X., 2022. A systematic review of immersive technology applications for medical practice and education - Trends, application areas, recipients, teaching contents, evaluation methods, and performance. *Educational Research Review*, 35.

Taniguchi, N., Fujibayashi, S., Takemoto, M., Sasaki, K., Otsuki, B., Nakamura, T., Matsushita, T., Kokubo, T. and Matsuda, S., 2016. Effect of pore size on bone ingrowth into porous titanium implants fabricated by additive manufacturing: An in vivo experiment. *Materials Science and Engineering: C*, 59, pp.690-701.

Tanji, A., Nagura, T., Iwamoto, T., Matsumura, N., Nakamura, M., Matsumoto, M. and Sato, K., 2022. Total elbow arthroplasty using an augmented reality–assisted surgical technique. *Journal of Shoulder and Elbow Surgery*, 31(1), pp.175-184.

Tareq, M.S., Rahman, T., Hossain, M. and Dorrington, P., 2021. Additive Manufacturing and the COVID-19 challenges: An in-depth study. *Journal of Manufacturing Systems*, 60, pp.787-798.

Tavassoli, S., 2018. *Adoption and Diffusion of Disruptive Technologies: The Case of 3D Printing in the Medical Device Industry*. *White paper I: Opportunity Areas, Stakeholder mapping and Road Mapping*. RMIT University. [Online] Available at: https://www.rmit.edu.au/content/dam/rmit/au/en/research/ecps/gbi/Medtech-3D-Report-2018.pdf [Accessed 9 March 2022].

Tavassoli, S., 2019. *Adoption and Diffusion of Disruptive Technologies: The Case of 3D Printing in the Medical Device Industry, White Paper II: Business Models, Barriers, and Solutions*. RMIT University. [Online] Available at: https://www.rmit.edu.au/content/dam/rmit/au/en/research/ecps/gbi/Medtech-3D-Report-2018.pdf [Accessed 9 March 2022].

Teatini, A., Kumar, R., Elle, O. and Wiig, O., 2021. Mixed reality as a novel tool for diagnostic and surgical navigation in orthopaedics. *International Journal of Computer Assisted Radiology and Surgery*, 16(3), pp.407-414.

Tejero, R., Anitua, E. and Orive, G., 2014. Toward the biomimetic implant surface: Biopolymers on titanium-based implants for bone regeneration. *Progress in Polymer Science*, 39(7), pp.1406-1447.

Telang, V., Pemmada, R., Thomas, V., Ramakrishna, S., Tandon, P. and Nanda, H., 2021. Harnessing additive manufacturing for magnesium-based metallic bioimplants: Recent advances and future perspectives. *Current Opinion in Biomedical Engineering*, 17.

Teo, A., Ng, D., Lee, P. and O'Neill, G., 2021. Point-of-Care 3D Printing: A Feasibility Study of Using 3D Printing for Orthopaedic Trauma. *Injury*, 52(11), pp.3286-3292.

Tezuka , T., Heckmann , N.D., Bodner, R.J. and Dorr, L.D., 2019. . Functional Safe Zone Is Superior to the Lewinnek Safe Zone for Total Hip Arthroplasty: Why the Lewinnek Safe Zone Is Not Always Predictive of Stability. *Journal of Arthroplasty*, 34(1), pp.3-8.

Thavornyutikarn, B., Chantarapanich, N., Sitthiseripratip, K., Thouas, G. and Chen, Q., 2014. Bone tissue engineering scaffolding: computer-aided scaffolding techniques. *Progress in Biomaterials*, 3(2-4), pp.61-102.

Thayaparan, G., Owbridge, M., Thompson, R. and D'Urso, P., 2018. Designing patient-specific solutions using biomodelling and 3D-printing for revision lumbar spine surgery. *European Spine Journal*, 28(S2), pp.18-24.

Thayaparan, G., Owbridge, M., Linden, M., Thompson, R., Lewis, P. and D'Urso, P., 2020b. Measuring the performance of patient-specific solutions for minimally invasive transforaminal lumbar interbody fusion surgery. *Journal of Clinical Neuroscience*, 71, pp.43-50.

Thayaparan, G., Owbridge, M., Thompson, R. and D'Urso, P., 2020a. Patient-specific processes for occipitocervical fixation using biomodelling and additive manufacturing. *Journal of Clinical Neuroscience*, 71, pp.251-256.

Thomas, D. and Gilbert, S., 2014. Costs and Cost Effectiveness of Additive Manufacturing: A Literature Review and Discussion. *NIST Special Publication 1176*.

Thompson, M., Moroni, G., Vaneker, T., Fadel, G., Campbell, R., Gibson, I., Bernard, A., Schulz, J., Graf, P., Ahuja, B. and Martina, F., 2016. Design for Additive Manufacturing: Trends, opportunities, considerations, and constraints. *CIRP Annals*, 65(2), pp.737-760.

Tibbits, S., 2014. 4D Printing: Multi-Material Shape Change. *Architectural Design*, 84(1), pp.116-121.

Tile, M., Helfet, D., Kellam, J. and Vrahas, M., 2015. *Fractures of the pelvis and acetabulum: Principles and Methods of Management*. 4th ed. Davos Platz: AO Foundation.

Tilton, M., Armstrong, A., Sanville, J., Chin, M., Hast, M., Lewis, G. and Manogharan, G., 2020b. Biomechanical Testing of Additive Manufactured Proximal Humerus Fracture Fixation Plates. *Annals of Biomedical Engineering*, 48(1), pp.463-476.

Tilton, M., Lewis, G., Bok Wee, H., Armstrong, A., Hast, M. and Manogharan, G., 2020a. Additive manufacturing of fracture fixation implants: Design, material characterization, biomechanical modeling and experimentation. *Additive Manufacturing*, 33.

Timercan, A., Sheremetyev, V. and Brailovski, V., 2021. Mechanical properties and fluid permeability of gyroid and diamond lattice structures for intervertebral devices: Functional requirements and comparative analysis. *Science and Technology of Advanced Materials*, 22(1), pp.285-300.

Todros, S., Todesco, M. and Bagno, A., 2021. Biomaterials and Their Biomedical Applications: From Replacement to Regeneration. *Processes*, 9(11).

Toh, W., Wang, P., Tan, X., Nai, M., Liu, E. and Tor, S., 2016. Microstructure and Wear Properties of Electron Beam Melted Ti-6Al-4V Parts: A Comparison Study against As-Cast Form. *Metals*, 6(11).

Tomiyama, T., Gu, P., Jin, Y., Lutters, D., Kind, C. and Kimura, F., 2009. Design methodologies: Industrial and educational applications. *CIRP Annals*, 58(2), pp.543-565.

Tong, Y., Kaplan, D., Spivak, J. and Bendo, J., 2020. Three-dimensional printing in spine surgery: a review of current applications. *The Spine Journal*, 20(6), pp.833-846.

Toro, M., Cardona, A., Restrepo, D. and Buitrago, L., 2021. Does vaporized hydrogen peroxide sterilization affect the geometrical properties of anatomic models and guides 3D printed from computed tomography images?. *3D Printing in Medicine*, 7(1).

Török, G., Gombocz, P., Bognár, E., Nagy, P., Dinya, E., Kispélyi, B. and Hermann, P., 2020. Effects of disinfection and sterilization on the dimensional changes and mechanical properties of 3D printed surgical guides for implant therapy – pilot study. *BMC Oral Health*, 20(1).

Tortora, G. and Derrickson, B., 2020. *Principles of anatomy and physiology*. 16th ed. Hoboken: Wiley.

Tran, M., Varzaly, J., Chan, J., Caplash, Y. and Worthington, M., 2018. Novel Sternal Reconstruction with Custom Three-Dimensional–Printed Titanium PoreStar Prosthesis. *Innovations: Technology and Techniques in Cardiothoracic and Vascular Surgery*, 13(4), pp.309-311.

Trovarelli, G., Angelini, A., Pala, E., Cappellari, A., Breda, A. and Ruggieri, P., 2019. Infection in orthopaedic oncology: crucial problem in modern reconstructive techniques. *European review for medical and pharmacological sciences*, 23(2), pp.271-278.

Trikoupis, I.G., Mavrodontis, I.I., Papadopoulos, D.V., Goumenos, S.D., Georgouli, D.A., Gavriil, P.A., Melissaridou, D., Savvidou, O.D., Kontogeorgakos, V.A. and Papagelopoulos, P.J., 2024. 3D-printed glenoid implant reconstruction, after partial scapulectomy for malignant tumors. a case series. *European Journal of Orthopaedic Surgery & Traumatology*.

Tsikandylakis, G., Mohaddes, M., Cnudde, P., Eskelinen, A., Kärrholm, J. and Rolfson, O., 2018. Head size in primary total hip arthroplasty. *EFORT Open Reviews*, 3(5), pp.225-231.

Tunn, P., 2009. *Treatment of Bone and Soft Tissue Sarcomas*. Berlin: Springer.

Turna, A., Kavakli, K., Sapmaz, E., Arslan, H., Caylak, H., Gokce, H. and Demirkaya, A., 2013. Reconstruction with a patient-specific titanium implant after a wide anterior chest wall resection. *Interactive CardioVascular and Thoracic Surgery*, 18(2), pp.234-236.

Uflacker, R., 2007. *Atlas of Vascular Anatomy*. Philadelphia: Wolters Kluwer Health.

Uhl, J., Jorge, J., Lopes, D. and Campos, P., 2021. *Digital Anatomy: Applications of Virtual, Mixed and Augmented Reality*, Cham: Springer.

Ujjie, A., 1971. *Method of and apparatus for constructing substantially circular cross section vessel by welding*. US Patent No. 3558846.

UK Intellectual Property Office, 2013. *3D Printing: A patent overview*.

United Nations, Department of Economic and Social Affairs, Population Division, 2019. *World Population Prospects 2019: Highlights*. [online] Available at: https://population.un.org/wpp/Publications/Files/WPP2019_Highlights.pdf [Accessed 9 March 2022].

Upex, P., Jouffroy, P. and Riouallon, G., 2017. Application of 3D printing for treating fractures of both columns of the acetabulum: Benefit of pre-contouring plates on the mirrored healthy pelvis. *Orthopaedics & Traumatology: Surgery & Research*, 103(3), pp.331-334.

Urschel, W., 1943. *Molding and depositing machine for solidifiable plastic materials*. US Patent No. 2314468.

Vakharia, V., Khan, S., Marathe, K., Giannis, T., Webber, L. and Choi, D., 2021. Printing in a Pandemic: 3D printing solutions for healthcare during COVID-19. A Protocol for a PRISMA systematic review. *Annals of 3D Printed Medicine*, 2.

Van den Brink, W. and Lamerigts, N., 2020. Complete Osseointegration of a Retrieved 3-D Printed Porous Titanium Cervical Cage. *Frontiers in Surgery*, 7.

Van der Stok, J., Koolen, M., de Maat, M., Amin Yavari, S., Alblas, J., Patka, P., Verhaar, J., van Lieshout, E., Zadpoor, A., Weinans, H. and Jahr, H., 2015. Full regeneration of segmental bone defects using porous titanium implants loaded with BMP-2 containing fibrin gels. *European Cells and Materials*, 29, pp.141-154.

Vaneker, T., Bernard, A., Moroni, G., Gibson, I. and Zhang, Y., 2020. Design for Additive Manufacturing: Framework and methodology. *CIRP Annals*, 69(2), pp.578-599.

Van Horn, M., Beard, R., Wang, W., Cunningham, B., Mullinix, K., Allall, M. and Bucklen, B., 2021. Comparison of 3D-printed titanium-alloy, standard titanium-alloy, and PEEK interbody spacers in an ovine model. *The Spine Journal*, 21(12), pp.2097-2103.

Vannucci, J., Scarnecchia, E., Potenza, R., Ceccarelli, S., Monopoli, D. and Puma, F., 2020. Dynamic titanium prosthesis based on 3D-printed replica for chest wall resection and reconstruction. *Translational Lung Cancer Research*, 9(5), pp.2027-2032.

Ventola, C., 2014. Medical Applications for 3D Printing: Current and Projected Uses. *Pharmacy and Therapeutics*, 39(10), pp.704-711.

Verboeket, V., Khajavi, S. H., Krikke, H., Salmi, M. and Holmström, J., 2021. Additive manufacturing for localized medical parts production: A case study. *IEEE Access*, 9, pp.25818-25834.

Verhey, J., Haglin, J., Verhey, E. and Hartigan, D., 2020. Virtual, augmented, and mixed reality applications in orthopedic surgery. *The International Journal of Medical Robotics and Computer Assisted Surgery*, 16(2).

Verma, J. and Paul, S., 2022. *Advances in augmented reality and virtual reality*. Singapore: Springer.

Viglialoro, R., Condino, S., Turini, G., Carbone, M., Ferrari, V. and Gesi, M., 2021. Augmented Reality, Mixed Reality, and Hybrid Approach in Healthcare Simulation: A Systematic Review. *Applied Sciences*, 11(5).

Vickers, O., Culmer, P., Isaac, G., Kay, R., Shuttleworth, M., Board, T. and Williams, S., 2021. Is in vivo sensing in a total hip replacement a possibility? A review on past systems and future challenges. *Progress in Biomedical Engineering*, 3(4).

Vincent, J., Bogatyreva, O., Bogatyrev, N., Bowyer, A. and Pahl, A., 2006. Biomimetics: its practice and theory. *Journal of The Royal Society Interface*, 3(9), pp.471-482.

Vivanco, F., Burgers, A., García-Rodríguez, S., Crookshank, M., Kunz, M., MacIntyre, J., Harrison, M., Bryant, T., Sellens, W. and Ploeg, L., 2014. Estimating the density of femoral head trabecular bone from hip fracture patients using computed tomography scan data. *Proceedings of the Institution of Mechanical Engineers, Part H: Journal of Engineering in Medicine*, 228(6), pp.616-626.

Vogt, M., Rips, A. and Emmelmann, C., 2021. Comparison of iPad Pro®'s LiDAR and TrueDepth Capabilities with an Industrial 3D Scanning Solution. *Technologies*, 9(2).

Walker, P. and Ewald, F., 1990. *Method of designing and manufacturing a human joint prosthesis*. US Patent No. 4936862.

Wallace, N., Schaffer, N., Aleem, I. and Patel, R., 2020. 3D-printed Patient-specific Spine Implants. *Clinical Spine Surgery: A Spine Publication*, 33(10), pp.400-407.

Walbron, P., Common, H., Thomazeau, H., Hosseini, K., Peduzzi, L., Bulaid, Y. and Sirveaux, F., 2020. Virtual reality simulator improves the acquisition of basic arthroscopy skills in first-year orthopedic surgery residents. *Orthopaedics & Traumatology: Surgery & Research*, 106(4), pp.717-724.

Wan, Z., Zhang, P., Liu, Y., Lv, L. and Zhou, Y., 2019. Four-Dimensional Bioprinting: Current Developments and Applications in Bone Tissue Engineering. *SSRN Electronic Journal*.

Wang, X., Xu, S., Zhou, S., Xu, W., Leary, M., Choong, P., Qian, M., Brandt, M. and Xie, Y., 2016. Topological design and additive manufacturing of porous metals for bone scaffolds and orthopaedic implants: A review. *Biomaterials*, 83, pp.127-141.

Wang, D., Wang, Y., Wu, S., Lin, H., Yang, Y., Fan, S., Gu, C., Wang, J. and Song, C., 2017. Customized a Ti6Al4V Bone Plate for Complex Pelvic Fracture by Selective Laser Melting. *Materials*, 10(1).

Wang, G., Shen, L., Zhao, J., Liang, H., Xie, D., Tian, Z. and Wang, C., 2018. Design and Compressive Behavior of Controllable Irregular Porous Scaffolds: Based on Voronoi-Tessellation and for Additive Manufacturing. *ACS Biomaterials Science & Engineering*, 4(2), pp.719-727.

Wang, J., Min, L., Lu, M., Zhang, Y., Wang, Y., Luo, Y., Zhou, Y., Duan, H. and Tu, C., 2019. Three-dimensional-printed custom-made hemipelvic endoprosthesis for primary malignancies involving acetabulum: the design solution and surgical techniques. *Journal of Orthopaedic Surgery and Research*, 14(1).

Wang, C., Chen, Y., Wang, L., Wang, D., Gu, C., Lin, X., Liu, H., Chen, J., Wen, X., Liu, Y., Huang, F., Yao, L., Fan, S., Huang, W. and Dong, J., 2020. Three-dimensional printing of patient-specific plates for the treatment of acetabular fractures involving quadrilateral plate disruption. *BMC Musculoskeletal Disorders*, 21(1).

Wang, J., Min, L., Lu, M., Zhang, Y., Wang, Y., Luo, Y., Zhou, Y., Duan, H. and Tu, C., 2020. What are the Complications of Three-dimensionally Printed, Custom-made, Integrative Hemipelvic Endoprostheses in Patients with Primary Malignancies Involving the Acetabulum, and What is the Function of These Patients?. *Clinical Orthopaedics and Related Research*, 478(11), pp.2487-2501.

Wang, W., Liang, Z., Yang, S., Feng, Q., Nie, X., Su, G., Yuan, W. and Han, Y., 2020. Three-dimensional (3D) -printed titanium sternum replacement: A case report. *Thoracic Cancer*, 11(11), pp.3375-3378.

Wang, X., Xu, H. and Zhang, J., 2020. Using personalized 3D printed Titanium sleeve-prosthetic composite for reconstruction of severe segmental bone loss of proximal femur in revision total hip arthroplasty. *Medicine*, 99(3).

Wang, X., Wang, C., Zhou, X., Wang, D., Zhang, M., Gao, Y. and Zhang, P., 2020. Evaluating lattice mechanical properties for lightweight heat-resistant load-bearing structure design. *Materials*, 13(21).

Wang, H., Liu, J., Wang, C., Shen, S., Wang, X. and Lin, K., 2021. The synergistic effect of 3D-printed microscale roughness surface and nanoscale feature on enhancing osteogenic differentiation and rapid osseointegration. *Journal of Materials Science & Technology*, 63, pp.18-26.

Wang, J., Zhang, Y., Aghda, N., Pillai, A., Thakkar, R., Nokhodchi, A. and Maniruzzaman, M., 2021. Emerging 3D printing technologies for drug delivery devices: Current status and future perspective. *Advanced Drug Delivery Reviews*, 174, pp.294-316.

Wasielewski, R., Cooperstein, L., Kruger, M. and Rubash, H., 1990. Acetabular anatomy and the transacetabular fixation of screws in total hip arthroplasty. *The Journal of Bone and Joint Surgery*, 72(4), pp.501-508.

Wasserthal, J., Breit, H.-C., Meyer, M.T., Pradella, M., Hinck, D., Sauter, A.W., Heye, T., Boll, D., Cyriac, J., Yang, S., Bach, M. and Segeroth, M., 2023. TotalSegmentator: Robust Segmentation of 104 Anatomic Structures in CT Images. *Radiology: Artificial Intelligence*.

Wauthle, R., Van der Stok, J., Yavari, S., Van Humbeeck, J., Kruth, J., Zadpoor, A., Weinans, H., Mulier, M. and Schrooten, J., 2015a. Additively manufactured porous tantalum implants. *Acta Biomaterialia*, 14, pp.217-225.

Wauthle, R., Vrancken, B., Beynaerts, B., Jorissen, K., Schrooten, J., Kruth, J. and Van Humbeeck, J., 2015b. Effects of build orientation and heat treatment on the microstructure and mechanical properties of selective laser melted Ti6Al4V lattice structures. *Additive Manufacturing*, 5, pp.77-84.

Wedemeyer, C. and Kauther, M., 2011. Hemipelvectomy- only a salvage therapy?. *Orthopedic Reviews*, 3(1).

Weems, A., Pérez-Madrigal, M., Arno, M. and Dove, A., 2020. 3D Printing for the Clinic: Examining Contemporary Polymeric Biomaterials and Their Clinical Utility. *Biomacromolecules*, 21(3), pp.1037-1059.

Wei, R., Guo, W., Ji, T., Zhang, Y. and Liang, H., 2016. One-step reconstruction with a 3D-printed, custom-made prosthesis after total en bloc sacrectomy: a technical note. *European Spine Journal*, 26(7), pp.1902-1909.

Weißmann, V., Bader, R., Hansmann, H. and Laufer, N., 2016. Influence of the structural orientation on the mechanical properties of selective laser melted Ti6Al4V open-porous scaffolds. *Materials & Design*, 95, pp.188-197.

Weller, C., Kleer, R. and Piller, F., 2015. Economic implications of 3D printing: Market structure models in light of additive manufacturing revisited. *International Journal of Production Economics*, 164, pp.43-56.

Wen, Y., Xun, S., Haoye, M., Baichuan, S., Peng, C., Xuejian, L., Kaihong, Z., Xuan, Y., Jiang, P. and Shibi, L., 2017. 3D printed porous ceramic scaffolds for bone tissue engineering: a review. *Biomaterials Science*, 5(9), pp.1690-1698.

Wegst, U. and Ashby, M., 2004. The mechanical efficiency of natural materials. *Philosophical Magazine*, 84(21), pp.2167-2186.

White, B., Garland, A., Alberdi, R. and Boyce, B., 2021. Interpenetrating lattices with enhanced mechanical functionality. *Additive Manufacturing*, 38.

Wild, M., Ghayor, C., Zimmermann, S., Rüegg, J., Nicholls, F., Schuler, F., Chen, T. and Weber, F., 2018. Osteoconductive Lattice Microarchitecture for Optimized Bone Regeneration. *3D Printing and Additive Manufacturing*, 6(1), pp.40-49.

Willeme, F., 1864. *Photo-Sculpture*. US Patent No. 43822.

Willemen, N., Morsink, M., Veerman, D., da Silva, C., Cardoso, J., Souto, E. and Severino, P., 2021. From oral formulations to drug-eluting implants: using 3D and 4D printing to develop drug delivery systems and personalized medicine. *Bio-Design and Manufacturing*, 5(1), pp.85-106.

Willemsen, K., Nizak, R., Noordmans, H., Castelein, R., Weinans, H. and Kruyt, M., 2019. Challenges in the design and regulatory approval of 3D-printed surgical implants: a two-case series. *The Lancet Digital Health*, 1(4), pp.163-171.

Wo, J., Huang, S., Wu, D., Zhu, J., Li, Z. and Yuan, F., 2020. The integration of pore size and porosity distribution on Ti-6A1-4V scaffolds by 3D printing in the modulation of osteo-differentation. *Journal of Applied Biomaterials & Functional Materials*, 18.

Wohlers Associates, 2021a. *Wohlers Report: 3D Printing and Additive Manufacturing Global State of the Industry*.

Wohlers Associates, 2021b. *Post-Processing of AM and 3D-Printed Parts*.

Wohlers, T. and Gornet, T., 2021. History of additive manufacturing. [Online] Available at: http://wohlersassociates.com/history2021.pdf [Accessed on 9 March 2022 with "Wohlers" key].

Wolff, J., 1986. The Law of Bone Remodeling. New York: Springer.

Wong, J., 2016. 3D Printing Applications for Space Missions. *Aerospace Medicine and Human Performance*, 87(6), pp.580-582.

Wong, K., Kumta, S., Cheung, K., Kwok, C., Lung, T., Ming, S. and Chi, L., 2010. Tumour Prosthetic Replacement in Paediatric Bone Cancer. *Hong Kong Journal of Paediatrics*. 15. pp.104-110.

Wong, K., Kumta, S., Geel, N. and Demol, J., 2015. One-step reconstruction with a 3D-printed, biomechanically evaluated custom implant after complex pelvic tumor resection. *Computer Aided Surgery*, 20(1), pp.14-23.

Wu, J. and Hochman, M., 2012. *Bone tumors: A Practical Guide to Imaging*. London: Springer.

Wu, J., Aage, N., Westermann, R. and Sigmund, O., 2018. Infill Optimization for Additive Manufacturing—Approaching Bone-Like Porous Structures. *IEEE Transactions on Visualization and Computer Graphics*, 24(2), pp.1127-1140.

Wu, Y., Chen, N., Xu, Z., Zhang, X., Liu, L., Wu, C., Zhang, S., Song, Y., Wu, T., Liu, H., Tang, M. and Wu, W., 2018. Application of 3D printing technology to thoracic wall tumor resection and thoracic wall reconstruction. *Journal of Thoracic Disease*, 10(12), pp.6880-6890.

Wu, H., Shao, Q., Song, C., Shang, R., Liu, X. and Cai, X., 2020. Personalized Three-Dimensional Printed Anterior Titanium Plate to Treat Double-Column Acetabular Fractures: A Retrospective Case-Control Study. *Orthopaedic Surgery*, 12(4), pp.1212-1222.

Wu, C., Deng, J., Pan, J., Li, T., Tan, L. and Yuan, D., 2020. Anatomical conditions and patient-specific locked navigation templates for transverse sacroiliac screw placement: a retrospective study. *Journal of Orthopaedic Surgery and Research*, 15(1).

Wu, Z., Narra, S. and Rollett, A., 2020. Exploring the fabrication limits of thin-wall structures in a laser powder bed fusion process. *The International Journal of Advanced Manufacturing Technology*, 110, pp.191-207.

Wu, H., Yang, S., Liu, J., Li, L., Luo, Y., Dai, Z., Wang, X., Yao, X., Zhou, F. and Li, X., 2021. 3D printing guide plate for accurate hemicortical bone tumor resection in metaphysis of distal femoral: a technical note. *Journal of Orthopaedic Surgery and Research*, 16(1).

Xi, W., Hegde, V., Zoller, S., Park, H., Hart, C., Kondo, T., Hamad, C., Hu, Y., Loftin, A., Johansen, D., Burke, Z., Clarkson, S., Ishmael, C., Hori, K., Mamouei, Z., Okawa, H., Nishimura, I., Bernthal, N. and Segura, T., 2021. Point-of-care antimicrobial coating protects orthopaedic implants from bacterial challenge. *Nature Communications*, 12(1).

Xie, X., Yu, X., Zeng, S., Du, R., Hu, Y., Yuan, Z., Lu, E., Dai, K. and Tang, T., 2010. Enhanced osteointegration of orthopaedic implant gradient coating composed of bioactive glass and nanohydroxyapatite. *Journal of Materials Science: Materials in Medicine*, 21(7), pp.2165-2173.

Xu, L., Qin, H., Cheng, Z., Jiang, W., Tan, J., Luo, X. and Huang, W., 2021. 3D-printed personalised prostheses for bone defect repair and reconstruction following resection of metacarpal giant cell tumours. *Annals of Translational Medicine*, 9(18), pp.1421-1421.

Xu, S., Guo, Z., Shen, Q., Peng, Y., Li, J., Li, S., He, P., Jiang, Z., Que, Y., Cao, K., Hu, B. and Hu, Y., 2022. Reconstruction of tumor-induced pelvic defects with customized, three-dimensional printed prostheses. *Frontiers in Oncology*, 12.

Yadav, D., Garg, R., Ahlawat, A. and Chhabra, D., 2020. 3D printable biomaterials for orthopedic implants: Solution for sustainable and circular economy. *Resources Policy*, 68.

Yam, M., Chao, J., Leong, C. and Tan, C., 2021. 3D printed patient specific customised surgical jig for reverse shoulder arthroplasty, a cost effective and accurate solution. *Journal of Clinical Orthopaedics and Trauma*, 21.

Yamazaki, A., Ito, T., Sugimoto, M., Yoshida, S., Honda, K., Kawashima, Y., Fujikawa, T., Fujii, Y. and Tsutsumi, T., 2021. Patient-specific virtual and mixed reality for immersive, experiential

anatomy education and for surgical planning in temporal bone surgery. *Auris Nasus Larynx*, 48(6), pp.1081-1091.

Yang, J., Cai, H., Lv, J., Zhang, K., Leng, H., Wang, Z. and Liu, Z., 2014. Biomechanical and Histological Evaluation of Roughened Surface Titanium Screws Fabricated by Electron Beam Melting. *PLoS ONE*, 9(4).

Yang, K., Zhu, J., Wang, C., Jia, D., Song, L. and Zhang, W., 2018. Experimental validation of 3D printed material behaviors and their influence on the structural topology design. *Computational Mechanics*, 61(5), pp.581-598.

Yang, Y., Song, X., Li, X., Chen, Z., Zhou, C., Zhou, Q. and Chen, Y., 2018. Recent Progress in Biomimetic Additive Manufacturing Technology: From Materials to Functional Structures. *Advanced Materials*, 30(36).

Yang, L., Mertens, R., Ferrucci, M., Yan, C., Shi, Y. and Yang, S., 2018. Continuous graded Gyroid cellular structures fabricated by selective laser melting: Design, manufacturing and mechanical properties. *Materials & Design*, 162(15), pp.394-404.

Yang, E., Leary, M., Lozanovski, B., Downing, D., Mazur, M., Sarker, A., Khorasani, A., Jones, A., Maconachie, T., Bateman, S., Easton, M., Qian, M., Choong, P. and Brandt, M., 2019. Effect of geometry on the mechanical properties of Ti-6Al-4V Gyroid structures fabricated via SLM: A numerical study. *Materials & Design*, 184.

Yang, J., Jin, X., Gao, H., Zhang, D., Chen, H., Zhang, S. and Li, X., 2020. Additive manufacturing of trabecular tantalum scaffolds by laser powder-bed fusion: Mechanical property evaluation and porous structure characterization. *Materials Characterization*, 170.

Yang, Q., Mu, M., Tao, X. and Tang, K., 2021. Three-dimensional printed talar prosthesis with biological function for giant cell tumor of the talus: A case report and review of the literature. *World Journal of Clinical Cases*, 9(13), pp.3147-3156.

Yang, S., Lin, H. and Luo, C., 2021. Meta-Analysis of 3D Printing Applications in Traumatic Fractures. *Frontiers in Surgery*, 8.

Yang, Y., Labus, K., Gadomski, B., Bruyas, A., Easley, J., Nelson, B., Palmer, R., McGilvray, K., Regan, D., Puttlitz, C., Stahl, A., Lui, E., Li, J., Moeinzadeh, S., Kim, S., Maloney, W. and Gardner, M., 2021. Osteoinductive 3D printed scaffold healed 5 cm segmental bone defects in the ovine metatarsus. *Scientific Reports*, 11(1).

Yeroushalmi, D., Singh, V., Maher, N., Gabor, J., Zuckerman, J. and Schwarzkopf, R., 2021. Excellent mid-term outcomes with a hemispheric titanium porous-coated acetabular component for total hip arthroplasty: 7–10 year follow-up. *HIP International*.

Yu, Z., Zhang, W., Fang, X., Tu, C. and Duan, H., 2021. Pelvic Reconstruction With a Novel Three-Dimensional-Printed, Multimodality Imaging Based Endoprosthesis Following Enneking Type I + IV Resection. *Frontiers in Oncology*, 11.

Zabala-Travers, S., 2021. Biomodeling and 3D printing: A novel radiology subspecialty. *Annals of 3D Printed Medicine*, 4.

Zadpoor, A., 2019. Mechanical performance of additively manufactured meta-biomaterials. *Acta Biomaterialia*, 85, pp.41-59.

Zafar, M., Zhu, D. and Zhang, Z., 2019. 3D Printing of Bioceramics for Bone Tissue Engineering. *Materials*, 12(20).

Zannoni, C., Mantovani, R. and Viceconti, M., 1998. Material properties assignment to finite element models of bone structures: a new method. *Medical Engineering and Physics*, 20(10), pp.735-40.

Zhang, B., Myers, D., Wallace, G., Brandt, M. and Choong, P., 2014a. Bioactive Coatings for Orthopaedic Implants—Recent Trends in Development of Implant Coatings. *International Journal of Molecular Sciences*, 15(7), pp.11878-11921.

Zhang, S., Wei, Q., Cheng, L., Li, S. and Shi, Y., 2014b. Effects of scan line spacing on pore characteristics and mechanical properties of porous Ti6Al4V implants fabricated by selective laser melting. *Materials & Design*, 63, pp.185-193.

Zhang, B., Pei, X., Zhou, C., Fan, Y., Jiang, Q., Ronca, A., D'Amora, U., Chen, Y., Li, H., Sun, Y. and Zhang, X., 2018. The biomimetic design and 3D printing of customized mechanical properties porous Ti6Al4V scaffold for load-bearing bone reconstruction. *Materials & Design*, 152, pp.30-39.

Zhang, X., Leary, M., Tang, H., Song, T. and Qian, M., 2018. Selective electron beam manufactured Ti-6Al-4V lattice structures for orthopedic implant applications: Current status and outstanding challenges. *Current Opinion in Solid State and Materials Science*, 22(3), pp.75-99.

Zhang, Z., Liu, R., Zepeda, H., Zeng, L., Qiu, J. and Wang, S., 2019a. 3D Printing Super Strong Hydrogel for Artificial Meniscus. *ACS Applied Polymer Materials*, 1(8), pp.2023-2032.

Zhang, C., Huang, Z., Jia, M., Chen, G., Ye, Y., Lin, Y., Liu, W., Chen, B., Shen, Q., Zhang, L. and Lavernia, E., 2019b. Additive manufacturing of functionally graded materials: A review. Materials Science and Engineering A. 762. 138209. 10.1016/j.msea.2019.138209. 2019. Additive manufacturing of functionally graded materials: A review. *Materials Science and Engineering: A*, 764.

Zhang, Y., Westerweel, B., Basten, R. and Song, J.S., 2020. 3D printing spare parts via IP licensing contracts, *SSRN Electronic Journal [Preprint]*.

Zhang, X., Yan, X., Fang, G. and Liu, M., 2020. Biomechanical influence of structural variation strategies on functionally graded scaffolds constructed with triply periodic minimal surface. *Additive Manufacturing*, 32.

Zhang, J., Yao, Y. and Deng, B., 2022. Fast and Robust Iterative Closest Point. *IEEE Transactions on Pattern Analysis and Machine Intelligence*, 44, pp.3450-3466.

Zhang, L., Lu, C., Lv, Y., Wang, X., Guo, S. and Zhang, H., 2021. Three-Dimensional Printing-Assisted Masquelet Technique in the Treatment of Calcaneal Defects. *Orthopaedic Surgery*, 13(3), pp.876-883.

Zhang, Y., Attarilar, S., Wang, L., Lu, W., Yang, J. and Fu, Y., 2021. A Review on Design and Mechanical Properties of Additively Manufactured NiTi Implants for Orthopedic Applications. *International Journal of Bioprinting*, 7(2).

Zhang, T., Wei, Q., Zhou, H., Jing, Z., Liu, X., Zheng, Y., Cai, H., Wei, F., Jiang, L., Yu, M., Cheng, Y., Fan, D., Zhou, W., Lin, X., Leng, H., Li, J., Li, X., Wang, C., Tian, Y. and Liu, Z., 2021. Three-dimensional-printed individualized porous implants: A new "implant-bone" interface fusion concept for large bone defect treatment. *Bioactive Materials*, 6(11), pp.3659-3670.

Zhang, X, Jiang, L., Yan, X., Wang, Z., Li, X. and Fang, G., 2023. Revealing the apparent and local mechanical properties of heterogeneous lattice: a multi-scale study of functionally graded scaffold. Virtual and Physical Prototyping, 18.

Zhao, S., Li, S., Hou, W., Hao, Y., Yang, R. and Misra, R., 2016. The influence of cell morphology on the compressive fatigue behavior of Ti-6Al-4V meshes fabricated by electron beam melting. *Journal of the Mechanical Behavior of Biomedical Materials*, 59, pp.251-264.

Zhao, H., Sigdel, A., Hou, X., Zhang, T., Zhang, G. and Sun, T., 2018. 3D-printed moulds facilitate making an anatomically matched cement spacer for reconstruction long bone defection after resection of tumors of humerous. *Nepalese Journal of Cancer*, 2(1), pp.27-31.

Zhao, D., Liang, H., Han, C., Li, J., Liu, J., Zhou, K., Yang, C. and Wei, Q., 2021. 3D printing of a titanium-tantalum gyroid scaffold with superb elastic admissible strain, bioactivity and in situ bone regeneration capability. *Additive Manufacturing*, 47.

Zhao, T., Feng, Y.T., Zhang, J., Wang, Z. and Wang, Z., 2021. Discrete Element Modelling of Dynamic Behaviour of Rockfills for Resisting High Speed Projectile Penetration. *Computer Modeling in Engineering and Sciences*, 127(2), pp.721-735.

Zheng, G., Tian, W. and Zhuang, X., 2018. *Intelligent Orthopaedics*. Singapore: Springer.

Zhou, Y., Yunus, A., Tian, Z., Chen, J., Wang, C., Xu, L. and Song, X., 2016. The pedicle screw-rod system is an acceptable method of reconstructive surgery after resection of sacroiliac joint tumours. *Współczesna Onkologia*, 1, pp.73-79.

Zhu, D., Fu, J., Wang, L., Guo, Z., Wang, Z. and Fan, H., 2021. Reconstruction with customized, 3D-printed prosthesis after resection of periacetabular Ewing's sarcoma in children using "triradiate cartilage-based" surgical strategy: a technical note. *Journal of Orthopaedic Translation*, 28, pp.108-117.

Zoltan, J., Popescu, D. and Sanei, S., 2023. A systematic review of follow-up results of additively manufactured customized implants for the pelvic area. *Expert Review of Medical Devices*, 20(4).

10. Published Articles

Trending in Orthopedics

Three-dimensional Technologies in Orthopedics

PANAYIOTIS J. PAPAGELOPOULOS, MD, DSC, FACS; OLGA D. SAVVIDOU, MD; PANAGIOTIS KOUTSOURADIS, MD; GEORGE D. CHLOROS, MD; IOANNA K. BOLIA, MD; VASILEIOS I. SAKELLARIOU, MD; VASILEIOS A. KONTOGEORGAKOS, MD; IOANNIS I. MAVRODONTIS, BSC, MSC; ANDREAS F. MAVROGENIS, MD; PANOS DIAMANTOPOULOS, DPHIL DRENG

abstract

New 3-dimensional digital technologies are revolutionizing orthopedic clinical practice, allowing structures of any complexity to be manufactured in just hours. Such technologies can make surgery for complex cases more precise, more cost-effective, and possibly easier to perform. Applications include preoperative planning, surgical simulation, patient-specific instrumentation and implants, bioprinting, prosthetics, and orthotics. The basic principles of 3-dimensional technologies, including imaging, design, numerical simulation, and printing, and their current applications in orthopedics are reviewed. [*Orthopedics*. 2018; 41(1):12-20.] VIDEO

New 3-dimensional (3D) digital technologies, including 3D imaging, design, numerical simulation, and printing, have valuable potential if efficiently integrated and applied in clinical practice.[1-3] The first and most important step is the acquisition of accurate image data. Acquired data are then imported and processed by specialized image-processing software packages with the aim of identifying and extracting specific tissue information. In general, it is possible to use processed medical images to design (computer-aided design [CAD]), evaluate (finite element analysis), and develop complex structures that are matched to a patient's anatomy (ie, patient-specific devices [3D printing]). This article presents the available technologies as an integrated 3D "toolkit" in orthopedics for effective diagnosis, preoperative planning, surgical simulation, surgical guidance, customized implant design, and patient-specific medical device development.

AVAILABLE TECHNOLOGY

Three-dimensional Imaging and Image Acquisition

Three-dimensional imaging consists of using various available techniques, including computed tomography, magnetic resonance imaging, and ultrasound, that each can provide raw data to be subsequently used in 3 dimensions (**Figure 1**). Once 3D imaging has been completed, the useful information is extracted. Every image has a collection of different gray values that are depicted by a sum of pixels or voxels, otherwise known as resolution (**Figure 2**, **Video 1**). For instance, in computed tomography, the gray values are expressed in Hounsfield units (HU). By default, air corresponds to -1024 HU, water to 0 HU, and any metal to 3072 HU. Thus, very dense materials have high values and will be displayed in white, whereas less dense materials have lower values and will be displayed in black. If the threshold value is varied, materials of different densities will stand out, permitting precise differentiation of the component tissues of the computed tomography scan (**Video 1**).[4] This process of tissue identification and classification is called segmen-

The authors are from the First Department of Orthopaedic Surgery (PJP, ODS, GDC, IKB, VIS, VAK, IIM, AFM), National and Kapodistrian University of Athens, School of Medicine, "ATTIKON" University General Hospital; "NIMTS" Veterans Hospital (PK, GDC); and the Department of Physiology (PD), National and Kapodistrian University of Athens, School of Medicine, Athens, Hellenic Republic, Greece.

The authors have no relevant financial relationships to disclose.

Correspondence should be addressed to: Panayiotis J. Papagelopoulos, MD, DSc, FACS, First Department of Orthopaedic Surgery, National and Kapodistrian University of Athens, School of Medicine, "ATTIKON" University General Hospital, 15 Neapoleos St, 15123, Amarousion, Athens, Hellenic Republic, Greece (pjportho@med.uoa.gr).

doi: 10.3928/01477447-20180109-04

COPYRIGHT © SLACK INCORPORATED

tation, which is the isolation of all pixels of the component of interest.

Three-dimensional Design

Once the segmentation process is complete, specific algorithms translate the pixel and/or voxel spatial information into its specific 3D geometry, containing specific points, lines, and surfaces. This is known as CAD, and this 3D geometry is usually represented by triangles (**Figure 3**, **Video 2**). Thus, CAD design functions can be applied for virtual surgical simulations (measurements, cuts, geometry alterations, procedures) or for creating anatomy-specific implants, instruments, and medical devices (**Figure 4**).[5]

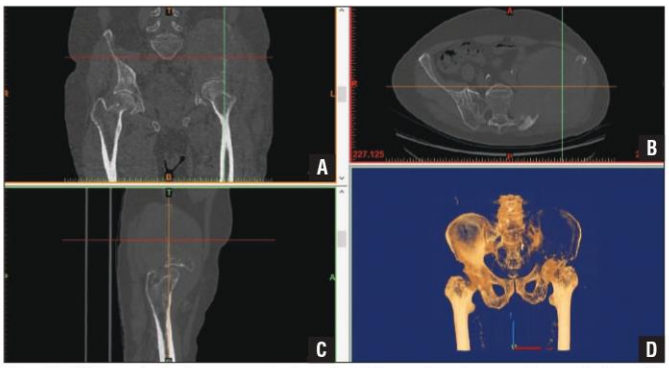

Figure 1: A 3-dimensional volume reconstruction of a pelvic mass based on raw data provided by multiplanar computed tomography. Coronal (A), transverse (B), and sagittal (C) views and 3-dimensional (D) reconstruction of the pelvis showing the osteolytic destruction of the left hemipelvis.

Three-dimensional Numerical Simulation

On the basis of the earlier segmentation process, various anatomical tissues have been differentiated and transferred to a CAD environment as different 3D geometric entities. As such, they can be easily transferred to a finite element analysis environment—a computer-based numerical simulation technique for studying the behavior of physical systems (eg, bone structures).[6] Within this environment, different material properties can be assigned to different structures. For example, the cancellous and cortical parts of the femur have been differentiated via the segmentation process (**Figure 5A**). The next step is to apply desired forces and study the stress risers within the structure in question (**Figure 5B**).

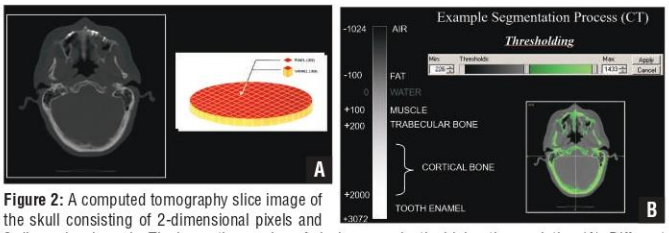

Figure 2: A computed tomography slice image of the skull consisting of 2-dimensional pixels and 3-dimensional voxels. The larger the number of pixels or voxels, the higher the resolution (A). Different types of tissues correspond to different gray values (B).

Three-dimensional Printing (Also Known as Rapid Prototyping or Additive Manufacturing)

Three-dimensional printing can include either a replica of the patient's anatomy, the manufacturing of surgical instruments, or the customized implant itself. It is a fast and accurate way to develop a 3D object by building up successive thin layers of raw material. Objects are produced from digital 3D files, once they have been designed with CAD and simulated by finite element analysis. Models of any complexity can usually be built within hours, significantly reducing the product development cycle. Recent 3D printing systems can combine multiple materials, colors, and textures. Three-dimensional printing involves several established manufacturing techniques, including but not limited to stereolithography (using photosensitive liquid polymer resin that is cured and solidified by ultraviolet laser), laminated object manufacturing (using layers of paper, plastic, or metal laminates that are fused under heat and pressure), fused deposition modeling (heating and extruding small beads of fused thermoplastic materials) (**Figure 6**), and selective laser sintering (using granules of thermoplastic, metal, ceramic, or glass powders that are melted and bonded by a high-power laser). It also

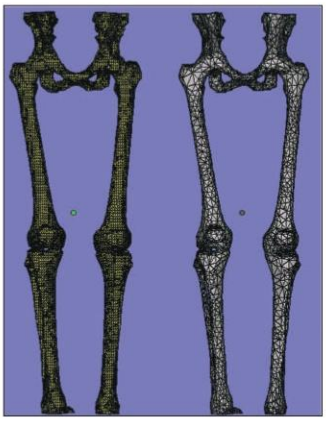

Figure 3: Geometric representation of the lower extremities using triangles. The image on the left has more triangles and thus is a more accurate (detailed) representation compared with the right.

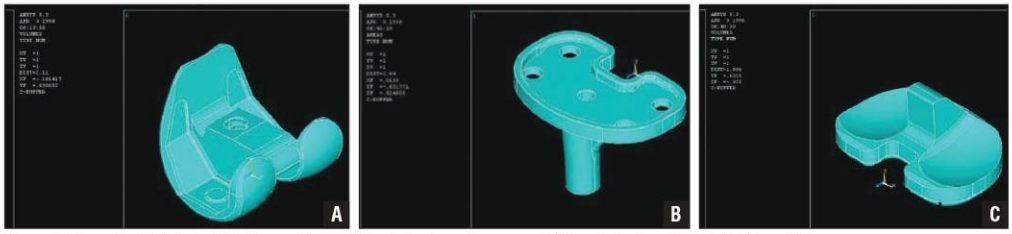

Figure 4: Computer-aided design total knee replacement implants: femoral component (A), polyethylene (B), and tibial tray (C).

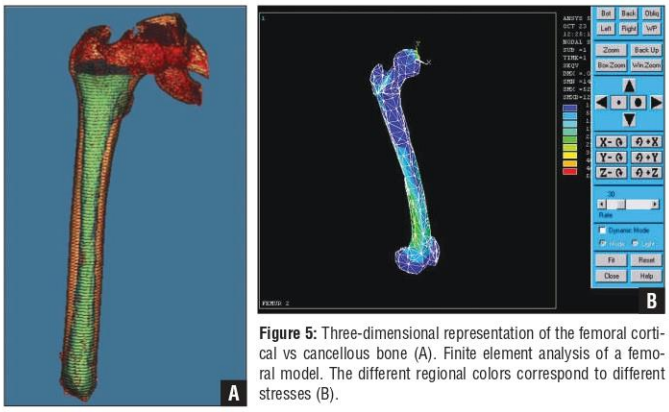

Figure 5: Three-dimensional representation of the femoral cortical vs cancellous bone (A). Finite element analysis of a femoral model. The different regional colors correspond to different stresses (B).

involves a multitude of experimental technologies under development, such as electron beam melting (using a computer-controlled electron beam under high vacuum to fully melt and bond metallic powder, including titanium). Each technique can be used for different clinical applications and for producing anatomical models, surgical guides, or even implants.

Technology Integration

The aforementioned technologies are part of an integrated process.[4] The acquisition of accurate image data is the first and most important step. Currently, most conventional hospital scanners can be used to provide medical imaging data in a DICOM (Digital Imaging and Communications in Medicine) format. Acquired data are then imported and processed by specialized image-processing software packages with the aim of identifying and extracting specific tissue information. Subsequently, CAD modeling allows the design of customized parts (ie, personalized implants and medical devices). Finite element analysis modeling allows the numerical simulation and validation of the designed parts. Rapid prototyping or additive manufacturing, both of which are commonly known as 3D printing currently, can actually build the previously designed and simulated parts. In general, virtual computer modeling and physical production can be combined as required, providing numerous advantages for achieving personalized therapy.

Clinical Applications in Orthopedics

Preoperative Visualization and Planning

The creation of 3D visualizations of the anatomy or exact 3D anatomical replicas to assist surgeons is revolutionizing the preoperative planning for many orthopedic procedures in situations ranging from complex trauma cases[7-19] to elective orthopedic surgery.[20-29]

Trauma. Chung et al were the first to report the use of 3D printing technologies for the preoperative visualization of and planning for a calcaneal fracture[9] and subsequently 4 complex distal tibial and 13 malleolar avulsion fractures.[10] The mirror imaging technique was used, which in this case consisted of printing a calcaneus of actual preinjury size by using the contralateral noninjured side as a reference.

Consequently, preoperative planning was achieved by applying preshaped locking plates to appropriately fit the model. This allowed accurate reduction and proper plate and hole position, thereby addressing possible intraoperative challenges and complications.

Bizzotto et al[7] used 3D modalities for complex articular fractures (distal radius, radial head, tibial plateau, talus, calcaneus, humeral head, and glenoid) of 102 patients from 6 hospitals. Three-dimensional printed replicas of the bones with the exact anatomy of the fracture were reproduced. These were subsequently used to establish the spatial geometry of the fragments as well as any articular displacement and to assist the surgeon in preoperatively determining the appropriate plates and screws. Additionally, the models were used when obtaining informed consent from patients and teaching medical students.

On the basis of the principles described above, including the mirror imaging technique of Chung et al[9,10] and the 3D printed

COPYRIGHT © SLACK INCORPORATED

replicas of the fractured bones of Bizzotto et al,[7] 3D technology has been successfully used in the preoperative planning for clavicle fractures,[12,19] complicated proximal humeral fractures,[16] trimalleolar and calcaneal fractures,[15] and complex acetabular fractures and pelvic surgeries.[8,11,17,18]

Elective Orthopedic Surgery. Three-dimensional computer-assisted preoperative planning for elective orthopedic cases has been performed in the setting of spinal disorders,[20,21] sports medicine,[22] adult reconstruction,[23] foot and ankle surgery,[24,25] pediatric orthopedics,[26] and orthopedic oncology.[27-29]

In spinal surgery, 3D printing for visualization and preoperative planning was first reported by Mizutani et al,[21] who created 3D replicas for 15 patients with rheumatoid cervical lesions. The appropriate occipitocervical angle was determined, as were the optimal contour and position of the plate-rod constructs. Li et al[20] retrospectively studied 37 patients undergoing revision lumbar diskectomy who were divided into 2 groups. In the first group (15 patients), 3D lumbar vertebral models were created that accurately replicated any complex or abnormal structures and the extent of osteoproliferation. The second group (22 patients) underwent the traditional procedure without the assistance of 3D technology. Although the first group had reduced operative time and perioperative blood loss, there was no difference in the other clinical outcomes.

Sheth et al[22] produced a solid 3D model of a young patient's glenohumeral joint for the preoperative planning of an arthroscopic Bankart repair. The replica was successfully used to assess the degree of bone loss (Hill-Sachs and Bankart lesions) and to determine the amount of external rotation and abduction required to engage the Hill-Sachs lesion. Furthermore, the optimal number and placement of the suture anchors required for the remplissage procedure were established.

Zerr et al[23] created a 3D replica of an acetabular cup that was used as a template in the preoperative planning of a complex total hip replacement revision. This permitted gauging the sizes of the acetabular defect and the cup, optimal screw placement, and trialing of the cup to evaluate stability, coverage, and appropriate anteversion and abduction.

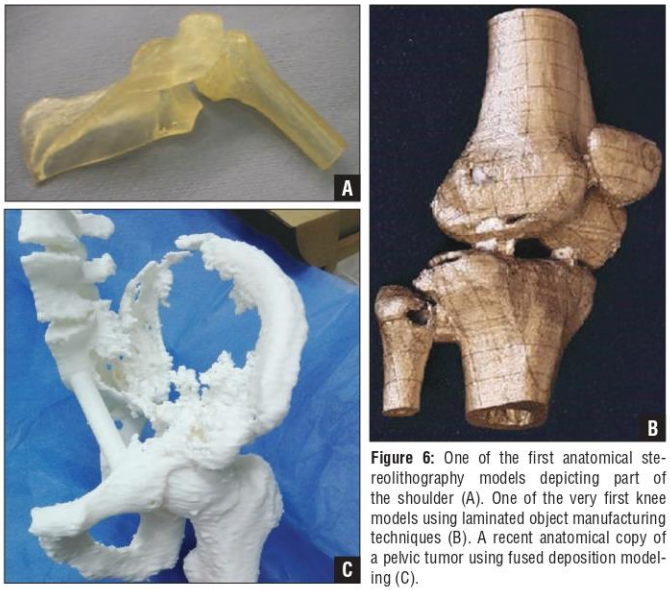

Figure 6: One of the first anatomical stereolithography models depicting part of the shoulder (A). One of the very first knee models using laminated object manufacturing techniques (B). A recent anatomical copy of a pelvic tumor using fused deposition modeling (C).

Giovinco et al[24] used 3D printed models in Charcot-Marie-Tooth foot reconstruction surgery. These models assisted them in terms of obtaining the optimal osteotomy and joint resection, instrumentation, and placement of internal and external fixation devices.

Jastifer and Gustafson[25] used a 3D printed anatomical replica for the preoperative planning for a malunited bimalleolar fracture. This replica increased understanding of the pathology, assisted with patient education, and permitted accurate preoperative measurement of the degree of corrective osteotomy and amount of bone wedge removal required.

Starosolski et al[26] used 3D printed replicas to evaluate pediatric disorders. In a case of Perthes disease, 3D printing allowed accurate evaluation of the deformity and simulation of the procedure, including exact placement of implants. In addition, 3D printed models were used in cases of tarsal coalition, Blount disease, and posttraumatic physeal bars to educate both patients and residents.

The application of 3D printing technologies for preoperative planning has also been well documented in orthopedic oncology. Xiao et al[28] used 3D printed replicas of cervical spinal malignant tumors for 5 patients. This enabled the surgeons to accurately localize the tumor and assess its shape, size, and relationship to surrounding structures. En bloc resection of the lesion was performed based on simulation using these models.

Ren et al[27] created a 3D replica to determine the exact position of an osteoid osteoma of the calcaneus in a 17-year-old girl. A surgical plate was manufactured using 3D technology to guide the trephine to make a bone window on the lateral aspect of the calcaneus. This permitted ac-

curate localization of the tumor, which can be challenging in the context of the complex anatomy of the foot, and complete resection of the lesion with minimal bone loss.

Zhang et al[29] used a 3D printed exact anatomical replica of a pelvic osteochondroma involving the ilium, sacrum, sacroiliac joint, and lumbar spine. The model provided a precise depiction of the tumor and the adjacent soft tissues at risk preoperatively. It was also sterilized and used intraoperatively to assist the surgeons in performing a hemipelvectomy for accurate en bloc resection of the osteochondroma.

Guidance (Surgical Instrumentation)

Once 3D technology has been used for preoperative planning as described above, it can further assist in the manufacture of customized surgical guides and tools (eg, appropriate jigs and cutting tools).

Patient-specific instruments are mostly used in total knee replacement, and most companies already manufacture 3D printed patient-specific guides. Three-dimensional models of the patient's knee are printed and then disposable cutting blocks are fabricated to match and replicate the patient's knee anatomy, thus theoretically optimizing the restoration of the mechanical axis of the knee and minimizing potential surgical errors. The proposed benefits of using patient-specific instrumentation include optimized functional outcomes and reduced surgical time, blood loss, fat embolism incidents, and costs. However, the use of 3D printed cutting guides in total knee replacement has not been shown to be superior to the use of traditional techniques.[30-35]

In recent years, the use of 3D printed patient-specific instrumentation has expanded beyond total knee replacements. Hirao et al[36] produced a custom-made surgical guide to correct a malunited pronation deformity after primary first metatarsophalangeal joint arthrodesis in a patient with rheumatoid arthritis. This provided an accurate index of rotation and alignment in complex revision fusion of the first metatarsophalangeal joint.

Storelli et al[37] produced patient-specific cutting jigs for precise planning and implementation of complex multiple osteotomies in the treatment of malunited forearm fractures in children. A wedge-shaped spacer was used both preoperatively and intraoperatively to achieve optimal osteotomy size and accurately correct the rotational malalignment of these fractures.

Pérez-Mañanes et al[38] used 3D printed surgical cutting guides for open wedge high tibial osteotomy in 8 patients with medial joint knee osteoarthritis. Twenty patients who underwent opening osteotomies with a traditional technique were used as controls. A patient-specific osteotomy positional guide and 3 polyhedral wedges were used to achieve the desired correction of the mechanical axis. Compared with the control group, the use of these 3D templates minimized intraoperative complications while reducing both surgical and fluoroscopic time.

Bellanova et al[39] used 3D printed patient-specific instrumentation for tibial bone sarcoma resection and allograft reconstruction in 4 pediatric patients. A custom-made surgical guide was fitted to the proper position on the affected tibia for accurate tumor resection with appropriate margins. Another 3D printed guide was manufactured to cut the selected bone allograft to fit the resection gap precisely. Patient-specific guides were similarly used to achieve proper tumor resection with accurate excision margins in a case of giant invasive sacral schwannoma[40] and a case of high-grade femoral osteosarcoma.[41]

Implants

Customized 3D printed implants have been used mainly in reconstruction surgery[42-44] and orthopedic oncology.[45-47] Stoffelen et al[44] used 3D printing technologies for the reconstruction of severe glenoid defects after failure of total shoulder arthroplasty. A custom-made titanium glenoid implant was manufactured that, after meticulous soft tissue debridement and with the aid of bone autografts, was successfully inserted and fixed in the glenoid component of the affected shoulder.

Li et al[42] and Mao et al[43] used 3D printing technologies for revision total hip arthroplasties with severe acetabular bone defects (Paprosky type 3B defects). After a series of preoperative trials, custom-made 3D printed cages were used. There was 1 case of cage loosening and 1 case of dislocation among 24 patients in the study of Li et al.[42] There were 2 cases of cage loosening and 2 cases of dislocation among 23 patients in the study of Mao et al.[43] Mean Harris hip score significantly improved from preoperatively to postoperatively in the study of Li et al[42] (36 vs 82 points) and in the study of Mao et al[43] (39.6 vs 80.9 points). Thus, it can be concluded that there are promising results in terms of hip pain and postoperative complications when using custom-made cages in cases where commercially available cages do not fit well to the host bone.

Wong et al[46] treated a patient with pelvic chondrosarcoma of the anterior column. First, the aforementioned mirror imaging technique and patient-specific instrumentation were used to appropriately cut the bone to resect the bone segment containing the tumor. Then, a custom-made pelvic implant designed to match the bone defect was 3D printed as a titanium monoblock. Imanishi and Choong[45] used a similar technique to perform total calcanectomy and calcaneus replacement with a 3D printed titanium implant in a patient with a grade 2 chondrosarcoma of the calcaneus.

The current authors recently reported the use of 3D printed implants of the talus and calcaneus after total talectomy and calcanectomy for Ewing's sarcoma in 3 patients, who had satisfactory 1- to 2-year follow-up results.[48]

Xu et al[47] used a 3D printed porous metal vertebral body to reconstruct the upper cervical spine of a young patient with Ewing's sarcoma after resection of

COPYRIGHT © SLACK INCORPORATED

the posterior elements of C2. The custom-made implant was manufactured according to a computer model, using titanium alloy powder.

Mobbs et al[49] reported 2 cases in which a 3D printed prosthesis was used for reconstruction following a C1/C2 chordoma resection and a custom-made titanium fusion cage was used to treat a congenital L5-hemivertebra deformity.

The idea behind the use of custom-made 3D printed implants in orthopedic oncology is that their shape matches the excised bone, thus decreasing the stresses on the existing bone compared with conventional implants. They can also help to address the significant challenges encountered in complex oncological surgery.

The mirror imaging technique for manufacturing 3D patient-specific implants has also been applied in orthopedic trauma. Shuang et al[50] used 3D printed custom-made osteosynthesis plates for 6 patients who had distal intercondylar humeral fractures. They found similar results in terms of elbow function and range of motion compared with 7 patients who were treated with conventional plates.

Orthopedic Fixators, Orthoses, and Prosthetics

Qiao et al[51] used 3D printing techniques to develop a novel customized external fixator for long bone fracture reduction of the lower limb. First, 3D images of the tibial and femoral diaphyseal fractures were reconstructed through computer software and virtual reductions were simulated. Subsequently, an external fixator with the appropriate frame size, connection rods, and pins was designed and manufactured, similar to the Ilizarov model, based on the data acquired by model reduction. The custom-made external fixator was later used to treat 3 patients with diaphyseal tibial fractures, showing excellent results in terms of reduction, fixation, union, and pain.[52]

Raux et al[53] prospectively compared custom-made orthoses for idiopathic scoliosis manufactured using a traditional plaster mold vs 3D printing among 29 children with moderate adolescent idiopathic scoliosis. Three-dimensional braces were made by optically scanning the patient, subsequently creating virtual molds, and using 3D printing for manufacturing. Each patient received 2 braces; radiographic correction and the patient's in-brace comfort were used to select the appropriate brace. Thirteen traditionally made and sixteen 3D printed braces were chosen, having comparable results in terms of correction and comfort. Although the results were comparable, 3D printing offered a less invasive and more hygienic procedure for the patient.

Dombroski et al[54] used 3D printing technologies to successfully manufacture low-cost, custom-made foot orthoses. Foot molds were created from both traditional plaster casting and 3D printing methods. Custom-made orthoses were then manufactured from each mold. Arch height index was measured during 10 gait cycles for both the traditional casting and the 3D method, with similar results shown.

In a recent review, Tanaka and Lightdale-Miric[55] highlighted how advances in 3D printing are altering the manufacture, customization, and accessibility of prosthetic hands for children with congenital or acquired upper extremity amputations. Because children rapidly damage and outgrow prostheses, they are ideal candidates for the currently available 3D printed devices. These custom-made prostheses are more affordable. The cost of materials for a 3D printed body-powered arm device ranges from $50 to $150, whereas the cost of a traditionally made body-powered prosthesis ranges from $4000 to $10,000. They are lightweight, easily manufactured and repaired, and designed to fit a specific size and activity.

Zuniga et al[56] used low-cost 3D printed prosthetic hands for 11 children with upper-limb traumatic or congenital amputations. These hands were manufactured either via laboratory visits or from a distance. They had a significantly lower cost compared with the available mechanical and myoelectric devices and thus represent an alternative for children and families in developing countries and with limited access to health care providers.

Galvez et al[57] used 3D printing to create various models from different potential donors in a case of bilateral surgical amputation in an 8-year-old child to determine the appropriate donor size for an acceptable result.

Lee et al[58] 3D printed a finger prosthesis for an adult patient with a right thumb amputation above the metacarpophalangeal joint. An image of the contralateral hand was used as a reference and rotated to the right side to design the appropriate thumb prosthesis.

Bioprinting

Bioprinting is defined as the manufacture and assembly of biological materials, such as molecules, biomaterials (including scaffolds), cells, and tissues, to accomplish one or more biological functions.[59] Three-dimensionally printed bioscaffolds have been used in laboratory studies for many orthopedic conditions. Zhu et al[60] 3D printed porous titanium within which a gelatine scaffold was implanted together with platelets derived from platelet-rich plasma, which induced cell migration into the titanium pores. The construct thus exhibited bioactivity and was successfully implanted in rabbits, significantly accelerating bone regeneration in osteonecrosis of the femoral head.

Zhang et al[61] 3D printed poly-epsilon-caprolactone meniscal scaffolds that were augmented with bone marrow–derived mesenchymal stem cells. Seventy-two New Zealand rabbits were divided into 4 groups: cell-seeded scaffold, cell-free scaffold, sham operation, and total meniscectomy alone. The regeneration of the implanted tissue, the articular cartilage degeneration, and the mechanical properties of the implants were assessed by

microscopic analysis at 12 and 24 weeks postoperatively. The results were significantly in favor of the cell-seeded scaffold group. The augmented poly-epsilon-caprolactone scaffolds showed increased fibrocartilaginous tissue regeneration and higher mechanical strength, thus providing a functional replacement to protect articular cartilage from damage after total meniscectomy.

Yang et al[62] 3D printed scaffolds composed of polylactide-co-glycolide and hydroxyapatite that were grafted with quaternized chitosan to produce biological scaffolds with increased antibacterial and osteogenic activity with advanced biocompatibility. It was shown that these scaffolds decreased biofilm formation and bacterial adhesion under both in vitro and in vivo conditions. Moreover, in experiments conducted on rats, hydroxyapatite-incorporated bioprinted scaffolds exhibited good neovascularization and enhanced tissue integration. Therefore, these results may indicate a great potential for both the prophylaxis and the treatment of bone infection.

Fedorovich et al[63] 3D printed heterogeneous, porous constructs by combining human osteogenic progenitors and human chondrocytes with a polysaccharide (alginate hydrogel) that promotes both osteogenic and chondrogenic differentiation. The various heterogeneous bioprinted scaffolds were then tested both in vitro and in vivo. The results indicated a stable cellular architecture of these 3D printed osteochondral grafts but also a lack of abundant osteogenic tissue formation; thus, further research is needed to improve the manufacture of cartilage implants and bone grafts.

To overcome the lack of tissue formation, Shim et al[64] manufactured 3D porous structures for building osteochondral tissues by using thermoplastic biomaterial polycaprolactone (poly-epsilon-caprolactone), based on its relatively higher mechanical properties compared with hydrogel. Although these 3D scaffolds, consisting of osteoblasts and chondrocytes, were successfully fabricated and retained their viability and initial position up to 7 days after being dispensed, they were tested only in vitro; therefore, further research is necessary to prove their efficacy and potential for use for osteochondral reconstruction and cartilage regeneration in humans.

CONCLUSION

The vast potential of 3D digital technologies, including imaging, design simulation, and printing, is becoming more apparent in clinical practice. Currently, complex structures, including replicas of patients' anatomy, surgical instruments, custom-made implants, and other medical devices, may be manufactured in a matter of hours. Preoperative visualization and education via the creation of a precise anatomical model may assist the surgeon in selecting the optimal surgical approach and the appropriate implant and position, thereby potentially optimizing patient outcomes and minimizing complications. Accurate planning has been demonstrated in complex trauma and elective cases of most orthopedic subspecialties. Surgical instrumentation and implants have also been developed using the aforementioned technologies, especially in the settings of adult reconstruction and orthopedic oncology. The application of such patient-specific guiding instruments can make surgery more precise, more cost-effective, and possibly easier in complex cases. Further implementation of these technologies in other areas of orthopedics is expected. However, patient-specific implants and instruments are expensive. Thus, research should focus on comparing patient outcomes when using 3D technology vs conventional preoperative planning. Braces, orthotics, and prosthetics have also been developed. Physicians should become more familiar with the technology to promote further implementation and research. Although 3D technologies have been used for printing biological scaffolds and have been successful when tested in in vitro and in vivo animal studies, human trials have not been performed.

REFERENCES

1. Eltorai AE, Nguyen E, Daniels AH. Three-dimensional printing in orthopedic surgery. *Orthopedics.* 2015; 38(11):684-687.
2. Mulford JS, Babazadeh S, Mackay N. Three-dimensional printing in orthopaedic surgery: review of current and future applications. *ANZ J Surg.* 2016; 86(9):648-653.
3. Arealis G, Nikolaou VS. Bone printing: new frontiers in the treatment of bone defects. *Injury.* 2015; 46(suppl 8):S20-S22.
4. Diamantopoulos P, Richardson JD. Integrating medical imaging, finite element analysis (FEA), computer aided design (CAD) and rapid prototyping. In: Middleton J, Jones ML, Shrive NG, Pande GN, eds. *Computer Methods in Biomechanics & Biomedical Engineering 3.* London, United Kingdom: Gordon & Breach; 2001:502-508.
5. Haglin JM, Eltorai AE, Gil JA, Marcaccio SE, Botero-Hincapie J, Daniels AH. Patient-specific orthopaedic implants. *Orthop Surg.* 2016; 8(4):417-424.
6. Pfeiffer FM. The use of finite element analysis to enhance research and clinical practice in orthopedics. *J Knee Surg.* 2016; 29(2):149-158.
7. Bizzotto N, Tami I, Santucci A, et al. 3D printed replica of articular fractures for surgical planning and patient consent: a two years multi-centric experience. *3D Printing in Medicine.* 2015; 2:2.
8. Chana-Rodríguez F, Mañanes RP, Rojo-Manaute J, Gil P, Martínez-Gómiz JM, Vaquero-Martin J. 3D surgical printing and pre contoured plates for acetabular fractures. *Injury.* 2016; 47(11):2507-2511.
9. Chung KJ, Hong DY, Kim YT, Yang I, Park YW, Kim HN. Preshaping plates for minimally invasive fixation of calcaneal fractures using a real-size 3D-printed model as a preoperative and intraoperative tool. *Foot Ankle Int.* 2014; 35(11):1231-1236.
10. Chung KJ, Huang B, Choi CH, Park YW, Kim HN. Utility of 3D printing for complex distal tibial fractures and malleolar avulsion fractures: technical tip. *Foot Ankle Int.* 2015; 36(12):1504-1510.
11. Duncan JM, Nahas S, Akhtar K, Daurka J. The use of a 3D printer in pre-operative planning for a patient requiring acetabular reconstructive surgery. *J Orthop Case Rep.* 2015; 5(1):23-25.
12. Kim HN, Liu XN, Noh KC. Use of a real-size 3D-printed model as a preoperative and intraoperative tool for minimally invasive plating of comminuted midshaft clavicle fractures. *J Orthop Surg Res.* 2015; 10:91.

COPYRIGHT © SLACK INCORPORATED

13. Kovler I, Joskowicz L, Weil YA, et al. Haptic computer-assisted patient-specific preoperative planning for orthopedic fractures surgery. *Int J Comput Assist Radiol Surg.* 2015; 10(10):1535-1546.
14. Wu XB, Wang JQ, Zhao CP, et al. Printed three-dimensional anatomic templates for virtual preoperative planning before reconstruction of old pelvic injuries: initial results. *Chin Med J (Engl).* 2015; 128(4):477-482.
15. Yang L, Shang XW, Fan JN, et al. Application of 3D printing in the surgical planning of trimalleolar fracture and doctor-patient communication. *Biomed Res Int.* 2016; 2016:2482086.
16. You W, Liu LJ, Chen HX, et al. Application of 3D printing technology on the treatment of complex proximal humeral fractures (Neer 3-part and 4-part) in old people. *Orthop Traumatol Surg Res.* 2016; 102(7):897-903.
17. Zeng C, Xiao J, Wu Z, Huang W. Evaluation of three-dimensional printing for internal fixation of unstable pelvic fracture from minimal invasive para-rectus abdominis approach: a preliminary report. *Int J Clin Exp Med.* 2015; 8(8):13039-13044.
18. Zeng C, Xing W, Wu Z, Huang H, Huang W. A combination of three-dimensional printing and computer-assisted virtual surgical procedure for preoperative planning of acetabular fracture reduction. *Injury.* 2016; 47(10):2223-2227.
19. Jeong HS, Park KJ, Kil KM, et al. Minimally invasive plate osteosynthesis using 3D printing for shaft fractures of clavicles: technical note. *Arch Orthop Trauma Surg.* 2014; 134(11):1551-1555.
20. Li C, Yang M, Xie Y, et al. Application of the polystyrene model made by 3-D printing rapid prototyping technology for operation planning in revision lumbar discectomy. *J Orthop Sci.* 2015; 20(3):475-480.
21. Mizutani J, Matsubara T, Fukuoka M, et al. Application of full-scale three-dimensional models in patients with rheumatoid cervical spine. *Eur Spine J.* 2008; 17(5):644-649.
22. Sheth U, Theodoropoulos J, Abouali J. Use of 3-dimensional printing for preoperative planning in the treatment of recurrent anterior shoulder instability. *Arthrosc Tech.* 2015; 4(4):e311-e316.
23. Zerr J, Chatzinoff Y, Chopra R, Estrera K, Chhabra A. Three-dimensional printing for preoperative planning of total hip arthroplasty revision: case report. *Skeletal Radiol.* 2016; 45(10):1431-1435.
24. Giovinco NA, Dunn SP, Dowling L, et al. A novel combination of printed 3-dimensional anatomic templates and computer-assisted surgical simulation for virtual preoperative planning in Charcot foot reconstruction. *J Foot Ankle Surg.* 2012; 51(3):387-393.
25. Jastifer JR, Gustafson PA. Three-dimensional printing and surgical simulation for preoperative planning of deformity correction in foot and ankle surgery. *J Foot Ankle Surg.* 2017; 56(1):191-195.
26. Starosolski ZA, Kan JH, Rosenfeld SD, Krishnamurthy R, Annapragada A. Application of 3-D printing (rapid prototyping) for creating physical models of pediatric orthopedic disorders. *Pediatr Radiol.* 2014; 44(2):216-221.
27. Ren X, Yang L, Duan XJ. Three-dimensional printing in the surgical treatment of osteoid osteoma of the calcaneus: a case report. *J Int Med Res.* 2017; 45(1):372-380.
28. Xiao JR, Huang WD, Yang XH, et al. En bloc resection of primary malignant bone tumor in the cervical spine based on 3-dimensional printing technology. *Orthop Surg.* 2016; 8(2):171-178.
29. Zhang Y, Wen L, Zhang J, Yan G, Zhou Y, Huang B. Three-dimensional printing and computer navigation assisted hemipelvectomy for en bloc resection of osteochondroma: a case report. *Medicine (Baltimore).* 2017; 96(12):e6414.
30. Bali K, Walker P, Bruce W. Custom-fit total knee arthroplasty: our initial experience in 32 knees. *J Arthroplasty.* 2012; 27(6):1149-1154.
31. Nam D, Park A, Stambough JB, Johnson SR, Nunley RM, Barrack RL. The Mark Coventry Award. Custom cutting guides do not improve total knee arthroplasty clinical outcomes at 2 years followup. *Clin Orthop Relat Res.* 2016; 474(1):40-46.
32. Ollivier M, Parratte S, Lunebourg A, Viehweger E, Argenson JN. The John Insall Award. No functional benefit after unicompartmental knee arthroplasty performed with patient-specific instrumentation: a randomized trial. *Clin Orthop Relat Res.* 2016; 474(1):60-68.
33. Zhu M, Chen JY, Chong HC, et al. Outcomes following total knee arthroplasty with CT-based patient-specific instrumentation. *Knee Surg Sports Traumatol Arthrosc.* 2017; 25(8):2567-2572.
34. Lombardi AV Jr, Berend KR, Adams JB. Patient-specific approach in total knee arthroplasty. *Orthopedics.* 2008; 31(9):927-930.
35. Spencer BA, Mont MA, McGrath MS, Boyd B, Mitrick MF. Initial experience with custom-fit total knee replacement: intra-operative events and long-leg coronal alignment. *Int Orthop.* 2009; 33(6):1571-1575.
36. Hirao M, Ikemoto S, Tsuboi H, et al. Computer assisted planning and custom-made surgical guide for malunited pronation deformity after first metatarsophalangeal joint arthrodesis in rheumatoid arthritis: a case report. *Comput Aided Surg.* 2014; 19(1-3):13-19.
37. Storelli DA, Bauer AS, Lattanza LL, McCarroll HR Jr. The use of computer-aided design and 3-dimensional models in the treatment of forearm malunions in children. *Tech Hand Up Extrem Surg.* 2015; 19(1):23-26.
38. Pérez-Mañanes R, Burró JA, Manaute JR, Rodriguez FC, Martin JV. 3D surgical printing cutting guides for open-wedge high tibial osteotomy: do it yourself. *J Knee Surg.* 2016; 29(8):690-695.
39. Bellanova L, Paul L, Docquier PL. Surgical guides (patient-specific instruments) for pediatric tibial bone sarcoma resection and allograft reconstruction. *Sarcoma.* 2013; 2013:787653.
40. Lin CL, Fang JJ, Lin RM. Resection of giant invasive sacral schwannoma using image-based customized osteotomy tools. *Eur Spine J.* 2016; 25(12):4103-4107.
41. Ma L, Zhou Y, Zhu Y, et al. 3D-printed guiding templates for improved osteosarcoma resection. *Sci Rep.* 2016; 6:23335.
42. Li H, Qu X, Mao Y, Dai K, Zhu Z. Custom acetabular cages offer stable fixation and improved hip scores for revision THA with severe bone defects. *Clin Orthop Relat Res.* 2016; 474(3):731-740.
43. Mao Y, Xu C, Xu J, et al. The use of customized cages in revision total hip arthroplasty for Paprosky type III acetabular bone defects. *Int Orthop.* 2015; 39(10):2023-2030.
44. Stoffelen DV, Eraly K, Debeer P. The use of 3D printing technology in reconstruction of a severe glenoid defect: a case report with 2.5 years of follow-up. *J Shoulder Elbow Surg.* 2015; 24(8):e218-e222.
45. Imanishi J, Choong PF. Three-dimensional printed calcaneal prosthesis following total calcanectomy. *Int J Surg Case Rep.* 2015; 10:83-87.
46. Wong KC, Kumta SM, Geel NV, Demol J. One-step reconstruction with a 3D-printed, biomechanically evaluated custom implant after complex pelvic tumor resection. *Comput Aided Surg.* 2015; 20(1):14-23.
47. Xu N, Wei F, Liu X, et al. Reconstruction of the upper cervical spine using a personalized 3D-printed vertebral body in an adolescent with Ewing sarcoma. *Spine (Phila Pa 1976).* 2016; 41(1):E50-E54.
48. Vottis C, Papagelopoulos PJ, Sarlikiotis T, Kontogeorgakos V, Mavrogenis AF, Savvidou OD. Limb salvage of the foot after tumor resection using 3D printed implants. Paper presented at: 19th International Society of Limb Salvage (ISOLS); May 10-12, 2017; Kanazawa, Japan.
49. Mobbs RJ, Coughlan M, Thompson R, Sutterlin CE III, Phan K. The utility of 3D printing for surgical planning and patient-specific implant design for complex spinal pathologies: case report. *J Neurosurg Spine.* 2017; 26(4):513-518.
50. Shuang F, Hu W, Shao Y, Li H, Zou H. Treatment of intercondylar humeral fractures with 3D-printed osteosynthesis plates. *Medicine (Baltimore).* 2016; 95(3):e2461.

51. Qiao F, Li D, Jin Z, et al. Application of 3D printed customized external fixator in fracture reduction. *Injury.* 2015; 46(6):1150-1155.
52. Qiao F, Li D, Jin Z, Hao D, Liao Y, Gong S. A novel combination of computer-assisted reduction technique and three dimensional printed patient-specific external fixator for treatment of tibial fractures. *Int Orthop.* 2016; 40(4):835-841.
53. Raux S, Kohler R, Garin C, Cunin V, Abelin-Genevois K. Tridimensional trunk surface acquisition for brace manufacturing in idiopathic scoliosis. *Eur Spine J.* 2014; 23(suppl 4):S419-S423.
54. Dombroski CE, Balsdon ME, Froats A. The use of a low cost 3D scanning and printing tool in the manufacture of custom-made foot orthoses: a preliminary study. *BMC Res Notes.* 2014; 7:443.
55. Tanaka KS, Lightdale-Miric N. Advances in 3D-printed pediatric prostheses for upper extremity differences. *J Bone Joint Surg Am.* 2016; 98(15):1320-1326.
56. Zuniga J, Katsavelis D, Peck J, et al. Cyborg beast: a low-cost 3D-printed prosthetic hand for children with upper-limb differences. *BMC Res Notes.* 2015; 8:10.
57. Galvez JA, Gralewski K, McAndrew C, Rehman MA, Chang B, Levin LS. Assessment and planning for a pediatric bilateral hand transplant using 3-dimensional modeling: case report. *J Hand Surg Am.* 2016; 41(3):341-343.
58. Lee KH, Kim SJ, Cha YH, Kim JL, Kim DK, Kim SJ. Three-dimensional printed prosthesis demonstrates functional improvement in a patient with an amputated thumb: a technical note [published online ahead of print December 20, 2016]. *Prosthet Orthot Int.* doi: 10.1177/0309364616679315.
59. Mironov V, Reis N, Derby B. Review: bioprinting. A beginning. *Tissue Eng.* 2006; 12(4):631-634.
60. Zhu W, Zhao Y, Ma Q, Wang Y, Wu Z, Weng X. 3D-printed porous titanium changed femoral head repair growth patterns: osteogenesis and vascularisation in porous titanium. *J Mater Sci Mater Med.* 2017; 28(4):62.
61. Zhang ZZ, Wang SJ, Zhang JY, et al. 3D-printed poly(ε-caprolactone) scaffold augmented with mesenchymal stem cells for total meniscal substitution: a 12- and 24-week animal study in a rabbit model. *Am J Sports Med.* 2017; 45(7):1497-1511.
62. Yang Y, Yang S, Wang Y, et al. Anti-infective efficacy, cytocompatibility and biocompatibility of a 3D-printed osteoconductive composite scaffold functionalized with quaternized chitosan. *Acta Biomater.* 2016; 46:112-128.
63. Fedorovich NE, Schuurman W, Wijnberg HM, et al. Biofabrication of osteochondral tissue equivalents by printing topologically defined, cell-laden hydrogel scaffolds. *Tissue Eng Part C Methods.* 2012; 18(1):33-44.
64. Shim JH, Lee JS, Kim JY, Cho DW. Bioprinting of a mechanically enhanced three-dimensional dual cell-laden construct for osteochondral tissue engineering using a multi-head tissue/organ building system. *J Micromech Microeng.* 2012; 22(8):085014.

COPYRIGHT © SLACK INCORPORATED

Current Oncology

MDPI

Article

Point-of-Care Orthopedic Oncology Device Development

Ioannis I. Mavrodontis *, Ioannis G. Trikoupis, Vasileios A. Kontogeorgakos, Olga D. Savvidou and Panayiotis J. Papagelopoulos

First Department of Orthopaedic Surgery, School of Medicine, National and Kapodistrian University of Athens, 11527 Athens, Greece; itrikoupis@med.uoa.gr (I.G.T.); vkonto@med.uoa.gr (V.A.K.); olgasavvid@med.uoa.gr (O.D.S.); pjportho@med.uoa.gr (P.J.P.)
* Correspondence: imavrodontis@med.uoa.gr

Abstract: Background: The triad of 3D design, 3D printing, and xReality technologies is explored and exploited to collaboratively realize patient-specific products in a timely manner with an emphasis on designs with meta-(bio)materials. Methods: A case study on pelvic reconstruction after oncological resection (osteosarcoma) was selected and conducted to evaluate the applicability and performance of an inter-epistemic workflow and the feasibility and potential of 3D technologies for modeling, optimizing, and materializing individualized orthopedic devices at the point of care (PoC). Results: Image-based diagnosis and treatment at the PoC can be readily deployed to develop orthopedic devices for pre-operative planning, training, intra-operative navigation, and bone substitution. Conclusions: Inter-epistemic symbiosis between orthopedic surgeons and (bio)mechanical engineers at the PoC, fostered by appropriate quality management systems and end-to-end workflows under suitable scientifically amalgamated synergies, could maximize the potential benefits. However, increased awareness is recommended to explore and exploit the full potential of 3D technologies at the PoC to deliver medical devices with greater customization, innovation in design, cost-effectiveness, and high quality.

Keywords: individualized; patient-specific; endo-prostheses; instruments; point of care; 3D technologies; 3D printing; virtual reality; augmented reality

check for updates

Citation: Mavrodontis, I.I.; Trikoupis, I.G.; Kontogeorgakos, V.A.; Savvidou, O.D.; Papagelopoulos, P.J. Point-of-Care Orthopedic Oncology Device Development. *Curr. Oncol.* **2024**, *31*, 211–228. https://doi.org/10.3390/curroncol31010014

Received: 14 November 2023
Revised: 8 December 2023
Accepted: 26 December 2023
Published: 29 December 2023

Copyright: © 2023 by the authors. Licensee MDPI, Basel, Switzerland. This article is an open access article distributed under the terms and conditions of the Creative Commons Attribution (CC BY) license (https://creativecommons.org/licenses/by/4.0/).

1. Introduction

In cases where no alternative options exist in cases such as bone reconstructions for limb salvage after oncologic resections, endo-prostheses must be tailored to the patient's unique anatomy and physiology. When and why artificial reconstructions of anatomical integrities are chosen depends on prognostic factors, technical considerations, short-to-long-term advantages and disadvantages, and other parameters [1]. Individualized implantable orthopedic parts have the potential to provide the following [2–4]:

1. Superior mechanical performance tailored to the anatomical area free from stress-shielding phenomena leading to osteolysis.
2. Superior biological performance that promotes bone ingrowth to achieve osseointegration.
3. Optimal aesthetic outcomes with perfect fit.
4. Optimal postoperative function with fast recovery and fewer complications and risks.

In contrast, compared with off-the-shelf counterparts, custom parts require a high level of expertise, careful handling, and quality control at all stages of their development, and they usually require higher costs and more time for pre-operative planning and development.

1.1. Enabling 3D Technologies

To facilitate the development of individualized medical devices at the point of care (PoC) and improve patient healthcare, it is necessary for certain emblematic 3D technologies to be utilized and appropriate synergies and workflows to be formed within scientifically

amalgamated and quality-controlled schemes. The term "3D technologies" refers to a broad gnostic field that includes the following elements, which enable the development of patient-specific solutions, including implantable medical devices (Figure 1):

1. **3D medical imaging:** Tomographs (internal and external forms) and 3D scanners (external shapes) are used to capture high-fidelity anatomical image data for 3D visualization.
2. **3D computer software:** These are used to (a) process medical image data; (b) plan pre-operatively and navigate intra-operatively; and (c) design, simulate, and optimize medical devices.
3. **xReality:** These are virtual (VR), augmented (AR), and mixed (MR) devices used for (semi)immersive experiences to support pre-surgical planning, simulation, and surgical navigation. With VR (headsets), the user has the feeling of being part of an artificial world (virtual presence) that is different from actual physical reality, while with AR and MR (headsets, monitors, projectors), the user has a semi-immersive experience in which computer-generated content (text, images, animations) is superimposed over the user's actual environment.
4. **3D printing:** This refers to (bio)material fabrication techniques for realizing physical medical devices from digital 3D models created with computer software.

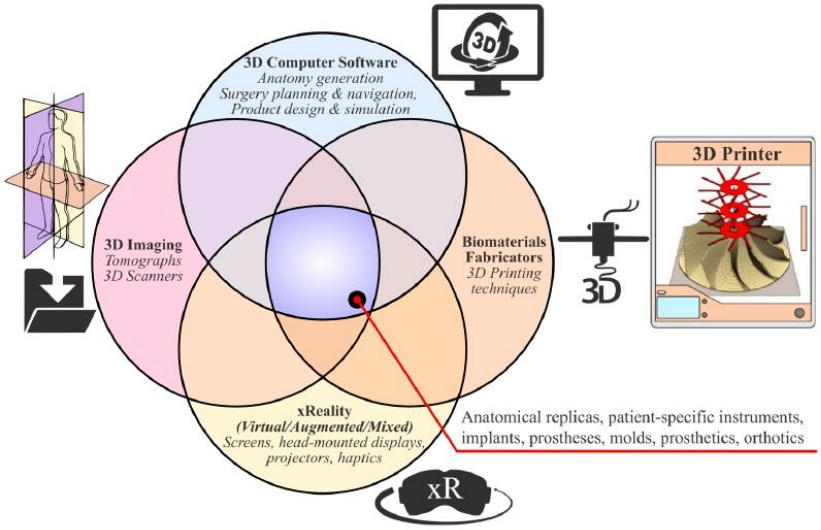

Figure 1. Three-dimensional technologies that enable the realization of individualized medical devices.

1.2. Three-Dimensional Printing of Individualized Medical Devices

According to ISO/ASTM [5], additive manufacturing (used synonymously with 3D printing) is defined as "a process of joining materials to make parts from 3D model data, usually layer upon layer, as opposed to subtractive manufacturing and formative manufacturing methodologies". There is a plethora of 3D printing techniques, each of which can be categorized into one of the seven classes: binder jetting, directed energy deposition, material extrusion, material jetting, powder-bed fusion, sheet lamination, and vat photo-polymerization.

Effectively, 3D printing is a tool-free method used for the primary shaping of complex freeform products. The 3D geometry emerges from the selective and successive layer-wise addition of material, with each layer corresponding to a cross-section of the product to be fabricated. This layer-by-layer principle enables almost unlimited and de novo design freedom to materialize extremely complex 3D geometries with intricate organic internal

and external features that vary in material density, geometry, and properties spatially across the part, per se. This way, manufacturing barriers are lifted, and the physical making of an object becomes easier than the digital 3D modeling of it. On the other hand, there can be technical flaws such as rough surfaces (the stair-stepping phenomenon), poor dimensional accuracy, anisotropic mechanical properties, micro-porosity, minimal feature size fabrication, and trapped powder particles (for powder-based techniques) [6].

Of the total value of 3D-printed products and services (USD 12.8 billion), the medical sector represents USD 1.65 billion [7]. Medical 3D printing has directly impacted more than 3 million patients and more than 5 million indirectly, with the largest growth expected in customized devices, surgical planning, and development and prototyping [8].

In medicine, intensive research is being conducted into 3D printing applications for making anatomical replicas, patient-specific instruments and molds, implants, (mega)endo-prostheses, orthotics and prosthetics, tissue-engineered constructs, and drug delivery products [9–11].

Numerous medically approved 3D printed devices have been implanted worldwide [12,13] with orthopedics and oncology being among the most common applications [14,15]. The process of 3D printing has been shown to provide beneficial solutions for bone substitution and limb salvage for oncological cases [16–18], and many breakthroughs have been achieved owing to the utilization of custom 3D designs followed by 3D printing [14,19–22]:

1. Physical replicas aid in better anatomic anticipation and physical surgical simulations for pre-operative planning, communication, teaching, and training. Particularly useful is the utilization of multi-material 3D printing where hard and soft structures are fabricated to mimic biological tissues [23,24].
2. Patient-specific solutions help
    a. To improve intra-operative navigation and surgical (biomechanics and functions) and aesthetic results.
    b. To decrease operating time, surgical risks and errors, blood loss, radiation exposure/fluoroscopy shots, and postoperative complications and infections.
    c. To lower cost and development times for one-off unique parts compared with traditional manufacturing methods.
    d. To create better coordination and communication between multi-disciplinary and inter-epistemic teams without disrupting their workflows.
3. Biomimetic weight, surface, and topology optimized structures with favorable interconnected porous geometries can be implemented to fabricate scaffolds for tissue engineering and bone grafts [25] or for artificial bone endo-prostheses for increased osseointegration and bone-matching mechanical properties [26,27]. Thus, properties are topologically and selectively tuned along the monolithic part, per se.
4. Novel medical devices are accelerated and design and/or timely manufacturing at the PoC is empowered.

The 3D printing of medical devices at the PoC can be useful for making patient-specific medical devices, resulting in savings; however, apart from the necessary inter-epistemic and multi-disciplinary synergy formation, the main issues are economic and regulatory, and qualified personnel are needed [28–36].

1.3. xReality Applications

xR technologies offer alternative tools for decision making that can improve patient healthcare outcomes and economic value [37]. Researchers report that xR leads to improved education, training, and surgical skill acquisition, outperforming classic sessions and training approaches [38–40], while xR systems for intra-operative navigation and information visualization are promising in complex surgical procedures requiring high precision and accuracy such as oncology (tumor resection) and spine surgeries [41,42], as xR is more or

equally reliable and accurate and less time-consuming than ultrasound and fluoroscopy with less or equal anesthesia time and blood loss [43–47].

1.4. Scope

This paper aims to fill the gap in the literature by presenting and unfolding, step by step, an inter-epistemic workflow for developing individualized orthopedic oncological devices at the PoC harnessing the above-mentioned 3D technologies. For this purpose, a case study on pelvic endo-prosthesis development with a suitable synergy that is centered around such 3D technologies is presented, and the potential and challenges are reported.

2. Materials and Methods

A systematic approach to engineering design [48] was tweaked and blended with other approaches to create a 15-step inter-epistemic end-to-end workflow for the development of patient-specific medical devices at the PoC (Figure 2). To fully explore and exploit the capabilities of 3D printing, design with 3D printing (Dw3DP) [49] was harnessed as a toolbox to expand conceptualization and boost creativity toward new design spaces. To overcome the associated issues of 3D printing and to maximize product performance through the synthesis of geometrical and material compositions, design for 3D printing (Df3DP) principles were considered [50,51]. Df3DP and Df3DP were inserted into a divergence–convergence model similar to the Double Diamond design process [52]. To support mimicking natural forms and functions, the Biomimicry Institute's design spiral and taxonomy of biological strategies were employed [53].

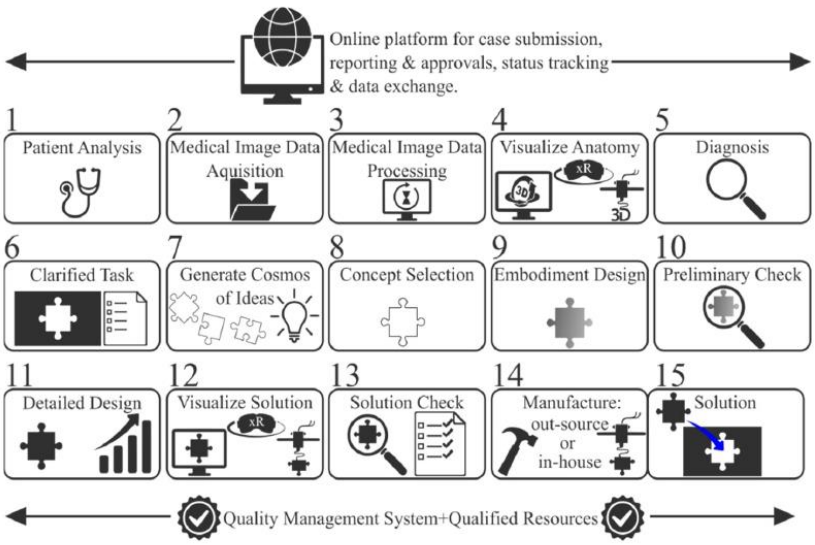

Figure 2. Inter-epistemic workflow for developing individualized orthopedic products.

Utilizing the aforementioned workflow, a case study of artificial pelvic reconstruction was carried out locally at a small 30-square-meter pilot PoC unit equipped with the hardware shown in Figure 3. In addition, an online platform was set up for status tracking and data exchange between the surgeon and the pilot PoC unit, supporting all phases described below.

Figure 3. PoC equipment.

2.1. Step 1—Patient Analysis

An adult male patient was diagnosed with pelvic osteosarcoma, and a two-step reconstruction approach was planned as per the prognostic factors and parameters and the tumor stage and site based on CT and MRI imaging (Figure 4). The ilium and sacroiliac joint were resected freehand en bloc (Type I plus partial IV plus partial II according to Enneking's classification [54]), and artificial reconstruction of the native bone structure with a non-bulky endo-prosthesis accompanied by patient-specific instruments was conducted.

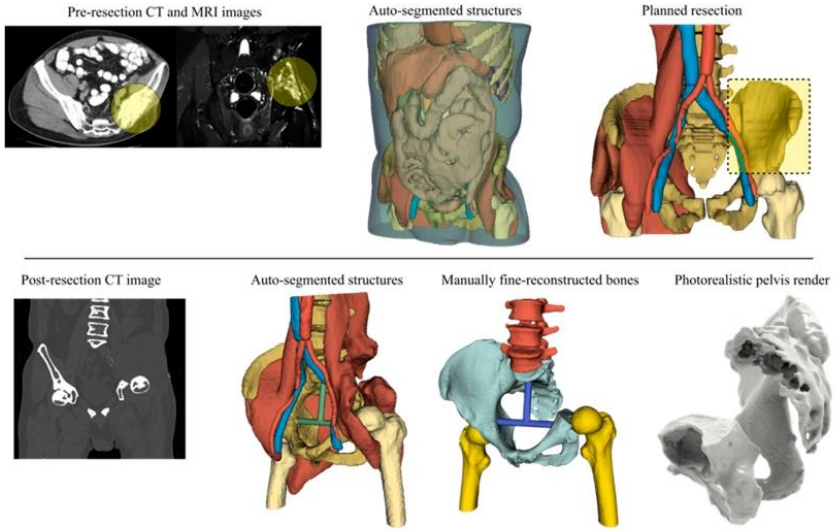

Figure 4. Pre- and post-resected 3D reconstructed anatomical models.

2.2. Step 2—Medical Image Acquisition

The patient's anatomy before and after resection was CT-scanned with a Somatom Definition Flash (Siemens Healthcare GmbH, Erlangen, Germany) with a slice thickness of

0.75 mm. The image data in both cases were anonymized before being shared with the PoC unit for segmentation and the generation of the anatomical 3D models.

2.3. Steps 3 and 4—Image Data Processing and Anatomy Visualization

For both pre- and post-resected CT scans, the free and open-source DICOM processing software 3D Slicer [55] was selected to generate the 3D anatomical structures and bony models by applying both manual and automatic tools, including trained algorithms for auto-segmentation (Figure 4). The structures were auto-segmented and generated in 3 min, while finer results of the post-resected pelvis required 170 min using manual tools to export the entire CT-scanned bony compartment. The pelvis was isolated, exported into a 33 MB .stl file, and re-meshed into a 20 MB .stl file using the free and open-source software Meshlab (version 5.2.2) [56].

The digital 3D anatomy was visualized in static photorealistic views and interactive 3D models (Figure 4) generated by KeyShot (Luxion Inc., Costa Mesa, CA, USA), and these, along with the .stl file itself, were transmitted to the surgeon. A 3D anatomical model was also prepared to be (semi)immersively viewed in (Figure 5) (a) virtual reality using the Oculus Rift S (Lenovo Group Limited, Beijing, China) headset running the Diffuse (now Specto Medical) (Specto Medical AG, Basel, Switzerland) and Medicalholodeck VR (Medicalholodeck AG, Zurich, Switzerland) software and (b) augmented reality using an Apple iPad 2021 Pro to augment the post-resected mesh model using both Augment AR Viewer (Augment SAS, Paris, France) and Medicalholodeck's Medical Imaging XR applications.

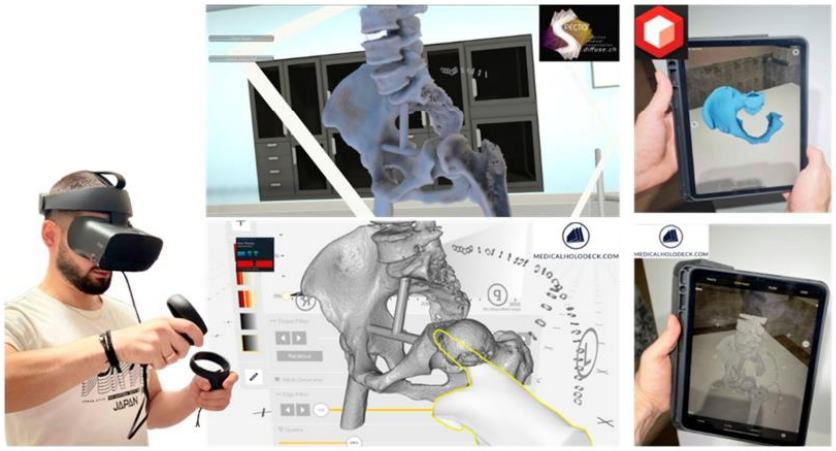

Figure 5. User immersed in virtual reality interacting with the post-resected pelvis in Specto and Medicalholodeck VR (**left**) and the post-resected model in AR Viewer and DICOM data in Medical Imaging XR (**right**).

A 248 × 231 × 168 mm pelvis was physically realized in a true-scale physical replica as a single monolithic piece (Figure 6) using the Creality (Shenzhen Creality 3D Technology Co., Ltd., Shenzhen, China) CR-10S 3D printer and ColorFabb's (Colorfabb B.V., Belfeld, the Netherlands) ivory-color PLA/PHA feedstock material. The free and open-source PrusaSlicer 2.4.2 was selected to plan the 3D printing process. In total, 663 g (EUR 23.2) of material was consumed in 3 days and 13 h. The pre-processing and post-processing took 15 and 20 min, respectively. The end product was more than acceptable, per se, in terms of surface finish and dimensional precision; measurements using a calibrated digital caliper revealed deviations of less than 0.3 mm.

Figure 6. Post-resected 3D-printed pelvic model.

2.4. Steps 5 and 6—Rehabilitation Strategy and Task Clarification

The ultimate goal was to preserve the patient's limb and retain favorable functions in the long term by re-establishing the continuity of the pelvic girdle to prevent subsequent collapses and deformations in the residual bony tissue under load-bearing activities. As pelvic endo-prostheses are fraught with difficulties, the developed solution had to mitigate as much complexity in the operating room as possible. By examining the patient's post-resected DICOM data, the 3D digital model, the virtual model, and the physical 3D-printed model, the surgeon was able to outline the need for a non-bulky, low-profile endo-prosthesis conforming to the inner form of the resected bone tissue, and together with the PoC unit, they set the rehabilitation strategy and clarified the task by defining the specifications and requirements of the solution. Certain product design specification elements were utilized by considering the application that the endo-prosthesis should adhere to. The specifications were filled collaboratively within a 1 h meeting session, and a 24 h window for amendments was agreed upon.

2.5. Steps 7 and 8—Conceptual Design and Evaluation

Working principles and ideas were explored by searching a knowledge database with inputs sourced from natural systems, industrial sectors, the orthopedic device market, and the literature. Matching products, forms, functions, and principles were captured as hypodigms for inspiration and mimesis to turn working ideas after analysis and synthesis into working concepts, adapting the concepts to the specification list. A mind map of concepts for each function was created by brainstorming, and a 24 h window for amendments was agreed upon. Under SWOT analysis, from which threats were considered for risk assessment, the generated concepts were evaluated collaboratively based on preset constraints and weighted (from 1 to 5) criteria. The deliverables were hand sketches (30 min required) and a corresponding tangible red modeling clay replica of the concept achieving the best score (40 min required), and 3D marking in computer modeling software and virtual reality were also explored (Figure 7).

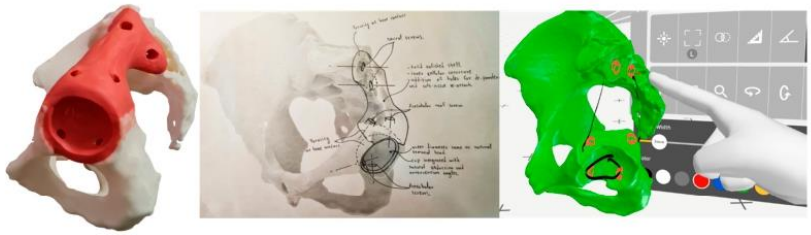

Figure 7. Physical clay modeling, hand sketching, and virtual reality sketching of the concept.

2.6. Steps 9, 10, and 11—Embodiment and Detailed Design

Then, 3D pre-operative planning and 3D modeling were conducted using the Spaceclaim 2022 R1 (Ansys Inc., Canonsburg, PA, USA), the cloud-based Fusion 360 (Autodesk Inc., San Fransisco, CA, USA), and Rhinoceros 7 (Robert McNeel and Associates, Seattle, WA, USA) software.

As patient-specific metrics have been suggested to be considered for cup placement instead of the typical "safe-zone" values reported in the literature decades ago [57], the anteversion (13.3°) and abduction angles (39.8°) were measured in 3D. A suitable off-the-shelf Ti alloy femoral stem with Ti coating that matched our needs, maintained the same symmetry, and eliminated leg-length discrepancy was selected along with a matching 22 mm diameter CoCrMo femoral head in combination with a UHMWPE 22/38 mm mobile liner within a stainless steel AISI 316L dual mobility 38/44 mm acetabular cup, which was cemented to the endo-prosthesis's 46/54 mm acetabular shell. The new left center of rotation had an 8.80 mm medial offset from the natural femoral head center and a 3 mm anterior offset from the right femoral head.

Six cancellous self-tapping Ti bone screws were positioned and oriented as per the bone morphology, surrounding soft tissue, and bone quality. Two 4 mm diameter cancellous screws were inserted 25 mm into the pubis and into the ischium as per the quadrant system described by Wasielewski et al. [58], two 6.5 mm diameter cancellous screws were inserted 30 mm from the acetabulum rooftop, and two 6.5 mm diameter cancellous screws were inserted 50 mm within the sacrum; most males and females can accommodate up to 8 mm diameter screws in S1 and S2 [59].

As hemispherical cups exhibit better stability with fewer complications compared with elliptic cups [60], a 46/54 mm diameter hemispherical acetabular shell was modeled with a spheroid-textured inner surface cup to facilitate better anchorage of the bone cement that fixed the cup in place. A solid endo-prosthesis was modeled and united with the acetabular shell into a single object. Unnecessary material was removed, and de-powdering holes were added for possible soft tissue suturing. Housings for all bone screw heads were added, and all features were blended into a smooth geometric result with no sharp edges.

Ancillary patient-specific instruments were also developed (Figure 8): (a) an acetabulum rooftop and sacrum side flat cutting jig; (b) an acetabulum reaming check tool used during reaming to guarantee a perfect fit, as the osseointegration of suitably interconnected porous implants depends on the minimization of micro-gaps, a reduction in micro-motions, and reaming for good vascularization and good bleeding [61]; (c) a femoral head cutting jig; and (d) bimodal bone screws, pilot hole drilling, and a trial endo-prosthesis replica.

By ignoring (a) the effects of all surrounding muscles, ligaments, and cartilage; (b) the threads of the bone screws and their tightening and reaction forces; and (c) the anisotropic characteristic of 3D-printed products, a mechanical static stress analysis was conducted in Fusion 360 (Nastran solver), as shown in Figure 9. Ti-6Al-4V material properties were assigned to the bone screws and endo-prosthesis, whereas the pelvic bones were assumed to behave as a single homogeneous, linear isotropic, elastic material with an averaged modulus of elasticity of $E = 7$ GPa and a Poisson's ratio of $\nu = 0.3$ [62,63]. The sacrum was fixed by constraining the top surfaces in all degrees of freedom, and a force four times the relevant body weight to simulate walking and stair-descending activities [64] (rounded at 3000 N) was applied individually and simultaneously at both hip joints. The bodies were volume-meshed with tetrahedral elements, and the simulation generated Von Misses stresses and displacement results. The stress distribution and displacement of the pelvic bones, endo-prosthesis, and bone screws differed considerably in each scenario with the peak stresses being considerably (16 times) lower (<60 MPa) than the yield stress of the endo-prosthesis and bone screws. As the relationship between load and stress is linear, a force eight times the body weight (to simulate the extreme event of stumbling [65]) could be easily borne by the endo-prosthesis and the bone screw materials.

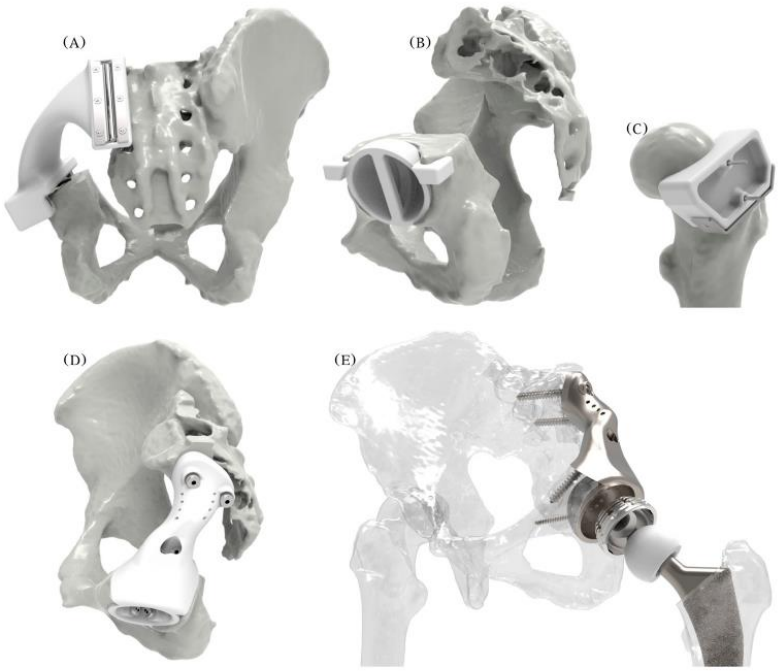

Figure 8. Photo-realistic models of the (**A**) cutting jig, (**B**) reaming check tool, (**C**) femoral head cutting jig, (**D**) drilling jig–trial endo-prosthesis instrument, and (**E**) endo-prosthesis and the total hip arthroplasty components.

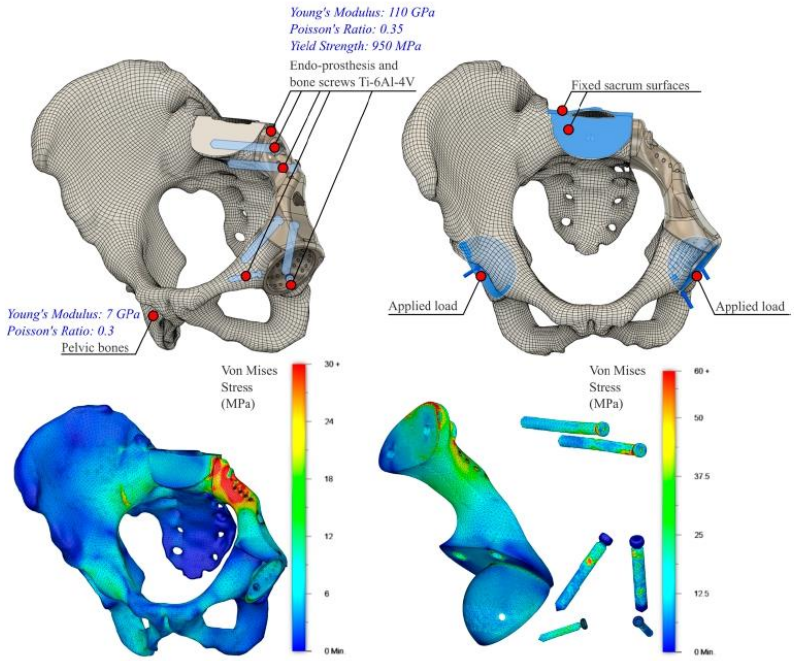

Figure 9. Mechanical static stress simulation and results for the combined hip-loading scenario.

The higher modulus of elasticity and the solid endo-prosthesis form result in a much stiffer endo-prosthesis compared with the host pelvic bone. Although topology optimization or generative design could have been employed to lighten the initially fully solid 416 g endo-prosthesis down to 292 g or 179 g, respectively (Figure 10) via stress-driven mass reduction, instead, we decided to introduce cellular architecture to the endo-prosthesis and keep a thin solid outer shell.

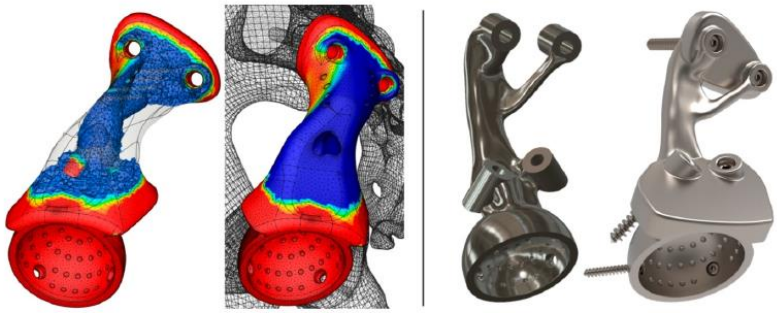

Figure 10. Topology-optimized (**left**) and generatively designed endo-prosthesis (**right**).

Toward the goal of "biologizing" the internal form and external surfaces that touch the host bone and obtaining optimal bimodal performance (bone ingrowth and stiffness reduction) within a suitable design space, it was concluded that the spongy complex of the natural bone can be mimicked by a functionally graded stochastic Voronoi foam pattern that can be assigned both internally and at bone-contact surfaces by considering (a) an optimal pore size of 0.3–0.6 mm for good cell colonization, vascularization, mechanical integrity, and permeability [66,67]; (b) manufacturability (laser beam powder bed fusion); and (c) the histomorphometric [27] properties of the trabecular bone at the iliac crest, i.e., 84% porosity, 0.15 mm feature thickness, and 0.75 mm pore size. Using nTopology 4.12.2 (nTopology Inc., New York, NY, USA), the endo-prosthesis was architected selectively and topologically with a gradient and conforming 3D stochastic Voronoi pattern. The total mass of the resultant optimized endo-prosthesis meta-(bio)material totaled 256 g, with 151 g being the scaffold structures and 105 g being the hollowed body with 1–1.5 mm wall thickness. The characteristics of the optimized biomimetic result are shown in Figure 11.

The generated stochastic Voronoi structure was assumed to be isotropic and homogeneous in terms of its elastic properties along any loading direction because of its randomized cell orientation [68]. Voronoi-based foams with open cells and high porosities are considered ideal bending-dominated structures, with a resultant modulus of elasticity calculated with the following formula [68,69]:

$$E_c = E_s * \rho \hat{} 2 \quad (1)$$

where E_c and E_s are the modulus of elasticity of the cellular and fully dense solids, respectively, and ρ is the relative density of the cellular solid, which is connected to the porosity (φ) of the cellular solid by the formula

$$\varphi = (1 - \rho) * 100 \quad (2)$$

In this case, as per Equations (1) and (2), the resultant modulus is E = 17.6 GPa, which is close to the modulus of elasticity of cortical bone [70]. To assess the mechanical performance of the final optimized form, only the hollowed body was used to carry out a similar mechanical static stress analysis as before. The hollowed body withstood the same loads as exerted previously on the fully solid endo-prosthesis, but in this case, under greater (three-fold) stresses and displacements. It was orthological to assume that introducing the

stochastic Voronoi infill would not compromise the mechanical performance of the solid shell and would not lead to mechanical failure, as plastic deformation is unlikely since the cellular structure is stiffened by the solid shell, though this claim should have been verified by suitable extra simulations.

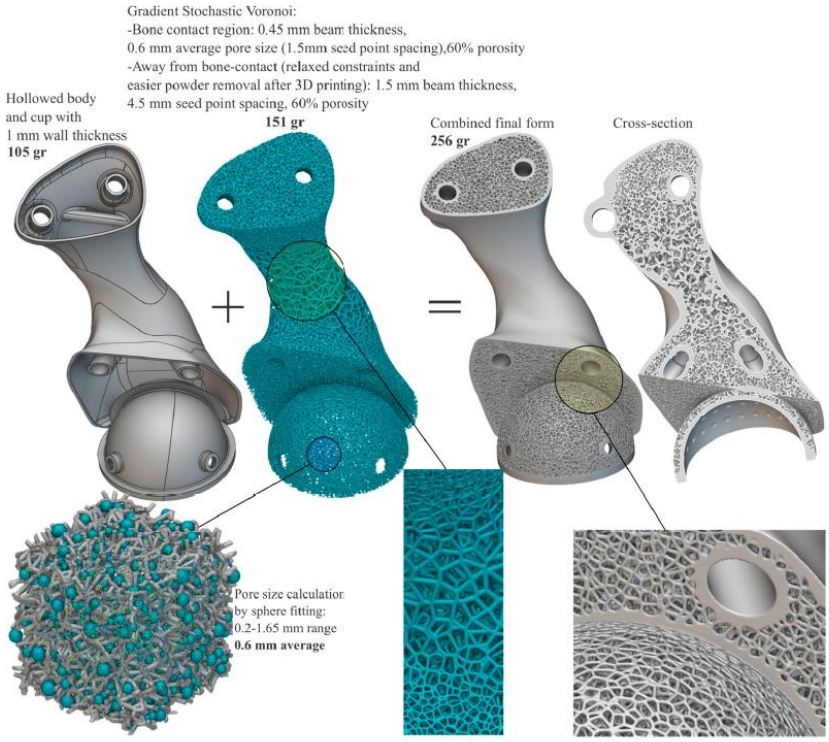

Figure 11. Mass and characteristics of the gradient stochastic Voronoi-optimized endo-prosthesis.

The total time to complete the embodiment and the detailed design was 3 days.

2.7. Step 12—Prototyping

Digital, virtual, and physical visualization was conducted for verification of all components of the solution (Figure 12). An anatomical model with a reamed acetabulum and flat-cut surfaces; a femoral head; a femoral head with a femoral stem and head inserted; a cemented cup; and prototypes of the cutting jig, reaming check tool, femoral head cutting jig, drilling jig–trial endo-prosthesis instrument, and endo-prosthesis were 3D-printed in three sessions using the Creality CR-10s 3D printer in 3 days and 13 h, 2 days and 4 h, and 22 h, consuming 663 g (ivory, EUR 23.2), 370 g (gray, EUR 13), and 280 g (black, EUR 10) ColorFabb PLA/PHA material, respectively. The total pre-processing and post-processing took 20 and 30 min, respectively. To better illustrate the details of the optimized endo-prosthesis, the Elegoo (Elegoo Inc., Shenzhen, China) Saturn S vat photopolymerization 3D printer and a clear plant-based photocurable resin were used. Chitubox Basic 1.9.4 (Chuangbide Technologies Co., Ltd., Shenzhen, China) was used to plan the process, which took 6 h, consuming 55 mL (EUR 3) of resin.

Figure 12. The 3D-printed prototype parts of the solution.

2.8. Steps 13, 14, and 15—Final Meeting, Manufacturing, and Implantation

All characteristics of the solution were documented, a final meeting with all required parties was arranged for final approval as per the applicable legal and standard procedures, and labels (unique numbers) were embossed on the surface of each unique part. The off-the-shelf components (total hip arthroplasty, bone screws, K-wires) were readily available on the market for purchase, whereas all custom parts were sent to a contract manufacturer; i.e.,

1. The cutting jig and drilling jig-trial endo-prosthesis instrument with all metal inserts, the reaming check tool, and the femoral head cutting jig were ordered to be 3D-printed out of surgical-grade PA12 with a suitable powder-bed fusion technology (laser sintering). The total cost was EUR 380 for 6 working days and delivery.
2. The endo-prosthesis was ordered to be 3D-printed out of surgical-grade Ti-6Al-4V with a suitable powder-bed fusion technology (laser melting), followed by glass bead blasting for satin surface finish. The total cost was EUR 1800 for 6 working days and delivery.

Once received and before application, all parts were carefully inspected, cleaned, and sterilized to prevent infection by applying the most suitable method [71], as erroneous or inadequate cleaning, post-processing, sterilization, and packaging can have serious performance and safety consequences.

3. Results and Discussion

The COVID-19 pandemic catalyzed the need to adopt a new model that embraces digital health tools [72], including xR devices, 3D design software, and 3D printing. As the weaknesses of modern healthcare systems were revealed, and their capacity, supply, and workforce were challenged, 3D printing proved to have suitable characteristics and potential, providing a glimpse into the future of healthcare by enabling the decentralized (localized) manufacturing of personal protective equipment and other critical parts at the PoC [73] despite some safety concerns and challenges [74]. Similarly, patient-specific medical devices can be designed and/or manufactured just in time at the PoC at affordable costs and with short lead times, provided that suitable equipment and infrastructure exist [30].

The operation of a PoC unit lies at the intersection of healthcare providers, regulatory groups, engineers, and manufacturers who contribute to the common goal of providing high-quality and safe solutions to each unique patient. In the quest to establish PoC units, non-technical challenges (regulatory compliance, lack of directives, standards and quality management systems, need for skilled personnel, intellectual property, and digital security

issues) and technical limitations still hold 3D technologies from springboarding and should be addressed [8]. PoC units must establish their best practices by implementing quality management systems while also conforming to applicable regulations and standards. In the USA and the EU, custom-made emergency devices can be exempted from regulatory control by allowing authorized healthcare professionals to provide design input and take responsibility for the safety and performance of customized medical devices. However, because existing regulations and standards oversee the way medical devices are manufactured, 3D technologies need further guidance to establish quality control measures as numerous parameters might lead to a low-quality 3D-printed product, i.e., data preparation variables, design features, feedstock materials, process and 3D printer parameters, personnel, documentation, infrastructure, and post-processing. Therefore, appropriate quality management systems, including strategies and processes for addressing errors and improving consistency, are important to controlling and assuring quality and safety. Otherwise, the uncontrolled rapid growth of 3D technologies and the increasing complexity might put patients at increased risk of potential errors, decreased quality, and sub-optimal performance for the solution. Ultimately, the evolution and synthesis of regulations, quality management systems, and accessibility to 3D technologies will define the maturation of PoC patient-specific device development. As necessity drives invention and innovation, once the readiness of 3D technologies stops remaining under question, data protection issues are addressed, and costs in tandem with medical device development time are further reduced, their PoC incorporation will accelerate healthcare into intelligent formats capable of unlocking mass customization with high-quality end results and increased patient satisfaction.

A plethora of trade-offs can be made for PoC units in terms of software and hardware equipment; infrastructure and layout organizational structure; and personnel. PoC fabrications of end parts could eliminate reliance on external partners, potentially reducing costs; however, it is recommended that in-house 3D designs and 3D printing should be commenced only for prototyping and outsourcing end parts. Only if sufficient demand exists is it orthological to increase capacity and implement in situ final manufacturing. Investments should be rationalized and driven by clinical needs so that collaboratively developed solutions are clinically and scientifically relevant and ultimately beneficial for each unique patient.

The developed patient-specific solution was successfully prototyped at the PoC within an acceptable clinical time and cost frame. The end polymer and metallic parts that required high-cost industrial-grade systems were outsourced to external partners, but 3D-printing polymer anatomical models, surgical guides, and implant prototyping, along with xReality systems for pre-operative planning and intra-operative (non-navigation) purposes, can be implemented at relatively low initial capital investments and operating and maintenance costs. The most time-consuming tasks were found to be the 3D printing of anatomical models and all prototype parts of the solution, but since much faster, low-budget 3D printers are currently available in the market, the time can be considerably reduced.

The custom meta-(bio)material-by-design endo-prosthesis developed for pelvic reconstruction after tumor resection featured interconnected porous architectures with gradient pore size and beam thickness. The areas away from the bone had a larger pore size and thicker beams to facilitate better manufacturability and the removal of trapped and un-melted powder particles after laser-based powder-bed fusion 3D printing, while the bone-contact regions had values as recommended in the literature, e.g., ~60–70% porosity with ~0.6 mm pore size [66,67]. Numerous 3D-printed implantable devices featuring cellular architectures have been researched, commercialized, and cleared by the FDA [12,13], and postoperative follow-ups of such porous morphologies have been proven to have good short- and mid-term outcomes [3,75–77], including hemi-pelvic endo-prostheses that have shown good oncological and functional outcomes with stable fixation and good osseointegration without severe complications [78–84].

With 3D printing, standard, modular, and patient-specific parts can be materialized that cannot or are extremely difficult to make using traditional methodologies. On the other hand, 3D printing is not a panacea, as it is prone to challenges when biomimetic porous structures and fine details are involved. Hence, appropriate design rules for ensuring manufacturability using the selected 3D printing technology must be adopted to avoid differences between as-designed and as-3D-printed products [85]. Appropriate methods should be implemented for the powder-bed fusion 3D printing of metals [86] as multi-scale, multi-physics phenomena occur that might lead to structural defects and implications if sub-optimal processing parameters are selected [27,87,88]. For example, the de-powdering of un-melted and trapped powder particles after the completion of laser-based powder-bed fusion 3D printing is critical, as there is a risk of particles entering the patient's body; air-jetting followed by dry ultrasonic vibration and/or chemical etching is important [89]. In addition, if the surface finish, dimensional accuracy, and fatigue properties have to be improved, post-processing methods such as machining and heat treatments can be applied.

Toward this direction, algorithmically driven and machine learning methodologies powered by trained datasets and sourced from the libraries of previous cases with an emphasis on design manufacturing process optimization for the highest mechanical and biological performance are highly sought in order to minimize errors and defects [90]. As image data acquisition and processing and design and manufacturing techniques are streamlined in tandem with artificial intelligence methods for decision-making and automating processes, the range of applications will widen, and ultimately the reliance on large, centralized manufacturing plants and the maintenance of expensive supply networks might be reduced.

This case study had several limitations that will be researched in the future:

1. To better define the endo-prosthesis form and its fixation points, directions, and lengths, multi-modal CT, MRI, magnetic resonance neurography (MRN), and computed tomography angiography (CTA) imaging are required to account for neurovascular tissue [91,92].
2. Extra-mechanical simulations considering anisotropic and inhomogeneous bone tissue properties [93,94] and surrounding soft tissue; the threads of bone screws and their tightening reaction forces; and dynamic fatigue analyses should be executed by considering more loading scenarios such as direct impacts caused by sideways falls.
3. Regarding the mechanical performance of the spongy architectures, alternative functionally graded structures could be explored and simulated while also investigating local stress concentrations, contact phenomena, and deformation levels on the nodes and beams to ensure that these can withstand the exerted loads without failure. Ideally, cellular structures should be generated by simulation-driven multi-objective and multi-scale tools that account for spatial variations in parameters across parts, per se.
4. Research on coating substances that can be applied to the porous surface for bacterial-fighting and osseointegration-boosting activities.
5. More case studies should enrich the portfolio, and follow-ups must be reported.

Future research can be extended toward scaffold-based or scaffold-free bioprinting for bone grafting; multi-material 3D printing of hard-soft composites; 4D (bio)printing of stimuli-responsive materials; drug delivery systems that elute under control; and "instrumented" endo-prostheses capable of sensing, measuring, and reporting real-time physical quantities.

4. Conclusions

Healthcare has traditionally been a non-engineering design and non-manufacturing sector, as neither design nor manufacturing usually takes place in situ. The entrance of 3D design and manufacturing technologies is transforming healthcare facilities into decentralized design and/or manufacturing sites. PoC units aiming at medical device development should be established accordingly to facilitate the symbiosis of healthcare professionals with skilled (bio)mechanical engineers to develop patient-specific devices at the PoC within acceptable lead times and costs.

Three-dimensional technologies are newly inserted tools into the modern digital cosmos of individualized healthcare delivery and introduce advanced abilities for delivering medical devices at the PoC with greater customization, innovation in design, cost-effectiveness, and high quality. Although related pitfalls are known to engineers, an increased awareness is suggested to explore and exploit the full potential of the 3D design–3D printing–xReality triad in realizing medical devices at the PoC under suitable quality management systems and as per the applicable regulations and standards.

Author Contributions: Conceptualization, I.I.M. and I.G.T.; methodology, I.I.M., I.G.T. and V.A.K.; software, I.I.M.; validation, V.A.K., O.D.S. and P.J.P.; formal analysis, V.A.K. and O.D.S.; investigation, I.I.M. and I.G.T.; resources, I.I.M. and P.J.P.; writing—original draft preparation, I.I.M. and I.G.T.; writing—review and editing, I.I.M., O.D.S. and P.J.P.; visualization, I.I.M.; supervision, V.A.K., O.D.S., and P.J.P.; project administration, I.I.M. and P.J.P. All authors have read and agreed to the published version of the manuscript.

Funding: This research received no external funding.

Institutional Review Board Statement: Not applicable.

Informed Consent Statement: Not applicable.

Data Availability Statement: No data are reported.

Conflicts of Interest: The authors declare no conflict of interest.

References

1. Özger, H.; Sim, F.; Puri, A.; Eralp, L. *Orthopedic Surgical Oncology for Bone Tumors*; Springer: Cham, Germany, 2022.
2. Li, X.; Feng, Y.; Wang, C.; Li, G.; Lei, W.; Zhang, Z.; Wang, L. Evaluation of Biological Properties of Electron Beam Melted Ti6Al4V Implant with Biomimetic Coating In Vitro and In Vivo. *PLoS ONE* **2012**, *7*, e52049. [CrossRef] [PubMed]
3. Regis, M.; Marin, E.; Fedrizzi, L.; Pressacco, M. Additive manufacturing of Trabecular Titanium orthopedic implants. *MRS Bull.* **2015**, *40*, 137–144. [CrossRef]
4. Taniguchi, N.; Fujibayashi, S.; Takemoto, M.; Sasaki, K.; Otsuki, B.; Nakamura, T.; Matsushita, T.; Kokubo, T.; Matsuda, S. Effect of pore size on bone ingrowth into porous titanium implants fabricated by additive manufacturing: An in vivo experiment. *Mater. Sci. Eng. C* **2016**, *59*, 690–701. [CrossRef] [PubMed]
5. *ISO/ASTM 52900:2021*; Additive Manufacturing—General Principles—Fundamentals and Vocabulary. ISO: Geneva, Switzerland, 2021.
6. Gibson, I.; Rosen, D.; Stucker, B.; Khorasani, M. *Additive Manufacturing Technologies*, 3rd ed.; Springer: Cham, Germany, 2021.
7. Wohlers Associates. *Wohlers Report: 3D Printing and Additive Manufacturing Global State of the Industry*; Wohlers Associates: Fort Collins, CO, USA, 2021.
8. ASME. *Medical Additive Manufacturing/3D Printing: Year in Review 2019–2020*; ASME: New York, NY, USA, 2020.
9. Ejnisman, L.; Gobbato, B.; de França Camargo, A.; Zancul, E. Three-Dimensional Printing in Orthopedics: From the Basics to Surgical Applications. *Curr. Rev. Musculoskelet. Med.* **2021**, *14*, 1–8. [CrossRef] [PubMed]
10. Charbonnier, B.; Hadida, M.; Marchat, D. Additive manufacturing pertaining to bone: Hopes, reality and future challenges for clinical applications. *Acta Biomater.* **2021**, *121*, 1–28. [CrossRef] [PubMed]
11. Salmi, M. Additive Manufacturing Processes in Medical Applications. *Materials* **2021**, *14*, 191. [CrossRef]
12. Lowther, M.; Louth, S.; Davey, A.; Hussain, A.; Ginestra, P.; Carter, L.; Eisenstein, N.; Grover, L.; Cox, S. Clinical, industrial, and research perspectives on powder-bed fusion additively manufactured metal implants. *Addit. Manuf.* **2019**, *28*, 565–584. [CrossRef]
13. Fogarasi, M.; Snodderly, K.L.; Di Prima, M.A. A survey of additive manufacturing trends for FDA-cleared medical devices. *Nat. Rev. Bioeng.* **2023**, *1*, 687–689. [CrossRef]
14. Levesque, J.; Shah, A.; Ekhtiari, S.; Yan, J.; Thornley, P.; Williams, D. Three-dimensional printing in orthopaedic surgery: A scoping review. *EFORT Open Rev.* **2020**, *5*, 430–441. [CrossRef]
15. Kermavnar, T.; Shannon, A.; O'Sullivan, K.; McCarthy, C.; Dunne, C.; O'Sullivan, L. Three-Dimensional Printing of Medical Devices Used Directly to Treat Patients: A Systematic Review. *3D Print. Addit. Manuf.* **2021**, *8*, 366–408. [CrossRef]
16. Angelini, A.; Trovarelli, G.; Berizzi, A.; Pala, E.; Breda, A.; Ruggieri, P. Three-dimension-printed custom-made prosthetic reconstructions: From revision surgery to oncologic reconstructions. *Int. Orthop.* **2018**, *43*, 123–132. [CrossRef] [PubMed]
17. Angelini, A.; Kotrych, D.; Trovarelli, G.; Szafrański, A.; Bohatyrewicz, A.; Ruggieri, P. Analysis of principles inspiring design of three-dimensional-printed custom-made prostheses in two referral centres. *Int. Orthop.* **2020**, *44*, 829–837. [CrossRef] [PubMed]
18. Park, J.; Kang, H.; Kim, J.; Kim, H. New 3-dimensional implant application as an alternative to allograft in limb salvage surgery: A technical note on 10 cases. *Acta Orthop.* **2020**, *91*, 489–496. [CrossRef]
19. Martelli, N.; Serrano, C.; van den Brink, H.; Pineau, J.; Prognon, P.; Borget, I.; El Batti, S. Advantages and disadvantages of 3-dimensional printing in surgery: A systematic review. *Surgery* **2016**, *159*, 1485–1500. [CrossRef]

20. Langridge, B.; Momin, S.; Coumbe, B.; Woin, E.; Griffin, M.; Butler, P. Systematic Review of the Use of 3-Dimensional Printing in Surgical Teaching and Assessment. *J. Surg. Educ.* **2018**, *75*, 209–221. [CrossRef]
21. Javaid, M.; Haleem, A. Additive manufacturing applications in orthopaedics: A review. *J. Clin. Orthop. Trauma* **2018**, *9*, 202–206. [CrossRef]
22. Kumar, L.; Haleem, A.; Javaid, M. Impact of three-dimensional printing in orthopedics. *J. Glob. Health* **2021**, *5*, 178–182. [CrossRef]
23. Goh, G.D.; Sing, S.L.; Lim, Y.; Thong, J.; Peh, Z.; Mogali, S.R.; Yeong, W.Y. Machine learning for 3D printed multi-materials tissue-mimicking anatomical models. *Mater. Des.* **2021**, *211*, 110125. [CrossRef]
24. Bezek, L.B.; Cauchi, M.P.; De Vita, R.; Foerst, J.R.; Williams, C.B. 3D printing tissue-mimicking materials for realistic transseptal puncture models. *J. Mech. Behav. Biomed. Mater.* **2020**, *110*, 103971. [CrossRef]
25. Brachet, A.; Bełżek, A.; Furtak, D.; Geworgjan, Z.; Tulej, D.; Kulczycka, K.; Karpiński, R.; Maciejewski, M.; Baj, J. Application of 3D Printing in Bone Grafts. *Cells* **2023**, *12*, 859. [CrossRef]
26. Benedetti, M.; du Plessis, A.; Ritchie, R.; Dallago, M.; Razavi, S.; Berto, F. Architected cellular materials: A review on their mechanical properties towards fatigue-tolerant design and fabrication. *Mater. Sci. Eng. Rep.* **2021**, *144*, 100606. [CrossRef]
27. McGregor, M.; Patel, S.; McLachlin, S.; Vlasea, M. Architectural bone parameters and the relationship to titanium lattice design for powder-bed fusion additive manufacturing. *Addit. Manuf.* **2021**, *47*, 102273. [CrossRef]
28. Frizziero, L.; Santi, G.; Liverani, A.; Giuseppetti, V.; Trisolino, G.; Maredi, E.; Stilli, S. Paediatric Orthopaedic Surgery with 3D Printing: Improvements and Cost Reduction. *Symmetry* **2019**, *11*, 1317. [CrossRef]
29. Pajot, T.; Benichou, L.; Moreau, E.; Tallon, V.; Meningaud, J.; Khonsari, R.; Ketoff, S. Implementation of a digital chain for the design and manufacture of implant-based surgical guides in a hospital setting. *J. Stomatol. Oral Maxillofac. Surg.* **2020**, *121*, 347–351. [CrossRef] [PubMed]
30. Teo, A.; Ng, D.; Lee, P.; O'Neill, G. Point-of-Care 3D Printing: A Feasibility Study of Using 3D Printing for Orthopaedic Trauma. *Injury* **2021**, *52*, 3286–3292. [CrossRef] [PubMed]
31. Popescu, D.; Marinescu, R.; Sandache, O. Upper Limbs Orthoses Production in 3D Printing Points-of-Care. In Proceedings of the 2021 International Conference on e-Health and Bioengineering (EHB), Iasi, Romania, 18–19 November 2021; pp. 1–4.
32. Calvo-Haro, J.; Pascau, J.; Asencio-Pascual, J.; Calvo-Manuel, F.; Cancho-Gil, M.; Del Cañizo López, J.; Fanjul-Gómez, M.; García-Leal, R.; González-Casaurrán, G.; González-Leyte, M.; et al. Point-of-care manufacturing: A single university hospital's initial experience. *3D Print. Med.* **2021**, *7*, 11. [CrossRef] [PubMed]
33. Keller, M.; Guebeli, A.; Thieringer, F.; Honigmann, P. In-hospital professional production of patient-specific 3D-printed devices for hand and wrist rehabilitation. *Hand Surg. Rehabil.* **2021**, *40*, 126–133. [CrossRef] [PubMed]
34. Honigmann, P.; Sharma, N.; Schumacher, R.; Rueegg, J.; Haefeli, M.; Thieringer, F. In-Hospital 3D Printed Scaphoid Prosthesis Using Medical-Grade Polyetheretherketone (PEEK) Biomaterial. *Biomed Res. Int.* **2021**, *2021*, 1301028. [CrossRef]
35. Andrés-Cano, P.; Calvo-Haro, J.; Fillat-Gomà, F.; Andrés-Cano, I.; Perez-Mañanes, R. Role of the orthopaedic surgeon in 3D printing: Current applications and legal issues for personalized medicine. *Rev. Esp. Cir. Ortop. Traumatol.* **2021**, *65*, 138–151. [CrossRef]
36. Czyżewski, W.; Jachimczyk, J.; Hoffman, Z.; Szymoniuk, M.; Litak, J.; Maciejewski, M.; Kura, K.; Rola, R.; Torres, K. Low-Cost Cranioplasty-A Systematic Review of 3D Printing in Medicine. *Materials* **2022**, *15*, 4731. [CrossRef]
37. Han, J.; Kang, H.; Kim, M.; Kwon, G. Mapping the intellectual structure of research on surgery with mixed reality: Bibliometric network analysis (2000–2019). *J. Biomed. Inform.* **2020**, *109*, 103516. [CrossRef] [PubMed]
38. Walbron, P.; Common, H.; Thomazeau, H.; Hosseini, K.; Peduzzi, L.; Bulaid, Y.; Sirveaux, F. Virtual reality simulator improves the acquisition of basic arthroscopy skills in first-year orthopedic surgery residents. *Orthop. Traumatol. Surg. Res.* **2020**, *106*, 717–724. [CrossRef] [PubMed]
39. Gerup, J.; Soerensen, C.; Dieckmann, P. Augmented reality and mixed reality for healthcare education beyond surgery: An integrative review. *Int. J. Med. Educ.* **2020**, *11*, 1. [CrossRef] [PubMed]
40. Tang, Y.; Chau, K.; Kwok, A.; Zhu, T.; Ma, X. A systematic review of immersive technology applications for medical practice and education—Trends, application areas, recipients, teaching contents, evaluation methods, and performance. *Educ. Res. Rev.* **2022**, *35*, 100429. [CrossRef]
41. Jud, L.; Fotouhi, J.; Andronic, O.; Aichmair, A.; Osgood, G.; Navab, N.; Farshad, M. Applicability of augmented reality in orthopedic surgery—A systematic review. *BMC Musculoskelet. Disord.* **2020**, *21*, 103. [CrossRef] [PubMed]
42. Casari, F.; Navab, N.; Hruby, L.; Kriechling, P.; Nakamura, R.; Tori, R.; de Lourdes dos Santos Nunes, F.; Queiroz, M.; Fürnstahl, P.; Farshad, M. Augmented Reality in Orthopedic Surgery Is Emerging from Proof of Concept Towards Clinical Studies: A Literature Review Explaining the Technology and Current State of the Art. *Curr. Rev. Musculoskelet. Med.* **2021**, *14*, 192–203. [CrossRef]
43. Pratt, P.; Ives, M.; Lawton, G.; Simmons, J.; Radev, N.; Spyropoulou, L.; Amiras, D. Through the HoloLens™ looking glass: Augmented reality for extremity reconstruction surgery using 3D vascular models with perforating vessels. *Eur. Radiol. Exp.* **2018**, *2*, 2. [CrossRef]
44. Al Janabi, H.; Aydin, A.; Palaneer, S.; Macchione, N.; Al-Jabir, A.; Khan, M.; Dasgupta, P.; Ahmed, K. Effectiveness of the HoloLens mixed-reality headset in minimally invasive surgery: A simulation-based feasibility study. *Surg. Endosc.* **2019**, *34*, 1143–1149. [CrossRef]
45. Peh, S.; Chatterjea, A.; Pfarr, J.; Schäfer, J.; Weuster, M.; Klüter, T.; Seekamp, A.; Lippross, S. Accuracy of augmented reality surgical navigation for minimally invasive pedicle screw insertion in the thoracic and lumbar spine with a new tracking device. *Spine J.* **2020**, *20*, 629–637. [CrossRef]

46. Elmi-Terander, A.; Burström, G.; Nachabé, R.; Fagerlund, M.; Ståhl, F.; Charalampidis, A.; Edström, E.; Gerdhem, P. Augmented reality navigation with intraoperative 3D imaging vs fluoroscopy-assisted free-hand surgery for spine fixation surgery: A matched-control study comparing accuracy. *Sci. Rep.* **2020**, *10*, 707. [CrossRef]
47. Tanji, A.; Nagura, T.; Iwamoto, T.; Matsumura, N.; Nakamura, M.; Matsumoto, M.; Sato, K. Total elbow arthroplasty using an augmented reality–assisted surgical technique. *J. Shoulder Elb. Surg.* **2022**, *31*, 175–184. [CrossRef] [PubMed]
48. Pahl, G.; Beitz, W.; Feldhusen, J.; Grote, K. *Engineering Design*, 3rd ed.; Springer: London, UK, 2007.
49. Floriane, L.; Frédéric, S.; Gianluca, D.; Marc, L. Enriching design with X through tailored additive manufacturing knowledge: A methodological proposal. *Int. J. Interact. Des. Manuf.* **2016**, *11*, 279–288. [CrossRef]
50. Kranz, J.; Herzog, D.; Emmelmann, C. Design guidelines for laser additive manufacturing of lightweight structures in TiAl6V4. *J. Laser Appl.* **2015**, *27*, S14001. [CrossRef]
51. Diegel, O.; Nordin, A.; Motte, D. *A Practical Guide to Design for Additive Manufacturing*; Springer: London, UK, 2019.
52. British Design Council. Available online: https://www.designcouncil.org.uk/fileadmin/uploads/dc/Documents/ElevenLessons_Design_Council%2520%25282%2529.pdf (accessed on 8 December 2023).
53. Biomimicry Institute. Available online: https://toolbox.biomimicry.org/methods/ (accessed on 8 December 2023).
54. Enneking, W.; Dunham, W. Resection and reconstruction for primary neoplasms involving the innominate bone. *J. Bone Jt. Surg.* **1978**, *60*, 731–746. [CrossRef]
55. Fedorov, A.; Beichel, R.; Kalpathy-Cramer, J.; Finet, J.; Fillion-Robin, J.C.; Pujol, S.; Bauer, C.; Jennings, D.; Fennessy, F.; Sonka, M.; et al. 3D Slicer as an Image Computing Platform for the Quantitative Imaging Network. *Magn. Reson. Imaging* **2012**, *30*, 1323–1341. [CrossRef] [PubMed]
56. Cignoni, P.; Callieri, M.; Corsini, M.; Dellepiane, M.; Ganovelli, F.; Ranzuglia, G. MeshLab: An Open-Source Mesh Processing Tool. In Proceedings of the Sixth Eurographics Italian Chapter Conference, Salermo, Italy, 2–4 July 2008; pp. 129–136.
57. Sharma, A.K.; Cizmic, Z.; Dennis, D.A.; Kreuzer, S.W.; Miranda, M.A.; Vigdorchik, J.M. Low dislocation rates with the use of patient-specific "Safe zones" in total hip arthroplasty. *J. Orthop.* **2021**, *21*, 41–48. [CrossRef] [PubMed]
58. Wasielewski, R.; Cooperstein, L.; Kruger, M.; Rubash, H. Acetabular anatomy and the transacetabular fixation of screws in total hip arthroplasty. *J. Bone Jt. Surg.* **1990**, *72*, 501–508. [CrossRef]
59. Wu, C.; Deng, J.; Pan, J.; Li, T.; Tan, L.; Yuan, D. Anatomical conditions and patient-specific locked navigation templates for transverse sacroiliac screw placement: A retrospective study. *J. Orthop. Surg. Res.* **2020**, *15*, 260. [CrossRef]
60. Hasegawa, K.; Kabata, T.; Kajino, Y.; Inoue, D.; Tsuchiya, H. Periprosthetic Occult Fractures of the Acetabulum Occur Frequently During Primary THA. *Clin. Orthop. Relat. Res.* **2017**, *475*, 484–494. [CrossRef]
61. Hsu, T.; Chang, H.; Huang, L.; Zobitz, E.; Chen, P.; Lai, A.; An, N. The number of screws, bone quality, and friction coefficient affect acetabular cup stability. *Med. Eng. Phys.* **2007**, *29*, 1089–1095. [CrossRef]
62. Ravera, P.; Crespo, J.; Guarnieri, A.; Braidot, A. Stress in human pelvis throughout the gait cycle: Development, evaluation, and sensitivity studies of a finite element model. In Proceedings of the IFMBE Proceedings, Toronto, ON, Canada, 7–12 June 2015; pp. 246–249.
63. Ricci, P.L.; Maas, S.; Kelm, J.; Gerich, T. Finite element analysis of the pelvis including gait muscle forces: An investigation into the effect of Rami fractures on load transmission. *J. Exp. Orthop.* **2018**, *5*, 33. [CrossRef] [PubMed]
64. Bergmann, G.; Bender, A.; Dymke, J.; Duda, G.; Damm, P. Standardized loads acting in hip implants. *PLoS ONE* **2016**, *11*, e0155612. [CrossRef] [PubMed]
65. Bergmann, G.; Graichen, F.; Rohlmann, A. Hip joint contact forces during stumbling. *Langenbeck's Arch. Surg.* **2004**, *389*, 53–59. [CrossRef] [PubMed]
66. Tan, X.; Tan, Y.; Chow, C.; Tor, S.; Yeong, W. Metallic powder-bed based 3D printing of cellular scaffolds for orthopaedic implants: A state-of-the-art review on manufacturing, topological design, mechanical properties and biocompatibility. *Mater. Sci. Eng. C* **2017**, *76*, 1328–1343. [CrossRef] [PubMed]
67. Barba, D.; Alabort, E.; Reed, R. Synthetic bone: Design by additive manufacturing. *Acta Biomater.* **2019**, *97*, 637–656. [CrossRef] [PubMed]
68. Mueller, J.; Matlack, K.; Shea, K.; Daraio, C. Energy Absorption Properties of Periodic and Stochastic 3D Lattice Materials. *Adv. Theory Simul.* **2019**, *2*, 1900081. [CrossRef]
69. Benedetti, M.; Klarin, J.; Johansson, F.; Fontanari, V.; Luchin, V.; Zappini, G.; Molinari, A. Study of the Compression Behaviour of Ti6Al4V Trabecular Structures Produced by Additive Laser Manufacturing. *Materials* **2019**, *12*, 1471. [CrossRef]
70. Yang, E.; Leary, M.; Lozanovski, B.; Downing, D.; Mazur, M.; Sarker, A.; Khorasani, A.; Jones, A.; Maconachie, T.; Bateman, S.; et al. Effect of geometry on the mechanical properties of Ti-6Al-4V Gyroid structures fabricated via SLM: A numerical study. *Mater. Des.* **2019**, *184*, 108165. [CrossRef]
71. Aguado-Maestro, I.; De Frutos-Serna, M.; González-Nava, A.; Merino-De Santos, A.; García-Alonso, M. Are the common sterilization methods completely effective for our in-house 3D printed biomodels and surgical guides? *Injury* **2021**, *52*, 1341–1345. [CrossRef]
72. Bini, S.; Schilling, P.; Patel, S.; Kalore, N.; Ast, M.; Maratt, J.; Schuett, D.; Lawrie, C.; Chung, C.; Steele, G. Digital Orthopaedics: A Glimpse into the Future in the Midst of a Pandemic. *J. Arthroplast.* **2020**, *35*, 68–73. [CrossRef]
73. Vakharia, V.; Khan, S.; Marathe, K.; Giannis, T.; Webber, L.; Choi, D. Printing in a Pandemic: 3D printing solutions for healthcare during COVID-19. A Protocol for a PRISMA systematic review. *Ann. 3D Print. Med.* **2021**, *2*, 100015. [CrossRef]

74. Singh, S.N.; Venkatesh, V.S.; Deoghare, A.B. A review on the role of 3D printing in the fight against COVID-19: Safety and challenges. *Rapid Prototyp. J.* **2021**, *27*, 407–420. [CrossRef]
75. Dall'Ava, L.; Hothi, H.; Henckel, J.; Di Laura, A.; Tirabosco, R.; Eskelinen, A.; Skinner, J.; Hart, A. Osseointegration of retrieved 3D-printed, off-the-shelf acetabular implants. *Bone Jt. Res.* **2021**, *10*, 388–400. [CrossRef] [PubMed]
76. Geng, X.; Li, Y.; Li, F.; Wang, X.; Zhang, K.; Liu, Z.; Tian, H. A new 3D printing porous trabecular titanium metal acetabular cup for primary total hip arthroplasty: A minimum 2-year follow-up of 92 consecutive patients. *J. Orthop. Surg. Res.* **2020**, *15*, 383. [CrossRef] [PubMed]
77. Huang, Y.; Zhou, Y.; Tian, H.; Wang, J.; Liu, W.; Li, H. Minimum 7-year Follow-up of A Porous Coated Trabecular Titanium Cup Manufactured with Electron Beam Melting Technique in Primary Total Hip Arthroplasty. *Orthop. Surg.* **2021**, *13*, 817–824. [CrossRef]
78. Wang, J.; Min, L.; Lu, M.; Zhang, Y.; Wang, Y.; Luo, Y.; Zhou, Y.; Duan, H.; Tu, C. What are the Complications of Three-dimensionally Printed, Custom-made, Integrative Hemipelvic Endoprostheses in Patients with Primary Malignancies Involving the Acetabulum, and What is the Function of These Patients? *Clin. Orthop. Relat. Res.* **2020**, *478*, 2487–2501. [CrossRef]
79. Han, Q.; Zhang, K.; Zhang, Y.; Wang, C.; Yang, K.; Zou, Y.; Chen, B.; Wang, J. Individual resection and reconstruction of pelvic tumor with three-dimensional printed customized hemi-pelvic prosthesis. *Medicine* **2019**, *98*, e16658. [CrossRef]
80. Durand-Hill, M.; Henckel, J.; Di Laura, A.; Hart, A. Can custom 3D printed implants successfully reconstruct massive acetabular defects? A 3D-CT assessment. *J. Orthop. Res.* **2020**, *38*, 2640–2648. [CrossRef]
81. Cao, J.; Zhu, H.; Gao, C. A Systematic Review and Meta-Analysis of 3D Printing Technology for the Treatment of Acetabular Fractures. *BioMed Res. Int.* **2021**, *2021*, 5018791. [CrossRef]
82. Hu, X.; Chen, Y.; Cai, W.; Cheng, M.; Yan, W.; Huang, W. Computer-Aided Design and 3D Printing of Hemipelvic Endoprosthesis for Personalized Limb-Salvage Reconstruction after Periacetabular Tumor Resection. *Bioengineering* **2022**, *18*, 400. [CrossRef]
83. Xu, S.; Guo, Z.; Shen, Q.; Peng, Y.; Li, J.; Li, S.; He, P.; Jiang, Z.; Que, Y.; Cao, K.; et al. Reconstruction of Tumor-Induced Pelvic Defects with Customized, Three-Dimensional Printed Prostheses. *Front. Oncol.* **2022**, *12*, 935059. [CrossRef] [PubMed]
84. Khal, A.A.; Apostu, D.; Schiau, C.; Bejinariu, N.; Pesenti, S.; Jouve, J.L. Custom-Made 3D-Printed Prosthesis after Resection of a Voluminous Giant Cell Tumour Recurrence in Pelvis. *Diagnostics* **2023**, *13*, 485. [CrossRef] [PubMed]
85. Vaneker, T.; Bernard, A.; Moroni, G.; Gibson, I.; Zhang, Y. Design for Additive Manufacturing: Framework and methodology. *CIRP Ann. Manuf. Technol.* **2020**, *69*, 578–599. [CrossRef]
86. Davoodi, E.; Montazerian, H.; Mirhakimi, A.; Zhianmanesh, M.; Ibhadode, O.; Shahabad, S.; Esmaeilizadeh, R.; Sarikhani, E.; Toorandaz, S.; Sarabi, S.A.; et al. Additively manufactured metallic biomaterials. *Bioact. Mater.* **2022**, *15*, 214–249. [CrossRef] [PubMed]
87. Maconachie, T.; Leary, M.; Lozanovski, B.; Zhang, X.; Qian, M.; Faruque, O.; Brandt, M. SLM lattice structures: Properties, performance, applications and challenges. *Mater. Des.* **2019**, *183*, 108137. [CrossRef]
88. Chen, L.; Liang, S.; Liu, Y.; Zhang, L. Additive manufacturing of metallic lattice structures: Unconstrained design, accurate fabrication, fascinated performances, and challenges. *Mater. Sci. Eng. Rep.* **2021**, *146*, 100648. [CrossRef]
89. Khrapov, D.; Paveleva, A.; Kozadayeva, M.; Evsevleev, S.; Mishurova, T.; Bruno, G.; Surmenev, R.; Koptyug, A.; Surmeneva, M. Trapped powder removal from sheet-based porous structures based on triply periodic minimal surfaces fabricated by electron beam powder bed fusion. *Mater. Sci. Eng. A* **2023**, *862*, 144479. [CrossRef]
90. Jin, Z.; Zhang, Z.; Demir, K.; Gu, G. Machine Learning for Advanced Additive Manufacturing. *Matter* **2020**, *3*, 1541–1556. [CrossRef]
91. Park, J.; Kwon, H.; Lee, W.; Yang, I.; Park, K. Anthropometric Measurement About the Safe Zone for Transacetabular Screw Placement in Total Hip Arthroplasty in Asian Middle-Aged Women: In Vivo Three-Dimensional Model Analysis. *J. Arthroplast.* **2021**, *36*, 744–751. [CrossRef]
92. Yu, Z.; Zhang, W.; Fang, X.; Tu, C.; Duan, H. Pelvic Reconstruction with a Novel Three-Dimensional-Printed, Multimodality Imaging Based Endoprosthesis Following Enneking Type I + IV Resection. *Front. Oncol.* **2021**, *11*, 629582. [CrossRef]
93. Helgason, B.; Perilli, E.; Schileo, E.; Taddei, F.; Brynjólfsson, S.; Viceconti, M. Mathematical relationships between bone density and mechanical properties: A literature review. *Clin. Biomech.* **2008**, *23*, 135–146. [CrossRef] [PubMed]
94. Vivanco, F.; Burgers, A.; García-Rodríguez, S.; Crookshank, M.; Kunz, M.; MacIntyre, J.; Harrison, M.; Bryant, T.; Sellens, W.; Ploeg, L. Estimating the density of femoral head trabecular bone from hip fracture patients using computed tomography scan data. *Proc. Inst. Mech. Eng. Part H J. Med. Eng.* **2014**, *228*, 616–626. [CrossRef] [PubMed]

Disclaimer/Publisher's Note: The statements, opinions and data contained in all publications are solely those of the individual author(s) and contributor(s) and not of MDPI and/or the editor(s). MDPI and/or the editor(s) disclaim responsibility for any injury to people or property resulting from any ideas, methods, instructions or products referred to in the content.

European Journal of Orthopaedic Surgery & Traumatology
https://doi.org/10.1007/s00590-024-03839-4

ORIGINAL ARTICLE

3D-printed glenoid implant reconstruction, after partial scapulectomy for malignant tumors: a case series

Ioannis G. Trikoupis[1] · Ioannis I. Mavrodontis[1] · Dimitrios V. Papadopoulos[2] · Stavros D. Goumenos[1] · Dimitrios A. Georgoulis[1] · Panagiotis Gavriil[1] · Dimitra Melissaridou[1] · Olga D. Savvidou[1] · Vasileios A. Kontogeorgakos[1] · Panayiotis J. Papagelopoulos[1]

Received: 28 October 2023 / Accepted: 18 January 2024
© The Author(s) 2024

Abstract

Purpose Glenoid tumors are extremely rare, and reconstruction remains very challenging. The aim of this study is to present the clinical and functional outcomes, of a new glenoid reconstruction method using 3-dimensional-printed implant.

Methods Four patients with primary glenoid tumors underwent reconstruction using 3-dimensional-printed glenoid implant linked with reverse shoulder arthroplasty. We retrospectively reviewed the clinical and functional outcome, using MSTS and DASH score, as well as complications' rate.

Results Wide excision was achieved in all patients. No local recurrence or distant metastasis was diagnosed at the follow-up period. The mean MSTS score was 80.5%, and DASH score was 15.2%. According to Hendersons' classification, there were no postoperative complications.

Conclusion The use of 3-dimensional-printed implants, can be a very reliable solution with satisfying clinical and functional outcomes for reconstruction, in patients with musculoskeletal malignancies of the glenoid.

Level of evidence IV Treatment Study.

Keywords 3D-printed implants · Partial scapulectomy · Glenoid tumor

Introduction

Although shoulder girdle area is the third most common anatomic location for musculoskeletal malignancies, scapular bone and soft tissue tumors are extremely rare [1]. The most common histopathological type of scapular malignancies

Ioannis G. Trikoupis and Ioannis I. Mavrodontis have contributed equally to this work.

✉ Panayiotis J. Papagelopoulos
pjporthopedic@gmail.com

Ioannis G. Trikoupis
giannistrikoupis@gmail.com

Ioannis I. Mavrodontis
i.i.mavrodontis@gmail.com

Dimitrios V. Papadopoulos
di_papadopoulos@yahoo.gr

Stavros D. Goumenos
stgoumenos@gmail.com

Dimitrios A. Georgoulis
jim.georgoulis@gmail.com

Panagiotis Gavriil
gavriilpan@gmail.com

Dimitra Melissaridou
dimitramelissaridi@gmail.com

Olga D. Savvidou
olgasavvidou@gmail.com

Vasileios A. Kontogeorgakos
vaskonto@gmail.com

[1] First Department of Orthopedic Surgery and Traumatology, National and Kapodistrian University of Athens, School of Medicine, "ATTIKON" University General Hospital, Rimini 1, Chaidari, 12462 Athens, Greece

[2] Second Department of Orthopedics, National and Kapodistrian University of Athens, 'Agia Olga' Hospital, Th. Konstantopoulou 3-5, Nea Ionia, 14233 Athens, Greece

Published online: 27 January 2024

include chondrosarcoma in adults, followed by Ewing sarcoma in children and young adolescents [2–5].

The development of endoprosthetic implants for the reconstruction of the resected bone tumors offered a reliable alternative to interscapular-thoracic resection (Tikhoff–Linberg operation) following total scapulectomy, providing better functional outcomes of these patients [6]. Recent advances in prostheses design offered an individualized strategy for every patient, thus nowadays endoprosthetic reconstruction is considered the gold standard for the surgical management of scapular tumors [1, 4, 7, 8].

However, surgical treatment of glenoid tumors remains controversial. Although partial scapulectomy and reconstruction using allografts or allograft-prosthetic composites is the mainstay for the management of glenoid tumors, the clinical results are suboptimal [5, 7, 9, 10]. Alone soft tissue reconstruction is another option for certain patients with preservation of the glenoid [11, 12]. 3D-printed implants have been widely used in orthopedic oncology over the past decade [13]. These implants are designed to reconstruct complex bone deficits in areas, such as the talus or calcaneus, the forearm, and the pelvic ring bones. Although larger studied are needed, the functional outcomes of these implants are promising [13–18].

The purpose of this study is to evaluate the short-term clinical and functional outcomes of enbloc resection and reconstruction using 3D-printed implant for the management of localized primary glenoid tumors.

Patients and methods

A retrospective observational study of prospectively collected data was performed between 2018 and 2021, including patients who underwent partial scapulectomy and reconstruction using 3D-printed implant for the treatment of localized glenoid tumors. All patients had extensive glenoid resection, including the glenoid fossa and the neck of the scapula. The study received approval by the Institutional Board Review, while an informed consent was obtained from all patients. The minimum follow-up period is 12 months.

All patients underwent preoperative CT-guided needle biopsy and histopathological confirmation of the lesion. Imaging evaluation included CT and MRI of the shoulder for tumor staging, and the treatment strategy was discussed and planned in accordance with the multidisciplinary tumor board of the hospital. Four patients were diagnosed with chondrosarcoma. In one patient with chondrosarcoma, the tumor was a local recurrence following curettage and cementation, and the recurrence occurred two years postoperatively. For the preoperative planning, high-resolution CT scan and MRI were performed [19] (Figs. 1, 2). According to the Malawer surgical classification system for shoulder girdle resections, one patient underwent extraarticular Type V resection and the remaining 3, intraarticular Type III partial scapulectomy [20]. The MUTARS® (Implantcast GmbH, Buxtehude, Germany) glenoid prosthesis and a reverse shoulder prosthesis were used for the reconstruction of glenoid and proximal humerus (Figs. 3, 4). In two patients, due to the extensive involvement of soft tissue, constrained liners

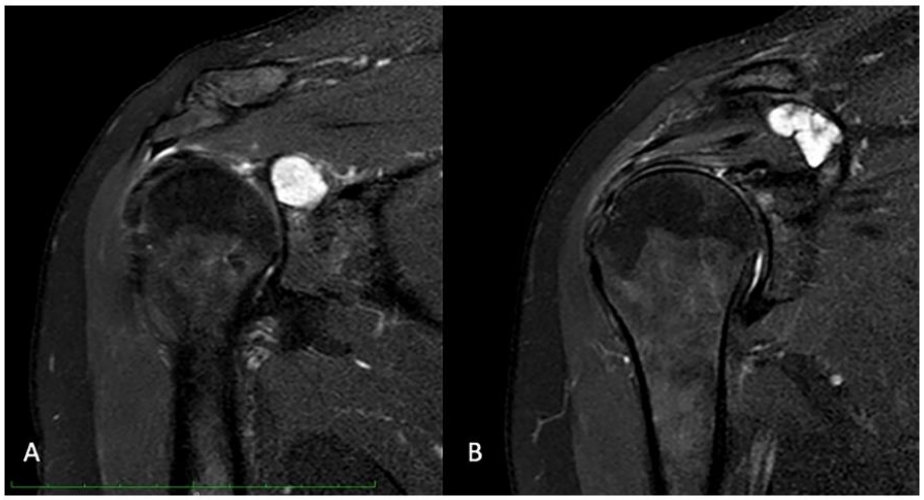

Fig. 1 Preoperative T2 signal MRI of 56-year-old patient with a recurrent Grade 2 Chondrosarcoma of glenoid (**A**) and coracoid process (**B**)

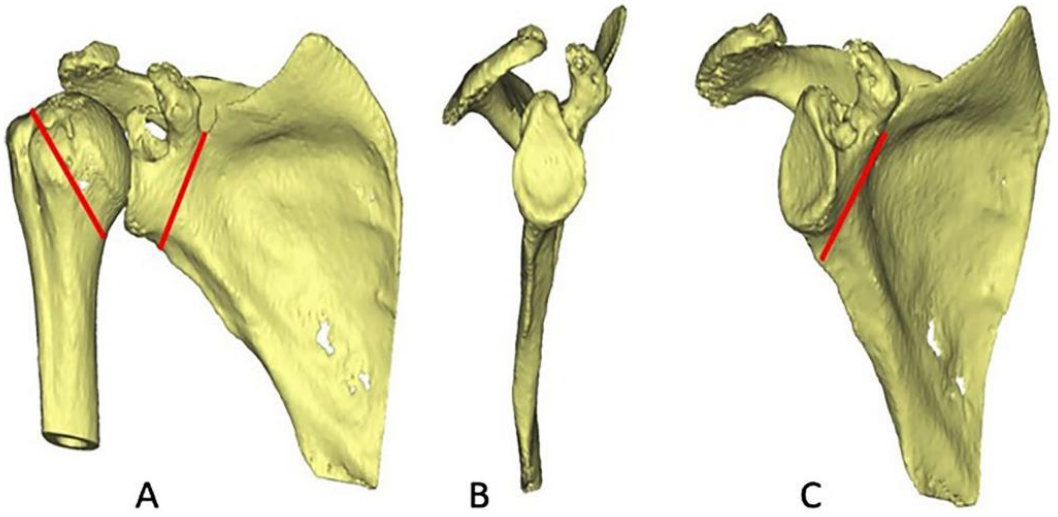

Fig. 2 3D-reconstruction of the preoperative CT-scan of the right shoulder. Osteotomy planning in anterior (**A**), coronal (**B**) and posterior view (**C**) of the scapula

Fig. 3 Final implant design. Modular fixation plate (**A**). Posterior (**B**) and anterior (**C**) view of the implant after plate assembling. Proximal humerus implants, humeral stem (**D**) and inverse cup (**E**)

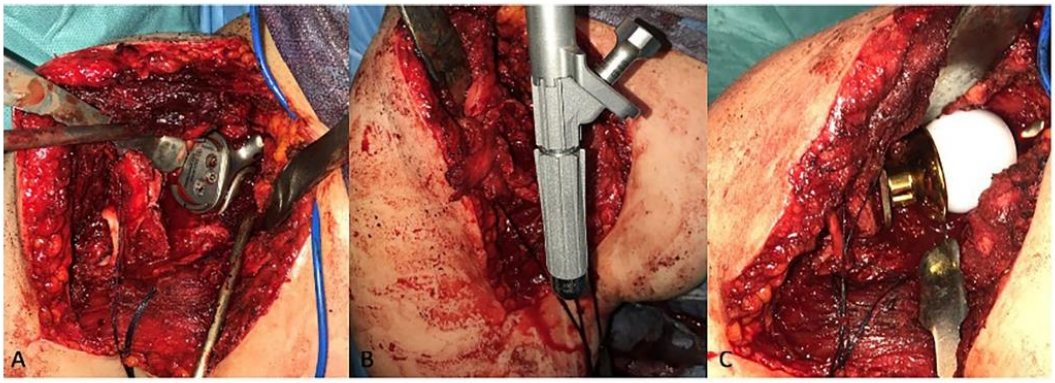

Fig. 4 Custom made glenoid implant in place after tumor resection (**A**), proximal humerus stem insertion in the humeral canal (**B**) and the final reduction of the humerus to the glenosphere (**C**)

were used, to increase the stability of the shoulder and to reduce the possibility of subluxation.

All patients underwent postoperative imaging including plain radiographs and MRI scan to evaluate implant fixation and local recurrence (Fig. 5). Clinical examination was performed to evaluate the postoperative shoulder range of motion (ROM) and the overall functional outcomes. The functional outcomes were assessed through the MSTS (Musculoskeletal Tumor Society Score) and DASH (Disabilities of the Arm Shoulder and Hand) scores [21, 22]. Moreover, patients were asked for their level of satisfaction (very satisfied, satisfied, moderate and poorly satisfied) [23]. Last, the presence of any complications based on the Henderson's classification system [24] was documented.

Overall, 4 patients were included in this study. There were 2 male patients and 2 females, while the mean age at the time of surgery was 56 (range 48–62) years. Wide resection with negative surgical margins was achieved in all patients according to the pathological examination of the surgical specimens, while the deltoid muscle along with the axillary nerve were preserved in all cases. The mean duration of surgery was 152.5 (range 110–200 min) minutes. The median follow-up period was 22 months (range 12–28 months).

Results

There were no local recurrences or distant metastases during the follow-up period in any of the included patients. Moreover, there were no postoperative complications based on the Henderson's Classification System, and no patient required reoperation.

Fig. 5 Plain radiograph of the right shoulder 28 months postoperatively

In terms of the functional outcome, the median MSTS score was 80.5% (range 65–94%) and the median DASH score was 15.2% (range 7.5–32.5%). Regarding the postoperative ROM at the latest follow-up, the median active

Table 1 Patients characteristics and functional outcome

Patient	Age	Surgery Time	MSTS	DASH	Abduction	Flexion	Liner
1	48	120	65	32.5	30	25	Constrained
2	56	110	94	7.5	120	110	Conventional
3	58	180	75	11.7	65	45	Constrained
4	62	200	88	9.2	100	100	Conventional

shoulder abduction was 78.75° (range 30–120), and the median active forward flexion was 70° (range 25–110). Three patients were very satisfied with the functional outcome of the procedure, while one was moderately satisfied (Table 1).

Discussion

Custom made 3D-printed prostheses have been recently introduced in tumor surgery and offer a patient's specific alternative reconstructive option. These implants are used to reconstruct complex bone defects following wide excision of musculoskeletal malignancies [25–27]. In our study, customized glenoid endoprosthesis combined with reverse shoulder arthroplasty were used to reconstruct the shoulder girdle and to restore the normal functional of the upper limb after extraarticular Malawer V type resections. The complication rate in our study was low during the short-term follow up, while the range of motion and the functional scores were significantly improved.

Studies regarding glenoid tumors are very limited. Capanna et al. retrospectively reviewed 12 patients who underwent transglenoid resection and reconstruction using prostheses. Although the authors of this study reported that the functional outcomes for this method were better compared to the traditional Tikhoff–Linberg procedure, the overall functional outcome was characterized as fair by most patients, while 25% of the patients underwent hardware removal due to infection [28]. Mnaymneh et al. reported good functional outcomes and a low complication rate using allograft reconstruction after resection of scapula sarcomas. However, in all 6 patients of this study, the rotator cuff muscles were preserved [10]. Similar outcomes were also reported by Zhang et at in 7 patients who underwent reconstruction with allograft [5]. In another study reported by Tsuda evaluated 21 patients who underwent Type V scapular resection followed by reconstruction with proximal humerus endoprosthesis and capture of the prosthesis head to the remaining scapula with either trevira tubes (Implantcast, Germany) or a Mersilene mesh (Ethicon) [29]. The postoperative functional outcomes were poor, while patients were not able to actively elevate their limb. Glenoid tumors are, and although wide excision of these localized lesions can be readily achieved, reconstruction of the residual bone defects is still very challenging [3]. Traditionally, resection of glenoid tumors is associated with poor functional outcomes [5]. The commonly used reconstructive methods include allografts and APCs with comparable results with regard to the functional outcomes and the complications rate. Although these reconstructive methods can result in an acceptable restoration of the upper limb function, they have been associated with a high complication rate (periprosthetic fractures, collapse and non-unions) [2, 3, 10]. Unfortunately, due to the rarity of these tumors, there are no high-quality studies to evaluate whether one reconstructive method is associated with better results compared to another one.

This study has also limitations. This is a retrospective study including a small number of patients with a short-term follow-up. However, due to the rarity of this tumors, there are only few studies evaluating these tumors with similar populations, while our study describes a novel reconstruction method, using 3D-printed implants that seems to offer better functional results.

3D printed, custom made glenoid prosthesis in combination to reverse shoulder arthroplasty can be used in extra-articular, Type V and intraarticular Type III partial scapulectomy excisions of shoulder girdle, with promising outcome. However, studies with larger number of patients and longer follow-up are needed, to establish the results of our study.

Funding Open access funding provided by HEAL-Link Greece. The authors did not receive support from any organization for the submitted work.

Declarations

Conflict of interest The author(s) declare that they have no competing interests.

Ethical approval Institutional Review Board (IRB) Number: EBΔ731/27-11-2019, 'Attikon' University General Hospital, Athens, Greece.

Open Access This article is licensed under a Creative Commons Attribution 4.0 International License, which permits use, sharing, adaptation, distribution and reproduction in any medium or format, as long as you give appropriate credit to the original author(s) and the source, provide a link to the Creative Commons licence, and indicate if changes were made. The images or other third party material in this article are included in the article's Creative Commons licence, unless indicated otherwise in a credit line to the material. If material is not included in the article's Creative Commons licence and your intended use is not

permitted by statutory regulation or exceeds the permitted use, you will need to obtain permission directly from the copyright holder. To view a copy of this licence, visit http://creativecommons.org/licenses/by/4.0/.

References

1. Puchner SE, Panotopoulos J, Puchner R et al (2014) Primary malignant tumours of the scapula—a review of 29 cases. Int Orthop (SICOT) 38:2155–2162. https://doi.org/10.1007/s00264-014-2417-8
2. Mayil Vahanan N, Mohanlal P, Bose JC et al (2007) The functional and oncological results after scapulectomy for scapular tumours: 2–16-year results. Int Orthop (SICO) 31:831–836. https://doi.org/10.1007/s00264-006-0261-1
3. O'connor MI, Sim FH, Chao EYS (1996) Limb salvage for neoplasms of the shoulder girdle. Intermediate reconstructive and functional results*. J Bone Jt Surg 78:1872–88. https://doi.org/10.2106/00004623-199612000-00011
4. Wittig JC, Bickels J, Wodajo F et al (2002) Constrained total scapula reconstruction after resection of a high-grade sarcoma. Clin Orthop Relat Res 397:143–155. https://doi.org/10.1097/00003086-200204000-00020
5. Zhang K, Duan H, Xiang Z, Tu C (2009) Surgical technique and clinical results for scapular allograft reconstruction following resection of scapular tumors. J Exp Clin Cancer Res 28:45. https://doi.org/10.1186/1756-9966-28-45
6. Wang B, Wu Q, Zhang Z et al (2018) Reconstruction with constrained scapular prosthesis after total scapulectomy for scapular malignant tumor. J Surg Oncol 118:177–183. https://doi.org/10.1002/jso.25118
7. Biazzo A, De Paolis M, Donati DM (2018) Scapular reconstructions after resection for bone tumors: a single-institution experience and review of the literature. Acta Bio Med Atenei Parm 89:415–422. https://doi.org/10.23750/abm.v89i3.5655
8. Mavrogenis AF, Papagelopoulos PJ (2012) Expandable prostheses for the leg in children. Orthopedics 35:173–175. https://doi.org/10.3928/01477447-20120222-03
9. Gibbons CLMH, Bell RS, Wunder JS et al (1998) Function after subtotal scapulectomy for neoplasm of bone and soft tissue. J Bone Jt Surg Br 80-B:38–42. https://doi.org/10.1302/0301-620X.80B1.0800038
10. Mnaymneh WA, Temple HT, Malinin TI (2002) Allograft reconstruction after resection of malignant tumors of the scapula. Clin Orthop Relat Res 405:223–229. https://doi.org/10.1097/00003086-200212000-00029
11. Houdek MT, Wilke BK, Barlow JD (2023) Management of scapular tumors. Orthop Clin N Am 54:101–108. https://doi.org/10.1016/j.ocl.2022.08.009
12. Xu S, Yu X, Xu M et al (2016) Functional results and emotional acceptance after scapulectomy for malignant shoulder tumors. Orthop Surg 8:186–195. https://doi.org/10.1111/os.12248
13. Fan H, Fu J, Li X et al (2015) Implantation of customized 3-D printed titanium prosthesis in limb salvage surgery: a case series and review of the literature. World J Surg Onc 13:308. https://doi.org/10.1186/s12957-015-0723-2
14. De Paolis M, Sambri A, Zucchini R et al (2022) Custom-made 3D-printed prosthesis in periacetabular resections through a novel ileo-adductor approach. Orthopedics. https://doi.org/10.3928/01477447-20211227-01
15. Wang J, Min L, Lu M et al (2020) What are the complications of three-dimensionally printed, custom-made, integrative hemipelvic endoprostheses in patients with primary malignancies involving the acetabulum, and what is the function of these patients? Clin Orthop Relat Res 478:2487–2501. https://doi.org/10.1097/CORR.0000000000001297
16. Papagelopoulos PJ, Sarlikiotis T, Vottis CT et al (2019) Total talectomy and reconstruction using a 3-dimensional printed talus prosthesis for Ewing's sarcoma: a 3.5-year follow-up. Orthopedics. https://doi.org/10.3928/01477447-20190523-05
17. Papagelopoulos PJ, Megaloikonomos PD, Korkolopoulou P et al (2019) Total calcaneus resection and reconstruction using a 3-dimensional printed implant. Orthopedics. https://doi.org/10.3928/01477447-20190125-07
18. Savvidou OD, Gavriil P, Trikoupis I et al (2022) Three-dimensional Printed endoprosthesis for reconstruction of the distal tibia and ankle joint after tumor resection. Orthopedics. https://doi.org/10.3928/01477447-20220706-07
19. Dalrymple NC, Prasad SR, Freckleton MW, Chintapalli KN (2005) Introduction to the language of three-dimensional imaging with multidetector CT. Radiographics 25:1409–1428. https://doi.org/10.1148/rg.255055044
20. Malawer MM (1991) Tumors of the shoulder girdle. Technique of resection and description of a surgical classification. Orthop Clin N Am 22:7–35
21. Enneking WF, Dunham W, Gebhardt MC et al (1993) A system for the functional evaluation of reconstructive procedures after surgical treatment of tumors of the musculoskeletal system. Clin Orthop Relat Res 286:241–246
22. Hudak PL, Amadio PC, Bombardier C et al (1996) Development of an upper extremity outcome measure: the DASH (disabilities of the arm, shoulder, and head). Am J Ind Med 29:602–608. https://doi.org/10.1002/(SICI)1097-0274(199606)29:6%3c602::AID-AJIM4%3e3.0.CO;2-L
23. Solomon DH, Bates DW, Horsky J et al (1999) Development and validation of a patient satisfaction scale for musculoskeletal care. Arthritis Care Res 12:96–100. https://doi.org/10.1002/1529-0131(199904)12:2%3c96::aid-art4%3e3.0.co;2-p
24. Henderson ER, O'Connor MI, Ruggieri P et al (2014) Classification of failure of limb salvage after reconstructive surgery for bone tumours: a modified system Including biological and expandable reconstructions. Bone Jt J 96-B:1436–1440. https://doi.org/10.1302/0301-620X.96B11.34747
25. Thadani VN, Riaz MJ, Singh G (2018) The evolution of three-dimensional technology in musculoskeletal oncology. J Clin Orthop Trauma 9:269–274. https://doi.org/10.1016/j.jcot.2018.07.020
26. Dong C, Beglinger I, Krieg AH (2022) Personalized 3D-printed guide in malignant bone tumor resection and following reconstruction: 17 cases in pelvic and extremities. Surg Oncol 42:101733. https://doi.org/10.1016/j.suronc.2022.101733
27. Schulze M, Gosheger G, Bockholt S et al (2021) Complex bone tumors of the trunk—the role of 3D printing and navigation in tumor orthopedics: a case series and review of the literature. JPM 11:517. https://doi.org/10.3390/jpm11060517
28. Capanna R, van Horn JR, Biagini R et al (1990) The Tikhoff-Linberg procedure for bone tumors of the proximal humerus: the classical "extensive" technique versus a modified "transglenoid" resection. Arch Orthop Trauma Surg 109:63–67. https://doi.org/10.1007/BF00439380
29. Tsuda Y, Fujiwara T, Evans S et al (2020) Extra-articular resection of shoulder joint for bone sarcomas: oncologic and limb-salvage outcomes of 32 cases compared with shoulder disarticulation and forequarter amputation. J Surg Oncol 121:612–619. https://doi.org/10.1002/jso.25838

Publisher's Note Springer Nature remains neutral with regard to jurisdictional claims in published maps and institutional affiliations.

11. Appendices

11.1 Appendix A: Timeline of Technology Advancements

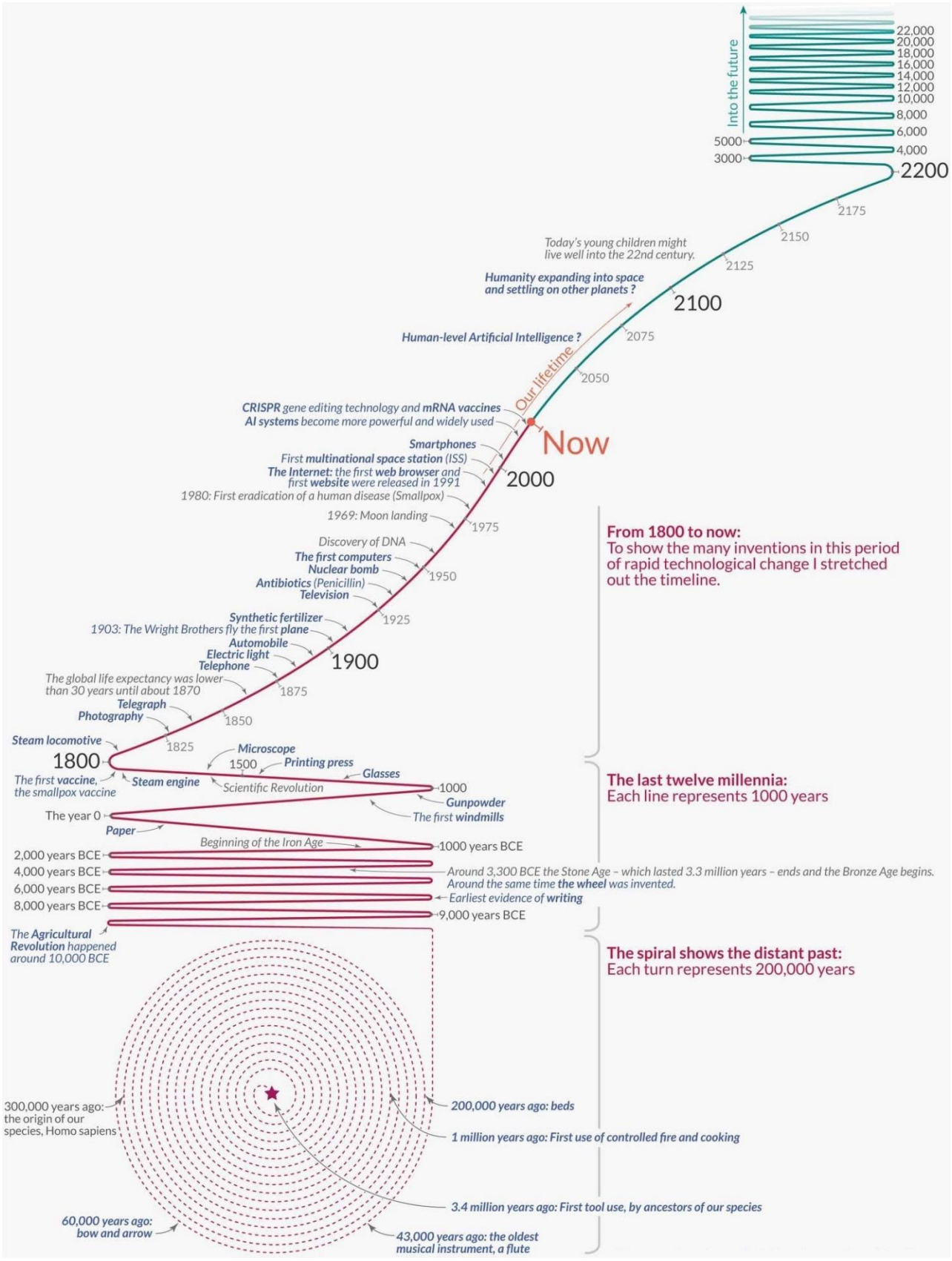

A long-term timeline of technology. Source: OurWorldinData.org

11.2 Appendix B: Modern Devices and Tools in Orthopaedics

Flat Head Syndrome Helmet

Source: Technology in Motion

Cervical Orthosis

Source: EOS Gmbh

Hand Casts & Splint

Source: Exiom

Source: Shapeways

Source: HP

Knee Brace

Source: Intamsys

Source: Crispin

Ankle Foot & Upper Body Braces

Source: Andiamo

Source: Onyq

Shoe Soles

Source: Under Armour

Source: Adidas

Foot Orthoses

Source: SuperFeet

3D printed custom orthotic products

Bespoke Running Prosthetic Leg

Source: Ottobock

Bespoke 3D Printed Prosthetic Foot

Source: EOS Gmbh

Smart Bionic Prosthetic Legs

Source: Biomechatronics Group @ MIT Media Lab

Bespoke 3D Printed Bionic Prosthetic

Source: Open Bionics

Smart Bionic Lower Body Exoskeleton

Source: Cyberdyne

Bionic Prosthetic Hand

Source: Ottobock

Smart Bionic Modular Prosthetic Limbs

Source: Applied Physics Lab @ Johns Hopkins University

Custom and standard prosthetic products

Arthroplasty and Tumour Prostheses

Source: Implantcast

Expandable Prostheses

Source: Implantcast

Modular Universal Tumor and Revision System (MUTARS)

Femoral components

Tibial components

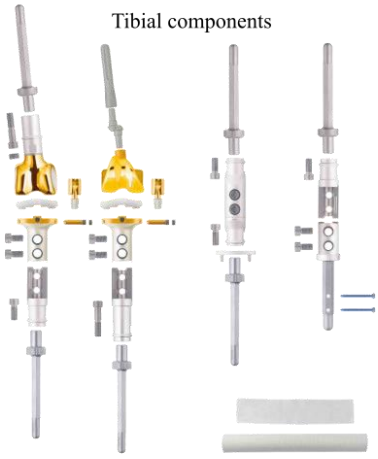

Humeral components

Revision components

Source: Implantcast

Expandable and fixed arthoplasty and tumor endo-prostheses

Model & Atlantoaxial Implant & PSI

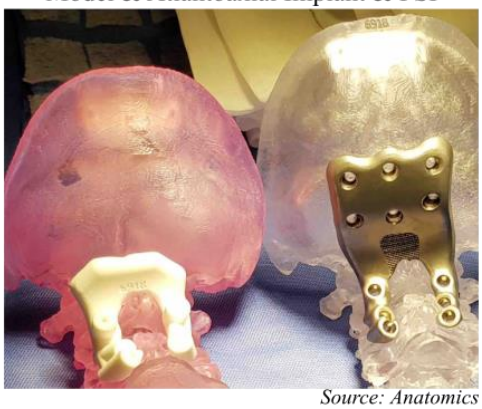

Source: Anatomics

Shoulder Tumour Prosthesis

Source: Implantcast

Radius & Ulna Prostheses

Source: (Park et al., 2020)

Sternal Prosthesis & PSI

Sternal Prosthesis

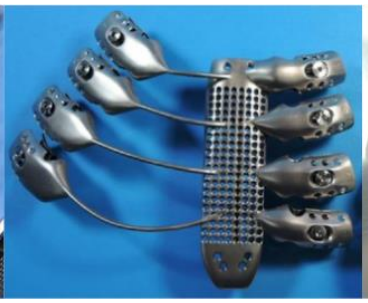

Sternal Prosthesis & Model

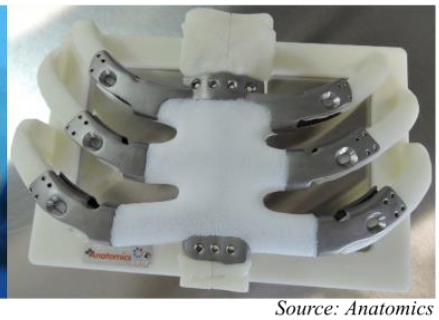

Source: Anatomics

Pelvic Prosthesis & Model

Source: Anatomics

Pelvic Prosthesis

Source: (Zeng and Nolte, 2015)

Acetabular Prosthesis

Source: Stryker

Pelvic Prosthesis & Model

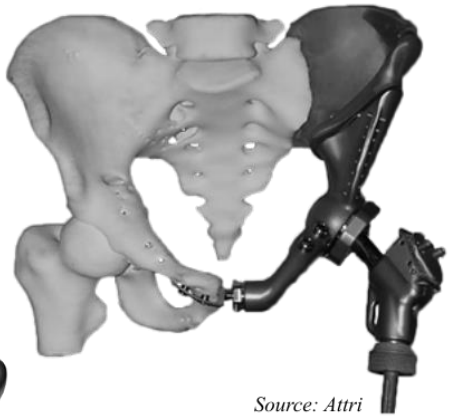

Source: Attri

Pelvic Prostheses & Models

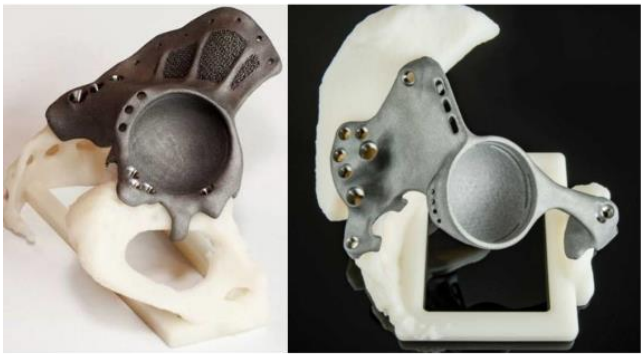

Source: Ossis

Acetabular Prosthesis & Model

Source: EOS Gmbh

3D printed patient-specific instruments, prostheses and models

Anatomical Model & PSI & Custom Plates

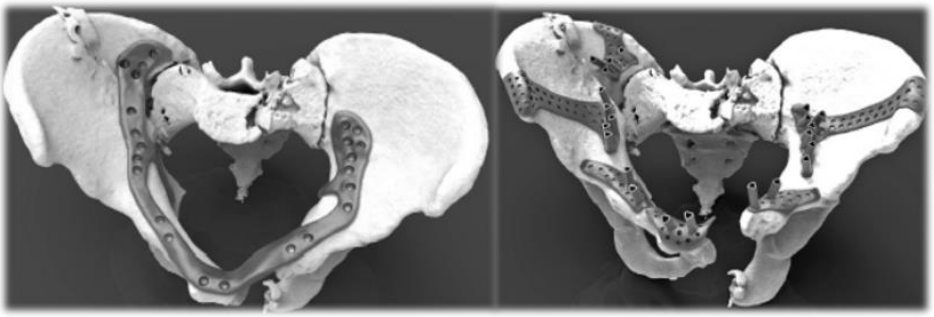

Source:

Acetabular Prosthesis & PSI

Source: Implantcast

Spine PSI Kit

Source: Anatomics

Multi-color Multi-material Anatomical Models

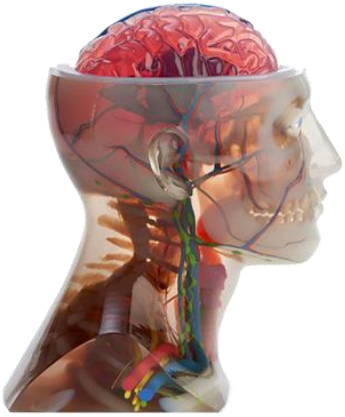

Source: Stratasys

Metacarpal Prosthesis & Model

Source: Anatomics

3D Printed Mold for PMMA

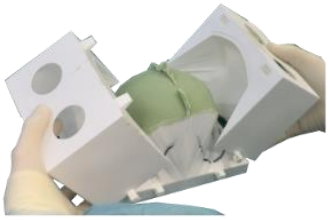

Source: 3D-Side

Knee PSI

Source: Medacta

Anatomical Model

Source: Formlabs

Anatomical Model for Plates Preparation

Source: St. Antonius Hospital @ Utrecht

Partial Femoral Prosthesis

Source: Virginia Cancer Specialists

Tibial Prosthesis

Source: DukeHealth

Talar Prosthesis

Source: PJ Papagelopoulos

Calcaneal Prosthesis

Source: Anatomics

3D printed patient-specific instruments, endo-prostheses and models

Occipito-Cervico-Thoracic Spinal System

Source: Zimmer Biomet

Spinal Fusion Cages

Source: Medtronic

Expandable Corpectomy

Source: Stryker

Bone Screws

Source: Stryker

Bone Plates

Source: DePuy Synthes

Source: Stryker

External Fixator Frame

Source: Stryker

Bone Nailing Systems

Source: Stryker

External Fixator Frame

Source: DePuy Synthes

Standard osteosynthesis products

Power Tools

Source: Stryker

Consumables

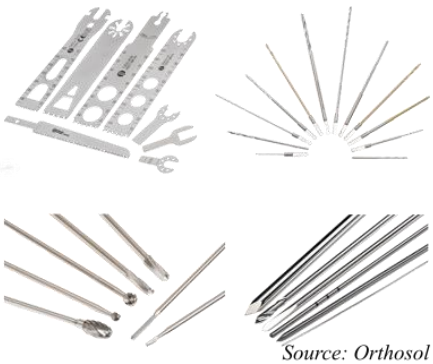

Source: Orthosol

Bone Fixation Instruments

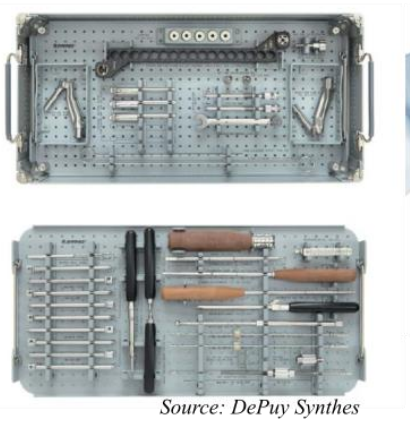

Source: DePuy Synthes

Source: DePuy Synthes

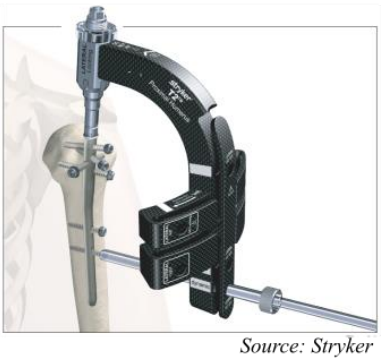

Source: Stryker

Arthroplasty Instruments

Robotic Surgery

Source: Intuitive Surgical

Source: Stryker

Surgery Navigation

Source: Stryker

Surgical tools used in orthopaedics

CT Scanner

Source: Siemens

MRI Scanner

Source: Siemens

PET/CT Full Body Scanner

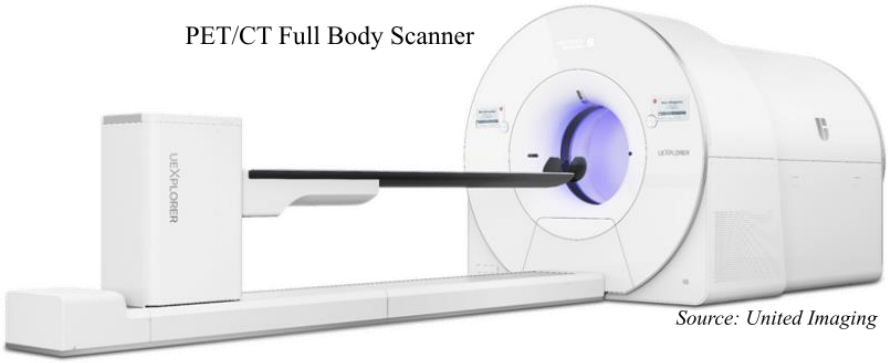

Source: United Imaging

Image-guided
Surgery Navigation

Source: 7D Surgical

Real-time 3D Fluoroscopy

Source: Medtronic

Real-time 3D CT-Scanner

Source: Samsung

Hand-held 3D Laser Scanners

Source: Artec

Source: 3D Systems

Anatomy imaging equipment used in orthopaedics

Scan Data 3D Viewer & Processing for Anatomical Model Generation

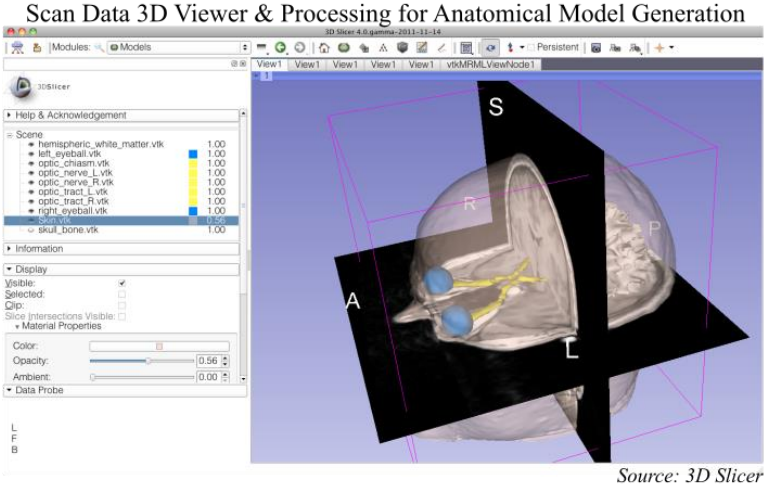

Source: 3D Slicer

Custom Implants & Prostheses Design
Digital Surgery Simulation

Source: 3D Systems

PSI Design

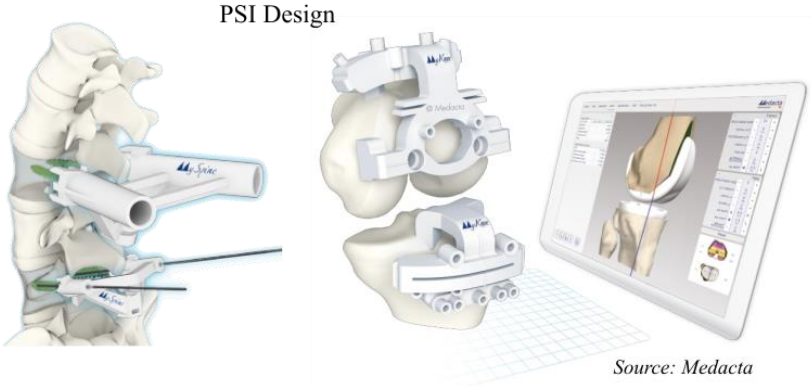

Source: Medacta

Prosthesis Optimisation

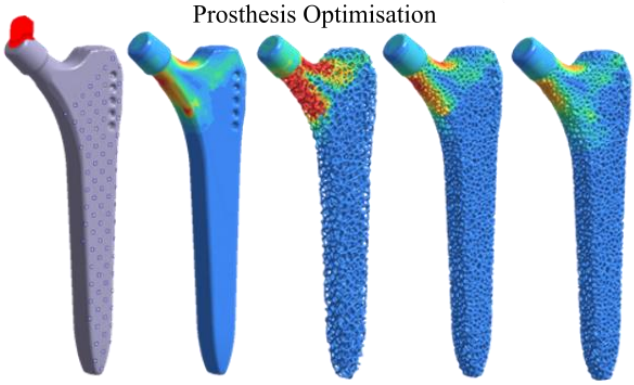

Source: nTop

Augmented/Mixed Reality Goggles

Source: Microsoft

Source: Augmedics

Intraoperative Augmented Assistance

Source: Augmedics

Virtual Reality Set

Source: Oculus

Physical Surgery Simulation

Source: 3D Systems

Haptic Device

Source: 3D Systems

Computer software, virtual and haptic devices used in orthopaedics

11.3 Appendix C: World Demographic Figures

World

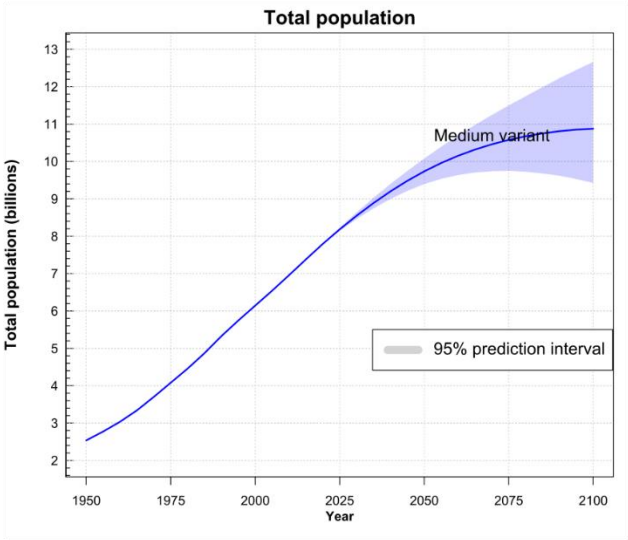

Europe

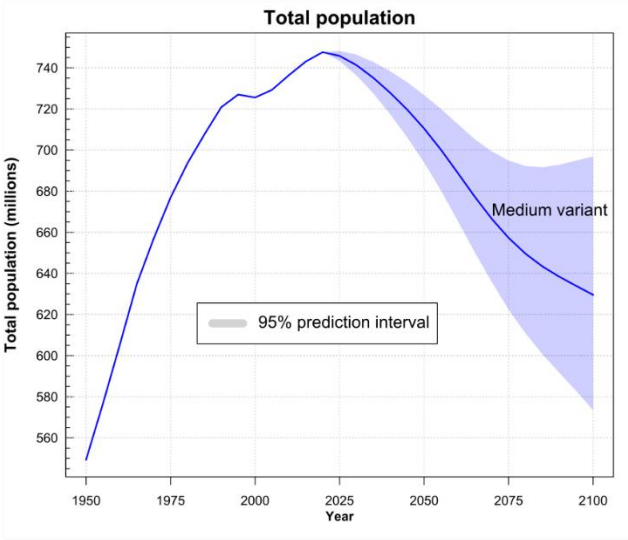

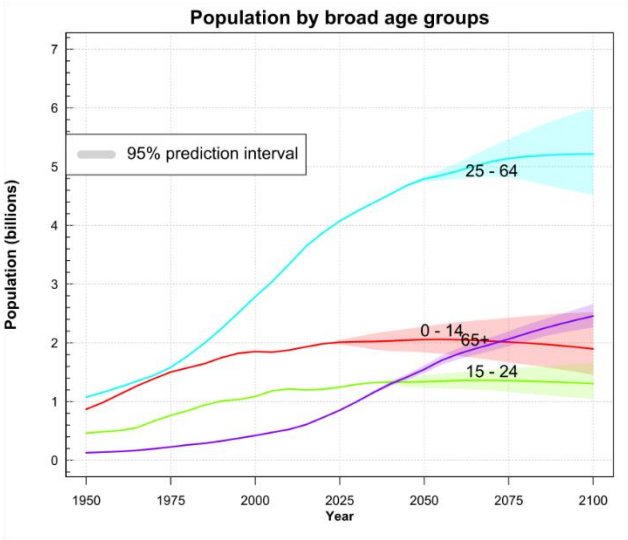

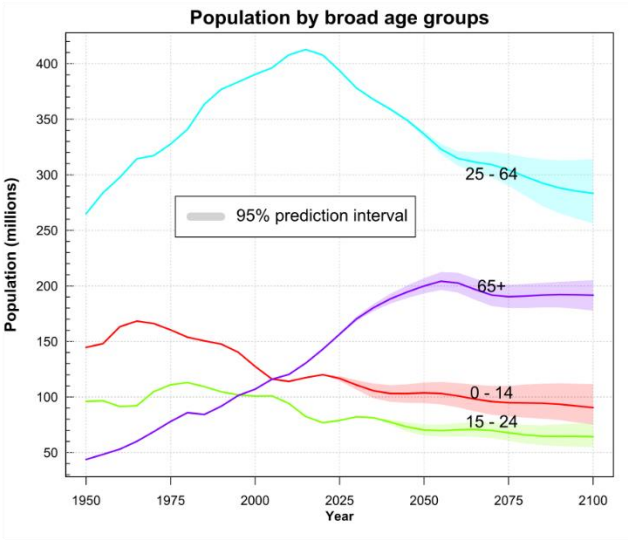

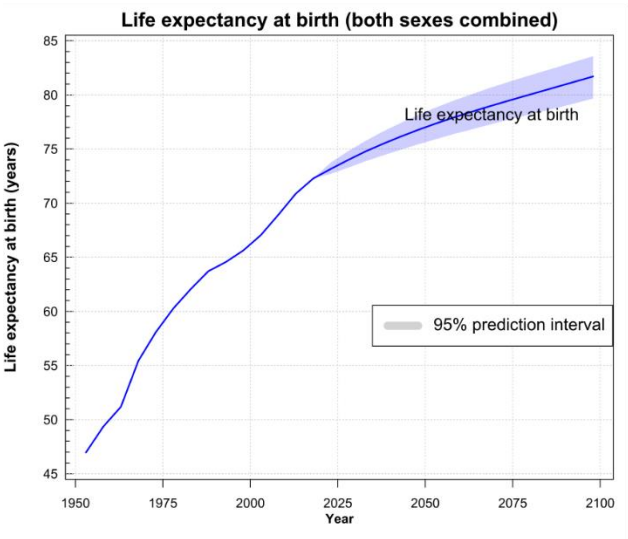

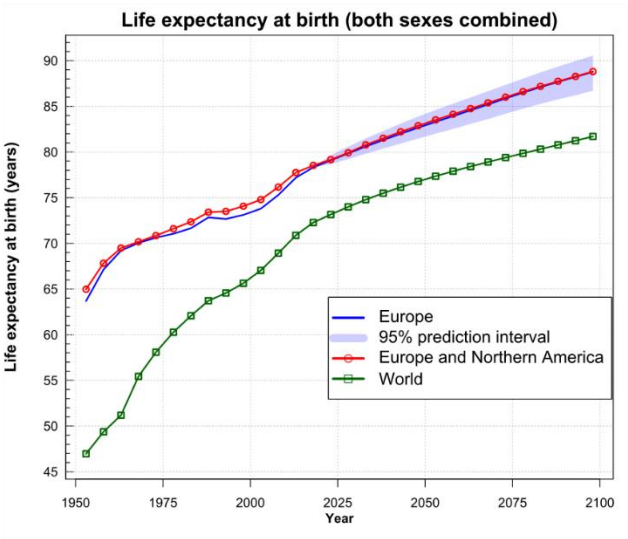

Source: United Nations, Department of Economic and Social Affairs,Population Division. World Population Prospects 2019, Volume II: Demographic Profiles

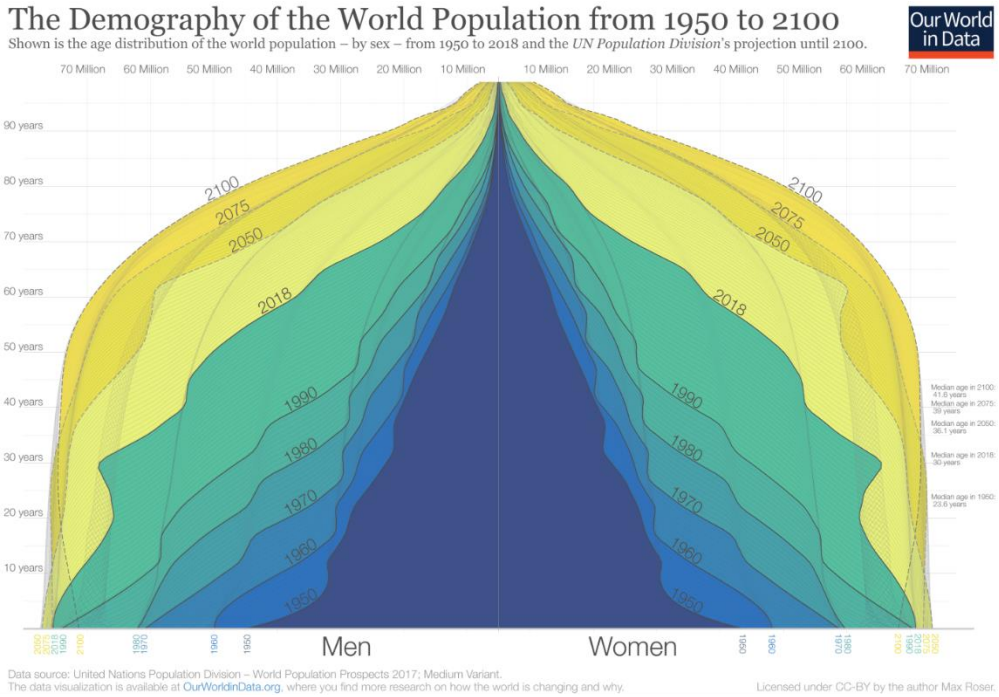
The Demography of the World Population from 1950 to 2100
Shown is the age distribution of the world population – by sex – from 1950 to 2018 and the UN Population Division's projection until 2100.
Our World in Data
70 Million 60 Million 50 Million 40 Million 30 Million 20 Million 10 Million
10 Million 20 Million 30 Million 40 Million 50 Million 60 Million 70 Million
90 years
80 years
70 years
60 years
50 years
40 years
30 years
20 years
10 years
2100
2075
2050
2018
1990
1980
1970
1960
1950
Men
Women
Data source: United Nations Population Division – World Population Prospects 2017; Medium Variant.
The data visualization is available at OurWorldinData.org, where you find more research on how the world is changing and why.
Licensed under CC-BY by the author Max Roser.

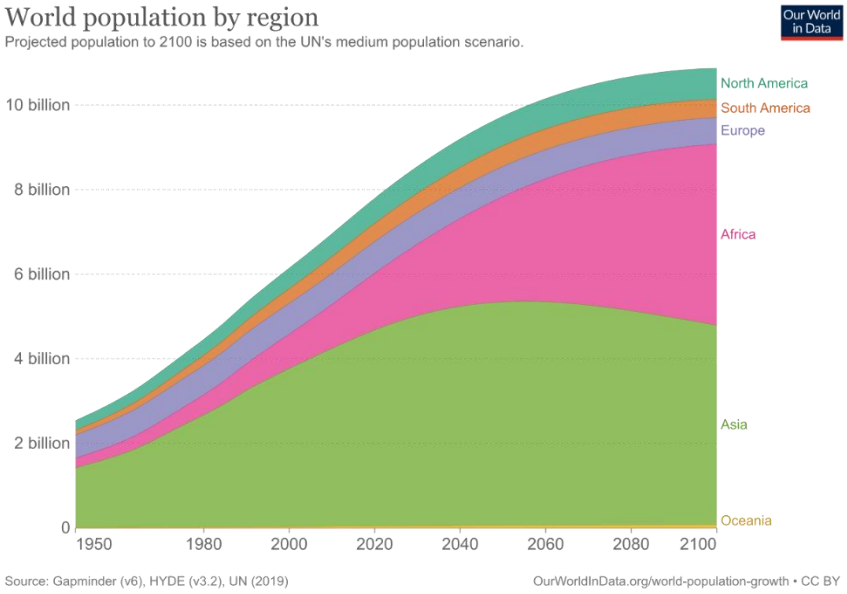
World population by region
Projected population to 2100 is based on the UN's medium population scenario.
Our World in Data
10 billion
8 billion
6 billion
4 billion
2 billion
0
1950
1980
2000
2020
2040
2060
2080
2100
North America
South America
Europe
Africa
Asia
Oceania
Source: Gapminder (v6), HYDE (v3.2), UN (2019)
OurWorldInData.org/world-population-growth • CC BY

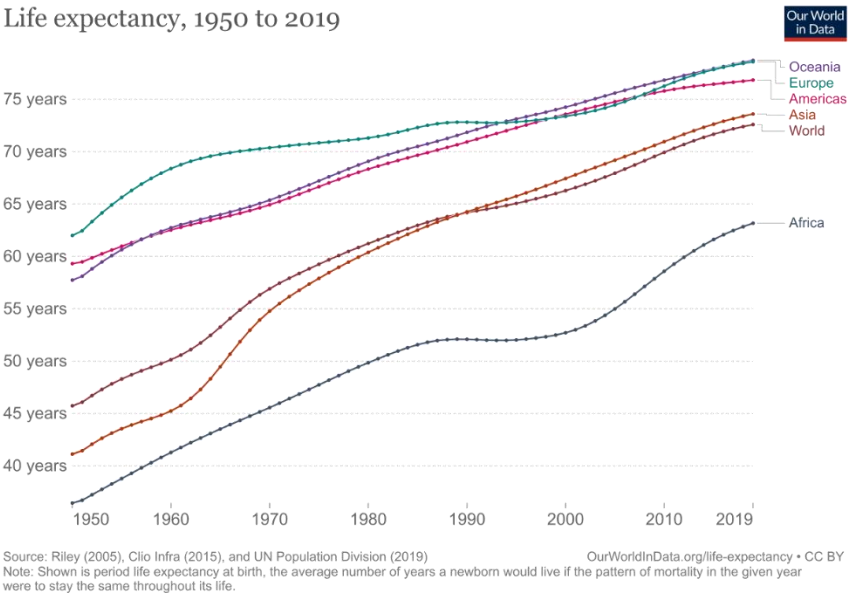
Life expectancy, 1950 to 2019
Our World in Data
75 years
70 years
65 years
60 years
55 years
50 years
45 years
40 years
1950
1960
1970
1980
1990
2000
2010
2019
Oceania
Europe
Americas
Asia
World
Africa
Source: Riley (2005), Clio Infra (2015), and UN Population Division (2019)
OurWorldInData.org/life-expectancy • CC BY
Note: Shown is period life expectancy at birth, the average number of years a newborn would live if the pattern of mortality in the given year were to stay the same throughout its life.

11.4 Appendix D: Table of Disabilities in Population

	Prevalence				Years of life lived with disability				Average disability weight
	All age (millions)		Age-standardised rate (per 1000)		All age (millions)		Age-standardised rate (per 1000)		
	2019	Percentage change*	2019	Percentage change*	2019	Percentage change*	2019	Percentage change*	2019
Overall total	**2412·0 (2338·0 to 2501·0)**	**63% (61 to 64)†**	**298·0 (289·0 to 309·0)**	**−5·6% (−6·1 to −5·1)†**	**310·0 (235·0 to 392·0)**	**69% (67 to 72)†**	**38·0 (29·0 to 49·0)**	**−5% (−6 to −3·9)†**	**0·13 (0·10 to 0·16)**
Musculoskeletal disorders									
Musculoskeletal disorders (total)	**1714·0 (1632·0 to 1800·0)**	**62% (60 to 64)†**	**210·0 (200·0 to 221·0)**	**−8·8% (−10 to −8·2)†**	**149·0 (108·0 to 199·0)**	**59% (55 to 64)†**	**18·0 (13·0 to 24·0)**	**−11% (−13 to −10)†**	**0·08 (0·06 to 0·11)**
Low back pain	568·0 (505·0 to 641·0)	47% (44 to 51)†	70·0 (62·0 to 79·0)	−16% (−17 to −16)†	64·0 (45·0 to 85·0)	47% (43 to 51)†	7·8 (5·5 to 10·0)	−16% (−17 to −16)†	0·11 (0·08 to 0·15)
Neck pain	223·0 (179·0 to 281·0)	79% (70 to 87)†	27·0 (22·0 to 34·0)	−0·45 % (−2·6 to 1·7)	22·0 (15·0 to 32·0)	78% (69 to 87)†	2·7 (1·8 to 3·8)	−0·31% (−2·5 to 1·8)	0·10 (0·07 to 0·14)
Fractures	436·0 (411·0 to 465·0)	69% (67 to 71)†	54·0 (51·0 to 57·0)	−6·9% (−7·8 to −6·0)†	26·0 (18·0 to 36·0)	66% (63 to 68)†	3·2 (2·2 to 4·4)	−8·3% (9·5 to −7·2)†	0·06 (0·04 to 0·08)
Other injuries	305·0 (282·0 to 336·0)	43% (40 to 46)†	38·0 (35·0 to 41·0)	−17% (−18 to −15)†	11·0 (7·5 to 15·0)	25% (19 to 31)†	1·3 (0·9 to 1·8)	−24% (−27 to −21)†	0·03 (0·02 to 0·05)
Osteoarthritis	344·0 (275·0 to 414·0)	114% (112 to 117)†	41·0 (33·0 to 50·0)	3·1 % (1·8 to 4·2)†	19·0 (10·0 to 38·0)	115% (112 to 117)†	2·3 (1·2 to 4·5)	3·3% (2 to 4·6)†	0·05 (0·03 to 0·1)
Amputation	176·0 (164·0 to 190·0)	52% (50 to 55)†	22·0 (20·0 to 23·0)	−13% (−14 to −12)†	5·5 (3·8 to 7·7)	36% (29 to 44)†	0·7 (0·5to 1·0)	−23% (−27 to −18)†	0·03 (0·02 to 0·04)
Rheumatoid arthritis	13·0 (12·0 to 15·0)	106% (104 to 109)†	1·6 (1·5 to 1·8)	8·1% (7·5 to 8·6)†	2·4 (1·7 to 3·3)	105% (102 to 108)†	0·3 (0·2 to 0·4)	8·3% (7·3 to 9·3)†	0·18 (0·13 to 0·24)
Neurological disorders									
Neurological disorders (total)	**255·0 (242·0 to 268·0)**	**106% (103 to 110)†**	**32·0 (31·0 to 34·0)**	**10% (8·4 to 12)†**	**51·0 (37·0 to 65·0)**	**104% (100 to 109)†**	**6·4 (4·7 to 8·2)**	**11% (8·5 to 13)†**	**0·20 (0·15 to 0·25)**
Cerebral palsy	50·0 (44·0 to 57·0)	159% (138 to 183)†	6·6 (5·8 to 7·6)	94% (78 to 111)†	11·0 (7·4 to 15·0)	155% (134 to 178)†	1·4 (1·0 to 1·9)	91% (76 to 108)†	0·21 (0·15 to 0·28)
Stroke	86·0 (79·0 to 94·0)	85% (82 to 88)†	11·0 (10·0 to 12·0)	−6·1% (−7·3 to −4·9)†	18·0 (13·0 to 23·0)	89% (85 to 93)†	2·2 (1·6 to 2·8)	−4·7% (−6·1 to −3·3)†	0·21 (0·15 to 0·26)
Traumatic brain injury	49·0 (47·0 to 51·0)	80% (78 to 82)†	6·0 (5·7 to 6·3)	−0·01% (−1·1 to 1·2)	7·1 (5·0 to 10·0)	79% (77 to 82)†	0·9 (0·6 to 1·2)	0·16% (−1 to 1·3)	0·14 (0·1 to 0·2)
Alzheimer's disease and dementia	52·0 (44·0 to 59·0)	161% (156 to 166)†	6·8 (5·9 to 7·8)	5·7% (4·3 to 6·9)†	7·4 (5·2 to 10·0)	165% (159 to 171)†	1·0 (0·7 to 1·3)	5·5% (4 to 6·8)†	0·14 (0·11 to 0·18)
Spinal cord injury	21·0 (19·0 to 24·0)	82% (74 to 87)†	2·5 (2·3 to 2·9)	5·8 % (2·7 to 10)†	6·2 (4·5 to 8·2)	65% (56 to 72)†	0·8 (0·6 to 1·0)	−1·6% (−5·6 to 3·3)	0·30 (0·22 to 0·38)
Parkinson's disease	3·9 (3·3 to 4·7)	156% (150 to 161)†	0·5 (0·4 to 0·6)	16% (13 to 18)†	1·2 (0·8 to 1·6)	155% (149 to 161)†	0·2 (0·1 to 0·2)	16% (13 to 19)†	0·30 (0·21 to 0·39)
Multiple sclerosis	1·4 (1·2 to 1·5)	72% (66 to 77)†	0·2 (0·1 to 0·2)	−6·1% (−8·7 to −3·8)†	0·5 (0·3 to 0·6)	71% (65 to 77)†	0·1 (0·04 to 0·07)	−5·8% (−8·6 to −2·9)†	0·33 (0·24 to 0·42)
Motor neuron disease	0·2 (0·2 to 0·3)	69% (62 to 76)†	0·03 (0·02 to 0·03)	1·9% (0·61 to 3·4)†	0·1 (0·0 to 0·1)	69% (62 to 76)†	0·01 (0 to 0·01)	1·9% (0·57 to 3·3)†	0·25 (0·17 to 0·32)
Guillain-Barré syndrome	0·1 (0·1 to 0·1)	67% (57 to 77)†	0·01 (0·01 to 0·02)	6·6 % (3·6 to 10)†	0·03 (0·02 to 0·04)	67% (57 to 77)†	0 (0 to 0·01)	6·5% (3·6 to 9·5)†	0·30 (0·20 to 0·41)
Sensory impairments									
Sensory impairments (total)	**677·0 (631·0 to 723·0)**	**77% (74 to 81)†**	**84·0 (79 to 90)**	**−4·5% (−5 to −4)†**	**45·0 (31·0 to 62·0)**	**70% (65 to 74)†**	**5·7 (3·9 to 7·7)**	**−9·4% (−11 to −7·9)†**	**0·07 (0·05 to 0·09)**
Hearing loss	403·0 (357·0 to 449·0)	79% (74 to 84)†	51·0 (45·0 to 56·0)	−5·4% (−6·2 to −4·8)†	24·0 (16·0 to 33·0)	69% (61 to 76)†	3·0 (2·0 to 4·2)	−7·3% (−8·3 to −6·3)†	0·06 (0·04 to 0·08)
Vision loss	329·0 (302·0 to 358·0)	80% (77 to 83)†	41·0 (38·0 to 44·0)	−3·8% (−4·5 to −3·1)†	21·0 (15·0 to 30·0)	71% (68 to 74)†	2·7 (1·9 to 3·7)	−12% (−14 to −9·5)†	0·06 (0·05 to 0·09)
Mental disorders									
Mental disorders (total)	**187·0 (147·0 to 229·0)**	**40% (36 to 47)†**	**24·0 (19 to 30)**	**0·52% (−2·1 to 4·2)**	**29·0 (22·0 to 37·0)**	**53% (49 to 58)†**	**3·7 (2·8 to 4·7)**	**1·7% (0·06 to 3·5)†**	**0·16 (0·12 to 0·20)**
Developmental intellectual disability	137·0 (97·0 to 177·0)	37% (32 to 46)†	18·0 (13·0 to 23·0)	1·2% (−2·5 to 7·1)	10·0 (6·1 to 14·0)	44% (37 to 54)†	1·3 (0·8 to 1·9)	6·5% (1·3 to 13)†	0·07 (0·05 to 0·1)
Schizophrenia	24·0 (20·0 to 27·0)	66% (63 to 69)†	2·9 (2·5 to 3·3)	−0·88% (−1·7 to −0·13)†	15·0 (11·0 to 19·0)	65% (62 to 69)†	1·8 (1·3 to 2·3)	−0·57% (−1·6 to 0·38)	0·64 (0·49 to 0·76)
Autism spectrum disorders	28·0 (24·0 to 34·0)	39% (39 to 40)†	3·7 (3·1 to 4·4)	−0·93% (−1·3 to −0·61)†	4·3 (2·8 to 6·2)	39% (38 to 40)†	0·6 (0·4 to 0·8)	−0·76% (−1·4 to −0·16)†	0·15 (0·11 to 0·21)
Chronic respiratory diseases									
Chronic respiratory diseases (total)	**118·0 (107·0 to 130·0)**	**89% (85 to 93)†**	**15·0 (13·0 to 16·0)**	**−6% (−7·7 to −4·1)†**	**20·0 (17·0 to 22·0)**	**89% (85 to 94)†**	**2·5 (2·1 to 2·8)**	**−4·8% (−6·6 to −3)†**	**0·17 (0·14 to 0·19)**
Chronic obstructive pulmonary disease	118·0 (107·0 to 130·0)	89% (85 to 93)†	15·0 (13·0 to 16·0)	−6% (−7·7 to −4·1)†	20·0 (17·0 to 22·0)	89% (85 to 94)†	2·5 (2·1 to 2·8)	−4·8% (−6·6 to −3)†	0·17 (0·14 to 0·19)
Cardiovascular diseases									
Cardiovascular diseases (total)	**37·0 (30·0 to 44·0)**	**106% (99 to 113)†**	**4·6 (3·9 to 5·6)**	**−7·2% (−10 to −4)†**	**4·2 (2·7 to 6)**	**106% (99 to 114)†**	**0·5 (0·4 to 0·8)**	**−6·9% (−10 to −3·7)†**	**0·11 (0·08 to 0·16)**
Heart failure	35·0 (29·0 to 43·0)	107% (99 to 115)†	4·5 (3·7 to 5·4)	−6·9% (−10 to −3·5)†	4·1 (2·6 to 5·8)	107% (99 to 115)†	0·5 (0·3 to 0·7)	6·7% (−10 to −3·3)†	0·11 (0·08 to 0·16)
Acute myocardial infarction	1·3 (1·1 to 1·5)	82% (80 to 84)†	0·2 (0·1 to 0·2)	−15% (−16 to −14)†	0·1 (0·1 to 0·2)	83% (79 to 86)†	0·01 (0·01 to 0·02)	−14% (−16 to −13)†	0·09 (0·06 to 0·12)
Neoplasms									
Neoplasms (total)	**18·0 (17·0 to 19·0)**	**118% (104 to 132)†**	**2·2 (2·0 to 2·3)**	**4·7% (−2·2 to 12)**	**1·9 (1·4 to 2·6)**	**129% (114 to 144)†**	**0·2 (0·2 to 0·3)**	**15% (7·5 to 22)†**	**0·11 (0·08 to 0·14)**

*Percentage change from 1990 to 2019. †Statistically significant.

Table: **Global prevalence and years of life lived with disability for health conditions in need of rehabilitation, all-age counts, and age-standardised rates for 2019, percentage change since 1990, and average disability weight for 2019**

Source: (Cieza et al., 2020)

11.5 Appendix E: Bone Architecture and Properties

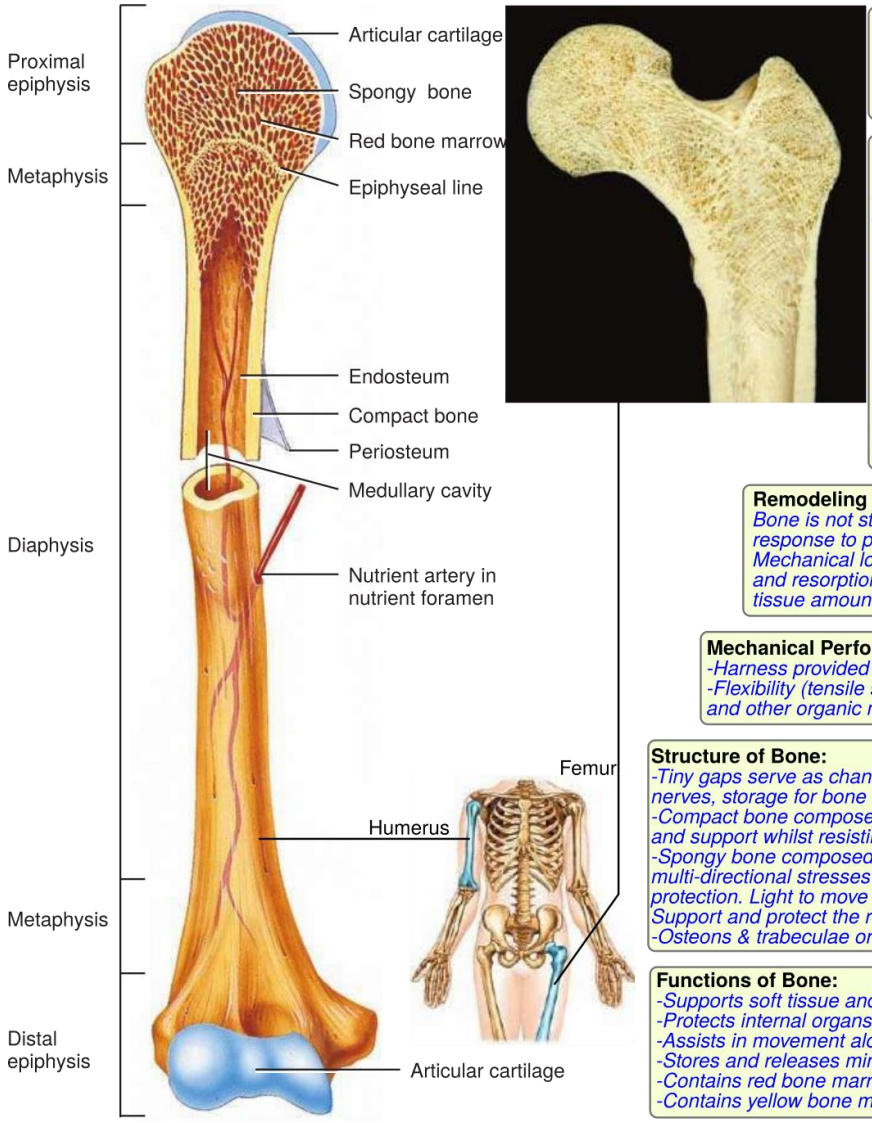

Histology of Bone Tissue:
Contains an abundant extracellular matrix (25% water, 25% collagen fibers, 50% crystallized mineral salts) that surrounds separated cells

Osteogenesis (Bone formation):
-Occurs: 1) in an embryo and fetus, 2) until adult size is reached, 3) throughout life during bone remodeling, 4) throughout life during repair of bone fractures.
-Responsible cells are: 1)Osteogenic: capable of division, originate from mesenchyme and transform into osteoblasts, 2) Osteoblasts: build bone tissue (deposition) and eventually transform into osteocytes, 3) Osteocytes: maintain normal bone tissue by guiding osteoblasts and osteoclasts, 4) Osteoclasts: breakdown bone tissue (resorption)

Remodeling of Bone:
Bone is not static but changes dynamically in response to physical demands placed on skeleton. Mechanical loading-driven deposition (osteoblast) and resorption (osteoclast) maintain optimum bone tissue amount and morphology

Mechanical Performance of Bone:
-Harness provided by crystallized inorganic mineral salts
-Flexibility (tensile strength) offered by collagen fibers and other organic molecules

Structure of Bone:
-Tiny gaps serve as channels for blood and lymphatic vessels, nerves, storage for bone marrow (red and yellow)
-Compact bone composed of osteons and provides protection and support whilst resisting stresses
-Spongy bone composed of trabeculae. Placed at low and/or multi-directional stresses Always covered by compact bone for protection. Light to move readily when pulled by a muscle. Support and protect the red marrow
-Osteons & trabeculae oriented along stress-lines (remodeling)

Functions of Bone:
-Supports soft tissue and provides skeletal muscle attachment
-Protects internal organs
-Assists in movement along with skeletal muscles
-Stores and releases minerals
-Contains red bone marrow, which produces blood cells
-Contains yellow bone marrow, which stores triglycerides (fats)

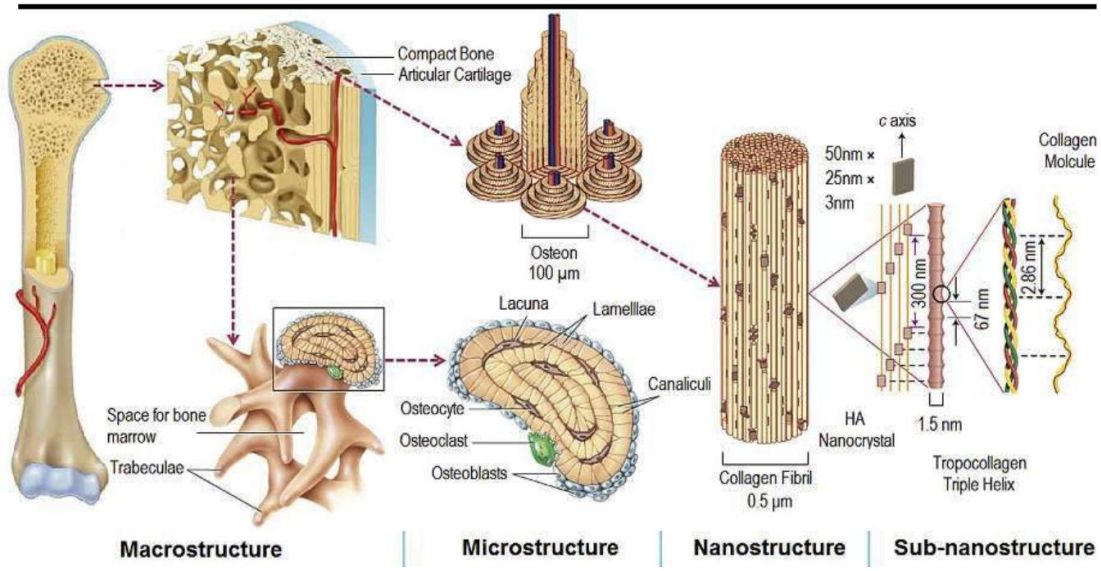

Source: (Tortora and Derrickson, 2020; Wang et al., 2016)

Bone	Age	Gender	Density	Condition	Ultimate Strain	Cross head (mm/min)	Yield (MPa)	Modulus (GPa)	UTS (MPa)	Source
Cortical bone tensile data										
Fibula	33	Male	1.91	Moist	2.1	1.1	– [a)]	19.2	100	EB
	59	Male	1.73	Moist	1.19	1.1	–	15.2	80	EB
Humerus	15–89	Male	1.77	Moist	1.2	0.5	–	15.6	149	–
	15–89	Female	1.72	Moist	1.9	0.5	–	16.1	151	–
Tibia	41.5	Male	1.96	Moist	1.76	1.1	–	18.9	106	EB
	71	–	1.83	Moist	1.56	1.1	–	16.2	84	EB
	20–29	–	–	Moist	4	–	126	18.9	161	Frozen
	30–39	–	–	Moist	3.9	–	129	27.0	154	Frozen
	40–49	–	–	Moist	2.9	–	140	28.8	170	Frozen
	50–59	–	–	Moist	3.1	–	133	23.1	164	Frozen
	60–69	–	–	Moist	2.7	–	124	19.9	147	Frozen
	70–79	–	–	Moist	2.7	–	120	19.9	145	Frozen
	80–89	–	–	Moist	2.3	–	131	29.2	156	Frozen
Femur	41.5	Male	1.91	Moist	1.32	1.1	–	14.9	102	EB
	71	Male	1.85	Moist	1.07	1.1	–	13.6	68	EB
	15–89	male	1.9	Moist	2	0.5	–	15.2	141	–
	15–89	female	1.8	Moist	1.8	0.5	–	15.0	134	–
	20–29	–	–	Moist	3.4	–	120	17.0	140	Frozen
	30–39	–	–	Moist	3.2	–	120	17.6	136	Frozen
	40–49	–	–	Moist	3	–	121	17.7	139	Frozen
	50–59	–	–	Moist	2.8	–	111	16.6	131	Frozen
	60–69	–	–	Moist	2.5	–	112	17.1	129	Frozen
	70–79	–	–	Moist	2.5	–	111	16.3	129	Frozen
	80–89	–	–	Moist	2.4	–	104	15.6	120	Frozen
Cortical bone compression data										
Tibia	20–29	–	–	Moist	–	–	– [a)]	–	–	Frozen
	30–39	–	–	Moist	–	–	–	35.3	213	Frozen
	40–49	–	–	Moist	–	–	–	30.6	204	Frozen
	50–59	–	–	Moist	–	–	–	24.5	192	Frozen
	60–69	–	–	Moist	–	–	–	25.1	183	Frozen
	70–79	–	–	Moist	–	–	–	26.7	183	Frozen
	80–89	–	–	Moist	–	–	–	25.9	197	Frozen
Femur	20–29	–	–	Moist	–	–	–	18.1	209	Frozen
	30–39	–	–	Moist	–	–	–	18.6	209	Frozen
	40–49	–	–	Moist	–	–	–	18.7	200	Frozen
	50–59	–	–	Moist	–	–	–	18.2	192	Frozen
	60–69	–	–	Moist	–	–	–	15.9	179	Frozen
	70–79	–	–	Moist	–	–	–	18	190	Frozen
	80–89	–	–	Moist	–	–	–	15.4	180	Frozen
Trabecular bone compression data										
Lumbar vertebra	14–89	Male	0.22	Dried	6.7	0.05	– [a)]	0.06	4.6	–
	14–89	Female	0.22	Dried	6.1	0.05	–	0.04	2.7	–
Tibial head	14–89	Male	0.22	Dried	8.3	0.05	–	0.03	3.9	–
	14–89	Female	0.22	Dried	6.9	0.05	–	0.02	2.2	–
Tibia	16–39	–	–	Moist	2.48	0.02	–	0.65	10.6	Frozen
	40–59	–	–	Moist	2.12	0.02	–	0.83	9.86	Frozen
	60–83	–	–	Moist	2.05	0.02	–	0.61	7.27	Frozen
Proximal tibia	59–82	–	0.29	Moist	–	–	–	0.45	5.33	Frozen
Femur	58–83	–	0.5	Moist	–	–	–	0.39	7.36	Frozen
Lumbar spine	15–87 (Vertical)	–	0.25	Moist	7.4	–	–	0.07	2.45	Frozen
	15–87 (Horizontal)	–	0.24	Moist	8.5	–	–	0.02	0.88	Frozen
	71–84	–	0.19	Moist	7.4	5	1.37	0.02	1.55	Frozen

Source: (Yang et al., 2019)

	Porosity	Modulus (GPa)		Strength (MPa)		Poisson's ration
Compact Bone	3–5%	Longitudinal	17.9 ± 3.9	Tension	135 ± 15.6	0.4 ± 0.16
				Compression	205 ± 17.3	
		Transverse	10.1 ± 2.4	Tension	53 ± 10.7	0.62 ± 0.26
				Compression	131 ± 20.7	
		Shear	3.3 ± 0.4	Shear	65 ± 4.0	
Trabecular Bone	Up to 90%	Vertebra	0.067 ± 0.045		2.4 ± 1.6	
		Tibia	0.445 ± 0.257		5.3 ± 2.9	
		Femur	0.441 ± 0.271		6.8 ± 4.8	

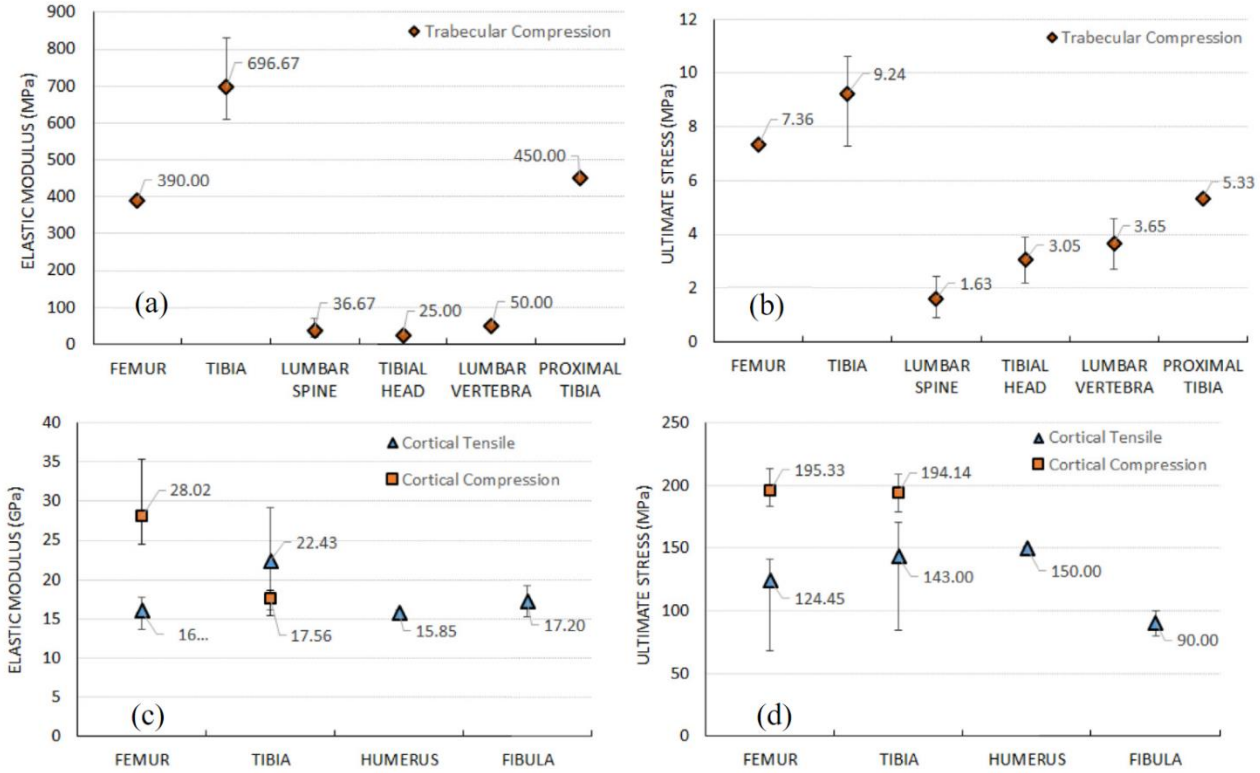

Source: (Wang et al., 2018; Yang et al., 2019)

11.6 Appendix F: Ashby's Material Property Charts

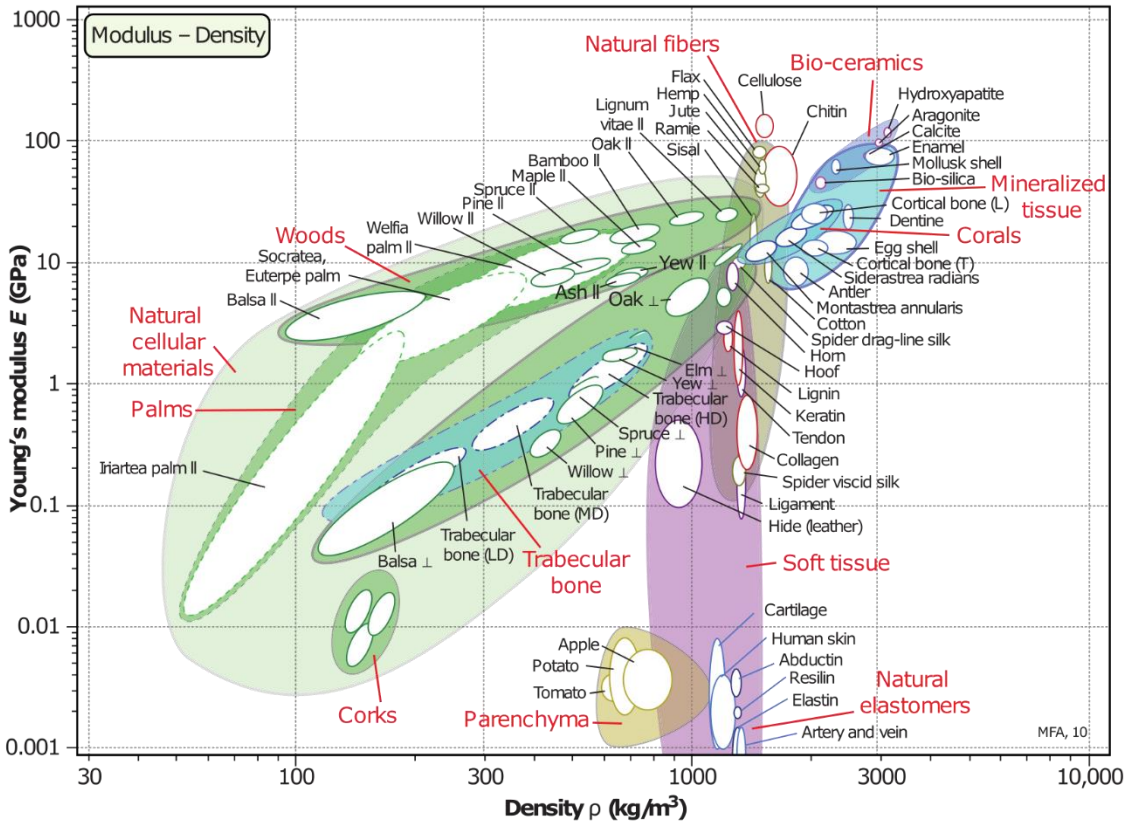

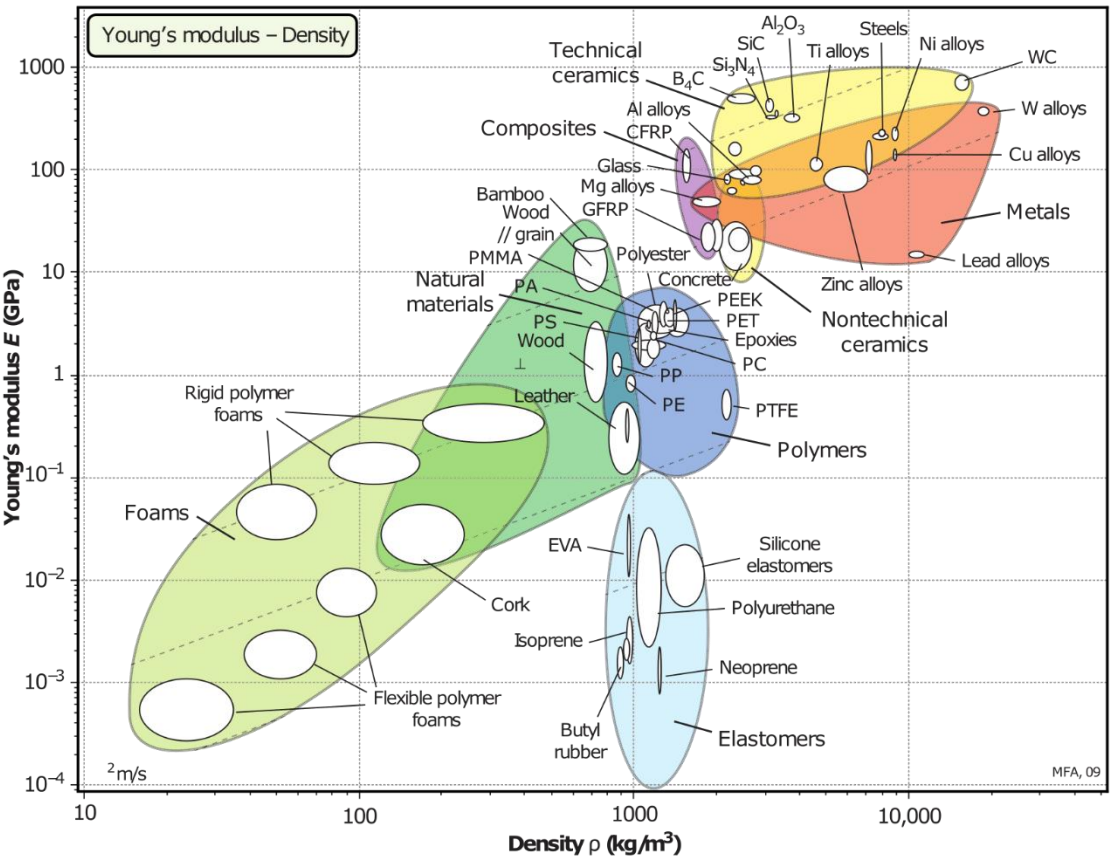

Source: (Ashby, 2016)

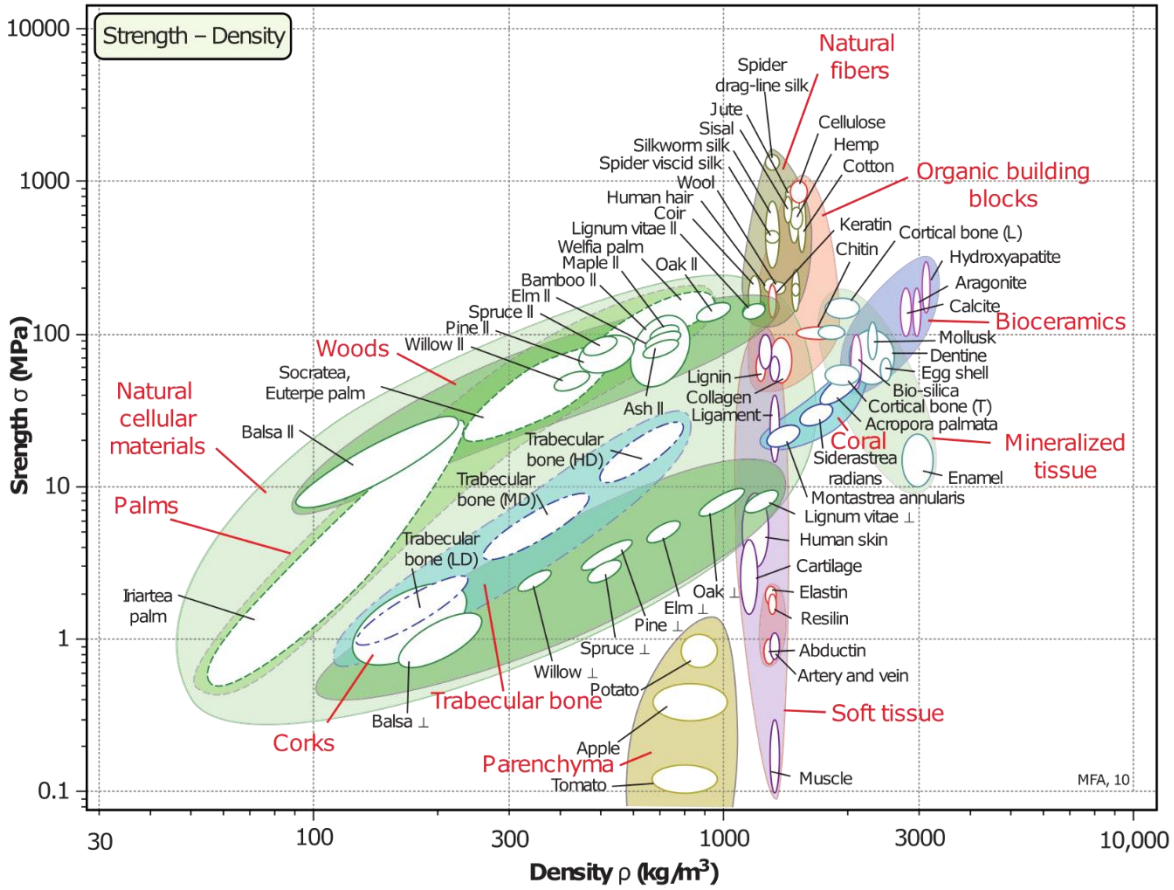

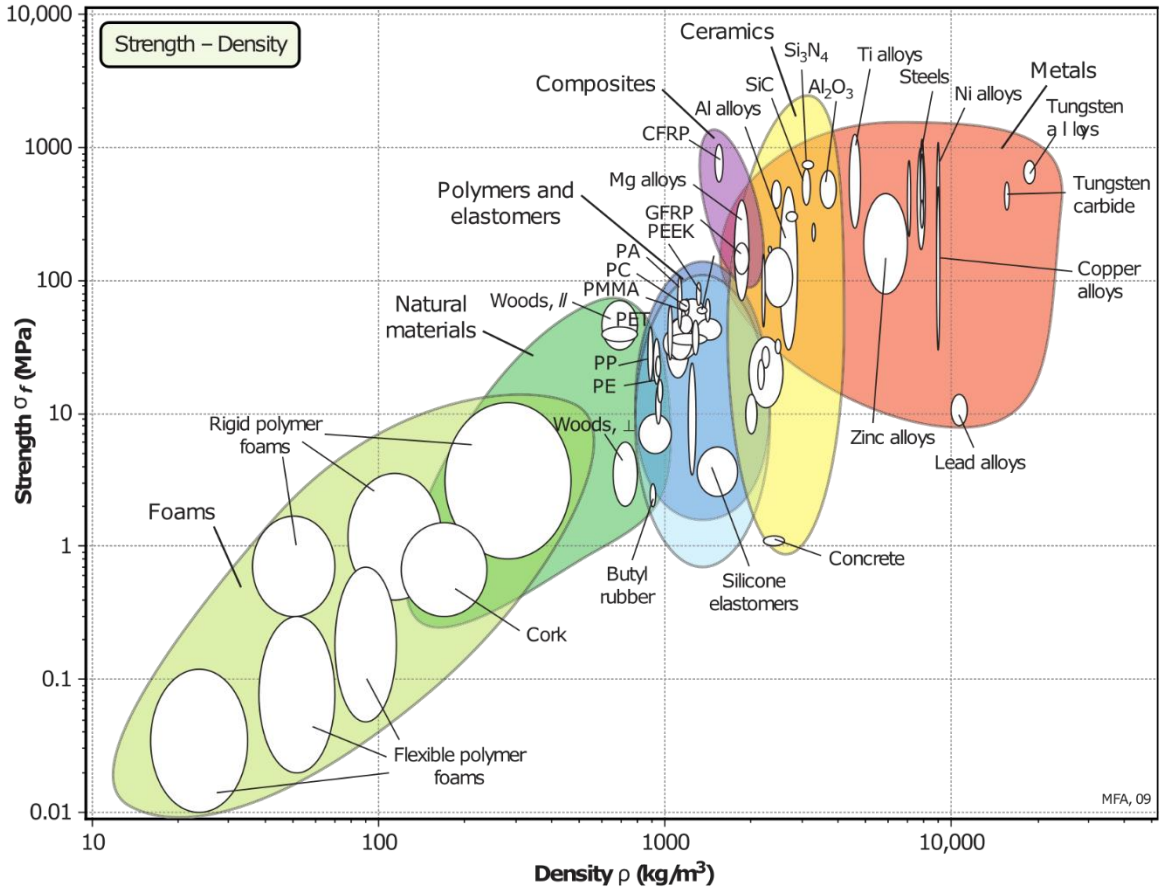

Source: (Ashby, 2016)

11.7 Appendix G: 3D Printing of Different Materials

Material processing capabilities and required steps for each 3D Printing category.

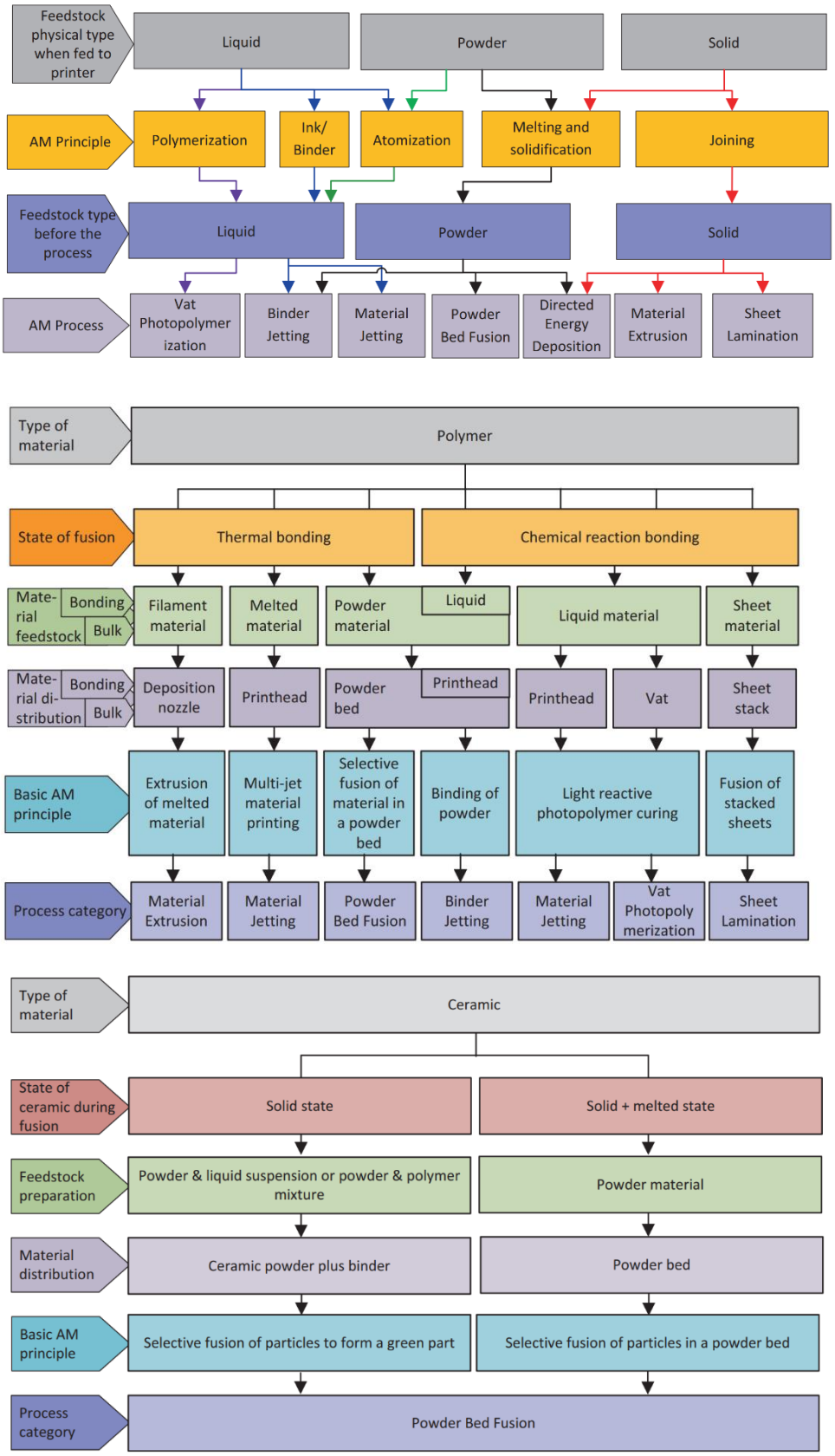

Source: (Gibson, Rosen and Stucker, 2021) according to ISO/ASTM

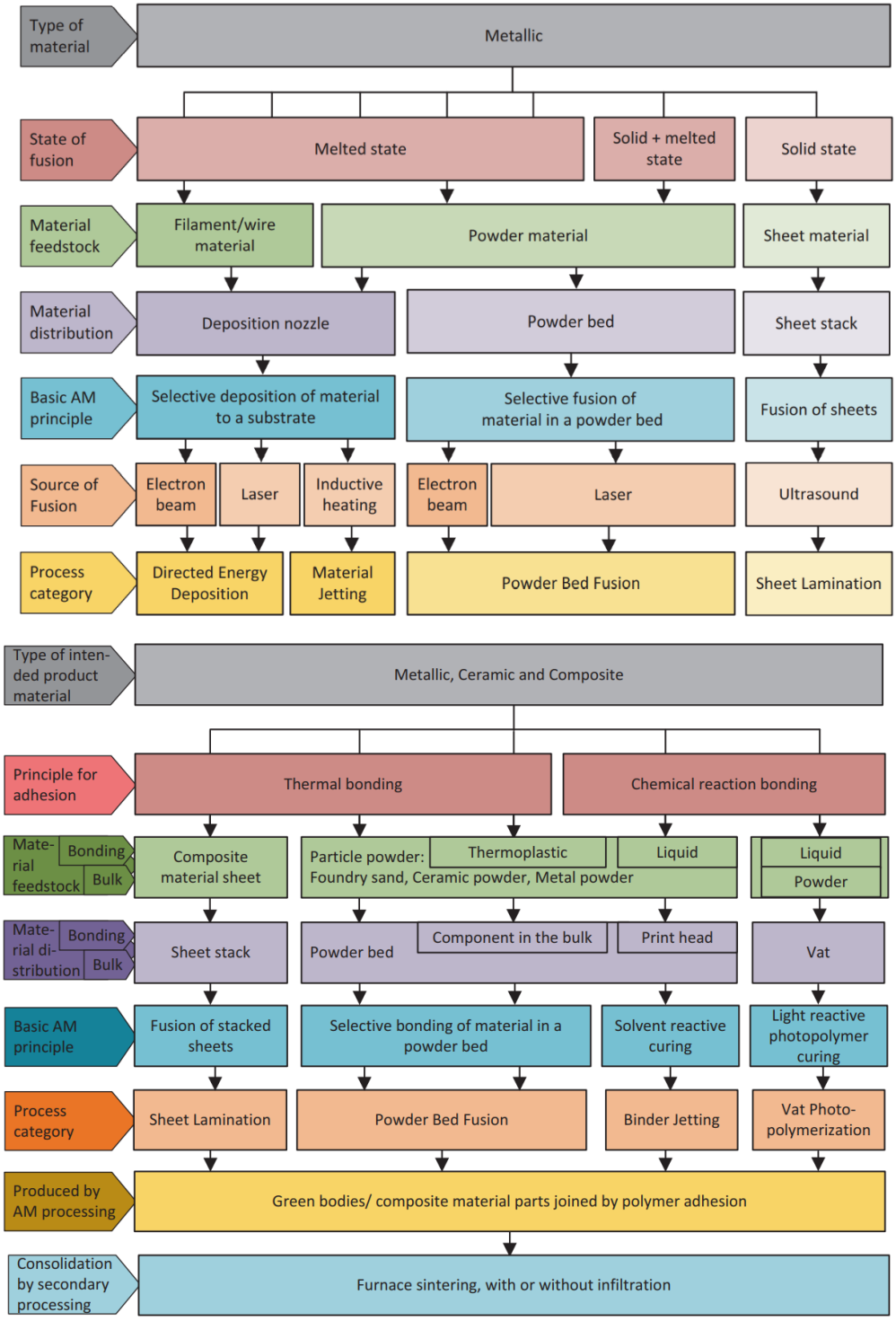

Source: (Gibson, Rosen and Stucker, 2021) according to ISO/ASTM

11.8 Appendix H: Anisotropy of Material Extruded Products

"Morpheas Extrusion 3D Printer"

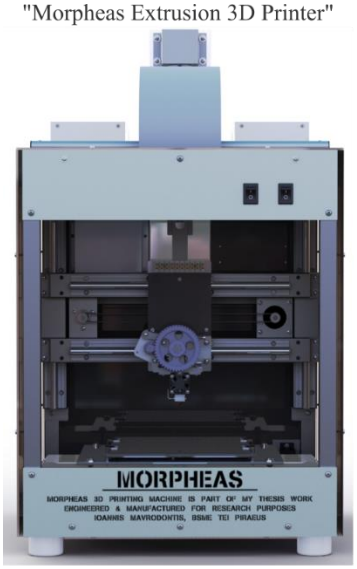

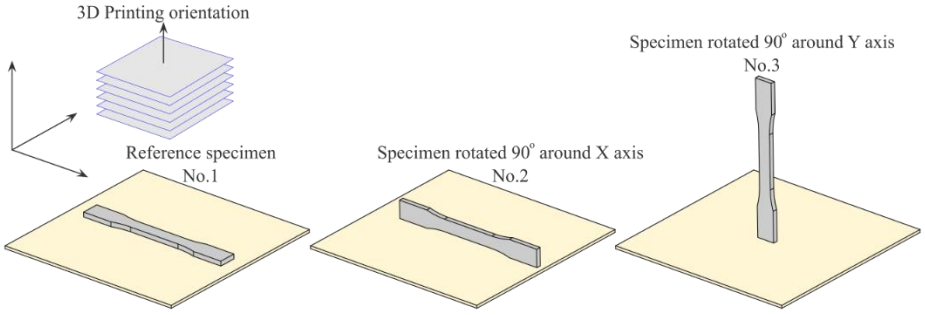

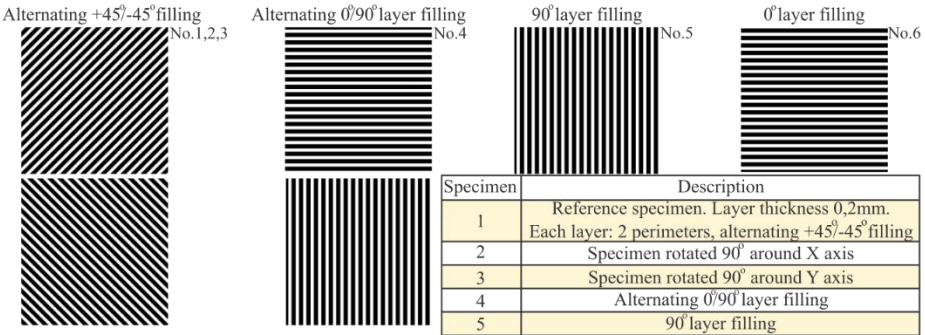

Specimen	Description
1	Reference specimen. Layer thickness 0,2mm. Each layer: 2 perimeters, alternating +45°/-45° filling
2	Specimen rotated 90° around X axis
3	Specimen rotated 90° around Y axis
4	Alternating 0°/90° layer filling
5	90° layer filling
6	0° layer filling

3D Printed PLA Specimens as per ASTM D 638-10 TYPE 1

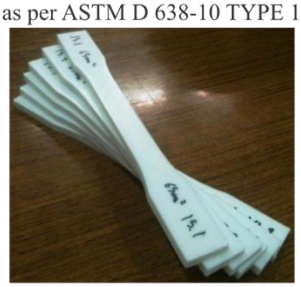

Tensile testing

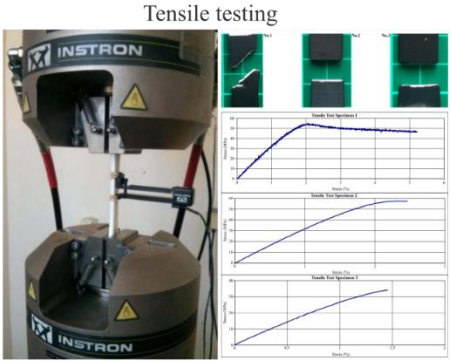

Fractured specimens

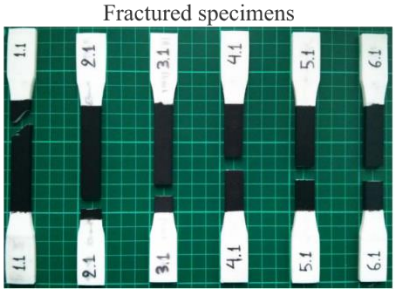

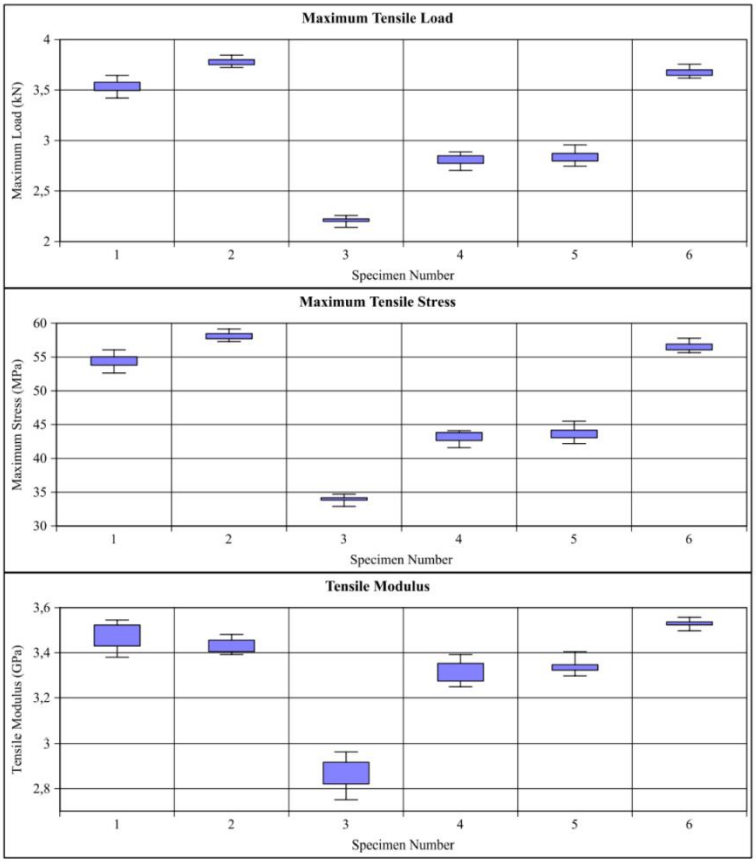

Source: (Mavrodontis, 2015)

11.9 Appendix I: 3D Printing and Software Market Landscape

Source: (AMFG, 2020)

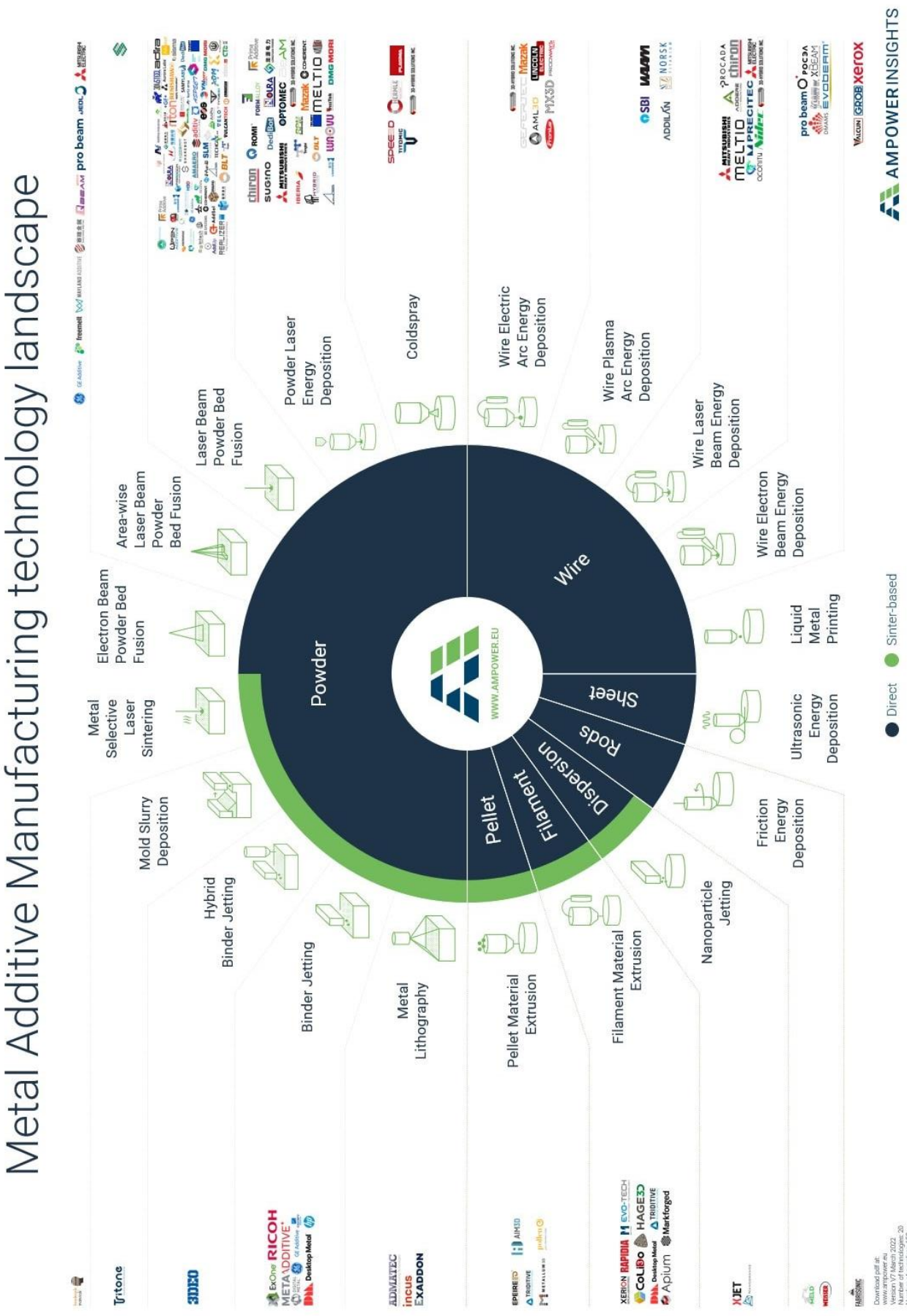

Source: ampower

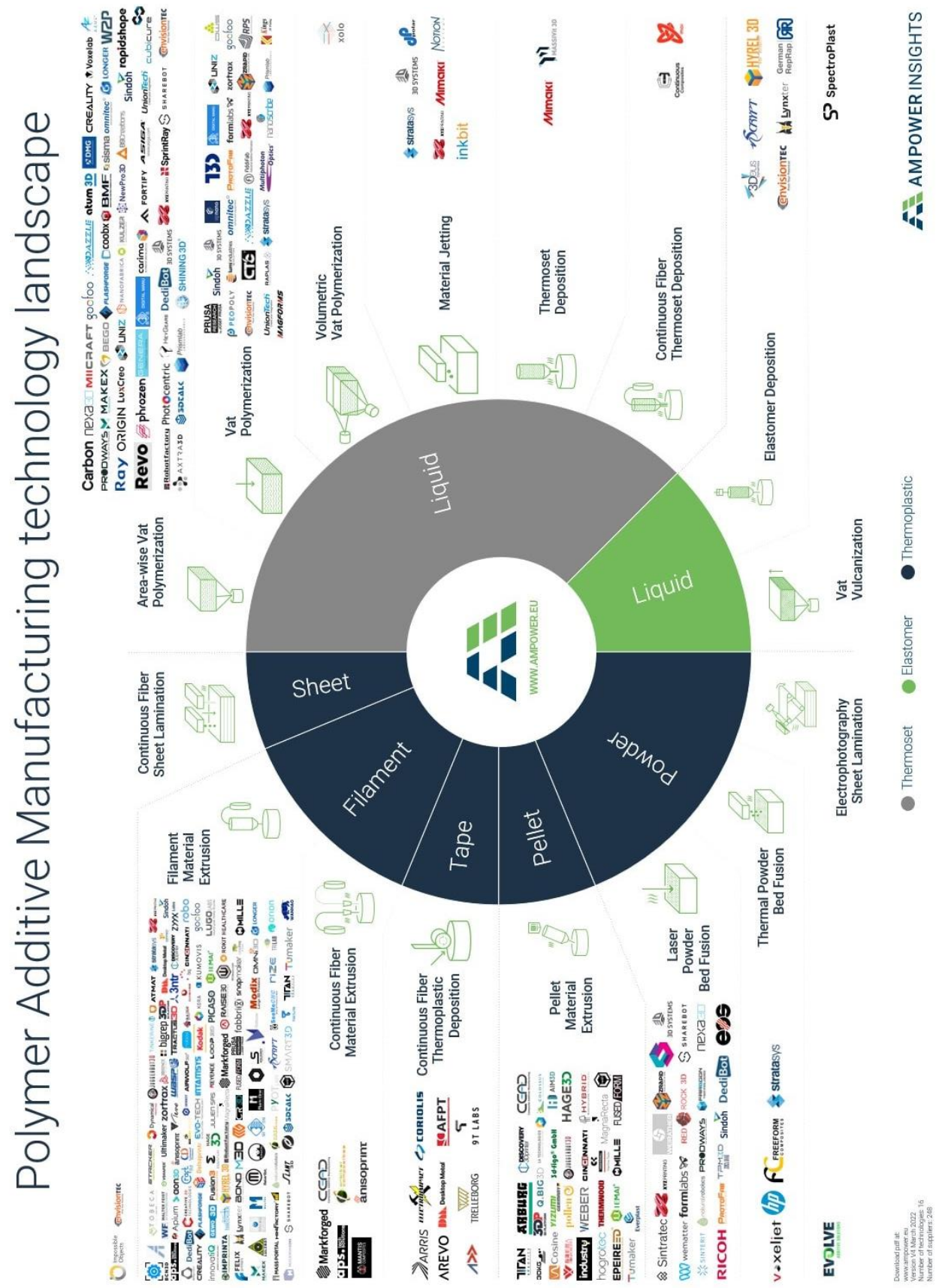

Source: ampower

Source: (AMFG, 2020)

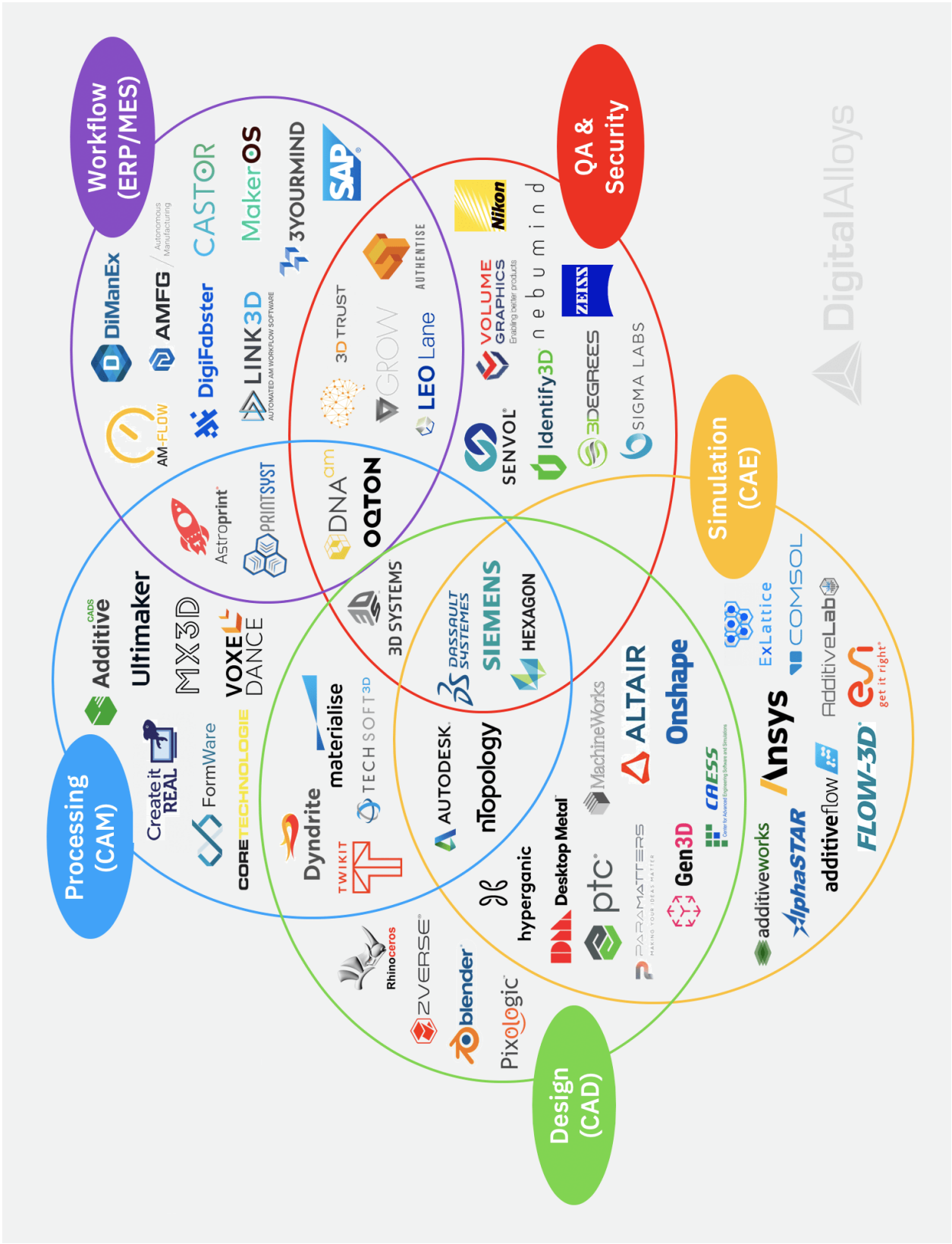

Design, simulation, workflow and processing software. Source: Digital Alloys

11.10 Appendix J: 3D Printing in Series of Severe Cases

Calcaneal Chondosarcoma.

Final titanium implant, unprocessed part, plastic prototype.

Missing sternum due to an unusual infection.

Composite PoreStar/3D-printed titanium implant.

Sternal Chondrosarcoma.

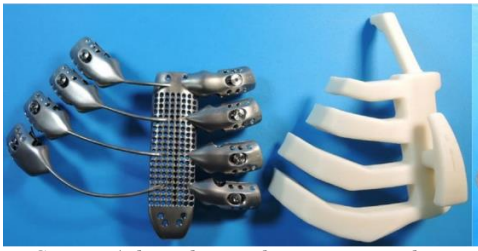

Sternum/rib implant and resection template.

Sternal germ cell tumor.

Part "as printed" and finished implant.

Spine surgery.

Polymer guides.

Chondroma.

Ti cervical fusion cage.

Severe trauma.

Ti metacarpal implant.

Pelvic Sarcoma.

Ti hemipelvic implant.

Deformity in lumbar vertebra.

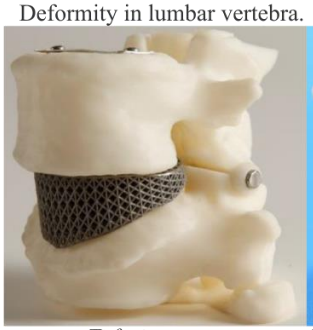

Ti fusion cage.

Cervical spine degeneration.

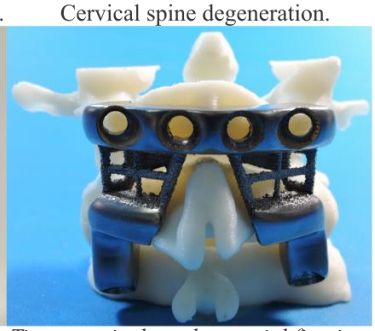

Ti transarticular atlantoaxial fixation.

C1 Fracture.

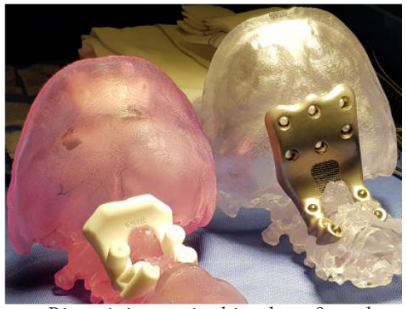

Ri occipitocervical implant & tools.

Revision lumbar spine surgery.

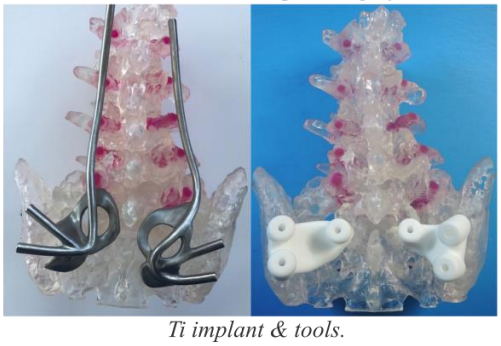

Ti implant & tools.
Source: Anatomics

Undifferentiated spindle cell sarcoma.
Solution: IIiac Plate, Combined with Total Hip Arthroplasty.

Pre-op CT & MRI *3DPed Biomodel & Cutting Guide*

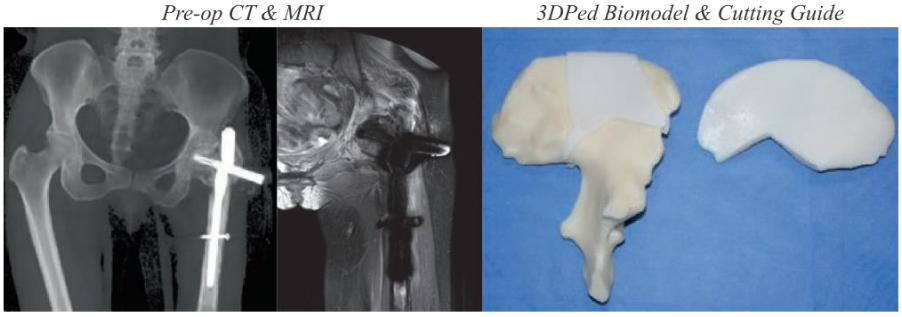

Post-op X-Ray *3DPed Endoprosthesis*

Grade 2 Chondrosarcoma.
Solution: Acetabulum for Easy Assembly of Total Hip Cup.

Pre-op CT & MRI *3DPed Cutting Guides*

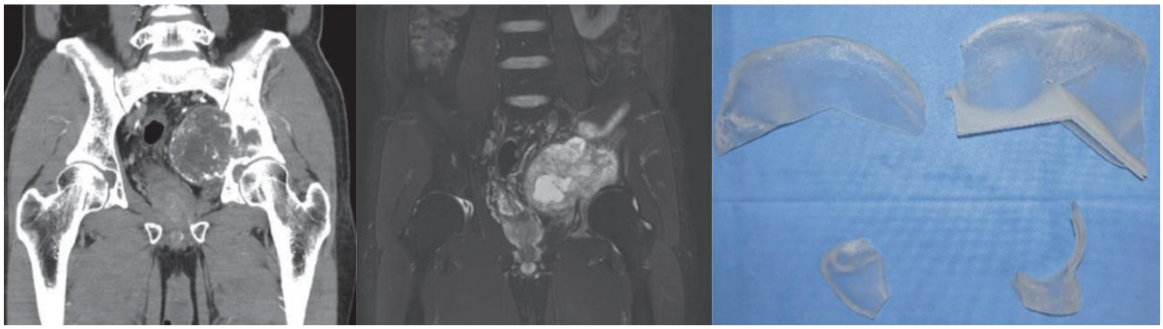

Post-op X-Ray *3DPed Endoprosthesis*

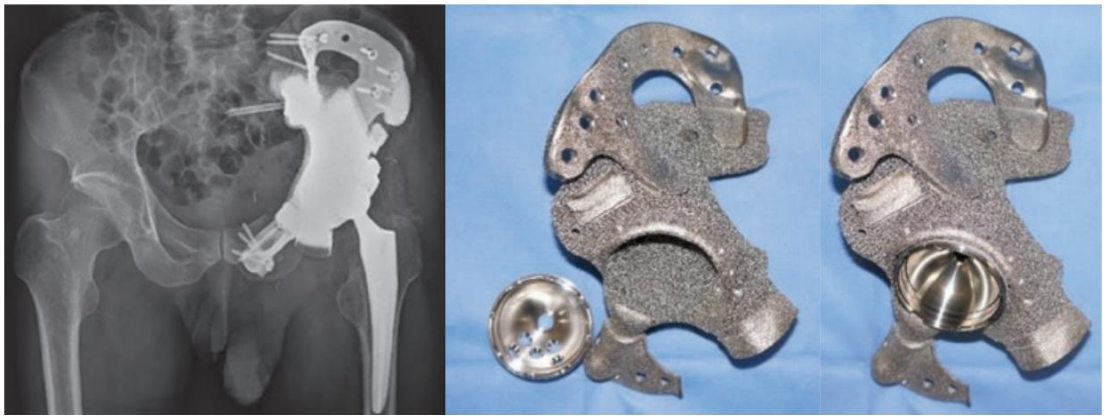

Source: (Kang, 2021)

Osteosarcoma. Solution: Mesh-Style Body Without Ischium.

Pre-op X-Ray & MRI *3DPed Biomodel & Cutting Guide*

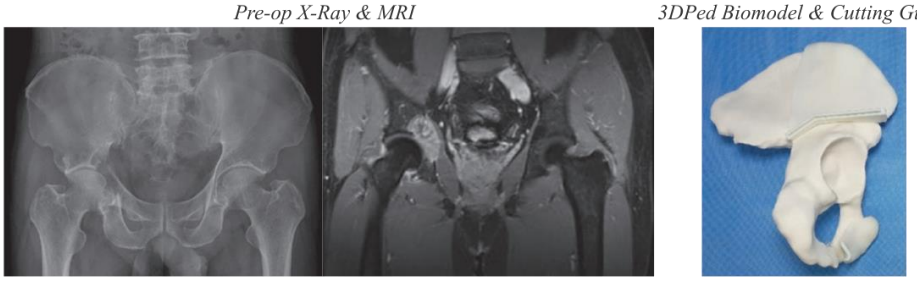

Post-op X-Ray *3DPed Endoprosthesis*

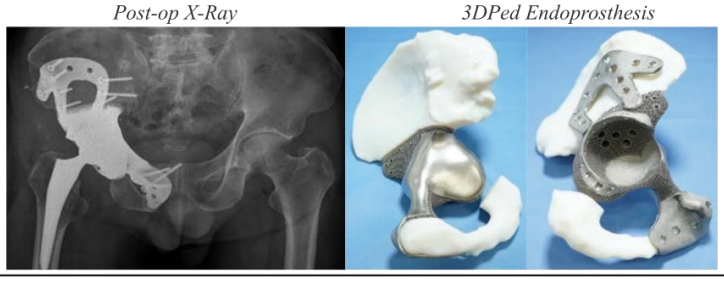

Ewing sarcoma. Solution: Omitting Pubis and Ischium.

Pre-op X-Ray & MRI *3DPed Biomodel & Cutting Guides*

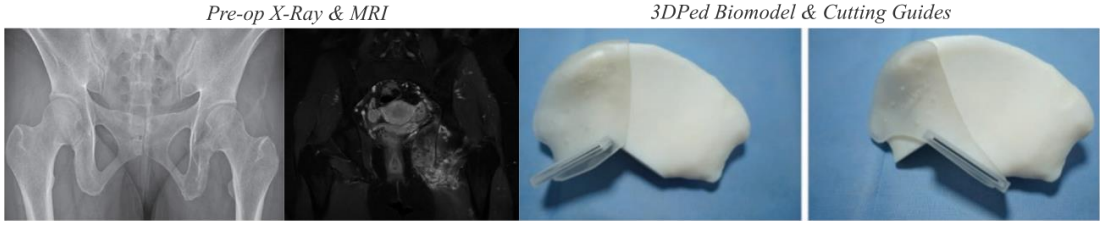

Post-op X-Ray *3DPed Endoprosthesis*

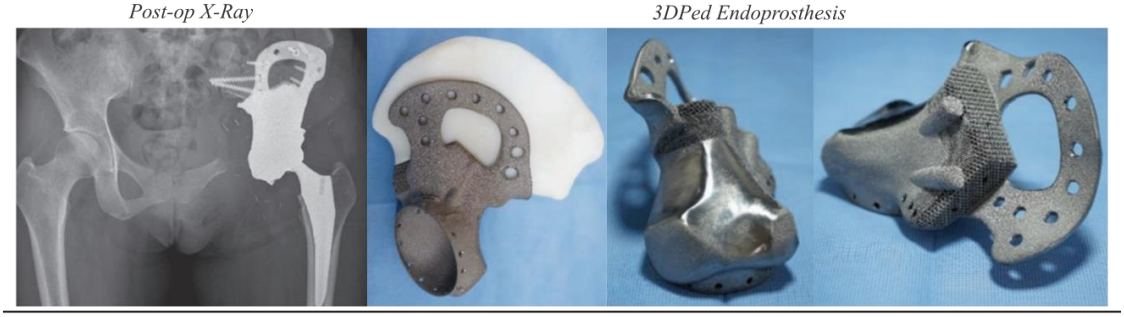

Grade 2 Chondrosarcoma. Solution: Iliac Wing.

Pre-op X-Ray & MRI *3DPed Biomodel & Cutting Guides*

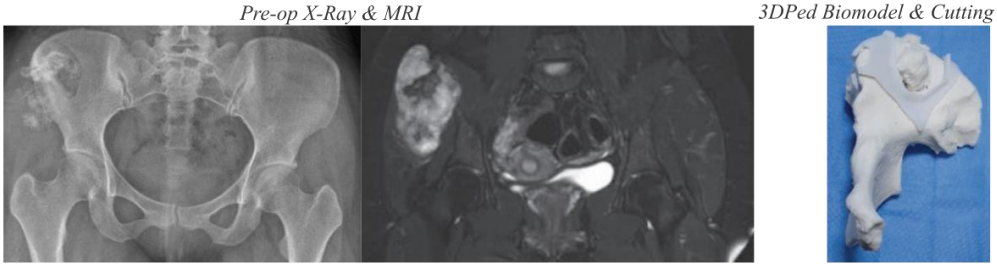

Post-op X-Ray *3DPed Endoprosthesis*

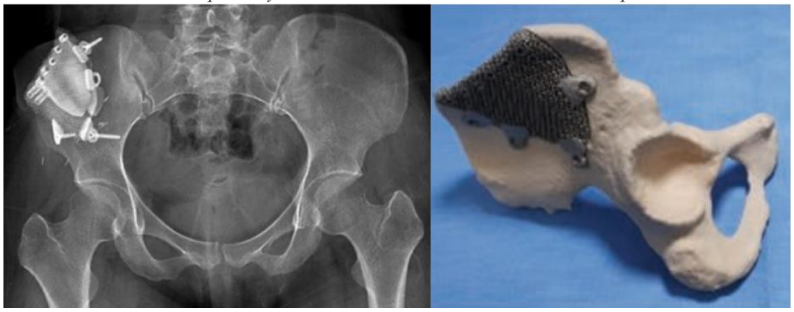

Source: (Kang, 2021)

Gastrointestinal stromal tumor. Solution: Iliac Spacer with Cavitary Resection.

Pre-op X-Ray & MRI *3DPed Biomodel & Cutting Guide*

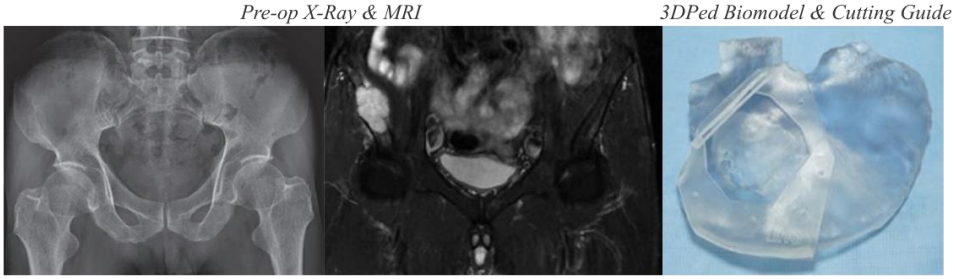

Post-op X-Ray *3DPed Endoprosthesis*

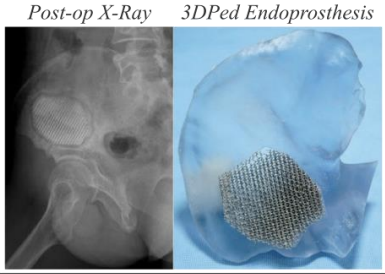

Osteosarcoma. Solution: Acetabular Subchondral Block.

Pre-op X-Ray & MRI *3DPed Biomodel & Cutting Guides*

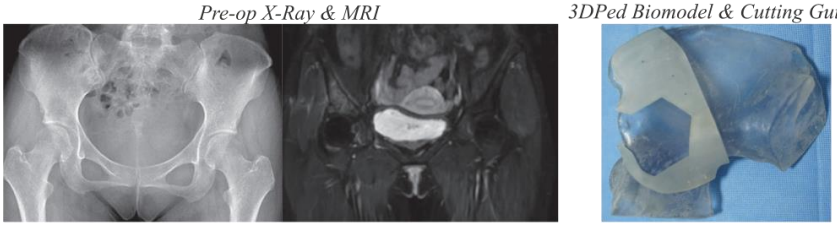

Post-op X-Ray *3DPed Endoprosthesis*

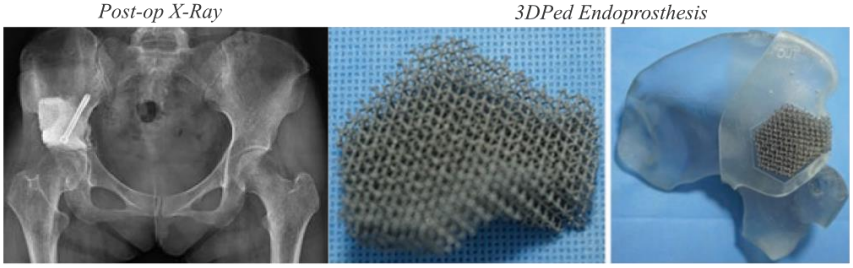

Osteosarcoma. Solution: Iliac Acetabular Block and Plate.

Pre-op X-Ray & MRI *3DPed Biomodel & Cutting Guides*

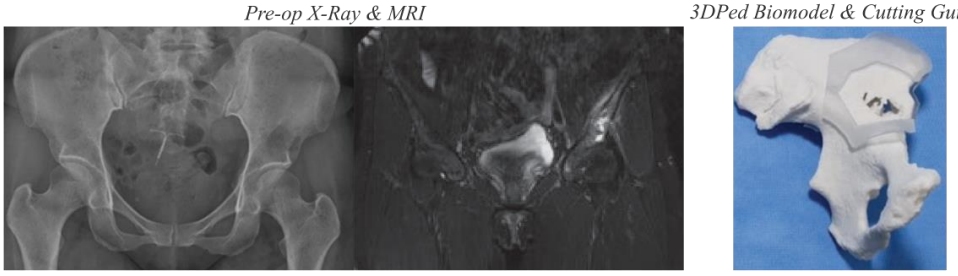

Post-op X-Ray *3DPed Endoprosthesis*

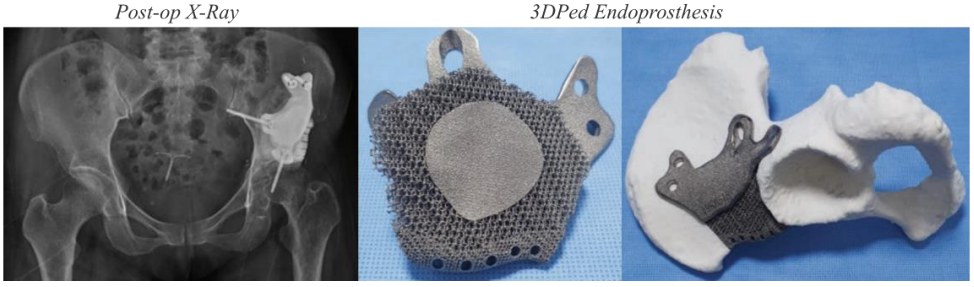

Source: (Kang, 2021)

Grade 2 Chondrosarcoma. Pubis Preventing Genital Deformity and Hernia.

Pre-op CT & MRI *3DPed Biomodel & Cutting Guide*

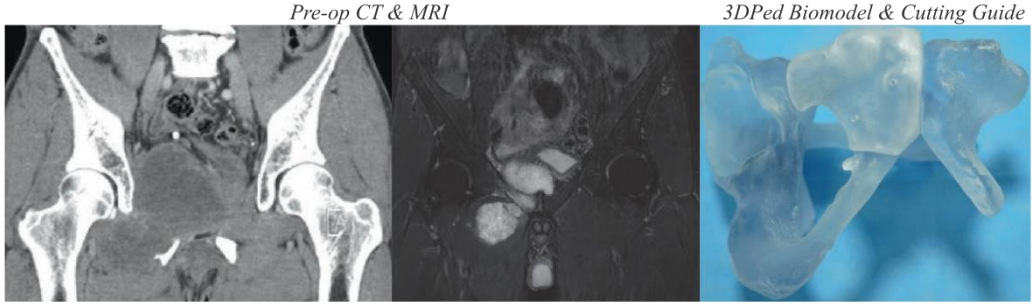

Post-op X-Ray *3DPed Endoprosthesis*

Ewing sarcoma. Solution: Pubis with Acetabular Preservation.

Pre-op X-Ray & MRI *3DPed Biomodel & Cutting Guides*

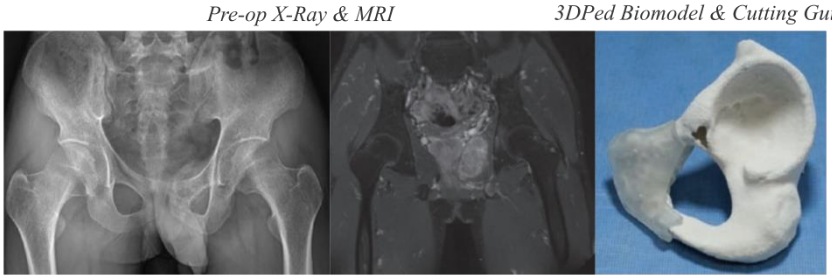

Post-op X-Ray *3DPed Endoprosthesis*

Acetabular fracture. Solution: Acetabular Reinforcement Cage.

Pre-op X-Ray *Post-op X-Ray* *3DPed Biomodel & Endoprosthesis*

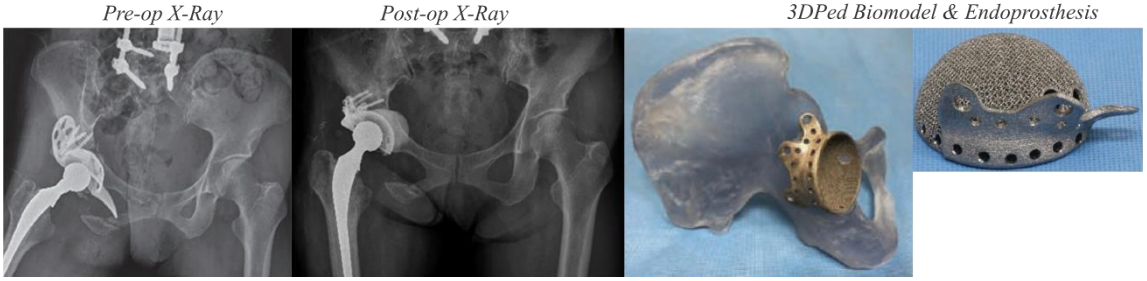

Source: (Kang, 2021)

Revision: Failed Allograft Bone Reconstruction.

Pre-op X-Ray *3DPed Biomodel & Cutting Guide*

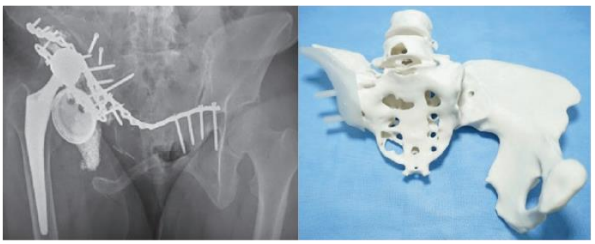

Post-op X-Ray *3DPed Endoprosthesis*

Revision: Failed Total Hip Arthroplasty.

Pre-op X-Ray *3DPed Biomodel & Cutting Guides*

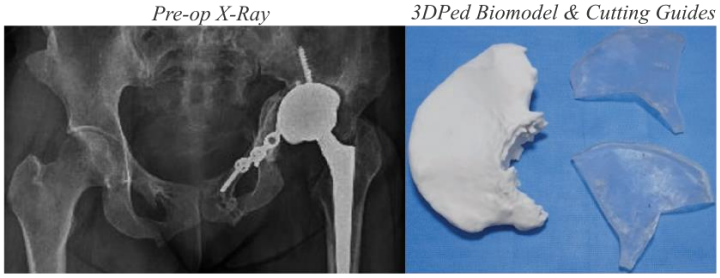

Post-op X-Ray *3DPed Endoprosthesis*

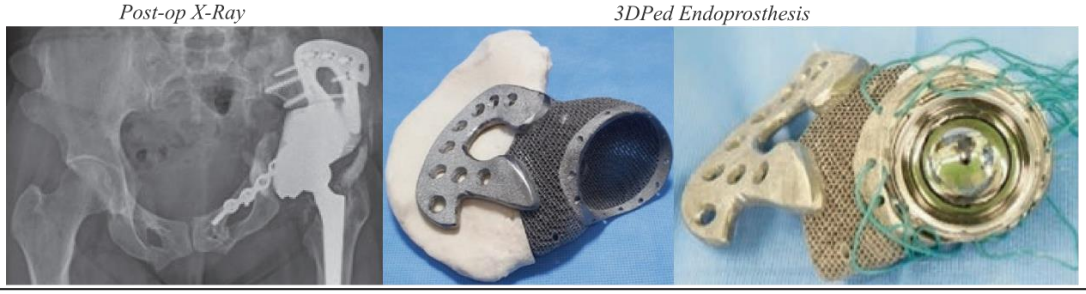

Revision: Complicated Saddle Prosthesis.

Pre-op X-Ray *3DPed Biomodel & Endoprosthesis*

Post-op X-Ray *3DPed Endoprosthesis*

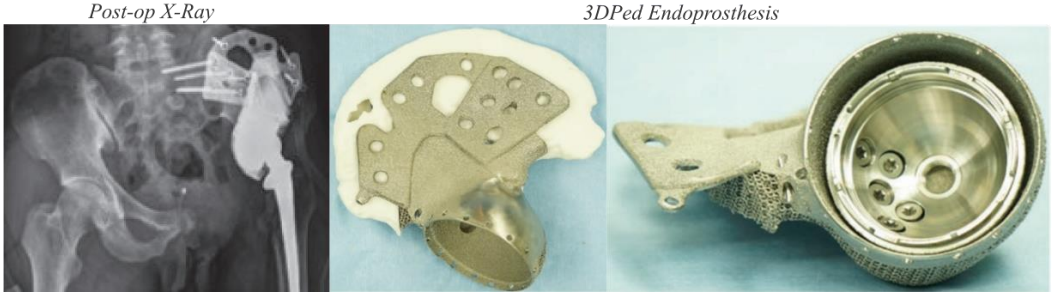

Source: (Kang, 2021)

Femoral Melorheostosis. Solution: Plate with Reinforcement Ridge.

Pre-op X-Ray *3DPed Biomodel & Cutting Guide* *Post-op X-Ray* *3DPed Endoprosthesis*

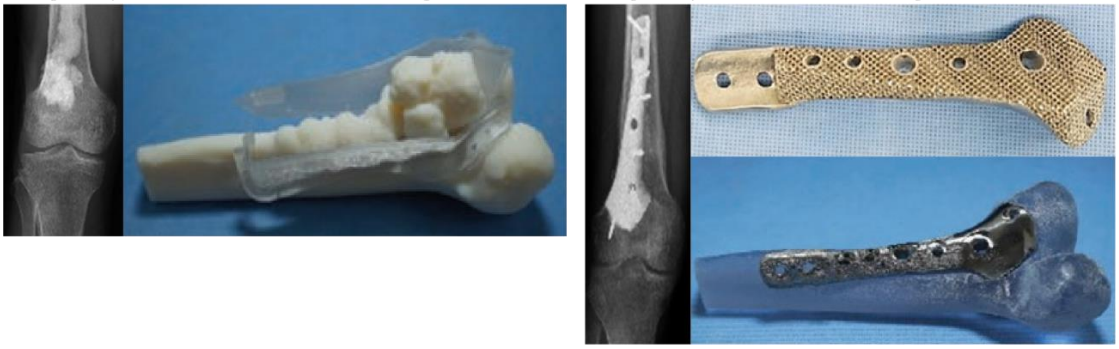

Femoral giant cell tumor. Solution: Posterior Intercondylar Y Plate.

Pre-op X-Ray *3DPed Biomodel & Cutting Guides* *Post-op X-Ray* *3DPed Endoprosthesis*

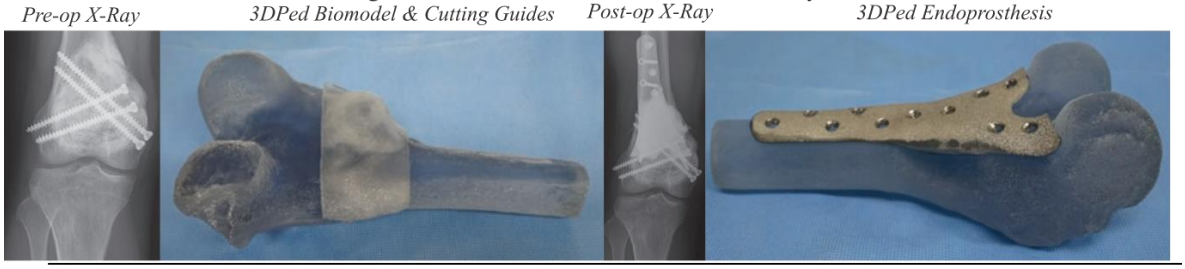

Femoral spindle cell sarcoma. Solution: Segmental Distal Femur Combined with IM Nail.

Pre-op X-Ray *3DPed Biomodel & Endoprosthesis* *Post-op X-Ray* *3DPed Endoprosthesis*

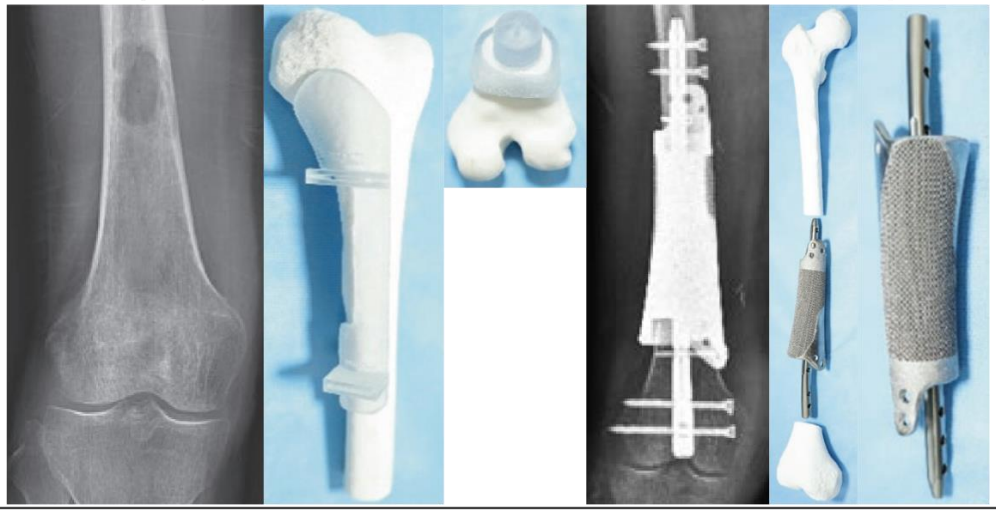

Femoral metastatic bone cancer. Solution: Cortical Mesh Covering IM Nail and Cement.

Pre-op X-Ray & MRI *3DPed Biomodel & Endoprosthesis* *Post-op X-Ray*

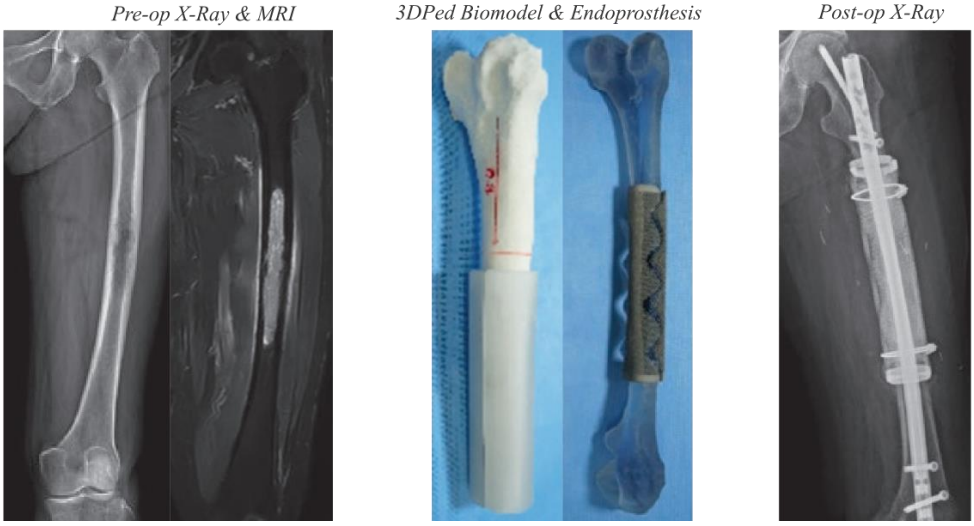

Source: (Kang, 2021)

Femoral fibrous dysplasia. Solution: Open Wedge Spacer and Supporting Plate.

Pre-op X-Ray *3DPed Cutting Guide* *Post-op X-Ray* *3DPed Endoprosthesis*

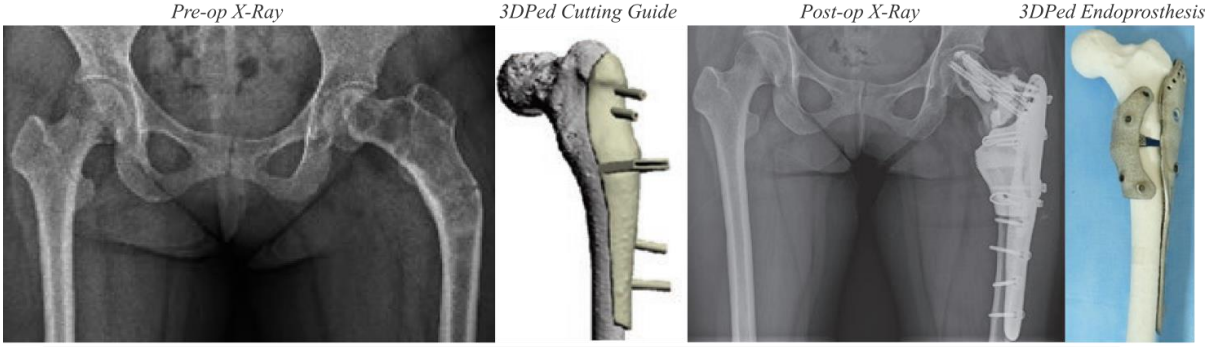

Tibial Adamantinoma. Segmental Tibia Diaphysis.

Pre-op X-Ray *3DPed Biomodel & Cutting Guides* *3DPed Endoprosthesis* *Post-op X-Ray*

Osteosarcoma. Proximal Tibia for Knee Joint Preserving.

Pre-op X-Ray *3DPed Biomodel & Endoprosthesis* *Post-op X-Ray* *3DPed Endoprosthesis*

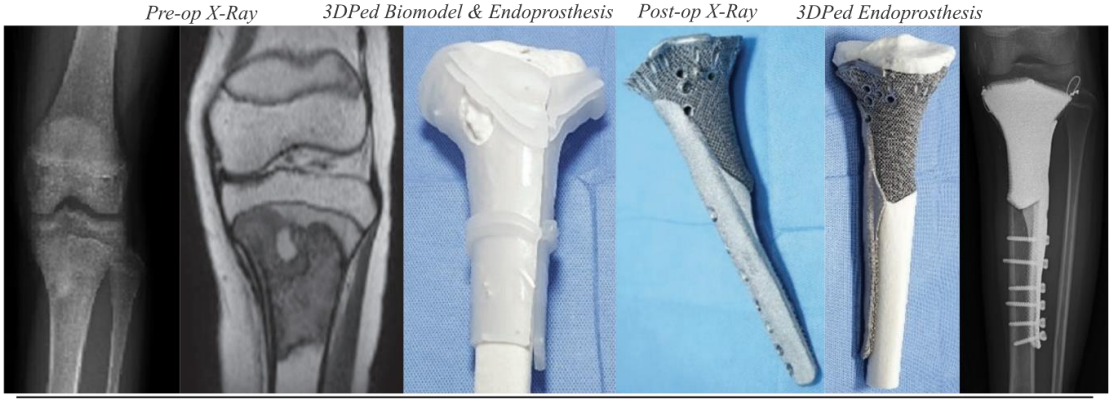

Osteosarcoma. Tibia Assembled with Knee Artifcial Joint Surface.

Pre-op X-Ray & MRI *3DPed Biomodel & Endoprosthesis* *Post-op X-Ray*

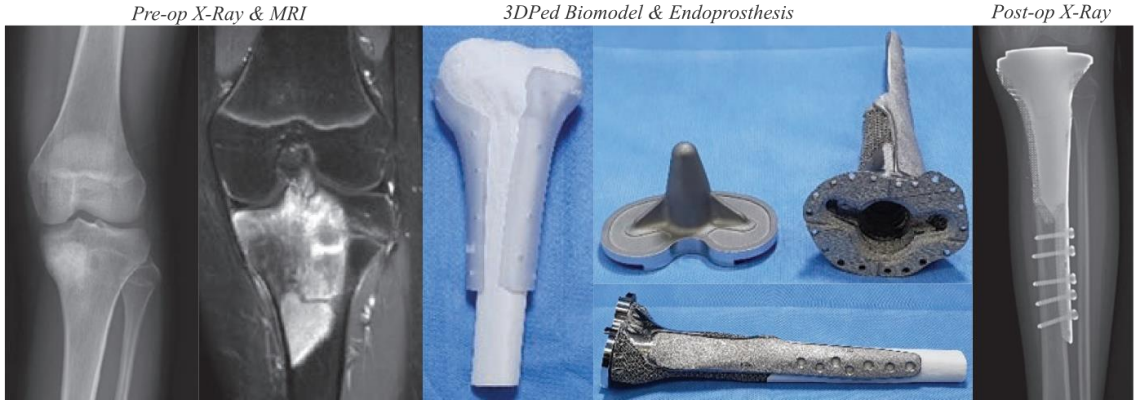

Source: (Kang, 2021)

Calcaneal Desmoid tumor.

Pre-op X-Ray & MRI *3DPed Endoprosthesis* *Post-op X-Ray*

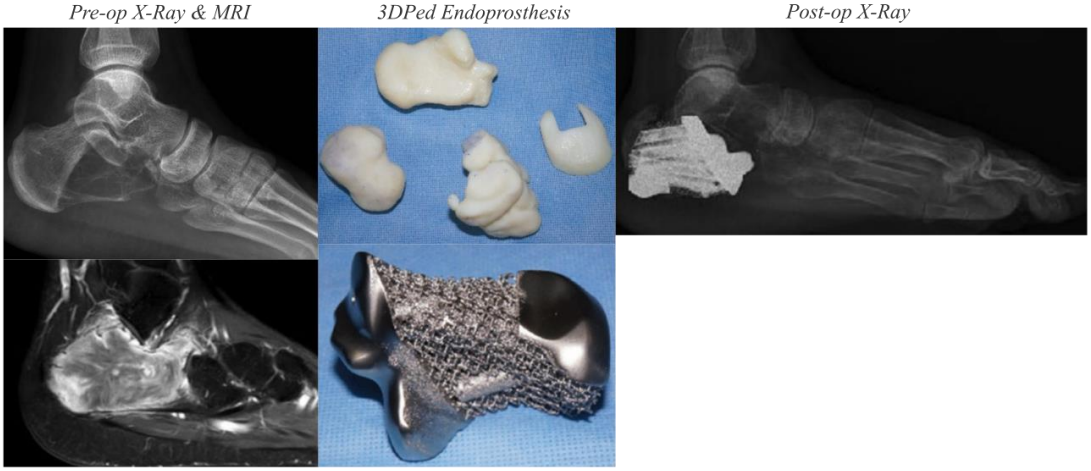

Scapular Grade 2 Chondrosarcoma. Scapula Combined with Reverse Shoulder Arthroplasty.

Pre-op X-Ray & MRI *3DPed Biomodel & Cutting Guides & Endoprosthesis* *Post-op X-Ray*

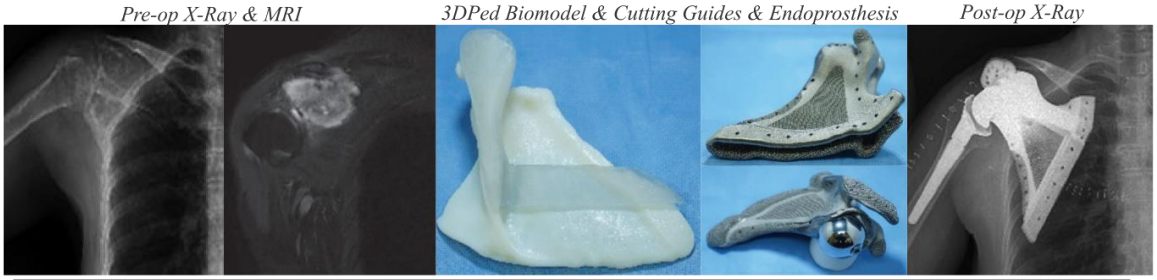

Ewing sarcoma. Scapula Combined with Glenoid of Conventional Shoulder System.

Pre-op X-Ray & MRI *3DPed Endoprosthesis* *Post-op X-Ray*

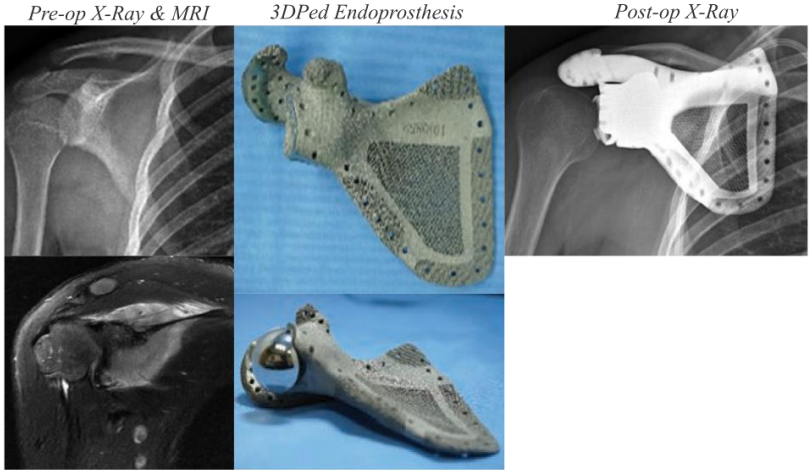

Osteosarcoma. Distal Humerus for Assembly with Tumor Prosthesis.

Pre-op X-Ray & MRI *3DPed Biomodel & Cutting Guides & Endoprosthesis* *Post-op X-Ray*

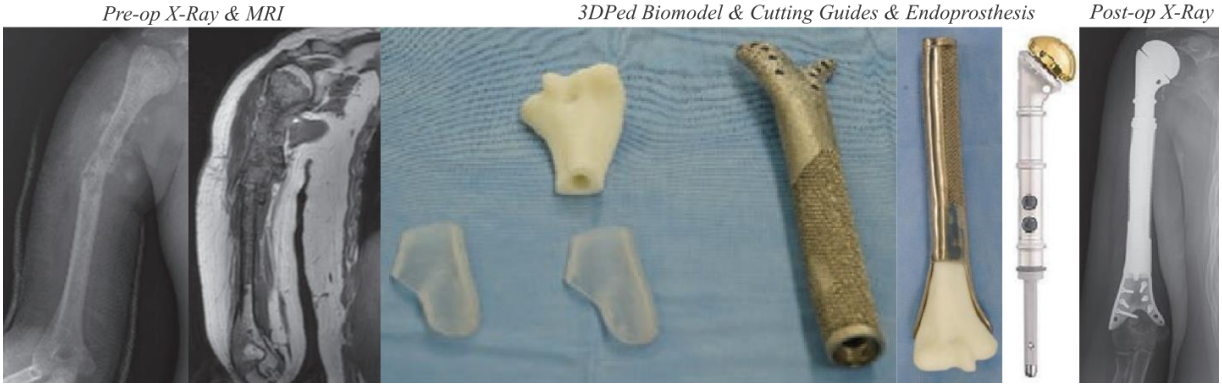

Source: (Kang, 2021)

Allograft failure. Partial Elbow Joint.

Pre-op X-Ray *3DPed Biomodel & Cutting Guides & Endoprosthesis* *Post-op X-Ray*

Aggressive fbromatosis. Radius & Ulna and Implant-Bone Connector.

Pre-op X-Ray & MRI *3DPed Biomodel & Cutting Guides & Endoprosthesis* *Post-op X-Ray*

Source: (Kang, 2021)

Defect of the left and right acetabulum.

Revision of a periprosthetic infection of the right knee joint.

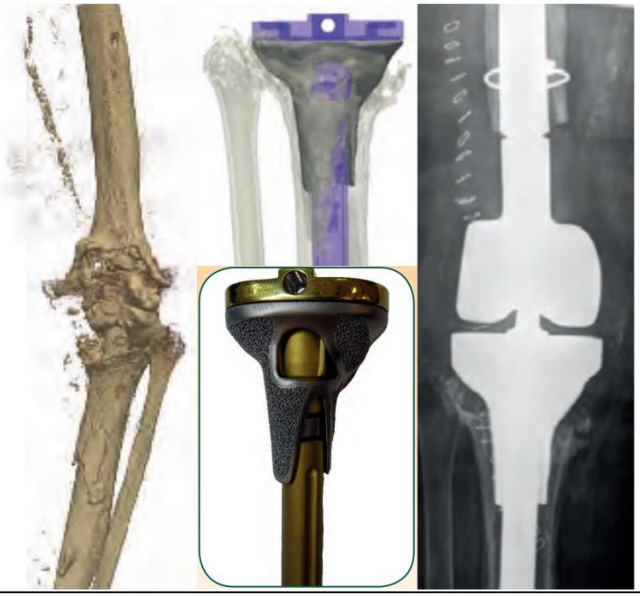

Osteosarcoma.

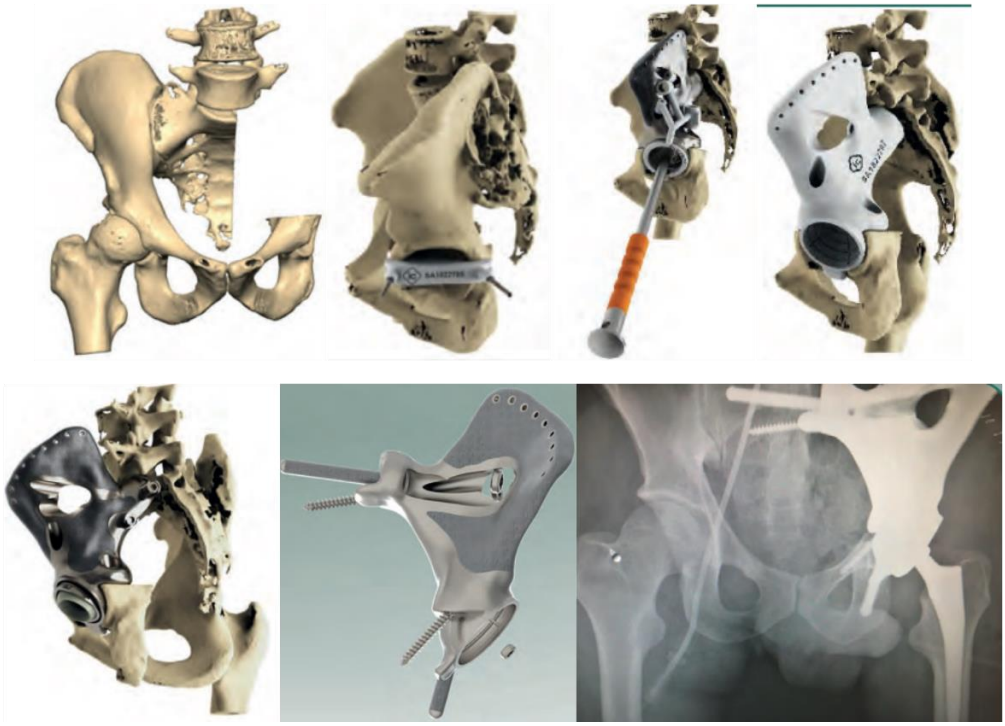

Source: (Implantcast, 2019)

Tumour in the distal femur.

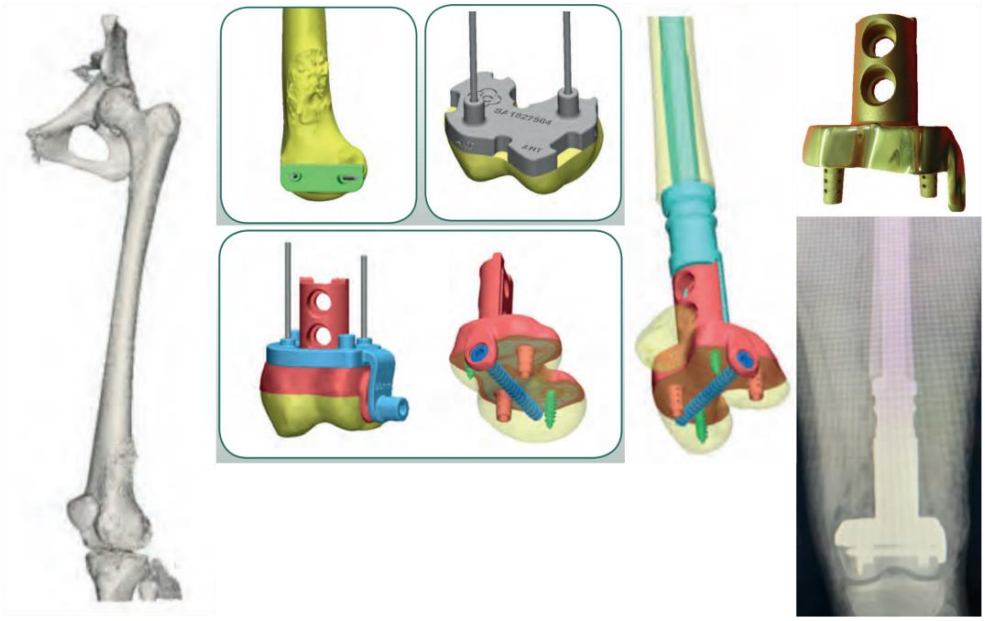

Recurrence of chondrosarcoma to the distal part of the humerus.

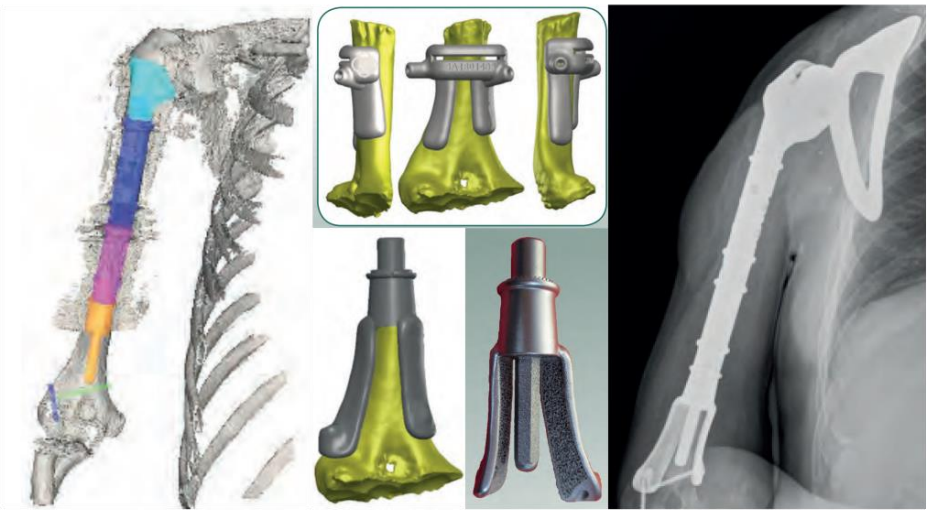

Revision of a large defect of the acetabulum after implant loosening.

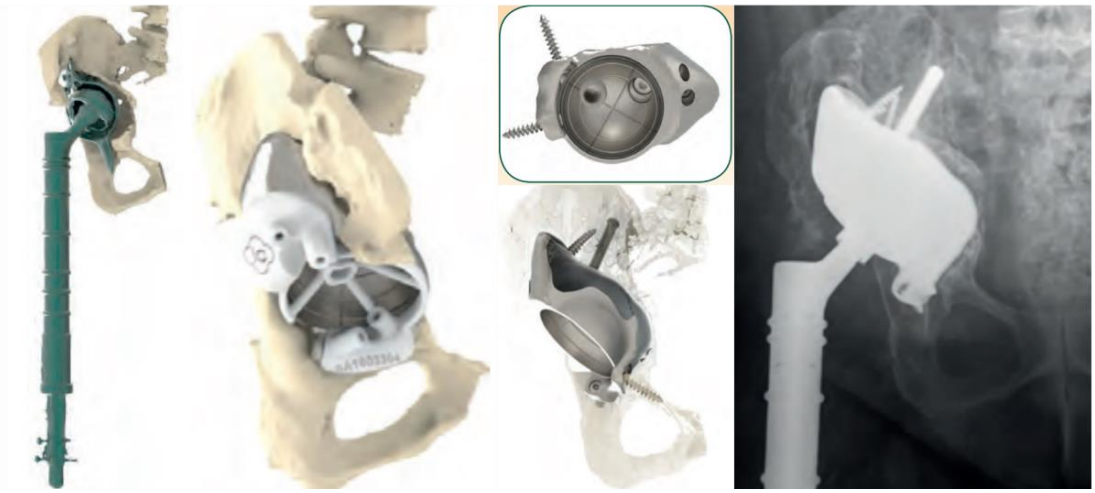

Source: (Implantcast, 2019)

Giant cell tumour of the second metacarpal bone.

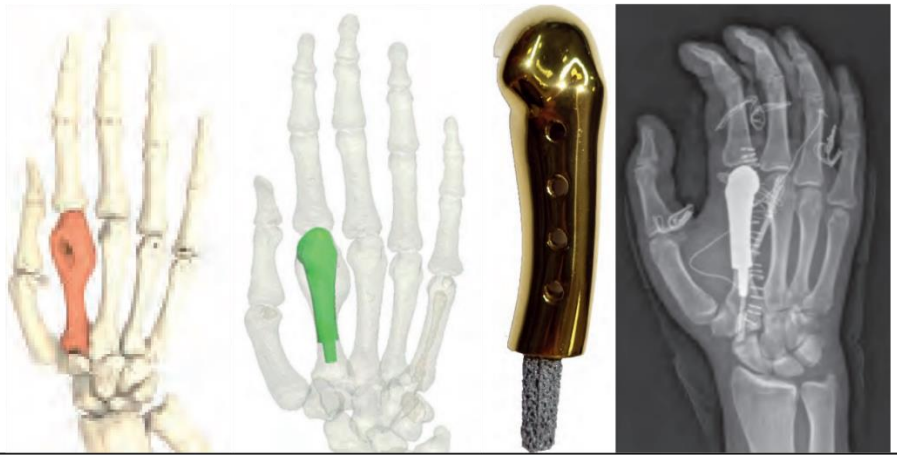

Chondrosarcoma of sternum.

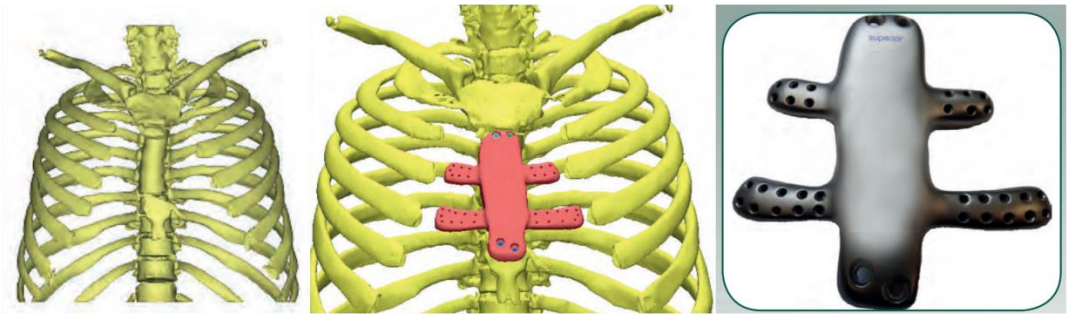

Osteosarcoma of the distal femur.

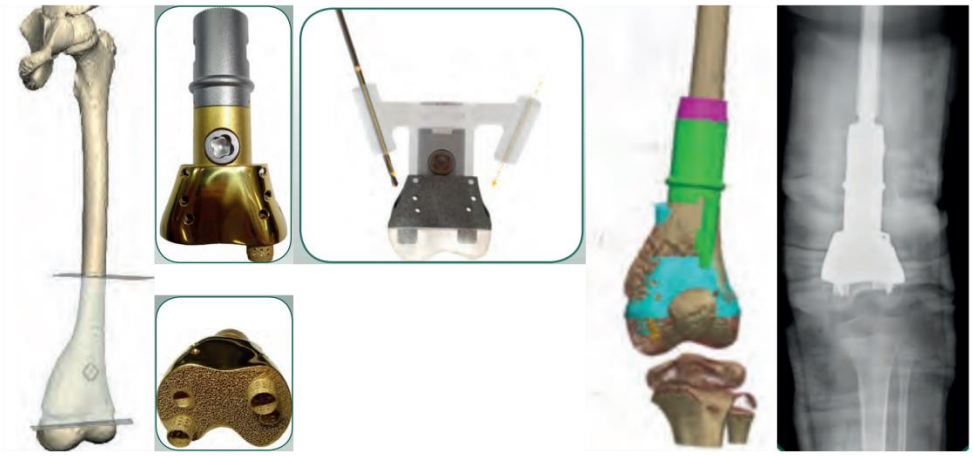

Osteosarcoma of the right distal tibia.

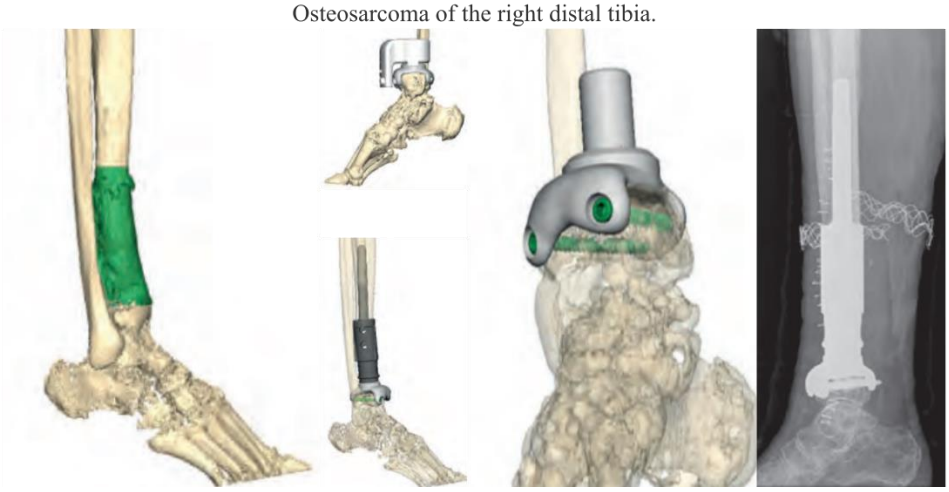

Source: (Implantcast, 2019)

Chondroblastoma of the glenoid.

Ewing´s sarcoma of the left scapula.

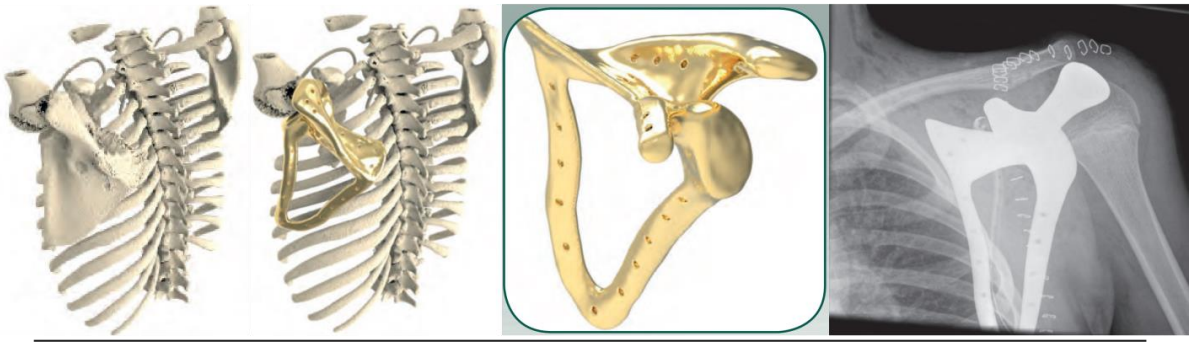

Bone loss of the distal humerus.

Osteosarcoma of distal left radius.

Source: (Implantcast, 2019)

Giant cell tumour.

Neuropathic osteoarthropathy, Charcot-Marie-Tooth-Syndrom.

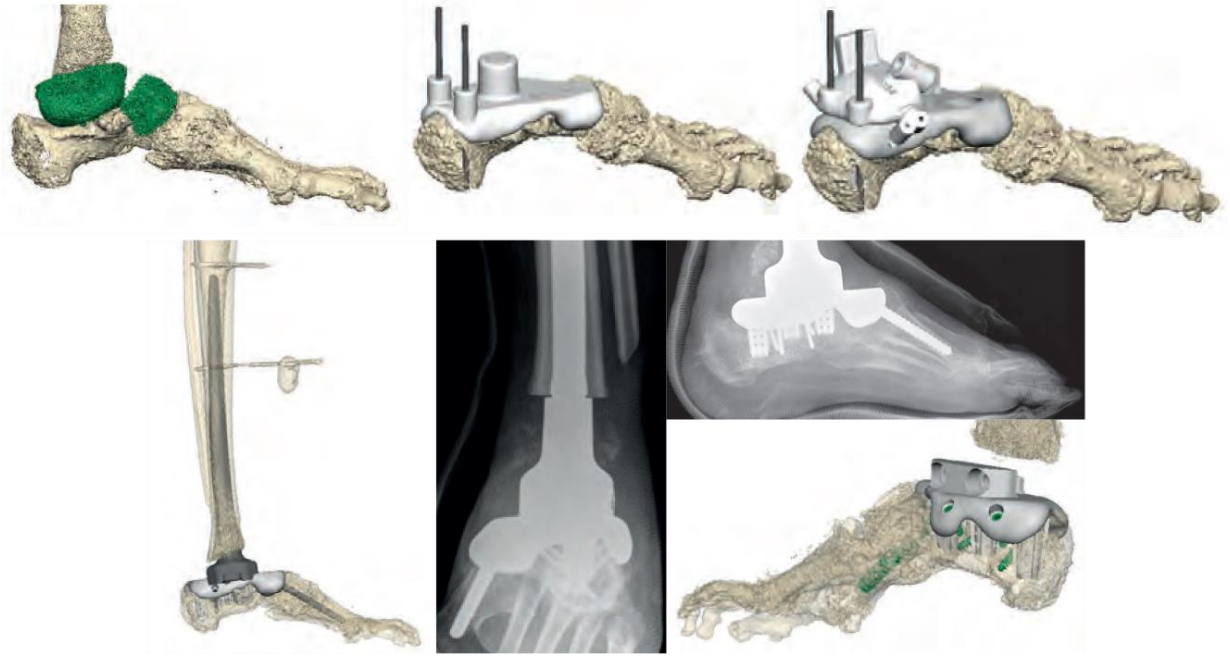

Ewing‘s sarcoma of the proximal phalanx.

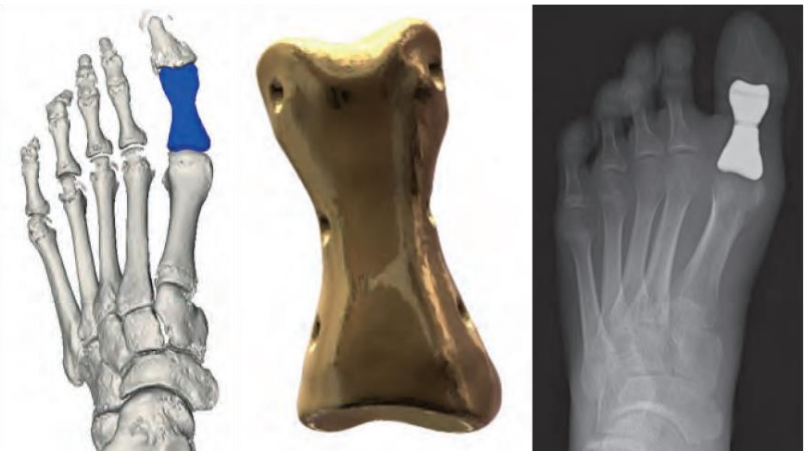

Source: (Implantcast, 2019)

Chondrosarcoma.

Chondrosarcoma.

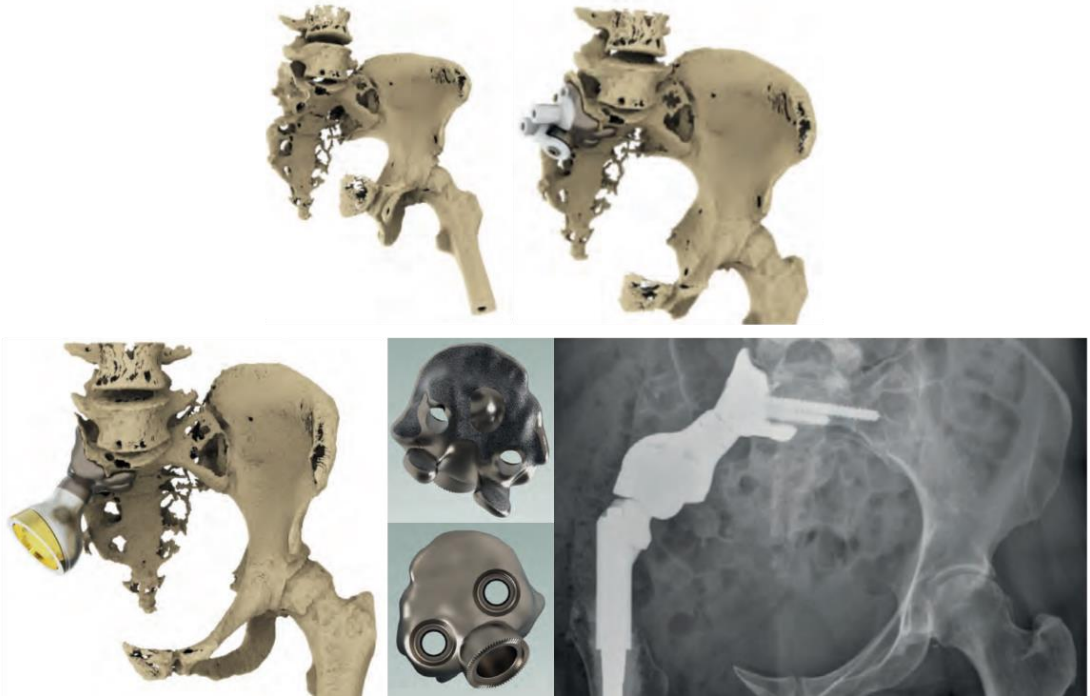

Source: (Implantcast, 2019)

11.11 Appendix K: Bone tumor types and statistics

Chondrogenic tumors
- *Benign*
  - Subungual exostosis
  - Bizarre parosteal osteochondromatous proliferation
  - Periosteal chondroma
  - Enchondroma
  - Osteochondroma
  - Chondroblastoma NOS
  - Chondromyxoid fibroma
  - Osteochondromyxoma
- *Intermediate (locally aggressive)*
  - Chondromatosis NOS
  - Atypical cartilaginous tumor
- *Malignant*
  - Chondrosarcoma, grades 1
  - Chondrosarcoma, grades 2
  - Chondrosarcoma, grades 3
  - Periosteal chondrosarcoma
  - Clear cell chondrosarcoma
  - Mesenchymal chondrosarcoma
  - Dedifferentiated chondrosarcoma

Osteogenic tumors
- *Benign*
  - Osteoma NOS
  - Osteoid osteoma NOS
- *Intermediate (locally aggressive)*
  - Osteoblastoma NOS
- *Malignant*
  - Low-grade central osteosarcoma
  - Osteosarcoma NOS
    - Conventional osteosarcoma
    - Telangiectatic osteosarcoma
    - Small cell osteosarcoma
  - Parosteal osteosarcoma
  - Periosteal osteosarcoma
  - High-grade surface osteosarcoma
  - Secondary osteosarcoma

Fibrogenic tumors
- *Intermediate (locally aggressive)*
  - Desmoplastic fibroma
- *Malignant*
  - Fibrosarcoma NOS

Vascular tumors of bone
- *Benign*
  - Hemangioma NOS
- *Intermediate (locally aggressive)*
  - Epithelioid hemangioma
- *Malignant*
  - Epithelioid hemangioendothelioma NOS
  - Angiosarcoma

Osteoclastic giant cell-rich tumors
- *Benign*
  - Aneurysmal bone cyst
  - Non-ossifying fibroma
- *Intermediate (locally aggressive, rarely metastasizing)*
  - Giant cell tumor of bone NOS
- *Malignant*
  - Giant cell tumor of bone, malignant

Notochordal tumors
- *Benign*
  - Benign notochordal cell tumor
- *Malignant*
  - Chordoma NOS
    - Chondroid chordoma
  - Poorly differentiated chordoma
  - Dedifferentiated chordoma

Other mesenchymal tumors of bone
- *Benign*
  - Chondromesenchymal hamartoma of chest wall
  - Simple bone cyst
  - Fibrous dysplasia
  - Osteofibrous dysplasia
  - Lipoma NOS
  - Hibernoma
- *Intermediate (locally aggressive)*
  - Osteofibrous dysplasia-like adamantinoma
  - Mesenchymoma NOS
- *Malignant*
  - Adamantinoma of long bones
    - Dedifferentiated adamantinoma
  - Leiomyosarcoma NOS
  - Pleomorphic sarcoma, undifferentiated
  - Bone metastases

Hematopoietic neoplasms of bone
- Plasmacytoma of bone
- Malignant lymphoma, non-Hodgkin, NOS
- Hodgkin disease NOS
- Diffuse large B-cell lymphoma NOS
- Follicular lymphoma NOS
- Marginal zone B-cell lymphoma NOS
- T-cell lymphoma NOS
- Anaplastic large cell lymphoma NOS
- Malignant lymphoma, lymphoblastic, NOS
- Burkitt lymphoma NOS
- Langerhans cell histiocytosis NOS
- Langerhans cell histiocytosis, disseminated
- Erdheim-Chester disease
- Rosai-Dorfman disease

NOS indicates not otherwise specified.

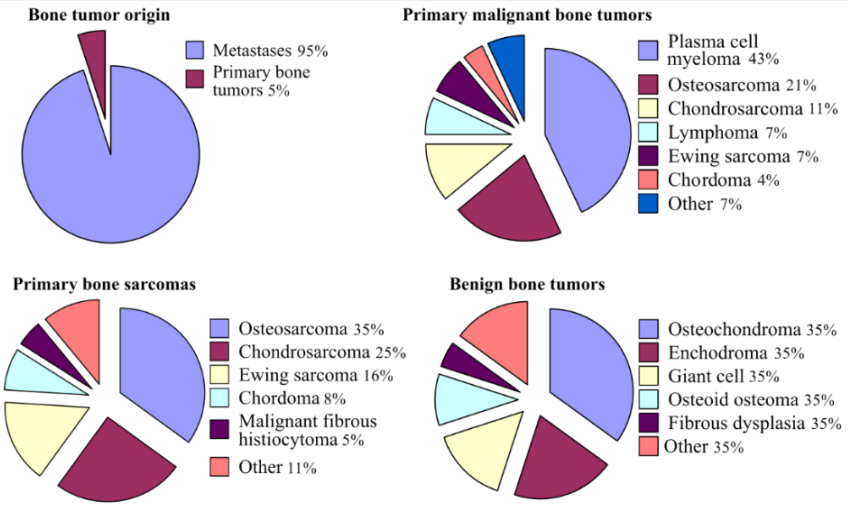

Source: (Choi and Ro, 2021) and (Murphey, 2006)

11.12 Appendix L: Anatomy of the pelvis

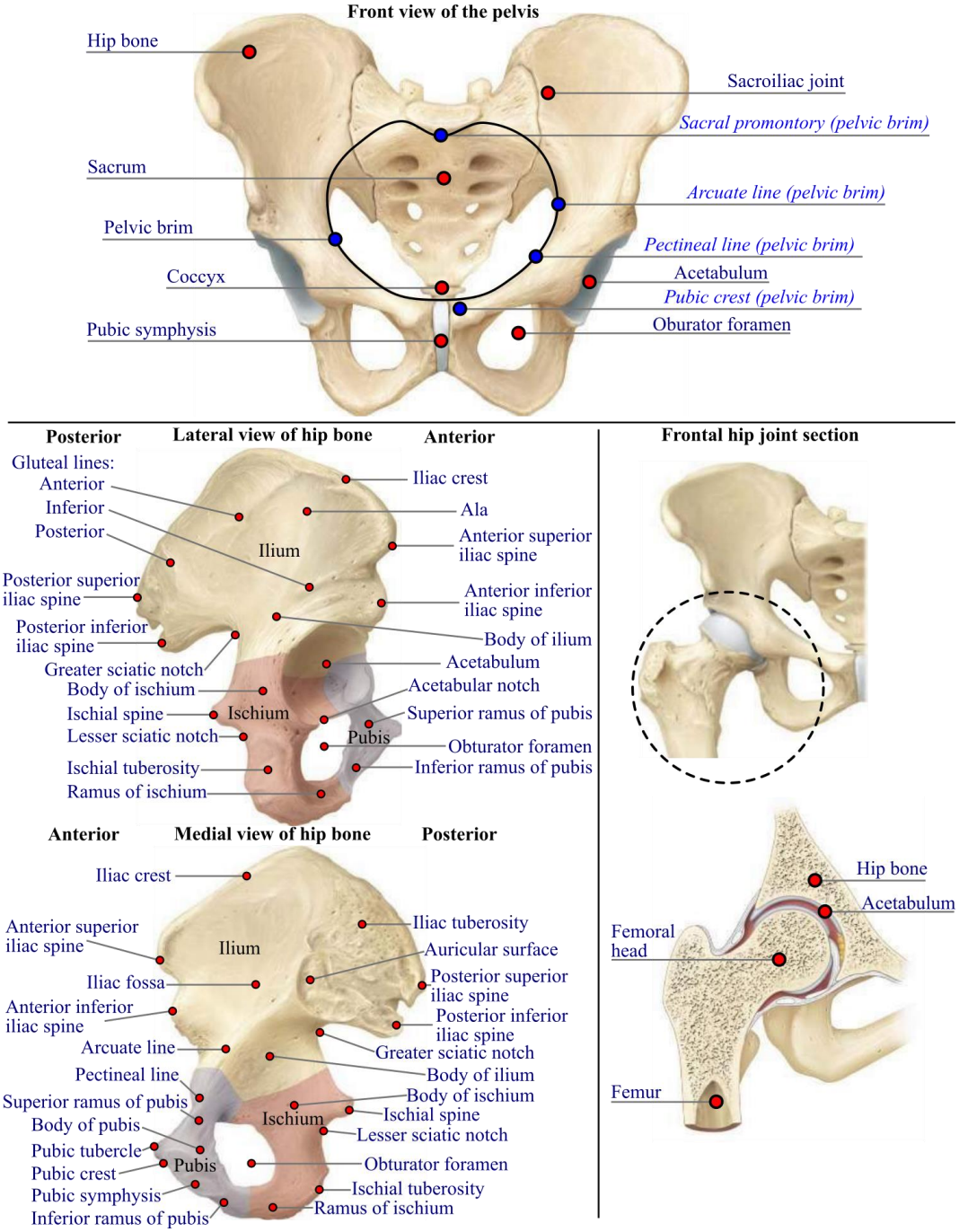

Bony pelvis. Source: (Tortora and Derrickson, 2020)

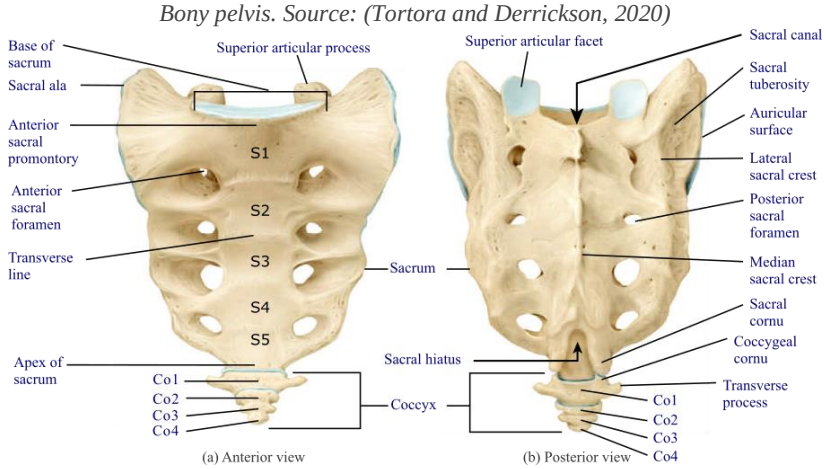

Sacrum anatomy. Source: (Tortora and Derrickson, 2020)

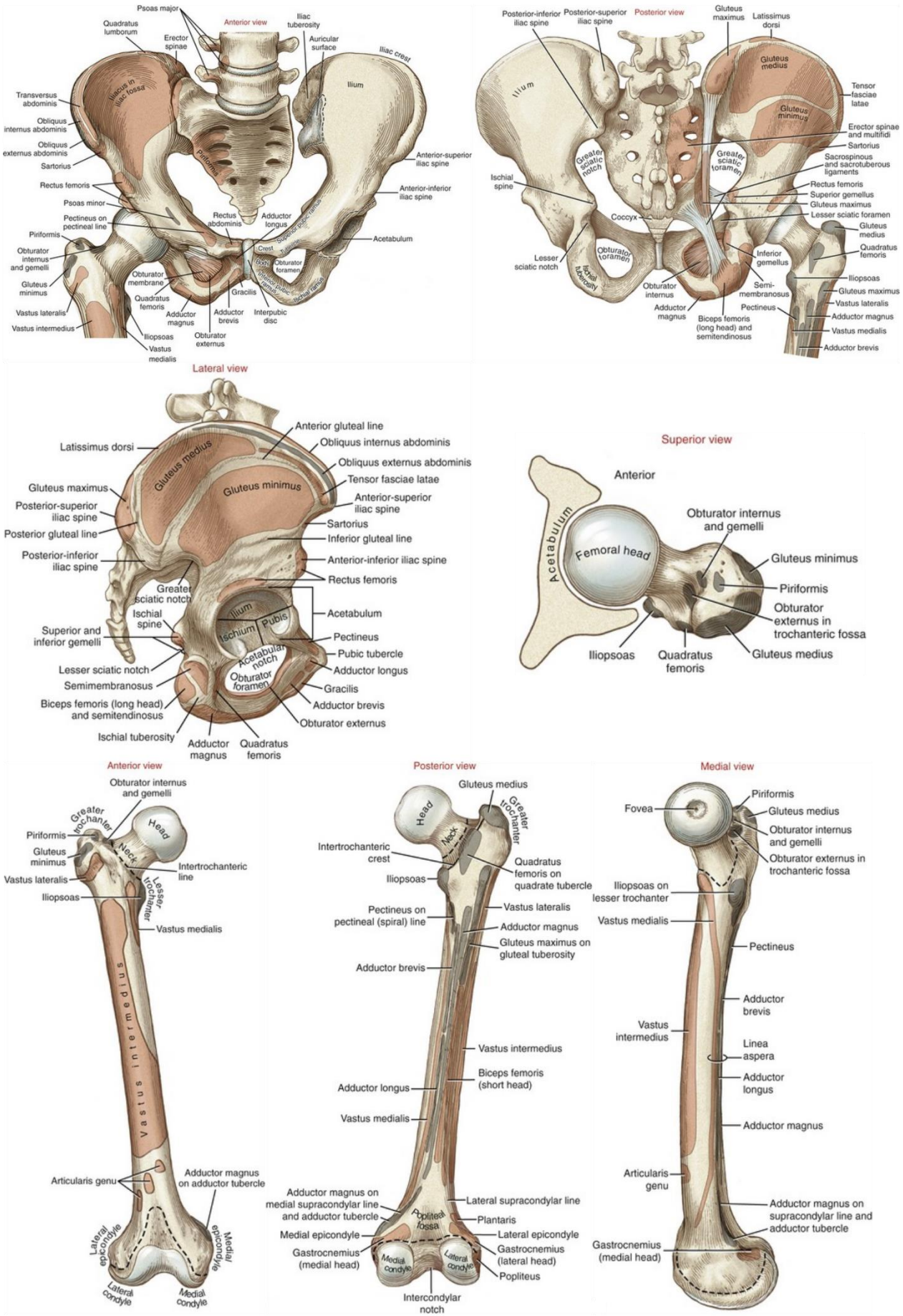

Muscle attachments on bony pelvis and femur. Source: clinicalgate.com

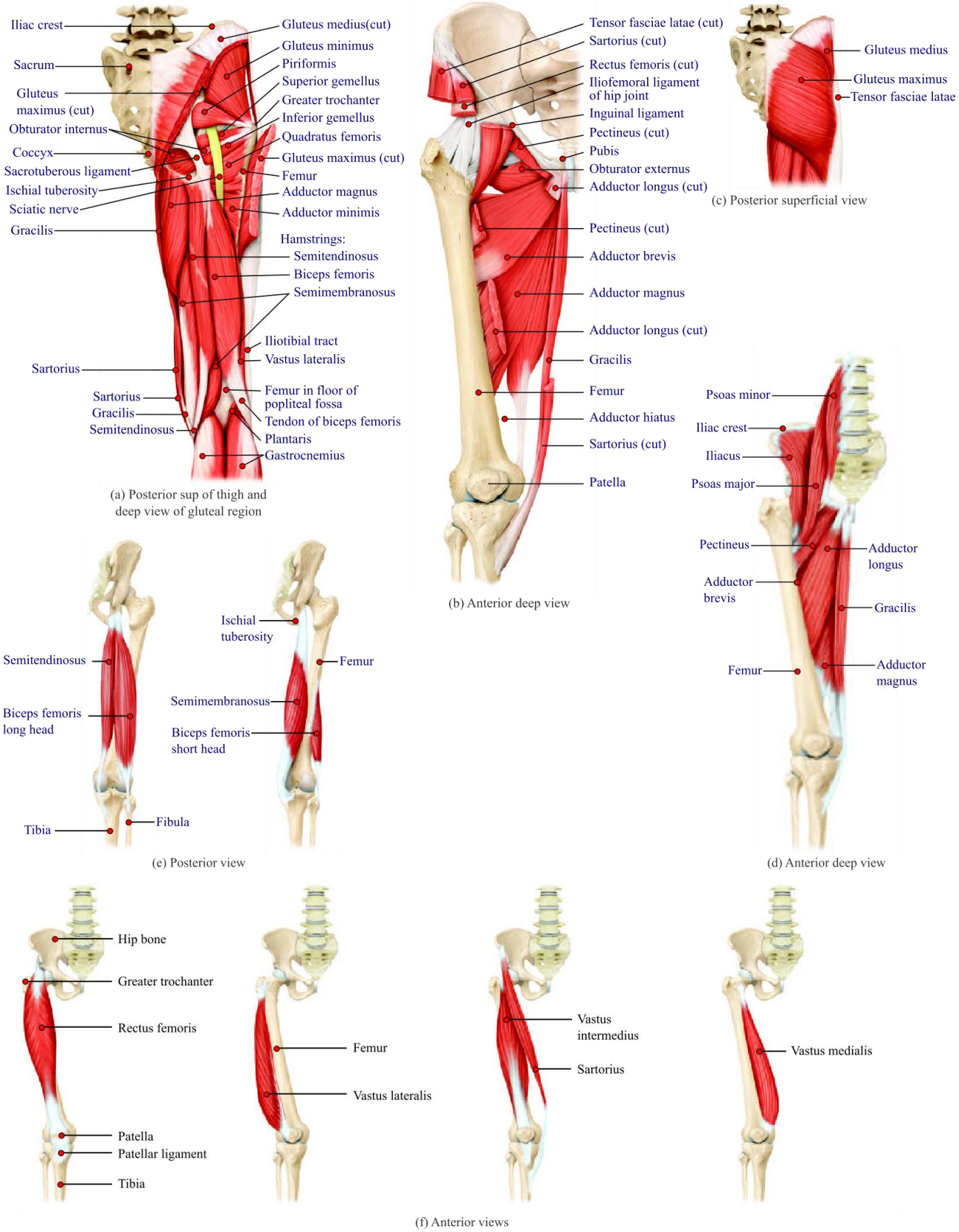

Muscles of the pelvis and femur. Source: (Tortora and Derrickson, 2020)

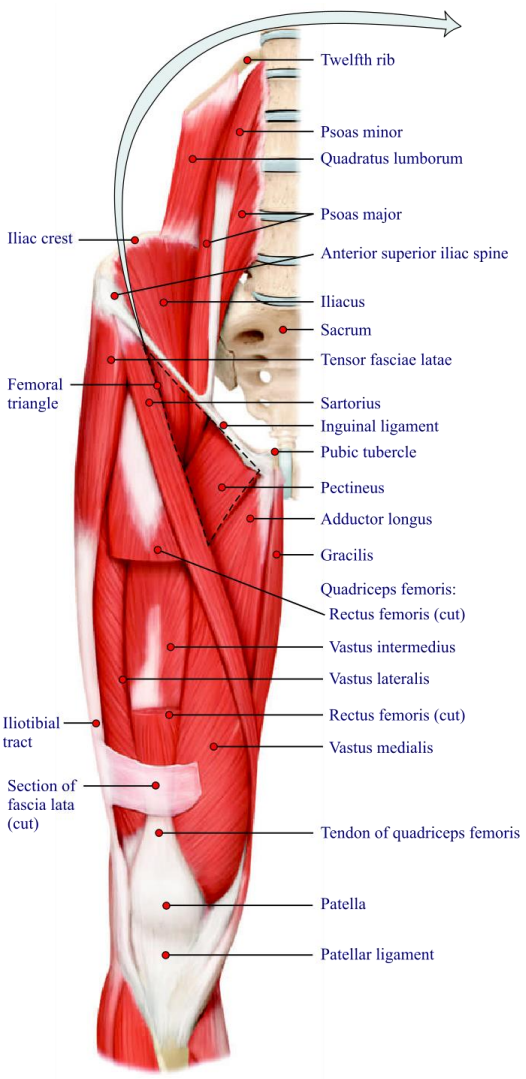

Anterior superficial view (the femoral triangle is indicated by a dashed line)

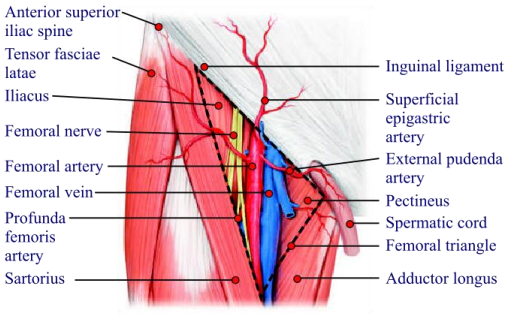

Details of femoral triangle

Muscles of the pelvis. Source: (Tortora and Derrickson, 2020)

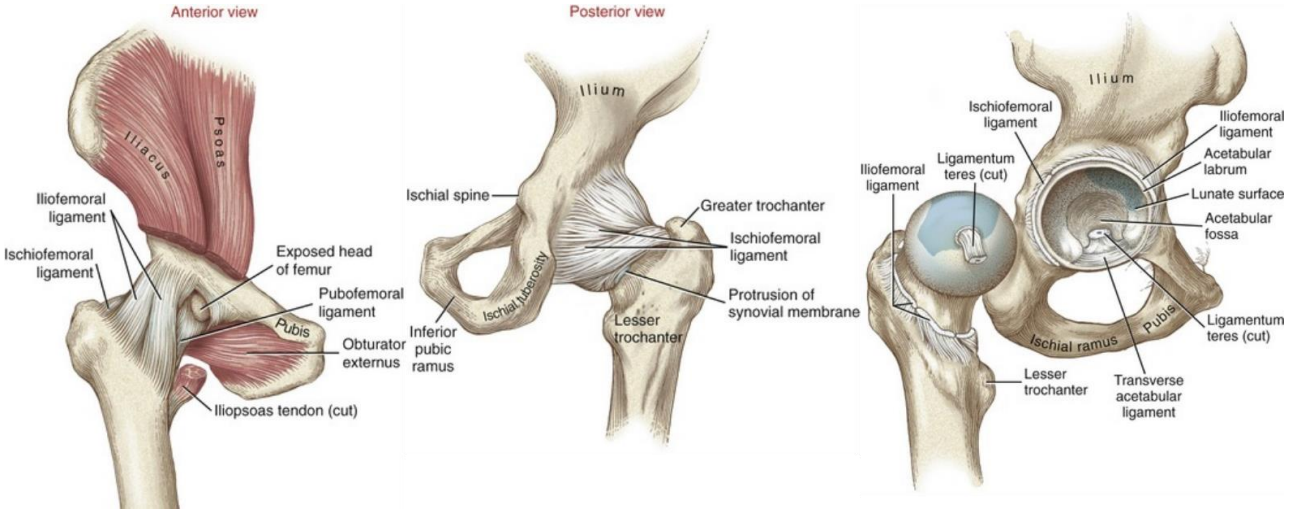

Hip joint mechanism and lignmaments. Source: clinicalgate.com

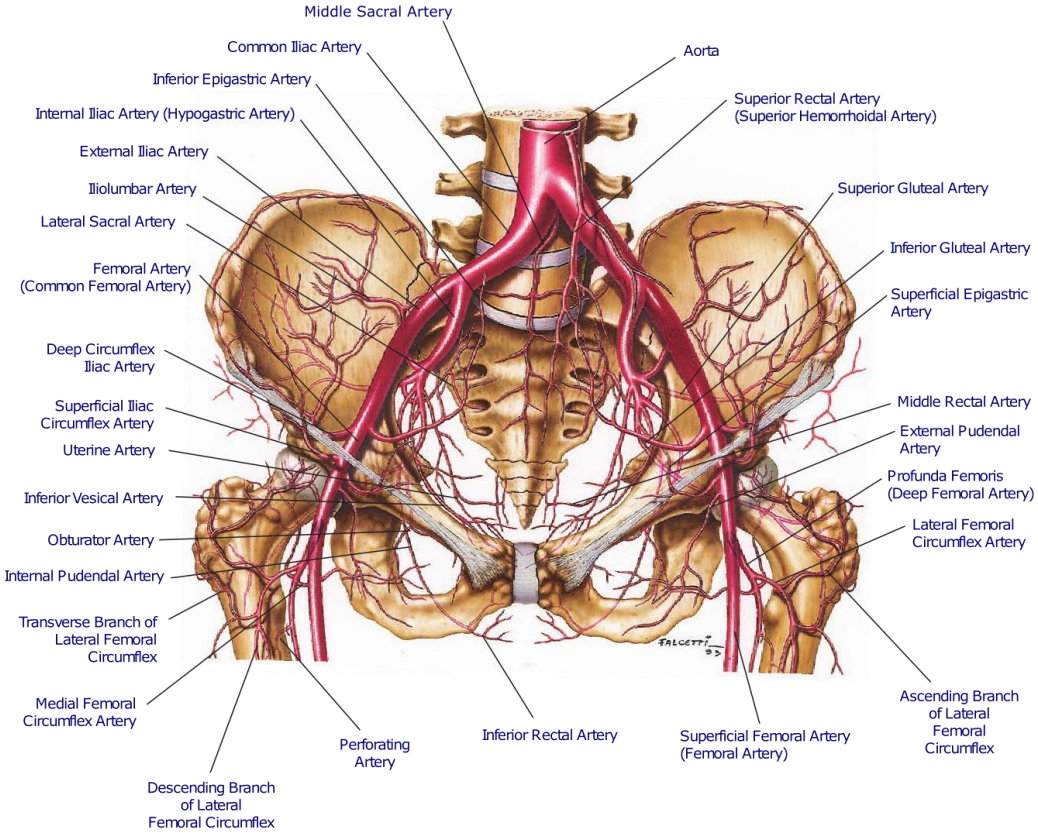

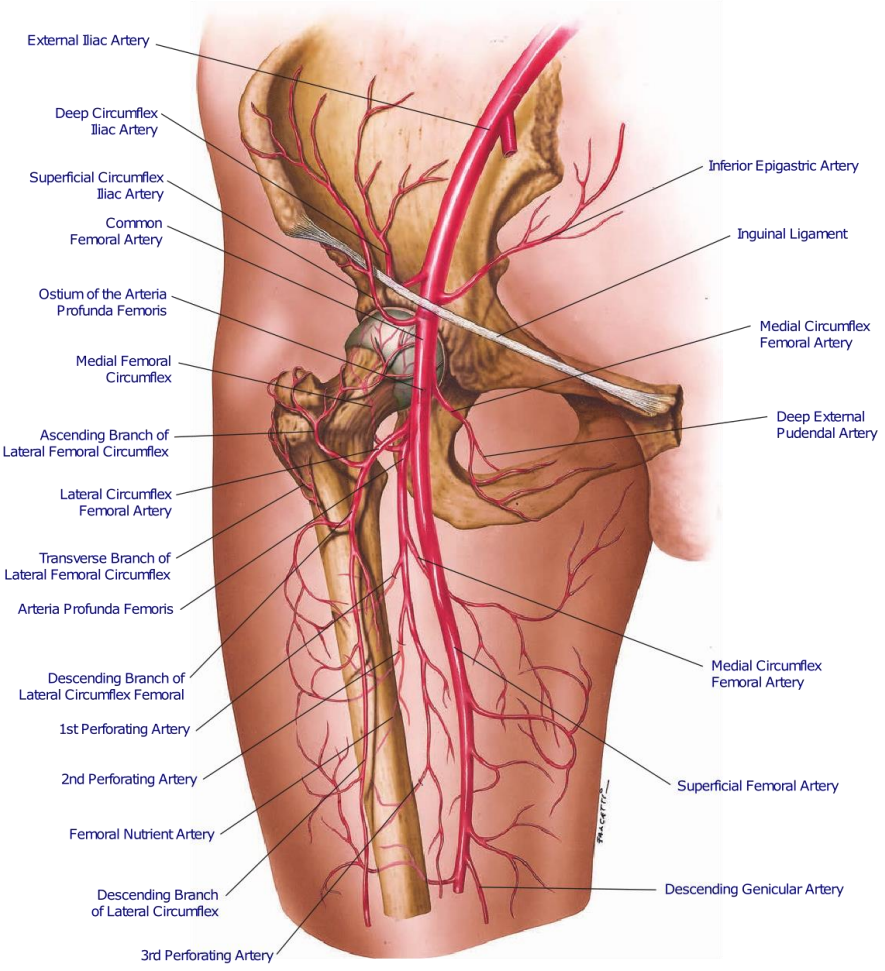

Vascular system (arteries) of the pelvis and femur. Source: (Uflacker, 2007)

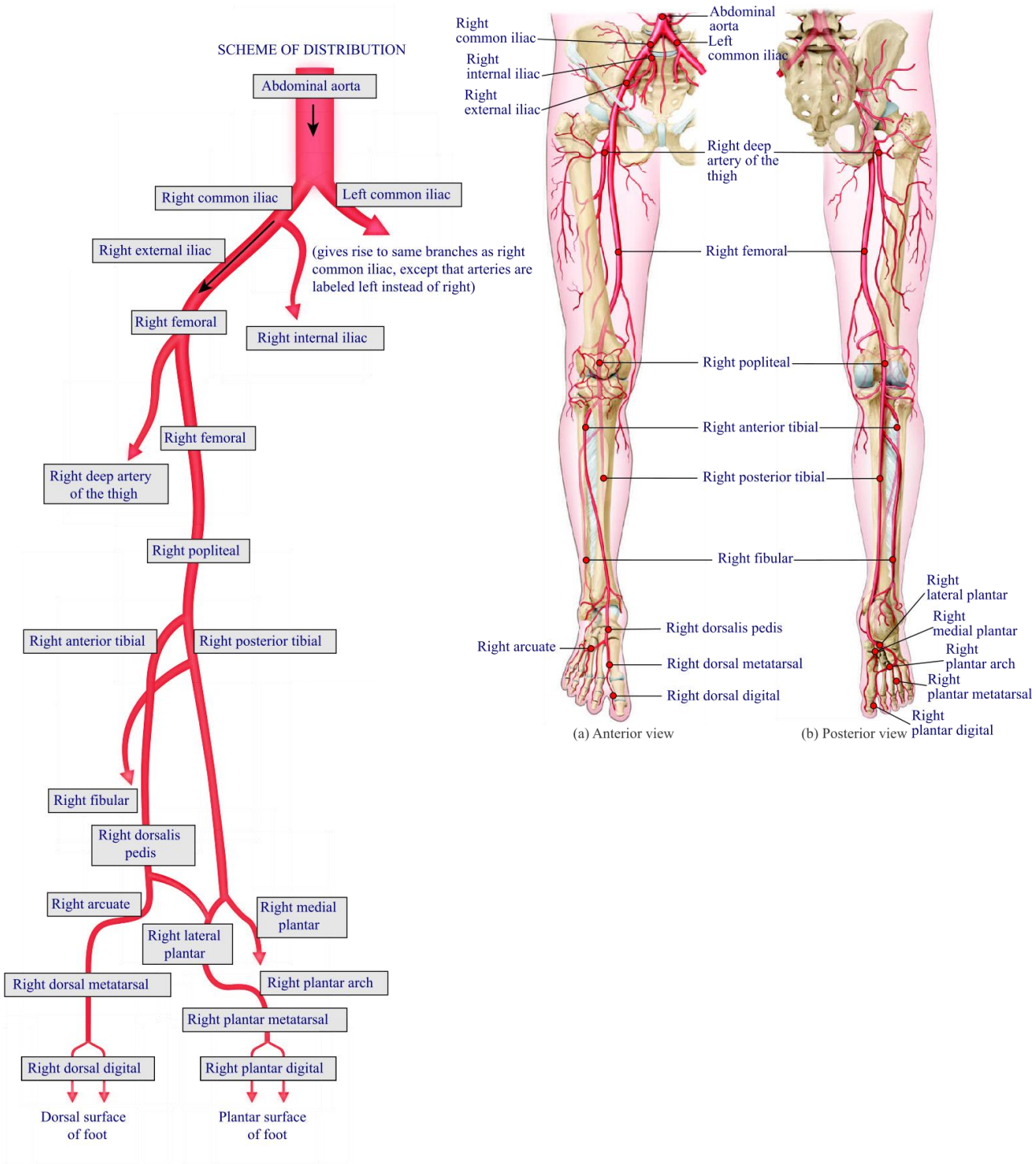

Vascular system (arteries) of the pelvis and lower limbs. Source: (Tortora and Derrickson, 2020)

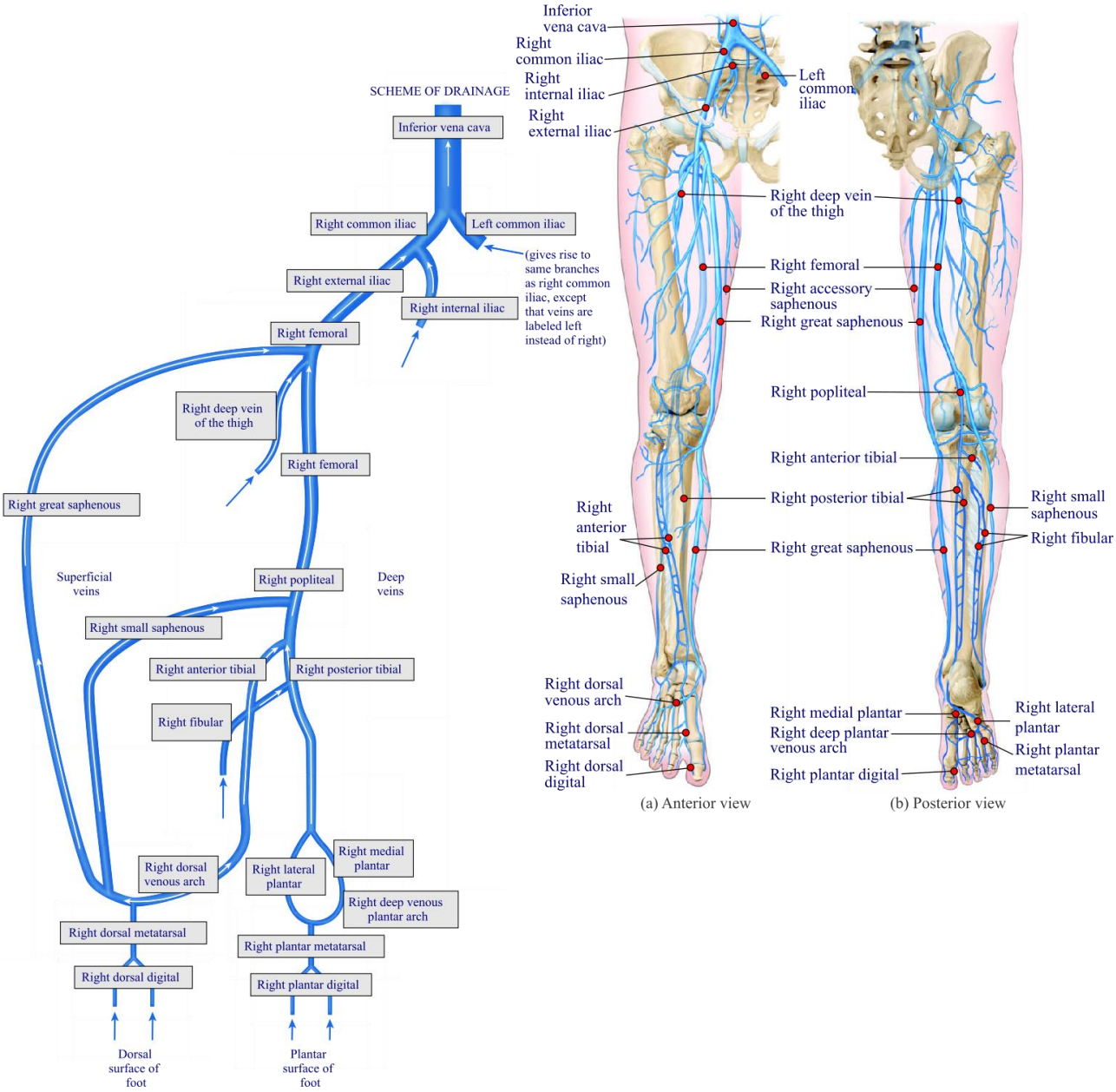

Vascular system (veins) of the pelvis and lower limbs. Source: (Tortora and Derrickson, 2020)

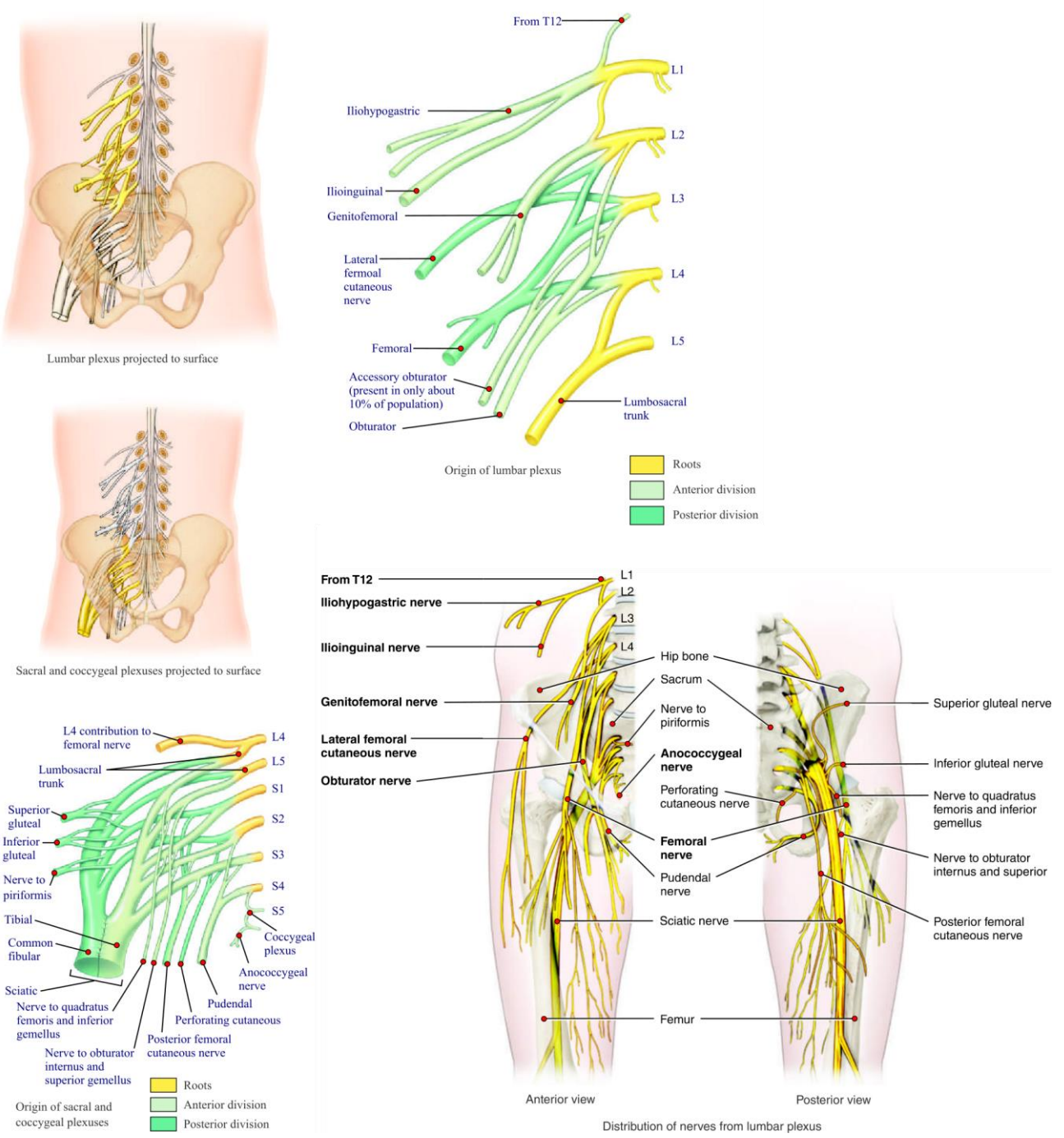

Nervous system of the pelvis. Source: (Tortora and Derrickson, 2020)

11.13 Appendix M: SkeletoMy website

Mission

SkeletoMy.com is an online platform supporting the *SkeletoMy* Point-of-Care 3D Unit set by the 1st Department of Orthopaedic Surgery, National and Kapodistrian University of Athens at Orthopaedic Research Center *"P.N. Soucacos", "Attikon"* University Hospital.

SkeletoMy emphasizes on delivering simple to extremely complex standard and/ or individualized orthopaedic solutions.

SkeletoMy's ultimate mission is to:

- Assist orthopaedists in musculoskeletal disorders rehabilitation by offering intangible services and/ or developing physical patient-specific orthopaedic products within or near the health care facility.
- Design and materialize optimal bespoke solutions and simplify orthopaedic operations by complex (bio)mechanical engineering design pre-operatively to mitigate as much risk from the operating room.

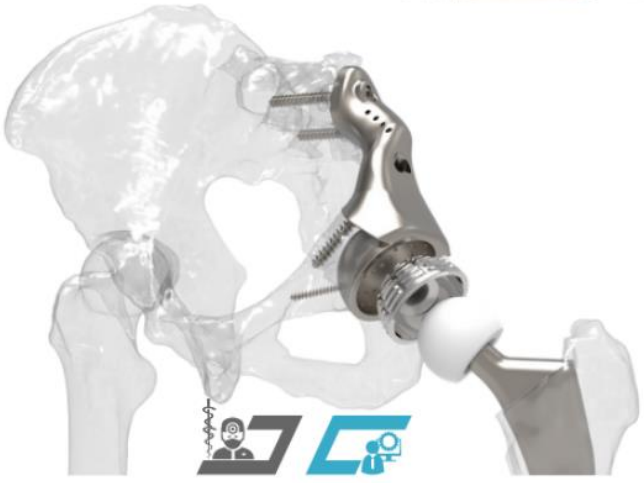

(continues)

(continued)

Inter-epistemic Synergy

Scientifically amalgamated schemes embracing engineering, powered by clinical expertise could categorically improve healthcare delivery and patient satisfaction. All patient-specific solutions emerge collaboratively from a de-novo systematic inter-epistemic orthopaedic product design methodology.

Orthopaedists "become the designers":

(Bio)mechanical design engineers develop and materialize each bespoke product as per the orthopaedist's guidelines.

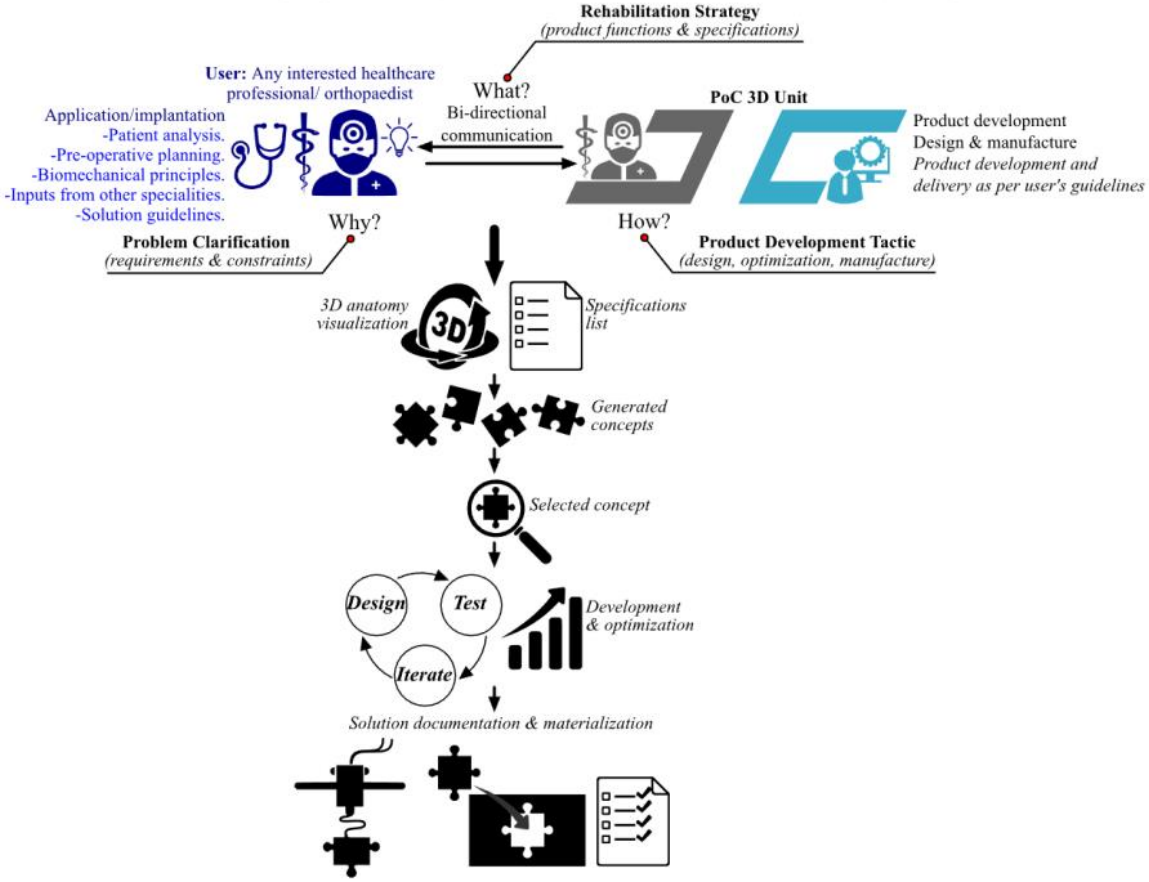

Services for End-to-End Workflow

SERVICE REQUEST & CASE SUBMISSION

Registered users request services, submit cases and upload anonymized patient data.

Development process status tracking and seamless data exchange.

Submission forms, guidelines provision, and reporting for efficient and fast collaboration.

MEDICAL IMAGE DATA PROCESSING

3D anatomical model reconstruction from Tomography (DICOM) and 3D scanned data.

COLLABORATIVE PATIENT-SPECIFIC ENGINEERING DESIGN

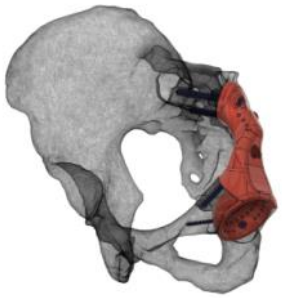

Utilization of a de-novo systematic inter-epistemic design methodology for off-the-shelf components selection and/ or custom solutions development as per the user's guidelines.

(continues)

(continued)

SkeletoMy's online platform home page

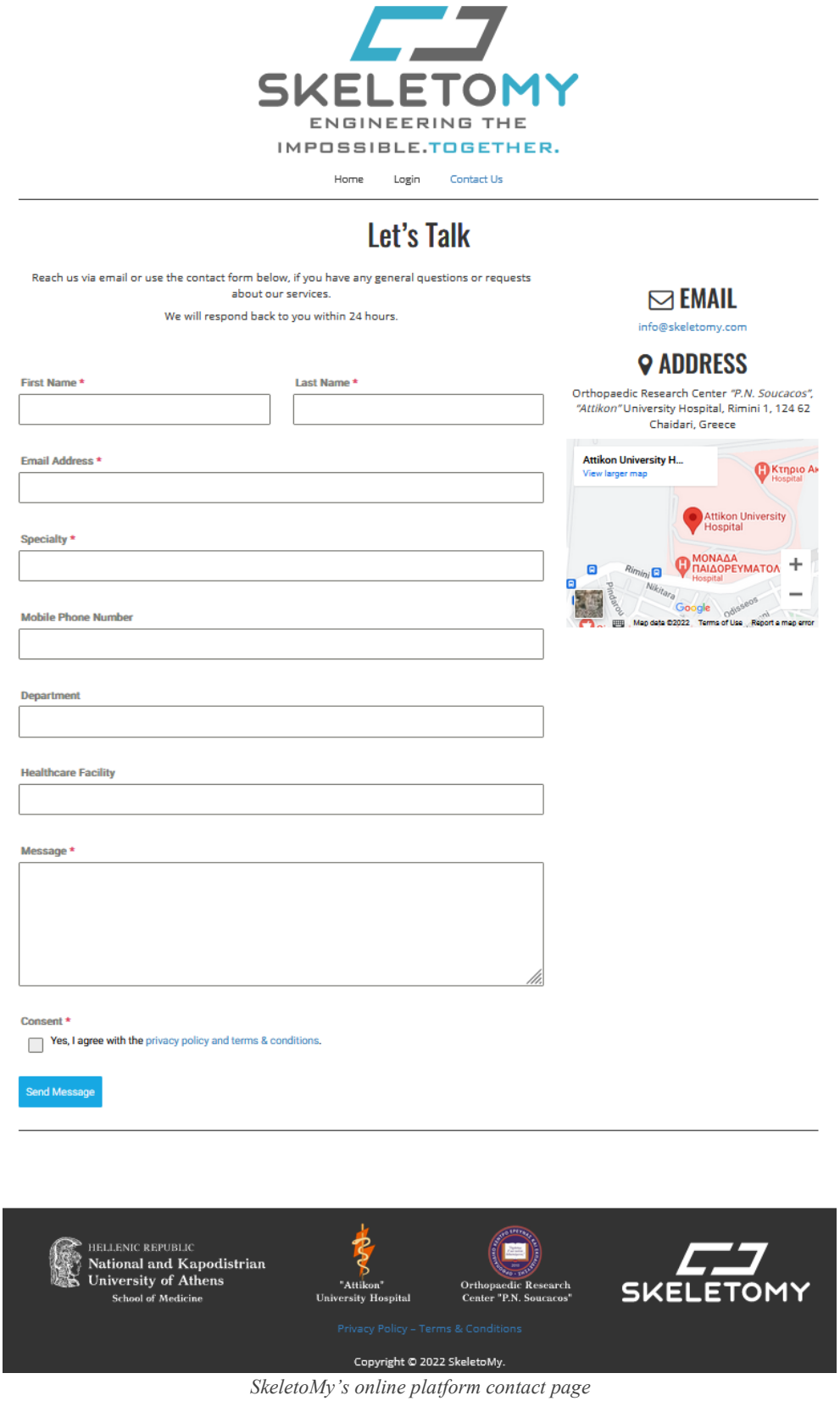

SkeletoMy's online platform contact page

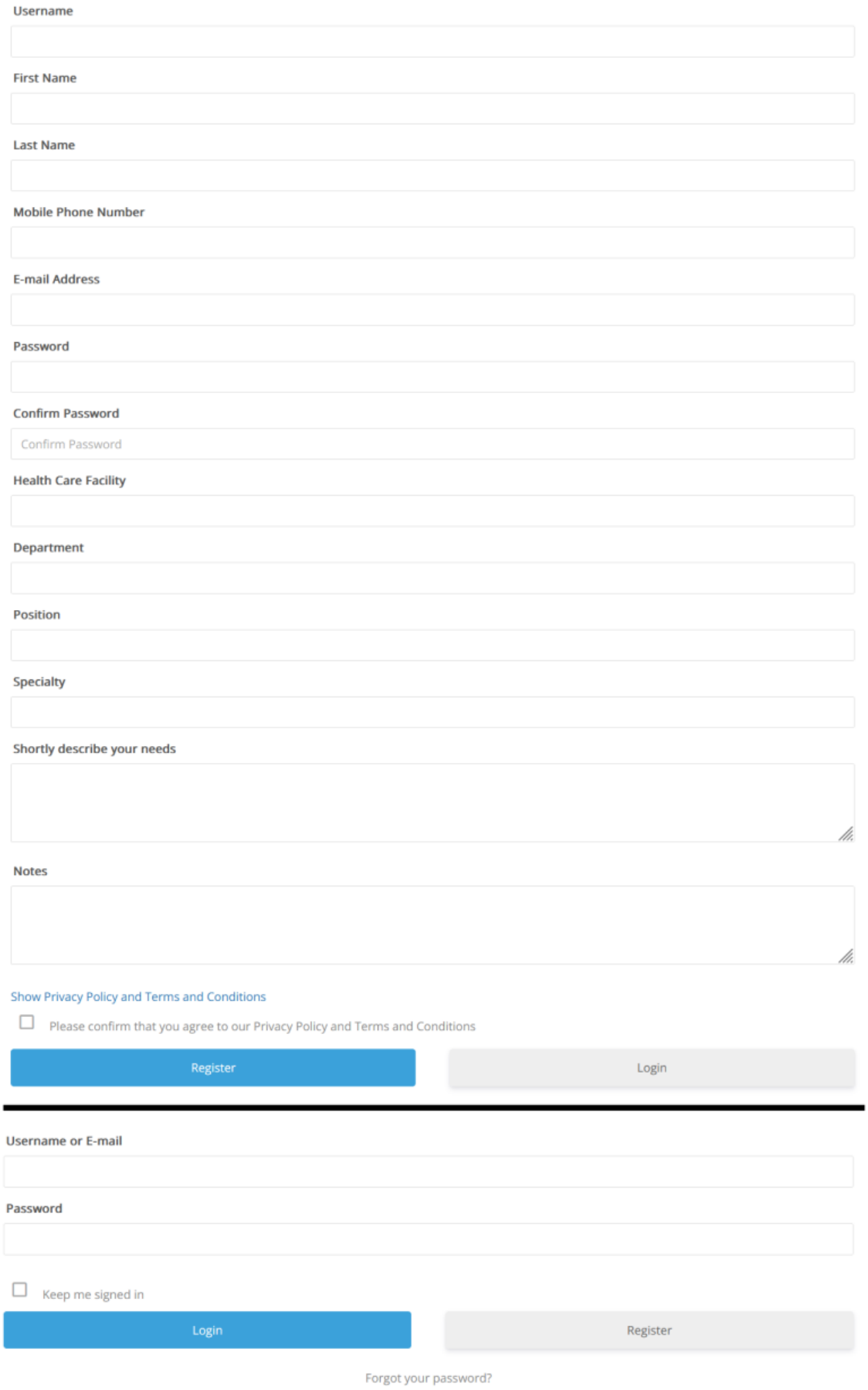

SkeletoMy's online platform login/registration pages

PRIVACY POLICY

This Privacy Policy applies to *SkeletoMy* Point-of-Care 3D Unit and to https://www.skeletomy.com website ("SkeletoMy", "we", "us", "our", "website") and outlines what, how and when personal information from individuals visiting our website are collected, handled, managed and protected in EU in the course of our operations. We are committed to protecting your privacy, and in cases we collect or deal with your personal information, we comply with the EU General Data Protection Regulation (GDPR) Articles, 12, 13 and 14. By providing your personal information to us you consent to the collection and usage of your information under the terms of this Privacy Policy.

It is advised that this Privacy Policy is to be read in conjunction with the Terms and Conditions.

This Privacy Policy was last updated on 12 December 2022. We reserve the right to update this Privacy Policy from time to time and post any updates on this page. Please review this Privacy Policy regularly so that you are updated on any changes.

SkeletoMy only collects information about individuals that is necessary for its operations and help you with better experience. We may collect among other things, your full name, address, telephone number, email address, and other personal information. In cases you do not provide the requested information that is essential for us, we may not be able to serve your needs. We collect personally identifiable information when you knowingly provide it to us, including:

- While you navigate through certain pages of our website via your browser.
- When you register to create a user account.
- When you participate by responding in surveys and send any kind of messages.
- When you fill out and submit forms via this website or send us information via email, via mobile phone, or deliver in person.

Before sending by any means or submitting via any forms any documents and files to us such as medical image data, any information pertaining to any patient under your supervision and responsibility, all such data must be anonymized. Guidelines for anonymizing such data is given to all registered users after they obtain account credentials to login to our website. Do not send us any patient data unless requested by us. Make sure that your patient(s) consent and provide(s) you the authority, whilst you comply with all applicable laws to send us such data after anonymization. Contact us for details.

We would like to send you information about products and services that we think you might like, though you may always opt out any time. Please contact us if you no longer wish to be contacted for marketing, promotional and surveying purposes.

SkeletoMy may use your personal information for the following purposes:

- To process and fulfil your request.
- To deal with any enquiries or complaints.
- To manage your account or support you.
- To provide you with information, products or services that you request from us, or which we feel may interest you.
- To administer and send you marketing, promotional and survey material.
- To improve our website, our strategies and our services and products to ultimately serve you better.

We securely store your data and take all reasonable steps to protect your personal information:

- We never ask for credit card numbers and bank account details.
- We use regular Malware scanning.
- We make sure that all collected personal information is accurate, complete and up to date.
- We protect all personal information from misuse, interference, loss or unauthorized access, modification or disclosure both physically and through computer security methods. All personal information is contained behind secured networks accessible to limited persons that keep all these information confidential.
- We destroy or permanently de-identify personal information if it is no longer needed or requested for any purpose.

We would like to make sure you are fully aware of all of your data protection rights:

- The right to access – You have the right to request for copies of your personal data. We may charge you a small fee for this service.
- The right to rectification – You have the right to request that we correct any information you believe is inaccurate. You also have the right to request us to complete the information you believe is incomplete.
- The right to erasure – You have the right to request that we erase your personal data, under certain conditions.
- The right to restrict processing – You have the right to request that we restrict the processing of your personal data, under certain conditions.
- The right to object to processing – You have the right to object to processing of your personal data, under certain conditions.
- The right to data portability – You have the right to request that we transfer the data that we have collected to another organization, or directly to you, under certain conditions.

If you would like to exercise any of the aforementioned rights, please contact us.

In addition to personal information, we collect "cookies". Cookies are small files stored on your computer to collect standard Internet logs and visitor behavior information. When you visit our website, we may collect information from you automatically through cookies. For further information, visit allaboutcookies.org. We use cookies in a range of ways to improve your experience on our website, including keeping you signed in and understanding and remembering your preferences for future visits to our website. You can set your browser not to accept cookies, and the above website tells you how to remove cookies from your browser. However, in a few cases, some of our website features may not function as a result.

Links to other third-party websites might be contained in our website. This Privacy Policy applies only to our website, so if you click on a link to another website, you should read their privacy policy and we have no responsibility or liability for the content and activities of these third-party websites. However, we welcome any feedback about these third-party websites.

If you have any queries or concerns about our Privacy Policy or the way we handle your personal information, please contact us. Should you wish to report a complaint or if you feel that *SkeletoMy* has not addressed your concern in a satisfactory manner, you may contact the Information Commissioner's Office.

Contact details:

Address: Orthopaedic Research Center *"P.N. Soucacos"*, *"Attikon"* University Hospital, Rimini 1, 124 62 Chaidari, Greece.

Email address: info@skeletomy.com

Telephone: +30 6981613476

Website: skeletomy.com

SkeletoMy's online platform privacy policy

TERMS AND CONDITIONS

User: any interested healthcare professional/ orthopaedist registered to *SkeletoMy* platform holding an active account with the ability to submit requests for services and/ or products in order to use these as aids in diagnosing and/ or treating his patient(s) for whom (patient(s)) he (user) is responsible for. Users a) provide design input, guidelines, notes and instructions for the development and delivery of the services and/ or products they request, b) approve in their whole the requested services and/ or products before realization and delivery by *SkeletoMy*, and c) take full responsibility for their performance, usage, risk, and safety of the requested services and/ or products.

SkeletoMy.com is an online platform supporting the *SkeletoMy* Point-of-Care 3D Unit established by the 1st Department of Orthopaedic Surgery, National and Kapodistrian University of Athens at Orthopaedic Research Center *"P.N. Soucacos"*, *"Attikon"* University Hospital. *SkeletoMy* delivers intangible services and physical products to the users to rehabilitate simple to extremely complex musculoskeletal disorders. Standard and/ or individualized orthopaedic solutions are developed collaboratively with the user within or near the health care facility, in order to simplify orthopaedic operations by complex (bio)mechanical engineering design pre-operatively and mitigate as much risk from (surgical) orthopaedic procedures.

This website is *SkeletoMy's* property and all content is protected by applicable copyright and trademark laws. Users may print single copies of the content for their own personal, non-commercial use. Further copying, redistribution or publication of any part of this website is prohibited.

We are not liable for any damages or injuries resulting from users' access to, or inability to access this website or from reliance on any information at this website. We make every effort to protect this website from malicious third-party access, it we will not be held responsible for any virus or third-party user damage sustained as a direct result of accessing this website.

Anyone accessing this website should not construe anything on the website as a promotion or solicitation for any product or service, or for the use of any product or service that is not authorized by the laws and regulations of the country in which they might be located. This website contains information about services and products that may or may not be available in any particular country or region and where applicable, may be approved or cleared by a government regulatory body for sale or use with different indications and restrictions in different countries. For more details, please contact us.

To send us documents and files such as medical image data pertaining to their patient(s), users must follow the instructions and send such data only when requested in our request forms. Such patient data must always be anonymized prior sent to us. Only registered users are allowed to upload and send such patient data. Do not send such data unless requested by us. Make sure that your patient(s) consent and provide(s) you the authority, whilst you comply with all applicable laws to send us such data after anonymization. Contact us for more details on how users can request services and/ or products offered by *SkeletoMy* and when and how to send patient data.

We are not responsible for the selection of any particular (surgical) technique and products to be used on a particular patient, or services and products to be used for diagnosing and/ or treating a particular patient. The user who performs the (surgical) technique is responsible for selecting suitable products, and deciding and implementing the appropriate techniques for all procedures, including products and procedures developed by *SkeletoMy*. We do not recommend any particular services or products developed by others than us and do not guarantee the validity and accuracy of their information.

SkeletoMy offers services and develops products collaboratively with and as per the user's guidelines, notes and instructions to aid in rehabilitating simple to complex musculoskeletal disorders. Before delivering a service and/ or a product, the user who requested that particular service and/ or product must fully accept and approve by his signature the service and/ or product to be delivered by *SkeletoMy* in its whole, and also fully agree and accept that he takes full responsibility for the performance, usage, risk, and safety of this service and/ or product to be delivered *SkeletoMy*.

Delivery time for services and/ or products will not start before the user fully approves for and agrees on all details, documentation and reports. We are free of the duty to compensate for transportation damages and costs. Delivery arrangement, and associated transportation risks and expenses are borne by the user. All products delivered by *SkeletoMy* to the user must be visually inspected before usage and any defects and damages to be reported to *SkeletoMy* as soon as possible.

Further terms of trade, terms of payments, as well as terms of warranty are made available to all users once they obtain active accounts and credentials to login in our website.

This site may contain information related to health conditions and their treatment. Such information is not meant to substitute advices and treatments given by healthcare professionals to their patients. Information and materials contained in this website must not be used for diagnosing and treating health problems. Any person suffering from any disorder should always consult a healthcare professional to determine what treatments might be appropriate for them.

If you have any questions at all regarding *SkeletoMy's* Terms and Conditions, please contact us.

Contact details:

Address: Orthopaedic Research Center *"P.N. Soucacos"*, *"Attikon"* University Hospital, Rimini 1, 124 62 Chaidari, Greece.

Email address: info@skeletomy.com

Telephone: +30 6981613476

Website: skeletomy.com

SkeletoMy's online platform terms and conditions

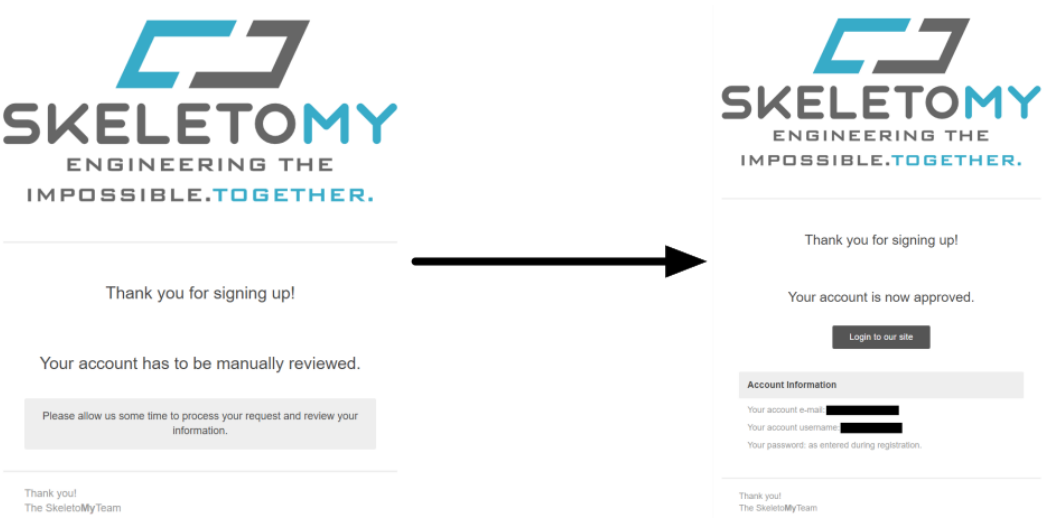

User account approval e-mail sent by SkeletoMy online platform

SkeletoMy's online platform service request page for registered users

11.14 Appendix N: Considerations for PoC manufacturers

OVERALL DEVICE DESIGN

GENERAL

[Market segment: medical device and POC]

- Compare desired feature sizes of the final finished device to the minimum possible feature size of your AM technique and the manufacturing tolerances of the individual machine.
  - This helps you compare build parameters and conditions under which the final device is expected to be made to your design.
  - The purpose of this comparison is to determine the reliability of the print.
- Pixelation of features (when smooth surfaces become stepped) can lead to rougher surface finishes.
  - Some devices require smooth surface finishes for patient safety
  - Surface finish requirements should be documented in specifications.

PATIENT-MATCHED DEVICE (PMD) DESIGN

INTRO

[Market segment: POC]

- PMDs may be produced within a defined design or performance envelope
  - This envelope is determined before patient matching can be initiated.
  - The envelope describes the minimum and maximum dimensions, mechanical performance limits, and other clinically relevant factors.
- PMDs are NOT customized devices meeting the FD&C Act custom device requirements.
  - Most PMDs fall under the requirements for their respective device type.
- Modifications of design may have direct consequences for the patient.
  - You should identify clinically relevant design parameters, the predetermined range for these parameters, and which of the parameters can be modified for patient-matching before the device can be used by any patient.

EFFECTS OF IMAGING

[Market segment: POC]

- Factors that may affect the fit and performance of AM image-based PMDs include: minimum image feature quality and resolution; smoothing or image processing algorithms that may alter dimensions when compared to reference anatomy; rigidity of anatomic structures being imaged; and clarity of anatomic landmarks used to match the device to the patient's anatomy.
- Small changes in size or geometry may be difficult to identify during visual inspection of the device and may only be detected once in use by a patient. It is also important to note the range of changes (e.g., deformation) that may be experienced by soft tissue at a target location when comparing true anatomy to a reference image. This should be considered when designing and testing your device.
- Anatomy can change over time (e.g., disease progression), even between the time the patient is imaged and the device used. This allowable time should be noted as an expiration date of the device

*You should employ a risk-based approach, taking into consideration the intended use of your device as well as your design methodologies to assess worst-case scenarios.

INTERACTING...*

[Market segment: POC]

- PMDs are often made by altering features of standard-sized devices. This is typically done through device manipulation software.
- Feature alterations can also be done by manual methods using key anatomic landmarks or specific measurements on radiographs.
- Any software or procedure used to make modifications to device design based on clinical input should include internal checks that prevent the operator from exceeding determined pre-established device specifications

COMPLEX DESIGN FILES

[Market segment: POC]

- PMDs that follow patient anatomy closely are especially vulnerable to errors in file conversion. For example, anatomic curves are typically geometrically or mathematically complex, increasing the likelihood of error.
- For PMDs, all file conversion steps are typically performed every time a device is built instead of once during the design phase of a standard-sized device. This means you should perform internal checks for each model to prevent inaccurate devices.
  - See Section V.C.I.A(1) on data integrity in the FDA guide for more information.

PATIENT-MATCHED DEVICE (PMD) DESIGN

CYBERSECURITY AND PII

[Market segment: Medical device and POC]

- Proper management and care of PII and PHI are essential to maintain patient privacy throughout the device design and manufacturing process.
  - See HHS Guidance on Significant Aspects of the Privacy Rule for more information on patient privacy.

SOFTWARE WORKFLOW

FILE FORMAT CONVERSIONS

[Market segment: Medical device and POC]

- Medical device design and manufacture typically involve interaction between several software packages, often from different manufacturers. This requires files to be compatible across the different software applications used to maintain design and file integrity.
- Errors in file conversion can negatively impact your final device and component properties, including dimensions and geometry.
  - Because of this, you should verify critical attributes and performance criteria of your final product as part of your software workflow validation.
- When possible, final device files for printing should be maintained and archived or referenced in robust, standardized formats that can store AM-specific information (i.e., AMF format).

DIGITAL DEVICE DESIGN TO PHYSICAL DEVICE

[Market segment: Medical device and POC]

- **Build volume placement**: The distance between each device or component in the build volume and whether they are identical or different designs can affect material properties, surface finish, and ease of post-processing. Build orientation of each device can also impact functional performance by affecting anisotropic properties. Many machines have areas of the build volume where they function optimally and areas where they do not. This affected region may be different for every machine.
  - Your operational qualification (OQ) should include challenging the build volume placement to establish control limits resulting in products that meet all requirements.
- **Addition of support material:** The location, type, and the number of supports in your print can affect a final finished device's geometric accuracy and mechanical properties. Each AM machine and technology have different support needs to produce a quality device. Most supports from any machine can be removed physically or by chemical means.
  - Automated algorithms can be used to choose the location and number of supports, but geometric complexities or printing limits often require manual intervention when adding supports to a print file.
  - Common structures that may need support include overhangs, high aspect ratio features that protrude from the main body of the device, internal features, and thin features prone to warping.
  - All manufacturing material removal processes should ensure that material residues are removed to the level where they do not impact the safety or effectiveness of the device.
- **Slicing:** Nominal layer thickness is determined by machine specifications and software capabilities. However, the machine's technical characteristics and the material' may further influence achievable layer thickness.
  - Choice of layer thickness should be documented and reflect a balance between the achievable and desired surface texture, bonding between and curing of each layer, sensitivity to power fluctuations, accuracy, quality, and printing speed.
- **Build Paths:** The path traced by the energy or material delivery system can impact the quality of your final device. The space between each line of the build path and the path speed change the amount of melting and remelting that the boundaries of each line of material will experience. Further, certain build path selections may result in an orientation or anisotropy in the device.

continues

continued

SOFTWARE WORKFLOW

DIGITAL DEVICE DESIGN TO PHYSICAL DEVICE

Before printing, you should assess whether differences in the build path have the potential to significantly affect the performance of your device (if so, it is essential to maintain consistency).
If a non-solid fill density is used, you should identify whether internal voids are externally accessible or sealed. If they are not sealed, you should assess the risk associated with patient exposure.
Machine Parameters and Environmental Conditions: Proper calibration and preventative maintenance are critical factors in achieving low rejection rates. To maintain the desired and acceptable calibration, machine parameters can be modified. Environmental conditions in the build volume can also affect final device quality; for those without a self-contained build volume, ambient temperature, atmospheric composition, and flow patterns can impact solidification, layer bonding, and mechanical properties. Finally, optimal settings and parameters for a single model of a machine can vary when printing different devices or for multiple models of a machine printing the same device.
Because of its effect on device quality, it is critical to establish and maintain procedures to control environmental conditions.
Parameters that may have a significant impact on the final device may include instantaneous power of the energy delivery system, build speed or beam speed, build path, total energy density, and focal point or nozzle diameter.

VALIDATING AND AUTOMATING SOFTWARE PROCESSES

[Market segment: Medical device and POC]
* Refer to FDA Guidance on "General Principles of Software Validation" if you use a workflow that automates one or more software steps.

MATERIAL CONTROLS

STARTING MATERIAL

[Market segment: Medical device and POC]
- Throughout the printing process, the material may undergo significant physical and/or chemical changes. This can significantly impact the success of the build cycle and properties of a final device.
- The following aspects of your starting material should be documented prior to printing: the identity of the material/chemical by common name, chemical name, trade names, Chemical Abstracts Service (CAS) number, recognized consensus material standard, material supplier, incoming material specifications, and material certificates of analysis (COAs) with any test methods used.
- Specifications for incoming materials or test methods should be based on the AM technology you use, the intended use of the final device, and the information available about the material or test methods. Specification examples include: particle size/distribution/relevant rheological performance for powders or filament diameter and diametric tolerances for filaments; viscosity or viscoelasticity and pot life for fluids; composition, purity, water content, molecular formula, chemical structure, molecular weight, molecular weight distribution, glass transition temperatures, melting/crystallization point temperatures, purity information for polymers; chemical composition and purity for metals/metal alloys/ceramics; mix ratio with specifications provided for each component for composite materials.
- When any material spec changes affect the build process, the effect on the final device should be understood and documented.

MATERIAL REUSE

[Market segment: Medical device and POC]
Unused material could be exposed to conditions that alter it from its virgin state. To account for this, the FDA recommends documenting any evidence that material reuse doesn't adversely affect the final device by describing the reuse process. This may include a description of processes like filtering, a limit on the percent of reused material, and monitoring for changes in chemistry, oxygen, or water content.

POST-PROCESSING

GENERAL

[Market segment: Medical device and POC]
- All post-processing steps should be documented and include a discussion of their effects on materials used and the final device. It is important to identify any potentially detrimental effects of post-processing and describe any mitigations implemented.
- Care should be taken to ensure the printing and post-processing processes maintain the required device performance.
- Following printing, the desired surface roughness of the device can be achieved through post-processing steps like mechanical polishing, but hard-to-reach spaces may remain in the as-built state. These spaces should be assessed for their effects on the mechanical performance of the device or component.

PROCESS VALIDATION AND ACCEPTANCE ACTIVITIES

PROCESS VALIDATION

[Market segment: Medical device and POC]
- Device quality is impacted by the AM process, and quality may vary for an identical device or component when built using different AM machines, even if the devices are the same model with the same print parameters. For this reason, knowledge of how variability affects the final device is critical to ensuring part quality.
- Process validation must be performed where the results of a process cannot be fully verified by subsequent inspection and test to ensure and maintain quality for all devices and components built in a single build cycle, between build cycles, and between machines.
- Criteria for acceptance must be established before testing.
- For validated processes, all monitoring and control methods and data must be documented.
  - Test methods used for process monitoring and control must also be validated.
- Types of factors to consider when performing process validation include in-process monitoring of process parameters, temperature melt pool data, build space environmental conditions, etc.), manual and automated visual inspection with defined acceptance criteria, non-destructive evaluation, and test coupon evaluation.

REVALIDATION

[Market segment: Medical device and POC]
- All process deviations and changes to your device or manufacturing process should be identified and analyzed for potential risks. Some changes and deviations may trigger the need for revalidation of the process.
  - Some triggers for revalidation include software changes, changes in material or material handling, changes in spacing or orientation of devices or components in the build volume, changes to software workflow, physical relocation of a machine, and changes to post-processing steps or parameters.
- When considering a change to a previously cleared or approved device that uses AM, rely on existing FDA guidance for their regulatory pathway.

ACCEPTANCE ACTIVITIES

[Market segment: Medical device and POC]
- Some acceptance activities for individual devices can be performed through non-destructive evaluation (geometry, morphology, some performance characteristics). Non-destructive techniques include calipers, ultrasound, computed tomography (CT) or micro-CT, x-ray, dye penetration, confocal microscopy, and hyperspectral imaging.
  - If a non-destructive evaluation technique is used in your process validation/acceptance activities, your choice of technique should be discussed and documented.

TEST COUPONS

[Market segment: Medical device and POC]
- It is recommended that test coupons be used to help with process validation and identify the print process's worst-case conditions. They can also be used for in-process monitoring.
  - Test coupons may not be needed if the process is validated and coupon testing is not a process-monitoring activity defined in the QMS.
- Test coupons suitable for destructive mechanical testing can be simple shapes, or they may contain one or more structural features representative of the component/device that can be assessed using destructive techniques.
- When used, the coupons should be validated to accurately and reproducibly represent the one or more printed parts within a specific build volume.

QUALITY DATA

GENERAL

[Market segment: Medical device and POC]
- Analysis of sources of quality data to identify existing and potential causes of a nonconforming product or other quality problems is essential to maintaining a quality process.
- It is important to consider whether it's necessary to keep track of the location of parts in the build volume. The answer to this question depends on the information you obtain during your process validation activities as well as design specifications.
- Level of specificity is important in identifying possible causes of failure when multiple different components are made in the same build volume at the same time. Quality data must be able to be analyzed to enable proper identification of quality problems and investigation of the cause of nonconformities.

Source: (Formlabs, 2021)

11.15 Appendix O: Biomimicry Taxonomy

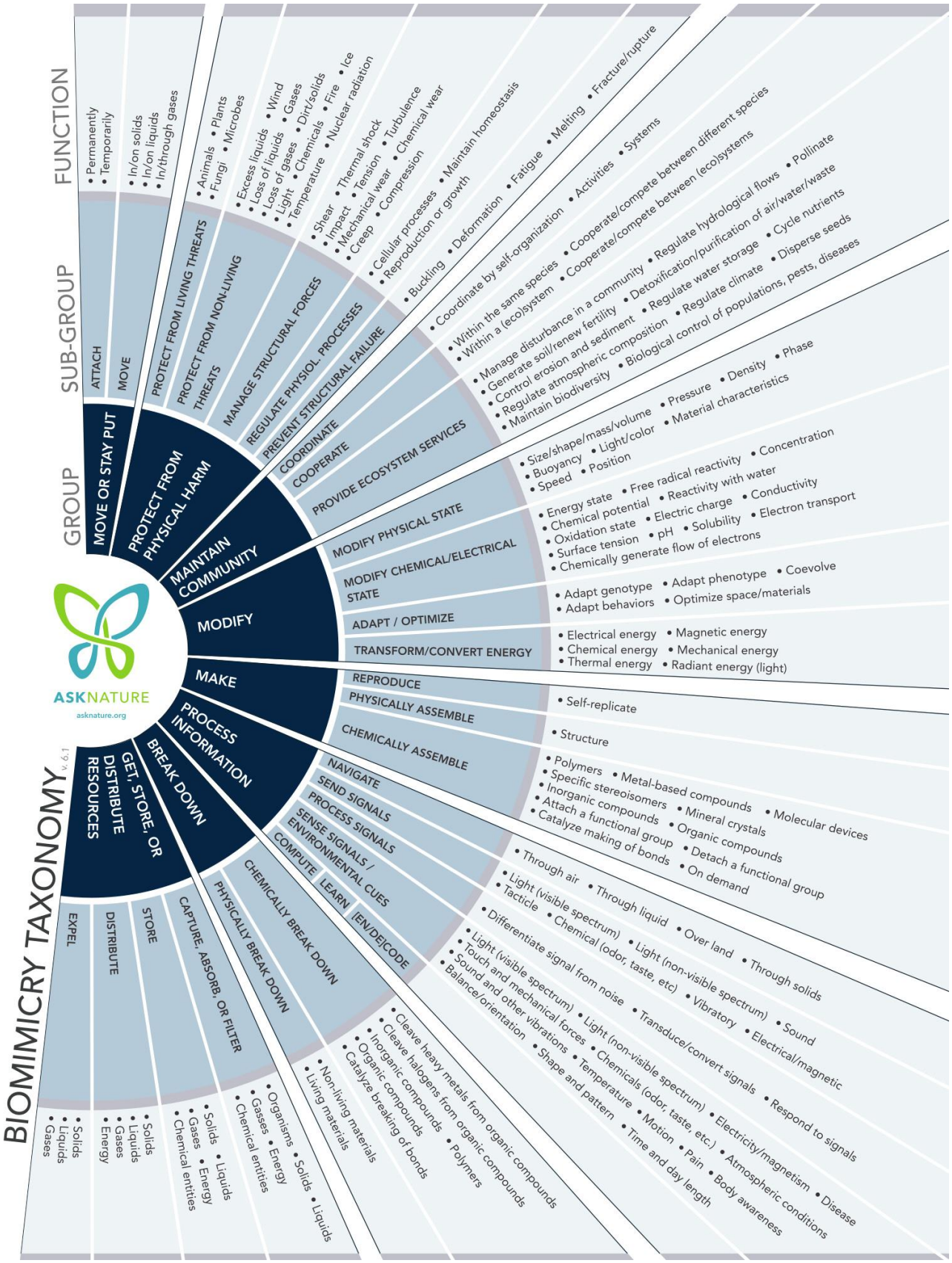

Biomimicry taxonomy of biological strategies as per their function. Source: Biomimicry Institute